INFORMATION TO USERS

This manuscript has been reproduced from the microfilm master. UMI films the text directly from the original or copy submitted. Thus, some thesis and dissertation copies are in typewriter face, while others may be from any type of computer printer.

The quality of this reproduction is dependent upon the quality of the copy submitted. Broken or indistinct print, colored or poor quality illustrations and photographs, print bleedthrough, substandard margins, and improper alignment can adversely affect reproduction.

In the unlikely event that the author did not send UMI a complete manuscript and there are missing pages, these will be noted. Also, if unauthorized copyright material had to be removed, a note will indicate the deletion.

Oversize materials (e.g., maps, drawings, charts) are reproduced by sectioning the original, beginning at the upper left-hand corner and continuing from left to right in equal sections with small overlaps.

ProQuest Information and Learning
300 North Zeeb Road, Ann Arbor, MI 48106-1346 USA
800-521-0600

DEFORMATION AND SEDIMENTATION ADJACENT TO CARBONIFEROUS DIAPIRIC SALT STRUCTURES, NOVA SCOTIA

By

John Paul Brown

Submitted in partial fulfillment of the requirements for the degree of Doctor of Philosophy

At

Dalhousie University
Halifax, Nova Scotia
July 1998

DALHOUSIE UNIVERSITY

FACULTY OF GRADUATE STUDIES

The undersigned hereby certify that they have read and recommend to the Faculty of Graduate Studies for acceptance a thesis entitled "Deformation and Sedimentation Adjacent to Carboniferous Diapiric Salt Structures, Nova Scotia"

by John Paul Brown

in partial fulfillment of the requirements for the degree of Doctor of Philosophy.

Dated: July 10, 1998

External Examiner

Research Supervisor

Examining Committee

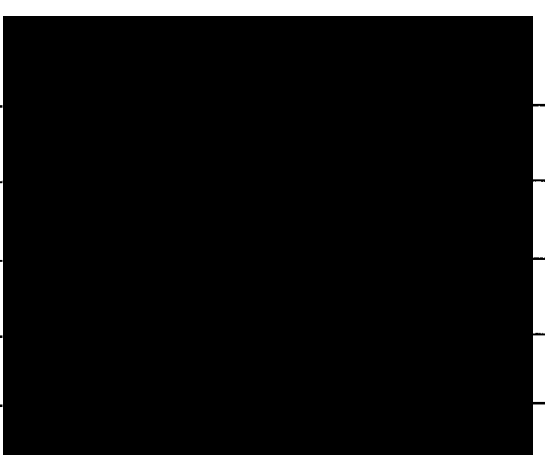

This thesis is dedicated to my mother,
for kicking me out of the house with a rucksack and a plane ticket to India
and to my father for teaching me to climb.

TABLE OF CONTENTS

LIST OF FIGURES

LIST OF TABLES

LIST OF APPENDICES TABLES AND FIGURES

LIST OF ENCLOSURES

1982 Chevron seismic line enclosures:

16 (i), 16 (ii), 67, 71, 75, 79 (i), 79 (ii), 83 (i), 83 (ii)

1978 Mabou seismic line enclosures:

2, 3, 4, 5, 6, 7, 8, 9, 11, 12, 13, 14, 15, 16

1985 Inverness seismic line enclosures:

A05, B03, B04, B06, B08, B10

ABSTRACT

Diapiric structures exposed within the Carboniferous rocks of western Cape Breton Island and on the Antigonish coast of Nova Scotia are unique and among the best exposed salt structures in the world. Complete sections through diapir structural carapaces and their associated drag zones are exposed as coastal cliff sections. The close tie between onshore exposures and near-shore seismic data provides a unique data set with which to examine halokinesis and salt tectonics at a scale over several orders of magnitude. The size, maturity, geometry and growth mechanism of the diapiric structures is directly related to the tectonics and sedimentary evolution of the field area which shows a division into three tectono-stratigraphic domains. Drag zone and the larger zone of rotation profiles are intimately related to the geometry of the diapir and the lithology of the strata adjacent to the diapir. Deformation within the drag zones was an interplay of brittle and ductile deformation mechanisms. Brittle faults exist as distinct generations that evolved in a systematic manner as the drag zone formed. Strain within the drag zones was biaxial, with horizontal extension parallel to the diapir margin being of similar magnitude to extension orthogonal to the diapir margin. Faults that developed late in the deformation history represent a localisation of extensional flexural slip. The distribution of competent and incompetent strata within a drag zone played a large role in determining the distribution of strain and deformation mechanisms within a drag zone. Deformation within the structural carapace mirrors the deformation within the underlying halite core of the diapir and reflects the maturity and geometry of the diapiric structure as a whole. The structural carapaces include curtain folds, which are bounded by curtain faults. Internal deformation was accommodated by a combination of brittle and ductile mechanisms and deformation was inherently triaxial. Halokinesis locally affected sedimentation by creating local sediment barriers source areas and depocentres in the form of diapiric exposures and withdrawal basins. This is indicated by local unconformities seen in outcrop and seismic profiles; conglomerates adjacent to some diapirs; progradational seismic facies adjacent to diapirs; and unusually variable paleoflow patterns. However, tectonic and eustatic events must be taken into account before the effects of halokinesis can be determined.

GLOSSARY OF SALT TECTONICS

CURTAIN FOLD. A cylindrical fold with radial axial trace and steeply plunging hinge within a diapir, possibly incorporating sheath folds originally in the source layer (Stier, 1915, Escher and Kuenen, 1929).

DRAG ZONE. The country rock strata adjacent to the diapir flank which has been deformed by the process of diapiric intrusion/growth. The rocks are typically deformed into a drag fold that extends for a few hundred metres away from the diapir (Davison, 1995). *Note*, the term drag zone is used in this thesis to describe a geometry, and does not attempt to describe the mechanism of formation.

EXTERNAL SHEAR ZONE. Located in the outermost part of a diapir where bedding curves in to parallelism with the external contact (Kupfer, 1976).

RIM SYNCLINE. A fold with an arcuate axial trace on the outer margin of a salt structure, typically resulting from salt withdrawal in the source layer (Nettleton, 1934).

PERIPHERAL SINK. Sediments that accumulate in a rim-syncline as a result of salt withdrawal (Trusheim, 1960).

SECONDARY PERIPHERAL SINK. Sediments that accumulate in a rim-syncline where the rim-syncline is formed as a result of salt withdrawal from a precursor pillow in to the diapir (Trusheim, 1960).

SALT DIAPIR. A mass of salt and evaporite minerals that has flowed in a ductile manner and appears to have discordantly pierced the overburden. An intrusion [of salt] emplaced discordantly against their country rocks (Posepny, 1871). A Fold cored by salt (Mrazec, 1907).

STRUCTURAL CARAPACE. A carapace that consists of a recognisable stratigraphic unit which has been transported vertically as part of a diapiric structure. Where present, a structural carapace is an intrinsic part of a diapiric structure (Schwerdtner, 1983).

SALT WALL. An elongate upwelling of diapiric salt, commonly forming sinuous, parallel rows (Trusheim, 1960).

SALT WITHDRAWAL. The process by which salt migrates from its original strataform position (or pre-existing salt structure) to form a (new) salt structure.

ZONE OF ROTATION (New Term) is similar to the drag zone but on a larger scale. In the context of this thesis the Zone of Rotation is seismically imaged and typically extends for up to 2.5 km from the external shear zone. The end of the Zone of Rotation is the closest point to the diapir of zero strata dip.

ACKNOWLEDGEMENTS

I would like to say a big thank you to Dr. Martin Gibling for his excellent support during my time at Dalhousie and also for intensifying my loathing of English grammar. A big thanks goes to several of my friends (Christina, Leslie, Brian, Robin, Deborah, Sandie and Jan) from Nova Scotia for making my time in Halifax a great experience. I would also like to thank Pan Canadian Petroleum for financial support and Midland Valley Services for giving me the time to finish this thesis.

I would also like to acknowledge funding from the Natural Sciences and Engineering Council of Canada (Grant to my supervisor, Dr M. R. Gibling) and federal funding from the Nova Scotia Minerals Development Agreement.

Lastly a huge thanks to Jan for all the page numbering, spelling corrections, seismic coloring and moral support.

CHAPTER 1, INTRODUCTION

1.1, THE FIELD AREA

The field area for this project is located within western Cape Breton Island (Port Hood to St. Rose), St. Georges Bay (Port Hood Island) and parts of the Antigonish coastline (Monks Head) (Figure 1.1.1). The project is therefore entirely contained within the province of Nova Scotia, which is part of the Atlantic Region of Eastern Canada. Fieldwork as part of this Ph.D project commenced in the fall of 1993 and initially concentrated upon the many sporadic exposures of the Upper Carboniferous Inverness Formation within western Cape Breton. The addition of the 1978 Mabou, 1982 Chevron and 1985 Inverness seismic surveys effectively extended the field area several kilometres offshore to incorporate the majority of St. Georges Bay (Figure 1.1.1). The seismic data clearly showed several large salt structures within the offshore areas of St. Georges Bay and western Cape Breton. From preliminary fieldwork it became obvious that the offshore salt structures may in fact be exposed onshore and that some of the coastal sections may represent sections through diapir drag zones as well as the diapirs themselves. The project was formulated to test this hypothesis and to examine the onshore diapir and drag zone exposures in detail.

1.2, PROJECT AIMS AND OBJECTIVES

Five objectives can be outlined for this project. Each objective concerns a specific aspect of the salt tectonics project, incorporating data and results from the other four stated objectives.

(i) To develop a tectono-stratigraphic framework for the field area based upon seismic data and onshore structural/stratigraphic information. Please note, however, that this thesis is focused upon salt tectonics and does not aim to resolve the detailed structural

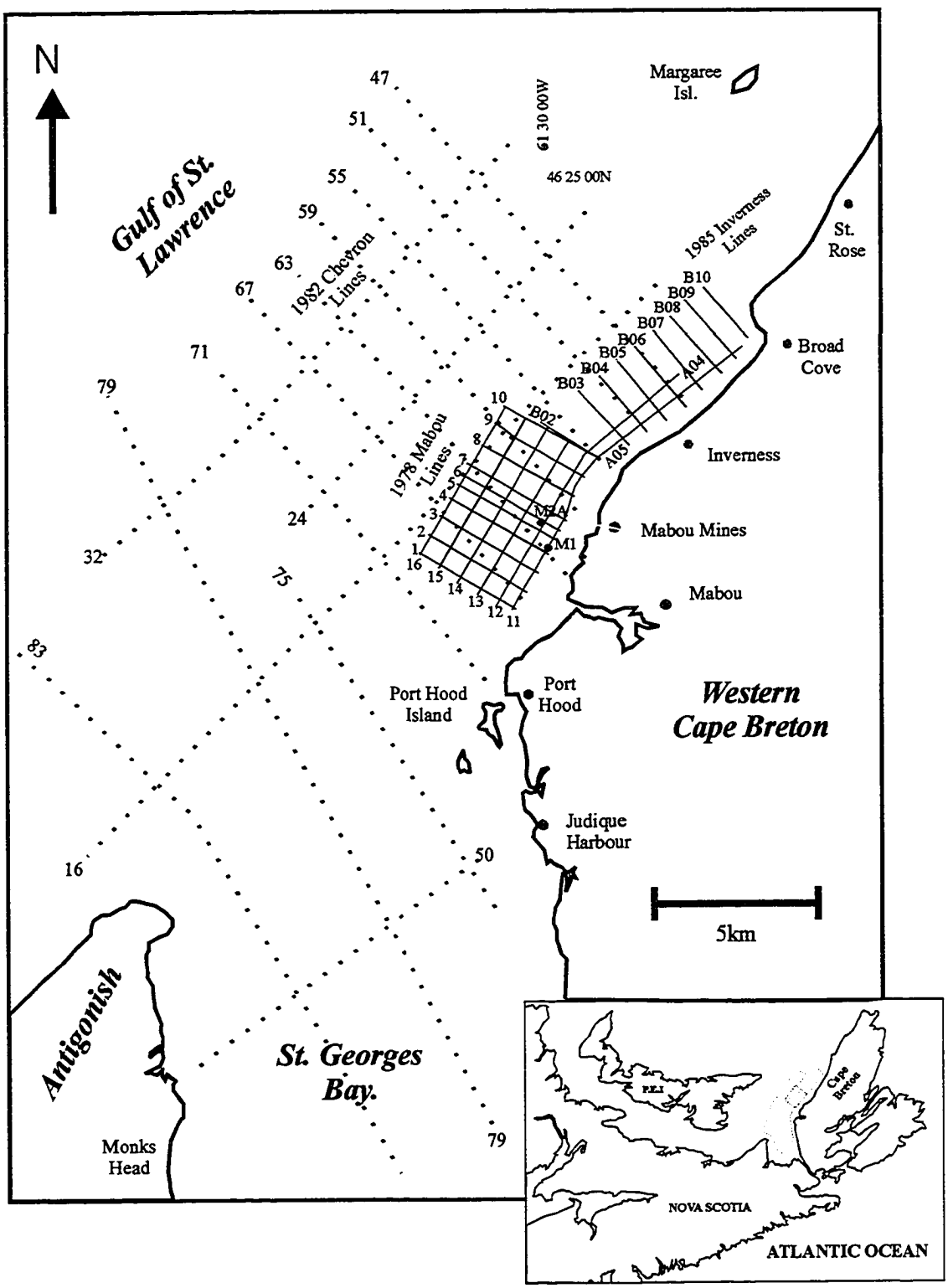

Figure 1.1.1. Field area location map and seismic coverage.

geology of western Cape Breton. In several areas the details required to produce a well constrained structural model for western Cape Breton are not available or would require exhaustive research that is outside the scope of this thesis.

(ii) To define the size, geometry, growth history and growth mechanism for the many salt structures which are either seismically imaged or exposed onshore within the project area.

(iii) To relate the tectono-stratigraphic framework of the field area to the evolution of the salt structures and to assess how tectonics and sedimentation have affected halokinesis.

(iv) To analyse the structure of onshore drag zones adjacent to diapiric structures. Broad objectives include: fault orientation analysis, examination of drag zone width and profile, and strain partitioning within drag zones. The objective of this structural analysis is to determine what geological factors control drag zone deformation.

(v) To examine the effects of halokinesis upon sedimentation and sedimentary architecture. This objective draws information from both the tectono-stratigraphic framework and the evolution of the salt structures and combines these data with onshore sedimentology and seismic facies analysis.

1.3, SALT TECTONICS: PAST, PRESENT AND FUTURE

Jackson et al. (1995) recently published a thorough review of the history of diapir studies and future directions, and this sections draws closely upon this analysis. Salt tectonics as a branch of geological research has, like any other branch of geology, undergone numerous conceptual revolutions in response to new theories and ideas that were (and still are) driven by economic necessity and advancements in technology. The discovery of economic hydrocarbons associated with diapiric structures, such as the Spindletop Diapir in Texas in 1901, greatly stimulated scientific research into salt tectonics. The advent of seismic data, in particular three-dimensional seismic data acquisition and processing, has allowed geologists to image sub-surface salt structures for the first time. Indeed, the conceptual leaps in our understanding of salt tectonics can be directly correlated with technological advances. Perhaps without the advent of modern technology our knowledge

would not have progressed significantly from the interpretation of Posepny's (1871) schematic cross section (Figure 1.3.1).

The conceptual difficulties within the realm of salt tectonics are all related to the unique geological properties of evaporites, coupled with the limitations of our current research tools. During the early years of salt tectonics research, several 'free-ranging' theories about the origin of salt diapirs were proposed. It was not until 1917 that Van der Gracht proposed that diapirs from the Gulf Coast of Mexico were pushed up as intrusive plastic masses through weaker spots in the overlying overburden. The application of buoyancy to salt diapirs by Lachmann (1910) and later by Arrhenius (1923) lent support to Van der Gracht's model for diapir growth. Buoyancy models for diapir growth were popular for over a decade despite acknowledgement of both mechanical and spatial difficulties involved with growing a diapir through a thick, lithified overburden. It was not until 1933 that Barton proposed the concept of a downbuilt diapir. His theory proposed that diapirs grew downwards from a relatively static top in response to basin subsidence and sediment accumulation. Inherent in this theory is the idea that the head of a diapiric structure would remain at or near the surface during much of the diapirs growth history. Barton's model was therefore in direct contradiction to the buoyancy theory, but it did succeed in solving the mechanical and spatial problems inherent in the buoyancy driven model.

The advent of analogue modelling was an important step in our understanding of salt tectonics. While analogue models can never truly reproduce the conditions or details of real geological situations, they can show a reasonable representation of the evolution or ontogeny of a geological system. Nettleton (1934) assumed that, when scaled down, salt and its overburden can be represented by two viscous fluids of negligible strength (oil and syrup). Nettleton (1934) demonstrated that gravity alone could generate a wide variety of diapir shapes and overburden geometries previously described from natural

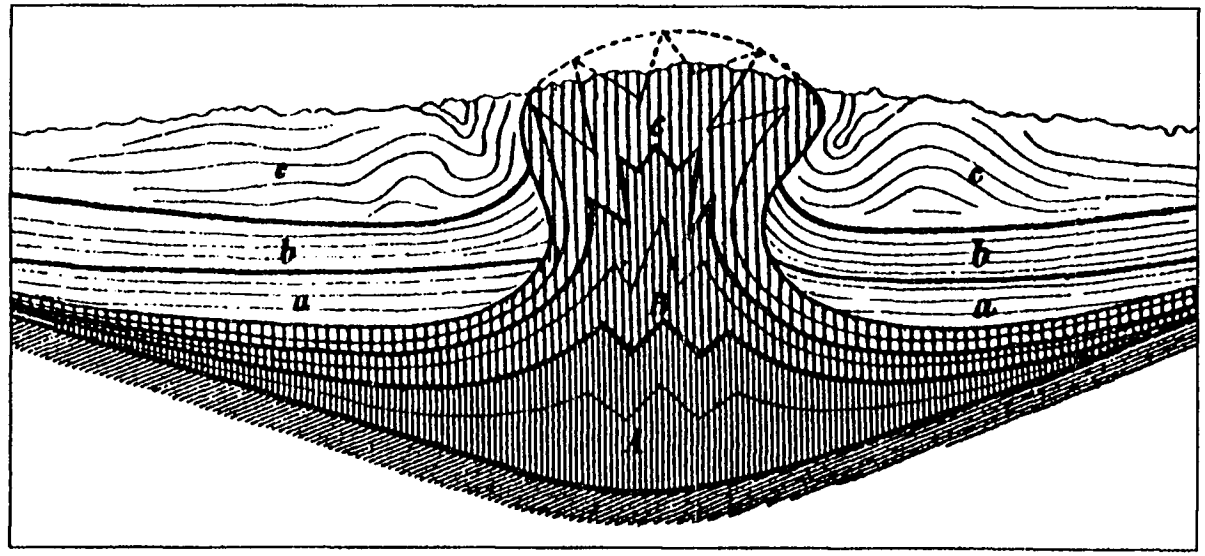

Figure 1.3.1. Posepny's (1871) schematic cross section. Note the discordant contact between the diapir and overburden, the overhanging geometry of the diapir head and the internal curtain fold structure. All these features are part of our modern understanding of diapiric salt structures.

examples. Later, Nettleton and Elkins (1947) used granular materials to simulate the behaviour of brittle overburdens. Their work shed light on how diapiric growth reacts to the addition of varying thicknesses of brittle overburden material. Their work was expanded on later by Parker and McDowell (1955) and Bishop (1978) and it forms a key aspect in how we interpret diapiric growth today. Due to its simple inexpensive nature and reproducibility, analogue modelling is still widely used today. Modern analogue models commonly use layers of quartz sand to simulate a brittle overburden with mica layers often inserted between sand layers to simulate bedding-parallel decollements and silicone putty to simulate the behaviour of salt. Analogue modelling has allowed scientists to investigate a wide range of geological factors that affect the growth and development of diapiric structures. For example, the development of mushroom diapirs (Jackson and Talbot, 1989a), Rayleigh-Taylor instability (Talbot et al. 1991), diapiric growth due to overburden extension (McGill and Stromquist, 1979; Vendeville and Cobbold, 1987; Cobbold et al., 1989; Weston et al., 1993), overburden deformation adjacent to evaporite diapirs (Davison et al., 1993; Alsop 1996), the growth of active salt diapirs (Schultz-Ela et al., 1993) and the effects of varying sediment aggredation rates (Venderville and Cobbold, 1988; Koyi, 1996) are but a few.

As analogue modelling progressed, new geological information was being added through both seismic and field based observations. Trusheim (1957, 1960) used seismic data covering German salt structures to examine the geometry of sedimentary units adjacent to salt diapirs. Trusheim formulated the concept of a peripheral sink, or rim-syncline with syn-kinematic sedimentation, that indicates salt withdrawal and diapir growth. The interaction of salt movement and sedimentation has received recent attention from petroleum geologists working within the Gulf of Mexico and elsewhere. In these areas, geologists have recognised that salt structures can create a variety of sediment barriers (due to the creation of surface topography) or sediment basins (due to salt withdrawal and/or dissolution) (Fletcher et al., 1995; Brown, 1995).

In 1989, Worrall and Snelson adapted computerized palinspastic reconstructions and section balancing techniques to salt tectonics. Inherent in the attempt to balance a salt terrain is the fact that salt, being entirely mobile, is free to migrate out of the plane of section and the fact that salt dissolution can commonly remove at least 50% of the original salt volume, thereby invalidating the assumption of constant volume or area for a restoration. Modern section balancing neatly sidesteps these problems by restoring only the sedimentary overburden in three dimensions and leaving the salt as 'void space'. In recent years the application of section balancing to several salt provinces (for example, Hossack and McGuinness (1990), Rowan (1994) and Hossack (1995)) has enabled geologists to sequentially restore the paleogeometry of salt provinces. This approach has allowed geologists to visualise the way in which salt migrates through geological time and enhances our understanding of salt-sedimentation interactions.

The immediate future of salt tectonics undoubtedly lies in continued advancements in seismic imaging of salt structures as well as more refined computer simulations. Poliakov et al. (1996) simulated simultaneous brittle faulting and viscous flow within overburden sediments by using two computer-based codes (an implicit Eulerian-Langrangian Finite-Element code and an explicit Langrangian Finite-Element code). From conclusions presented in this thesis it appears that the simulation of simultaneous brittle and viscous overburden behaviour may be more realistic than assuming a purely brittle overburden, yet the overburden parameters in themselves represent only one of the numerous variables that must be taken into account. Perhaps the most important contribution that computer modelling can make in the future is to allow multiple parameters, such as overburden behaviour and thermal modelling (both within the diapir and the surrounding country rocks) to be modelled simultaneously.

1.4, WESTERN CAPE BRETON ISLAND AND ITS RELEVANCE TO MODERN SALT TECTONICS

The presence of salt structures throughout the Maritime region of Atlantic Canada has been well known for at least 50 years. Periodic work has been carried out to identify salt structures for salt and potash extraction (Bancroft, 1957; Bidgood, 1970; Carbonneau, 1977; Boehner, 1980b, 1981, 1983, 1984, 1986; Howie, 1988) or to define salt structures as part of the general regional structure (Haites, 1952; Grant, 1994) (Figure 1.4.1). With a few notable exceptions, for example Carter (1990a, b and c), no research has yet focused solely upon the salt structures.

In comparison with other geological structures, well-preserved and well-exposed salt structures are rare. In terms of their exposure and tectonic environment, the western Cape Breton Island diapir exposures are apparently unique in the world. Although a wide variety of salt structures are exposed in the world today, the author is not aware of any other examples of salt structures that show continuous cross sections through both diapir drag zones and the diapir itself.

Within western Cape Breton Island, both diapirs and their associated drag zones (see Glossary of Salt Tectonics) are exposed as continuous cliff sections. These exposures allow diapir drag zones to be examined in great detail so that the temporal and spatial distribution of deformation and deformation mechanisms can be evaluated. Previous analysis of fault patterns and deformation associated with diapiric structures has focused on analogue modelling. The models of Link (1930), Parker and McDowell (1955) and Alsop et al. (1996) emphasise the presence of radial extensional faults within the overburden of active diapiric structures. Withjack and Scheiner (1982) analysed the importance of a regional stress field upon fault orientation, again from clay-based analogue models. This project will analyse drag zone deformation in far greater detail than is possible with analogue models. The quantification of internal drag zone

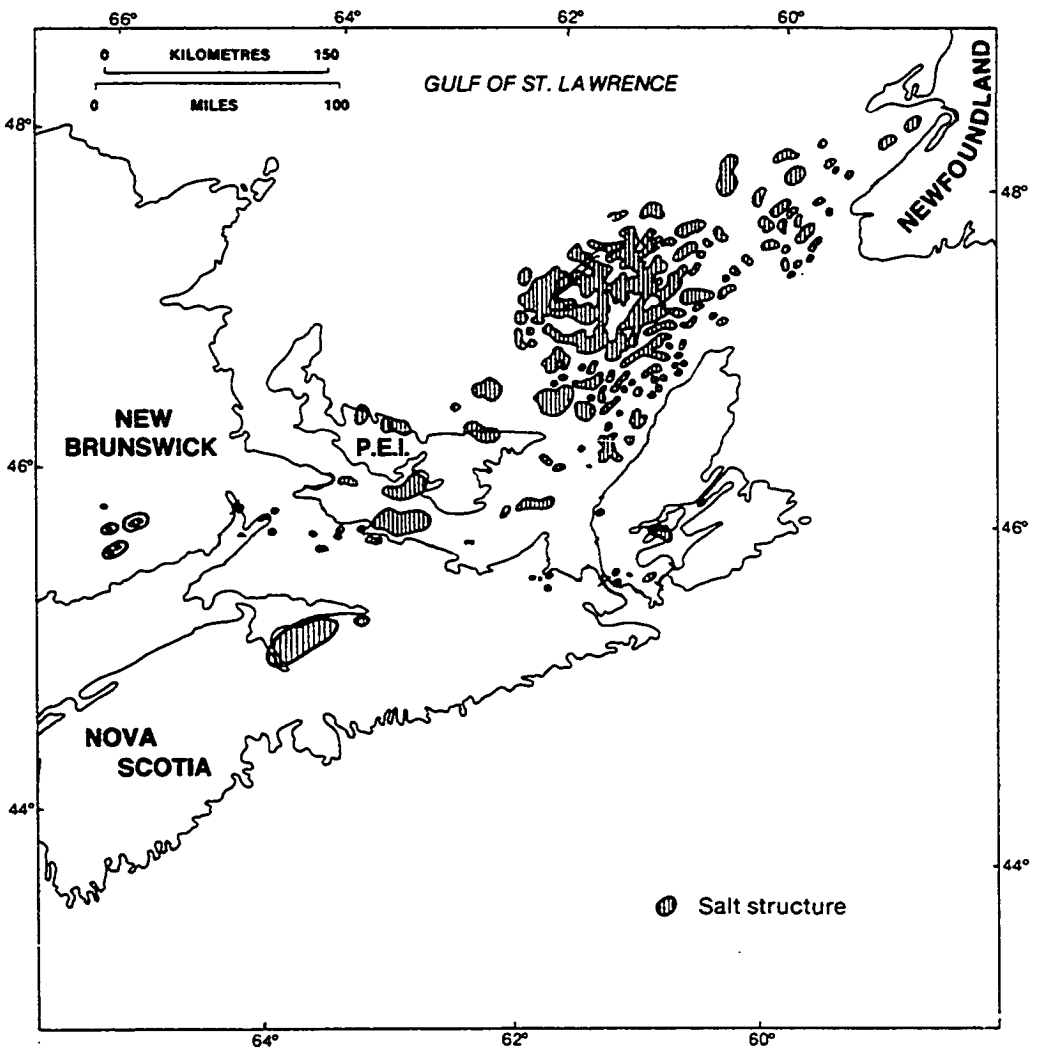

Figure 1.4.1. Position of previously documented salt structures from within the Gulf of St. Lawrence and adjacent onshore areas. From Boehner (1986).

deformation in terms of deformation concentration and distance over which deformation extends could be applied to hydrocarbon reservoir modelling, since high fault concentration can adversely affect hydrocarbon recovery potential.

Hydrocarbon exploration relies heavily upon seismic data to target wells. Although salt diapirs are frequently ideal targets, seismic resolution is generally poor in the crucial drag zone/diapir contact zone. The steep diapir/stratal dips, combined with the unusually high velocity of salt, produces diffraction and refraction of the seismic wavelet and poor migration solutions. A quantitative estimate of drag zone geometry and length therefore has very real implications for seismic interpretation and the positioning of exploration wells.

The diapiric structures themselves consist of Middle Windsor Group or Hood Island Formation structural carapaces, overlying a predominantly halite core. The structural carapaces have a well-constrained stratigraphy that can be used to reconstruct the configuration of the structural carapace. In this thesis, an attempt will be made to compare the structures seen within the structural carapaces to structures commonly observed within the halite diapir core. This analysis will aim to establish whether or not the structural carapace is a dynamic part of the diapir, or if the deformation observed is related to non-diapiric deformation, such as regional compression.

Recently, geologists have attempted to understand how syn-kinematic sediments are distributed around diapiric structures. Approaches taken include analogue modelling, seismic interpretation and fieldwork observations. The chief aim is to produce a predictive model for the distribution of sandstone hydrocarbon reservoirs adjacent to diapiric structures. The near-shore area of western Cape Breton is covered by several high resolution/shallow penetration seismic surveys that can be tied directly to the on-shore outcrops using cored exploration wells. The combination of on-shore sedimentology and seismic facies analysis provides a good data set with which to interpret paleoflow,

sediment transport mechanisms and sedimentary architecture. This information can then be integrated with the movement history of the diapiric structures to evaluate what effect halokinesis had upon sediment transport and sedimentary architecture.

The aim of this project is therefore focused upon aspects of salt tectonics that have received little attention in the past, in Atlantic Canada and worldwide - the internal deformation and characterisation of drag zones. Furthermore, the project contributes to a current research objective of salt tectonics - the distribution of syn-kinematic sediments adjacent to salt structures. In addition, the project will provide new data concerning the internal geometry of diapirs that will be more detailed and comprehensive than existing models formulated from mine plans or 2D plan sections. Due to the close association of on-shore exposures and seismic profiles, the salt structures and their associated drag zones can be examined over a wide variety of scales. This excellent data set has enabled several new ideas and concepts to be drawn out and evaluated. These concepts would not have been elucidated if either the seismic data or on-shore exposures had been examined alone.

On a more local scale, the presence of 4 km high, 35 km long diapiric structures within the Maritimes Basin of Atlantic Canada has received little geological attention from scientists, apart from their value for local salt production. However, as modern analysis of the Gulf of Mexico shows, salt is often the medium that controls both deformation and sedimentation on a basinal scale. This project will hopefully increase awareness of salt tectonics within Nova Scotia so that future structural and stratigraphic models will incorporate the idea of salt tectonics more completely.

1.5, THESIS STRUCTURE

- In order to fully examine the many diapiric structures contained within the field area, it is important to place the growth and evolution of the diapirs within a

regional and local tectono-stratigraphic framework. Chapter 2 therefore gives a brief background to the Gulf of St. Lawrence Basin before developing a tectono-stratigraphic model for the formation and evolution of the St. Georges Bay Sub-Basin and adjacent areas within western Cape Breton and the Gulf of St. Lawrence. It should be noted that the information required to define a precise structural model for western Cape Breton and the immediate offshore area is not available at this time. Chapter 2 also describes several previously undocumented salt structures which were defined from the seismic data.

- Chapter 3 describes the onshore diapiric structures and correlates these structures with the seismically defined structures (Chapter 2). Chapter 3 focuses upon the internal geometry of the onshore salt structures, the nature of the external shear zones, drag zone deformation mechanisms and drag zone length/profile relationships.

- Chapter 4 discusses the growth mechanism of the many salt structures within the field area. Evidence is drawn from seismic and onshore data presented in Chapters 2 and 3. Following this a general model for drag zones is presented.

- Chapter 5 briefly describes the sedimentology of the Inverness Formation (a widely distributed rock unit that lies adjacent to many of the diapirs) before focusing upon the effects of halokinesis upon the sedimentary architecture of the Inverness Formation and related syn-halokinetic and syn-tectonic sediments. Seismic facies defined from the 1978 Mabou seismic survey are combined with sedimentology to illustrate some of the effects of diapir growth upon syn-kinematic sedimentation.

- Chapter 6 draws together the many ideas, concepts and models, then presents some general conclusions as well as emphasising future areas of research.

- A great deal of information related to the project, including the seismic database, palynological dating results and seismic velocity analysis, could not be included within the chapters and is located in the appendices and referenced within the main text.

CHAPTER 2, BASINAL SETTINGS: STRUCTURAL EVOLUTION, SEISMIC STRATIGRAPHY AND SALT STRUCTURES

2.1, INTRODUCTION

This chapter provides a brief overview of the Carboniferous basins of the Maritimes region of Atlantic Canada. The overview is included in order to place the study area within a regional framework. A tectono-stratigraphy for the study area is then developed. The tectono-stratigraphic evolution of the study area draws heavily upon the 1982 Chevron seismic survey and is therefore a seismic stratigraphy, although the onshore stratigraphy developed by Giles et al. (1997a and b) is used as the stratigraphic framework. In particular, the role of the Hollow Fault (a major crustal lineament that was reactivated during the Carboniferous) in the structural and stratigraphic development of the study area is examined. The chapter then describes the geographic distribution and geometry of the salt structures based upon the available seismic data, proposes a growth history for the salt structures and relates this growth history to the tectono-stratigraphic evolution of the study area.

2.2, THE MARITIMES BASIN OF ATLANTIC CANADA

The Maritimes Basin (Roliff, 1962; Williams, 1974; Knight, 1983) of Atlantic Canada is considered to be a successor basin that developed immediately after the Early to Middle Devonian Acadian Orogeny (McCutcheon and Robinson, 1987). The Maritimes Basin covers 150,000 km^2 (Hacquebard, 1986) and contains a Late Devonian - Early Permian sedimentary basin fill. It consists of numerous sub-basins distinguished by their relative size and mode of formation. Although these sub-basins are technically component depocentres of the regional Maritimes Basin, in this thesis they are referred to as "basins" in their own right, for purposes of convenience.

The Gulf of St. Lawrence Basin (Hacquebard, 1986) is the largest depocentre of the Maritimes Basin, covering an area of approximately 46000 km^2 centred beneath the Magdalen Islands. The nature and mode of formation of the Gulf of St. Lawrence Basin remains uncertain. Belt (1968) proposed an extensional model, whereas Bradley (1982) proposed a pull-apart model based on the assumption of through-going strike-slip faults between Newfoundland and New Brunswick. McCutcheon and Robinson (1987) presented field and magnetic data suggesting that strike-slip faults did not pass beneath the Gulf of St. Lawrence but were displaced 30 - 200 km to the south on the Canso Fault. More recently, the analysis of deep crustal seismic data as part of the Lithoprobe project suggests that the Gulf of St. Lawrence Basin may be an extensional basin related to relaxation of the Acadian thrust front during the Late Devonian. This model involves extensional reactivation and hangingwall collapse of the Acadian thrust front between the Central and Grenville Lower Crustal Blocks. This resulted in extension within the upper crustal portion of the Central Lower Crustal Block, creating a large extensional basin (Stockmal et al. 1990). Similar basins formed by extensional reactivation of pre-existing thrust fronts have been interpreted from other deep crustal seismic data, such as the Celtic Sea Basin of the offshore U.K. that was imaged on the MOIST and BIRPS lines (Brewer and Smythe, 1984) and the Tucano and Jatoba Basins of Brazil (Kusznir et al., 1987). During the Carboniferous, the Windsor Group evaporites within the Gulf of St. Lawrence Basin underwent halokinesis, resulting in a diapir field covering some 16800 km^2 (Howie, 1988; Grant, 1994; Durling and Marillier, 1993). The tallest salt structures are centred beneath the Magdalen Islands and consist of cylindrical salt diapirs between 6 and 8 km high.

In addition to the Gulf of St. Lawrence Basin, numerous smaller basins were created within the Maritimes Basin area during the Upper Carboniferous, such as the Cumberland Basin, Minas Basin, Stellarton Graben, the Bay St. George Basin (Newfoundland) and the St. Georges Bay Basin (which forms the major part of this thesis). Bradley (1982) noted

that these basins are located adjacent to major Late Devonian - Carboniferous strike-slip faults, especially the Cobequid - Chedabucto Fault and the Hollow Fault systems in Nova Scotia (Figure 2.2.1). These basins have structural and sedimentological histories related to movement of the faults, although their sedimentary fills show similarities that reflect the overall sedimentary architecture of the Maritimes Basin. Some of these tectonic, basin-forming events may be correlated with phases of the Alleghanian Orogeny that had its main impact to the south within continental U.S.A. Subsidence curves calculated from the Gulf of St. Lawrence Basin (Rehill, 1996) show a rapid subsidence phase during the Namurian and Early Westphalian that corresponds to a phase of active tectonic subsidence of several smaller basins, as well as to the onset of Alleghanian deformation to the south (Gibling, 1995).

2.3, STRATIGRAPHIC FRAMEWORK OF THE GULF OF ST. LAWRENCE BASIN AND WESTERN CAPE BRETON

2.3.1, Introduction

The Gulf of St. Lawrence Basin of Atlantic Canada preserves the thickest and most widespread Late Paleozoic deposits in eastern Canada (Bell and Howie, 1990). Most stratigraphic work has been conducted in the onshore area. However, as the vast majority of Gulf of St. Lawrence Basin strata lie beneath the present day Gulf of St. Lawrence, regional stratigraphic research has relied upon biostratigraphic, chronostratigraphic and lithostratigraphic correlation of the disjunct onshore outcrops (Boehner and Giles, 1986). A recent comprehensive review of Gulf of St. Lawrence strata using seismic and well log data has only recently been completed (Rehill, 1996).

Within western Cape Breton, early work by Norman (1935) defined six stratigraphic units: the Horton Group, Windsor Group, Hawkesbury Group (Mabou Formation, Port

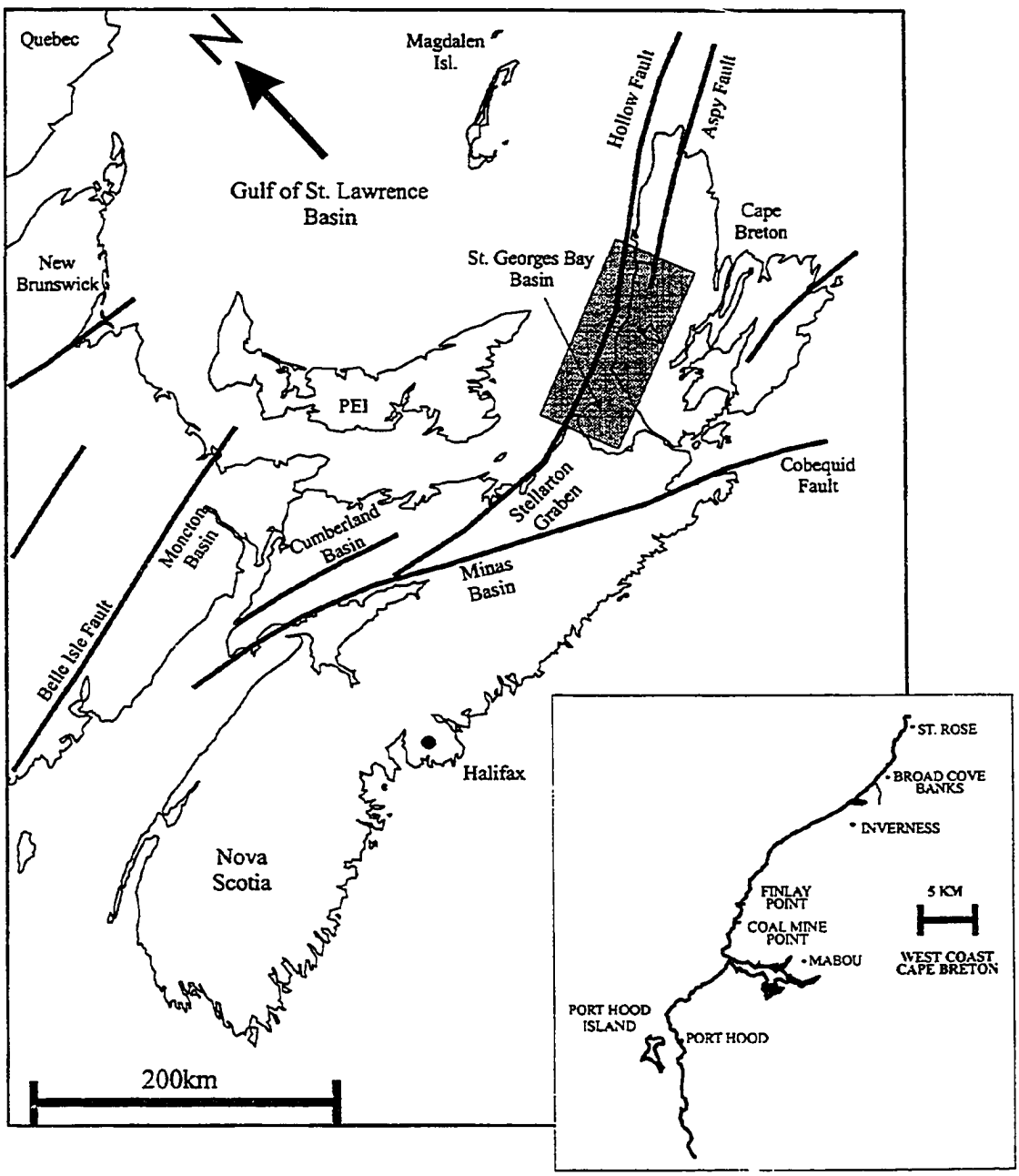

Figure 2.2.1. Simplified map of the Maritimes region to show the geographic location of Carboniferous Basins and major faults which were active during the Carboniferous.

Hood Formation), and the Pictou Group (Inverness Formation and Broad Cove Formation). The most recent stratigraphic work within western Cape Breton by Giles et al. (1997a and b) uses Norman's 1935 stratigraphic framework with some modifications (Figure 2.3.1).

On a regional scale, Bell (1944, 1948, 1958) and Ryan et al. (1991) developed a comprehensive stratigraphic nomenclature for the Late Paleozoic fill of the Maritimes Basin, recognising six stratigraphic units: the Horton, Windsor, Canso, Riversdale, Cumberland and Pictou. Subsequent stratigraphic work by Belt (1964, 1965) revised part of the basin stratigraphy, replacing the Canso Group and part of the Riversdale Group with the Mabou Group.

2.3.2, Stratigraphic Overview

Horton Group. The Horton Group was defined by Bell (1929) from a type section located in the Minas Basin, Nova Scotia. The Horton Group consists of alluvial and lacustrine sediments, which are generally grey to black (Kelley, 1967; Hacquebard, 1972). The stratigraphic thickness is highly variable, ranging from less than 10m to a maximum of 3291m on Cape Breton Island (Kelley, 1967). The sedimentary architecture of the Horton Group is attributed to deposition within intermontane, graben-style basins (Hamblin and Rust, 1989). The Horton Group rests conformably to unconformably on the Devonian Fountain Lake Group or, in the absence of the Fountain Lake Group, upon older basement rocks.

Within western Cape Breton, Giles et al. (1997a and b) divided the Horton Group into three formations: the Creignish, Strathlorne and Ainslie Formations (in chronological order). The thickness of the Horton Group within western Cape Breton is not well constrained, but is estimated to be in the order of 2000m (Giles et al., 1997a and b).

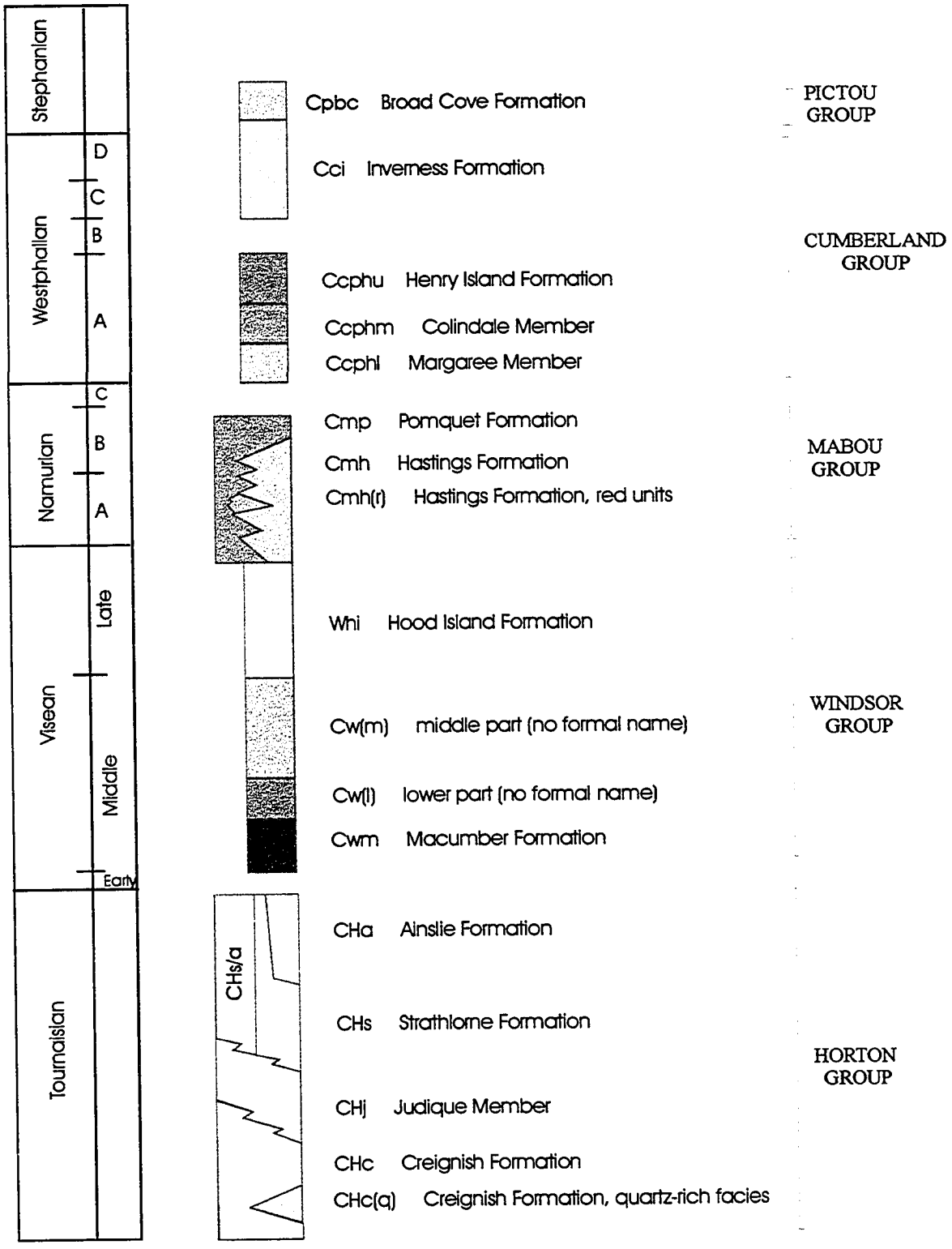

Figure 2.3.1. Carboniferous Stratigraphy, western Cape Breton, Nova Scotia. From Giles et al., 1997a.

Windsor Group. The Windsor Group was defined originally by Bell (1929), then a type section in the Minas Basin, Nova Scotia, was subsequently defined by Kelley (1967) and Boehner (1984). The Windsor Group is characterised by thick units of red mudstone, siltstone, shale and limestone intercalated with gypsum, anhydrite and halite. Local fanglomerate units are associated with basin-margin facies (Boehner and Giles, 1986; Howie and Barss, 1975; Kelley, 1967). Estimates by Ryan and Boehner (1994) suggest that the Windsor Group was originally 1000-1500m thick in the type area. The Windsor/Horton contact is generally disconformable although local angular unconformities have been recorded (Giles et al., 1997a and b).

The Windsor Group within western Cape Breton and Antigonish County has been described by Stacy (1953), Sage (1954) and Schenk (1969) and more recently by Giles et al. (1997a and b). The more recent studies form the basis for the diapir descriptions in this thesis, although the work of Stacy (1953), Sage (1954) and Schenk (1969) is considered for two specific diapir outcrops (Monks Head and Port Hood Island, Chapter 3).

The base of the Windsor Group is defined by the Macumber Formation, a 3-10m thick laminated limestone. The Macumber Limestone is overlain by a thick gypsum unit that is in turn overlain by a thick halite unit, which is the source of halokinesis and salt tectonics within the field area. Based upon a 2D restored salt volume calculation (calculating the volume of salt contained within the salt structures and restoring that volume to a strataform layer) (Appendix 1), the Windsor Group is estimated to be 1500-2000m thick within St. Georges Bay, of which about 540m was originally strataform halite.

The remainder of the Windsor Group is informally divided into the Middle Windsor and the Hood Island Formations based largely upon lithostratigraphy (Figure 2.3.2). One of the key features of the Middle Windsor and Hood Island Formations is the presence of

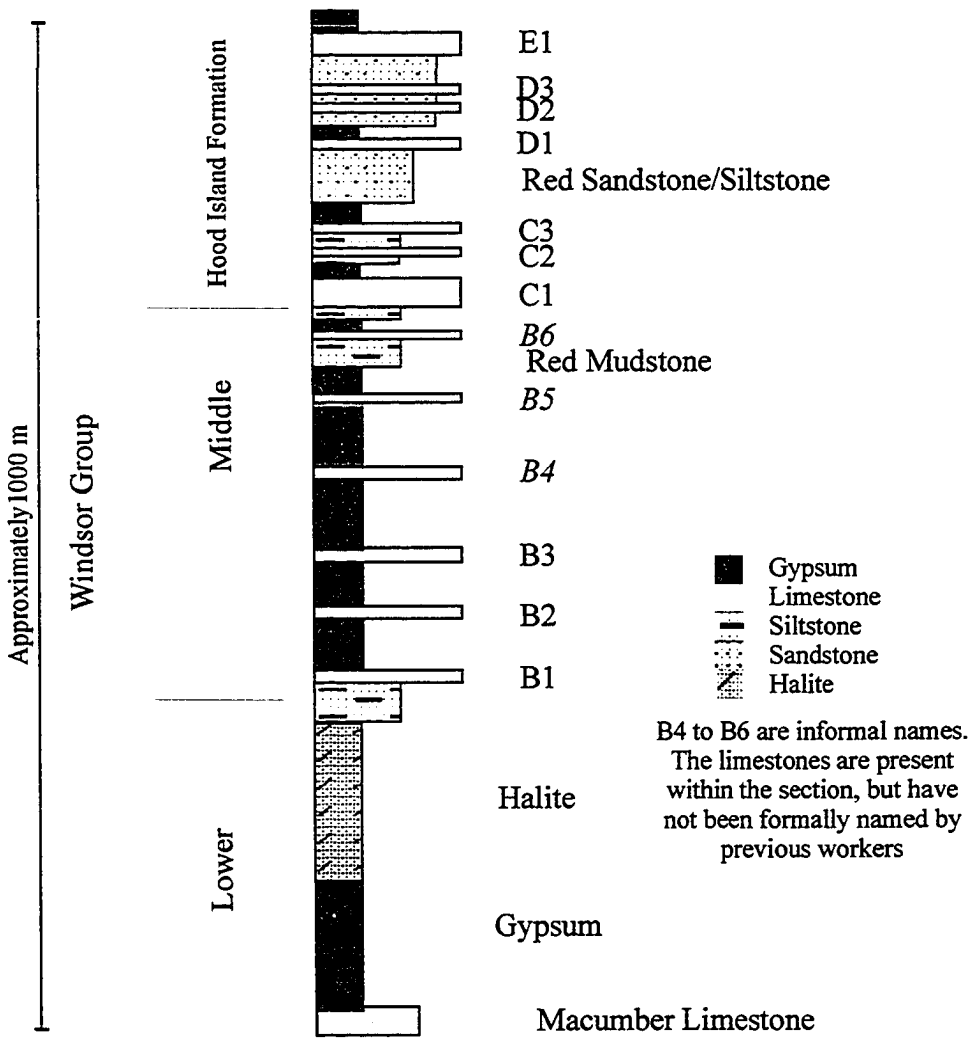

Figure 2.3.2, Windsor Group Stratigraphy.
Modified from Giles and Boehner, 1982

limestone marker horizons. Stacy (1953) and Stacy (1954) introduced an alpha-numeric notation to denote each of these units and this system is adopted in this thesis (Figure 2.3.2). The Middle Windsor Formation includes the B1 to B5 limestone units and the Hood Island Formation includes the C1-C3, D1-D3 and E1 limestone units. In general, the Middle Windsor limestones are thinner than those within the Hood Island Formation. Also, the Middle Windsor limestones tend to be separated by thick gypsum units while the Hood Island Formation limestones are separated by thinner gypsum units, intercalated with mudstones and siltstones. In this thesis, the main Windsor Group limestone associated with the structural carapaces is the E1 limestone. The E1 limestone is characterised by its relatively greater thickness as compared to the underlying limestones, the presence of rugose corals and by its association with red sandstones and siltstones that are rare in the underlying section. The type section for the E1 limestone within the field area is at Broad Cove (P. Giles, pers. comm. 1995), where it is exposed as four repeated sections within the Broad Cove Diapir. The E1 limestone is also an important stratigraphic marker within the Monks Head Diapir and the Port Hood Island Diapir.

Mabou Group. The Mabou Group type section, defined by Belt (1964, 1965), is located within western Cape Breton. The Mabou Group consists of up to 2000m of red and grey sandstones, siltstones and mudstones deposited in a range of fluvial, floodplain and lacustrine environments (Belt, 1964; Ryan and Boehner, 1994). The Mabou Group conformably to unconformably overlies the Windsor Group and represents the transition from marine to continental facies (Utting, 1978).

Within western Cape Breton, the Mabou Group is divided into the Hastings and Pomquet Formations based upon lithostratigraphic characteristics; the two units are in part laterally equivalent. The Mabou Group reaches a maximum stratigraphic thickness of 2400m within St. Georges Bay, as interpreted from seismic data.

Cumberland Group. The type section for the Cumberland Group is located within the western part of the Cumberland Basin (Ryan and Boehner, 1994). The Cumberland Group locally exceeds 5000m in thickness, consisting predominantly of red and grey conglomerates, sandstones, mudstones, coal seams and thin bituminous limestones. Depositional environments of the Cumberland Group include alluvial fans, meandering and braided rivers, lakes and restricted marine tracts. The Cumberland Group conformably to unconformably overlies the Mabou Group and locally onlaps older basement rocks (Ryan et al., 1991).

Within western Cape Breton, the Cumberland Group is divided into the Port Hood Formation and Inverness Formation. The Port Hood Formation is divided into the Margaree, Colindale and Henry Island Members based upon lithostratigraphy and palynological dating. The members do not appear to be strongly diachronous and their contact relationships are generally conformable. The contact between the Inverness and Port Hood Formations is not seen onshore but appears to be conformable to locally unconformable in seismic profiles, with disconformity related to syn-sedimentary halokinesis. The Port Hood and Inverness Formations are each about 700m thick, as interpreted from seismic data.

Pictou Group. The type section for the Pictou Group is located within the western part of the Cumberland Basin (Ryan et al., 1991). The Pictou Group consists of up to 3000m of red fluvial sandstones and mudstones (Ryan and Boehner, 1994) with the thickest sequence being located beneath Prince Edward Island. The Pictou Group blankets older Carboniferous or basement rocks with disconformity, angular unconformity or nonconformity (Ryan and Boehner, 1994).

Within western Cape Breton, the Pictou Group is represented by the Broad Cove Formation, which consists of red mudstones and sandstones assigned to the Stephanian

by Barss and Hacquebard (1967). The contact with the underlying Inverness Formation is not exposed and appears to be conformable based on stratal dips; however, it may be unconformable to disconformable locally based upon its relationship to the Broad Cove Diapir (see below, Chapter 4). The Broad Cove Formation is restricted to the immediate area around the Broad Cove Diapir and no sedimentary rocks of comparable lithology are found elsewhere within western Cape Breton.

2.4, SEISMIC STRATIGRAPHY

2.4.1, General Statement

In order to investigate the tectono-stratigraphic development of the St. Georges Bay Basin and how it relates to the adjacent onshore stratigraphy and Gulf of St. Lawrence Basin stratigraphy, a seismic stratigraphic framework was developed using principally the 1982 Chevron seismic survey. This framework recognises and uses the on-land stratigraphic divisions outlined above. A full description of the 1982 Chevron seismic survey (and other seismic data used as part of this project) is given in Appendix 2, Seismic Database. The reflector colour scheme used when interpreting the seismic data is shown in Table 2.4.1. The Inverness Formation and parts of the Port Hood Formation can be tied to the seismic data by using the Mabou-1, Mabou-2a and Port Ban-1, Port Ban-2 and Inverness I-2 drill cores described by Hacquebard et al. (1989) (Figure 2.4.1). The well data to seismic tie is well constrained and the onshore to well tie is described fully in Chapter 5. The underlying Mabou Group strata are not tied to any well data and the stratigraphic tie becomes increasingly uncertain with depth below the Port Hood Formation.

In order to use the seismic profiles for stratigraphic analysis, a seismic velocity profile is required to make depth conversions from two-way travel time. As explained in Appendix 3, a velocity of 3500m/sec (11,483 ft/sec) was used in this study.

Stratigraphic Horizon	Reflector	Colour
Inverness Formation	D1	
Inverness Formation	D2	
Inverness Formation	D3	
Inverness Formation	D4	
Inverness Formation	D5	
Inverness Formation	C1	
Inverness Formation	C3	
Inverness Formation	C3	
M.Member, Port Hood Fm.	Coal Seam Interval	
Windsor/Mabou	R2	
Windsor/Mabou	Gillis Fan	
Upper Windsor Group	Top Salt	
Lower Windsor Group	Salt Structure	
	Faults	
	Unconformity	
Seismic facies	Down Lap	
Seismic facies	Pinch Out	
Seismic facies	Sandstone	
Seismic facies	Conglomerate	
Seismic facies	Rim-Syncline	

Table 2.4.1, Seismic Reflector Color Scheme.

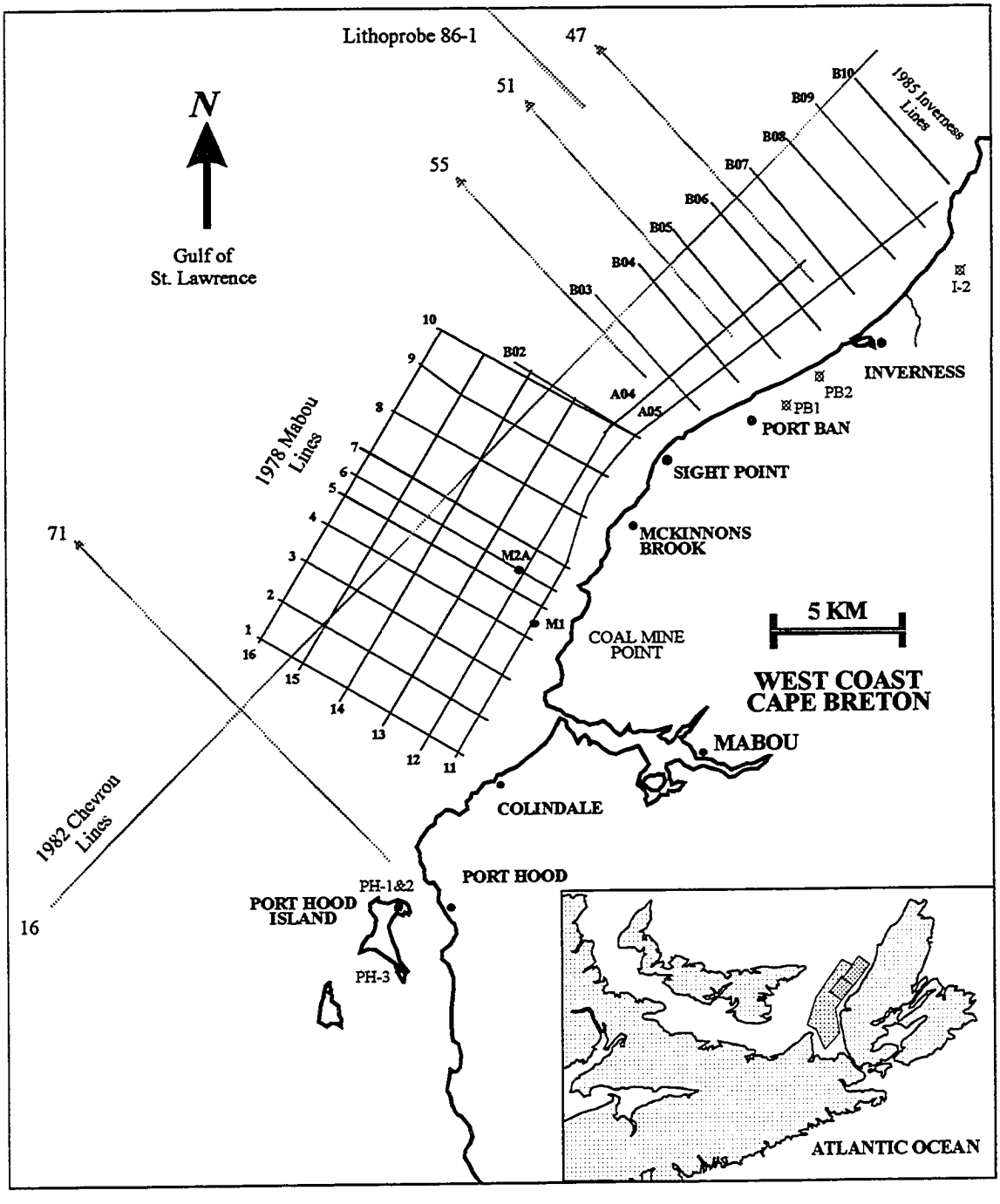

Figure 2.4.1. Map of western Cape Breton showing the tie lines between the seismic surveys and the position of the 86-1 Lithoprobe line.

2.4.2, Seismic Stratigraphy

The Chevron survey consists of 580 km line length (10 inlines and 4 diplines), covering an area of 2500 km^2. The survey grid partially overlaps the 1978 Mabou and 1985 Inverness geophysical surveys and covers the greater part of St. Georges Bay (Figure 2.4.1).

The 1982 Chevron seismic survey penetrates to a depth of 2.2-2.5 sec TWT and images presumed Windsor Group reflectors, but not Horton or basement reflectors. The stratigraphy described below is a general stratigraphy which is in part superseded by a more detailed stratigraphy interpreted from the 1978 Mabou seismic survey and presented in Chapter 5 as part of the correlation of the Inverness Formation exposures.

(Seismic reflector colour scheme is shown on Table 2.4.1, refer to Figure 2.4.2 for TWT values)

0-300 ms. A largely seismically transparent zone lies above the Inverness Formation coal measure reflectors. This interval is approximately equivalent to the 200-800 ms interval described for the 1978 Mabou survey (Chapter 5). This zone on the Chevron profiles has far less resolution than on the 1978 Mabou and 1985 Inverness surveys and little useful information was obtained from this zone. Exceptions to this are high-amplitude reflectors which represent strata uplifted on the flanks of salt structures and brought to shallower depths, e.g. line 75, 1982 Chevron survey.

300-1000 ms. The Inverness Formation and Port Hood Formation coal seam reflectors are contained within this interval. A reflector that is inferred to represent the 15'0" (D2) coal seam is always present as a high-amplitude, high-coherency reflector. The D1 and D3 reflectors are also imaged and usually have a very high-amplitude with slightly less coherency than the R2 reflector; they are also inferred to represent coal seams. Above

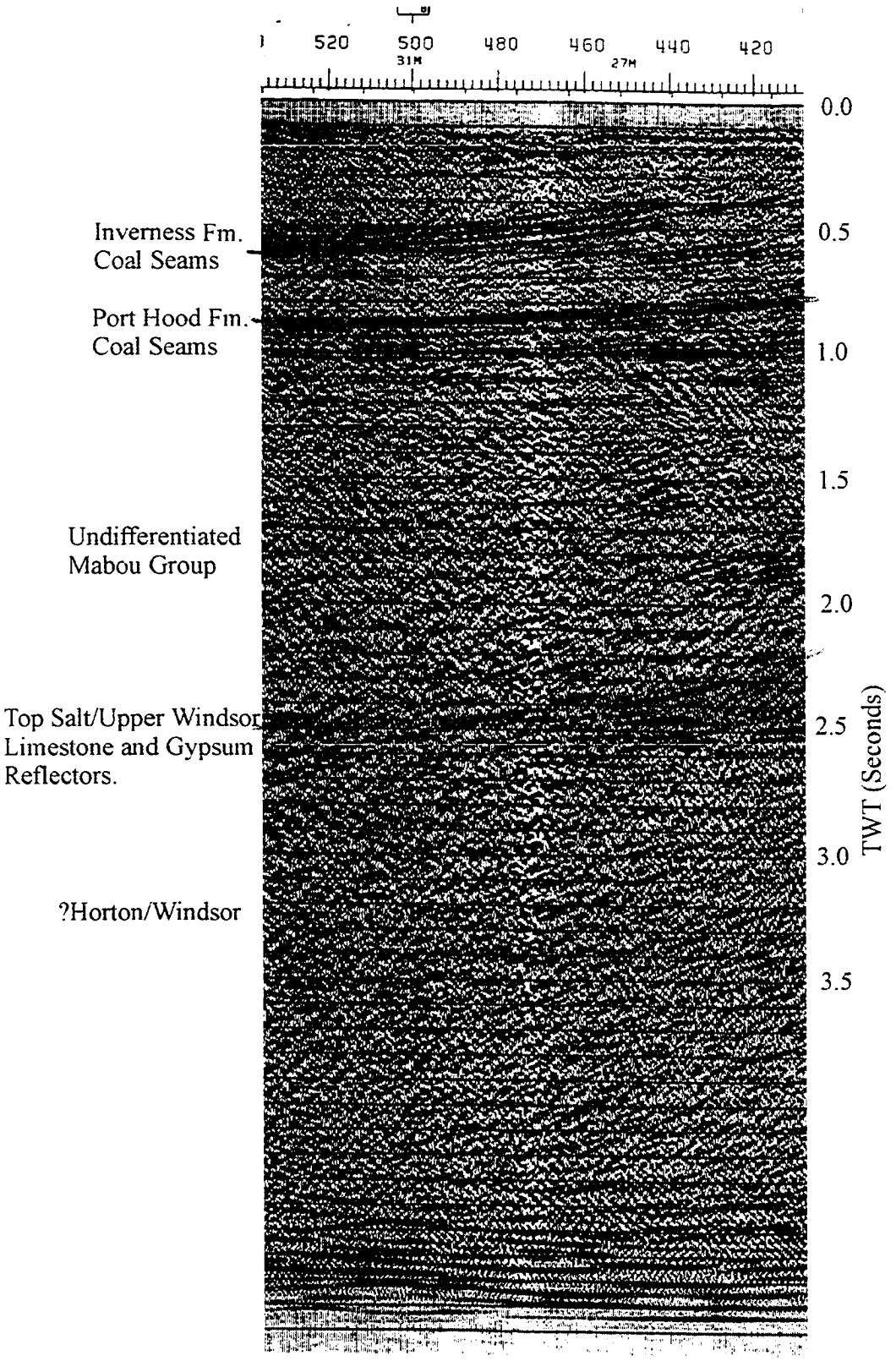

Figure 2.4.2. Example seismic section to show reflector characteristics. Line 75, shot points 520 to 420, Chevron survey.

and below the coal seam reflectors, one or two additional reflectors are also present. They are of lower amplitude and coherency and cannot be traced for more than a few kilometres.

The coal seam reflectors (D1, D2 and D3) are tied directly to the 1978 Mabou and 1985 Inverness surveys where the Chevron survey grid intersects the Mabou and Inverness survey grids. In turn, the Mabou and Inverness surveys are tied to two cored off-shore coal exploration wells, Mabou 1 and Mabou 2a. After depth conversion, the 1978 Mabou and 1982 Chevron seismic surveys can be tied directly to the Mabou-1 and Mabou 2a lithological well logs of Hacquebard (1986). The 6' Port Hood coal seam is penetrated by three drill holes (PH1, 2 & 3) and is inferred to be the principal seismic reflector identified from the 1985 Port Hood survey (McGregor, 1985). The 6' coal seam is one of several coal seams that can be tied from well data and the 1985 Port Hood survey onto the 1982 Chevron survey. The 6' coal seam cannot be tied to the Chevron survey as a single reflector but is apparently one of several coal seam reflectors of the Port Hood coal measures. The coal measure reflectors are high-amplitude, moderate-coherency reflectors. Individual reflectors can be traced for several kilometres and the coal measures as a whole can be traced regionally. This interval is approximately equivalent to the Colindale Member of the Port Hood Formation.

The seismic stratigraphy for this interval is therefore well constrained. The Inverness Formation coal seams are the most regionally extensive seismic reflectors that can be traced along western Cape Breton (Inverness to Port Hood) and into St. Georges Bay (lines 63, 16, 71 and 75).

1000-15000 ms. This interval is largely seismically transparent. Seismic reflectors are of moderate amplitude and low coherency. The reflectors cannot be traced laterally for more than 1-2 km.

1000-2000 ms. This time interval spans the Margaree Member of the Port Hood Formation (below the Port Hood coal measures) and the Mabou Group. The interval contains few seismic reflectors and the top of the Mabou Group is not imaged. Reflectors from within this interval are of low/moderate amplitude and low coherency. The poor nature of the seismic reflectors within this interval is not surprising, given the sedimentology of the Mabou Group. The Mabou Group essentially consists of fine-grained argillaceous and arenaceous sediments with mean bed thicknesses of a few metres at most. These strata are not likely to have a large impedance contrast across sedimentary interfaces, especially where mudstone grades to siltstone and sandstone. A similar lack of prominent reflectors in the Mabou Group was noted across the Gulf of St. Lawrence by Rehill (1996).

2000-2500 ms. The stratigraphy below 2000 ms is largely uncertain. No wells within western Cape Breton penetrate the Mabou Group and onshore exposures do not provide accurate thickness estimates for the Mabou Group and Windsor Group. In addition, as noted above, salt withdrawal from the Windsor Group halite has undoubtedly altered the original stratigraphic thickness of the Windsor Group. The seismic stratigraphy below ~2.0 seconds TWT is therefore inferred from the expected seismic character of reflectors described from onshore logged sections.

At about 2000-2500 ms, a series of very high-amplitude, high-coherency reflectors are imaged over a vertical thickness of ~200ms TWT. The reflectors are interpreted to represent Hood Island Formation limestone and gypsum, the juxtaposition of which would result in a strong impedance contrast. In addition, the number of reflectors (7 or 8) corresponds approximately to the number of Hood Island Formation limestones. Further support for this interpretation is seen on line 79 (1982 Chevron survey) where the reflectors are rotated and uplifted by a salt structure from 2000 ms to 200 ms TWT as coherent reflectors. This configuration suggests that the salt structure has uplifted the

strata directly overlying the salt structure, a situation that is directly analogous to the formation of a structural carapace. There is no consistent top salt reflector. The Hood Island FormationGroup reflectors are used as a top salt horizon with the caveat that the 'real' top salt horizon is located several hundred meters below.

2.4.3, Salt

The seismic character of salt is hard to define precisely and is something of a 'black art' among geophysicists. Salt is commonly identified in seismic sections by its lack of coherent reflection events and by an intermittent diffraction pattern within the salt body. This appearance is due in part to the steep dips within a salt diapir, the high velocity of salt (~15,000 ft/sec), the steep dips of most diapir flanks and the refraction of the seismic signal at salt/overburden interfaces.

2.5, TECTONO-STRATIGRAPHIC DIVISION OF THE FIELD AREA

2.5.1, Introduction

The field area for this project is divided into three tectono-stratigraphic domains. Most of the study area is located within the St. Georges Bay Basin, which is preserved under the present day St. Georges Bay (Figure 2.5.1). The project area also includes immediately adjacent areas within western Cape Breton and the Gulf of St. Lawrence (Figure 2.5.1). The western Cape Breton extension of the field area (Port Hood to St. Rose) includes both onshore coastal outcrops and near-shore areas covered by marine seismic data. The Gulf of St. Lawrence extension of the project area is defined as the area immediately north of St. Georges Bay, within the Gulf of St. Lawrence Basin, and covered by the 1982 Chevron seismic survey.

The division of the field area into the three tectono-stratigraphic domains described below is based upon the stratigraphic framework developed earlier in this chapter. This

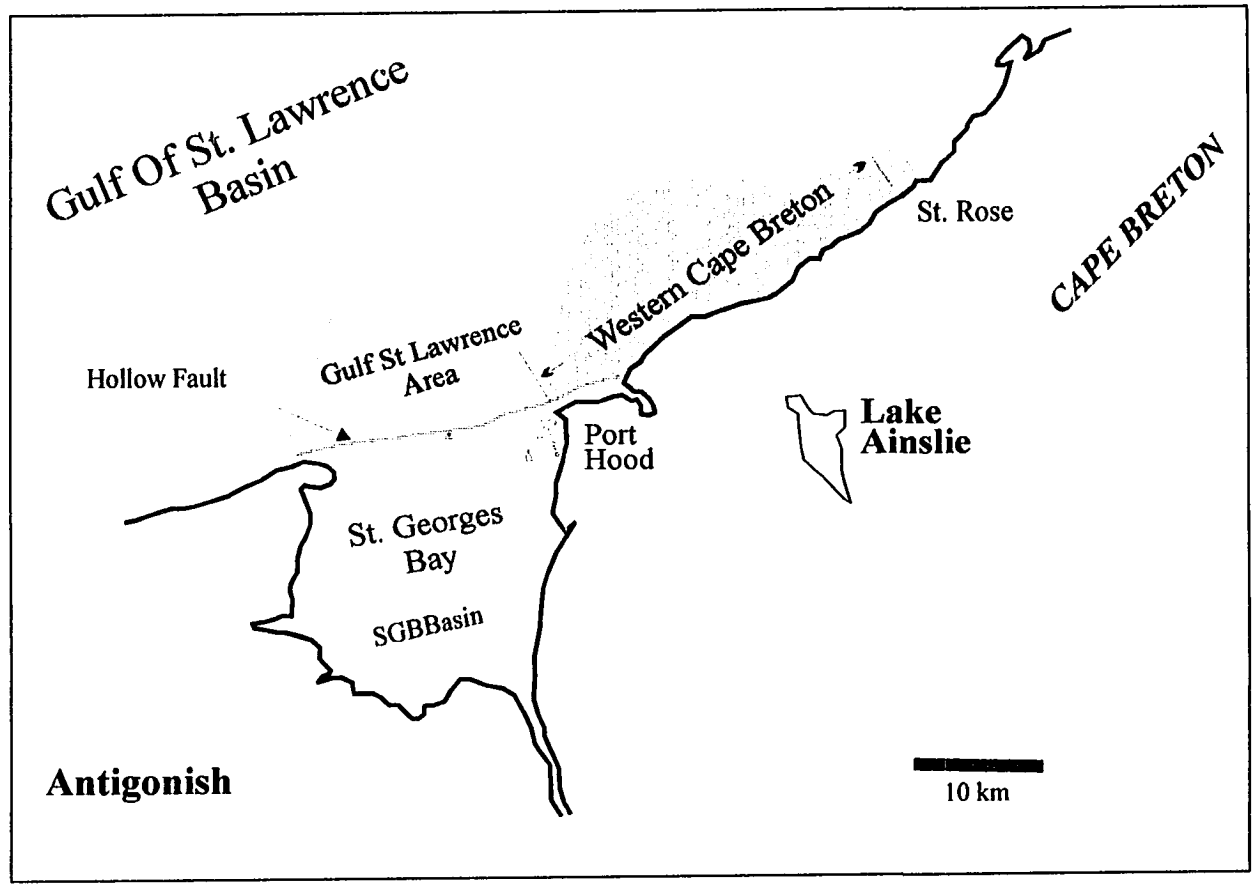

Figure 2.5.1. Tectono-stratigraphic division of the field area. The St. Georges Bay Basin area is mostly located beneath the present day St. Georges Bay, but includes adjacent onshore Port Hood Formation and Mabou Group strata exposed near Antigonish and Port Hood. The western Cape Breton area extends from Port Hood to St. Rose. The Gulf of St. Lawrence area is bounded to the south by the Hollow Fault and to the north-east by the Gillis Fan .

framework is intimately related to the superimposed effects of subsidence of the large Gulf of St. Lawrence Basin (late Devonian-Stephanian) and localised Late Carboniferous tectonic subsidence related to the formation of the St. Georges Bay Basin (Namurian - Westphalian A) (Figure 2.5.1). Division of the field area is important in order to consider the evolution of the salt structures. An analysis of diapiric structures would be largely invalid if the prevailing tectonic and sedimentary regimes at the time of halokinesis were not considered.

The key element in delineating these three domains is the Hollow Fault, which separates the St. Georges Bay Basin from the Gulf of St. Lawrence Basin. In addition, the stratigraphic development of the western Cape Breton outcrop belt may be associated with strands of the Hollow Fault. The Hollow Fault may also be a key element in the structural development of the study area. For this reason, the Hollow Fault and its influence upon basin development is described first, followed by the geographic division of the study area.

2.5.2, The Hollow Fault

During the Palaeozoic, the Hollow Fault has a documented movement history ranging from the Middle Devonian to the Westphalian C – D. During this period, it was responsible for the formation of numerous syn-kinematic sedimentary formations related to repeated cycles of uplift and source area rejuvenation (Bradley, 1982; Dostal et al., 1983; Fralick and Schenk, 1981; Keppie, 1982b; Ryan et al., 1987; Yeo and Ruixiang, 1987) (Figure 2.5.2). Several workers have suggested that the Hollow Fault was active as a dextral strike-slip fault during the Late Carboniferous (Eisbacher, 1967; Webb, 1969; Benson, 1974). More recent work on fracture patterns within mainland Nova Scotia by Yeo and Ruixiang (1987) appears to confirm that the Hollow Fault had a dextral sense of movement within Nova Scotia during the Late Carboniferous. The Hollow Fault within Nova Scotia forms the north-west margin of the Antigonish Highlands (Figure 2.5.3);

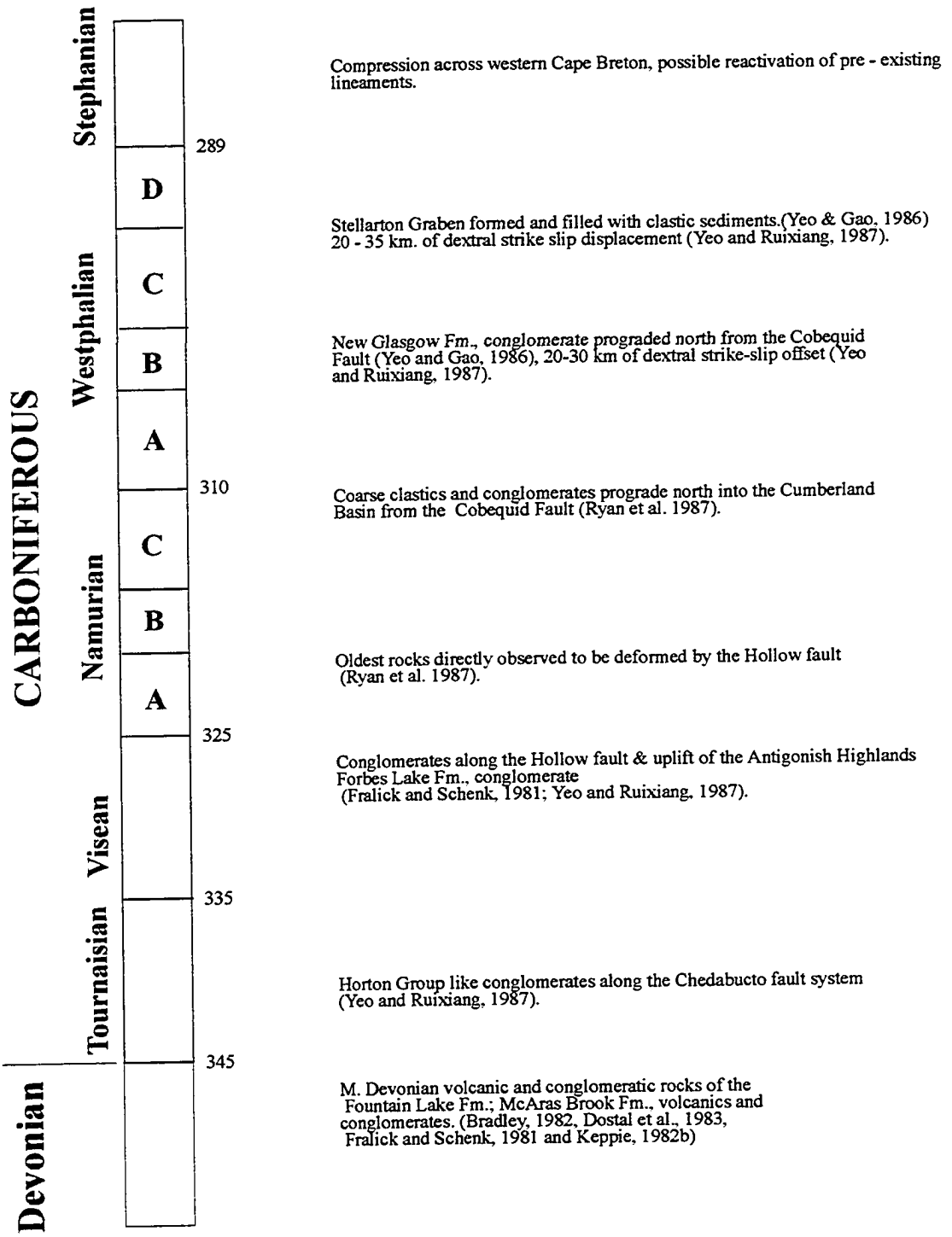

Figure 2.5.2. Kinematic history of the Hollow-Cobequid fault system from Nova Scotia. Absolute ages from Van Eysinga (1970).

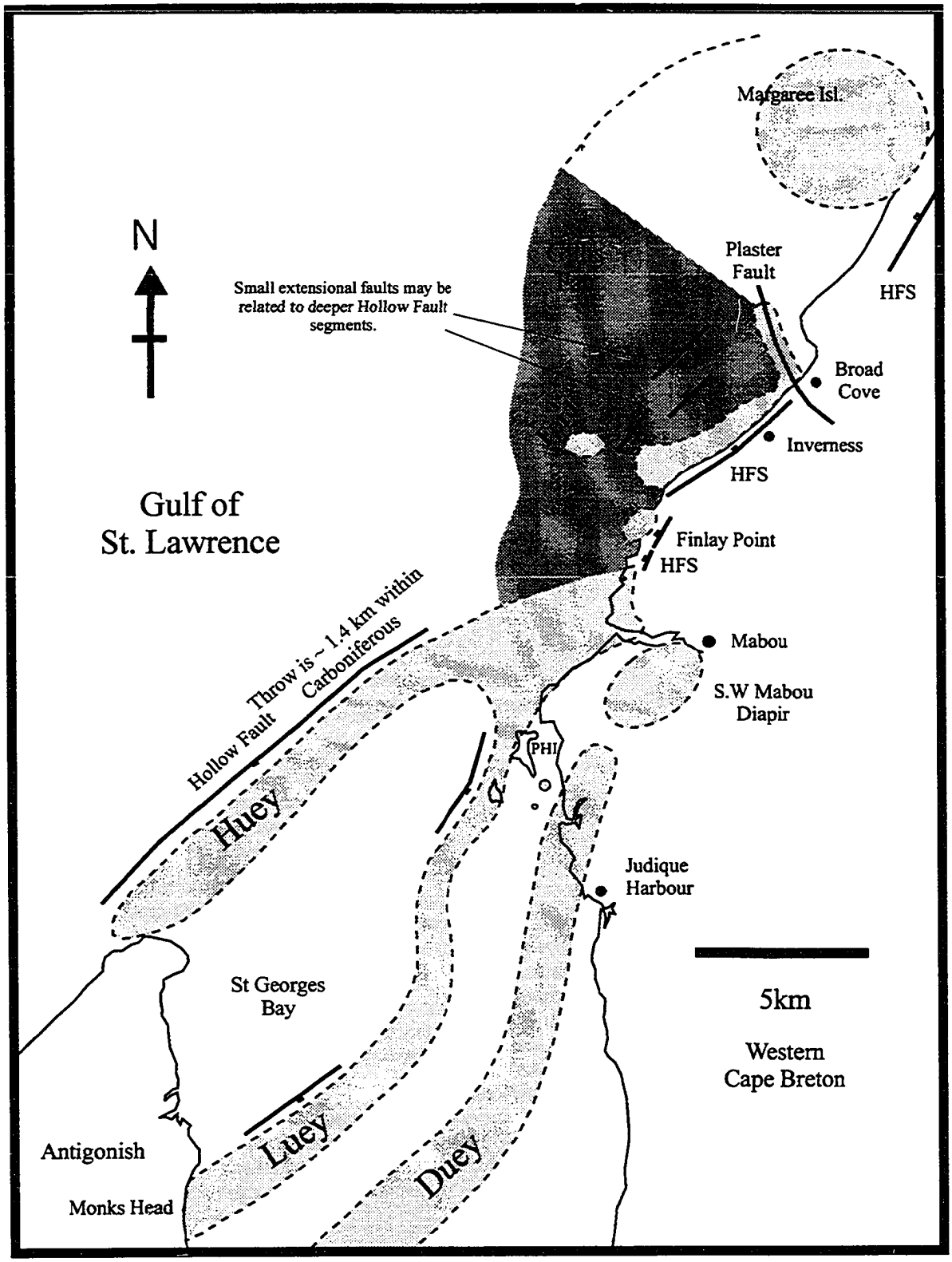

Figure 2.5.3. Position of interpreted Carboniferous extensional faults. Lighter shaded areas are salt structures.

however, its path is less certain when traced north-eastward towards Cape Breton Island. It is inferred to strike either along the coast of western Cape Breton (Howie and Barss, 1975a) or just inland from the coast through the Mabou area (P.S. Giles, pers. comm. 1995; Durling et al., 1995). These two projected paths of the Hollow Fault pass through or immediately north of St. Georges Bay (Figure 2.5.3).

2.5.3, Position and Geometry of the Hollow Fault within the Study Area

Within St. Georges Bay, three salt walls are evident from seismic profiles (Huey, Luey and Duey: Figure 2.5.3). These salt walls are described fully later in this chapter. Immediately to the north of the Salt Wall Huey (Figure 2.5.3), the Upper Carboniferous strata (Mabou Group to Inverness Formation) are about 1.6 sec TWT (2.4km) thick, whereas immediately to the south of the Salt Wall Huey, the equivalent Carboniferous strata are 2.5 sec TWT (~3.8km) thick (see seismic lines 83, 79, 75). Thus the Carboniferous strata thicken by approximately 1.4 km over a horizontal distance of 3 km. There is therefore a need to create 1.4 km of additional accommodation space to the south of the Salt Wall Huey (i.e. within St. Georges Bay) during the Upper Carboniferous. Two mechanisms are proposed which combined could have created the required accommodation space.

- Although poorly imaged, a fault with a throw of approximately 0.8 sec (TWT), (~1.4 km) which dips to the south is interpreted on lines 79 and 83 (Figure 2.5.4) immediately to the north of the Salt Wall Huey. The Upper Carboniferous strata appear to be occupying a hangingwall basin and the Salt Wall Huey is located partially within the hangingwall of the fault. The value of 1.4 km for the fault offset would be a maximum as salt withdrawal subsidence would reduce this offset (see below).

- Salt withdrawal from the Windsor Group into the growing salt structures would have

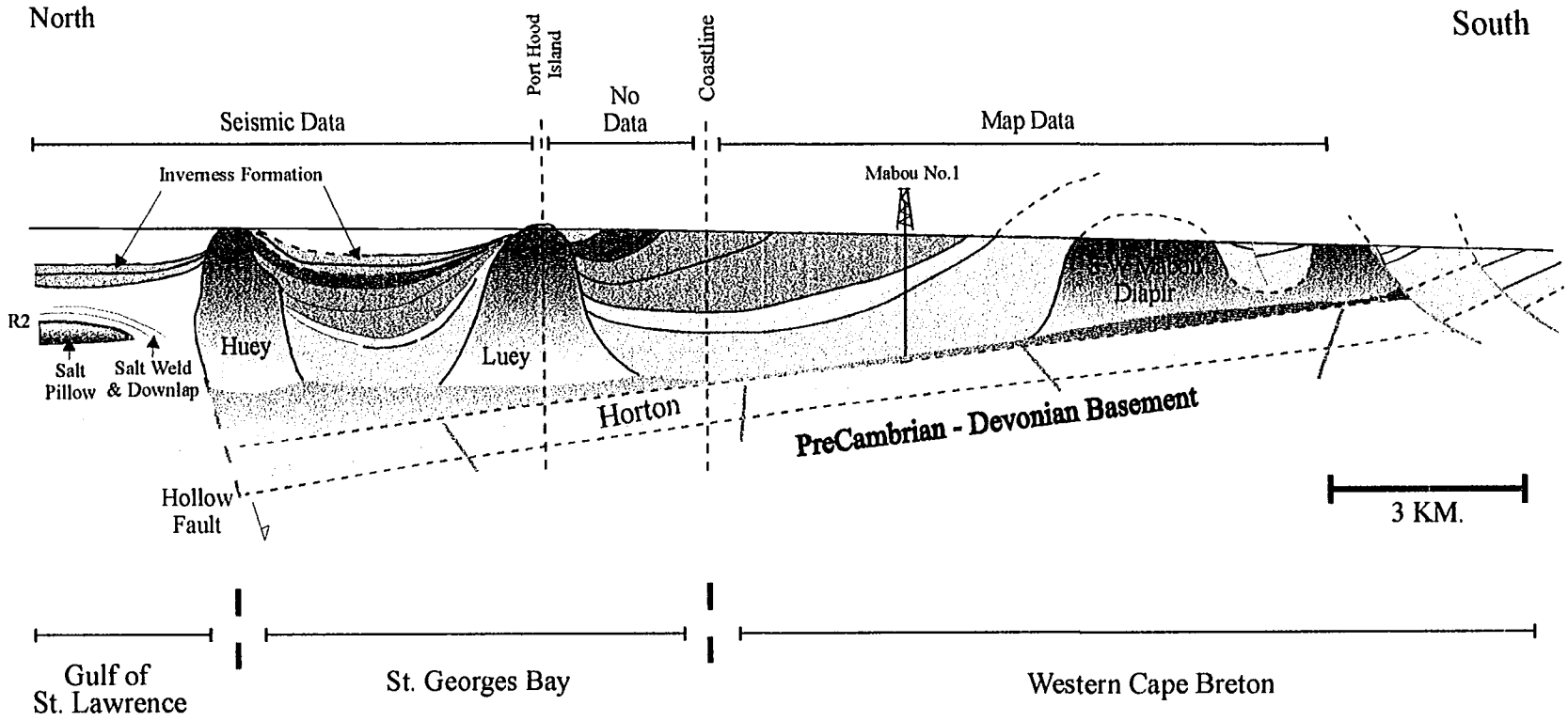

Figure 2.5.4. Cross-section constructed from line 75 (1982 Chevron survey) and onshore geological data from Giles et al. (1997). The Mabou number 1 well gives a depth to the top of the Horton Group but otherwise the depth to the top Horton is unconstrained. The rapid thickness changes of the U. Carboniferous strata between the SW Mabou Diapir and Luey may be caused by inaccurate depth conversio and/or poorly constrained surface contacts. Despite this all of the U. Carboniferous strata to the left of the SW Mabou diapir have been uplifted and folded. This may be related to post Carboniferous inversion..

resulted in subsidence of the Upper Carboniferous section as the salt was withdrawn. This subsidence would have been independent of and in addition to tectonic subsidence. The thickness of the salt layer needed to form the observed salt structures is estimated to be about 540 m (see Appendix 1). This suggests that up to 540 m of salt related-subsidence was created during the Namurian to Stephanian (a major growth period of the salt walls, see Chapter 4). Salt-withdrawal subsidence has been previously documented for the Gulf Coast of Mexico, where up to several thousand metres of salt-withdrawal subsidence allowed the accumulation of an equivalent thickness of Cenozoic clastic sediments (Rowan, 1994; Hossack, 1995).

The fault described above is interpreted to represent a segment of the Hollow Fault. The position of this proposed segment is on strike with the north-west margin of the Antigonish Highlands and is also the most feasible location for the Hollow Fault within St. Georges Bay. The position of the Hollow Fault also corresponds to the position of the Hollow Fault Zone described by Durling et al. (1995). The geometrical information that is available from the seismic data indicates that the Hollow Fault within St. Georges Bay is a south-east dipping fault. However, the information that is available is by no means conclusive. The Hollow Fault within St. Georges Bay may have a dextral offset as well as an extensional offset (a transtensional strike-slip fault). Because the Hollow Fault is only imaged on widely spaced two-dimensional seismic data, the lateral offset (if one exists) may not be seen. The indicative features of strike-slip faults that can be imaged on seismic data are most easily seen on time-slices (or coherency data) that are generated from three-dimensional seismic data. The rapid changes in stratal thickness across the Hollow Fault indicate that the fault was active during the Upper Carboniferous (Namurian to Westphalian). The movement history of the Hollow Fault cannot be constrained more precisely as there is no well data available below the Port Hood Formation to tie the seismic data across the Hollow Fault. In addition, the large salt structures mask any evidence for syn-tectonic sedimentation, or similar evidence to

indicate fault movement. The Hollow Fault may well have been moving before the Namurian; however, the lack of seismic resolution below the Windsor Group prevents an interpretation of this earlier movement. It should be noted that if the Hollow Fault has a large lateral offset as described earlier, then the changes in stratigraphic thickness across the fault are not true stratigraphic features and may be exaggerated or reduced by structural juxtaposition.

At Coal Mine Point, Finlay Point, and Inverness (Figure 2.5.3), Upper Carboniferous strata are juxtaposed against Devonian to Precambrian basement or basement/Horton rocks along the coastline. In the immediate offshore area (<1 km offshore), the Upper Carboniferous strata are over 1 km thick. In order to accommodate over 1 km of Upper Carboniferous sediments juxtaposed against the basement rocks, over 1 km of accommodation space must have been created during the Upper Carboniferous. The model proposed to explain this accommodation space is similar to that proposed above for St. Georges Bay. The Upper Carboniferous strata may be occupying basins of one or more major faults with a throw of ~1km, faults that lie along the present day coast of western Cape Breton. If these faults exist, they would be a logical extension of the Hollow Fault into western Cape Breton.

A major difference between western Cape Breton and St. Georges Bay is that within western Cape Breton, the fault segments would have to dip to the north-west (opposite polarity) if they are interpreted to be extensional faults. From a fault geometry standpoint, this configuration is problematic as it would require the Hollow Fault to switch polarity over a relatively short distance. However, there is evidence to support the existence of north-west dipping extensional faults within western Cape Breton. Marillier et al. (1989) interpreted north-west dipping extensional faults on line 86-1 of the Lithoprobe East seismic data at shot point 4500, ~1-3 sec TWT. (Figure 2.5.5). While the Lithoprobe line does not intersect any of the seismic data used in this project and stops

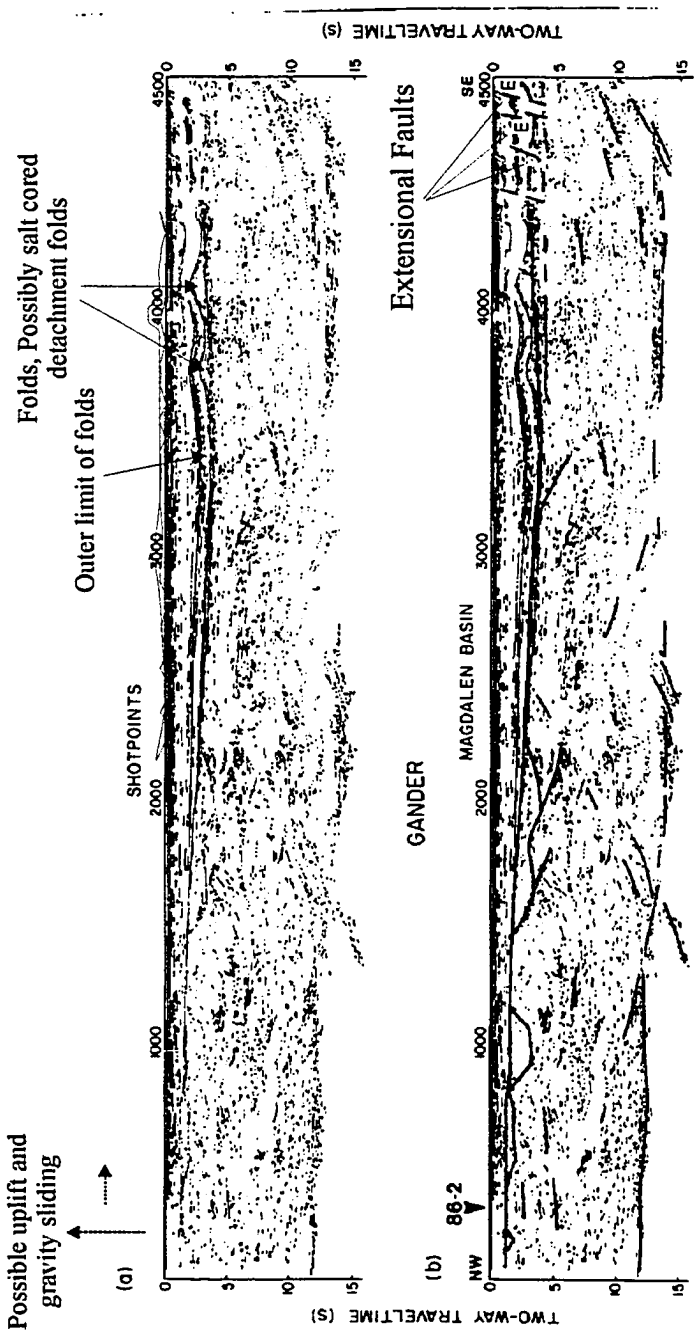

Figure 2.5.5. Line 86-1 of the Lithoprobe East transect and line diagram interpretation by Marillier et al. (1988). The upper 1.5 - 5.0 seconds TWT represents the Carboniferous basin fill within the Gulf of St. Lawrence Basin. At the south-eastern end of the section, beneath shot point 4500, extensional faults are interpreted. These faults downthrow to the NW and offset the Windsor and Horton Groups. Note the folding of the Windsor Group Beneath shot point 4500. See Figure 2.4.1 for the location of this line relative to western Cape Breton.

several kilometres from the Cape Breton coast, the extensional faults appear to have the same dip direction and vertical offset as those interpreted from the Chevron seismic data from St. Georges Bay. Alternatively, if the Hollow Fault is a strike-slip fault, then the geometric problem of opposite polarity extensional faults is negated. A transtensional strike-slip fault commonly has a negative flower structure consisting of numerous extensional (and less commonly reverse) fault segments (Harding and Lowell, 1979; Harding, 1985). The various fault segments do not have a consistent polarity and the direction of the downthrown side switches frequently along the fault zone. Unfortunately, the data that is required to determine whether the Hollow Fault was an extensional or strike-slip fault during the Late Carboniferous is not available (see above). The proposed Hollow Fault segments within western Cape Breton are not imaged on any of the available seismic data because the seismic lines stop short of the coastline by approximately 1 km.

Given the data available, the Hollow Fault can be extrapolated from the Antigonish coastline across the northern margin of St. Georges Bay. It cannot be proven that the Hollow Fault extends along the west coast of Cape Breton, although it would be unreasonable to terminate such a major fault so abruptly and the juxtaposition of Precambrian to Devonian rocks against Upper Carboniferous sediments is most easily explained as a fault offset. The exact nature and geometry of the Hollow Fault is also unconstrained by the available data. While it can be shown that the Hollow Fault has a major normal offset in St. Georges Bay, this does not rule out the strong possibility that the Hollow Fault has a significant lateral offset as described elsewhere within mainland Nova Scotia. If the Hollow Fault was a strike-slip fault during the Upper Carboniferous, some of the faults along the coastline of western Cape Breton could be reverse faults.

The fault model proposed in this thesis is that the Hollow Fault extends along the west coast of Cape Breton and gave rise to a number of small basins. The sedimentary rocks

deposited within these basins are now mainly preserved in the immediate offshore area along the west coast of Cape Breton. Isolated outcrops of Mabou Group, Port Hood Formation and Inverness Formation sedimentary rocks at Port Hood, Mabou Mines, Inverness and St. Rose represent onshore exposures of these small Carboniferous basins. As in the St. Georges Bay scenario, salt withdrawal subsidence probably occurred, reducing the tectonic subsidence required.

Within the Cabot Strait to the north-east of Cape Breton Island, up to 6 km of Devonian to Carboniferous strata are preserved in two north-east/south-west trending linear graben. The formation and subsequent deformation of these graben are related to several major north-east/south-west trending strike-slip faults: the Cabot Fault, the Cape Ray Fault, the Hollow Fault, the Mid-Bay Fault and the Red Island Fault (Figure 2.5.6). Most of these major extensional faults were important in the Middle to Late Carboniferous deformation of the basin fill (Langdon and Hall, 1994). Langdon and Hall (1994) also identified numerous salt structures within the Cabot Strait, often localised along major faults, which probably began to grow during the first post-Visean deformation, perhaps in the Namurian (Langdon and Hall, 1994).

Assuming that the Hollow Fault extends into the Cabot Strait (Langdon and Hall, 1994), it may be possible that the Hollow Fault can be extrapolated from the Stellarton Graben, across St. Georges Bay, along the west coast of Cape Breton and into the Cabot Strait. Previously documented basins formed as a result of movement on the Hollow Fault have similar basin styles. For example, the Stellarton Graben, the Cape Ray Graben and the Searston Graben (Figure 2.5.6) are all relatively small, pull-apart basins related to wrench tectonics which were formed during the Namurian to Stephanian (Langdon and Hall, 1994). This evidence of basin formation was used to support the available data when examining the St. Georges Bay Basin.

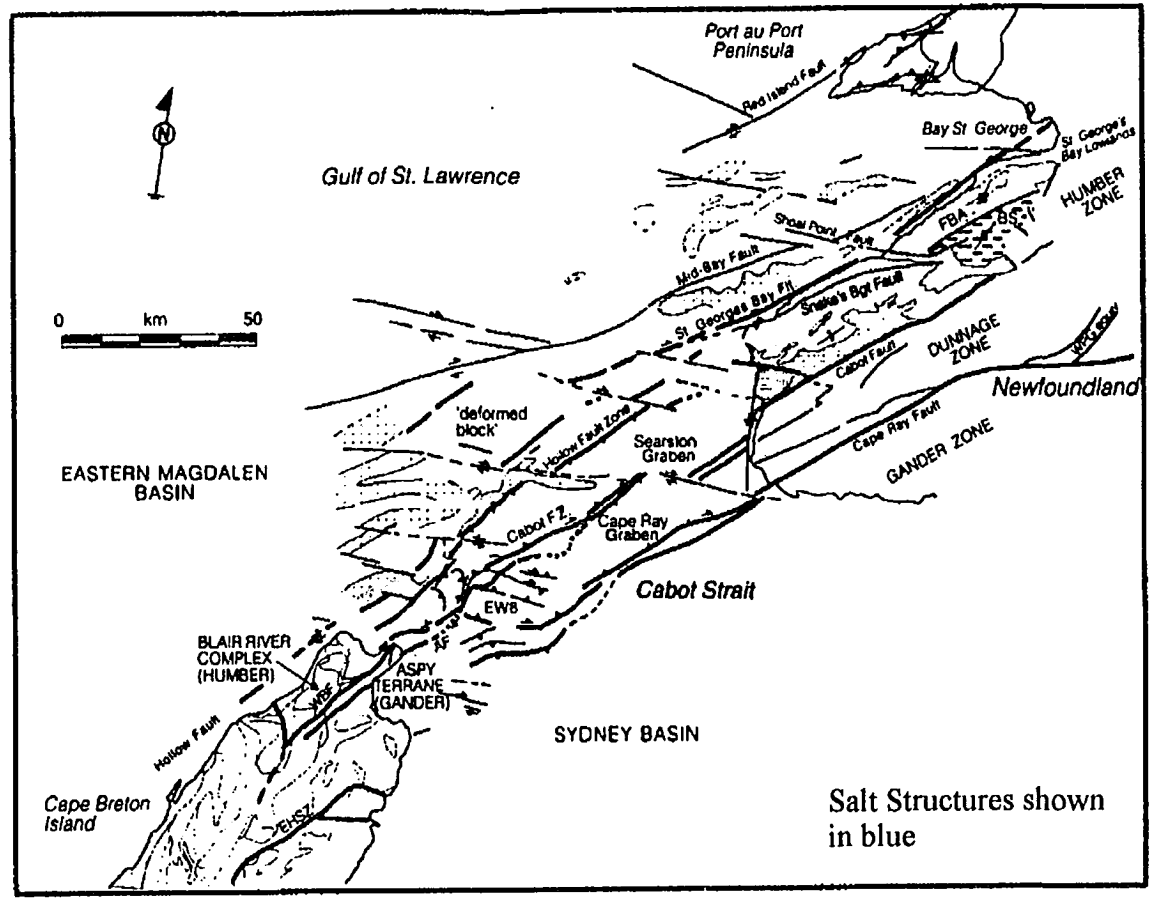

Figure 2.5.6. Diagram to show the distribution of major Carboniferous faults within the Cabot Strait between Nova Scotia and Newfoundland. The basement and Carboniferous strata have been deformed by a series of strike-slip faults with a major extensional component. Syn-kinematic sediments were deposited within a series of fault bounded grabens and salt withdrew into the faults to form salt walls and diapirs. Modified from Langdon and Hall, 1994.

Further descriptions of proposed segments of the Hollow Fault are described in Chapter 3. These descriptions highlight the specific displacement configuration required for each of the proposed Hollow Fault segments.

2.5.4, The St. Georges Bay Basin: A Late Carboniferous Tectonic Basin

The St. Georges Bay Basin (Figure 2.5.3) contains approximately 3.6 km of Upper Carboniferous strata (Late Visean - Westphalian D) and, based upon present-day preserved dimensions and those of basins along the Hollow Fault in the Cabot Strait (Langdon and Hall, 1994), would be classified as a small tectonic basin. If the Carboniferous basin did not extend significantly beyond its present limits, the Carboniferous basin would have measured 33.5 km by 28 km (Canso Causeway to the Hollow Fault and Monks Head to Port Hood) (Figure 2.5.1). These dimensions combine to give an aspect ratio for the St. Georges Bay Basin of approximately 6.5:1 (length/depth, or width/depth). This is an extremely high aspect ratio for a sedimentary basin, indicating that the St. Georges Bay Basin was probably a tectonically controlled basin as opposed to a thermal sag basin. The high aspect ratio of the St. Georges Bay Basin has implications for its subsidence history related to its thermal characteristics. The lateral heat flow gradient in small, tectonic basins is generally high because heat is rapidly transferred through the basin margins; the basin therefore remains in thermal equilibrium with the surrounding lithosphere (Allen and Allen, 1990). Since the basin remains at or close to thermal equilibrium, the post-tectonic thermal subsidence phase commonly associated with larger basins is severely attenuated or absent (Figure 2.5.7a and b). The critical basin length below which lateral heat loss becomes important is approximately 100 km.

From the evidence available from adjacent areas and the apparent displacement on the Hollow Fault, it is probable that movement of the Hollow Fault during the Late Carboniferous played an important role in the tectonic development of the St. Georges

Figure 2.5.7a. Calculated subsidence curves for small extensional basins (length or width < 100 km). Note the rapid tectonic subsidence followed by a subdued thermal subsidence phase. From Allen and Allen, 1990.

Figure 2.5.7b. Calculated subsidence curves for large extensional basins. Yc = crustal thickness. Yl = lithospheric thickness, Beta = strain. Note the pronounced thermal subsidence phase associated with large extensional basins. From Allen and Allen, 1990.

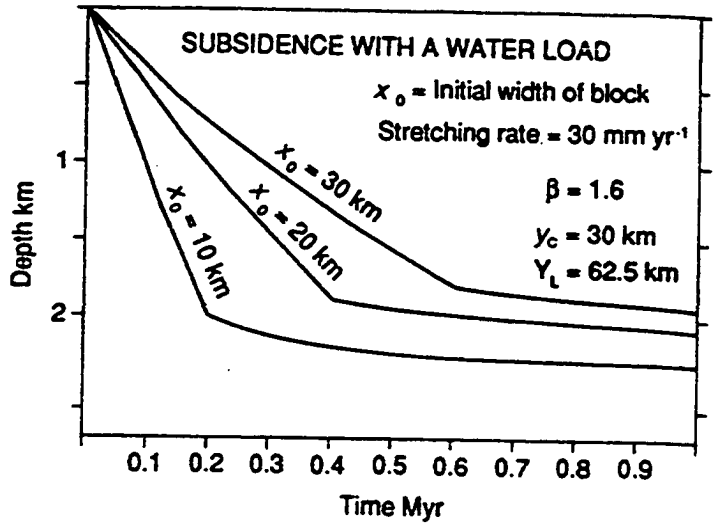

Figure 2.5.7a

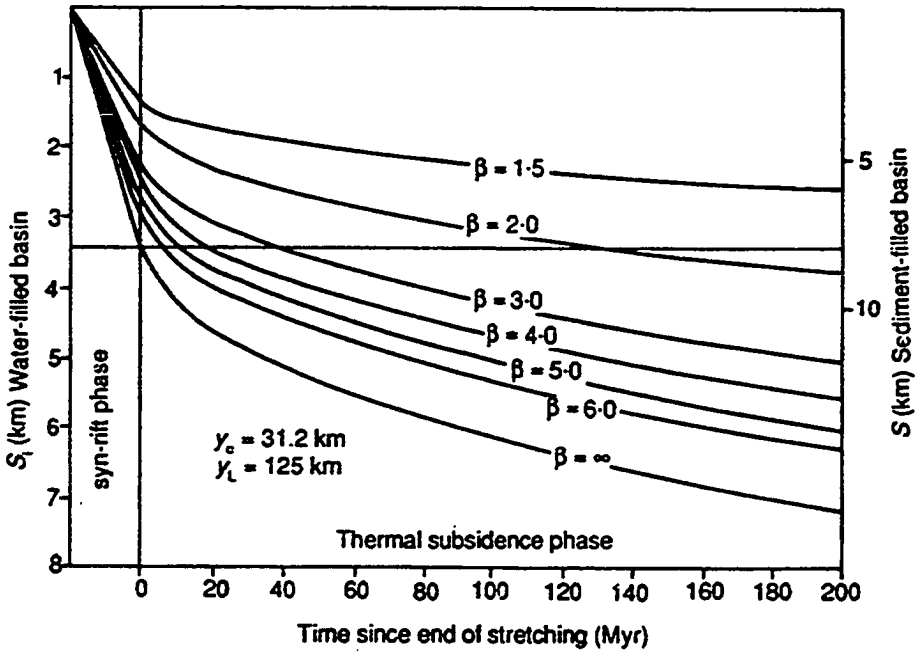

Figure 2.5.7b

Bay Basin. However, because few basement reflectors are seen within the seismic data, the precise structure of the basin can only be speculated and no unique basin description can be proposed. The basin could be a pull-apart basin similar to the Stellarton Graben, related to transtension associated with a releasing bend within the Hollow Fault. Alternatively, the St. Georges Bay Basin could be an extensional half-graben with the basin-bounding fault (the Hollow Fault) located immediately to the north of the Salt Wall Huey. In reality, the St. Georges Bay Basin is likely to have formed by a combination of wrench and extensional tectonics related to movement of the Hollow Fault over a protracted period during the Carboniferous.

2.5.5, The St. Georges Bay Basin Fill (Figures 2.5.1 and 2.5.8)

(The text below details the threefold division of the field area into tectono-stratigraphic domains).

The St. Georges Bay Basin fill is defined as the package of Upper Carboniferous strata and associated basement rocks that underlies the present day St. Georges Bay and the onshore exposures which extend south-west to Antigonish and which border St. Georges Bay to the north-east on the Judique coastline (Figure 2.5.1). The St. Georges Bay Basin is separated from the Gulf of St. Lawrence Basin by a basin-bounding fault, which is interpreted to be the main structural expression of the Hollow Fault in this area.

Within the St. Georges Bay Basin, ~2.9 km of Mabou Group and Port Hood Formation sediments were deposited. The approximate depocentre for the Mabou - Port Hood interval within the project area is imaged on line 83 to the south of the Salt Wall Huey. Within the St. Georges Bay Basin, the Inverness Formation has been severely disrupted by salt tectonics. Sedimentary pinch-outs, rafting and erosional truncation, possibly due to inversion (see below), make determination of gross thickness trends very difficult (Figure 2.5.9).

Figure 2.5.8. Tectono-stratigraphic division of the field area. As interpreted from the 1982 Chevron seismic survey, the Mabou Group and Port Hood Formation are approximately 0.7 km thick within the Gulf of St. Lawrence area and between 0 – 0.5 km thick within the western Cape Breton area (although local thickness variations exist). The Gulf of St. Lawrence and western Cape Breton areas were probably platform areas during much of the Namurian. While thick Mabou Group sediments were deposited within St. Georges Bay Basin, the 2R and Gillis Fan units were deposited within the Gulf of St. Lawrence and western Cape Breton areas. The 2R and Gillis Fan units are probably indicative of much slower sedimentation rates on the platform areas.

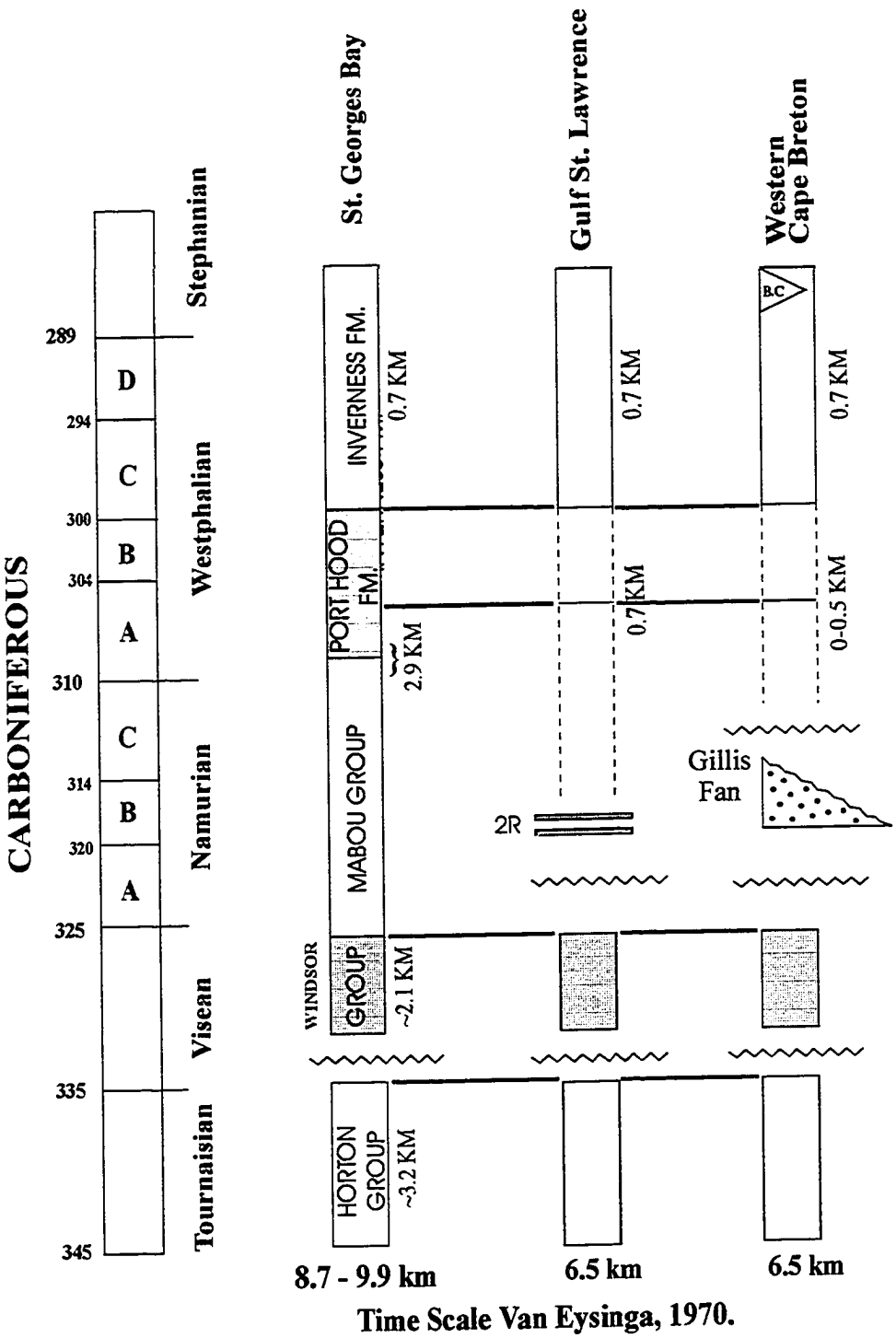
CARBONIFEROUS
Stephanian
Westphalian
Namurian
Visean
Tournaisian
289
294
300
304
310
314
320
325
335
345
D
C
B
A
C
B
A
St. Georges Bay
Gulf St. Lawrence
Western Cape Breton
INVERNESS FM.
PORT HOOD FM.
MABOU GROUP
WINDSOR GROUP
HORTON GROUP
0.7 KM
2.9 KM
~2.1 KM
~3.2 KM
0.7 KM
0.7 KM
0.7 KM
0-0.5 KM
B.C
2R
Gillis Fan
8.7 - 9.9 km
6.5 km
6.5 km
Time Scale Van Eysinga, 1970.

Figure 2.5.8

Figure 2.5.9. TWT contour map of the Inverness Formation 15' coal seam reflector interpreted from the 1982 Chevron survey. The contours show that the Inverness Formation has been folded and uplifted within the St. Georges Bay area. Within the Gulf of St. Lawrence area the contours reflect salt withdrawal to create a salt pillow. Within the western Cape Breton area the contours show a simple thickening towards the north-east.

Figure 2.5.10. TWT contour map of the 2R reflector. The reflector defines a dome and swell topography associated with salt withdrawal. The topography has an amplitude of 500-600m (0.5-0.6 sec TWT).

Figure 2.5.11. TWT contour map of the Top Windsor reflector. Note that when combined with the Inverness Formation contour map (Figure 2.5.9) the thickness of the Mabou Group and Port Hood Formation strata are dramatically reduced over the Gillis Fan in western Cape Breton.

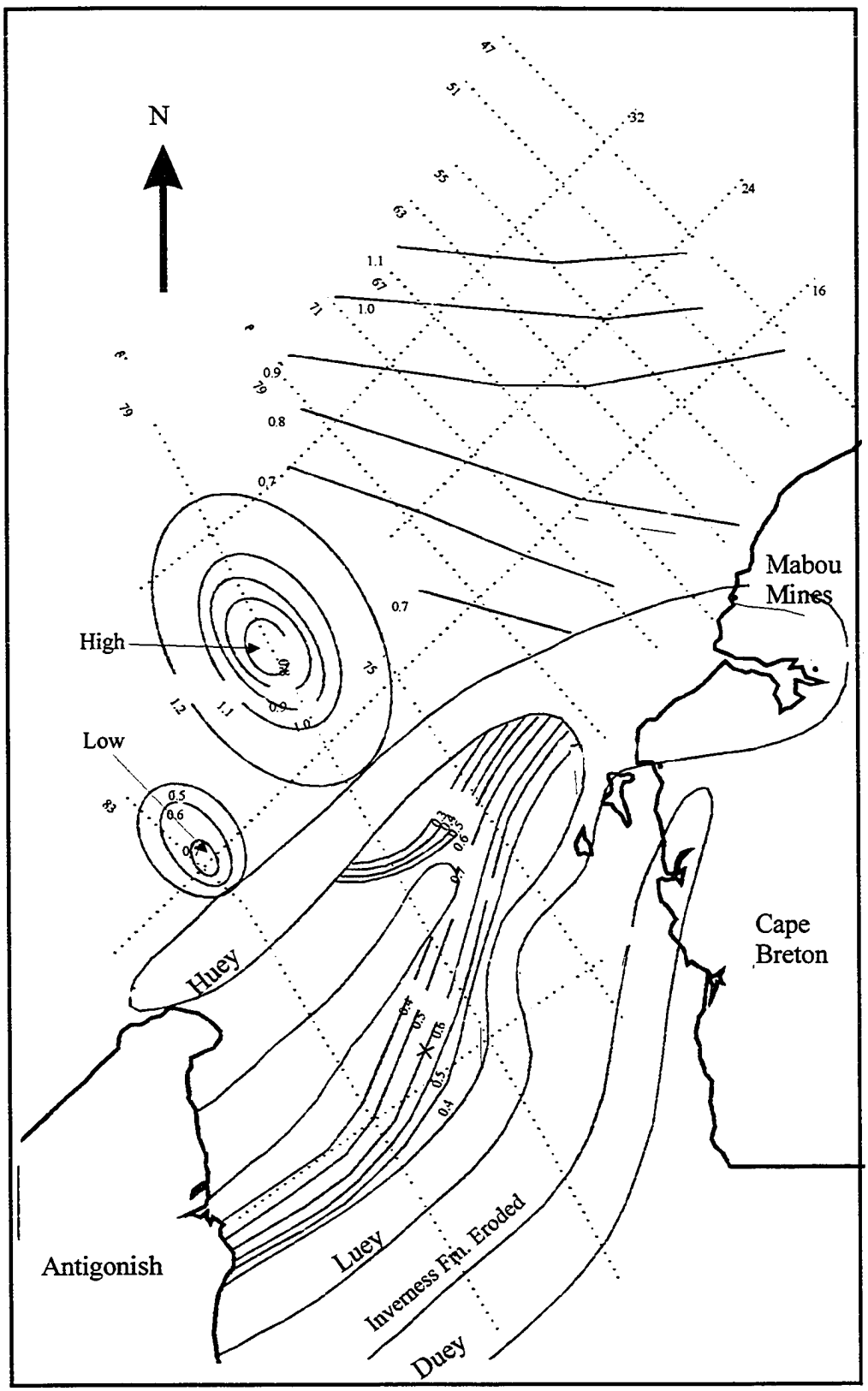

Figure 2.5.9. TWT contour map of the 15' coal seam of the Inverness Formation.

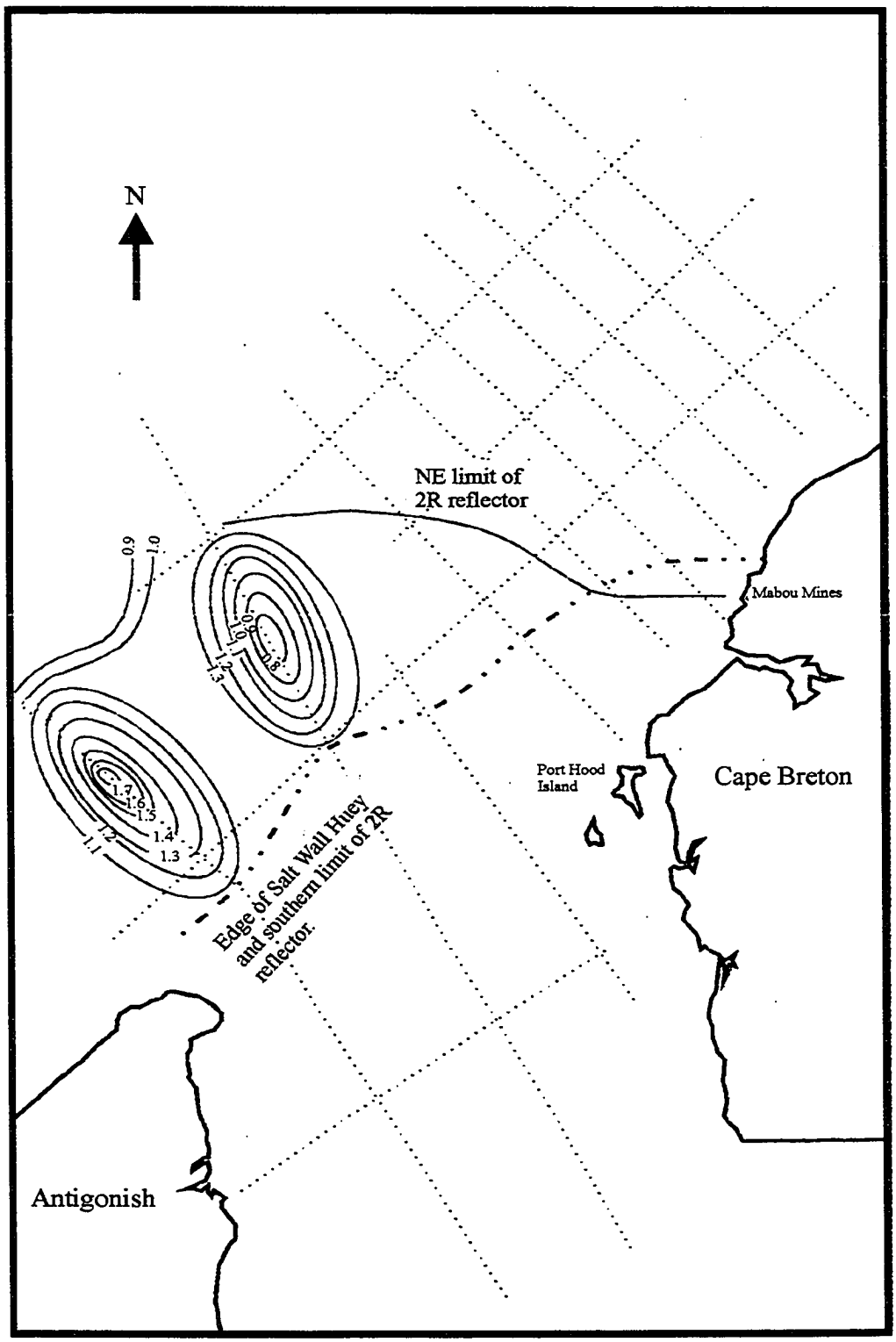

Figure 2.5.10. TWT contour map of the 2R reflector. Contour interval = 100 ms.

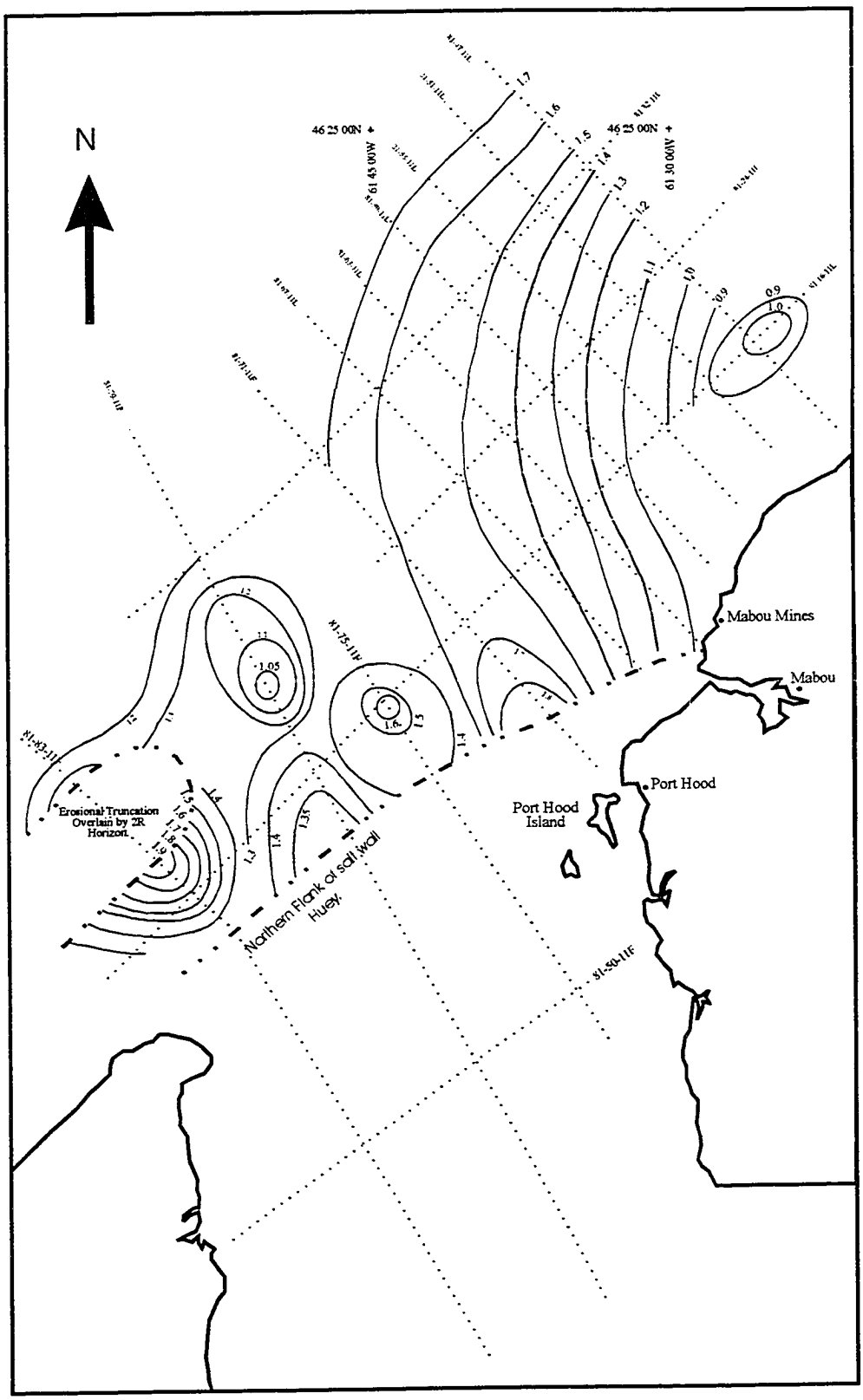

Figure 2.5.11 . TWT Contour Map for the Top Windsor Reflector.

2.5.6, The Gulf of St. Lawrence Area (Figure 2.5.1 and 2.5.8)

Within the Gulf of St. Lawrence area immediately north of St. Georges Bay and close to the Nova Scotian coast, 0.7 - 1.8 km of Mabou Group and Port Hood Formation sediments are preserved (Figure 2.5.8). A distinct seismic reflector (2R reflector, see seismic stratigraphy), probably representing a sedimentary unit, is imaged directly above the Top Windsor reflector (Figure 2.5.10). The stratigraphic position of the 2R reflector implies an early Namurian age; however, no well penetrations exist in this area and so the age and sedimentology of the 2R unit remains tentative. The 2R seismic reflector is a continuous, high-amplitude reflector throughout most of the Gulf of St. Lawrence area but progressively loses coherency and amplitude towards the north-east until it is no longer distinguishable. This 'fading' of the 2R reflector coincides with the appearance of a set of seismic reflectors interpreted to be a north-westward prograding clastic wedge (the Gillis Fan). The interface of the clastic wedge and the 2R reflector forms the north-eastern boundary of the Gulf of St. Lawrence area against the western Cape Breton area (Figure 2.5.1).

Examination of the TWT contour map for the Henry Island Member of the Port Hood Formation coal measure reflectors shows a distinctive dome and trough within the Gulf of St. Lawrence area (Figures 2.5.9 and 2.5.11). This topography is related to an underlying salt pillow. Downlapping relationships indicate that this structure probably formed as a result of salt withdrawal and rollover of the overlying strata as the salt withdrew to form a salt pillow and salt weld. The salt pillow is described in more detail in section 2.7.

2.5.7, The Western Cape Breton Area (Figure 2.5.8)

The western Cape Breton area forms an elongated strip approximately 7 km wide and 35 km long that extends from Port Hood to St. Rose and includes both the offshore area and the adjacent coastline. The western Cape Breton area follows the interpreted path of the Hollow Fault.

The Gillis Fan is a previously undocumented, 300-500 m thick stratigraphic unit with a wedge-shaped cross section. It covers an area of 150 km^2 with a semi-circular geometry centred upon the town of Inverness, western Cape Breton (Figure 2.5.12) (see below, Chapter 5). The stratigraphic position of the Gillis Fan is equivalent to the 2R seismic reflector and therefore it is also assigned to the Namurian. The Mabou - Port Hood interval recognised from the St. Georges Bay area thins rapidly into the western Cape Breton area as the sediments overstep the ~500 m thick Gillis Fan. At the extreme north-eastern edge of the 1982 Chevron seismic grid (line 47), the Mabou - Port Hood interval is <100 ms (150 m) thick. This rapid thinning over the Gillis Fan suggests that the western Cape Breton area was a shallow platform area adjacent to the Gulf of St. Lawrence area during the Namurian-early Westphalian. Isolated depocentres that contain a thicker Mabou - Port Hood interval are present; for example, at St. Rose. In these areas, the thicker sedimentary succession is probably related to offset of an isolated segment of the Hollow Fault. The lithology and age of the Gillis Fan strata is too poorly defined to warrant stratigraphic ascription at present.

To the north-east and outboard of the Gillis Fan, the Mabou Group interval is approximately 900 m thick and thickens rapidly in the St. Rose area. Within the Henry Island Member of the Port Hood Formation exposed onshore, one or more distinctive horizons (ostracod rich, high TOC black shales) palynologically dated as Westphalian A are present at numerous locations within western Cape Breton. This indicates possible sedimentological continuity between the St. Georges Bay (St. Georges Bay Basin) and the western Cape Breton area during the Westphalian A. This, in turn, may imply movement on segments of the Hollow Fault within western Cape Breton, allowing the deposition of Port Hood Formation sediments within western Cape Breton. Within the western Cape Breton area, the Inverness Formation thickens progressively from

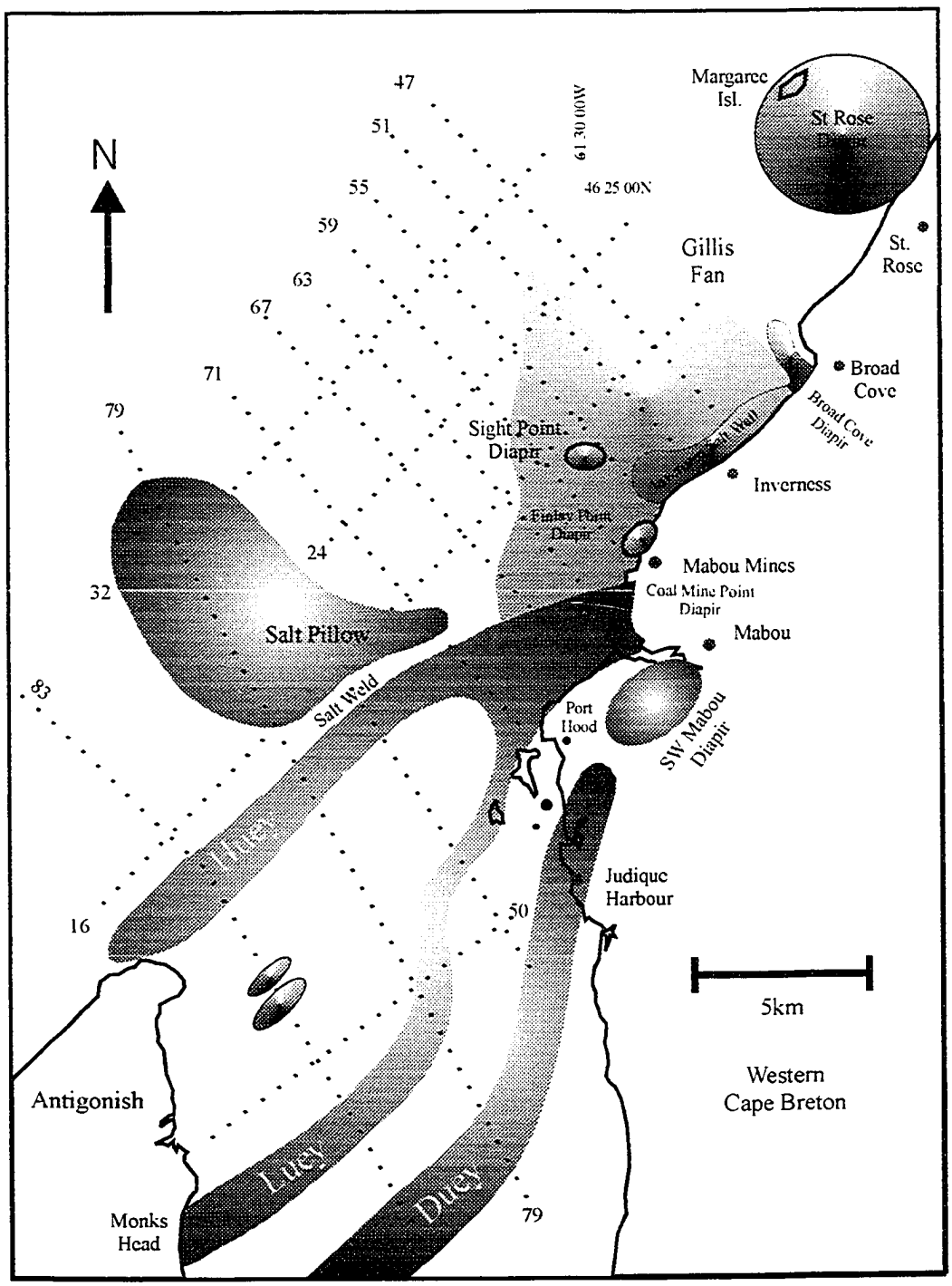

Figure 2.5.12. Geographic location of salt structures. Salt structures shown as darker shaded areas. Gillis Fan shown as lighter shade.

approximately 0.7 sec TWT (~1.05km) in the southern portion (Mabou Mines) to 1.1 sec TWT (~1.6km) at the northern margin of the seismic coverage (St. Rose) (Figure 2.5.9). The thickness of the Inverness Formation does not appear to be affected by the Gillis Fan. However, it is clear from onshore exposures that the Inverness Formation is onlapping basement rocks to the east; for example, at Port Ban. The thickening of the Inverness Formation towards the north could be the result of thickening towards the Gulf of St. Lawrence Basin depocenter located beneath the Magdalen Islands.

2.6, BASIN INVERSION

There is strong evidence to suggest that large regions of the Maritimes Basin have undergone inversion both during the Carboniferous and after the Carboniferous. Within Atlantic Canada, workers have described both structures and sedimentation related to compressional phases of deformation during the Carboniferous (Webb, 1963; Poole, 1967; Belt, 1968; Currie and Nance, 1983; Plint and van de Poll, 1984; Caudill and Nance, 1986; Nance, 1987). The structures described by these workers vary considerably in terms of style, geometry and timing but a review by Nance (1987) drew together several of the tectonic elements to propose a tectonic model for southern New Brunswick that extends into north-central Nova Scotia. The model proposes that the various thrust faults, strike-slip faults and extensional faults can be explained as component parts of a regional dextral transpression within southern New Brunswick and north-central Nova Scotia during the Late Carboniferous. The dextral transpression was driven by a north-west/south-east orientated compression that reactivated pre-existing faults. Documented evidence for Carboniferous tectonic inversion within Cape Breton is sparse. Bradley and Bradley (1986) described a small basin (Big Pond Basin) located in eastern Cape Breton that they interpret to be a pull-apart basin formed as a result of dextral strike-slip offset on a through going fault. The age of movement is not fully constrained but at least some of the movement occurred during the Visean, which correlates the faulting associated with

the Big Pond Basin to similar Visean faulting documented in New Brunswick and Newfoundland.

As well as tectonic evidence for Carboniferous inversion, there is evidence (vitrinite reflectance data and apatite fission track data) to indicate post-Carboniferous sedimentation and inversion. Hacquebard (1984) proposed that vitrinite reflectance levels of ~ 0.6% R_0 obtained from coal samples in the Sydney Basin indicated that the Sydney Basin coal seams were buried by a thick overburden and that subsequently 3700 m of strata overlying the coal seams has been eroded.

On a more regional scale, Ryan (1993) and Grist et al. (1995) used apatite fission track analysis to model the subsidence and inversion history of the Maritimes Basin. Grist et al. (1995) concluded that, although uplift rates were not uniform over the region, large areas of the Maritimes Basin underwent up to 4 km of post-Carboniferous uplift and erosion. The apatite fission track analysis provides information about the retrograde thermal history of a sample whereas vitrinite reflectance data provides prograde burial history information that can be used to determine the maximum depth of burial. The results from the two techniques complement each other and indicate that large areas of the Maritimes Basin were covered by 3-4 km of post-Carboniferous sedimentary rock and that up to 4 km of this sedimentary cover has been eroded. Marillier et al. (1989) interpreted two large folds at the Windsor Group level on line 86-1 of the Lithoprobe East seismic data (Figure 2.5.5). The folds can be interpreted to be salt-cored detachment folds that have uplifted and folded overlying reflectors. Folds of this nature could be the result of Late or post-Carboniferous inversion, or be related to thin-skinned gravity spreading of the Upper Carboniferous strata along a Windsor Group evaporite decollement due to uplift and tilting of the Magdalen Basin (Figure 2.5.5). In either case, the folds may be explained as inversion related structures.

Within the field area, Inverness Formation coal seam samples taken from the Mabou 1 and Mabou 2a wells have an average vitrinite reflectance of 0.62% R_0 (Hacquebard, 1986), similar to those reported from the Sydney Basin (Haquebard, 1984). This implies that the Inverness Formation within western Cape Breton has also been buried under approximately 3-4 km of overburden sediments and that subsequently this overburden has been eroded to place Upper Carboniferous rocks at or near the surface today.

Recent geological mapping of western Cape Breton has highlighted features that support inversion within western Cape Breton. Lynch and Brisson (1994) documented the Ainslie Detachment, which they described as a low-angle fault that detached along the Macumber Limestone and transported the overlying Carboniferous strata to the south-west within the Denys River area. Based on stratigraphic evidence, Lynch and Brisson (1994) proposed that displacement on the Ainslie Detachment occurred after the Namurian and before the Westphalian C. Giles et al. (1997a and b) extended the Ainslie Detachment into western Cape Breton. As indicated on the regional maps/cross-sections (Giles et al. 1997a and b), the Ainslie Detachment is now strongly folded. Although there is no upper age constraint, this folding must have occurred after the Westphalian C.

A number of pieces of structural data were collected from the coastal outcrops in the field area that could indicate both Carboniferous and post-Carboniferous inversion. This evidence is described briefly below and a full discussion of each point is included in Chapter 3.

- To the south of the town of Inverness, Giles et al. (1997b) mapped an angular unconformity between the Inverness Formation and the underlying Horton and Windsor Groups (Figure 3.1.2). The Horton and Windsor Groups in this location have been folded in to broad open folds indicating that a pulse of deformation, possibly due to compression, took place in the time interval between the deposition of the Windsor

Group and the Inverness Formation (Namurian–Westphalian C).

- At Mabou Mines Beach, a thrust fault is exposed that repeats the Macumber Formation. Striations on the fault surface and vergence of thrust-related folds indicate transport of the hangingwall towards the NNW. Timing of the thrust is only constrained to be after the deposition of the Macumber Formation.

- At Green Point, the Horton Group is deformed by numerous small brittle faults. The faults contain calcite shear veins, which indicate that the majority of the faults are strike-slip or reverse faults. A stereographic plot of these faults indicates that they could have been formed by a north-west/south-east orientated compression (i.e. sigma 1 = NW/SE). This set of faults must have been formed after the deposition/lithification of the Horton Group.

- At MacKinnons Brook, there are numerous faults that cut, and therefore post-date, the Inverness Formation. The faults are dominantly strike-slip faults orientated north-south or east-west (approximately the same orientation as the strike-slip faults at Green Point). The formation of these faults could be explained by an approximately north-west/south-east orientated compression taking place after the Carboniferous (i.e. sigma 1 = NW/SE).

2.7, HALITE DISSOLUTION

In many of the salt provinces around the world, such as the Gulf Coast of Mexico, it is estimated that up to 50% of the original salt volume has been lost due to dissolution at the surface (Hossack, 1995). This salt volume loss makes balancing and restoration of structural cross-sections inherently difficult. Boehner (1983, 1986) concluded that there are no solution cap rocks (similar to those described from onshore Texas and Louisiana,

e.g. Martinez, 1974, 1978) within Nova Scotia and Cape Breton, although there is good evidence for halite dissolution. Boehner (1993) reported many examples of collapse breccia that consist of blocks of gypsum and carbonate in a mudstone matrix that form an irregular zones overlying a diapir. These residual zones appear to be associated with areas where halite has reached the surface. Within Cape Breton, Giles (1981a) described Windsor Group sections from the Canso-Bras d'Or area in which halite has been removed to a depth of 200-300 m, leaving a telescoped Windsor section. Salt springs are common within Nova Scotia and Cape Breton and are direct evidence for modern halite dissolution. The location of salt springs is not always associated with a diapiric structure or fault. Boehner (1983, 1986) described areas from Nova Scotia and Cape Breton where a fault or salt structure is not associated with salt springs and suggested that the diapir or fault may have been sealed from groundwater flow by residual clay. Howie (1988) documented many occurrences of salt springs from Antigonish county, the Denys Basin – Canso area and western Cape Breton. There is evidence that halite dissolution has affected the salt structures within the field areas. The evidence for this is described in Chapter 3 and a discussion is presented in Chapter 4.

2.8, DISTRIBUTION OF SALT STRUCTURES AND RELATIONSHIP BETWEEN ONSHORE AND OFFSHORE DIAPIRS

Figure 2.5.12 shows the present distribution of salt structures within St. Georges Bay, along the west coast of Cape Breton and in the immediate onshore area of western Cape Breton and Nova Scotia. The onshore salt structures examined in this thesis do not consist of halite but of a deformed package of Middle Windsor Group and/or Hood Island Formation strata. Schwerdtner (1983) described structural carapaces from Arctic Canada that consisted of gypsum and anhydrite that had been carried above the halite diapir core as the diapir penetrated the overburden. Numerical modelling by Weinberg (1993) indicated that diapirs in which the halite acted as a power-law fluid would be capable of

lifting inclusions up to 3-6 km^2. These numerical calculations are backed up by field observations from Iran where large rafts of Hormuz sediments and volcanic rocks appear to have been lifted by the salt from depth to be exposed at the surface. In all cases, the onshore exposures of deformed Middle Windsor Group and Hood Island Formation strata can be tied to a seismically imaged salt structure. From this close association and from previously documented examples around the world, the Middle Windsor Group and Hood Island Formation strata can be interpreted to be structural carapaces that have been uplifted as part of a diapiric structure. It is possible that the Windsor Group strata were carried as an inclusion within the halite prior to exposure at surface. The surrounding halite would have to dissolve since no halite is presently associated with the carapaces. In this scenario, halite dissolution would probably cause collapse or rollover of the overburden. In only one case (the St. Rose Diapir) is there evidence of overburden deformation related to dissolution of halite and in this case overburden deformation may well be related to deep salt withdrawal instead of surface dissolution (see below, Chapter 3.2). The available field and theoretical evidence indicate that the most likely model to explain the Middle Windsor Group and Hood Island Formation exposures that are associated with seismically imaged salt structures is that they are structural carapaces that have been transported vertically as an intrinsic part of the diapir. Detailed descriptions of the onland diapir exposures are given in Chapter 3.

As well as describing the many salt structures, this section also describes structural and stratigraphic features associated with the salt structures and makes some interpretation of these features. These interpretations are incorporated into later sections that deal with the onshore salt structures.

2.8.1, Salt Structures within the St. Georges Bay Basin

Within St. Georges Bay, three north-east / south-west trending salt walls (Huey, Luey and Duey) are interpreted from the 1982 Chevron data. The salt walls cross cut St. Georges

Bay and are exposed as coastal sections in western Cape Breton (Coal Mine Point and Finlay Point), Port Hood Island and on the Antigonish coast (Monks Head).

Salt Wall Huey. The Salt Wall Huey lies parallel and adjacent to the northern boundary of the St. Georges Bay Basin (the Hollow Fault) and has a complex geometric form that progressively becomes simpler towards the north-east (western Cape Breton).

Line 83: The northern flank of the salt wall is 2.1 km high with a vertical to slightly overhanging geometry. The southern flank of the salt wall is ~3.2 km high. The base of the southern flank is near-vertical, whereas the upper portion shows a lateral protrusion that extends into the surrounding sedimentary rocks (Figure 2.8.1). The lateral protrusion may have intruded the surrounding overburden at a shallow burial depth or extruded onto the surface, forming a salt glacier, before being buried by onlapping sediments. It is unlikely that the salt would have had sufficient mechanical force to intrude compacted and lithified sediments at depth (Nelson and Fairchild, 1989). No salt is imaged to the left of the Salt Wall Huey on the footwall of the Hollow Fault. It appears that the entire section to the left of the salt wall (shot point 1720 – 1380, ~1.5 sec TWT) was either devoid of salt or the salt has migrated to form a weld (Figure 2.8.1). Between shot point 1060 and 1020, ~0.3 sec TWT (Figure 2.8.2), reflectors interpreted to be Inverness Formation coal seam reflectors show strong folding and faulting above a small diapir. The isopach nature of the folded reflector package indicates that most of the rocks were lithified prior to folding. It is unlikely that the small diapir could exert sufficient mechanical force to fold the observed thickness of overburden (~500 m) (for example see Schultz-Ela et al., 1993). Unfortunately, the seismic resolution in this area is poor and so only the top 500 ms of the diapir are imaged. With this in mind, it would be over ambitious to argue the precise mechanics of this situation. Having stated the limitations of the data, the folding can be interpreted to be the result of rejuvenation of diapir growth related to inversion. A compressive force would squeeze the diapir, greatly increasing the

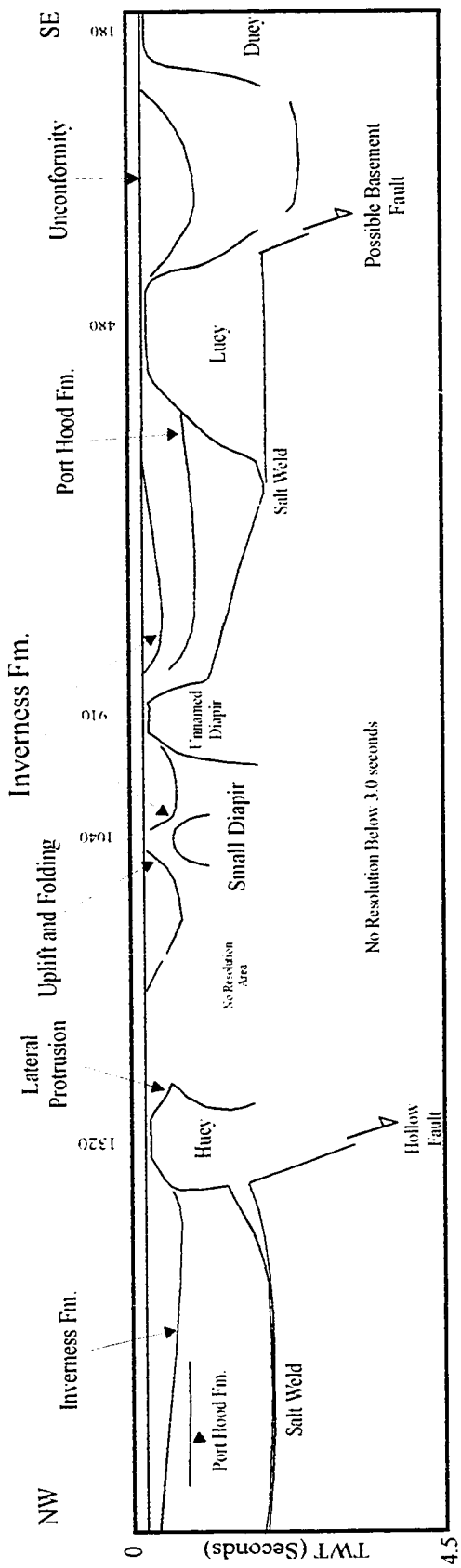

Figure 2.8.1. Line Diagram of Chevron Line 83.

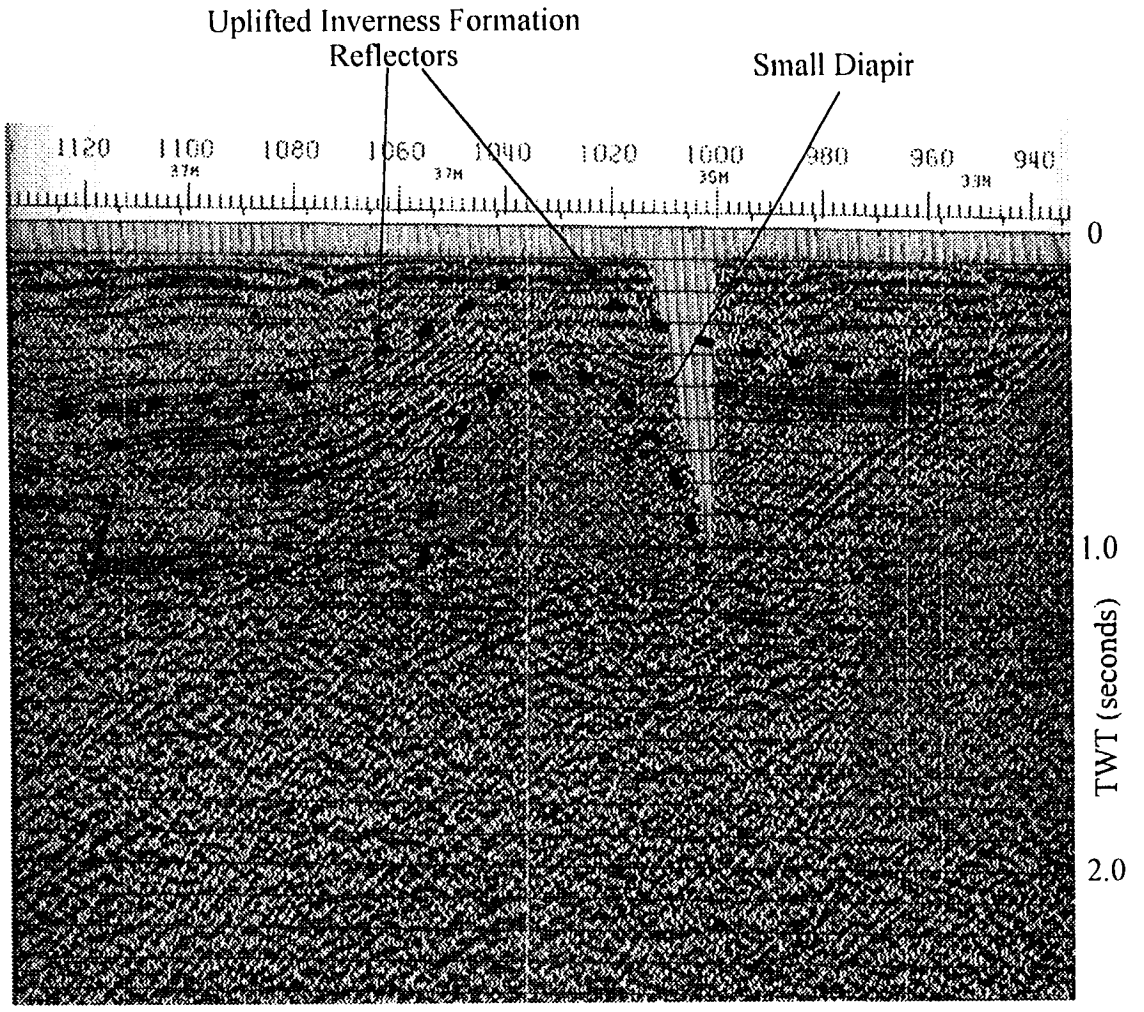

Figure 2.8.2. Part of line 83 showing uplifted and folded strata above a small diapir.

upward mechanical force exerted by the halite on its overburden. If the increased deviatoric stresses at the diapir/overburden interface exceed the strength of the overburden, then the diapir may force its way through the overburden as an active diapir (Vendeville and Nilsen, 1995). Rejuvenation of this kind would uplift and fold the overburden rocks but tends to preserve the internal geometry of the uplifted units. The fact that Inverness Formation rocks are uplifted and folded implies that rejuvenation of the diapir did not occur until after the Westphalian D.

Line 79: On line 79, Huey has a similar geometry to that imaged on line 83 (see above). The northern flank is 1.4 km high with a rounded to quasi-shouldered geometry (average dip ~71 degrees) (Figure 2.8.3). The southern flank is ~3.2 km high with a lateral protrusion that extends into the surrounding Carboniferous strata. To the left of the Salt Wall Huey, in the footwall of the Hollow Fault, a salt weld is imaged between shot points 1580 – 1520 at ~ 1300 ms., to the right of a large salt pillow. An angular unconformity overlying the salt weld can be seen between reflectors that are interpreted to be Mabou Group and Inverness Formation strata. The angular unconformity may be caused by subsidence and folding (rotation) of the Mabou Group strata as the salt evacuated to form the salt weld. Subsequent erosion followed by deposition of the Inverness Formation would produce the geometry seen today. This relationship constrains the timing of weld formation to be between the Late Namurian and Westphalian C. The salt pillow to the right of the salt weld is located above a shallow anticlinal structure. The formation of this fold structure may be the reason for the formation of the salt pillow in this area and may relate pillow formation to Carboniferous inversion. The formation of the fold structure due to inversion may have caused differential loading of the salt layer due to sedimentation on the flanks of the uplifted area. In turn, this may have focused salt withdrawal away from the depocenters and into the crest of the fold. The slight thickening of the Mabou Group sediments over the salt weld to the right of the pillow supports this idea.

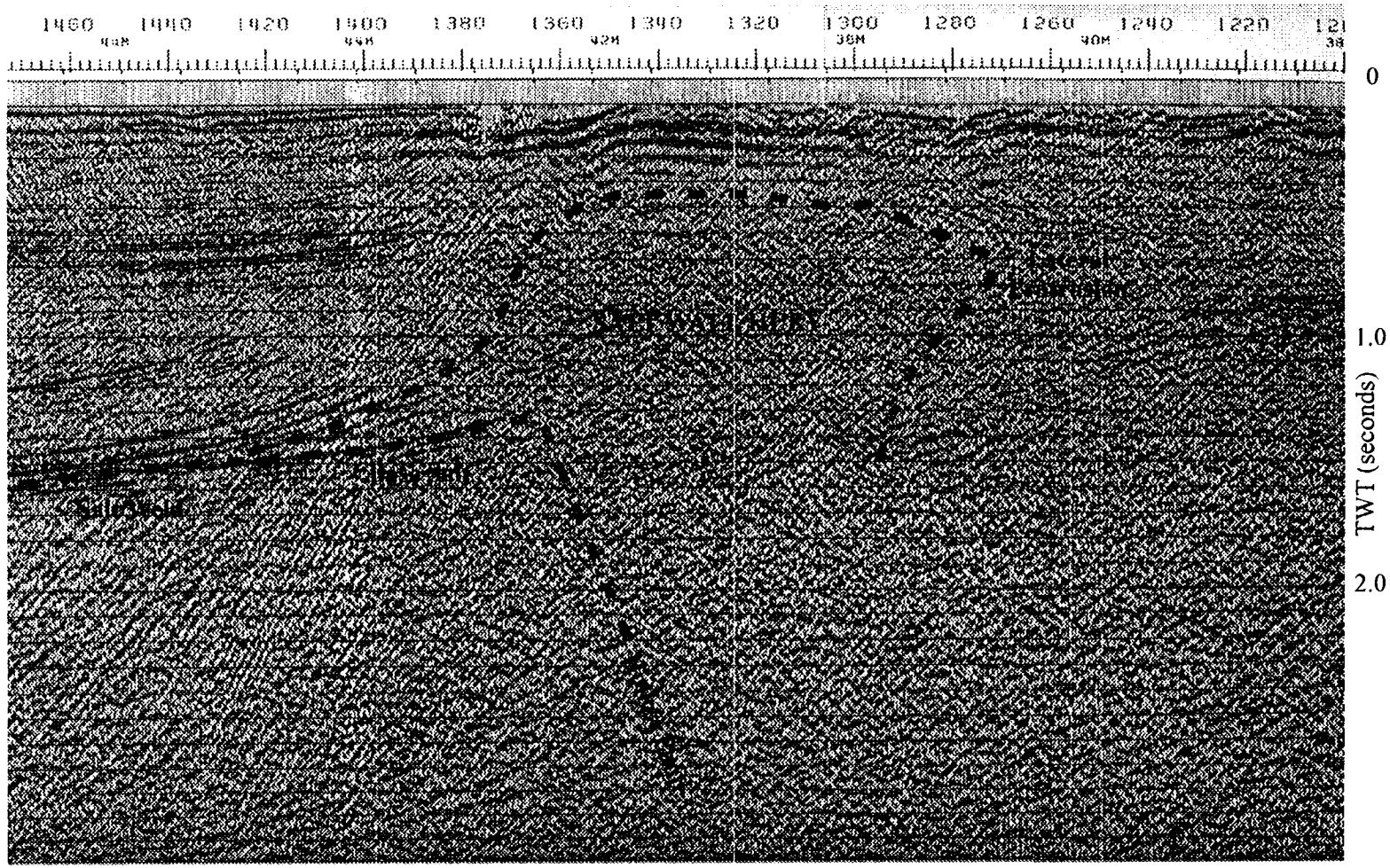

Figure 2.8.3. Part of line 79 showing the Salt Wall Huey, the Hollow Fault, a salt weld in the footwall of the Hollow fault and a lateral protrusion on the right hand side of the salt wall.

Between shot points 1280 – 1060 and 600 – 260, the Inverness and Port Hood Formation reflectors have been uplifted and folded over the crests and flanks of salt structures (the salt walls Huey and Duey) (Figure 2.8.4). The package of strata that has been uplifted is relatively isopachous and varies in thickness from approximately 1800 m to 2600 m. Previous workers have shown that the thickness of overburden that a diapir can uplift due to buoyancy alone is relatively thin and is approximately 1/3 of the diapir's height (Vendeville and Jackson, 1992a; Schultz-Ela et al., 1993). For salt walls Huey and Duey to lift the observed overburden, they would have to be approximately 5.4 km and 7.8 km high respectively. Both salt walls are around ½ the height needed to lift the overburden by buoyancy. The only way for the salt walls to lift so thick an overburden is by rejuvenation resulting from compression or inversion. A compressive force would squeeze the diapir, greatly increasing the upward mechanical force exerted by the halite on its overburden. Rejuvenation of this kind would uplift and fold the overburden rocks. The fact that Inverness Formation rocks are uplifted and folded implies that rejuvenation of the diapir did not occur until after the Westphalian D.

Line 75: On line 75, Huey has a strongly asymmetrical geometry. The northern flank is planar, steeply dipping (78 degree dip) and ~1.5 km high. The southern flank is 3.6 km high and has a pronounced shoulder that protrudes laterally into the adjacent overburden. To the left of the Salt Wall Huey, between shot points 1160 – 1040 at ~1.5 sec TWT, a package of seismic reflectors can be seen that downlap onto the basal Windsor to the right of a salt pillow (Figures 2.8.5 and 2.8.6). The configuration of reflectors is interpreted to represent a salt weld. When restored to horizontal (approximate sedimentary datum), the reflectors would represent onlap surfaces onto the flanks of a salt structure. Withdrawal of the salt from beneath the onlap surfaces caused them to rollover on to the basal Windsor to form a salt weld. The reflectors within the strata overlying the salt weld features are chaotic and so the timing of salt movement cannot be established although it may be equivalent to the salt weld seen on line 79.

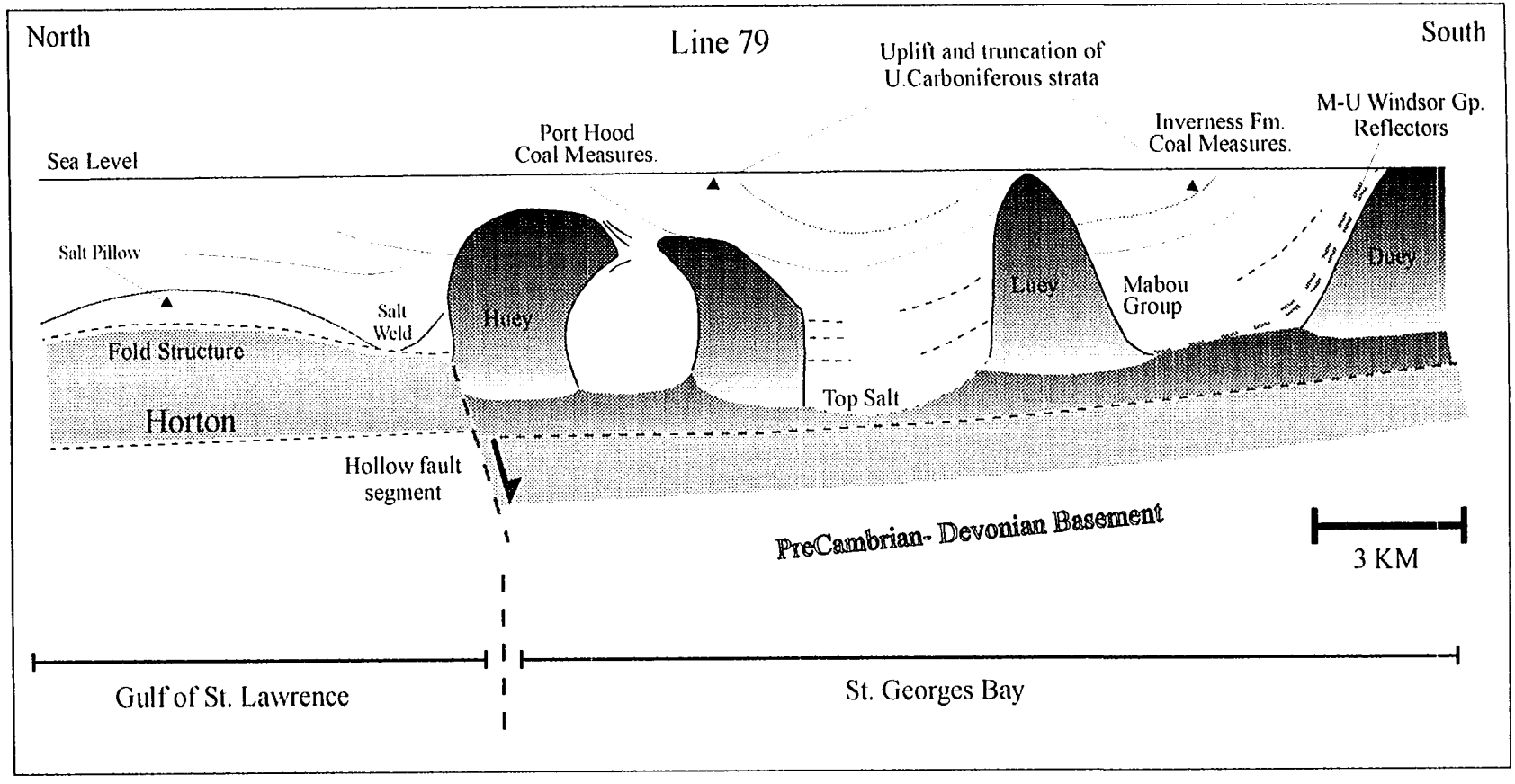

Figure 2.8.4. Interpretation of line 79 (Chevron survey). The position of the Inverness Formation coal seam reflectors is shown in grey and the Port Hood Formation coal seam reflectors are shown in black. Geophysical basement is at the top salt level. The depth to base salt is relatively unconstrained as is the thickness of the Horton Group. The un-named diapir shown between Huey and Luey is an isolated salt structure which only appears on line 79 (see seismic data).

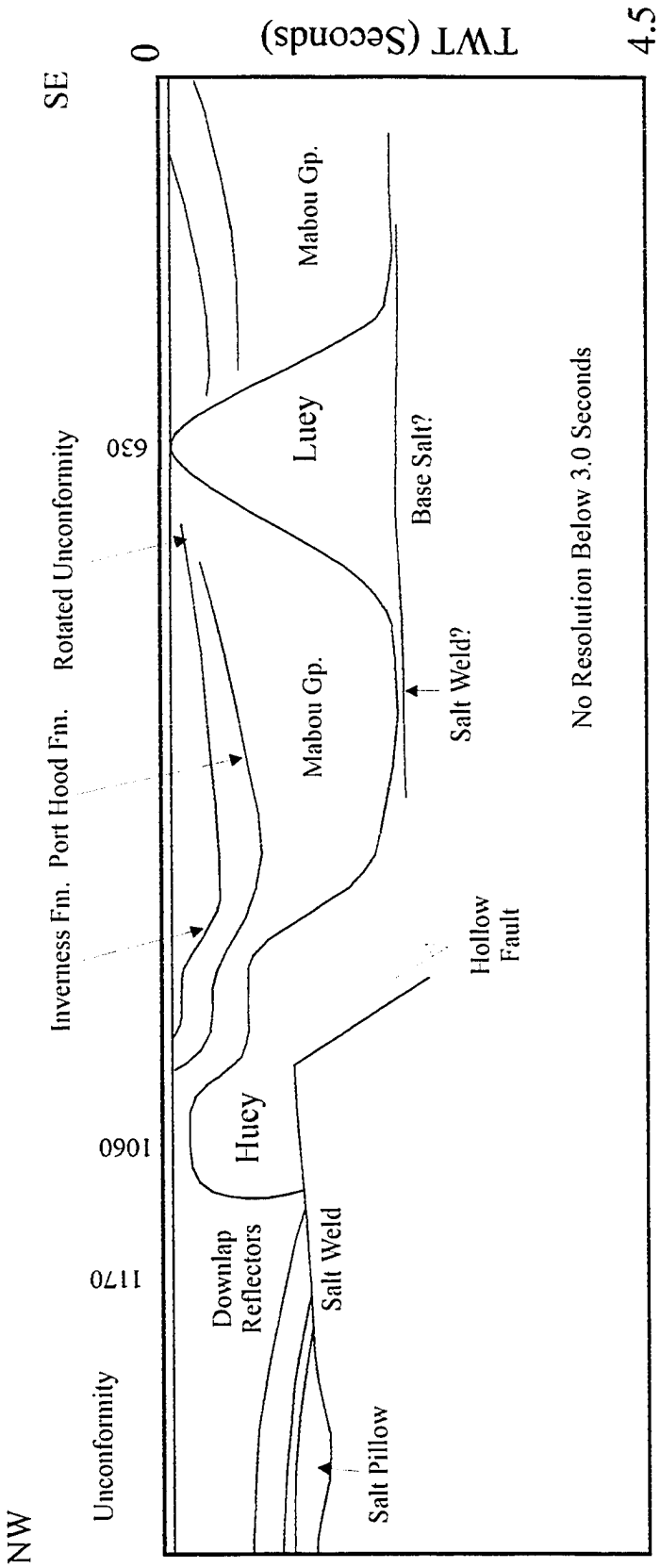

Figure 2.8.5. Line Diagram of Chevron Line 75.

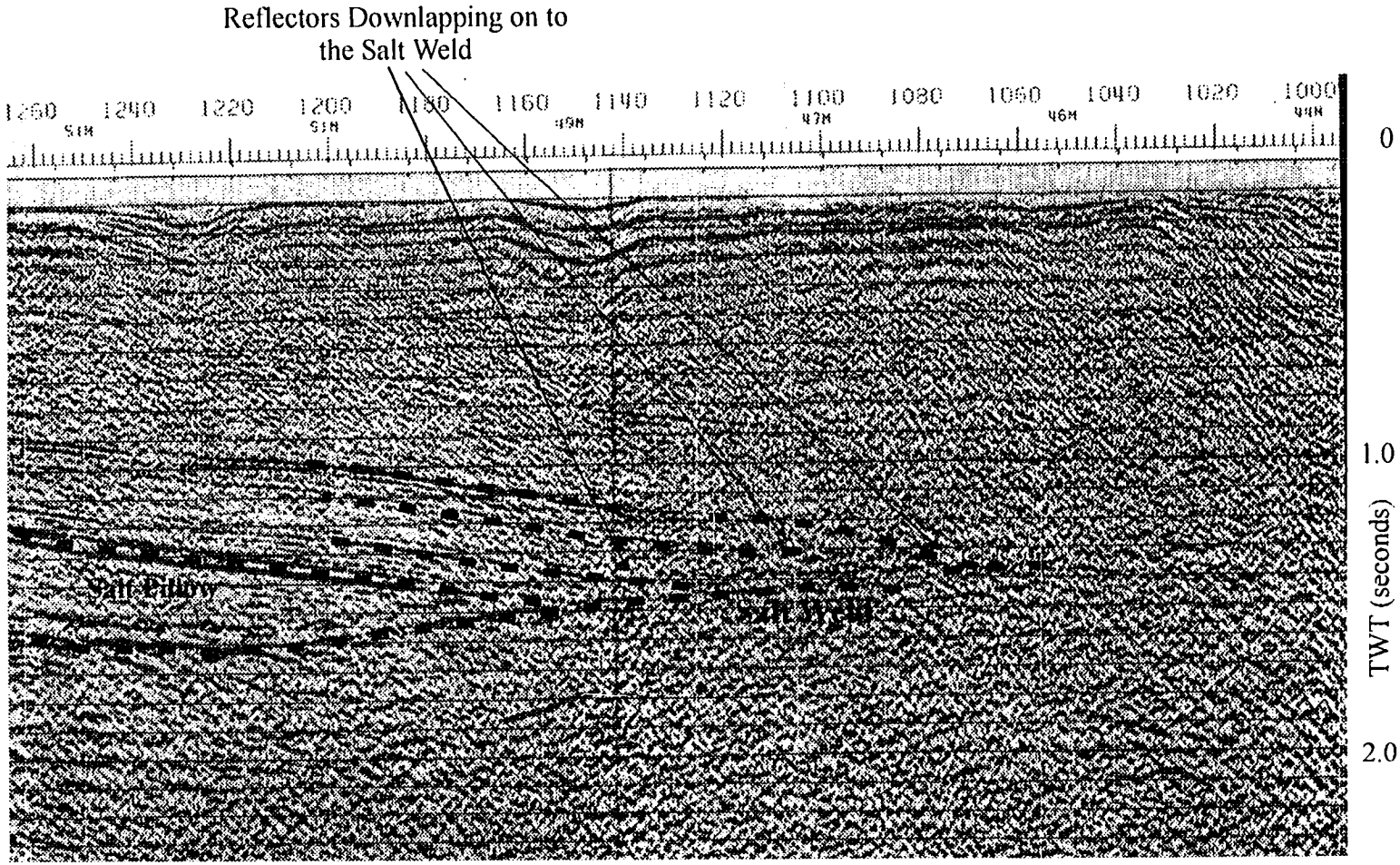

Figure 2.8.6. Part of line 75 showing reflectors downlapping on to the base salt reflector to form a salt weld.

Line 71: On line 71, only the northern flank of Huey is imaged. The northern flank is ~2.5 km high with a rounded geometry (average dip 58 degrees). The salt wall is very broad at this location, which may be due to the intersection of Huey with the Salt Wall Luey. Line 71 finishes just north of Port Hood Island and therefore does not extend far enough south to image the southern flank of the Salt Wall Huey/Luey.

Extending from shot points 300 – 980, the Inverness Formation reflectors dip to the north-west while over the same distance, the underlying Windsor Group reflectors dip to the south-east (Figure 2.8.7). If the Hollow Fault in this location has an extensional displacement that downthrows to the north-west (see above), then the dip of the Inverness Formation reflectors (and the underlying wedge of strata) indicates that inversion has taken place on the Hollow Fault, although the fault is still in net extension for the Inverness Formation strata. No onlapping sedimentary surface onto the back of the inverted strata are visible and so it is not possible to constrain the timing of inversion, except to say that it was post Westphalian D. It should be noted that the geometry of the Hollow Fault at this location is not accurately constrained. Although unlikely, the Hollow Fault may downthrow to the south-east, in which case the dip of the Inverness Formation may be explained as footwall uplift due to continued extension.

Also imaged on line 71 is a salt weld that separates a small salt pillow from the Salt Wall Huey (Figure 2.8.8). The salt weld was probably formed by salt withdrawal into the pillow and diapir, resulting in subsidence of the overlying strata, and is similar to the salt weld seen on lines 79 and 75.

Line 67: On line 67, as on line 71, only the northern flank of the diapir is imaged. The northern flank is ~2.5 km high and at least ~3.5 km wide (seismic grid stops short of southern flank). The northern flank has a very irregular geometry, best described as an upturned wineglass. (For more information on this portion of the salt wall, see Coal Mine

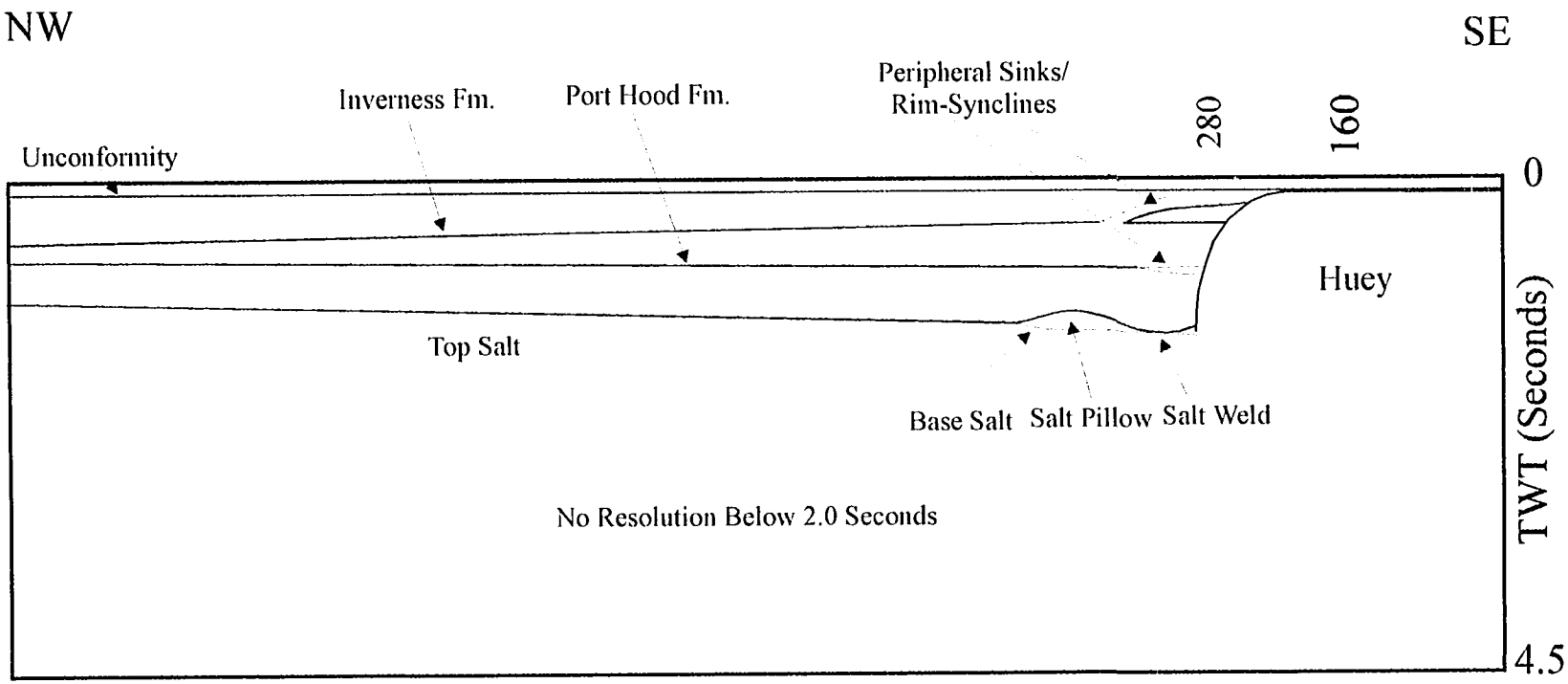

Figure 2.8.7. Line Diagram of Chevron Line 71.

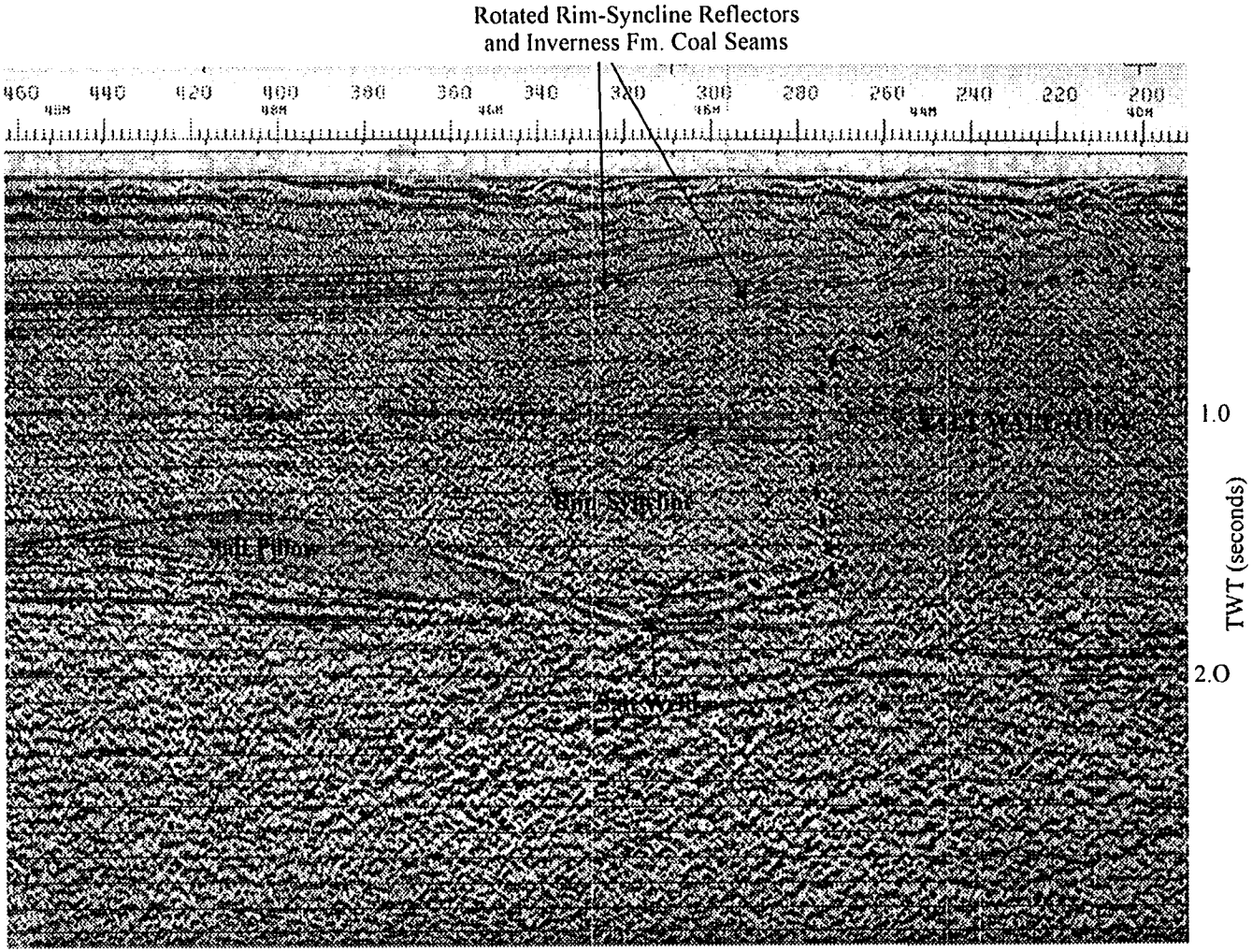

Figure 2.8.8. Part of Line 71 showing two rim-synclines, a salt weld and salt pillow located on the right hand side of the Salt Wall Huey.

Point Diapir, Chapter 3).

In a similar way to line 71, the Inverness Formation reflectors dip to the north-west. In addition, the Inverness Formation reflectors adjacent to the diapir have been folded into a monoclinal fold that has been uplifted adjacent to the diapir. Underneath the Inverness Formation is a package of high-amplitude reflectors. Around shot point 140, several of these reflectors dip upwards towards the Inverness Formation reflectors. Although the intersection of the two reflector packages is not imaged, the lower reflectors may be truncated by the overlying Inverness Formation reflectors. To the right of shot point 140, the reflectors that make up the lower reflector package diverge to increase the apparent stratal thickness represented by this reflector package. The apparent truncation of the lower reflectors by the Inverness Formation reflectors indicates pre-Westphalian C folding (pre-Inverness Formation) while the isopach nature of the Inverness Formation implies post-Carboniferous folding (post-Inverness Formation). The folding of the lower reflector package could be explained by the presence of a reverse fault dipping to the south-east (shown in dotted line on seismic) or a small salt structure located in the same area. Unfortunately, the resolution in this area is poor and no fault plane or salt structure is imaged. As described earlier, the overall dip of the Inverness Formation towards the north-west can be interpreted as inversion of the Hollow Fault. In a similar way, the uplift and folding of the Inverness Formation as an intact package adjacent to the diapir is likely to be the result of compression that could easily be related to inversion of the Hollow Fault. Uplift of the Inverness Formation indicates a post-Westphalian D age for inversion.

It is unfortunate that in lines 71 and 67, the Hollow Fault is not imaged and that the seismic data does not image features below the Windsor Group. For these reasons, the interpretations presented above must be considered to be somewhat speculative.

Interpretation of the Salt Wall Huey

The Salt Wall Huey has a complex geometric shape. The geometry of a diapiric intrusion is usually a good indication of the maturity of a salt structure.

Numerous factors, both tectonic and sedimentary in origin, play a fundamental role in controlling this growth history. These factors determine *how* and *if* a salt structure will grow and develop and to a certain extent will control its geometry. Some examples are described below which show the diverse nature of salt diapirs and how external factors can affect a diapir's ontogeny.

- An embryonic diapir starved of overburden sediment may grow to pillow stage by hydration diapirism (Hoyos et al., 1996), but cannot develop further to the diapir stage, simply because it has no overburden to intrude. Conversely, a salt diapir can be prevented from growing if too much overburden is deposited; that is, if sufficient lithostatic load is added to overcome the diapir's buoyancy force, it effectively stalls the diapir.

- Diapirs of the Great Kavir salt basin of Iran are dominantly mature salt structures with a well-developed salt canopy formed from the coalescing of several salt diapirs with mushroom-shaped heads (Jackson et al., 1990). A salt canopy probably forms by extrusion of halite onto the surface to form salt glaciers. The coalescing of two or more salt glaciers forms a salt canopy. The salt canopy may be preserved in the geological record if sedimentation buries the canopy. In contrast, diapirs of the Zagros Mountains derived from the Hormuz salt do not develop into mushrooms or canopies but remain as symmetrical cylinders or cone-shaped diapirs. This is probably due to the rheology of the overburden, which consists of competent carbonate strata that could not yield in a ductile manner (Gansser, 1960). The Hormuz diapirs were prevented from extruding and were

forced to intrude as ductile pistons by lifting the brittle overburden along concentric faults.

The shape of the Salt Wall Huey represents a moderately mature diapir. The diapir may not have progressed to a more mature shape due to the lack of available halite. The original (strataform) Windsor Group salt layer may not have been sufficiently thick to supply the required volume of salt to the diapir to sustain growth. The presence of a salt weld to the north-west of the Salt Wall Huey on lines 79, 75 and 71 attests to the fact that the salt wall has been at least partially cut off from its salt supply. Similar salt welds may exist within the St. Georges Bay Basin, for example on line 75 between shot points 820-760 at ~2.6 sec TWT, although the resolution at this depth makes interpretation difficult. The Salt Wall Huey is currently located within the footwall and hangingwall of the Hollow Fault within St. Georges Bay (lines 83, 79 and 75). Salt was probably supplied from both the hangingwall and footwall of the Hollow Fault until the formation of the salt weld seen on lines 79 and 75. After formation of this salt weld, salt supply from the footwall of the Hollow Fault was at least partially restricted. A complete cut off of the footwall salt supply cannot be proven because the large line spacing of the Chevron survey allows for spatial aliasing of salt-related structures.

The Eocene salt that is the source of the Kavir salt diapirs of north-west Iran is estimated to be 3-4 km thick (Jackson et al., 1990) while balanced sections across the Gulf of Mexico indicate that the Jurassic salt is at least 3 km thick (Digel et al., 1995; Peel et al., 1995). The Windsor Group halite within the project area is estimated to have been 540 m thick (Appendix 1). The volume of salt available to feed diapiric growth within Cape Breton is, therefore, very much smaller than that of the Kavir Salt Basin or the Gulf of Mexico.

Analogue modelling indicates that thin-skinned extension generally leads to the

development of diapirs and salt walls that are located in the footwall of listric extensional faults (commonly extensional growth faults) (Jackson and Talbot, 1994). In contrast, analogue modelling of thick-skinned extension, where a basement fault offsets the base of the salt layer, leads to the development of diapirs and salt walls that are located in the hangingwall and footwall of the extensional fault (Jackson and Talbot, 1994). The latter case has obvious similarities to the Hollow Fault within St. Georges Bay.

The geometry of Huey is similar to two diapirs (Machar and Medan diapirs) from the South Central North Sea (Figure 2.8.9). Remmelts (1995), Hossack (1995) and Stewart et al. (1996) postulated a model whereby the Machar and Medan diapirs grew above major basement faults with salt initially supplied from both the hangingwall and footwall. In the latter stages of diapiric growth, the salt supply to the diapirs from the hangingwall and footwall was either partially or completely cut off by grounding of the Triassic sediments on to the basal salt/basement units to form a salt weld. Hossack (1995) used two-dimensional restoration techniques to propose that Triassic extension allowed the diapirs to initially form as reactive diapirs. On reaching the surface, the diapirs continued to grow as passive salt structures for approximately 260 m/y. The final growth stage of the Medan diapir was as an active diapir. This final active stage may be connected to the Alpine inversion in the North Sea (Ziegler, 1990) that "squeezed" and rejuvenated the diapir (Nilsen et al., 1995).

The position of the Machar and Medan diapirs above basement faults, their geometry and their salt supply history are broadly similar to that of the Salt Wall Huey. The Machar and Medan diapirs can therefore be used as broad analogues for the Salt Wall Huey. The following growth history is proposed for the Salt Wall Huey:

- Initial reactive growth due to offset of the Hollow Fault as a thick-skinned extensional fault. While there is no direct evidence for a reactive phase of growth,

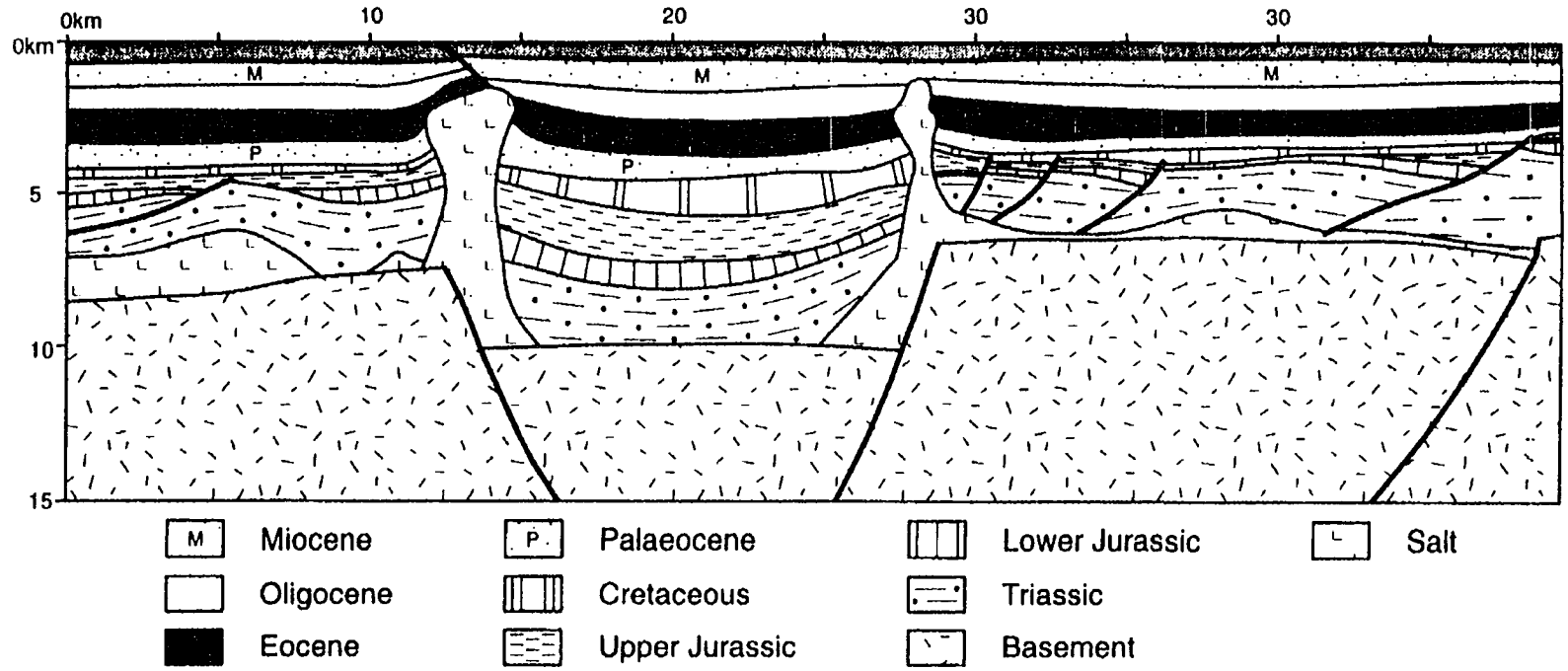

Figure 2.8.9. The Machar (left) and Medan (right) diapirs from the Eastern Trough, Central Graben, North Sea. The diapirs probably grew initially in response to basement extension. Following the termination of basement extension, the diapirs continued to grow as passive diapirs until the Oligocene. Modified from Hossack, 1995.

there is evidence of extension (the Hollow Fault) that could initiate reactive diapirism (for example, Vendeville and Jackson, 1992a).

- Salt supply from both the hangingwall and footwall during at least the initial growth phase. Salt supply may have been restricted in the later growth history as indicated by the formation of an elongate salt weld on the footwall of the Hollow Fault.

- Once parts of the salt wall reached the surface, they could continue to grow as passive salt structures. Syn-kinematic conglomerates exposed on Port Hood Island indicate that at least some of the diapirs were at surface during the Late Carboniferous. Evidence for shallow marine, or sub-arial, exposure of the diapirs is described in Chapter 3.5.

- Carboniferous inversion may have played a role in diapir growth as indicated by the structures imaged on line 67 (see above). There is no evidence for large-scale inversion within St. Georges Bay at this time, although this evidence may well have been obscured by later inversion or by poor seismic resolution of the stratigraphy below the Port Hood Formation level.

- Inversion after the Westphalian D resulted in rejuvenation of the diapiric structures and caused the overlying Inverness Formation to be uplifted and folded. It is possible that the heads of the diapiric structures intruded into the Inverness Formation at this time (see below, Chapter 3.3).

Salt Wall Luey. The Salt Wall Luey extends from the Monks Head diapir exposure on the Antigonish coast, north-east across St. Georges Bay, beneath Port Hood Island to the tip of western Cape Breton where it joins the Salt Wall Huey. The salt wall is approximately 25 km long.

Line 83: On line 83, the Salt Wall Luey has an almost symmetrical geometry. The northern flank of the salt wall is ~2.8 km high and dips moderately (~45 degrees) to the north. The opposite, southern flank, is ~3.9 km high and dips steeply (~67 degrees) to the south. The discrepancy in the height of the two flanks of the diapir highlights a possible basement structure beneath the southern flank of the diapir. The depth to the Windsor reflector increases from ~2.8 km to ~3.9 km over a horizontal distance of ~1.0 km. This increase in depth is interpreted to represent a fault with a vertical throw of 1.1 km that dips to the south. The fault probably offsets Windsor, Horton and basement rocks; however, these units are not imaged and so the point must remain speculative. The Salt Wall Luey on line 83 is located at the crest of the footwall. Salt walls and diapirs occupying the footwall of an extensional fault are not unusual and have been previously described from analogue models (Jackson and Talbot, 1994).

Line 79: On line 79, the Salt Wall Luey has a triangular cross section. The northern flank is ~2.2 km high and is planar with a constant dip of ~66 degrees. The southern flank is also planar, but dips more gently at ~39 degrees. The upward turn of the Windsor reflector beneath the diapir may indicate a basement fault that would correlate with the fault interpreted on line 83. However, the upturn of the Windsor reflector may be a velocity pull-up due to the overlying high velocity salt. Assuming the velocity of salt to be 15000ft/sec, the velocity pull-up from the overlying salt diapir equals ~0.5 sec TWT. This is approximately the amount of upturn of the Windsor reflector beneath Luey.

Line 75: On line 75, the Salt Wall Luey is a symmetrical diapir with a triangular cross section. The northern flank is ~2.4 km high, planar, and dips steeply (~60 degrees). The southern flank is also ~2.4 km high, planar, and dips steeply (~71 degrees). There is no evidence of basement perturbations that could be interpreted as faults. On the northern flank, the Inverness Formation coal seam reflectors approach the diapir flank at almost 90

degrees whereas the Port Hood Formation coal seam reflectors intersect the diapir flank at a more oblique angle. This angular discordance is interpreted to represent an angular unconformity surface between the Inverness and Port Hood Formation (Figure 2.8.10). A similar rotated unconformity is exposed at Bruces Cove on Port Hood Island (see Chapter 3.5). The unconformity indicates diapir growth during the Westphalian B.

The salt wall is not imaged on the Chevron lines to the north-east as a discrete salt wall. On lines 71 and 67, it is imaged as part of the combined Salt Walls Huey and Luey (see above, Salt Wall Huey, for description).

Salt Wall Duey. Only the northern flank of the Salt Wall Duey is imaged on lines 83 and 79. The seismic coverage stops short of the southern flank on these two lines and the salt wall is not imaged at all on lines 75 and 71.

Line 83: On line 83, the northern flank of the Salt Wall Duey is ~3.5 km high, planar, and dips steeply (~ 81 degrees). The salt wall is imaged at the extreme edge of line 83 where the fold of the seismic data begins to drop off. This makes interpretation of details of the salt diapir difficult.

Line 79: The southern flank of Duey is ~2.6 km high, planar, and dips moderately (~58 degrees). The flank appears to have a concordant contact with the Middle Windsor Group and Hood Island Formation reflectors. The Windsor Group reflectors can be traced from about 2.0 sec TWT to 0.2 sec TWT as a continuous reflector set that are sub-parallel to the diapir flank. In addition, the overlying Port Hood and Inverness Formation reflectors appear to have been uplifted and rotated in a similar way to the Windsor Group reflectors. This configuration implies that the Upper Carboniferous strata have been uplifted and rotated to the near surface as the salt wall grew and that diapir growth did not occur until after the Westphalian D. From a mechanical standpoint, it is unlikely that

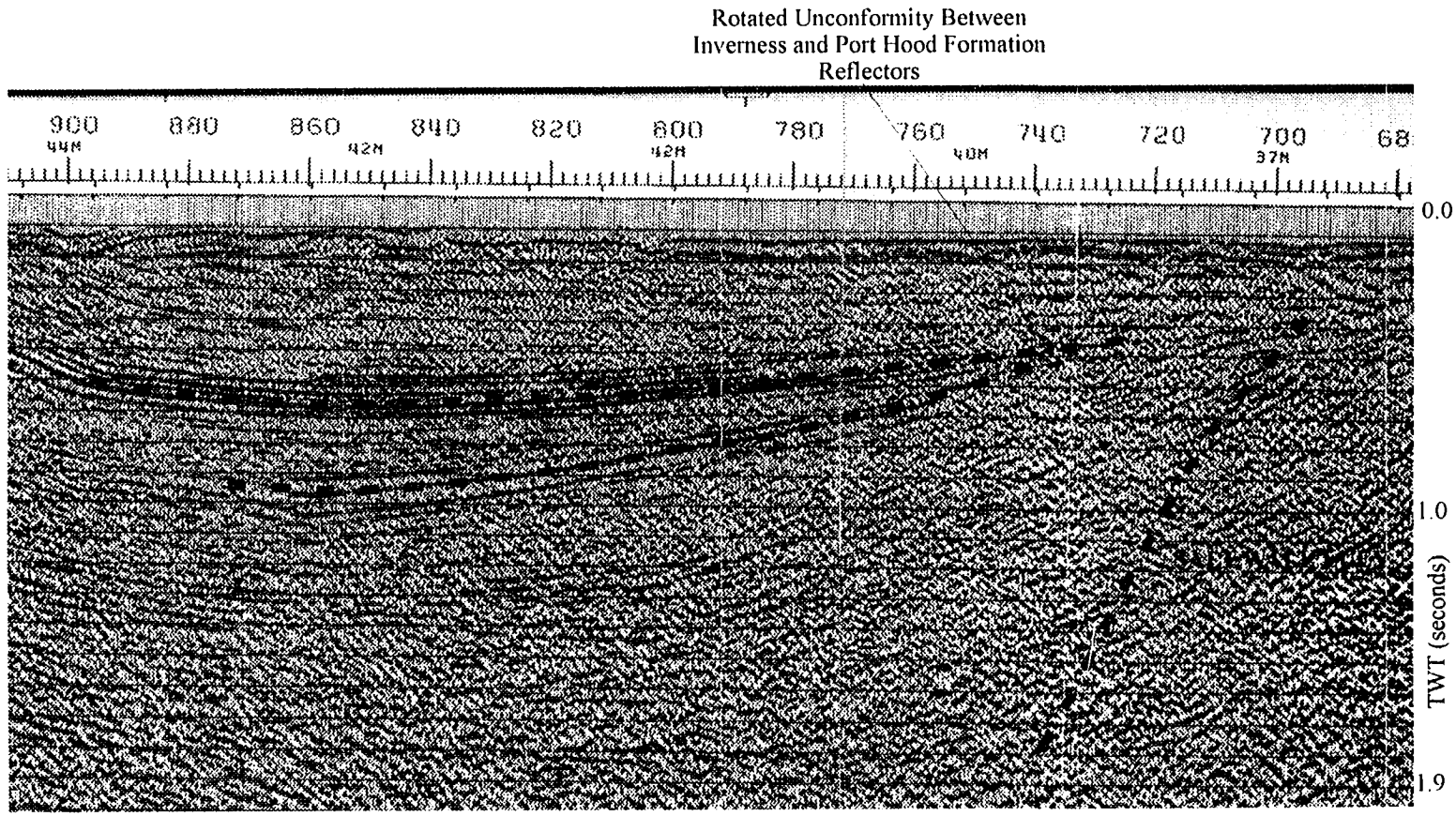

Figure 2.8.10. Part of seismic line 75 showing a rotated unconformity between two sets of seismic reflectors interpreted to be Inverness Formation (upper) and Port Hood Formation (lower).

Duey grew as an active diapir. Schultz-Ela et al. (1993) demonstrated that in order for a diapir to actively lift its roof, the diapir height must be at least two-thirds the thickness of the overburden. This relationship can not be demonstrated for Duey. It is most likely that Duey grew in response to post-Carboniferous inversion.

Possible Fault Control upon the Location of the Salt Walls

The salt walls Huey, Luey and Duey clearly cross St. Georges Bay in a north-east/south-west direction with a pronounced swing to the north by the salt walls Luey and Duey towards the eastern side of the bay (Figure 2.5.3). Durling et al. (1995) suggested that salt-cored anticlines mapped within St. Georges Bay could be correlated with onshore faults and were the seismic expression of these faults. The salt-cored anticlines of Durling et al. (1995) are equivalent to the salt walls Huey, Luey and Duey described above. The preferred interpretation presented as part of this thesis is that the salt walls are true diapiric structures. Some of the onshore faults, correlated with offshore salt-cored anticlines by Durling et al. (1995), for example, at Monks Head and Port Hood Island, are interpreted here as the onshore expression of the salt walls. The Monks Head Fault and Port Hood Island Fault are interpreted as external shear zones where Upper Carboniferous overburden strata are juxtaposed against Windsor Group diapiric structures.

Despite the lack of firm correlation between onshore faults and offshore faults, it is by no means unreasonable to propose that the St. Georges Bay salt walls are localised on basement/Horton faults. From analogue modelling, Vendeville and Jackson (1992a) and Jackson and Talbot (1994) concluded that overburden faults and basement faults were two criteria that can result in the development of parallel salt walls. The Salt Wall Huey and part of the Salt Wall Luey are interpreted to be associated with extensional faults (see above) and it may be that other segments of the salt walls are associated with similar faults. The lack of seismic resolution below the Windsor group reflectors prevents basement or Horton faults from being imaged.

2.8.2, Seismically Imaged Salt Structures, Western Cape Breton

(This section describes only the seismic expression of the many salt structures offshore western Cape Breton. Onshore exposures are described in Chapter 3).

Sight Point Diapir. The Sight Point Diapir is a small salt diapir located 3 km offshore from Sight Point (Figure 2.5.12). The salt structure is imaged on line 16 of the 1982 Chevron survey as well as lines 9, 10, 13 and 14 of the 1978 Mabou survey. The Sight Point Diapir is approximately 1 km high and 2.1 km wide at the base with a rounded cross section. The fact that the diapir is not imaged on lines 59 or 63 of the 1982 Chevron survey suggests that it has a near-circular geometry. The Sight Point Diapir has intruded through the Gillis Fan and the Inverness Formation coal measures but has not penetrated to the surface. Lines 13 and 14 of the 1978 Mabou Survey show that the diapir is currently overlain by ~ 600m of overburden.

The Sight Point Diapir is positioned at the toe of the Gillis Fan. This position, combined with the lack of obvious faulting adjacent to the salt structure, may imply that differential loading and not tectonics triggered salt movement. The progradation of the Gillis Fan may have forced salt movement ahead of the advancing clastic wedge, thereby triggering diapirism. The Sight Point Diapir shows no evidence of post-Carboniferous rejuvenation as has been demonstrated for the St. Georges Bay salt walls. A possible explanation for this may be that the tectonic stress at this location was not sufficient to allow the diapir to penetrate its roof.

Inverness Salt Wall. The existence of the Inverness Salt Wall is inferred from both onland and seismic data.

Lines A05, B03 and B06 of the 1985 Inverness seismic survey clearly image diapiric

structures where the seismic coverage extends far enough inshore to cross the northern margin of the Inverness Salt Wall. Lines B04, B05, B07, B08 and B10 do not extend far enough inshore to cross the Inverness Salt Wall; however, these lines image rotated and upturned strata at their southern ends. The rotated and upturned strata have very similar geometries to the Inverness Salt Wall drag zones imaged on lines A05, B03 and B06 and indicate that the salt structures imaged on lines A05, B03 and B06 may extend along the coastline to form an elongate salt wall (Inverness Salt Wall). The Inverness Salt Wall would be a 17 km long salt wall extending from Broad Cove to Sight Point (Figure 2.5.12).

The onshore outcrop of the Inverness Formation exposed between Inverness and Sight Point has a variable dip of 11-33 degrees to the north-west. The shore section contains the 7' coal seam (Haites, 1952) that can be approximately located on the seismic data by tying the seismic data to sub-sea mine plans. The seismic data show the approximated 7' coal seam rotated and uplifted within the Inverness Salt Wall drag zone, and on line B06 the 7' coal seam can be traced to within 100 ms (~150m) of the surface. Uplift of the Inverness Formation strata has resulted in erosional truncation of the Inverness Formation (see Line B06). The variation in the stratal dip in the Inverness Shore section may be due to the proximity of the postulated Inverness Salt Wall. The exposed Inverness Formation section would therefore be a continuous section through the Inverness Salt Wall drag zone. Strata with low dips would be located in the outer portion of the drag zone (i.e. where the diapir is some distance away from the exposed strata) and strata with higher dips would be located in the inner portion of the drag zone (i.e. where the diapir is located quite close to the exposed strata). This inner to outer drag zone relationship is readily seen on seismic lines B03-B10 which run orthogonally offshore.

To the south-east, the Inverness Formation unconformably overlies basement rocks. In order for there to be a salt wall adjacent to the present day coastline, a major basement

involved fault must exist between the basement rocks and the salt wall. This scenario is similar to that proposed for the Finlay Point and Coal Mine Point Diapirs (see below, Chapter 3). Unfortunately, the proposed fault is not imaged on the seismic data and so its existence and geometry must remain speculative.

The Inverness seismic data can be correlated with the onshore Inverness to Sight Point section and both lines of evidence can be interpreted to support the existence of the Inverness Salt Wall. However, the seismic lines stop short of the proposed location of the salt wall and so its existence is unproven. The only way to prove the existence of the Inverness Salt Wall is by drilling or by acquisition of more seismic data.

Broad Cove Diapir. The Broad Cove Diapir is located at the north-east end of the Inverness Salt Wall. It is not clear whether or not the Broad Cove Diapir is actually part of the Inverness Salt Wall, although the close proximity of the two salt structures suggests that they are intimately related. The Broad Cove Diapir was first identified by Haites (1952) and a seismic survey acquired by the Lion Oil Company identified a salt structure in the offshore area that probably corresponds to the Broad Cove Diapir (Lake, 1969).

The south-west margin of the Broad Cove Diapir is clearly imaged in line A05 of the 1985 Inverness seismic survey. The line does not extend to the north-east margin and so the overall geometry of the diapir remains uncertain. The south-west margin of the Broad Cove Diapir corresponds to the location of the Plaster Fault (Figure 2.5.3), which is interpreted to be a south-trending high-angle reverse fault (P.S. Giles, pers. comm, 1994 and 1995) with a displacement of ~900m (Maclean, 1939; Haites, 1952). As interpreted from seismic data (1985 Inverness survey), the Plaster Fault is simply the south-west margin of the Broad Cove Diapir, which is approximately 900m high. The extrapolation of the Plaster Fault and the Broad Cove Diapir inland has not been attempted due to the poor exposure onshore.

2.9, DIAPIR GROWTH MECHANISMS AND TIMING

It is important to establish both the timing and mechanism of diapir growth, as several of the concepts discussed in later chapters rely on this information. Evidence used to propose a growth mechanism and timing for the many diapiric structures draws together data from a large number of sources. Where specific evidence is used from diapirs not previously mentioned, the reader is referred to the appropriate chapter.

2.9.1, Current Theories

Current theories regarding diapir growth mechanisms focus on passive or downbuilt diapirism, first described by Barton (1933), and the reaction of salt to a regional or applied stress field. Buoyancy driven diapirism, first described by Lachmann (1910) and later by Arrhenius (1913), has fallen into disfavour due to the severe mechanical difficulties in uplifting and 'removing' a rigid, lithified overburden. Recent work has placed numerical boundary conditions upon active diapirism (Schultz-Ela et al. 1993).

Modern ideas focus on the reaction of salt to a regional or applied stress field. Extension within the basement, thin-skinned overburden extension, basement compression, decoupled compression of a cover sequence and differential sediment loading are all recent examples of geological phenomena which have been proposed as triggers for salt migration and diapirism. Once faulting weakens the overburden, reactive diapirism can lift the overburden, allowing salt to reach the surface. Once at the surface, the diapir can grow over an extended period of time by passive diapirism. During this passive phase, the head of the diapir remains at or near surface and is fed from the mother salt layer, which is subsiding with the basement. Continued sedimentation imposes a load on the mother salt layer, maintaining salt withdrawal and hence diapiric growth. This rather simplified version of diapir growth cannot begin to include the multitude of input variables which

can control the shape, growth rate, distribution, size or growth mechanism of diapiric structures. For more information on diapir growth mechanisms, the reader is directed to several recent publications: Vendeville and Jackson (1992a,b), Talbot (1993), Davison et al. (1993), Schultz-Ela et al. (1993), Petersen and Lerche (1993), Jackson and Talbot (1994), Poliakov et al. (1993, 1996), Rowan (1994), Demercian et al. (1993), Vendeville and Nilsen (1995) and Hoyos et al. (1995).

2.9.2, Diapiric Structures within the Project Area

The project area has been divided into three tectono-stratigraphic domains based upon seismic interpretation. Each domain represents an area of similar tectonics and stratigraphy that has marked differences from the other two adjacent domains. It is therefore not surprising that the diapiric structures located within the St. Georges Bay, western Cape Breton and Gulf of St. Lawrence domains show very different growth histories that can be related to the tectono-stratigraphic evolution of the St. Georges Bay Basin and western Cape Breton.

2.9.3, St. Georges Bay Basin

The three salt walls (Huey, Luey and Duey) probably grew as passive diapirs through most of their growth history, which extended from the early Namurian to the Stephanian. This interpretation is supported by a number of lines of evidence.

- St. Georges Bay Basin underwent rapid tectonic subsidence throughout the Namurian and Westphalian A. This tectonic subsidence is indicated by the presence of a thick Mabou Group and Port Hood Formation sequence within St. Georges Bay Basin compared to the thin succession to the north within the Gulf of St. Lawrence domain. Subsidence was accommodated in part on the Hollow Fault, but undoubtedly involved displacement on basement faults located below geophysical basement within St. Georges Bay Basin. Given our present understanding of the behaviour of salt in

response to extension, it is highly unlikely that the Windsor Group halite would have remained as a strataform layer during tectonic subsidence of the St. Georges Bay Basin. Once at or near the surface, the diapirs could continue to grow as passive diapirs. This situation is analogous to numerous examples from the North Sea, Central Graben area where Triassic and Jurassic extension gave rise to salt diapirs located within the hangingwall and footwall of major basement faults (examples include Hossack, 1995 - Machar and Medan diapirs, Eastern Trough, Central Graben (Figure 2.8.9)).

- The rim-syncline seismic facies identified from line 71, ~1.0 sec TWT (see below, Chapter 5) indicates diapiric growth and possible exposure at, or near, the surface of part of the Salt Wall Huey during deposition of the Mabou Group (Namurian). The alluvial fan seismic facies identified from line 71, ~0.5 sec TWT (see below, Chapter 5) suggests diapiric growth and possible sub-aerial exposure of part of the Salt Wall Huey just prior to the deposition of the Inverness Formation coal seams during the Westphalian C - Stephanian interval. The two seismic facies suggest that the salt wall was growing from the Namurian to the Westphalian C.

- On-shore exposures of the Salt Wall Luey on Port Hood Island and at Monks Head have very short associated drag zones (80 m within Westphalian B strata, Port Hood Island Diapir, and 32 m in Namurian C strata, Monks Head Diapir). Short, relatively attenuated drag zones are indicative of passive diapirism (Davison et al., 1995). The onshore outcrops therefore support passive rather than active diapirism.

- Carboniferous inversion may have played a role in diapir growth although the exact extent of this inversion can only be speculated.

- Inversion after the Westphalian D resulted in rejuvenation of the diapiric structures

and caused the overlying Upper Carboniferous rocks to be folded. It is possible that the heads of the diapiric structures intruded into or through the Inverness Formation and Broad Cove Formation at this time.

- Evidence from the onshore exposures (Chapter 3) indicates that the diapirs in general did not penetrate very far through the Upper Carboniferous rocks. All the onshore diapir exposures consist of Middle Windsor Group or Hood Island Formation rocks transported as a structural carapace (see below, Chapter 3). These carapaces show modest penetration into the topmost Carboniferous (Inverness Formation/Broad Cove Formation). If the diapirs had penetrated the Inverness Formation by a greater amount, the structural carapace would be well above the Inverness Formation level and erosion would have removed the structural carapace and exposed the underlying halite. Exposed to a humid climate, the halite would have undergone massive dissolution, resulting in structural collapse of the surrounding overburden.

- Vitrinite reflectance data and apatite fission track data indicate that the entire area was covered by 3-4 km of post-Carboniferous overburden. The deposition of such a thick overburden probably halted or stalled diapir growth. Buoyancy would have been insufficient to allow the diapirs to grow through a thick overburden and the position of the structural carapaces at or near the top of the Carboniferous indicates that inversion did not cause rejuvenation and growth of the diapirs through the post-Carboniferous overburden. Subsequent erosion has returned the diapirs to the surface or near-surface. If overburden roofs were thinned enough and halite was available in the source layer, the diapirs may have been rejuvenated at this time. However, since the structural carapaces have remained largely intact, any rejuvenation at this stage must have been modest.

2.9.4, Western Cape Breton

- Within parts of western Cape Breton, the Mabou Group is very thin, consisting of only 50-100 ms (<100m) on seismic sections. The Gillis Fan (see above) rests directly upon the Windsor reflector and so is occupying the Mabou Group stratigraphic level. It is probable that only small, localised depocentres existed within western Cape Breton during the Namurian and the western Cape Breton area may have been a platform area for much of the Namurian period. Only during the Westphalian (Port Hood Formation) were thick sequences of sediments deposited within western Cape Breton in response to displacement on various segments of the Hollow Fault. Despite the thin cover of Mabou Group sediments, differential loading could have played a role in driving salt migration and diapiric growth. In particular, the development of the Gillis Fan could well have induced salt migration if it developed as a series of lobate fan units.

- The Finlay Point (see Chapter 3) and Broad Cove diapirs are interpreted to be strongly asymmetrical diapirs that resemble trap doors and are similar to those described as asymmetric intrusions by Trusheim (1960) and Nelson (1989). In this model, the halite lifts and rotates a package of intact strata and syn-kinematic sediments are deposited outboard of the uplifted strata. Such diapirs can be initiated over an extensional basement fault, where upward growth of the diapir is often assisted by coeval extension in the cover related to flexure over the basement fault. Figure 2.9.1 shows a model of a 'trap door' diapir, similar to the Finlay Point diapir and possibly the Broad Cove diapir, developed from a seismically imaged diapir in the North Sea (Remmelts, 1995). The later growth history of the Finlay Point and possibly the Broad Cove diapirs may also be linked to inversion. The Finlay Point Diapir uplifts an intact stratigraphic package that includes Inverness Formation coal seam reflectors without apparent thinning onto the diapir flanks. The onshore

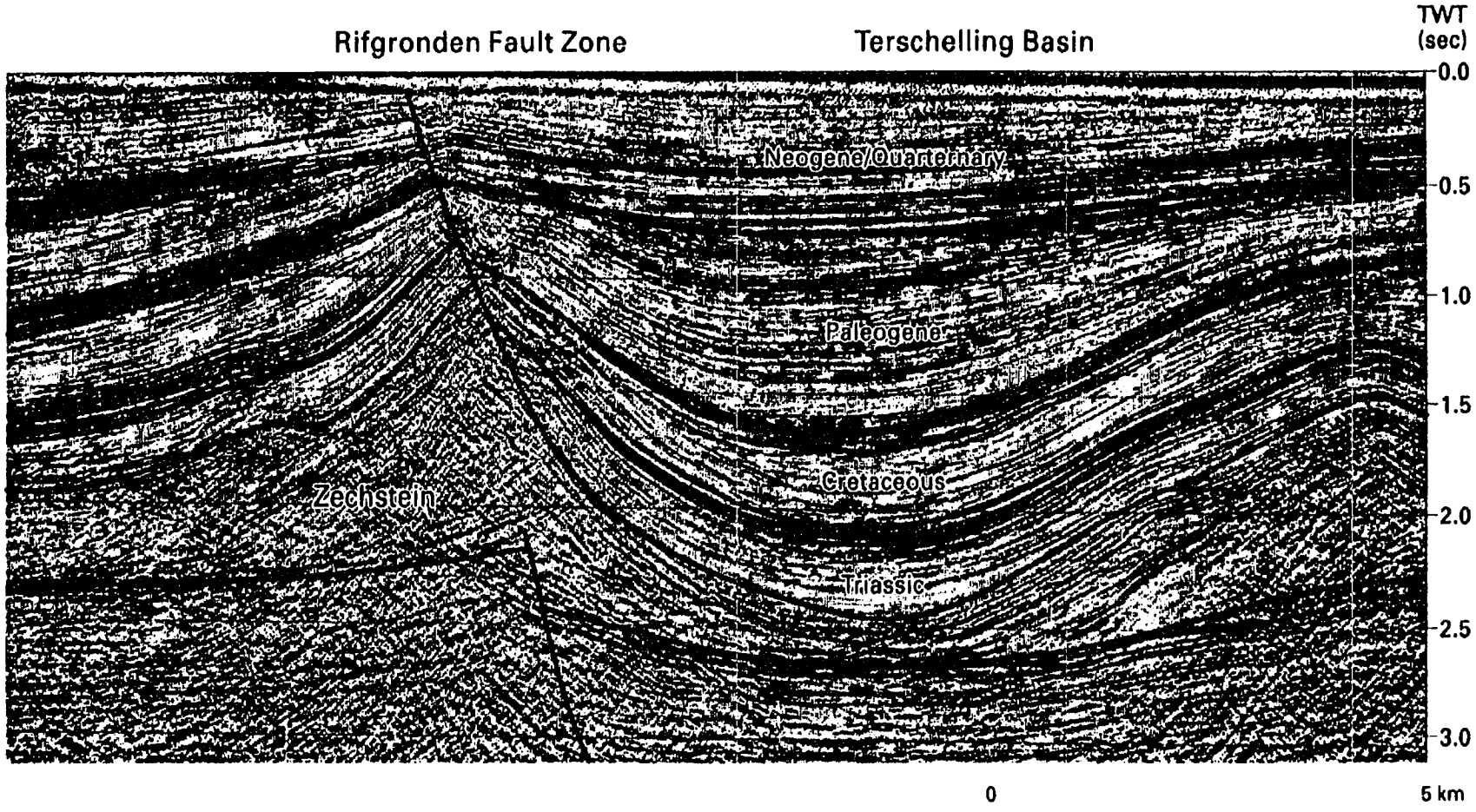

Figure 2.9.1a. Seismic example of a trap door diapir formed over a basement extensional fault. Example is from the Southern North Sea, Netherlands Sector. Modified from Remmelts (1995).

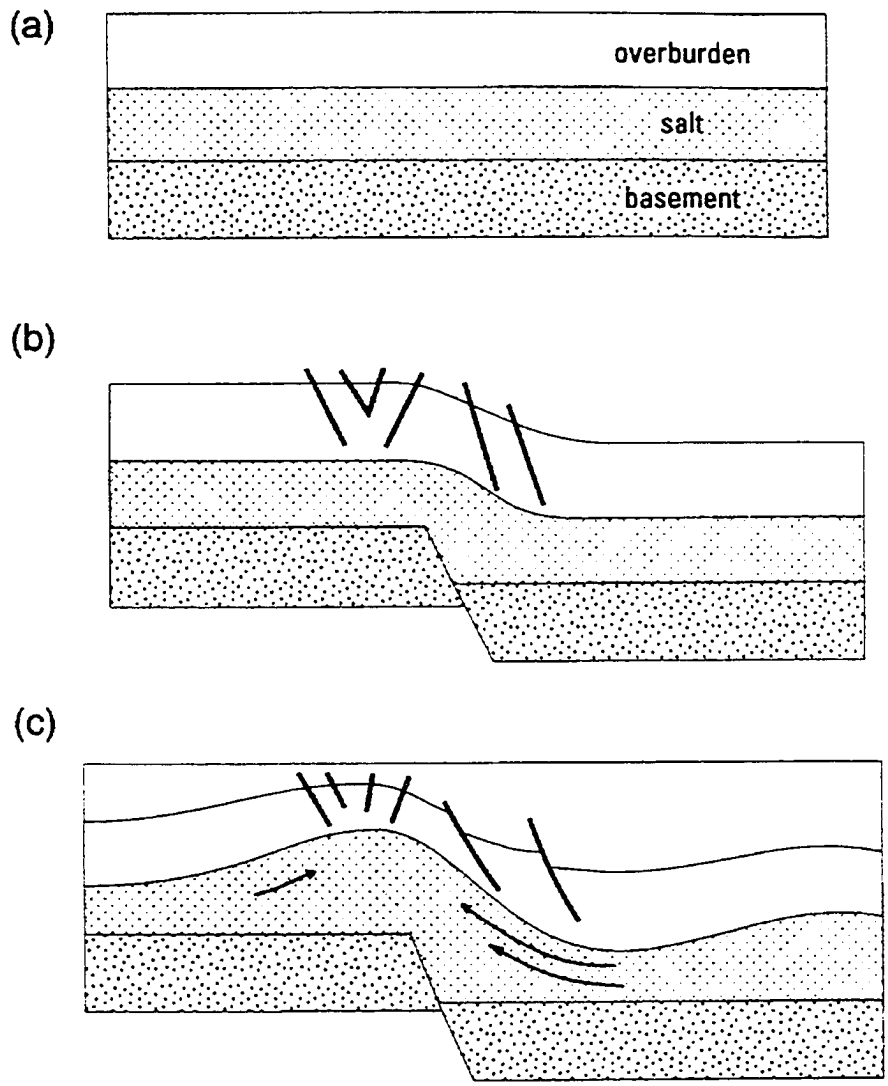

Figure 2.9.1b. The evolution of a reactive diapir to produce a trap door geometry. (a) Original strataform layers. (b) basement extension leads to the formation of a drape fold within the cover rocks. Extensional faults are formed where the cover rocks fold over the basement faults. (c) differential loading caused by differential sedimentation and/or compaction leads to salt withdrawal. Salt withdraws towards the fault plane where it moves vertically through the weakened cover rocks to form an asymmetrical trap door diapir. Seismic example shown in Figure 2.7.2a. Modified from Remmelts (1995).

exposure of the Finlay Point Diapir confirms that the diapir has locally penetrated the Inverness Formation (see below, Chapter 3.3). This growth phase did not occur until after the Westphalian D. The timing of this growth links the development of the Finlay Point Diapir to post-Carboniferous inversion that has been demonstrated from elsewhere in the field area. Diapir growth that lifts a thick overburden is more mechanically feasible during compression (Vendeville and Nilsen, 1995). Compression can increase the deviatoric stresses at the salt/rock interface to a point where it exceeds the strength of the overburden rocks. At this point, the diapir can actively penetrate the overburden. Unfortunately, without seismic coverage over the Hollow Fault, the precise nature of the Finlay Point Diapir must remain speculative.

- The age of the intact stratigraphic package uplifted by a diapir gives an indication of the maximum age of diapiric growth. It does not in any way constrain the minimum age of growth. The St. Rose Diapir (see below, Chapter 3) uplifts part of the Colindale Member of the Port Hood Formation, giving a maximum age of top Westphalian A for diapir growth, while the Broad Cove Diapir uplifts part of the Hastings Formation, giving a maximum age of Namurian B. The Finlay Point Diapir uplifts a package of Inverness Formation reflectors indicating a maximum age for diapirism of Westphalian D.

- Seismic facies analysis indicates that a pulse of diapir movement occurred during the Stephanian (see below, Chapter 5). Although seismic facies analysis gives no indication of a maximum age constraint, it does support late (post-Westphalian) diapir growth within the western Cape Breton domain. This Stephanian pulse of diapiric activity may be related to the rejuvenation of the diapirs by inversion.

2.10 SUMMARY

St. Georges Bay. These are dominantly passive (downbuilt) salt walls that may have had an initial reactive growth stage in response to tectonic subsidence of St. Georges Bay Basin. The diapirs and salt walls probably began to grow soon after the onset of basin subsidence (early Namurian) and continued to grow throughout the Namurian, Westphalian and into the Stephanian with passive growth being driven by continuous sedimentation. Post-Carboniferous inversion caused rejuvenation of the diapirs resulting in uplift and folding of the overlying Upper Carboniferous strata. Diapir growth was stalled by the deposition of a thick overburden sometime after the Carboniferous.

Western Cape Breton. These are dominantly asymmetrical salt diapirs that probably grew initially as reactive diapirs in response to displacement on segments of the Hollow Fault and differential loading due to uneven sedimentation. The timing of early diapiric growth is not well constrained. Later diapiric growth is linked to post-Carboniferous compression that allowed the diapirs to lift and penetrate the overlying Inverness and Broad Cove Formations. At the end of diapiric growth, the western Cape Breton diapirs were still relatively embryonic.

In both St. Georges Bay and western Cape Breton, diapiric growth may have been strongly influenced by inversion. There is evidence that inversion definitely occurred after the Carboniferous and that this inversion rejuvenated some of the salt structures. There is also a strong indication that inversion occurred during the Upper Carboniferous (Namurian to Westphalian B) and that this may have affected diapir growth. The effects of inversion on the salt structures will be examined in detail in Chapter 3.

CHAPTER 3, ONSHORE DIAPIR AND DRAG ZONE EXPOSURES

3.1, THE BROAD COVE DIAPIR

3.1.1, Geographic Data

The start of the north-east drag zone is at Broad Cove Brook, latitude 46N,16,25 longitude 61W,16,50, that is shown on topographic map 11K/6.The north-east external shear zone of the Broad Cove Diapir is at Plaster Rocks, latitude 46N,16,00 longitude 61W,16,50. The south-west external shear zone is located at the north-east end of Inverness Beach, latitude 46N,16,00 longitude 61,16,49. The Broad Cove Diapir is exposed over a length of ~285m north-east to south-west. (Figures 3.1.1 and 3.1.2).

3.1.2, General Information

The Broad Cove structure was first described as a diapir by Haites (1952). Haites described the western Cape Breton diapirs between St. Rose and Mabou as salt-cored anticlinal folds that penetrated through the overlying strata. Haites also described diapir drag zones as synclines adjacent to diapiric structures and went on to suggest that the diapirs were growing during sedimentation. Haites' interpretation was remarkably accurate in terms of what is now understood about salt tectonics and diapiric intrusion.

3.1.3, Seismic Coverage over the Broad Cove Diapir

The Broad Cove Diapir forms the north-eastern end of the Inverness Salt Wall (see Inverness Salt Wall, Chapter 2). The south-west flank of the Broad Cove Diapir is imaged on Inverness line A05 as a sub-vertical discontinuity between diapiric Windsor Group halite and the adjacent Mabou Group, Port Hood Formation, Inverness Formation and Broad Cove Formation strata. The overburden rocks appear to intersect the diapir margin with little or no upturn (drag) of the strata between 0.9 and 0.3 sec TWT. Near the head of the diapir (0.3-0.05 sec TWT), the Carboniferous strata are draped over the head of the

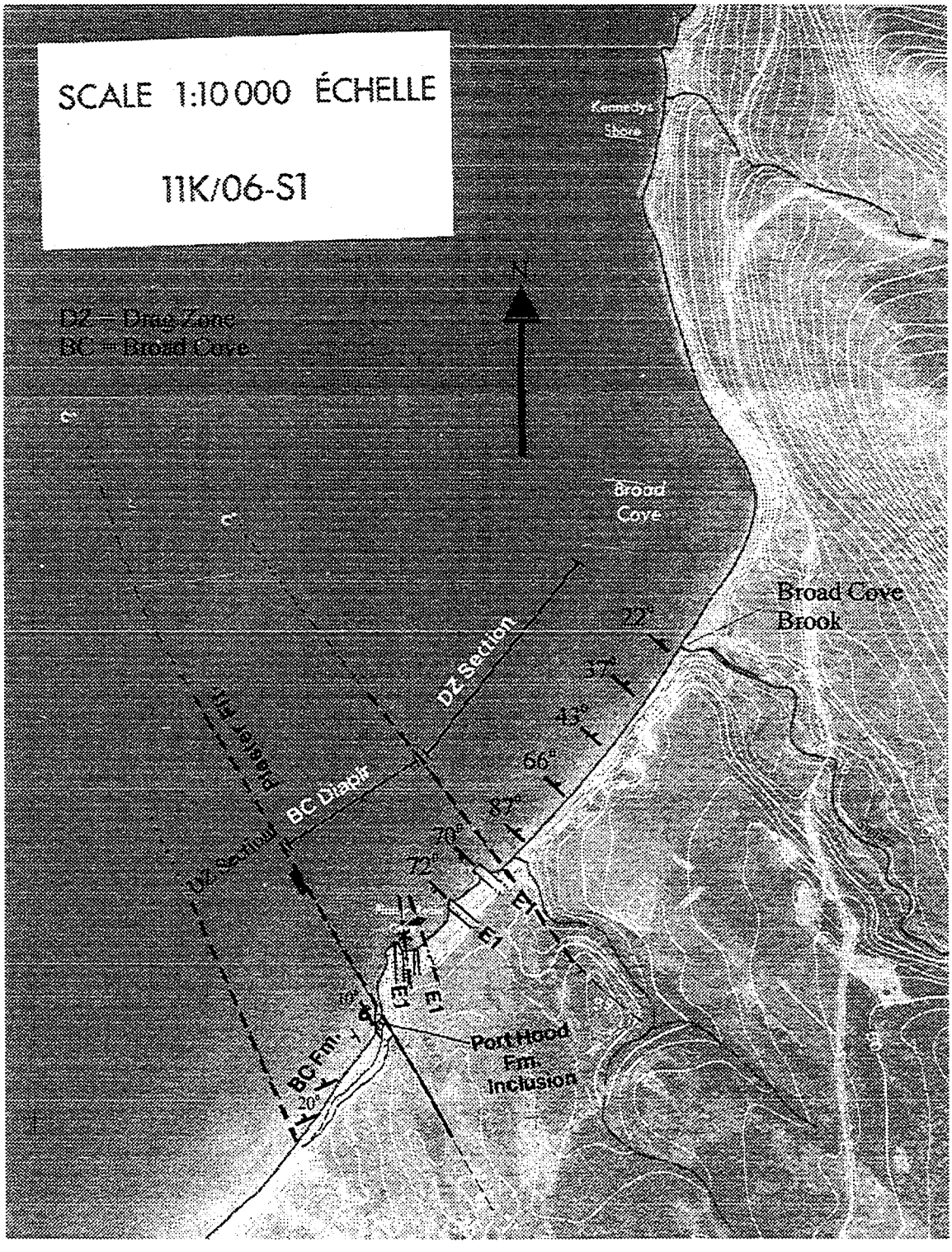

Figure 3.1.1. Orthophotograph to show the position of the Broad Cove Diapir and associated drag zones on the west coast of Cape Breton. Symbols follow standard geological notation.

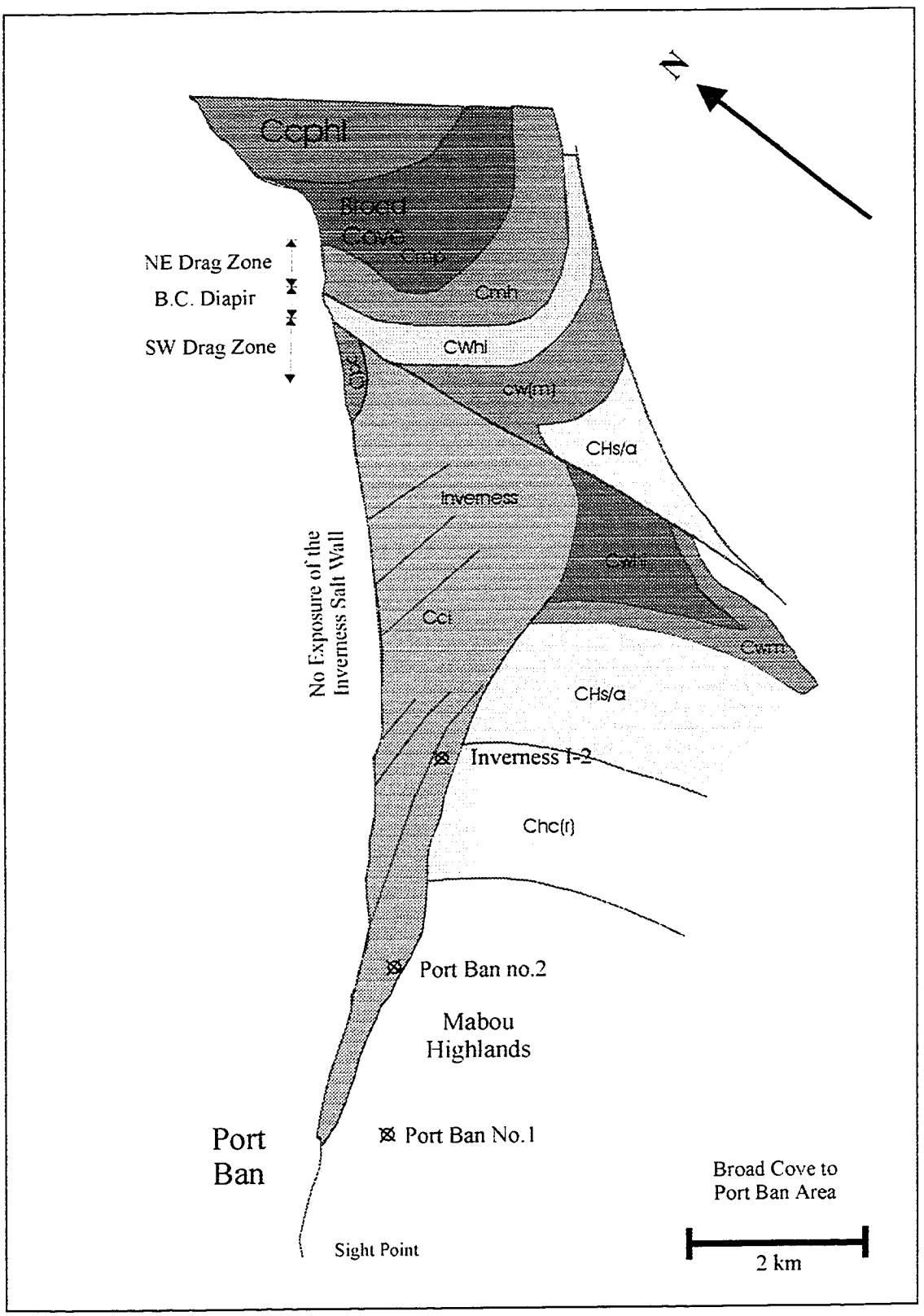

Figure 3.1.2. Geological Map of the Broad Cove and Inverness Area. (Modified from Giles et al. (1997a and b) (See Figure 2.3.1 for Key)

diapir, forming a monoclinal drape fold.

The geometry of the north-western flank of the diapir is imaged on Inverness line B10. The Carboniferous strata have a smooth, curved drag zone profile with the degree of diapir-induced drag decreasing progressively with depth. Within the Inverness Formation level, the drag zone is ~1.6 km wide and has a vertical (drag) displacement of ~450m.

Based upon seismic depth conversion (see Depth Conversion, Appendix 3), the Broad Cove Diapir is ~0.9 km high (1.0 sec TWT) and has a diameter of approximately 1.0 - 1.5 km. The diapir's geometry in the subsurface cannot be accurately constrained because only the south-west and north-west flanks are covered by seismic data. From the available seismic coverage, the Broad Cove Diapir appears to have an asymmetric geometry with a sub-vertical south-west flank and a more gently dipping north-east flank (Figure 3.1.3).

3.1.4, Relationship of the Broad Cove Diapir to the Hollow Fault

The apparent juxtaposition of at least 900m of Carboniferous strata against Precambrian to Ordovician basement rocks to the east requires that at least 900m of accommodation space was created after formation of the basement and prior to the deposition of the Upper Carboniferous strata. The seismic data does not image any coherent reflector below ~1.0 sec TWT and does come within 700 m of the shoreline. There is therefore no way to constrain the geometry of the Broad Cove Diapir with respect to faulting except from theoretical considerations and extension of data from adjacent areas, for example St. Georges Bay. Perhaps the simplest way to create the required accommodation space is on an extensional fault with the Carboniferous strata being deposited on the subsiding hangingwall of a basement-involved extensional fault (the Hollow Fault). Salt withdrawal from the footwall and hangingwall (possibly due to differential loading) could lead to diapiric growth. An example of this configuration is imaged on the 1982 Chevron seismic survey forming the boundary between the St. Georges Bay and Gulf of St. Lawrence

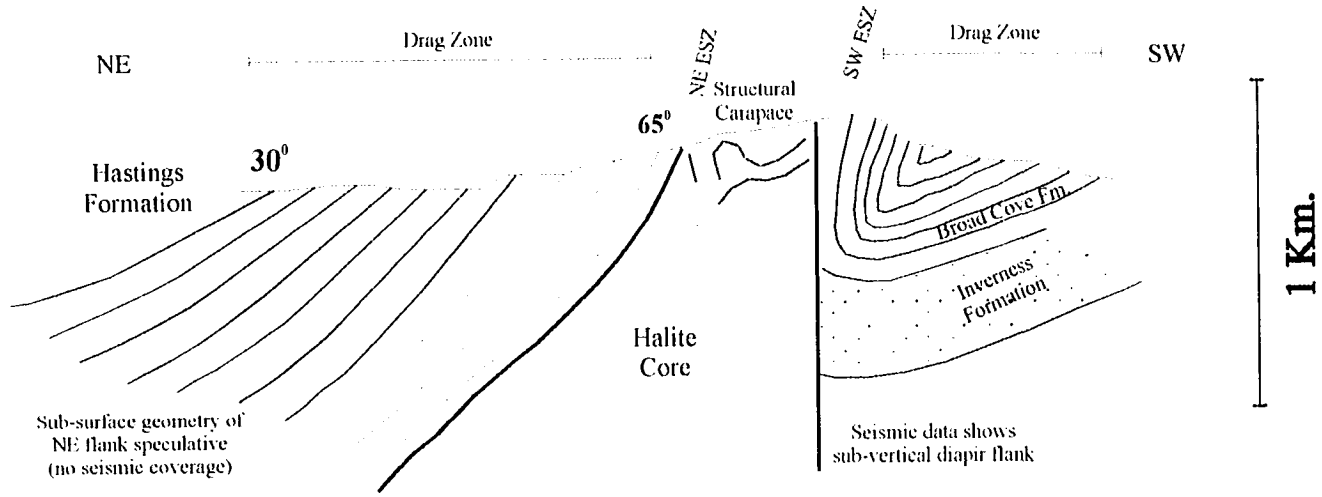

Figure 3.1.3. A schematic model of the Broad Cove Diapir constructed from seismic and in-shore data.

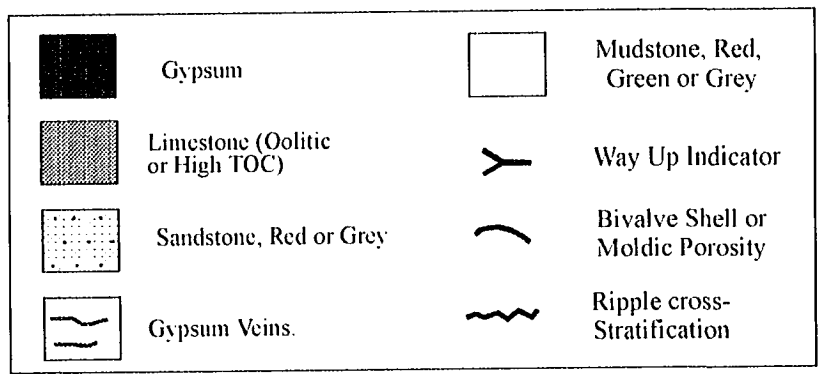

Figure 3.1.4. Key for diapir sections and structural carapaces.

areas (see above, Chapter 2). An alternative explanation is that the Broad Cove Diapir is located in the hangingwall of a thrust or reverse fault that dips to the south-east. In this situation, the diapir would grow in response to regional compression either during or after the Carboniferous. Compression undoubtedly did play a role in the evolution of the Broad Cove Diapir, as will be described later in this section.

3.1.5, Onshore Exposure of the Broad Cove Diapir

The onshore exposure of the Broad Cove Diapir is the most complete exposure of a diapir and its associated drag zones within the project area. The exposure forms a complete 2D profile through the Broad Cove Diapir and through two mutually opposite diapir drag zones (north-east and south-west drag zones) (Figure 3.1.3).

3.1.6 The Hood Island Formation Structural Carapace

The Broad Cove Diapir exposure consists of Hood Island Formation strata, which have been transported as a structural carapace (see Glossary of Salt Tectonics) above Lower Windsor Group halite (Figure 3.1.3). A stratigraphic package of Hood Island Formation strata including the C3, D1, D2, D3 and E1 limestones (P. Giles, pers. comm. 1995, 1996) can be recognised within the structural carapace.

The Hood Island Formation carapace consists of alternate units of gypsum, limestone, red mudstone and red siltstone (Figures 3.1.4 and 3.1.5). From the top down (youngest to oldest), the stratigraphic package consists of:

1. 5-8m of white gypsum with variable textures (rosette, chickenwire and mylonitic).
2. The E1 limestone. 7-9m of sparsely oolitic limestone and grainstone containing sporadic bivalve shells used as way-up indicators. Very rare ripple cross-stratification was also noted.
3. 3-4m of red mudstone. Homogeneous and brecciated.
4. 50cm of red sandstone/siltstone containing rare ripple cross-stratification and erosional

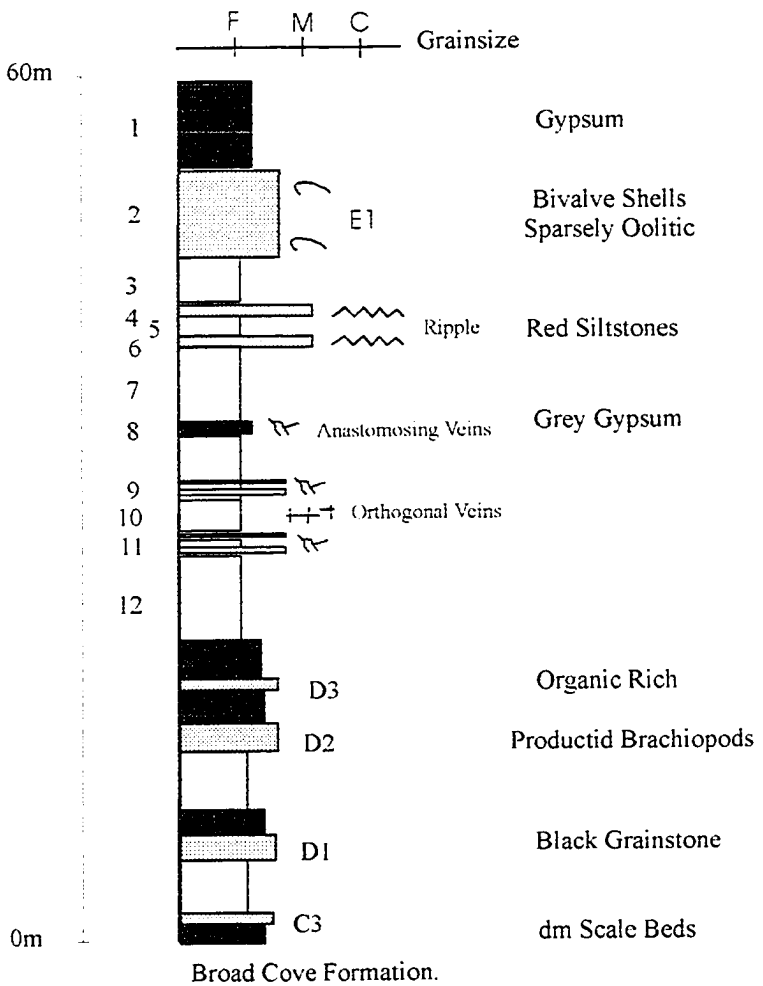

Figure 3.1.5. Stratigraphy of the Broad Cove Diapir structural carapace. The numerical designationis used to describe repeated sections. Strata below unit 12 are not repeated and are therefore not given a number. (Legend for this figure shown in Figure 3.1.4).

surfaces used as way-up evidence.

5. 2-3m of red mudstone. Homogeneous and brecciated.

6. 50cm red sandstone/siltstone containing rare ripple cross-stratification and erosional surfaces used as way-up evidence.

7. 5-8m of red/green mudstone. Homogeneous and brecciated.

8. 1.0m grey gypsum. Foliated grey gypsum is cut by many anastomosing gypsum veins.

9. 1.5m stratal package consisting of three 5-10cm thick grey siltstone beds separated by 10-20cm of red mudstone. Siltstones are predominantly homogeneous with extremely rare ripple cross-stratification. Layer-parallel gypsum veins are common.

10. 2-3m of red mudstone shot through with two sets of gypsum veins in a mutually orthogonal orientation.

11. 1.5m stratal package consisting of two or three 5-10cm thick grey siltstone beds separated by 10-20cm of red mudstone. Siltstones are predominantly homogeneous with extremely rare ripple cross-stratification. Layer-parallel gypsum veins are common.

12. 5-8m of red mudstone. Homogeneous and brecciated.

Repeated occurrences of this stratigraphic package were used to identify faults and folds within the Broad Cove exposure. Below the red mudstone (Unit 12 above), the stratigraphic package continues with the D3, D2, D1 and C3 Hood Island - Middle Windsor limestones separated by white gypsum and red/green mudstones (P. Giles, pers. comm. 1995, 1996).

Throughout the stratigraphic package, way-up evidence ranged from unequivocal to questionable. The available evidence was sufficient to constrain the orientation of the repeated stratigraphic package and is in accordance with the structural reconstruction presented below.

The structural carapace of the Broad Cove Diapir is similar to those described by Schwerdtner (1983) for diapirs of the Queen Elizabeth Islands, Arctic Canada. In

particular, the position of a recognisable stratigraphic sequence that has been uplifted on top of halite-cored diapiric structure is closely analogous to the Broad Cove Diapir structural carapace. There is no evidence to suggest that the strata overlying the Broad Cove Diapir represents a solution cap composed of an insoluble residue similar to that described for the Gulf of Mexico diapirs. A solution cap may exist below the level of exposure at the interface of the halite with the carapace, although there is no evidence for this. From a regional study of the Windsor Group, Boehner (1983) concluded that there were no examples within Nova Scotia or Cape Breton of solution caprocks similar to those described from the Gulf Coast.

Configuration of the Structural Carapace

By using the stratigraphic package, and in particular the limestones, as structural markers, the configuration of the structural carapace can be reconstructed. The structural carapace is described below from the north-east to the south-west (Figures 3.1.4 and 3.1.6).

- An overturned stratigraphic package consisting of the gypsum mylonite unit 1 to the red mudstone unit 12 (see above). The units dip ~70 degrees to the west. This package is a repetition of the stratigraphic unit immediately to the west.

  Interpretation. The units are inferred to have been repeated on a curtain fault (see Glossary of Salt Tectonics) that has cut up through the stratigraphic section causing repetition of stratigraphic units 1 to 12. This curtain fault is interpreted to be a layer-parallel decollement except where it cuts up stratigraphy (Figure 3.1.6). The decollement surface for the fault is the lower surface of the gypsum (unit 1).

- A tight to isoclinal anticline with units 1 to 12 repeated in the north-east and south-west limbs (Figures 3.1.6 and 3.1.7). The fold geometry and age relationships of the two limbs are constrained by good way-up evidence (ripple

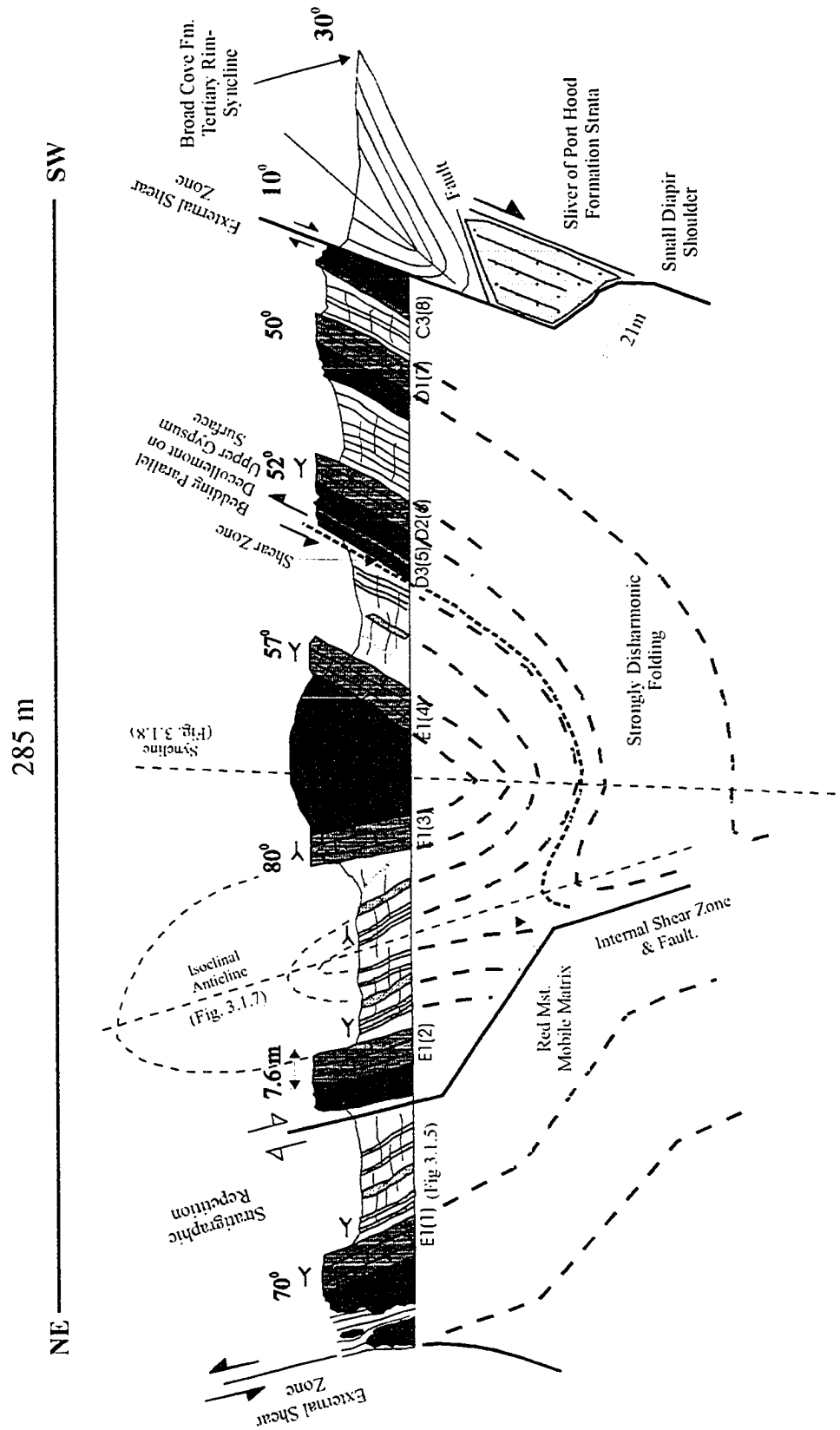

Figure 3.1.6. The structural carapace of the Broad Cove Diapir.

Figure 3.1.7. The isoclinal anticline within the structural carapace of the Broad Cove Diapir. The beds can be matched on both limbs of the fold and way up evidence is sufficient to constrain the structure as an anticline. The fold limbs are not planar, but show parasitic folding which makes accurate determination of dip and strike difficult.

Figure 3.1.8. The syncline within the structural carapace of the Broad Cove Diapir. The E1 limestone can be seen on both limbs of the fold and bivalve moldic porosity provides unequivocal way up evidence. The gypsum unit overlying the E1 limestone has been squeezed in to an antiform within the hinge region.

(Note, for fold axis, read fold axial trace)

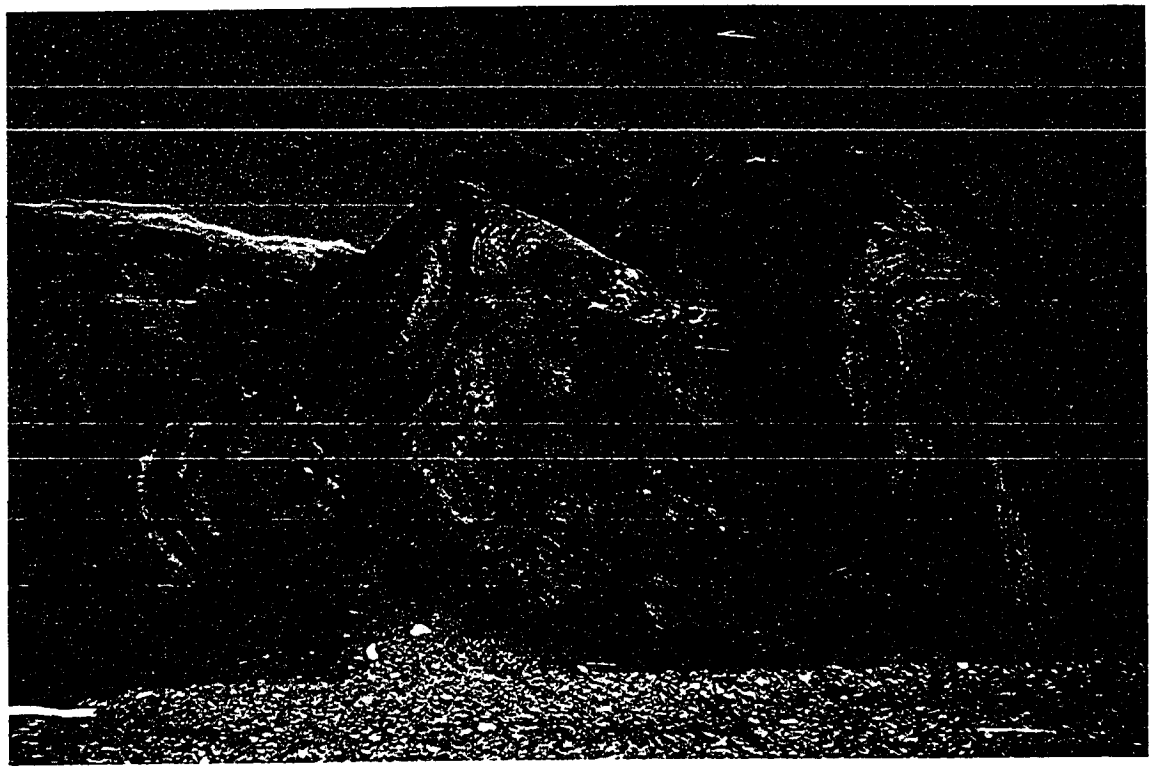

Figure 3.1.7

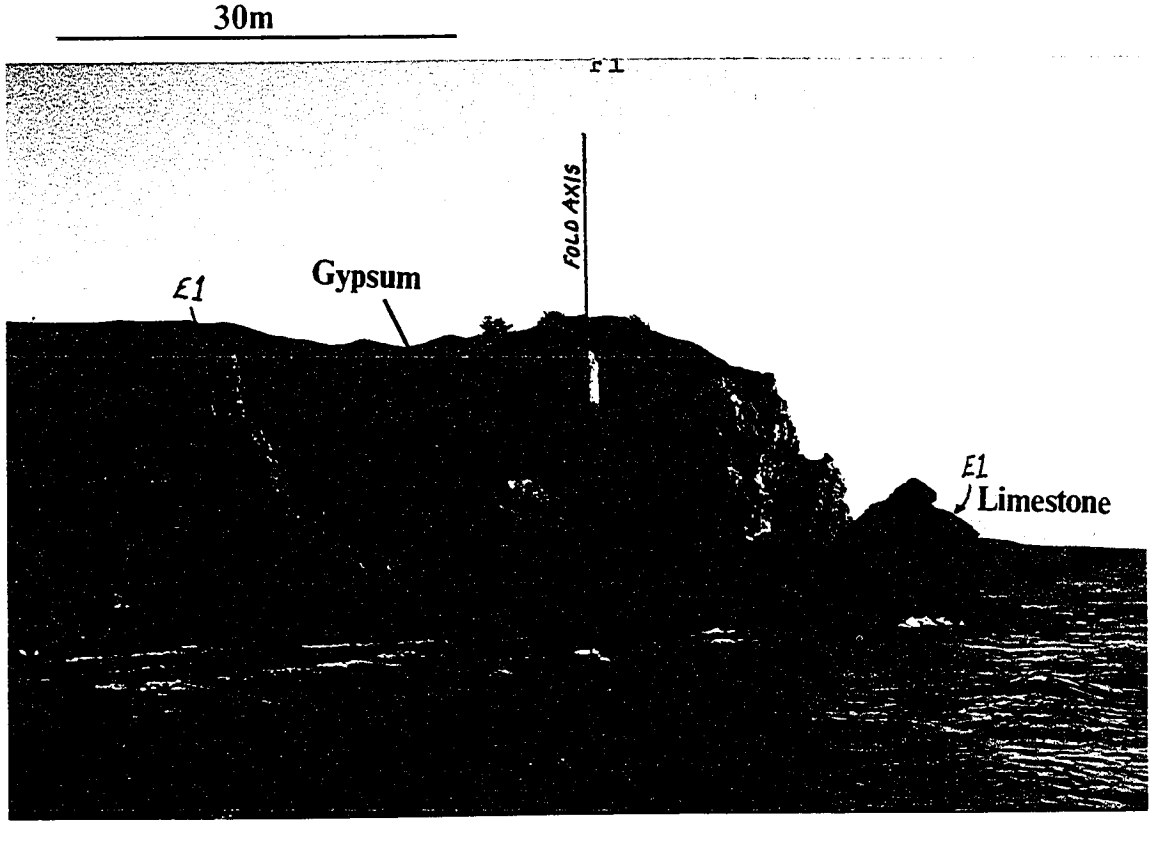

Figure 3.1.8

laminations). Where exposed in the cliff section, the fold limbs are not planar but are deformed by parasitic folds. In addition, the red mudstone strata in the fold shows rapid thickness and rare colour banding is highly deformed and displaced by many small faults. Both of these features indicate that the mudstone strata are highly deformed. It is suspected that the mudstone strata have acted as a mobile matrix that has been mobilised during the formation of the anticline. The fold axis plunges 70 degrees to the SSE (160 degrees).

- A tight synclinal structure with units 1 to 12 repeated in the south-west and north-east limbs of the fold (Figure 3.1.8). The synclinal structure is clearly seen where the E1 limestone crops out near the fold hinge. The fold plunges at 30 degrees towards the SSW (195 degrees) and the fold has an interlimb angle of 58 degrees. The white gypsum overlying the E1 limestone has been squeezed between the E1 limestones in the hinge region into an antiform within the core of the syncline.

- Beneath unit 12 on the south-western limb of the syncline, the stratigraphic package continues as intact stratigraphy through the D3, D2, D1 and C3 limestones, separated by gypsum and red/green mudstone strata (Figure 3.1.6). This stratigraphic succession is in structural concordance with the south-western limb of the syncline; however, the D3, D2, D1 and C3 limestones are not present anywhere within the exposed anticline to the north-east. The upper contact of the gypsum overlying the D3 limestone is highly foliated with a lineation dipping 52 degrees to the north-north-east.

Interpretation. This configuration suggests that the folding in the sub-surface is strongly disharmonic (Figure 3.1.6) and that a bedding-parallel decollement exists between the red mudstone (12) and the gypsum overlying the D3 limestone. The existence of the decollement at this position is indicated by the well-developed shear zone seen on the upper surface of the gypsum that overlies the D3 limestone

(see above). This decollement would accommodate the bedding-parallel slip required to form disharmonic folds. The development of disharmonic folding was probably accompanied by migration of incompetent red mudstone strata as a mobile matrix. The red mudstone strata in the isoclinal anticline are highly deformed (see above), which can be interpreted as evidence that the red mudstone has been mobilised during deformation.

The strongly folded nature of the structural carapace indicates that a large amount of lateral contraction has taken place. In addition, the exposed diapir flanks verge outwards from the diapir (Figure 3.1.6). Both of these features imply lateral contraction of the structural carapace. Unfortunately, because only a small part of each fold and fault is exposed, a strain value (Beta value) for contraction cannot be estimated. A number of possible explanations for this lateral contraction can be proposed:

- The folding could be an intrinsic part of the growing diapir. In this scenario, the structural carapace would be mirroring the deformation of the underlying halite core. However, the structures observed within the carapace do not compare well with those within halite diapir cores (for example, those within the Pugwash mine (Carter, 1990a, b and c)), where the most typical structures are curtain folds with steeply plunging (sub-vertical) fold axes. In addition, this model cannot easily explain sub-horizontal compression as the main fabric should indicate vertical stretching.

- The folding could be related to Carboniferous and/or post-Carboniferous inversion. Evaporite minerals are generally weaker than the surrounding sedimentary rocks. They therefore act as stress risers that can absorb regional compression by thinning and by modification of the diapir geometry. Compression across the structural carapace could account for the folding of the structural carapace, either by amplifying pre-existing folds or generating new folds (M. Jackson Pers. Comm. 1997). It is felt that compression related to Carboniferous or post-Carboniferous inversion is the most

likely explanation for observed folding within the Broad Cove structural carapace.

- The anhydrite to gypsum reaction involves a 42 % volume increase due to the absorption of water. Typically, this reaction takes place at a shallow depth of a few meters down to a depth of 200 m (M. Zentilli, Pers. Comm. 1996). The water needed for the anhydrite to gypsum reaction may be taken from pore waters or supplied by groundwater. The expansion of anhydrite could cause folding or fold amplification within the carapace, especially if the carapace is partially confined by the surrounding overburden. The folding related to volume expansion is hard to distinguish from tectonic folds, and so it is hard to quantify the effects of volume expansion. It can be inferred that, given the thickness of gypsum within the Broad Cove carapace, not all of the folding can be attributed to volume expansion.

3.1.7, The North-East External Shear Zone

The north-eastern external shear zone (Figure 3.1.9) is a sheared contact that forms the boundary between overburden rocks of the Hastings Formation and the Hood Island Formation structural carapace. The external shear zone is a 'pencil thin' (~1-2cm) contact with no tectonic interleaving between diapir and overburden rocks. Intact, vertically oriented siltstones of the Hastings Formation can be traced only a few centimetres from the sheared contact. The Windsor Group strata at the external shear zone consist of red mudstone with included gypsum lozenges up to 50 cm in length. A sporadic limestone breccia consisting of angular, organic-rich limestone clasts up to 10 cm long is located at the contact on the diapir side of the external shear zone. The dominant deformation mechanism within the external shear zone is plastic shearing.

Interpretation. Within western Cape Breton, the Hastings Formation stratigraphically overlies the Hood Island Formation. This stratigraphic tie suggests that there is very little displacement across the external shear zone. This hypothesis is supported by the relatively minor deformation seen within the external shear zone. If the external shear zone is a semi-concordant contact between diapir and overburden, this implies that the

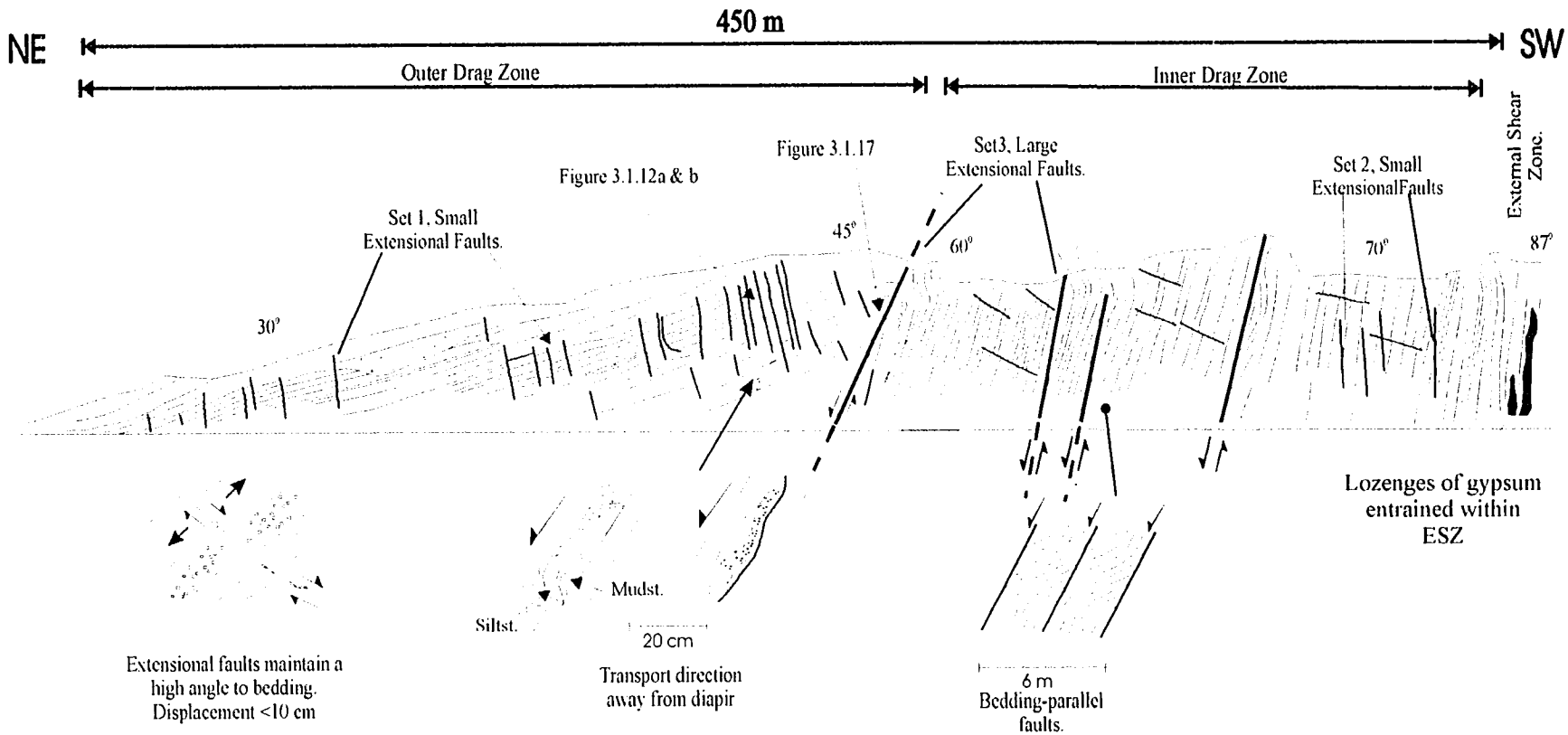

Figure 3.1.9. The North-East Drag Zone, Broad Cove Diapir.

north-east flank of the Broad Cove Diapir may dip towards the north-east and that the flank is overlain by a rotated, intact stratigraphic package rather than a sub-vertical surface (Figure 3.1.3).

3.1.8, North-East Drag Zone of the Broad Cove Diapir

*(**Note**: This section references a number of graphs that show structural data. In all cases, the graphs have been standardised so that the diapir is located on the left-hand side at 0m).*

The north-east drag zone is exposed as a 450 m continuous section. The structural deformation that has affected the drag zone consists of three separate structural styles (Figure 3.1.9).

Folding

The Hastings Formation strata within the north-east drag zone form a dip fan, within which the dip of the strata increases from approximately 22-30 degrees at the outer drag zone to 87 degrees at the diapir/overburden contact (external shear zone) (Figure 3.1.10). The total amount of rotation within the drag zone is approximately 70 degrees.

The rotation and deformation of the strata within the drag zone has not resulted in a smooth folding profile. The dip profile has been disrupted by faulting, which has partitioned the drag zone into three units (outer drag zone, inner drag zone and external shear zone), with each unit having a different amount of stratal rotation/folding.

Within the outer drag zone (280-600m), the stratal dip increases smoothly from 20-40 degrees. The outer drag zone is separated from the inner drag zone by the first of the set 3 faults (see below) at 280m, across which there is a sharp, 40 degree change of the stratal dip. Although some of this 40 degree dip change is undoubtedly related to fault drag, an overall 5-10 degree dip change can be seen across the fault. Within the inner drag zone

Figure 3.1.10. Stratal dip within the north-east drag zone of the Broad Cove Diapir. Total amount of stratal rotation is approximately 70 degrees. The perturbation of the drag zone profile is caused by fault drag related to the Set 3, Large Extensional faults. The best-fit line is an estimated mean through the data points.

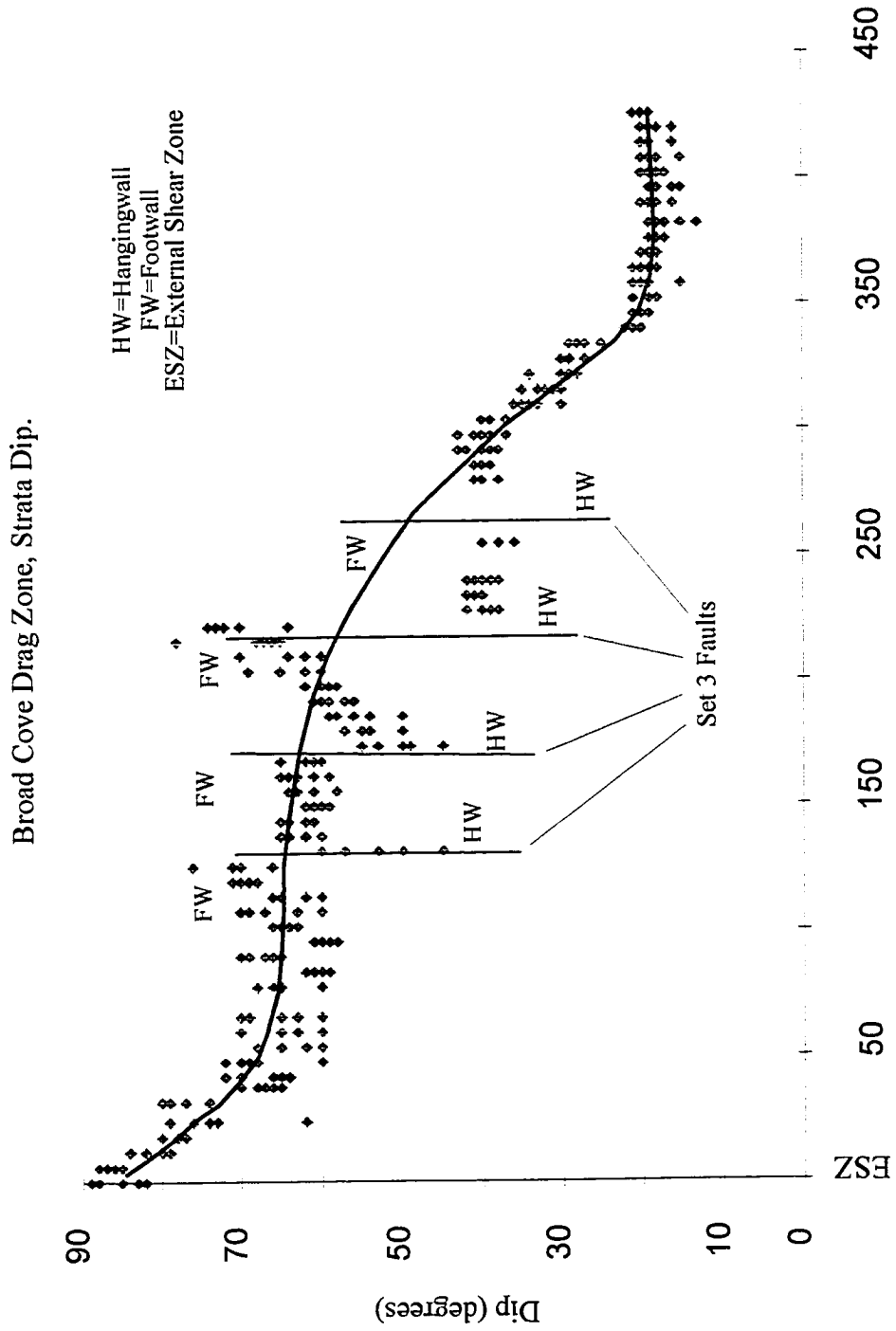
Broad Cove Drag Zone, Strata Dip.
HW=Hangingwall
FW=Footwall
ESZ=External Shear Zone
Dip (degrees)
90
70
50
30
10
0
ESZ
50
150
250
350
450
Horizontal Distance from Diapir (m)
FW
HW
Set 3 Faults

Figure 3.1.10.

(280-0m), the stratal dip increases moderately from ~55 to 70 degrees. The stratal dip increases markedly from 70 to 87 degrees from a distance of 0 to 20m from the external shear zone. Throughout the drag zone, the stratal strike is constant at 140-160 degrees (Figure 3.1.11).

Interpretation. The increase in the amount of stratal rotation near the external shear zone seems to be characteristic of diapir drag zones in general (e.g. Alsop, 1995, 1996). The constant strike of the drag zone strata (150-160 degrees) implies that there has been no forced rotation of strata along strike due to diapiric intrusion.

Faulting

Three sets of faults were recorded from the north-east drag zone. The fault sets are distinguished by their fault characteristics: offset, fault plane angle, length/width, relationship to hangingwall and footwall strata and orientation. The faults are described below as Small Faults (Set 1), Small Faults (Set 2), and Large Faults (Set 3).

Set 1, Small Faults

A pervasive set of faults is clearly seen throughout the north-east drag zone (Figure 3.1.9, 3.1.12a and b). These faults are characterised by:

- A small dip-slip offset. The maximum observed offset was ~20cm and, in most cases, displacement was <1-2 cm. In rare cases, gypsum had infilled the fault plane. The gypsum fibre orientation always showed a dip-slip offset with no strike-slip or reverse offset. No slickensides are associated with this set of faults.

- Little or no fault drag. The faults appear to be entirely brittle fractures showing mode 1 tensile fracturing within competent siltstones and mode 2 shearing within incompetent mudstones.

Figure 3.1.11. Strike of the strata within the north-east drag zone of the Broad Cove Diapir. The strike is almost constant at between 140-165 degrees. The strata within the drag zone are orientated sub-parallel to the adjacent diapir margin. The perturbation at around 250m is probably related to rotation caused by a Set 3, Large Extensional Fault.

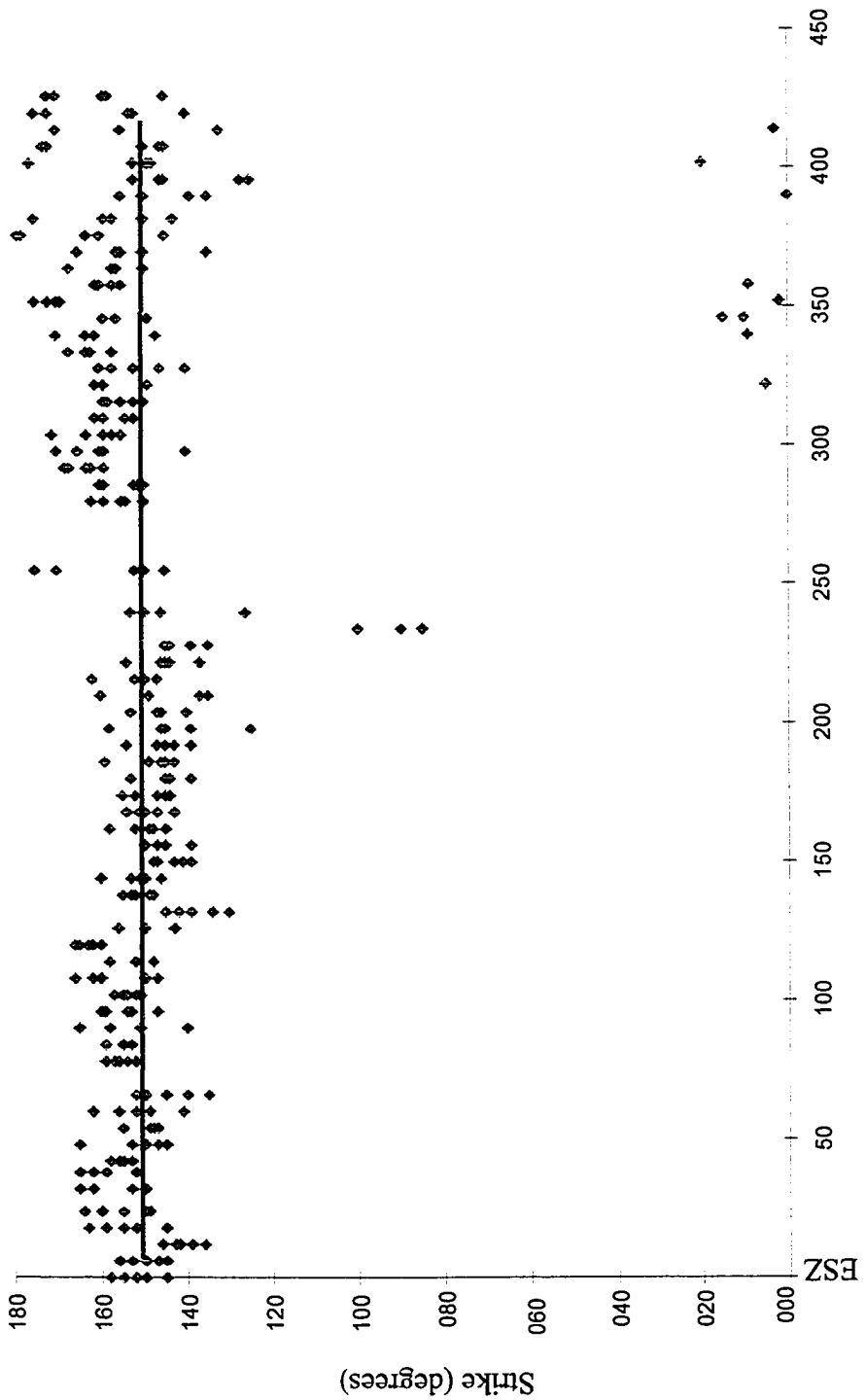
Broad Cove Drag Zone, Strike of the Drag Zone Strata vs Distance
Strike (degrees)
180
160
140
120
100
080
060
040
020
000
ESZ
50
100
150
200
250
300
350
400
450
Horizontal Distance from Diapir (m)

Figure 3.1.11.

Figure 3.1.12a. Examples of Set 1, Small Extensional Faults. Three clear faults can be seen (two on the left in shadow, one to the right marked by a rubbly gash). The faults have an offset of <1cm. Fault spacing is approximately 30cm.

Figure 3.1.12b. Photograph of a cliff section approximately 8m high from the north-east drag zone of the Broad Cove Diapir. Faults marked (i) are parallel Set 1 faults. Faults marked (ii) are orthogonal Set 1 faults. Orthogonal faults are hard to distinguish because they strike sub-parallel to the cliff face.

Figure 3.1.12a

Figure 3.1.12b

- The faults generally do not extend for more than a few metres. Faults commonly terminate at a bedding plane intersection.

Based on the orientation of the rare gypsum veins, the Set 1 faults are interpreted to be extensional faults, although it should be noted that kinematic indicators are scarce. Set 1, small extensional faults, show a progressive change in dip of the fault plane as the external shear zone is approached (Figures 3.1.13 and 3.1.14). Within the outer drag zone, the faults dip at 70-80 degrees and have an approximately 60 degree angle to bedding. Adjacent to the external shear zone (<10m from diapir/overburden contact), the fault planes dip at 25-35 degrees, maintaining a 50-60 degree angle to bedding. Thus the fault planes are inferred to have been progressively rotated to lower dip angles as the external shear zone is approached. The total amount of fault plane rotation is 50 +/- 15 degrees.

Set 2, Small Faults

Within 50 m of the external shear zone, a new set of extensional faults can be distinguished. These faults are identical to the Set 1 faults described above except that they maintain a high angle to bedding of 65-90 degrees. More common gypsum vein fibres in the inner drag zone indicate that these faults are extensional faults. No slickensides are associated with these faults.

Strike of Set 1 and Set 2 Small Extensional Faults

The strikes of Set 1 and Set 2 small extensional faults have a polarised distribution with faults striking orthogonal to and parallel to the adjacent margin of the diapir, which strikes at 140 degrees (Figure 3.1.15). The strikes of Set 1 and Set 2 faults also have parallel or orthogonal orientations with respect to bedding within the drag zone which strikes at 140 degrees (+/- 10 degrees) (Figure 3.1.11). Within the outer drag zone, both orthogonal and parallel faults exist with approximately the same density. The faults within the outer drag zone therefore consist of two mutually orthogonal fault sets. Both

Figure 3.1.13. Graph to show the fault plane dip for the Set 1 and Set 2, Small Extensional Faults. The estimated best-fit fault plane rotation is approximately 55 degrees with a range of +/- 15 degrees. The large spread of the data may be related to fault drag associated with Set 3, Large Extensional Faults. This data set has been statistically averaged to calculate the arithmetic mean for fault plane dip (see Figure 3.1.14).

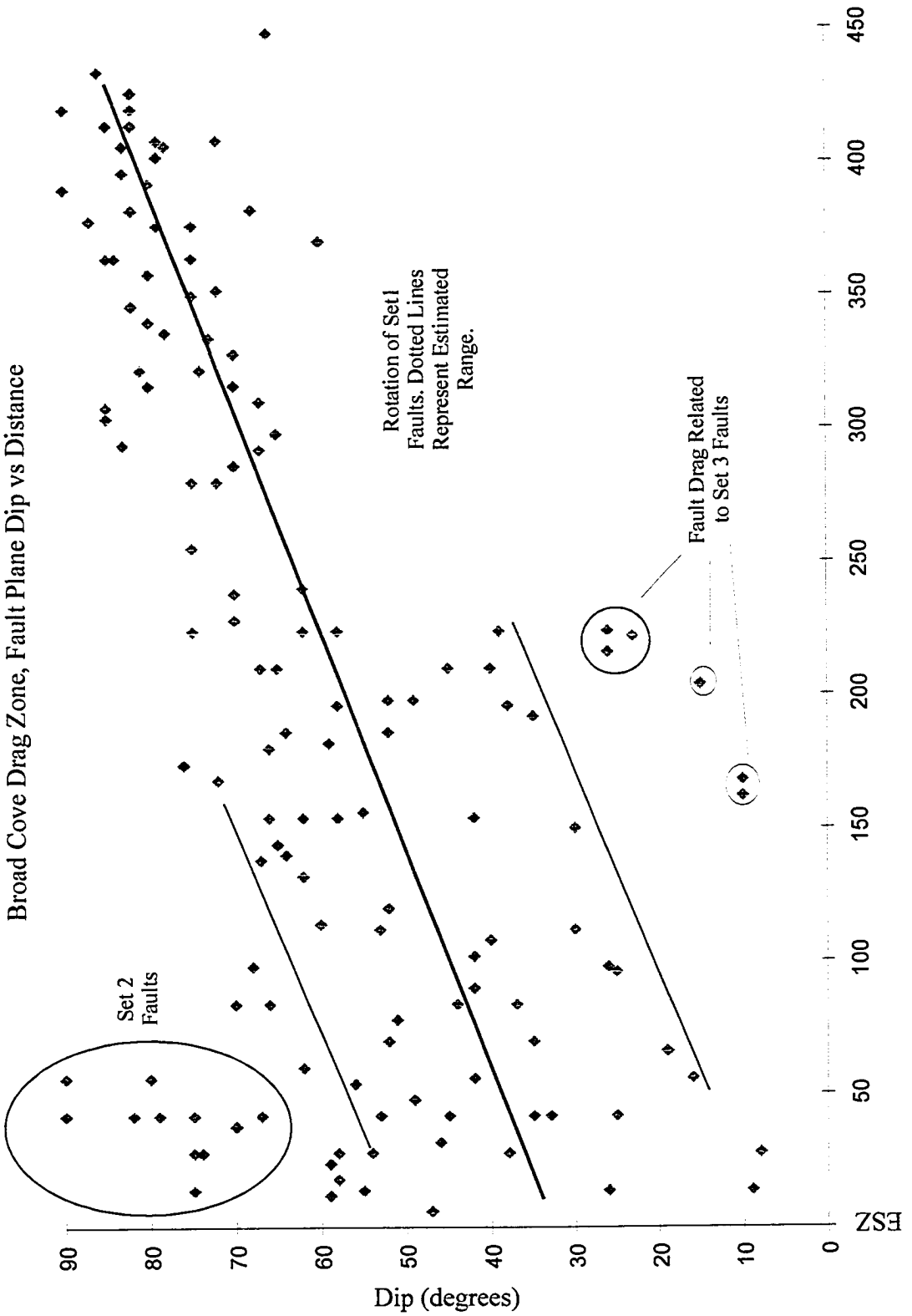
Broad Cove Drag Zone, Fault Plane Dip vs Distance
Set 2
Faults
Rotation of Set1
Faults. Dotted Lines
Represent Estimated
Range.
Fault Drag Related
to Set 3 Faults
Dip (degrees)
90
80
70
60
50
40
30
20
10
0
ESZ
50
100
150
200
250
300
350
400
450
Horizontal Distance from Diapir (m)

Figure 3.1.13.

Figure 3.1.14. Graph to show the rotation of Set 1, Small Extensional Faults. The points shown on the graph are calculated arithmetic mean values. The fault plane dip data, collected at each station was summed and divided by the number of faults to produce a mean value. Averaging the dip data reduces some of the extreme data values, which were caused by fault drag and by Set 2 faults (see Figure 3.1.13). The overall trend still shows a fault plane rotation of approximately 50 degrees.

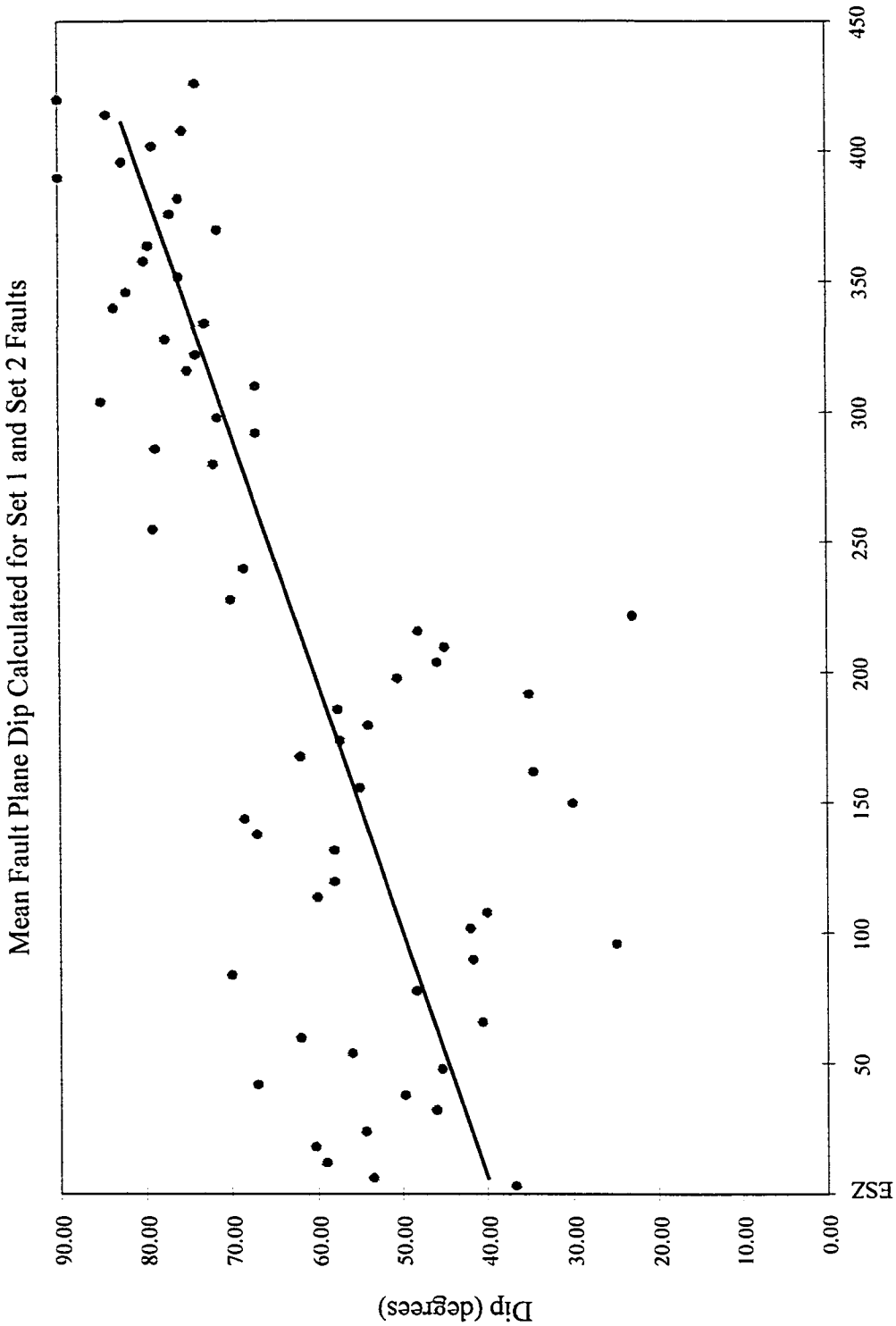
Mean Fault Plane Dip Calculated for Set 1 and Set 2 Faults
Dip (degrees)
90.00
80.00
70.00
60.00
50.00
40.00
30.00
20.00
10.00
0.00
ESZ
50
100
150
200
250
300
350
400
450
Horizontal Distance from Diapir (m)

Figure 3.1.14.

Figure 3.1.15. Graph to show the strike of Set 1 and Set 2, Small Extensional Faults. The graph shows that the fault orientations are very systematic with faults striking either ~140-160 degrees or ~080- 040 degrees. These orientations are approximately parallel to and orthogonal to the adjacent margin of the Broad Cove Diapir which strikes at ~140 degrees. These orientations are also parallel to and orthogonal to the strike of the drag zone strata.

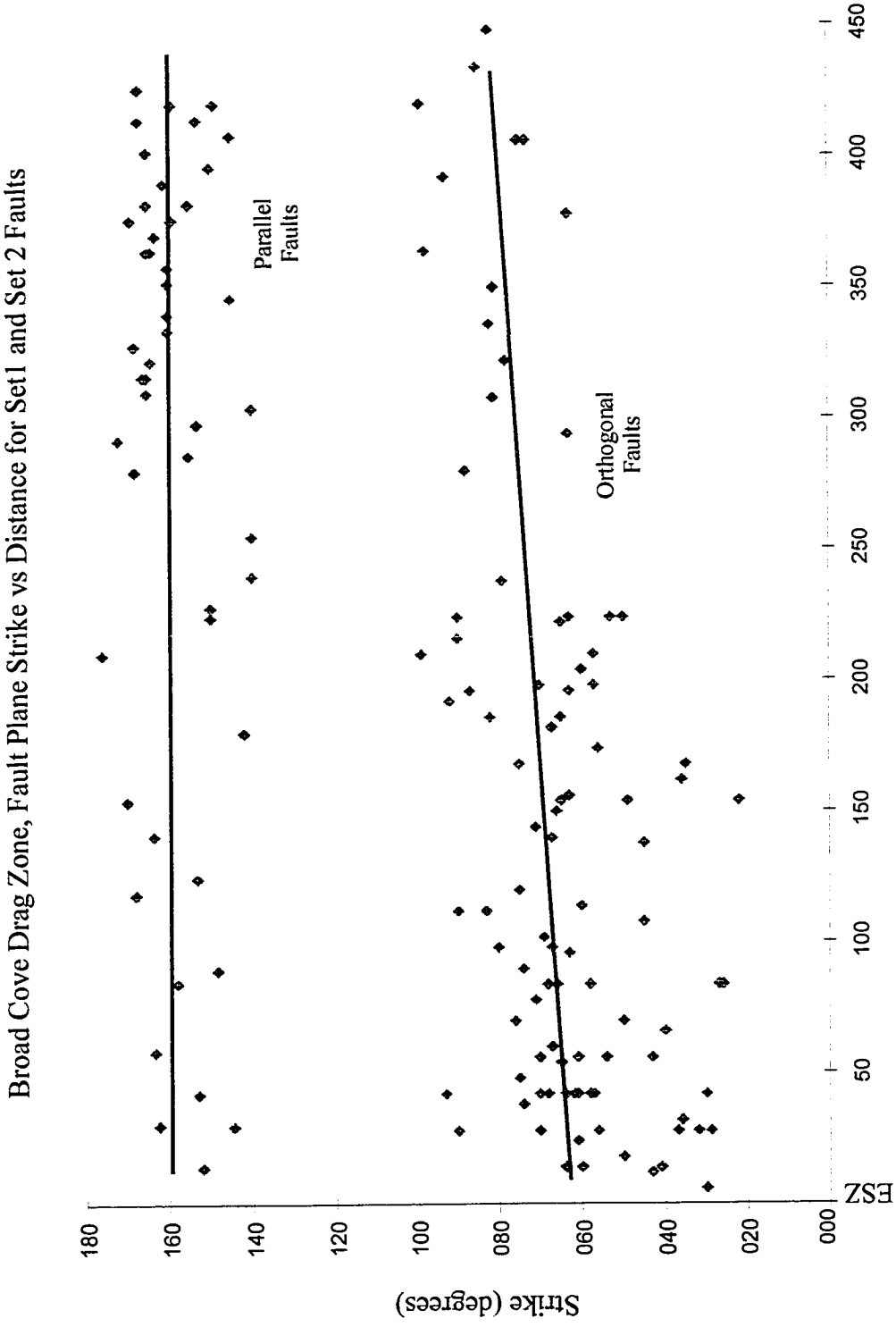
Broad Cove Drag Zone, Fault Plane Strike vs Distance for Set1 and Set 2 Faults
Strike (degrees)
180
160
140
120
100
080
060
040
020
000
ESZ
50
100
150
200
250
300
350
400
450
Horizontal Distance from Diapir (m)
Parallel Faults
Orthogonal Faults

Figure 3.1.15

the orthogonal and parallel faults appear to have been rotated and no difference in rotation angle can be discerned between the two fault orientations (Figure 3.1.16).

Set 3, Large Faults

Set 3 faults are observed within the north-eastern drag zone (Figure 3.1.17). These faults are characterised by:

- A relatively large displacement estimated to be 5-10 m. The strata in the hangingwall and footwall cannot be matched, suggesting that the fault displacement is at least equal to the height of the cliff.

- Kinematic indicators are only exposed at one location in the drag zone and consist of small drag folds (<10 cm long) that are in contact with the fault plane. The drag folds indicate an extensional dip-slip offset for this fault. By inference, the other Set 3 faults are also interpreted to be extensional faults. No slickensides or shear veins were observed in any of the Set 3 faults, which are generally poorly exposed.

- Strata in the hangingwall have been rotated (rollover) onto the fault plane so that they dip at a slightly lower angle than the adjacent hangingwall strata. Strata in the footwall have been rotated to a higher angle as the fault plane is approached (Figure 3.1.10). Set 1 small extensional faults show the same amount of rotation as the strata as the fault plane is approached, indicating an older/younger genetic relationship between the Set 1 and Set 3 faults (Figure 3.1.13).

- An orientation sub-parallel to the surrounding drag zone strata and diapir margin. There are four definite and three probable Set 3 faults located within the inner portion of the drag zone that dips between 55 and 70 degrees. Set 3 faults are not seen within the outer drag zone (250m to 450m) or adjacent to the external shear

Figure 3.1.16. Graph to show fault plane rotation of Set 1 and Set 2 faults divided into orthogonal and parallel fault sets. The graph shows that parallel faults and orthogonal faults have been rotated by approximately the same angle. The relative concentration of data points does not represent fault density, but the ease with which fault orientations could be determined and measured.

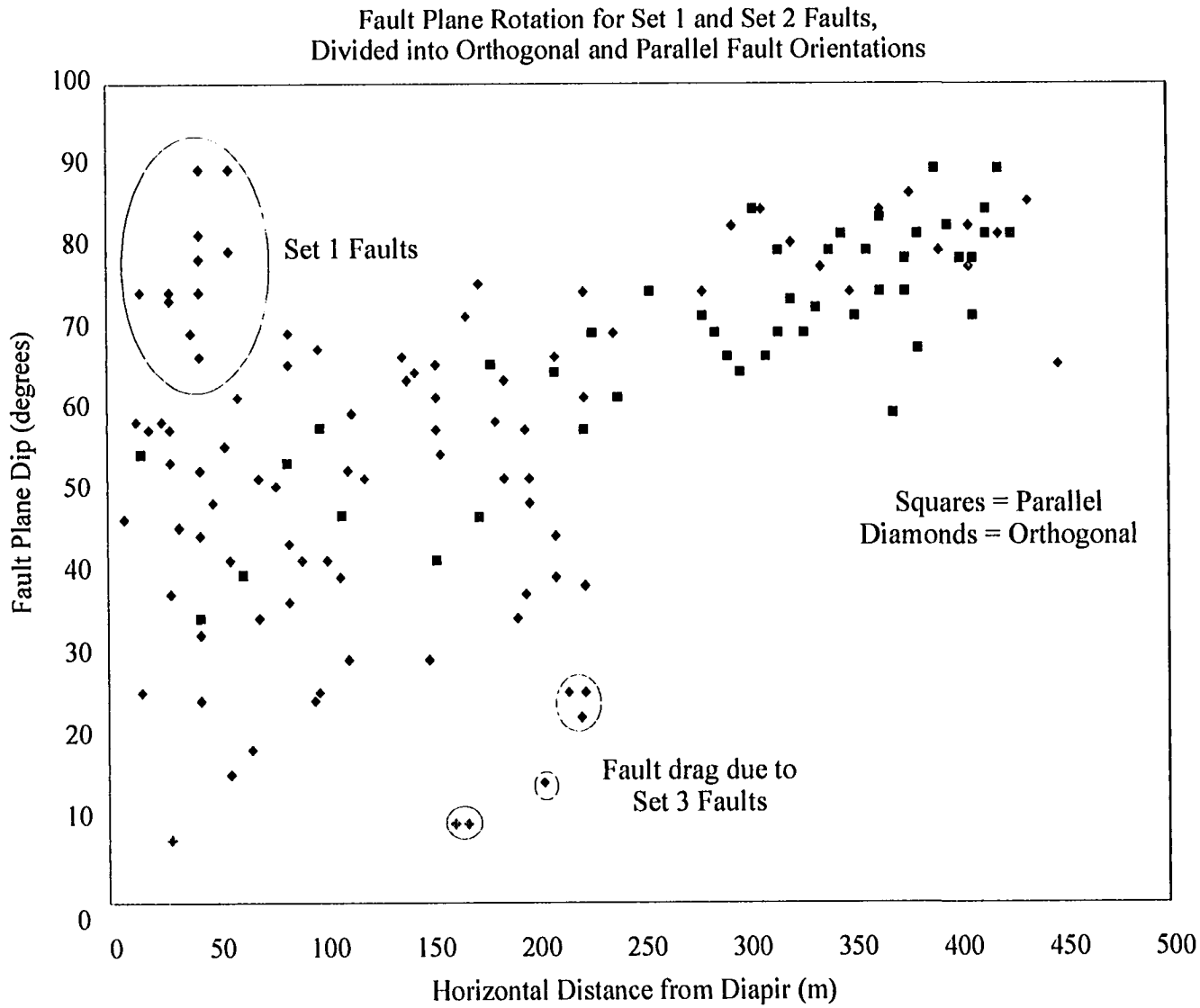
Fault Plane Rotation for Set 1 and Set 2 Faults,
Divided into Orthogonal and Parallel Fault Orientations
Fault Plane Dip (degrees)
100
90
80
70
60
50
40
30
20
10
0
Set 1 Faults
Squares = Parallel
Diamonds = Orthogonal
Fault drag due to
Set 3 Faults
0
50
100
150
200
250
300
350
400
450
500
Horizontal Distance from Diapir (m)

Figure 3.1.16.

Figure 3.1.17. A Set 3, Large Extensional Fault exposed within the north-east drag zone of the Broad Cove Diapir. The fault plane is marked by a sheared clay gouge and steps within the fault plane show that the fault is locally cutting up stratigraphy. Within the hangingwall (right hand side), the bedding dip increases from ~42 degrees to 65 degrees due to fault drag. The strata within the footwall dip at ~80 degrees. As the stratal dip increases towards the diapir this set of faults become orientated sub-parallel to bedding. See Figure 3.1.18 for the interpreted fault plane geometry.

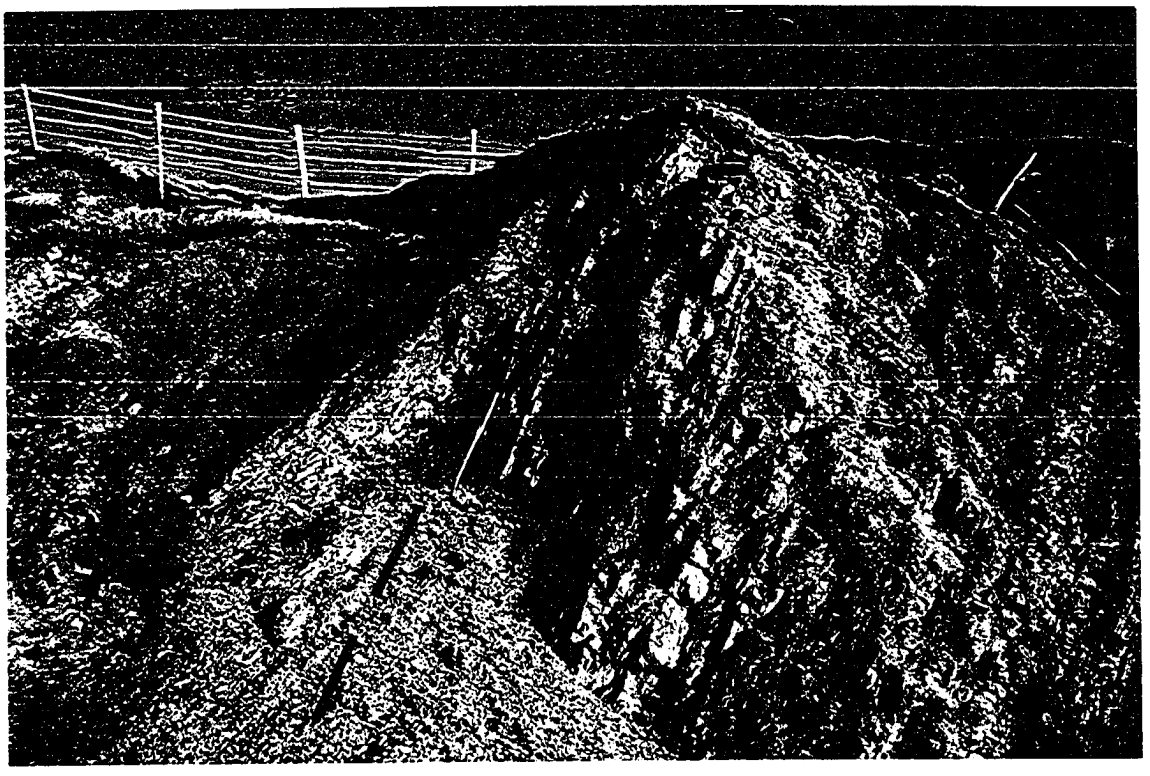

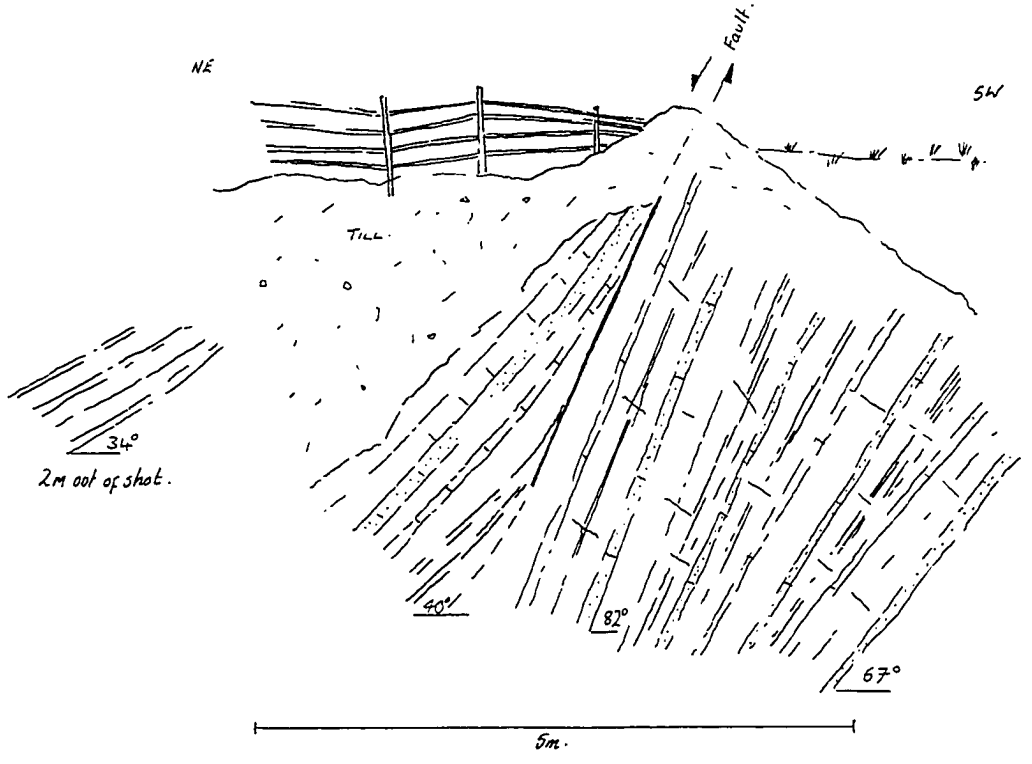

Figure 3.1.17

zone. The drag zone exposure does not show a complete fault, i.e. from tip to tip. However, from the geometry and stratal relationships observed, a geometry for the whole fault can be proposed (Figure 3.1.18). The fault is interpreted to have a listric geometry such that the exposed fault plane is the steeper portion of the fault and the bedding-parallel portion is located below the cliff section. The evidence to support this interpretation and its implications for drag zone deformation are discussed in Chapter 4.

3.1.9, Subordinate Drag Zone Structures

Numerous small-scale, bedding-parallel slip surfaces were recorded within the more steeply dipping portion of the drag zone (55-70 degrees). The slip surfaces all show transport of strata away from the diapir and the slip surfaces commonly end at small-scale compressional features. In rare cases, a centimetre scale duplex was formed. The slip surfaces mostly displaced more competent siltstone units over incompetent mudstones in a down dip direction.

3.1.10, South-Western Drag Zone and External Shear Zone

The south-western drag zone and external shear zone, imaged on Inverness line A05, is exposed as an onshore section at the north-east end of Inverness Beach. The external shear zone is a poorly exposed fault contact between Hood Island Formation gypsum and red, medium-grained sandstone of the Broad Cove Formation. The sandstone at the external shear zone has been overturned by ~12 degrees (as indicated by way-up evidence from graded bedding and overturned cross-stratification). The folding of the Broad Cove strata defines a narrow overturned syncline (~30m wide), to the south of which the dip of the Broad Cove Formation decreases rapidly to a regional dip of ~20 degrees. The entire south-western drag zone is approximately 100 m wide, considerably narrower than the north-eastern drag zone. Away from the diapir, the Broad Cove Formation conformably or disconformably overlies the Inverness Formation (Figure 3.1.6).

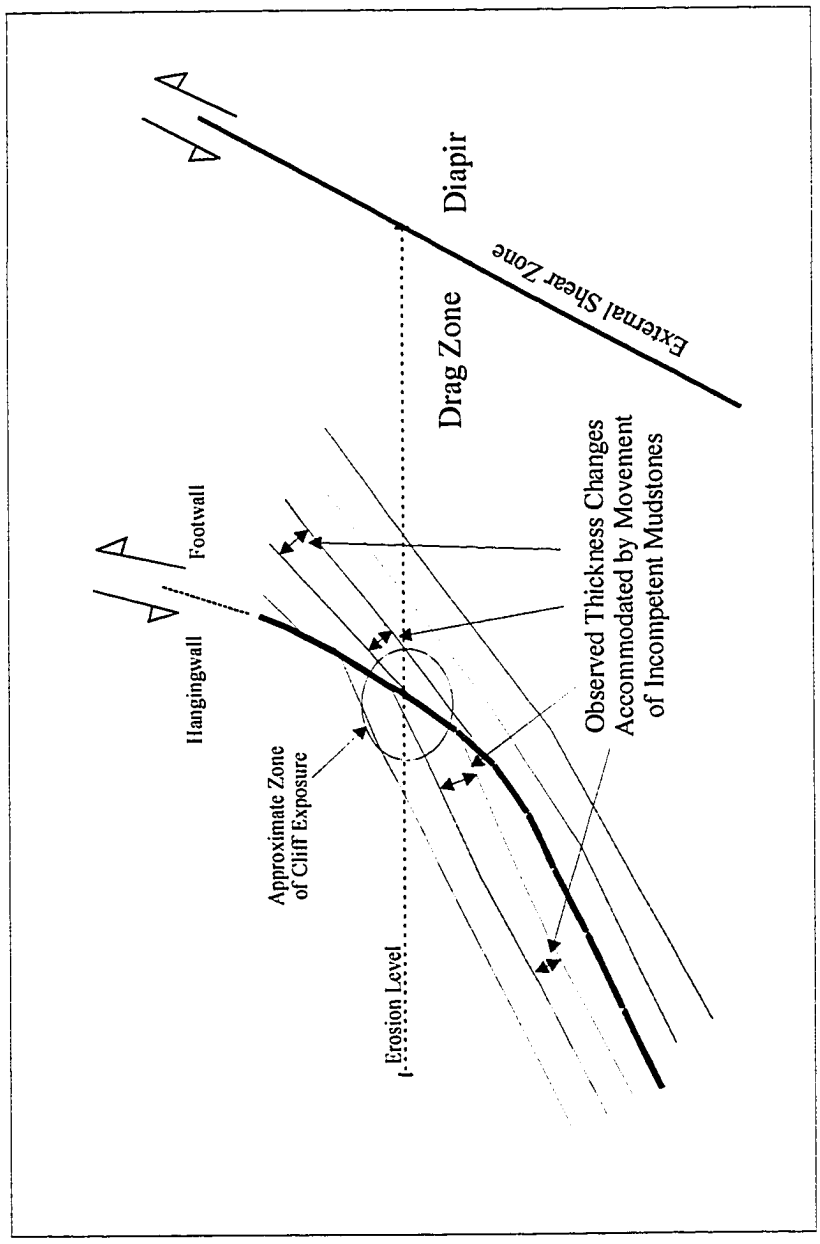

Figure 3.1.18. Model for the Set 3, large extensional faults.

3.1.11, Port Hood Formation Tectonised Fragment

Exposed on the beach beneath the Broad Cove Formation is a sliver of grey/green, arkosic sandstone that contains abundant coalified plant fragments (Figure 3.1.6). The stratigraphic attribution of the sandstone is indicated by several cylindrical carbonate-cemented tree stems, which are apparently unique to the Port Hood Formation within the Upper Carboniferous strata of western Cape Breton. The sandstone outcrop is approximately 21 m wide and can be traced across the beach to within 2 m of the Broad Cove Formation adjacent to the south-west external shear zone of the Broad Cove Diapir. The contact between the Broad Cove and Port Hood Formations is not exposed but must be abrupt.

Interpretation. The apparent juxtaposition of the Port Hood and Broad Cove Formations and the concordance of both units with the margin of the Broad Cove Diapir suggest that the Port Hood Formation sandstone is a fault-bounded sliver that has been transported vertically to its present position by the upward growth of the Broad Cove Diapir. The Inverness Formation in the Broad Cove area is estimated to be 700 to 900 m thick (see Seismic Stratigraphy, Chapter 2). The Port Hood Formation sliver has, therefore, probably been uplifted by approximately 700 m through the Inverness Formation.

3.1.12, The Broad Cove Formation – Secondary Peripheral Sink

The Broad Cove Formation conformably to disconformably overlies the Inverness Formation adjacent to the south-west margin of the Broad Cove Diapir (Figure 3.1.3). The Broad Cove Formation is unique within the field area, consisting of intercalated red sandstones, siltstones and red mudstones. The red sandstones are medium to coarse-grained, are typically 1-2 m thick and are apparently either structureless or trough-cross-stratified. The red oxidised state of the Broad Cove Formation may indicate deposition within arid, continental conditions that are typically associated with Stephanian to Permian sediments in Atlantic Canada. The oxidised (red) state of the Broad Cove Formation precludes palynological dating and no macrofossils have been found. This has

made dating the Broad Cove Formation problematical. The Broad Cove Formation is clearly younger than Westphalian D, and Bell (1944) assigned the Broad Cove Formation to the lowest Permian based upon its sedimentology and stratigraphic position.

A rim-syncline is a structural term used to describe a fold that has an arcuate axial trace. Rim-synclines associated with diapirs are commonly filled by syn-kinematic sediments referred to as primary and secondary peripheral sinks. A secondary peripheral sink is associated with a diapir that is growing by withdrawing salt from its precursor pillow. Several lines of evidence suggest that the Broad Cove Formation is a secondary peripheral sink with respect to the Broad Cove Diapir:

- The Broad Cove Formation is restricted to the area immediately adjacent to the south-west flank of the Broad Cove Diapir and is not exposed elsewhere within Cape Breton. This may imply that the Broad Cove Diapir in some way controlled the deposition of the Broad Cove Formation.

- On seismic section A05, a reflector interval that is correlated with the Broad Cove Formation is imaged as a wedge of strata that thins progressively away from the diapir to a maximum distance of 5.5 km.

- Analogue models show secondary peripheral sinks juxtaposed against the steeply dipping flanks of asymmetric diapirs (for example Lemon, 1985). During continued growth, the synclines are progressively deformed by continued diapiric intrusion into tight, overturned synclines.

Interpretation. The position of the Broad Cove Formation adjacent to the steeply dipping south-western flank of the asymmetric Broad Cove Diapir corresponds to the position of secondary peripheral sinks from analogue models; for example, Lemon (1985). In addition, the wedge shape of the Broad Cove Formation indicates that it may have been

deposited within a rim-syncline adjacent to the diapir. The lack of any other exposures of the Broad Cove Formation (or its equivalent) within western Cape Breton implies that it was deposited as a local sedimentary feature, further tying its depositional environment to the Broad Cove Diapir. For these reasons, the Broad Cove Formation is interpreted to be a secondary peripheral sink that was deposited within a rim-syncline adjacent to the Broad Cove Diapir.

3.2, THE ST. ROSE DIAPIR

3.2.1, Geographic Data

The start of the diapir drag zone is at latitude 46N,20,05 longitude 61W,13,00 - MacLeods Pond. The north-east external shear zone begins at latitude 46N,19,40 longitude 61W,13,30 - Near MacRaes Beach. The south-west end of diapir exposure is located at latitude 46N,20,54 longitude 61W,11,57 (Figure 3.2.1).

3.2.2, General Information

The St. Rose Diapir was first described as a diapiric structure by Haites (1952). Haites described the diapir as a doubtful piercement structure that was bounded on its eastern border by a fault contact between Hood Island Formation gypsum and Canso beds (remapped as the Colindale Member, Port Hood Formation by Giles et al. (1997b).

3.2.3, The St. Rose Diapir Geometry Constrained from Onshore Map Pattern and Mine Plan Data

The St. Rose Diapir is not covered by any of the seismic surveys used in this project or by any available seismic data. The overall geometry of the St. Rose Diapir is therefore inferred from its onshore map pattern and by comparison of the onshore exposures with other diapirs (principally the Broad Cove Diapir) which have similar structural features.

Onshore Map Pattern

The interpretation presented below uses data from the most recent geological map of western Cape Breton (Giles et al., 1997b) (Figure 3.2.1).

The Upper and Middle Windsor strata of the St. Rose Diapir describe a crescent-shaped map pattern that defines the south-east margin of the diapiric structure with a length of 3.5 km (Figure 3.2.1). The offshore extent and geometry of the St. Rose diapir is

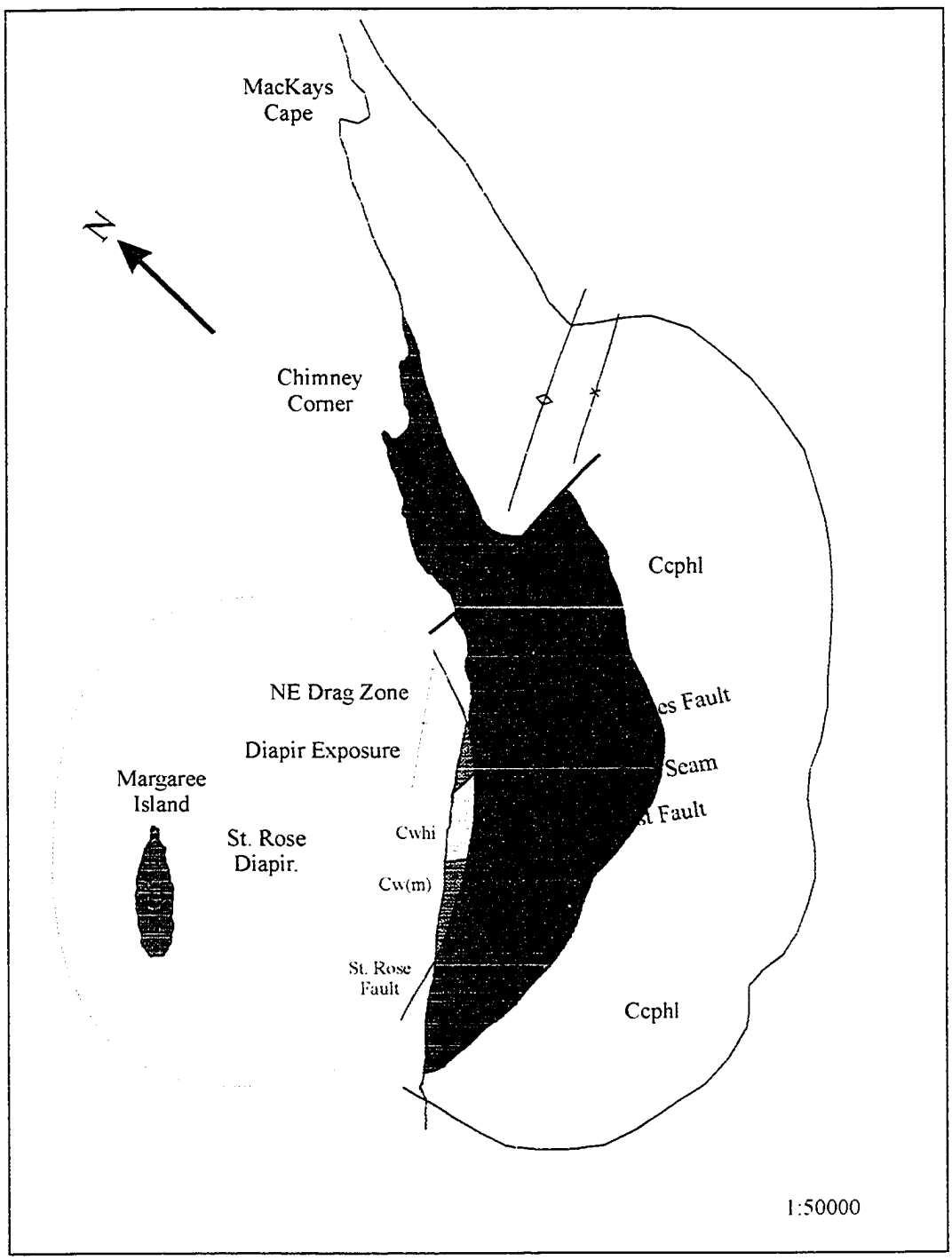

Figure 3.2.1. Geological map of the St. Rose area. Modified from Giles et al. (1997b). (See Figure 2.3.1 for Key).

uncertain. If the crescent-shaped section is extrapolated into the offshore area, assuming a cylindrical diapir, then the diameter of the St. Rose Diapir is approximately 6.5 km. If this diameter is correct, then the St. Rose Diapir extends beneath Margaree Island and Margaree Island may be a raft of Upper Carboniferous strata (probably Inverness Formation: P.S. Giles, pers. comm. 1994) supported from beneath by the St. Rose Diapir. This interpretation closely resembles that of the Port Hood Island diapir (see below, Chapter 3.5) where much of Port Hood Island is interpreted to be a raft of Upper Carboniferous strata supported from beneath by the Port Hood Island Diapir. It should be noted, however, that there is no seismic data to support this interpretation which must therefore be regarded as speculative.

The Carboniferous strata (Hastings Formation, Pomquet Formation, Margaree and Colindale Members of the Port Hood Formation) exposed inland of the St. Rose Diapir have a sub-circular map pattern that extends approximately 4-5 km around the St. Rose diapir. The stratigraphic units generally dip towards the St. Rose Diapir except where deformed within the diapir drag zone immediately adjacent to the diapir (<500m) (Figures 3.2.1 and 3.2.2). The circular map pattern and the dip of the strata towards the diapir may indicate that the St. Rose Diapir has affected erosion of the Carboniferous overburden by a combination of diapiric uplift followed by subsidence. During growth, the St. Rose Diapir may have lifted overlying strata above the regional datum to form a dome. Erosion of the domal structure would produce a circular map pattern centred on the diapir within the overburden strata. The present day dip of the strata towards the diapir indicates partial deflation of the source layer to form a rim-syncline.

Structural features inland support the interpretation of the St. Rose structure as an intrusive diapir. A cross-section constructed using the SR-4, SR-5 and SR-1 drill holes indicates that the No.5 coal seam may have been deformed into a drag zone structure within 200-350 m of the St. Rose Diapir (between drill holes SR-4 and SR-1) (Figure

Figure 3.2.2. Map to show the position of coal exploration drill holes. Contour interval are constructed on the 5' coal seam with 100' intervals. The coal seam contours define a bowl-shaped depression, centered approximately on the St. Rose Diapir. This bowl-shaped depression is reflected in the surface geological map of Giles et al. (1997).

Modified from MacNeil (1985)

Figure 3.2.3. Cross-section constructed from the coal exploration drill holes. The St. Rose Fault shown on the cross-section is interpreted to be the external shear zone of the St. Rose Diapir. The drag zone width on this section is approximately 200-250m wide (shown as the region adjacent to the diapir where the dip direction changes from north-west to south-east).

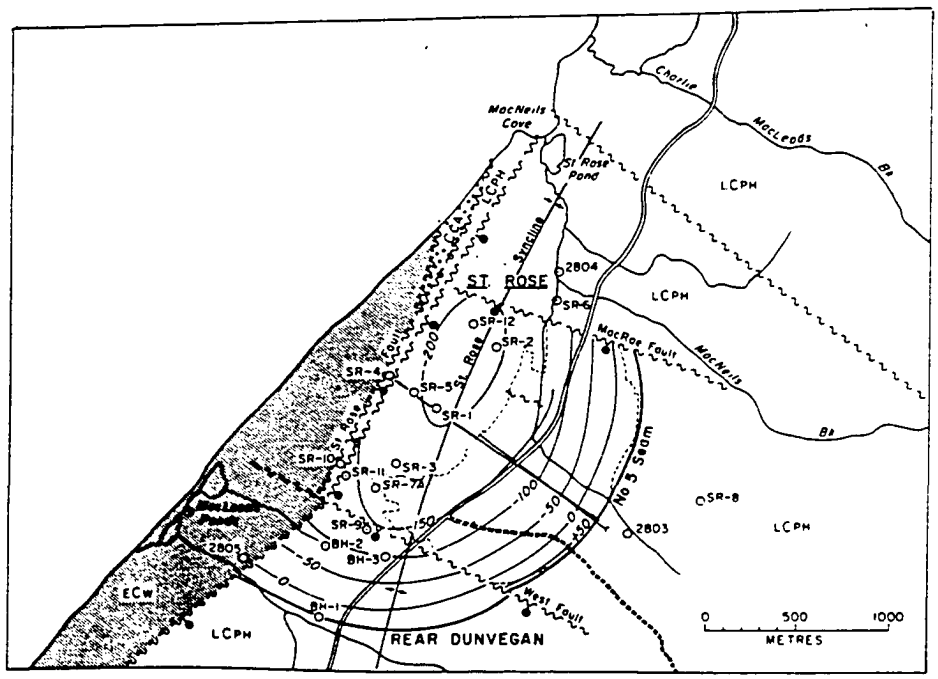

Figure 3.2.2

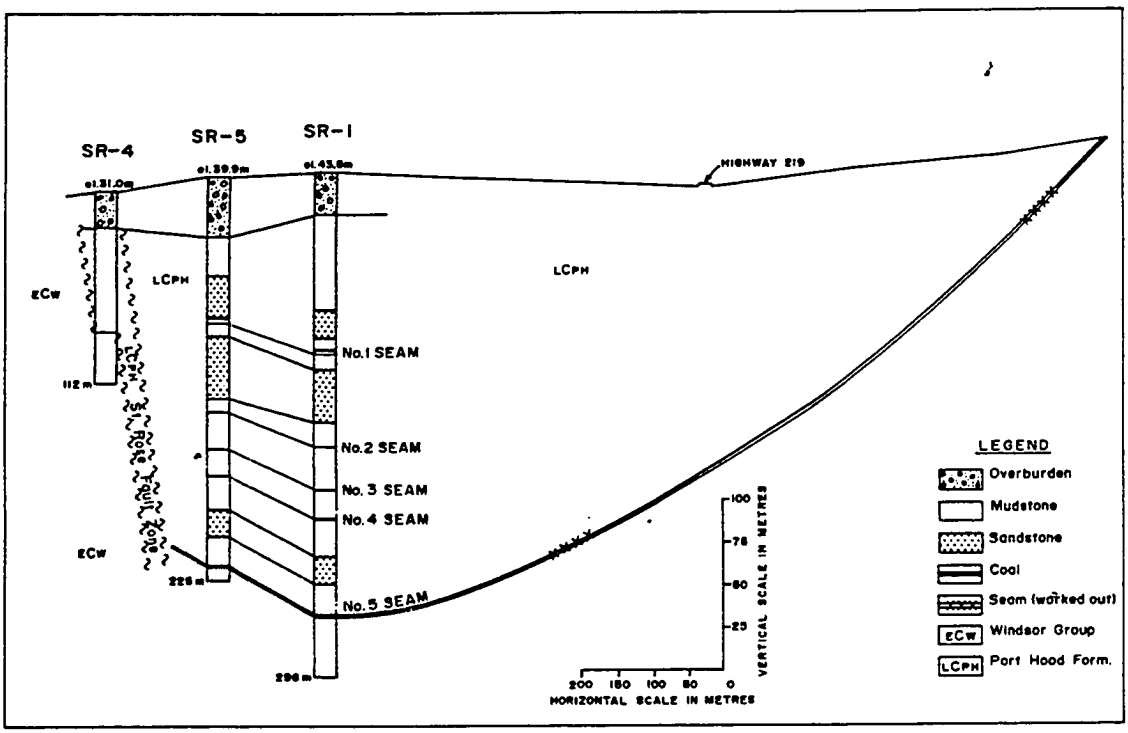

Figure 3.2.3

3.2.3). This drag zone structure is interpreted to be the eastern drag zone of the St. Rose Diapir, which has a geometry similar to the north-east drag zone exposed on MacRaes Beach (see below). The St. Rose fault is interpreted to represent the external shear zone of the St. Rose Diapir. From mine plans and mine drill hole data, the fault has been described as an extensional fault that dips at 70 degrees to the east (Hacquebard et al., 1989). This geometry therefore describes the approximate geometry of the eastern external shear zone of the St. Rose Diapir (Figure 3.2.3).

Two extensional faults that intersect the St. Rose Diapir at approximately 90 degrees - the MacRae Fault and the West Fault - have been mapped from field and mine data (Figure 3.2.1). These faults are probably orthogonal faults formed when the St. Rose Diapir intruded through the Carboniferous strata (see St. Rose drag zone). The offset of the West Fault has been calculated to be 12 m (Hacquebard et al., 1989); the offset of the MacRae Fault has not been calculated. Orthogonal faults extending from the margins of evaporite diapirs appear to be a common feature of diapir intrusion and have previously been described from analogue modelling (Link, 1930; Parker and McDowell, 1955; Alsop, 1996).

St. Rose Diapir - Vertical Profile

Due to the lack of seismic coverage, the 3D geometry of the St. Rose Diapir remains speculative. The north-east drag zone of the St. Rose Diapir (Figures 3.2.1 and 3.2.6) is very similar in both profile and structural features to the north-east drag zone of the Broad Cove Diapir. However, unlike the Broad Cove example, the Middle Windsor strata of the St. Rose Diapir are juxtaposed against the Colindale Member of the Port Hood Formation and so the diapir is not in stratigraphic continuity with the surrounding overburden. This suggests that the St. Rose Diapir has penetrated through the Carboniferous overburden as well as rotating the strata as an intact unit adjacent to the diapir (see Broad Cove Diapir, Chapter 3.1).

The lack of exposure of the south-west drag zone of the St. Rose Diapir precludes further interpretation of the overall geometry of the St. Rose Diapir.

3.2.4, The St. Rose Diapir, Coastal Exposure

The north-east drag zone section is 450 m long. The south-west flank of the diapir and its associated drag zone are not exposed due to severe beach erosion. The diapir is exposed for 480 m in a north-east to south-west direction (Figures 3.2.4 and 3.2.5). The onshore exposure of the St. Rose Diapir represents only a fragment of the entire diapir. As described above, the coastal section is a crescent-shaped slice through the south-east margin of the diapir. Measurable data can only be obtained from the northern third of the Windsor exposure, which represents approximately 1/12 of the entire diapir width. The remaining two thirds are heavily eroded by wave action.

In line with Giles et al. (1997b), the exposure over which measurable data can be collected is interpreted to be Middle Windsor Group strata. This interpretation is based upon the predominance of gypsum within the outcrop and the lack of any distinctive Hood Island Formation limestones. Limestones within the exposure are thin (<1m) and are separated by thick gypsum units. The lack of red mudstone/siltstone strata also suggests a Middle Windsor age.

3.2.5, Structural Carapace.

The Middle Windsor Group exposure is interpreted to be part of a structural carapace overlying the halite core of the St. Rose Diapir. The exposed carapace consists mostly of white gypsum with minor, brecciated limestones and red mudstones (Figure 3.2.4).

The deformation within the diapir exposure is asymmetric, with deformation decreasing progressively from the north-east to south-west. The north-east end of the exposure contains highly foliated gypsum units in a sub-vertical orientation (dip 70 - 85 degrees).

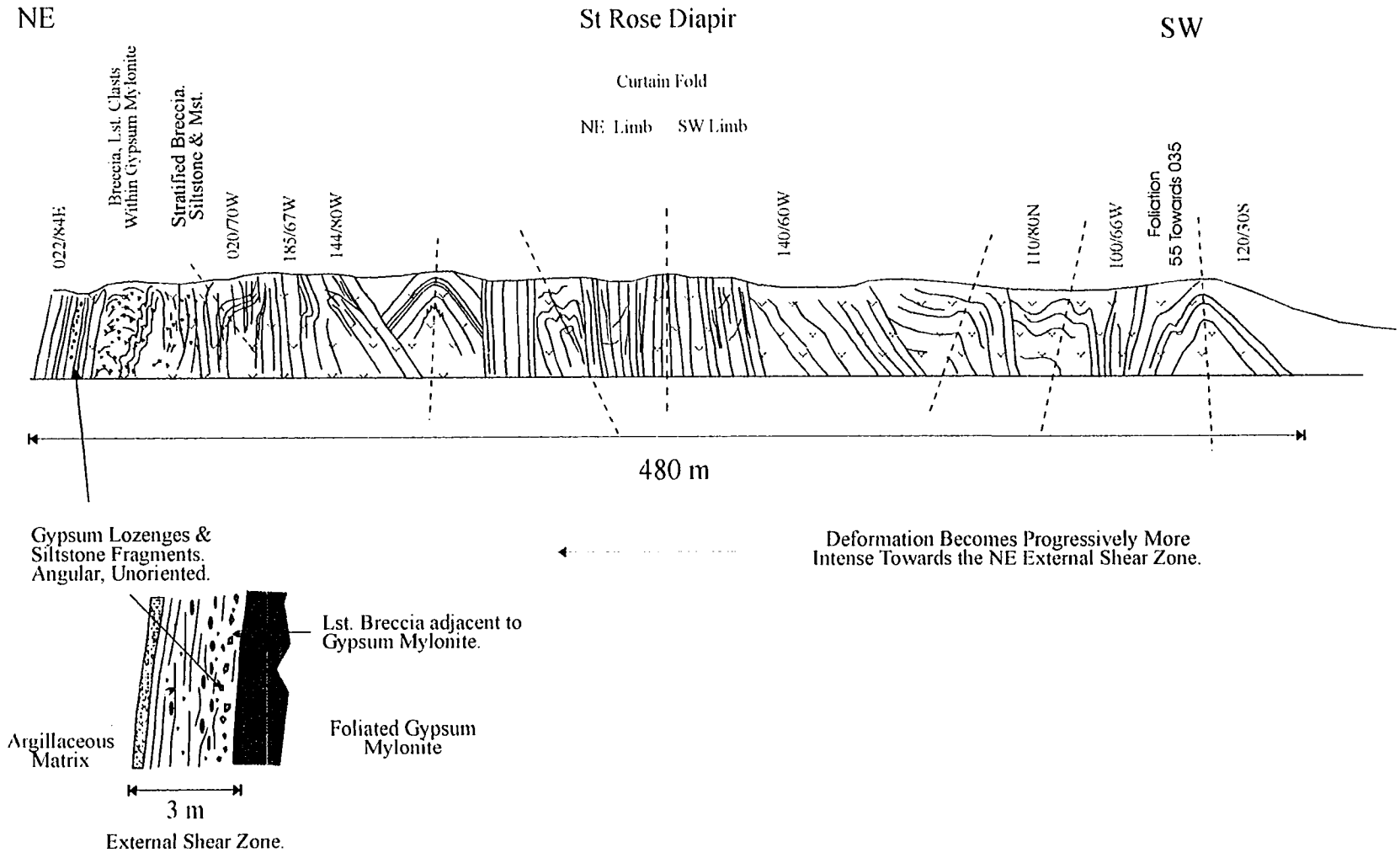

Figure 3.2.4. The St. Rose Diapir.

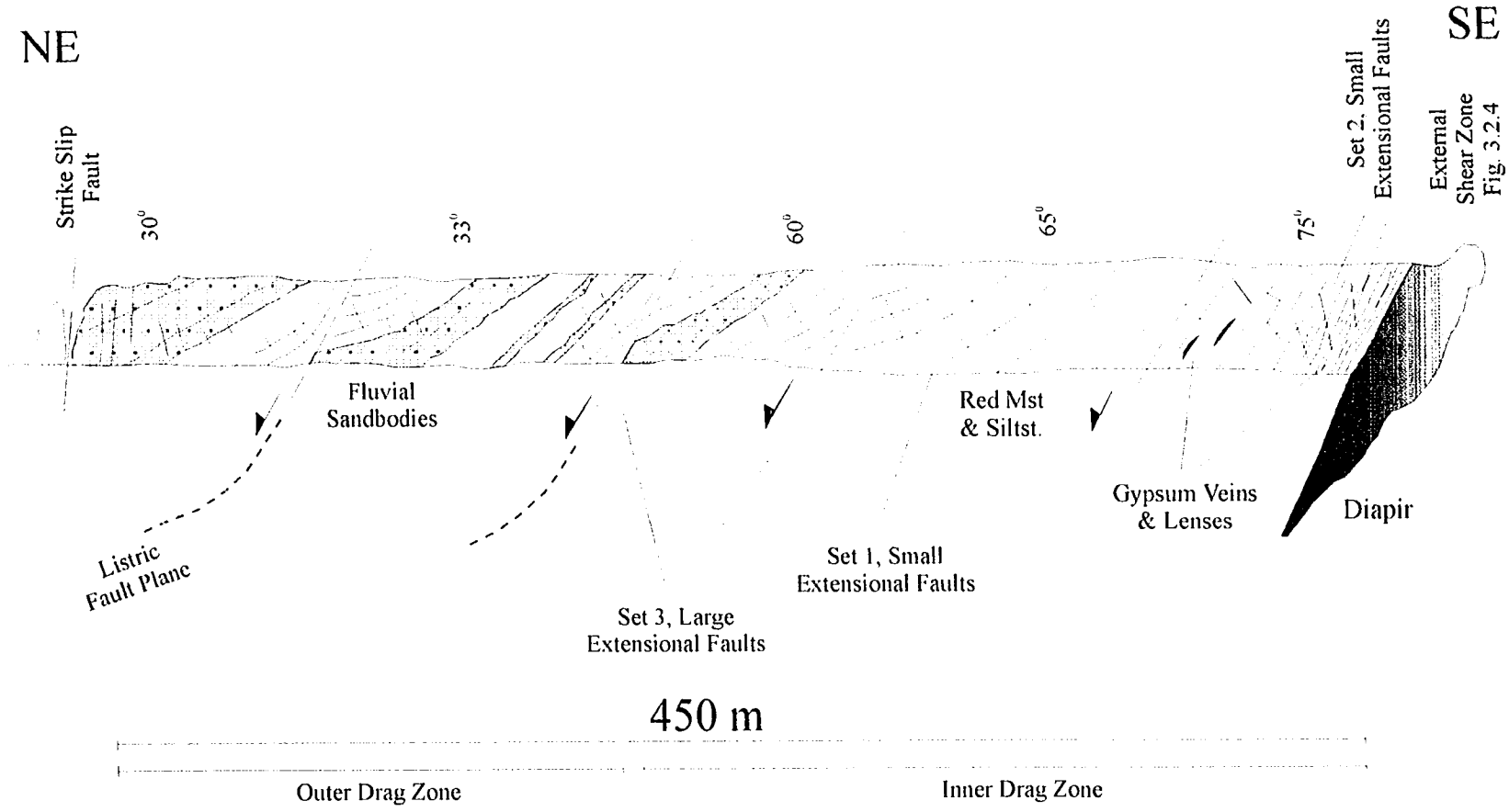

Figure 3.2.5. The North-East Drag Zone of the St. Rose Diapir.

Towards the south-west, the stratigraphic units dip more gently (~60 degrees) and fold hinges are observed. The folds have interlimb angles of 30 - 50 degrees, with moderate plunges of ~10-20 degrees (Figure 3.2.4).

Fold Geometry

Interpretation. At first glance, there appears to be no overall structural pattern to the diapir exposure. However, the outcrop can be interpreted to be part of a large, kilometre scale fold similar to that proposed for the Monks Head Diapir exposure of the Salt Wall Luey (see below, Chapter 3.6). The north-eastern portion of the diapir exposure strikes north-south with a sub-vertical stratal dip, whereas the south-western portion of the diapir units dip either south-east or north-west at between 66 and 33 degrees. If the two portions of the diapir exposure are considered to be opposite limbs of a fold, then the structural data define an anticline, plunging at between 33 and 66 degrees to the SSE (Figure 3.2.4).

3.2.6, The North-East External Shear Zone

The north-east external shear zone is a 3 m wide shear zone that forms the contact between Middle Windsor Group strata of the St. Rose Diapir and the surrounding Colindale Member, Port Hood Formation overburden (Figure 3.2.4). The external shear zone is zoned and a progressive increase in strain towards the diapir was noted.

- The outermost zone of the external shear zone consists of highly sheared mudstones that have a sub-vertical foliation parallel to bedding. Rare prolate gypsum lozenges (5-10 cm diameter) are included within the sheared mudstone. The prolate lozenges are aligned with their long axes dipping sub-vertically.

- The central zone of the external shear zone consists of prolate gypsum lozenges and angular siltstone fragments (~2-3cm) within a sheared mudstone matrix. The

concentration of gypsum lozenges and siltstone fragments increases across this zone towards the diapir margin. The orientation of the prolate lozenges indicates a sub-vertical shear at this location that is appropriate for the margin of a diapiric structure.

- The innermost zone of the external shear zone consists of a limestone breccia in contact with a gypsum unit of the St. Rose Diapir. The limestone breccia consists of angular Windsor Group limestone clasts (2-5 cm) which show no preferred orientation despite being entrained within a shear zone. The limestone breccia is effectively a layer one clast thick. It was noted at several locations within the field area that units of relatively unstrained rocks could be found within the external shear zone of a diapir. These rock units are typically surrounded by highly sheared rocks and it is thought that the unstrained units represent pieces of rock that have been entrained within the shear zone but transported in a relatively undeformed state, perhaps due to lithological/rheological properties.

3.2.7, The North-East Drag Zone

The north-east drag zone of the St. Rose Diapir is well exposed throughout its entire 450 m length and has yielded a large amount of structural data.

The north-east drag zone of the St. Rose Diapir contains structural features that are very similar to those found within the Broad Cove Diapir (north-east drag zone). Four separate deformation styles were observed, each of which is distinct in space and time (Figure 3.2.5).

Drag Zone Folding

The Colindale Member, Port Hood Formation strata form a dip fan within which the dip of the strata increases from approximately 30 degrees at the start of the drag zone to 87

degrees at the external shear zone (Figures 3.2.5 and 3.2.6).

The folding of the strata within the drag zone is not a smooth folding profile. Fault drag associated with Set 3 extensional faults (see below) has disrupted the drag zone profile at 55m, 90m, 145m, 165m and 250m (Figures 3.2.6 and 3.2.7). The stratal dip increases markedly within 20m of the external shear zone from 68 to 87 degrees. The total amount of stratal rotation within the drag zone is approximately 48 degrees +/- 8 degrees. The stratal rotation quoted above is a visually estimated value, not a statistically derived value (see above, Chapter 3.1).

The strike of the drag zone strata is almost constant at 030 degrees. This strike is parallel to the assumed margin of the St. Rose Diapir but slightly oblique to the coastal section, which is oriented north-east/south-west (Figure 3.2.7).

Faulting

Set 1, Small Extensional Faults

A pervasive set of extensional faults is present throughout the north-east drag zone. These faults are characterised by:

- A small displacement. The maximum observed displacement was ~20cm. In most cases, displacement is 1-2 cm.

- Little or no fault drag. The faults appear to be entirely brittle fractures showing mode 1 fracturing within competent siltstones and mode 2 shearing within incompetent mudstones. The mode 1 fracturing suggests that the faults formed at shallow burial depths with small confining pressures.

- The faults generally do not extend for more than a few metres. Faults commonly terminate at a bedding plane intersection.

The Set 1 extensional faults show a progressive rotation of the fault plane as the external shear zone is approached (Figures 3.2.8 and 3.2.9). Within the outer part of the drag zone, the faults dip at 88-60 degrees and have a 50 to 60 degree angle to bedding. Within the inner drag zone, the faults dip at 32 to 52 degrees, giving a total fault plane rotation of 33 to 40 degrees. The rotation of the fault planes is approximately the same as strata folding (~48 degrees) so that the faults maintain a 50 to 60 degree angle to bedding.

The strike of the Set 1, small extensional faults does not show any systematic orientation. Throughout the drag zone, the faults show a spectrum of orientations between orthogonal to and parallel to the diapir margin, with a range of ~80 degrees. An empirical observation would be that the majority of faults tend to have an orthogonal trend (Figure 3.2.7).

Set 2, Small Extensional Faults

Within 50 m of the external shear zone, a new set of extensional faults can be distinguished (Figure 3.2.5). These faults are identical to the Set 1 extensional faults, except they do not appear to have been rotated since they maintain a high fault plane dip of 73-77 degrees (Figure 3.2.8).

Set 3, Large Extensional Faults

A third set of extensional faults is observed within the north-east drag zone. These faults are characterised by:

- A relatively large offset. The strata in the hangingwall and footwall cannot be

Figure 3.2.6. Dip of the strata within the north-east drag zone of the St. Rose Diapir. The best-fit line is a visual estimate of the stratal dip. Set 3, large extensional faults have disrupted the strata in such a way that a large proportion of the drag zone strata are affected by fault drag. Footwalls and hangingwalls of Set 3 faults are indicated (FW and HW respectively).

Figure 3.2.7. Strike of the Set 1 and Set 2 faults and strata within the north-east drag zone of the St. Rose Diapir. Best-fit lines are visual estimates. The stratal strike is approximately constant at 020 degrees. Set 1 and Set 2 faults do not appear to have a consistent orientation.

Figure 3.2.8. Fault plane dip for the Set 1 and Set 2 faults. The best fit line is a visual estimate. Set 1 faults are seen to have been rotated by Set 3 faults, which can be seen graphically as anomalously high fault plane dips.

Figure 3.2.9. Arithmetic mean of the fault plane dips for the Set 1 and Set 2 faults. For each outcrop measurement location the recorded fault plane dip values were summed and divided by the number of readings to produce a mean value. This mean value incorporates fault planes, which are rotated by Set 3 faults.

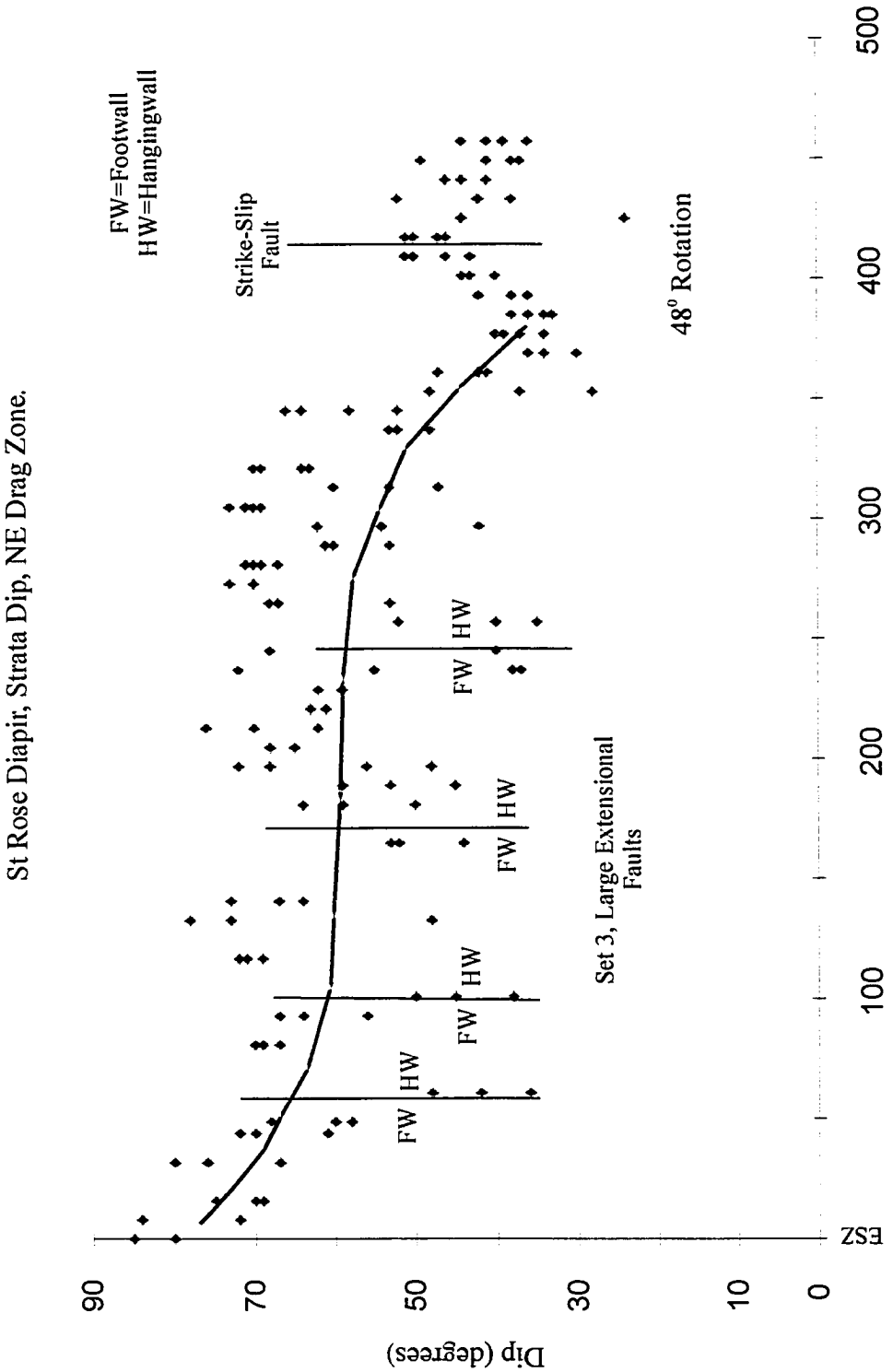
St Rose Diapir, Strata Dip, NE Drag Zone.
FW=Footwall
HW=Hangingwall
Strike-Slip Fault
48° Rotation
Set 3, Large Extensional Faults
FW
HW
Dip (degrees)
90
70
50
30
10
0
ESZ
100
200
300
400
500
Horizontal Distance from Diapir (m)

Figure 3.2.6

St Rose Diapir, Strike of the Set 1 and Set 2 Small Extensional faults.

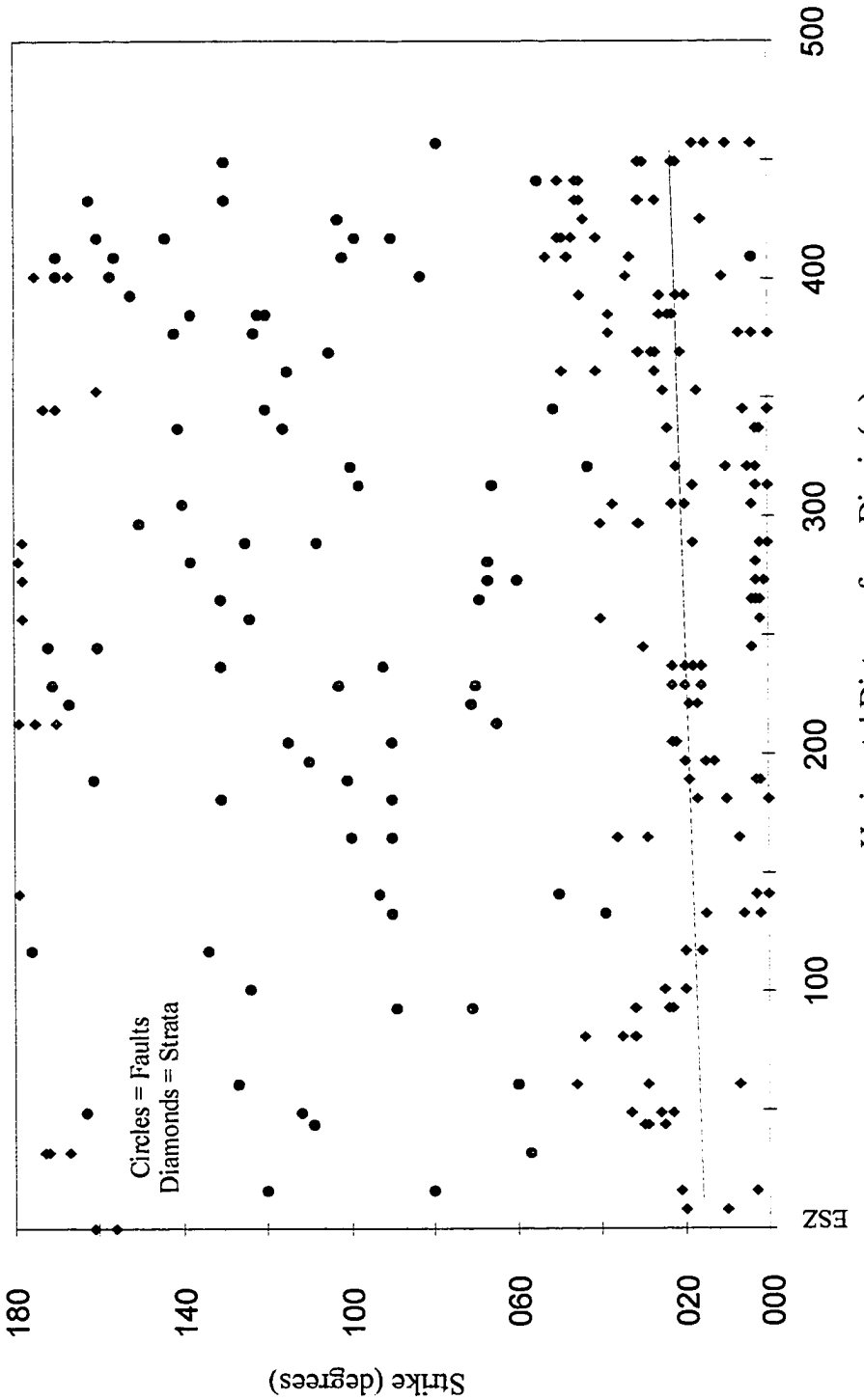

Figure 3.2.7

St. Rose Diapir, Fault Plane Dip, Set 1 and Set 2, Small Extensional Faults.

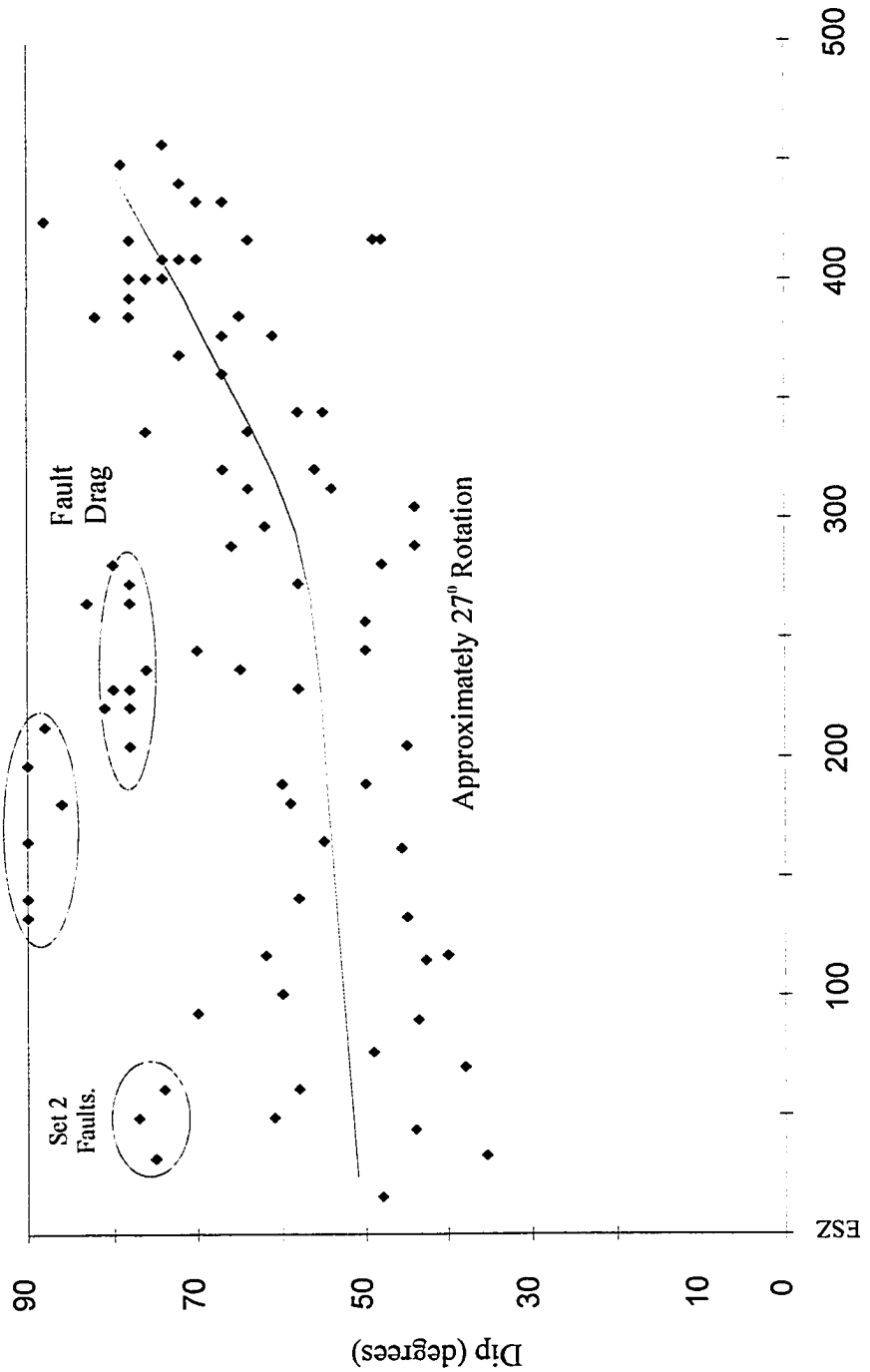

Figure 3.2.8

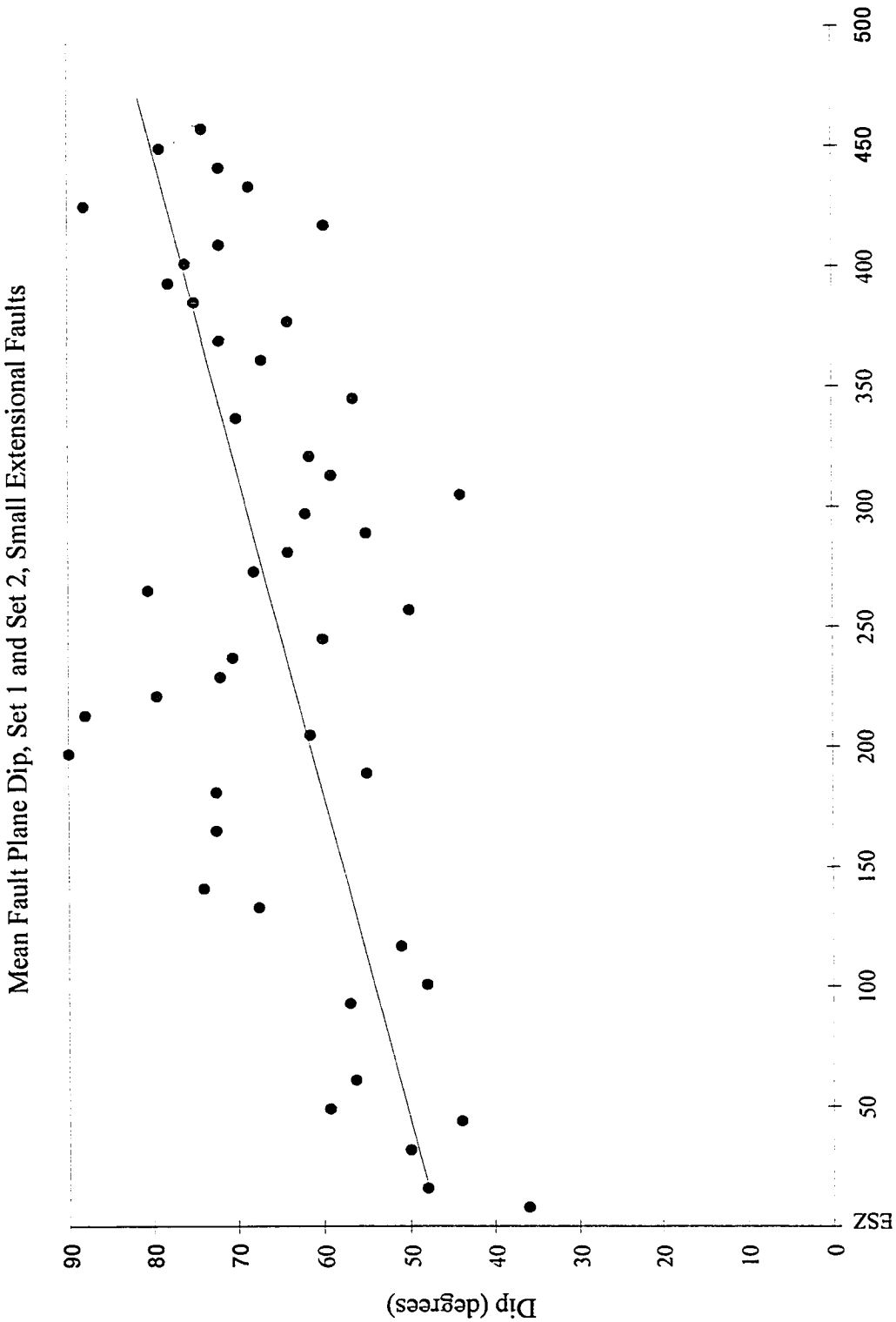
Mean Fault Plane Dip, Set 1 and Set 2, Small Extensional Faults
Dip (degrees)
0
10
20
30
40
50
60
70
80
90
ESZ
50
100
150
200
250
300
350
400
450
500
Horizontal Distance from Diapir (m)

Figure 3.2.9

matched, suggesting that the fault displacement is at least equal to the height of the cliff (>5-10m).

- Extensive fault drag. Strata in the hangingwall appear to have been rotated onto the fault plane so that they dip at a slightly lower angle than the adjacent footwall strata away from the fault. Strata in the hangingwall appear to have been rotated to a higher angle as the fault plane is approached (Figure 3.2.6). Set 1, small extensional faults have been rotated with the fault drag, indicating an older/younger genetic relationship (Figure 3.2.8).

- An orientation sub-parallel to the surrounding drag zone strata and diapir margin.

There are four Set 3, large extensional faults located within the drag zone. The Set 3 extensional faults are found throughout the width of the drag zone and do not partition the drag zone into an inner and outer drag zone, as is the case at Broad Cove (see Chapter 3.1).

Subordinate Drag Zone Structures

Numerous small scale, bedding-parallel slip surfaces were recorded within the more steeply dipping portion of the drag zone (55-70 degrees). The slip surfaces often end in small-scale compressional duplexes and commonly displace more competent siltstone units over incompetent mudstones. The orientation of the duplexes indicates transport of strata away from the diapir. No other kinematic indicators, for example slickensides, were observed in connection with the slip surfaces.

3.2.8, General Conclusion

The drag zone deformation described above for the St. Rose Diapir is very similar to the deformation described for the north-east drag zone of the Broad Cove Diapir (see Chapter

3.1). The folding, and in particular the faulting, fault sets and fault orientations, are very similar in both drag zones. An obvious exception to the similarity is that the small extensional faults (Set 1) at St. Rose do not show the polarised strike orientations that are seen at Broad Cove. The lack of a consistent strike orientation may be related to the deflation of the diapir described earlier. If the diapir or the source layer is undergoing deflation, the overburden (including the drag zone) must be reacting to the change in salt volume. If salt is withdrawn at depth, the overburden must subside to take up the volume space. Subsidence may well involve folding, fracturing and rotation of portions of the overburden that could affect the orientation of pre-existing structures, for example faults. Also, folding may create new fractures that overprint pre-existing fractures. These new fractures will have an orientation that is related to the pattern of salt withdrawal, not diapiric growth.

3.3. THE FINLAY POINT DIAPIR

3.3.1, Geographic Data

The Finlay Point Diapir is located at the northern end of Mabou Mines beach, immediately behind the fishing wharf at latitude 46N,22,30 longitude 61W,21,10 (Figures 3.3.1 and 3.3.2). The drag zone section is approximately 350 m long and is located on the WNW flank of the diapir. Finlay Point is covered by the 11K/3 topographical map.

3.3.2, General Information

Haites (1952) correlated the Coal Mine Point section with Finlay Point and described both the Finlay Point Diapir and Coal Mine Point Diapir as a single salt structure. This interpretation was entirely reasonable, given the lack of seismic data at the time.

3.3.3, The Finlay Point Diapir - Seismic Data

A north-east/south-west cross-section through the Finlay Point Diapir is imaged on Mabou lines 11 and 12. These seismic sections show that the Finlay Point Diapir has a strongly asymmetric geometry. The south-western diapir/overburden contact is a steeply dipping fault contact with Inverness Formation sedimentary rocks, whereas the north-eastern contact is a gently dipping (~41 degrees) semi-concordant contact between Inverness Formation sedimentary rocks and the diapiric strata (see Mabou line) (Figure 3.3.3). By tying line 11 to line 12 in an east/west direction, it can be shown that the western flank of the Finlay Point Diapir dips to the west at a similar angle to the north-east flank (~41 degrees) (Figure 3.3.3). The eastern flank of the Finlay Point Diapir is not exposed and is not covered by seismic data. In addition, the Mabou seismic data is only shown to 1.0 sec TWT and so the base of the Finlay Point Diapir is not imaged. As with the other diapiric structures within western Cape Breton, the relationship of the diapir to basement faulting cannot be constrained. The Finlay Point Diapir may be located adjacent to a strand of the Hollow Fault, which may be either an extensional, reverse or

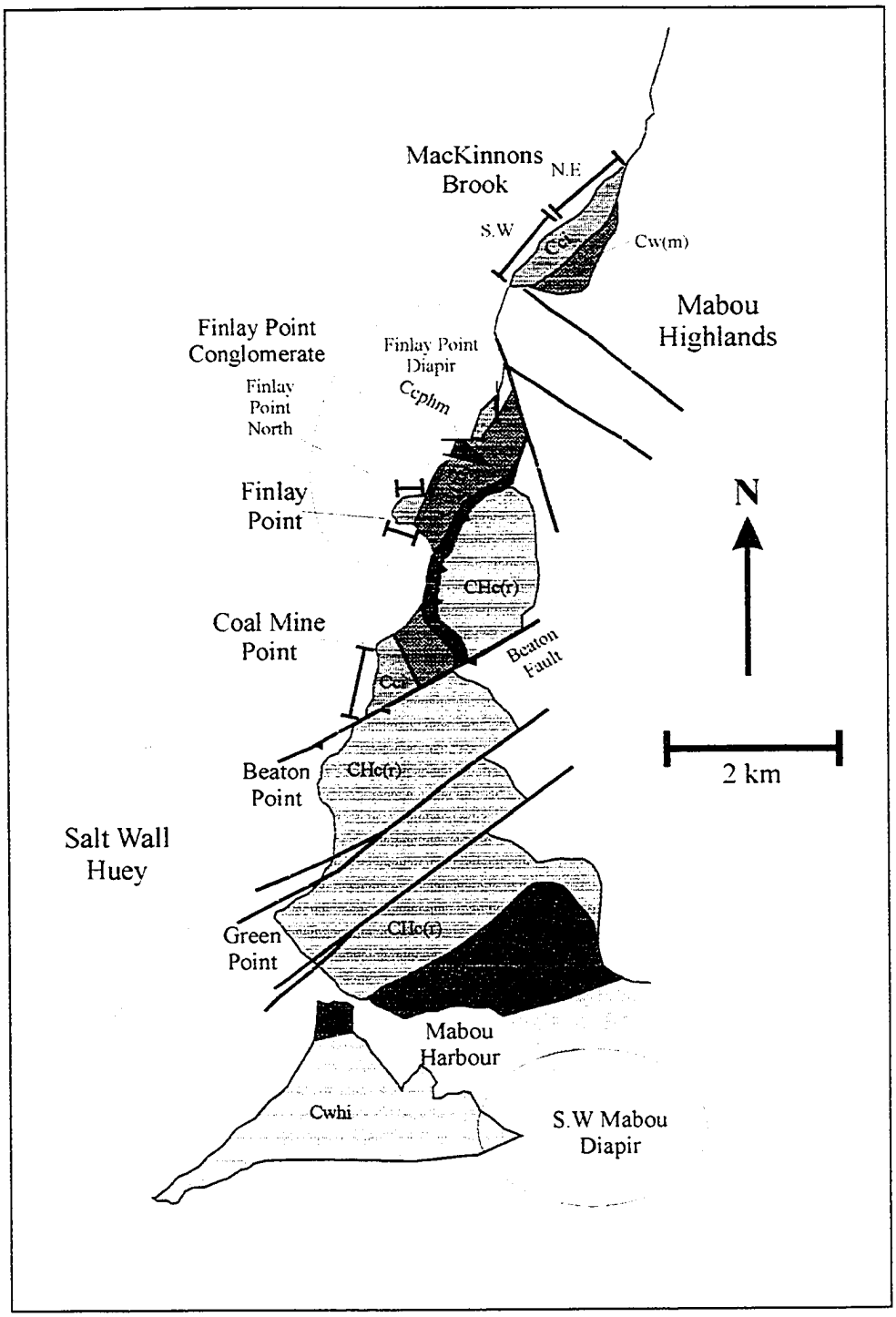

Figure 3.3.1. Geological map of the Mabou Mines area. Also shown are the outlines of the Finlay Point Diapir, the Salt Wall Huey and the Southwest Mabou Diapir. Modified from Giles et al. (1997b).

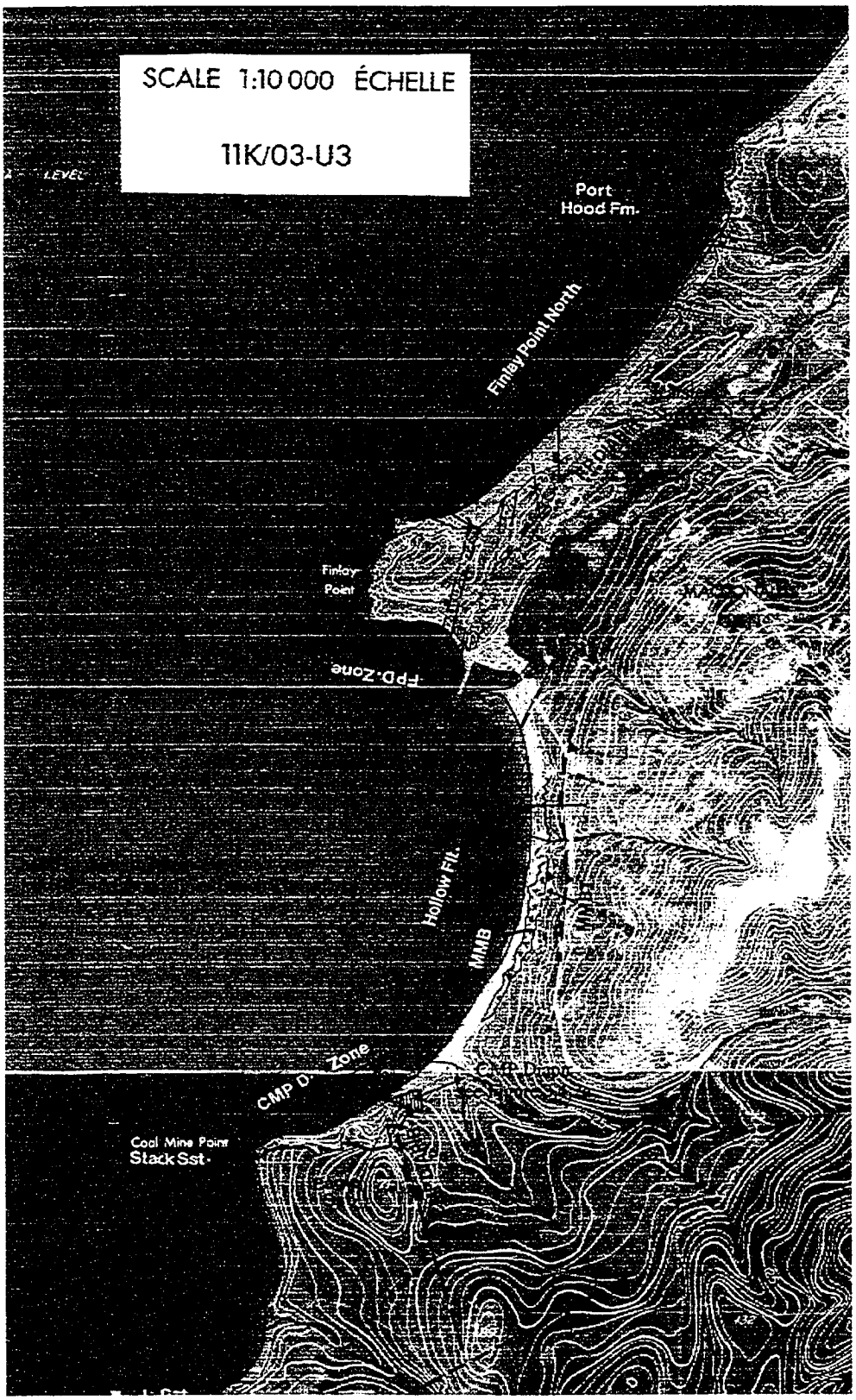

Figure 3.3.2. Orthophotograph of the Mabou Mines area to show the positions of the Coal Mine Point Diapir and the Finlay Point Diapir.

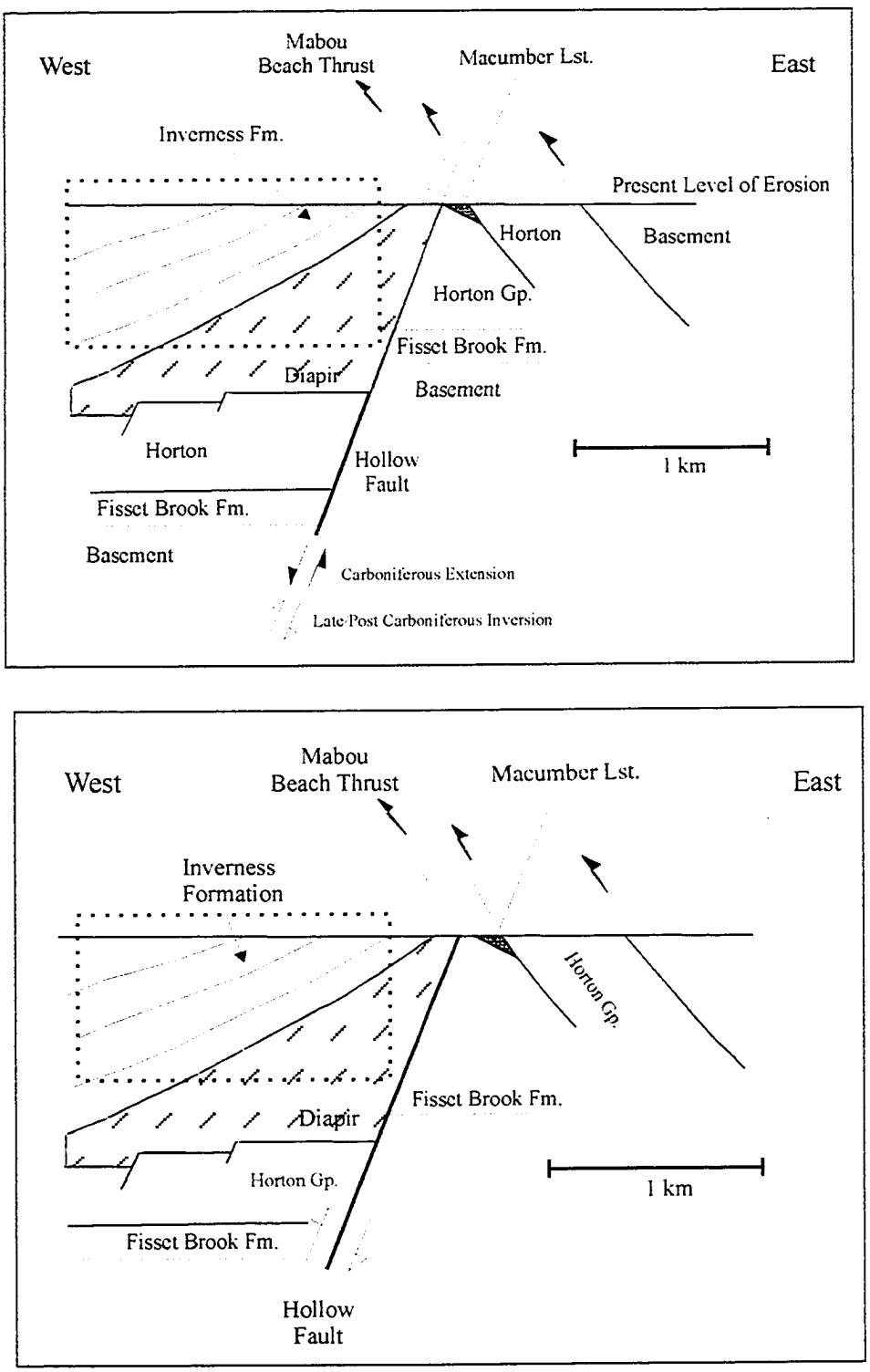

Figure 3.3.3. Schematic cross-sections across the Finlay Point Diapir, and the Hollow Fault to show two possible configurations . Top model assumes that the Hollow Fault is an extensional fault. Bottom model assumes the Hollow Fault is a reverse fault. Dotted box shows extent of seismic coverage.

strike-slip fault at this location.

On the north-eastern and western flanks, the Carboniferous strata (probably Port Hood Formation and Inverness Formation) have been lifted actively above the rising salt. The geometry can be visualised as a trap door where the hinged door surface actively lifts and rotates the Carboniferous overburden, while the door opening is defined by steep faults (Figure 3.3.4). While the seismic data does not constrain the maximum age for growth of the diapir, it does indicate that the Finlay Point Diapir had a significant growth phase after the deposition of the Inverness Formation (Westphalian D).

3.3.4, Geology of the Finlay Point Area (Figures 3.3.1 and 3.3.2)

In order to fully describe the Finlay Point Diapir, the surrounding geology of the Finlay Point area must be described and placed in context with the diapir.

The Finlay Point diapir exposure is described as two sections. The Finlay Point section extends 500 m west from the fishing wharf to Finlay Point. This section is oriented orthogonal to the trend of the Finlay Point Diapir and so can be thought of as a dip section. The Finlay Point North section extends 1.75 km NNE from Finlay Point to the contact of the Inverness Formation with Ordovician basement rocks of the Mabou Highlands. This section is oriented parallel to the western margin of the Finlay Point Diapir and so can be thought of as a strike section (Figure 3.3.2).

Inland of the coastal exposure, the Finlay Point Diapir is poorly exposed along a karsted surface. Numerous sinkholes extend from the exposed gypsum at Finlay Point in a NNE direction towards the faulted contact of Carboniferous rocks with Ordovician basement rocks of the Mabou Highlands.

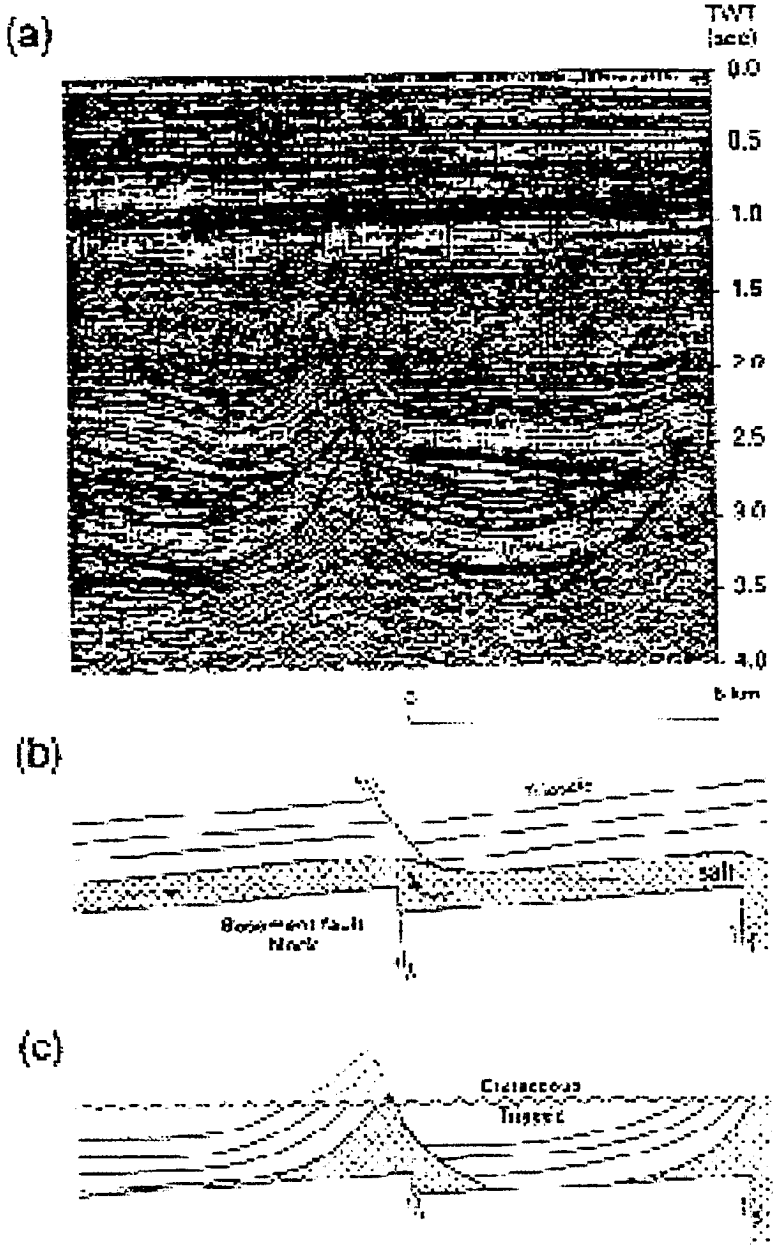

Figure 3.3.4. An example of a reactive/active diapir. (A) is a seismic section across a trap-door diapir and (B) and (C) show an interpretation of how the diapir developed. Basement faulting (extension) creates differential loading of the salt layer and faulting within the overburden. Differential loading initiates salt withdrawal while the overburden faults allow the salt to migrate vertically. Footwall strata are rotated to form the trap-door geometry. From Remmelts, 1995.

Relationship of the Finlay Point Diapir to the Hollow Fault

On its eastern flank, the Finlay Point Diapir is juxtaposed against Horton and basement rocks. On its western flank, it is juxtaposed against at least 1.5 km of Upper Carboniferous strata (Port Hood Formation and Inverness Formation, defined on seismic data) that lie within 1 km of the present shore line (Figures 3.3.1 and 3.3.3). This geological configuration requires that at least 1.5 km of subsidence must have occurred during the Westphalian A - Westphalian C/D adjacent to the coastline in order to allow deposition of the Port Hood and Inverness Formation strata and to allow growth of the Finlay Point Diapir into these sediments. A simple way to create the required accommodation space is as a hangingwall basin to an extensional fault. As outlined in Chapter 2, this fault could represent a segment of the Hollow Fault. The fault would have a similar geometry to the Hollow Fault segment imaged on line 79 of the 1982 Chevron seismic survey, although with opposite polarity. As described above and in Chapter 2, the seismic data does not cover the Hollow Fault (or any faults adjacent to the coastline of Cape Breton). The Finlay Point Diapir could be located in the footwall of a reverse fault. The exact configuration of the diapir relative to a basement fault and indeed the existence of a basement fault in the Finlay Point area therefore remains speculative.

The value of 1.5 km of tectonic subsidence does not take into account subsidence related to salt withdrawal. The estimated thickness of the Lower Windsor halite is 540 m for the St. Georges Bay area (see Chapter 2), so approximately 540 m of salt withdrawal subsidence could have occurred. The value of salt withdrawal subsidence should be subtracted from the sediment accommodation space required so that the value of 1.5 km is a maximum estimate for tectonic subsidence.

3.3.5, The Finlay Point Diapir, Onshore Exposure (Figures 3.3.5 and 3.3.6)

The Finlay Point Diapir is exposed as a massive, white gypsum unit that contains a pervasive sub-vertical foliation striking approximately east/west. No Windsor Group limestone or disseminated limestone is contained within the gypsum, which makes

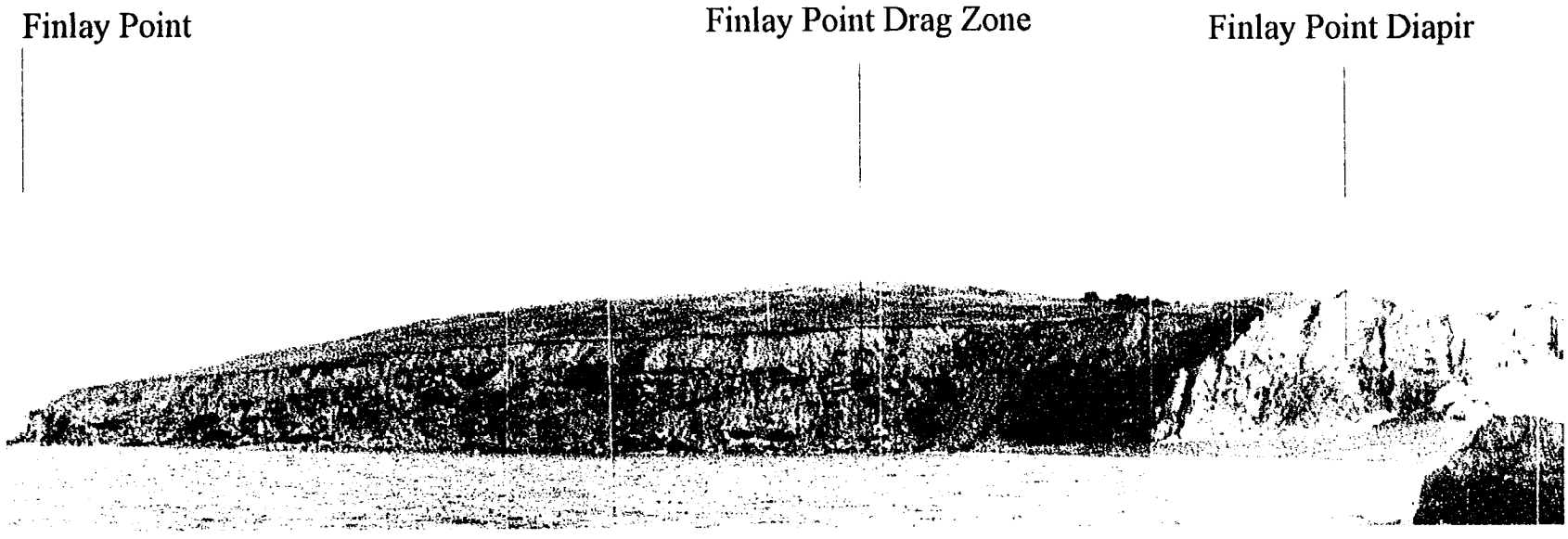

Figure 3.3.5. The Finlay Point Diapir and drag zone (see Figure 3.3.6 for interpretation).

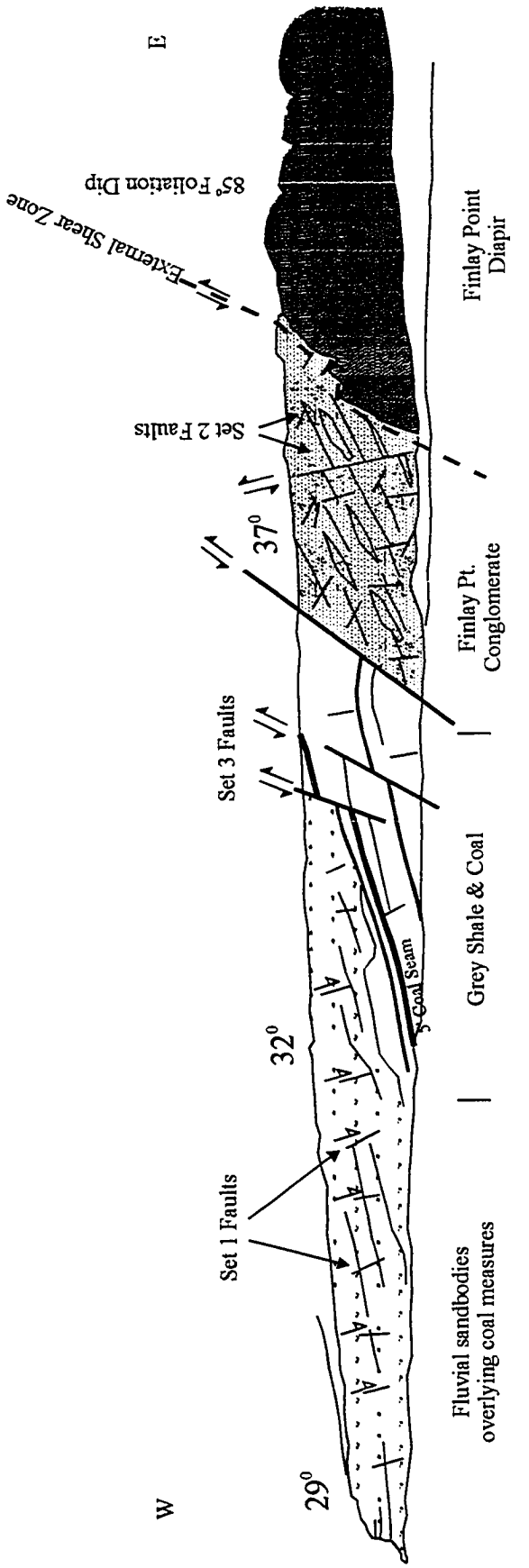

Figure 3.3.6 The Finlay Point Diapir and Drag Zone Section.

stratigraphic correlation difficult and subjective. The Finlay Point Diapir exposure is assigned to the Middle Windsor based upon the lack of thick Hood Island Formation limestones and the absence of the Lower Windsor Macumber limestone at the wharf. Giles et al. (1997a) assigned the Finlay Point Windsor strata to the Lower Windsor based upon its proximity to the Macumber limestone exposed on Mabou Mines beach (the beach between the Finlay Point Diapir and the Coal Mine Point Diapir). However, as described above, the Lower Windsor exposed on Mabou Mines Beach (Macumber Limestone) is probably separated from the Finlay Point Diapir by a segment of the Hollow Fault and therefore the Lower Windsor assessment for the wharf strata may be invalid (Figure 3.3.3).

The North-West External Shear Zone

The Finlay Point diapir is juxtaposed against the Finlay Point Conglomerate by a discrete fault that dips at ~75 degrees to the north-west (Figures 3.3.6 and 3.3.7). Across the fault contact, the gypsum and conglomerate are deformed into small-scale drag folds, indicating an extensional offset across the fault. Deformation is confined to a narrow, 10-15 cm zone adjacent to the fault plane and there is no intercalation of the juxtaposed units.

The Finlay Point Conglomerate

The outcrop of the Finlay Point Conglomerate is ~35 m wide and the unit is a red, polymict conglomerate containing coarse sand, basement (granitic and dioritic), sandstone, siltstone and mudstone clasts. The quartz sand grains are predominantly sub-rounded, whereas the basement clasts are angular to sub-angular. The predominant grain size is 1 - 2.5 mm, although pebble-sized clasts are also present. Graded bedding is common and lenses of coarse sediment resemble minor channel fills.

The Finlay Point Conglomerate is located beneath the Inverness Formation. Although the Finlay Point Conglomerate is a fault-bounded unit, it is only weakly deformed, which

Figure 3.3.7. The faulted contact between Middle Windsor gypsum of the Finlay Point Diapir and the Finlay Point Conglomerate. The contact is a discrete extensional fault with little interleaving of the two stratal units. Reverse faults within the Finlay Point Conglomerate are probably extensional faults, which have been rotated through the vertical.

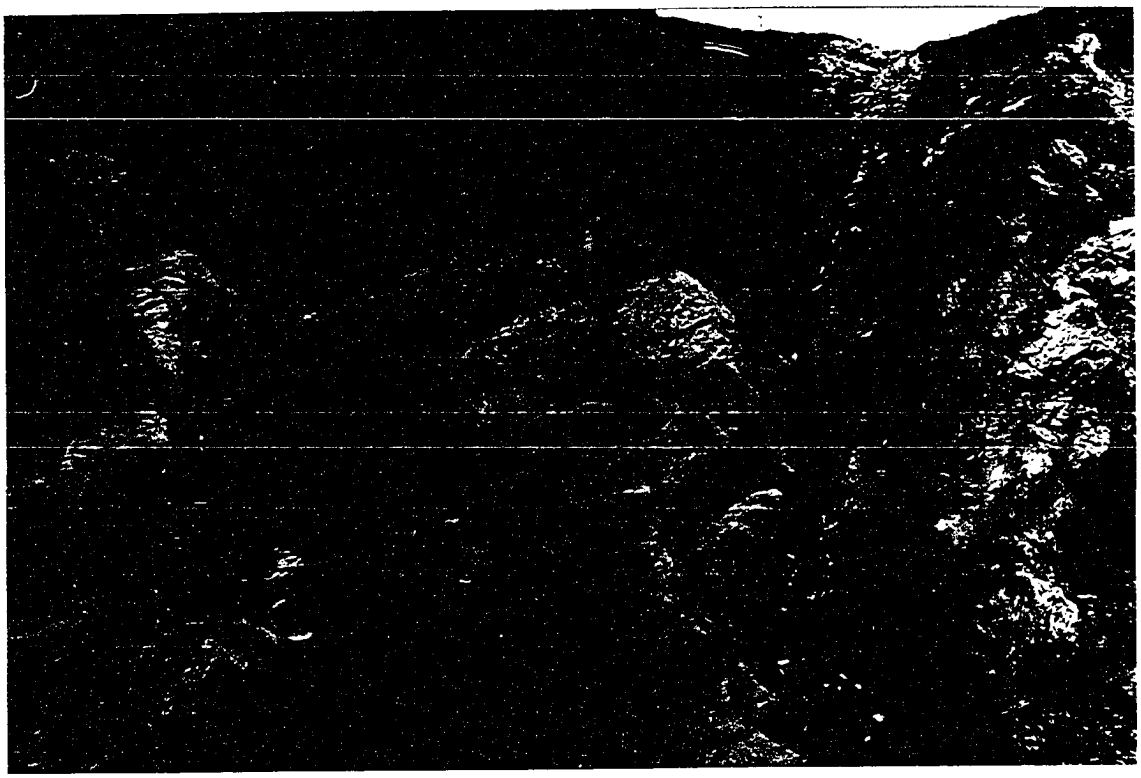

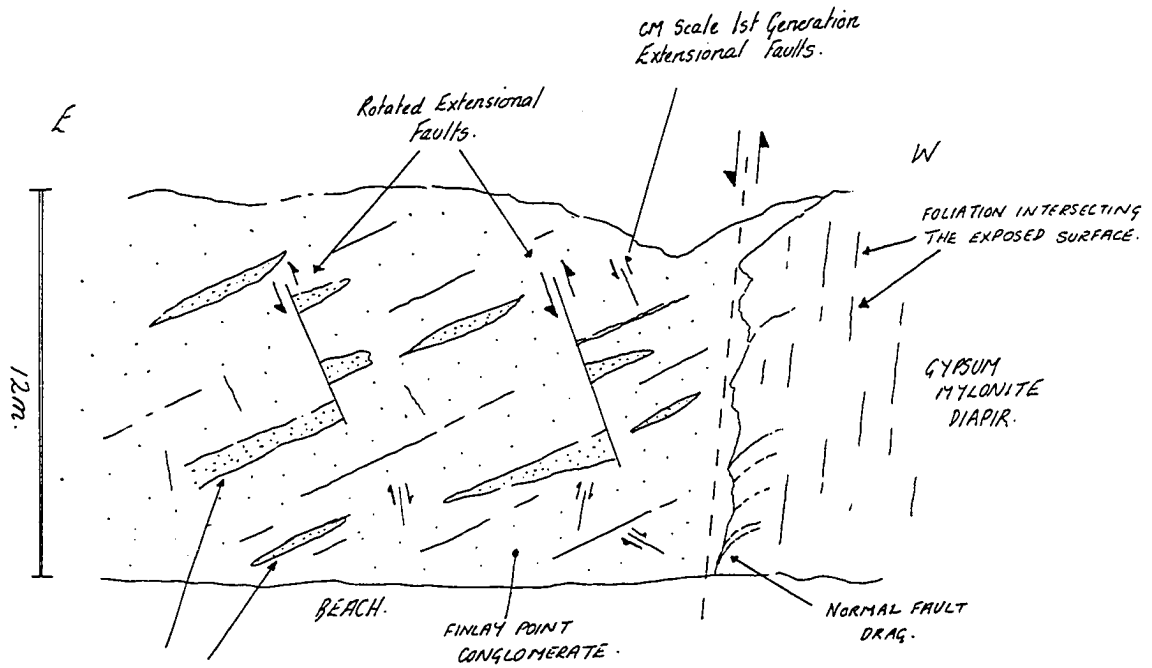

THE FAULT CONTACT BETWEEN THE FINLAY POINT CONGLOMERATE AND THE FINLAY POINT DIAPIR.

Figure 3.3.7

suggests a relatively small displacement from its original stratigraphic position. The Finlay Point Conglomerate is therefore tentatively assigned to the Henry Island Member of the Port Hood Formation (Westphalian A - Westphalian B).

Interpretation. The Finlay Point Conglomerate is interpreted to be a fault scarp clastic wedge that was sourced from the uplifted footwall of the Hollow Fault and adjacent basement massifs. The presence of angular basement fragments suggests that the Mabou Highlands, located ~1.5 km to the north-east, may have been the source area for the basement clasts. This interpretation accords well with the existence, geographic position and timing of movement of the proposed segment of the Hollow Fault to the east of the Finlay Point Diapir.

Following deposition of the Finlay Point Conglomerate, the Finlay Point Diapir intruded the Carboniferous sediments. As the diapir intruded through the conglomerate and the overlying Inverness Formation, the sediments were deformed into the drag zone that is exposed today.

3.3.6, The North-West Drag Zone

The north-west drag zone of the Finlay Point Diapir is well exposed throughout its 250 m length. The drag zone exposure consists of the Finlay Point Conglomerate in fault contact with grey shales, coals and fluvial sandstone bodies (principally the Eagle Sandstone, Dickie, 1986) of the Inverness Formation.

The north-west drag zone contains similar structural features to those described for the Coal Mine Point drag zone (see below) except that the deformation at Finlay Point is considerably less intense. Three separate deformation styles were recorded.

Drag Zone Folding (Figure 3.3.8)

The dip of the Inverness Formation strata is relatively constant at 19 degrees from Finlay

Point to a distance of 24 m from the external shear zone. From this point to the external shear zone, the stratal dip increases rapidly from 19 to 37 degrees. The overall geometry of the drag zone is therefore very different from the Coal Mine Point drag zone, which shows a greater amount of stratal folding within the drag zone.

Interpretation. The small amount of folding throughout most of the drag zone probably reflects the geometry of the underlying diapir (see above). The drag zone exposed onshore corresponds to the northern flank of the Finlay Point Diapir imaged on the Mabou line 11. As described above, the northern flank of the diapir has a simple trap-door-like geometry that has simply rotated the overlying Carboniferous strata as an intact package of strata. There has therefore been little penetration of the diapir through the sedimentary overburden.

Extensional Faults within the Finlay Point Diapir Drag Zone

The distribution of brittle deformation within the Finlay Point diapir drag zone is heterogeneous and is used to divide the drag zone into an inner drag zone (0-40 m from the diapir) and an outer drag zone (40-250 m from the diapir).

Within the drag zone, three sets of faults can be distinguished based upon the dip of the fault plane and displacement across the fault.

Set 1, Small Extensional Faults

Set 1, small extensional faults are characterised by:

- Gypsum vein fibres providing kinematic information of fault offsets. The vein fibres indicate that the majority of the Set 1 faults are extensional faults, although rare reverse and strike-slip fault offsets were recorded.

- A small offset. Maximum displacement recorded was <10 cm, mean displacement

was <2 cm.

- Little or no fault drag. The majority of the faults are simple mode 1 tension fractures with no vein infilling the fault plane.

- A short length, usually less than 1.5 m. The faults are pervasive throughout the drag zone, although their concentration falls significantly in the outer drag zone.

- Low angle fault planes with recorded dips of between 15 and 50 degrees within the inner drag zone (Figure 3.3.9). No low angle extensional faults were recorded at greater than 40 m from the external shear zone and so the Set 1, small extensional faults are restricted to the inner drag zone (Figure 3.3.9).

Set 2, Small Extensional Faults

A second set of small faults can be defined based on their angle to bedding (Figure 3.3.9). The criteria are similar to that used at Broad Cove (see above, Chapter 3.1). Set 2, small extensional faults are characterised by:

- A small displacement. Maximum displacement recorded was <10 cm, mean displacement is <2 cm.

- An extensional offset as indicated by gypsum veins.

- Little or no fault drag. The majority of the faults are simple mode 1 tension fractures.

- A short length, usually less than 1.5 m.

Density and Strike of Small Extensional Faults (Set 1 and Set 2)

The density of Set 1 and Set 2 faults is greatest within the inner drag zone (4-6 faults per metre) and decreases progressively away from the diapir margin to about 1 fault per metre. The Set 1 extensional faults have a very specific orientation with respect to the margin of the Finlay Point Diapir. Faults strike either parallel to or orthogonal to the margin of the diapir (Figure 3.3.10). The faults therefore consist of two fault sets orientated at 90 degrees to one another in a similar way to those described from the Broad Cove drag zone.

Set 3, Large Extensional Faults

Set 3, large extensional faults are characterised by:

- An offset in the order of metres to tens of metres.
- An orientation sub-parallel to the NNE/SSW margin of the Finlay Point Diapir.
- A high fault plane angle of 52-65 degrees.

These large extensional faults cross-cut the more shallowly dipping drag zone strata, displacing the Inverness Formation sandbodies and the two exposed Inverness Formation coal seams (15' and 5' equivalent) by 3-5 m (Figure 3.3.6). The Finlay Point Conglomerate is juxtaposed against the Inverness Formation by one of these large extensional faults. Although the true displacement of this fault cannot be seen, the displacement across this fault must be at least 10 m (the full height of the cliff), as the Finlay Point Conglomerate is not exposed in the hangingwall of the fault.

Micro-Faults

Micro-faults identical to those described for Coal Mine Point (Chapter 3.4) were recorded from the Finlay Point drag zone. The micro-faults have a density of 10-25 faults per metre within the inner drag zone (<40m) (Figure 3.3.11), which is about half the value recorded

for the Coal Mine Point drag zone. The micro-fault density falls abruptly within the outer drag zone to approximately 1-3 faults per metre. This fall in fault density corresponds to the lithological change from the Finlay Point Conglomerate to Inverness Formation shales, coals and sandstones. It is likely that the fall in micro-fault density is related to buffering of deformation by the incompetent shales and coals. This rapid decrease in the number of micro-faults stratigraphically above the grey shale facies and away from the external shear zone is similar to that observed at Coal Mine Point (see Coal Mine Point, Chapter 3.4).

Figure 3.3.8. Stratal Dip within the Finlay Point Diapir Drag Zone. Approximately 12-15 degrees of stratal rotation has occurred. The large range is probably caused by fault drag associated with Set 3 faults. The stratal rotation is a visual estimate and not a statistical average.

Figure 3.3.9. Fault Plane Dip of the Set 1 and Set 2 faults within the Finlay Point Diapir Drag Zone. The fault plane dips separate into two groups, which differentiate the Set 1 (rotated) faults from the Set 2 (non-rotated) faults.

Figure 3.3.10. Strike data for the Set 1 and Set 2 faults and the drag zone strata. The strike of the drag zone strata (diamonds) is relatively constant at ~080 degrees, parallel to the trend of the diapir margin. The faults (squares) have an orientation either orthogonal to or parallel to the trend of the diapir margin and the strike of the drag zone strata. Within the inner drag zone (<40m from the diapir) the majority of faults are orthogonal.

Figure 3.3.11. Micro-fault density within the inner drag zone is relatively constant at approximately 18 faults per metre. Fault density falls abruptly within the outer drag zone to 1-3 faults per metre. The high number of faults in the coal seam probably reflects the tendency of coal to form micro-faults during diagenesis.

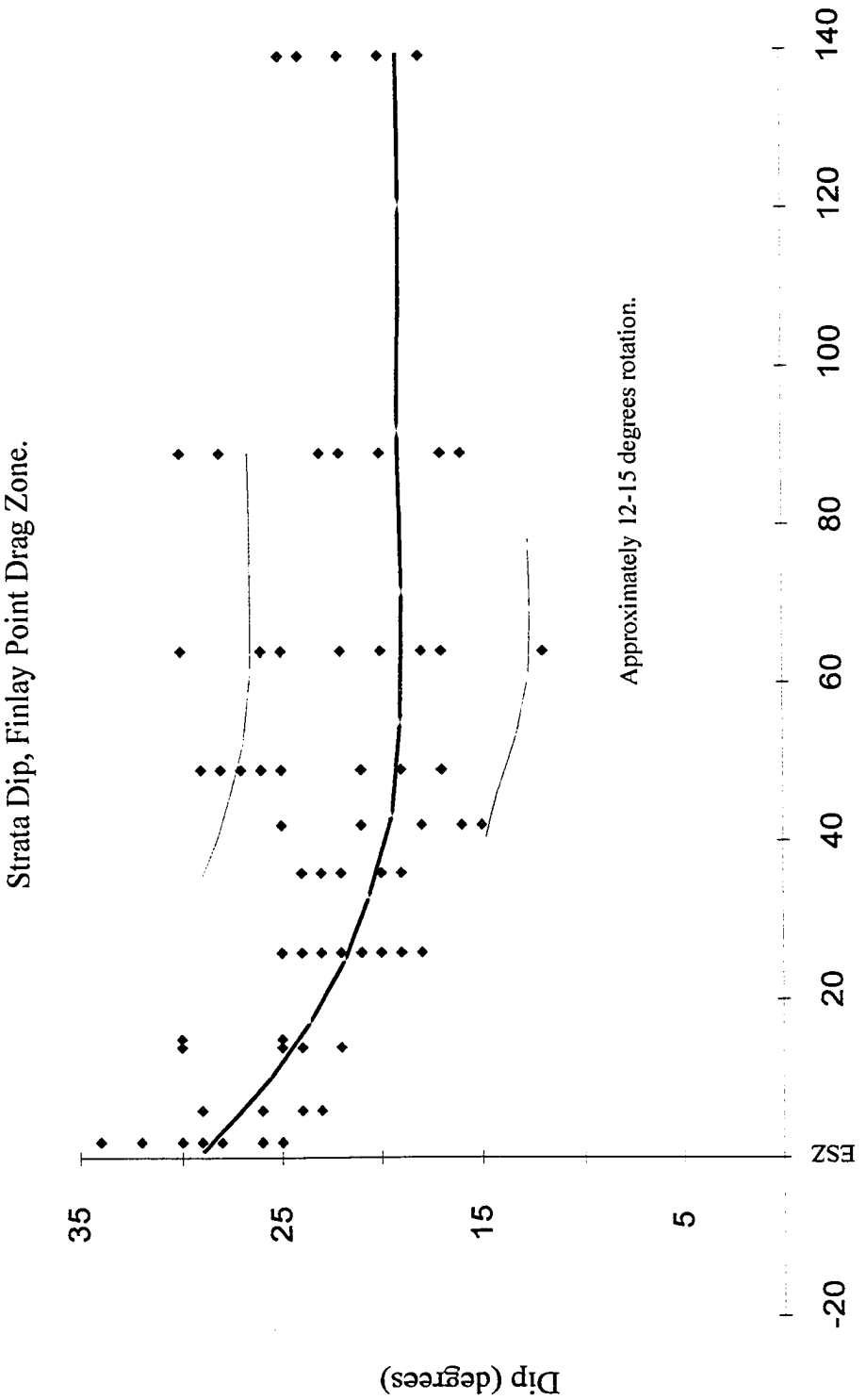
Strata Dip, Finlay Point Drag Zone.
Approximately 12-15 degrees rotation.
Dip (degrees)
35
25
15
5
ESZ
-20
20
40
60
80
100
120
140
Horizontal Distance from Diapir (m)

Figure 3.3.8

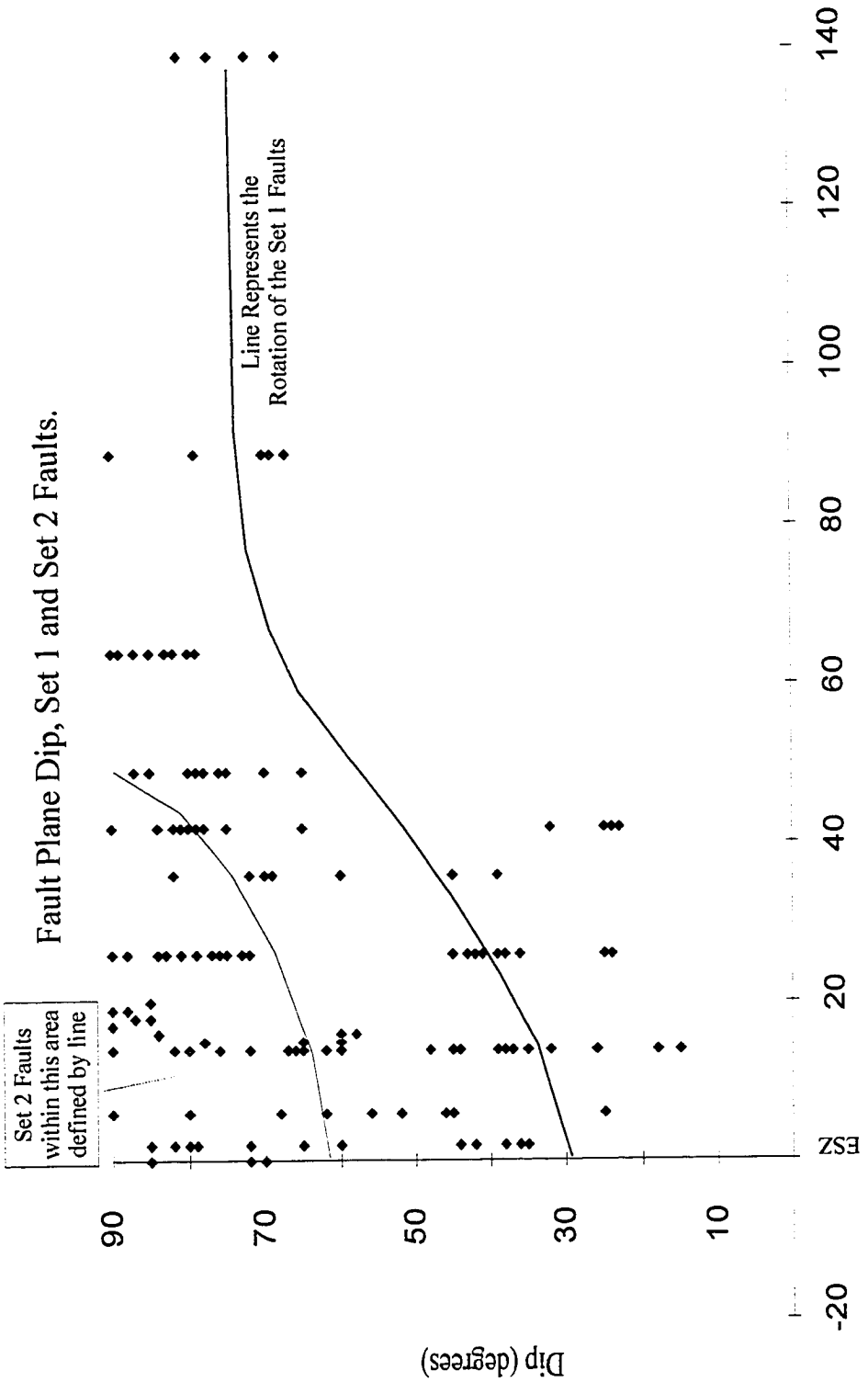
Fault Plane Dip, Set 1 and Set 2 Faults.
Set 2 Faults within this area defined by line
Line Represents the Rotation of the Set 1 Faults
Dip (degrees)
90
70
50
30
10
-20
ESZ
20
40
60
80
100
120
140
Horizontal Distance from Diapir (m)

Figure 3.3.9

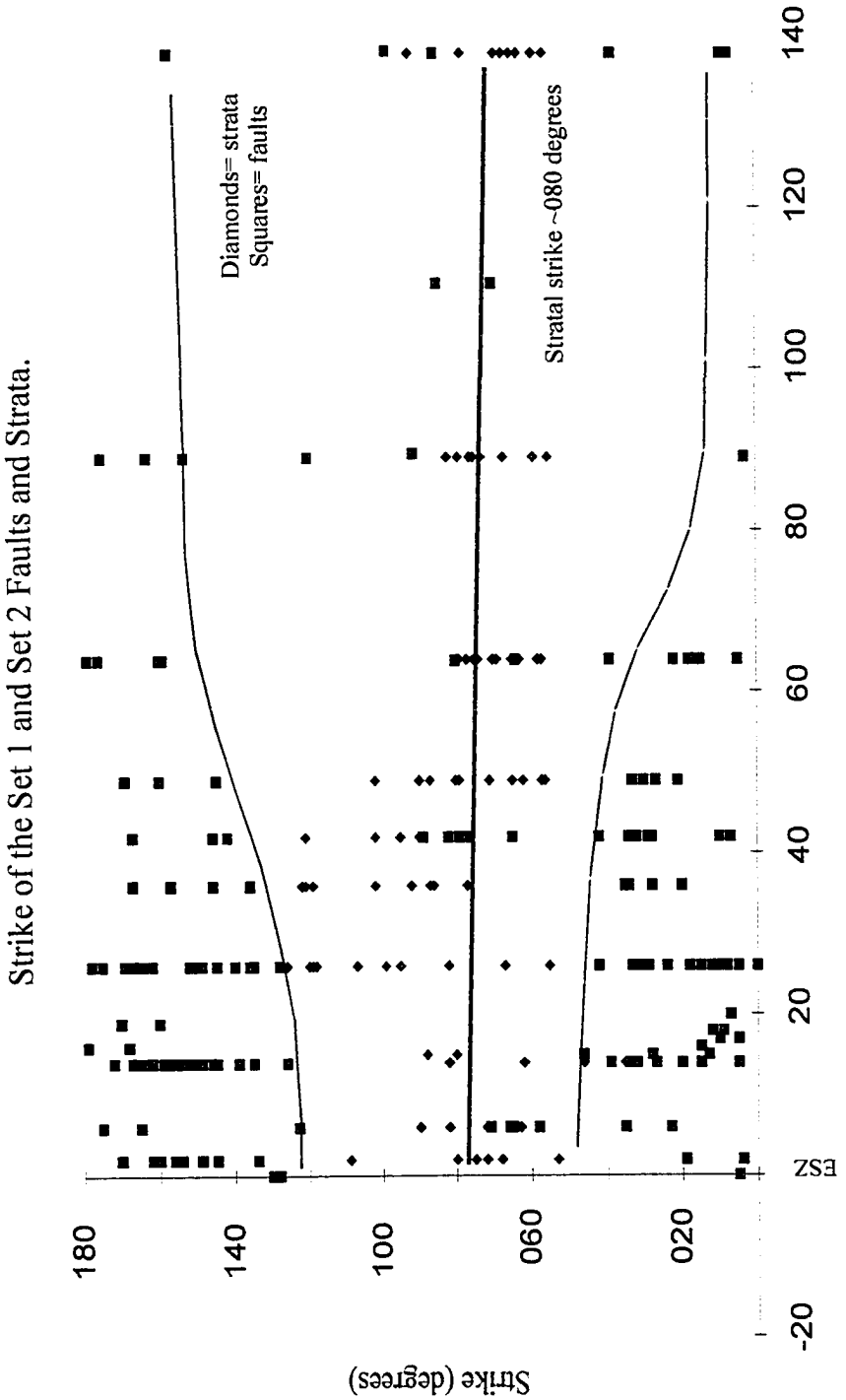
Strike of the Set 1 and Set 2 Faults and Strata.
Diamonds= strata
Squares= faults
Stratal strike ~080 degrees
ESZ
180
140
100
060
020
-20
Strike (degrees)
20
40
60
80
100
120
140
Horizontal Distance from Diapir (m)

Figure 3.3.10

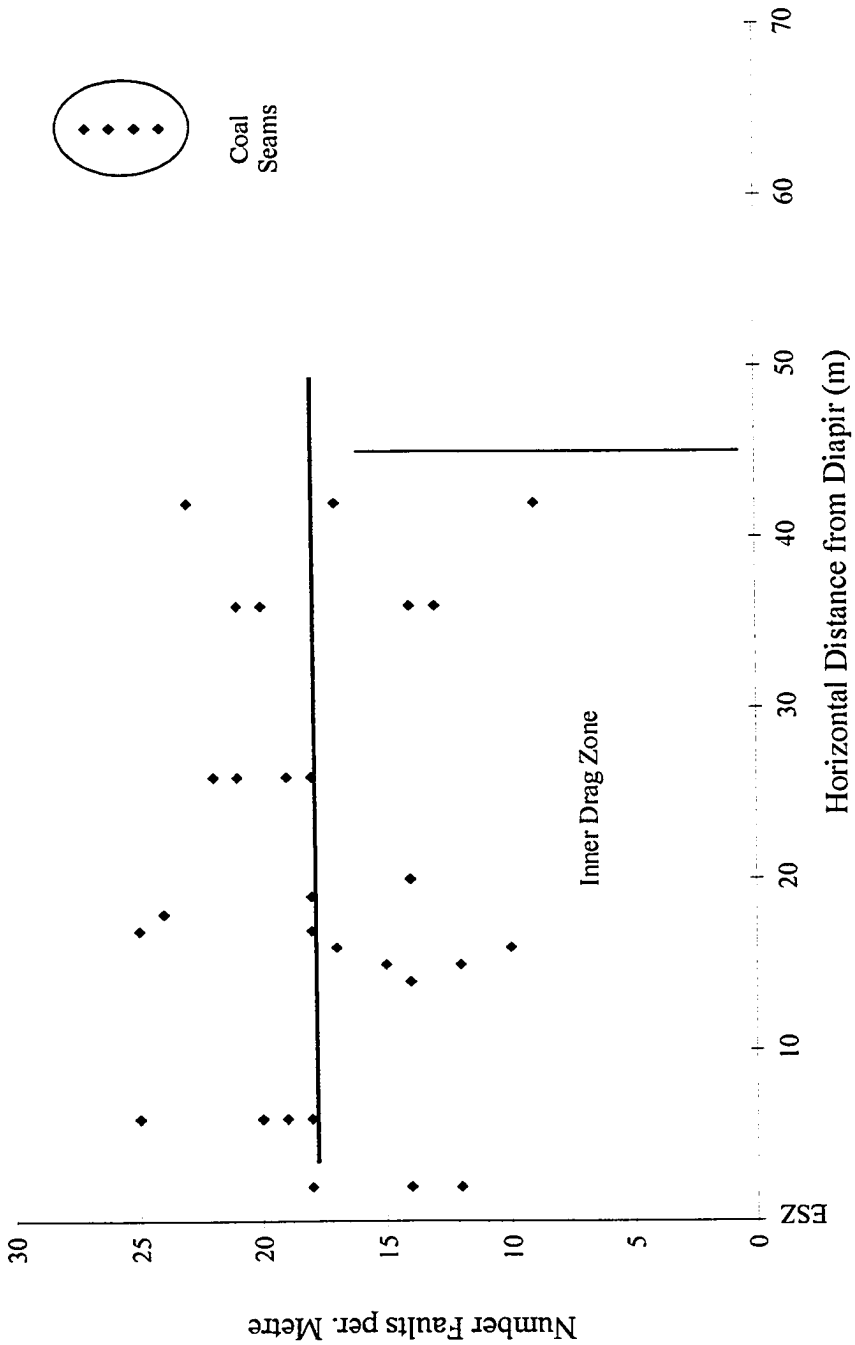
Micro-Fault Density Finlay Point Drag Zone.
Number Faults per. Metre
30
25
20
15
10
5
0
ESZ
10
20
30
40
50
60
70
Horizontal Distance from Diapir (m)
Inner Drag Zone
Coal
Seams

Figure 3.3.11

3.3.7, Finlay Point North

The Finlay Point North section extends in a NNE/SSW direction from Finlay Point to the contact of the Inverness Formation with Ordovician basement rocks (Figures 3.3.1 and 3.3.2).

The Finlay Point North section is important because it is the only drag zone section within the field area that is oriented parallel to the margin of a diapir. The section lies along the external shear zone of the western flank of the Finlay Point Diapir.

Structure of the Finlay Point North Section

The structure of the Finlay Point North section is characterised by a number of dip-slip and strike-slip faults which offset the margin of the Finlay Point Diapir and juxtapose a multitude of stratigraphic units (Figure 3.3.12). Apart from the Inverness Formation, all the lithological units are fault-bounded. This has made reconstruction of the section subjective, as a number of the units, particularly the conglomerates, cannot be placed stratigraphically. All the tectono-stratigraphic units dip towards the west (seawards) at an angle of 12-30 degrees. The units are therefore dipping away from the western margin of the Finlay Point Diapir, as might be expected for strata that have been deformed by a rising diapir. Although the high degree of deformation and poor exposure makes accurate strike measurements difficult to collect, the lithological units appear to strike sub-parallel to the beach and the flank of the Finlay Point Diapir. The structure is described below from SSW to NNE (right to left in Figure 3.3.12):

- The Eagle Sandstone (Dickie, 1986) overlies grey shales and coals of the Inverness Formation and the Finlay Point Conglomerate. The exposure is poor and so the precise stratigraphic relationships between these units cannot be determined. A coal seam exposed beneath the Eagle Sandstone consists of an isolated block surrounded by grey shale. The coal seam has been folded and

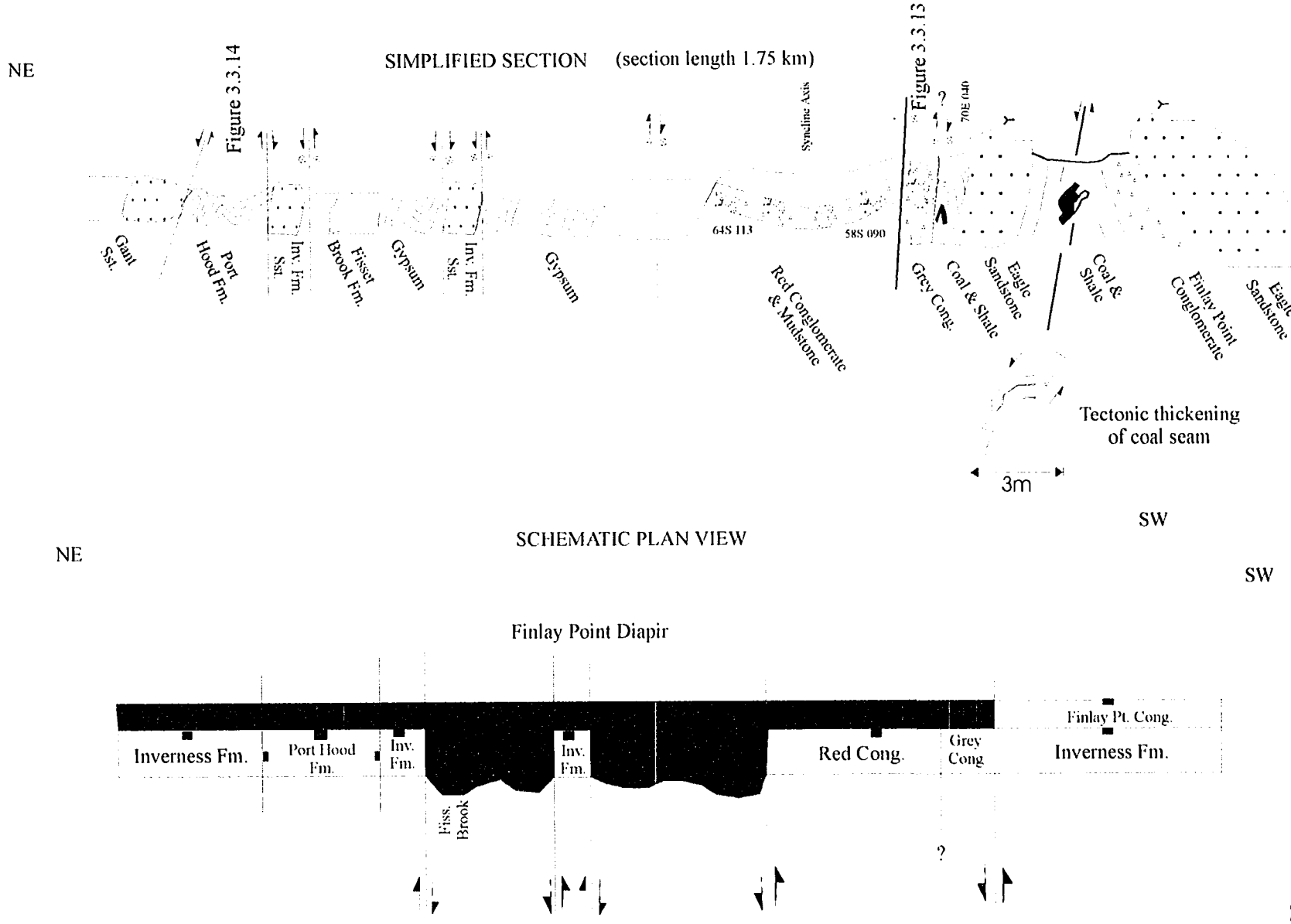

Figure 3.3.12. Section and plan view of the Finlay Point North section.

tectonically imbricated to approximately three times its stratigraphic thickness. This tectonic thickening suggests that extensive bedding-parallel slip has occurred within the grey shales as the Eagle Sandstone was translated downwards relative to the rising Finlay Point Diapir.

- A grey to yellow polymict conglomerate which contains basement and Carboniferous sedimentary clasts within a coarse sand matrix (Figure 3.3.13). The clasts are angular, relatively unsorted and the strata show very poor graded bedding. The conglomerate is of unknown affinity but has a similar texture and composition to the Finlay Point Conglomerate. The distinctive grey and yellow coloration, however, implies that it is not part of the Finlay Point conglomerate. The conglomerate unit dips sub-vertically and strikes orthogonally to the diapir margin. Although the contacts are not exposed, it is likely that the unit is fault-bounded. Its stratigraphic relationship to the Eagle Sandstone to the immediate SSW and the Finlay Point Conglomerate to the immediate NNE is not known.

- A red conglomeratic mudstone unit that is interpreted to be part of the Finlay Point Conglomerate based upon its colour and the presence of basement clasts within the conglomeratic portion of the unit. This unit is probably fault-bounded between the grey/yellow conglomerate to the SSW (see above) and gypsum of the Finlay Point Diapir (although the contact is not exposed). The conglomerate band within the unit defines a syncline that plunges at 50 degrees towards 097. The fold hinge of the syncline is orthogonal to the diapir margin.

- 50 m of no exposure. This section was probably occupied by gypsum since a karsted gypsum surface is exposed immediately to the east; however, a small stream now runs through this area.

Figure 3.3.13. Grey/yellow polymict conglomerate exposed on the Finlay Point North section. Conglomerate is of unknown affinity, but is interpreted to be derived from the uplifted footwall of the Hollow Fault segment located 0.75 km to the south-east. For Location see Figure 3.3.12.

Scale. Figure in photo is 4'8" (1.42m)

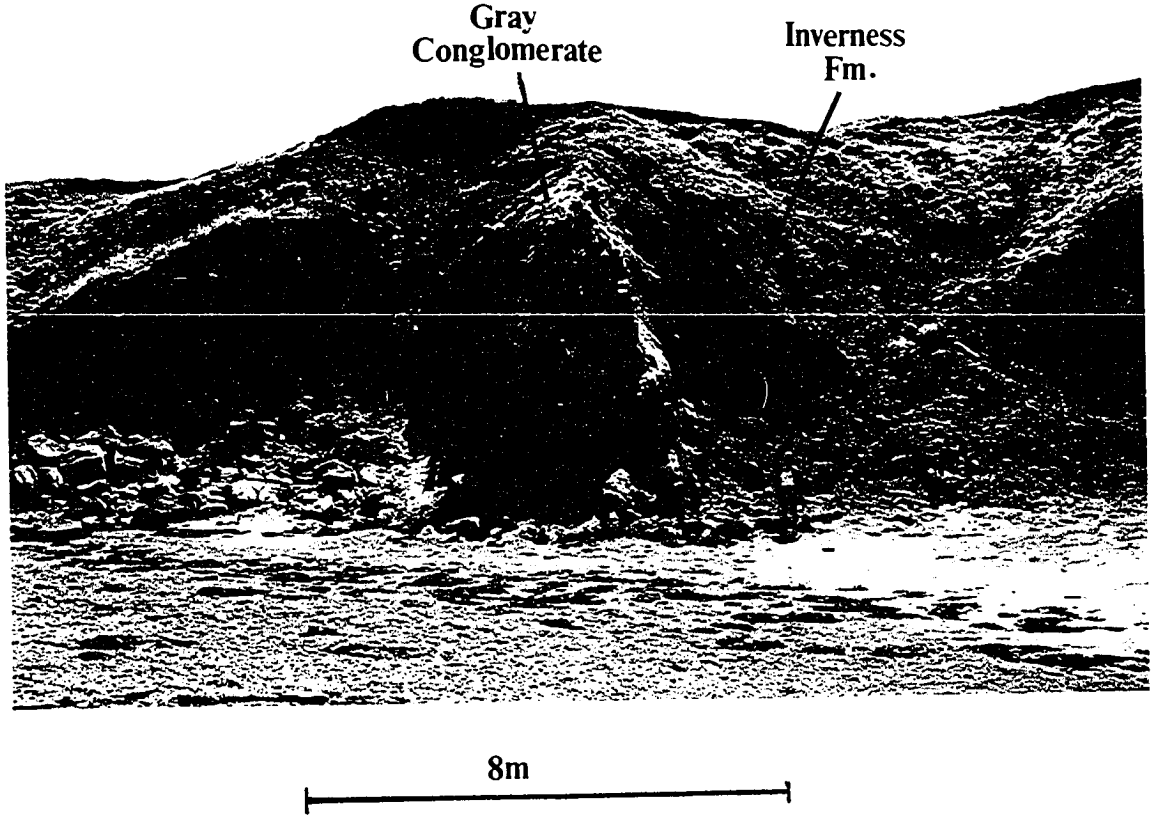

Figure 3.1.13

- 100 m of gypsum representing part of the Finlay Point Diapir. The gypsum is bounded by two faults with both dip-slip and strike-slip offsets and is therefore a westward protrusion of the diapir, forming a step in the diapir margin (Figure 3.3.12). The gypsum unit is heavily eroded but contains many blocks containing meso-scale fold hinges. Two intact folds were measured; the first plunges 21 degrees towards 010 degrees and the second plunges 42 degrees towards 250 degrees. The hinges of the folds are therefore oriented parallel to and orthogonal to the diapir margin.

- An isolated allochthonous block of Inverness Formation sandstone, bounded by gypsum, which may be part of the Eagle Sandstone.

- A poorly exposed section of gypsum mylonite containing a block of Fisset Brook Formation meta-sedimentary rock.

- An isolated sandstone unit of the Inverness Formation which may be part of the Eagle Sandstone. Palynological dates taken from minor shale horizons within the sandstone yielded a Westphalian C-D age (G. Dolby, pers. comm. 1994 and 1995) that is equivalent to the age of the Eagle Sandstone (G. Dolby, pers. comm. 1994 and 1995) and so supports a correlation of this exposure with the Eagle Sandstone. Palynological age data is fully described in Chapter 5.

- A fault-bounded unit consisting of laminated grey/black petroliferous shales and grey limestones. The shales contain abundant ostracods, fish-scale fragments and fish teeth. Palynological analysis of the grey shales indicates an Upper Yeodonian - Westphalian A age (G. Dolby, pers. comm. 1994 and 1995). The unit contains tight to isoclinal metre-scale folds with many internal flexural slip decollements and faults related to over-tightening of fold structures (Figure 3.4.14a and b). The distinctive lithology and palynological age date indicate that this unit is part of the

Figure 3.3.14a. The north-east contact of Middle Member, Port Hood Formation strata with Inverness Formation sandstone units. The contact is a sharp fault contact which may have up to ~700m displacement.

Figure 3.3.14b. Tight to isoclinal folds within the Middle Member Port Hood Formation unit. The fold pattern is convoluted and the folds have been faulted, typically through the fold hinge region. The fold hinge plunges ~15 degrees to the west.

(Scale, hammer is 32 cm long).

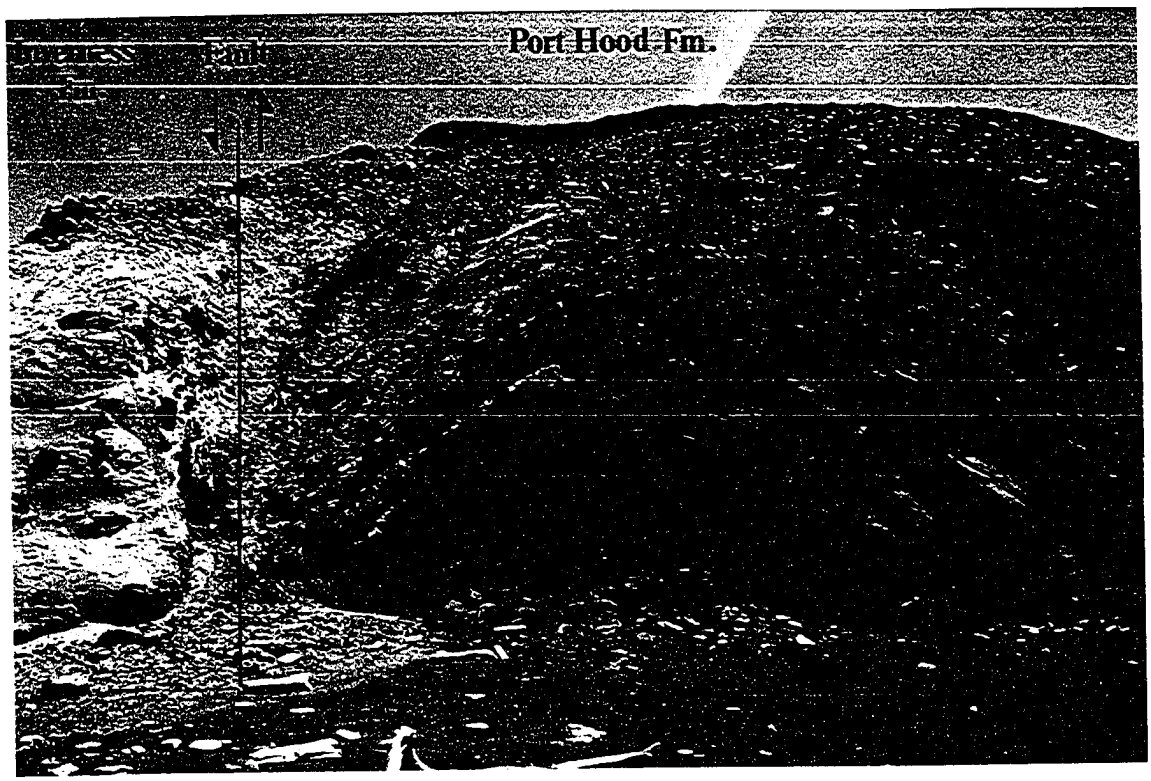

Figure 3.3.14a

Figure 3.3.14b

Colindale Member of the Port Hood Formation. This stratigraphic unit is distinctive and closely resembles lithological units with comparable age dates at Port Hood (Ismuth Point) and Coal Mine Point. The block is faulted against Inverness Formation sandstone units to the north-east and south-west and so is entirely fault-bounded.

- The remainder of the section consists of Inverness Formation sandstones with minor shale horizons. As with the other Inverness Formation sandstones in this section, the exact stratigraphic relationship to the Eagle Sandstone is uncertain, although palynological dating of the shale horizons indicates a Westphalian C-D age comparable to the Eagle Sandstone.

Interpretation. The presence of a Fisset Brook Formation block within the section is problematical since the Fisset Brook Formation lies stratigraphically beneath the Windsor Group and can therefore not have been transported solely by the Finlay Point Diapir. Some mechanism is required to place the Fisset Brook Formation block above the Windsor Group prior to diapirism. The preferred explanation proposed here is that the Fisset Brook Formation block represents a fragment of rock which spalled off the footwall of the Hollow Fault prior to the onset of diapirism. The block could thereby lie as an allochthonous block above the Windsor Group. Subsequent halokinesis and diapirism entrained the block within the diapir, which transported it to its present elevation. The tightly folded Port Hood Formation unit is interpreted to be an inclusion of Port Hood Formation strata that became entrained within an enclave on the margin of the diapir. The unit was transported by the diapir some several hundred metres vertically through the Inverness Formation to its current stratigraphic position. The extreme deformation of the unit reflects this transportation.

General Conclusion

The Finlay Point North section reveals the extremely complex along-strike structure

associated with the Finlay Point Diapir margin. All other sections described in this chapter are dip sections through drag zones.

The strike section must be considered as a three dimensional structure and not as a two dimensional interface between the diapir and its overburden since lithostratigraphic units have been shuffled into their present arrangement by a combination of vertical and horizontal displacement associated with diapir growth. The displacement of the lithostratigraphic units has been accommodated on a series of faults, which have large dip-slip and strike-slip offset components. These faults give the diapir an irregular, stepped margin that contrasts with the smooth margin that is more characteristic of halite diapir exposures. The faulted/stepped margin indicates that the gypsum/anhydrite structural carapace underwent brittle faulting as well as ductile deformation.

3.4, THE COAL MINE POINT DIAPIR

3.4.1, Geographical Data

Coal Mine Point is located at latitude 46N,22,30 longitude 61W,21,10, on topographical map 11K/3 (Figures 3.3.1 and 3.3.2). The Coal Mine Point Diapir drag zone section is approximately 250 m long and is located on the south-west flank of the diapir. The Coal Mine Point Diapir exposure is approximately 75 m long and is located at the south-eastern end of Mabou Mines Beach.

3.4.2, General Information

The Coal Mine Point structure was first interpreted as a diapir by Haites in 1952. Haites also described the adjacent Mabou Mines area as an anticline and correlated the Inverness Formation sections at Coal Mine Point and Finlay Point. Haites considered that the flanks of the Mabou Mines anticline had been faulted, but did not discuss whether the faults played a role in accommodating the Coal Mine Point and Finlay Point diapirs. Haites' interpretation is very similar to that presented in this thesis. Authors subsequent to Haites interpreted the juxtaposition of the Upper Carboniferous Inverness Formation sediments against Windsor Group sediments as the result of an extensional fault (e.g. Hacquebard, 1986) or a low-angle detachment (the Ainslie Detachment, Lynch and Brisson, 1994; Giles et al., 1997a).

3.4.3, The Coal Mine Point Diapir - Seismic Data

The Coal Mine Point Diapir is the northernmost extension of the Salt Wall Huey (see Salt Wall Huey, Chapter 2 and Figure 2.8.2). The Coal Mine Point Diapir is assigned a separate name because of its excellent onshore exposure at Coal Mine Point.

The Coal Mine Point Diapir is imaged on Mabou lines 3, 4, 11 and 12 and lines 63 and 67 of the 1982 Chevron seismic survey *(see relevant seismic lines)*.

Line 67, 1982 Chevron Seismic Survey & Lines 3 and 4 of the 1978 Mabou Seismic Survey

Seismic data covering the north-west flank of the Coal Mine Point Diapir show a structure ~2.5 km high and 3.5 km in width. However, the south-east flank of the Coal Mine Point Diapir is not covered by seismic data and the width is therefore a minimum estimate.

The north-west flank of the Coal Mine Point Diapir has an irregular geometry best described as a section through an upturned wine glass. The broad diapir base at 1.7 sec TWT narrows sharply to a 'neck' between 0.8 - 0.3 sec TWT before broadening again from 0.3 - 0.05 sec TWT (*see line 67)*. The top of the diapir can be described as a salt overhang, a common feature of salt diapirs, e.g. Kavir Salt Basin of Iran (see Jackson et al., 1990).

Outside the immediate drag zone, within the broader zone of rotation (see Glossary of Salt Tectonics) (>250 m westwards of the external shear zone), the Upper Carboniferous strata extend away from the diapir with an almost homoclinal dip of 15-19 degrees (calculated from depth-converted seismic section, Appendix 3). This angle of dip changes abruptly at a distance of 2000 m where the strata cross a prominent fold hinge. Strata to the west of the hinge are not affected by the diapir, whereas all strata to the east of the hinge show rotation and folding. The fold structure is hereafter referred to as the Clayton Fold. The fold is persistent along strike and can be traced throughout the 1978 Mabou survey as a fold whose hinge strikes parallel to the Salt Wall Huey (Coal Mine Point Diapir) and the Finlay Point Diapir. The isopach nature of the uplifted Inverness Formation strata indicates that they were not affected by diapirism until after the Westphalian D, although this does not preclude diapiric growth before then. The Clayton Fold may be related to active uplift of the Inverness Formation strata by the Coal Mine Point Diapir, although line 67 also shows evidence of inversion (see above, Chapter 2). The formation of the Clayton Fold could be explained by active uplift of the overburden

strata by diapiric rejuvenation related to post-Carboniferous inversion.

Lines 11 and 12, 1978 Mabou Seismic Survey

The north-west flank of the Coal Mine Point Diapir is imaged on Mabou lines 11 and 12. The intersections of the seismic lines 11 and 12 with the diapir flank are, respectively, 2.5 and 4.0 km north of and orthogonal to the line 67 intersection. It should be noted that the Mabou seismic data were only recorded to 1.0 sec TWT and so the base of the diapir is not imaged. None of the 1982 Chevron lines lie close enough to shore to image the Coal Mine Point Diapir at this location.

As imaged, the north-west flank of the Coal Mine Point Diapir is planar and dips steeply to the north-west, although it should be noted that only the upper portion of the diapir is covered by the seismic data. The oblique intersection of the seismic line with the strike of the diapir margin probably causes the flank to appear to be dipping less steeply than it actually is.

The Carboniferous strata adjacent to the diapir show sharp contacts with the diapir margin and appear to have a smoothly varying drag zone profile. However, the drag zone of the Coal Mine Point Diapir is truncated by the Finlay Point Diapir ~2 km to the north and so the entire drag zone is not seen.

3.4.4, Geology of the Mabou Mines Area

In order to fully describe the Coal Mine Point Diapir exposure, it is necessary to describe its relationship to the surrounding geology of the Mabou Mines to Beaton Point area (Figures 3.3.1 and 3.3.2). This approach places the Coal Mine Point Diapir in a regional context.

From Green Point to Beaton Point (Figure 3.3.1), Horton Group strata are exposed at surface as extensive coastal cliffs. These Horton Group strata have been thrust north-

westwards over the Coal Mine Point Diapir along the Beaton Fault, which is exposed on the coastal section ~500 m south of Coal Mine Point. The Horton Group strata occupy the hangingwall of the fault, whereas the Inverness Formation and Windsor gypsum occupy the footwall. The Beaton Fault is therefore a thrust fault.

The Beaton Fault apparently truncates the Coal Mine Point Diapir ~750 m inland from Mabou Mines Beach, where it has overridden part of the south-eastern flank of the Coal Mine Point Diapir.

Between Green Point and Beaton Point, large numbers of small extensional, reverse and strike-slip faults deform the Horton Group strata. These faults typically have a displacement of <50 cm and contain sparse calcite mineral veins. Stereographic paleostress analysis of nineteen faults (one extensional and eighteen strike-slip) indicates a north-west to north compression direction could produce the recorded faults (Figure 3.4.1).

The structural relationship between the Coal Mine Point Diapir and the Beaton Fault could be explained by a north-west oriented compressional phase of deformation (i.e. sigma 1 orientated ~325/135 degrees). This interpretation is supported by analysis of faults from MacKinnons Brook (Figure 3.3.1) where north-west and NNW orientated strike-slip faults are exposed which juxtapose basement rocks against Inverness Formation. These faults could also be formed by an approximately north-west orientated compression, although in this case deformation occurred after deposition and lithification of the Inverness Formation sediments, i.e. post-Stephanian. From the combination of the Mabou Mines, Green Point and MacKinnons Brook fault data, it seems reasonable to suggest that the project area was affected by a compressional phase of deformation that produced faults related to a north-west/south-east compression. The phase of compression occurred after the Stephanian and may have reactivated pre-existing basement structures as well as creating new faults within the Carboniferous cover rocks.

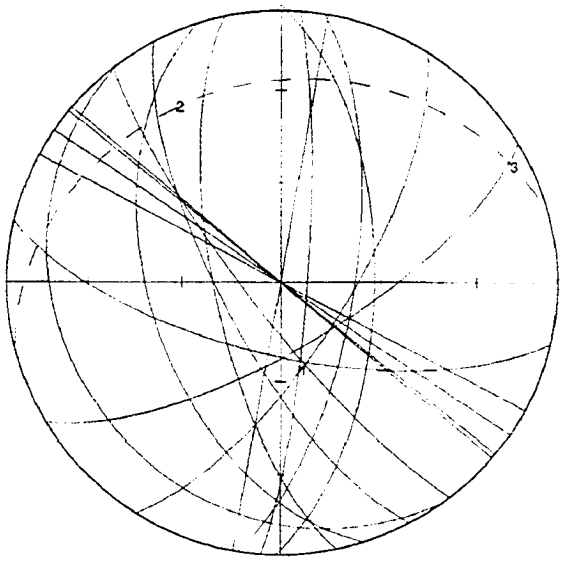

Figure 3.4.1a. A lower hemisphere great circle projection of sixteen small-scale faults (extensional and strike-slip). The data was collected from outcrops between Green Point and Beaton Point (see Figure 3.3.1).

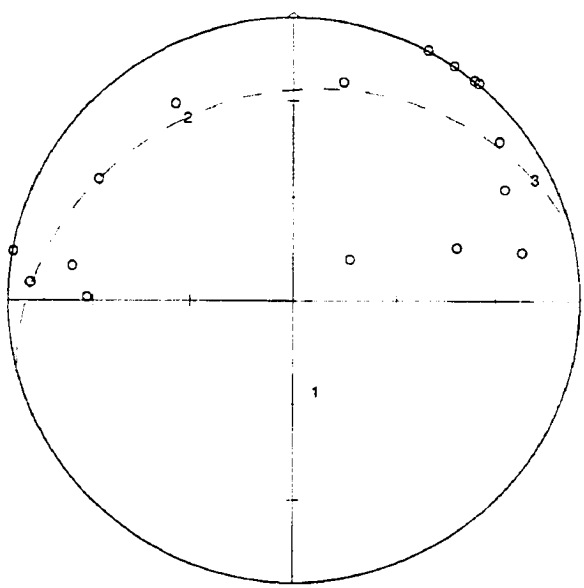

Figure 3.4.1b. A lower hemisphere projection showing the poles to the small-scale faults. Although the range of the fault orientations is large, the data indicates that the fault pattern could be produced by a north-west compression, i.e maximum compressive stress was sub-horizontal and orientated towards the north-west.

The hypothesis of a post-Carboniferous north-west orientated phase of deformation is supported by evidence from the offshore seismic data (see above, Chapter 2).

3.4.5, Relationship of the Coal Mine Point Diapir to the Hollow Fault

As imaged on the 1978 Mabou and 1982 Chevron surveys, the Coal Mine Point Diapir is 2.5 km high within 1 km of the present shoreline. Onshore exposures of the basal Windsor strata (Macumber Limestone) at Mabou Mines require that approximately 2.5 km of accommodation space be created in order to accommodate deposition of the Upper Carboniferous strata and growth of the Coal Mine Point Diapir. The simplest and most logical way to create the required accommodation space is on an extensional fault. The interpretation preferred in this thesis is that a major extensional fault lies along the present coastline adjacent to Mabou Mines and that this fault represents a segment of the Hollow Fault. This segment of the Hollow Fault probably bounds the Coal Mine Point Diapir as well as the Finlay Point Diapir 1.5 km to the north-east, so that the diapirs have grown vertically up the fault plane from the hangingwall. As noted earlier, the effects of salt withdrawal subsidence must be considered when calculating overall subsidence. The estimated tectonic subsidence of 2.5 km must therefore be a maximum value.

3.4.6, The Coal Mine Point Diapir

The Coal Mine Point Diapir is exposed at the southern end of Mabou Mines beach as a massive block of white gypsum with horizons containing disseminated limestone clasts (Figure 3.4.2a and b). No intact Windsor Group limestones are exposed within the diapir, which makes precise stratigraphic determination difficult. The diapir was assigned to the Lower Windsor by Giles et al. (1997a) based on the lack of Middle Windsor or Hood Island limestones and the proximity of the outcrop to the Macumber Limestone exposed on Mabou Beach. However, the massive gypsum within the Lower Windsor lies stratigraphically beneath the halite and so could not have been transported as a structural carapace at the top of the diapir. The gypsum is therefore interpreted to be a Middle Windsor gypsum unit. The absence of Middle Windsor limestones may reflect tectonic

Figure 3.4.2a. The Coal Mine Point Diapir as seen from Finlay Point. The Eagle Sandstone forming Coal Mine Point can easily be distinguished as can the 2nd sandstone unit and the Stack sandstone. Note the steep dip of the Stack sandstone and the shallow dip of the Eagle sandstone. The Coal Mine Point Diapir can be seen as the white unit located towards the left of the photograph.

Figure 3.4.2b. The Coal Mine Point Diapir as seen from the Mabou Mines Road. On the extreme left of the picture gypsum karst topography marks the position of the Coal Mine Point Diapir inland.

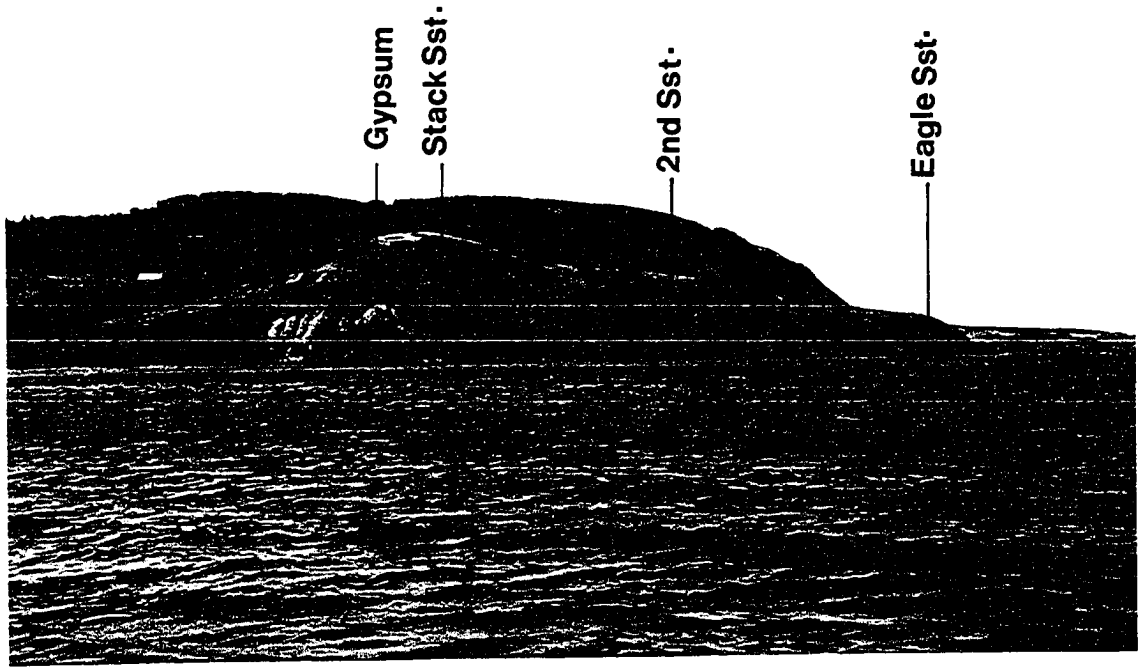

Figure 3.4.2a

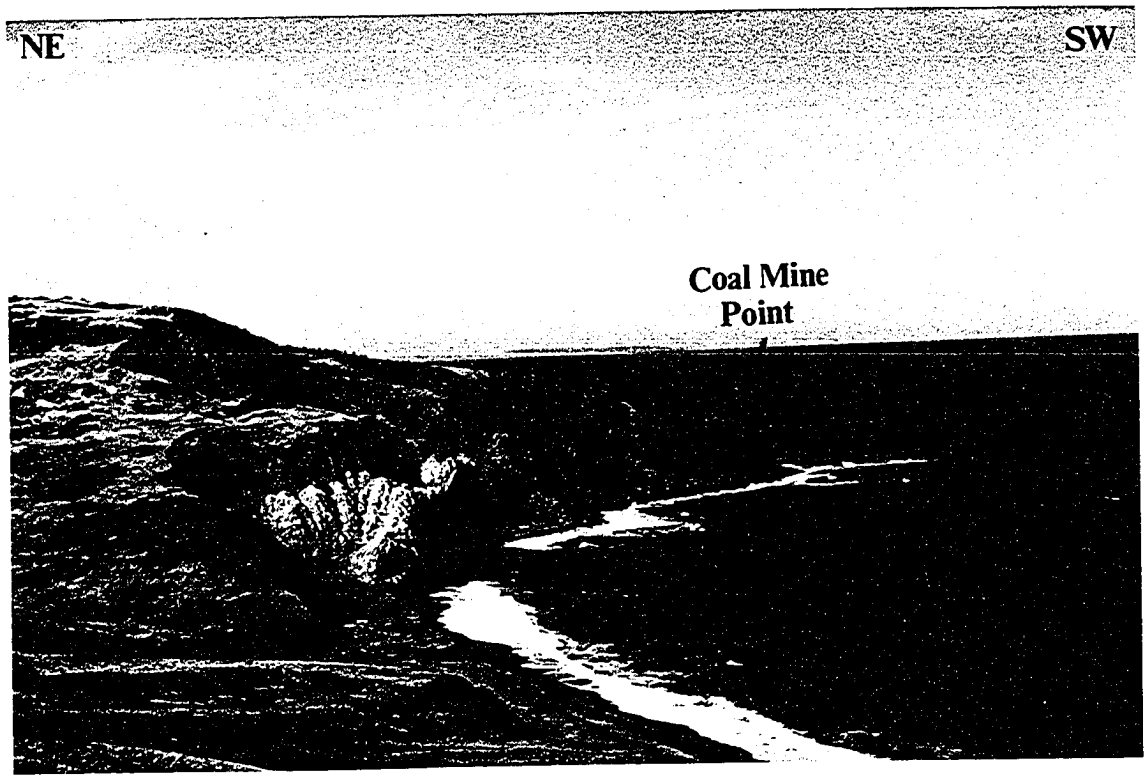

Figure 3.4.2b

brecciation during diapir intrusion (see below Chapter 4).

3.4.7, The Southern External Shear Zone

The southern external shear zone is a 1 m wide shear zone that forms the contact between Windsor Group gypsum of the Coal Mine Point Diapir and the Inverness Formation overburden (Figure 3.4.3). The external shear zone is best exposed at beach level but is also poorly exposed on the steep vegetated bank that rises from the beach.

The external shear zone is a mixture of rock fragments that have undergone brittle faulting and plastic shearing. Fragments of Windsor Group limestone as well as siltstone, sandstone and conglomerate clasts of unknown affinity form a polymict breccia approximately 60 cm thick that has been sheared against the flank of the diapir. The breccia is crosscut by numerous faults (extensional, compressional and strike-slip) that have a small displacement (<10 cm) and no apparent preferred orientation. Slickensides developed in mud-rich fragments show a vertical shear sense sub-parallel to the adjacent diapir margin.

Exposed at beach level, the southern margin of the diapir becomes sub-horizontal for several metres, forming a shoulder that extends outwards below the surrounding Inverness Formation. Resting on top of this shoulder is a block of laminated grey/black shale and limestone measuring 3 m long by 2 m high (width not exposed) (Figure 3.4.4). The black shales are petroliferous and contain abundant ostracods as well as fish fragments (scales and teeth), while the limestones are grey and thinly laminated. Stratigraphically, the block is interpreted to be part of the Colindale Member of the Port Hood Formation which is also exposed at Finlay Point North (see Finlay Point North, Ch. 3.3) and Ismuth Point, Port Hood (see below, Chapter 3). In both locations, the Port Hood Formation has been palynologically dated as latest Yeadonian - Westphalian A (G. Dolby, pers.comm., 1994 and 1995).

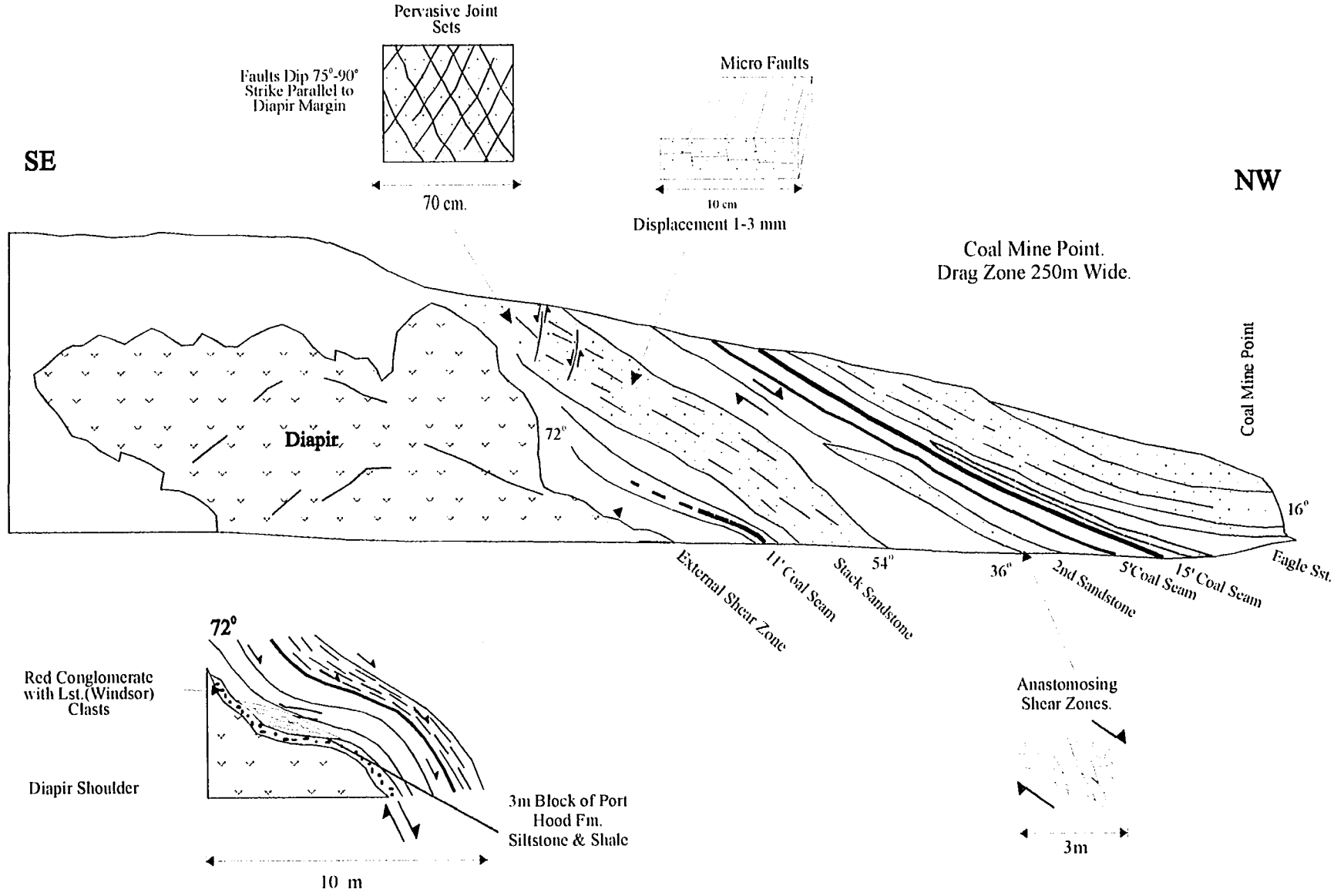

Figure 3.4.3. The Coal Mine Point Diapir and Drag Zone.

Figure 3.4.4. The Port Hood Formation tectonised fragment resting upon the protruding shoulder of the Coal Mine Point Diapir. Note that the shoulder extends sub-horizontally outwards from the diapir flank. The tectonised fragment is highly faulted and detaches easily as breccia. It is not known how far the fragment extends along the diapir margin.

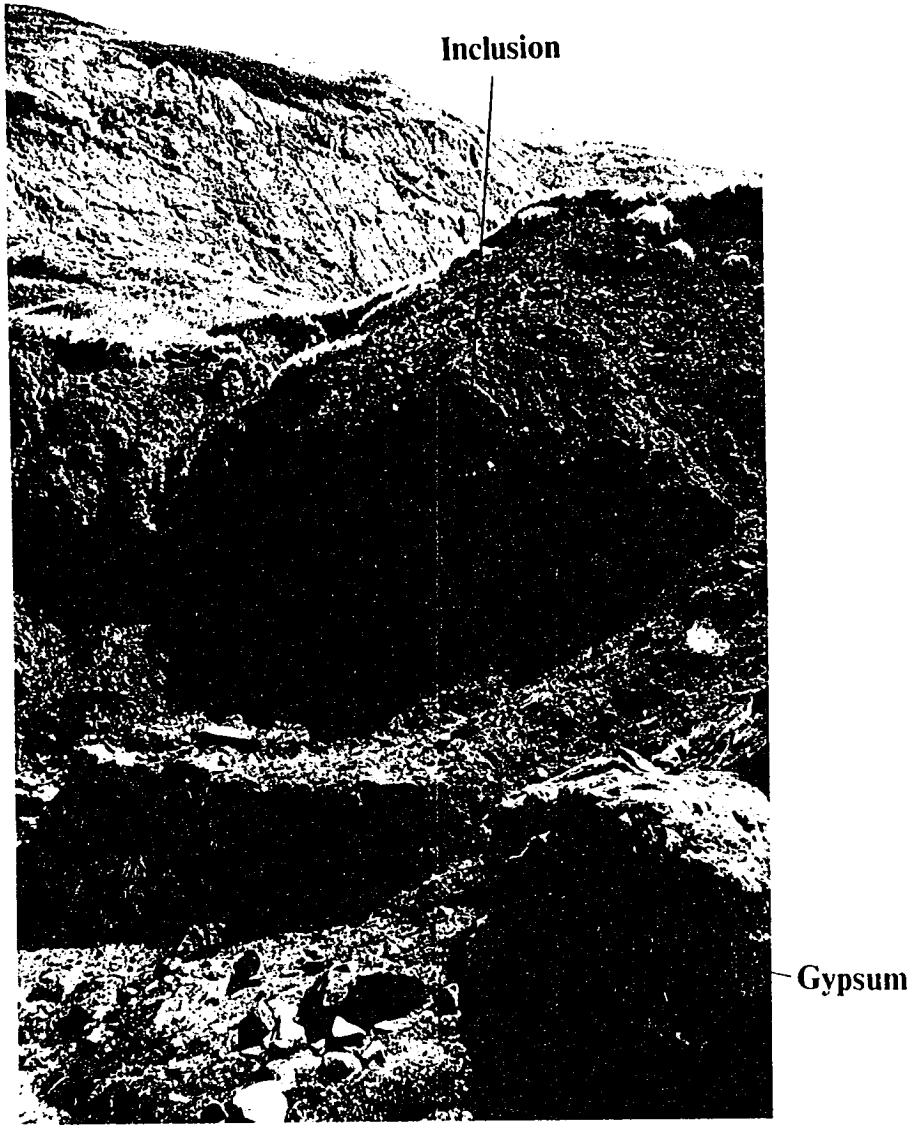
Inclusion
Gypsum

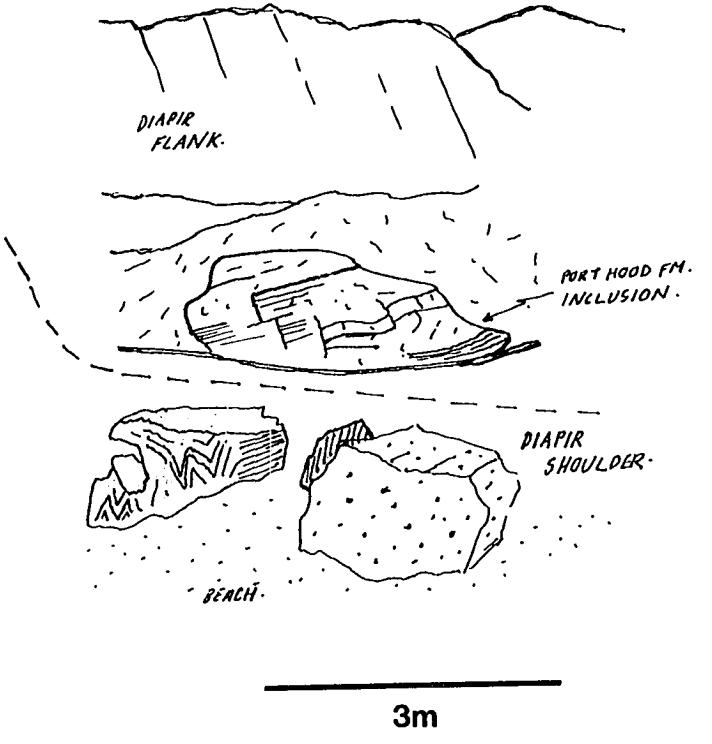
DIAPIR FLANK.
PORT HOOD FM. INCLUSION.
DIAPIR SHOULDER.
BEACH.
3m

Figure 3.4.4

Interpretation. The block is interpreted to be a fragment of Port Hood Formation strata which has been entrained on top of the diapir shoulder and transported vertically as an inclusion on the diapir margin in a similar way to other Port Hood Formation fragments exposed at Finlay Point North. From available seismic data, it is estimated that the parent Port Hood Formation strata are located approximately 900-1200 m beneath the present location of the tectonised fragment. The exposure of the shoulder beneath the inclusion demonstrates how a fragment of strata can be carried vertically for several hundred metres through the overlying Inverness Formation. The block of strata is intensely deformed by faults that are probably related to the transport of the block within the outer margin of the diapir.

3.4.8, The Southern Drag Zone

The southern drag zone is moderately well exposed throughout its entire 250 m length (Figures 3.4.2a/b and 3.4.3). The Eagle Sandstone (Dickie, 1986) forms the Coal Mine Point headland and marks the outermost part of the drag zone. The Eagle Sandstone is the highest stratigraphic level exposed and the section beneath the Eagle Sandstone (towards the Coal Mine Point Diapir) is a repetition of the section exposed to the south-east of Coal Mine Point, previously described by Keating (1950) and Hacquebard et al. (1989) (see below, Chapter 3). Stratigraphically, beneath the Eagle Sandstone the southern drag zone of the Coal Mine Point Diapir consists of:

- ~20 m of intercalated grey and black shale, siltstone and nodular siderite horizons.

- A 75 cm thick coal seam that is correlated with the 15' coal seam exposed to the south-east of Coal Mine Point.

- A 40 cm thick coal seam which is correlated with the 5' coal seam to the south-east of Coal Mine Point.

- ~15 m of grey shale with sporadic nodular siderite bands.

- 3.5 m of medium sandstone containing spectacular anastomosing shear zones (second sandstone on Figure 3.4.3).

- A non-exposed section covered by vegetation. Correlation with the section to the south-east of Coal Mine Point suggests that the unexposed strata consist of coal, grey/black shales and nodular siderite horizons.

- The Stack Sandstone (Hacquebard, 1980), which is approximately 55 m thick as described for the section to the south-east of Coal Mine Point.

- Approximately 25 m of grey shales, minor sandstone and a single coal seam that would correlate with the 11' coal seam described by Hacquebard (1980) for the section to the south-east of Coal Mine Point. The section is truncated by the Coal Mine Point Diapir 5-6 m beneath the 11' coal seam.

Due to the degree of brecciation of the sandbodies and vegetation cover over the grey shale and coal seam intervals, dip and strike measurements were difficult to take and faults were extremely hard to distinguish.

Five separate sets of structures were recorded from the Coal Mine Point drag zone.

3.4.9, Drag Zone Folding

From Finlay Point (1.5 km to the north), the Inverness Formation can be seen to be draped off the north-west flank of the Coal Mine Point Diapir in a smooth dip fan (Figure 3.4.5). In contrast to the smooth dip fan profile, the individual sandstone units do not appear to be strongly folded but are somewhat homoclinal when viewed from Finlay Point. Actual dip and strike data from the drag zone were extremely hard to obtain and

only twenty dip/strike measurements were recorded from sandstone units. The drag zone profile shows a rapid decrease in the stratal dip angle within the inner drag zone from 72 degrees adjacent to the external shear zone to 45 degrees at a distance of 75-80 m from the diapir.

Within the outer drag zone (80m-250m), the stratal dip decreases more slowly, such that the dip angle at 80 m (45 degrees) decreases to 16 degrees at 250 m (Coal Mine Point).

3.4.10, Faults

Many faults were recorded from each of the three sandbodies. It is suspected that many faults exist within the Stack Sandstone; however, the severe brecciation of the Stack Sandstone probably prevented many faults from being recorded as they could not be distinguished from the pervasive joint sets (see below).

No kinematic indicators were recorded from the faults. For this reason, it cannot be said for certain what the sense of movement on the faults is. By inference from other faults in similar structural locations within the field area, the faults are tentatively interpreted to be extensional faults.

The faults that could be defined strike between 080 and 180 degrees and therefore range between parallel and orthogonal faults with respect to the trend of the diapir margin (090 degrees). The fault planes dip between 44 and 85 degrees, with no preferred dip direction. The 41 degree range of fault plane dip could imply multiple generations of faults, similar to Broad Cove and St. Rose drag zones; however, the quantity and quality of the data are insufficient to prove this hypothesis (Figure 3.4.6).

3.4.11, Conjugate Joint Sets

The Stack Sandstone has been deformed by the formation of two conjugate joint sets (Figure 3.4.3). This style of deformation is not seen in other diapir outcrops and so is

described here as a separate structural style. The joint sets strike sub-parallel to the peripheral shear zone of the Coal Mine Point Diapir (140-180 degrees) and dip 65-90 degrees west and 40-60 east, respectively. The joint sets have a cumulative joint density of 10-12 joints per metre. The density of jointing is such that the Stack Sandstone has been virtually reduced to a breccia (Figure 3.4.8). Original sedimentary features, e.g. bedding and cross-stratification, as well as tectonic structures such as faults are almost impossible to identify.

The second sandstone (Figure 3.4.3) is less intensely jointed than the Stack Sandstone. Although joint sets have approximately the same dip angle as those contained within the Stack Sandstone, the strike of the joint sets shows a much wider range (040-170 degrees). Original sedimentary structures and later tectonic structures are easily recognisable within the second sandbody. The Eagle Sandstone contains no joint/fault sets. The development of joint sets is therefore restricted to within 80 horizontal meters of the diapir/overburden contact.

3.4.12, Micro Faults

These structures are extensional faults with a displacement of 1-3 mm with a clear extensional geometry. In thin section, the structures are brittle faults with no dynamic grain size reduction along the fault plane. Iron oxide minerals (hematite) have been deposited along the fault plane.

All the micro-faults strike sub-parallel to the diapir margin (160-010 degrees). Based upon dip direction, two conjugate sets of micro-faults can be defined. The dominant set dips 69-80 degrees west (away from the diapir) and the subordinate set dip 65-70 degrees east (towards the diapir).

The micro-faults have a high density within the Stack Sandstone of 11-82 faults per metre and a lower density within the second sandbody (13-55 seams per metre). A high micro-

fault density is only found within the basal 20 m of the Eagle Sandstone, where the density is 13-55 faults per metre, which is comparable to the density observed within the Stack Sandstone. Above the basal 20 m, no micro-faults were identified. The micro-faults are therefore restricted to within 120 m of the diapir/overburden contact (Figure 3.4.7).

The concentration of micro-faults within individual sandstone bodies appears to have no systematic distribution, although the highest density was recorded at the diapir/overburden contact. This is undoubtedly due to a higher finite strain within the external shear zone.

3.4.13, Anastomosing Shear Zones

The second sandstone (Figure 3.4.3) contains spectacular anastomosing shear zones. The anastomosing shear zones define lozenges of intact sandstone surrounded by thin (<2cm wide) brittle shear zones (Figure 3.4.9). The lozenges and shear zones are all aligned sub-parallel to bedding, which is oriented at 350E/160. This style of deformation is very similar to the Port Hood Island diapir external shear zone exposed at Bruces Cove, Port Hood Island (see below, Chapter. 3.5). The style and orientation of deformation with respect to the Coal Mine Point Diapir is an indication that intense shearing has occurred within the sandstone and it also indicates that similar shearing occurred within the surrounding mudstones and coals.

Interpretation. The mudstones and coal seams surrounding the second sandstone are relatively homogeneous and incompetent. These units probably accommodated drag zone folding by layer-parallel slip. This may account for the lack of visible evidence for penetrative strain in the incompetent units.

Figure 3.4.5. Stratal Dip of the Coal Mine Point Diapir Drag Zone. From Coal Mine Point to the external shear zone approximately 56 degrees of rotation was recorded.

Figure 3.4.6. Dip of Extensional Faults within the Coal Mine Point Diapir Drag Zone. The range of fault plane dips can be interpreted to represent multiple generations of faults, however, the number of faults recorded is insufficient to prove this hypothesis.

Figure 3.4.7. Density of Micro Faults within the Coal Mine Point Diapir Drag Zone. Micro faults are only found within the sandstone units. No micro faults were recorded from the mudstone and coal-bearing intervals.

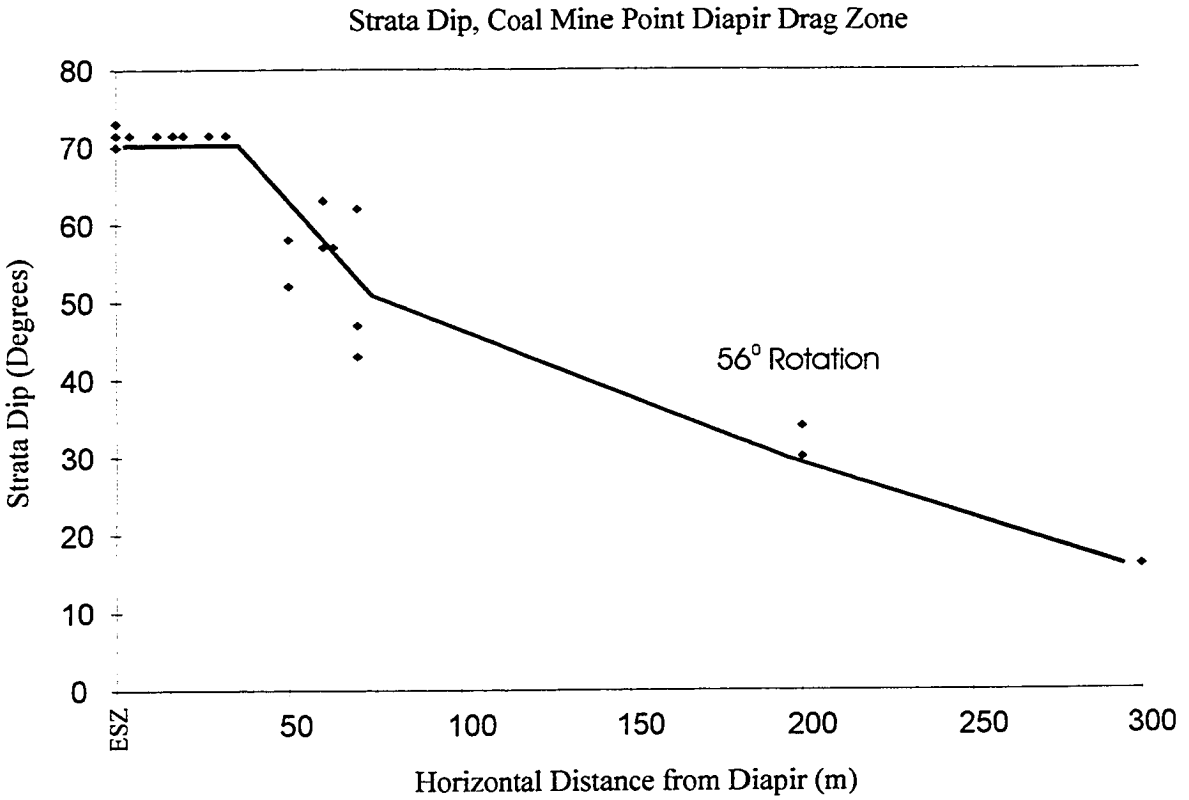

Figure 3.4.5.

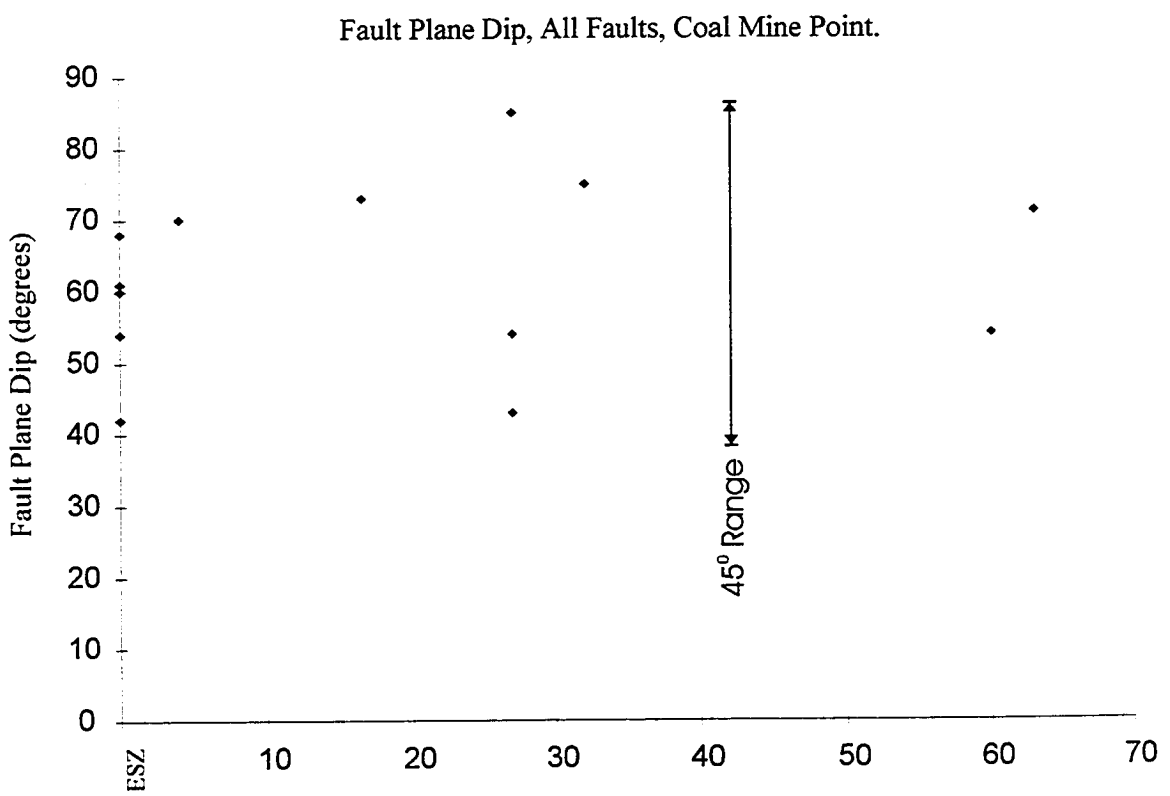

Figure 3.4.6.

Micro Fault Density, Coal Mine Point Diapir

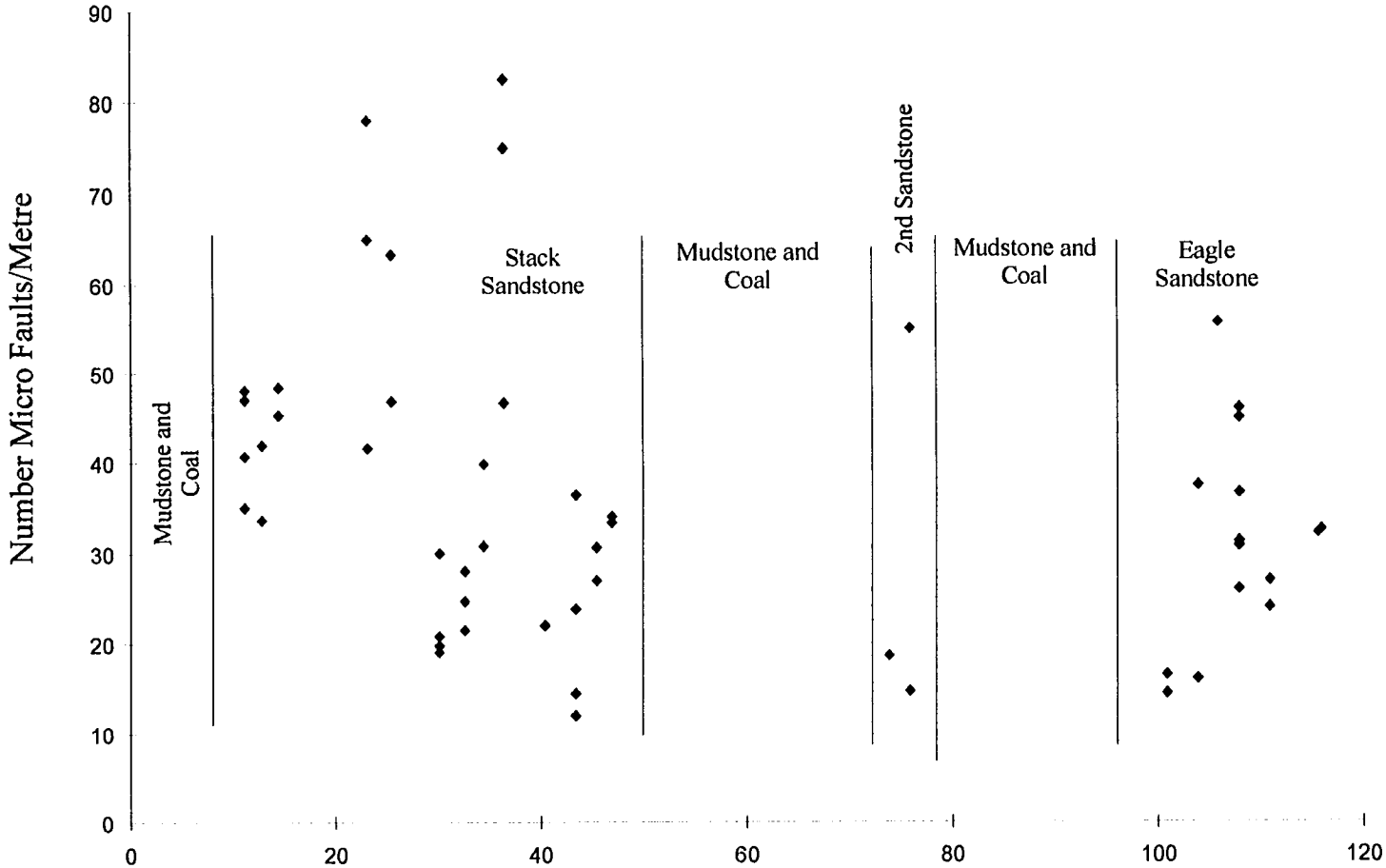

Figure 3.4.7.

Figure 3.4.8. The Stack Sandstone exposed on the southern flank of the Coal Mine Point Diapir. The Stack Sandstone has been reduced to a breccia by a combination of conjugate joint sets, micro faults and extensional faulting. On the top left of the photograph the contact of the diapir flank (white gypsum) and the Stack Sandstone can be seen. Approximate field of view 100m.

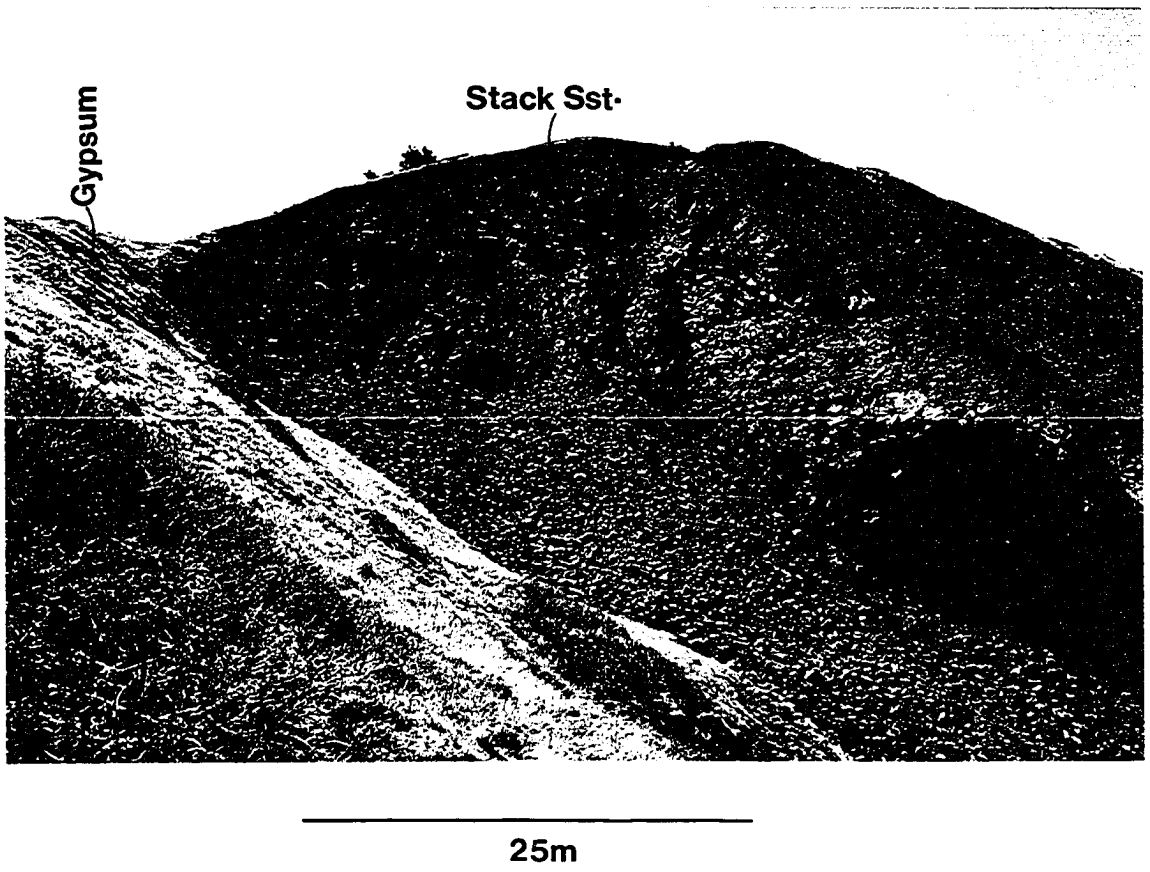

Figure 3.4.8

Figure 3.4.9a. The second sandstone unit within the southern drag zone of the Coal Mine Point Diapir. Meter-scale anastomosing shear zones can be seen in the outcrop. The shear zones bound lozenge-shaped units of rock which have little internal deformation.

(Scale, camera case is 17 cm long)

Figure 3.4.9b. Larger-scale photograph of the second sandstone unit. In outcrop, the anastomosing shear zones can be observed at a centimeter and millimeter scale. This style of deformation was also observed on Port Hood Island (see Chapter 3.5).

(Scale, car key ring is 4.2 cm long)

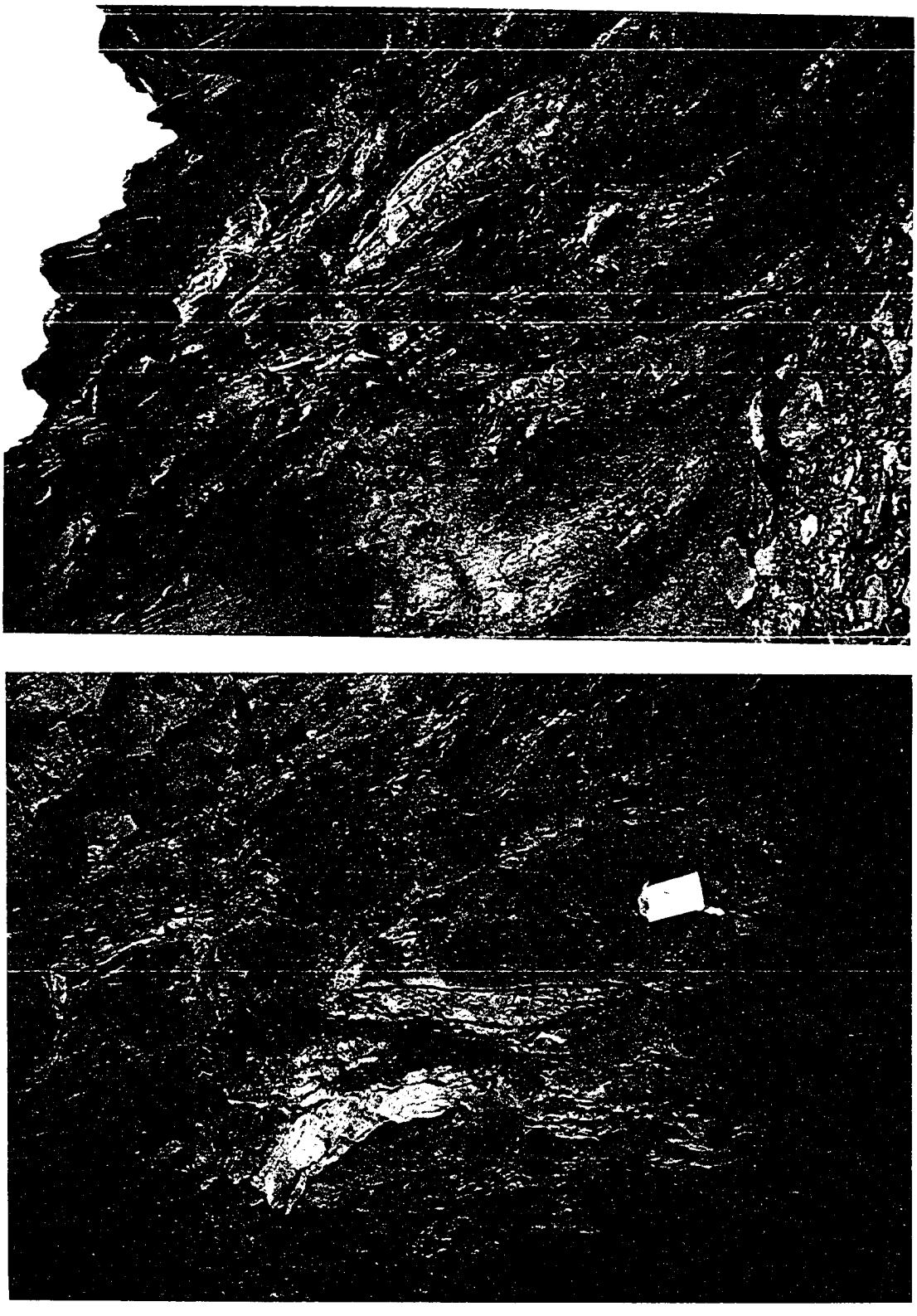

Figure 3.4.9a (right), 3.4.9b (left)

3.5, THE PORT HOOD ISLAND DIAPIR

3.5.1, Geographic Data

The south-east external shear zone of the Port Hood Island Diapir is exposed at latitude 46N,01,13 longitude 61W,33,47 - Bruces Cove - and latitude 46N,00,40 longitude 61W,34,25 - Bear Cove. The Port Hood Island Diapir exposure forms the north-west promontory of Port Hood Island – topographical map 11K/4 (Figures 3.5.1 and 3.5.2).

3.5.2, General Information

The Port Hood Island Diapir has not previously been described as a diapiric structure. Previous interpretations described Port Hood Island as a fault-bounded horst (Hacquebard et al., 1989). Recent palynological dating indicates that the Upper Carboniferous strata exposed on Port Hood Island are of Westphalian B age, placing them within the Henry Island Formation (Giles et al., 1997a).

3.5.3, Port Hood Island Diapir - Seismic Data

The Port Hood Island Diapir is an onshore exposure of the Salt Wall Luey (see above, Chapter 2). Line 75 of the 1982 Chevron seismic survey is the closest line to Port Hood Island, crossing the Salt Wall Luey approximately 5 km south-west of Port Hood Island. On line 75, the Port Hood Formation and Inverness Formation coal seam reflectors are interpreted to pinch out against the northern flank of the Salt Wall Luey. Although the quality of the seismic data degenerates near the pinch-out at the diapir margin, the Inverness Formation is interpreted to lie with angular unconformity upon the Port Hood Formation at the diapir margin. This interpretation is reasonable in light of evidence suggesting Westphalian diapiric growth (see above, Chapter 2) and the exposure onshore of a similar unconformable relationship within the Port Hood Island drag zone at Bruces Cove, Port Hood Island (see below). At Bruces Cove, palynologically dated Westphalian B sediments lie above the angular unconformity.

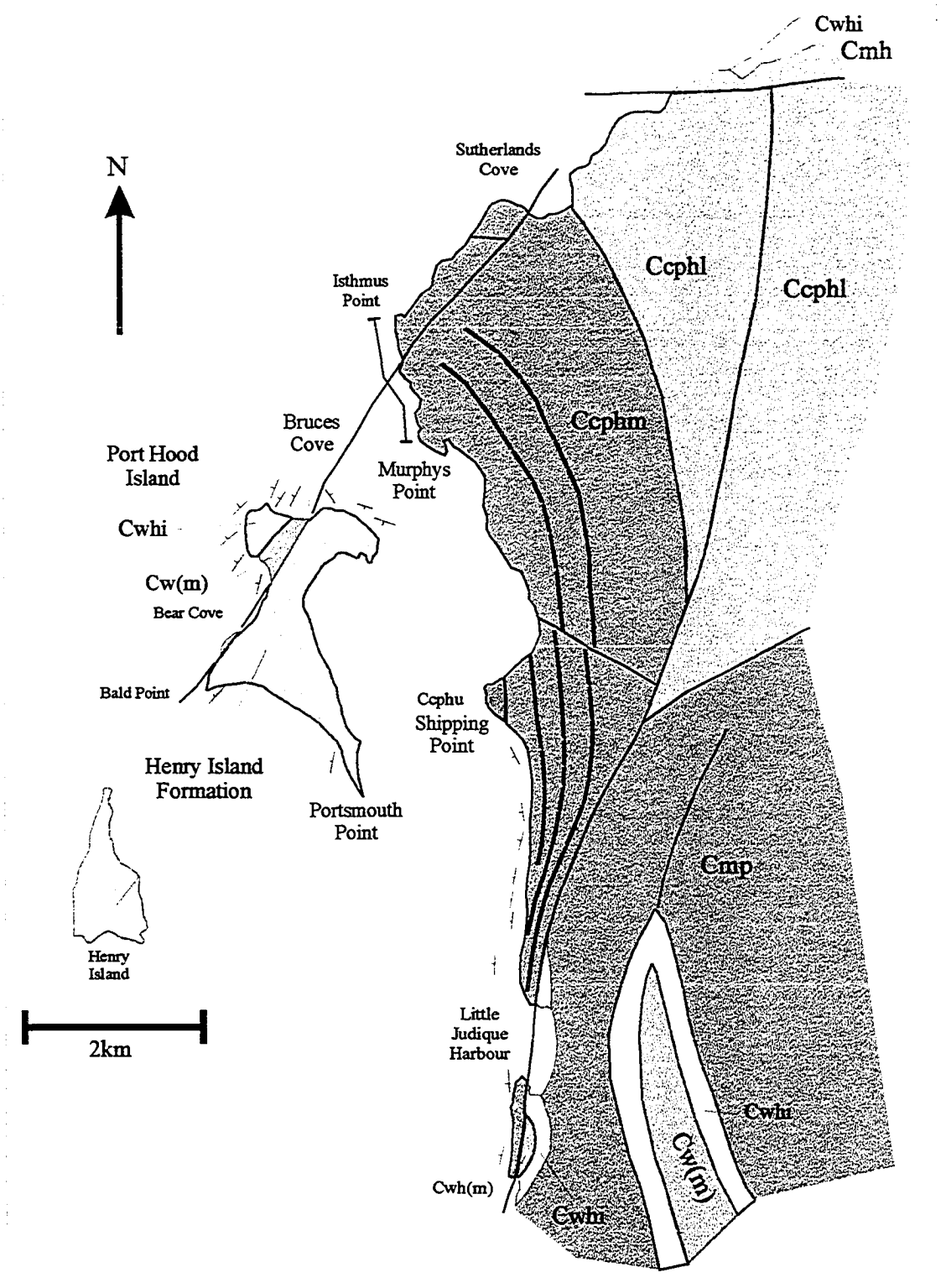

Figure 3.5.1. Geological map of the Port Hood area. For key see Figure 2.3.1 (Modified from Giles et al. (1997a)

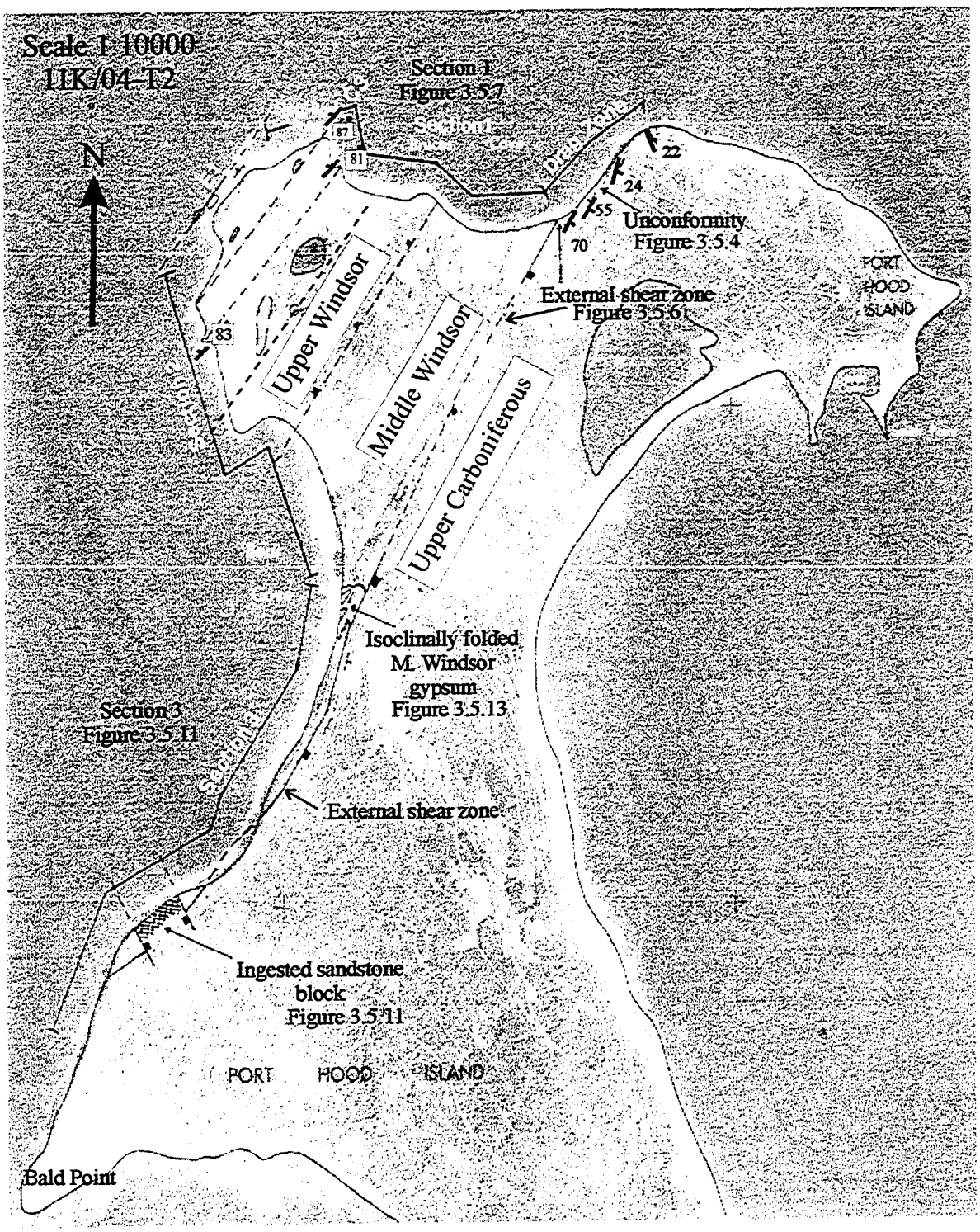

Figure 3.5.2. Orthophotograph of Port Hood Island to show the position of geological sections referred to in text.

Interpretation. The seismic to onshore correlation suggests that the majority of the clastic sediments that make up Port Hood Island belong to the Henry Island Formation. The folded red strata that lie stratigraphically beneath the unconformity at Bruces Cove (see below) appear, on seismic line 75, to correspond to the Port Hood Formation coal seam reflectors. A tentative Westphalian A age date can therefore be assigned to the strata immediately beneath the unconformity.

3.5.4, The Port Hood Island Diapir - Onshore

Figure 3.5.1 shows that Middle Windsor Group and Hood Island Formation strata make up the north-west corner of Port Hood Island and that the Windsor Group rocks are separated from the Upper Carboniferous strata by a sharp discontinuity previously described as a reverse fault (Hacquebard et al., 1989). This discontinuity is re-interpreted here as the south-eastern external shear zone of the Port Hood Island Diapir. The Windsor Group strata to the north-west of the external shear zone are therefore interpreted to be diapiric and the Upper Carboniferous strata to the south-east are interpreted as the deformed overburden adjacent to the diapir. The Windsor Group strata exposed are interpreted to be part of a structural carapace that has been transported above the halite core of the Port Hood Island Diapir. This interpretation is similar to that of the other diapirs within the field area (Figure 3.5.3).

The overall strike of the Windsor Group strata is approximately north-east/south-west, parallel to the external shear zone. The orientation of the Port Hood Island coastline therefore results in exposure through two dip sections and one strike section. The Windsor Group strata are repeated in the two north-east/south-west oriented dip sections; however, the sections are not identical and the difference between the two sections helps to define some aspects of diapir-related deformation (see below).

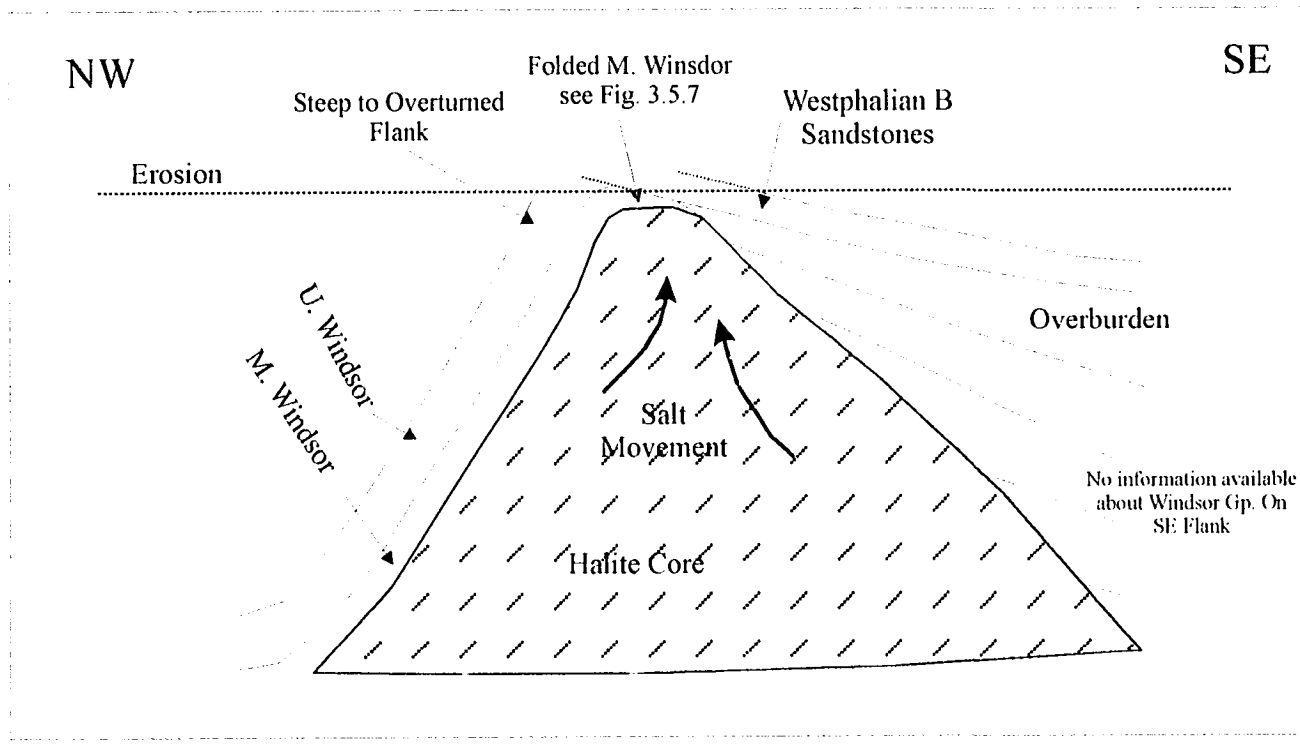

Figure 3.5.3. Schematic model for the configuration of the Port Hood Island Diapir and the adjacent sedimentary rocks which make up the majority of Port Hood Island.

3.5.5, Port Hood Island Diapir – South-East Drag Zone

The south-east drag zone is exposed as an 85 m section at Bruces Cove (Figures 3.5.2, 3.5.4 and 3.5.5). From the outer drag zone to the diapir margin, the dip of the strata increases from 14 degrees to 70 degrees at the external shear zone. The poor exposure within the drag zone prevents detailed structural analysis. The strata exposed to the south-east of Bruces Cove are gently dipping and relatively undeformed and are interpreted to be outside the diapir drag zone. Deformation of these rocks is probably related to rafting of the sedimentary cover on top of the Salt Wall Luey as part of the zone of rotation.

The drag zone at Bruces Cove is very narrow (85m) in comparison to drag zones associated with the Broad Cove, St. Rose and Coal Mine Point diapirs, but is similar to the south-west drag zone of the Monks Head Diapir, which is approximately 22 m long (see below, Chapter 3.6). The implications of drag zone width in relation to diapir size and growth mechanism are discussed in Chapter 4.

The most prominent feature within the drag zone is an angular unconformity between distinctive red sandstones and conglomerates (below unconformity) and buff sandstones and conglomerates (above unconformity). The strata above the unconformity consist of buff channel sandstones, mudstones and numerous conglomeratic units. The conglomerate units are typically ~1 m thick and are dominated by clasts of reworked limestones (stromatolites, grainstones and oolites) as well as rare siltstone clasts. The limestone clasts are rounded and range from 5-45 cm in diameter. Individual conglomerate units are normally graded and rest upon erosional surfaces. The strata below the unconformity comprise coarse red sandstone and red mudstone containing carbonate nodules (1-3cm). Associated conglomerates are polymict and contain a variety of sedimentary clasts (limestones, siltstones, mudstones and sandstones) as well as basement clasts of granitic and mafic rocks (Figure 3.5.4). The polymict conglomerates are poorly sorted and the basement clasts are mainly angular. The strata above and below

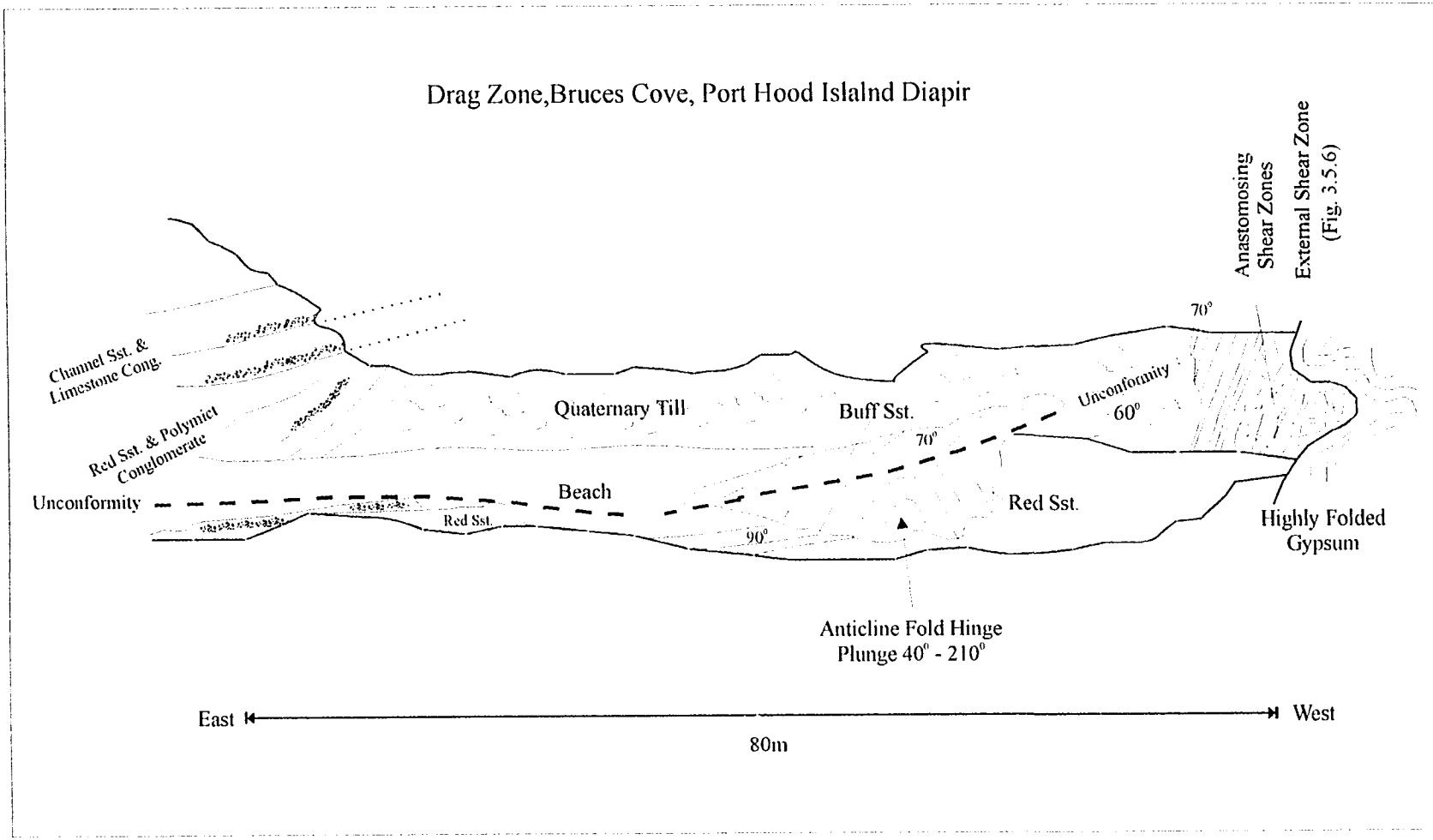

Figure 3.5.4. The drag zone section exposed at Bruces Cove, Port Hood Island. See Figure 3.5.2 for location.

Figure 3.5.5. Rotated unconformity, Bruces Cove, Port Hood Island. Strata beneath the unconformity consists of red sandstones and polymict conglomerates whereas the strata above the unconformity consist of buff channel sandstones and monomict conglomerates. The red strata beneath the unconformity have been tightly folded.

(Scale, hammer = 32cm long)

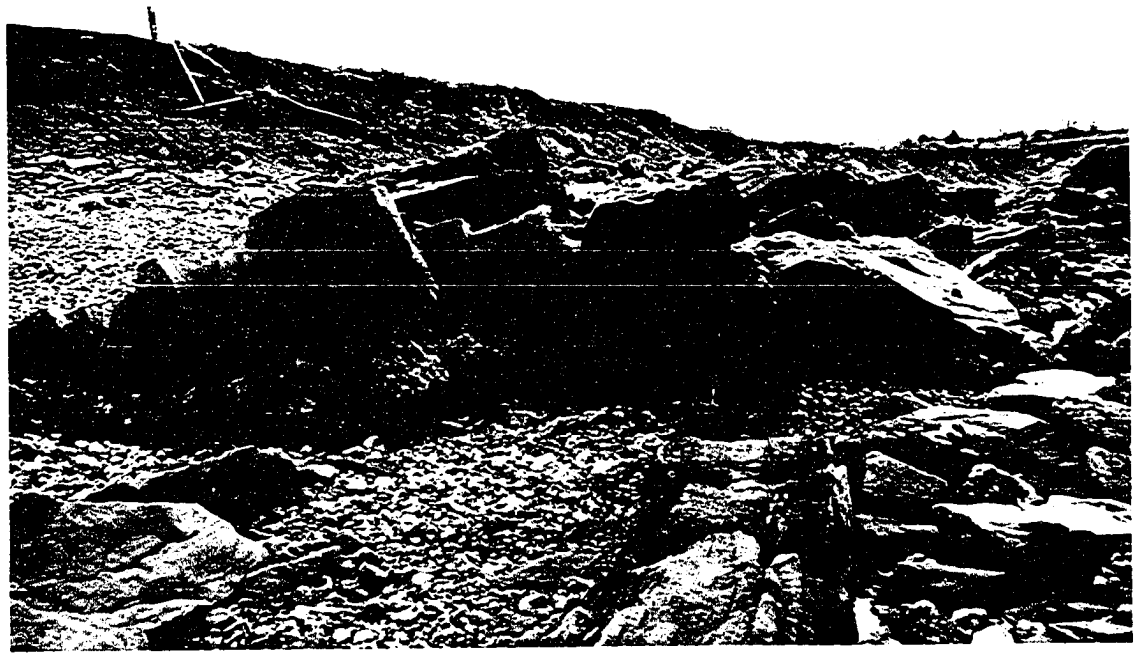

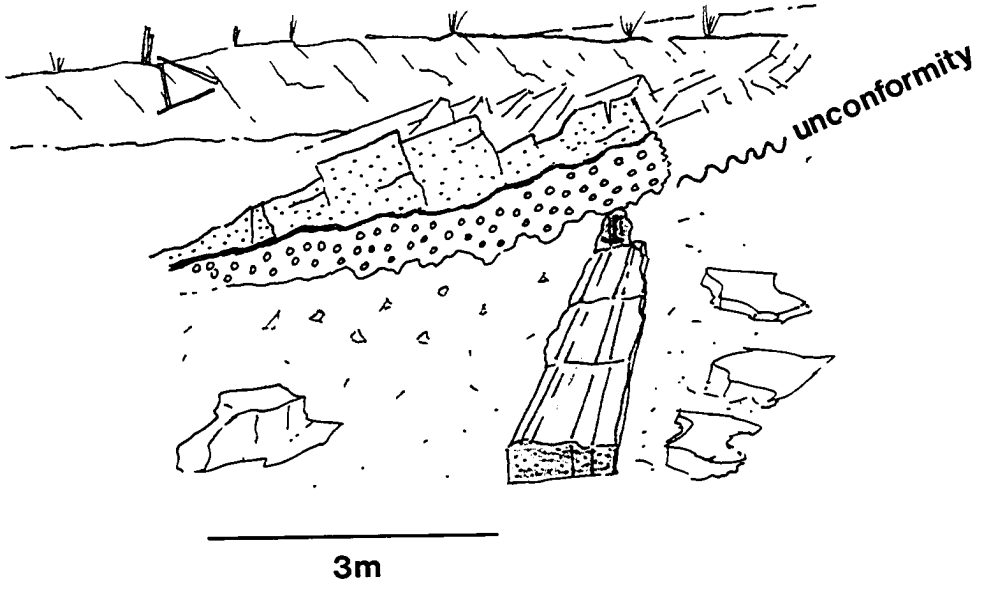

Figure 3.5.5

the unconformity are distinguished by the distinctive colour of the sandstones and the clast composition of the conglomerates.

The red strata beneath the unconformity surface were folded prior to erosion and so the precise discordance across the unconformity is hard to determine. The angular unconformity has approximately 25 degrees of discordance (Figure 3.5.3).

The unconformity surface has been folded within the drag zone so that the dip of the unconformity surface increases from 12 degrees (outer drag zone) to 60 degrees adjacent to the external shear zone. The fact that the unconformity is folded within the drag zone implies that it is a pre- or early drag zone structure that has been folded as the diapir intruded the overburden sediments, forming the drag zone.

The South-East External Shear Zone

The south-east external shear zone is a 5 m wide shear zone consisting of grey siltstones which contain spectacular anastomosing shear zones (Figures 3.5.4 and 3.5.6). The exposure comprises siltstone lozenges with little internal deformation surrounded by brittle shear zones less than 2 cm wide. Deformation within the lozenges is restricted to conjugate brittle faults whose orientation mirrors that of the surrounding shear zones. The pattern of lozenges surrounded by shear zones can be distinguished over several orders of magnitude (m scale to mm scale) within the outcrop. No joint sets or micro-faults were recorded within the external shear zone. The anastomosing shear zones are separated from weakly deformed siltstone by a bedding-parallel (dip 70 degrees) fault.

The external shear zone is very irregular. The external shear zone and the adjacent gypsum of the Port Hood Island Diapir have been folded together into tight, convoluted folds. Large numbers of small thrust, strike-slip and extensional faults with no apparent preferred orientation are associated with this folding (Figure 3.5.6).

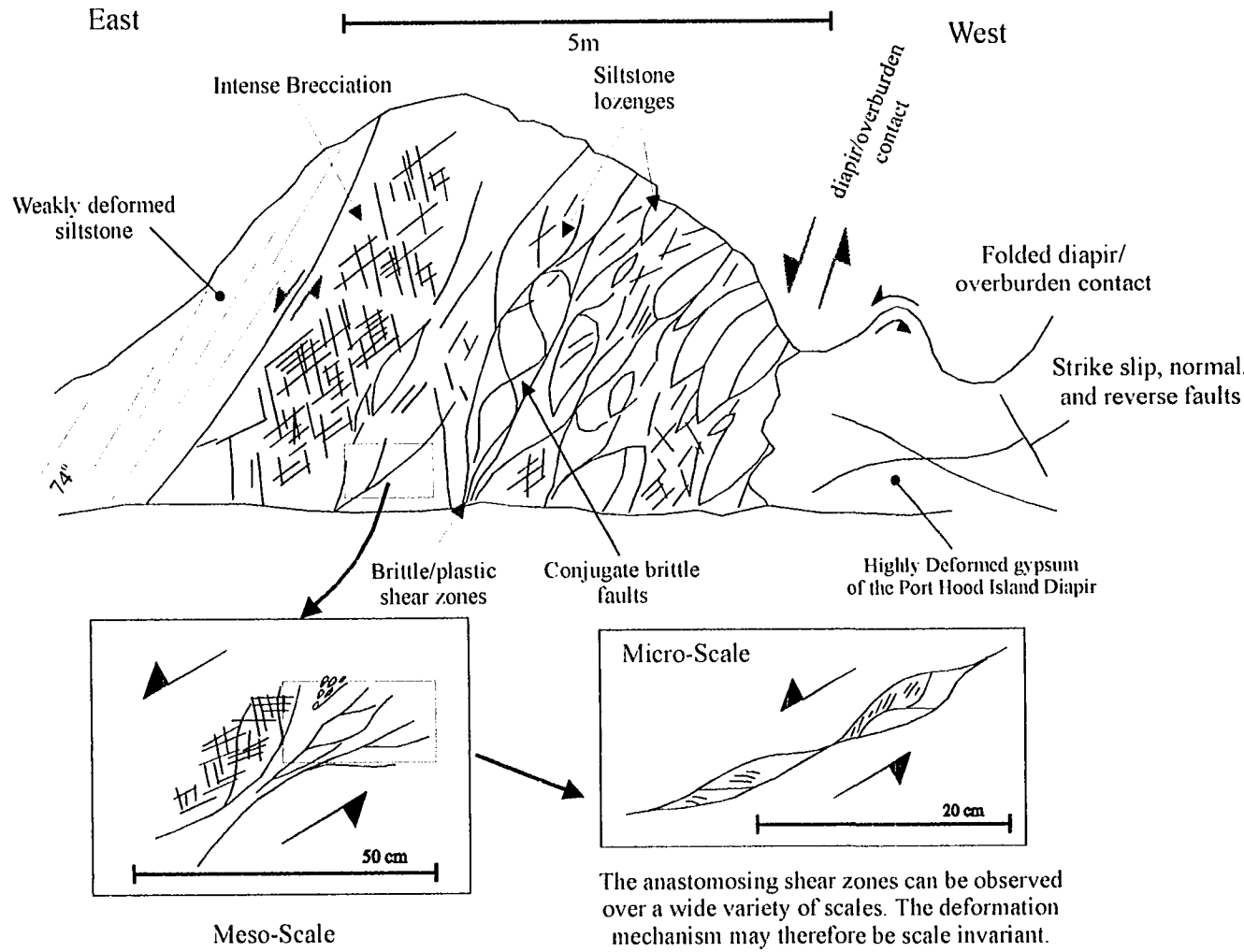

Figure 3.5.6. The External Shear Zone of the Port Hood Island Diapir exposed at Bruces Cove, Port Hood Island (see Figure 3.5.4).

The external shear zone can be correlated across Port Hood Island to Bear Cove, where it again separates Upper Carboniferous strata from Middle Windsor gypsum. The strike of the external shear zone is relatively constant at 045 degrees (Figures 3.5.1 and 3.5.2).

3.5.6, The Port Hood Diapir

The Port Hood Island Diapir is exposed for a continuous length of 1.75 km along the north-west promontory of Port Hood Island. The orientation of the coastline changes through the section, exposing dip and strike sections through the diapir. For this reason, the description of the Port Hood Island Diapir is divided into three sections (Figure 3.5.2).

Section 1, Northern Dip Section

This section is exposed from Bruces Cove to Shag Rock Point in a south-east to north-west direction. The section is a dip section through Middle Windsor Group and Hood Island Formation strata (Figure 3.5.7).

The Middle Windsor strata consist of massive gypsum units with intercalated thin limestones and subordinate red siltstones and mudstones. Although the gypsum units are poorly preserved due to intense coastal erosion, several folds are exposed. The folds are generally tight and have fold hinges oriented parallel to the diapir margin, plunging moderately (18 - 30 degrees) to the south-west or north-east.

The limestones are generally less than 30 cm thick and often show intense brecciation. The upper and lower surfaces of the limestones are commonly brecciated and angular fragments of the limestone are included within adjacent gypsum units. The included limestone fragments are interpreted to be the result of progressive dissemination of limestone units, which is a common feature of diapiric deformation within the project area (see Coal Mine Point, St. Rose and Monks Head diapirs). Stacy (1953) identified the limestones within this section as the B2 and B3 Middle Windsor limestones. The thickest

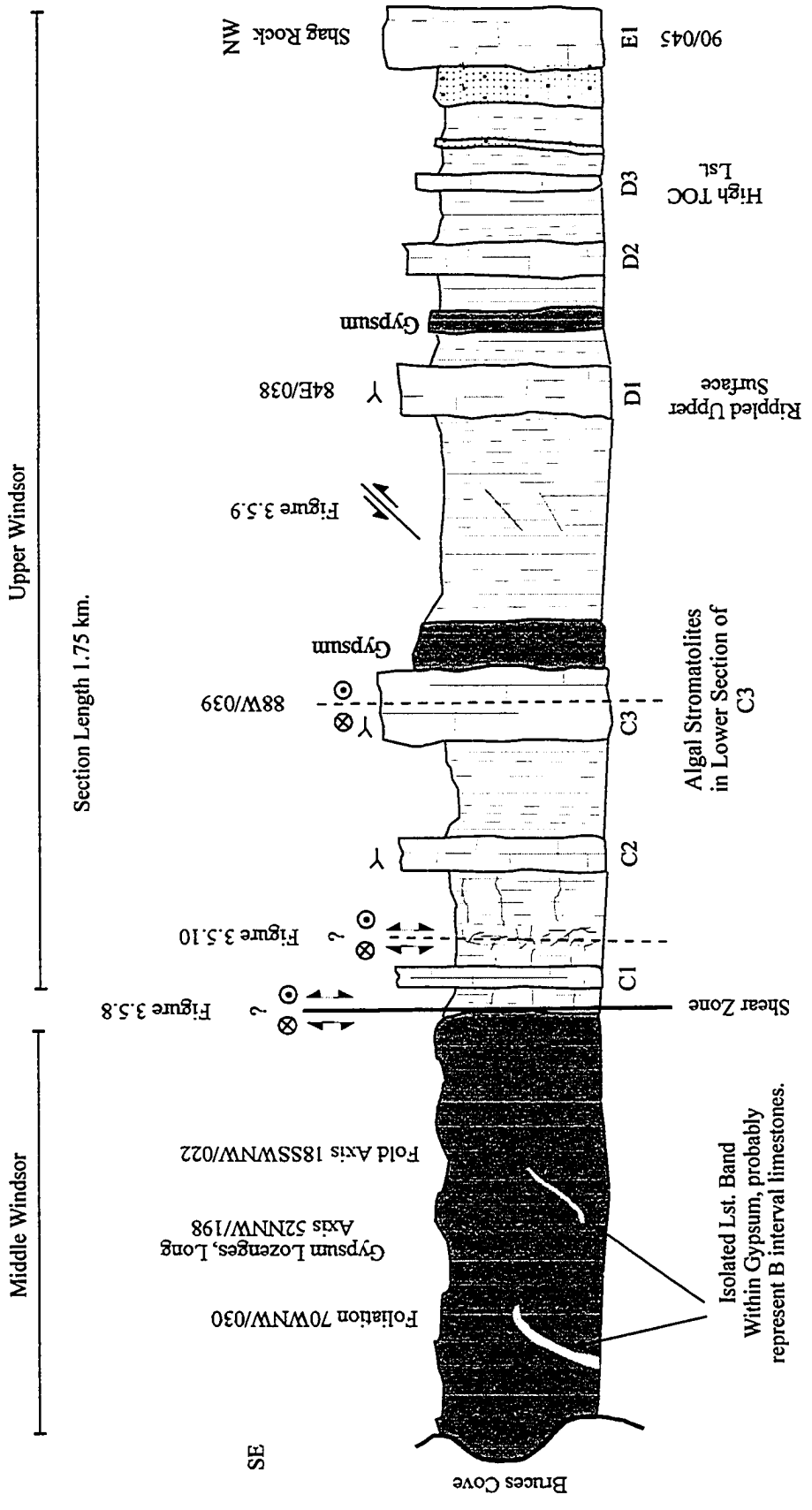

Figure 3.5.7. Section 1, Bruces Cove to Shag Rock, Port Hood Island.

limestone observed today is 28 cm thick and consists of a fine grained micritic mudstone. Other limestone units are intensely brecciated and appear as limestone fragments within a gypsum matrix. Within this thesis, the Middle Windsor limestones observed are not assigned to be a specific limestone unit. However, there is no obvious reason not to adopt Stacy's identification since it has no impact upon the results of this thesis.

A portion of the Middle Windsor strata is absent (P.S. Giles, pers. comm. 1995) and the Middle Windsor Group/Hood Island Formation contact is marked by a bedding-parallel shear zone (Figures 3.5.7 and 3.5.8). The displacement across the shear zone could be vertical or horizontal or a combination of both. No oriented shear sense indicators were recorded from the shear zone and so the displacement is not known.

The Hood Island Formation strata exposed within section 1 consist of thick grey limestones, white gypsum, red siltstones and red mudstones. The section is a complete Hood Island Formation stratigraphic section from the C1 limestone to the E1 limestone (Figure 3.5.7). Although the section is highly deformed (see below), no stratigraphic repetitions were recorded and so the section is probably not folded. For a complete lithological and paleontological review of this section, see Stacy (1953), Sage (1954), Schenk (1969) and Giles and Boehner (1982).

Specific Deformation within Section 1

Within the Hood Island Formation strata of section 1, various deformation styles illustrating typical diapir-related deformation were observed. The deformation is described below in a south-east to north-west direction (see Figure 3.5.7)

- The red strata are cross cut by numerous fibrous gypsum veins. The majority of the veins have a sub-horizontal orientation but, in some locations, the gypsum veins are orientated parallel to the steeply dipping bedding. All of the gypsum veins are relatively undeformed and cross-cut some of the shear zones and smaller

Figure 3.5.8. The shear zone (fault) contact between the Middle Windsor Group and Hood Island Formation strata. No shear sense indicators were recorded from the shear zone and so the true displacement is not known. The offset is shown assuming that the Middle Windsor has been upthrown, truncating part of the Hood Island Formation (see Figure 3.5.3).

A. View of the shear zone which consists of sheared gypsum and mudstone.

B. Cliff section view of the shear zone (fault) contact.

(Scale, hammer is 32cm long)

For location of this figure, see Figure 3.5.7.

Figure 3.5.8 (A) top (B) below

- faults. Where the veins are sub-horizontal, the vein fibres have a sub-vertical orientation, indicating a vertical opening direction. Veins that are orientated parallel to bedding tend to have sub-horizontal vein fibres, indicating a horizontal opening direction.

- The red mudstone strata are relatively uniform and distinguishable faults are rare throughout most of the section. Where the strata are banded red and green, small-scale faults can be distinguished (Figure 3.5.9). It is not known when the faults formed with respect to the rotation of the bedding. The faults may therefore be extensional faults (if they formed post-rotation) or contractional faults (if they formed pre-rotation).

- Figure 3.5.10 shows a zone of highly deformed green strata and gypsum veins some 3 m wide. Within the deformed zone, no original sedimentary features can be determined and fold and fault structures are juxtaposed in several orientations. The deformed zone separates two relatively intact units and is interpreted to be a fault zone separating two stratigraphic units that have been displaced vertically or horizontally relative to one another. All deformation caused by this displacement was accommodated within the strain zone so that the stratigraphic units to either side remained relatively undeformed.

- Although highly faulted, the limestones are still intact and can be assigned to specific stratigraphic units based upon sedimentology. The limestones exposed within this Hood Island Formation section are the C1, C2, C3, D1, D2, D3 and E1 limestones (stratigraphic nomenclature of Stacy (1953), Sage (1954), Giles and Boehner (1982). The C3 limestone is easily recognised by the presence of 1 m tall club-shaped algal stromatolites (Giles and Boehner, 1982). These stromatolites have a pervasive dextral displacement of the top of each stromatolite by ~10 cm with respect to the lower surface. This displacement could be the result of dextral

Figure 3.5.9. Small faults within the Hood Island Formation, section1. It is not known when the faults formed with respect to the dip of the strata. In their current position the upper two faults are steeply dipping contractional faults and the lower most fault is a sub-horizontal contractional fault. The fault planes have been mineralized by gypsum. It is suspected that many more small-scale faulting exists but was not observed due to the homogeneous nature of the red mudstones.

For location of figure see Figure 3.5.7.

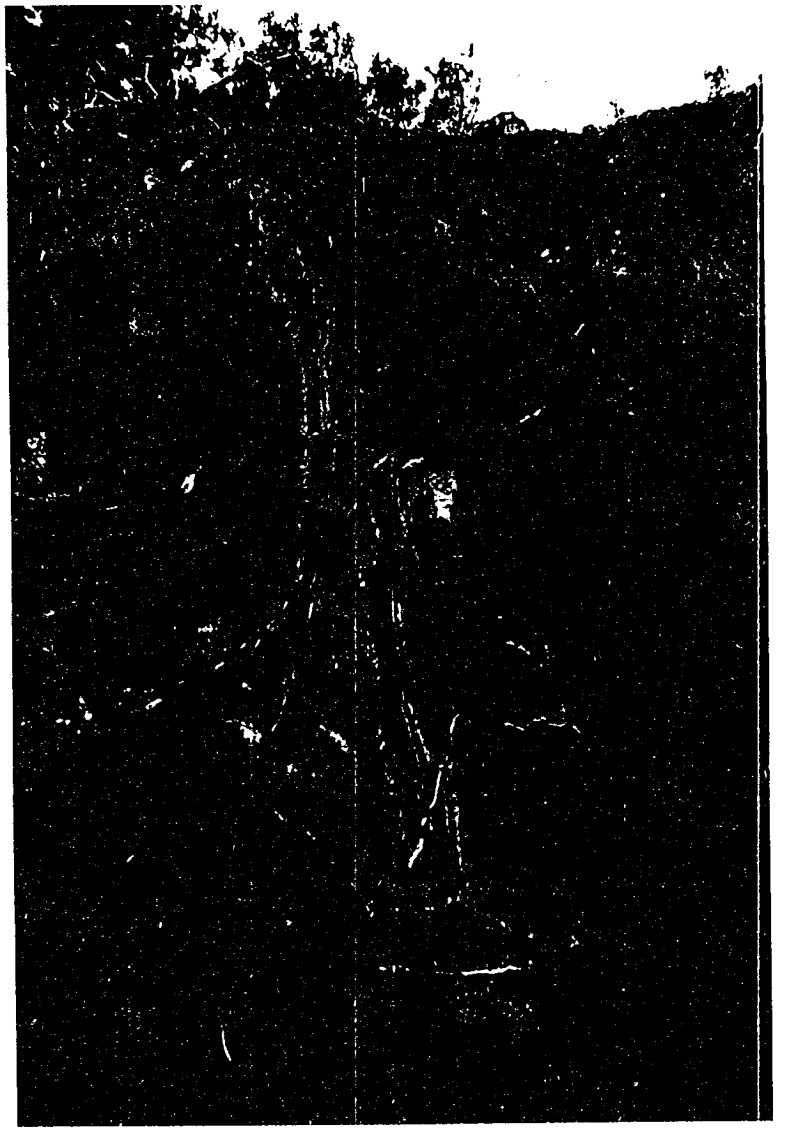

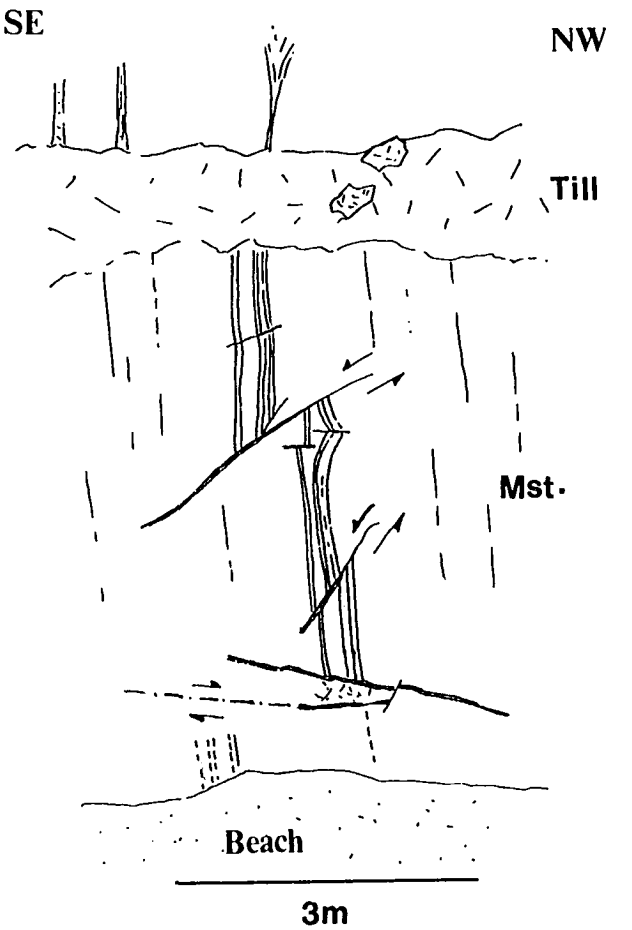

Figure 3.5.9

Figure 3.5.10. A Deformation Zone within Green Mudstone of the Hood Island Formation. The deformation zone separates two relatively undeformed units of red mudstone which have been displaced relative to one another. Note the sub-horizontal gypsum veins within the weakly deformed red mudstone and the folded gypsum veins within the deformed green strata. For location see Figure 3.5.7.

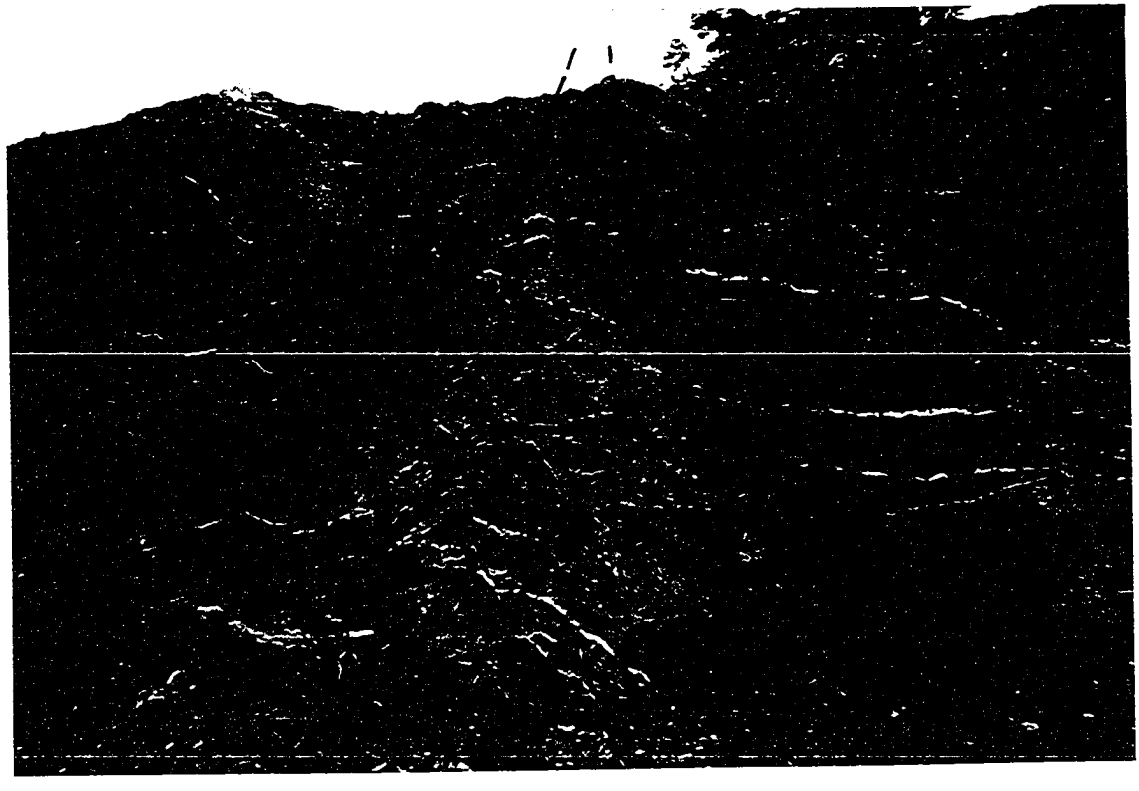

3m

Figure 3.5.10

shearing of the strata, with the shear direction oriented parallel to the external shear zone/diapir margin. Alternatively, the offset could be a growth feature of the stromatolites related to water current or ambient sunlight conditions.

The dip and strike of the strata within section 1 are roughly constant. Stratal dip is sub-vertical or dips steeply north-west and the strike ranges from 028 to 045 degrees, sub-parallel to the external shear zone/diapir margin.

Section 2, Southern Dip Section

This poorly exposed section extends from Shag Rock to Bear Cove (Figures 3.5.1 and 3.5.2). The limited exposure prevents a precise stratigraphic description of the Windsor Group strata, although it can be stated that the Hood Island Formation strata exposed in Section 1 appear to be repeated in Section 2.

The brecciation of the limestones within Section 2 may reflect more intense deformation of the strata in this area. Localization and variations of deformation (finite strain and/or strain rate) within the Port Hood Island Diapir (see above) and other diapir outcrops are common within the field area, for example the Monks Head and St. Rose diapirs. The limestone units exposed in Section 2 may have become fragmented in response to a higher finite strain or higher strain rate in this area, whereas the intact limestone units of Section 1 represent an area of lower strain rate or lower finite strain. Any horizontal or vertical extensional stress applied to the brecciated limestones would draw the limestone out into a mega-boudinage similar to that observed at Monks Head (see below, Chapter 3.6).

Section 3, Strike Section

Section 3 is a 1.25 km strike section along the external shear zone of the Port Hood Island Diapir from Bear Cove to Bald Point (Figures 3.5.1 and 3.5.2). The orientation of the external shear zone with respect to the coastline causes the section to repeatedly step

between the hangingwall and footwall of the external shear zone, alternately exposing diapir and drag zone strata. The section is described from Bear Cove to Bald Point (north-east – south-west).

- Middle Windsor strata are exposed at the northern end of Bear Cove and have been folded into tight to isoclinal folds (Figures 3.5.11, 3.5.12 and 3.5.13). The fold axes are oriented parallel to the external shear zone/diapir margin. This Middle Windsor section is probably stratigraphically equivalent to the Middle Windsor strata exposed at Bruces Cove. Folding within the gypsum has preserved the bed thickness throughout the folds (class 1b folds). Angular inclusions of Windsor Group limestone up to 20 cm in diameter are contained within the gypsum units. Zones of limestone fragments with an average clast size of ~1 cm are also found within the gypsum. These zones are typically less than 1 m thick.

- To the south-west of the folded gypsum units, Henry Island Formation sandstone units overlie Windsor Group red mudstone, which in turn overlies the highly folded Middle Windsor Group gypsum (Figure 3.5.12). The external shear zone in this section is therefore the shallowly dipping (22 degrees south-east) contact between the red Windsor Group mudstone and the Henry Island Formation sandstone. The exposed external shear zone is a discrete surface with very little associated brittle deformation.

- 500 m north-east of Bald Point is a block of Henry Island Formation sandstone, measuring approximately 100 m long by 30 m high, that has been ingested into the gypsum (Figure 3.5.11). Although the edges of the sandstone block can easily be recognised, the block has been completely brecciated into decimeter scale fragments so that original sedimentary structures can no longer be distinguished.

  Interpretation. The block of sandstone probably collapsed into a solution hole

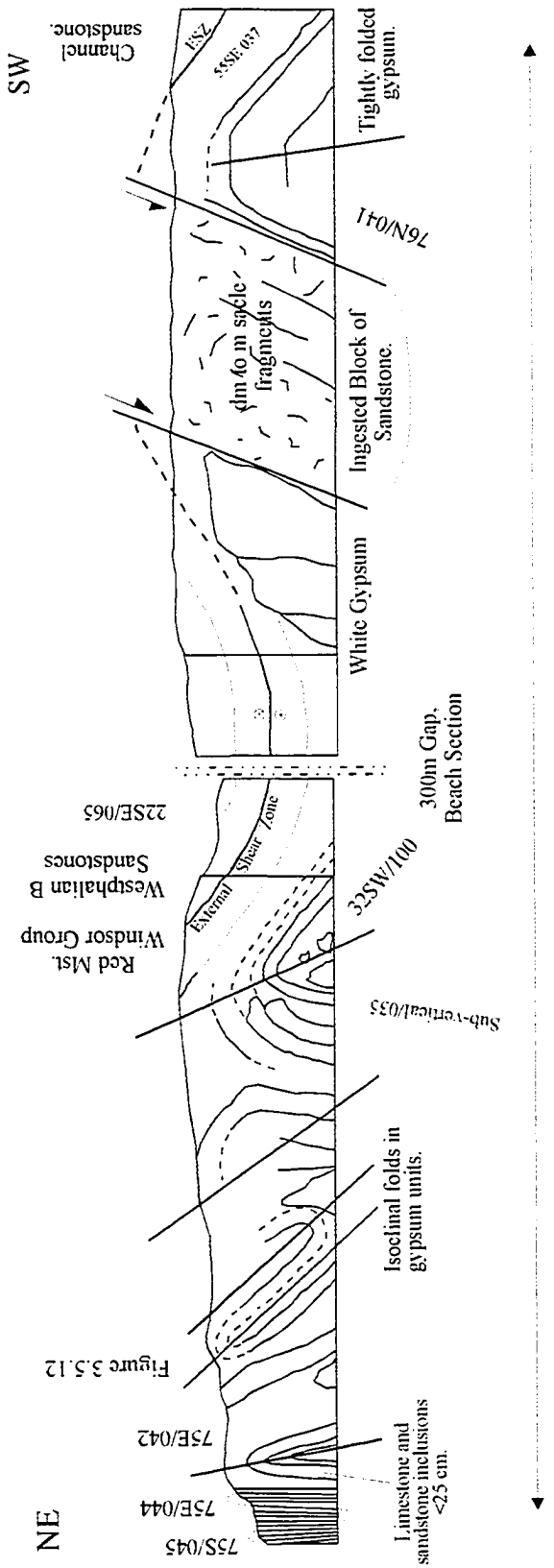

Figure 3.5.11. Section 3, Bear Cove to Bald Point (see Figure 3.5.2 for location).

Figure 3.5.12. Isoclinal fold within gypsum, Bear Cove, Port Hood Island. Note that bed thickness is preserved despite the fact that the gypsum has been folded into an isoclinal fold. This outcrop collapsed during the winter of 1994.

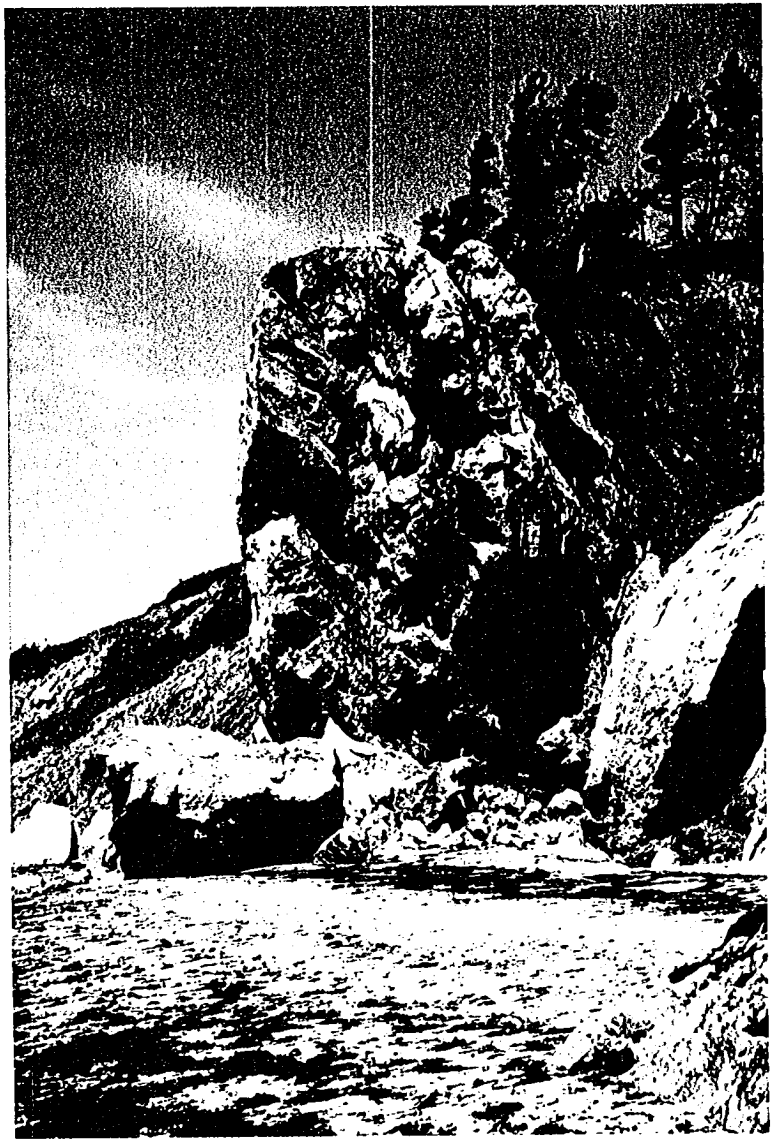

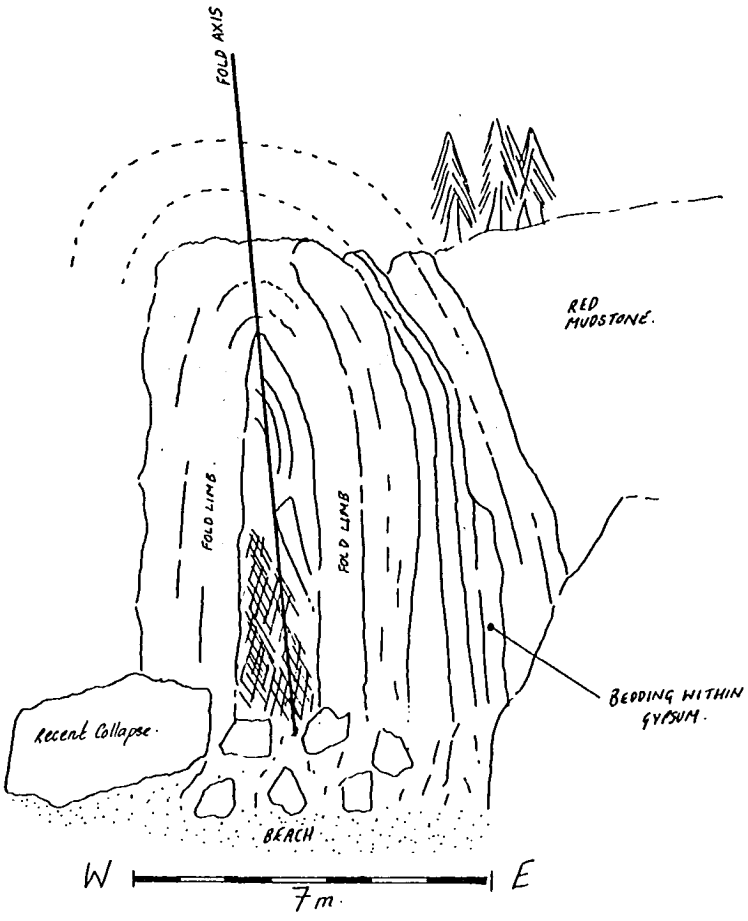

ISOCLINAL FOLD, BEAR COVE, PORT HOOD ISLAND.

Figure 3.5.12

Figure 3.5.13. Bear Cove, Port Hood Island, (Section 3). Tight to isoclinally folded gypsum can be seen on the left of the photograph (see Figure 3.5.12). In the centre and at the right buff channel sandstones of the Port Hood/Inverness Formation overlie purple/red mudstone of the Windsor Group. The mudstone/ sandstone contact forms the external shear zone in this location which dips gently (22 degrees) towards the north-east.

(Scale of view, approximately 1000m)

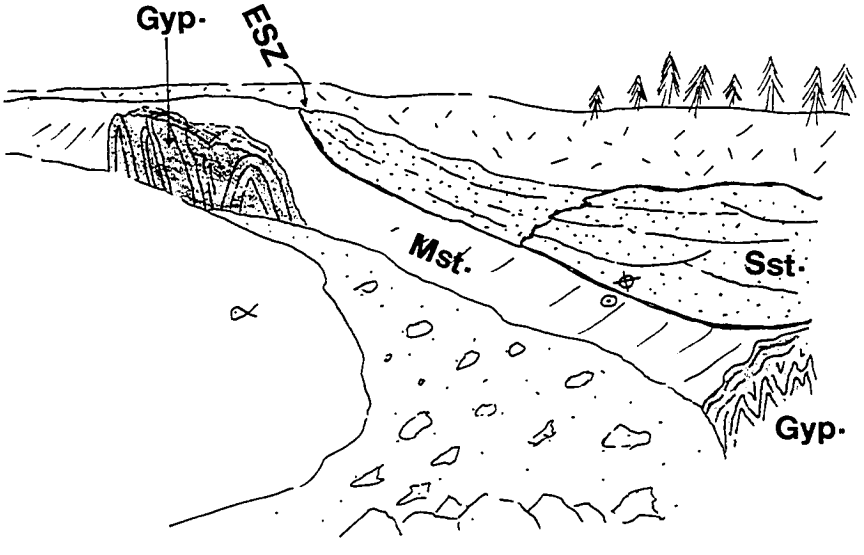

Figure 3.5.13

within the gypsum. This resulted in the almost complete brecciation of the sandstone unit. Ingestion and fragmentation of overlying overburden may be an important mechanism of diapiric growth that allows a diapir to grow vertically. This mechanism is similar to that described for diapirs from the Red Sea Coast of Yemen (Davison et al., 1995). Alternatively, the collapse of the block could have been caused by more recent dissolution of underlying halite that created a cavity into which the block collapsed. Unfortunately, there is no way to conclusively prove which of the two mechanisms is correct.

- At Bald Point, the Henry Island Formation sandbodies are well exposed and dip steeply (41 degrees) to the south-east. Unfortunately, the remainder of the section to the south-east of Bald Point is covered by recent mud washover and bank collapse. The drag zone section from Bald Point to Portsmouth Point is therefore unexposed and no detailed structural measurements were recorded.

3.5.7. General Structural Features Associated with the Intrusion of the Port Hood Island Diapir

All of the Middle Windsor Group rocks on Port Hood Island are strongly folded into tight to isoclinal folds that have generally steeply dipping or vertical limbs and gently plunging fold axes. In contrast, the Hood Island Formation rocks, although highly deformed, are not folded, and have an almost homoclinal dip on Port Hood Island. Throughout the exposure of the Port Hood Island Diapir, almost all fold axes and foliations have orientations parallel to the margin of the Port Hood Island Diapir (045 degrees). The folds within the Middle Windsor could have been formed in response to a north-west orientated compression (i.e. sigma 1 = 325 degrees). In addition, the folding indicates that the rocks were probably at a shallow depth of burial when the rocks were folded. The oligomict conglomerates exposed at Bruces Cove indicate that the structural carapace was at surface at some time during the Late Carboniferous. The orientation of the compression that could have produced the folds in the Middle Windsor is very similar to the north-west

orientated compression determined from paleostress analysis at Green Point, Mabou Mines and MacKinnons Brook (see above, Chapter 3.3). The folding within the Middle Windsor rocks can therefore be correlated to inversion that probably took place during the Late Carboniferous. Another line of evidence to support inversion and lateral shortening of the structural carapace can be inferred from the position of the Westphalian B sandstone unit which now rests directly on top of the Middle Windsor. The sandstone unit shows no evidence of thinning onto the diapir and so may be a post-kinematic unit that has been actively uplifted by diapir rejuvenation during inversion. An interpretation of the Port Hood Island Diapir is shown in Figure 3.5.3. Fibrous gypsum veins cross-cut a lot of the deformation (folding and faulting) but remain relatively undeformed. This indicates that the veins were not emplaced until after most of the deformation of the structural carapace had taken place. The reasons and implications of this are discussed in Chapter 4.

3.6, THE MONKS HEAD DIAPIR

3.6.1, Geographic data

The north-west external shear zone is located at Monks Head, latitude 45N,50,36 longitude 61W,50,20. The south-east external shear zone is located at latitude 45N,40,16 longitude 61W,49,46. The diapir section is 496 m long. Monks Head is shown on topographic map 11E/16 (Figure 2.7.1).

3.6.2, General Information

The existence of salt springs and salt ponds has been known within the Antigonish area for over 100 years (Cole, 1930; Pohl, 1931). In 1866, the Nova Scotia Salt Works and Exploration Company conducted drilling operations to define sub-surface salt bodies at Town Point, 9 km north-east of Antigonish. Since that time, repeated attempts have been made to locate salt bodies around Antigonish using a combination of drilling, seismic data, gravity surveys and aeromagnetic surveys. Figure 3.6.1 shows the position of some of the salt exploration wells. In 1969, Novasel Limited drilled NSDM 4862 and penetrated 114 m of salt between 242 m and 365.8m. Further exploration wells within the area (BASSH-1, NSDM 1708 and NSDM 1835) (Figure 3.6.1) encountered minor amounts of salt but failed to penetrate a significant thickness of salt. The position of the NSDM 4862 well is significant since it is located only 3.5 km inland from the Monks Head Diapir described below. Approximately 10 km to the south of Monks Head at Pomquet River, NSDM 2554 and NSDM 2555 were drilled in 1958 over a strong gravity low (MacNeil, 1959). Although both wells failed to encounter significant salt bodies, a seismic line shot by the Nova Scotia Research Foundation in 1958 confirmed the presence of an antiformal structure interpreted to represent a salt dome (Blanchard, 1959). The history of salt exploration around Antigonish lends support to the interpretation of the Monks Head exposure as a diapir. The failure of drilling programmes to locate a salt structure may be due to the presence of a Hood Island Formation structural carapace, which commonly overlies the diapirs. The majority of

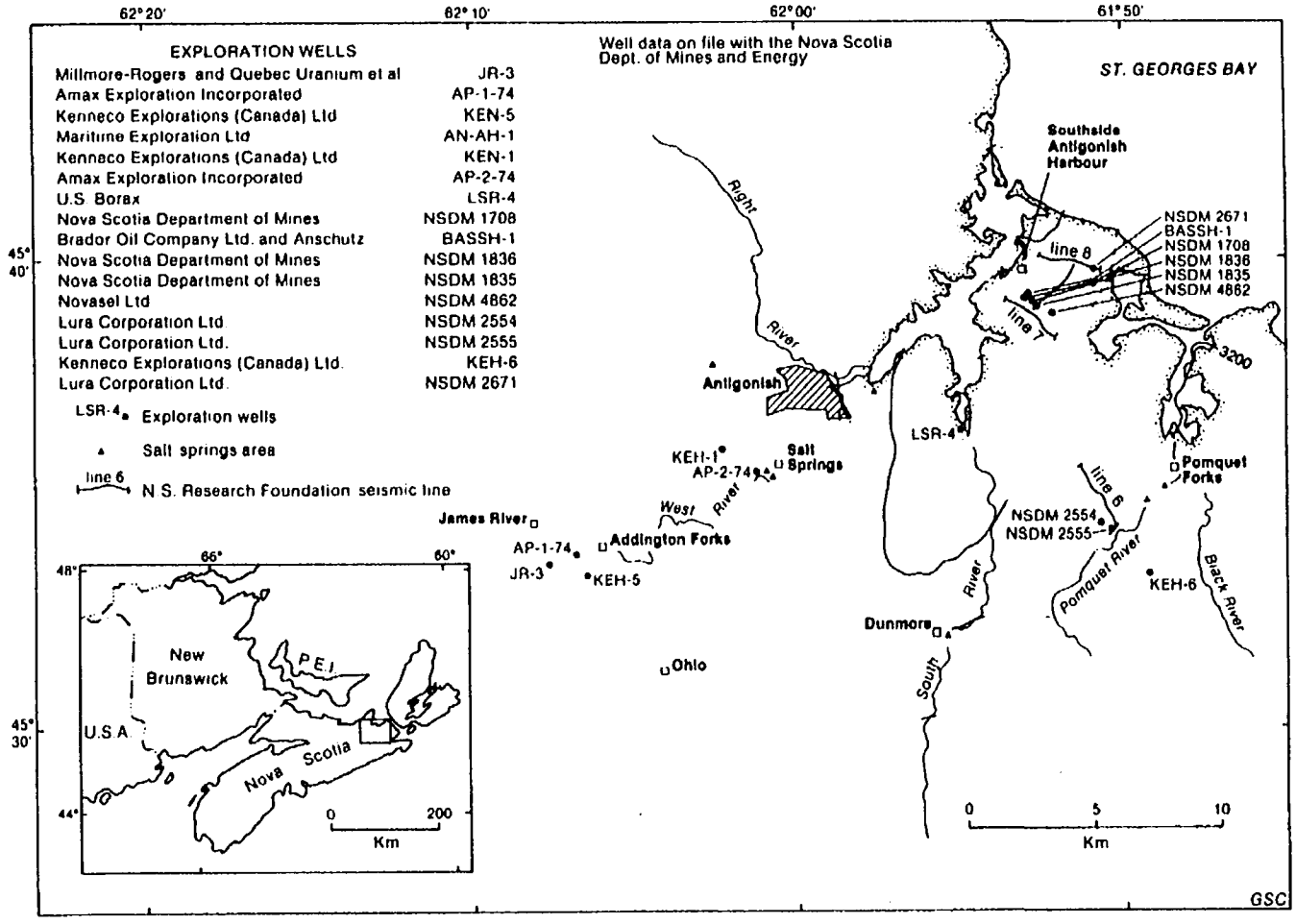

Figure 3.6.1. Map to show the position of the salt exploration wells and seismic lines within Antigonish County which are referred to in the text. Modified from Howie (1988).

wells were completed at a shallow depth of a few hundred metres and may have failed to penetrate the carapace, which may be hundreds of metres thick at Monks Head.

The Monks Head Diapir is the onshore exposure of the Salt Wall Luey. Although the Monks Head Diapir is the longest continuous diapiric exposure within the field area, the exposure represents only a fragment of the entire diapiric structure. As in the case of all diapir exposures within the field area, the exposed part of the diapir is the structural carapace that overlies the halite core of the diapir.

3.6.3, The Monks Head Diapir - Seismic Data

The Salt Wall Luey is imaged on lines 50, 75, 79 and 83 of the 1982 Chevron seismic survey and is fully described in Chapter 2, Salt Wall Luey. An abbreviated description is given here in order to place the Monks Head Diapir exposure in context.

The Salt Wall Luey is a symmetrical diapir with a near-triangular cross section. Luey ranges in height from ~3.5 km on line 75 to ~2.9 km on line 83, with a progressive decrease in height towards the south-west (the Antigonish coastline). The fact that Luey strikes north-east/south-west and is a continuous salt wall rather than a cylindrical diapir suggests that the salt wall may be a fault-controlled salt structure. The salt wall is probably following a basement fault similar to the extensional fault immediately north of the Salt Wall Huey. A possible fault offset at Horton/Basement level is imaged beneath the Salt Wall Luey on line 83 of the 1982 Chevron seismic survey. This fault has a throw of ~0.5 sec TWT and could represent part of the diapir-controlling fault.

The deformation of the surrounding Carboniferous sedimentary rocks is relatively uniform. In general terms, the Carboniferous strata have been deformed into broad drag zones up to 2.5 km wide. The drag zones generally have a smooth profile (see above, Chapter 2).

3.6.4, The Monks Head Diapir - Onshore

The exposure of the Monks Head Diapir consists of a highly deformed Hood Island Formation structural carapace. The section is assigned to the Hood Island Formation based upon the presence of the E1 limestone. The Monks Head section is therefore stratigraphically equivalent to that of the Broad Cove Diapir. A small stratigraphic interval of the Hood Island Formation is repeated several times throughout the section. The E1 limestone is a 7-10 m thick oolitic limestone containing bivalve moldic porosity which can be used to indicate structural inversion (way-up evidence). Another limestone, presumed to be the D3 limestone (based upon its stratigraphic position beneath the E1 limestone), is a black, organic-rich limestone that has a distinct petroliferous smell when pulverised. The two limestones are, therefore, sedimentologically distinct and are used as marker horizons to decipher the structure of the diapir exposure.

The intervening strata separating the E1 and D3 limestones consist of red and green mudstone, red siltstone and gypsum. The gypsum is usually located stratigraphically on top of the limestones, though exceptions to this are present. The gypsum is intensely foliated and the foliation almost always has a sub-vertical orientation.

As part of a stratigraphic review, Sage (1954) measured the Monks Head section and identified a range of Windsor Group limestones including the B1-B3, C1-C3 and D1-D3. Sage's identification is therefore at odds with the interpretation presented in this thesis. However, Sage pointed out that his map was constructed largely by assuming a stratigraphic spacing similar to the neighbouring Saw Mill section to piece together the disjointed stratigraphy. The resulting map juxtaposes several Windsor stratigraphic units and requires an extremely complex structural model to produce the observed map. Sage (1954) does not include a section in his report and so it is hard to envisage how Sage has interpreted his map in terms of a structural model. Sage (1954) delineated the Windsor Group limestones using macro and micro fauna assemblages. No attempt was made as part of this thesis to carry out a detailed paleontological investigation and so the apparent

disparity between the two interpretations cannot be rigorously assessed. However, the distinctive 'algal club' stromatolites which characterise the C3 limestone were not observed anywhere in the section. A possible explanation for this is the rapid rate of cliff erosion observed at several outcrops within the field area. Cliff sections were observed to erode by up to 5 m in one year. Given the 43 year gap between Sage's (1954) report and this thesis, considerable changes in cliff profile can be expected.

The North-West External Shear Zone

The north-western external shear zone is exposed as a 3-4 m wide shear zone and consists of four distinct units described below from north-west to south-east, i.e. from external margin inwards (Figure 3.6.2).

- Unit 1. A 1.75 m thick, highly foliated gypsum unit with secondary anastomosing gypsum veins. Foliation within the gypsum is sub-vertical (041/78NW). The gypsum also contains many centimeter to decimeter scale chevron folds.

- Unit 2. Red mudstone. A 1 m thick, weakly brecciated mudstone with pervasive sub-horizontal gypsum veins. The gypsum veins cross-cut the mudstone but are sheared into a sub-vertical orientation at the contact with the gypsum units (Figure 3.6.2). This vein geometry may indicate that the mudstone is a passive inclusion sandwiched between two dynamic gypsum units within the external shear zone. This passive transport may explain the relatively minor internal deformation of the mudstone.

- Unit 3. A highly sheared gypsum unit similar to unit 1 (see above)

- Unit 4. A limestone breccia. This unit is ~25 cm wide and consists of Windsor Group limestone that has been brecciated into gravel to cobble sized fragments surrounded by a mudstone matrix. The mudstone matrix is highly sheared with a

Figure 3.6.2. The north-east External Shear Zone of the Monks Head Diapir consists of four units. The two visible gypsum units (1 and 3) are highly foliated and contain small-scale chevron folds and shear zones (not visible on photograph scale). The gypsum units are separated by a red mudstone/siltstone (2),which contains undeformed, sub-horizontal gypsum veins. The innermost unit (4) consists of a limestone breccia consisting of E1 and D3 Upper Windsor Group limestone clasts. The photograph is orientated north-east to south-west (right to left). The notebook scale in the photograph measures 12cm on its longest axis.

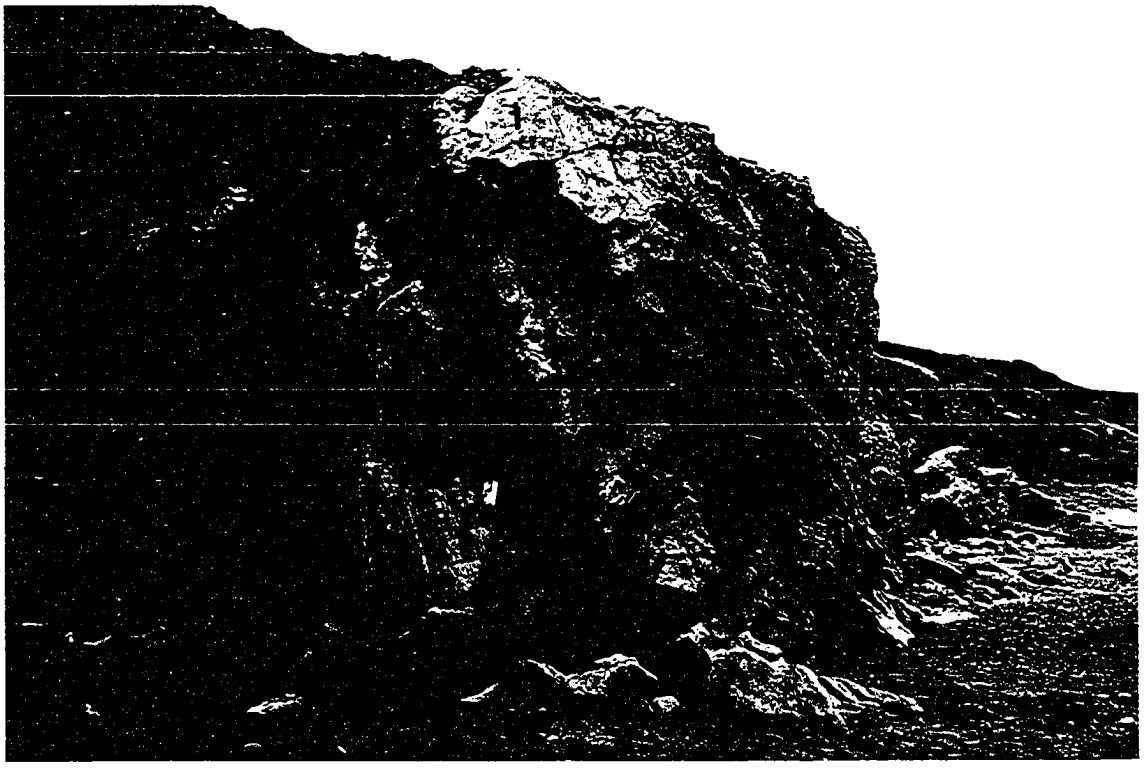

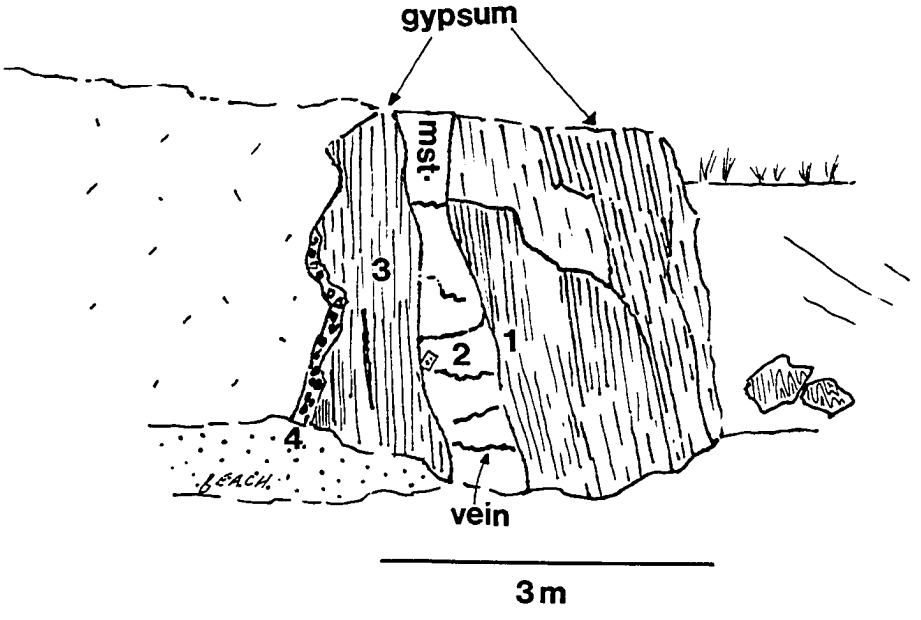

Figure 3.6.2

sub-vertical foliation. Although highly brecciated, it is clear that the breccia contains two populations of limestone clasts. One set of clasts can be confidently recognised as D3 limestone, while the other set resembles E1 limestone.

Fibrous Gypsum Veins

The majority of the diapir units are cross-cut by sub-horizontal fibrous gypsum veins (Figure 3.6.3a,b & c). These veins cross-cut almost all exposed internal portions of the structural carapace and commonly have a vertical opening direction. Rarely, within well-bedded siltstone units, the gypsum veins follow the sub-vertical bedding with a horizontal opening direction. Most of these siltstone units show evidence of shearing as indicated by small duplexes within the siltstone beds around which some of the veins are folded, although for the most part the gypsum veins cut directly across folds and faults. Within 20 m of the south-eastern external shear zone, the gypsum veins are orientated in three mutually orthogonal planes (one horizontal and two vertical) with the vein fibres orientated normal to the vein margin (Figure 3.6.3a,b & c). The fact that the gypsum veins cross-cut deformation features indicates that the veins formed after most of the deformation of the structural carapace had taken place.

3.6.5, Reconstruction of the Structural Carapace

The Monks Head Diapir section is shown in Figures 3.6.3 a, b and c. Throughout the section dip and strike measurements, the distinctive sedimentology of the E1 and D3 limestones and way-up evidence deduced from bivalve moldic porosity were recorded and used to constrain the configuration of the carapace.

Within the Monks Head section, the E1 and D3 limestones are repeated three times. An interpretation of the structural configuration that could cause repetition of the limestones is shown in Figure 3.6.7.

The E1 limestone units become progressively more deformed towards the south-east,

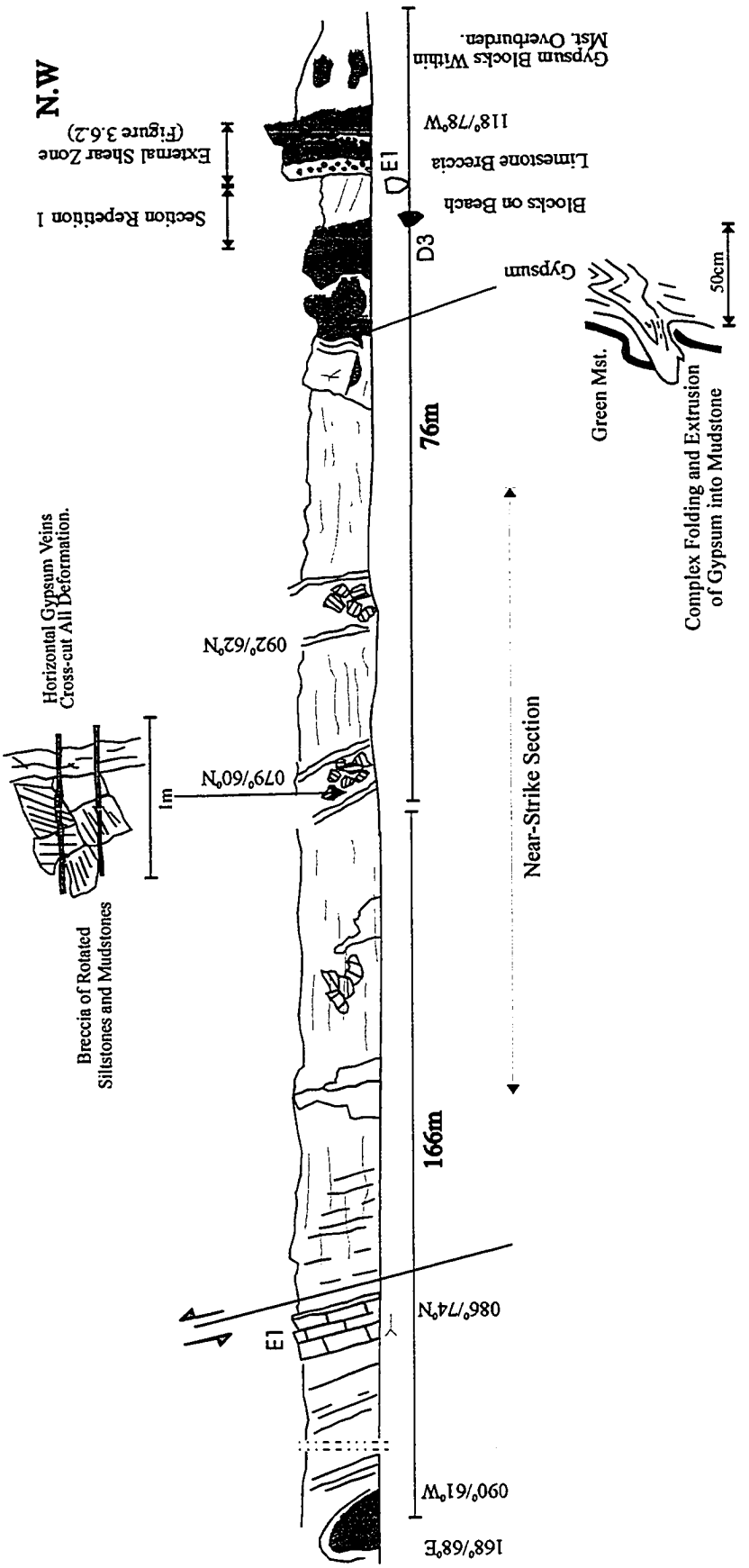

Figure 3.6.3a. The Monks Head Diapir, Section 1.
Note Sections 1,2 and 3 are a continuous section.

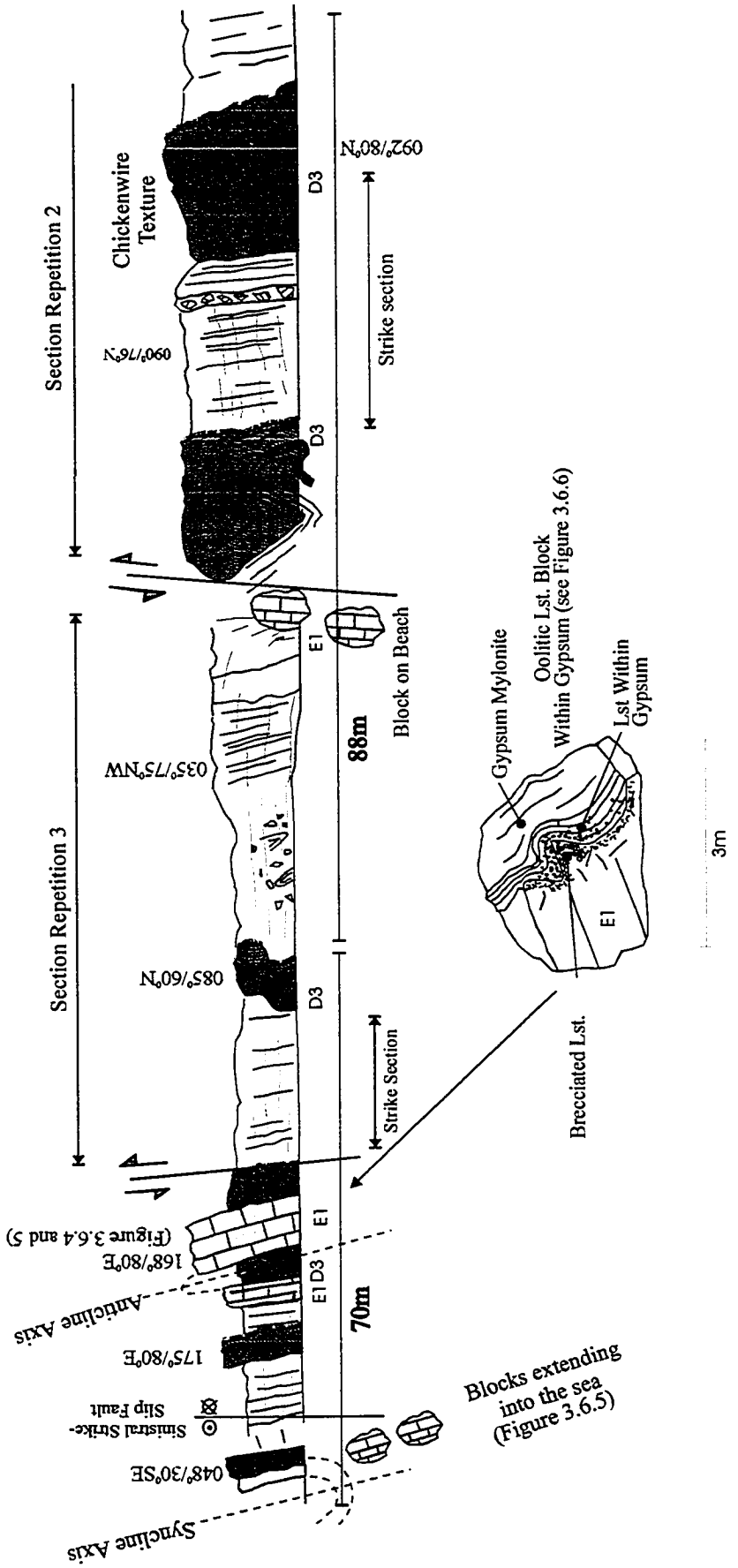

Figure 3.6.3b. The Monks Head Diapir, Section 2.

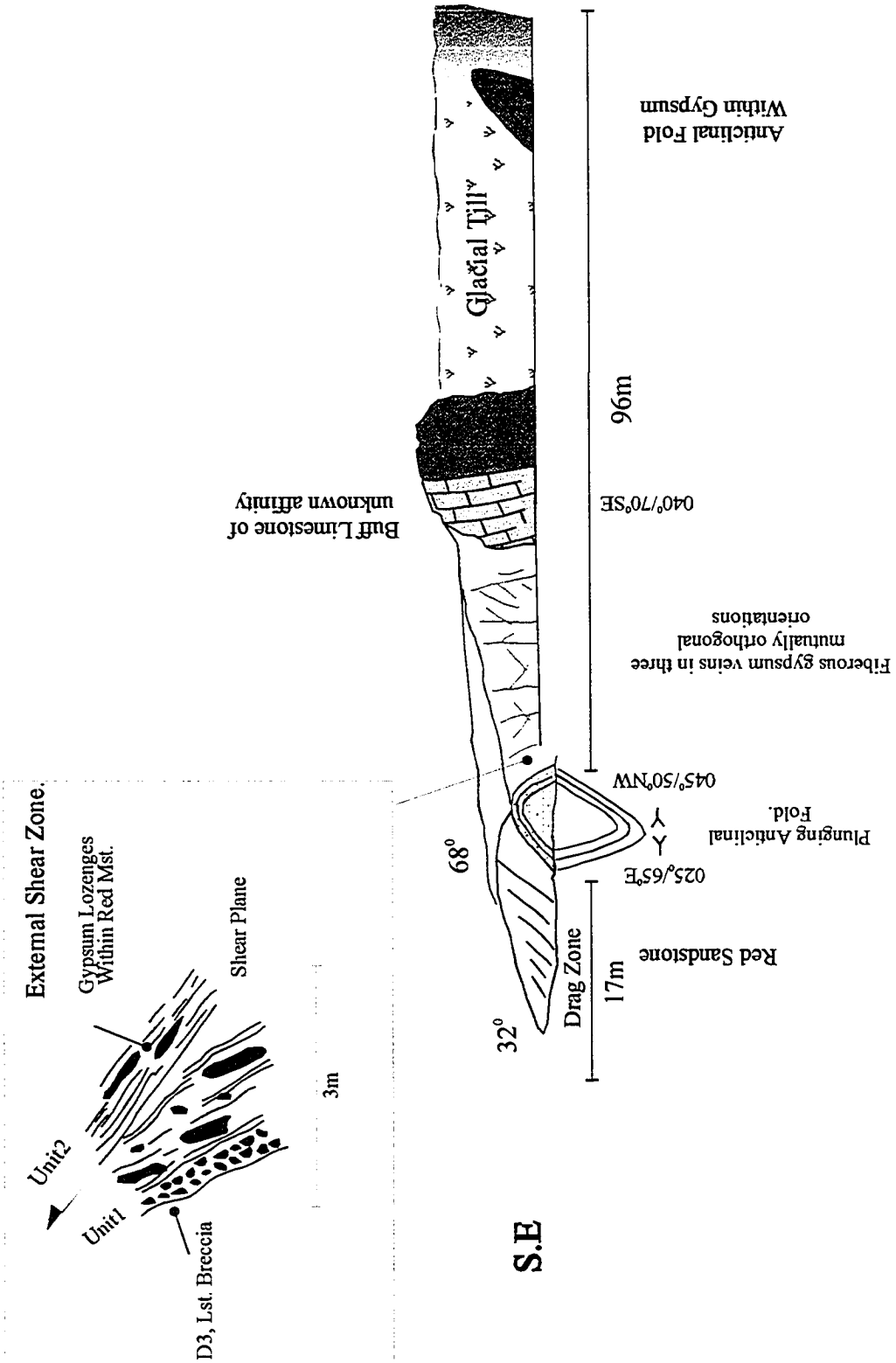

Figure 3.6.3c. The Monks Head Diapir, Section 3.

where the limestone is fragmented into blocks up to 15 m high by 10 m wide and 8 m thick (Figure 3.6.4). At one location, individual limestone blocks form a line of blocks that extends for ~200 m sub-parallel to shore (Figure 3.6.5). The limestone blocks all appear to be aligned along strike (048 degrees). Where the line of blocks intersect the cliff section, the intervening space between individual limestone blocks has been invaded by gypsum with well-developed foliation. The surface of these limestone blocks is commonly brecciated, with the interstitial joints being filled with amorphous gypsum. The gypsum surrounding the limestone blocks contains angular fragments of limestone. Brecciation can be seen in all stages of development, from initial joint/fault invasion to complete brecciation (Figure 3.6.6). The D3 limestone seems to be particularly prone to brecciation. In two localities, gypsum units contain zones of disseminated D3 limestone fragments up to 50 cm thick. These zones may represent part of the D3 limestone that has been so completely brecciated and disseminated by deformation that the original limestone is no longer recognisable.

Interpretation. The strike orientated limestone blocks are interpreted to represent a limestone unit that has undergone strike-parallel extension. This can be envisaged as boudinage on a large scale (macro-boudinage), in which the limestone units deformed in a brittle manner, probably in response to high strain rates within the diapir. The surrounding gypsum units probably deformed in a ductile manner, as indicated by the pervasive foliation, and invaded the small fractures within the limestones by solution and precipitation of gypsum as indicated by the amorphous gypsum texture.

Towards the south-east end of the section where the E1 and D3 limestones have been strongly folded (Figure 3.6.3b), the gypsum and red mudstone strata (estimated to be initially ~70 m thick) separating the limestone units are seen to thin progressively. At the south-east end of the exposure, the E1 and D3 limestone are folded together into a steeply plunging (68-75 degrees) anticline and syncline pair. The intervening ~70 m of red mudstone and gypsum has been completely removed (Figure 3.6.3a, b & c). This

Figure 3.6.4. Limestone block that contains a core of buff coloured E1 limestone around which the darker D3 limestone has been folded. The red mudstone strata, which originally separated the E1 and D3 limestones has been tectonically removed. The limestone units are surrounded by gypsum. This block is an example of macro-boudinage. The stratal package containing the two limestones has been strongly folded as part of the Monks Head curtain fold (see text below). During this deformation the limestone unit have been fragmented in to large blocks and the space created between the blocks has been invaded by gypsum.

MEGA BOUDINAGE

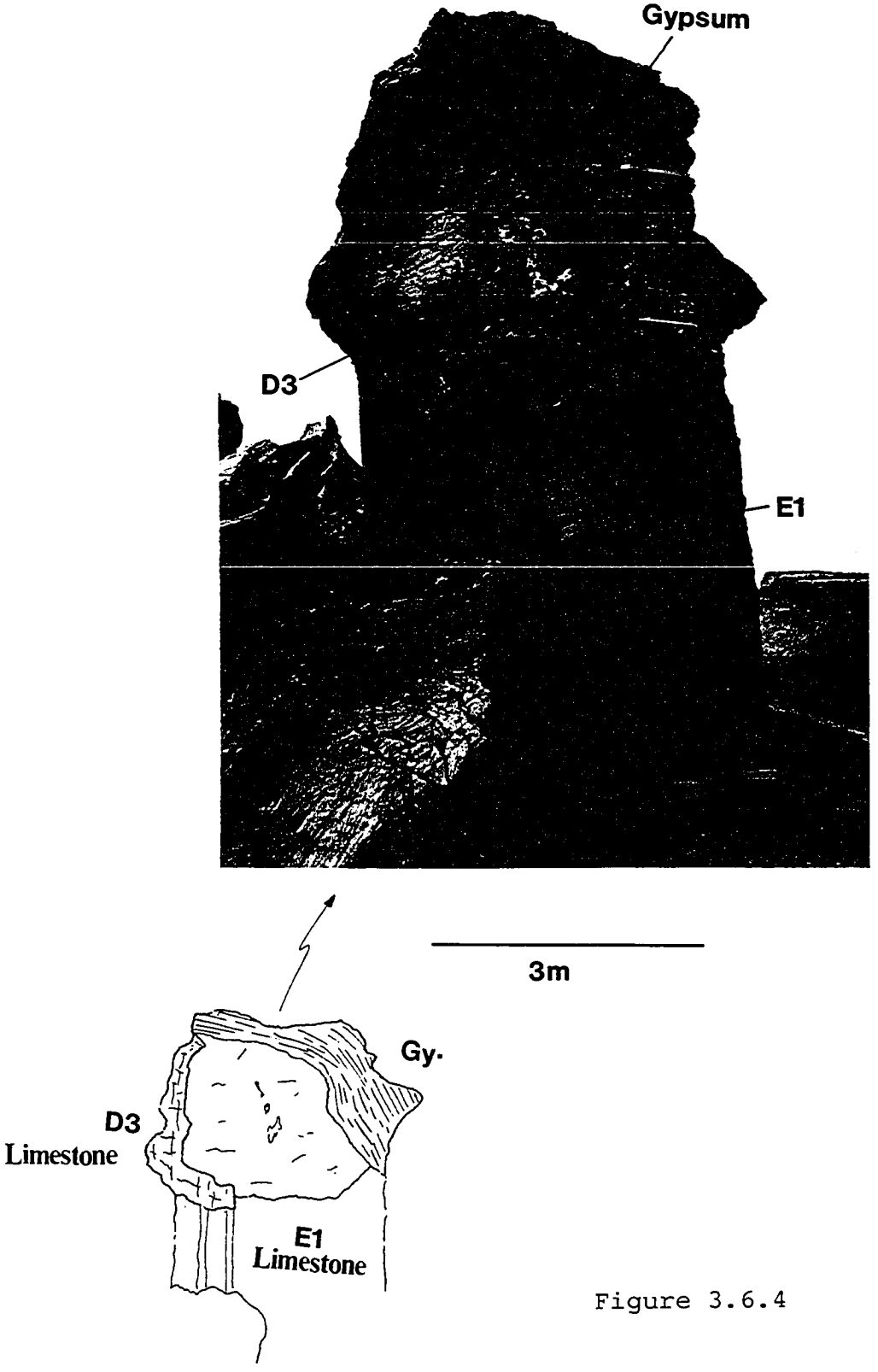

Figure 3.6.4

Figure 3.6.5. A series of limestone blocks representing macro-boudinage. The blocks are predominantly of E1 limestone, although some of the blocks show D3 limestone folded around the E1 limestone. The blocks are all aligned along the same strike. The blocks are interpreted to represent an original limestone unit (E1 or D3) which has been fragmented in to blocks by both vertical and horizontal extension. On the extreme left of the figure the block standing upright on the beach is the limestone block shown in Figure 3.6.4. This block is separated from the line of blocks by a left lateral strike-slip fault (see Figure 3.6.3b).

Field of view is approximately 200m.

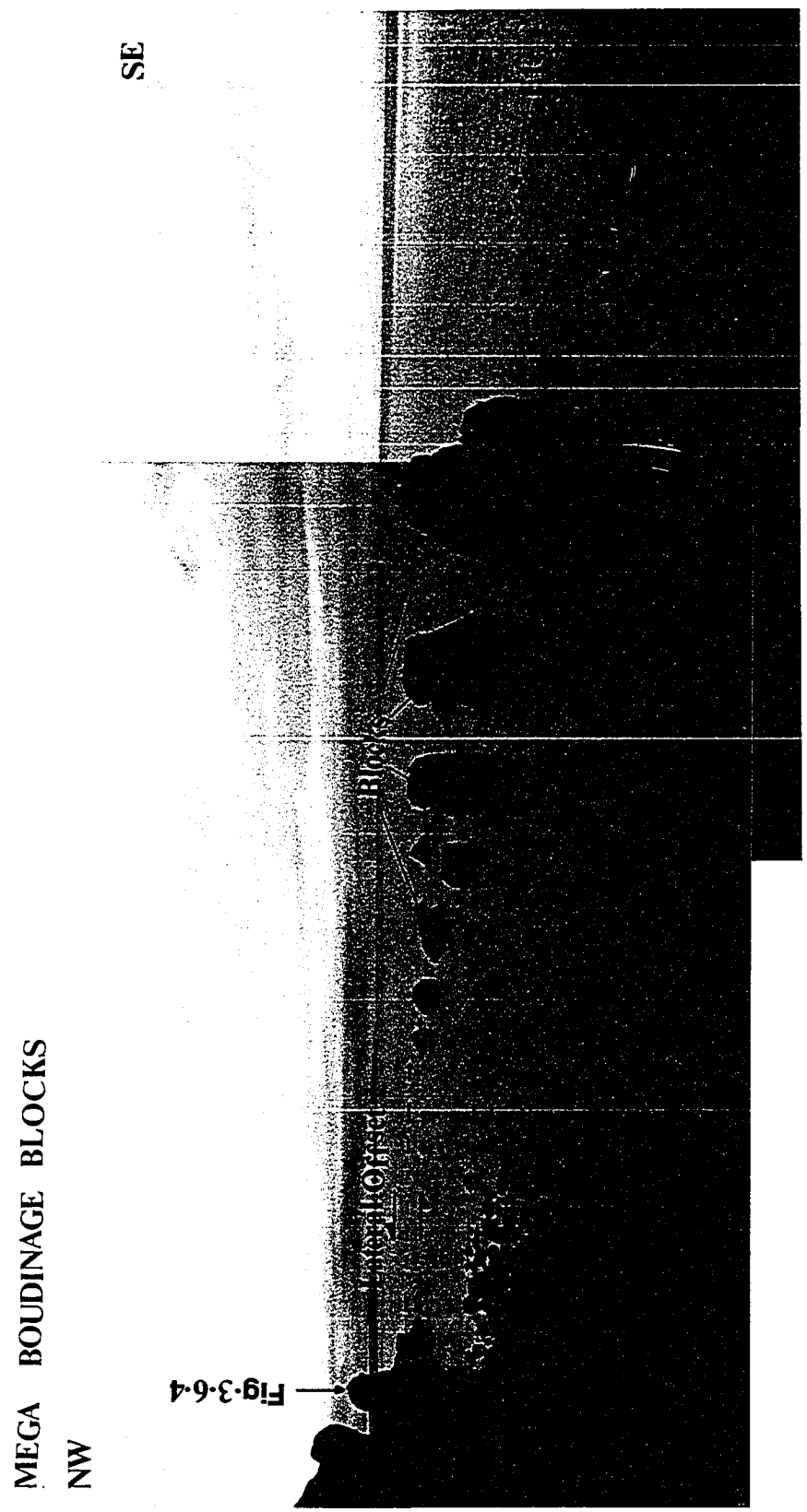

Figure 3.6.5

Figure 3.6.6. Two examples of limestone brecciation and invasion of gypsum along joints and fractures. The gypsum is probably able to invade the limestones by a combination of pressure solution and creep processes (although this can not be proven without detailed microscopic examination). The upper-most photograph shows an early stage of brecciation while the lower photograph shows a more advanced stage. It is possible that the brecciation process was assisted by the anhydrite to gypsum reaction, which involves a 42% volume increase. Such a reaction would apply stress to fractures which contained anhydrite, thereby aiding fracturing.

Scale, lens cap is 52mm in diameter.

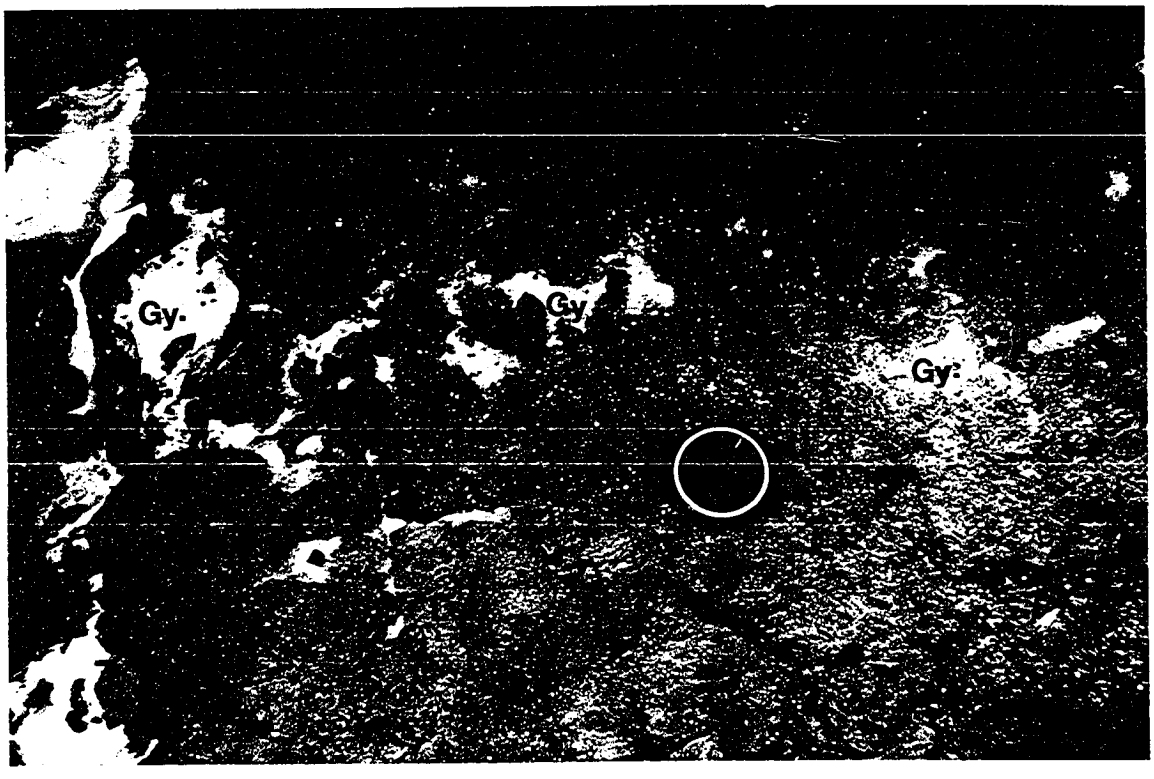

Figure 3.6.6

stratigraphic thinning corresponds to the position of sheared contacts between gypsum units and red mudstone units within the structural carapace. Strain observed within the gypsum units decreases rapidly away from the mudstone/gypsum contact, whereas shearing within the mudstone is not discernible more than 40 cm away from the contact.

Interpretation. The sheared gypsum/mudstone contacts probably represent discrete layer-parallel-slip decollements within the structural carapace. The stratigraphic thinning combined with the presence of sheared contacts probably indicates that the incompetent red mudstone and gypsum strata have been progressively removed by tectonic 'squeezing'. The incompetent strata were probably forcibly extruded from between the more competent limestones as the stratigraphic package was folded into tight to isoclinal folds.

3.6.6, Fold Geometry

The structural features described above must be placed in context with an overall structure model for the Monks Head Diapir. Important facts that pertain to the structure model include:

- The fold axes of the anticlinal and synclinal folds located at the south-eastern end of the section plunge at 68-75 degrees towards the north-east.

- The recorded dip and strike information indicates that all of the stratigraphic units within the section are steeply dipping. No horizontal or shallowly dipping units were recorded.

- The E1 and D3 limestones have been repeated three times and the way-up evidence indicates that the repetition was caused by faulting rather than by folding.

- A large thickness of red mudstone strata has been removed from the hinge regions of the folds.

- The macro-boudinage of the E1 limestone may indicate high strain rates as well as mobilisation of the surrounding gypsum.

The Monks Head section has several features which are similar to those associated with curtain folds. Steeply plunging fold axes are commonly associated with curtain folds and several examples can be seen in the Pugwash salt mine and were interpreted by Carter (1990a, b and c). The steeply plunging anticline and syncline at the north-western end of the section can be interpreted as either parasitic folds or re-folding of the curtain fold. Again, similar re-folding or parasitic folds can be seen in the Pugwash salt mine and were mapped on a large scale by Carter (1990a, b and c). The macro-boudinage of the limestone units could represents bedding-parallel (strike and/or dip) extension in the limb area of the curtain fold. Bedding-parallel extension resulting in boudinage of more competent units is characteristic of meso-scale diapir folds observed within the field area and of meso-scale folds within the Pugwash Diapir. Tectonic removal of incompetent strata from the limbs of folds is also common within diapir folds observed throughout the field area and from 3D exposures within the Pugwash salt mine. In these exposures, the more incompetent strata appear to have been forced from the hinge areas into the limbs of the fold (Carter, 1990a, b and c).

By considering the Monks Head Diapir as a section through a curtain fold, the various structural features of the diapir exposure can be explained in a logical manner. The scale of the curtain fold exposed is comparable to curtain folds within the Pugwash Diapir, which have kilometre to decimetre scale wavelengths.

A major problem with the model is that it would be mechanically very hard for a series of gypsum, limestone and mudstone strata to form a curtain fold structure. These structures are most commonly associated with the halite core of a diapir, where the salt movement results from processes such as thermal convection and buoyancy. A second problem

relates to the position of the carapace within the diapir. The E1 limestone represents the top of the Windsor Group and therefore the top of any diapiric structure. It might be expected that the head of a diapiric structure would have a strong flattening fabric related to upward growth of the diapir through an overburden and to the overall movement of evaporite material within the diapir. There is no evidence of a flattening fabric within the Monks Head section. The apparent conflict between the structure model and the points described above are explored in Chapter 4.

The north-east and south-west margins of the diapir exposure show multiple repetition of the E1 and D3 limestones (Figure 3.6.7) by faults. Unfortunately, the faults that cause the stratigraphic repetition are not well exposed and so the geometry of these faults is speculative. The sub-vertical orientation of the foliation in the gypsum units adjacent to the faults indicates a dip-slip movement rather than a strike-slip movement. The faults have been modelled as sub-vertical thrust faults (Figure 3.6.7) and are referred to hereafter as curtain faults. The curtain faults increase the width of the carapace by repetition of the stratigraphy in a similar way to that interpreted at Broad Cove. The large increase in carapace width may not be mechanically feasible, especially since the shear sense on the faults is opposite to the adjacent external shear zone. The proposed faults only represent a geometrical solution for the repetition. They do not address the mechanical feasibility of repetition or of expanding the carapace. Given the inherently 3D strain typically associated with diapirs, no attempt has been made to balance the model.

3.6.7, The South-East External Shear Zone

The south-east external shear zone is well exposed as a 3 m wide outcrop of sheared gypsum, mudstone and limestone. The external shear zone is divided into two units described from south-east to north-west, i.e. external to internal with respect to the diapir (Figure 3.6.3c).

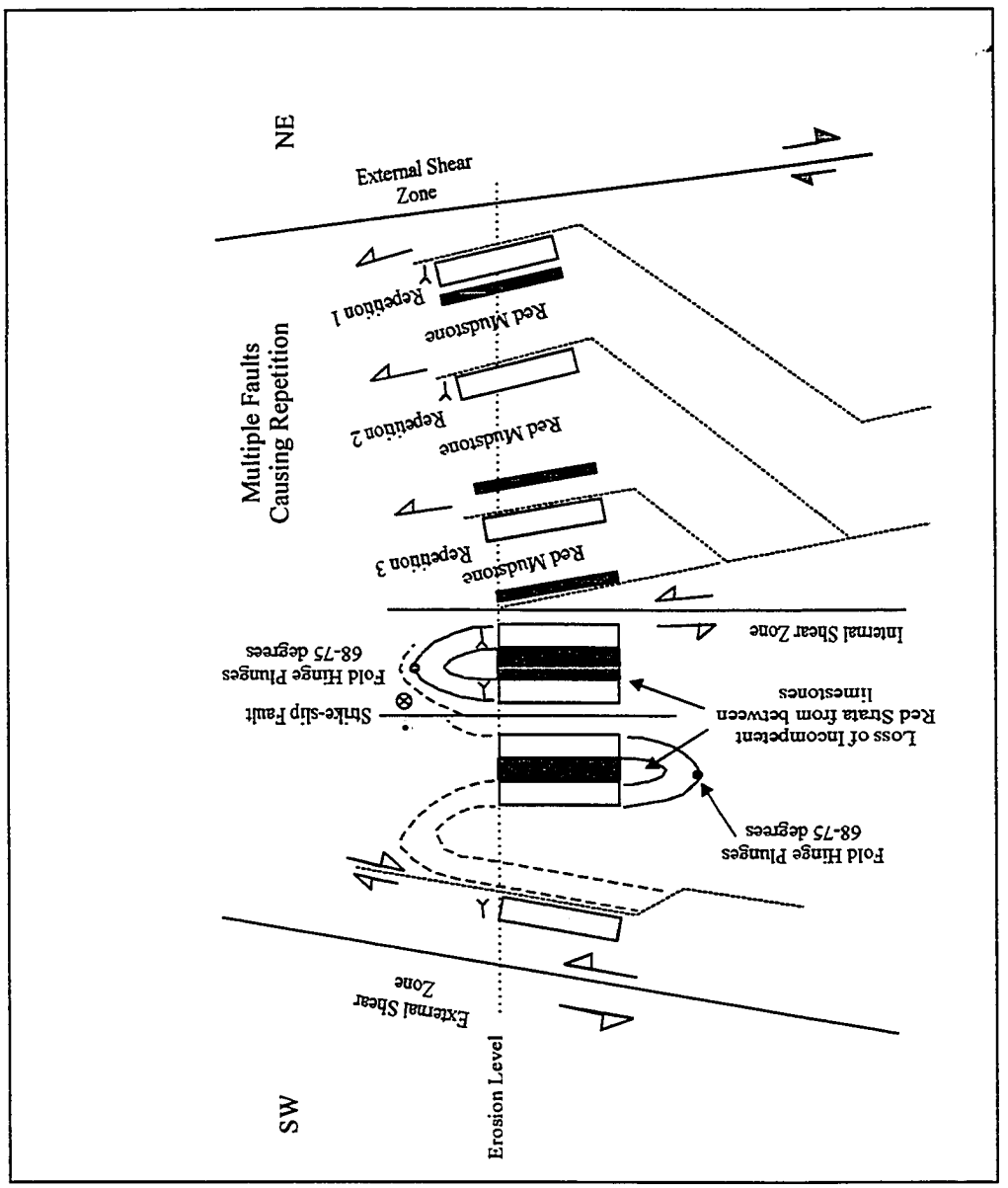

Figure 3.6.7. Schematic model for the structural carapace of the Monks Head Diapir (Not To Scale)

- Unit 1. Limestone breccia. A 50 cm wide breccia consists of Windsor Group limestone clasts up to 7 cm in diameter within a sheared mudstone matrix. The limestone clasts are sub-angular and have no apparent preferred orientation.

- Unit 2. A 2.5 m wide unit consisting of sheared mudstone with intercalated red gypsum lozenges. The mudstone foliation is steeply inclined and a shear plane is seen to cut across the mudstone foliation. The gypsum lozenges have a prolate shape and are aligned with their long axes parallel to the inclined mudstone foliation.

The actual contact of the external shear zone with the drag zone has been washed out and covered with glacial till.

3.6.8, The South-Eastern Drag Zone

The south-eastern drag zone is poorly exposed as isolated Port Hood Formation sandstone beds protruding through the present day beach (Figure 3.6.3c). The exposed drag zone is ~22 m long and consists of an anticline plunging 14 degrees north, followed by a short (17 m) dip fan. The dip within the dip fan decreases rapidly from 68 degrees adjacent to the anticline to 32 degrees at the end of the exposure.

Two pervasive sets of small faults can be distinguished within the exposed drag zone. The faults have a maximum displacement of 1 cm and are all extensional faults. In most cases, no displacement could be determined. Although no detailed measurements were recorded, the fault sets are clearly oriented parallel to and orthogonal to the adjacent diapir margin.

Interpretation. The drag zone profile is extremely short and the deformation is relatively minor considering the height and maturity of the Monks Head Diapir. This apparently highly attenuated drag zone may reflect the lower strain associated with a passive mode

of diapiric intrusion (see above, Chapter 2). However, the exposed drag zone may be part of a much larger drag zone structure that is not exposed and it would be inappropriate to draw any major conclusions based upon this outcrop.

CHAPTER 4, DRAG ZONE AND DIAPIR DEFORMATION; DISCUSSION

Introduction

This section of the thesis draws together both onshore and seismic information described in previous chapters to propose a number of conclusions regarding drag zone folding and internal drag zone deformation as well as describing the deformation of the structural carapaces within the study area.

This chapter presents:

(1) A model for the fold profile observed within drag zones. This model relies upon interpretation of the drag zone profiles, which are exposed as cliff sections and described in Chapter 3. This model is then extended to include the larger 'zones of rotation' (see Glossary of Salt Tectonics) that were interpreted from the offshore seismic data.

(2) A model for faulting within diapir drag zones.

(3) A model for deformation within structural carapaces. This model attempts to relate the structure seen within the structural carapaces to: structures described for more internal parts of the diapir, the effects of halite dissolution, the hydration of anhydrite to gypsum and horizontal shortening due to compression and inversion.

When formulating the models and conclusions, it was noted that several geological factors were applicable to any one model or conclusion. The text for each model therefore describes several geological factors and attempts to illustrate how each factor affects the model or conclusion. Where possible, examples are used to illustrate conclusions.

4.1, MODEL FOR DEFORMATION OF SEDIMENTARY ROCKS ADJACENT TO EVAPORITE DIAPIRS

4.1.1, Drag Zone Folding

This section attempts to categorise the drag zones and then to illustrate the geological factors that control drag zone morphology and geometry. Drag zone folding is described in terms of drag zone width and drag zone profile and is based upon information derived from the on-shore diapir exposures (see Table 4.1.1). In the subsequent section, the analysis is extended to a larger scale using depth converted seismic sections. The analysis allows drag zone folding to be divided into three categories:
(For drag zone profiles please refer to the graphs in relevant sections of Chapter 3)

Drag Zone Categories

(i) *Broad drag zone folds* (450-600m wide) with a smooth drag zone profile, e.g. the north-east Broad Cove Diapir drag zone and the north-east St. Rose Diapir drag zone.

(ii) *Intermediate drag zone folds* (250-300m wide) with a high degree of stratal rotation within the inner drag zone and a lower degree of stratal rotation within the outer drag zone, e.g. the Coal Mine Point Diapir drag zone (250m) and the Finlay Point Diapir drag zone (300m).

(iii) *Narrow drag zone folds* (<100m wide) e.g. the south-east Port Hood Island Diapir drag zone (Bruces Cove) and the south-west Broad Cove Diapir drag zone. These drag zones typically show intense deformation and folding within 20m of the diapir margin. Beyond this zone, the drag zone profile is almost homoclinal.

Controls Upon Drag Zone Profile

What geological factors control the width/profile of diapir drag zones? From the drag zone outcrops, two main controls upon drag zone fold profile were identified: lithology

Drag Zone	Length (m)	1st Generation Fault Rotation (Degrees)	Stratal Rotation (Degrees)	Growth Mechanism	See Chapter
NE Broad Cove	450	46 +/-12	57 +/-5	Reactive	3.1
SW Broad Cove	100	NA	102	Reactive	3.1
St. Rose	450	45 +/-10	48 +/-10	Reactive	3.2
Finlay Point	290	30 +/-5	19 +/-7	Reactive	3.3
Coal Mine Point	250	NA	72	Reactive	3.4
Port Hood Island (Bruces Cove)	85	NA	58	Passive	3.5
Monks Head	~22	NA	~40	Passive	3.6
Zone of Rotation					
79, left hand side, SW Luey	2000	-	-	Passive	App 6.
79, left hand side, SW Huey	4500	-	-	Passive	App 6.
A03, Inverness Salt Wall	200	-	-	Reactive	App 6.
A10, Broad Cove Diapir	400	-	-	Reactive	App 6.
2, Coal Mine Point Diapir	1600	-	-	Reactive	App 6.
63, Salt Wall Huey	3500	-	-	Reactive	App 6.
67, Salt Wall Huey	2700	-	-	Reactive	App 6.
79, right hand side, SW Huey	1600	-	-	Passive	App 6.
71, right hand side, SW Huey	1500	-	-	Passive	App 6.
75, left hand side, SW Luey	3500	-	-	Passive	App 6.
83, right hand side, SW Huey	800	-	-	Passive	App 6.

Table 4.1.1. Drag Zone and Zone of Rotation Data.

and diapir geometry.

Lithology

Both the north-east Broad Cove and north-east St. Rose diapir drag zones (division (i) above) consist of incompetent mudstones, siltstones and subordinate sandstones (Hastings Formation and Margaree Member of the Port Hood Formation, respectively). The mean bed thickness of the drag zone strata is <1m and the stratigraphic package is relatively homogeneous throughout.

Both of these packages of strata would have been able to deform by ductile/plastic creep processes under relatively low strain conditions. As the drag zone was folded, incompetent mudstones were probably acting as bedding-parallel slip decollements, allowing the more competent siltstone units to slip above and below the incompetent mudstones. Bedding-parallel slip is indicated by the many small-scale asymmetric folds and duplex structures that were recorded (see above, Chapter 3.1). These structures all show vergence and hence transport material away from the diapir. Because of the thin bed thickness, many bedding-parallel slip decollements probably existed so that a broad area of strata could undergo bedding-parallel slip penecontemporaneously. These factors probably allowed strain to be distributed over a wide area since there are few obvious locations where strain could be preferentially concentrated. This relatively even strain distribution would tend to result in a broad drag zone with a smooth dip fan profile (Figure 4.1.1a).

In contrast, the lithology of the intermediate drag zones is strongly inhomogeneous and consists of thick channel sandstone bodies (up to 93m thick, the Eagle Sandstone) separated by thick grey mudstone and coal seam intervals, e.g. the Coal Mine Point Diapir drag zone. At high strain, the competent sandstones would be unlikely to have deformed by ductile or plastic mechanisms. In response to a high strain rate, the thick sandstones would probably deform by brittle fracture, as is evident from the high

Incompetent and Homogeneous Strata

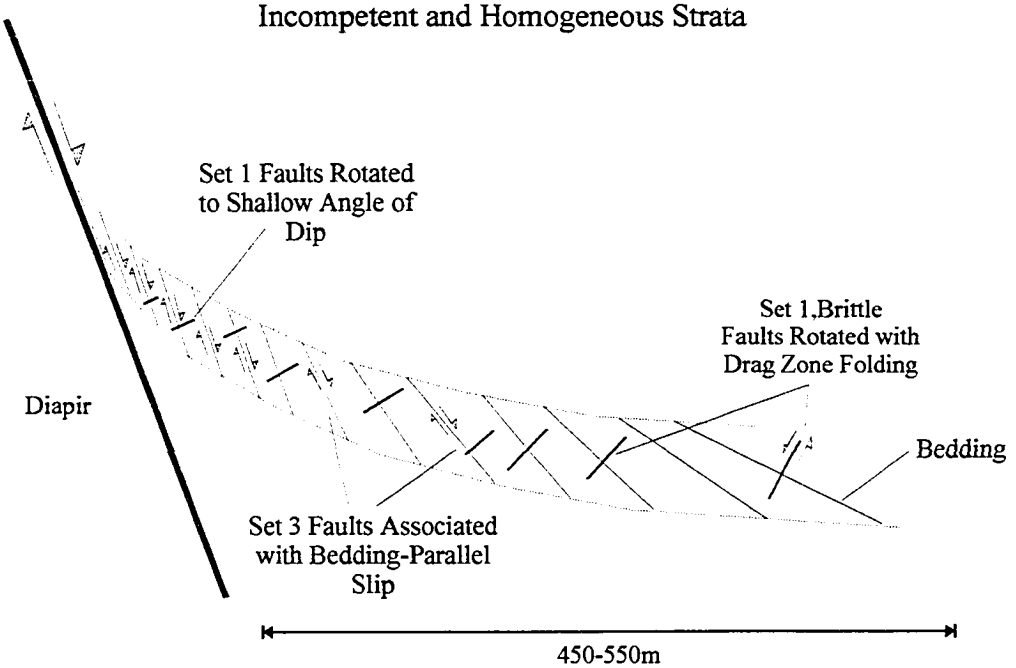

Figure 4.1.1a

Competent/Incompetent and Heterogeneous Strata

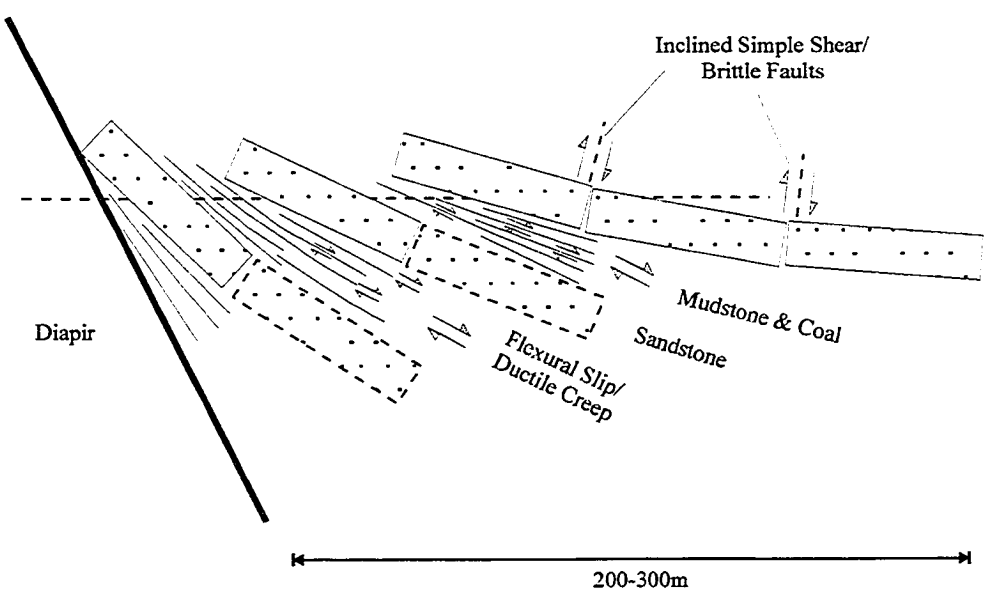

Figure 4.1.1b

concentration of joints, micro-faults and extensional faults (see above, Chapter 3.3 and 3.4). The intercalated incompetent mudstone and coal intervals that separate the sandstone units deformed primarily by plastic creep and flexural slip, as indicated by the pervasive anatomosing shear zones recorded from the 2nd sandstone unit at Coal Mine Point (see above, Chapter 3.3).

The whole stratigraphic package therefore would deform as a series of large lubricated slabs. Deformation within the sandstone units (slabs) not immediately adjacent to the diapir shows relatively minor deformation because the incompetent shales (the lubricant) have accommodated most of the strain (Figure 4.1.1b). Although the weakly deformed sandstone units can dip steeply (up to 52 degrees), much of the 'dip' may be due to simple rotation which is accommodated by brittle faults (inclined simple shear) and not to folding (Figure 4.1.1b). The required volume/thickness change to accommodate this rotation was probably provided by ductile creep within the intercalated mudstones.

By examining the drag zones from St. Rose, Broad Cove, Finlay Point and Coal Mine Point, it can be shown that lithology and bed thickness play important roles in determining the strain mechanisms within a drag zone. In turn, the relative importance and interplay of the deformation mechanisms play a role in controlling drag zone profile.

The observation that lithology is a major factor that controls rock deformation mechanism, fold style and fold wavelength has long been understood by geologists. Currie et al. (1962) used a combination of laboratory models and field examples to illustrate that the intercalation of competent and incompetent strata and the relative thickness of these units controlled fold amplitude and wavelength. In essence, they suggested that thick stratal units promote larger amplitude/wavelength folds. In a similar way, Beloussov (1962) and Pritchett (1997) described triple-bed sequences that consisted of two ductile beds and an interlayer of brittle rock as sites for preferential fracturing within the brittle rock unit. Beloussov (1962) concluded that the overlying ductile

material was likely to become over-pressured, which was translated into tension within the underlying brittle rock unit. Ramsey (1974) suggested that chevron folds with sharp fold hinges and planar limbs were only stable for homogeneously mechanically competent stratal units of similar unit thickness. The intercalation of incompetent material or a significantly thicker unit would promote folds with curved limbs and expel the incompetent material from the limbs into the hinge of the fold. Boyer (1986) described folds from the Appalachian and Rocky Mountain fold belts where he observed that kilometre scale kink-band folds with sharp fold hinges and planar limbs developed within thick carbonate strata and that strain associated with folding was confined to the hinge region.

Applying this previous work to the diapir drag zones exposed within the field area supports the drag zone interpretations presented in this thesis. The thick Inverness Formation sandstone units resemble kink-band folds in that the sandstone units appear to have folded (or faulted) around a sharp fold hinge while maintaining relatively planar limbs (Figure 4.1.1b and Mabou line 4). This deformation has produced a stepped drag zone profile where volume changes are accommodated by migration of intercalated incompetent strata; for example, the Coal Mine Point Diapir drag zone. In contrast, the more incompetent stratal packages, such as the Hastings Formation at Broad Cove, allow an evenly distributed strain throughout the drag zone to produce a smoother drag zone profile. The work of Pritchett (1997) and Beloussov (1962) on fracturing within interlayered ductile and brittle rock units appears to correlate well with the north-east Broad Cove and St. Rose diapir drag zone. At these locations, it was observed that sandstone and siltstone sandwiched between mudstones were intensely deformed by tensile (mode I) fractures, while the surrounding mudstones did not show brittle deformation.

An apparent exception to the above conclusions is the division (iii) narrow drag zones, examples of which are exposed at Port Hood Island (Bruces Cove) and on the south-west

side of the Broad Cove Diapir (see above). These drag zones consist of either thick competent sandstone units or intercalated sandstones and mudstones and yet have extremely narrow drag zone profiles. Clearly some geological factor other than lithology is controlling drag zone profile. These factors are discussed below under the sections dealing with diapir geometry and diapir growth mechanism.

Diapir Geometry

The control which diapir geometry exerts upon drag zone folding can be demonstrated by comparing the south-west Broad Cove drag zone, the Finlay Point drag zone and the Coal Mine Point drag zone. For these diapirs, the geometry of the diapir is well constrained by seismic data.

South-West Broad Cove Drag Zone. This is a narrow (division (iii)) drag zone that extends no more than 100m from the diapir margin and consists primarily of an overturned syncline (see above, Chapter 3.1). As imaged on Inverness line A05, the south-west flank of the Broad Cove Diapir is a sub-vertical contact between the Inverness Formation and Broad Cove Formation and diapiric Windsor Group. The steep dip of the diapir flank has two implications for drag zone profile:

- The overburden adjacent to the steeply dipping contact is not supported from beneath by a diapir shoulder extending beneath the overburden at depth (Figure 4.1.2). During diapir growth, as the diapir grew upward relative to the adjacent overburden, the overburden is free to subside. This relative subsidence can take the form of basement subsidence, vertical diapir growth or a combination of both. Because the overburden adjacent to the diapir is not supported by the diapir, little folding results.

- The steep flank of the diapir exerts a relatively small frictional force upon the adjacent sediments as the diapir moves relative to the sedimentary rocks. A simple mathematical relationship is shown in Figure 4.1.3 and shows that the frictional

1. Trap Door Diapir, e.g. Finlay Point Diapir

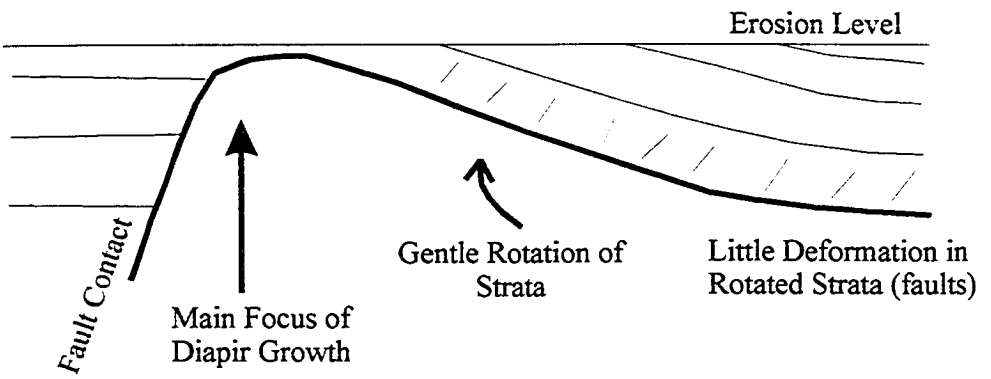

2. Steeply Dipping Diapir Flanks, e.g. South-West Broad Cove Diapir

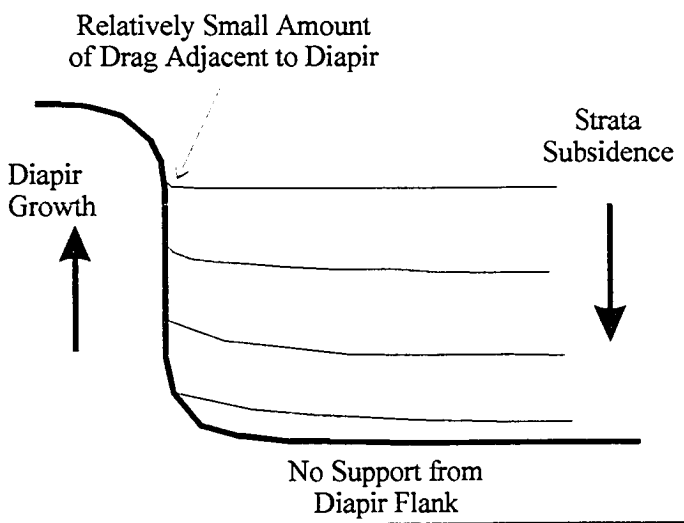

3. Diapir Flank Supports Overlying Strata, e.g. The Coal Mine Point Diapir

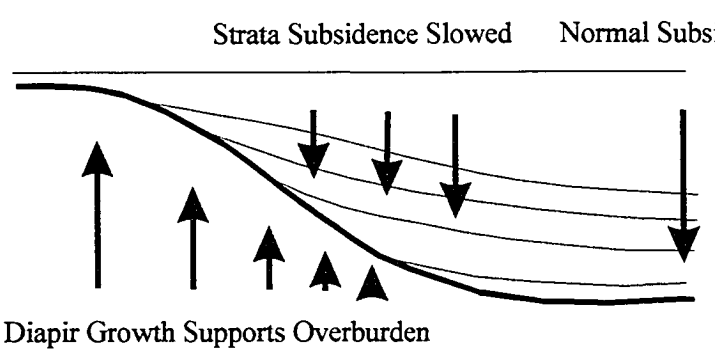

Figure 4.1.2. Diagram to show how diapir geometry controls drag zone profile.

The hypothesis that drag zone folding is related to the dip of the diapir flank is based upon two assumptions:

1. Shear stress on fault plane is proportional to tangent of the dip of the fault plane

2. Shear stress is proportional to hangingwall deformation

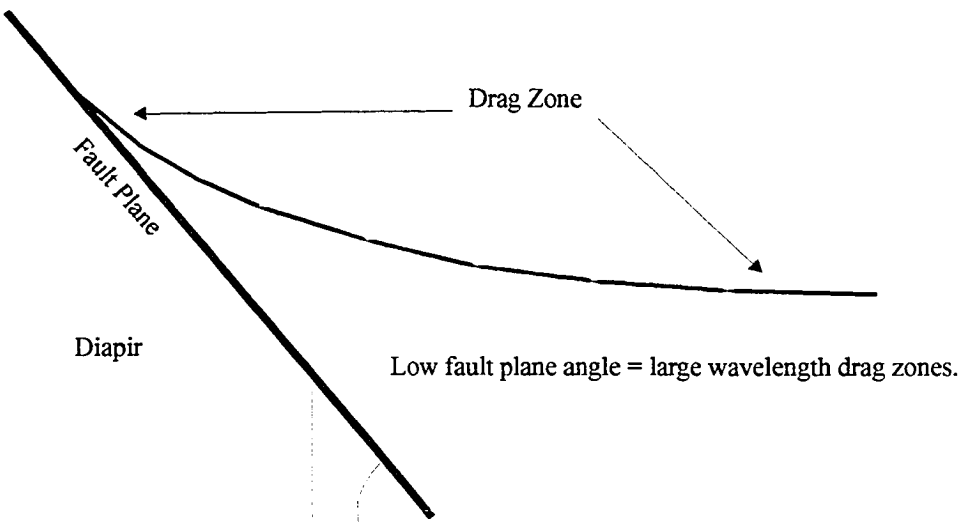

Figure 4.1.3a.

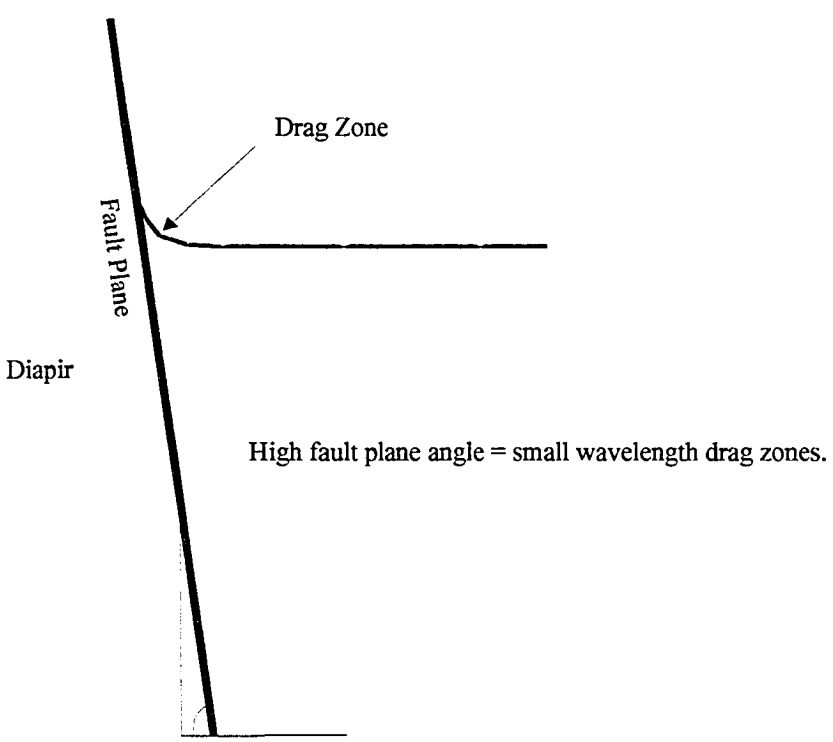

Figure 4.1.3b.

resistance to sliding of the diapir relative to its overburden is related to the angle of the diapir flank. Simply stated, steep flanks produce less friction and therefore less deformation (folding) than gently dipping diapir flanks.

Finlay Point Diapir Drag Zone. The Finlay Point Diapir is an asymmetrical diapir whose geometry can be described as a trap door (see Chapter 3.3). The Finlay Point Diapir drag zone is located above the 'door' of the diapir so that drag zone exposure represents a package of strata that has a gentle, homoclinal dip. In this location, the Inverness Formation overburden has simply been uplifted and rotated as the 'door' of the diapir 'opened' during diapir growth. The drag zone fold reflects this 'gentle' rotation. The maximum dip of the drag zone strata is 37 degrees adjacent to the external shear zone and the majority of the drag zone dips homoclinally at 29-32 degrees, reflecting the passive rotation of the strata above the trap door (Figure 4.1.2).

The Coal Mine Point Diapir Drag Zone. The Coal Mine Point Diapir is described here to illustrate the drag zone fold produced by a more typical diapir geometry in contrast to the south-west Broad Cove drag zone and the Finlay Point drag zone. It should be noted that the fold profile of the Coal Mine Point Diapir is also affected by a strong lithological control (see above). The north-west flank of the Coal Mine Point Diapir dips moderately at approximately 55-70 degrees and the diapir has penetrated through the Inverness Formation overburden. The diapir geometry is dissimilar to both the Finlay Point and Broad Cove drag zones described above. The drag zone produced by the Coal Mine Point Diapir is an intermediate division (ii) drag zone, which has steeply dipping drag zone strata extending for 250m away from the diapir.

The geometry of the Coal Mine Point drag zone can be explained using the same lines of reasoning used for the south-west Broad Cove drag zone described above. The moderate dip of the diapir flank implies that the frictional force exerted by the translation of the overburden (hangingwall) relative to the diapir (footwall) would have been considerable

(Figure 4.1.3). Also, the dip of the diapir flank implies that some portion of the drag zone is underlain at depth by the diapir flank (Figure 4.1.2). This would have restricted the diapir subsidence by supporting the sedimentary rocks from beneath if the salt within the diapir flank had remained relatively stationary over time.

Using this reasoning, it can be explained why the drag zone fold associated with the Coal Mine Point Diapir is wider than the south-west Broad Cove drag zone.

Diapir Growth Mechanism

In Chapter 2, the idea was developed that the evolution of the salt structures within the field area could be divided into two groups: passive and reactive diapirs. The onshore drag zone data reveal that drag zones associated with reactive diapirs are between 100 - 450m long whereas drag zones associated with passive diapirs are between 22 and 85m long (Table 4.1.1). It should be borne in mind that the south-west Broad Cove Diapir drag zone is by far the shortest drag zone (~100 m) associated with a reactive diapir and that the short drag zone length may be attributed to the diapir geometry. Also, the 22m length that was stated for the Monks Head Diapir drag zone is a minimum estimate because of poor exposure. However, even taking into consideration these caveats, it is reasonable to propose that the diapir growth mechanism is a controlling factor on drag zone length. This hypothesis is reasonable in light of the geological processes that give rise to reactive and passive diapirs. Passive diapirs grow by remaining for extended periods at or close to surface. In effect, the diapir remains stationary and sediments deposited against the diapir flank subside due to the effects of compaction, isostasy and salt withdrawal. Much of the 'drag' associated with passive diapiric intrusion is, therefore, a slow, relatively un-dynamic process that takes place over an extended time frame. Also, the initial stages of drag zone formation may well occur while the drag zone sediments are unlithified and therefore have no flexural rigidity. In contrast, reactive diapirs rely on a vertical intrusion of salt through either a weakened or intact overburden and, in most cases, the intruded overburden rocks will be fully lithified and therefore have a significant flexural rigidity. It

is therefore reasonable to propose that the different diapir growth mechanisms will be controls for the length of diapir drag zones as demonstrated by the exposures within the field area.

4.1.2, Seismic Analysis of Diapir Geometry as a Control upon Zone of Rotation Profile

The analysis of folding adjacent to salt structures has been extended to a larger scale using depth converted seismic sections. This analysis deals with a more general zone of rotation (new term) (see Glossary of Salt Tectonics) which includes the drag zone immediately adjacent to the diapir. The zones of rotation observed in the study area extend out from the diapir to a distance of approximately two or three kilometres. These features are therefore much larger than the drag zones exposed onshore. Recent quantitative work on large-scale folding adjacent to diapirs has focused on sandbox analogue models; for example, Alsop (1996). This work has highlighted the importance of diapir geometry as a controlling factor upon large-scale fold profile. These ideas are incorporated below. The sandbox analogue model folds described by Alsop (1996) are approximately equivalent in scale to the zone of rotation used in this thesis.

The analysis presented below attempts to relate the profile of the zone of rotation to the geometry of the associated diapir. Lithology could not be examined as a factor because of the lack of well data and by the fact that only the Inverness Formation was imaged clearly enough in the seismic data. The analysis shows a good correlation between diapir geometry and zone of rotation profile.

Eleven seismic sections of diapir drag zones were interpreted in order to define the geometry of the 15' coal seam within the Inverness Formation (see Seismic Stratigraphy, Chapter 2). The 15' coal seam reflector was depth converted (see Appendix 3) to examine the fold geometry within the zone of rotation (200-2500m from the diapir). All of the

seismic sections intersected the diapirs approximately normal to the strike of the diapir margin. The way in which zones of rotation were defined is shown in Figure 4.1.4 and the zone of rotation profile data are included in Appendix 6. In some cases, mutual diapir interference or the end of a seismic line meant that a zero or regional dip could not be defined to mark the end of the fold. In these cases, the end of the zone of rotation was defined as the minimum observed dip.

All the diapiric structures in this data set pierce the Inverness Formation (Westphalian C-Stephanian). As a whole, the Inverness Formation is mechanically homogeneous over the study area, consisting predominantly of coal measure facies (~50 m) and thick (30-200 m) fluvial sandstone units. The homogeneity of the Inverness Formation effectively normalises the lithological control upon the zone of rotation folding so that the diapir geometry control can be examined independently.

Results

The eleven zones of rotation can be divided into three categories associated with specific diapir geometries. The categories are described below along with examples of the associated zones of rotation. The data used to calculate the drag zone profiles are included in Appendix 5.

1. Zones of rotation associated with steep (planar) (70 degrees) to slightly overhanging (12 degrees) diapir margins e.g. Salt Wall Luey on Line 79: Folding of the Inverness Formation is characterised by a wide (400-2300 m), but low angle (<20 degrees) zone of rotation and a small (<120 m) drag zone with a high angle of dip (30-50 degrees) adjacent to the salt/sediment contact (Figure 4.1.5).

2. Steep to gently dipping (50 degrees) diapir margins. Zone of rotation folding is characterised by a smooth 'dip fan' profile that extends 1600 - 3500 m from the salt/sediment contact, e.g. the Salt Wall Luey, right-hand side, Chevron Line 75:

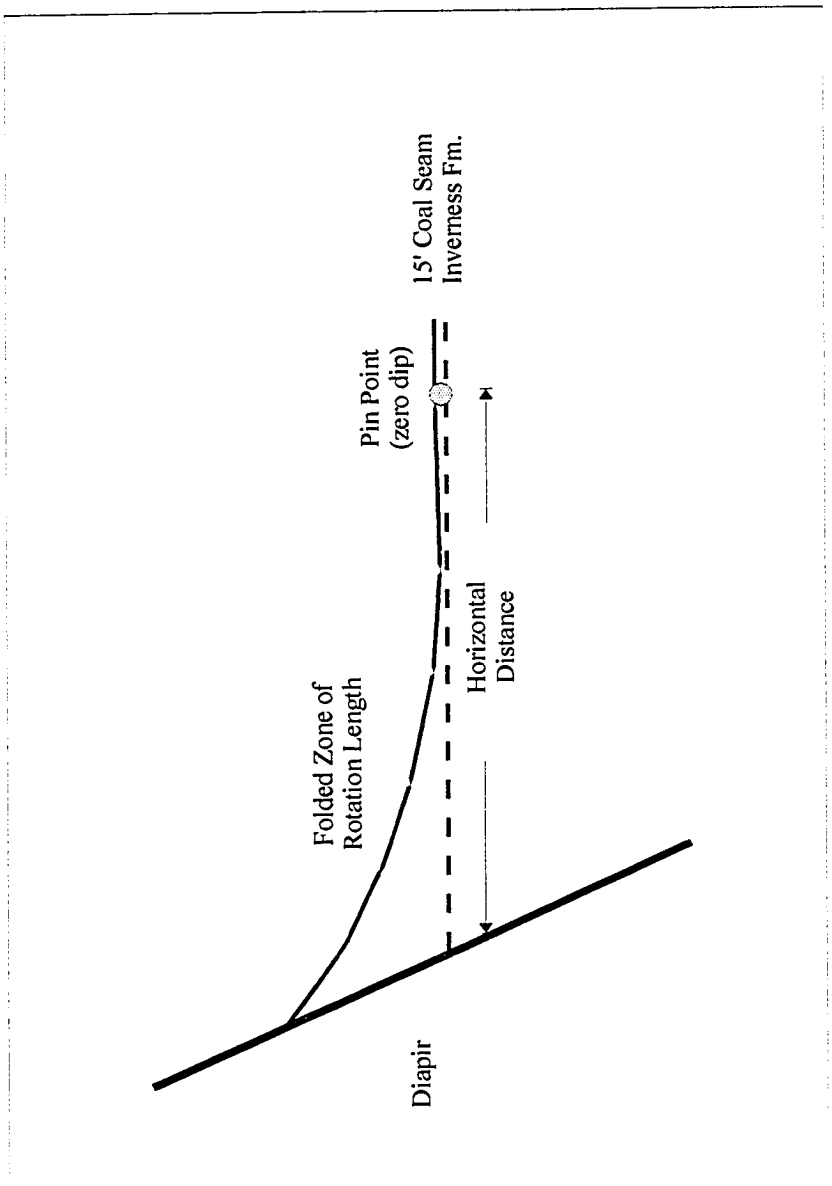

Figure 4.1.4. Schematic diagram to show how a zone of rotation is defined.

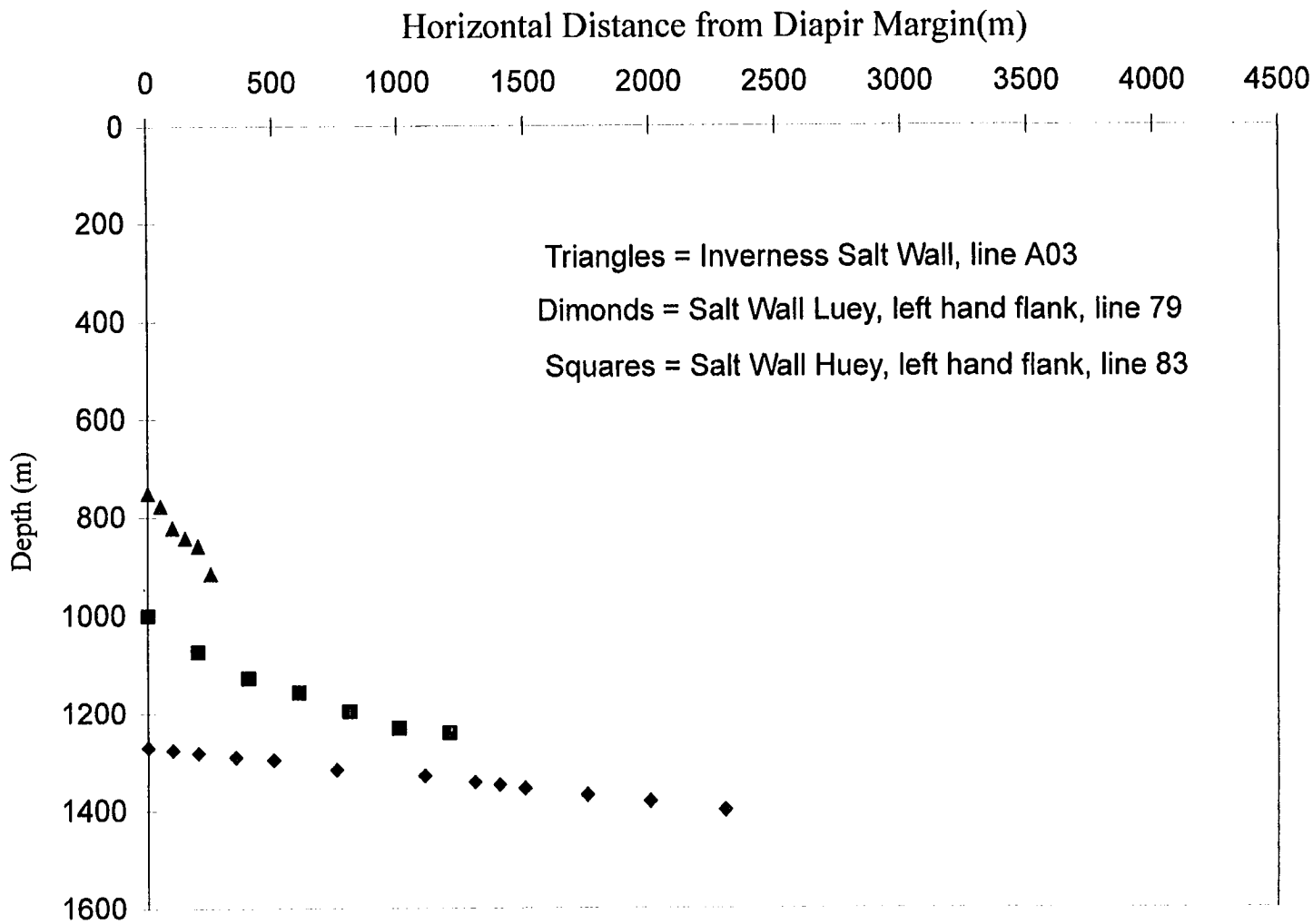

Figure 4.1.5. Group 1, steep/planar diapir margins.

Maximum dip at the salt/strata contact ranges from 35-63 degrees. In all cases, the folding of the strata within the drag zone was unable to accommodate the stress induced by diapiric intrusion and a normal fault formed at the outer limit of the zone of rotation which accommodated part of the rotational torque induced by intrusion (Figure 4.1.6).

3.Gently dipping (58 degrees) and diapir margins with pronounced shoulders, for example, the right-hand side of the Salt Wall Huey on line 75: Zone of rotation folding around these diapirs is characterised by an extremely steeply dipping (65-74 degrees) inner zone above the protruding shoulder. Outside of this inner zone, a smooth 'dip fan' (similar to 1 above) extends away from the diapir to a maximum distance of 4500m (Figure 4.1.7).

The above analysis shows that a positive correlation exists between the geometry of a diapir and the zone of rotation profile. Presented below are lines of reasoning to explain this correlation. In part, this reasoning is similar to that presented for the smaller drag zone exposures (see above).

(i) The zone of rotation probably reflects the slope of the diapir flank. Shallow diapir flanks, probably associated with an embryonic pillow stage (Davison et al., 1996), extend beneath the sedimentary overburden at depth and geometrically support the overburden. Thus, shallow diapir flanks will tend to be associated with broad zones of rotation (Alsop et al., 1995). In contrast, steep diapir flanks do not extend beneath the overburden and so provide no support to the overburden. For this reason, steep-sided diapirs are associated with relatively narrow drag zones. This reasoning is very similar to that presented for the smaller drag zones.

(ii) If the strata contained within the zone of rotation have a high flexural rigidity, such as thick sandstones, then the fold profile is more likely to be broad than if the strata have a low flexural rigidity, such as mudstones and shales. This reasoning postulates a

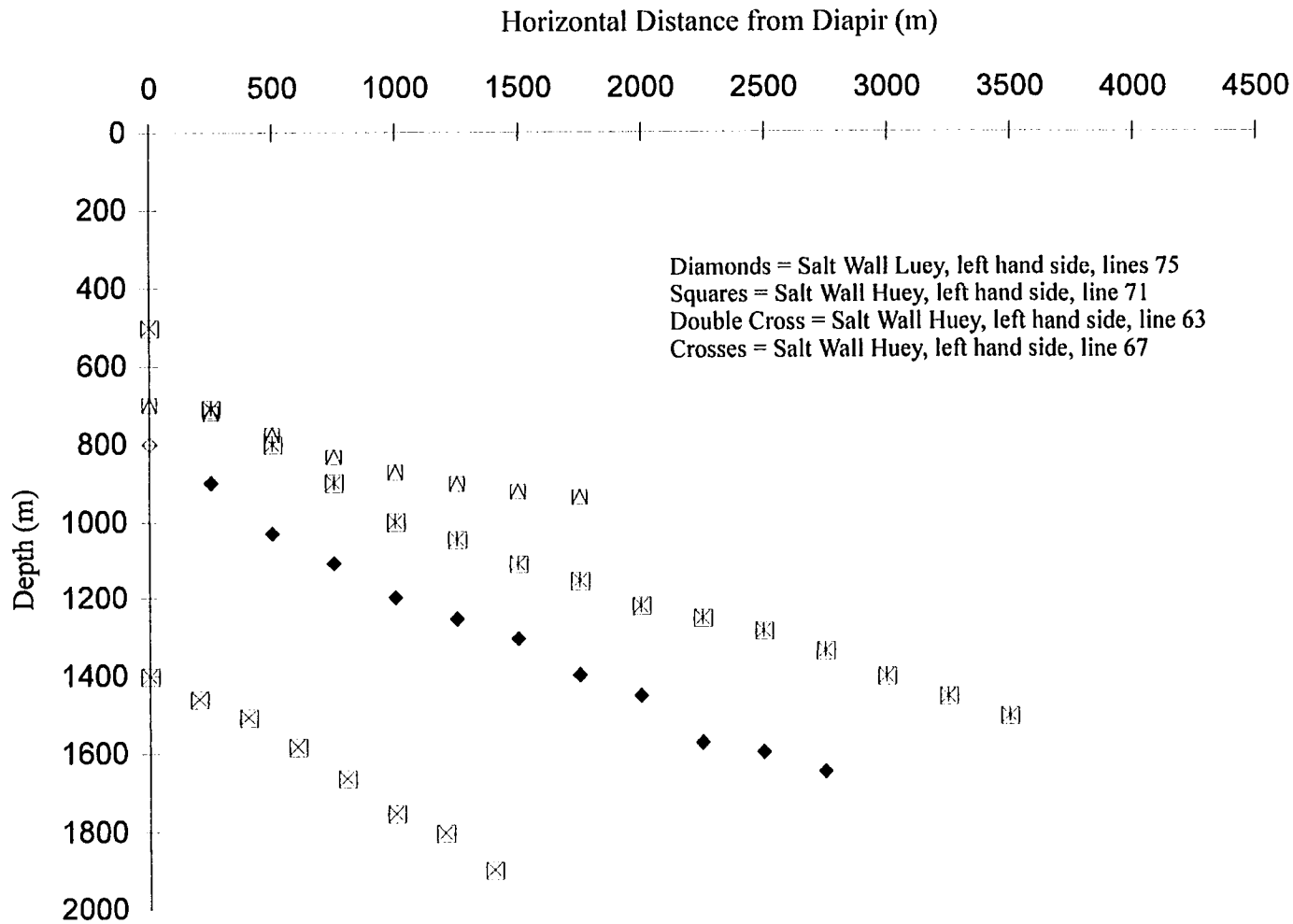

Figure 4.1.6. Group 2, gently dipping/irregular diapir margins.

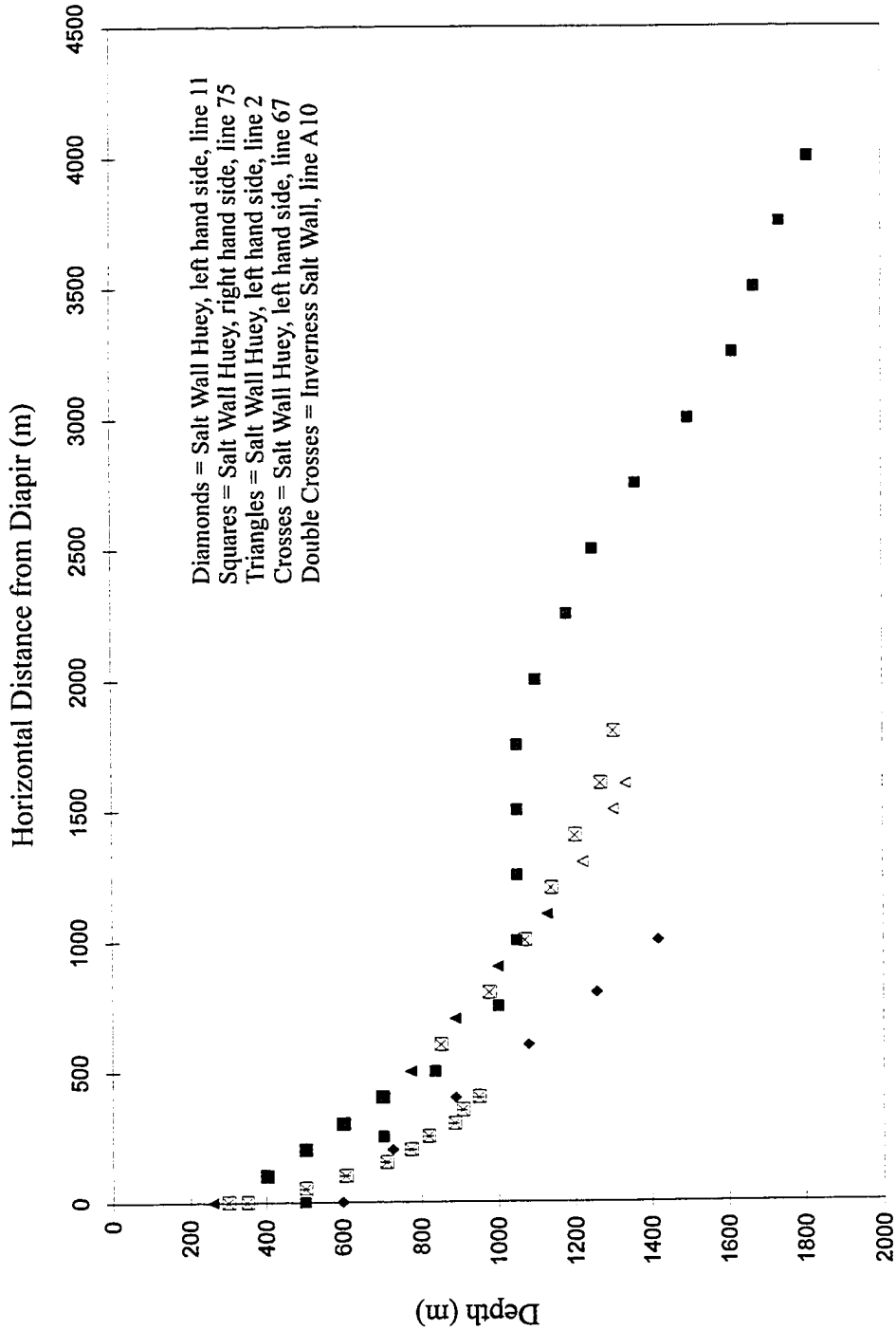

Figure 4.1.7. Group 3, irregular/shouldered diapir margins.

lithological control upon zone of rotation profile that is similar to that proposed for the smaller drag zone. However, this hypothesis can not be rigorously tested as only the Inverness Formation could be used in this analysis.

Both mechanisms (i) and (ii) above are valid explanations for the zone of rotation profile. In reality, the actual control is probably an interplay between the two mechanisms.

4.1.3, General Conclusion

From the above discussions, it has been shown that no single factor controls drag zone and zone of rotation folding. For an individual diapir, at least three factors (lithology, diapir geometry and growth mechanism) contribute to produce the final fold profile.

1. It can be demonstrated that for a single diapir, the drag zone profile can be largely controlled by diapir geometry, for example the Broad Cove Diapir and the Finlay Point Diapir. Diapir growth mechanism appears to have a direct control upon drag zone length. This is related to the fact that passive and reactive diapirs affect the surrounding rocks and sediments in fundamentally different ways. It can also be shown that lithology exerts a very strong control upon the drag zone profile, although it is probably secondary to diapir geometry and growth mechanism.

2. Drag zone lithology, lithological unit thickness and the intercalation of competent and incompetent units are probably the most important factors that control internal drag zone deformation (see below). The deformation mechanisms that are controlled by lithology are directly related to drag zone profile (see above).

3. A good correlation exists between diapir geometry and zone of rotation profile. The present study allows lithology as a controlling factor to be normalised and thereby allows the diapir geometry factor to be analysed in isolation. A future study of other diapir provinces may allow diapir geometry to be normalised,

allowing the lithological control for zones of rotation profiles to be examined. In the present study, an examination of how the diapir growth mechanism may control zone of rotation profiles was not attempted.

4.2, DEFORMATION WITHIN DIAPIR DRAG ZONES

4.2.1, Faulting

This section of the thesis discusses faulting within diapir drag zones and attempts to draw conclusions based upon the large amount of fault data that was collected. No single drag zone exposure displays all of the fault-related conclusions that are described below. Where possible, an example is used to illustrate a conclusion or line of evidence. The two most common categories of faults that were recorded from diapir drag zones are extensional and strike-slip faults. These two types of faults are described separately below.

4.2.2, Extensional Faults

Extensional faults were by far the most common type of fault observed with diapir drag zones. The extensional faults described in Chapter 3 were divided into three sets based upon their physical characteristics. The discussion below focuses on evidence suggesting that the extensional fault sets formed as fault generations that can be related to specific aspects of drag zone deformation.

4.2.3, Orientation of Extensional Faults

Perhaps the most noticeable aspect of the extensional faults is the systematic orientation of these faults in relation to the strike of the adjacent diapir margin. The vast majority of faults recorded from the diapir drag zones are orientated either orthogonal to or parallel to the strike of the diapir margin. Thus the faults form two conjugate sets of faults that intersect at about 90 degrees. The best example of this systematic fault orientation is the north-east drag zone of the Broad Cove Diapir (see above, Chapter 3), although similar

relationships were also recorded in the Coal Mine Point Diapir and the Finlay Point Diapir drag zones. An exception to this systematic fault orientation was recorded from the St. Rose Diapir drag zone. Within the St. Rose Diapir drag zone, many faults clustered around the orthogonal and parallel orientations; however, a spread of fault orientation between orthogonal and parallel is also evident (see above, Chapter 3). Given the current data available for the St. Rose Diapir, the reason for the spread of fault orientations cannot be stated; however, some possible reasons can be postulated. If the Carboniferous overburden strata overlying the Windsor Group have undergone any gravity sliding on a residual Windsor Group salt layer, faults in the overburden could well be rotated and new faults could form as a result of translation. Similarly, if the St. Rose Diapir has undergone a small amount of deflation, the overburden may have collapsed to a small extent. Evidence to support partial deflation of the St. Rose Diapir is described in Chapter 3.2. Overburden collapse could easily rotate pre-existing faults as well as creating new faults. Both of the scenarios described above could explain the observed spread in fault orientations.

4.2.4, Fault Plane Rotation of the Set 1, Small Extensional Faults

Where reliable fault data could be collected, it was noted that the Set 1, small extensional faults have been rotated as the strata within the drag zone were folded. Table 4.1.1 shows rotations calculated for the Set 1, small extensional faults, and the overall stratal rotation for the north-east drag zone of the Broad Cove Diapir, the north-east drag zone of the St. Rose Diapir and the drag zone of the Finlay Point Diapir.

The amount of fault plane rotation was calculated by taking an estimated mean through the graphed fault plane dips. Fault plane dips above or below the estimated mean are expressed as a range (+/-) about the mean value. Extreme values for fault plane rotation are discounted from this mean as it can be shown that these values correspond to local rotation produced by Set 3, large extensional faults, and are not due to drag zone stratal rotation. A second approach was to calculate an arithmetic mean for the fault plane dips

recorded at each measurement station. Both of these methods produced approximately the same value for fault plane rotation.

From Table 4.1.1, it can be shown that a relationship exists between the rotation of the Set 1, small extensional faults and the dip increase, or folding, of the drag zone strata. The St. Rose Diapir drag zone shows that faults have been rotated by 45 +/- 10 degrees while over the same drag zone section, the strata show a dip increase (folding) of 48 +/- 10 degrees. The north-east Broad Cove Diapir drag zone shows that the fault rotation (46 degrees +/- 12 degrees) is similar to the stratal dip increase (folding) of 57 +/-5 degrees. The Finlay Point Diapir drag zone shows that the fault rotation of the Set 1 faults (30 degrees, +/- 5 degrees) is greater that the folding of the drag zone strata (19 degrees, +/- 7 degrees) over the same drag zone interval.

Two questions that must be addressed regarding the relationship between fault and stratal rotation are what was the stratal dip when the faults formed and did the faults form synchronously? Anderson (1951) used fault mechanic principles to predict the orientation and angle at which faults will form if the upper surface to faulting is the earth's surface. For extensional faults, Anderson concluded that fault planes will form at an angle of between 60-80 degrees from the horizontal. Applying this value to the drag zone faults suggests that the faults within the outer drag zone, which dip between 70 and 80 degrees, have not undergone significant rotation. This in turn implies that those faults within the Broad Cove and St. Rose Diapir drag zones did not form until approximately 45 degrees of drag zone folding had occurred. An alternative solution to the drag zone/fault relationship would be to assume that the faults formed immediately after the drag zone started to form. The total amount of fault rotation would therefore be equal to the stratal dip at the present time and would imply that the faults are reverse faults that have been rotated past the vertical. Given that the process of forming a diapir drag zone is an extensional process (see below), it would be unlikely that reverse faults would form with such a high concentration and in such a systematic manner.

The drag zone folding/fault rotation relationship is different for the Set 1, small extensional faults recorded from the Finlay Point Diapir drag zone. The faults show a rotation of approximately 30 degrees while the change in drag zone dip from the Finlay Point headland to the diapir contact is only 19 degrees. However, in this case the maximum amount of stratal rotation (approximately 35 degrees) is almost equal to the observed fault plane rotation (30 degrees, +/-5 degrees). This is interpreted to indicate that some of the Set 1 faults formed soon after the initiation of folding. If this was the case, the initial dip of these faults would have been approximately 60 degrees (30 degrees fault rotation, plus 30 degrees folding), which is within the range predicted by Anderson (1951). This relationship only applies to the faults located within 40 m of the external shear zone that show approximately 30 degrees of rotation. Beyond 40 m, faults are dipping at approximately 70 degrees, suggesting that these faults formed after most of the drag zone folding had occurred. The different timing of faulting relative to folding can be explained by considering the lithology of the drag zones. Both the Broad Cove and St. Rose drag zones are developed in stratal packages that consist of intercalated siltstone, sandstone and mudstone, whereas the Finlay Point drag zone is developed in a stratal package consisting of thick sandstone units, conglomerates and mudstone rich coal-bearing intervals. The relatively incompetent strata of the Broad Cove and St. Rose drag zones may have allowed the strain induced by folding to be accommodated by a deformation mechanism other than faulting, for example bedding-parallel slip (see below). In contrast, the thick sandstone and conglomeratic units of the Finlay Point drag zone are unlikely to deform by a mechanism other than brittle faulting (Figure 4.1.1).

4.2.5, Relative Timing of the Set 1, Small Extensional Faults

The interpretation presented above indicates that the Set 1 faults formed either at the onset of folding or within the early stages of folding. Similarly, the fact that Set 1 faults are rotated by fault drag associated with Set 3 faults, and that Set 2 faults offset Set 1 faults indicates that the Set 1 faults were the first faults to form. For these reasons, the Set 1 faults are designated as the 1st generation faults (Figure 4.2.1).

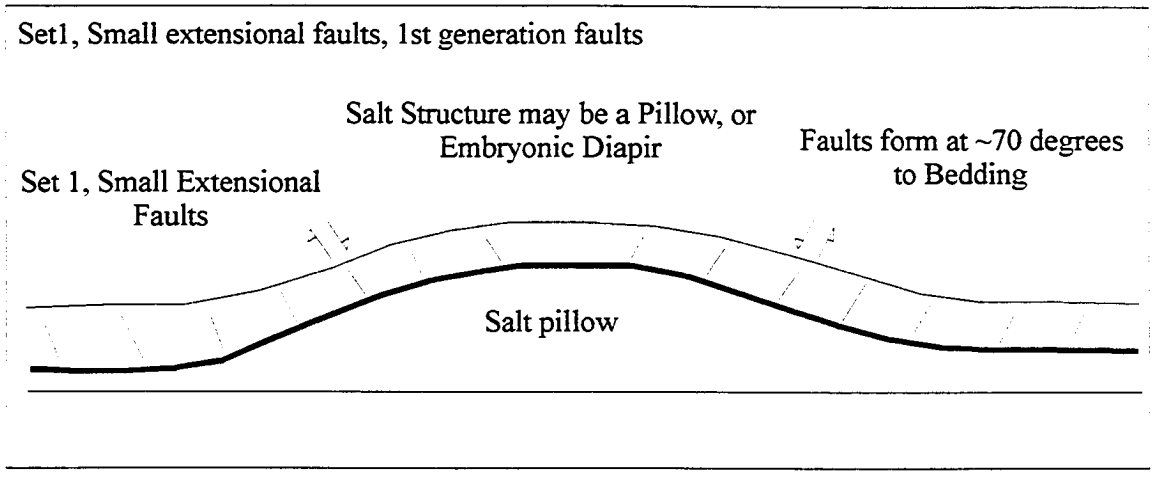

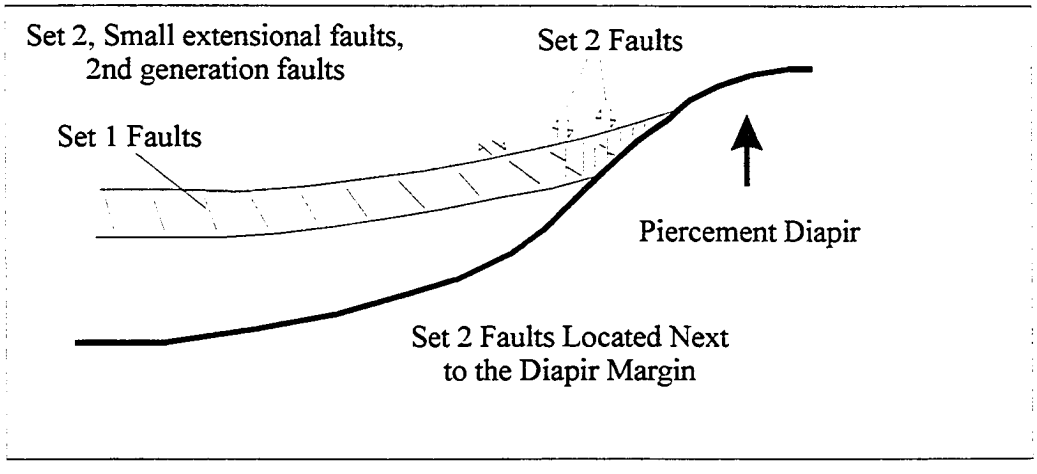

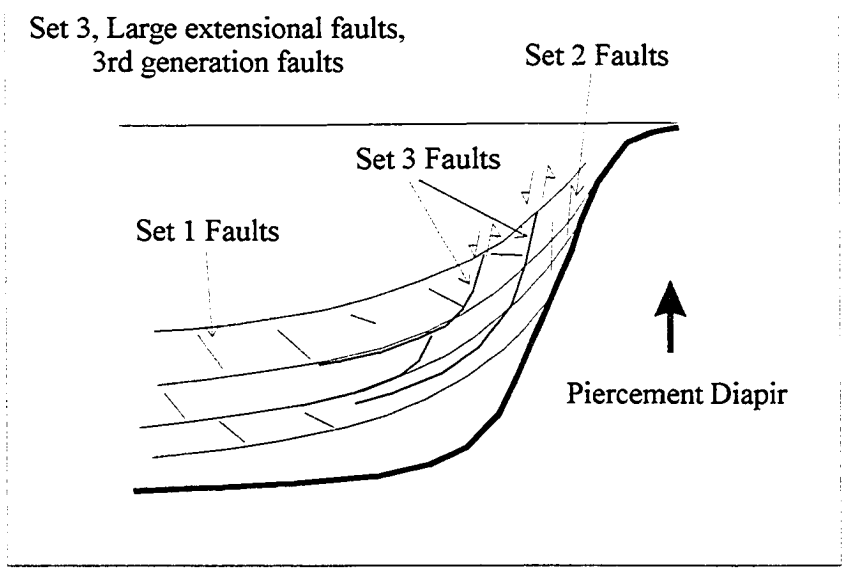

Figure 4.2.1. Diagram to show three generations of faulting associated with drag zones.

4.2.6, Mutually Orthogonal Fault Sets with Diapir Drag Zones

With the exception of the St. Rose Diapir, small brittle faults recorded from the diapir drag zones have a very systematic orientation with respect to the adjacent diapir margin. The faults tend to form two groups that strike either parallel to or orthogonal to the adjacent diapir margin. In addition, it was shown in Chapter 3 that the rotation of the Set 1 faults was approximately equal for orthogonal and parallel faults (with respect to the diapir margin), suggesting that overburden extension (strain) orthogonal to the diapir is approximately equal to overburden extension (strain) parallel to the diapir. The orientation and rotation of the Set 1, small extensional faults, probably reflects the 3D stress field created by diapiric growth. Extensional faults tend to form normal to the sigma 3 direction (the least compressive stress direction) (Anderson, 1951). The fact that two groups of faults are recorded with a 90 degree difference in strike implies that the orientation of sigma 3 and sigma 2 switched periodically during the formation of the drag zone, thereby allowing the formation of the two groups of faults. The reason why sigma 2 and sigma 3 switched orientations may be related to the effects of fault generation on the strength of the rock. The formation of fractures with a consistent orientation may result in a reduction of the effective rock strength in a direction perpendicular to the fault plane. This would cause sigma 3 to switch with sigma 2, so that any new fractures formed will form normal to the new sigma 3 direction, orthogonal to the previous fault set. This process of switching sigma 2 for sigma 3 could occur several times. Previous work using natural examples (Jackson et al., 1990) and analogue models (Link, 1930; Parker and McDowell, 1955; Alsop, 1996) emphasised radial faults (with respect to the diapir) and therefore extension orientated parallel to the diapir margin. In comparison with western Cape Breton, the faults described from other natural examples and analogue models probably represent faults similar to the West Fault at St. Rose, which has an offset of approximately 12 m. This fault is the only orthogonal faults that can be seen at map scale (1:250000). Note that the discussion above does not attempt to describe faults within the overburden that are located over the top of a diapiric structure.

4.2.7, Set 2, Small Extensional Faults

Set 2, small extensional faults, are only found within the inner drag zone, typically no more that 40 m from the external shear zone. In terms of physical characteristics, they are very similar to the Set 1 faults (see above). Set 2 small extensional faults are interpreted to be 2nd generation faults. This interpretation is supported by two lines of evidence: firstly, the faults do not show rotation to lower angles of dip and secondly, Set 1 faults are offset by Set 2 faults, indicating a clear genetic relationship. The majority of Set 2 faults are oriented orthogonally with respect to the trend of the diapir margin. Very few Set 2 faults oriented parallel to the diapir margin were recorded. In terms of the diapir intrusion process, Set 2 faults are interpreted to reflect the intense shear stress within the inner drag zone that results from the penetration of the diapir through the Carboniferous strata (Figure 4.2.2).

4.2.8, Set 3, Large Extensional Faults

Set 3 extensional faults are distinguished from Set 1 and Set 2 faults by their size, displacement, orientation with respect to the diapir and by their distribution within the drag zone.

The main characteristics of the Set 3 extensional faults are:

- A metre scale displacement (>3m). Only at Finlay Point could the footwall and hangingwall of a Set 3 fault be matched, with a displacement of ~3m. In all other cases, the hangingwall and footwall could not be matched. This indicates that the displacement across the fault would have to be equal to or greater than the height of the cliff (approximately 3-10m).

- The faults are oriented sub-parallel to the diapir margin and the folded drag zone strata.

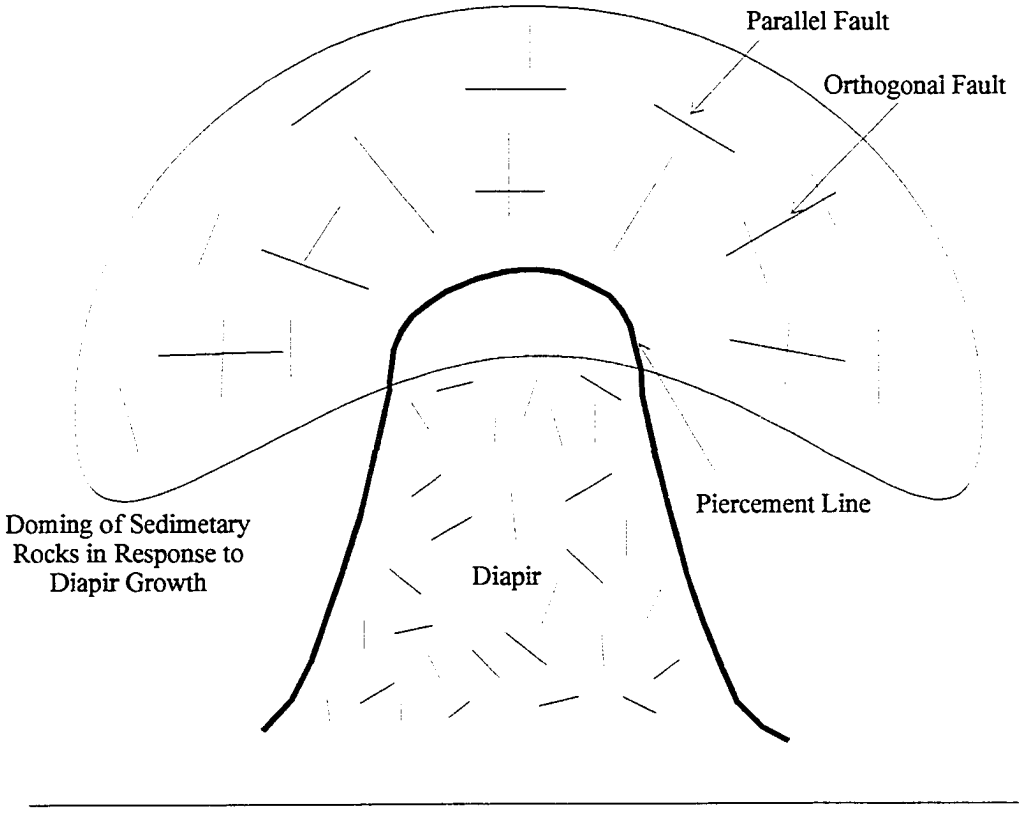

Orientation of principal stress axes changes around the diapir margin

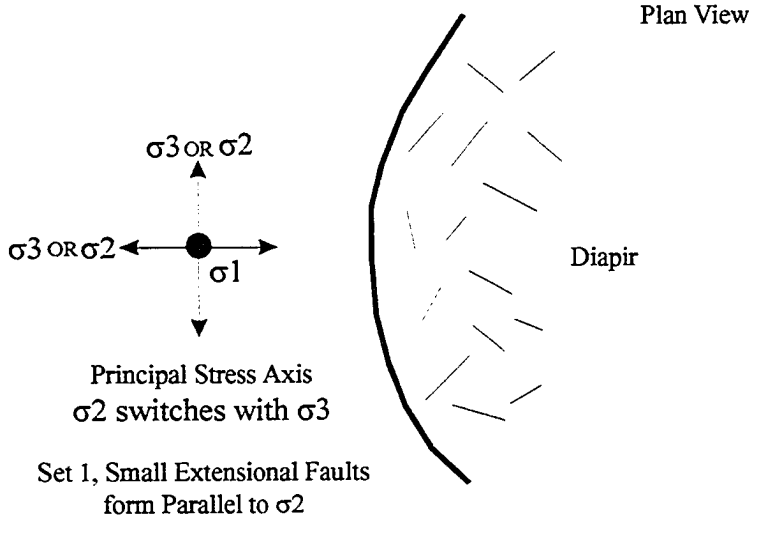

Figure 4.2.2. Schematic Diagram to show the orientation of Set 1 Faults in relation to the Principal stress axes.

- Set 3 faults are generally associated with the inner drag zone where the strata dip at 50-60 degrees.

- The faults are orientated sub-parallel to the folded drag zone strata, which dip at approximately 60 degrees.

- Set 1 faults are rotated within the hangingwalls and footwalls of the larger Set 3 faults. The amount of rotation of the faults is approximately equal to the change in strata dip due to fault drag.

Because the Set 1 faults are rotated within the hangingwalls and footwalls of the Set 3 faults, Set 3 faults are interpreted to have formed relatively late in the deformation history of the drag zone. For this reason, they are designated as 3rd generation faults, although their relationship to the 2nd generation faults is not clear.

4.2.9, Fault Plane Geometry

A complete section through a Set 3 fault (i.e. tip to tip) is not exposed in any of the drag zone sections. From the exposures available, a fault plane geometry can be proposed, which is presented below. It should be noted that this is by no means a unique solution and some of the more reasonable alternative models are also described.

Figure 4.2.3 shows the preferred interpretation for the Set 3 faults. The fault plane has a listric geometry such that the fault becomes a bedding-parallel decollement at depth. Within the coastal section, only the portion of the fault that cut through stratigraphic section was recorded, probably because the bedding-parallel decollement would not be recognised as a fault plane.

The outcrop exposure of the faults shows that both the hangingwall and footwall have deformed during faulting. The footwall and hangingwall deformation is also apparent if

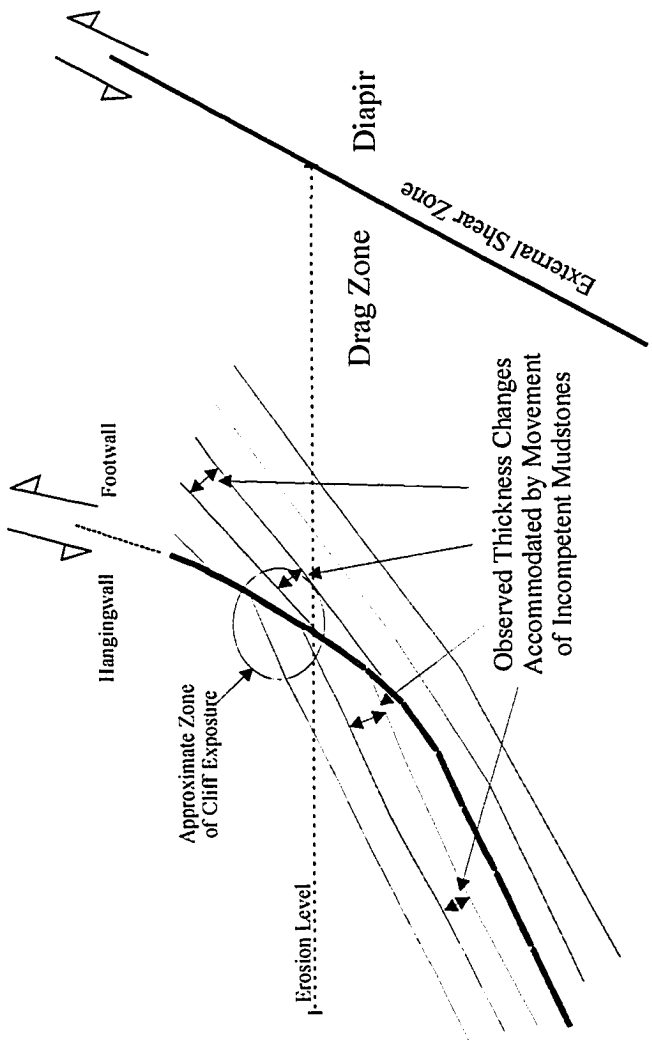

Figure 4.2.3. Model for the Set 3, large extensional faults.

the strata dip profile from the north-east Broad Cove drag zone is examined (see above, Chapter 3). The profile shows that the dip of the footwall usually increases while the dip of the hangingwall decreases. In order to allow this hangingwall and footwall deformation, the hangingwall and footwall strata must undergo thickness changes. These thickness changes are probably accommodated by ductile/plastic processes, which locally thicken or thin the mudstone strata. Because the process of this deformation probably occurs on a microscopic scale, field evidence for such processes would be enigmatic and no evidence of this kind was collected in the field.

An alternative model for the Set 3 faults is that they formed early in the drag zone deformation history and are rotated listric extensional faults with hangingwall rollover. Although the gross geometry of this model fits the available data, the interpretation is rejected because:

- The rotation of the Set 1 faults suggests that the Set 3 faults formed after formation and partial rotation of the Set 1 faults.

- If a listric fault plane had formed early and been rotated, it would show a reverse offset with the fault plane dipping towards the diapir.

4.2.10, Bedding-Parallel Slip within Diapir Drag Zones

Bedding-parallel slip appears to be an important deformation mechanism within the diapir drag zones exposed in western Cape Breton. The development of bedding-parallel slip within drag zones appears to occur over a range of scales, which is dependent upon the presence and distribution of incompetent strata.

For highly competent strata such as the thick sandstone units within the Inverness Formation (e.g. the Eagle Sandstone and the Stack Sandstone), stress is absorbed by pervasive brittle deformation; for example, within the Coal Mine Point Diapir drag zone.

However, where incompetent mudstone separates the sandstone units, evidence of large-scale bedding-parallel slip is evident. At Coal Mine Point, the second sandstone unit contains anastomosing shear zones that are interpreted to be the results of bedding-parallel slip occurring within mudstone units above and below the sandstone unit (see above, Chapter 3). Bedding-parallel slip has allowed the sandstone bodies to 'slide' in a down dip direction away from the diapir and bedding-parallel slip has been confined to one or two thick mudstone units (Figure 4.1.1b).

Pervasive bedding-parallel slip appears to be associated with thinly bedded intercalated mudstones, sandstones and siltstones. At Broad Cove, the drag zone consists largely of incompetent strata and bedding-parallel slip appears to be much more pervasive. Numerous small duplex structures were observed which show vergence away from the diapir indicating transport of strata away from the diapir. Once the drag zone strata have been folded to around 60 degrees, they become orientated sub-parallel to the diapir margin. In this orientation, it may become easier for the drag zone strata to deform by bedding-parallel slip, rather that brittle faulting (Figure 4.2.2). The individual sedimentary units would begin to slip relative to one another, with the incompetent mudstone units acting as decollements. The whole stratal package begins to deform as a sheared pack of playing cards. The lithology of the drag zone strata probably plays a large role in determining whether or not bedding-parallel slip will occur. Thick, competent sandstones, for example, the Eagle Sandstone, are unlikely to deform by bedding-parallel slip. However, if mudstone units are present between the sandstone units then bedding-parallel slip may occur in these units. This style of deformation was noted at the Coal Mine Point Diapir drag zone (see below). Similarly, the Set 3 faults are interpreted to represent a localisation of bedding-parallel slip since their timing, displacement orientation and geometry is consistent with extensional bedding-parallel slip (Figure 4.1.1a).

4.2.11, Summary of Faults within Diapir Drag Zones

Drag zone deformation is an interplay of brittle (faulting) and plastic (bedding-parallel

slip) deformation. Not surprisingly, lithology and the intercalation of competent and incompetent strata play fundamental roles in determining the localisation or partitioning of strain (and hence faults) within diapir drag zones.

From crosscutting relationships and rotation of passive markers, it can be shown that the faults formed as distinct generations. The 1st generation formed as a result of the initial folding within the drag zone. These faults tend to be distributed throughout the drag zone. 2nd generation faults formed adjacent to the external shear zone and were probably related to the shear stress induced as the diapir penetrated through the sedimentary rocks. 3rd generation faults appeared to form relatively late in the drag zone formation process and may represent a localisation of bedding-parallel slip.

In nearly all drag zones, the orientation of the fault sets is either parallel to or orthogonal to the diapir margin.

4.2.12, Relationship of Western Cape Breton to Modern Concepts of Salt Tectonics

The lack of suitable field examples of diapir drag zones coupled with advances in computer and analogue modelling techniques have given rise to a number of drag zone models that are based solely upon computer or analogue models. One of the fundamental features of all analogue and computer models is the assumption of how the overburden will behave in response to stress. Authors typically assume that the overburden will behave as either a viscous fluid, a brittle solid, an elastoplastic medium (Schultz-Ela et al., 1993), an isotropic granular brittle overburden (Davison et al., 1993), or Power-Law Fluids (Davison et al., 1996). All these assumptions are approximations to actual geological conditions. Only recently has it become possible to computer model simultaneous brittle-plastic deformation within a single drag zone (Poliakov et al., 1996) by using an implicit Eulerian-Lagrangian Finite-Element code to simulate viscous flow (Poliakov et al., 1993a) and an explicit Lagrangian Finite-Element code to simulate brittle

failure (Poliakov et al., 1993a).

Observations from western Cape Breton show that overburden rocks deform by plastic/ductile (viscous) mechanisms and by localised shear zones or faults (brittle behaviour). Plastic and brittle deformation commonly co-exist within the same rock unit in space and time. The observations from western Cape Breton therefore support the use of brittle/viscous deformation algorithms used in the most recent computer models of Poliakov et al. (1996).

4.3. DEFORMATION WITHIN STRUCTURAL CARAPACES

This section attempts to draw together the interpretations from the seismic data and onshore diapir outcrops to account for the overall configuration of the structural carapaces. Factors that will be taken into account include: relating the structural carapaces to structures commonly seen within halite diapirs, the effects of regional compression and inversion, halite dissolution and the gypsum to anhydrite reaction.

4.3.1, Internal Structure of Evaporite Diapirs

The purpose of this section is to compare the structural carapaces exposed within the field area to internal structures previously described for halite diapirs.

Structures commonly formed within diapirs are curtain folds, which are characterised as a cylindrical fold with a radial axial trace and steeply plunging fold hinge (Jackson and Talbot, 1994) (Figure 4.3.1). A diapir can contain either a single curtain fold (Figure 4.3.2), or many curtain folds (Figure 4.3.3).

There is no exposure of the internal structure (halite core) of the diapirs within the study area. However, salt exploration wells and underground mining have been able to define

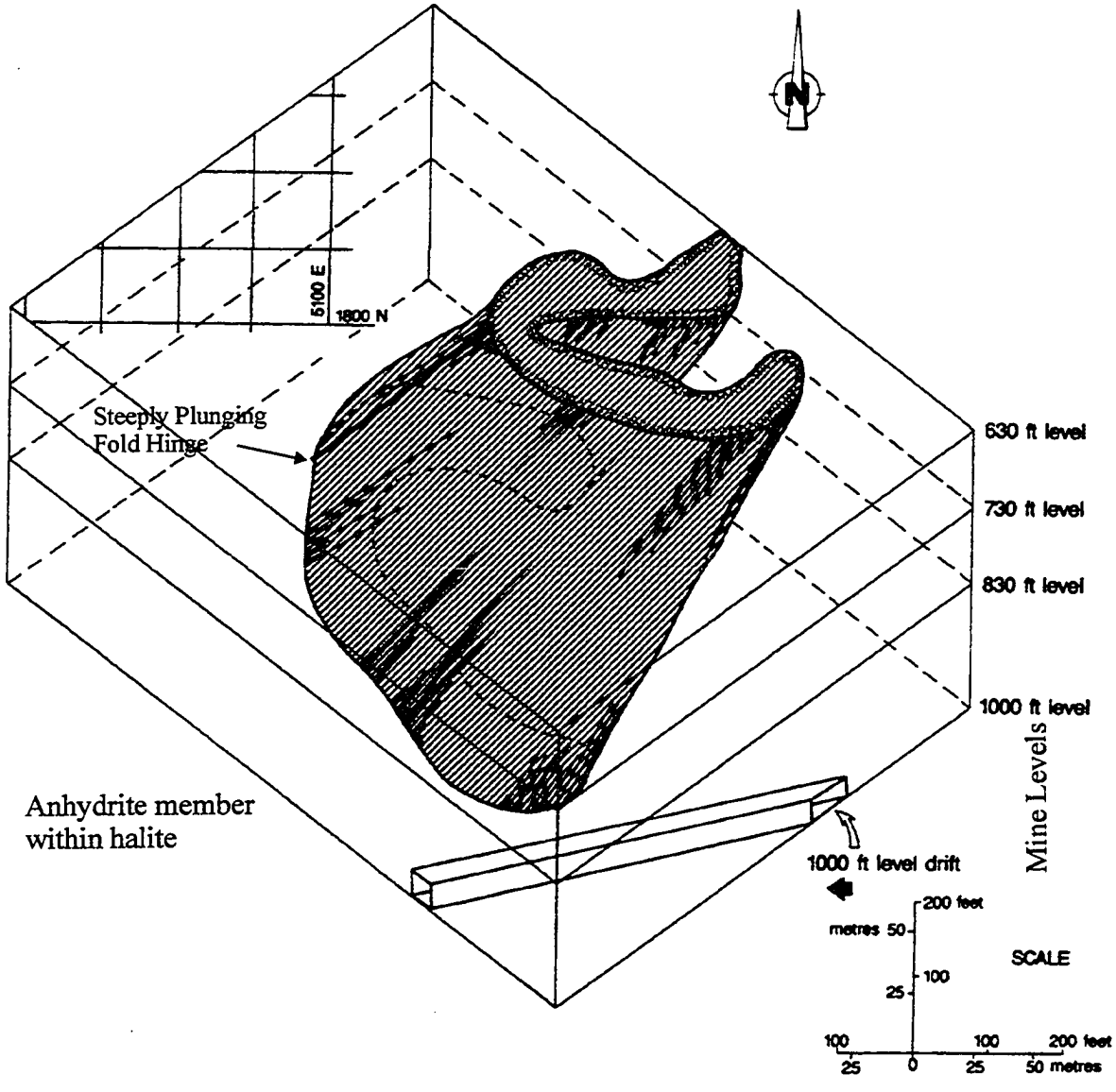

Figure 4.3.1. A simple curtain fold from the Pugwash Diapir. Note the steeply plunging fold axis which can be traced for at least 300 ft vertically. The curtain fold is defined by a distinctive anhydrite member.

Modified from Carter (1990)

Example section which would expose repeated stratal units.

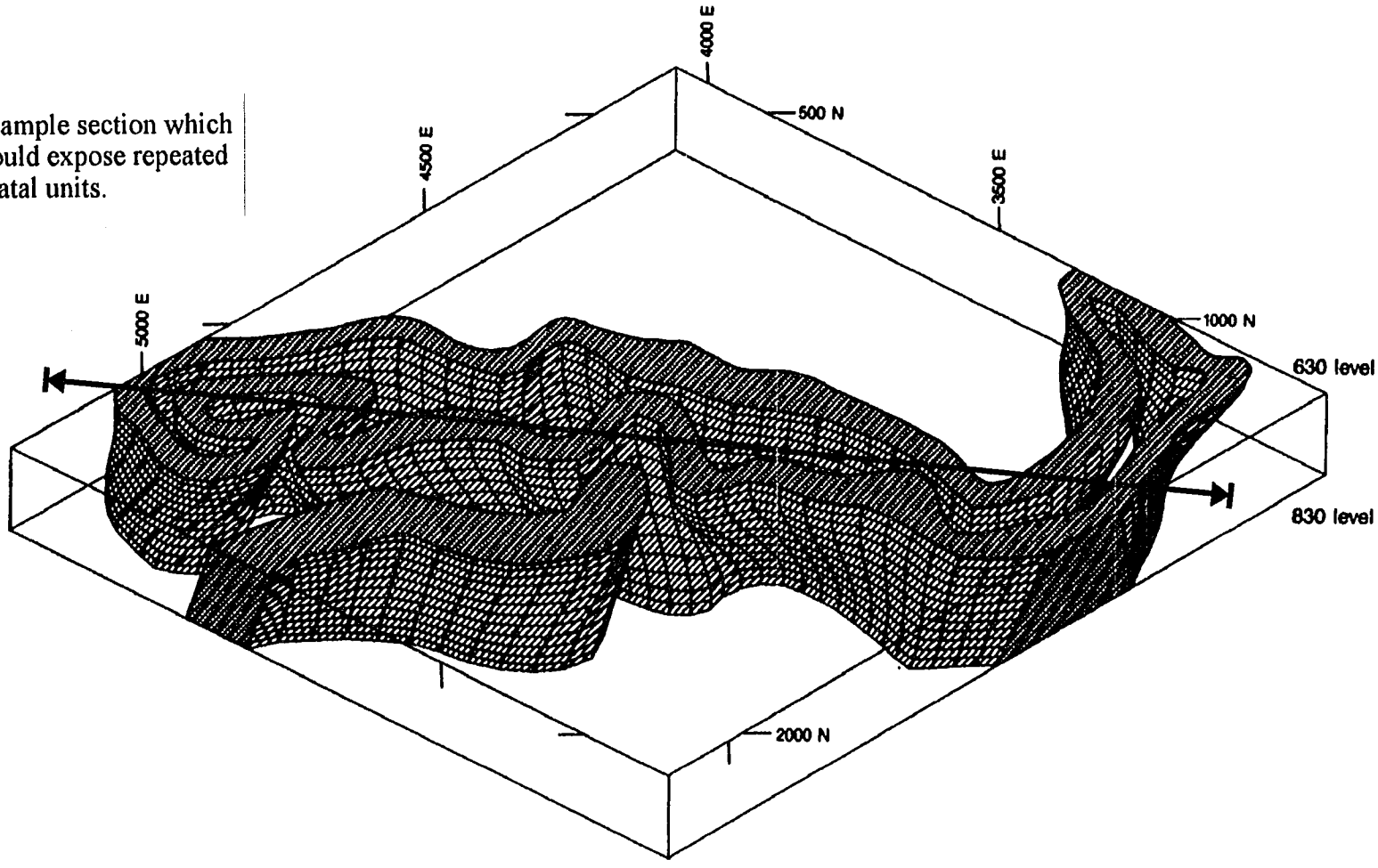

Figure 4.3.2. A refolded curtain fold from the Pugwash Diapir. The refolding has produced a complex fold geometry. A section through such a curtain fold would expose repeated stratal units.

Modified from Carter (1990)

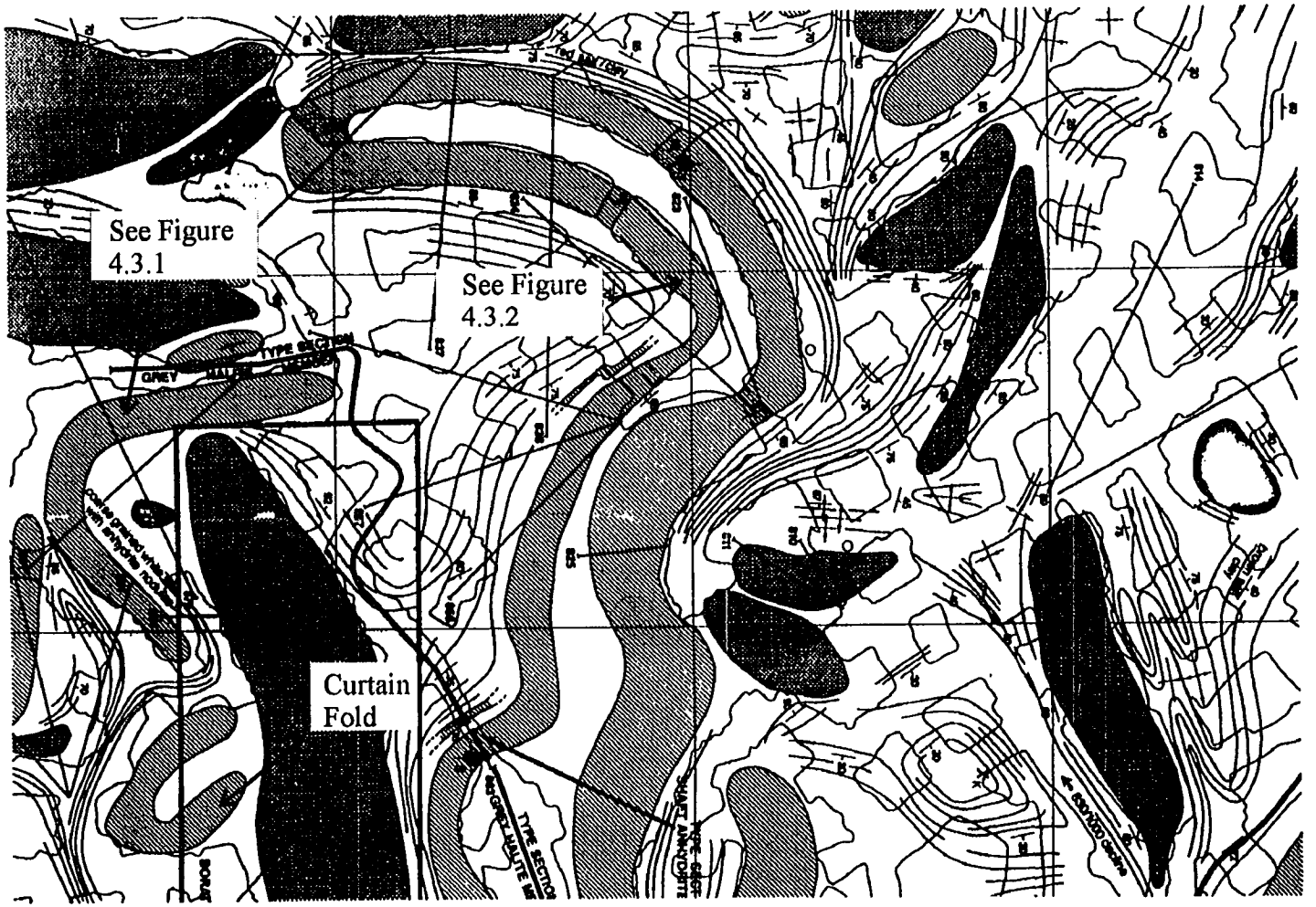

Figure 4.3.3. Interpretation of part of the 730' level from the Pugwash salt mine. Multiple curtain folds are evident, the majority of which can be traced through to the underlying 830' and overlying 630' level can be seen. The presence of borate and anhydrite marker horizons (light and dark grey areas) make it possible to interpret the fold structures. Modified from Carter 1990.

the gross internal structure of two salt diapirs within Nova Scotia: the Pugwash Diapir at the Pugwash salt mine and an unnamed diapir at Malagawatch, Cape Breton Island.

The Pugwash Diapir is currently mined for halite and potash. The mine is developed on three levels (630ft, 730ft and 830ft) using a room and pillar system. Horizontal and vertical pre-extraction drilling on the three levels have defined over 20 individual curtain fold structures based on mapping of anhydrite "marker" layers (Carter, 1990a,b,c) (Figure 4.3.3). Individual structures vary in cross-sectional width from 200 – 2000 m and the larger curtain folds can be correlated through all three mine levels.

From 1979 to 1981, a Chevron-Irving consortium drilled eleven exploration wells to define the structure of an evaporite diapir at Malagawatch (Howie, 1988). Three marker horizons (the borate horizon, the potash horizon and a breccia zone) were repeatedly intersected in the wells and the well intersections were used to define the internal structure of the diapir (Figure 4.3.4). The interpreted internal structure consists of two folds that are separated by a narrow synclinal structure. The fold hinges in the lower parts of the folds are interpreted to be steeply dipping, while the upper parts of the fold hinges are gently dipping. The geometry of the folds at Malagawatch does not correspond to the definition of a curtain fold but may represent curtain folds that have been modified by compression or folds formed as a result of convection. Unfortunately, the interpretation from the wells is poorly constrained and so a definitive interpretation is probably inappropriate. The Malagawatch diapir is, however, good evidence for large-scale folds within a diapir.

It is apparent from the two available examples that large folds within diapiric structures are present within Nova Scotia and that some of these folds are curtain folds.

4.3.2, Structural Carapaces within the Study Area

There is little doubt that the diapir outcrops within the study area have very complex

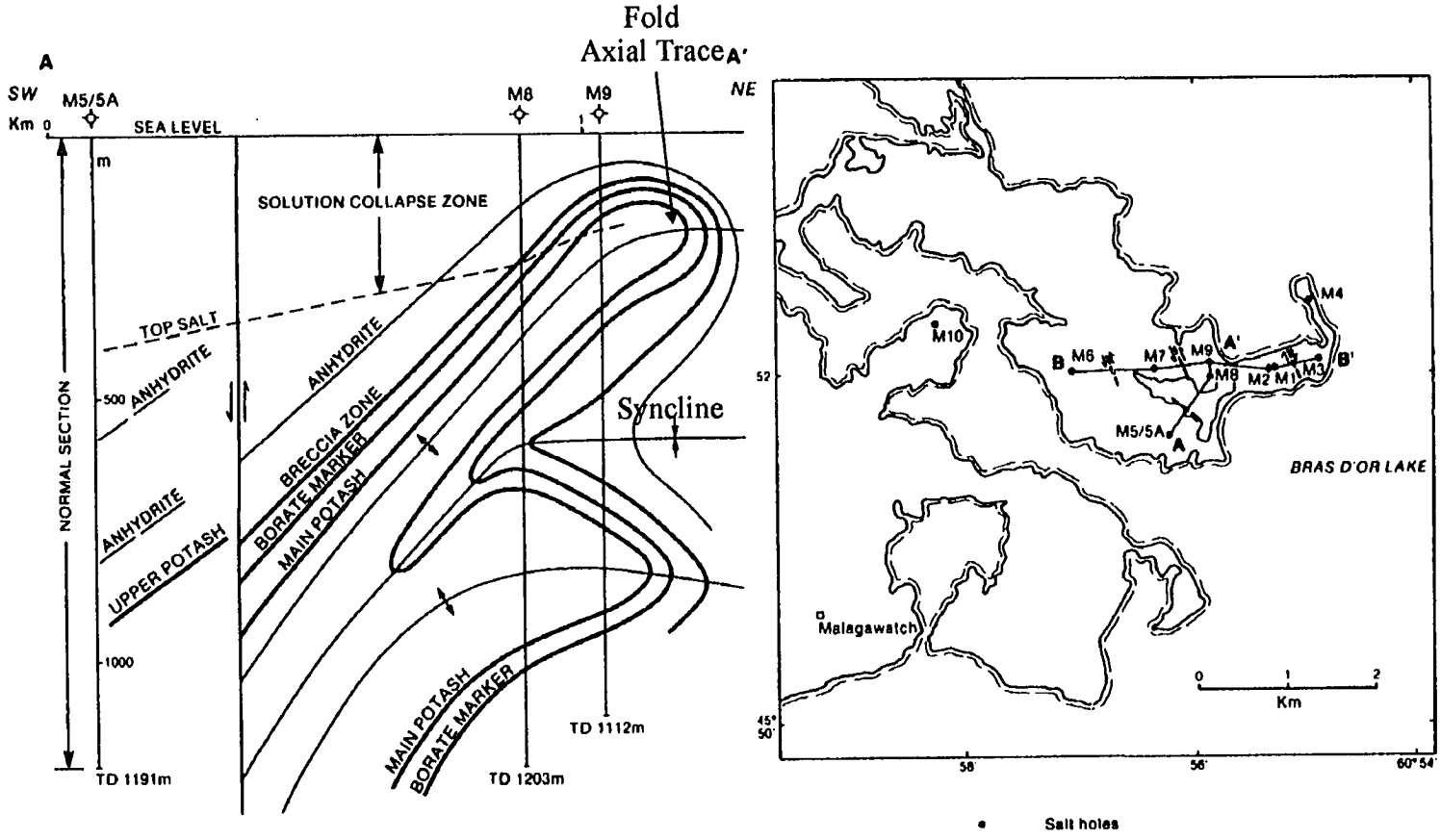

Figure 4.3.4. An un-named diapir near to Malagawatch, Cape Breton. Right-hand diagram shows the location of the salt exploration wells. Left-hand diagram shows an interpretation of the diapir geometry based upon the well data. Modified from Howie (1988).

structural configurations. However, by constructing detailed structural cross-sections and by realising that the outcrops represent diapiric structures, the structural configuration of each outcrop can be logically reconstructed.

The Monks Head and St. Rose diapirs represent the two largest diapiric structures exposed within the study area. Their structural carapaces have been interpreted to represent partially exposed folds that have steeply plunging fold axes. The scale, wavelength and fold-axis orientation of these folds are similar to some of the smaller folds described from the Pugwash salt mine and to those at Malagawatch. The folds can be interpreted to represent portions of curtain folds or may be compressional folds related to inversion. If the Monks Head and St. Rose carapaces do represent curtain folds, this indicates that the structural carapace overlying the halite core is mirroring the deformation of the halite core and is not being transported as a passive cap rock. The formation of a curtain fold relies to a large extent upon buoyancy and thermal convection, which are able to operate because of the unusual properties of halite as compared to other sedimentary/evaporitic rocks (for example, its viscous behaviour). It therefore seems implausible that a structural carapace that is devoid of halite would be able to form a curtain fold.

While it can be shown in two cases that the deformation within the structural carapace is similar in some respects to the style of deformation typical of the halite core, it is very unlikely that the gypsum/anhydrite, mudstone and limestone that make up the structural carapace could have flowed in a similar way to halite.

4.3.3 Deformation Related to the Hydration of Anhydrite to form Gypsum

The anhydrite to gypsum reaction involves a 42% volume increase (and vice versa). Typically, this reaction takes place at a shallow depth of a few meters, down to a depth of 200 m (M. Zentilli, pers. comm. 1996). This indicates that, as a diapir approaches the surface, any anhydrite within the structural carapace will expand by 42% (assuming

sufficient pore water or phreatic water is available). At the same time, the structural carapace is likely to be confined laterally and from beneath by the surrounding sedimentary rocks and underlying halite core. It may also be confined from above if there is an overburden overlying the carapace. This will be particularly true for active or reactive diapirs. Confining the gypsum volume change might well result in folding or in tightening of pre-existing folds. Good examples of where this may have occurred are the Broad Cove Diapir and Port Hood Island Diapir. Both of these structural carapaces show tight to isoclinal folds.

Folds related to diapiric deformation or horizontal shortening due to compression are hard to distinguish from volume expansion folds, so it is hard to quantify the effects of volume expansion. While it is very likely that some deformation related to volume expansion did occur, it can be inferred that, given the relatively small amount of gypsum within the Broad Cove carapace, not all of the folding can be attributed to volume expansion.

4.3.4, Horizontal Shortening of a Structural Carapace Due to Inversion or Compression

Another potential form of non-diapiric deformation relates to Carboniferous and post-Carboniferous compression that could have caused horizontal shortening of the structural carapaces. Chapters 2 and 3 discussed the evidence for both Carboniferous and post-Carboniferous compression and inversion. The section below describes how this compression and inversion may be represented in the structural carapaces.

A halite diapir can absorb either extension or compression by changing its geometry (Jackson and Carmez, 1989; Vendeville and Nilsen, 1995). Extension of the overburden may lead to the diapir becoming fatter, with diapir expansion being equal to extension. Compression may lead to rejuvenation of growth, thinning of the diapir, and possibly to halite being extruded at surface (Vendeveille and Nilsen, 1995). The physical evidence of both extension and compression is hard to detect in halite diapirs but may be more

obvious in structural carapaces. A compressional event may lead to thinning of the diapir and coeval diapir growth (effectively redistributing the halite) or extrusion of halite at surface. The structural carapace may react to thinning of the underlying halite diapir by horizontal shortening. Two obvious examples of structural carapaces that may have been affected by horizontal shortening are the Port Hood Island Diapir and the Broad Cove Diapir.

The Middle Windsor strata exposed on Port Hood Island show pervasive tight to isoclinal folding with fold axes orientated towards the north-east/south-west. This orientation corresponds to the orientation of fold axes that would be produced by a north-west directed compression. In addition, the Middle Windsor strata are interpreted to be located on the crestal region of the Salt Wall Luey. If the salt wall underwent thinning due to compression, the crestal region should also undergo horizontal shortening. The pervasive folding within the Middle Windsor is interpreted to represent horizontal shortening due to compression in the Late Carboniferous or post-Carboniferous. The exposed Hood Island Formation strata are interpreted to be located on the north-west flank of the salt wall and are dipping at >80 degrees. In this orientation, a north-west orientated compression would cause strain approximately orthogonal to bedding and would not result in folding (Figure 4.3.5).

The carapace of the Broad Cove Diapir is strongly folded into a number of meso-scale fold structures (wavelength ~ 50m). On the south-west flank of the diapir, the structural carapace is now above the level of the Inverness Formation and juxtaposed against the Broad Cove Formation, indicating post-Carboniferous growth. In addition, the exposed flanks of the carapace verge outwards from the diapir, while the south-west flank imaged on the Inverness seismic line A05 has an almost vertical flank. This geometry may indicate that the Broad Cove Diapir has been thinned and rejuvenated by compression. Horizontal shortening of the diapir would logically be accompanied by horizontal

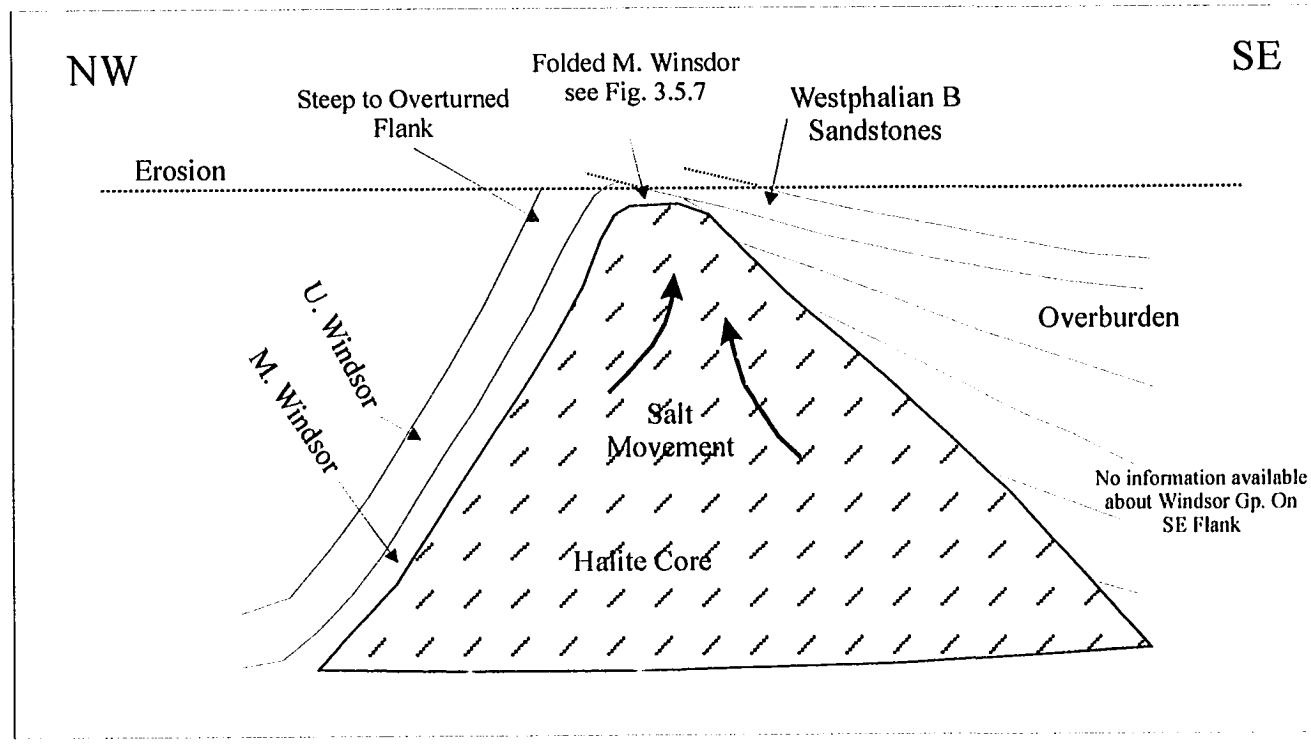

Figure 4.3.5. Schematic model for the configuration of the Port Hood Island Diapir and the adjacent sedimentary rocks which make up the majority of Port Hood Island.

shortening of the carapace. However, if the carapace was unable to accommodate an equivalent amount of shortening, this would lead to a carapace that was marginally wider than the underlying diapir and, hence, vergence of the carapace sides outwards from the diapir. The carapace consists of stratal units that are considerably more competent than halite and so it is likely that they could not react to horizontal shortening by viscous flow. On the south-east flank, the diapir has penetrated through the Inverness Formation. This is evidence of post-Carboniferous growth and may well be contemporaneous with post-Carboniferous inversion (see above). While it can not be proven categorically that the folding within the structural carapace is related to inversion and/or compression, the bulk of evidence tends to support this conclusion. The fold axes of the Broad Cove Diapir structural carapace strike north-west/south-east. The orientation of these folds does not correspond to the regional north-west orientated compression proposed in Chapter 2. However, the fold axes do plunge steeply to the south-east and this may be evidence of refolding of pre-existing folds by the north-west directed post-Carboniferous compression. The cause of the original north-west/south-east striking fold axis remains uncertain but it may be the result of either dissolution, the hydration of anhydrite or movement of the underlying diapir.

4.3.5, Halite Dissolution

Boehner (1993) reported many examples of collapse breccia that consist of blocks of gypsum and carbonate in a mudstone matrix that form an irregular caprock overlying a diapir. These residual caprocks appear to be associated with areas where halite has reached the surface. Within Cape Breton, Giles (1981a) described Windsor Group sections from the Canso-Bras d'Or area in which halite has been removed to a depth of 200-300 m, leaving a telescoped Windsor section. Salt springs are common within Nova Scotia and Cape Breton and are direct evidence for modern halite dissolution. The location of salt springs is not always associated with diapiric structures. Boehner (1983, 1986) describes areas from Nova Scotia and Cape Breton where a fault or salt structure is not associated with salt springs and suggested that the diapir or fault may have been

sealed from groundwater flow by residual clay. Howie (1988) documented many occurrences of salt springs from Antigonish county, the Denys Basin – Canso area and western Cape Breton. None of these salt springs are located close to one of the salt structures described in this thesis. There is therefore evidence for regional halite dissolution but this cannot be tied to a specific salt structure without a detailed understanding of the regional hydrogeology. Having stated this, there is evidence for halite dissolution affecting the salt structures within the field area. On Port Hood Island, a block of Upper Carboniferous sandstone has collapsed so that it is now exposed as a breccia surrounded by gypsum (see above, Chapter 3.5). Halite dissolution underneath the caprock/overburden could result in collapse of the caprock and overburden to produce the structure exposed today. At St. Rose, the regional map pattern and structures within the drag zone of the St. Rose Diapir suggest that the diapir has undergone/is undergoing a reduction in salt volume related to salt migration or dissolution (see above, Chapter 3.2). The structural carapaces within the field area do not contain any halite, although it is possible that halite was originally present. Boehner (1986) showed that, while the thickest halite unit within the Windsor Group is located in the Lower Windsor, halite units up to 91 m thick are present in the Hood Island Formation within the Lake Bras d'Or area of Cape Breton. Removal of this halite may result in a telescoped section similar to those described by Giles (1981a). It may also result in some folding of the insoluble carapace material if halite dissolution was not at an even rate throughout the carapace. The structural carapaces do not resemble collapse breccias similar to those described by Boehner (1983), although the Mabou mega-breccia that was interpreted to be associated with halite dissolution is similar to Boehner's collapse breccia. J. Waldron (pers. comm. 1998) suggested that dissolution of halite beneath the structural carapace could lead to a passive subsidence of the carapace and account for the position of the carapaces at surface today. While this could well be so (and is indicated by the collapsed block on Port Hood Island), the volume of halite dissolution must be relatively small since it has not affected the map pattern of the surrounding overburden, for example at St. Rose (see above, Chapter 3.2).

4.3.6, Faults within Structural Carapaces

In two locations (Broad Cove and Monks Head), repeated stratigraphic sections were recorded whose way-up evidence and dip/strike orientation indicated that faulting and not folding were the cause of repeated sections. These faults are located within the structural carapace, most commonly within the portion of the carapace that is adjacent to the external shear zone. Within the Monks Head diapir, the faults repeat the E1 to D3 stratigraphy three times with no apparent folding or significant change in stratal dip. From the available data, the geometry of these faults can best be described as a sub-vertical thrust fault. An extensional fault geometry would not cause the observed stratal repetition. Where the strata are repeated more than once, the faults are modelled as a vertically oriented thrust stack, for example the Monks Head Diapir (Figure 4.3.6). Within this thesis, the faults have been described using a ramp/flat geometry that assumes no bed length or bed thickness changes. This is obviously an over-simplification when dealing with evaporite rocks, which patently show bed length and bed thickness changes. However, since none of the curtain fault 'ramps' are exposed and the cliff sections only provide limited, two-dimensional structural control, the approximation is reasonable. A problem with the interpretation of the faults within the carapace relates to their expansion of the structural carapace. The repetition of stratigraphic units on faults implies that the width of the carapace has increased. This seems hard to explain since the surrounding overburden would tend to restrict expansion and also it has been demonstrated that horizontal shortening of structural carapaces related to compression has occurred in the field area. The formation of repeated units could be explained by removal of large volumes of material from the more internal portion of the carapace (moving laterally or vertically). This would create space to allow repetition of stratal units without expanding the carapace. There is evidence of removal of ~70 m of red mudstone strata from the structural carapace (see above, Chapter 3.6). However, the connection between removal of mudstone strata and the formation of the faults is only speculative.

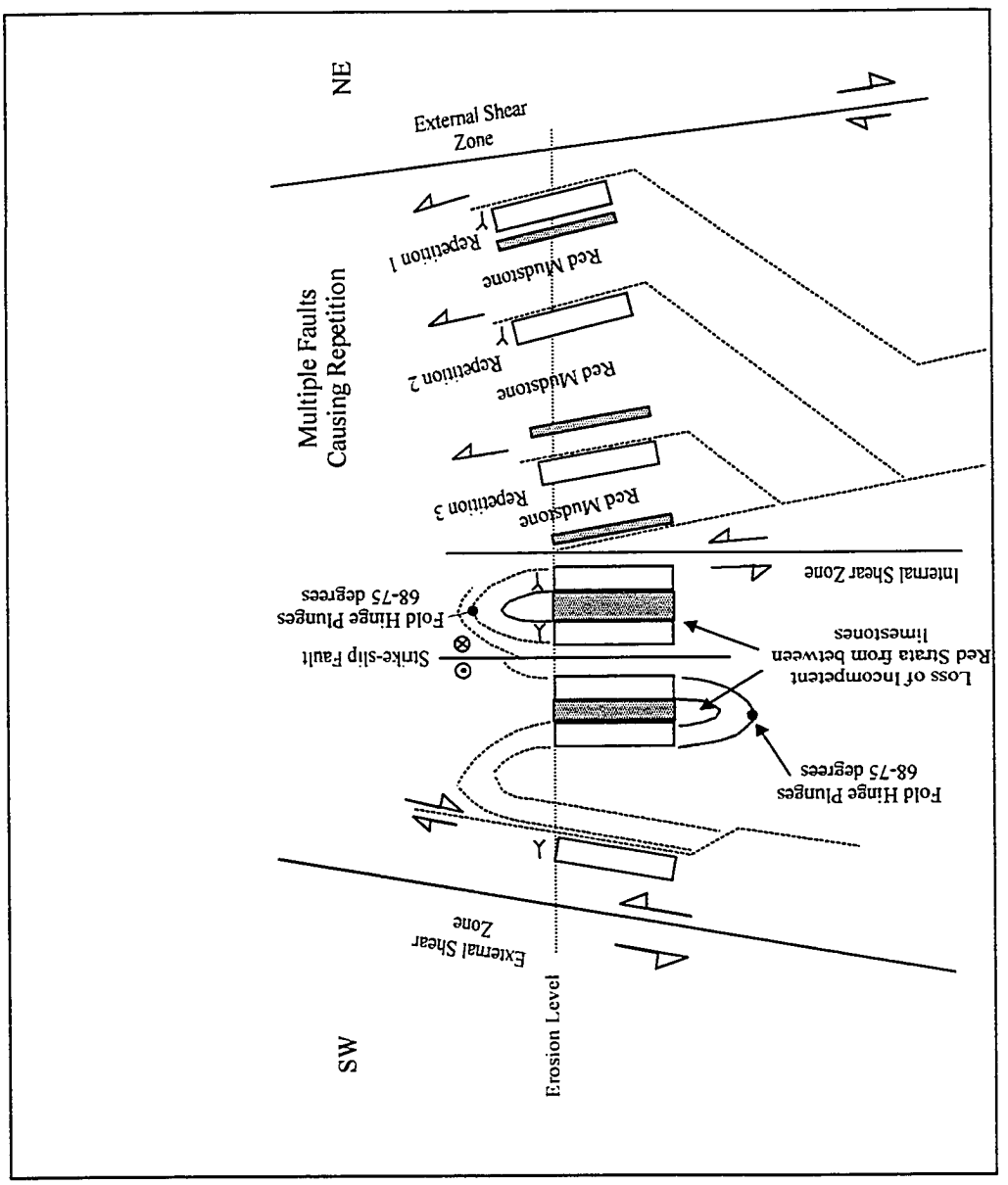

Figure 4.3.6. Schematic model for the structural carapace of the Monks Head Diapir (Not To Scale)

4.3.7, Mega-Boudinage

Mega-boudinage may be associated with the formation of folds within diapirs or structural carapaces (Figure 4.3.6). As exposed at Monks Head (Antigonish County), mega-boudinage is typified by blocks (up to 15m square) of competent limestone surrounded by gypsum with the blocks lining up along strike, resembling giant stepping stones (Figure 3.5.11). Structural reconstruction of the Monks Head Diapir section shows that the mega-boudinage blocks are located within the limbs of steeply plunging folds. These folds are interpreted to be similar-style folds, which implies that extension has occurred within the fold limbs during folding. Mega-boudinage takes place in the fold limbs when the vertical and horizontal strain rates are greater than can be absorbed plastically by the limestone units, with the result that the limestone units (originally intact beds) are fractured both horizontally and vertically. Laboratory experiments show that, under a steady strain rate of 10^{-14}/sec, sulphate evaporites weaken rapidly at 150-200 deg.C; under the same conditions, limestones do not begin to weaken until 300-400 deg.C. (Muller and Briegel, 1978; Muller et al., 1981). Although estimates of strain rates in natural diapirs are different from laboratory experiments, the dichotomy in the brittle/plastic transition should still apply. As folding continues, the limestone unit is pulled apart along the fractures in a vertical and horizontal direction and gypsum invades the growing fractures. The end result is isolated blocks of limestone which have a common orientation and are surrounded by gypsum. Similar, though smaller scale, structures associated with folding have been previously described for fractured and rotated dolomites within anhydrite from the Jurassic of the Overthrust Belt of the Rocky Mountains (Picard, 1980), and for micro-scale folds of dolomite within gypsum from the Italian Alps (Helman and Schreiber, 1983). More local examples of mega-boudinage were observed within the Pugwash salt mine. Within the halite, blocks of anhydrite can be seen that are completely surrounded by halite. On longer tunnel sections, several such blocks can be seen, forming a line of blocks similar to those observed at Monks Head. The mega-boudinage deformation mechanism can be used to explain one of the geometric problems in forming folds within

a diapir. As a diapir grows and forms internal folds, it does so using a relatively small volume of rock from beneath the diapir plus halite that migrates into the diapir. In order for competent units to form folds within a diapir, they must increase their surface area dramatically. This is mechanically hard to do unless the rocks are extremely ductile. A geometric solution to this problem is to have the rock units fracture both vertically and horizontally so that the resulting blocks can separate (Figure 4.3.7). The mega-boudinage deformation is therefore a way of allowing competent rock units to 'expand' as they are deformed into folds (Figure 4.3.6). The process of forming mega-boudinage with a diapir is a three-dimensional extrapolation of Beloussov's (1962) work on chevron and similar class folds in which a competent rock unit is surrounded by incompetent rock units. Beloussov (1962) showed how thick limestone and sandstone rock units were fractured and separated into discrete blocks during folding, while surrounding mudstones deformed plastically to accommodate spaces between the separated blocks. Beloussov's (1962) model has obvious similarities to the mega-boudinage example where the Hood Island Formation limestones are surrounded by mudstone and anhydrite.

4.3.8, Progressive Brecciation

No limestone unit found within the structural carapaces is undeformed and all the limestones contain many joints and fractures. These joints and fractures are exploited by gypsum, which invades the smallest of joints, probably by a precipitation from gypsum bearing fluids, pressure solution or plastic creep. The gypsum found in the joints is typically amorphous, which would tend not to support a crack-seal type of infilling. Once joint planes and fractures are invaded by gypsum, the gypsum may encourage hydrofracturing, which widens the existing joint plane and creates new planes. Hydrofracturing could result from the volume changes associated with the gypsum to anhydrite transition. If the carapace was elevated to the near surface, percolating ground water could initiate the anhydrite to gypsum reaction, resulting in expansion of the anhydrite by 42%. This process of gypsum invasion leads to the progressive brecciation of stratigraphic units - typically limestones. The process continues until the limestone is

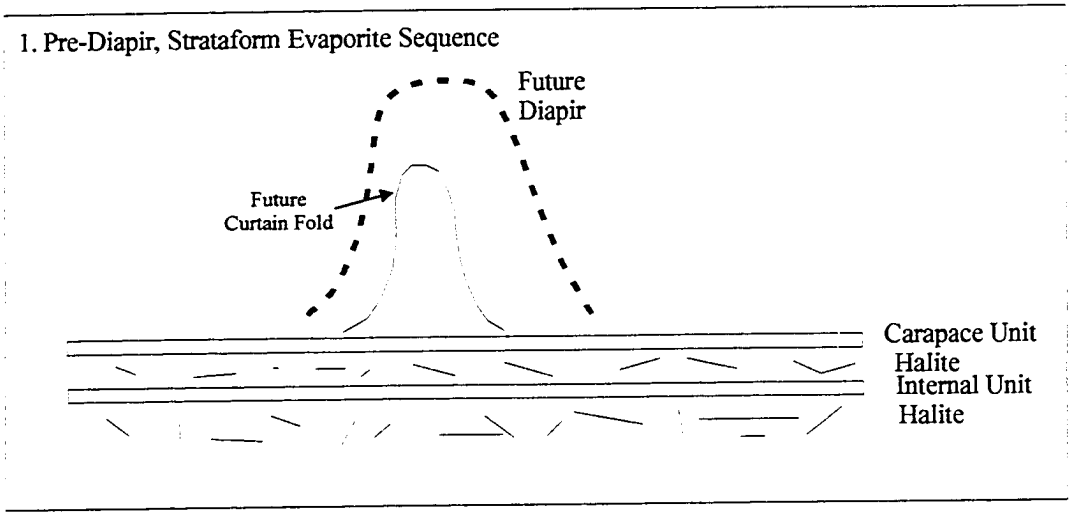

The formation of a curtain fold or structural carapace requires rapid extension and/or thinning of the strata. Mega-boudinage is a mechanism whereby competent stratal units, for example the Upper Windsor limestones can accommodate such extension.

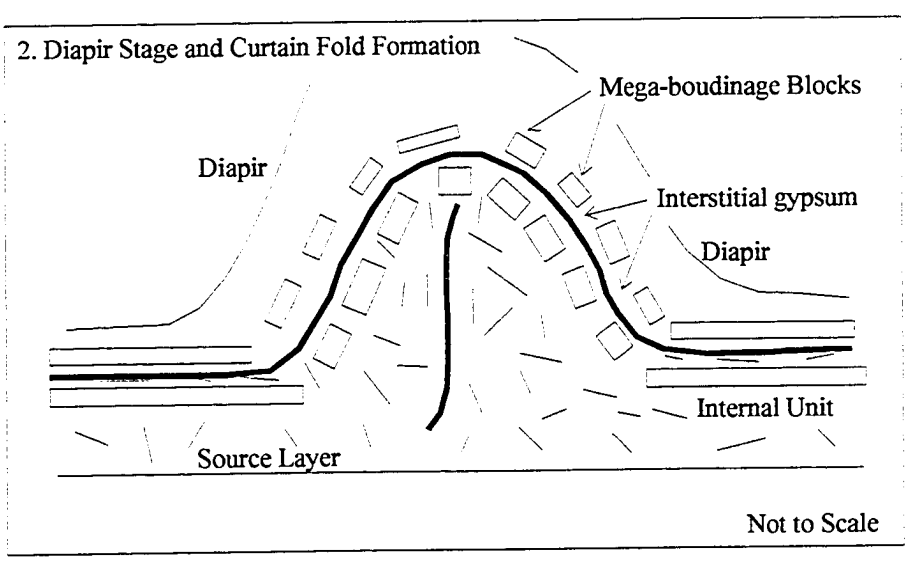

Figure 4.3.7. Schematic Diagram to show the Development of Mega-Boudinage. As the diapir grows, the limestone units become separated into large blocks that are surrounded by gypsum and mudstone (see Chapter 3.6).

reduced to a breccia with a mean clast size of a few centimetres. The progressive brecciation process can destroy stratigraphic horizons, making stratigraphic interpretation difficult.

4.3.9, Disharmonic Folding

In order to reconstruct the structure of the diapirs from the coastal outcrops, it is necessary to assume that folding of the Upper/Middle Windsor strata was strongly disharmonic on a large-scale, for example the Broad Cove Diapir (see above, Chapter 3). This also requires that layer-parallel decollements exist within the diapir carapace in order to accommodate the disharmonic folding. Although the scale of the outcrops precludes observation of large-scale disharmonic folds, complete micro- and meso-scale disharmonic folds are abundant. The interpretation used to reconstruct the diapir carapaces is therefore an extrapolation of the micro/meso-scale folds by assuming that a scale invariant or fractal relationship exists between the various sizes of folds.

4.3.10, Gypsum Veining

Two of the diapir outcrops (Monks Head and Port Hood Island) contain numerous sub-horizontal gypsum veins with a vertical opening direction. The formation of these veins is clearly related to gypsum-rich fluids migrating through the carapace, but questions remain as to when the veins formed and how vein formation relates to diapir growth. The veins indicate a degree of overpressure within the carapaces such that the hydrostatic force exceeded the lithostatic force (weight of the overburden) plus the intrinsic rock strength. Conditions of overpressure require that the movement of fluids be restricted so that the fluids cannot migrate to re-equilibrate with the surrounding environmental conditions. Hydrofracturing and vein formation can therefore be associated with either burial or uplift. During burial, trapped fluids may become overpressured and cause fracturing if the overpressure exceeds the lithostatic load plus the intrinsic rock strength. Alternatively, buried rocks containing overpressured fluids may undergo fracturing and vein formation if tectonic uplift or erosion reduces the effective lithostatic load to a point where

hydrostatic pressure exceeds the lithostatic load plus the intrinsic rock strength. The fact that the veins within the structural carapaces cross-cut most of the deformation indicates that they formed later than most of the deformation within the structural carapaces. This indicates that they formed after the post-Carboniferous inversion, although there is no upper age constraint for vein formation. The veins could therefore have formed during deposition of the Mesozoic sedimentary cover (see above, Chapter 2), or formed later during uplift and erosion of the Mesozoic cover. It is also possible that the veins formed as a result of glaciation, which could have loaded and unloaded the diapirs. The origin of the gypsum-rich fluids can only be partially answered by the present study. Clearly, the gypsum-rich fluids could have derived gypsum from a local source, but why gypsum-rich fluids should be circulating is not certain. The fluids may be a result of dissolution of the underlying halite, in which case the gypsum may represent a relatively low solubility component to the brine solution that was precipitated within the carapace. The study of fluid migration through diapirs and structural carapaces is a potential area for new research, with opportunities to apply geochemical and petrological techniques as well as structural analysis.

4.3.11, Summary of Deformation within Structural Carapaces

Although some features of the structural carapaces are similar to those associated with curtain folds, it is highly unlikely that gypsum, anhydrite, mudstone and limestone will be able to deform in a similar way to halite. For this reason, the structural carapaces probably do not represent curtain folds. The structural carapaces do not, therefore, mirror the internal deformation of the halite core, but act as a more rigid carapace. Having said that, some of the deformation seen within the structural carapace may be related to dissolution of the underlying halite, leading to foundering of carapace/overburden material and possibly to folding. Some of the deformation within the carapaces is undoubtedly intrinsic to the carapace. For example, the volume change associated with the hydration of anhydrite to gypsum in a restricted setting could produce some of the observed folding. Probably the most important factor that resulted in deformation or modification of

existing deformation of the carapaces was horizontal shortening related to compression and inversion. Compression and inversion rejuvenated the diapirs and probably caused thinning of the diapirs and horizontal shortening of the carapace. Horizontal shortening of the carapace was accommodated by the formation of tight to isoclinal folds.

4.4, A GLOBAL PERSPECTIVE

The Cape Breton salt structures examined in this thesis are in many ways unique. However, it is not that the Cape Breton diapirs exhibit an especially unusual form of salt tectonics, but rather it is their excellent state of preservation that is the main reason why these diapirs are important. Many salt provinces around the world undoubtedly produce diapirs with similar configurations to the Cape Breton examples. However, the timeframe over which they can remain at surface prior to erosion is relatively short. The fact that several intact yet completely exposed structural carapacess are preserved in the humid Cape Breton climate must be something of a geological fluke. Typically, salt structures that are exposed at surface today consist of halite glaciers that are the result of active extrusion on to a peneplain, for example the diapirs of the Zagros in Iran (Talbot and Jarvis, 1984). Other diapirs are represented by halite uplifting a thin cap of sedimentary overburden, for example the diapir province in north-west Yemen described by Davison et al. (1996). In rare cases, the embryonic pillow stage of diapirism that can result from anhydrite hydrating to gypsum is exposed, for example those described by Hoyos et al. (1996), from central Spain. In all of the cases described above, one specific component of a diapir's evolution is exposed. Our understanding of salt tectonics is therefore an amalgamation of these snapshots in time.

The Windsor Group, which forms the structural carapace, has a clearly defined and distinctive stratigraphy. This has allowed detailed reconstruction of the carapaces, which has in turn shed light on the relationship between a structural carapace and processes such as regional compression and inversion, the hydration of anhydrite and dissolution.

Although Schwerdtner (1983) described structural carapaces from the Queen Elizabeth Islands of arctic Canada, his descriptions did not allow for detailed structural reconstruction of the carapaces.

For many years, the term 'drag zone' has been used informally by geologists to describe the deformation of sedimentary rocks adjacent to a diapir. The author can find no reference to its first usage. Bearing this in mind, drag zones have received very little scientific attention despite the fact that drag zones form many giant oil and gas fields around the world. This lack of attention is due in part to the lack of suitable field outcrops. The author is not aware of any other diapir province in the world that contains continuous cross-sections through diapir drag zones. Recent work on drag zones has used analogue models to simulate deformation within diapir drag zones (Alsop, 1996). However, analogue models suffer from an inherent scaling limitation in that a single sandgrain is approximately equivalent to a 10 m boulder if scaled to the real-world. This scaling limitation means that analogue models can only model large-scale structures. Alsop (1996) described several prominent faults within his analogue models that had a radial orientation around the diapir. In terms of the Cape Breton examples, these faults may be equivalent to the West Fault at St. Rose. These faults have an approximate throw of 12 m. Analogue models cannot re-create the small-scale fracturing observed within the Cape Breton drag zones. For this reason, the importance of faults orientated parallel to the diapir during diapir growth has not been previously described. Similarly, the lack of good drag zone exposures has prevented scientists from evaluating the roles of lithology and mechanical competency during the formation of drag zones. The Cape Breton drag zones are developed in a variety of lithologies and it is obvious that these lithological contrasts lead to the development of very different drag zones, both in terms of geometry and internal deformation.

CHAPTER 5, UPPER CARBONIFEROUS STRATA IN WESTERN CAPE BRETON: CORRELATION, MECHANICAL PROPERTIES AND EVIDENCE FOR HALOKINETIC INFLUENCE DURING DEPOSITION

Aims. This chapter has two main aims. The first is to attempt to establish *if*, *how* and *when* halokinesis affected the sedimentology and sedimentary architecture of the Inverness Formation. The Inverness Formation is the best choice for this halokinetic/sedimentation analysis for a number of reasons. Firstly, the Inverness Formation has good, though disjunct, exposure within western Cape Breton, thereby providing a large sedimentological database. Secondly, shale units within the Inverness Formation allow palynological age dating so that, when combined with seismic and well data, a good correlation of the outcrops can be obtained. Thirdly, the Inverness Formation contains thick sandstone bodies which contain abundant cross-strata. Large numbers of paleocurrent orientations can therefore be collected and used to analyse the sediment transport direction during diapir growth. Lastly, the Inverness Formation is well represented on available seismic data, which allows the sedimentology and paleocurrent data to be correlated with seismic facies interpreted from the 1978 Mabou seismic survey. Although the available seismic data suggest that the underlying Port Hood Formation was also deposited while halokinesis was in progress, the formation is not imaged well on the seismic data and was not penetrated by the Mabou 1 and Mabou 2a drill holes. In addition to the analysis of the Inverness Formation, several Westphalian conglomeratic units are described and are used to constrain both fault movements and halokinesis.

A second aim of this chapter is to establish the gross sedimentary architecture of the Inverness Formation so that its mechanical properties with regards to structural deformation can be established. It is important to do this in order to understand how the Inverness Formation can be expected to deform when it becomes involved in a drag zone.

This chapter also describes several conglomeratic units that are not part of the Inverness Formation. These conglomerates are described because they shed light on the timing of diapir growth and basin forming fault movements.

Approach

- Sedimentological facies analysis was used in order to define the sedimentology and sedimentary architecture of the Inverness Formation.

- Paleocurrent directions for individual sandstone units from each of the Inverness Formation exposures within western Cape Breton were recorded to detect paleocurrent variations through time.

- Seismic data were combined with limited well data and palynological age dating to correlate the Inverness Formation exposures and to define the internal stratigraphy of the Inverness Formation.

- The sedimentary architecture, paleocurrent data and stratigraphic correlation were then integrated with seismic facies analysis of the Inverness Formation. This extensive sedimentological database was then compared to the known movement history of the diapiric structures within the study area (see above, Chapter 2) in order to examine what effect halokinesis had upon synhalokinetic sedimentation of the Inverness Formation.

5.1, ONSHORE EXPOSURES OF THE INVERNESS FORMATION

Carboniferous rocks are well exposed in the Port Hood to Inverness area along the coast of western Cape Breton Island (Figures 5.1.1, 5.1.2, 5.1.3, and 5.1.4). The Inverness

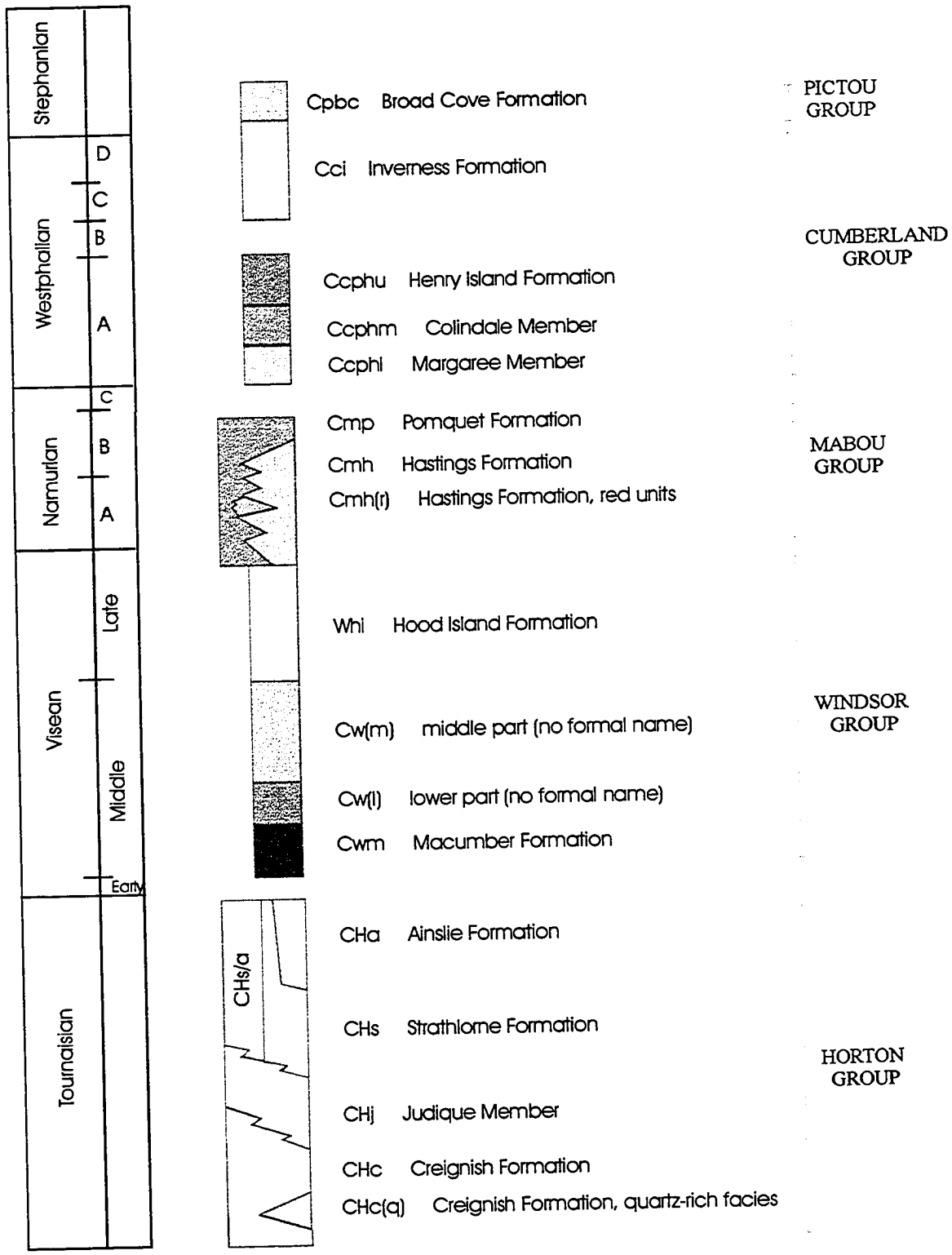

Figure 5.1.1. Carboniferous Stratigraphy, western Cape Breton, Nova Scotia. From Giles et al., 1997a and b.

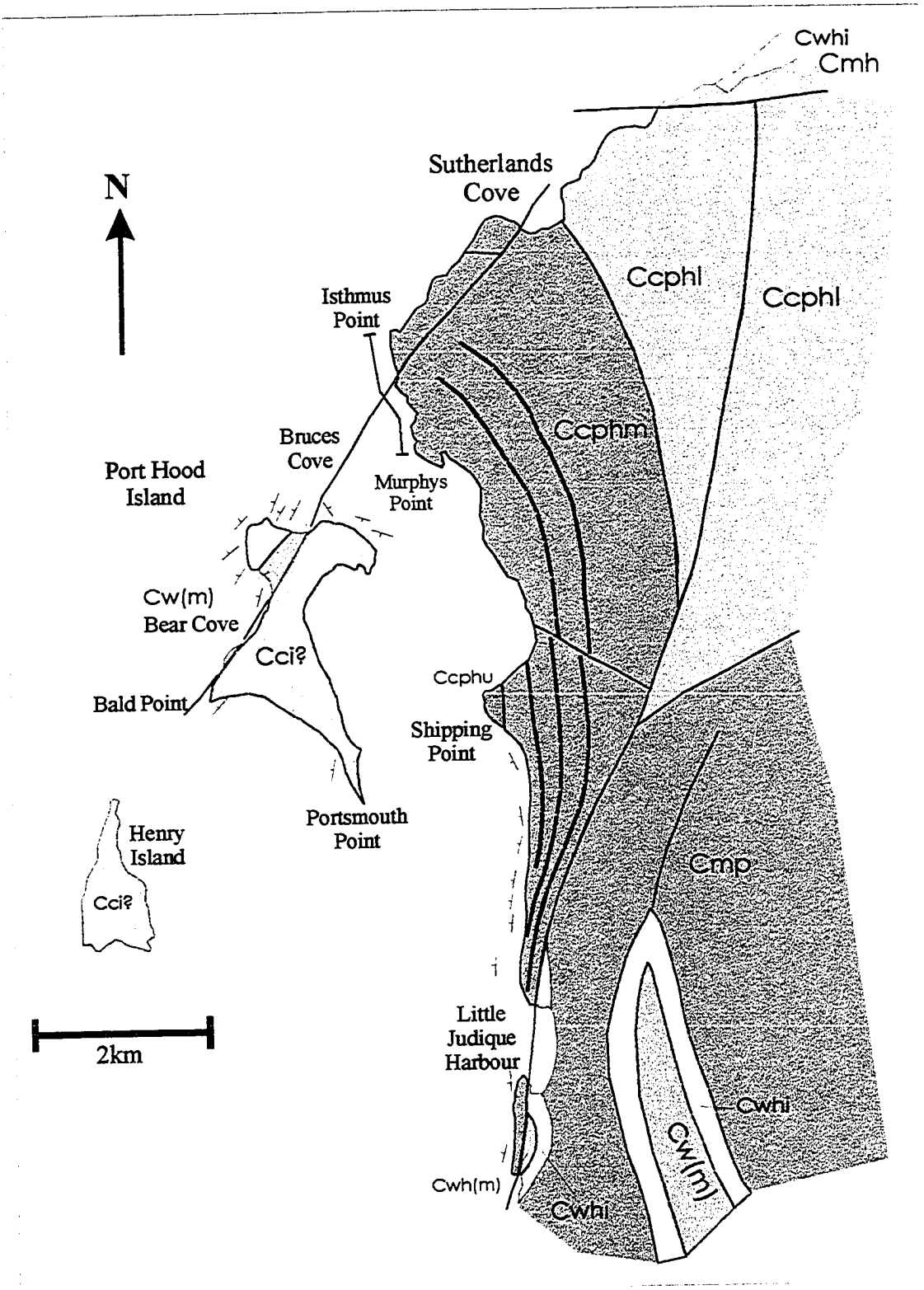

Figure 5.1.2. Geological map of the Port Hood area, western Cape Breton. See Figure 5.1.1 for stratigraphy. Modified from Giles et al. (1997b).

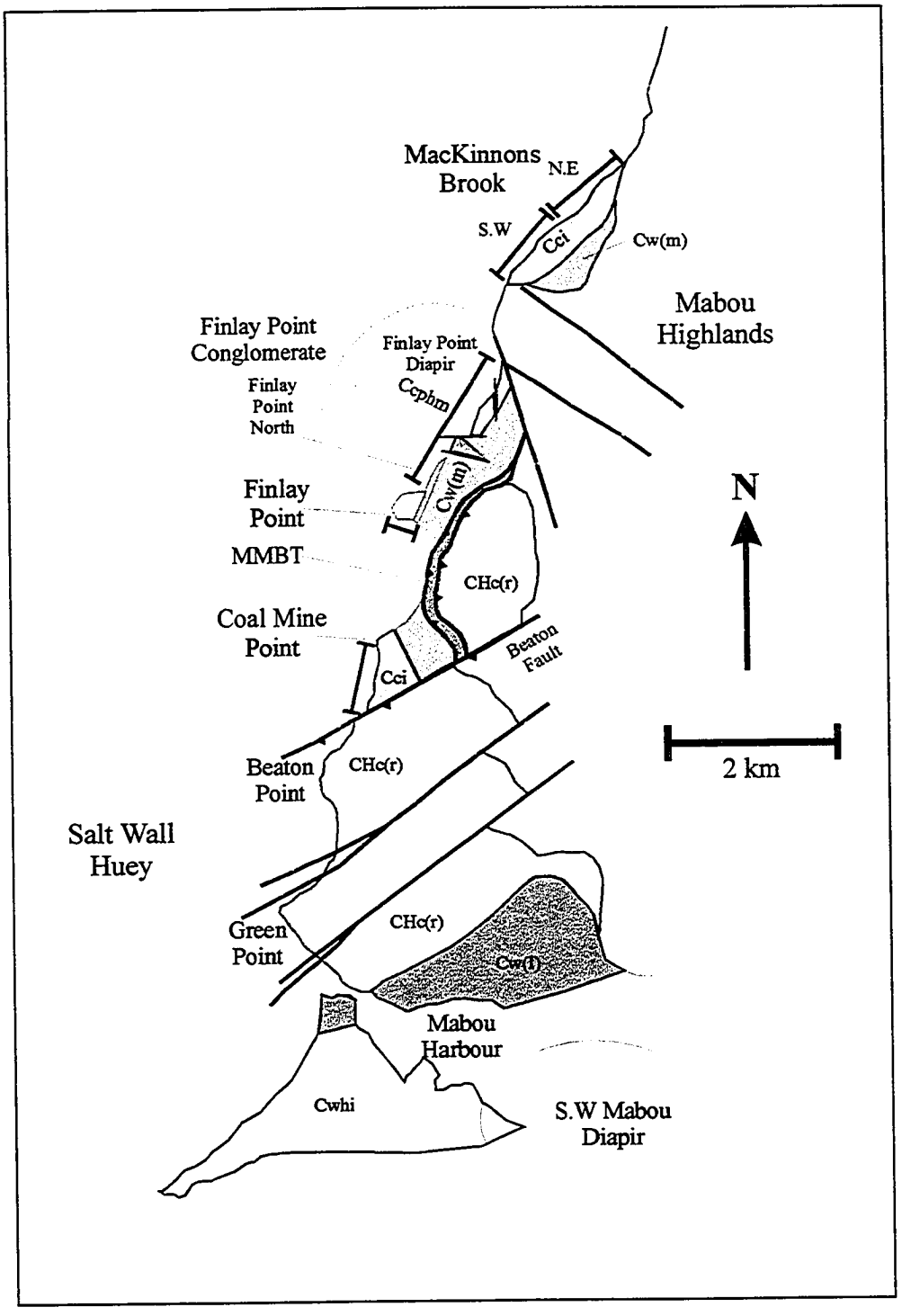

Figure 5.1.3. Geological map of the Mabou Mines area. Also shown are the outlines of the Finlay Point Diapir, the Salt Wall Huey and the Southwest Mabou Diapir. Modified from Giles et al. (1997b).

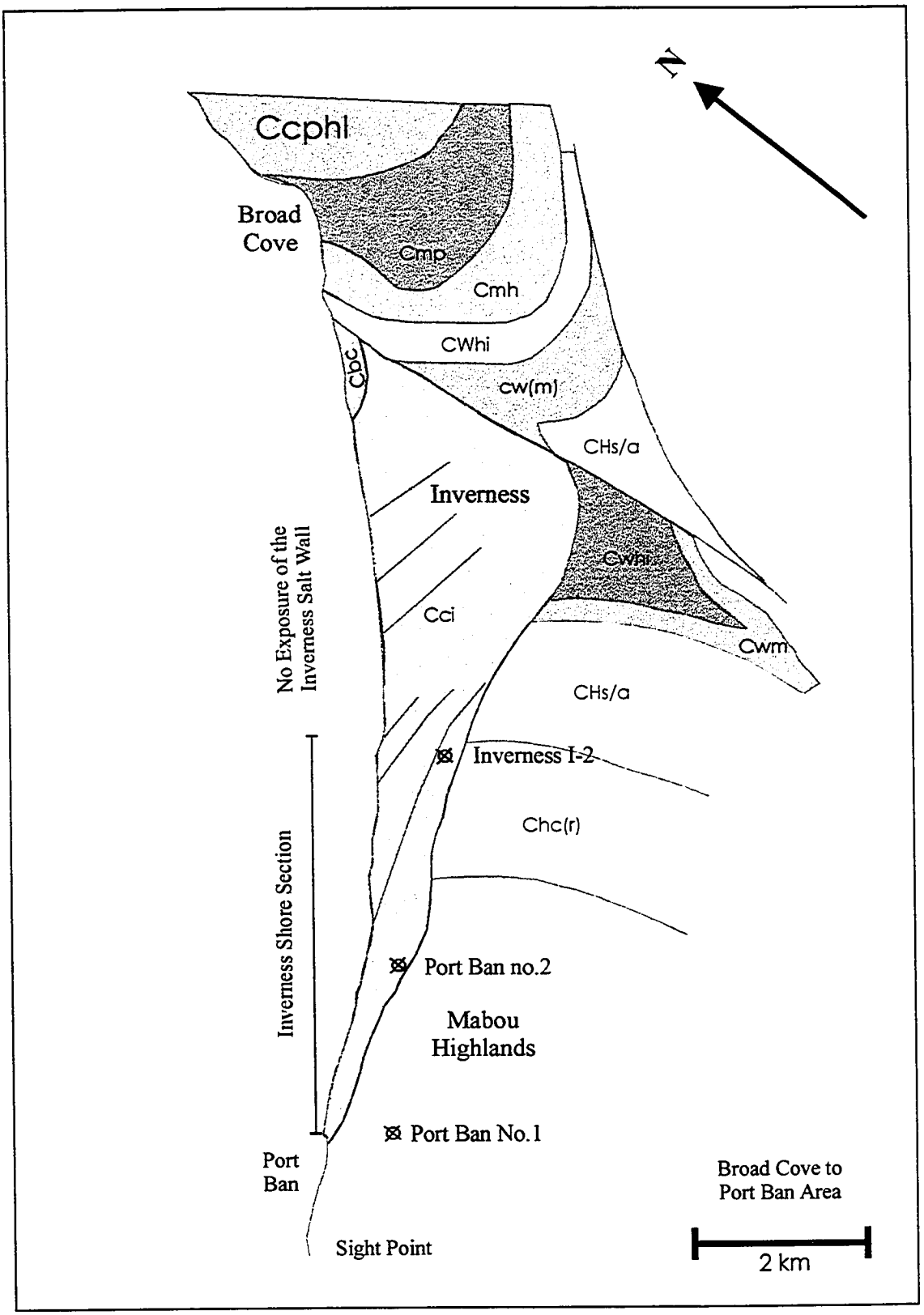

Figure 5.1.4. Geological Map of the Broad Cove and Inverness Area.
(Modified from Giles et al. (1997a and b)

Formation is a Westphalian C to Stephanian rock unit (see palynological dating, below) that is exposed in a series of disjunct and locally strongly deformed coastal sections at Coal Mine Point, Finlay Point, MacKinnon's Brook and Inverness. Detailed location information for the coastal sections used as part of this thesis is given in Appendix 6. Previous stratigraphic studies include those of Norman (1935), Keating (1950), Haites (1952), Hacquebard (1962, 1980, 1986), Hacquebard et al. (1989) and Gibling and Kalkreuth (1991). The surface distribution of the Inverness Formation is shown on Figures 5.1.1, 5.1.2, 5.1.3, and 5.1.4, which are modified from a recent map produced under a Mineral Development Agreement (Giles et al., 1997a and b). Strata of equivalent age cover an extensive area of the adjacent Gulf of St. Lawrence (Hacquebard et al., 1989; Grant and Moir, 1992; Grant, 1994; Rehill et al., 1995), where they form a considerable resource of coal, coal-bed methane and possibly of hydrocarbons. The Inverness Formation overlies the Port Hood Formation, although the contact is not exposed in the study area, and locally (as at Port Ban) rests unconformably on pre-Carboniferous rocks. The Broad Cove Formation overlies the Inverness Formation north of Inverness with apparent structural conformity but with a marked lithological change.

5.1.1, Stratigraphic Sections

Measured sections through the Inverness Formation are shown in Figures 5.1.5 to 5.1.13. No single section was encountered that gives a complete stratigraphic section through the Inverness Formation.

In the Mabou Mines area, the Coal Mine Point section is locally steeply dipping and deformed but a relatively complete section could be measured (Figure 5.1.7). The basal strata are exposed close to the Beaton Fault at the southern end of the outcrop belt; a stratigraphic basal contact was not observed. In addition, the true thickness of several mined coals could not be established with certainty and channel-sandstones are locally thickly bedded and highly fractured so that dip measurements were unreliable. The sedimentology and organic petrology of the section was discussed by Gibling et al.

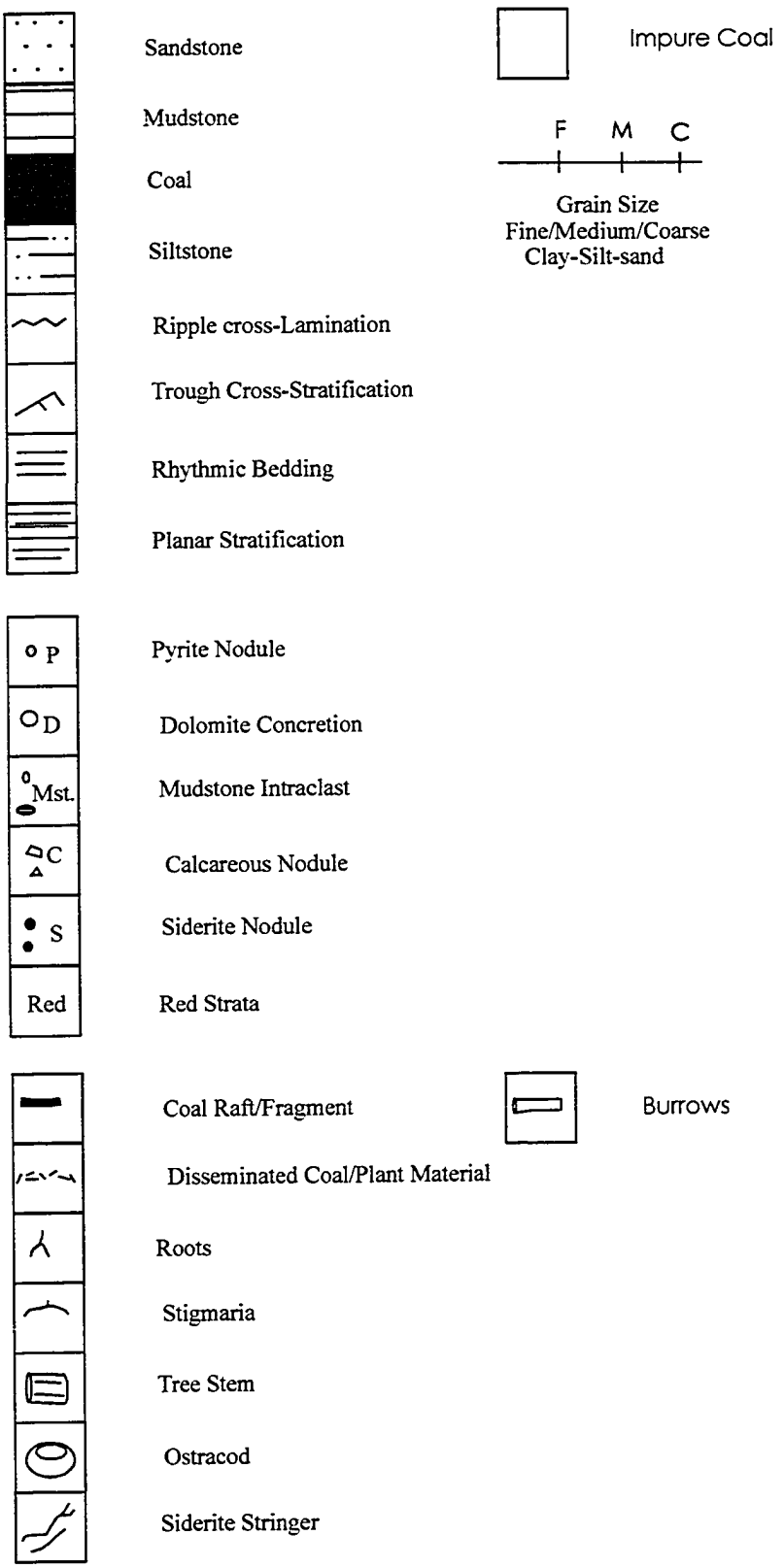

Figure 5.1.5. Sedimentological key for the stratigraphic logs.

Stratigraphic Logs

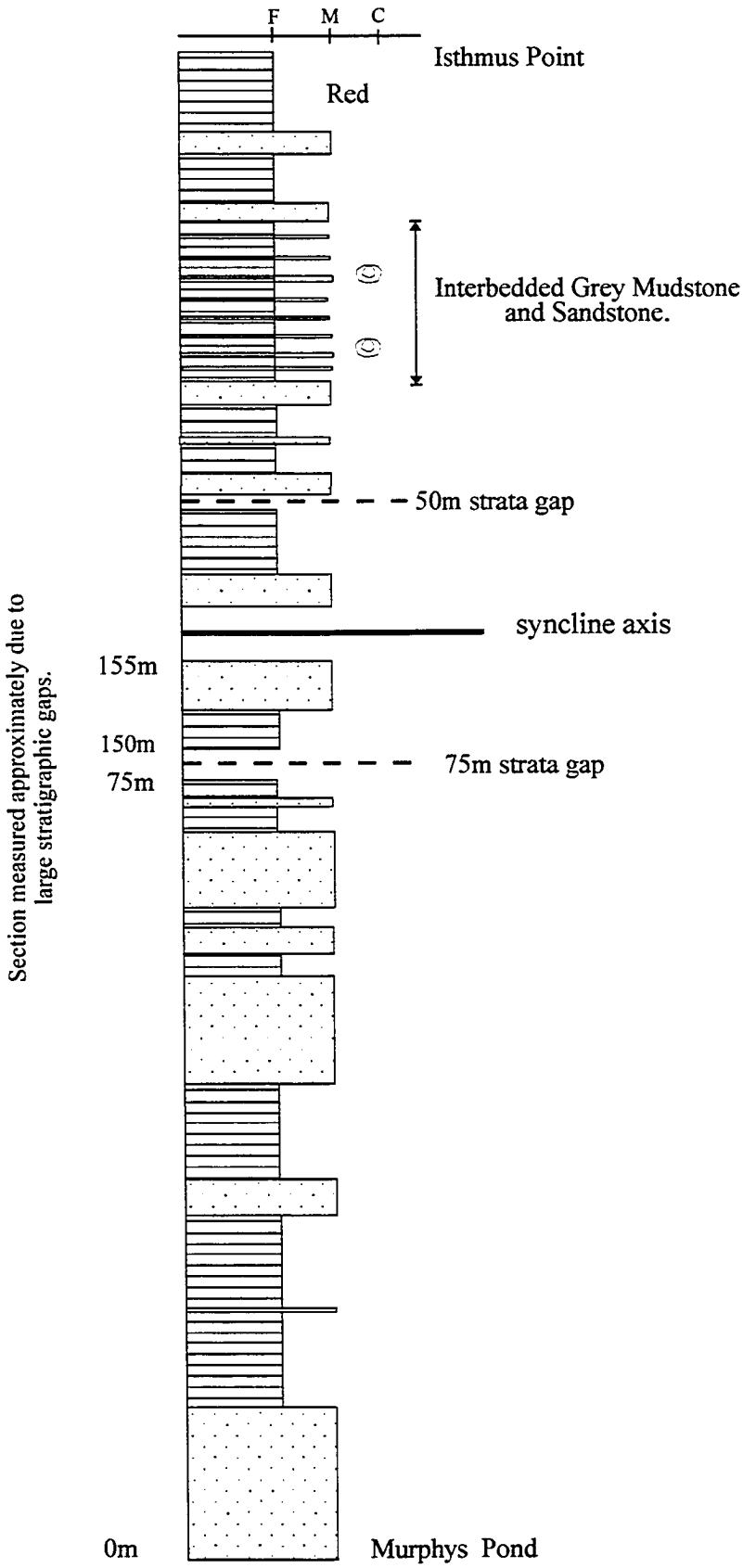

Figure 5.1.6. Strata Log 1, stratigraphic log of the Port Hood Section.

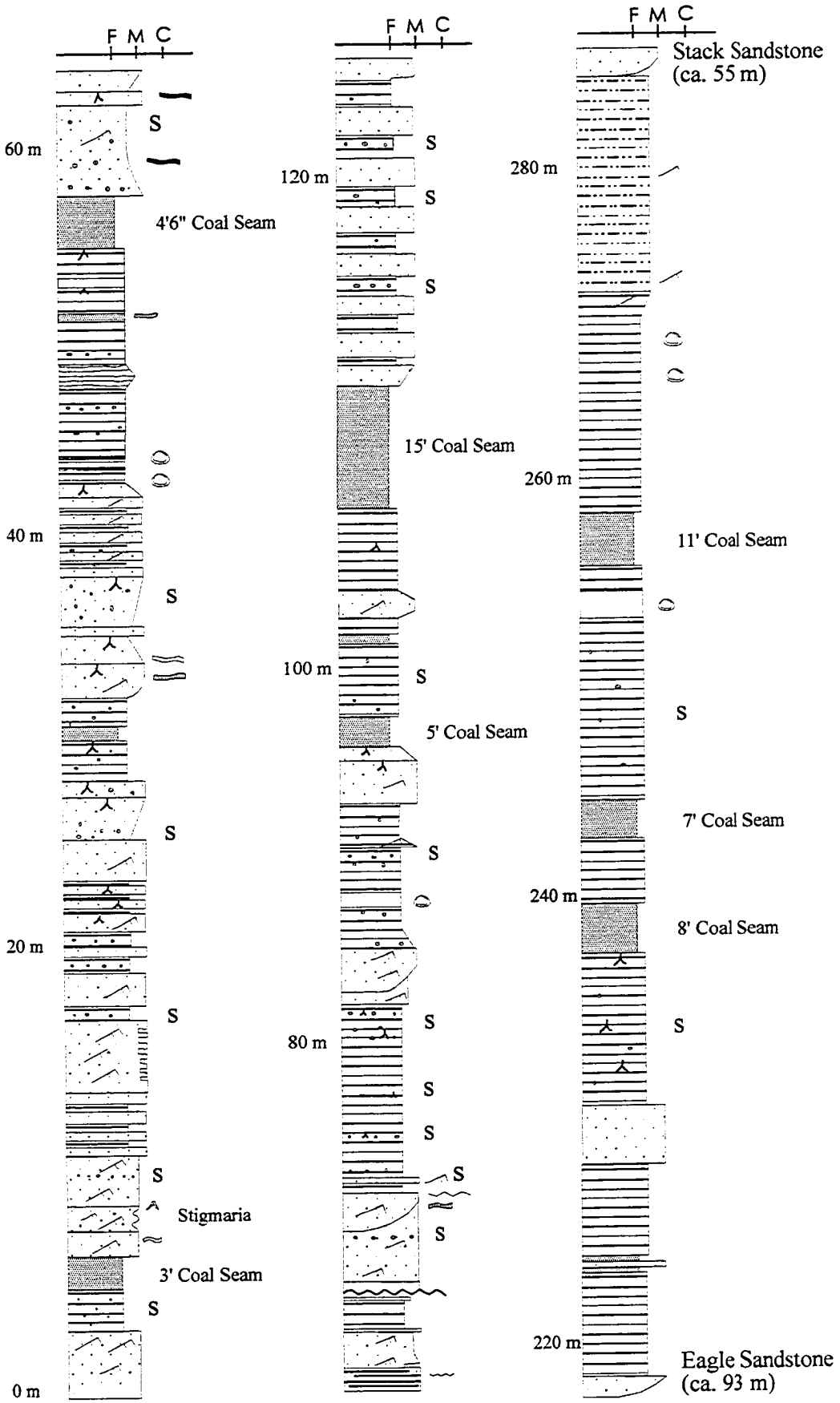

Figure 5.1.7. Strata log 2, Stratigraphic log for the Coal Mine Point section.

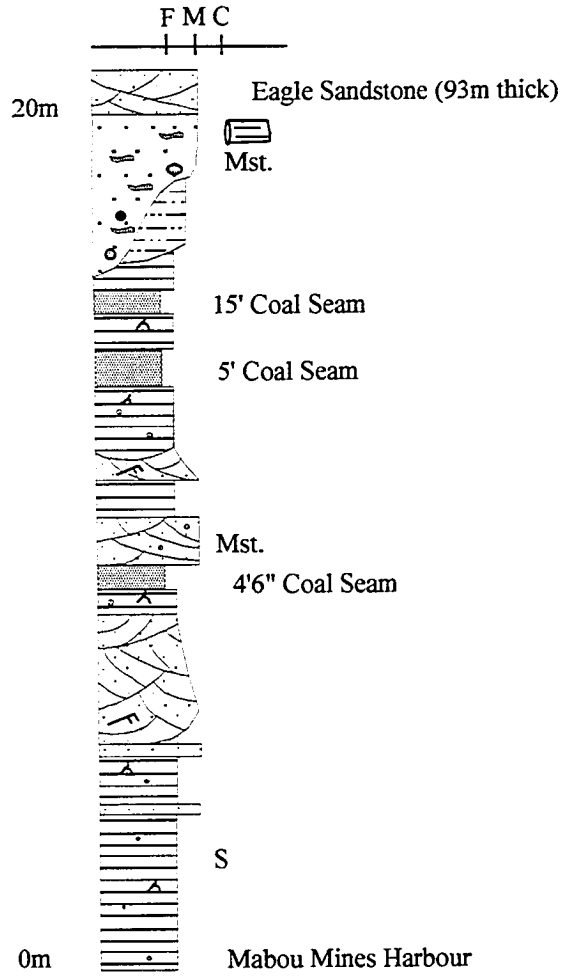

Figure 5.1.8. Strata Log 3, Stratigraphic log of the Finlay Point Section.

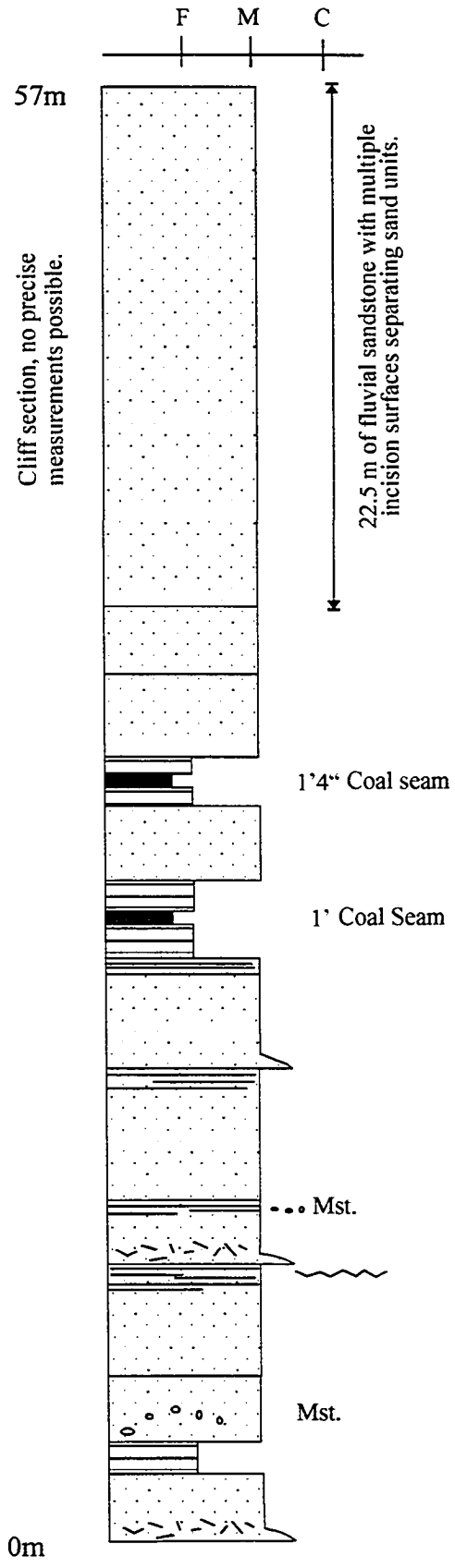

Figure 5.1.9. Strata Log 4,
stratigraphic log of the Northeast MacKinnons Brook section.

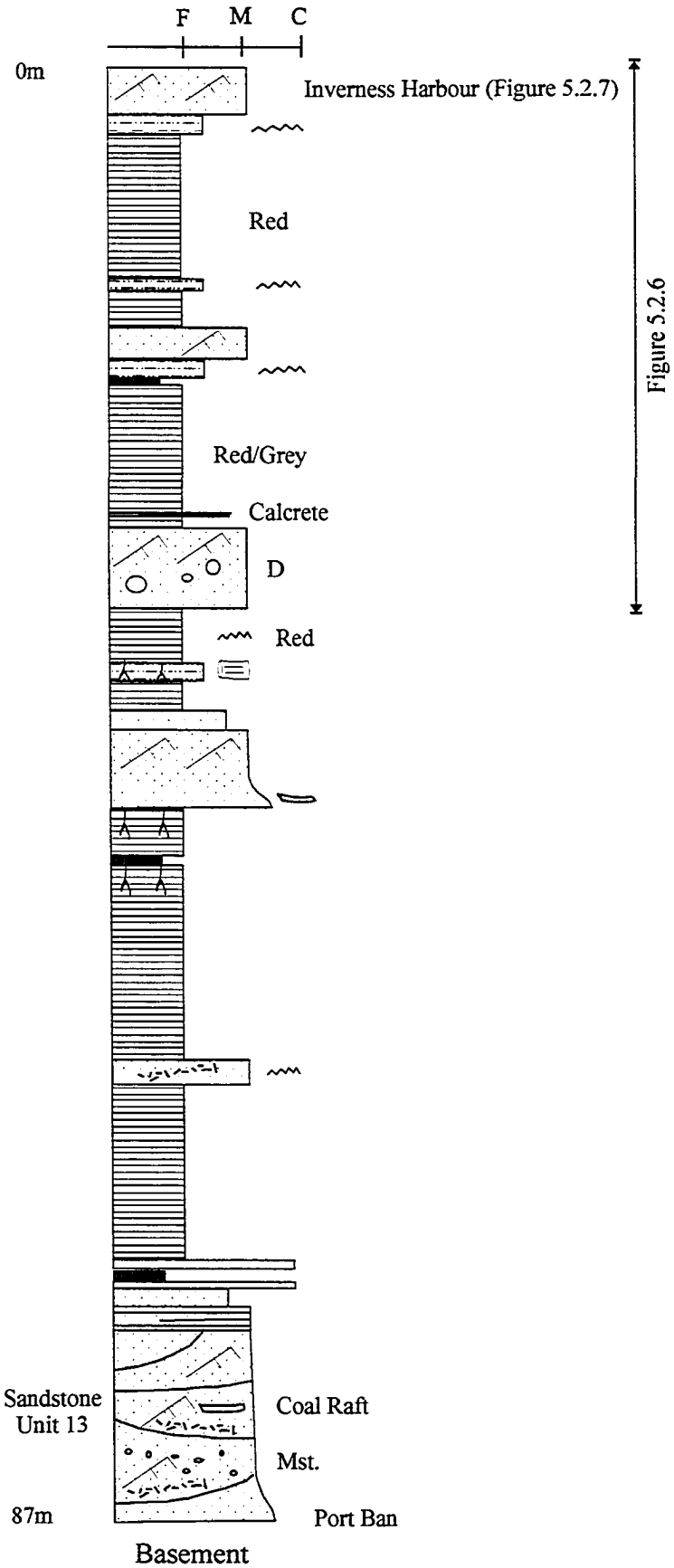

Figure 5.1.10. Strata Log 5, stratigraphic log of the Inverness Shore Section.

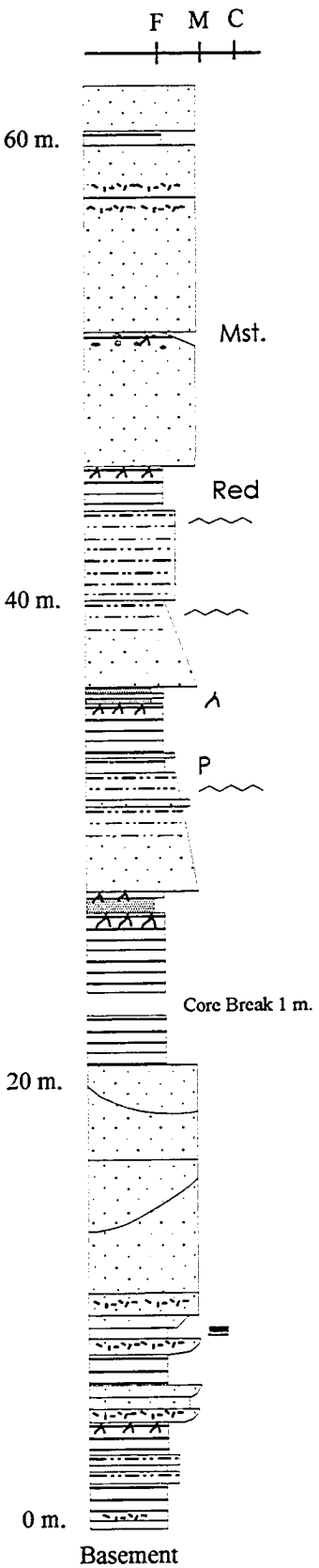

Figure 5.1.11. Strata Log 6, stratigraphic log of the Port Ban No.1 Core.

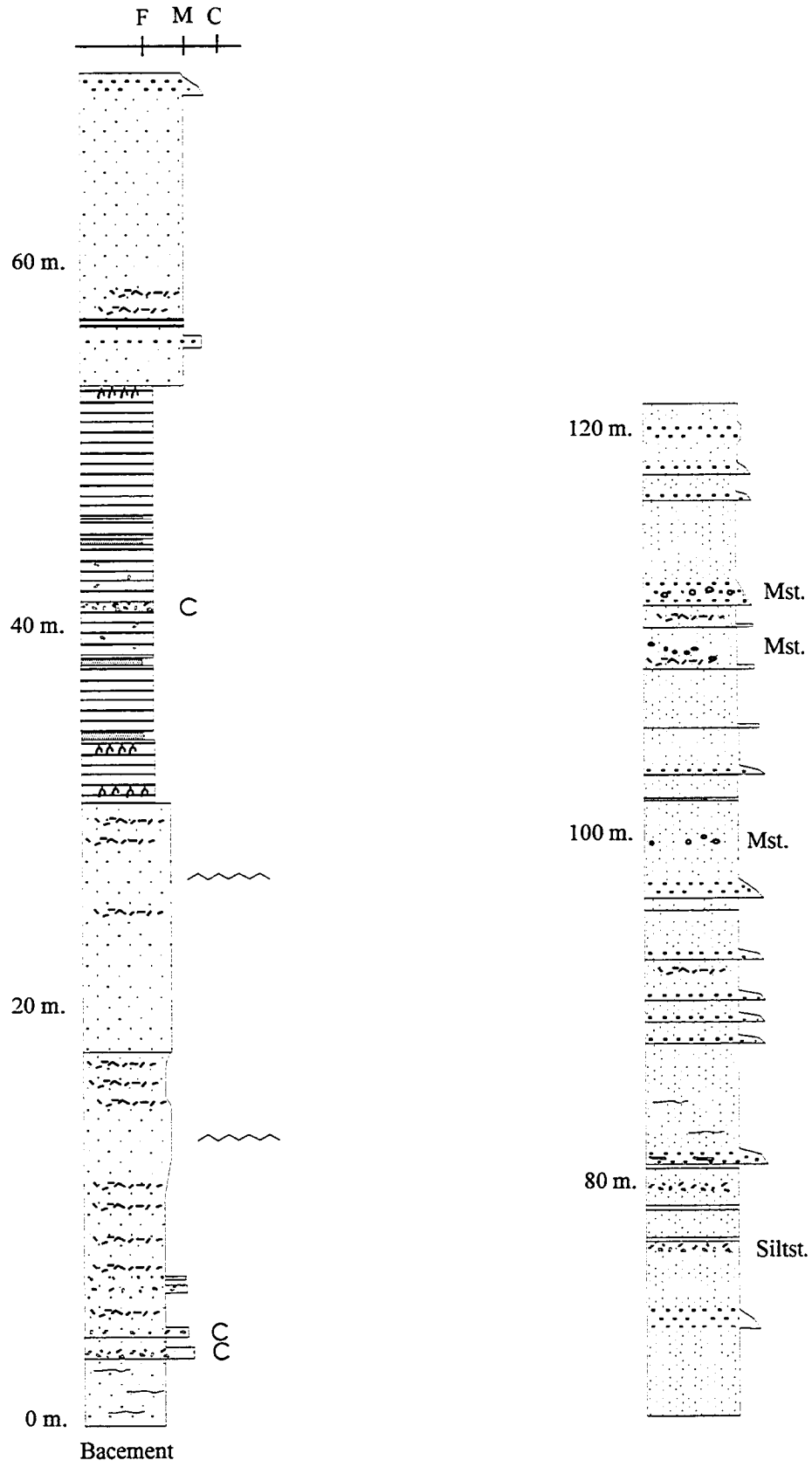

Figure 5.1.12. Strata Log 7. Stratigraphic log of the Port Ban No. 2 well.

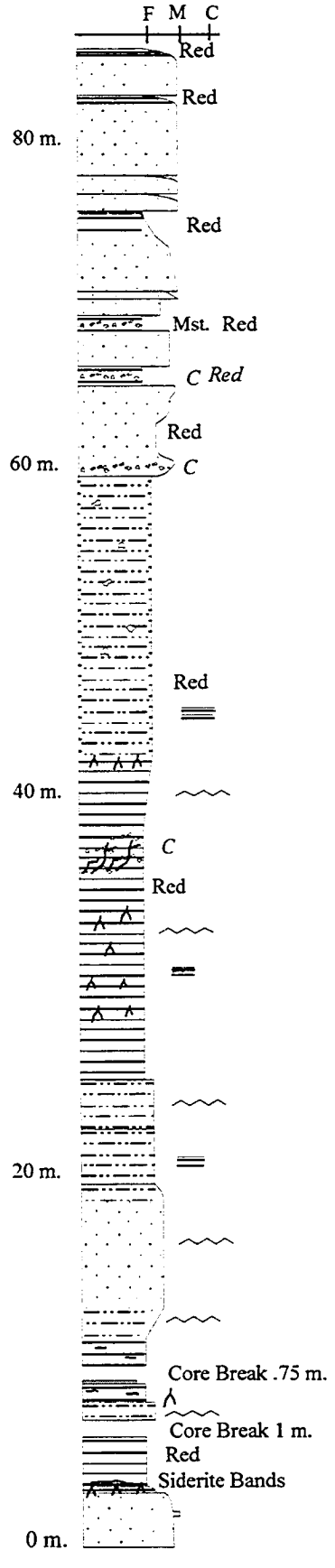

Figure 5.1.13. Strata Log 8, stratigraphic log of the Inverness I-2 well.

(1994), and a detailed account of the siliciclastic and organic facies was given in Dickie (1986), Gibling and Kalkreuth (1991) and Hacquebard (1993). A basal 125 m of strata comprises shales, coals and thin sandstone bodies, with workings visible on the 15-Foot Seam. These strata are overlain by a thickly bedded channel body, informally termed the Eagle Sandstone, that is estimated to be 93 m thick (125-218 m in the measured section). The channel body is predominantly medium-grained sandstone, with thin conglomeratic layers and one thin shale, and is multi-storeyed with numerous erosional surfaces. Sedimentary structures are mainly trough cross-stratification, ripple cross-lamination and planar stratification. Above, an additional 68 m of shale, coal and sandstone is present (218-286 m in the measured section), with workings visible on the 8-Foot and 7-Foot Seams. The section is capped by approximately 55 m of channel sandstone, informally termed the Stack Sandstone, composed of trough cross-bedded, medium-grained sandstone. The total thickness of the section is 341 m.

At Finlay Point, the Inverness Formation strata dip gently seaward, generating a section approximately 113 m thick (Figure 5.1.8). Siliciclastic and organic facies were discussed by Deal (1986) and Hacquebard (1993). The basal strata are in fault contact with the purple Finlay Point conglomerate (informal name) of uncertain affinity close to the wharf. Approximately 19 m of shale, coal and sandstone are present along the south side of Finlay Point. These strata are overlain by a thick channel-sandstone body, probably equivalent to the Eagle Sandstone of the Coal Mine Point section, that is estimated to be 93 m thick (Keating, 1950). The basal surface of the channel body has several metres of relief and is deeply incised into the underlying strata; the lowermost channel fill includes a spectacular conglomerate composed mainly of coal clasts up to 1.5 m long, coalified plant debris and intrabasinal mudclasts. The sandstone body is multi-storeyed, composed of at least ten erosionally-based storeys of medium- to very coarse-grained sandstone that typically fine upward slightly from a basal gravel lag. Conglomeratic layers up to 1 m thick are present locally. The sandstones are predominantly massive (apparently devoid of sedimentary structures) but some strata contain trough and planar cross-stratification,

ripple cross-lamination and planar stratification. The sandstone body also contains two thin, fine-grained intervals: 3 m of grey shale capped by 0.5 m of coal (52-55.5 m above section base) and 1.5 m of shale (103-104.5 m above section base).

At MacKinnon's Brook, a north-east and south-west section are delineated on either side of the brook, which drains into the Gulf of St. Lawrence and approximately follows the axis of a shallow syncline. The Inverness Formation strata rest unconformably on older pre-Carboniferous rocks to the south-west and are in fault contact with pre-Carboniferous rocks to the north-east. The north-east section (Figure 5.1.9) comprises 57 m of strata, principally medium-grained sandstone in the form of multi-storeyed channel bodies with lagged erosional surfaces and some planar stratification. Thin, finer-grained units including two thin coals, siltstones and grey shales are present. The south-western section appears to be equivalent to the north-east section to the south of the synclinal axis.

Between Port Ban and Inverness, 87 m of strata were measured (Figure 5.1.10). The basal strata at Port Ban rest unconformably on pre-Carboniferous rocks. A basal channel-sandstone body about 30 m thick forms a strike section that extends for about 3 km along the coast. The channel body is multi-storeyed with trough cross-bedding and abundant mudstone intraclasts, plant material and coal fragments. The overlying 100 m of strata are much finer grained in aggregate and comprise grey and red mudstone, thinner channel bodies, thin floodplain sandstones, thin coal seams and a calcrete. Red shales are increasingly prominent at higher levels. The section terminates with an 8-10 m thick channel-sandstone body at Inverness Harbour. A considerable interval (about 3 km) with virtually no exposure is present northwards along Inverness beach; mine dumps behind the beach indicate the presence of the workable Inverness coals in this part of the section. Strata of the Broad Cove Formation appear at the northern end of Inverness beach.

Logs for the three wells are shown in Figures 5.1.11, 5.1.12 and 5.1.13. The Port Ban No. 1 and No. 2 wells penetrated 62 m and 122 m of strata, respectively, to terminate in pre-

Carboniferous rocks. The strata include thick, multi-storeyed channel bodies, grey shales, one thin, red shale (No. 1 well), and thin coals. The Inverness I-2 well penetrated 88 m of strata but did not reach "basement"; red shales form a significant part of the section.

The section near Port Hood is shown in simplified version in Figure 5.1.13 and has been described in detail by D. Keighley (Ph.D. thesis, 1996) and Gersib and McCabe (1981).

5.2, SEDIMENTOLOGY OF THE INVERNESS FORMATION

The sedimentology of the Inverness Formation can be divided into three broad facies: the channel sandstone facies, the coal-bearing facies and the red mudstone and calcrete facies. Each of these facies is described separately below.

5.2.1, Inverness Formation - Channel Sandstone Facies

Sandstone bodies makes up approximately 50-70% of the Inverness Formation. The resistant nature of the sandstone means that the sandstone bodies are preferentially preserved and exposed relative to the weak, easily eroded coal-bearing facies. The actual outcrop of the Inverness Formation is therefore dominated by the channel sandstone facies.

The sandstones are mainly medium-to-coarse grained with subordinate units of pebble conglomerate, siltstone and grey shale. Individual sandstone units are either trough cross-stratified (troughs sets typically 0.5 - 2.0 m thick) or apparently structureless, though rare planar trough cross-stratified units were recorded. Sandstone units are laterally discontinuous and typically have a concave upwards (incisional) basal surface and a planar upper surface (where not removed by incision). They form lensoid sandstone bodies up to 3 m thick and 100 m in length. Ripple laminated sandstones are rare within the exposed sections and typically form thin (<0.5 m thick) planar sandstone or siltstone units.

Major erosional surfaces are defined by extremely coarse channel lags (Figure 5.2.1a and b) that contain coal fragments, mudstone intraclasts up to 15 cm in diameter, extrabasinal pebbles up to 3 cm in diameter, fragmented plant debris (Figure 5.2.2) and larger tree stems and branches up to 5 m in length (Figure 5.2.2). The coal fragments range in size from disseminated coal 'flecks' up to rafts 10 m long by 1 m thick. The margins of the coal rafts have commonly been extruded into the surrounding sediments and resemble coal 'veins'. The major erosional surfaces define the base of channelised sandstone units that eroded into the underlying strata. These surfaces are present throughout the sandstone bodies such that a major erosional surface can usually be defined every 10-15 m (stratigraphic thickness).

Minor siltstone units within the channel sandstone bodies are typically thin (<1m) units that are planar and laterally continuous until they are truncated by incision below a sandstone unit. Internally, the siltstones may be massive, planar cross-stratified or ripple cross-laminated. Within the ripple cross-laminated units, climbing ripples are common. Some of the siltstones contain vertical burrows.

Grey shales are rare and tend to form thin, isolated interstitial units between thick sandstone units. The upper surfaces of the shales are commonly eroded below the overlying sandstone, which suggests that the shales are an erosional remnant of formerly more extensive fine-grained units.

Vertical Sequences

Several individual lensoid sandstone units combine to produce sandstone storeys up to 10-15 m thick bounded above and below by major erosional surfaces (Figure 5.2.3). The top strata of a sandstone storey may fine upwards into siltstone and/or shale; however, the majority of the sandstone storeys consist uniformly of trough cross-stratified sandstone. The thickness of the trough sets generally decreases towards the top of the sandstone storey.

Figure 5.2.1a. Major channel lag from the Finlay Point section. Note the elongate coal fragments which probably represent reworked peat mats. The channel lag has eroded approximately 2.5 m of the underlying cross-stratified sandstone. The present dip of the channel lag is due to compaction associated with the organic material.

(Hammer 32cm long).

Figure 5.2.1b. A second major channel lag from the Finlay Point section. As well as the reworked peat fragments, intrabasinal siderite nodules and mudclasts are also included within the channel lag.

(Hammer 32cm long).

Figure 5.2.1a

Figure 5.2.1b

Figure 5.2.2a. Calcified Lycopsid tree stem exposed in sandstone unit 13 of the Inverness shore section (see Figure 5.1.10). Note that the internal ring structure has been well preserved indicating early calcite cementation.

(Lens cap 5.2cm diameter)

Figure 5.2.2b. Well-preserved Calamites plant debris exposed on a bedding plane within the Eagle Sandstone at Finlay Point (see Figure 5.1.8). Plant material has been replaced by siderite.

(Lens cap 5.2cm diameter)

Figure 5.2.2a

Figure 5.2.2b

Figure 5.2.3. Channel Sandstone Body at Port Ban. Two major erosional surfaces (i and ii) separate three sandstone storeys. The three storeys are part of sandbody 13 of the Inverness-Port Ban section (see Strata Log 4, Figure 5.1.10). Relief on erosional surface (ii) is approximately 6m. Individual sandstone units can be clearly seen within each sandstone storey.

(Dr. M.R. Gibling 1.80m tall).

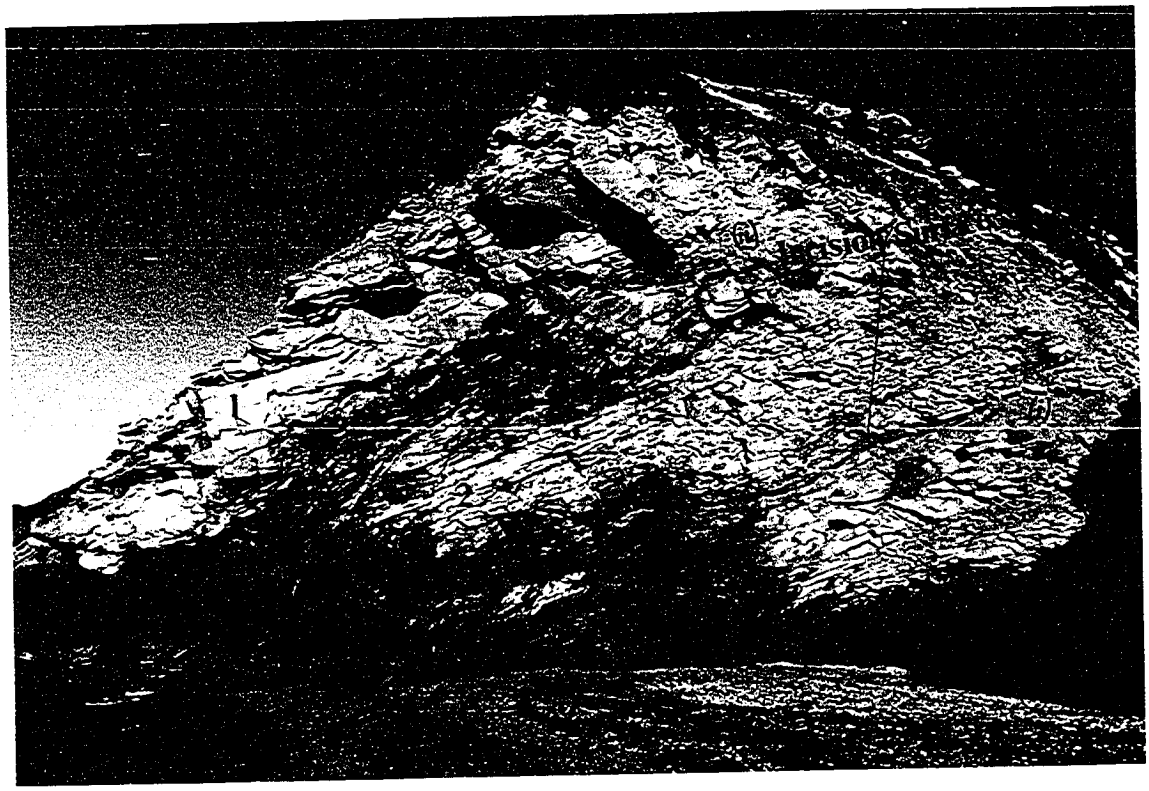

15m

Figure 5.2.3

Sandstone storeys are stacked vertically to produce sandstone bodies up to 200 m thick, e.g. the Gant Sandstone (200 m thick), the Eagle Sandstone (93 m thick) and the Stack Sandstone (63 m thick) (Keating, 1950). Shale within a sandstone body is concentrated within the lower portion of the sandstone body as discontinuous horizons between individual sandstone units. Within the upper two-thirds of the Gant Sandstone, shale is restricted to partings less than 20 cm thick and a few metres wide.

Interpretation. The repeated incision within the sandstone bodies and the lack of well established (or preserved) overbank facies indicate a high-energy environment with a high temporal discharge variability. This interpretation is supported by the absence of trace fossil assemblages within the sandstone units, which may indicate that the depositional environment was too dynamic to establish and/or preserve faunal assemblages (G. Pemberton, pers. comm. 1995).

No lateral accretion surfaces indicative of point bar formation were recorded. This apparent absence, combined with the lack of significant overbank facies and fining upwards sequences within storeys and the high-energy depositional environment, suggests that the fluvial system was a low-sinuosity (braided) as opposed to a high-sinuosity (meandering) fluvial system.

The channels probably filled rapidly by vertical aggradation that contributed to avulsion of the fluvial system and channel abandonment. Subsequent avulsion resulted in re-occupation of the channel, incision and removal of any fine-grained overbank facies. The floor of the channel was probably covered by sinuous-crested dunes, now preserved as trough cross-strata, while emergent bars and overbank areas may have been covered by ripples formed as waning flow bedforms (Figure 5.2.4).

The vertical stacking of trough sets within cross-stratified sandstones and the decrease in trough set thickness towards the top of a sandstone storey or channel sandstone body

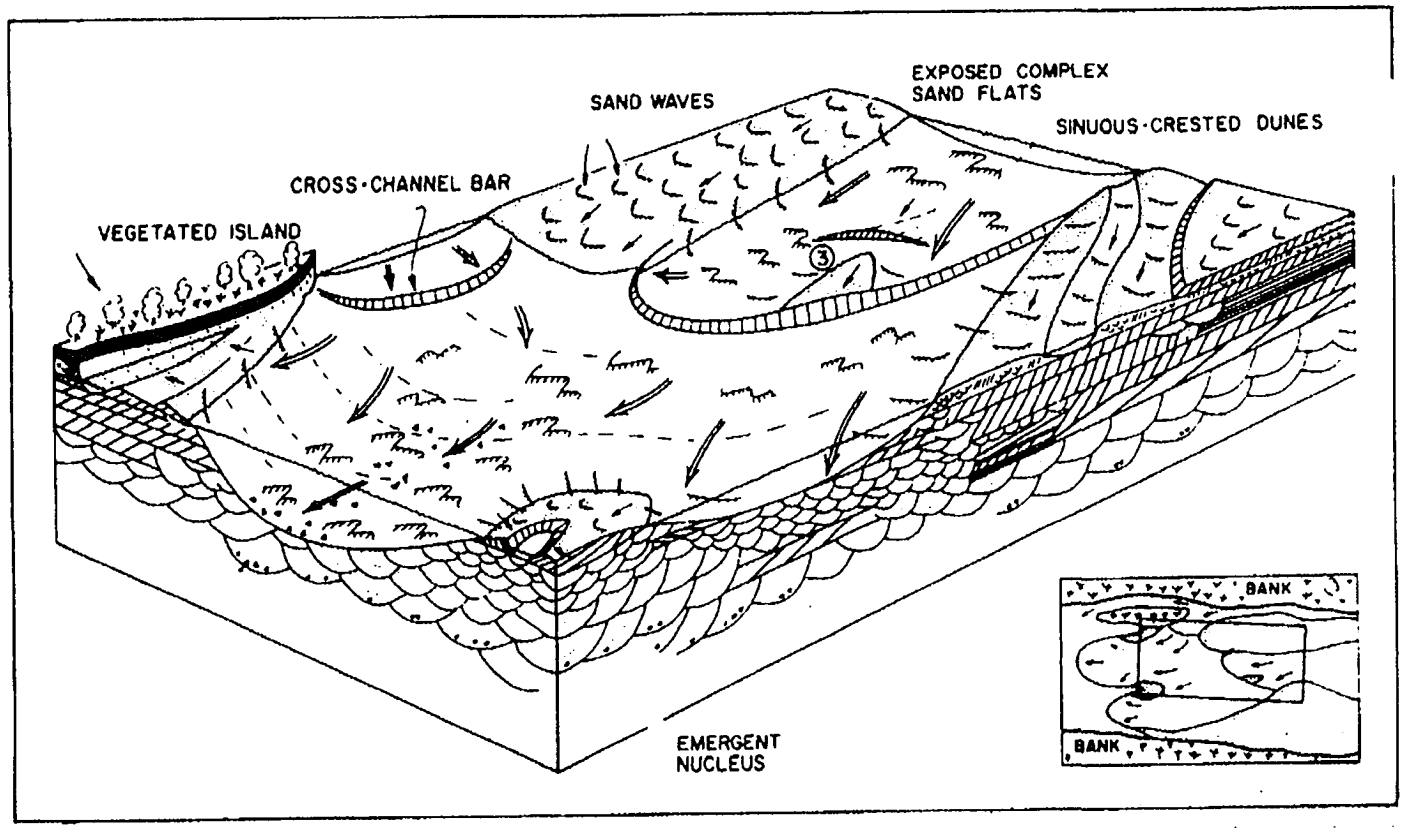

Figure 5.2.4. A model for braided fluvial channels (based on the South Saskatchewan River) applicable to the Inverness Formation, Channel Sandstone Facies. Note the aggredation of trough cross-stratified sandstone units due to the migration of sinuous crested dunes. Also the formation of mid-channel and bank-attached bars which may coalesce to produce aerially extensive sandflats. Sandflats may become vegetated and accumulate peat. Note, however, that the planar cross-strata shown as part of the sandflats in the South Saskatchewan River were not observed in the Inverness Formation. Modified from Cant and Walker (1976).

compare well with examples of braided fluvial systems described by Cant and Walker (1975) for the Battery Point Sandstone of Gaspé, Quebec. The major difference between the Inverness Formation and the Battery Point Sandstone is the paucity of planar trough cross-stratified sandstones within the Inverness Formation. Planar cross-stratified strata were inferred by Cant and Walker (1978) to represent cross-channel migration of foreset bars.

The preservation of coal fragments and 'rafts' within coarse channel lags suggests that vegetated bar tops may have formed within the channel belt, but that channel avulsion resulted in cannibalisation of the bar tops. The vegetated bar tops were reworked and the peat fragments were deposited in the channel lags. Similar modern examples of vegetated bar tops that have accumulated 1-4 m of peat are found within the Brahmaputra river system (Coleman, 1969). Modern vegetated bar tops probably grow from a coalescence of bar forms around a nucleus sand bar to produce a bar complex or sandflat. The sandflats have a relatively high topography which is emergent at anything but flood stage and is able to accumulate peat locally (Figure 5.2.4). Sandflats reported from modern braided rivers vary in size from 1-2 km across, e.g. the South Saskatchewan River (Cant and Walker, 1978), to 10 km or more (the Brahmaputra River, Coleman, 1969). Another possible source for the peat is from underlying coal seams (previously peat bogs) of the coal-bearing facies (see below). However, seismic stratigraphy indicates that the coal-bearing facies occupy regional stratigraphic levels and are not, for the most part, laterally equivalent to the channel sandstone bodies (see above, Chapter 2). From the seismic data, it appears that the channel sandstone bodies incised into the coal facies only locally. However, the vertical resolution of the seismic data is in the order of 10-20 m and so it is possible that minor incision into the coal-bearing facies could be the source of the reworked peat, especially for accumulations at the base of channel bodies.

The physical characteristics of the Inverness Formation sandstones have several similarities to the modern Brahamputra River of Bangladesh described by Coleman

(1969). The braided channel system of the Brahamputra varies in width from 1-10 km and the actual channel belt is highly unstable with annual lateral migration rates of up to 2600 ft/yr. In-channel physiography is dominated by mid-channel and bank-attached braid bars that rapidly aggrade during falling stage flow when the sediment load is greater than the transport capacity of the channel. Rapid aggradation results in 'choking' of the channel with barforms and promotes frequent avulsion of the channel. The modern Brahmaputra/Ganges/Meghna alluvial plain covers an area of approximately 23,000 square miles in Bangladesh. The Carboniferous Inverness Formation can be traced across the Gulf of St. Lawrence on seismic data, indicating a Carboniferous depositional surface area of at least 18,000 square miles (Hacquebard, 1986; Grant, 1994; Rehill, 1996). In terms of surface area, the Inverness Formation is comparable to the modern Brahmaputra system. A major difference is that the Inverness Formation was probably sourced from several areas, including the Appalachians to the west and the exposed Cape Breton basement massifs as well as uplifted basement units surrounding the Maritimes Basin. The Brahmaputra is entirely sourced from the modern Himalaya. While it is true that the individual channels and bedforms of the Inverness Formation are not as large as those found in the Brahmaputra, the overall sedimentary characteristics and physiographic details show considerable similarity.

5.2.2, Coal-Bearing Facies

The coal-bearing facies make up approximately 30-50% of the Inverness Formation. The coal-bearing facies are important economically both for potential coal production and for potential coal-bed methane sources. The coal-bearing facies are significant to this project because the coal seams are excellent seismic reflectors that can be used to tie on-shore outcrops to seismic sections (see below). Detailed work on the coal composition, facies relationships and depositional environments of the western Cape Breton coal seams and related sediments has been carried out over the past 50 years (Keating, 1950; Haites, 1952; Hacquebard, 1951, 1972, 1980, 1986, 1989; Hacquebard et al., 1978; Gibling et al., 1994). Only a brief review of the coal-bearing facies is presented in this thesis.

(i) Detrital Sediments

Grey shale and siltstone form the bulk of the coal-bearing intervals. The fine-grained strata tend to be massive but locally laminated. Roots including *Stigmaria* and plant fragments are present throughout the coal-bearing intervals. Bivalves are common and *Anthracomya* was identified by Keating (1950). Siderite nodules are present at many levels both as nodule-rich layers and siderite bands up to 5 cm thick.

Dark shale units up to 1 m thick are interbedded with the grey shales and coals (Figure 5.2.5). Most of these units are rich in bivalves and ostracods, the flattened tests of which impart a stratification to the rocks. Three dark shale samples from Coal Mine Point were analysed by Gibling and Kalkreuth (1991) and are composed of illite, kaolinite and chlorite, with quartz silt and variable amounts of pyrite, siderite, and fine-grained calcite as well as fish fragments and shells. Total organic carbon content ranges from 2.3 to 13.2%. Vitrinite predominates in two of the samples and sporinite in the third. The organic matter is characterised as Type III kerogen consistent with a terrestrial plant source. The samples show a modest oil and gas potential of 2.7 to 42.6 kg/tonne and vitrinite reflectance of one sample was 0.62% Ro. Four shales analysed by Smith and Naylor (1990) yielded similar results.

(ii) Coals

Eight major coal seams are present in the Coal Mine Point section and are named according to their approximate thicknesses. Maximum seam thickness is 3.9 m with six seams greater than 1.4 m.

The coals are highly volatile B/C coals with vitrinite reflectance levels of 0.6 to 0.7% Ro. Within the coal seams, predominantly bright coal alternates with coal that has a considerable dull coal component. Microlithotype analysis shows a predominance of the

Figure 5.2.5. Coal-Bearing Facies, Inverness Formation, Coal Mine Point.

1. Three, black, organic-rich shales separated by grey mudstones.

2. Minor sandstone units. The units are thin (<30 cm), planar and laterally continuous beds with rare ripple cross-lamination. The sandstone units probably represent deposition within an interchannel area.

3. A 5 cm thick coal seam which is underlain by a seat earth.

Stratigraphic top is to the left. The photograph corresponds to the 50-55m interval shown on Figure 5.1.7.

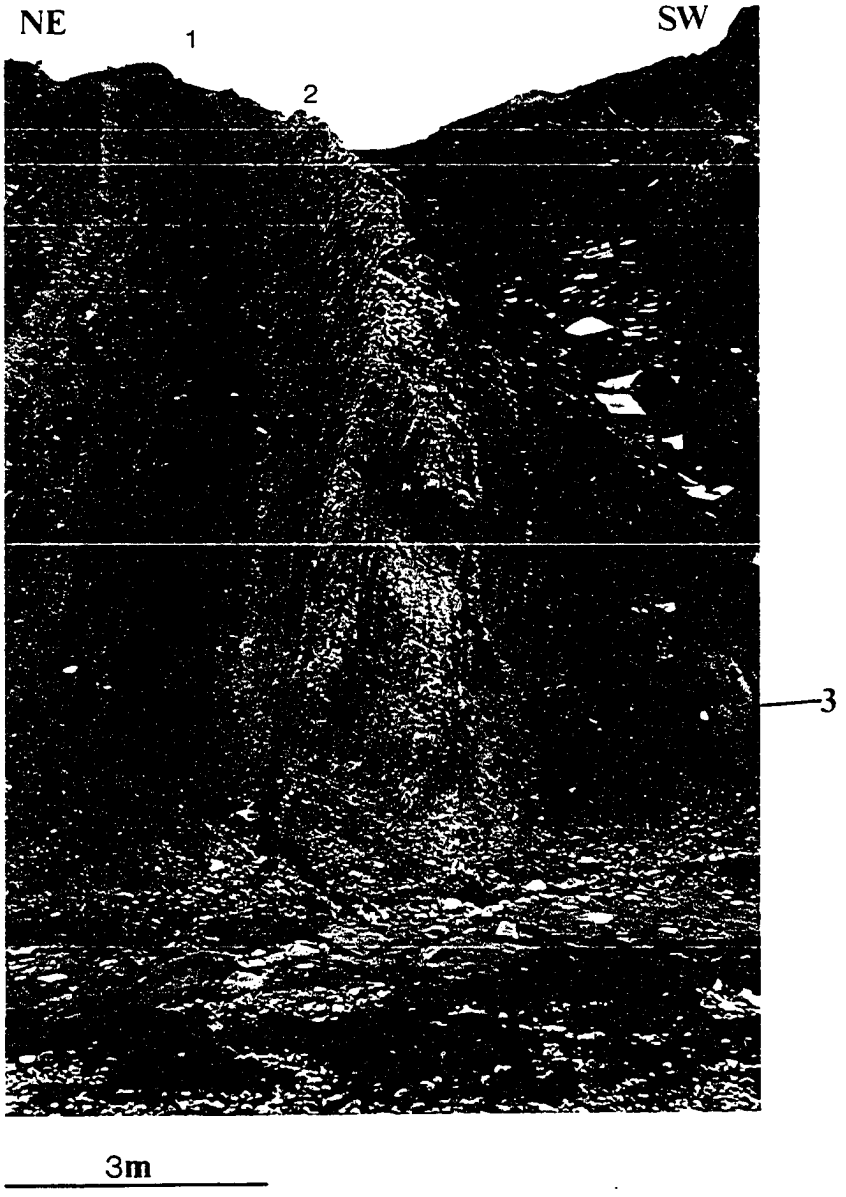

Figure 5.2.5

reed moor facies, with lesser proportions of open moor and forest moor facies. Small monolete miospores with sphenopsid (horsetail) affinity are present in great abundance.

As part of a regional study of Late Carboniferous coals in Atlantic Canada, six of the Mabou coal seams were sampled and their maceral proportions determined on full-seam composites (Gibling et al., 1994). On maceral-ratio diagrams (Diessel, 1986), the coals show moderate values of Gelification and Tissue Preservation Index and their plotted positions correspond to Diessel's upper delta plain to alluvial plain zone as determined from the Newcastle Coal Measures of Australia.

5.2.3, Red Mudstone and Calcrete Facies

The youngest strata of the Inverness Formation are exposed adjacent to Inverness Harbour as part of the Inverness-Port Ban section (Figure 5.2.6). The top ~35 m of this section shows a distinctive sedimentological change from the underlying sandstone and coal facies that may indicate a significant climatic and sedimentological change (see below).

This interval is dominated by thin, single-storey channel sandstones up to 8 m thick that are intercalated with grey and red mudstones and a single calcrete horizon (Figure 5.2.7). Within the channel sandstone bodies, lateral accretion surfaces are exposed. Lateral accretion surfaces were not recorded from any of the underlying multi-storey channel sandstone bodies (see above, Channel Sandstone Facies). The red mudstone is non-stratified, has a red/green mottled texture and contains abundant slickensided surfaces and calcite nodules. A similar sedimentological sequence was recorded from the Inverness I-2 well that is located 3 km to the south. Although the channel sandstones incise into the underlying mudstone by 1.5 m (Figure 5.2.7), the presence of thick mudstones and ripple laminated siltstones indicates that incision was not as intensive as that associated with the multi-storey channel sandstone bodies. Some thin, impure coals are also present in these strata.

Figure 5.2.6. Photograph showing the section to the south-east of Inverness Harbour (part of the Inverness shore section) (see Figure 5.1.10).

1. Single storey channel sandstone body. (see Figure 5.1.10) and shown in detail in Figure 5.2.7.

2. A calcrete horizon overlying an 8m thick channel sandstone body. The calcrete is exposed on the wave cut platform at low tide and is 50-70 cm thick.

3. Red mudstones, interpreted to be paleosols, become increasingly common towards the top of the section at Inverness Harbour.

(Section view is approximately 750m long).

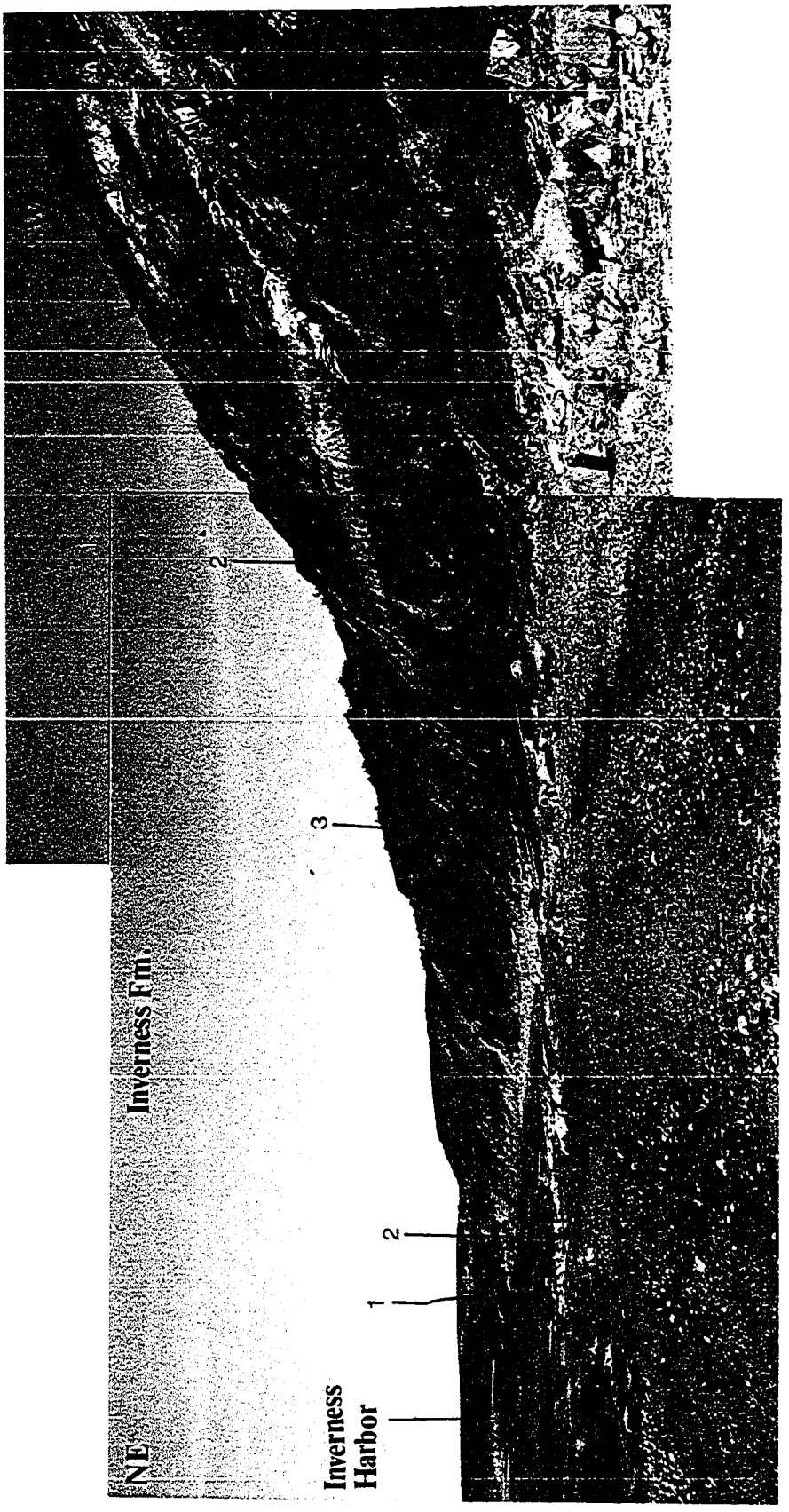

Figure 5.2.6

Figure 5.2.7. Single storey channel sandstone exposed at Inverness Harbour (see Figure 5.1.10). The base of the channel sandstone has approximately 1.5m of erosional relief. The channel base is defined by a coarse channel lag that consists almost entirely of reworked siderite nodules and coarse sand grains.

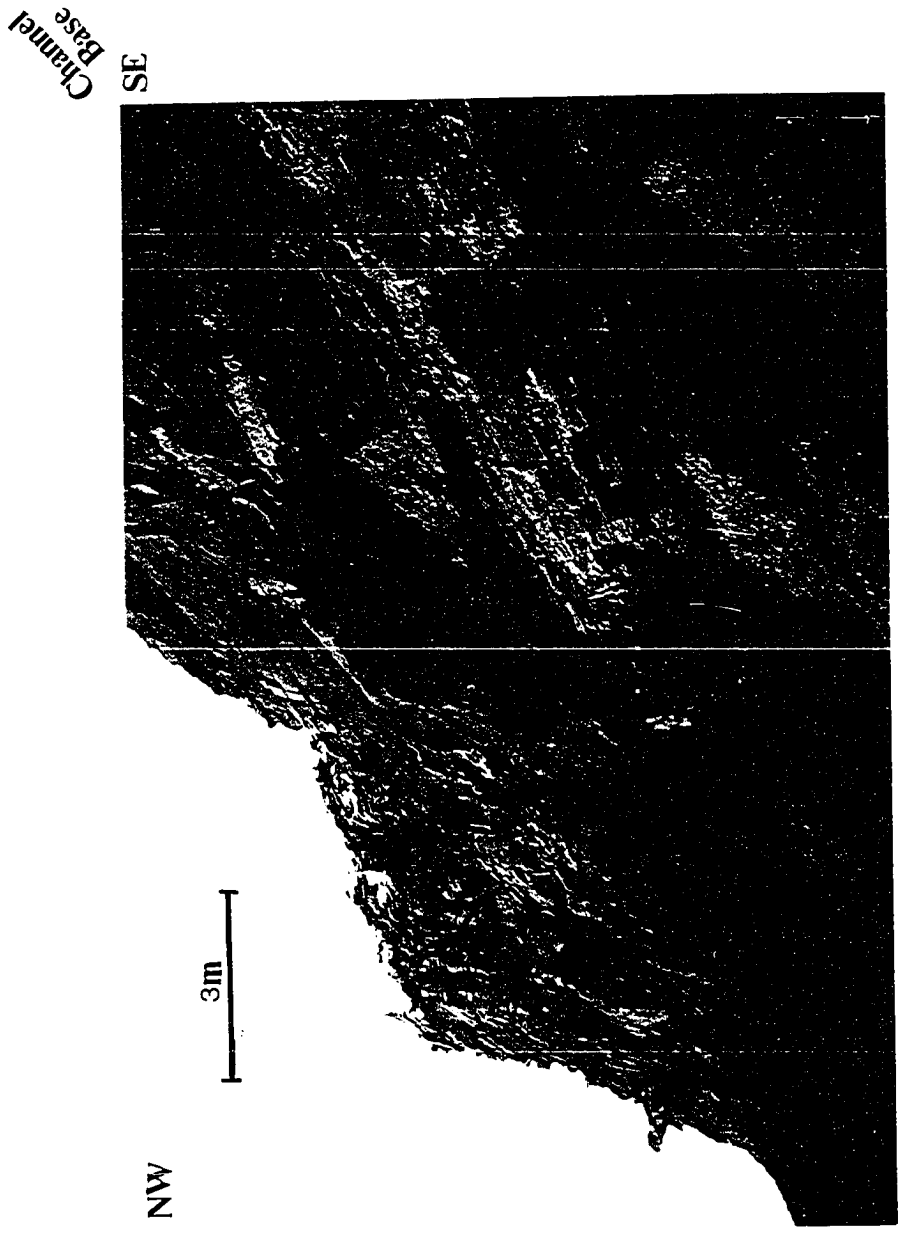

Figure 5.2.7

Interpretation. The decrease in channel incision and thickness as well as the presence of poorly developed lateral accretion surfaces in the uppermost sandstone unit may indicate a change to a lower energy channel system. The textural features of the red mudstones suggest that they are paleosols. From modern examples, paleosols of this kind are typically developed in highly seasonal climatic conditions with pronounced wet and dry seasons (Dudal and Eswaran, 1988). Similarly, the presence of a well developed calcrete indicates a highly seasonal climate requiring a long dry season followed by a short wet season in an equatorial climate (Cecil, 1990). The climatic conditions favourable to the formation and preservation of red paleosols and calcrete horizons normally preclude the deposition and preservation of peat, which requires more continuous precipitation throughout the year. The presence of the red mudstone-calcrete facies at the top of the Inverness Formation indicates a climatic change to a highly seasonal climate.

5.2.4. Mechanical Properties of the Inverness Formation

From a mechanical standpoint, the Inverness Formation can be considered to be a stack of rigid beams (the thick sandstone bodies) separated by plastic units (the coals and shales). A mechanical unit such as the Inverness Formation can be expected to deform by both bedding-parallel slip and inclined shear, but not necessarily at the same time. The thick sandstone units will have a large bending moment and a high flexural rigidity. When an applied stress exceeds its mechanical strength, the rigid sandstone units will tend to break into long, planar beams, separated by discrete faults rather than by forming folds. An example of this is imaged on the Mabou seismic line 2, where the intrusion of the Coal Mine Point Diapir has rotated part of the Inverness Formation as a relatively planar beam. The beam is broken around the Clayton Fault, which acts as the hinge. Although the intercalated mudstone strata must be accommodating bedding-parallel slip during the deformation described above, the role of bedding-parallel slip is more easily illustrated by using a smaller scale example. Within the drag zone of the Coal Mine Point Diapir (see Chapter 3.4), the Inverness Formation is deformed into a short drag zone structure. In this situation, the rigid sandstone units still have a high flexural rigidity and so tend to remain

as planar beams separated by faults. In order to fill void space created by rotating planar beams, the plastic shales must accommodate strain by migrating into the void space. This mode of deformation is illustrated by the anastomosing shear zones within the second sandstone unit at Coal Mine Point, which are the result of a shear couple acting across the sandstone unit.

5.2.5, Paleoenvironmental Protozoan Analysis

A widely held belief concerning Nova Scotia's Upper Carboniferous coal basins over the last 150 years was that they were sites of freshwater deposition. In 1986, however, scientists working at Dalhousie University's Centre for Marine Geology discovered microfossils that were believed to be foraminifera in the coal-bearing strata of the Sydney Basin. This discovery has changed the way these coal basins are interpreted, for it is becoming accepted that many of the North American coal basins were influenced by marine waters to varying degrees. The analysis of fossil foraminifera has become refined so that the protozoan content of fine-grained sedimentary rocks can be used to indicate a depositional paleoenvironment.

A sample suite of 89 shale samples was analysed for fossil protozoans by Dr. W.G. Wightman under a short-term contract as part of the present project. Details of sample location, sample preparation and results are included in Appendix 7.

Summary of Protozoan Analysis

For the Inverness Formation, 40 samples yielded agglutinated foraminifera of the genera Trochammina, Ammotium, Ammobaculites and Textularia, and 9 samples yielded thecamoebians (arcellaceans) that could not be identified to the genus level (of 89 samples analysed, see Appendix 7). For the Port Hood Formation, 10 samples yielded agglutinated foraminifera of the genus Trochammina and one yielded thecamoebians (of 21 samples analysed, see Appendix 7). Deformed strata on the east side of Finlay Point were also analysed, and foraminifera and thecamoebians were extracted from strata of

both Namurian to Westphalian A age (Port Hood Formation equivalent) and Westphalian C-D age (Inverness Formation equivalent).

The distribution of protozoan fossils within the measured sections is illustrated in Figures 5.2.8 and 5.2.9. Foraminifera are well represented throughout the Coal Mine Point and basal Finlay Point sections and in certain intervals of the MacKinnon's Brook section. Fewer samples were productive in the I-2 well and the Inverness coastal section (where sampling was restricted to the basal strata). Distribution in the Port Hood section is sporadic in the upper portion of the section, but good specimens were obtained from the section just north of Murphys Pond.

The foraminiferal genera are extant and represent an opportunistic, conservative assemblage that is well adapted to modern restricted-marine environments (Wightman et al., 1993, 1994a; Gibling and Wightman, 1994; Rehill et al., 1994). The Trochammina assemblage of foraminifera is especially common in estuarine and salt marsh settings, whereas the thecamoebians are characteristic of freshwater settings. Although agglutinated foraminifera do occur rarely in modern saline lakes, their presence in such a setting is regarded as anomalous and probably explained by avian transport (e.g. Patterson et al., 1990). The relative abundance of agglutinated foraminifera in many samples of the present suite implies a periodic restricted marine connection to the depositional basin. The only possible indication of more fully marine conditions is the occurrence of Textularia in one sample near the base of the Coal Mine Point section.

5.3, STRATIGRAPHIC CORRELATION OF THE INVERNESS FORMATION

Introduction

In order to correlate the isolated Inverness Formation exposures within western Cape Breton, palynological age dating has been combined with a detailed seismic stratigraphy of the Inverness Formation. This correlation relies upon tying the 1978 Mabou seismic

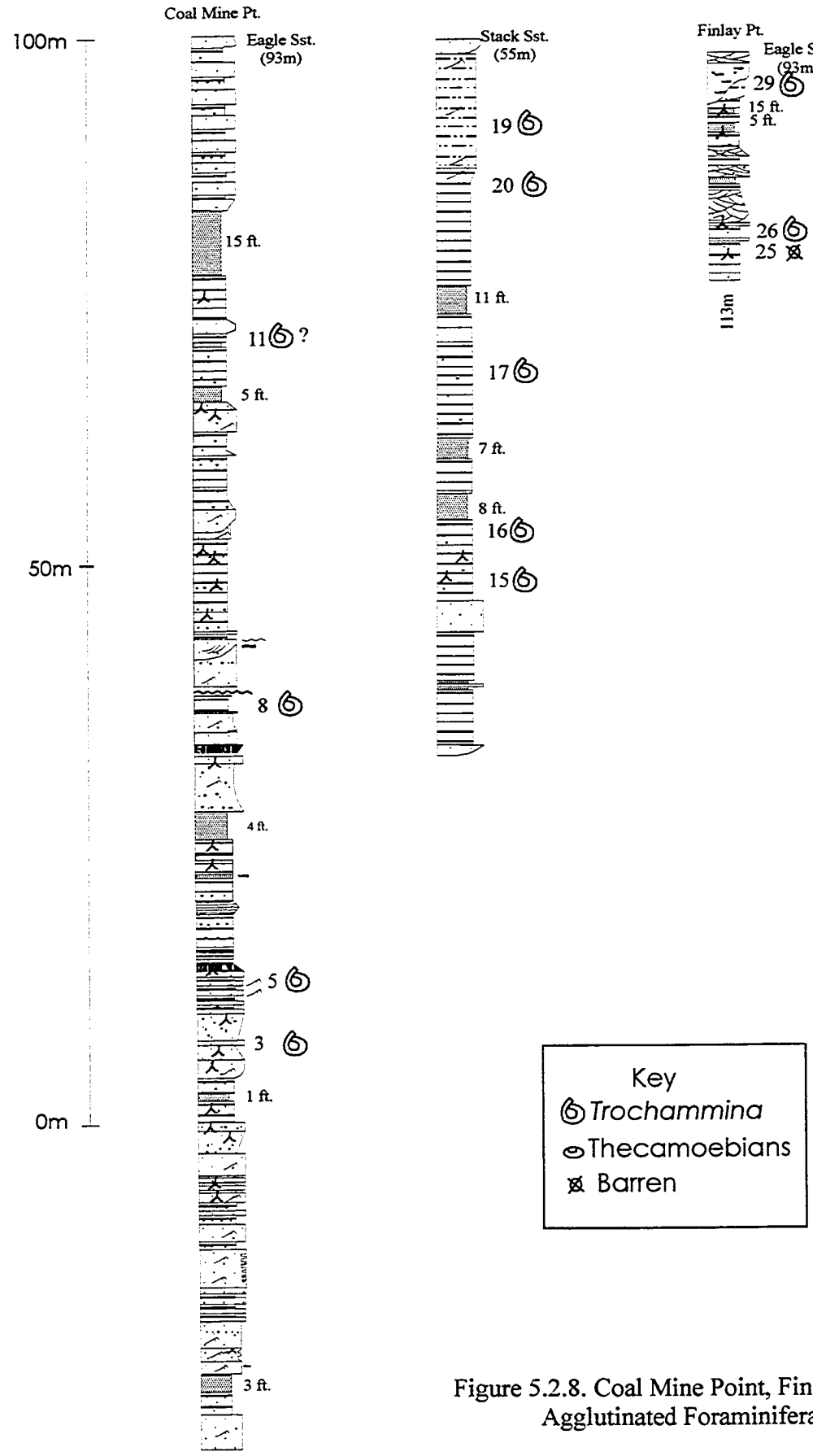

Figure 5.2.8. Coal Mine Point, Finlay Point, Agglutinated Foraminifera.

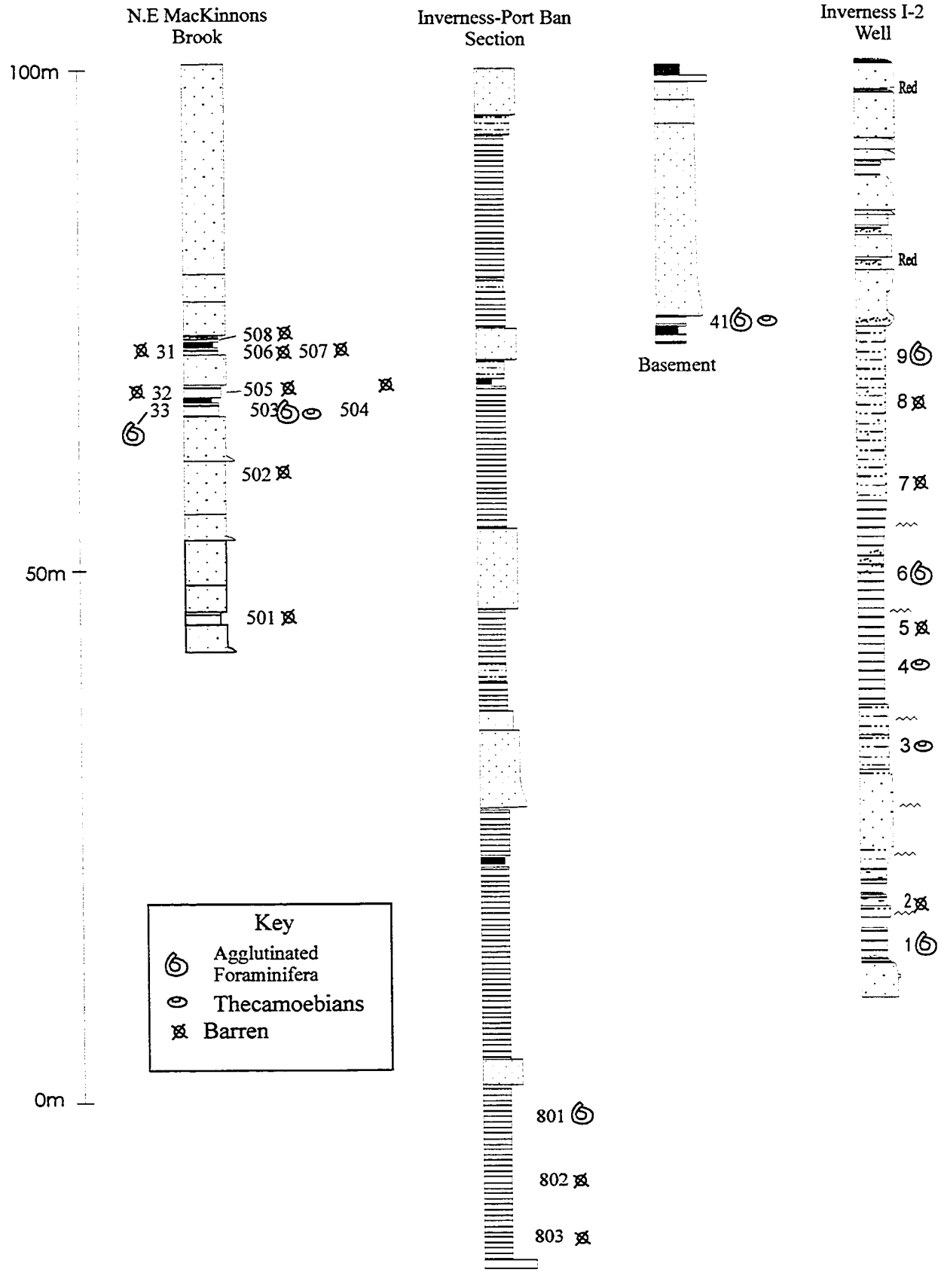

Figure 5.2.9. Inverness and MacKinnons Brook, Fossil Protozoan Samples.

survey and the two Mabou wells (Mabou 1 and Mabou 2a) to the coastal section at Coal Mine Point. Unlike the 1982 Chevron survey, the individual Inverness Formation coal seams can be identified on the 1978 Mabou data. Identification of individual seams allows a precise seismic to well to shore tie, which is not possible from the Chevron data. For this reason, stratigraphic correlation of the Inverness Formation onshore exposures with offshore data is well constrained. The Inverness Formation correlation is important because much of the subsequent paleocurrent and seismic facies analysis relies upon accurate correlations between exposures themselves and between exposures and the seismic data.

5.3.1, Palynological Dating

Previous Palynological Dating

Barss and Hacquebard (1967) and Hacquebard (1972) defined four biostratigraphic zones (A-D) based upon analysis of fossil plant spores contained within 6000 ft (1829 m) of Upper Carboniferous strata of the Sydney Basin and other outcrop belts. Subsequent work on the Mabou and Inverness coal-bearing strata, using the Sydney Basin spore zones for reference, suggested that the Inverness coal measures are stratigraphically younger than the Mabou Mines coal measures. The Inverness coal measures were assigned to the B (*Torispora*) and C (*Thymospora*) spore zones, whereas the Mabou Mines coal measures were assigned to the B (*Torispora*) spore zone, placing the Mabou Mines coal measures stratigraphically beneath those of the Inverness coal field (Hacquebard, 1986, 1989; Barss et al., 1979) (Figure 5.3.1). However, the interpretation that the Mabou Mines coal seams lie stratigraphically beneath the Inverness coal seams is not supported by recent palynological age dating carried out in conjunction with this thesis.

Palynological Age Dating (1993 and 1994)

Ninety-two shale samples collected from the Inverness and Port Hood Formations were

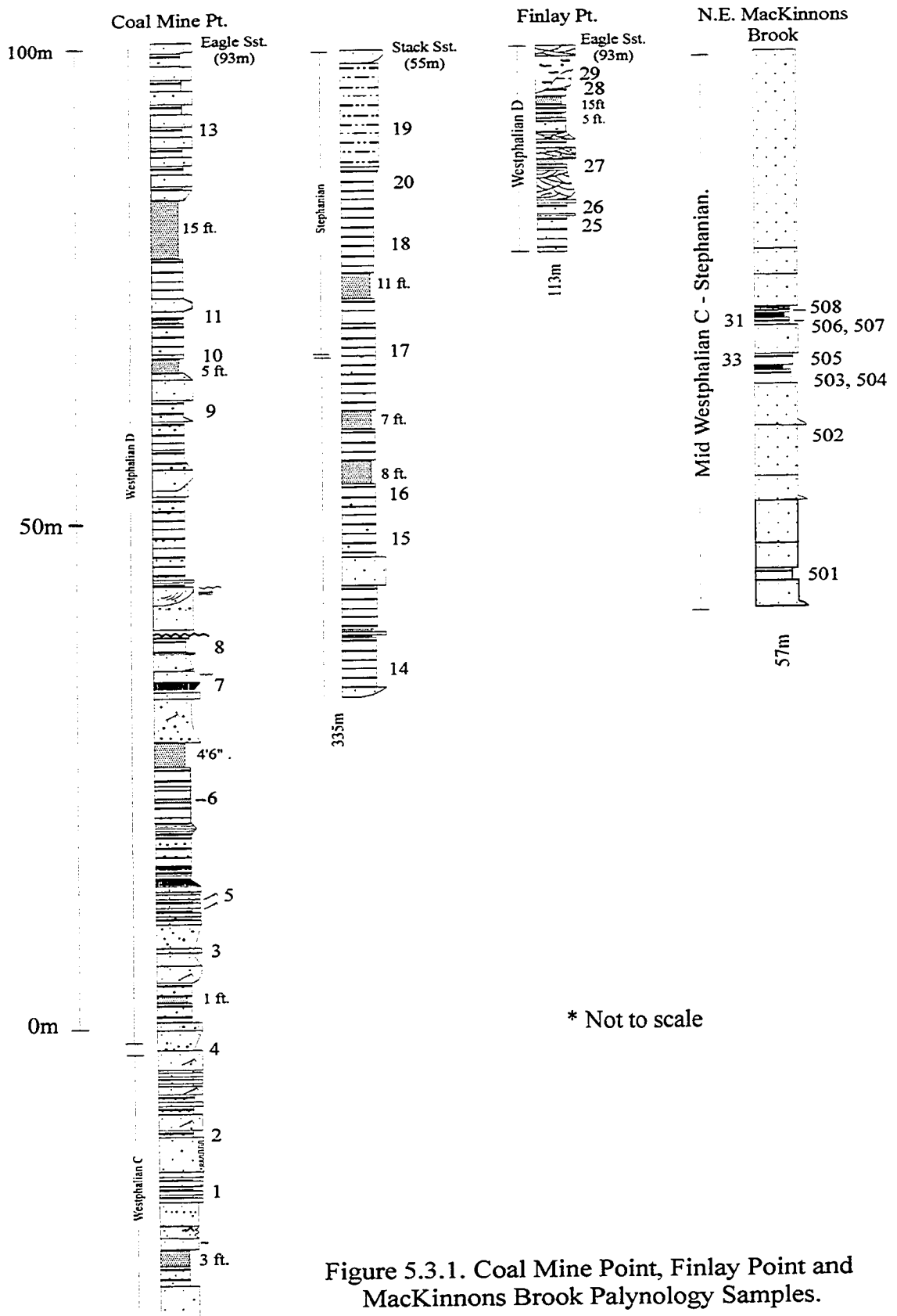

Figure 5.3.1. Coal Mine Point, Finlay Point and MacKinnons Brook Palynology Samples.

submitted for analysis to Dr. G. Dolby as part of the NATMAP project for stratigraphic study in Atlantic Canada. Seventy-six samples yielded reliable age dates and the age data are shown on Figures 5.3.1 and 5.3.2 (Appendix 8 contains tabulated results of the palynological analysis). As well as dating the Inverness Formation exposures, palynological dating has been used to date allochthonous sedimentary rock units that have been transported as diapir inclusions (see above, Chapter 3). Detailed discussions of the sampled sections are included in Appendix 8 and a summary of the ages is presented below.

Summary of Palynological Results

Note. *Age bars shown on Figures 5.3.1 and 5.3.2 represent probable stratal ages based on the palynological results. For this reason, the ages shown on Figures 5.3.1 and 5.3.2 may not match those of individual samples set out in Appendix 8 (see Palynological Data, Appendix 8).*

The Inverness Formation exposed between Mabou Mines and Inverness are predominantly of Westphalian D age with only the Coal Mine Point section showing a stratigraphic section that ranges from the Westphalian C through the Westphalian D and into the Stephanian (Figures 5.3.1 and 5.3.2).

The palynological age data indicate that the coal-bearing facies and channel sandstone bodies exposed sporadically between Mabou Mines and Inverness are approximately stratigraphically equivalent. The Inverness coal seams appear to be age equivalent to the Mabou Mines coal seams. This palynological interpretation is also supported by re-interpretation of offshore seismic data (see below).

5.3.2, Seismic Stratigraphic Correlation

Introduction

In order to assess undersea mining potential, a series of seismic surveys were acquired

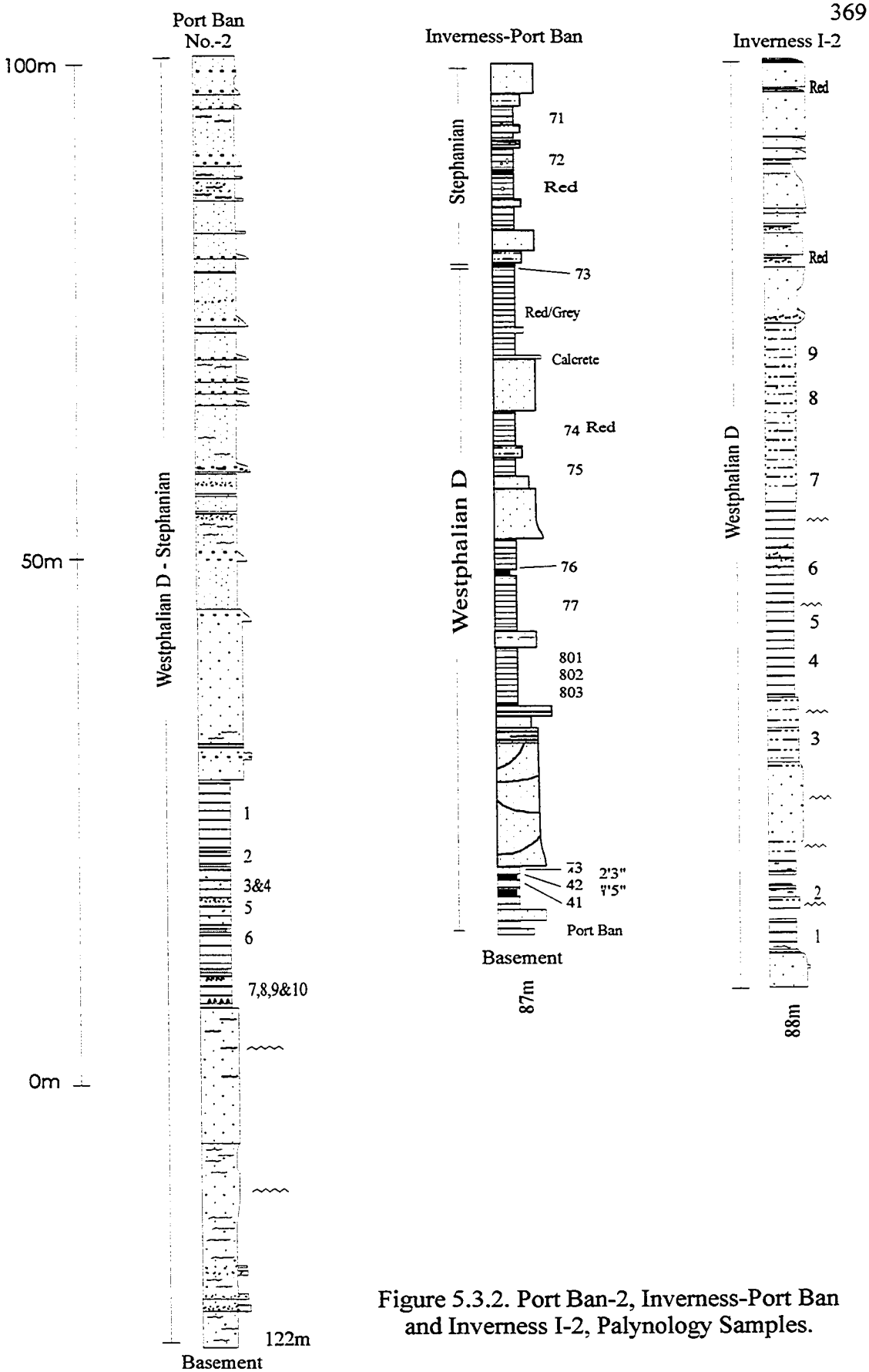

Figure 5.3.2. Port Ban-2, Inverness-Port Ban and Inverness I-2, Palynology Samples.

between 1978 and 1985 in the near shore areas of Inverness and Mabou Mines (see Seismic Database, Appendix 2). Two exploration drill holes, Mabou-1 and Mabou-2a, were subsequently drilled in support of the 1978 Mabou seismic survey. Both drill holes were cored and subsequently described by Hacquebard (1986) and Hacquebard et al. (1989).

Both the 1978 Mabou and 1985 Inverness NSDME seismic surveys are partially overlapped by the 1982 Chevron survey (Figure 5.3.3). By tying coal seams within the two Mabou cores (M-1 and M-2a) to the 1978 Mabou survey and then tying the three seismic surveys to each other, a seismic stratigraphic correlation of the Inverness Formation in the offshore area can be formulated.

The correlation can be extended to the onshore area at Mabou Mines by tying the Mabou-1 and Mabou-2a wells to the Coal Mine Point Shore section using palynological dating (Dolby, 1994, 1995) and extrapolation of sub-sea mine plans prepared by Keating (1950). At Inverness, the correlation can be extended onshore by tying the coal seam reflectors imaged on the 1985 Inverness seismic survey to the Inverness sub-sea mine plans prepared by Haites (1952).

One Dimensional Sedimentological Profile from Cores M-1 and M-2a

Mabou - 2A is located 2.4 km offshore from Mabou Mines and is the deeper of the two cored Mabou wells (TD 1464 m), thereby giving the most complete section through the Inverness Formation. M-1 is located 1.6 km offshore from Mabou Mines and is therefore a closer tie to shore sections (Figure 5.3.3). For this reason, the vertical sedimentological profile described below is from the Mabou-1 core, based upon core descriptions of Hacquebard (1986) (Figure 5.3.4).

The vertical lithological profile shows an overall upwards fining, a decrease in sedimentary unit thickness, a decrease in the sand:shale ratio and a decrease in coal seam

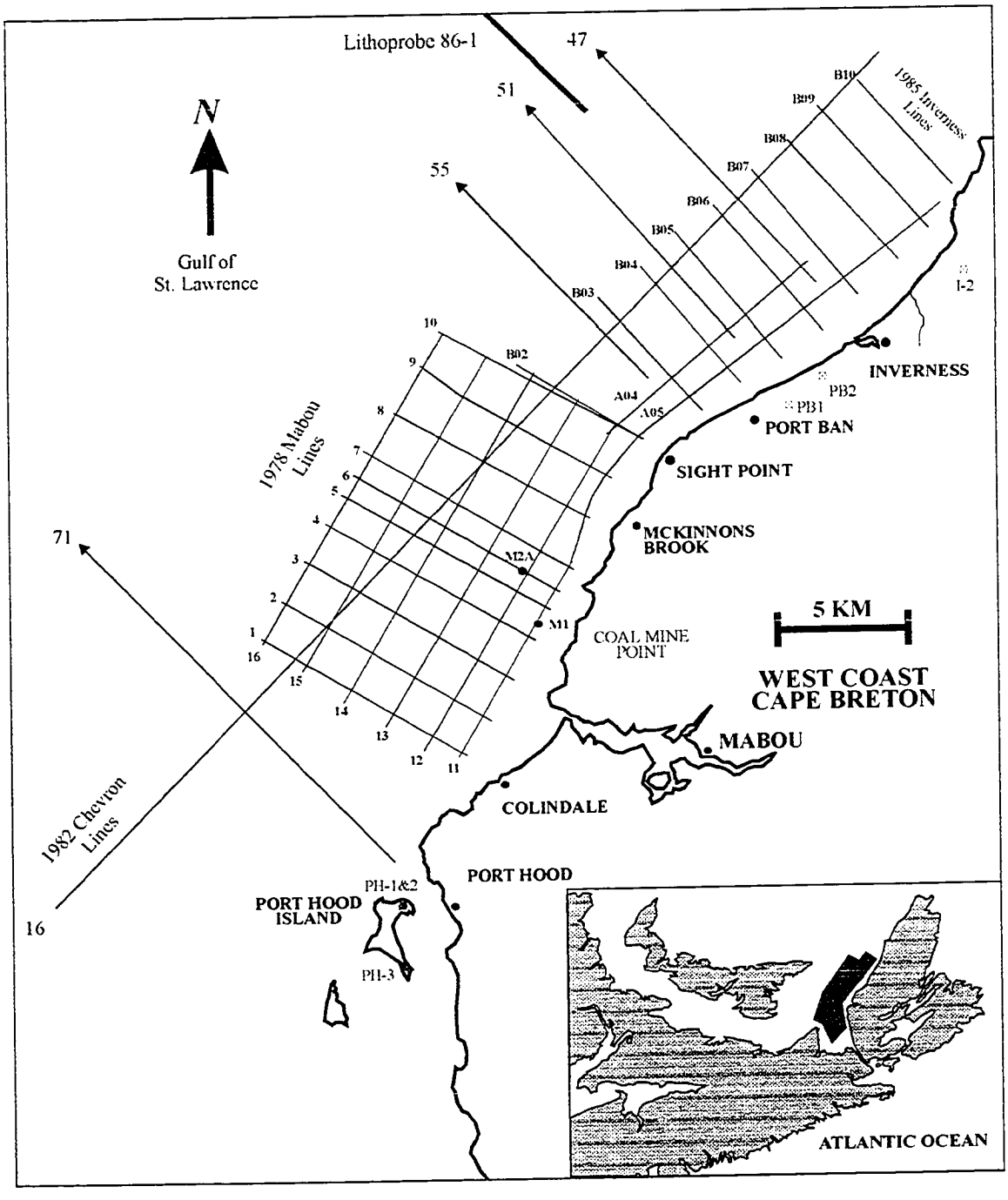

Figure 5.3.3.. Map of western Cape Breton showing the tie lines between the seismic surveys and the position of the 86-1 Lithoprobe line.

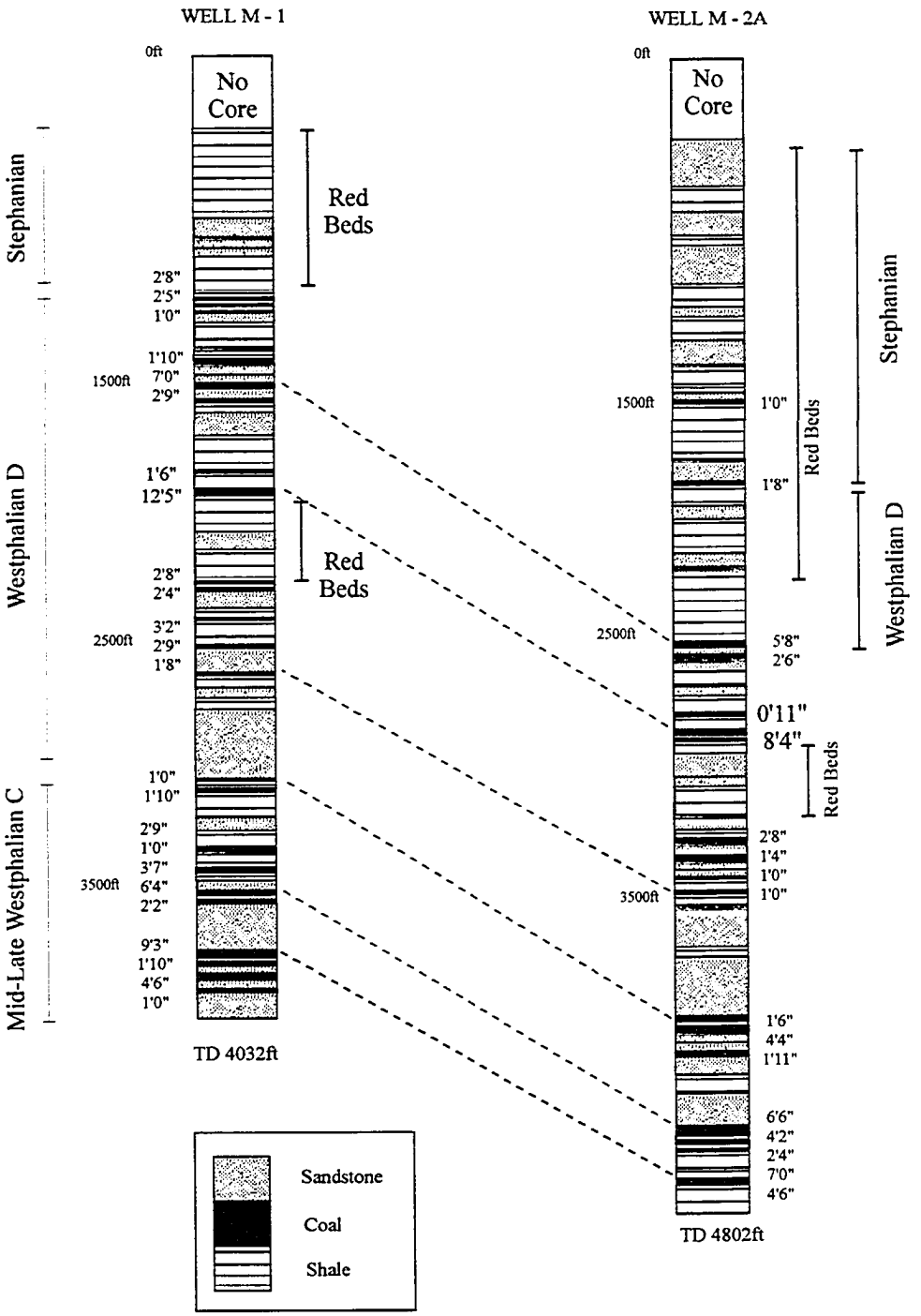

Figure 5.3.4. Lithological well logs for Mabou 1 and Mabou 2A, (modified from Hacquebard et al., 1989) and palynological age data (G. Dolby, 1994).

thickness and number of seams.

Basal Section (4032 - 2500 ft) M-1

This interval contains three major sandstone bodies that are 63 m, 19 m and 88 m thick, respectively. These sandbodies are separated by two coal-bearing zones consisting of intercalated coal seams, shale units and impure coal seams. Each coal-bearing zone contains 3 to 6 individual coal seams and associated impure coal seams.

Central Section (2500 - 1500 ft) M-1

This interval consists of a single thick coal seam (12'5" seam) and two coal zones consisting of multiple thin coal seams, intercalated with sandstones, siltstone and shales. The sandstone horizons are thinner than those of the basal section with a maximum thickness of 38 m.

Upper Section (1500 - 0 ft) M-1

This interval consists of interbedded sandstone, siltstone and shales but no thick coal seams. The average vertical thickness for any lithology is < 40 m and there is only one thick sandstone body (~30 m). The strata within this interval are predominantly red and are therefore distinct from the Central and Basal sections.

Vertical Reflection Profile - 1978 Mabou Seismic Survey

(Described from line 3, Shot Points 0-300)

0 - 150 ms TWT. Parallel reflectors. High amplitude and moderate to good continuity. It is suspected that the majority of high amplitude reflectors from the original Mabou seismic data are seabed multiples. Sediments above the regional unconformity (see below) are of unknown age and are not considered as part of this thesis.

~ 200 ms TWT. Regional erosional unconformity. The unconformity is sub-horizontal except where affected by the Clayton Fault. Dipping reflectors below the unconformity

are truncated to form truncation reflection events.

200 - 400 ms TWT. Variable reflectors. High amplitude with moderate continuity (1 - 3 km) intercalated with seismically transparent horizons. This reflector package is typical of coal measure sequence and probably represents sandstone-filled channels, minor coal seams and thick shale horizons. The bulk of the seismic facies units are identified within this interval (see Seismic Facies, Chapter 5).

400 - 800 ms TWT. Seismically transparent. Few reflectors are identifiable within this interval and they are of low amplitude and continuity. This may be due to poor seismic processing or acquisition as clear, high-amplitude reflectors from the overlying interval can be seen to lose amplitude and continuity if they are uplifted to ~400 ms. An alternative explanation may be that the sedimentary unit thickness within the upper sections of the M-1 and M-2a wells (< 2000 ft.) decreases markedly from that of the lower section. The thinner unit thickness may cause interference of reflected seismic wavelets with the result that no coherent reflectors are imaged.

800 - 1000 ms TWT. The three principal reflectors D1, D2 and D3 are imaged within this zone. These three 'bright', high-amplitude and high-coherency reflectors can be traced throughout the seismic data. The three reflectors maintain a constant separation throughout the survey area, except where affected by diapiric uplift.

In addition to the above reflectors, Line 11 (1978 Mabou survey) images three seismic reflectors within an uplifted stratal package which are below the 1 sec TWT cut-off throughout the majority of the seismic survey. The reflectors are high-amplitude reflectors that maintain a constant separation within the short distance over which they are imaged. These reflectors are penetrated by the Mabou-1 and Mabou-2a drill holes (see below).

Mabou-1 and Mabou-2a Core Ties to the 1978 Mabou Geophysical Survey

The seismic reflectors identified from lines 11, 12, 5 and 6 were tied to the Mabou 1 and Mabou 2a cores. In order to tie the lithological core descriptions from M-1 and M-2a to the seismic data, the seismic reflectors were depth converted (see Depth Conversion, Appendix 3) and the depths, measured in feet below seabed, were correlated with the M-1 and M-2a drill cores. The reflectors are designated as either C or D reflectors and then assigned a number (deepest to shallowest) e.g., D1, D2 and D3 etcetera.

The seismic to well tie is complicated by the fact that the reflector characteristics change with depth. The Mabou-1 and Mabou-2a wells were drilled in an area of uplifted strata. At this shallow depth, vertical seismic resolution is good and individual coal seams and some sandstone/shale reflectors can be recognised and tied to the wells. Unfortunately, the vertical seismic resolution deteriorates with depth so that at depths of 800 to 1000 ms only three high-amplitude reflectors are imaged (D1-D3, see above). These three high-amplitude reflectors probably represent amalgamations of the coal seam reflectors as the high frequency component of the seismic wavelet is attenuated and vertical resolution is reduced with depth. Each of the three reflectors imaged at 800 to 1000 ms (see above) probably represents reflections from two or more closely spaced coal seams. Examination of the lithological logs from Mabou-1 and Mabou-2a (Figure 5.3.4) shows that the coal seams typically exist in 'coal zones' containing two or more closely spaced coal seams. The coal zones are separated from the overlying and underlying coal zones by a relatively thicker sequence of sandstone and shale. The assumption that the three 'D' reflectors represent reflections from two or more closely spaced coal seams is therefore supported from a geophysical and lithological perspective.

The D1, D2 and D3 reflectors are the principal seismic reflectors that can be traced throughout the 1978 Mabou survey and correlated with similar reflectors imaged on the 1982 Chevron survey. Reflectors D4 and D5 (not shown on tie diagrams) probably represent reflections from single, thin coal seams that cannot be interpreted at depth and

are therefore not regional seismic reflectors. The following suggested correlations from reflectors to coal seams are made:

From the Mabou-1 Core (1000-2500 ft) (Table 5.3.1, Figure 5.3.5)

D1: 2'8", 2'4", 3'2", 2'9" and 1'8" coal seams.

D2: 12'5" and 1'6" coal seams.

D3: 1'10", 7'0" and 2'9" coal seams.

From the Mabou-2a Core (2000-3000 ft) (Table 5.3.1, Figure 5.3.6)

D1: 2'8", 1'4", 1'0" and 1'0" coal seams

D2: 0'11" and 8'4" coal seams

D3: 5'8" and 2'6" coal seams.

D4: 1'8" coal seam.

D5: 1'0" coal seam.

The C seismic reflectors are high-amplitude reflection events that represent coal seam reflectors from the deeper portion of the seismic record (>700ms) on line 11, 5 and 6 (1978 Mabou survey). Throughout the rest of the Mabou seismic survey, these reflectors are below the 1.0 sec TWT cut-off and are therefore not imaged. These reflectors are imaged on the 1982 Chevron survey, where they form the lower part of the Inverness Formation coal zone (see Seismic Stratigraphy, Ch.2). The C reflector seismic to well tie is not very accurate. The C1, C2 and C3 reflectors appear to be consistently deeper than indicated after depth conversion. This is probably due to a combination of poor depth conversion, well deviation and/or inaccurate well or seismic line location. An excellent tie is obtained if a velocity of 10,000 ft/sec is used to depth convert the seismic data, but available data suggest that a higher velocity is preferable (Appendix 3).

From the Mabou-1 Core (3000-4032 ft) (Table 5.3.1, Figure 5.3.5)

C1: 9'3", 1'10", 4'6" and 1'0" coal seams.

C2: 6'4" and 2'2" coal seams.

C3: 2'9", 1'0" and 3"7" coal seams.

From the Mabou-2a Core (4000-4802 ft) (Table 5.3.1, Figure 5.3.6)

C1: 7'0" and 4'6" coal seams

C2: 6'6", 4'2", 2'4" and 2'0" coal seams

C3: 1'6", 4'4" and 1'11" coal seams

Mabou-1 and Mabou-2a Core Correlation to the Coal Mine Point Shore Section

The M-1 and M-2a drill cores are correlated to the Coal Mine Point shore section by extrapolation of sub-sea mine plans and by palynological dating.

Extrapolation of Mine Plans. Keating (1950) estimated the dip of the Mabou coal seams to be 17 degrees and that the dip was almost homoclinal over the entire sub-sea mining area. Extrapolation of the top of the Eagle Sandstone (Keating, 1950) to the Mabou-1 well, located 1800 m north of Coal Mine Point, gives an approximate tie to both drill core and seismic data. The mine plan extrapolation correlates the top of the Eagle Sandstone to a depth of 1805 ft (550 m) in the Mabou-1 well, which is located between the 1'6" and 2'9" coal seams close to a 33 m thick sandstone unit (Figure 5.3.4). If this sandstone unit is the Eagle Sandstone, then the overlying coal seams in the Mabou-1 well (2'9", 7'0" and 1'10") would correlate with the 8'0", 7'0" and possibly the 11'0" coal seams at Coal Mine Point. The underlying coal seams in the Mabou-1 well (1'6" and 12'5") would correlate with the 15'0" and 5'0" coal seams at Coal Mine Point.

A 95 m thick sandstone unit is located at a depth of 2880 ft (877 m) within the Mabou-1 well and would seem to be a good candidate for the Eagle Sandstone. However, in order

Mabou-1 Reflector	TWT(ms)	Depth(ft)	Depth(m)	Sediment Interface
D1	380	2150-2350	655-716	2'8",2'4",3'2" & 2'9"
D2	320	1870	570	12'5" & 1'6"
D3	240	1402	427	1'10",7'0" & 1'0"
D4	Absent			
D5	Absent			
C1	660	3770	1150	9'3",1'10",4'6" & 1'0"
C2	610	3550	1082	6'4" & 2'2"
C3	580-600	3350	1021	2'9",1'0" & 3'7"
Mabou2a Reflector	**TWT(ms)**	**Depth(ft)**	**Depth(m)**	**Sediment Interface**
D1	570-610	3313-3537	1009-1078	2'8", 1'4", 1'0", 1'0"
D2	500	2865	873	0'11", 8'4"
D3	410	2358	718	5'8", 2'6"
D4	310	1805	550	1'8"
D5	250	1447	441	1'0"
C1	1050	4737	1443	2'0", 7'0", 4'8"
C2	1000	4531	1380	6'6", 4'2", 2'4"
C3	950	4088	1245	1'6", 4'4", 1'11"

Table 5.3.1. Coal Seam to Seismic Correlations.

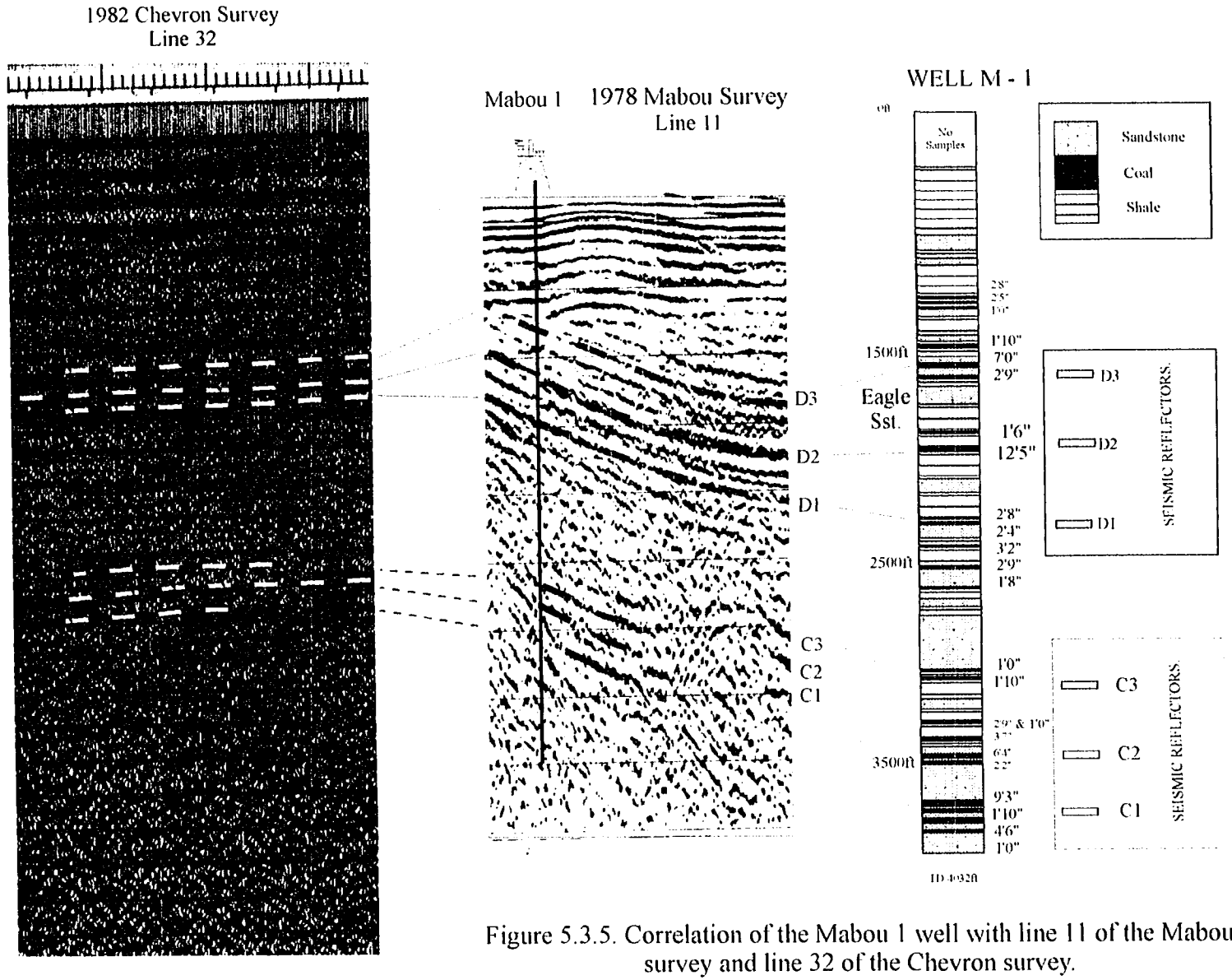

Figure 5.3.5. Correlation of the Mabou 1 well with line 11 of the Mabou survey and line 32 of the Chevron survey.

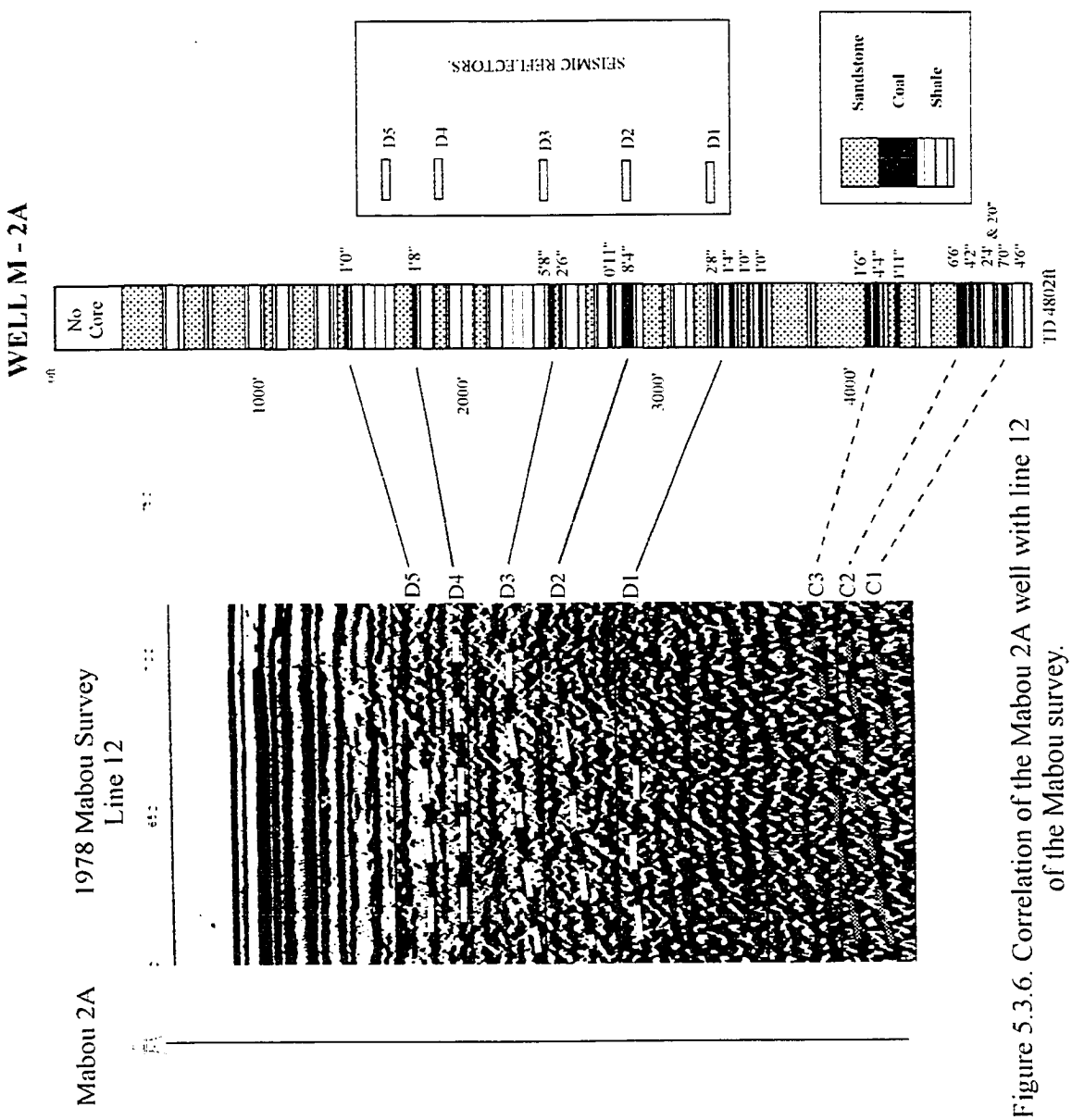

Figure 5.3.6. Correlation of the Mabou 2A well with line 12 of the Mabou survey.

to tie this sandstone to the Eagle Sandstone at Coal Mine Point, a strata dip of 26 degrees would have to be used. This dip is significantly steeper than that estimated by Haites (1952).

Palynology. The M-1 and M-2a drill cores were sampled for palynological dating (Dolby, 1994). Using this palynological data in conjunction with the Coal Mine Point palynology data gives a good shore section to drill core tie.

Seventy-three shale samples from Mabou-1 and seven shale samples from Mabou-2a were used for palynological dating (Dolby, 1994). The results are summarised below and plotted on Figure 5.3.4:

Mabou-1		
Interval (below sea-level)	320'-1050'	Stephanian A
Interval (BSL)	1050'-3050'	Westphalian D
Interval (BSL)	3050'-4032'	Mid-Late Westphalian C
Mabou-2a.		
Interval (BSL)	1450'	Stephanian
Interval (BSL)	1775'-3298'	Westphalian D

(For palynological data and specimen details, see Appendix 5, Palynological Data)

The palynological dating confirms the core to core correlation proposed by Hacquebard (1986) and suggests the following seismic to Mabou-1 to Coal Mine Point shore section correlation:

Seismic		Mabou-1 Core		Coal Mine Point
D1	-	2'8", 2'4", 3'2", 2'9"	-	1'0" and 4'6"
D2	-	12'5", 1'6"	-	5'0" and 15'0"
D3	-	1'10", 7'0", 1'0"	-	8'0", 7'0"

C1 - 2'9", 1'0", 3'7" - 3'0" (end of shore section strata)

The mine plan data and the palynology data provide two independent lines of evidence to support the correlation of the off-shore section as imaged on seismic data and within Mabou-1 and 2a with the onshore section at Coal Mine Point.

Mabou Mines to Inverness Correlation of the Inverness Formation Coal Seams

The three seismic reflectors D1-D3 and the underlying set of high coherency/high amplitude reflectors defined from the 1978 Mabou geophysical survey and Mabou-2a well also appear as strong reflectors on the 1982 Chevron geophysical survey. The three coal seam reflectors D1-D3 can be tied from the 1978 Mabou survey to line 16 of the 1982 Chevron survey which runs for 40.8 km parallel to the coast of Cape Breton, intersecting the 1985 Inverness geophysical survey (Figure 5.3.3). Lines 55, 51 and 47 of the 1982 Chevron survey can then be used to tie the D1-D3 coal seam reflectors to both the 1985 Inverness survey and to the Inverness mine plans of Haites (1952). The mine plans can then be correlated with the Inverness shore section to give a complete Mabou to Inverness correlation (Figure 5.3.7 and 5.3.8).

The D coal seam reflectors can be tied from the 1982 Chevron survey to a reflector zone of approximately 50 ms TWT on the 1985 Inverness seismic data (the data quality of the 1985 Inverness survey is poor and so the coal seams cannot be tied to a specific reflector). The 1985 Inverness lines can be traced to within 850 m of the shore and to within 200 m of sub-sea mine plans for the 7' coal seam mined at Inverness (Haites, 1952). Hacquebard et al. (1989) constructed structure contours on the 7' coal seam that projected the 7' coal seam into the area covered by the 1985 Inverness seismic survey. In this way, the 7' coal seam can be tied with reasonable accuracy to the 1985 Inverness survey.

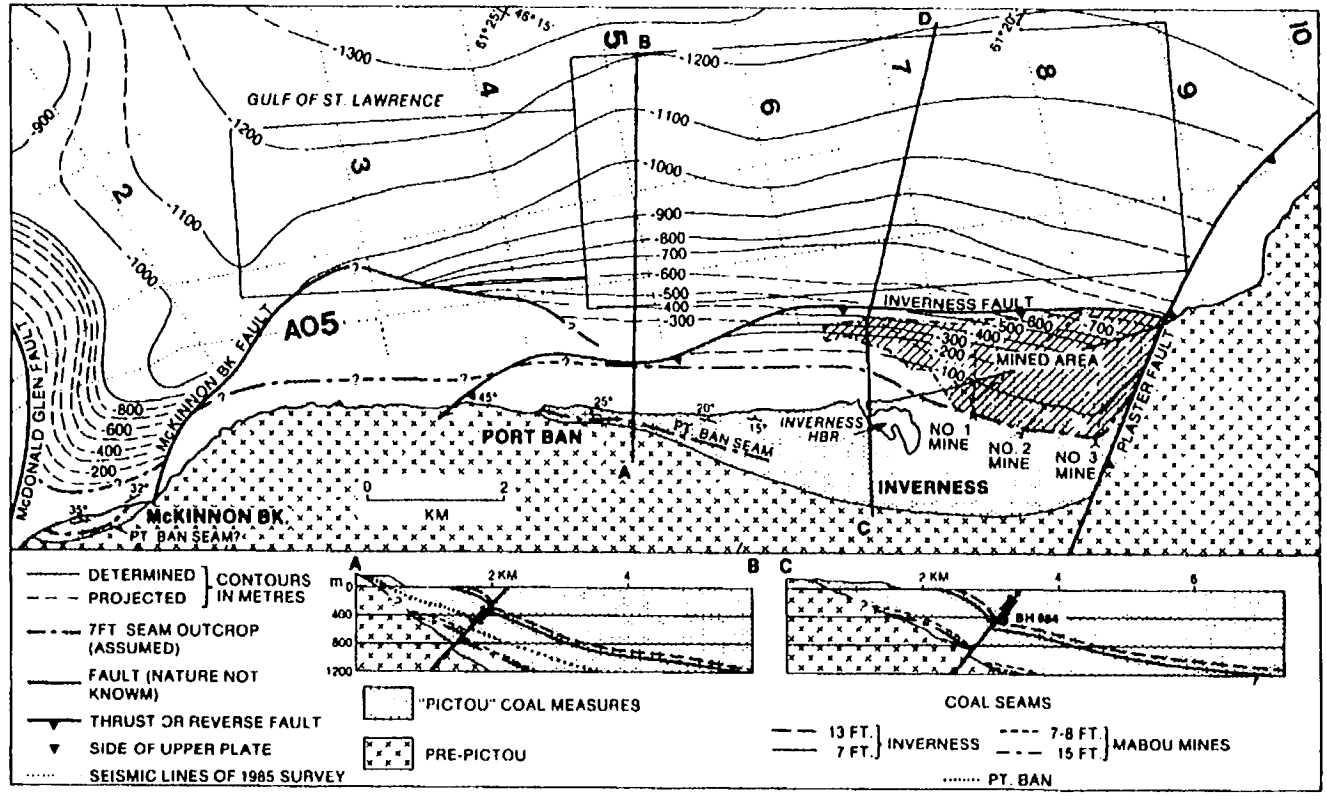

Figure 5.3.7. Structure contours on the interpreted position of the 7 ft coal seam in the Inverness area, based on the 1985 Inverness seismic survey and sub-sea mine data. Contour interval is 100m. Modified from LaPierre, (1986b).

Figure 5.3.8a. Correlation of the Inverness Formation

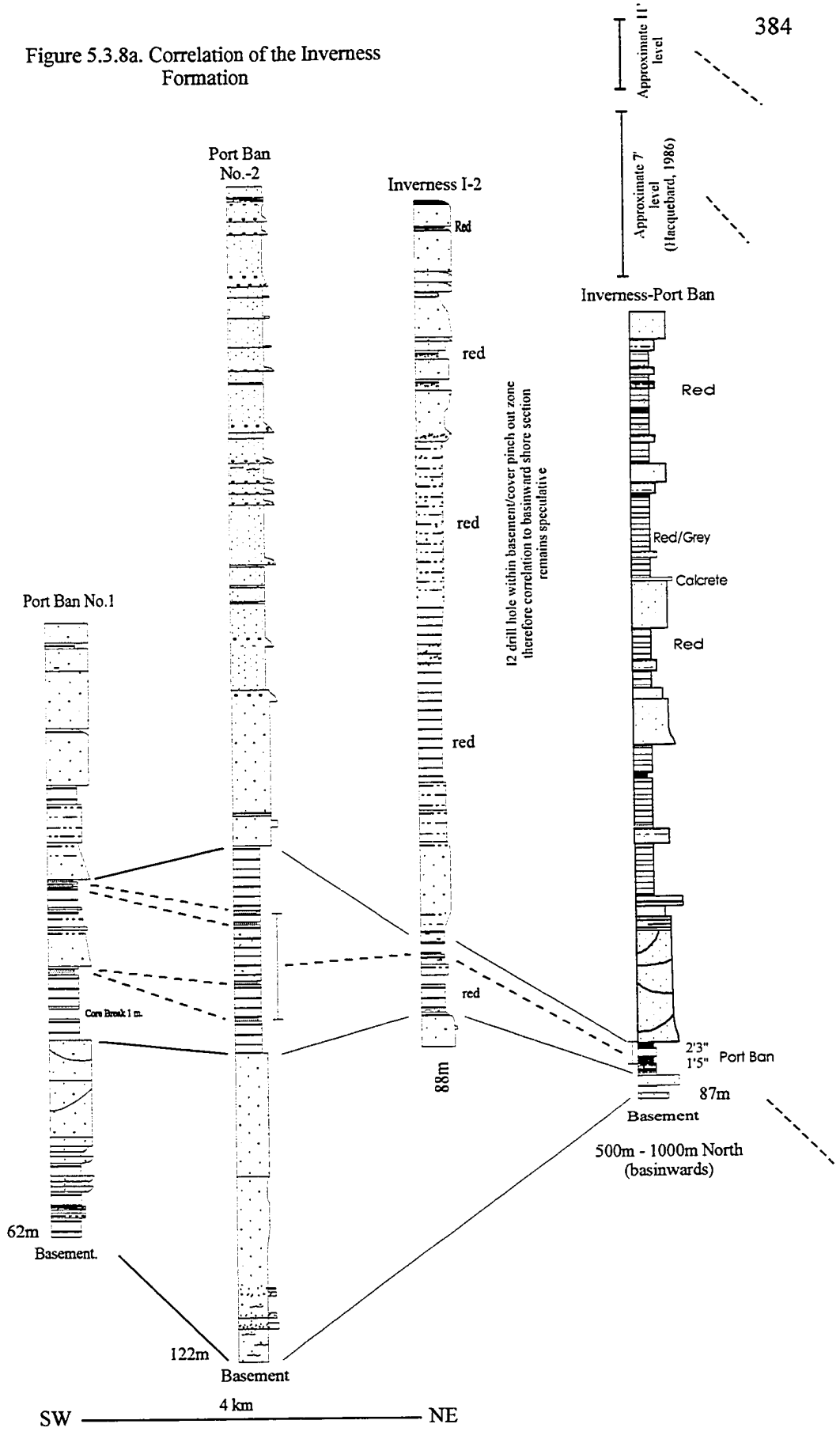

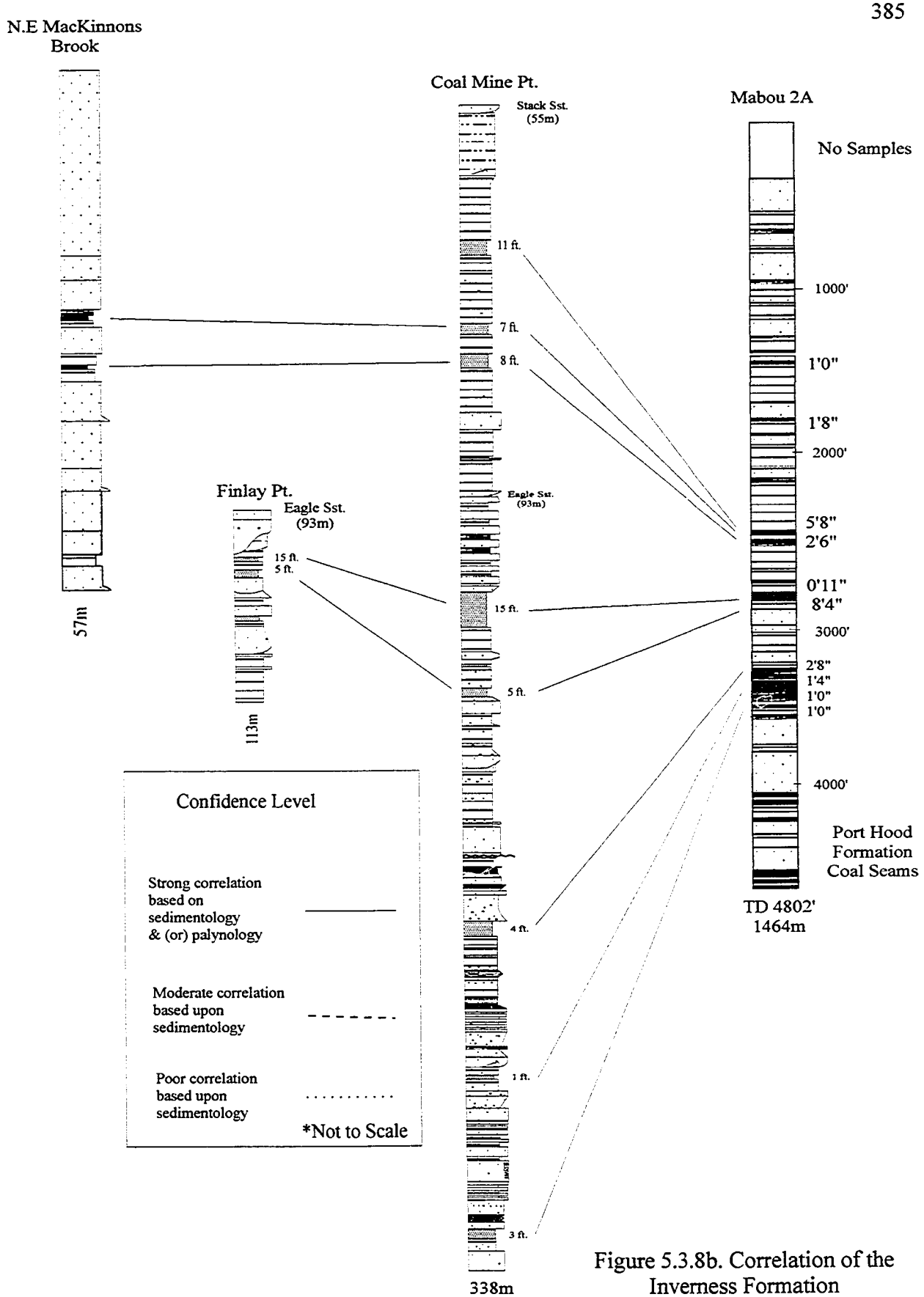

Figure 5.3.8b. Correlation of the Inverness Formation

Summary of Correlation

Coal Mine Point to Inverness Correlation. The 7' and 8' coal seams at Coal Mine Point can be correlated to the 12'5" and 1'6" coal seam in the Mabou-1 well, which can be tied to the D2 seismic reflector on the 1978 Mabou seismic survey. The D2 seismic reflector from the Mabou survey can be tied to the D2 reflector in the 1982 Chevron seismic survey, which can be tied to the 1985 Inverness seismic survey. From the Inverness survey, the seismic reflector can be correlated to the 7' coal seam at Inverness.

Onshore Correlation. A correlation of the onshore exposures of the Inverness Formation is shown on Figure 5.3.8. The correlation is constrained by both the palynological age dating and the seismic interpretation.

Regional Correlation of the Inverness and Port Hood Coal Seams

Although highly disrupted by salt tectonics, the Mabou-Inverness coal reflectors can also be recognised consistently within St. Georges Bay (see lines 75, 79 and 83). In addition, geophysical well correlations of coal intersections and seismic data from the Gulf of St. Lawrence indicate that the Inverness Formation coal measures extend beneath the present day Gulf of St. Lawrence as distinct coal seam reflector horizons (Hacquebard, 1986; Grant, 1994; Rehill, 1996).

5.4, CONGLOMERATE FACIES

At sporadic locations and stratigraphic levels, conglomerates form significant lithological units. While the conglomerates are volumetrically insignificant, they may be important indicators of halokinetic movement phases. The conglomerates are divided into three facies based upon their composition and sedimentological significance.

5.4.1, Red/Grey Polymict Conglomerate Facies

Examples: *the Finlay Point conglomerate (Figure 5.4.1), the grey/yellow conglomerate*

Figure 5.4.1. The Finlay Point Conglomerate exposed at Mabou Mines Harbor.

1. Lenses of coarser material which stand proud of the surrounding rock due to preferential cementation.

2. Stratification is poorly developed throughout the Finlay Point Conglomerate.

The planar feature in the top right of the photograph is interpreted to be an extensional fault which has been rotated through the vertical (counter clockwise as seen in photograph).

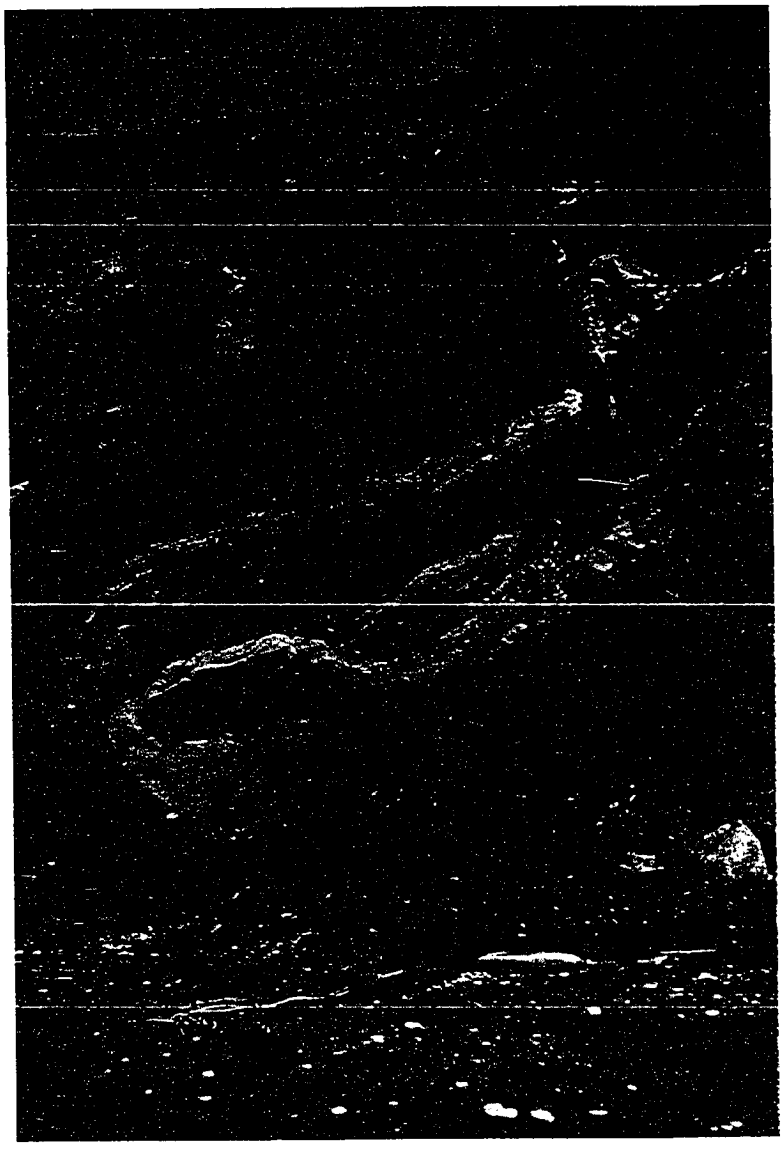

Figure 5.4.1

at Finlay Point North and the red conglomerates at Bruces Cove, Port Hood Island.

This conglomeratic facies is characterised by a red/purple or grey/yellow coloration and by the presence of basement clasts. The conglomerates are polymict, consisting of angular/sub-angular basement (mafic and granitic) clasts and sub-rounded to rounded Carboniferous sedimentary rock clasts. The proportion of basement to sedimentary clasts varies greatly, but in any one sample, basement and sedimentary clasts are always present. Size ranges from 0.5 to 4 cm for both basement and sedimentary clasts. The matrix of the conglomerates varies from coarse sand to red/green mud and the texture varies from clast to matrix supported, with poorly developed grading. Layering within the conglomerates is variable. In rare cases, distinct bedding planes can be defined, but most bedding planes are vague and laterally discontinuous (Figure 5.4.1). No cross-stratification or clast imbrication is present within the conglomerates. The lateral extent and the geometry of these conglomerates cannot be precisely defined because of the restriction imposed by cliff sections. However, the Finlay Point conglomerate can be traced for 300-400 m to the Finlay Point North section, which gives some indication as to scale. The thickness of the conglomeratic units is also hard to define. The Finlay Point conglomerate and Finlay Point North conglomerate are entirely fault-bounded and so their present thicknesses (20 m, Finlay Point conglomerate, and 4.5 m, Finlay Point North conglomerate) may not represent depositional thickness. The Bruces Cove conglomerate is only partially exposed at low tide beneath beach debris.

Interpretation. The red/grey polymict conglomerate facies are interpreted to be fault-scarp alluvial fan conglomerates deposited from stream and debris flows. The conglomerates were probably eroded off uplifted footwalls and deposited within hangingwall basins adjacent to fault scarps. This interpretation is supported by the composition of the conglomerates and by their geographic location with respect to known (or interpreted) fault locations. The Finlay Point conglomerate was interpreted in Chapter 3 to be located within the hangingwall of and adjacent to the paleo-fault scarp of a strand

of the Hollow Fault that lies to the east of the Finlay Point Diapir. In this location, the Finlay Point conglomerate would have been deposited within the hangingwall basin before it was forcefully intruded by the Finlay Point Diapir. The Mabou Highlands, located 1.5 km to the north, may possibly be the source of the basement clasts and the sedimentary clasts could have been derived from the Upper Carboniferous sedimentary rocks.

A similar 'fault scarp' scenario can be postulated for the red conglomerates exposed on Port Hood Island. The composition and texture of these conglomerates is similar to that of the Finlay Point conglomerate. The Port Hood Island conglomerate suggests the presence of a previously undetected basement fault located in the Port Hood area.

The rounded nature of the sedimentary clasts suggests that some transport has occurred, but the angular nature of the basement clasts suggests that the transport distance was relatively short (assuming the same source area for both clast groups). It is possible that, following deposition, some fluvial reworking of the conglomerates took place. Limited fluvial transport would have abraded the sedimentary clasts and may have produced the variable stratification and grading that typifies the conglomerates. Similarly, the lack of outsized clasts and the small clast size range implies some reworking and sorting of the sediments. Fluvial reworking could have taken the form of interaction with the prevailing braided fluvial system of the channel sandstone bodies or could have been an autocyclic process whereby fault scarp run-off through the conglomerate partially reworked the sediments. Similar fault-derived conglomerates that show evidence of partial fluvial re-working have been documented from the Lower Miocene Pickhandle Basin of the central Mojave Desert (Fillmore and Walker, 1996; Fillmore, 1993; Fillmore, pers. comm. 1996).

The stratigraphic level of the red/grey polymict conglomerates could give an indication of when the adjacent fault was active. Unfortunately for all of the red/grey polymict conglomerates, the stratigraphic position is only known approximately. The Finlay Point

and Finlay Point North conglomerates are in fault contact with Westphalian C-D strata and the oldest strata in the same sections are dated at Westphalian A. The stratigraphic age of the conglomerate (and hence fault movement) can therefore only be constrained to the Westphalian A to Westphalian C-D. The stratigraphic age of the Port Hood Island red/grey polymict conglomerate is also poorly constrained. The red strata are undatable (palynologically) although the overlying strata give a Westphalian B upper age constraint (see below, Chapter 3.5). The Port Hood Island red/grey polymict conglomerate could therefore be Namurian to Westphalian B in age, indicating Namurian to Westphalian B fault movement.

5.4.2, The Mega-Breccia Facies

Example. *The Mabou mega-breccia (Figure 5.4.2)*

The Mabou mega-breccia (informal name) is exposed for approximately 500 m at the back of Mabou Mines beach, between Finlay Point and Coal Mine Point. The Mabou mega-breccia is an uncemented polymict breccia that contains angular lithic fragments dominated by Windsor Group limestone clasts up to 15 cm in diameter, as well as mudstone and siltstone (up to 3 m in length) of unknown affinity, in a coarse arkosic sand matrix. Subordinate clasts consist of rounded granitic and mafic basement rocks up to 6 cm in diameter, as well as rare rounded quartz pebbles. The conglomerate unit shows little indication of stratification, grading and sorting and no imbrication was recognised.

The Mabou mega-breccia rests upon the Macumber Limestone with a highly tectonised contact. The contact between the Macumber Limestone and the Mabou mega-breccia is a west verging thrust (not shown). Therefore, the Mabou mega-breccia is inferred to be allochthonous and to have been deformed and translated as part of the post-Stephanian compressional event (see below, Chapter 3). The fact that the Mabou mega-breccia is deformed by the post-Stephanian deformation implies that the Mabou mega-breccia was deposited some time between the Visean (after the Macumber Limestone) and prior to

Figure 5.4.2. The Mabou mega-breccia exposed on Mabou Mines beach. The bulk of the breccia consists of coarse sand matrix which surrounds blocks of sedimentary rock up to 3m in length. The blocks consist of sandstone, mudstone and limestone lithologies.

1. A 3m long sandstone block (center of photograph) and a fragmented sandstone block (center left of photograph).

2. Clasts of Windsor Group limestone which are approximately 25cm in diameter. Similar clasts can be found on the beach where wave action has separated the limestone clasts from the sand matrix.

3. The grey bed at the base of the photograph may be part of the Macumber Limestone that has been faulted into the breccia during the post-Carboniferous compression (see Chapter 2).

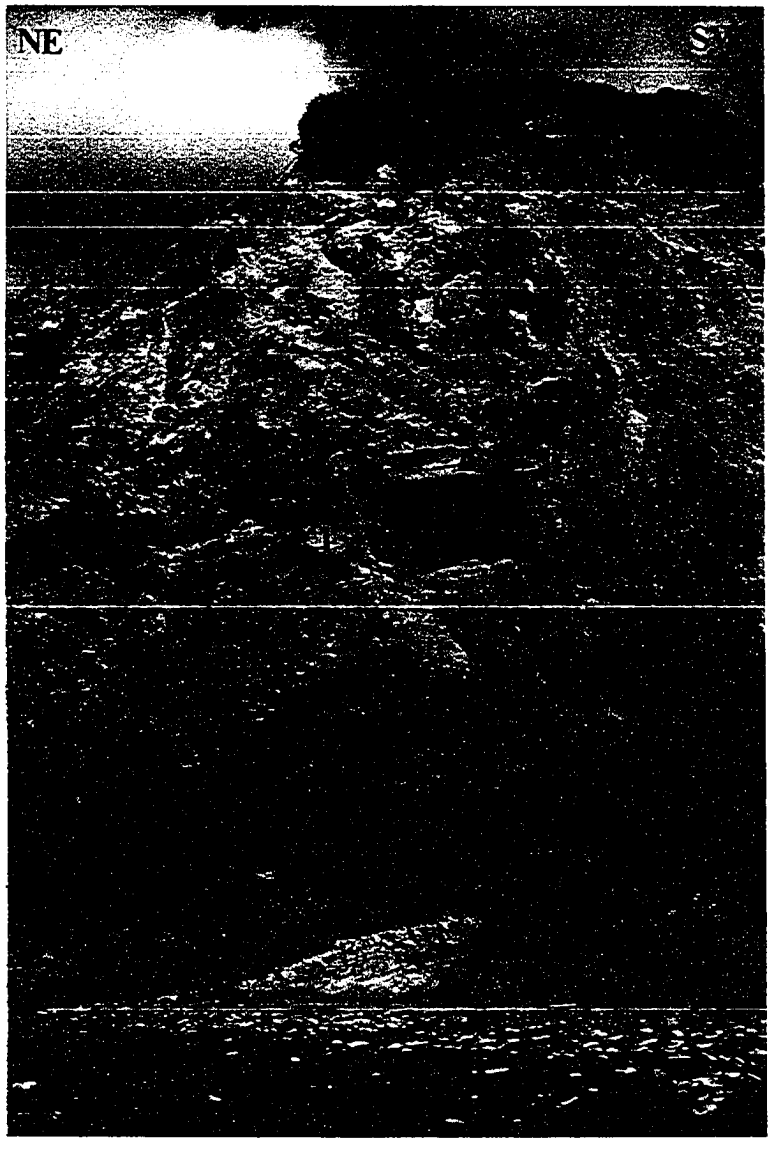

Figure 5.4.2

the post-Stephanian deformation. Palynological dating of the mega-breccia is not possible and since no other stratigraphic information is available, the precise age of the Mabou mega-breccia cannot be established.

Interpretation. The Mabou mega-breccia is interpreted to be either the remnant of a collapse breccia related to dissolution of the Lower Windsor halite or a catastrophic alluvial fan sourced from erosion of a diapir. Three scenarios are postulated for the evolution of the Mabou mega-breccia.

(i) Fault Model

The Mabou mega-breccia may be located within the footwall of the Hollow Fault (see above, Chapter 3). Footwall uplift during the Carboniferous on this fault or a related fault followed by erosion could have resulted in exposure of the Lower Windsor strata. Percolating groundwater would rapidly have dissolved the Lower Windsor halite, resulting in dissolution collapse of the overlying gypsum/mudstone sequence. The Mabou mega-breccia might therefore be related to fault-induced erosion, dissolution and collapse. This interpretation complements the present stratigraphic location of the Mabou mega-breccia, which rests upon the Macumber Limestone. The strataform halite of the Lower Windsor lies stratigraphically on top of the Macumber Limestone (Boehner 1983). Dissolution of the halite followed by collapse would place the breccia directly on top of the Macumber Limestone. However, the Mabou mega-breccia is at present an allochthonous unit and so its stratigraphic relationship to the Macumber Limestone is not well constrained.

The composition of the Mabou mega-breccia corresponds to the composition of the Lower Windsor Group and the overlying Upper Carboniferous sedimentary rocks. The high concentration of Windsor Group limestone clasts and the coarse sand matrix of the Mabou mega-breccia imply that the Middle Windsor Group, Hood Island Formation and some overlying Upper Carboniferous clastic formations were involved in the 'collapse'.

This model might also explain the presence of basement clasts within the breccia, since basement units would also be uplifted in the footwall of the fault.

(ii) Diapir Model

The South-West Mabou Diapir (Haites, 1952; Howie, 1988) is located 4 km to the south-east of Mabou Mines beach (see above, Chapter 3). Vertical growth of the South-West Mabou Diapir could have exposed Hood Island - Middle Windsor strata of the structural carapace as well as adjacent uplifted Carboniferous sedimentary rocks. Rapid erosion of the topographic high could have resulted in a collapse breccia or a catastrophic debris flow, especially if the underlying halite core was dissolved by groundwater. The clasts would have been transported away from the diapir, perhaps to a distance of only a few kilometres. Similar erosional products of diapirs are described from the Great Kavir Salt Basin of Iran (Jackson et al., 1990), where emergent diapirs and their adjacent overburden are eroded to form peripheral fan deltas or piedmont sediments between diapiric structures.

The composition of the Mabou mega-breccia is consistent with the composition of sediments that are exposed today within diapir cap rocks and overburden sediments in western Cape Breton. Erosion of a Windsor Group diapir carapace would result in dissolution of the gypsum and fragmentation of the Windsor limestone. Brecciation would be enhanced if halite dissolution resulted in collapse of the overlying strata. Erosion of uplifted Mabou Group, Port Hood Formation or Inverness Formation overburden sediments would supply medium to coarse sand matrix as well as the siltstone/mudstone clasts associated with the mega-breccia. The overall angular nature of the clasts and the presence of large blocks of siltstone imply a short transport distance and so a local source for the conglomerate is appropriate. The poor sorting, lack of stratification, lack of grading and the presence of large blocks of strata suggest a disordered transport mechanism, possibly a debris flow.

At the present level of erosion, the Lower Windsor is exposed over the location of the South-West Mabou Diapir. This implies that the carapace has been eroded to expose the gypsum and halite of the Lower Windsor. The timing of erosion can only be inferred, but could have been associated with diapir growth. If this is the case, much dissolution and collapse would have occurred between the Namurian and Stephanian.

(iii) Salt Glacier Moraine

The Mabou mega-breccia could be the remnant of a salt glacier – a glacial moraine. If a diapir grew to a point where the Lower Windsor halite was extruded onto the surface, the halite would tend to move away from the diapir as a salt glacier, taking advantage of the local topography. As well as halite, the salt glacier would consist of various overburden and carapace rocks that have either foundered into the halite or been entrained from the surrounding overburden. The halite within the salt glacier would be undergoing dissolution at surface and so at some point the halite would be completely dissolved, leaving the insoluble material as a moraine. At present, the Lower Windsor is exposed at surface in the South-West Mabou Diapir. This is therefore a potential source of extruded salt.

All three models can account for the timing, composition and sedimentary architecture of the Mabou mega-breccia since all of the models involve erosion of the Windsor group strata and adjacent clastic overburden. There is currently no obvious way to prove one model over the other and so the origin of the Mabou mega-breccia remains speculative. A breccia at a similar stratigraphic level (Pembroke Breccia) described from the Bay of Fundy has been attributed to evaporite solution collapse (Clifton, 1967).

5.4.3, Oligomict Conglomerate Facies

Examples. *The limestone conglomerates at Bruces Cove, Port Hood Island (see Figure 5.4.3, Chapter.3).*

Figure 5.4.3. A conglomerate exposed at Bruces Cove, Port Hood Island which is an example of the Oligomict Conglomerate facies. The conglomerate is moderately well sorted and rests upon a red mudstone (possible paleosol) horizon. All clasts seen are of Middle or Upper Windsor Group limestone. The conglomerate is clast supported and is almost devoid of interstitial matrix material.

(Lens cap is 52mm in diameter).

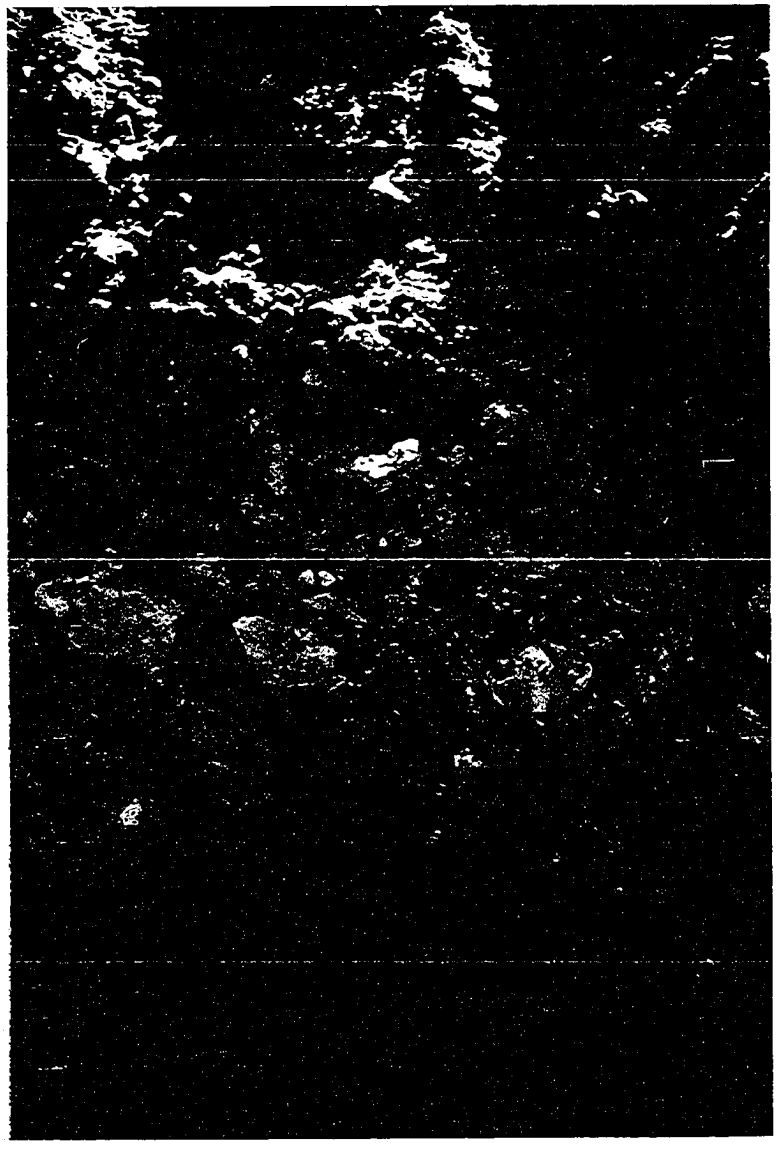

Figure 5.4.3

The oligomict conglomerate facies are distinguished by the dominance of Hood Island Formation limestone clasts, which comprise some 70-90% of the clasts, and by the absence of basement clasts. Subordinate clasts consist of siltstone, sandstone and mudstone. The limestone clasts are rounded to sub-rounded and range in size from 2-45 cm. Within individual conglomerate units, normal grading is well developed and interstitial mud and silt are virtually absent. Two conglomerate units are exposed that are up to 2.5 m thick and are located stratigraphically within the buff sandstones and red mudstones above the unconformity surface exposed at Bruces Cove, Port Hood Island (see above, Chapter 3). Their lateral extent and geometry is hard to determine within the cliff sections, although the conglomerate units appear to taper laterally, suggesting a lensoid geometry. The base of each conglomeratic unit may be erosional, as individual clasts are inset into the underlying mudstone, although this could be purely a loading feature. No shear zone or evidence of dynamic grain-size reduction was noted beneath the conglomerates to indicate a rock avalanche or debris flow.

Interpretation. The oligomict conglomerates are interpreted to be the product of fluvially reworked diapir cap rock material or cap rock collapse breccia. Erosion of the Middle Windsor Group-Hood Island Formation and weathering by fluvial processes could have lead to erosion of the soft gypsum and separation of the argillaceous mudstone from the limestone breccia by winnowing during transport. The limestone breccia clasts could have become rounded during bedload transport before being deposited as an oligomict conglomerate largely devoid of fines. The excellent grading of the conglomerates at Bruces Cove and their proximity to Westphalian B channel sandstones suggests that fluvial transport was involved.

The proximity of the conglomerates exposed at Bruces Cove, Port Hood Island, to the Port Hood Island Diapir suggests a genetic link between diapir and conglomerate as well as providing the most logical mechanism to bring the Hood Island Formation limestones to surface during the Westphalian B.

If the oligomict conglomerates are the product of reworked diapir material, then the stratigraphic position of the conglomerate gives an indication of when the adjacent diapir was exposed at surface. In the case of the conglomerate at Bruces Cove, Port Hood Island, the conglomerate indicates that the diapir was at surface and undergoing erosion during the Westphalian B.

5.5, PALEOCURRENT DATA

The paleocurrent data presented below (Table 5.5.1) were collected almost exclusively from the channel sandstone bodies of the Inverness Formation. In all but a few cases, the recordings were taken from trough cross-stratified sandstones exposed on wave-cut platforms at low tide (Figure 5.5.1). Where possible, paleocurrent data were tied to specific sandstone units. This rigorous approach was undertaken in order to assess the variability of paleocurrent direction (i) between individual sandstone units within a larger sandstone storey and (ii) between channel sandstone bodies. This analysis was conducted to detect any unusual paleocurrent changes that might reflect the effects of salt withdrawal/diapirism or fault movement upon sediment transport. A small number of paleocurrent data were collected from the Port Hood Formation at Port Hood. Keighley (1996) published paleocurrent data from the same section. Keighley's data was not incorporated with the data presented, as it was not known how the data was collected.

Paleocurrent Orientation

(Table 5.5.1 shows the paleocurrent data set, n = 128)

St. Rose. (n = 10). Paleocurrent data from St. Rose could only be recorded from the thick channel sandstones at MacLeods Beach that are part of the Colindale Member of the Port Hood Formation (Westphalian A). The paleocurrents show a wide spread with a poorly defined east-west trend and a dominant south-east trend (Figure 5.5.2). Paleocurrent orientations were relatively consistent within individual sandstone units, but switched

Paleocurrent	Indicator	Lithology	Location
117	Trough	M.S	Inverness.
95	Trough	M.S	Inverness.
97	Trough	M.S	Inverness.
120	Trough	M.S	Inverness.
319	Trough	M.S	Inverness.
346	Trough	M.S	Inverness.
313	Trough	M.S	Inverness.
357	Trough	M.S	Inverness.
317	Trough	M.S	Inverness.
321	Trough	M.S	Inverness.
310	Trough	M.S	Inverness.
310	Trough	M.S	Inverness.
340	Trough	M.S	Inverness.
354	Trough	M.S	Inverness.
168	Trough	M.S	McKinnons B.West
188	Trough	M.S	McKinnons B.West
238	Trough	M.S	McKinnons B.West
95	Trough	M.S	McKinnons B.West
27	Trough	M.S	McKinnons B.West
275	Trough	M.S	McKinnons B.West
21	Trough	M.S	McKinnons B.West
72	Trough	M.S	McKinnons B.West
68	Trough	M.S	McKinnons B.West
65	Trough	M.S	McKinnons B.West
18	Trough	M.S	Port Hood
205	Trough	M.S	Port Hood
11	Ripple	F.S	Port Hood
110	Trough	M.S	Port Hood
310	Ripple	F.S	Port Hood
298	Ripple	F.S	Port Hood
29	Trough	M.S	Port Hood
302	Trough	M.S	Port Hood
326	Trough	M.S	Port Hood
16	Trough	M.S	Port Hood
110	Trough	M.S	McKinnons B.East
23	Trough	M.S	McKinnons B.East
105	Trough	M.S	McKinnons B.East
84	Trough	M.S	McKinnons B.East
15	Trough	M.S	McKinnons B.East
316	Trough	M.S	McKinnons B.East
62	Trough	M.S	McKinnons B.East
45	Trough	M.S	McKinnons B.East
88	Trough	M.S	McKinnons B.East
128	Trough	M.S	McKinnons B.East
192	Trough	M.S	McKinnons B.East
215	Trough	M.S	McKinnons B.East
92	Trough	M.S	McKinnons B.East
145	Trough	M.S	McKinnons B.East
81	Trough	M.S	McKinnons B.East
285	Trough	M.S	St. Rose
300	Trough	M.S	St. Rose
210	Trough	M.S	St. Rose
145	Trough	M.S	St. Rose
140	Trough	M.S	St. Rose
147	Trough	M.S	St. Rose
40	Trough	M.S	St. Rose
60	Trough	M.S	St. Rose
110	Trough	M.S	St. Rose
90	Trough	M.S	St. Rose
81	Trough	M.S	Coal Mine Point
99	Trough	M.S	Coal Mine Point
105	Trough	M.S	Coal Mine Point

Table 5.5.1. Paleocurrent Data

Paleocurrent	Indicator	Lithology	Location
93	Trough	M.S	Finlay Point
67	Trough	M.S	Finlay Point
87	Trough	M.S	Finlay Point
190	Trough	M.S	Finlay Point
101	Trough	M.S	Finlay Point
85	Trough	M.S	Finlay Point
64	Trough	M.S	Finlay Point
64	Trough	M.S	Finlay Point
43	Trough	M.S	Finlay Point
62	Trough	M.S	Finlay Point
363	Trough	M.S	Finlay Point
245	Trough	M.S	Finlay Point
155	Trough	M.S	Finlay Point
235	Trough	M.S	Finlay Point
158	Trough	M.S	Finlay Point
76	Trough	M.S	Finlay Point
207	Trough	M.S	Finlay Point
137	Trough	M.S	Inverness.
140	Trough	M.S	Inverness.
8	Trough	M.S	Inverness.
172	Trough	M.S	Inverness.
125	Trough	M.S	Inverness.
45	Flute	Siltstone	Inverness.
63	Ripple	Siltstone	Inverness.
69	Trough	M.S	Inverness.
68	Trough	M.S	Inverness.
52	Trough	M.S	Inverness.
50	Trough	M.S	Inverness.
37	Trough	M.S	Inverness.
46	Trough	M.S	Inverness.
34	Trough	M.S	Inverness.
58	Trough	M.S	Inverness.
142	Trough	M.S	Inverness.
168	Trough	M.S	Inverness.
53	Trough	M.S	Inverness.
72	Trough	M.S	Inverness.
63	Trough	M.S	Inverness.
83	Trough	M.S	Inverness.
82	Trough	M.S	Inverness.
82	Trough	M.S	Inverness.
70	Trough	M.S	Inverness.
81	Trough	M.S	Inverness.
354	ripple	M.S	Inverness.
60	Trough	M.S	Inverness.
88	Trough	M.S	Inverness.
61	Trough	M.S	Inverness.
87	Trough	M.S	Inverness.
180	Ripple	F.S	Inverness.
69	Trough	M.S	Inverness.
81	Trough	M.S	Inverness.
60	Trough	M.S	Inverness.
95	Trough	M.S	Inverness.
63	Trough	M.S	Inverness.
45	Trough	M.S	Inverness.
93	Trough	M.S	Inverness.
46	Ripple	F.S	Inverness.
100	Trough	M.S	Inverness.
119	Trough	M.S	Inverness.
100	Trough	M.S	Inverness.
125	Trough	M.S	Inverness.
45	Trough	M.S	Inverness.
119	Trough	M.S	Inverness.
72	Trough	M.S	Inverness.
73	Trough	M.S	Inverness.
150	Trough	M.S	Inverness.
125	Trough	M.S	Inverness.

Table 5.5.1. Paleocurrent Data.

Figure 5.5.1. Trough cross-stratified sandstone within a channel sandstone unit of the Inverness Formation. Paleocurrent direction is into the photograph.

(Lens cap 5.2cm diameter).

Figure 5.5.1

All Paleocurrent Data

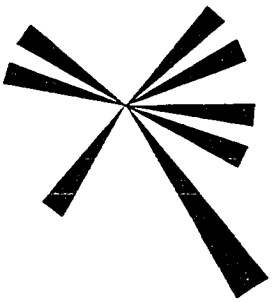

St. Rose

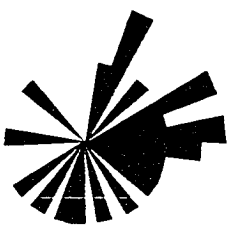

MacKinnons Brook

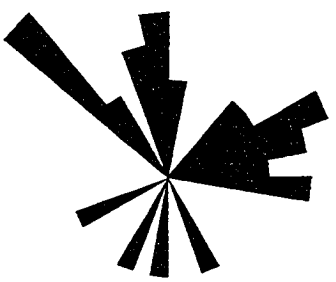

Finlay point and Coal Mine Point

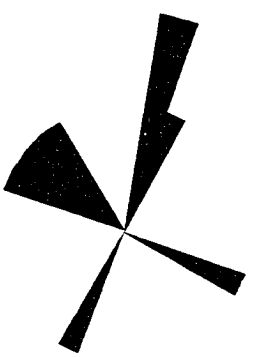

Port Hood

Figure 5.5.2. Paleocurrent Data

orientation between larger channelised sandstone bodies.

MacKinnon's Brook. (n=25). The MacKinnon's Brook section is split into the MacKinnon's Brook East and West sections. However, evidence indicates that the two sections are equivalent. For this reason, the paleocurrent data are presented as a single rose diagram. Paleocurrent orientations show a wide spread from north-east to north-west with a dominant direction towards the north-east and east (Figure 5.5.2). Access at MacKinnon's Brook was poor, so paleocurrents could not be tied to individual sandstone units.

Finlay Point and Coal Mine Point (n=17 and 3). Paleocurrent orientation from Finlay Point and Coal Mine Point shows a division into three main trends: north-east/east, north and north-west. A subordinate trend lies within the south-east/south-west sector (Figure 5.5.2). Paleocurrents were noted to be fairly consistent within sandstone units, with more dramatic changes taking place between the larger sandstone bodies, e.g. the Eagle and Stack Sandstones (Keating, 1950).

Inverness Shore Section (Inverness Harbour to Port Ban). (n = 81). The Inverness shore section provided the most extensive paleocurrent data set. In all cases, the paleocurrent data could be tied to a specific sandbody and, for sandbody 13 (see Figure 5.1.9), the paleocurrents could be tied to individual sandstone units (Table 5.5.2). This was possible because of the orientation of the coastline/sandbody, which exposes a 3 km strike section with an adjacent wave cut platform.

(Figure 5.5.3 shows paleocurrent rose diagrams for individual sandbodies and sandstone units).

Sandbody 1. (n = 6) Paleocurrents are confined to trends ranging from north to south in the eastern sector (Figure 5.5.3). Within this sector, there is no preferred orientation and

Sandstone Body.	Sandstone Unit	Paleocurrent	Bedform	Lithology	Location	Sandstone Body.	Sandstone Unit	Paleocurrent	Bedform	Lithology	Location
1	(i)	137	Trough	M.S	Inverness.	13	(iii)	69	Trough	M.S	Inverness.
1	(i)	140	Trough	M.S	Inverness.	13	(iv)	81	Trough	M.S	Inverness.
1	(i)	8	Trough	M.S	Inverness.	13	(iv)	60	Trough	M.S	Inverness.
1	(i)	172	Trough	M.S	Inverness.	13	(iv)	95	Trough	M.S	Inverness.
1	(i)	125	Trough	M.S	Inverness.	13	(v)	63	Trough	M.S	Inverness.
1	(ii)	45	Flute	Siltstone	Inverness.	13	(vi)	45	Planar	M.S	Inverness.
1	(ii)	63	Ripple	Siltstone	Inverness.	13	(vi)	93	Trough	M.S	Inverness.
6	(i)	69	Trough	M.S	Inverness.	13	(vi)	46	Ripple	F.S	Inverness.
6	(i)	68	Trough	M.S	Inverness.	13	(vi)	100	Trough	M.S	Inverness.
6	(i)	52	Trough	M.S	Inverness.	13	(vi)	119	Trough	M.S	Inverness.
6	(i)	50	Trough	M.S	Inverness.	13	(vi)	100	Trough	M.S	Inverness.
11	(i)	37	Trough	M.S	Inverness.	13	(vi)	45	Trough	M.S	Inverness.
11	(i)	46	Trough	M.S	Inverness.	13	(vi)	119	Trough	M.S	Inverness.
11	(i)	34	Trough	M.S	Inverness.	13	(vi)	72	Trough	M.S	Inverness.
11	(i)	58	Trough	M.S	Inverness.	13	(vi)	73	Trough	M.S	Inverness.
11	(ii)	142	Trough	M.S	Inverness.	13	(vi)	150	Trough	M.S	Inverness.
11	(ii)	168	Trough	M.S	Inverness.	13	(vi)	125	Trough	M.S	Inverness.
13	(i)	53	Trough	M.S	Inverness.	13	(vi)	117	Trough	M.S	Inverness.
13	(i)	72	Trough	M.S	Inverness.	13	(vii)	95	Trough	M.S	Inverness.
13	(i)	63	Trough	M.S	Inverness.	13	(vii)	97	Trough	M.S	Inverness.
13	(i)	83	Trough	M.S	Inverness.	13	(viii)	120	Trough	M.S	Inverness.
13	(i)	82	Trough	M.S	Inverness.	13	(ix)	319	Trough	M.S	Inverness.
13	(i)	82	Trough	M.S	Inverness.	13	(ix)	346	Trough	M.S	Inverness.
13	(i)	70	Trough	M.S	Inverness.	13	(ix)	313	Trough	M.S	Inverness.
13	(i)	81	Trough	M.S	Inverness.	13	(ix)	357	Trough	M.S	Inverness.
13	(i)	354	ripple	M.S	Inverness.	13	(ix)	317	Trough	M.S	Inverness.
13	(i)	60	Trough	M.S	Inverness.	13	(ix)	321	Trough	M.S	Inverness.
13	(i)	88	Trough	M.S	Inverness.	13	(ix)	310	Trough	M.S	Inverness.
13	(i)	61	Trough	M.S	Inverness.	13	(ix)	310	Trough	M.S	Inverness.
13	(i)	87	Trough	M.S	Inverness.	13	(ix)	340	Trough	M.S	Inverness.
13	(ii)	180	Ripple	F.S	Inverness.	13	(ix)	354	Trough	M.S	Inverness.

Table 5.5.3, Paleocurrent Data from the Inverness Shore Section.

All Inverness Shore Section Data

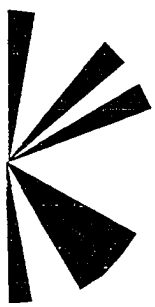

Inverness Shore Section, Sandstone Unit 1

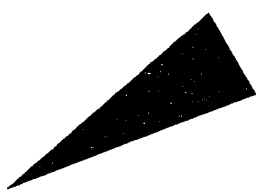

Inverness Shore Section, Sandstone Unit 6

Inverness Shore Section, Sandstone Unit 11

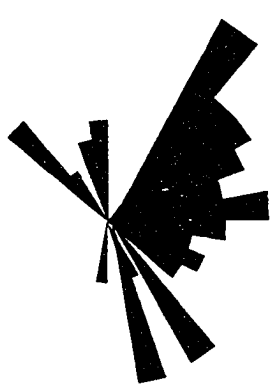

Inverness Shore Section 13

Figure 5.5.3. Paleocurrent Data for the Inverness Shore Section.

dramatic paleocurrent changes of up to 130 degrees were noted between vertically adjacent sandstone units.

Sandbody 6. (n = 4) All paleocurrents were orientated towards the north-east.

Sandbody 11. (n = 6). The dominant orientation is towards the east-north-east with a subordinate south-east orientated set.

Sandbody 13. (n = 62) As a whole, the dominant orientation is towards the north-east sector, which accounts for approximately 68% of the paleocurrent data. The subordinate orientation is towards the north-north-west and south-east, which accounts for approximately 25% of the paleocurrent data. For sandbody 13, the paleocurrents could be precisely tied to individual sandstone units or stacked sandstone units (see above, Chapter 5). Approximately 60% of the paleocurrent data were recorded from three stacked sandstone units with the remaining 40% coming from intercalated sandstone units. Within individual sandstone units and sandstone storeys, the paleocurrent data are relatively consistent with only a 35-53 degree range, while between vertically adjacent sandstone units/stacked sandstone units, the paleocurrent generally changes by 30-100 degrees. Two extreme paleocurrent changes of 130 and 150 degrees were recorded between vertically adjacent sandstone units.

Interpretation. By tying the paleocurrents to specific sandstone bodies, stacked sandstone units (storeys) and individual sandstone units, a high resolution paleocurrent evolution can be determined. The bulk of the data set (84%) was recorded from the Inverness Formation channel sandstone bodies (Westphalian C - Stephanian) and the remainder was recorded from the Colindale Member of the Port Hood Formation (Westphalian A). Taken as a whole, the paleocurrent data indicate that the dominant paleocurrent orientation was towards the north-east and east throughout the Westphalian A and Westphalian C - Stephanian. There is no strong subsidiary orientation but rather

the paleocurrents box the compass. Where paleocurrents could be tied to specific sandstone units (Inverness shore section - sandbody 13), the paleocurrents within an individual sandstone unit showed a moderate range (35-53 degrees) whereas between vertically adjacent sandstone units changes of up to 150 degrees were common.

Discussion. The 35-53 degree paleocurrent range for individual sandstone units is similar to the range associated with both modern and ancient braided fluvial systems. Miall (1976) reported a paleocurrent range of 41-61 degrees within individual braided channel sandbodies (probably equivalent to stacked sandstone units) for Cretaceous braided channel sandstones of Banks Island, Arctic Canada, and Williams and Rust (1969) reported a mean 40 degree paleocurrent range for the low sinuosity, braided Donjek river of the Yukon Territory. The modern Brahmaputra river of Bangladesh has an in-channel paleocurrent range of 15-112 degrees with an average range of approximately 50 degrees (Coleman, 1969).

The dominant north-east/east paleocurrent orientation may reflect the effects of the Hollow Fault. Figure 5.5.2 shows inferred positions of the Hollow Fault strands and the position of known diapiric structures. The Hollow Fault was probably active during the Namurian-Stephanian and would therefore have affected sediment transport by creating hangingwall basins as well as sediment barriers behind the uplifted footwalls. Modern and ancient examples of major faults controlling drainage patterns include Miall (1976).

The dominant north-east/east paleocurrent direction is in accordance with a regional paleocurrent analysis of Westphalian B to Early Permian strata of Atlantic Canada (Gibling et al., 1992). Gibling et al. (1992) suggested that the dominant paleocurrent direction for the Maritimes region during this period was towards the north-east, following the strike of Appalachian structural lineaments. The north-east/east paleocurrent orientation from western Cape Breton, following the path of the Hollow Fault, is in accord with this regional study.

Additionally, diapir growth and salt withdrawal occurred throughout the Upper Carboniferous (Westphalian A/B - Stephanian) (see above, Chapter 2) and these diapiric structures may have had some control upon paleocurrents. An active diapir will usually create a domal structure within the overlying overburden during growth. Passive diapirs may create a topographic high due to the diapir growing above the surrounding surface (Jackson et al., 1990; Davison et al., 1993; Schultz-Ela et al., 1993; and Hoyos et al., 1996). Diapir-related topography can act as local sediment barriers, diverting flow around the dome and providing a local sediment source area for conglomeratic debris flows. Some of the conglomeratic units described earlier in this chapter are interpreted to be the product of re-worked diapir material, e.g. the grey oligomict conglomerate exposed at Bruces Cove, Port Hood Island. This interpretation supports the hypothesis that diapirs were affecting sedimentation during the Carboniferous. It is likely that some of the subsidiary paleocurrent directions and the rapid shifting of paleocurrents noted within vertically adjacent sandstone units are due to salt movement. The rise of diapirs during compression may be episodic (Vendeville and Nilsen, 1995), which may lead to episodic creation of relief and hence deflection of paleocurrents from the regional trend. Further evidence to support this argument is presented below in the section dealing with seismic facies analysis. The effect of salt diapirism for an individual diapir is usually a second order control superimposed upon the first order control (in this case, the Hollow Fault). The deflection of fluvial channels by salt diapirs in the modern environment is evident from satellite images and aerial photographs, e.g. Jackson et al. (1990).

The subordinate paleoflow may also be related to sediment supply from local basement massif areas within western Cape Breton, e.g. the Mabou Highlands and the Creignish Highlands. The Inverness shore section is located between Gillis Mountain and the northern end of the Mabou Highlands. This paleotopographic flow would therefore have been a natural fluvial conduit from inland Cape Breton and the Maritimes Basin. Similarly, the Mabou Mines and Port Hood area is located adjacent to the southern end of

the Mabou Highlands with the Creignish highlands 10 km to the north-east. Erosion of these basement massifs could have supplied sediments that were transported northwards into the Maritimes Basin through the Mabou-Port Hood area.

5.6, SEISMIC FACIES ANALYSIS

Introduction

Seismic facies analysis attempts to derive sedimentological information from packages of seismic reflection data. Information is derived from interpretation of reflector geometry, amplitude, continuity and the overall reflector characteristics within a package of reflectors. Typical information that can be obtained from seismic facies analysis concerns sediment transport direction, lithological information and sedimentary architecture. The method cannot be used in place of traditional sedimentology for the simple reason that the average seismic reflector represents approximately 30-50 m of geologic strata. Seismic facies analysis and sedimentology are therefore different analytical tools and should not be confused. However, if sedimentological analysis has already defined an accurate depositional environment for the strata in question, then seismic facies analysis becomes a powerful tool for obtaining relatively large scale information that may not be obvious at outcrop scale.

5.6.1, Seismic Facies, Western Cape Breton

As part of the project, seismic facies analysis was primarily used to evaluate the sediment transport and sedimentary architecture of the Inverness Formation. Seismic facies analysis was therefore a logical and useful addition to the onshore sedimentology and paleocurrent data. The technique was most rigorously applied to the 1978 Mabou seismic survey, since this is the highest resolution/quality data set. The 1985 Inverness seismic survey is of poorer quality and seismic facies could not be defined using this data. Unexpected seismic facies were imaged by the 1982 Chevron seismic survey and these provided

valuable information concerning basin dynamics as well as the movement history of certain diapirs.

5.6.2, Seismic Data Processing

In order to improve the resolution and "interpretability" of the 1978 Mabou survey, line 9 was re-processed at the Lithoprobe Data Processing Centre at the University of Calgary. The original data processing dominantly imaged the low frequency signal produced by the Inverness Formation coal seam reflectors (D1-D3) (see above, Chapter 5). In addition, severe seabed multiples and interbed multiples obscured the true reflected signal within the top 500 ms of the seismic record. Data re-processing successfully removed the majority of seabed multiples and reduced the random noise within the data considerably (see Appendix 2 for data processing parameters). The re-processed line 9 was used as a template to interpret the remaining lines so that it was largely possible to interpret through the seabed and interbed multiples contained within the remaining 15 lines.

The results of reprocessing can be seen by comparing the original Mabou line 9 and the reprocessed line, which are included in the enclosures section of this thesis.

5.6.3, Seismic Facies, the 1978 Mabou Survey

Line 9 (re-processed).

Within the time interval interpreted to represent the Inverness Formation, line 9 contains multiple pinch out and downlap terminations of high amplitude/moderate coherency reflectors located between 250-400 ms (see Seismic Stratigraphy, Chapter 5), 10000-11000 common depth points (CDP). Additional downlap terminations of high amplitude/moderate coherency reflectors are located between 350-450 ms, 1000-4500 CDP. Above 350 ms, the reflectors are parallel and continuous and do not show downlap or pinch out terminations.

The same features can be recognised on the original line 9, although the presence of

seabed and interbed multiples makes interpretation harder.

Lines 2-8 and 11-16

The remaining un-reprocessed lines were interpreted in light of the seismic facies imaged on the re-processed line 9. The interpreted seismic facies are shown in the enclosures section. Lines 10 and 1 are of very poor quality and no attempt was made to define seismic facies from these lines. Lines 2-8 and 11-16 contain few reliable seismic facies reflectors. Some downlap and rare pinch-out terminations were interpreted, but the majority of these were obscured by high amplitude multiples.

Interpretation. Although the seismic facies are not well imaged (except on the re-processed line), they are nevertheless significant. On the re-processed line 9, the pinch-out reflector terminations are all located within the uplifted and folded drag zone strata associated with the Finlay Point and Sight Point diapirs. This relationship can be interpreted to represent possible syn-kinematic sedimentation on an actively deforming stratal base. As the Finlay Point Diapir and Sight Point Diapir intruded the overburden, the overburden was uplifted. The resulting topography may have affected the prevailing sedimentary system, causing pinch out of the syn-kinematic sediments against the emerging topographic high. The downlap reflector terminations all downlap away from the diapirs, suggesting progradation of sedimentary packages away from the diapirs. Examples of similar progradational synkinematic sedimentation are numerous in the literature, for example Jackson et al. (1990) described piedmont and alluvial fan deposits that were sourced from diapiric structures. Possible examples of synkinematic, diapir-related alluvial sediments from western Cape Breton have also been described, for example the grey, oligomict conglomerate located at Bruces Cove, Port Hood Island (see above, Chapter 5).

All the seismic facies are located within a common time horizon of 250-400 ms over the area of the Mabou seismic grid. This implies that both sediment pinch out and

progradation were occurring penecontemporaneously. The seismic facies show an overall westward sediment transport away from the region that includes the Finlay Point Diapir, Sight Point Diapir and Coal Mine Point Diapir. The combined uplift effects of these diapirs may have resulted in an ephemeral topographic high. The folded nature of the drag zone strata observed on-shore and imaged on seismic data support this suggestion. Outside of the drag zone and away from the diapir, salt withdrawal may have resulted in accelerated subsidence of the Carboniferous strata. The combination of uplift and subsidence could have produced a shallow mini-basin located between the three diapiric structures. The mini-basin would have been in a favourable position to accumulate diapir-derived material that would have been eroded from the diapir topographic high.

5.6.4, Correlation with Onshore Sedimentology

Although the westward sediment transport direction derived from the seismic facies analysis corresponds to one of the major sediment transport directions derived from the on-shore paleocurrent data, it would be inappropriate to tie the two data sets together directly. The on-shore paleocurrent data were recorded from metre-scale sets of trough cross-stratified sandstone, whereas the seismic facies analysis sediment transport direction was recorded from reflectors interpreted to be fluvial and/or alluvial sediments. Furthermore, the time interval over which the seismic facies were interpreted is not exposed on shore as they have all been uplifted and eroded due to diapir growth (see Mabou line 4, Enclosures section).

The seismic facies analysis interpretation does indicate that the Finlay Point Diapir, Sight Point Diapir and Coal Mine Point Diapir were growing during deposition of the 250-400 ms time interval and that the growth of these diapirs affected the sedimentary architecture of the synkinematic sediments of the Inverness Formation. The creation of a mini-basin would represent a short-lived perturbation of the dominant sediment transport direction that was probably related to the effects of the Hollow Fault and the development of the Gulf of St. Lawrence Basin (see above, Chapter 5).

5.6.5, Seismic Facies, 1982 Chevron Data

The Gillis Fan

On lines 63, 55, 51 and 47 a package of high/moderate amplitude reflectors defines a large, convex upward wedge that tapers towards the west. The wedge has a maximum thickness of 500 ms (~500 m after depth conversion) and a maximum horizontal length of approximately 12 km. The westernmost reflectors appear to downlap onto older strata, suggesting that these reflectors represent progradational surfaces. In plan view, the wedge has a semi-circular shape that extends off the north-east end of the 1982 Chevron seismic coverage. Extrapolation of the plan view as a semi-circle indicates an approximate surface area of 150 km^2 centred on the town of Inverness.

Interpretation. The wedge of reflectors is interpreted to represent a large alluvial fan or clastic wedge that may have resulted from erosion of an emergent diapir in a similar way to the Mabou mega-breccia (see above, Chapter 5). The Gillis Fan is positioned directly between Gillis Mountain and the Mabou Highlands. These two basement massifs are likely to have been Carboniferous highs and so the Gillis Fan is positioned at the mouth of a possible Carboniferous paleovalley. In addition, a segment of the Hollow Fault is inferred to be located close to the town of Inverness and so the Gillis Fan could be a thick fault-scarp breccia. Examples of coarse clastic material associated with movement of the Hollow Fault are exposed near Antigonish, Nova Scotia (Fralick and Schenk, 1981).

The stratigraphic position of the Gillis Fan is equivalent to the 2R seismic reflector and therefore it is also assigned to the early Namurian.

Chevron Survey, Line 71

At approximately 1.0 sec TWT, between shot points 260-320, three high-amplitude reflectors define a shallow, concave upward wedge. The wedge is truncated by the right hand edge of the Salt Wall Luey.

Interpretation. The reflector package is interpreted to represent either a secondary or tertiary rim-syncline. Rim-synclines are associated with salt withdrawal from the source layer into the diapir, producing subsidence of the surrounding strata and thickening of syn-kinematic sediments. The presence of a rim syncline within the Mabou Group strata implies that diapirism was occurring during Mabou Group deposition (Namurian).

Chevron Survey, Line 71

At 400-600 ms between shot points 240-340, a package of high amplitude, low coherency reflectors define a flat-bottomed, convex upwards wedge tapering towards the west. All of the reflectors dip westwards and the Inverness coal seam reflectors have been folded into a shallow syncline over the western end of the wedge.

Interpretation. The wedge of reflectors and the overlying Inverness Formation reflectors have been rotated so that the reflectors do not represent the depositional geometry of the sedimentary units. Within the wedge, the reflectors look like downlap progradational reflectors. However, restoration of these reflectors to horizontal (an approximate depositional surface) indicates that the sediments probably deposited in a rim-syncline similar to that described above. The presence of a rim-syncline directly beneath the Inverness Formation implies that diapirism was occurring during the Westphalian B-C. The rotation of the reflectors from their depositional geometry may be related to post-Carboniferous inversion.

5.6.6, Halokinesis and Sedimentation

At first glance, the prediction of sediment dispersal around growing diapiric structures appears relatively straightforward. For example, salt structures produce a topographic expression, forming adjacent structural (drag-related) basins and salt withdrawal basins which attract sedimentary systems and in which sediments are deposited. However, the dynamic nature of salt diapirism combined with the effects of erosion, sedimentation,

mutual diapir interference and diapir morphology complicate this simplistic sediment dispersal pattern to the point that it becomes a 'complex system'.

The effect of diapir-induced topography upon sediment distribution and sediment dispersal is usually a second order control superimposed upon the first order control, for example, outflow from a mountain range, overall basin geometry, major faults and fold trends. As a second order control, diapirs cause a localised modification of the first order sediment transport/depositional system. In order to predict the effect of diapir topography upon such phenomena as sandbody distribution, the first order sediment transport/dispersal system needs to be evaluated. Only then can the second order diapir effects be superimposed and examined.

Since diapirs as topographic features may be ephemeral, in order to predict the reaction of a sedimentary system to diapiric intrusion we need to know when (temporally) each individual diapir was either buried beneath a sedimentary cover or exposed at surface (creating local topography) in relation to all other adjacent diapirs/salt structures. Only then can we attempt to understand how this diapir configuration affected sedimentation.

(i) It is probable that halokinesis played a role in controlling the sedimentation of the Inverness Formation. In particular, the seismic facies analysis appears to tie sedimentation to halokinesis. However, the available seismic data 'window' in terms of space and time over which this relationship can be demonstrated is very small (250 ms over a 10 km by 15 km grid) and the seismic facies cannot be tied to the onshore exposures due to erosion onshore.

(ii) The Inverness Formation exposures are located within the hangingwall of a major extensional fault (the Hollow Fault). The tectono-stratigraphy presented in this thesis indicates that segments of the Hollow Fault were active during deposition of the Inverness Formation.

There are therefore at least two separate variables that could cause base level fluctuations and shifts in sedimentation patterns. Outside of the seismic facies window, it cannot be determined which of the two mechanisms was actively affecting base level and hence sedimentation. The relative timing of halokinesis and tectonics would suggest that both mechanisms were active at the same time and so both probably affected sedimentation. Given the current data set, the relative importance of tectonics and halokinesis cannot be determined. Additional information could probably be derived from the analysis of modern salt structure and sediment interactions. The interpretation of conglomerates as either syn-tectonic (red polymict conglomerates) or syn-halokinetic (grey oligomict conglomerates) may be a useful tool that can be used to constrain the timing and position of tectonic and halokinetic events, which adds valuable information to the tectono-stratigraphic framework.

CHAPTER 6, CONCLUSIONS

Evaporite-bearing strata of the Lower Windsor Carboniferous Group are widely distributed in mainland Nova Scotia and Cape Breton Island, Atlantic Canada, where they are overlain by thick Upper Carboniferous continental and restricted-marine strata. The present study integrates near-shore seismic data from the Gulf of St. Lawrence with structural and stratigraphic analysis of adjacent cliff exposures. The results indicate that many intensely deformed outcrop belts of Lower and Upper Carboniferous rocks represent the structural carapaces and associated drag zones of large diapirs, some of which have intruded along strands of the Hollow Fault. Stratigraphic evidence constrains the major phase of halokinesis to the Middle and Upper Carboniferous. The excellent exposures permit an unusually detailed analysis of the diapirs' internal geometry and drag zones. Five main groups of conclusions are presented below:

(i) The St. Georges Bay Basin

The St. Georges Bay Basin is a small, half-graben style tectonic basin which underwent rapid tectonic subsidence during the Namurian to Westphalian B. Subsidence was intimately related to extensional offset of a segment of the Hollow Fault that forms the northern basin bounding fault. The St. Georges Bay Basin probably existed in some form prior to the Namurian and there is abundant evidence for continued subsidence, in the form of sedimentation, after the early Westphalian B. However, from the available evidence, it can be shown that the main tectonic subsidence phase was restricted to the Namurian to Westphalian B interval.

Western Cape Breton was a platform area to the St. Georges Bay Basin for much of the Namurian and early Westphalian. The Hollow Fault is interpreted to extend into western Cape Breton as indicated by the repeated juxtaposition of Late Carboniferous rocks against Lower Carboniferous and older rocks along the west coast of Cape Breton. However, the Hollow Fault is not imaged on any of the seismic data and so its geometry

and mode of displacement remain unconstrained. Sedimentation within western Cape Breton was probably controlled by offset of segments of the Hollow Fault to the north-east of St. Georges Bay and sediment accumulation remained modest until the late Namurian-Westphalian A. Offset along the Hollow Fault was therefore diachronous.

(ii) Relationship Between Tectonics, Sedimentation and Halokinesis

The diapiric structures within the St. Georges Bay Basin form elongate salt walls whose location and geometry may be controlled by north-east/south-west striking basement faults. The salt walls are interpreted to have grown as passive diapirs from the early Namurian to the Stephanian, during which time diapiric growth was probably sustained by continuous sedimentation and tectonic subsidence.

The western Cape Breton diapiric structures are dominantly small 'trap door' diapirs, short salt walls or isolated cylindrical diapirs which are smaller and less mature than the St. Georges Bay salt walls. Uplift and penetration of the Inverness Formation (Westphalian D) indicate an upper age constraint for reactive diapirism (see below). Timing of initial growth is hard to determine from the available seismic and onshore data. Early growth of the western Cape Breton salt structures may have been related to basement faulting (Hollow Fault segments), in which case the diapirs grew as reactive diapirs, probably from the late Namurian/early Westphalian to the Late Westphalian. Diapir growth may also have been driven by differential loading, either by uneven sediment accumulation of the Mabou Group and Port Hood Formation or by progradation of the Gillis Fan into the Gulf of St. Lawrence.

(iii) Modification of Diapir Geometry during Inversion

There is a large body of evidence derived from interpretation of seismic data and onshore exposures of faults that indicates that the western Cape Breton area underwent post-Carboniferous inversion. This conclusion is also supported by previous geological research that was able to quantify the amount of post-Carboniferous inversion (e.g. Grist et al.,

1995; Hacquebard, 1984). As well as regional inversion, there is evidence for tectonic inversion. Fault orientation analysis indicates a phase of post-Carboniferous compression occurred, orientated within sigma 1 towards the north-west/south-east, and created numerous small faults within the field area. Correlation of previous geological research from elsewhere in the Maritimes Basin indicates that Late Carboniferous inversion may also have taken place (e.g. Nance, 1987). However, the evidence for Late Carboniferous inversion within the field area is inconclusive and will require future research.

The large salt walls within St. Georges Bay have uplifted and rotated thick stratal units that can only be explained by rejuvenation during compression. Similarly, in western Cape Breton, the Finlay Point Diapir uplifts and penetrates the Inverness Formation. Here, due to the lack of seismic penetration, it cannot be proven that uplift of the Inverness Formation is a result of compression, although it is by far the most likely scenario. The post-Carboniferous growth of the diapiric structures is therefore linked to compression.

Tight to isoclinal folds within the Port Hood Island, Broad Cove and St. Rose diapir structural carapaces are interpreted to be the result of horizontal shortening during compression which may have been coeval with cryptic horizontal shortening and rejuvenation of the underlying diapir. Compression may have tightened pre-existing folds or formed new folds. Pre-existing folds may be related to deformation of the structural carapace by the underlying halite diapir, to the hydration of anhydrite to form gypsum or subsidence due to halite dissolution. From the field evidence, it is hard to distinguish different fold generations or the mechanism by which the folds originally formed. Although the Monks Head structural carapace shares some features that are associated with curtain folds (for example, steeply plunging fold hinges, the formation of mega-boudinage and removal of incompetent strata from fold limbs), these features can also be explained by folding processes related to compression, hydration of anhydrite and dissolution (see above).

dissolution (see above).

Two of the structural carapaces (Broad Cove and Monks Head) contain stratigraphic packages that have been repeated by faults. The repetitions are well constrained, although the geometry of the fault responsible for repetition is not. The faults are modelled as sub-vertical faults with a ramp and flat geometry. Because of their geometry (see Figure 4.3.6), these faults cause widening of the structural carapace which contradicts evidence for horizontal shortening of the carapace. In addition, there is no evidence that the two structures (folds and faults) were formed at different times. A possible explanation for the formation of the strata repeating faults is that they are related to diapir rejuvenation during compression. If, during rejuvenation, the diviatoric stress at the halite/carapace interface exceeds the strength of the carapace rocks, the halite may fault the carapace, pushing it upwards and causing the repetition (carapace widening). Although the net effect is carapace shortening, this hypothesis may explain the apparent contradiction of coeval carapace shortening and widening.

Apatite fission track and vitrinite reflectance data indicate that the Maritimes Basin was covered by 3-4 km of post-Carboniferous sediments. It is highly unlikely that the observed salt tectonics could have taken place beneath this overburden. Given this, the compression and inversion event that modified the salt structures could have taken place either prior to burial or after exhumation. While there is no upper age constraint for inversion within the field area, several workers have suggested that a Permian phase of compression affected the Maritimes Basin (M. R. Gibling, pers. comm. 1998).

(iv) Dissolution

While is certainly true that halite dissolution has occurred within western Cape Breton and Antigonish, there is no evidence that large-scale dissolution has affected the salt structures within the study area. The St. Rose Diapir does show evidence for partial deflation that may be related to either dissolution or re-migration of halite at depth, but so

leading to collapse of the surrounding overburden and carapace. The Mabou mega-breccia may be the remnants of this dissolution and collapse. On a smaller scale, features such as the brecciated sandstone exposed on Port Hood Island may be the result of localised halite dissolution, although these features are small in comparison to the whole carapace.

(iv) Drag Zones Adjacent to Evaporite Diapirs

(a) Faulting and Fault Generations

Where fault data could be collected, the faults within a drag zone could usually be divided into three fault generations. Each fault generation is interpreted to reflect a specific deformation in space and time:

- 1st Generation Faults reflect early faulting due to folding of the drag zone strata as the diapir began to deform the overburden adjacent to the diapir. The faults are pervasive throughout the drag zone. The monogenetic nature of the faults implies that, after formation, the faults were passively rotated as the drag zone strata were folded. The equal rotation of orthogonal and parallel faults suggests that extension parallel to the diapir was equal to extension orthogonal to the diapir. This is an important point that has not been previously recognised for drag zone faulting. Previous work emphasised radial faults that represent extension parallel to the diapir margin.

- 2nd Generation Faults are localised adjacent to the external shear zone. They are interpreted to be caused by the intense shear stress across the external shear zone when the diapir penetrates through the stratigraphic horizon in which the faults are located.

- The 3rd Generation Faults are only recorded in strata that have been rotated to an angle of dip of ~60 degrees. This angle of dip is approximately sub-parallel to the

external shear zone and the faults are spatially associated with small-scale layer-parallel slip horizons. 3rd Generation Faults are modelled as extensional faults.

Although a small number of strike-slip and reverse fault offsets were recorded, the vast majority of faults appear to be extensional faults. In addition, some of the reverse offsets may in fact be extensional faults that have been rotated through the vertical. Therefore, the faults within the drag zones do not show evidence of inversion during compression. In contrast to this, faults that are not associated with a diapir drag zone commonly showed strike-slip or reverse offsets. This observation suggests that the diapirs themselves may have preferentially absorbed the compression by horizontal shortening while the drag zone strata remained unaffected by compression. A similar conclusion was proposed by Vendeville and Nilsen (1995), who concluded that the evaporite rocks contained within a diapir will deform under compression in preference to the stronger sedimentary rocks surrounding the diapir. It should also be noted that the formation of extensional faults within the drag zone may be temporally separated from horizontal shortening within the structural carapace. Diapir growth and formation of drag zones may have been occurring from the Namurian through to the post-Carboniferous, while the bulk of evidence indicates post-Carboniferous compression.

(b) Drag Zone/Zone of Rotation Profile

The width and profile of drag zones and zones of rotation is dependent on at least two factors (in order of importance):

- Diapir geometry: There is a strong correlation between the dip of the diapir flank and the width of the drag zone. This correlation is related to two principles. (i) The frictional resistance to movement is proportional to the dip of the external shear zone. Higher frictional forces are associated with more intense deformation within the hangingwall (the overburden). (ii) A gently dipping diapir flank will support the drag zone because the flank extends beneath the drag zone at depth. Hence gently

dipping diapir flanks are associated with broad drag zones.

- Overburden lithology: Incompetent lithologies such as shales, mudstones and coals will tend to deform by plastic deformation under relatively low stress conditions within a drag zone. The incompetent strata therefore tend to absorb a large proportion of the strain and buffer deformation within more competent units such as sandstones and siltstones. If the drag zone is composed entirely of incompetent strata, the deformation tends to be evenly distributed and the drag zone is relatively broad with a smooth dip profile. However, if incompetent strata are intercalated with competent strata, strain tends to be absorbed within the mudstones and coals. The competent strata remain relatively undeformed (except where in direct contact with the diapir) and the drag zone tends to be relatively narrow with a rapid decrease of dip away from the diapir. Competent lithological units, for example thick fluvial sandstone sheets, tend to deform by brittle deformation processes such as faulting and fracturing. This brittle deformation tends to be localised, either where the unit abuts directly on to a diapir flank or at fold hinges in large-scale folds. In the latter case, the competent unit 'breaks' at the fold hinge by faulting, while the limbs of the folds undergo solid body rotation as well as folding.

(v) Halokinesis and Sedimentation

It can be demonstrated that halokinesis did affect the sediment distribution of the Inverness Formation. The Coal Mine Point, Sight Point and Finlay Point diapirs all created local topography. Coeval sedimentation resulted in sedimentary pinch outs against the rising topography and may have led to progradation away from the diapirs.

However, such relationships can only be demonstrated where high-resolution seismic data are available. In the absence of this information, relying upon paleocurrent patterns, seismic data with insufficient resolution and sedimentary architecture, the effects of

halokinesis cannot be distinguished unequivocally from the effects of eustatic sea-level fluctuations or tectonic activity.

FUTURE RESEARCH

The main avenue for future research would be a fault density study and the application of fractal mathematics to the fault density. The faults within the diapir drag zones are well exposed, isolated and are not associated with parasitic faults that are common around larger faults. The collection of fault density data would therefore be relatively easy and straightforward. The fault data could be scaled to determine if any fractal relationship existed between diapir growth mechanism, diapir geometry and lithology. A relationship between these factors and fault density/fault spacing seems likely, given the relationships demonstrated within this thesis. Such quantitative relationships would be of great use to hydrocarbon reservoir engineers who have to estimate fault densities and fault sizes within hydrocarbon reservoirs to assess permeability damage or enhancement.

APPENDIX 1, SALT THICKNESS RESTORATION

The presence of an intact Upper/Middle Windsor structural carapace exposed at surface implies that little or no salt dissolution has occurred from the underlying halite core of the diapirs. Thus an estimate of the strataform halite thickness for the Windsor Group can be obtained by performing a 2D area balancing restoration The restoration calculation assumes total salt withdrawal of the Lower Windsor halite to form diapiric structures. Since total salt withdrawal is unlikely, the estimated thickness should be regarded as a minimum.

CALCULATED AREA OF SALT STRUCTURES (imaged on line 79)

The area of salt is calculated by measuring the base length and height of each salt wall and assuming that the salt walls have a triangular cross sectional geometry. The height of each salt wall is calculated using the velocity analysis described in Chapter 3.

Calculated area of salt = 14.04 km^2

LENGTH OF THE ST. GEORGES BASIN

The length of the St. Georges Bay Basin is calculated by measuring the distance from the Hollow Fault (located at the northern margin of the basin) to the eastern margin of the Salt Wall Duey.

Calculated distance = 26km

THICKNESS OF LOWER WINDSOR HALITE

An estimate of the strataform thickness of the Lower Windsor halite is calculated by dividing the area of salt by the length of the St. Georges Bay Basin. The value obtained can only be regarded as a minimum estimate due to a number of caveats.

- The calculation assumes no salt dissolution.
- The calculation assumes only plane strain for the salt volume.
- The physical boundaries of the St. Georges Bay Basin are poorly constrained and the calculation assumes that no salt migrated into or out of the immediate area.

Thickness of Lower Windsor halite = 14.04/26 = 540m.

APPENDIX 2, SEISMIC DATABASE

1978 Mabou Survey

Data acquired by Geomarine Associates Ltd. Acquired June 18 to July 11. A total of 200km of seismic data were acquired as 10 NW-SE lines and 6 NE-SW lines over a 10 by 15 km grid. Data processing by Geodigit Ltd. of Calgary. Recording time was 1.0 sec (TWT). Streamer used 12 channels with an 8.33m spacing. 6 fold CDP coverage.

Reference, Stewart and Meagher (1978); Hacquebard et al. (1989).

1982 Chevron Survey

Data acquired by Chevron Ltd. 96 channel streamer with a 25m group interval. Data used in this thesis consists of 580km of seismic data over 10 NW-SE lines (83,79,75,71,67,63,59,55,51,47) and 4 SE-SW lines (50,32,24,16). Recording time 6.0 sec (TWT). 48 fold coverage.

Reference, Durling et al. (1995).

1985 Inverness Survey

Data acquired by Geomarine Associates Ltd. 84km of seismic data acquired as 9 NW-SE lines and two NE-SW lines over a 12 by 7 km grid. Data processing by Geodigit Ltd. of Calgary. Recording time was 2.5 sec (TWT). Survey used a 24 channel streamer with a 16.7m group spacing. 12 fold CDP coverage.

Reference, Hacquebard et al. (1989)

1978 Mabou Survey, Line 9, Re-processing Perimeters

Re-Processing of the seismic data was carried out using the Landmark ITA Insight system at the University of Calgary, Lithoprobe Data Processing Centre during June of 1996.

In the course of re-processing the seismic data a number of specific techniques were applied which improved certain aspects of the data quality.

(i) In order to suppress sea-bed multiples an autocorrelation was performed to calculate the gap length required for a short gap deconvolution filter.

(ii) An automatic gain control function was applied to counteract spherical divergence and attenuation of the seismic wavelet. The optimum AGC was 0.5.

(iii) A sliding bandpass filter of 5-250 Hz was applied to the data. This broad filter retained the high frequency component of the signal and therefore enhanced resolution from the shallow reflection events.

(iv) F-K Migration was applied to the stacked data and significantly enhanced resolution.

APPENDIX 3, VELOCITY ANALYSIS

Velocity used for Time to Depth Conversion

As outlined above, the seismic velocity used to depth-convert the seismic data was:

3500 m/sec or 11483 ft/sec

Corresponding to a straight line function:

$$Y = MX + C$$

$$X = Y/0.0005714$$

(Where X is depth and Y is two way travel time)

Velocity Data

Table A1 summarises the velocity information used in this thesis. The table shows depth vs TWT (sec). Graph A1 shows the velocity data, presented graphically.

Horizon Time, Inverness Survey (Horizon T. Inverness). This data represents two way travel time to the reflector Horizons 1, 2 and 3 identified by LaPierre (1986b) from the 1985 Inverness seismic survey.

Horizon Time, Port Hood Survey (Horizon T. Port H.). This data was taken from LaPierre's (1986a) report of the 1985 Port Hood seismic survey. The data appears as a graph with no reference in the text. It is not known how this data was obtained.

Stack Velocity, Line 71, 1982 Chevron Survey (Vstack71 Chevron). This data was taken from the stacking velocity used to process the 1982 Chevron survey. As expected the stacking velocities do not match well with the interval or check shot velocities.

Port Hood, Vertical Velocity Profile (Port H. V. Profile). This data was extracted from the velocity graph included in the Port Hood seismic survey report (La Pierre, 1986a). No reference to the data is made in the text and so it is not known how the velocity profile was calculated.

Mabou-1 and Mabou-2a Interval Velocity (M1 & M2a Int. Vel.). This velocity information was obtained from down hole compensated sonic logs (Stewart, 1978). The interval transit time is an average value over 200 ft intervals. The sonic log was only recorded from 30 to 1432 m.

Northumberland Strait F-52 Well (F052 Chk. Sht.). This velocity information was obtained from down hole compensated sonic logs at a depth of 1200ft. Calculated velocity = 13,124 ft/sec.

H-3 Well, Sydney Basin, Check Shot Velocity (H-3 Chk. Sht.). This velocity information was obtained from a check shot fired at 1700ft. Calculated velocity = 12,467 ft/sec.

The majority of the velocity information presented in Table A3 and Figure 3.1 approximates to a straight line velocity function with a velocity of 11,483 ft/sec. The H-3 and F-52 wells both record higher velocities although they were both drilled into Upper Carboniferous strata. The horizon times from the 1985 Port Hood survey do not match the straight line velocity function. Because it is not known how this data was obtained this data was not used to calculate velocity. The stack velocity from line 71 in the 1982 Chevron survey do not match the interval velocities. This is to be expected since stacking velocities are approximations to real interval velocities which are used primarily for data processing. The interval velocities obtained from the Mabou-1 and Mabou-2a wells provide the best constrained velocity profile with a reasonable velocity. For this reason and the fact that the two wells are located within the field area, and intersect the 1978 Mabou and 1982 Chevron survey grids, this velocity data was used to calculate the velocity of 11,483 ft/sec.

Depth (m)	Horizon T. Inverness	Horizon T Port H.	VStack71 Chevron	Port H. V. Profile	M1 & M2a Int. Vel.	F-52 Chk. Sht.	H-3 Chk. Sht.
100	0.11						
1100	0.642						
375	0.22						
1500	0.843						
250	0.218						
320	0.175						
30		0.03					
80		0.06					
145		0.14					
310		0.42					
500		0.78					
2200		1.3					
2600		1.5					
1500			0.12				
2485			0.32				
3204			0.76				
3406			0.96				
3881			1.4				
500				0.38			
1000				0.63			
1500				0.91			
2000				1.2			
2500				1.45			
30					0.04		
91					0.09		
152					0.14		
213					0.18		
274					0.22		
335					0.25		
396					0.29		
457					0.32		
518					0.35		
579					0.39		
640					0.42		
701					0.45		
762					0.48		
823					0.51		
884					0.54		
945					0.57		
1006					0.59		
1067					0.62		
1128					0.65		
1189					0.68		
1250					0.71		
1310					0.74		
1372					0.76		
1432					0.8		
365						0.18	
518							0.27

Table A1, Seismic Velocity Data.

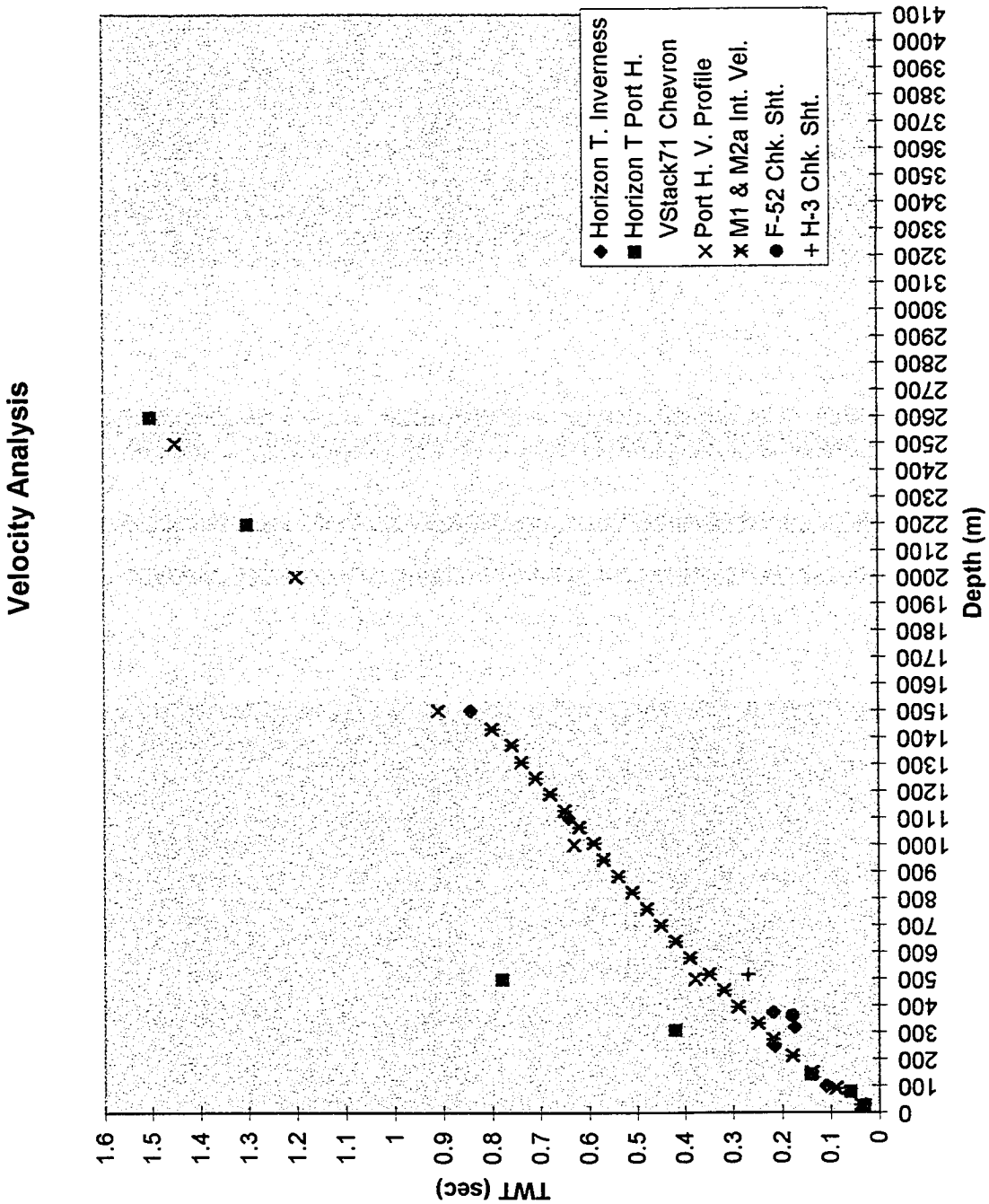
Velocity Analysis
TWT (sec)
Depth (m)
Horizon T. Inverness
Horizon T Port H.
VStack71 Chevron
Port H. V. Profile
M1 & M2a Int. Vel.
F-52 Chk. Sht.
H-3 Chk. Sht.

APPENDIX 4, STRUCTURAL DATA FOR THE ONSHORE DIAPIR OUTCROPS.

(i) Broad Cove Diapir (Table A2). This data was collected from the north-east drag zone of the Broad Cove Diapir (Chapter 3.1). For each outcrop station, four or five stratal dip and strike readings and two or three fault dip and strike readings were recorded. For each station the arithmetic mean was calculated for both fault plane dip and stratal dip. The faults were assigned to groups based upon the strike of the fault plane. Faults were assigned to either an east-west or north-south group with each group encompassing a region of plus or minus 45 degrees from the indicated compass orientation.

(ii) St. Rose Diapir (Table A3). This data was collected from the north-east drag zone of the St. Rose Diapir. For the most part four stratal dip and strike readings and two fault dip and strikes were recorded at each outcrop station. For each station the arithmetic mean was calculated for both stratal dip and fault plane dip.

(iii) Coal Mine Point Diapir (Table A4). This data was collected from the southern drag zone of the Coal Mine Point Diapir. Due to the brecciated nature of the outcrop dip and strike measurement were difficult to obtain. Measurements were therefore taken wherever possible. Micro-fault data was collected by locating an insitu sandstone rock unit, measuring a fixed length (ideally 1m) and recording the number of micro-faults within that distance. The location of the reading was calculated using a 17m tape to measure the distance of the outcrop from the external shear zone.

(iv) Finlay Point Diapir (Table A5). This data was collected from the drag zone of the Finlay Point Diapir. Fault and strata measurements were recorded at fixed station along the drag zone. Micro-fault data was collected using the same technique as described for the Coal Mine Point Diapir drag zone.

KEY

Distance = Distance from the diapir/overburden contact in metres.
Dist. Inv. = Inverse distance, used to orientate the external shear zone to the left hand side of the graphs.

M. Strata D. = Arithmetic mean strata dip (degrees)
M. Fault D. = Arithmetic mean fault plane dip (degrees)
E/W F. dip = Fault plane dip for east/west striking faults.
N/S F. dip = Fault plane dip for north/south striking faults.

The faults that were recorded from the Broad Cove and St. Rose diapir drag zones were binned in to one of two groups based upon the strike of the fault plane. The fault bins have a 90 degree range around the stated compass direction. For example an east-west fault would be one with a strike of 045 to 135 degrees. Where a fault fell outside the range of a bin, the fault was not binned.

Station	Distance	Dist. Inv.	Strata Dip	Dip Dir.	Strike	Fault dip.	Dip.Dir	Strike.
A	0	426	19	E	159	82	W	167
	0	426	20	E	158			
	0	426	21	E	170			
	0	426	20	E	145			
	0	426	21	E	172			
B	5	420	16	E	172	90		149
	5	420	20	E	153	90		159
	5	420	18	E	175			
	5	420	19	E	152			
	5	420	19	E	140			
C	11	414	20	E	170	82	W	153
	11	414	16	NE	132	85	W	167
	11	414	19	E	3			
	11	414	19	E	155			
	11	414	20	E	155			
D	17	408	15	E	150	79	W	145
	17	408	18	E	146	72	W	145
	17	408	20	E	172			
	17	408	19	E	173			
	17	408	20	E	145			
E	23	402	20	E	20	79	E	165
	23	402	18	E	148			
	23	402	19	E	149			
	23	402	18	E	152			
	23	402	17	E	176			
F	30	396	16	NE	125	83	W	150
	30	396	18	NE	127			
	30	396	15	E	146			
	30	396	19	E	145			
	30	396	15	E	152			
G	36	390	16	E	139	90		161
	36	390	18	E	135			
	36	390	19	E	155			
	36	390	20	E	0			
	36	390	16	E	150			
H	42	382	13	E	143	82	W	165
	42	382	19	E	175	68	W	155
	42	382	17	E	157			
	42	382	18	E	159			
	42	382	15	E	150			
I	48	376	19	E	160	75	W	159
	48	376	17	E	163	79	W	169
	48	376	18	E	178			
	48	376	19	E	145			
	48	376	17	E	179			
J	54	370	19	E	155	60	W	163
	54	370	19	E	135			
	54	370	20	E	156			
	54	370	18	E	165			
	54	370	20	E	150			
K	60	364	21	E	157	75	W	164
	60	364	19	E	167	84	W	165
	60	364	18	E	150			
	60	364	20	E	157			
	60	364	20	E	156			
L	66	358	19	E	155	80	W	160
	66	358	21	E	161			
	66	358	15	E	160			
	66	358	19	E	9			
	66	358	20	E	157			
M	72	352	18	E	172	72	W	160
	72	352	21	E	169			
	72	352	18	E	2			
	72	352	19	E	170			
	72	352	21	E	175			
N	78	346	20	E	156	82	W	145
	78	346	19	E	149			
	78	346	19	E	10			
	78	346	21	E	159			
	78	346	20	E	15			
O	84	340	20	E	147	80	W	160
	84	340	21	E	163			
	84	340	21	E	161			
	84	340	22	E	170			
	84	340	20	E	9			
P	92	334	27	E	167	73	W	160
	92	334	28	E	162			
	92	334	29	E	162			

Table A2, The Broad Cove Diapir, Structural Data.

	92	334	25	E	163			
	92	334	25	E	157			
Q	98	328	29	E	157	70	W	168
	98	328	27	E	146			
	98	328	30	E	140			
	98	328	30	E	160			
	98	328	27	E	152			
R	104	322	28	E	149	74	W	164
	104	322	29	E	161			
	104	322	30	E	5			
	104	322	29	E	161			
	104	322	34	E	159			
S	110	316	33	E	155	70	W	166
	110	316	32	E	150	80	W	165
	110	316	35	E	158			
	110	316	30	E	152			
	110	316	31	E	159			
T	116	310	36	E	161	67	W	165
	116	310	33	E	152			
	116	310	34	E	159			
	116	310	30	E	159			
	116	310	35	E	154			
U	122	304	37	E	157	85	W	140
	122	304	39	E	163			
	122	304	37	E	155			
	122	304	40	E	159			
	122	304	39	E	171			
V	128	298	40	E	140	65	W	153
	128	298	39	E	159			
	128	298	41	E	160			
	128	298	43	E	165			
	128	298	37	E	170			
W	134	292	39	E	159	67	W	172
	134	292	42	E	168			
	134	292	40	E	163			
	134	292	38	E	167			
	134	292	43	E	162			
X	140	286	40	E	159	70	W	155
	140	286	41	E	160			
	140	286	39	E	150			
	140	286	40	E	151			
	140	286	40	E	152			
Y	146	280	40	E	150	72	W	168
	146	280	38	E	155			
	146	280	41	E	159			
	146	280	40	E	154			
	146	280	41	E	162			
Z	171	255	36	E	150	75	W	140
	171	255	36	E	175			
	171	255	36	E	152			
	171	255	38	E	145			
	171	255	40	E	170			
A1	186	240	39	E	126	62	W	140
	186	240	40	E	146			
	186	240	41	E	150			
	186	240	42	E	153			
	186	240	38	E	150			
B1	192	234	40	N	85			
	192	234	41	N	90			
	192	234	42	N	100			
C1	198	228	39	E	145	70	W	150
	198	228	40	NE	135			
	198	228	42	NE	135			
	198	228	38	E	139			
	198	228	42	NE	144			
D1	204	222	70	E	145	23	S	65
	204	222	74	E	146			
	204	222	72	E	137			
	204	222	73	E	144			
	204	222	64	E	154			
E1	210	216	67	E	150	26	S	90
	210	216	68	E	147			
	210	216	66	E	162			
	210	216	78	E	147			
	210	216	65	E	152			
F1	216	210	60	E	160	45	S	57
	216	210	62	E	149			
	216	210	64	E	149			
	216	210	70	E	137			

Table A2, The Broad Cove Diapir, Structural Data.

	216	210	60	E	135			
G1	222	204	62	E	146	15	S	60
	222	204	69	E	153			
	222	204	62	E	147			
	222	204	65	E	140			
	222	204	60	E	153			
H1	228	198	62	E	139	49	S	70
	228	198	59	E	125	52	S	57
	228	198	60	E	158			
	228	198	59	E	146			
	228	198	58	E	145			
I1	234	192	60	E	154	35	S	92
	234	192	59	E	143			
	234	192	57	E	145			
	234	192	61	E	139			
	234	192	56	E	147			
J1	240	186	54	E	146	64	S	65
	240	186	58	E	159			
	240	186	50	E	143			
	240	186	59	E	145			
K1	240	186	56	E	149	52	S	82
	246	180	57	E	153	66	W	142
	246	180	50	E	144			
	246	180	54	E	145			
	246	180	55	E	139			
L1	252	174	53	E	152	76	S	56
	252	174	49	E	144			
	252	174	50	E	145			
	252	174	55	E	147			
	252	174	45	E	155			
M1	258	168	61	E	147	10	SE	35
	258	168	62	E	150			
	258	168	60	E	151			
	258	168	62	E	143			
	258	168	65	E	154			
N1	264	162	64	E	148	10	SE	36
	264	162	65	E	145			
	264	162	61	E	149			
	264	162	59	E	152			
	264	162	63	E	158			
O1	270	156	61	E	139	55	S	63
	270	156	58	E	145			
	270	156	63	E	150			
	270	156	64	E	147			
	270	156	63	E	145			
P1	276	150	60	E	141	30	S	66
	276	150	61	E	143			
	276	150	59	E	147			
	276	150	62	E	139			
	276	150	61	E	148			
Q1	282	144	62	E	146	65	S	71
	282	144	61	E	150			
	282	144	62	E	160			
	282	144	64	E	153			
	282	144	65	E	151			
R1	288	138	62	E	153	67	S	45
	288	138	62	E	148			
	288	138	60	E	152			
	288	138	64	E	155			
	288	138	65	E	149			
S1	294	132	60	E	145	62		
	294	132	50	E	139			
	294	132	53	E	134			
	294	132	57	E	130			
	294	132	45	E	142			
T1	300	126	66	E	150			
	300	126	76	E	156			
	300	126	70	E	150			
	300	126	71	E	156			
	300	126	71	E	143			
U1	306	120	69	E	162	52	S	75
	306	120	71	E	166			
	306	120	68	E	165			
	306	120	70	E	160			
	306	120	69	E	163			
V1	312	114	66	E	148	60	S	60
	312	114	62	E	158			
	312	114	65	E	152			
	312	114	66	E	152			

Table A2, The Broad Cove Diapir, Structural Data.

	312	114	60	E	152			
W1	318	108	67	E	166	40	SE	45
	318	108	70	E	160			
	318	108	69	E	162			
	318	108	60	E	150			
	318	108	63	E	147			
X1	324	102	63	E	152	42	S	69
	324	102	64	E	154			
	324	102	65	E	157			
	324	102	64	E	151			
	324	102	66	E	155			
Y1	330	96	59	E	160	25	S	63
	330	96	60	E	153			
	330	96	60	E	147			
	330	96	58	E	154			
	330	96	61	E	159			
Z1	336	90	69	E	151	42	S	74
	336	90	70	E	165			
	336	90	65	E	140			
	336	90	66	E	158			
	336	90	67	E	158			
A2	342	84	62	E	155	70	S	68
	342	84	62	E	153			
	342	84	60	E	159			
	342	84	61	E	153			
	342	84	59	E	159			
B2	348	78	66	E	154	51	S	71
	348	78	68	E	156			
	348	78	60	E	152			
	348	78	68	E	159			
	348	78	65	E	157			
C2	360	66	65	E	145	19	S	40
	360	66	63	E	152			
	360	66	69	E	150			
	360	66	60	E	135			
	360	66	70	E	140			
D2	366	60	60	E	156	62	S	67
	366	60	70	E	149			
	366	60	70	E	152			
	366	60	65	E	162			
	366	60	63	E	141			
E2	372	54	62	E	147	56	S	65
	372	54	62	E	148			
	372	54	60	E	148			
	372	54	65	E	149			
	372	54	68	E	155			
F2	378	48	69	E	150	49	S	75
	378	48	60	E	147			
	378	48	70	E	153			
	378	48	68	E	165			
	378	48	72	E	145			
G2	384	42	65	E	156	67	S	57
	384	42	64	E	153			
	384	42	66	E	155			
	384	42	70	E	158			
	384	42	72	E	153			
H2	391	38	67	E	162	70	S	74
	391	38	66	E	152			
	391	38	70	E	159			
	391	38	68	E	162			
	391	38	65	E	165			
I2	397	32	80	E	165	46	S	36
	397	32	74	E	150			
	397	32	79	E	162			
	397	32	74	E	153			
	397	32	77	E	162			
J2	403	24	74	E	164	59	S	61
	403	24	73	E	150			
	403	24	62	E	149			
	403	24	76	E	155			
	403	24	79	E	160			
K2	409	18	77	E	159	58	S	50
	409	18	77	E	155			
	409	18	78	E	145			
	409	18	80	E	152			
	409	18	78	E	163			
L2	415	12	79	E	143	59	S	43
	415	12	80	E	146			
	415	12	79	E	139			

Table A2. The Broad Cove Diapir, Structural Data.

	415	12	84	E	142			
	415	12	82	E	136			
M2	421	6	85	E	150	47	SE	30
	421	6	88	E	153			
	421	6	86	E	156			
	421	6	85	E	145			
	421	6	87	E	147			
N2	427	0	88	E	150			
	427	0	82	E	152			
	427	0	89	E	158			
	427	0	83	E	145			
	427	0	85	E	155			
	434	14				75	S	60
	434	14				26	S	64
	434	14				9	S	41
	434	14				55	SW	152
	420	28				38	NW	32
	420	28				58	S	37
	420	28				8	SW	90
	420	28				54	S	56
	420	28				75	S	29
	420	28				74	S	29
	420	28				74	S	70
	406	42				82	N	62
	406	42				45	S	64
	406	42				53	S	58
	406	42				33	S	68
	406	42				35	S	153
	406	42				90		70
	406	42				79	S	93
	406	42				25	SE	30
	406	42				75	SW	61
	392	56				42	S	70
	392	56				16	S	61
	392	56				90		43
	392	56				80	S	54
	378	70				35	S	50
	378	70				52	S	76
	364	84				66	S	66
	364	84				44	NNW	26
	364	84				37	S	58
	364	84				37	NW	27
	350	98				68	S	67
	350	98				26	S	80
	336	112				53	S	83
	336	112				30	S	90
	308	140				64	S	67
	294	154				58	S	49
	294	154				66	S	65
	294	154				62	S	22
	294	154				42	W	170
	280	168				72	S	75
	266	182				59	E	67
	252	196				58	S	87
	252	196				38	S	63
	238	210				40	SSW	99
	238	210				67	SSE	99
	238	210				65	NW	176
	224	224				62	SW	90
	224	224				58	W	150
	224	224				75	S	53
	224	224				39	S	50
	224	224				26	SSW	63
	210	238				70	S	79
	182	280				75	S	88
	168	294				83	S	63
	154	308				85	N	81
	140	322				81	N	78
	126	336				78	S	82
	112	350				75	N	81
	98	364				85	N	98
	84	378				87	S	63
	70	392				80	N	93
	56	406				83	N	75
	42	406				78	NE	73
	28	420				82	S	99
	14	434				86	NW	85
	0	448				66	SW	82

Table A2, The Broad Cove Diapir, Structural Data.

Distance	Inv. Dist.	Dip	Dip Dir.	Strike.	Fault Dip	Dip Dir.	Strike.	M.Fault D	M.StrataD
0	457	36	E	18	74	S	79		
0	457	41	E	4					40
0	457	39	E	15				74	
0	457	44	E	10					
8	449	41	E	31	79	S	130		
8	449	38	E	23					
8	449	37	E	22				79	41.25
8	449	49	E	30					
16	441	44	E	45	72	S	55		
16	441	41	E	50					
16	441	46	E	46				72	43.75
16	441	44	E	46					
24	433	38	E	45	70	E	130		
24	433	52	E	46	67	E	162		
24	433	42	E	27				68.5	43.5
24	433	42	E	31					
32	425	24	E	16	88	W	103		
32	425	44	E	44				88	37.33333
32	425	44	E	44					
40	417	46	E	41	78	E	160		
40	417	50	E	47	49	S	90		
40	417	51	E	49	64	E	144	59.75	48.5
40	417	47	E	50	48	S	99		
48	409	43	S	53	72	E	156		
48	409	50	SE	33	72	S	102	72	47.5
48	409	51	S	48	74	E	170		
48	409	46	S	53	70	E	4		
56	401	44	SE	34	76	E	157		
56	401	43	SE	11					
56	401	40	SE	175	74	SW	170	76	41.75
56	401	40	SE	167	78	SW	83		
64	393	42	E	45					
64	393	36	SE	20	78	W	152		
64	393	38	E	26				78	38
64	393	36	E	22					
72	385	33	S	24	65	W	120		
72	385	36	S	23	82	NW	138	75	35.25
72	385	34	S	38	78	W	122		
72	385	38	S	26					
80	377	40	S	7					
80	377	37	SE	0	67	SW	142		
80	377	39	SE	38	61	NE	123	64	37.5
80	377	34	SE	4					
88	369	28	SE	21	72	NE	105		
88	369	36	SE	28				72	32
88	369	30	S	27					
88	369	34	S	31					
96	361	47	SE	41	67	SW	115		
96	361	41	SE	27					
96	361	42	SE	49				67	43.33333
104	353	37	S	160					
104	353	28	S	25					37.66667
104	353	48	S	17					
112	345	58	SE	170	55	SW	120		
112	345	52	SE	6	58	SE	51		
112	345	64	E	173				56.5	60
112	345	66	SE	0					
120	337	53	E	24	76	W	141		
120	337	52	E	2	64	W	116		
120	337	48	SE	3				70	51
136	321	64	SE	10	56	S	43		
136	321	70	SE	22	67	NE	100		
136	321	69	SE	5				61.5	66.5
136	321	63	SE	3					
144	313	53	SE	3	54	S	66		
144	313	60	SE	0	64	SE	98		
144	313	47	SE	18				59	53.33333
152	305	71	E	4	44	SW	140		
152	305	70	E	23				44	70.75
152	305	69	E	37					
152	305	73	E	20					
160	297	62	E	40	62	SW	150		
160	297	54	E	31				62	52.66667
160	297	42	E	40					

Table A3. The St. Rose Diapir, Structural Data.

168	289	60	E	0	44	W	108		
168	289	61	E	2	66	E	125		
168	289	53	E	178					
168	289	60	E	18				55	58.5
176	281	67	E	3					
176	281	69	E	3	80	N	67		
176	281	71	E	3	48	SW	138	64	69.25
176	281	70	E	179					
184	273	70	E	1	78	NW	60		
184	273	73	E	178	58	S	67	68	71
184	273	70	E	3					
192	265	68	E	3	78	NW	69		
192	265	53	E	2	83	E	131	80.5	62.66667
192	265	67	E	4					
200	257	52	E	2	50	W	124		
200	257	40	E	178				50	42.33333
200	257	35	E	40					
212	245	68	SE	30	70	NW	160		
212	245	40	E	4	50	NW	172	60	54
220	237	55	E	18					
220	237	72	E	23	76	W	131		
220	237	38	E	16	65	SW	92	70.5	55
220	237	37	E	20					
228	229	62	E	16	58	SW	103		
228	229	59	E	23	80	W	171		
228	229	62	E	20	78	S	70	72	61
236	221	63	SE	17	78	W	167		
236	221	61	SE	19	81	S	71	79.5	62
244	213	76	SE	175					
244	213	62	SE	179	88	S	65		
244	213	70	SE	170				88	69.33333
252	205	68	SE	23	78	W	115		
252	205	65	SE	22	45	SW	90	61.5	66.5
260	197	56	SE	20					
260	197	48	SE	15	90		110		
260	197	72	E	13				90	61
260	197	68	E	13					
268	189	59	SE	3	50	W	161		
268	189	53	SE	19	60	NE	101	55	52.33333
268	189	45	SE	2					
276	181	50	SE	17	86	N	90		
276	181	59	SE	0	59	SW	131	72.5	57.66667
276	181	64	E	10					
292	165	53	SE	36	90		90		
292	165	44	SE	7	55	S	100	72.5	49.66667
292	165	52	SE	29					
316	141	64	SE	3	90		50		
316	141	67	SE	179	58	S	93	74	68
316	141	73	SE	0					
324	133	73	E	2	90		39		
324	133	78	E	6	45	NW	90	67.5	66.33333
324	133	48	E	15					
340	117	71	E	16	40	S	176		
340	117	72	E	16	62	W	134	51	70.66667
340	117	69	E	20					
356	101	38	SE	25	60	NE	124		
356	101	50	SE	20	36	S	84	48	44.33333
356	101	45	SE	25					
364	93	56	SE	23	44	SW	89		
364	93	64	SE	32	70	NE	71	57	62.33333
364	93	67	SE	24					
376	81	67	SE	44					
376	81	70	SE	35					68.66667
376	81	69	SE	32					
396	61	48	SE	46	74	S	60		
396	61	42	SE	7	58	NE	127	56.33333	42
396	61	36	SE	29	37	S	69		
408	49	58	SE	26	77	NE	112		
408	49	60	SE	23	61	E	163	59.33333	62
408	49	68	SE	33	40	S	77		
413	44	61	SE	29	44	SW	109		
413	44	72	SE	25				44	67.66667
413	44	70	SE	30					
425	32	76	E	173	75	S	57		
425	32	67	E	172	41	S	66	50	74.33333

Table A3. The St. Rose Diapir, Structural Data.

425	32	80	E	167	34	S	82		
441	16	69	E	21	48	S	80		
441	16	75	E	3	48	SW	120	48	71.33333
441	16	70	E	21					
449	8	72	E	20	39	S	92		
449	8	84	E	10	33	S	101	36	78
457	0	80	E	161					
457	0	85	E	156					82.5

Table A3. The St. Rose Diapir, Structural Data.

									COAL MINE POINT						MICRO-FAULT DATA						
Distance	Dis. Invers	Dip	Dip Dir.	Strike	Faults.Dip	Dip Dir.	Faults.Strike	Foliation	Fol. Dip	Dip Dir.	Joint Dip	Dip Dir.	Strike	Distance	Number	length	per metre.	Dip	Dip. Dir.	Strike
0	300	73			61	E	146	170	90					11.1	48	100	48	77	W	157
0	300	70			54	W	130							11.1	35	100	35	69	W	154
0	300	71.5			68	N	95							11.1	47	100	47			
0	300	71.5			42	W	180							11.1	37	90	40.7			
0	300	71.5			60	E	155							12.8	30	60	42	70	W	166
4	296	71.5			70	W	160							12.8	24	60	33.6			
12	288	71.5									46	E	183	14.4	44	90	48.4	72	W	178
12	288	71.5									65	W	155	14.4	34	75	45.322			
16.5	283.5	71.5			73	W	154							17.1						
19.5	280.5	71.5									60	E	140	23.1	32	70	41.6	80	W	176
19.5	280.5	71.5									70	W	161	23.1	26	40	65			
27	273	71.5			85	S	85				90		180	23.1	39	50	78			
27	273	71.5			43	SW	114				55	NE	141	25.4	39	80	46.8			
27	273	71.5			54	N	74							25.4	19	30	63.327			
32	268	71.5			75	W	2				75	W	165	30.1	22	110	19.8	80	W	172
32	268	71.5									40	E	5	30.1	19	100	19			
50	250	58	NW	42		2nd sst23m								30.1	12	40	30			
50	250	52	W	45										30.1	16	70	20.8			
60	240	63	173		54	S	90				60	E	171	32.6	14	65	21.532			
60	240	57									52	SE	45	32.6	20	60	28			
63	237	57			71	SW	141				72	S	90	32.6	19	70	24.7	90		3
70	230	62	W	158							76	NW	164	34.4	17	55	30.77			
70	230	47	W	152		3sst 4m								34.4	22	55	39.82			
70	230	43		148										36.4	33	40	82.5			
200	100	30												36.4	30	40	75			
200	100	34	N	35										36.4	21	45	46.662			
300	0	16												40.4	11	50	22	90		29
														43.4	10	80	12			
														43.4	12	80	14.4			
														43.4	26	60	36.4	77	W	163
														43.4	17	60	23.8			
														45.4	34	110	30.6			
														45.4	27	100	27			
														46.9	17	50	34			
														46.9	25	70	33.325			
														73.9	14	70	18.62			
														75.9	11	75	14.663			
														75.9	22	40	55			
														100.9	16	110	14.4			
														100.9	15	90	16.5	65	E	11
														103.9	16	100	16			
														103.9	30	80	37.5			
														105.9	39	70	55.692			
														107.9	26	100	26	70	E	10
														107.9	23	50	46			
														107.9	22	60	30.8			
														107.9	45	100	45			
														107.9	33	90	36.63			
														107.9	22	70	31.24			
														110.9	24	100	24			
														110.9	27	100	27			
														115.9	26	80	32.5			
														115.6	29	90	32.19			

Table A4. The Coal Mine Point Diapir, Structural Data.

FINLAY	POINT	DIAPIR				
Distance(m)	Strata Dip	Dir.	Strike	Fault Dip.	Dir.	Strike.
0				85	E	130
0				70	E	128
0				72	W	5
2	32	NW	53			
2	34	N	68	66	N	83
2	26	N	72	36	E	134
2	28	N	68	38	E	134
2	30	N	80	35	E	156
2	29	N	75	42	W	19
2	25	N	109	80	E	162
2				82	E	4
2				44	E	145
2				72	E	74
2				60	E	160
2				79	S (REV.)	170
2				65	E	154
2				85	W	93
6	26	N	90			
6	29	N	72	55	S	87
6	24	N	63	66	S	91
6	23	N	82	70	N	82
6				45	SE	58
6				46	SE	65
6				68	N	123
6				56	S	71
6				62	S	66
6				90		165
6				25	E	175
6				80	W	23
6				52	W	35
6				56	S	71
14	22	NW	35			
14	25	N	82			
14	30	NW	62	68	S	75
14	24	N	46	60	N	60
14				38	E	172
14				44	E	162
14				65	E	165
14				35	E	153
14				66	W	5
14				90		166
14				60	NE	135
14				39	NE	146
14				67	E	167
14				38	E	149
14				15	E	167
14				60	E	150
14				45	E	155
14				80	S	70

Table A5. The Finlay Point Diapir, Structural Data.

14				35	E	164
14				90		34
14				38	E	159
14				18	E	172
14				32	E	152
14				48	N	100
14				39	NE	126
14				26	E	154
14				26	E	157
14				62	W	27
14				60	S	93
14				72	W	32
14				76	W	39
14				37	E	139
14				82	E	15
15	25	N	80	65	NW	46
15	30	N	88	60	E	13
15				78	W	28
16				60	E	168
16				58	E	179
16				84	W	15
17				45	N	86
17				90		5
18				85	W	12
18				87	W	9
19				90		160
19				88	W	170
20				85	W	7
26	20	N	95	75	W	9
26	19	N	82	81	W	10
26	22	N	99	73	E	5
26	23	N	67	24	E	175
26	22	N	107	76	E	166
26	25	N	126	77	E	30
26	19	N	119	41	E	168
26	18	N	118	72	W	29
26				77	E	8
26				79	W	18
26				70	N	63
26				88	W	11
26				39	E	140
26				41	E	136
26				36	E	151
26				72	E	152
26				83	W	178
26				84	W	12
26				79	E	0
26				39	E	145
26				36	E	164
26				83	E	31
26				90		15

Table A5. The Finlay Point Diapir, Structural Data.

26				43	S	80
26				39	E	135
26				38	E	128
26				25	E	162
26				42	E	128
26				43	E	169
26				45	E	149
26	21	NE	120	81	W	33
26	24	N	55	76	W	42
36	19	N	92	72	W	35
36	23	N	87	39	E	146
36	20	N	121	45	S	89
36	22	N	102	69	W	34
36	23	N	119	82	E	167
36	24	N	122	70	W	20
36	23	N	86	60	W	28
36	20	N	77	72	N	94
42	21	N	79	80	E	34
42	25	N	121	84	W	42
42	15	N	95	78	W	28
42	16	N	102	84	W	29
42	18	N	90	79	W	32
42				24	N	82
42				25	N	65
42				32	N	79
42				23	N	89
42				25	N	77
42				75	W	146
42				90		167
42				82	W	10
42				81	W	7
42				65	W	142
49	26	N	87	76	W	30
49	21	N	79	78	W	33
49	27	N	57	79	W	21
49	25	N	102	75	W	27
49	25	N	90	70	S	77
49	28	N	65	85	W	169
49	27	N	62	65	W	145
49	17	N	71	87	N	96
49	19	N	80	80	W	160
49	29	N	56	70	S	74
64	26	N	77	82	E	39
64	30	N	69	90		15
64	25	N	58	89	W	18
64	22	N	63	87	W	160
64	26	N	70	83	W	159
64	17	N	65	82	W	179
64	12	N	57	79	W	22
64	18	N	75	85	W	5
64	20	N	79	80	E	17

Table A5. The Finlay Point Diapir, Structural Data.

64	17	N	74	90		176
89	30	N	79	79	W	175
89	28	N	82	70	N	120
89	16	N	79	67	W	163
89	17	N	75	69	W	3
89	16	N	76	90		153
89	22	NW	59	73	N	82
89	23	N	67	77	N	86
89	17	N	55	66	S	92
89	20	N	73			
139	22	N	63	72	W	7
139	24	N	69	77	W	157
139	18	N	92	81	W	9
139	24	N	78	68	E	38
139	20	N	59	74	S	79
139	25	N	65	82	S	88
139	18	N	56	71	N	92
139	24	N	56	69	E	168
139	20	N	67	83	E	18

Table A5. The Finlay Point Diapir, Structural Data.

APPENDIX 5, SEISMIC INTERPRETATION OF THE 15' COAL SEAM FROM THE INVERNESS FORMATION

The data included in this appendix (Table A6) was used to construct the zone of rotation profiles described in Chapter 4.2.

Abbreviations key, for use with Table A6.

A03, ISW	=	Line A03, 1985 Inverness Survey, Inverness Salt Wall
79,L,RHS	=	Line 79, 1982 Chevron Survey, Salt Wall Luey, Right Hand
Side.		
LHS	=	Left Hand Side
H	=	Salt Wall Huey
D	=	Salt Wall Duey
FPD	=	Finlay Point Diapir

- The terms right-hand side and left-hand side refer to diapir flanks on the relevant seismic sections.
- A prefix number refers to the seismic line number. Although three surveys were used, then numbers are unique to a seismic section.

A03,ISW		A10,ISW		79,L,RHS		79,CSC,RHS		2,H,LHS,Idz		63,H,LHS,Idz		67,H,LHD,Idz		75,L, LHS		63,H,RHS		11,FPD
Dist (m)	depth (m)	Dist. (m)	Depth (m)	Dist. (m)	Depth (m)	Dist. (m)	Depth (m)	Distance	Depth (m)	Dist. (m)	Depth (m)	Distance	Depth	Dist. (m)	Depth (m)	Dist. (m)	Depth (m)	Dist. (m)
0	717.5	0	350	0	1618.75	0	1382.5	0	227.5	0	595	0	306.25	0	787.5	0	1015	0
31.2	770	31.2	455	108	1601.25	108	1417.5	40	315	108	682.5	108	393.75	108	848.75	108	1058.75	80
62.4	805	62.4	525	216	1583.75	216	1461.25	80	385	216	761.25	216	507.5	216	892.5	216	1085	160
93.6	822.5	93.6	595	432	1575	432	1505	120	446.25	324	805	324	630	324	962.5	324	1120	240
124.8	840	124.8	656.25	540	1566.25	540	1557.5	160	507.5	432	857.5	432	700	432	1006.25	432	1137.5	320
156	848.75	156	717.5	648	1548.75	648	1596	200	560	540	901.25	540	787.5	540	1050	540	1155	400
187.2	848.75	187.2	761.25	756	1540	756	1645	240	603.75	648	953.75	648	875	648	1076.25	648	1172.5	480
218.4	866.25	218.4	796.25	864	1522.5	864	1688.75	280	665	756	1015	756	927.5	756	1120	756	1190	560
249.6	927.5	249.6	831.25	972	1505	972	1723.75	320	717.5	864	1050	864	997.5	864	1155	864	1198.75	640
280.8	953.75	280.8	857.5	1080	1487.5	1080	1758.75	360	757.75	972	1102.5	972	1050	972	1190	972	1207.5	720
312	796.25	312	892.5	1188	1470	1188	1811.25	400	815.5	1080	1146.25	1080	1085	1080	1225	1080	1216.25	800
343.2	813.75	343.2	910	1296	1452.5	1296	1863.75	440	840	1188	1190	1188	1120	1188	1251.25	1188	1225	880
374.4	805	374.4	927.5	1404	1443.75	1404	1890	480	883.75	1296	1225	1296	1163.75	1296	1268.75	1296	1233.75	960
405.6	805	410.8	945	1512	1435	1512	1907.5	520	927.5	1404	1251.25	1404	1190	1404	1295	1404	1242.5	1040
		416	953.75	1620	1426.25	1620	1750	560	962.5	1512	1268.75	1512	1225	1512	1321.25	1512	1242.5	1120
		447.2	962.5	1728	1417.5	1728	1750	600	1006.25	1620	1303.75	1620	1242.5	1620	1356.25	1620	1242.5	
				1836	1408.75	1836	1758.75	640	1032.5	1728	1330	1728	1260	1728	1400			
				1944	1400			680	1058.75	1836	1356.25	1836	1260	1836	1417.5			
				2052	1391.25			720	1085	1944	1382.5			1944	1435			
				2160	1382.5			760	1107.75	2052	1408.75			2052	1461.25			
								800	1120	2160	1426.25			2160	1487.5			
								840	1120	2268	1443.75			2268	1531.25			
								880	1120	2376	1470			2376	1575			
										2484	1487.5			2484	1592.5			
										2592	1505			2592	1618.75			
										2700	1522.5			2700	1636.25			
										2808	1522.5			2808	1662.5			
										2916	1522.5			2916	1688.75			
														3024	1715			
														3132	1732.5			
														3240	1750			

Table A6, Zone of Rotation Data.

2,H,RHS			63,H,LHS		67,H,LHS,Idz		71,H,LHS		75,H, RHS		79,H,LHS	
Depth (m)	Dist. (m)	Depth	Dist. (m)	Depth (m)	Dist. (m)	Depth (m)	Dist. (m)	Depth (m)	Dist. (m)	Depth (m)	Dist. (m)	Depth (m)
560	0	271.25	0	525	0	1837500	0	691.25	0	490	0	437.5
630	80	385	108	595	2160	2082500	108	708.75	108	577.5	108	490
700	160	455	216	673.75	4320	2358125	216	717.5	216	700	216	560
752.5	240	560	324	717.5	6480	2511250	324	735	432	787.5	432	612.5
813.75	320	630	432	743.75	8640	2603125	432	761.25	540	875	540	665
901.25	400	700	540	805	10800	2817500	540	787.5	648	945	648	700
971.25	480	757.75	648	840	12960	2940000	648	813.75	756	997.5	756	735
1032.5	560	822.5	756	875	15120	3062500	756	840	864	1032.5	864	787.5
1102.5	640	866.25	864	927.5	17280	3246250	864	862.75	972	1050	972	840
1172.5	720	910	972	980	19440	3430000	972	875	1080	1058.75	1080	875
1242.5	800	953.75	1080	1006.25	21600	3521875	1080	892.5	1188	1058.75	1188	892.5
1295	880	997.5	1188	1032.5	23760	3613750	1188	901.25	1296	1058.75	1296	901.25
1365	960	1023.75	1296	1058.75	25920	3705625	1296	910	1404	1058.75	1404	910
1435	1000	1050	1404	1085	27000	3797500	1404	910	1512	1058.75	1512	927.5
1505	1040	1071	1512	1111.25	28080	3889375	1512	927.5	1620	1058.75	1620	945
	1080	1093.75	1620	1128.75	29160	3950625	1620	936.25	1728	1058.75	1728	1006.25
	1120	1128.75	1728	1155	30240	4042500	1728	945	1836	1067.5	1836	1050
	1160	1160.25	1836	1181.25	31320	4134375	1836	945	1944	1076.25	1944	1067.5
	1200	1172.5	1944	1207.5	32400	4226250	1944	953.75	2052	1093.75	2052	1085
	1240	1190	2052	1225	33480	4287500	2052	962.5	2160	1128.75	2160	1102.5
	1280	1207.5	2160	1233.75	34560	4318125			2268	1172.5		
	1320	1225	2268	1251.25	35640	4379375			2376	1207.5		
	1360	1233.75	2376	1268.75	36720	4440625			2484	1242.5		
	1400	1246	2484	1286.25	37800	4501875			2592	1277.5		
	1440	1268.75	2592	1303.75	38880	4563125			2700	1330		
	1480	1282.75	2700	1321.25	39960	4624375			2808	1400		
	1520	1303.75	2808	1347.5	41040	4716250			2916	1435		
	1560	1321.25	2916	1365	42120	4777500			3024	1487.5		
	1600	1340.5	3024	1400	43200	4900000			3132	1540		
	1640	1347.5	3132	1417.5	44280	4961250			3240	1592.5		
	1680	1347.5	3240	1429.75					3348	1618.75		
	1720	1347.5	3348	1443.75					3456	1636.25		
			3456	1461.25					3564	1671.25		
			3564	1487.5					3672	1680		
			3672	1505					3780	1715		
			3780	1522.5					3888	1750		
			3888	1522.5					3996	1767.5		
			3996	1522.5					4104	1785		
									4212	1802.5		
									4320	1811.25		
									4428	1802.5		
									4536	1793.75		
									4644	1776.25		

Table A6, Zone of Rotation Data.

APPENDIX 6, GEOGRAPHIC LOCATION OF COASTAL SECTIONS AND COAL EXPLORATION WELLS

Stratigraphic sections were measured for five coastal sections and three onshore wells through the Inverness Formation. One additional coastal section in the Port Hood Formation near the town of Port Hood was sampled for shales. The geographic location and stratal thickness of each section and well is given below. The sections are presented from south (Port Hood) to north (Inverness) along with a section key (Figure 5.1.5).

Port Hood Shore section (155m stratigraphic thickness)

Murphys Pond; Latitude 46,03,40N Longitude 61,32,40W

Isthmus Point; Latitude 46,02,00N Longitude 61,32,20W

This section traverses the exposed Middle Member of the Port Hood Formation near the town of Port Hood (Figure 5.1.6). The section begins at the first sandstone body north of Murphys Pond and continues to the sandstone body forming Isthmus Point. The section traverses the Port Hood syncline and so the section is repeated to the north and south of the syncline axis.

Coal Mine Point Section (335m stratigraphic thickness)

Latitude 46,07,30N Longitude 61,27,50W

This section traverses the exposed Inverness Formation between the Beaton Fault and Coal Mine Point (Figure 5.1.7). The section is continuous but has been rotated as a footwall syncline beneath the Beaton Fault so that the strata dip steeply near the Beaton Fault. The highest stratigraphic unit is the Eagle Sandstone (Keating, 1950) exposed at Coal Mine Point after which the section is repeated from Coal Mine Point to the Coal Mine Point Diapir (see below, Chapter 3).

Finlay Point Section (113m stratigraphic thickness)

Latitude 46,14,51N Longitude 61,17,08W

This section traverses the ~300m long section of exposed Inverness Formation between Mabou Mines Harbour and Finlay Point (Figure 5.1.8). The Inverness section begins where the Inverness Formation sandstones, coals and grey shales are juxtaposed against the purple Finlay Point conglomerate. The section is continuous out to Finlay Point and a repeated (although tectonised) section is exposed 300m to the north at the Finlay Point North section (see above, Chapter 3). The extensional faults within the Finlay Point section have relatively small displacements and do not cause large stratigraphic omission.

North-East MacKinnons Brook Section (57m stratigraphic thickness)

North-east MacKinnons Brook; Latitude 46,10,20N Longitude 61,25,50W

MacKinnons Brook; Latitude 46,10,00N Longitude 61,26,20W

This section traverses the Inverness Formation section from MacKinnons Brook, north-east to the faulted contact of the Inverness Formation with basement rocks (Figure 5.1.9). This section contains ~30m high cliffs which drop directly into the sea. Access to this section is only possible at low tide, and little structural or sedimentological information could be gained from the cliff sections.

South-West MacKinnons Brook Section (~57m stratigraphic thickness)

South-west MacKinnons Brook; Latitude 46,09,43N Longitude 61,26,35W

MacKinnons Brook; Latitude 46,10,00N Longitude 61,26,20W

This section traverses the Inverness Formation section between MacKinnons Brook, south-west to the exposed unconformity between the Inverness Formation and basement rocks. The section is intensely brecciated and contains steep, loose cliff sections. Little structural or sedimentological information could be gained from this section. From photomosaics taken from offshore, this section appears to be a repetition of the north-east MacKinnons Brook section. *(This section is not shown on a separate log).*

Inverness Harbour to Port Ban Section (87m stratigraphic thickness)

Inverness Harbour; Latitude 46,13,45N Longitude 61,19,48W

Port Ban; Latitude 46,12,35N Longitude 61,22,40W

This section traverses the exposed Inverness Formation section between the south-western side of Inverness Harbour and Port Ban, ~5km to the south-west (Figure 5.1.10). The section begins on the seafront at the first sandstone body to the south-west of Inverness Harbour. The section is largely a strike section and therefore only ~87m of strata are exposed. The base of the section at Port Ban unconformably overlies basement rocks.

Port Ban No.1 Core (62m stratigraphic thickness)

Latitude 46,12,23N Longitude 61,22,18W

This well is located approximately 600m inland of Port Ban. The drill hole penetrates approximately 62m of Inverness Formation strata (Figure 5.1.11).

Port Ban No.2 Core (122m stratigraphic thickness)

Latitude 46,12,53N Longitude 61,21,06W

This well is located 1.5 km north-east of Port Ban. The well penetrates approximately 122m of Inverness Formation strata. The location of this well obtained from the government core store library (Stellarton) locates the well on basement rocks. This is probably an error and the true well location probably lies seawards within the Inverness Formation outcrop (Figure 5.1.12).

Inverness I-2 Core (88m stratigraphic thickness)

Latitude 46,14,51N Longitude 61,17,08W

This well is located ~1km south-west of the town of Inverness. The drill hole penetrates approximately 88m of Inverness Formation strata (Figure 5.1.13).

APPENDIX 7, PROTOZOAN ANALYSIS, SAMPLE LOCATIONS, PREPARATION AND RESULTS

Sample Preparation and Analysis

Each shale sample consisted of approximately 250 cm^3. The samples were split into two equal portions with one portion being kept in reserve while the other was processed. Prior to chemical processing the coarser samples were crushed in a mortar to provide a greater surface area for the chemicals to work on. The softer samples were treated with industrial soap, which acts as a surfactant. Harder samples were treated with sodium sulphite. A fuller description of the techniques is provided in Wightman et al. (1994a).

Samples disaggregated relatively well and most were in processing for four to five days until sufficient breakdown had taken place. The harder samples were treated for a period of 2-4 weeks. Residues from the harder samples were quite small because of incomplete breakdown, however enough material was available to provide a qualitative overview of the microfossils. The softer samples provided plenty of material. Residues were sieved into various size components and examined with a binocular microscope using the optical techniques (low-angle source of light and glycerine immersion) described in Wightman et al. (1994a).

Sample Locations and Results

Sample locations and the results obtained from each sample are given in Appendix Table A7.

Sample	Section / Log Location	latitude / longitude	Metres Above Base	Agglutinated Foraminifera	Paleoenvironment
110	Port Hood	lat.46/03/40 long.61/32/40	14m	*Trochammina (few)*	Estuary
109	Port Hood	(Cape Linzee)	18m	*Barren*	
108	Port Hood		22m	*Trochiammina (few)*	Estuary
107	Port Hood		27m	*Trochiammina (few)*	Estuary
106	Port Hood		31m	*Barren*	
105	Port Hood		35m	*Trochammina (good Samples)*	Estuary / Marsh
104	Port Hood		37m	*Barren*	
103	Port Hood		42m	*Barren*	
102	Port Hood		46m	*Trochiammina (common)*	Upper Estuary / marsh
101	Port Hood		51m	*Barren*	
100	Port Hood		55m	*Thecamoebians (rare)*	Transported ?
99	Port Hood		60m	*Barren*	
98	Port Hood		77m	*Barren*	
97	Port Hood		93m	*Barren*	
96	Port Hood		100m	*Barren*	
95	Port Hood		123m	*Trochiammina (few)*	Estuary
94	Port Hood		150m	*Trochiammina (few)*	Estuary
93	Port Hood		180m	*Trochiammina (Seat Earth Fauna)*	Upper Estuary / Marsh
92	Port Hood		205m	*Trochiammina (Seat Earth Fauna)*	Upper Estuary / Marsh
91	Port Hood	(Isthmus Point)	200m	*Trochammina ?*	
90	Port Hood	lat.46/02/00 long.61/32/20	155m	*Trochiammina (common)*	Upper Estuary
71	Inverness - Port Ban	lat.46/13/45 long.61/19/48	8m		
72	Inverness - Port Ban	(Inverness)	18m		
73	Inverness - Port Ban		40m		
74	Inverness - Port Ban		55.5m		
75	Inverness - Port Ban		64m		
76	inverness - Port Ban		78.5m		
77	Inverness - Port Ban		95m		
801	Inverness - Port Ban		101m	*Trochiammina (Good)*	Upper Estuary
802	Inverness - Port Ban		107m	*Barren*	
803	Inverness - Port Ban		115m	*Barren*	
41	Port Ban	(Port Ban)	130m		
42	Port Ban	lat.46/12/35 long.61/22/40	*125m*	*Thecamoebians, Trochiammina & Ammotium*	Upper Estuary
50	Finlay Point, East Side	lat.46/09/0 long.61/27/0		*Trochiammina (few)*	Upper Estuary / Marsh
51	Finlay Point, East Side			*Barren*	
52	Finlay Point, East Side			*Ostracods & Tecamoebians*	Freshwater
53	Finlay Point, East Side			*Barren*	
54	Finlay Point, East Side			*Barren*	
55	Finlay Point, East Side		*section is*	*Barren*	
fp -1	Finlay Point, East Side		*structurally*		
56	Finlay Point, East Side		*complex*	*Trochammina ?*	
fp - 2	Finlay Point, East Side		*dating is needed*		
fp - 3	Finlay Point, East Side		*in order to constrain*		
fp - 4	Finlay Point, East Side		*juxtaposition of*		
57	Finlay Point, East Side		*strata units. no log*	*Ostracods*	
fp - 5	Finlay Point, East Side		*of the strata was*		
58	Finlay Point, East Side		*possible.*	*Barren*	
59	Finlay Point, East Side			*Trochiammina (common) & Ammotium*	Upper Estuary
60	Finlay Point, East Side			*Barren*	
61	Finlay Point, East Side			*Trochiammina (large)*	Estuary
62	Finlay Point, East Side			*Trochiammina (few)*	Estuary
63	Finlay Point, East Side			*Trochiammina ?*	
2001	Finlay Point, East Side			*Trochiammina (rare)*	Estuary
2002	Finlay Point, East Side			*Thecamoebians (rare)*	Transported
2004	Finlay Point, East Side			*Thecamoebians (rare)*	Transported
2005	Finlay Point, East Side			*Trochammina (rich)*	Upper Estuary / Marsh
2009	Finlay Point, East Side			*Ostracods*	
2010	Finlay Point, East Side			*Ostracods*	
2014	Finlay Point, East Side			*Ostracods*	
2015	Finlay Point, East Side	lat.46/08/15 long.61/27/35		*Trochammina ?*	
25	Finlay Point	lat.46/14/51 long.61/17/08		*Barren*	
26	Finlay Point			*Trochiammina (common)*	Upper Estuary / Marsh
27	Finlay Point				
28	Finlay Point				
29	Finlay Point			*Barren*	
1	Inverness Core I - 2	lat.46/14/51 long.61/17/08	3.1	*Trochiammina (few)*	Upper Esturine / Salt Marsh
2	Inverness Core I - 2		8.3	*Barren*	
3	Inverness Core I - 2		22.5	*Thecamoebians (abundant)*	Freshwater Marsh
4	Inverness Core I - 2		27.6	*Thecamoebians (abundant)*	Freshwater Marsh
5	Inverness Core I - 2		31.6	*Barren*	
6	Inverness Core I - 2		37	*Throchiammina (few)*	Upper Estuary / Marsh
7	Inverness Core I - 2		44.1	*Barren*	
8	Inverness Core I - 2		54.3	*Barren*	
9	Inverness Core I - 2		58.5	*Trochammina (abundant) & Ammotium (few)*	Upper Estuary

Table A7, Protozoan Samples and Results

Sample	Section / Log Location	latitude / longitude	Metres Above Base	Agglutinated Foraminifera	Paleoenvironment
501	NE MacKinnons Brook	lat.46/10/20.long.61/25/50	4	*Barren*	
502	NE MacKinnons Brook		21.5	*Barren*	
503	NE MacKinnons Brook		27	*Thecamoebians & Trochiammina (few)*	Freshwater
504	NE MacKinnons Brook		28	*Barren*	
505	NE MacKinnons Brook		29.5	*Barren*	
506	NE MacKinnons Brook		34	*Barren*	
507	NE MacKinnons Brook		35	*Barren*	
508	NE MacKinnons Brook	lat.46/10/0 long.61/26/20	36	*Barren*	
31	MacKinnons Brook			*Barren*	
32	MacKinnons Brook			*Barren*	
33	MacKinnons Brook			*Trochiammina ?*	
601	SW McKinnons Brook	lat.46/10/0 long.61/26/20	section is intensly		
602	SW McKinnons Brook		brecciated with		
603	SW McKinnons Brook	lat.46/09/43 long.61/26/35	poor access.		
701	Port Hood Island.	lat.46/00/30 long. 61/34/50		*Barren*	
702	Port Hood Island.			*Barren*	
703	Port Hood Island.			*Barren*	
704	Port Hood Island.		No log,	*Barren*	
705	Port Hood Island.		complex section	*Barren*	
706	Port Hood Island.		uplifted above	*Thecamoebians (rare)*	Transported
707	Port Hood Island.		salt diapir	*Trochiammina ?*	
708	Port Hood Island.			*Trochiammina (few)*	Estuary
1	Coal Mine Point	lat.46/07/30 long.61/27/50	9		
2	Coal Mine Point		16		
3	Coal Mine Point		27	*Trochiammina*	Upper - Middle Estuary
4	Coal Mine Point		22		
5	Coal Mine Point		40	*Trochiammina & Textularia*	Middle Estuary
6	Coal Mine Point		50		
7	Coal Mine Point		61.5		
8	Coal Mine Point		63	*Trochiammina (rare)*	Upper Marsh
9	Coal Mine Point		89.5		
10	Coal Mine Point		97		
11	Coal Mine Point		100	*Trochiammina ?*	
13	Coal Mine Point		127		
14	Coal Mine Point		219		
15	Coal Mine Point		231	*Trochammina, Ammobachies & Ammonium*	Lower - Middle Estuary
16	Coal Mine Point		237	*Trochiammina & Ammotium*	Upper Estuary
17	Coal Mine Point		250	*Trochiammina (abundant)*	Upper Estuary / Marsh
18	Coal Mine Point		260.5		
19	Coal Mine Point		272	*Trochiammina & Ammotium*	Upper Estuary
20	Coal Mine Point	lat.46/07/30 long.61/27/50	277	*Trochiammina (few)*	Transported ?

Table A7, Protozoan Samples and Results.

APPENDIX 8, PALYNOLOGY RESULTS

Palynological Results

(Palynological sample locations are show in Table A8)

Coal Mine Point. The Coal Mine Point section is arguably the thickest and most complete of the five coastal sections, containing eight major coal seams within 335m of stata.

Bell (1944) correlated the Coal Mine Point section with his *Linopteris obliqua* zone of mid to late Westphalian C age, whereas Barss and Hacquebard (1967) and Hacquebard (1972) assigned the section to the approximately equivalent *Torispora* zone. Zodrow and Vasey (1986) assigned a late Westphalian C to early Westphalian D age to the section and noted that it is equivalent in age to much of the South Bar Formation of the Sydney Basin. The more recent palynological data from this study indicate that the Coal Mine Point section is considerably younger.

Mid to late Westphalian samples from Coal Mine Point yielded a wide variety of species including *Torispora securis*, *Punctatosporites granifer*, *P. minutus*, *Triqutrites sculptilis* and *Vestispora* with smaller numbers of *Triquitrites additus, T. spinosus, T. tribullatus, V. fenestrata* and *Striatosporites spp.*

Westphalian D samples commonly have a Westphalian C background assemblage but are assigned to the Westphalian D based upon the presence of several species. *Cadispora magna* is present in significant numbers in several samples (no. 4,6,10,16,17). Peppers (1985) considered that this species appears in the very latest Westphalian C along with a group of species, all of which Smith and Butterworth (1967) and Smith (1987) considered to appear at the base of the Westphalian D. *Mooreisporites inusitatus* is present in the 4'6" coal seam and *Raistrickia aculeata* is present in the 7' coal seam. Both of these

species are part of the Westphalian D group of species of Smith and Butterworth (1967) and Smith (1987).

Stephanian samples are defined by large amounts of striate pollen including *Illinites unicus, I. boehneri, I. annosus, Protohaploxypinus spp., Straitoabieites spp., Straitopodocarpites spp. and Striomonosaccites spp.* The sacs in *Striatoabietes* are sometimes indiscernible so that the palynomorph resembles *Vittatina nova*, a taxon recorded from the late Stephanian of France (Alpern, 1958; Liabeuf and Alpern, 1969, 1970) and of Germany (Helby, 1966). *Vittatina spp.* first appear in the early Stephanian of Europe (Clayton et al., 1977).

Finlay Point is located approximately 1.25 km north of Coal Mine Point. It has long been speculated that the Finlay Point and Coal Mine Point sections are equivalent (Haites, 1952) and that the 15' and 5' coal seams exposed at Finlay Point can be correlated with the 15' and 5 ' coal seams of Coal Mine Point. The new palynological data presented here support this hypothesis. Four samples were taken from Finlay Point (FP 26-29) and all yielded mid-Westphalian C to D background assemblages. A poor specimen of *Mooreisporites insusitatus* in sample FP29 confirms a Westphalian D age, but there are no other markers. Also present in FP29 are specimens of *Densosporites sphaerotriangulus*. The only occurrences of this species at Coal Mine Point are in samples CMP13 and CMP14. The palynological data therefore support a correlation of the stratigraphic interval containing the 15' and 5' coal seams from Coal Mine Point with the coal-seam interval exposed at Finlay Point based upon stratigraphic age and the presence of *Densosporites sphaerotriangulus*.

North-East MacKinnons Brook is an isolated outlier of Inverness Formation strata which has a well exposed onlapping contact with the underlying basement (see Chapter 5). The samples were collected from two sections, north-east of MacKinnons Brook and south-west of MacKinnons Brook (see above, Chapter 4). The north-east MacKinnons Brook samples are divided between a tentative Late Westphalian C assemblage and a younger Westphalian D to Stephanian assemblage. The stratigraphic thickness between

the two age assemblages is small (<2 m) which may imply that a depositional hiatus exists between them. The lower productive samples are rich in the Mid Westphalian C to Stephanian background assemblage but there are no 'marker species' specimens to confirm a Westphalian C or D age.

South-West MacKinnons Brook. The in situ assemblage contains elements of the mid Westphalian C - D background assemblage while the presence of *Torispora securis*, *Punctatosporite granifer*, *P. oculus, Triquitrites tribullatus* and striate pollen including *Illinites unicus* indicate an age no older that early middle Westphalian C. Specimens of *Vestispora pseudoreticulata* in 601 indicate that the sample is no younger than earliest Westphalian D (Table A8).

Sample 31 taken from MacKinnons Brook yielded a Stephanian age defined by a specimen of the fungal body *Centonites symmetricus* which appears to be a Missourian-Virgilian marker in the U.S.A (Peppers, 1964) and which is also present in the type section of Liabeuf and Alpern (1969). This implies that the coal seams exposed at MacKinnons Brook may be equivalent to the 7' or 11' coal seam at the top of the Coal Mine Point section.

Port Ban forms the southern end of the Inverness shore section. Of the three samples submitted for analysis, only one contained usable palynomorphs. The sample 41 is rich and contains a specimen of *Striatoabietes* which is characteristic of the Stephanian at Coal Mine Point.

Inverness Shore Section. Of the ten samples analysed from the Inverness shore section, eight samples yielded rich assemblages of mid-Westphalian D to earliest Stephanian specimens. The section has been tentatively divided into three zones based upon the palynological assemblages (see Appendix 5). The oldest zone contains a rich Westphalian C background assemblage but is assigned to the Westphalian D based upon samples of *Vestispora witneyensis, V. cf. witneyensis, V. colchesterensis and V. cf. colchesterensis.* Good specimens of *Vestispora witneyensis and V. colchesterensis* are typical of the mid

Westphalian D in both England (Smith, 1987) and Illinois (Peppers, 1970). The equivalent in the Sydney Basin extends from approximately 25m above the Phalen Seam to the Hub Seam. The second interval yielded generally poor samples of *Cadiospora magna and Thymospora obscura* which are Westphalian D-Stephanian species. The lack of *Vestispora witneyensis* and data from the overlying zone suggests that this interval is of latest Westphalian D age. The youngest zone contains specimens of striate bisaccate pollen which appear in the latest Westphalian B but which are thought to be more consistently numerous in Stephanian and younger sediments. Three specimens in the 18 m (no. 73) sample resemble *Vittatina*, a predominantly Permian genus which can occur sporadically in the Stephanian. Based upon this evidence and the ages of the underlying strata, this interval is tentatively assigned to the Stephanian.

Coal Exploration Core Samples

Inverness I-2. Nine samples were analysed from well Inverness I-2 located 3 km north of Inverness. Of the nine samples only the two oldest samples yielded reasonable assemblages. Both samples yielded a rich Westphalian C to Stephanian background assemblage, but also contained specimens of *Cadiospora magna* and *Raistrickia cf. aculeata* which indicate an age no older that the Westphalian D. The presence of *Vestispora witneyensis and V. cf. witneyensis* similar to those found in the Inverness shore section zone 1 also confirm a Westphalian D age for these two samples.

The majority of the I-2 core penetrated red strata similar to those exposed adjacent to Inverness Harbour (see Chapter 5). Since red strata within the Inverness Formation are distinctive, a possible correlation exists between the I-2 core and the top of the Inverness Shore section. The correlation is partly supported by the palynological results.

Port Ban 2. Ten samples from the Port Ban 2 well were analysed and all yielded rich assemblages typical of the Westphalian D to Stephanian. Specimens of *Thymospora* suggest that the samples are not of early Westphalian D age and the lack of *Vestispora witneyensis and V. colchesterensis* also precludes a middle to early Westphalian D age. The abundance of *Torispora spp.* and *Punctatosporites spp.* is significant. These species

typically peak in the late Westphalian C to earliest D, but within the Sydney Basin there is a second peak abundance for both these species in the late Westphalian D to Stephanian. Based on this evidence the samples are assigned to the late Westphalian D to Stephanian. This age is approximately equivalent to that of the Inverness shore section samples which were collected only 0.25 km north of the PB-2 well.

Sample	Section / Log Location	Metres Above Base	latitude / longitude	Stratagraphic Age
110	Port Hood	14m	lat.46/03/40 long.61/32/40	*Late Namurian - Westphalian A*
109	Port Hood	18m	(Cape Linzee)	*Late Namurian - Westphalian A*
108	Port Hood	22m		*Late Namurian - Westphalian A*
107	Port Hood	27m		*Late Namurian - Westphalian A*
106	Port Hood	31m		*Late Namurian - Westphalian A*
105	Port Hood	35m		*Late Namurian - Westphalian A*
104	Port Hood	37m		*Late Namurian - Westphalian A*
403	Port Hood	42m		*Late Namurian - Westphalian A*
402	Port Hood	46m		*Late Namurian - Westphalian A*
401	Port Hood	51m		*Late Namurian - Westphalian A*
100	Port Hood	55m		*Late Namurian - Westphalian A*
99	Port Hood	60m		*Late Namurian - Westphalian A*
98	Port Hood	77m		*Late Namurian - Westphalian A*
97	Port Hood	93m		*Late Namurian - Westphalian A*
96	Port Hood	100m		*Late Namurian - Westphalian A*
95	Port Hood	123m		*Late Namurian - Westphalian A*
94	Port Hood	150m		*Late Namurian - Westphalian A*
93	Port Hood	180m		*Late Namurian - Westphalian A*
92	Port Hood	205m		*Late Namurian - Westphalian A*
91	Port Hood	200m	(Isthmus Point)	*Late Namurian - Westphalian A*
90	Port Hood	155m	lat.46/02/00 long.61/32/20	*Late Namurian - Westphalian A*
		depth from top section		
71	Inverness - Port Ban	8m	lat.46/13/45 long.61/19/48	*Westphalian D*
72	Inverness - Port Ban	18m		*Westphalian D*
73	Inverness - Port Ban	40m		*Westphalian D*
74	Inverness - Port Ban	55.5m		*Westphalian D*
75	Inverness - Port Ban	64m		*Westphalian D*
76	Inverness - Port Ban	78.5m		*Westphalian D*
77	Inverness - Port Ban	95m		*Westphalian D*
801	Inverness - Port Ban	101m		*Westphalian D*
802	Inverness - Port Ban	107m		*Westphalian D*
803	Inverness - Port Ban	115m	lat.46/12/35 long.61/22/40	*Westphalian D*
50	Finlay Point, East Side		lat.46/09/0 long.61/27/0	*Westphalian C*
51	Finlay Point, East Side			*Late Namurian - Westphalian A*
52	Finlay Point, East Side			*Late Namurian - Westphalian A*
53	Finlay Point, East Side			*Barren*
54	Finlay Point, East Side			*Barren*
55	Finlay Point, East Side	*section is*		*Late Namurian - Westphalian A*
fp -1	Finlay Point, East Side	*structurally*		*Late Namurian - Westphalian A*
56	Finlay Point, East Side	*complex*		*Late Namurian - Westphalian A*
fp - 2	Finlay Point, East Side	*dating is needed*		*Barren*
fp - 3	Finlay Point, East Side	*in order to constrain*		*Late Namurian - Westphalian A*
fp - 4	Finlay Point, East Side	*juxtaposition of*		*Late Namurian - Westphalian A*
57	Finlay Point, East Side	*strata units. no log*		*Late Namurian - Westphalian A*
fp - 5	Finlay Point, East Side	*of the strata was*		*Westphalian C*
58	Finlay Point, East Side	*possible.*		*Westphalian C*
59	Finlay Point, East Side			*Westphalian C*
60	Finlay Point, East Side			*Westphalian C*
61	Finlay Point, East Side			*Westphalian C*
62	Finlay Point, East Side			*Westphalian D*
63	Finlay Point, East Side		lat.46/08/15 long.61/27/35	*Westphalian D*
1	Inverness Core I - 2	3.1	lat.46/14/51 long.61/17/08	*Westphalian D*
2	Inverness Core I - 2	8.3	lat.46/14/51 long.61/17/08	*Westphalian D*
3	Inverness Core I - 2	22.5	lat.46/14/51 long.61/17/08	*Barren*
4	Inverness Core I - 2	27.6	lat.46/14/51 long.61/17/08	*Barren*
5	Inverness Core I - 2	31.6	lat.46/14/51 long.61/17/08	*Barren*
6	Inverness Core I - 2	37	lat.46/14/51 long.61/17/08	*Barren*
7	Inverness Core I - 2	44.1	lat.46/14/51 long.61/17/08	*Barren*
8	Inverness Core I - 2	54.3	lat.46/14/51 long.61/17/08	*Barren*
9	Inverness Core I - 2	58.5	lat.46/14/51 long.61/17/08	*Barren*

Table A8, Palynology Samples and Results.

Sample	Section / Log Location	Metres Above Base	latitude / longitude	Stratagraphic Age
	NE of McKinnons Brook			
501	NE McKinnons Brook	4	lat.46/10/20 long.61/25/50	*Mid - Westphalian C*
502	NE McKinnons Brook	21.5		*Mid - Westphalian C*
503	NE McKinnons Brook	27		*Mid - Westphalian C*
504	NE McKinnons Brook	28		*Westphalian D*
505	NE McKinnons Brook	29.5		*Westphalian D*
506	NE McKinnons Brook	34		*Westphalian D*
507	NE McKinnons Brook	35		*Westphalian D*
508	NE McKinnons Brook	36	lat.46/10/0 long.61/26/20	*Westphalian D*
	SW of McKinnons Brook			
601	SW McKinnons Brook	section is intensly	lat.46/10/0 long.61/26/20	*Mid - Westphalian C*
602	SW McKinnons Brook	brecciated with		*Mid - West. C or West D*
603	SW McKinnons Brook	poor access.	lat.46/09/43 long.61/26/35	*Mid - Westphalian C*

Table A8, Palynology Samples and Results.

REFERENCES

Albrecht, H. and Hunsche, U. 1980. Gebirgsmechanische Aspekte bei der Endlagerung Radioaktiver Abfalle unter besonderer Berucksichtigung des Fliebverhaltens von Steinsalz. Fortschr Miner. V. 58, p. 212-247.

Allen, P.A. and Allen, J.R. 1990. Basin Analysis, Principles and Applications. Blackwell Scientific Publications.Oxford, London. 451 p.

Alsop, G.I., Jenkins, G., and Davison, I. 1995. A Preliminary Study of Drag Zone Geometry Adjacent to Salt Diapirs. 16th Annual Research Conference, Salt, Sediments and Hydrocarbons, December 3-6, 1995, p. 1-9.

Alsop, G.I. 1996. Physical Modelling of Fold and Fracture Geometries Associated with Salt Diapirism. Salt Tectonics, Geological Society Special Publication no. 100. eds. Alsop. G.I., Blundell, D.J., and Davison, I. p. 227-243.

Anderson, E. M. 1951. The Dynamics of faulting, Oliver and Boyd, Edinburgh.

Arrhenius, S. 1913. Zur Physik der Salzlagerstatten Meddelanden Vetensskapkademiens Nobelinstitut, v. 2, No. 20, p. 1-25.

Balk, R. 1949. Structure of the Grand Saline Dome, Van Zandt County, Texas. AAPG Bulletin, v. 33, p. 1792-1829.

Balk, R. 1953. Salt Structure of the Jefferson Island Salt Dome, Iberia and Vermillion Parishes, Louisiana. AAPG Bulletin, v. 37, p. 2455-2474.

Bancroft, M.F. 1957. Salt Deposits of Pugwash and Malagash, Nova Scotia. Geology of Canadian Industrial Minerals Deposits. Canadian Institute of Mining and Metallurgy. p. 215-218.

Barton, D.C. 1933. Mechanics of Formation of Salt Domes with Special Reference to Gulf Coast Salt Domes of Texas and Louisiana. AAPG Bulletin, v. 17, p. 1025-1083.

Barss, M.S. and Hacquebard, P.A. 1967. Age and Stratigraphy of the Pictou Group in the

Maritime Provinces as Revealed by Fossil Spores. Geological Association of Canada, Special Paper No. 4, p. 267-282.

Barss, M.J., Bujak, J.P. and Williams, G.L. 1979. Palynological Zonation and Correlation of Sixty-Seven Wells, Eastern Canada. Geological Survey of Canada, Paper 78-24, p. 4-10.

Bell, W.A. 1929. Horton Windsor District, Nova Scotia. Geological Survey of Canada, Memoir 155, 268p.

Bell, W.A. 1944. Carboniferous Rock and Fossil Flora of Northern Nova Scotia. Geological Survey of Canada, Memoir 238, 119p.

Bell, W.A. 1948. Early Carboniferous Strata of St. Georges Bay Area, Newfoundland. Geological Survey of Canada, Bulletin No. 10, 45p.

Bell, W.A. 1958. Possibilities for Occurrence of Petroleum Reservoirs in Nova Scotia. Nova Scotia Department of Mines Paper, 177p.

Bell, J.S. and Howie, R.D. 1990. Paleozoic Geology, in Keen, M.J. and Williams, G.L. eds. Geology of the Continental Margin of Eastern Canada. Geological Survey of Canada, Geology of Canada, no. 2, p. 141-165.

Beloussov, V. V. 1962. Basic Problems in Geotectonics: New York, eds. McGraw-Hill, 809p.

Belt, E.S. 1964. Revision of Nova Scotia Middle Carboniferous Units. American Journal of Science, v. 262, p. 653-673.

Belt, E.S. 1965. Stratigraphy and Paleogeography of the Mabou Group and Related middle Carboniferous Facies, Nova Scotia, Canada. Geological Society of America Bulletin, v. 76, p. 777-802.

Belt, E.S. 1968b. Post - Acadian Rifts and Related Facies, Eastern Canada, in Zen, E.A., White, W.S., Hadley, J.B., and Thompson, J.B., eds., Studies of Appalachian Geology, Northern Maritimes: New York, Wiley, p. 95 - 117.

Benson, D.G. 1974. Geology of the Antigonish Highlands, Nova Scotia. Geological Survey of Canada, Memoir 376, 92p.

Bishop, R.S. 1978. Mechanism for Emplacement for Piercement Diapirs. AAPG Bulletin. V. 62, p. 1561-1583.

Blanchard, J.E. 1959. Geophysical Exploration Antigonish County 1952-1958, Prepared for Lura Corporation, Montreal, by Nova Scotia Research Foundation. Assessment File 11F/12, 39-B-05(05), 10p.

Boehner, R.C. 1980b. Geology, Geochemistry and Geophysics of the Shubenadacie-Stewiake Salt Deposit, Hants and Colchester Counties, Nova Scotia. Mineral Resources Devision, Report of Activities, 1979. Nova Scotia Department of Mines and Energy, Report 80-1, p. 165-186.

Boehner, R.C. 1981. A History of Potash Exploration in Nova Scotia. Mineral Resources Devision, Report of Activities, 1980. Nova Scotia Department of Mines and Energy, 81-1, p. 141-153.

Boehner, R.C. 1983. Windsor Group Salt and Potash in Nova Scotia, Canada. Sixth International Symposium on Salt, v. 1, p. 141-153.

Boehner, R.C. 1984. Carboniferous Basin Studies, Salt, Potash, Celestite and Barite - New Exploration Potential in the Sydney Basin, Cape Breton Island. Nova Scotia Department of Mines and Energy, Information Series No. 7, p. 75-77.

Boehner, R.C. 1986. Salt and Potash Resources in Nova Scotia. Nova Scotia Department of Mines and Energy, Bulletin No. 5, 246 p.

Boehner, R.C. and Giles, P.S. 1986. Geological Map of the Sydney Basin. Nova Scotia Department of Mines and Energy. Map 86-1.

Bidgood, D.E.T. 1970. The Distribution and Nature of Some Nova Scotia Evaporites - a geophysical Evaluation. Third Symposium on Salt, v. 1, p. 298-305.

Bradley, D.S. 1982. Subsidence in Late Paleozoic Basins in the Northern Appalachians. Tectonics, V. 1, p. 107 - 123.

Bradley, D.S. and Bradley, L.M. 1986. Tectonic Significance of the Carboniferous Big Pond Basin, Cape Breton Island, Nova Scotia. Canadian Journal of Earth Sciences, V. 23, p. 2000-2011.

Brewer, J.A. and Smythe, D.K. 1986. Deep Structure of the Foreland to the Caladonian Orogen, NW Scotland: Results of the BIRPS WINCH Profile. Tectonics, V. 5, p. 171-194.

Brown, J.P. 1995. Halokinetic Controls on the Sedimentary architecture of the Inverness Formation, Western Cape Breton, Nova Scotia. Current Research 1995 - D, Geological Survey of Canada,p. 39 - 43.

Brown J.P., 1992. Fault Segmentation and Hangingwall Deformation of the Cormorant Field, Northern North Sea. Unpublished MSc thesis. Royal Holloway University of London.

Cant, D.J., and Walker, R.G. 1975. Development of a Braided-Fluvial Facies MOdel for the Devonian Battery Point Sandstone, Quebec. Can. J. Earth Sci., v. 13, p. 102-119.

Cant, D.J., and Walker, R.G. 1978. Fluvial Processes and Facies Sequences in the Sandy Braided South Saskatchewan River, Canada. Sedimentology, v. 25, p. 625-648.

Caputo, M.V., and Crowell, J.C. 1985. Migration of Glacial Centres Across Gondwana During the Paleozoic Era. Geological Society of America Bulletin, v. 96, p. 1020-1036.

Carbonneau, C. 1977. Geology and Possible Utilization of Salt Structures in the Central Gulf of St. Lawrence. Salt Dome Utilization and environmental Considerations. eds. Martinez, J.D., and Thoms, R.L. p. 57-75.

Carter, D.C. 1990. Pugwash Salt Mine, 630 Level, Pugwash, Nova Scotia. Nova Scotia Department of Mines and Energy, Map 90-1.

Carter, D.C. 1990. Pugwash Salt Mine, 730 Level, Pugwash, Nova Scotia. Nova Scotia Department of Mines and Energy, Map 90-2.

Carter, D.C. 1990. Pugwash Salt Mine, 830 Level, Pugwash, Nova Scotia. Nova Scotia Department of Mines and Energy, Map 90-3.

Cecil, C.B. 1990. Paleoclimate Controls on Stratigraphic Repetition of Chemical and Siliciclastic Rocks, Geology v. 18, p. 533-536.

Caudill, M.R. and Nance, R.D. 1986. Variscan tectonostratigraphy of the Mispec Group, southern New Brunswick: Stratigraphy and Depositional Setting. In Current Research, Part A, Geological Survey of Canada. Paper 86-1A, p. 343-350.

Clifton, H.E. 1967. Solution Collapse and Cavity Filling in the Windsor Group, Nova Scotia, Canada. Geological Society of America Bulletin, v. 78, p. 819-832.

Cobbold, P., Rossello, E. and Vendeville, B.C. 1989. Some Experiments on Interacting Sedimentation and Deformation Above Salt Horizons. Societe Geologique de France Bulletin. V. 8, no. 3, p. 453-460.

Cole, L.H. 1930. Salt Industry of Canada, Salt Occurrences in the Maritimes Provinces; Mines Branch, Department of Mines, Canada, No. 716, p. 2-25.

Coleman, J.M. 1969. Brahmaputra River: Channel Processes and Sedimentation. Sedimentary Geology, v. 3, p. 129-239.

Collier, R.E., Leeder, M.R., and Maynard, J.R. 1990. Transgressions and Regressions: a Model for the Influence of Tectonics, Deposition and Eustacy, with Application to Quaternary Examples. Geological Magazine, v. 127, p. 117-128.

Crowell, J.C. 1978. Gondwana Glaciation, Cyclotherms, Continental positioning and Climate Change. American Journal of Science, v. 278, p. 1345-1372.

Currie, K.L. and Nance, R.D. 1983. A Reconsideration of the Carboniferous Rocks of St. John, New Brunswick. In. Current Research, Part A, Geological Survey of Canada, Paper 84-1A, p. 193-201.

Davison, I., Insley, M., Harper, M., Weston, P., Blundell, D., MaClay, K., and Quallington, A. 1993. Physical Modelling of Overburden Deformation around Salt Diapirs. Tectonophysics v. 228, p. 255-274.

Davison, I., Bosence, D., Alsop, G.I. and Al-Aawah, M.H. 1996. Deformation and Sedimentation around Active Miocene Salt Diapirs on the Tihama Plain, NW Yemen. In Salt Tectonics, Geological Society Special Publication no. 100. eds. Alsop. G.I., Blundell, D.J., and Davison, I. p. 23-41.

Demercian, S., Szatmari, P. and Cobbold, P.R. 1993. Style and Pattern of Salt Diapirs due to Thin-Skinned Gravitational Sliding, Campos and Santos Basins, Offshore Brazil. Tectoniphysics, V. 228, p. 393-433.

Dickie, J.R. 1986. Upper Carboniferous Sedimentation in the Gulf of St. Lawrence Coal Basin, Nova Scotia. Unpublished B.Sc. Hons.thesis,Dalhousie University, Halifax, Nova Scotia, 118p.

Diesael, C.F.K. 1986. The Correlation Between Coal Facies and Depositional Environments. in Advances in the Study of the Sydney Basin, Proceedings 20th Symposium, University of Newcastle, New South Wales, Australia. P. 19-22.

Diegel, F.A., Karlo, J.F., Schuster, D.C., Shoup, R.C. and Tauvers, P.R. 1995. Cenozoic Structural Evolution and tectono-Stratigraphic Framework of the Northern Gulf Coast Continental Margin. In M.P.A. Jackson, D.G. Roberts and S. Snelson, eds. Salt tectonics: a Global Prospective. AAPG Memoir 65, p. 109-151.

Dostal, J., Keppie, J.D. and Dupuy, C. 1983. Petrology and Geochemistry of Devono-Carboniferous Volcanic Rocks in Nova Scotia. Maritime Sediments and Atlantic Geology. V. 19, p. 59.

Dudal, R., and Eswaran, H. 1988. Distribution, Properties and Classifiecation of Vertisols in Vertisols, Their Distribution, Properties, Classification and Management eds. Wilding, L.P., and Puentes, R. College Station, Texas A&M University, p. 105-117.

Durling, P. and Marillier, F. 1993. Structural Elements of the Magdalen Basin, Gulf of St. Lawrence, from Seismic Reflection Data. In Current Research, Part D. Geological Survey

of Canada, Paper 93-1D, p. 147-154.

Durling, P., Harvey, P., and Howells, K. 1995. Geophysical Evidence for Thrust Faulting in the Carboniferous Antigonish-Mabou Sub-Basin, Nova Scotia. Atlantic Geology, v. 31, p. 183-196.

Eisbacher, G.H. 1967. Tectonic Analysis of the Cobequid Mountains, Nova Scotia, Canada. Unpublished Ph.D Thesis, Geological Department of Princeton, New Jersey, 108p.

Fletcher, R.C., Hudec, M.R. and Watson, I.A. 1995. Salt Glacier and Composite Sediment-Salt Glacier Models for the Emplacement and Early Burial of Allocthonous Salt Sheets. In M.P.A. Jackson, D.G. Roberts and S. Snelson, eds. Salt tectonics: a Global Prospective. AAPG Memoir 65, p. 77-109.

Fillmore, R.P. 1993. Sedimentation and Extensional Basin Evolution in a Miocene Metamorphic Core Complex Setting, Alvord Mountain, Central Mojave Desert, California, USA. Sedimentology v. 40, p. 721-742.

Fillmore, R.P., and Walker, J.D. 1996. Evolution of a Supradetachment Extensional Basin: The Lower Miocene Pickhandle Basin, Central Mojave Desert, California. Geological Society of America, Special Paper 303. p. 107-126.

Fralick, P.W., and Schenk, P.E. 1981. Molasse Deposition and Basin Evolution in a Wrench tectonic Setting: The Late Paleozoic, Eastern Cumberland Basin, Maritimes Canada. in Sedimentation and Alluvial Basins. eds. A.D. Miall. Geological Association of Canada, Special Paper 23, p. 77-97.

Gansser, A. 1960. Uber Schlammvulkane und Saklzdome. Viertejahrsschrift der Naturforsschenden, V. 105, p. 825-846.

Gibling, M.R. and Kalkreuth, W.D. 1991. Petrology of Selected Limestones and Shales in Late Carboniferous Coal Basins of Atlantic Canada. International Journal of Coal Geology, V. 17, p. 239-271.

Gibling M.R., Calder J.H., Ryan R., Van De Poll H.W., & Yeo G.M., 1992. Late Carboniferous and Early Permian Drainage Patterns of Atlantic Canada. CJES. 29 p.338 - 352.

Gibling, M.R., Marchioni, D.L. and Kalkreuth, W.D. 1994. Detrital and Organic Facies of Upper Carboniferous Strata at Mabou Mines, Western Cape Breton Island, Nova Scotia; GSC current report of activities 1994 - D.

Gibling, M.R. and Bird, D.J. 1994. Late Carboniferous Cyclotherms and Alluvial Paleovalleys in the Sydney Basin, Nova Scotia. Geol. Soc. Am. Bull. V. 106, p. 105-117.

Gibling, M.R. and Wightman, W.G. 1994. Paleovalleys and Protozoan Assemblages in a Late Carboniferous Cyclotherm, Sydney Basin, Nova Scotia. Sedimentology, V. 41, p. 699-719.

Gibling, M.R. 1995. Upper Paleozoic Rocks, Nova Scotia. In, Geology of the Appalachian-Caledonian Orogen in Canada and Greenland, eds. Williams, H. Geological Survey of Canada, Geology of Canada, no. 6, p. 493-523.

Giles, P.S. and Boehner, R.C. 1979. The Windsor Group Stratigraphy in the Schubenacadie and Musquodobiot Basins of Central Nova Scotia. Nova Scotia Department of Mines and Energy, Paper 79-6, 56 p.

Giles, P.S. 1981a. The Windsor Group of the Mahone Bay Area, Nova Scotia. Nova Scotia Department of Mines and Energy. Paper 81-3, 27 p.

Giles, P.S. 1981b. Major Transgressive-Regressive Cycles in Middle to Late Visean Rocks of Nova Scotia. Nova Scotia Department of Mines and Energy. Paper 81-2, 27 p.

Giles, P.S. 1982. Geological Map of the Eureka Area, Central Nova Scotia. Nova Scotia Department of Mines and Energy, Map 82-3.

Giles, P.S., Hein, F.J. and Allen, T.L. 1997a. Bedrock Geology of Port Hood-Lake Ainslie (11K04, 11K03, 11F13), Cape Breton Island, Nova Scotia. Geological Survey of Canada Open File 3253, 1:50 000 Map with Marginal Notes.

Giles, P.S., Hein, F.J. and Allen, T.L. 1997b. Bedrock Geology of Margaree (11K06), Cape Breton Island, Nova Scotia. Geological Survey of Canada Open File 3254, 1:50 000 Map with Marginal Notes.

Giles, P.S. and Boehner, R.C. 1982. Subdevision and Regional Correlation of Strata of the Upper Windsor Group, Cape Breton Island and Central Nova Scotia. Nova Scotia Department of Mines and Energy, Report 82-1.

Grant, A.C. and Moir, P.N. 1992. Observations on Coalbed Methane Potential, Prince Edward Island. In, Current Research, Part E, Geological Survey of Canada, Paper 92-1E, p. 269-278.

Grant, A.C. 1994. Aspects of Seismic Character and Extent of Upper Carvboniferous Coal Measures, Gulf of St. Lawrence and Sydney Basins. Paleogeography, Paleoclimatology, Paleoecology. 106, p. 271 - 285.

Grist, A.M., Ryan, R.J. and Zentilli, M. 1995. The Thermal Evolution and Timing of Hydrocarbon Generation in the Maritimes Basin of Eastern Canada: Evidence from Apatite Fission Track Data. Bulletin of Canadian Petroleum Geology, V. 43, no. 2, p. 145-155.

Hacquebard, P.A. 1951. The Correlation by Petrographic Analysis of the No.5 Seam, St. Rose and Chimney Corner Coalfields. Geological Survey of Canada Bulletin, v. 19, 29p.
Hacquebard, P.A. 1962. Palynological Studies of Some Upper and Lower Carboniferous Strata in Nova Scotia. Third Coal Conference, Crystal Cliffs, Nova Scotia, p. 227-253.

Hacquebard, P.A. 1972. The Carboniferous of Eastern Canada. 7th International Congress on Carboniferous Stratigraphy and Geology, Compte Rendu, v. 1, p. 63-90.

Hacquebard, P.A., Cameron, A.R., Forgeron, S.V., Potter, W.C, Shaw, W.S., and Smith, E.W. 1978. Geology of the Carboniferous Coal Deposits in Nova Scotia. in Toronto 1978 Field Trip Guidebook, Geological Association of Canada, p. 43-64.

Hacquebard, P.A. 1980. Geology of Carboniferous Coal Deposits in Nova Scotia: Field Trip Guide Book. Geological Association of Canada, 37 p.

Hacquebard, P.A. 1984. Coal Rank Changes in the Sydney and Pictou Coalfields of Nova Scotia, Causes and Significance. Canadian Institute of Mining and Metallurgy, Bulletin, V. 77, p. 33-40.

Haquebard, P.A. 1986, The Gulf of St. Lawrence Basin; the largest Coalfield of Eastern Canada. CIM Bulletin, p. 67-78.

Hacquebard, P.A., Gillis, K.S., and Bromley, D.S. 1989. Re-Evaluation of the Coal Resources of Western Cape Breton Island; Nova Scotia Department of Mines and Energy,

Paper 89-3, 47 p.

Hacquebard, P.A. 1993. Petrology and Facies Studies of the Coal Seams in the Carboniferous Section of the Mabou and Inverness Coal Fields, Cape Breton Island, Nova Scotia. International Journal of Coal Geology.

Hamblin, A.P., and Rust, B.R. 1989. Tectono-Sedimentary Analysis of Alternate-Polarity Half Graben Basin-Fill Successions: Late Devonian-Early Carboniferous Horton Group, Cape Breton Island, Nova Scotia. Basin Research, v. 2, p. 239-255.

Harding, T.P. and Lowell, J.D. 1979. Structural Styles, their Plate Tectonic Habitats and Hydrocarbon Traps in Petroleum Provinces. AAPG Bulletin, V. 63, p. 1016-1058.

Harding, A.P. 1985. Seismic Characteristics and Identification of Negative Flower Structures, Positive Flower Structures and Positive Inversion Structures. AAPG Bulletin, V. 69, p. 582-600.

Hays, J.D., Imbrie, J., and Shackleton, N, J. 1976. Variations in the Earths Orbit: Pacemaker of the Ice Ages. Science, v. 194, p. 1121-1131.

Heard, H.C. 1972. Steady-State Flow in Polycrystaline Halite at Pressure of 2 Kilobars. In, Flow and Fracture of Rocks. American Geophysical Union, Washington, D.C. p. 191-208.

Heckel, P.H. 1986. Sea Level Curve for Pennsylvannian Eustatic Marines Transgressive Depositional Cycles along the Midcontinental Outcrop Belt, North America. Geology, v. 14. p. 330-334.

Helman, M.L. and Schreiber, B.C. 1983. Permian Evaporite Deposits of the Italian Alps: the Development of Unusual and Significant Fabrics. Sixth International Symposium on Salt, V. 1, p. 57-66.

Hossack, J.R. and McGuinness, 1990. Balanced Sections and the Development of Fault and Salt Structures in the Gulf of Mexico (GOM) (abs) GSA Abstracts with Programs, V. 22, no. 7, p. A48.

Hossack, J. R. 1995. Geometric Rules of Section Balancing for Salt Structures. . In M.P.A. Jackson, D.G. Roberts and S. Snelson, eds. Salt tectonics: a Global Prospective. AAPG Memoir 65, p. 29-41.

Howie R.D., 1988. Upper Paleozoic Evaporites of Southeastern Canada. *GSC* Bulletin 380.

Hoyos, M., Doblas, M., Sanchez-Moral, S., Canaveras, J.C., Ordonez, S., Sese, C., Sanz, E., and Mahecha, V. 1996. Salt Tectonics, Geological Society Special Publication No. 100, p. 49-63.

Howie, R.D., and Barss, M.S. 1975a. Upper Paleozoic Rocks of the Atlantic Provinces, Gulf of St. Lawrence, and Adjacent Continental Shalf. Geological Survey of Canada, Paper 74 - 30, p. 35 - 55.

Haites, T.B. 1952. Some Geological Aspects of the Inverness County Coalfields in Comparison with those of the Sydney Coalfield. 2nd Conference on the Orogin and Constitution of Coal, Crystal Cliffs, 1952. Nova Scotia Department of Mines and Energy Research Foundation, Halifax, p. 112 - 135.

Jackson, M.P.A., Cornelius, R.R., Craig and Talbot, C.J. 1987. The Great Kavir Salt Canopy: a Major New Class of salt structures (abs):GSA Abstracts with Programs, v. 19, no. 7, p. 714.

Jackson, M. P. A and Talbot, C.J. 1989a. Anatomy of Mushroom-Shaped Diapirs. Journal of Structural Geology. V. 11, p. 211-230.

Jackson, M.P.A., Cornelius, R.R., Craig, C.H., Gansser, J., Stocklin, J. and Talbot, C.J. 1990. Salt Diapirs of the Great Kavir, Central Iran. Geological Society of America Memoir 177, pp. 139.

Jackson, M.P.A. and Talbot, C.J. 1994. Advances in salt Tectonics. In Hancock, P.L. ed. Continental Deformation. Pergamon Press, p. 159-179.

Jackson, M.P.A., Roberts, D.G., and Snelson, S. 1996. Salt Tectonics a Global Prospective. AAPG Memoir 65. pp. 454.

Johnson, A.M. 1970. Physical Processes in Geology. Freeman, Cooper and Co.

Keating, B.J. 1950. Mabou Coal Area Inverness County, Nova Scotia. Unpublished report for the Nova Scotia Research Foundation. 60 pages.

Kelly, D.G. 1967. Some Aspects of Carboniferous Stratigraphy and depositional history in the Atlantic Provinces. Geological Association of Canada, Special Paper 4, p. 213-229.

Keppie, J.D. 1982. The Minas Geofracture. in Major Structural Zones and Faults of the Northern Appalachians. Eds P. Saint Jullien and J. Beland. Geological Association of Canada, Special Paper 24, p. 263-280.

Knight, I. 1983. Geology of the Carboniferous Bay of St. George Sub-Basin, Western Newfoundland, Newfoundland Department of Mines and Energy, Memoir 1, 358p.

Koyi, H. 1996. Salt Flow by Aggrading and Prograding Overburdens. In. Salt Tectonics, Geological Society Special Publication no. 100. eds. Alsop. G.I., Blundell, D.J., and Davison, I. p. 243-258.

Kupfer, D.H. 1976. Shear Zones Inside Gulf Coast Stocks Help Delineate Spines of Movement. AAPG Bulletin, v. 60, p. 1434-1447.

Kusznir, N.J., Karner, G.D., and Egan, S. 1987. Geometric , Thermal and Isostatic Consequences of Detatchments in Continental Lithosphere Extension and Basin Formation.in Beaumont, C., and Tankard, A.J., eds., Sedimentary Basins and Basin Forming Mechanisms: Canadian Society of Petroleum Geologists, Memoir 12, p.185 - 203.

Lachmann, R. 1910. Uber Autoplaste (Nichttektonische) Formelemente im Bau der Salzgesteine, Norddeutschlands. Deutschen Geologischen Gesellschaft Monatsberict, v. 62. p. 113-116.

Langdon, G.S., and Hall, J. 1994. Devonian-Carboniferous Tectonics and Basin Deformation in the Cabot Strait Area, Eastern Canada. AAPG Bulletin, v. 78, No. 11, p. 1748-1774.

LaPierre, T. 1986a. Marine Seismic Survey, Port Hood Area, Cape Breton Island, Nova

Scotia; McGregor Geoscience Ltd. Geological Survey of Canada Project 85-74.1, 42p.

LaPierre, T. 1986b. Marine Seismic Survey, Inverness Area, Cape Breton Island, Nova Scotia; McGregor Geoscience Ltd. Geological Survey of Canada, Project 85-74.2, 47p.

Leeder, M.R. 1988. Recent Deveploments in Carboniferous Geology: A Critical Review with Implications for the British Isles and North West Europe. Proceedings of the Geological Association, v. 99. p. 73-100.

Lemon, N. M. 1985. Physical Modelling of Sedimentation Adjacent to Diapirs and Comparison with Late Precambrian Oratunga Breccia Body in Central Flinders Range, South Australia. AAPG Bulletin, v. 69, p. 1327-1338.

Link, T.A. 1930. Experiments Relating to Salt Dome Structures. AAPG Bulletin, v. 14, p. 483-508.

Lynch, G. and Brisson, H. 1994. Ainslie Detachment in the Carboniferous River Denys Basin of Cape Breton Island, Nova Scotia, with Regional Implications for Pb-Zn Mineralization. In Current Research 1994-D, Geological Survey of Canada, p. 57-62.

McGill, G.E. and Stromquist, A.W. 1979. The Grabens of Canyonlands National Park, Utah: Geometry, Mechanics and Kinematics. Journal of Geophyscical Research, V. 84, no. B9, p. 4547-4563.

MacLean, J.H. 1939. Geology and Coal Resources of the Inverness Area. Annual Report of the Nova Scotia Department of Mines, Part 2, 26p.

MacNeil, D.J. 1959. The Geology of an Area Near Antigonish, Nova Scotia, and a Report on the Drilling Program Sponsored by Lura Corporation Ltd. within that Area. Nova Scotia Department of Mines and Energy, Assessment File 11/F12C 39-B-05(06).

McGregor Geoscience Ltd. 1985. Marine Geophysical Survey Offshore Inverness, Cape Breton Island, Nova Scotia. McGregor Geoscience Project 85-74.1, 64 p.

Marillier, F., Keen, C.E., Stockmal, G.S., Quinlan, G., Williams, H., Colman-Sadd, S.P.,

and O'Brien, S.J. 1989. Crustal Structure and Surface Zonation of the Canadian Appalachians: Implications of Deep Seismic Reflection Data. Can. J. Earth. Sci, v. 26, p. 305-321.

Martinez, J.D. 1974. Tectonics behaviour of Evaporites. In, Fourth Symposium on Salt. V. 1, p. 155-168. North Ohio Geological Society.

Martinez, J.D. 1978. Salt Dome Caprock – A Reccord of Geological Process. In, Fifth Symposium on Salt. V. 1, p. 143-151. North Ohio Geological Society.

Maynard, J.R., and Leeder, M.R. 1992. On the Periodicity and Magnitude of Late Carboniferous Glacio-Eustatic Sea-Level Changes. Journal of the Geological Society of London, v. 149, p. 303-311.

McCutcheon, S.R., and Robinson, P.T.1987. Geological Constriants on the Genesis of the Maritimes Basin, Atlantic Canada. in Sedimentary Basins and Basin Forming Mechanisms. eds. C. Beaumont and A.J. Tankard. Canadian Society of Petroleum Geolgists, Memoir 12, p. 287 - 297.

Miall, A.D. 1976. Paleocurrent and Hydrologic Analysis of some Vertical Profiles through a Cretaceous Braided Stream Deposit, Banks Island, Artic Canada. Sedimentology, v. 23, p. 459-483.

Muller, W.H. and Briegel, U. 1978. The Rheological Behaviour of Polycrystaline Anhydrite. Ecolg. Geol. Helv. V. 71/2, p. 397-407.

Muller, W.H., Schmid, S.H. and Briegel, U. 1981. Deformation Experiments on Anhydrite Rocks of Different Grain Sizes: Rheology and Microfabric. Tectonophysics, V. 78, p. 527-543.

Nance, R.D. 1987. Dextral Transpression and Late Carboniferous Sedimentation in the Fundy Coastal Zone of Southern New Brunswick. In. Beaumont, C. and Tankard, A.J. eds. Sedimentary Basins and Basin Forming Mechanisms. Canadaian Society of Petroleum Geologists, Memoir 12, p. 363-377.

Nelson, T.H. 1989. Style of Salt Diapirs as a Function of the Stage of Evolution and the Nature of Encasing Sediments. GCS-SEPM 10th Annual Conference, Program with Abstracts, p. 109-110.

Nettleton, L.L. 1934. Fluid Mechanics of Salt Domes. AAPG Bulletin, v. 18. p. 1175-1204.

Nettleton, L.L. 1943. Recent Experimental and Geophysical Evidence of Mechanics of Salt Dome Formation. AAPG Bulletin, v. 27, No. 1, p. 51-63.

Nettleton, L.L and Elkins, T. A. 1947. Geological Models made from Granular Materials. American Geophyscical Union Transacrions, V. 28, p. 451-466.

Nilsen, K.T., Vendeville, B.C. and Johansen, J.T. 1995. Influence of Regional Tectonics on Halokinesis in the Nordkapp Basin, Barents Sea. In M.P.A. Jackson, D.G. Roberts and S. Snelson, eds. Salt tectonics: a Global Prospective. AAPG Memoir 65, p. 413-437.

Norman, G.W.H. 1935. Lake Ainslie Map Area. Geological Survey of Canada., Memoir 177, 103 p.

Parker, T.J., and McDowell, A.N. 1955. Model Studies of Salt Dome Tectonics. AAPG Bulletin, v. 39, p. 2384-2470.

Peel, F.J., Travis, C.J. and Hossack, J.R. 1995. Genetic Structural Provinces and salt Tectonics of the Cenozoic Offshore U.S. Gulf of Mexico: A Preliminary Analysis. In M.P.A. Jackson, D.G. Roberts and S. Snelson, eds. Salt tectonics: a Global Prospective. AAPG Memoir 65, p. 153-177.

Petersen, K. and Lerche, I. 1993. Interactive Salt and Sediment Evolution: Self-Consistent Quantative Models. Tectonophysics, V. 228, p. 211-238.

Plint, A.G. and Van de Pohl, H.W. 1984. Structural and Sedimentary History of the Quaco Head Area, Southern New Brunswick. Canadian Journal of Earth Sciences, V. 21, p. 753-761.

Picard, M.D. 1980. Stratigraphy, Petrography and Orogin of Evaporites in Jurassic Arapien Shale, Central Utah. Utah Geological Association, Henry Mountains Symposium, p. 129-150.

Pohl, E.R. 1931. Windsor Rocks of the Antigonish Basin and Knoydart District. in

Report on the Potash Possibilities of Nova Scotia by A.O. Hayes. Province of Nova Scotia, Department of Public Works and Mines, 1930, Part 2, p. 85-94.

Poliakov, A.N.B., Cundall, P., Podladchikov, Y., and Laykhovsky, V. 1993a. An Explicit Inertial Method for the Simulation of Viscoelastic Flow: An Evaluation of Elastic Effects on Diapiric Flow in Two and Three Layer Models. In: Stone, D.B. and Runcorn, S.K. (eds), Flow and Creap in the Solar System: Observations, Modelling and Theory. Kluwer, Dordretcht, 175-195

Poliakov, A.N.B., Podladchikov, Y.Y., Dawson, E.C., amd Talbot, C.J. 1996. Salt Diapirism with Simultaneous Brittle Faulting and Viscous Flow. Salt Tectonics, Geological Society Special Publication No. 100. eds. Alsop, G.I., Blundel, D.J., and Davison, I. p. 291-302.

Poole, W.H. 1967. Tectonic Evolution of Appalachian Region of Canada. In Neale, E.R.W. and Williams, H. eds. Geological Association of Canada, Special paper no. 4, p. 9-51.

Posepny, F. 1871. Studien aus dem Salinargebiete Siebenburgens: Kaiserlich-Koniglichen Geloogischen Reichsanstalt Jahrbuch, V. 21, p. 123-186.

Pritchett, R. W. 1997. Fracture Prediction in Triple-Bed Strata. In, Natural Fracture Systems in the Southern Rockies. Eds. Close, J. C. And Casey, T. A. Pub. Four Corners Geological Society.

Rehill, T.A. 1996. Late Carboniferous Nonmarine Sequence Stratigraphy and Petroleum Geology of the Central Maritimes Basin, Eastern Canada. Unpublished Ph. D thesis, Dalhousie University, Nova Scotia.

Rehill, T. A., Gibling, M.R. and Williamson, M.A. 1995. Stratigraphy of the Central Maritimes Basin, Eastern Canada: Nonmarine Sequence Stratigraphy. In, Current Research 1995-E. Geolohical Survey of Canada, p. 221-231.

Roliff, R.A., 1962. The Maritimes Basin of Eastern Canada. Geological Assosiation of Canada, Proceedings, V. 14, p. 21 - 41.

Rowan, M.G. 1994. A Systematic Technique for the Sequential Restoration of Salt Structures. Tectonophysics, V. 228, p. 331-348.

Ryan, R.J., Calder, J.H., Donahoe, H.V. and Naylor, R. 1987. Late Palaeozoic Sedimentation and Basin Development Adjacent to the Cobequid Highlands Massif,

Eastern Canada. In Beumont, C. and Tankard, A, eds. Sedimentary Basins and Basin Forming Mechanisms. Canadian Society of Petroleum Geology, Memoir 12, p. 311-317.

Ryan, R.J., Boehner, R.C., and Calder, J.H. 1991. Lithostratigraphic Revision of the Upper Carboniferous to Lower Permian Strata in the Cumberland Basin, Nova Scotia and Regional Implications for the Maritimes Basin in Atlantic Canada. Bulletin of Canadaian Petroleum Geology, v. 39, no. 4, p. 289-314.

Ryan, R.J. 1993. Metallogenetic and Thermal Evolution of the Maritimes Basin, Evidence from the Cumberland Basin. Unpublished Ph.D thesis, Dalhousie University, 333 p.

Ryan, R.J., and Boehner, R.C. 1994. Geology of the Cumberland Basin, Cumberland, Colchester and Pictou Counties, Nova Scotia, Nova Scotia Department of Mines and Energy, Memoir 10, 222p.

Sage, N.M. 1954. The Stratigraphy of the Windsor Group in the Antigonish Quadrangle and the Mahone bay-St. Margaret Bay Area, Nova Scotia. Memoir No. 3. Nova Scotia Department of Mines and Energy.

Schenk, P.E. 1969. Carbonate-Sulphate-Redbed Facies and Cyclic Sedimentation of the Windsorian Age (Middle carboniferous), Maritime Provinces. Canadian Journal of earth Sciences, v.6, p. 1037.

Schultz, D.D, Jackson, M.P.A., and Vendeville, B.C. 1993. Mechanics of Active Diapirism. Tectonophysics v. 228, p. 275-312.

Stacy, M.C. 1953. Stratigraphy and Paleontology of the Windsor group (Upper Mississippian) in parts of Cape Breton Island, Nova Scotia. Memoir No. 2. Nova Scotia Department of Mines and Energy.

Schwerdtner, W.M. 1983. Gypsum-Anhydrite Caps of the Artic Salt Domes, Queen Elizabeth Islands: Products of Active and Passive Diapirism. Sixth International Symposium on Salt, v. 1, p. 311-314.

Smith, W.D., and Naylor, R.D. 1990. Oil Shale Reseources of Nova Scotia. Nova Scotia Department of Mines and Energy, Economic Geology Series, 90-3, 73p.

Stockmal, G.S., Colman - Sadd, S.P., C.E. Keen, Marillier, F., O'Brian, S.J., and Quinlan, G.M. 1990. Deep Seismic Structure and Plate Tectonic Evolution of the Canadian Appalachians. Tectonics, Vol 9, No.1, P. 45 - 62.

Talbot, C.J. and Jarvis, R.J. 1984. Age, Budget and Dynamics of an Active Salt Extrusion in Iran. Journal of Structural Geology, V. 6. P. 521-533.

Talbot, C. J., Ronnlund, P., Schmeling, H., Koyi, H. and Jackson, M.P.A. 1991. Diapiric Spoke Patterns. Tectonophyscics, V. 188, p. 187-201.

Talbot, C.J. 1993. Spreading of Salt Structures in the Gulf of Mexico. Tectonophysics, V. 228, p. 151-166.

Trusheim, F. 1957. Uber Halokinese und ihre Bedeutung fur die Strukturelle Entwicklung Norddeutschlands. Deutschen Geologischen Gesellschaft Zeitschrift, v. 109, p. 111-151.

Trusheim, F. 1960. Mechanism of Salt Migration in Northern Germany. AAPG Bulletin, v. 44, p. 1519-1540.

Utting, J. 1978. Palynological Investigation of the Windsor Group (Mississippian) of Port Hood Island and other Localities on Cape Breton Island, Nova Scotia. Geological Survey of Canada, Paper 78-1A, pp. 205-207.

Yeo, G.M. and Ruixiang, G. 1987. Stellarton Graben: an Upper Carboniferous Pull - Apart Basin in Northern Nova Scotia. in Sedimentary Basins and Basin Forming Mechanisms. eds. C. Beaumont and A.J. Tankard. Canadian Society of Petroleum Geologists, Memoir 12, p. 299 - 309.

Van Eysinga, F.W.B. 1970. Geological Time Table, 1st edition, Elsevier Amsterdam.

Van Der Gracht, W.A.I.M.v.W. 1917. The Saline Domes of North-West Europe: Southwestern Association of Petroleum Geology, v. 1, p. 85-92.

Veevers, J.J., and Powell, C.M.C.A. 1987. Late Paleozoic Glacial Episodes in Gondwanaland Reflected in Transgressive-Regressive Depositional Sequences in Euroamerica. Geological Society of America Bulletin, v. 98, p. 475-487.

Vendeville, B.C. and Cobbold, P.R. 1987. Synsedimentary Gravitational Sliding and Listric Growth Faults: Insights from Scales Physical Models. Comptes Rendus de l'Academie des Sciences de Paris, s. II, V. 305, p. 1313-1319.

Vendeville, B.C. and Cobbold, P.R. 1988. How Normal Faulting and Sedimentation Interact to Produce Listric Fault Profiles and Stratigraphic Wedges. Journal of Structural Geology. V. 10, p. 649-659.

Vendeville, B.C., and Jackson, M.P.A. 1992a. The rise of Diapirs during Thin-Skinned Extension: Marine and Petroleum Geology, v. 9, p. 331-353

Vendeville, B.C., and Jackson, M.P.A. 1992b. The Fall of Diapirs During Thin-Skinned Extension. Marine and Petroleum Geology, v. 9, p. 354-371.

Vendeville, B.C. and Nilsen, K.T. 1995. Episodic Growth of Salt Domes Driven by Horizontal Shortening. GCSSEPM Foundation 16th Annual Research Conference. Salt, Sediment and Hydrocarbons, p. 285-295.

Walkden, G.M. 1987. Sedimentary and Diagenetic Styles in Late Devonian Carbonates in Britain. in European Dinantian Environments, eds. Miller, J., Adama, A.E., and Wright, V.P. p. 131-155.

Walker, C.W. 1974. Nature and Orogin of Caprock Overlying Gulf Coast Salt Domes. In, Fouth International Symposium on Salt. V. 1, p. 169-195. North Ohio Geological Society.

Webb, G.W. 1963. Occurrence and Exploration Significance of Strike-Slip Faults in Southern New Brunswick. AAPG Bulletin, V. 47, p. 1904-1927.

Webb, G.W. 1969. Palaeozoic Wrench Faults in Canadian Appalachians. In M. Kay, ed. North Atlantic Geology and Continental Drift. AAPG Memoir 12, p. 754-786.

Weinberg, R.F. 1993. The Upward Transport of Inclusions in Newtonian and Power-Law Salt Diapirs. Tectoniphysics, V. 228, p. 141-150.

Worrall, D.M., and Snelson, S. 1989. Evolution of the Northern Gulf of Mexico, with Emphesis on Cenozioc Growth Faulting and the Role of Salt. in The Geology of North America - an Overview, eds. Bally, A.W., and Palmer, A.R, GSA, Boulder, Colorado, v. A, p. 97-138.

Wightman, W.G., Grant, A.C., and Rehill, T.A. 1994. Paleontotlogical Evidence for Marine Influence During Deposition of the Westphalian Coal Measures in the Gulf of St. Lawrence-Sydney Basin Region, Atlantic Canada. in Current Research 1994-D; Geological Survey of Canada, p. 41-50.

Wightman, W.G., Scott, D.B., Medioli, F.S., and Gibling, M.R. 1993. Carboniferous Marsh Formainifera from Coal-Bearing Strata at the Sydney Basin, Nova Scotia: A New Tool for Identifying Paralic Coal-Forming Environments. Geology 21, p. 631-634.

Wightman, W.G. 1994. Cable Head E-95 and Brion Island No.1 Wells: Agglutinated Formainifera and Thecamoebian Assemblages. Paleotec Geological Consulting, unpublished report, 3p.

Williams, E.P. 1974. Geology and Petroloeum Possibilities in and around the Gulf of St. Lawrence. AAPG Bulletin, v. 58, p. 1137-1155.

Withjack, M.O., and Scheiner, C. 1982. Fault Patterns Associated with Domes - an Experimental and Analytical Study. AAPG Bulletin, v. 66, p. 302-316.

Zeigler, P.A. 1990. Geologic Atlas of Western and Central Europe. The Hague, Shell International Petroleum.

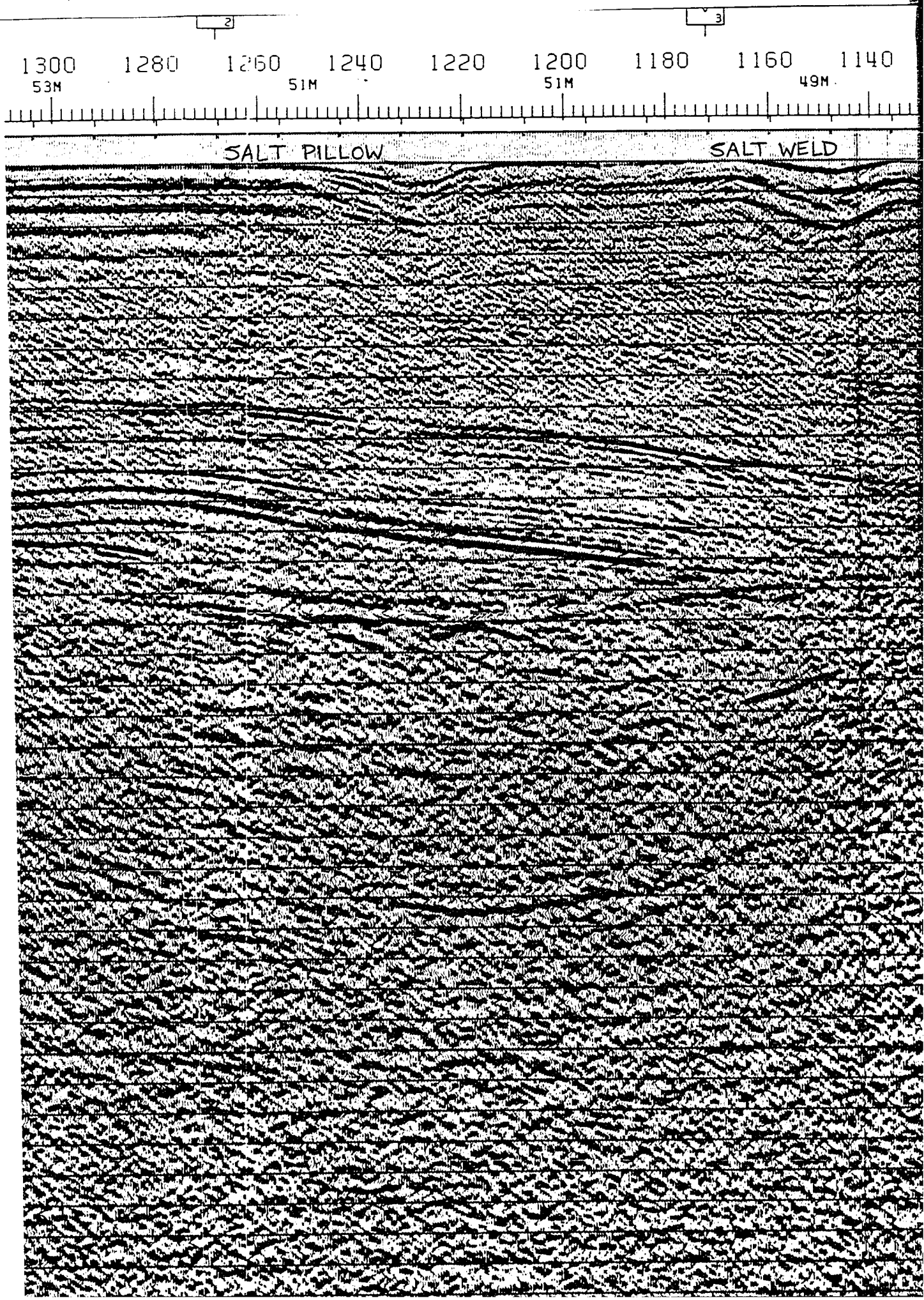
2
3
1300
1280
1260
1240
1220
1200
1180
1160
1140
53M
51M
51M
49M
SALT PILLOW
SALT WELD

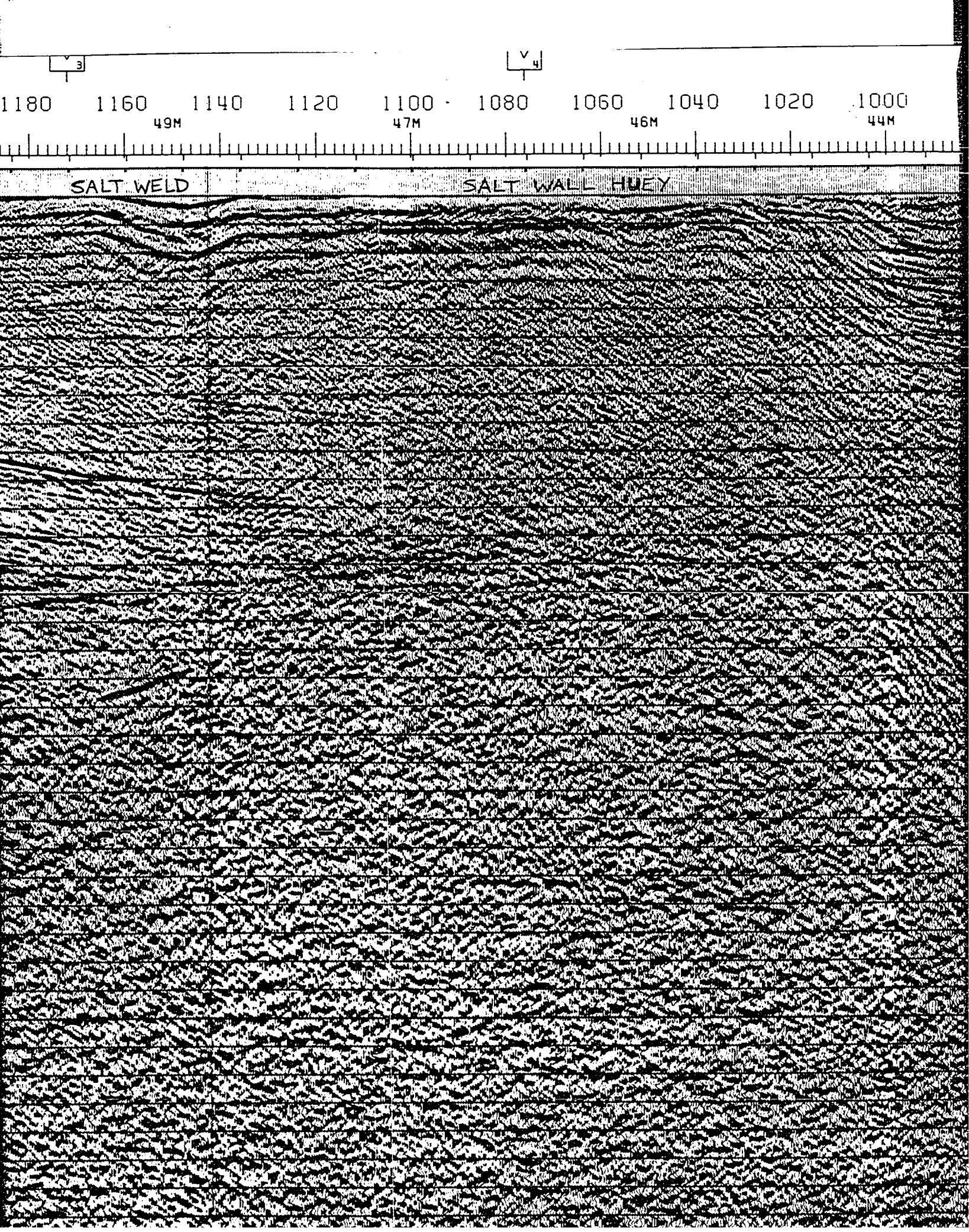
V 3
V 4
1180
1160
1140
1120
1100
1080
1060
1040
1020
1000
49M
47M
46M
44M
SALT WELD
SALT WALL HUEY

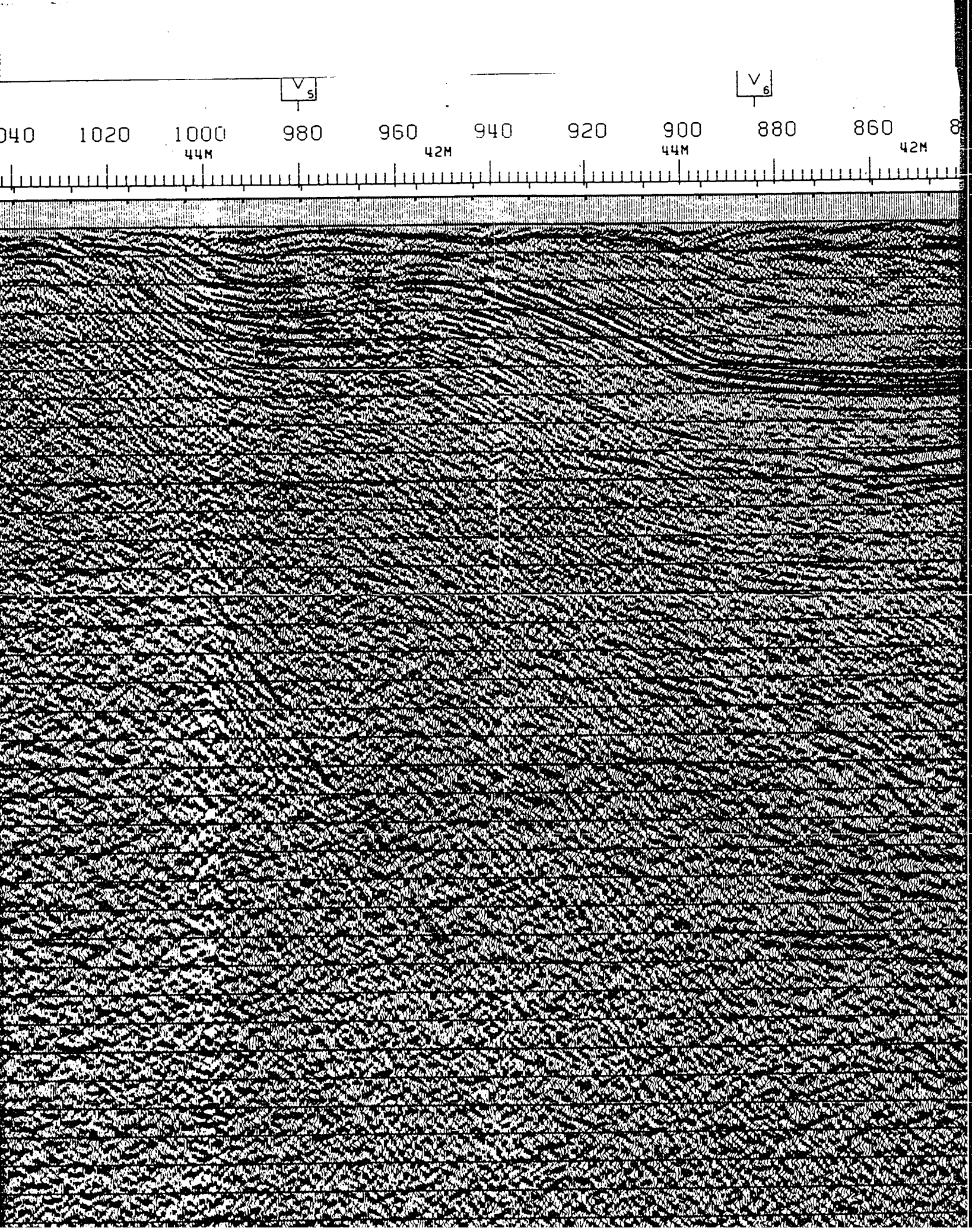
V5
V6
040
1020
1000
980
960
940
920
900
880
860
44M
42M
44M
42M

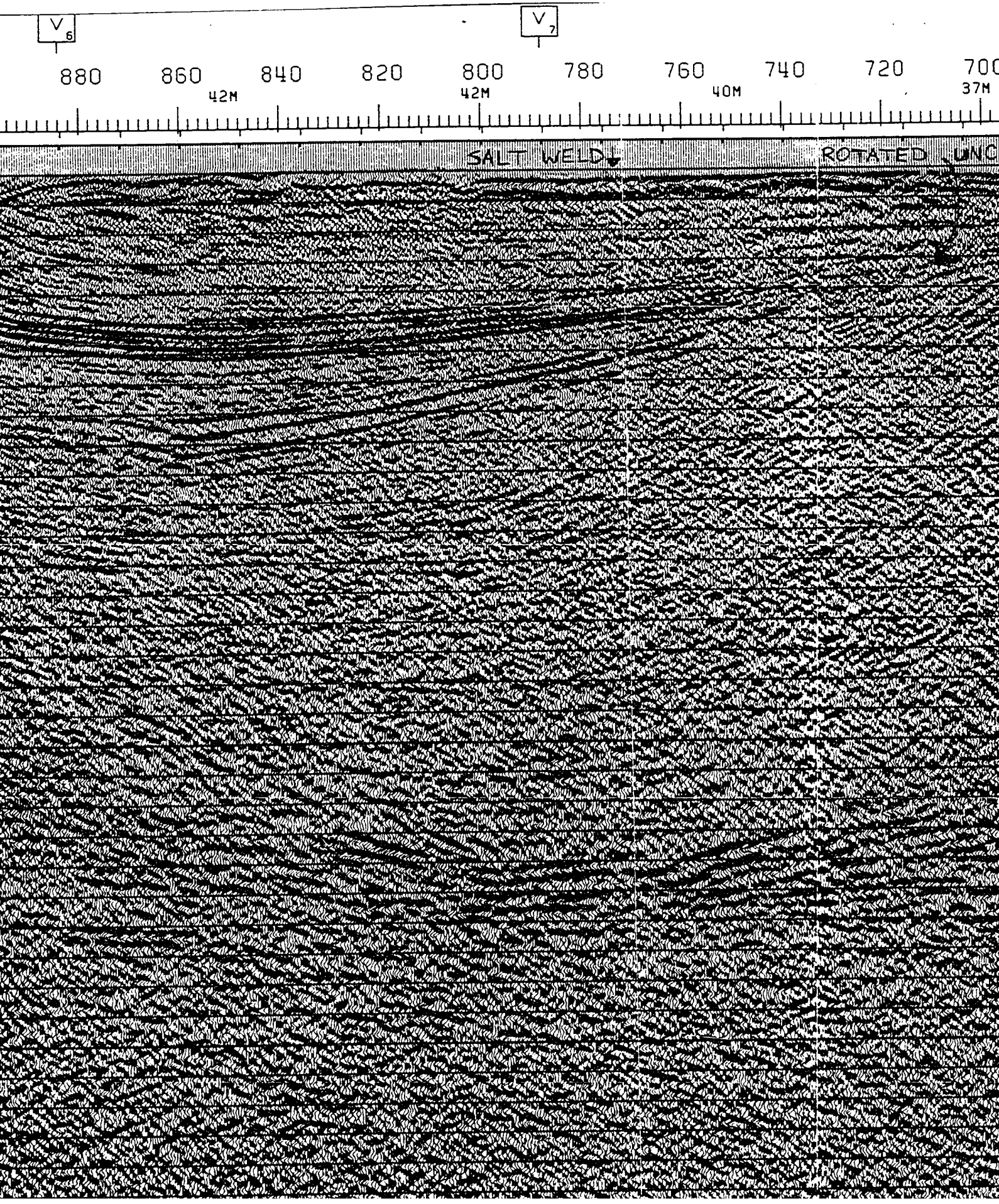
V6
V7
880
860
840
820
800
780
760
740
720
700
42M
42M
40M
37M
SALT WELD
ROTATED

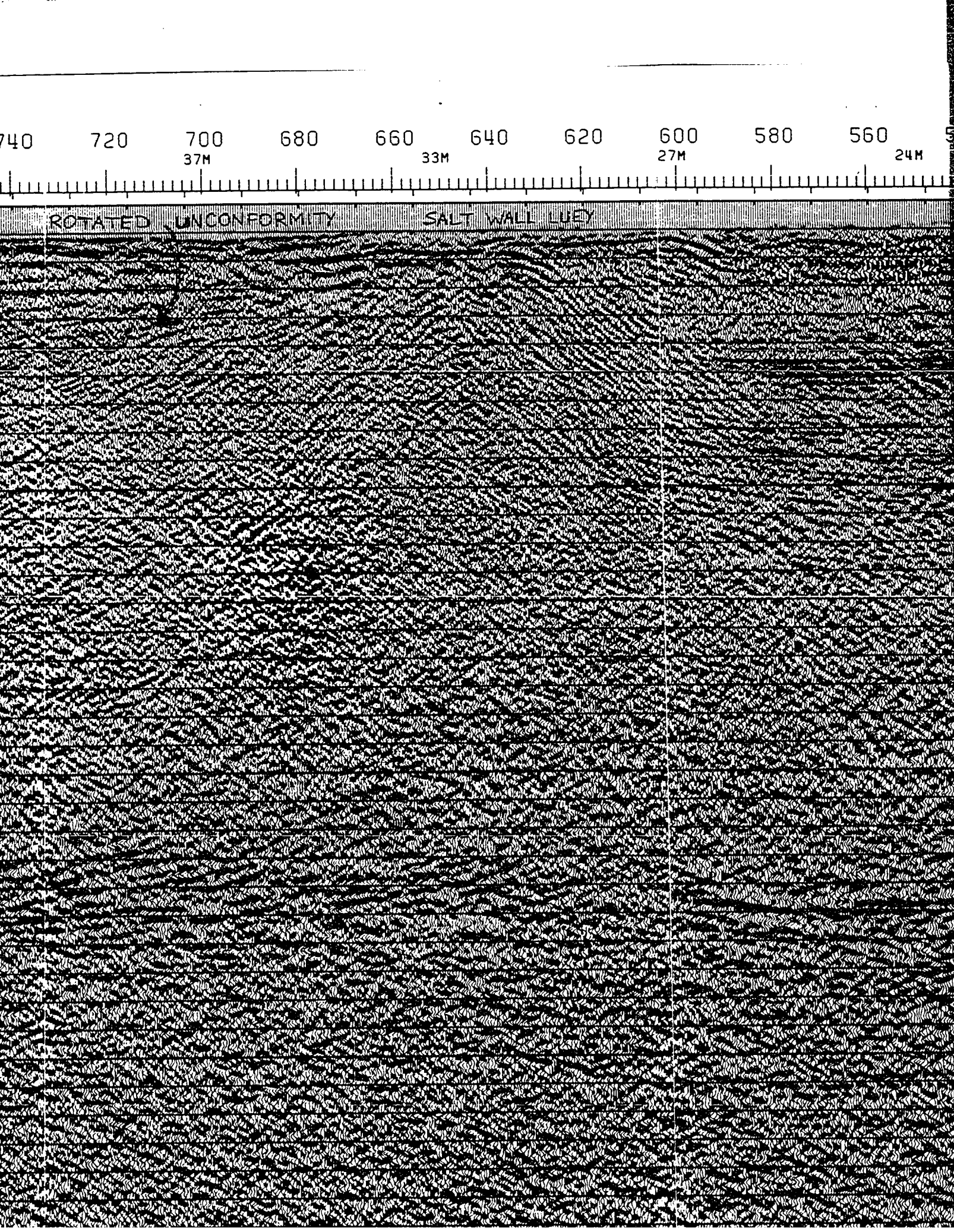
740
720
700
37M
680
660
33M
640
620
600
27M
580
560
24M
ROTATED UNCONFORMITY
SALT WALL LUEY

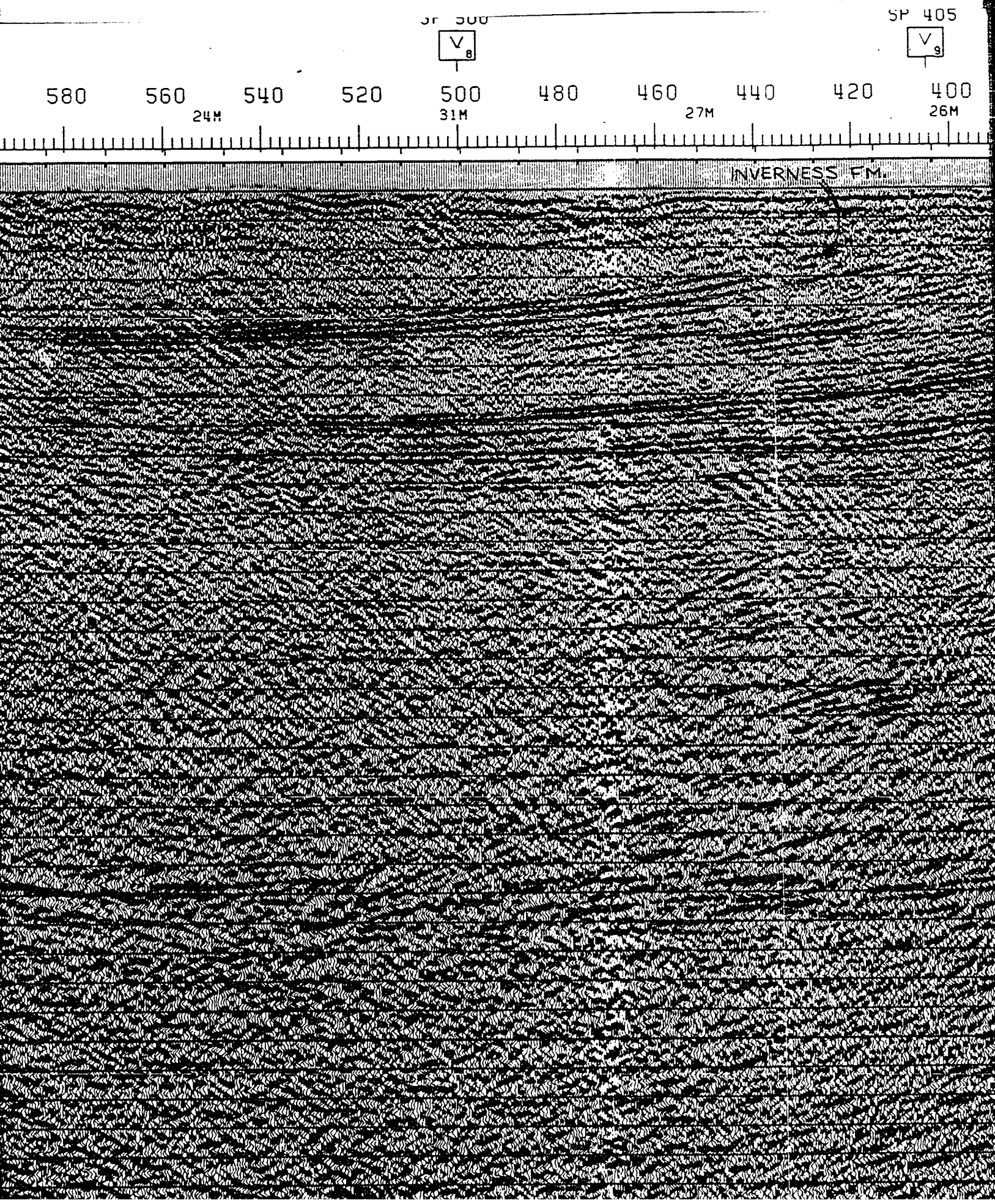
SP 405
V9
580
560
540
520
500
480
460
440
420
400
24M
31M
27M
26M
INVERNESS FM.

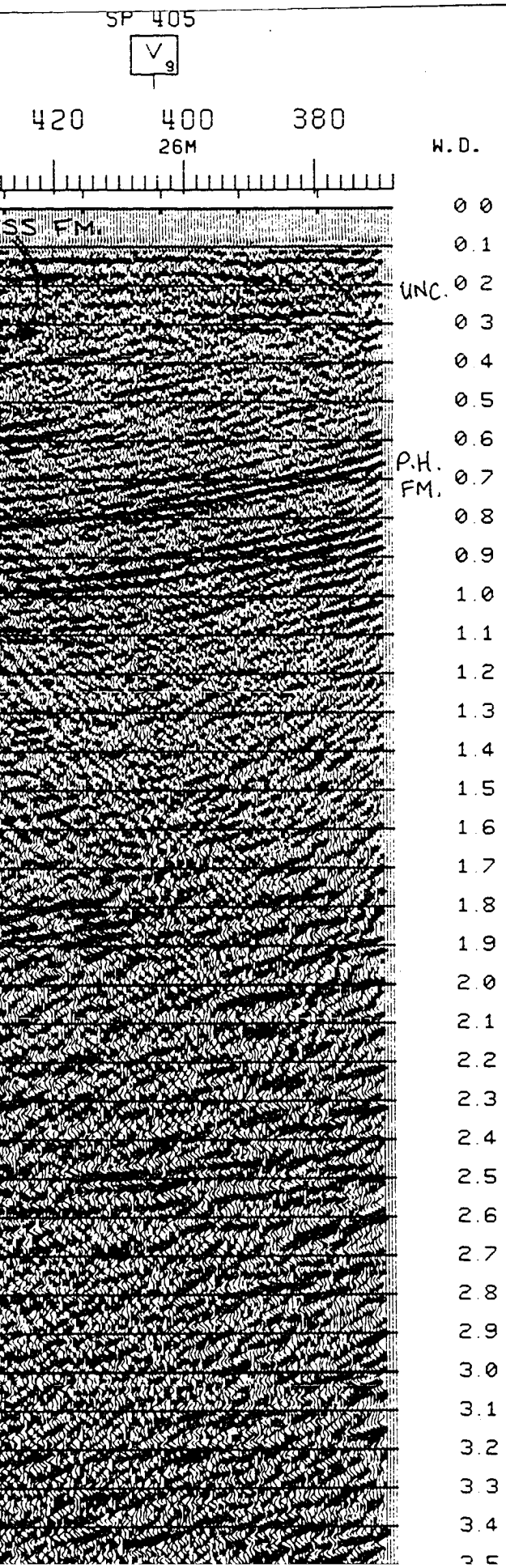

891-1364

SOUTHEAST

CHEVRON STANDARD LTD.

AREA: NORTHUMBERLAND STRAIT

SHOT BY WESTERN GEOPHYSICAL COMPANY PARTY 127 JULY
PROCESSED BY WESTERN GEOPHYSICAL (CALGARY) GROUP 6 OCT

RECORDING DATA

SOURCE

ENERGY SOURCE	AIR GUNS
CHARGE SIZE	1050 CU.IN
NUMBER OF GUNS	15
GUN DEPTH	6 M
FIRING INTERVAL	27 M
SHOT POINT INTERVAL	27 M
DISTANCE OF SOURCE TO ANTENNA	47 M

INSTRUMENTS

SYSTEM	KILOSEIS
AMPLIFIER	INST. FLOATING POINT
FILTER	L/9-H/450
SAMPLING INTERVAL	1 MS
RECORD LENGTH	5.0 SEC
FORMAT	SEG-D

CABLE

TYPE CABLE	STREAMER
CABLE LENGTH	2565 M
CABLE DEPTH	8 M
LEAD IN	187 M
GROUP INTERVAL	27 M
NUMBER OF GROUPS RECORDED	96
SPREAD	2752 M

ARRAY PARAMETERS

ROMS	7/21
CHANNELS PER ARRAY	8.50% OVERLAP
WEIGHTS	32.32.32.32.32.32.32
NUMBER OF DATA CHANNELS RECORDED	384
CHANNEL INTERVAL	6.67 M

PROCESSING SEQUENCE AND PARAMETERS

PROCESSING SAMPLING INTERVAL 4 MS

1. SIGNATURE DECONVOLUTION
2. DECONVOLVED BEFORE STACK
   - WINDOW LENGTH 2 ZONES OF 2500 MS
   - LENGTH OPERATOR 280 MS
   - PREDICTION DISTANCE 4 MS
3. NMO STACK 4800 %
4. RELATIVE AMP. COMPENSATION
5. F-K DOMAIN FILTER
6. DECONVOLVED AFTER STACK
   - WINDOW LENGTH 2 ZONES OF 2500 MS
   - LENGTH OPERATOR 300 MS
   - PREDICTION DISTANCE 20 MS
7. FINITE DIFFERENCE MIGRATION
8. TIME VARIANT FILTER

TIME	L.C. (HZ)	H.C.

~~SEG-D~~ 891-1364 11-F-NW
891-1364 11-K-SW

SOUTHEAST

W.D.

UNC. P.H. FM.

CHEVRON STANDARD LTD.

AREA: NORTHUMBERLAND STRAIT

SHOT BY WESTERN GEOPHYSICAL COMPANY PARTY 127 JULY 1981
PROCESSED BY WESTERN GEOPHYSICAL (CALGARY) GROUP 6 OCT 1981

RECORDING DATA

SOURCE

ENERGY SOURCE	AIR GUNS
CHARGE SIZE	1050 CU.IN
NUMBER OF GUNS	15
GUN DEPTH	6 M
FIRING INTERVAL	27 M
SHOT POINT INTERVAL	27 M
DISTANCE OF SOURCE TO ANTENNA	47 M

INSTRUMENTS

SYSTEM	KILOSEIS
AMPLIFIER	INST. FLOATING POINT
FILTER	L/9-H/450
SAMPLING INTERVAL	1 MS
RECORD LENGTH	5.0 SEC
FORMAT	SEG-D

CABLE

TYPE CABLE	STREAMER
CABLE LENGTH	2565 M
CABLE DEPTH	8 M
LEAD IN	187 M
GROUP INTERVAL	27 M
NUMBER OF GROUPS RECORDED	96
SPREAD	2752 M

ARRAY PARAMETERS

ROMS	7/21
CHANNELS PER ARRAY	8.50% OVERLAP
WEIGHTS	32.32.32.32.32.32.32.32
NUMBER OF DATA CHANNELS RECORDED	384
CHANNEL INTERVAL	6.67 M

PROCESSING SEQUENCE AND PARAMETERS

PROCESSING SAMPLING INTERVAL 4 MS

1. SIGNATURE DECONVOLUTION
2. DECONVOLVED BEFORE STACK
   - WINDOW LENGTH 2 ZONES OF 2500 MS
   - LENGTH OPERATOR 280 MS
   - PREDICTION DISTANCE 4 MS
3. NMO STACK 4800 %
4. RELATIVE AMP. COMPENSATION
5. F-K DOMAIN FILTER
6. DECONVOLVED AFTER STACK
   - WINDOW LENGTH 2 ZONES OF 2500 MS
   - LENGTH OPERATOR 300 MS
   - PREDICTION DISTANCE 20 MS
7. FINITE DIFFERENCE MIGRATION
8. TIME VARIANT FILTER

TIME	L.C. (HZ)	H.C.

SEG. D 91-1364 11-F-NW
891-1364 11-K-SW

SOUTHEAST

75

PROJ NO: 8624 C4 9E LINE NO:

STANDARD LTD.

HUMBERLAND STRAIT

COMPANY	PARTY 127	JULY 1981
SICAL (CALGARY)	GROUP 6	OCT 1981

RDING DATA

SOURCE
- AIR GUNS
- 1053 CU.IN
- 15
- 6 M
- 27 M
- 27 M
- NA 47 M

NSTRUMENTS
- KILOSEIS
- INST. FLOATING POINT
- L/9-H/450
- 1 MS
- 5.0 SEC
- SEG-D

CABLE
- STREAMER
- 2565 M
- 8 M
- 187 M
- 27 M
- 96
- 2752 M

Y PARAMETERS
- 7/21
- 8.50% OVERLAP
- 32.32.32.32.32.32.32.32
- CORDED 384
- 6.67 M

EQUENCE AND PARAMETERS

SAMPLING INTERVAL 4 MS
CONVOLUTION
BEFORE STACK
- 2 ZONES OF 2500 MS
- OR 280 MS
- STANCE 4 MS

300 %
. COMPENSATION
ILTER
AFTER STACK
- 2 ZONES OF 2500 MS
- OR 300 MS
- STANCE 20 MS

RENCE MIGRATION
FILTER
- L.C. (HZ) H.C.

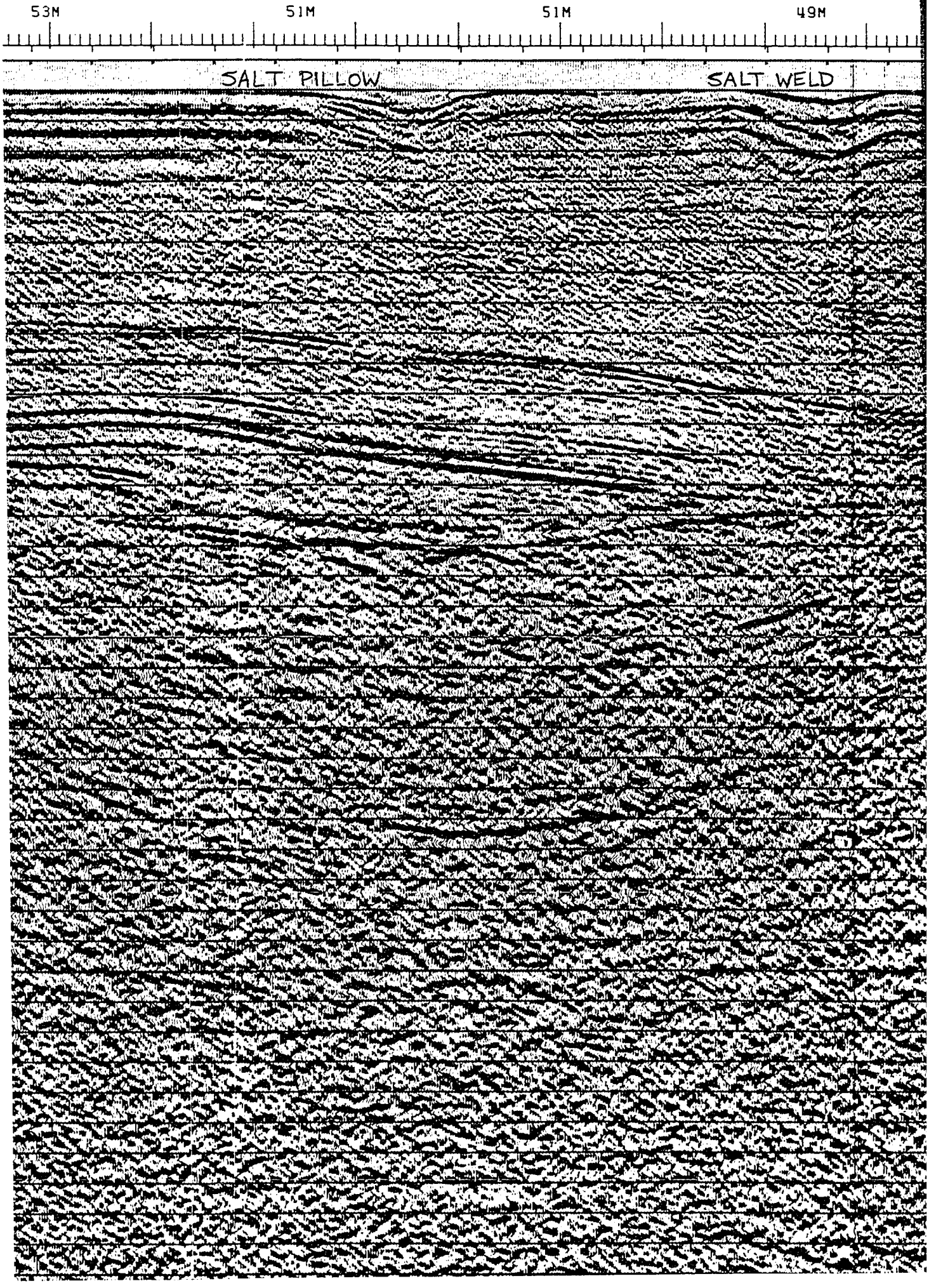
53M
51M
51M
49M
SALT PILLOW
SALT WELD

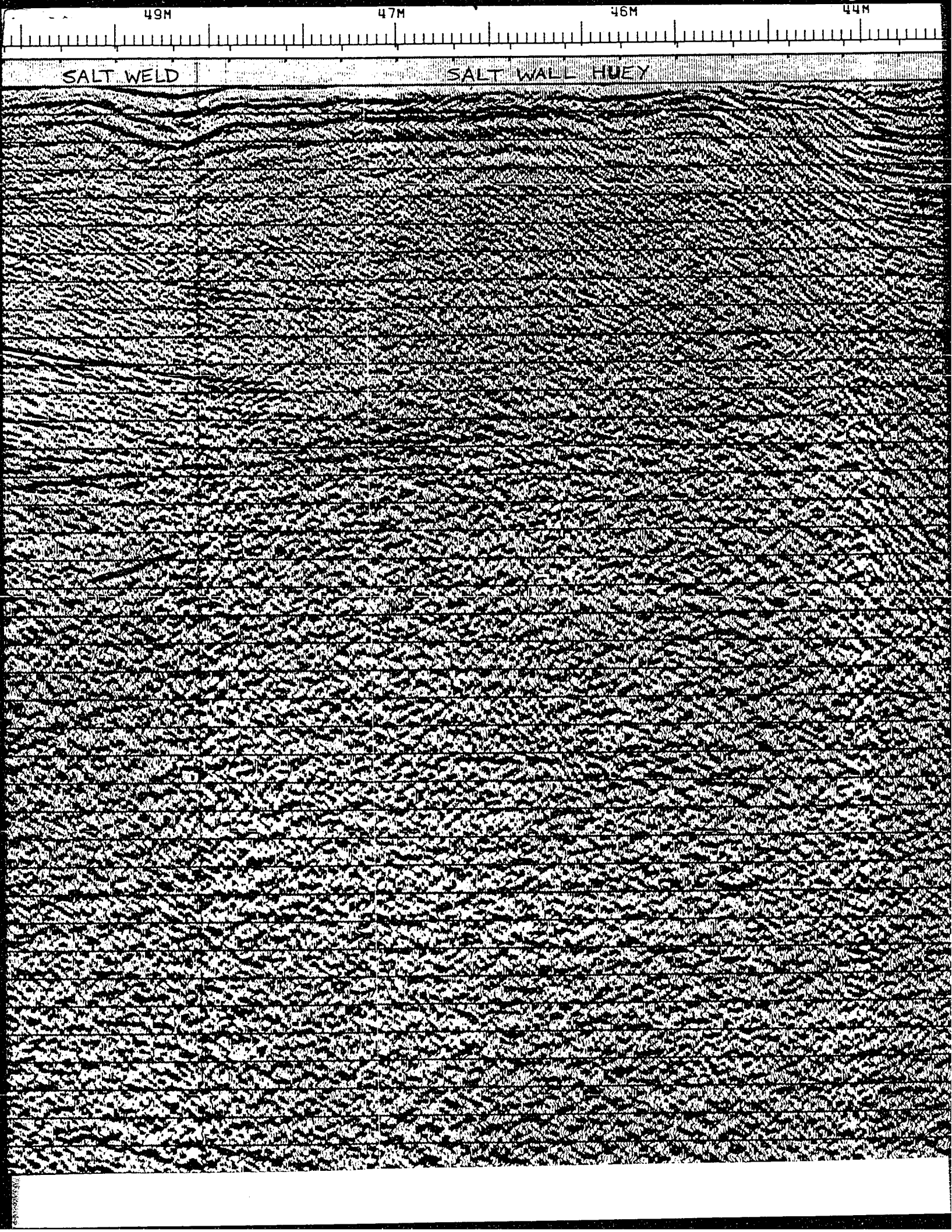
49M
47M
46M
44M
SALT WELD
SALT WALL HUEY

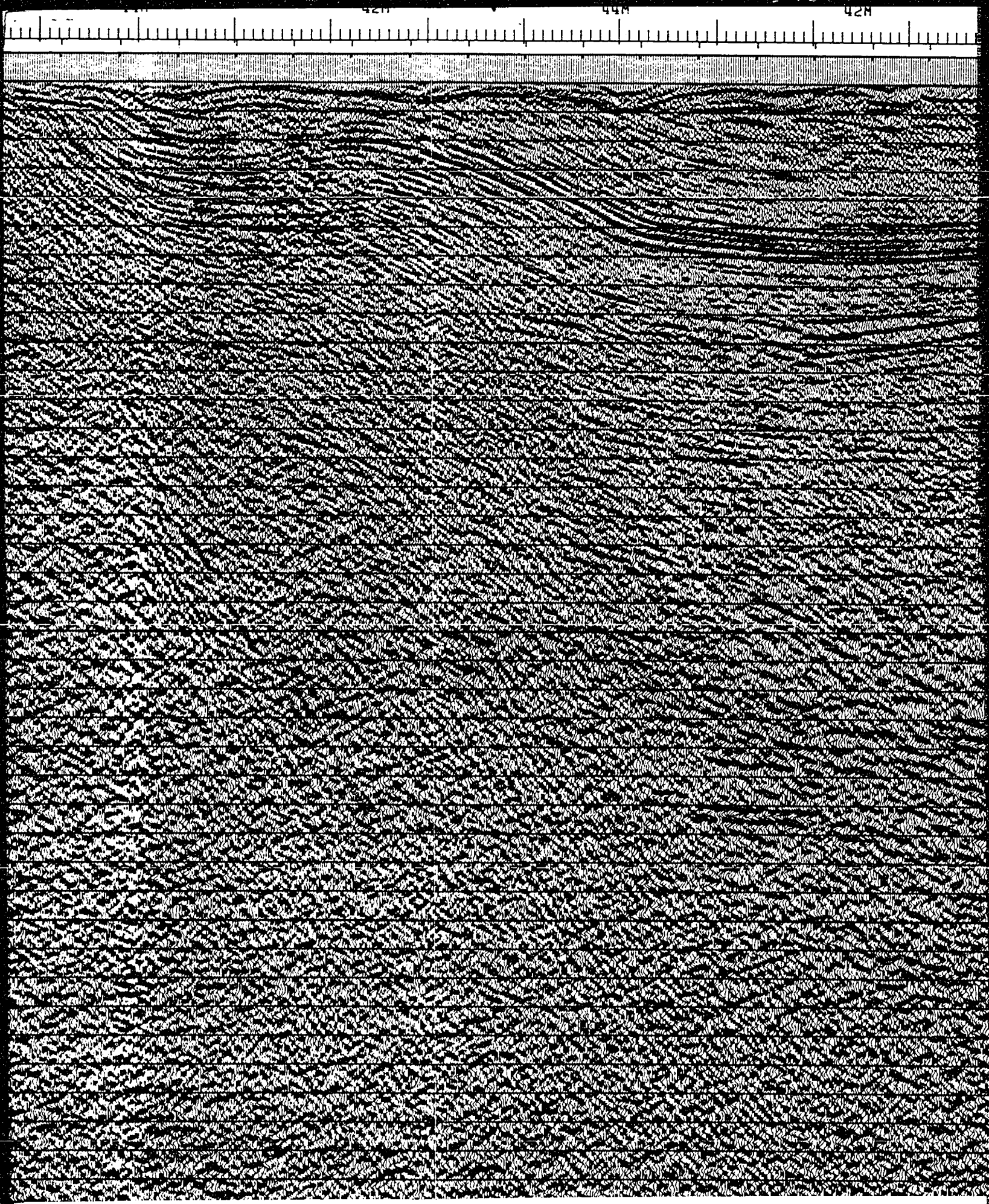
42M
44M
42M

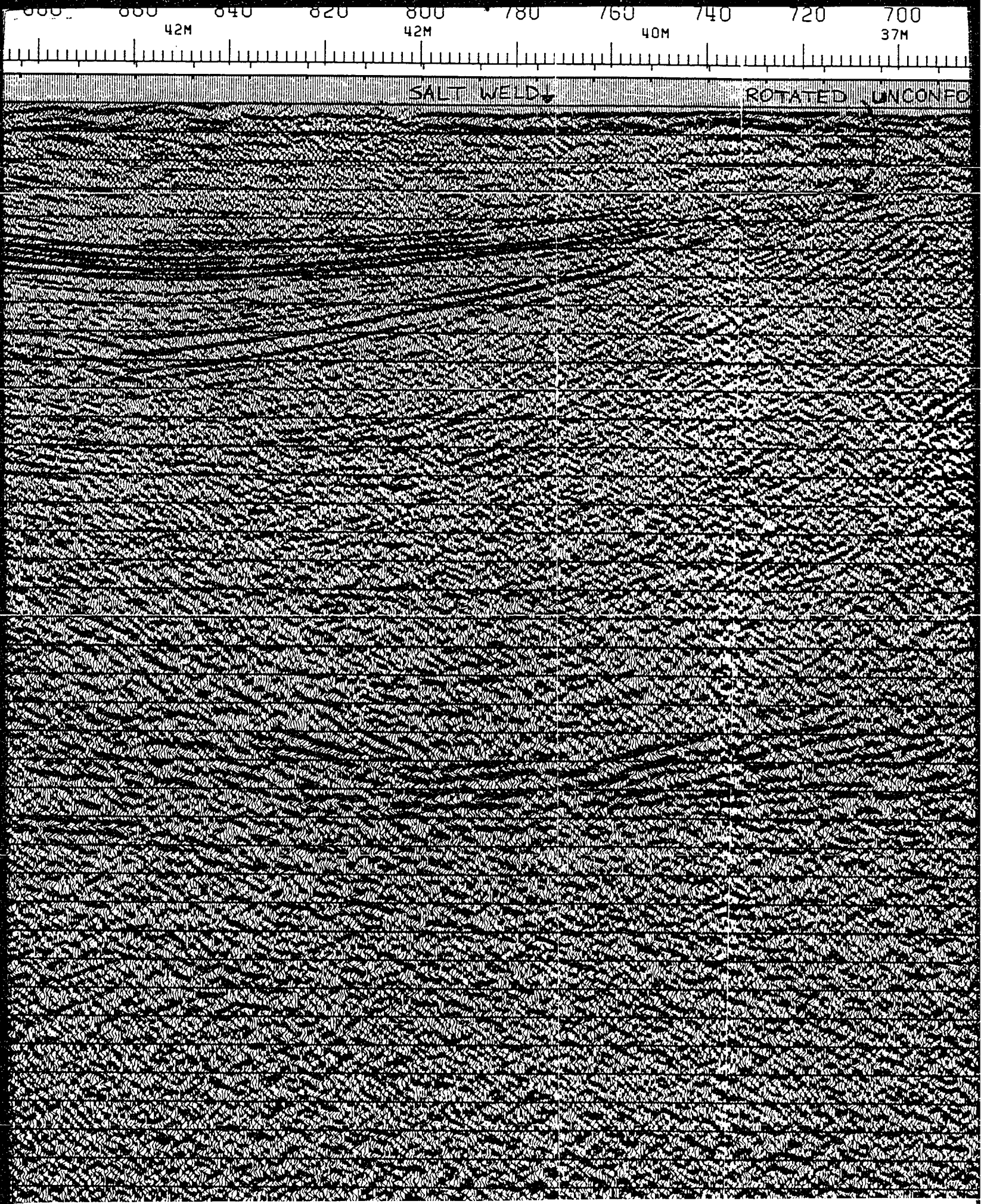
860
840
820
800
780
760
740
720
700
42M
42M
40M
37M
SALT WELD
ROTATED, UNCONFO

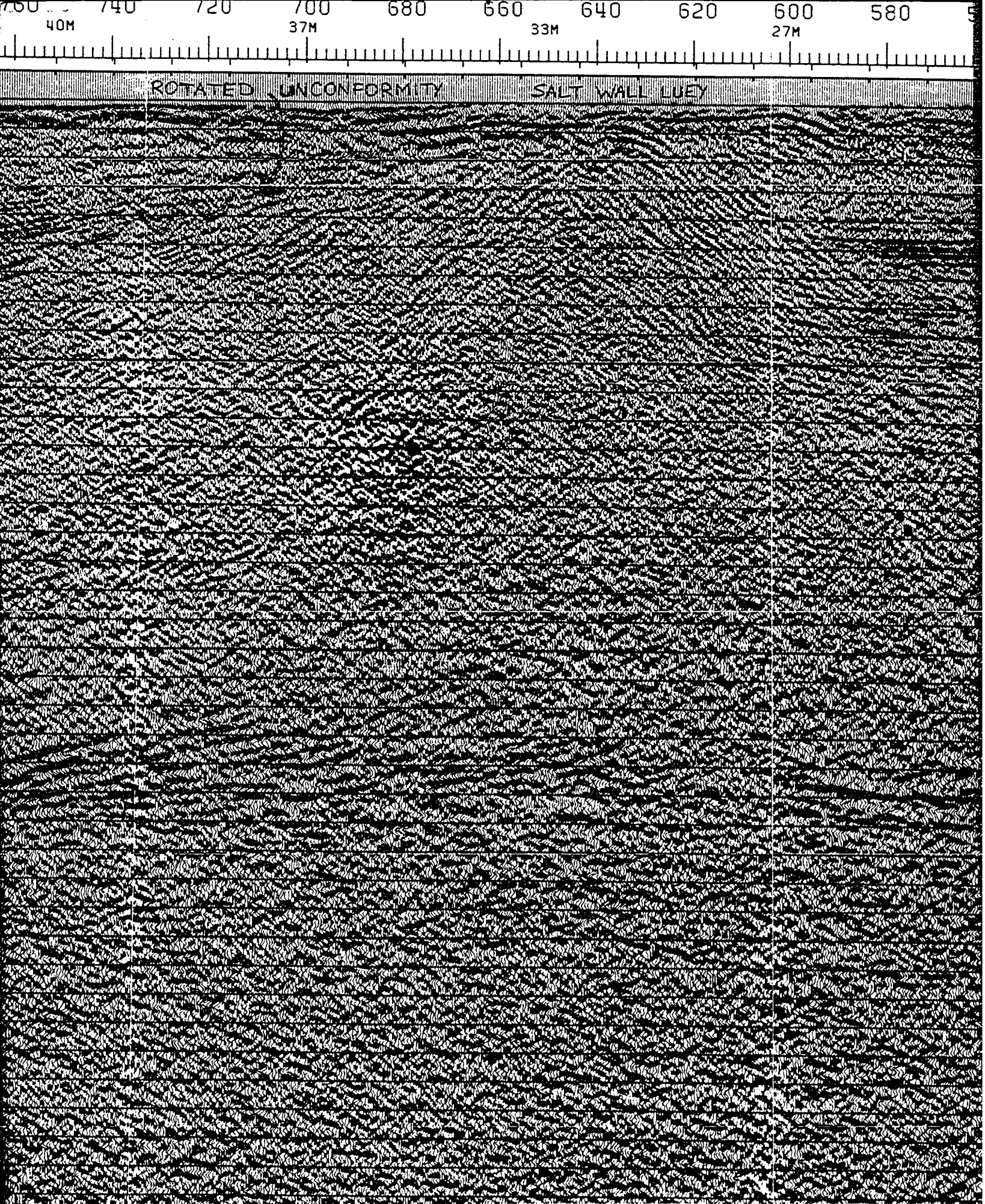
760
740
720
700
680
660
640
620
600
580
40M
37M
33M
27M
ROTATED UNCONFORMITY
SALT WALL LUEY

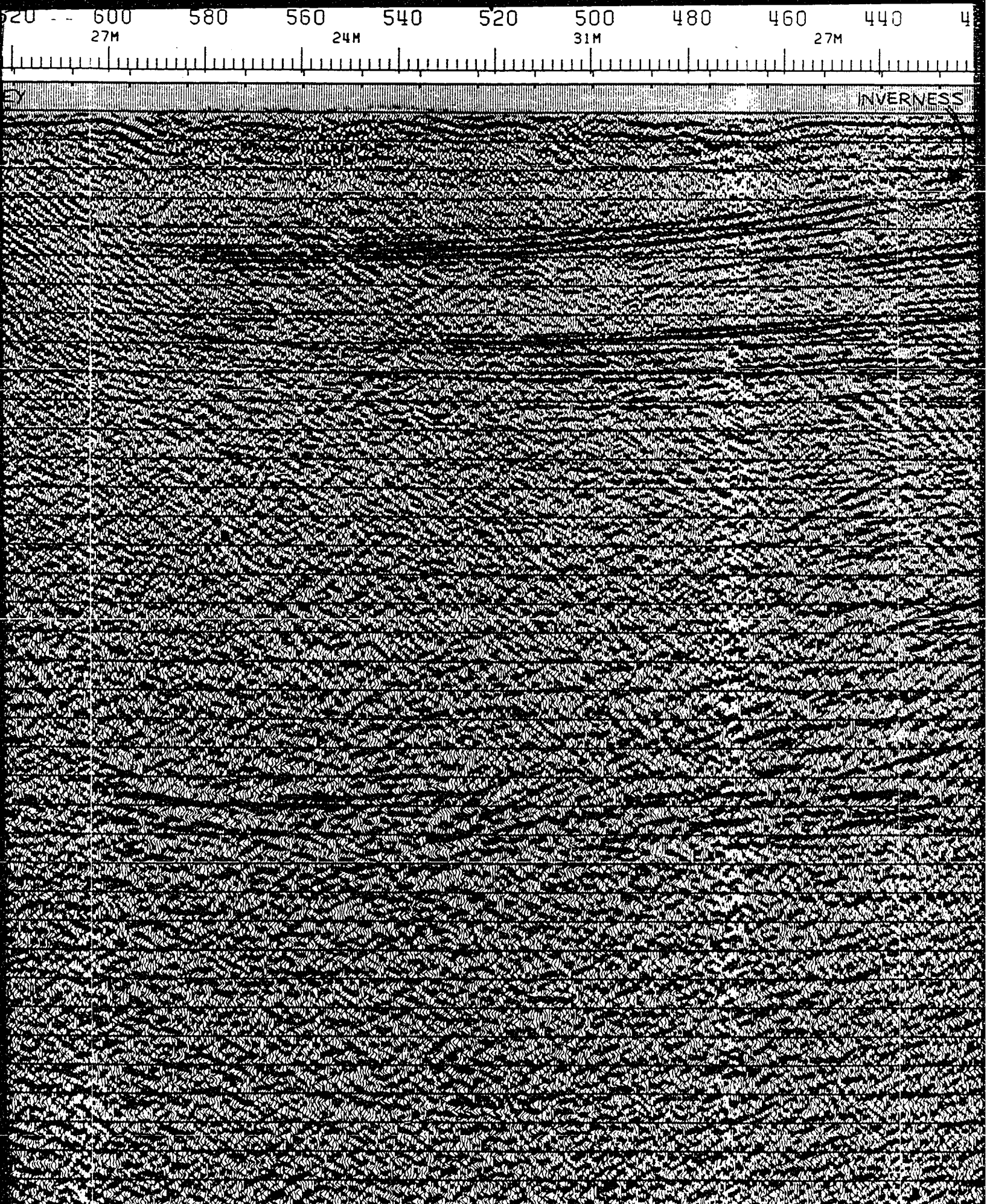
620
600
580
560
540
520
500
480
460
440
27M
24M
31M
27M
INVERNESS

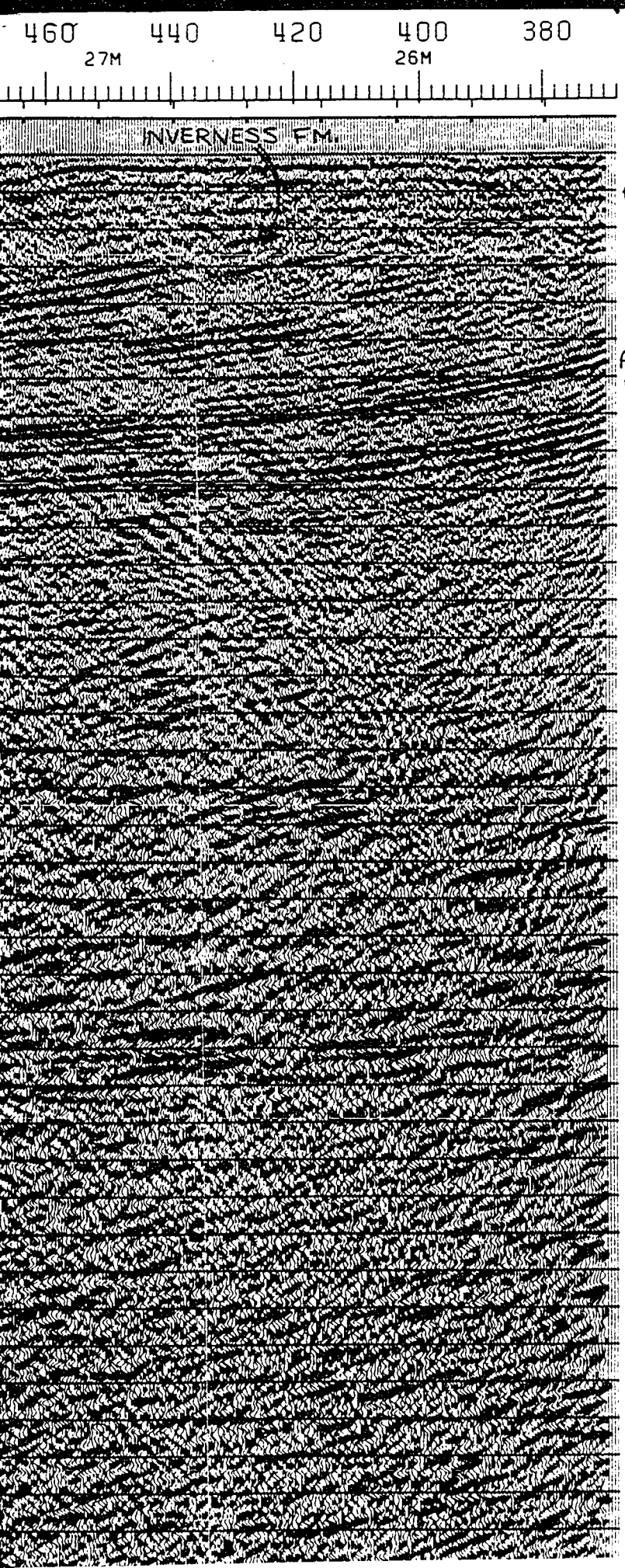

CHEVRON STANDA

AREA: NORTHUMBERLAND

SHOT BY WESTERN GEOPHYSICAL COMPANY
PROCESSED BY WESTERN GEOPHYSICAL (CALGA

RECORDING DA

SOURCE

ENERGY SOURCE	AIR
CHARGE SIZE	105
NUMBER OF GUNS	15
GUN DEPTH	6 M
FIRING INTERVAL	27 M
SHOT POINT INTERVAL	27 M
DISTANCE OF SOURCE TO ANTENNA	47 M

INSTRUMENTS

SYSTEM	KILO
AMPLIFIER	INST
FILTER	L/9-
SAMPLING INTERVAL	1 MS
RECORD LENGTH	5.0
FORMAT	SEG-C

CABLE

TYPE CABLE	STREA
CABLE LENGTH	2565
CABLE DEPTH	8 M
LEAD IN	187 M
GROUP INTERVAL	27 M
NUMBER OF GROUPS RECORDED	96
SPREAD	2752

ARRAY PARAMETERS

ROMS	7/21
CHANNELS PER ARRAY	8.50
WEIGHTS	32.32
NUMBER OF DATA CHANNELS RECORDED	384
CHANNEL INTERVAL	6.67

PROCESSING SEQUENCE AND

PROCESSING SAMPLING IN

1. SIGNATURE DECONVOLUTION
2. DECONVOLVED BEFORE STA
   - WINDOW LENGTH 2 Z
   - LENGTH OPERATOR
   - PREDICTION DISTANCE
3. NMO STACK 4800 %
4. RELATIVE AMP. COMPENSA
5. F-K DOMAIN FILTER
6. DECONVOLVED AFTER STACK
   - WINDOW LENGTH 2 Z
   - LENGTH OPERATOR
   - PREDICTION DISTANCE
7. FINITE DIFFERENCE MIGRA
8. TIME VARIANT FILTER

TIME		L.C. (HZ
1.00	SEC	12
3.00	SEC	8
5.00	SEC	8

9. RMS GAIN (128-512 MS W

47 M

LEGE

W.D.

UNC.

P.H.
FM.

CHEVRON STANDARD LTD.

AREA: NORTHUMBERLAND STRAIT

SHOT BY WESTERN GEOPHYSICAL COMPANY PARTY 127 JULY 1981
PROCESSED BY WESTERN GEOPHYSICAL (CALGARY) GROUP 6 OCT 1981

RECORDING DATA

SOURCE

ENERGY SOURCE	AIR GUNS
CHARGE SIZE	1050 CU.IN
NUMBER OF GUNS	15
GUN DEPTH	6 M
FIRING INTERVAL	27 M
SHOT POINT INTERVAL	27 M
DISTANCE OF SOURCE TO ANTENNA	47 M

INSTRUMENTS

SYSTEM	KILOSEIS
AMPLIFIER	INST. FLOATING POINT
FILTER	L/9-H/450
SAMPLING INTERVAL	1 MS
RECORD LENGTH	5.0 SEC
FORMAT	SEG-D

CABLE

TYPE CABLE	STREAMER
CABLE LENGTH	2565 M
CABLE DEPTH	8 M
LEAD IN	187 M
GROUP INTERVAL	27 M
NUMBER OF GROUPS RECORDED	96
SPREAD	2752 M

ARRAY PARAMETERS

ROMS	7/21
CHANNELS PER ARRAY	8.50% OVERLAP
WEIGHTS	32.32.32.32.32.32.32.32
NUMBER OF DATA CHANNELS RECORDED	384
CHANNEL INTERVAL	6.67 M

PROCESSING SEQUENCE AND PARAMETERS

PROCESSING SAMPLING INTERVAL 4 MS

1. SIGNATURE DECONVOLUTION
2. DECONVOLVED BEFORE STACK
   - WINDOW LENGTH 2 ZONES OF 2500 MS
   - LENGTH OPERATOR 280 MS
   - PREDICTION DISTANCE 4 MS
3. NMO STACK 4800 %
4. RELATIVE AMP. COMPENSATION
5. F-K DOMAIN FILTER
6. DECONVOLVED AFTER STACK
   - WINDOW LENGTH 2 ZONES OF 2500 MS
   - LENGTH OPERATOR 300 MS
   - PREDICTION DISTANCE 20 MS
7. FINITE DIFFERENCE MIGRATION
8. TIME VARIANT FILTER

TIME		L.C. (HZ)	H.C.
1.00	SEC	12	60
3.00	SEC	8	45
5.00	SEC	8	30

9. RMS GAIN (128-512 MS WINDOW)

47 M

LEGEND

STANDARD LTD.

THUMBERLAND STRAIT

L COMPANY PARTY 127 JULY 1981
YSICAL (CALGARY) GROUP 6 OCT 1981

ORDING DATA

SOURCE
AIR GUNS
1050 CU.IN
15
6 M
27 M
27 M
NNA 47 M

INSTRUMENTS
KILOSEIS
INST. FLOATING POINT
L/9-H/450
1 MS
5.0 SEC
SEG-D

CABLE
STREAMER
2565 M
8 M
187 M
27 M
96
2752 M
AY PARAMETERS
7/21
8.50% OVERLAP
32.32.32.32.32.32.32.32
CORDED 384
6.67 M

EQUENCE AND PARAMETERS

SAMPLING INTERVAL 4 MS
ECONVOLUTION
BEFORE STACK
2 ZONES OF 2500 MS
TOR 280 MS
ISTANCE 4 MS
800 %
P. COMPENSATION
FILTER
AFTER STACK
2 ZONES OF 2500 MS
TOR 300 MS
ISTANCE 20 MS
ERENCE MIGRATION
T FILTER

	L.C. (HZ)	H.C.
EC	12	60
EC	8	45
EC	8	30

28-512 MS WINDOW)

LEGEND

NO: 8624 C4 9E LINE NO: 81

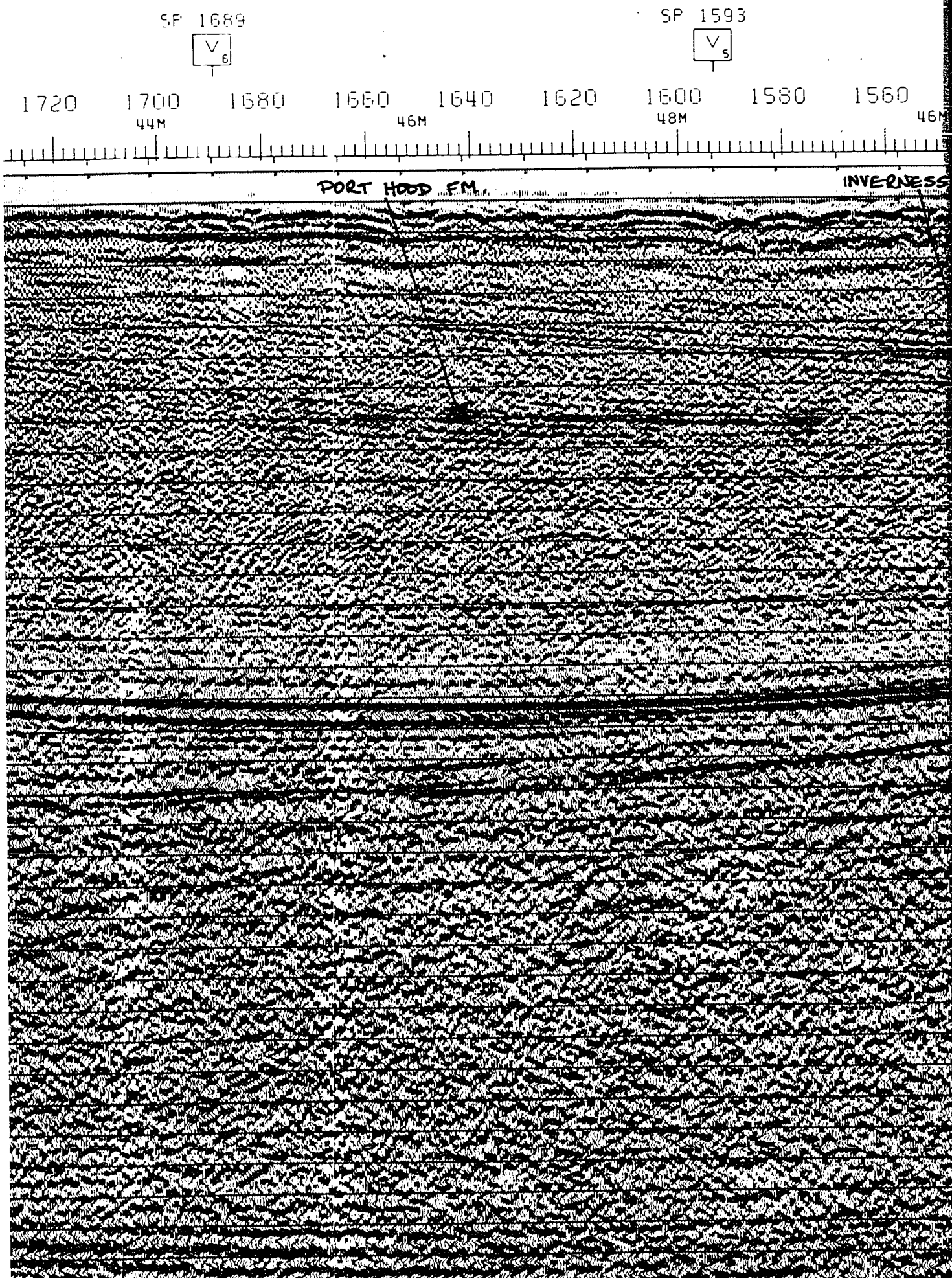
SP 1689
V6
SP 1593
V5
1720
1700
1680
1660
1640
1620
1600
1580
1560
44M
46M
48M
46M
PORT HOOD FM.
INVERNESS

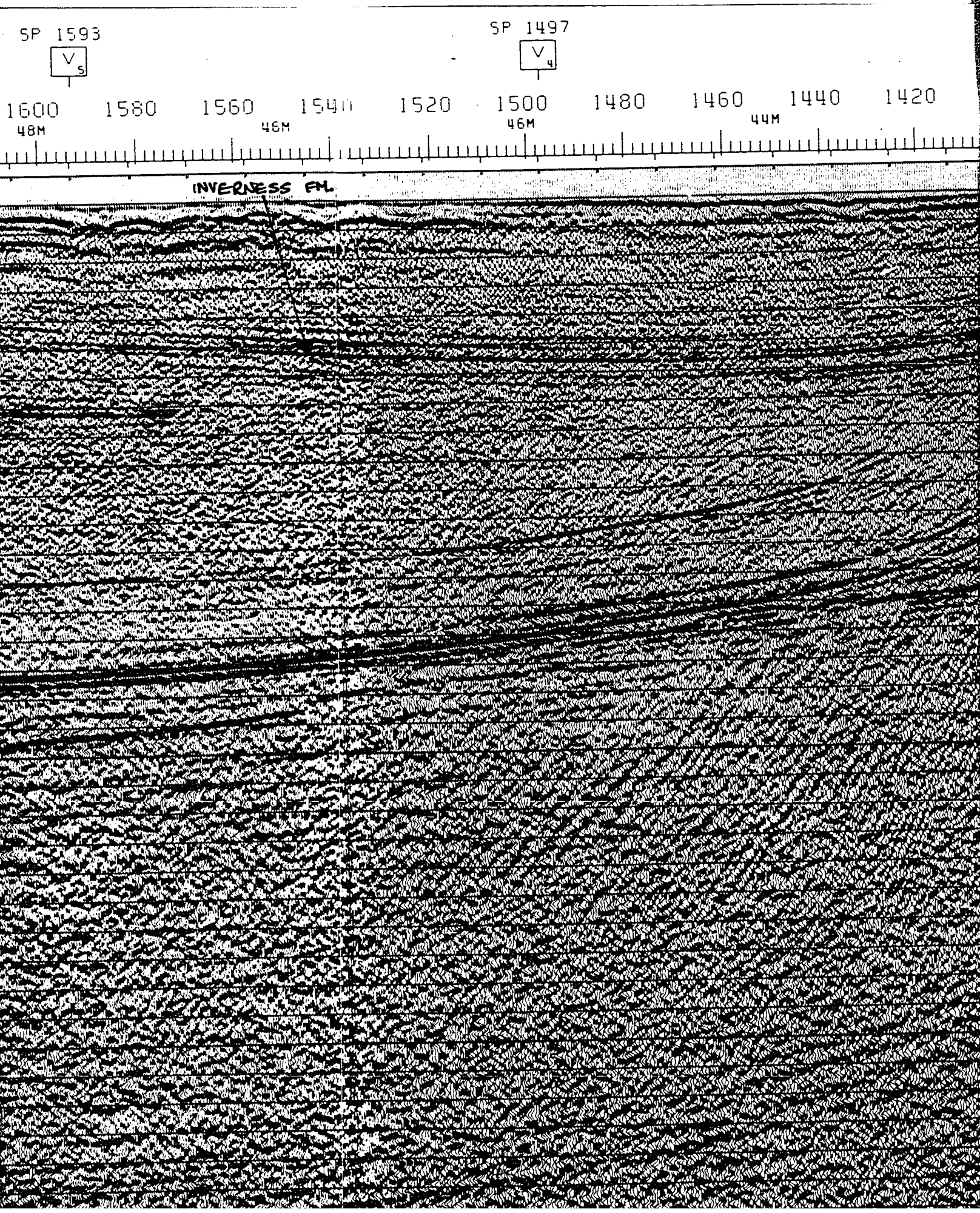
SP 1593
V5
SP 1497
V4
1600
1580
1560
1540
1520
1500
1480
1460
1440
1420
48M
46M
46M
44M
INVERNESS FM.

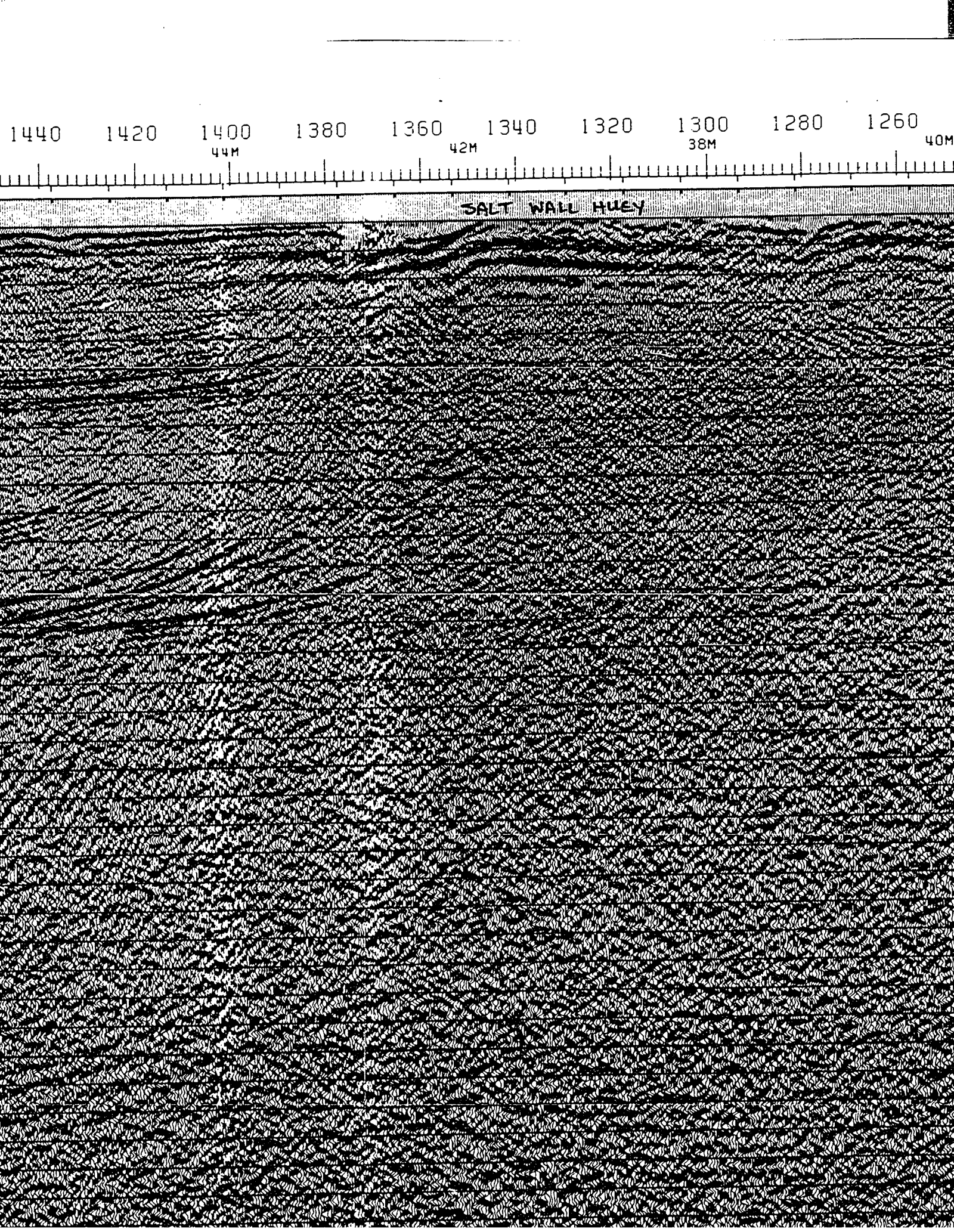
1440
1420
1400
44M
1380
1360
42M
1340
1320
1300
38M
1280
1260
40M
SALT WALL HUEY

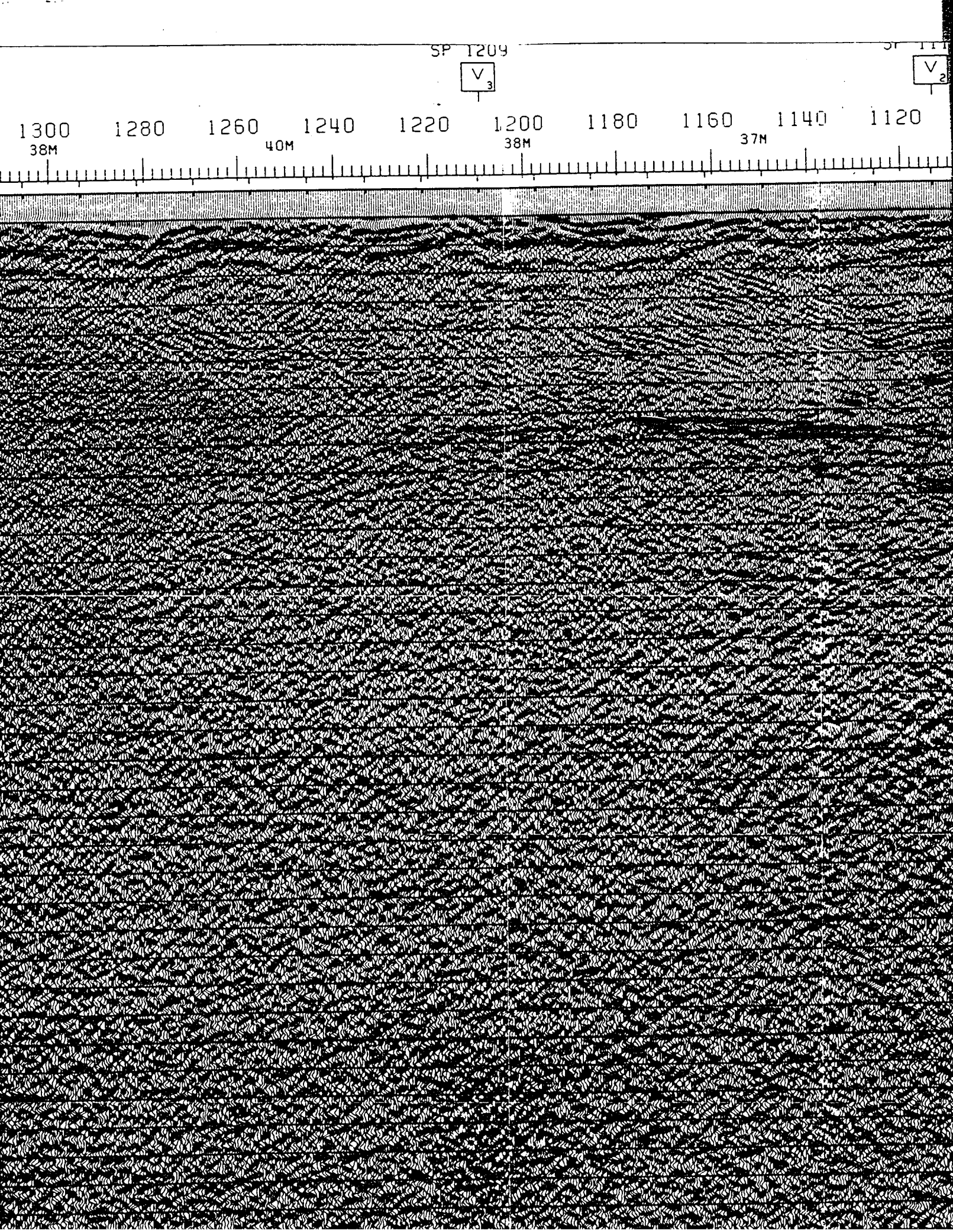
SP 1209
V3
V2
1300
1280
1260
1240
1220
1200
1180
1160
1140
1120
38M
40M
38M
37M

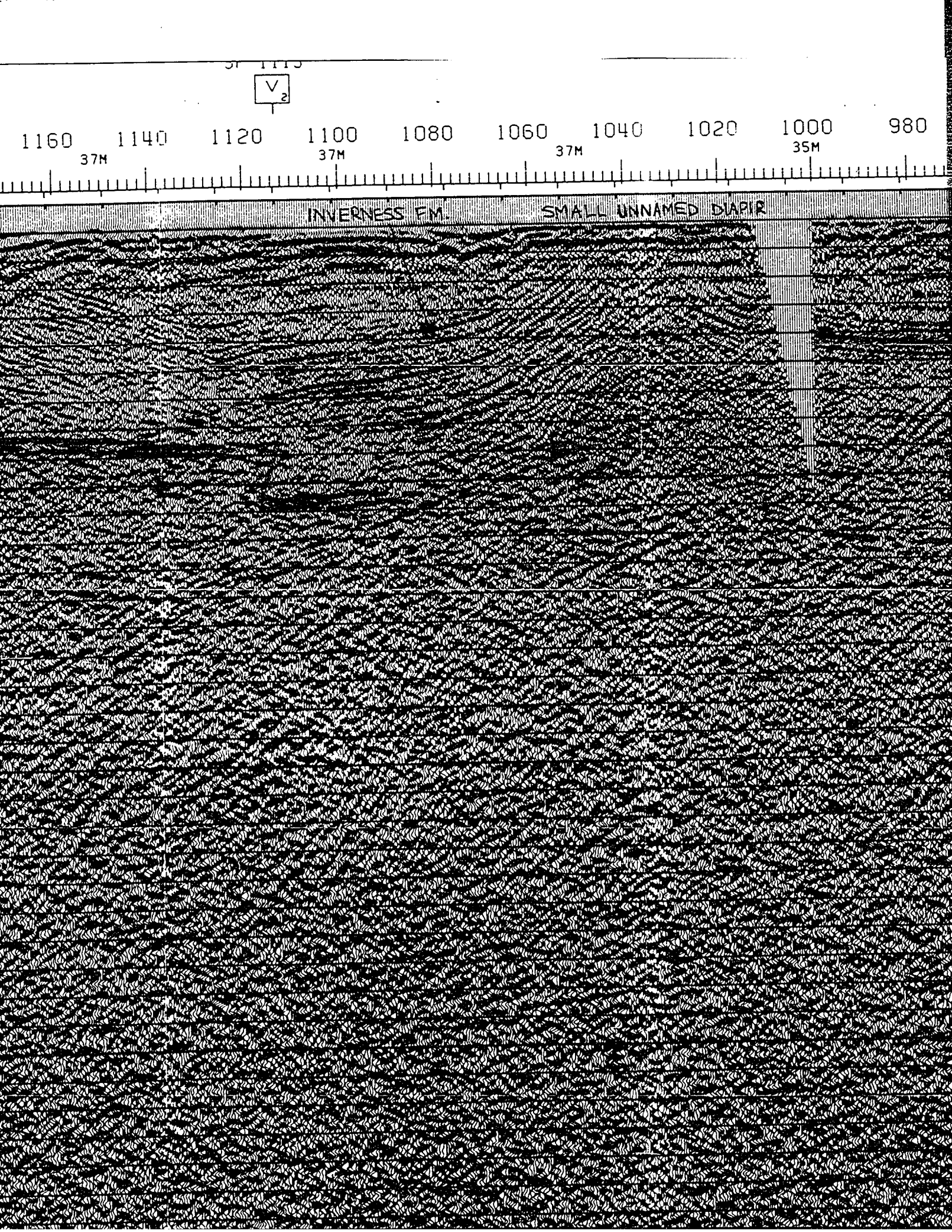
V2
1160
1140
1120
1100
1080
1060
1040
1020
1000
980
37M
37M
37M
35M
INVERNESS FM.
SMALL UNNAMED DIAPIR

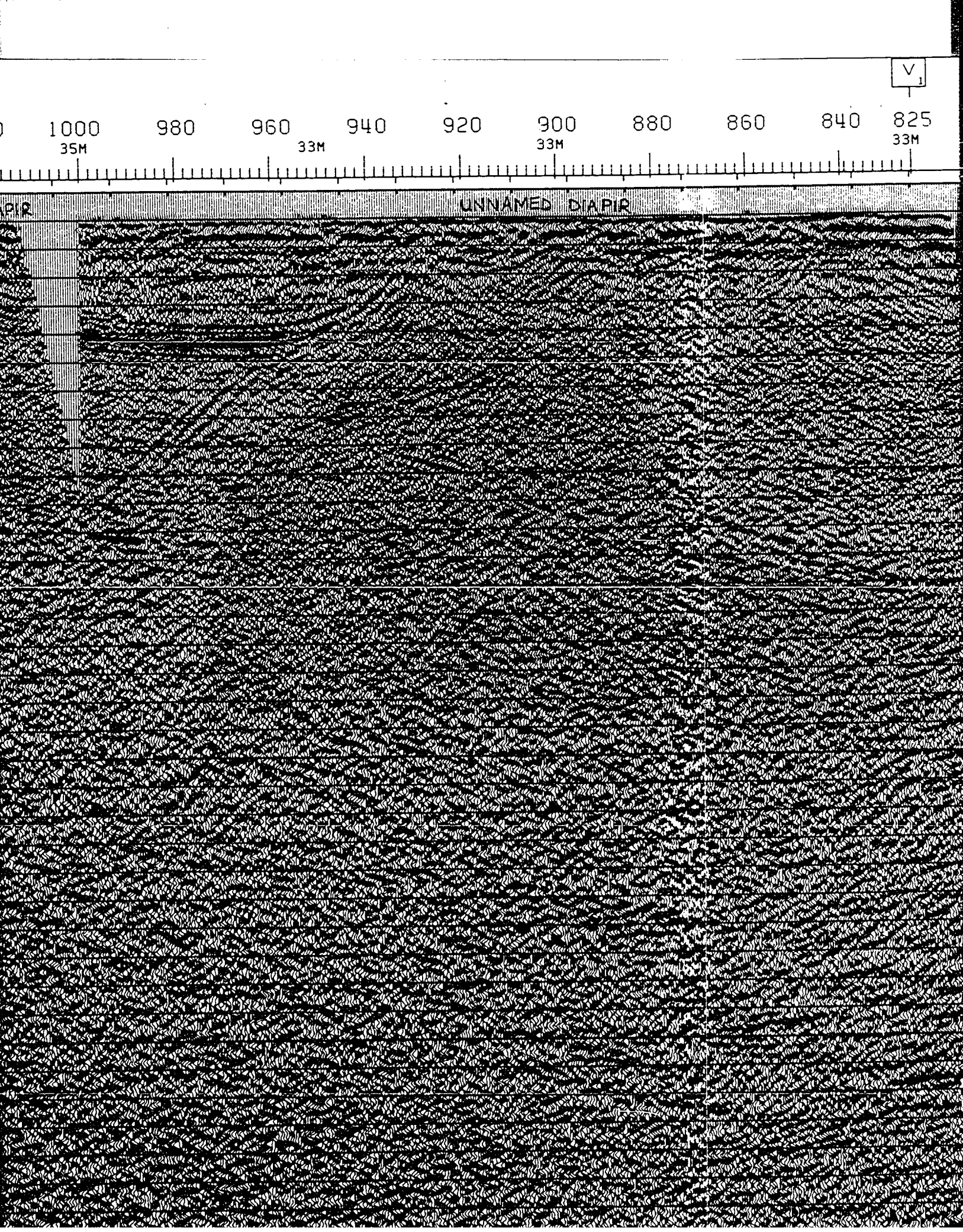
V1
1000
980
960
940
920
900
880
860
840
825
35M
33M
33M
33M
UNNAMED DIAPIR

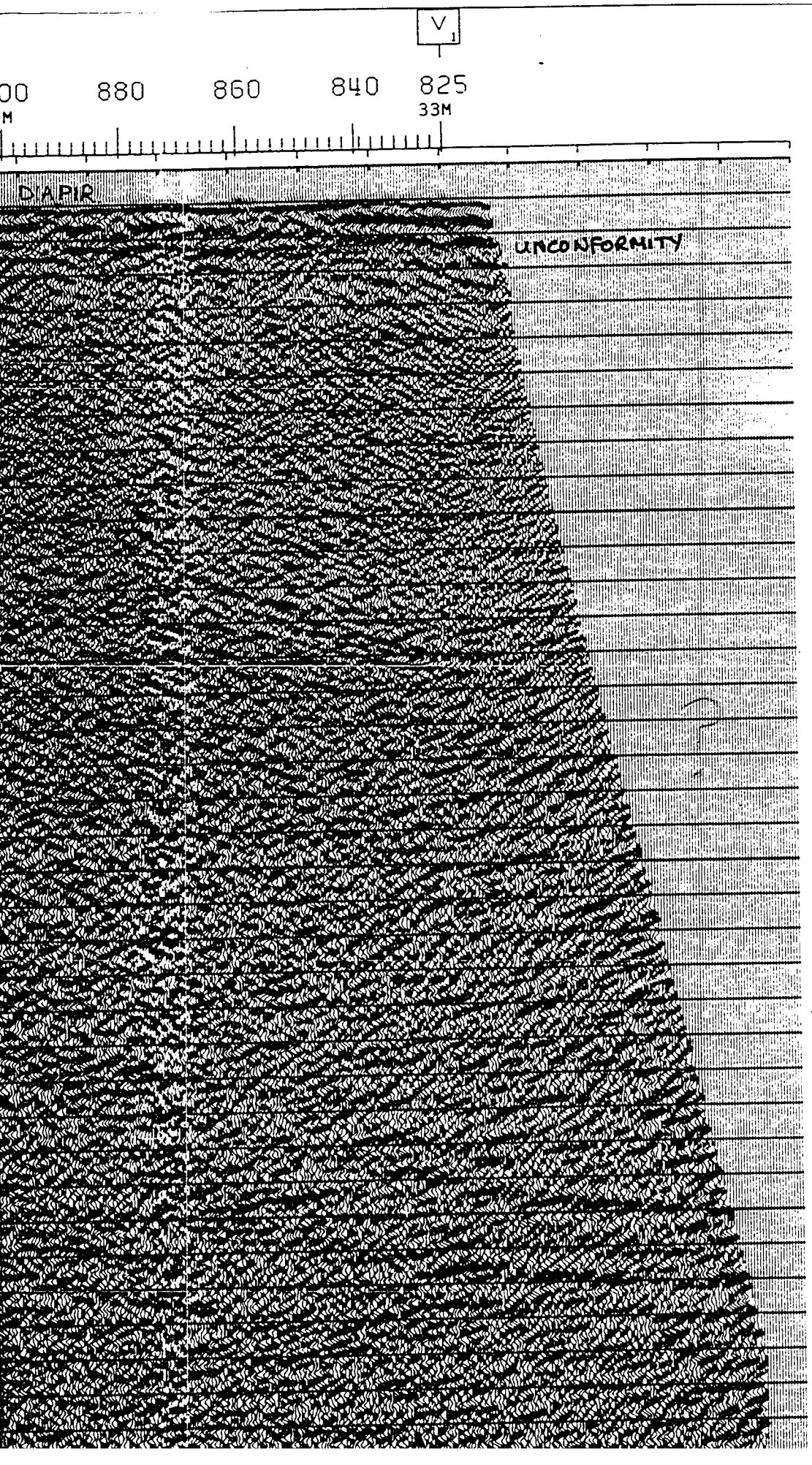

CHEVRON

AREA: N

SHOT BY WESTERN GEOPHY
PROCESSED BY WESTERN GE

ENERGY SOURCE
CHARGE SIZE
NUMBER OF GUNS
GUN DEPTH
FIRING INTERVAL
SHOT POINT INTERVAL
DISTANCE OF SOURCE TO R

SYSTEM
AMPLIFIER
FILTER
SAMPLING INTERVAL
RECORD LENGTH
FORMAT

TYPE CABLE
CABLE LENGTH
CABLE DEPTH
LEAD IN
GROUP INTERVAL
NUMBER OF GROUPS RECORI
SPREAD

ROMS
CHANNELS PER ARRAY
WEIGHTS
NUMBER OF DATA CHANNEL
CHANNEL INTERVAL

PROCESSIN

PROCESSI
1. SIGNATUR
2. DECONVOL
WINDOW L
LENGTH O
PREDICTI
3. NMO STAT
4. RELATIVE
5. F-K DOMA
6. DECONVOL
WINDOW L
LENGTH O
PREDICTI
7. FINITE
8. TIME VA
TI

1.00
3.00
5.00

9. RMS GAI

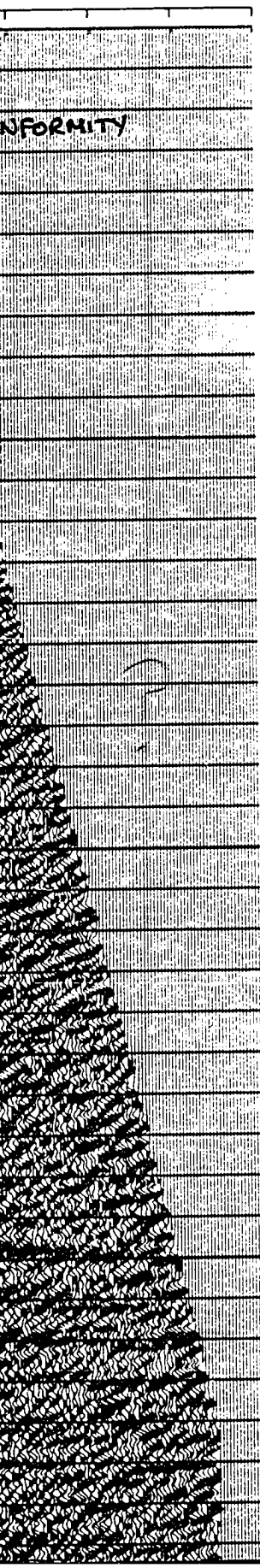

W.D.

0 0
0 1
0 2
0 3
0 4
0 5
0 6
0 7
0 8
0 9
1 0
1 1
1 2
1 3
1 4
1 5
1 6
1 7
1 8
1 9
2 0
2 1
2 2
2 3
2 4
2 5
2 6
2 7
2 8
2 9
3 0
3 1
3 2
3 3
3 4
3 5
3 6
3 7

CHEVRØN STANDARD LTD.

AREA: NORTHUMBERLAND STRAIT

SHOT BY WESTERN GEOPHYSICAL COMPANY PARTY 127 JULY 1981
PROCESSED BY WESTERN GEOPHYSICAL (CALGARY) GROUP 6 OCT 1981

RECORDING DATA

SOURCE

ENERGY SOURCE	AIR GUNS
CHARGE SIZE	1050 CU.IN
NUMBER OF GUNS	15
GUN DEPTH	6 M
FIRING INTERVAL	27 M
SHOT POINT INTERVAL	27 M
DISTANCE OF SOURCE TO ANTENNA	47 M

INSTRUMENTS

SYSTEM	KILOSEIS
AMPLIFIER	INST. FLOATING POINT
FILTER	L/9-H/450
SAMPLING INTERVAL	1 MS
RECORD LENGTH	5.0 SEC
FORMAT	SEG-D

CABLE

TYPE CABLE	STREAMER
CABLE LENGTH	2565 M
CABLE DEPTH	8 M
LEAD IN	187 M
GROUP INTERVAL	27 M
NUMBER OF GROUPS RECORDED	96
SPREAD	2752 M

ARRAY PARAMETERS

ROMS	7/21
CHANNELS PER ARRAY	8.50% OVERLAP
WEIGHTS	32.32.32.32.32.32.32.32
NUMBER OF DATA CHANNELS RECORDED	384
CHANNEL INTERVAL	6.67 M

PROCESSING SEQUENCE AND PARAMETERS

PROCESSING SAMPLING INTERVAL 4 MS

1. SIGNATURE DECONVOLUTION
2. DECONVOLVED BEFORE STACK
   - WINDOW LENGTH 2 ZONES OF 2500 MS
   - LENGTH OPERATOR 280 MS
   - PREDICTION DISTANCE 4 MS
3. NMØ STACK 4800 %
4. RELATIVE AMP. COMPENSATION
5. F-K DOMAIN FILTER
6. DECONVOLVED AFTER STACK
   - WINDOW LENGTH 2 ZONES OF 2500 MS
   - LENGTH OPERATOR 300 MS
   - PREDICTION DISTANCE 20 MS
7. FINITE DIFFERENCE MIGRATION
8. TIME VARIANT FILTER

TIME		L.C. (HZ)	H.C.
1.00	SEC	12	60
3.00	SEC	8	45
5.00	SEC	8	30

9. RMS GAIN (128-512 MS WINDOW)

NORTHWEST

VRON STANDARD LTD.

AREA: NORTHUMBERLAND STRAIT

ERN GEOPHYSICAL COMPANY — PARTY 127 — JULY 1981
WESTERN GEOPHYSICAL (CALGARY) GROUP 6 — OCT 1981

RECORDING DATA

SOURCE

E	AIR GUNS
	1050 CU.IN
NS	15
	6 M
VAL	27 M
NTERVAL	27 M
SOURCE TO ANTENNA	47 M

INSTRUMENTS

	KILOSEIS
	INST. FLOATING POINT
	L/9-H/450
TERVAL	1 MS
TH	5.0 SEC
	SEG-D

CABLE

	STREAMER
H	2565 M
	8 M
	187 M
VAL	27 M
ROUPS RECORDED	96
	2752 M

ARRAY PARAMETERS

	7/21
R ARRAY	8.50% OVERLAP
	32.32.32.32.32.32.32.32
ATA CHANNELS RECORDED	384
ERVAL	6.67 M

PROCESSING SEQUENCE AND PARAMETERS

PROCESSING SAMPLING INTERVAL 4 MS

1. SIGNATURE DECONVOLUTION
2. DECONVOLVED BEFORE STACK
   - WINDOW LENGTH 2 ZONES OF 2500 MS
   - LENGTH OPERATOR 280 MS
   - PREDICTION DISTANCE 4 MS
3. NMO STACK 4800 %
4. RELATIVE AMP. COMPENSATION
5. F-K DOMAIN FILTER
6. DECONVOLVED AFTER STACK
   - WINDOW LENGTH 2 ZONES OF 2500 MS
   - LENGTH OPERATOR 300 MS
   - PREDICTION DISTANCE 20 MS
7. FINITE DIFFERENCE MIGRATION
8. TIME VARIANT FILTER

TIME		L.C. (HZ)	H.C.
1.00	SEC	12	60
3.00	SEC	8	45
5.00	SEC	8	30

83/11

NO: 8624 C4 9E LINE NO: 81

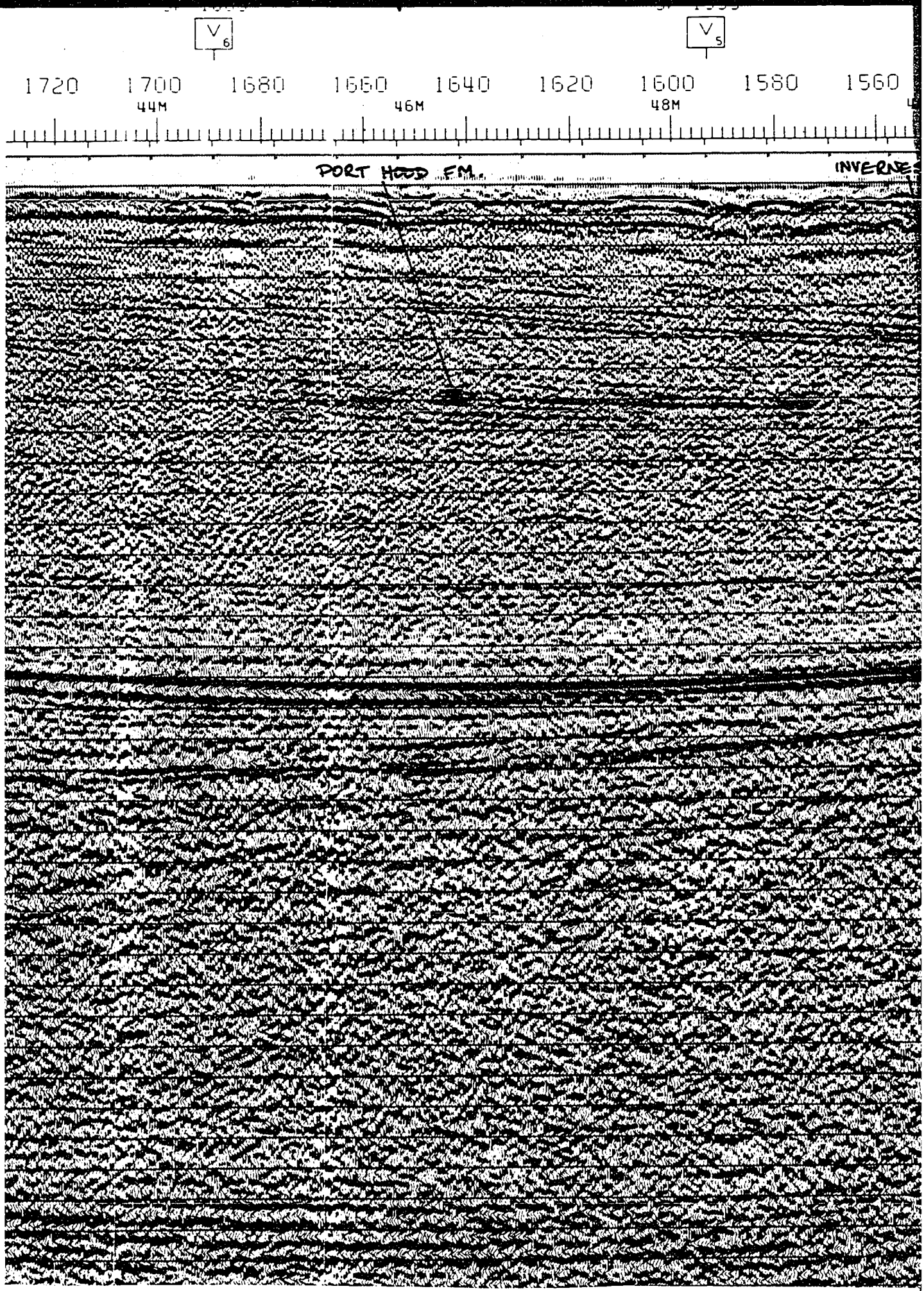
V6
V5
1720
1700
1680
1660
1640
1620
1600
1580
1560
44M
46M
48M
PORT HOOD FM.
INVERNE

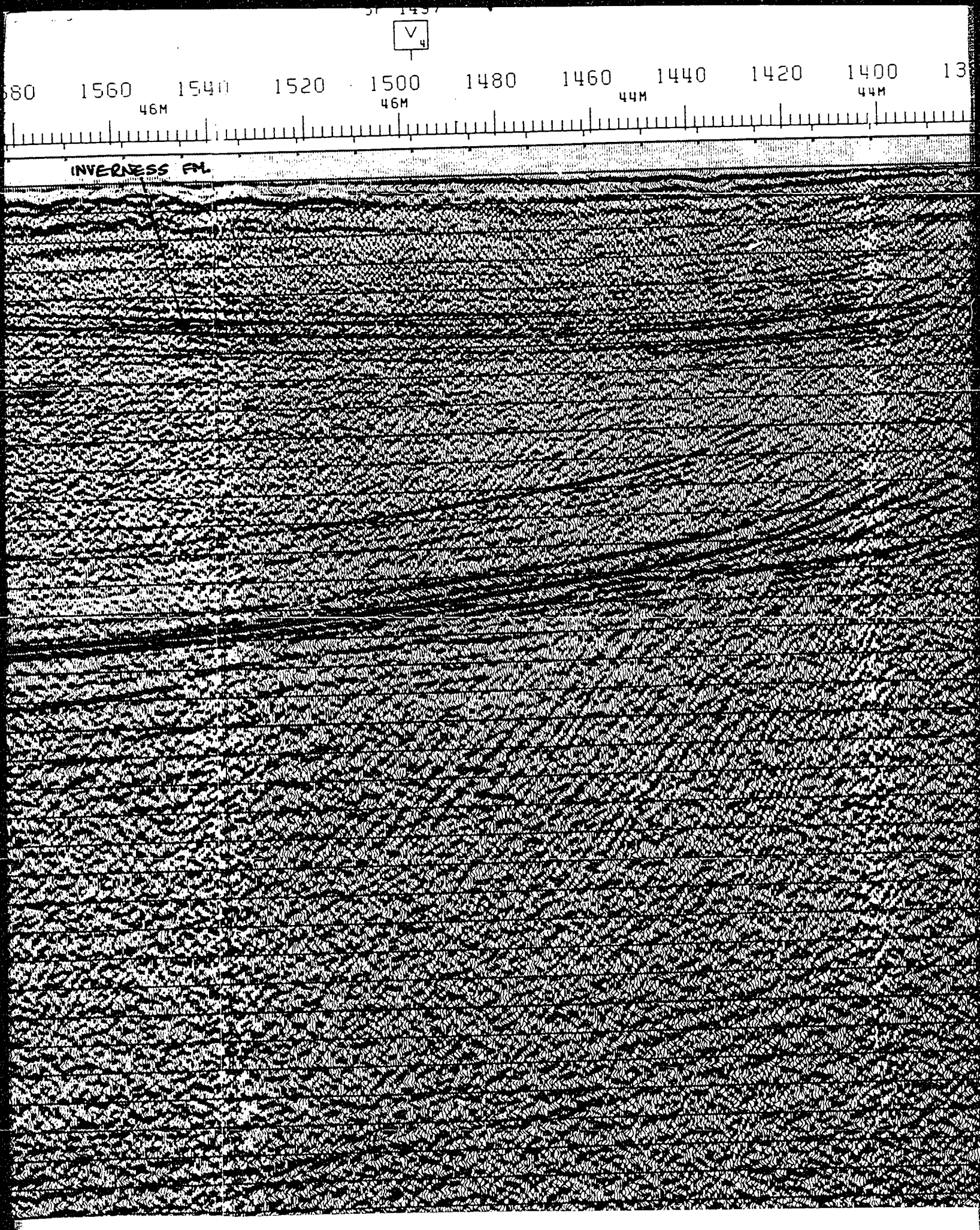
V4
1560
1540
1520
1500
1480
1460
1440
1420
1400
46M
46M
44M
44M
INVERNESS FM.

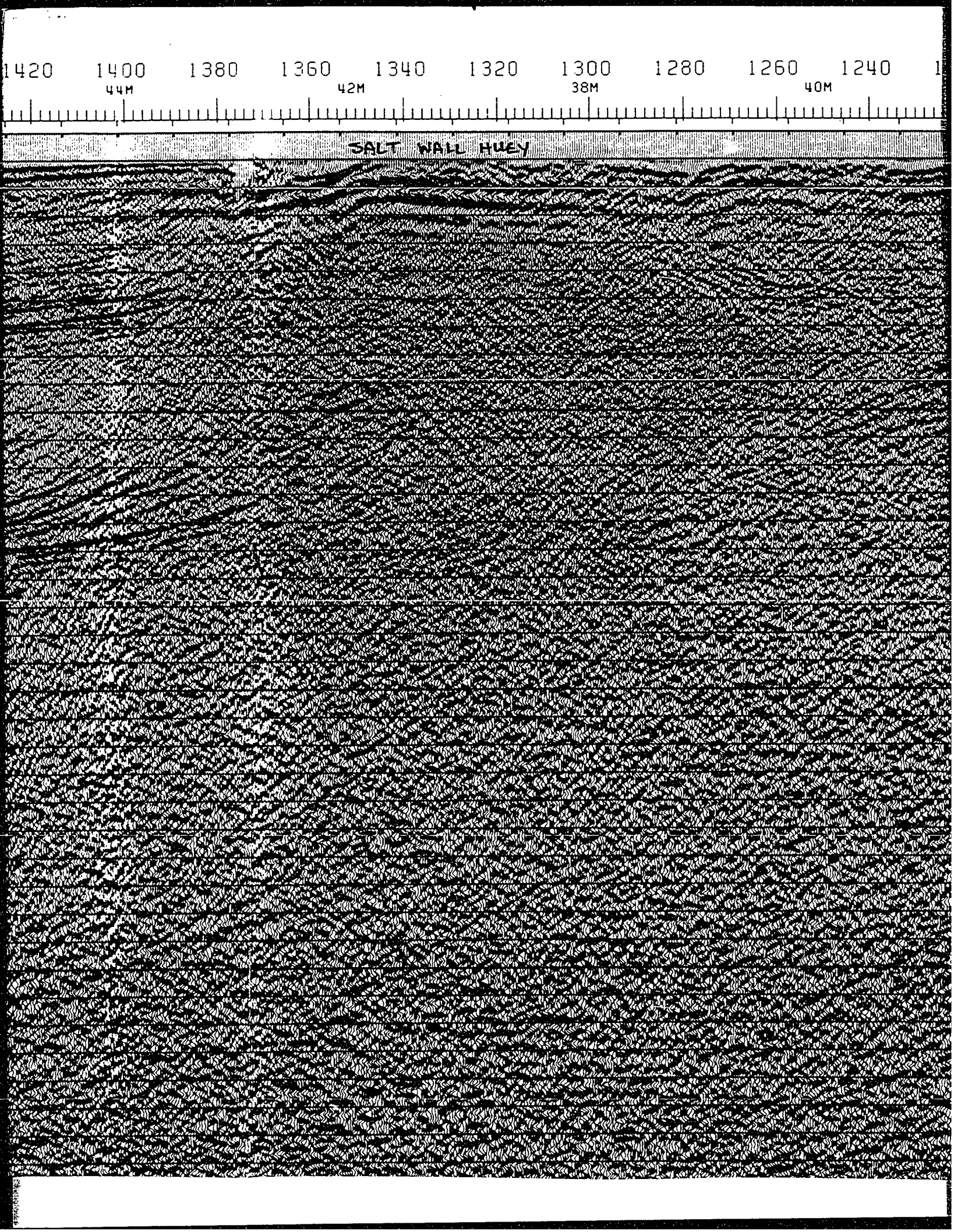
1420
1400
1380
1360
1340
1320
1300
1280
1260
1240
44M
42M
38M
40M
SALT WALL HUEY

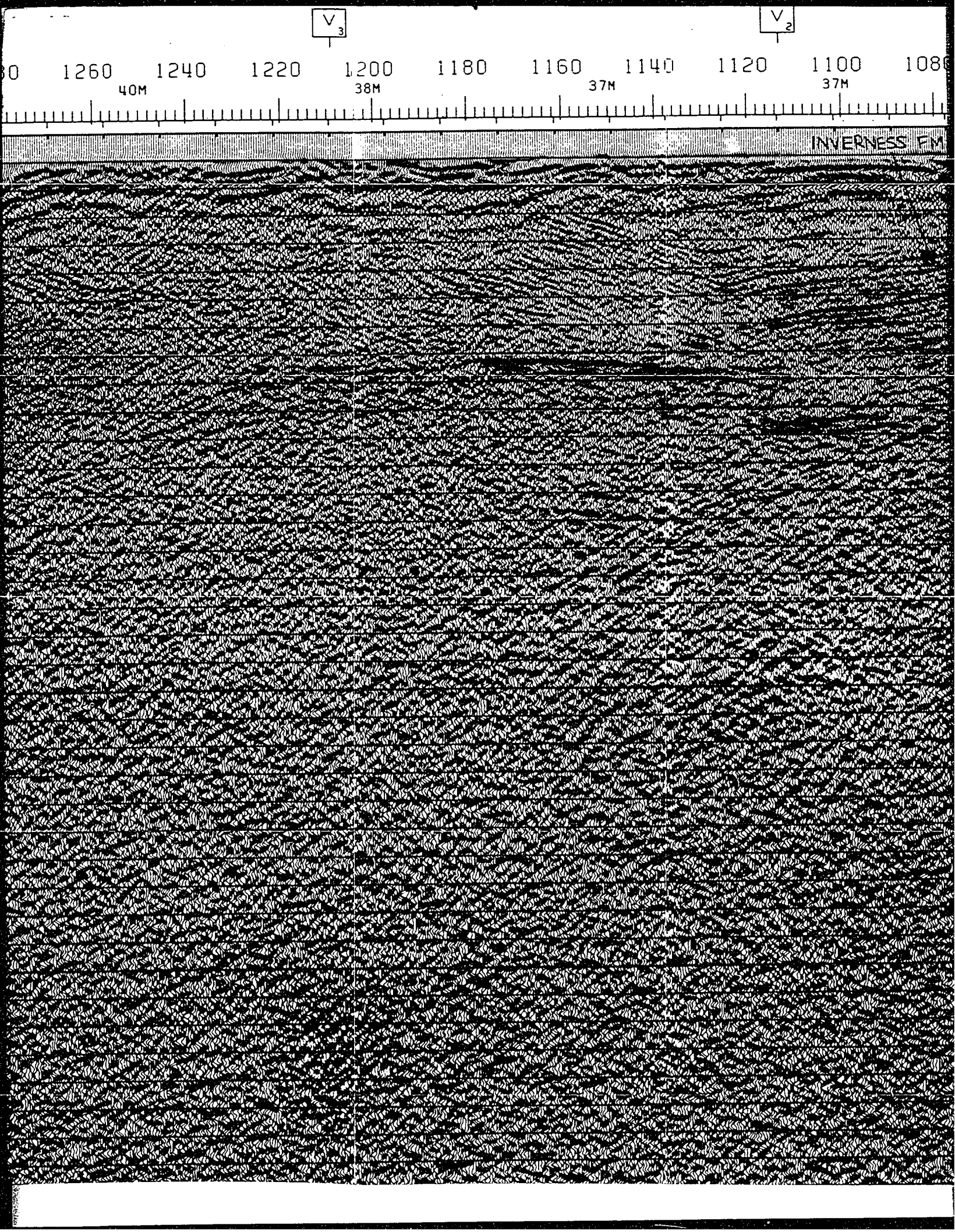
V3
V2
1260
1240
1220
1200
1180
1160
1140
1120
1100
40M
38M
37M
37M
INVERNESS FM

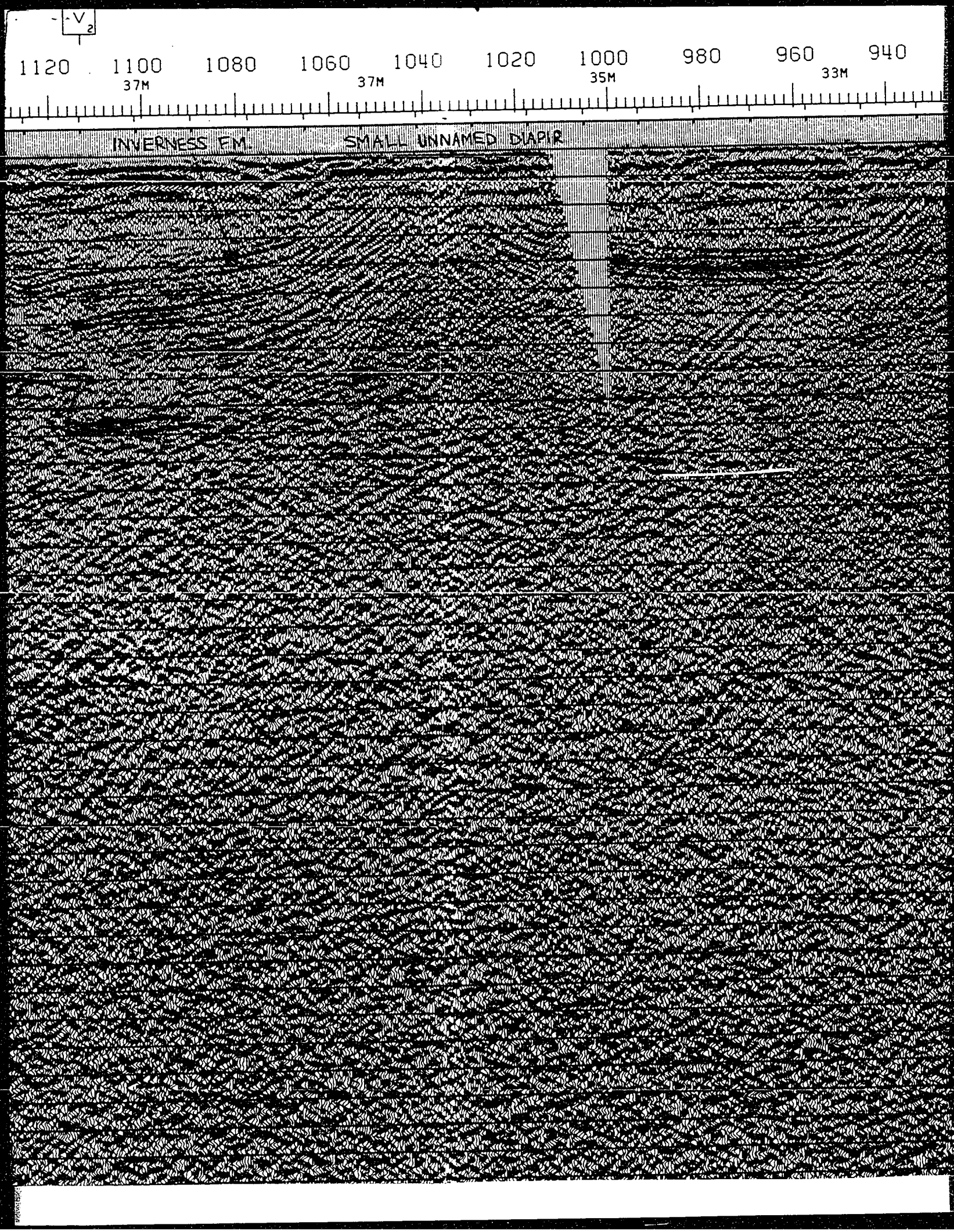
V2
1120
1100
37M
1080
1060
37M
1040
1020
1000
35M
980
960
33M
940
INVERNESS F.M.
SMALL UNNAMED DIAPIR

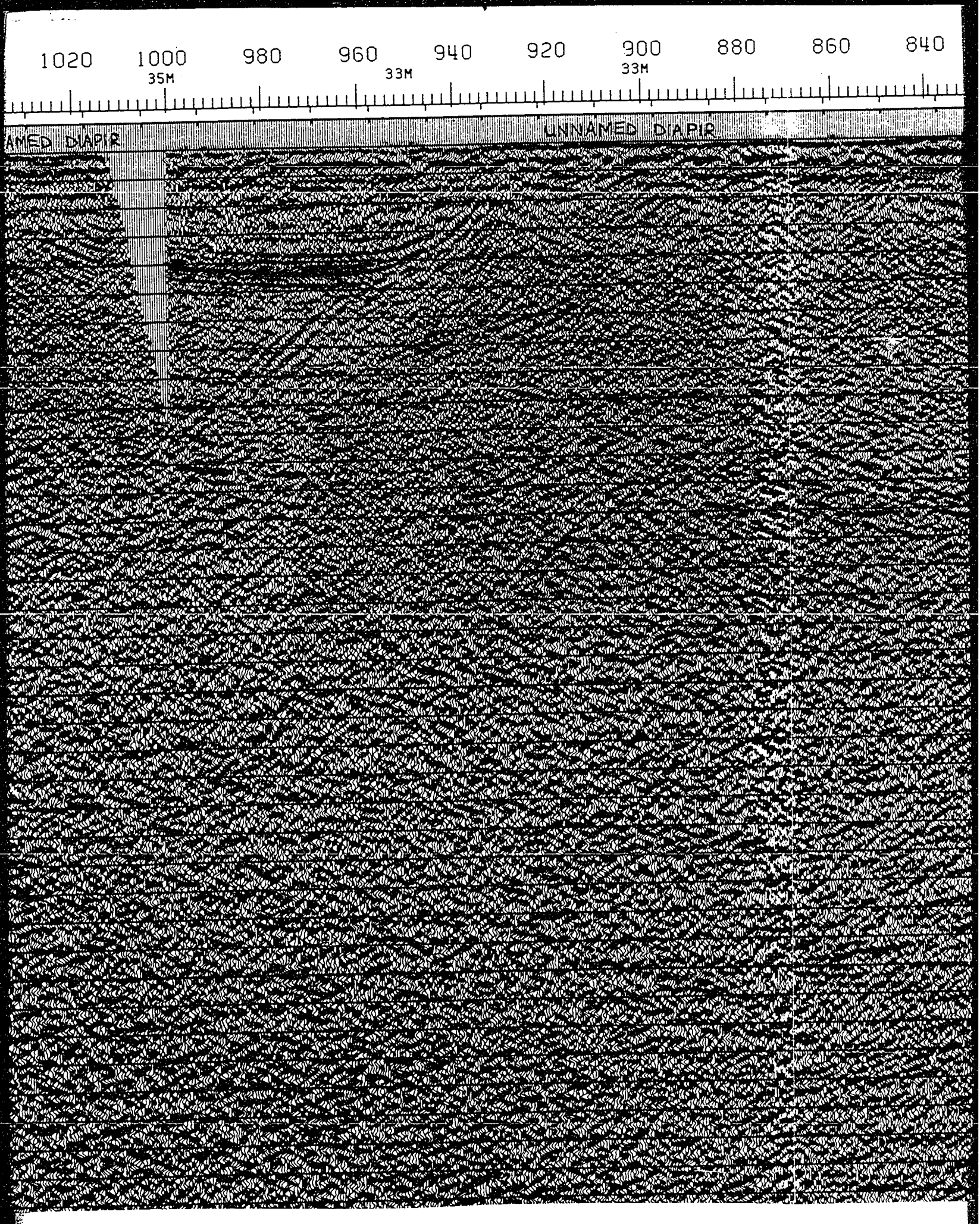
1020
1000
35M
980
960
33M
940
920
900
33M
880
860
840
AMED DIAPIR
UNNAMED DIAPIR

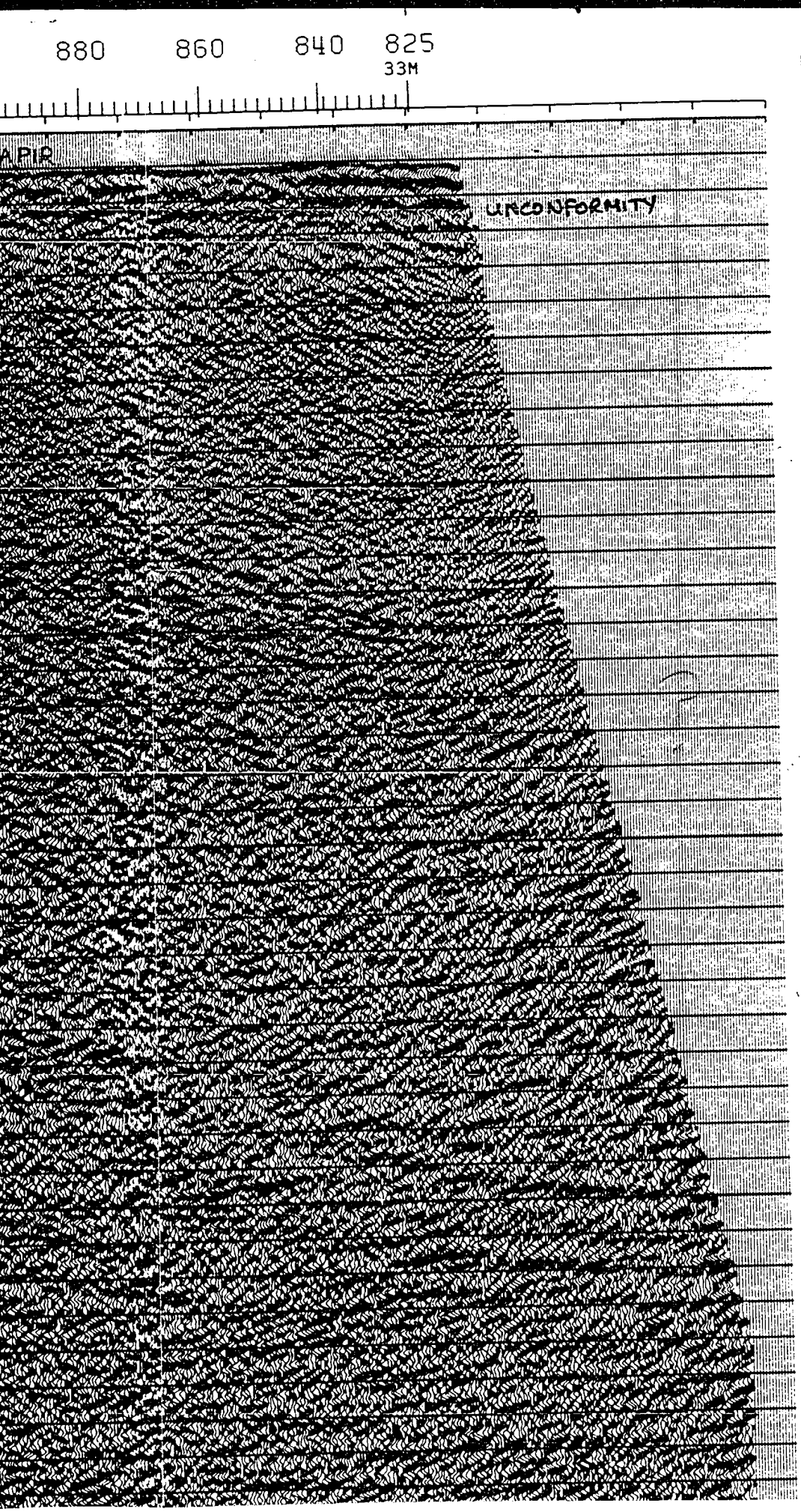

CHEVRON

AREA: NO

SHOT BY WESTERN GEOPHYSIC
PROCESSED BY WESTERN GEOP

RE

0 0	
0 1	
0 2	
0 3	
0 4	
0 5	
0 6	ENERGY SOURCE
0 7	CHARGE SIZE
0 8	NUMBER OF GUNS
0 9	GUN DEPTH
1 0	FIRING INTERVAL
1 1	SHOT POINT INTERVAL
1 2	DISTANCE OF SOURCE TO AN
1 3	
1 4	SYSTEM
1 5	AMPLIFIER
1 6	FILTER
1 7	SAMPLING INTERVAL
1 8	RECORD LENGTH
1 9	FORMAT
2 0	
2 1	TYPE CABLE
2 2	CABLE LENGTH
2 3	CABLE DEPTH
2 4	LEAD IN
2 5	GROUP INTERVAL
2 6	NUMBER OF GROUPS RECORDE
2 7	SPREAD
2 8	A
2 9	ROMS
3 0	CHANNELS PER ARRAY
3 1	WEIGHTS
3 2	NUMBER OF DATA CHANNELS
3 3	CHANNEL INTERVAL
3 4	
3 5	
3 6	
3 7	
3 8	

PROCESSING

PROCESSIN
1. SIGNATURE
2. DECONVOLV
WINDOW LEN
LENGTH OPE
PREDICTION
3. NMO STACK
4. RELATIVE
5. F-K DOMAI
6. DECONVOLV
WINDOW LEN
LENGTH OPE
PREDICTION
7. FINITE DI
8. TIME VARI
TIM
1.00
3.00
5.00
9. RMS GAIN

47 M

W.D.

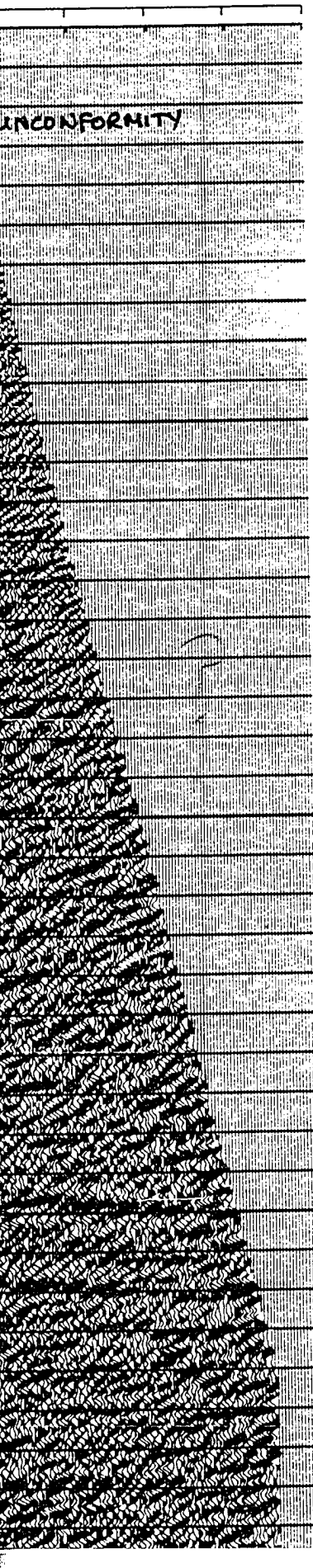

0.0
0.1
0.2
0.3
0.4
0.5
0.6
0.7
0.8
0.9
1.0
1.1
1.2
1.3
1.4
1.5
1.6
1.7
1.8
1.9
2.0
2.1
2.2
2.3
2.4
2.5
2.6
2.7
2.8
2.9
3.0
3.1
3.2
3.3
3.4
3.5
3.6
3.7
3.8

CHEVRON STANDARD LTD.

AREA: NORTHUMBERLAND STRAIT

SHOT BY WESTERN GEOPHYSICAL COMPANY PARTY 127 JULY 1981
PROCESSED BY WESTERN GEOPHYSICAL (CALGARY) GROUP 6 OCT 1981

RECORDING DATA

SOURCE

ENERGY SOURCE	AIR GUNS
CHARGE SIZE	1050 CU.IN
NUMBER OF GUNS	15
GUN DEPTH	6 M
FIRING INTERVAL	27 M
SHOT POINT INTERVAL	27 M
DISTANCE OF SOURCE TO ANTENNA	47 M

INSTRUMENTS

SYSTEM	KILOSEIS
AMPLIFIER	INST. FLOATING POINT
FILTER	L/9-H/450
SAMPLING INTERVAL	1 MS
RECORD LENGTH	5.0 SEC
FORMAT	SEG-D

CABLE

TYPE CABLE	STREAMER
CABLE LENGTH	2565 M
CABLE DEPTH	8 M
LEAD IN	187 M
GROUP INTERVAL	27 M
NUMBER OF GROUPS RECORDED	96
SPREAD	2752 M

ARRAY PARAMETERS

ROMS	7/21
CHANNELS PER ARRAY	8.50% OVERLAP
WEIGHTS	32.32.32.32.32.32.32.32
NUMBER OF DATA CHANNELS RECORDED	384
CHANNEL INTERVAL	6.67 M

PROCESSING SEQUENCE AND PARAMETERS

PROCESSING SAMPLING INTERVAL 4 MS

1. SIGNATURE DECONVOLUTION
2. DECONVOLVED BEFORE STACK
   - WINDOW LENGTH 2 ZONES OF 2500 MS
   - LENGTH OPERATOR 280 MS
   - PREDICTION DISTANCE 4 MS
3. NMO STACK 4800 %
4. RELATIVE AMP. COMPENSATION
5. F-K DOMAIN FILTER
6. DECONVOLVED AFTER STACK
   - WINDOW LENGTH 2 ZONES OF 2500 MS
   - LENGTH OPERATOR 300 MS
   - PREDICTION DISTANCE 20 MS
7. FINITE DIFFERENCE MIGRATION
8. TIME VARIANT FILTER

TIME		L.C. (HZ)	H.C.
1.00	SEC	12	60
3.00	SEC	8	45
5.00	SEC	8	30

9. RMS GAIN (128-512 MS WINDOW)

47 M

LEGEND

NORTHWEST

EVRON STANDARD LTD.

AREA: NORTHUMBERLAND STRAIT

STERN GEOPHYSICAL COMPANY PARTY 127 JULY 1981
BY WESTERN GEOPHYSICAL (CALGARY) GROUP 6 OCT 1981

RECORDING DATA

SOURCE

RCE	AIR GUNS
E	1050 CU.IN
GUNS	15
	6 M
ERVAL	27 M
INTERVAL	27 M
F SOURCE TO ANTENNA	47 M

INSTRUMENTS

	KILOSEIS
	INST. FLOATING POINT
	L/9-H/450
NTERVAL	1 MS
NGTH	5.0 SEC
	SEG-D

CABLE

	STREAMER
TH	2565 M
H	8 M
	187 M
RVAL	27 M
GROUPS RECORDED	96
	2752 M

ARRAY PARAMETERS

	7/21
ER ARRAY	8.50% OVERLAP
	32.32.32.32.32.32.32.32
DATA CHANNELS RECORDED	384
NTERVAL	6.67 M

PROCESSING SEQUENCE AND PARAMETERS

PROCESSING SAMPLING INTERVAL 4 MS

1. SIGNATURE DECONVOLUTION
2. DECONVOLVED BEFORE STACK
   - WINDOW LENGTH 2 ZONES OF 2500 MS
   - LENGTH OPERATOR 280 MS
   - PREDICTION DISTANCE 4 MS
3. NMO STACK 4800 %
4. RELATIVE AMP. COMPENSATION
5. F-K DOMAIN FILTER
6. DECONVOLVED AFTER STACK
   - WINDOW LENGTH 2 ZONES OF 2500 MS
   - LENGTH OPERATOR 300 MS
   - PREDICTION DISTANCE 20 MS
7. FINITE DIFFERENCE MIGRATION
8. TIME VARIANT FILTER

TIME		L.C. (HZ)	H.C.
1.00	SEC	12	60
3.00	SEC	8	45
5.00	SEC	8	30

9. RMS GAIN (128-512 MS WINDOW)

LEGEND

83

NO: 8624 C4 9E LINE NO: 81-

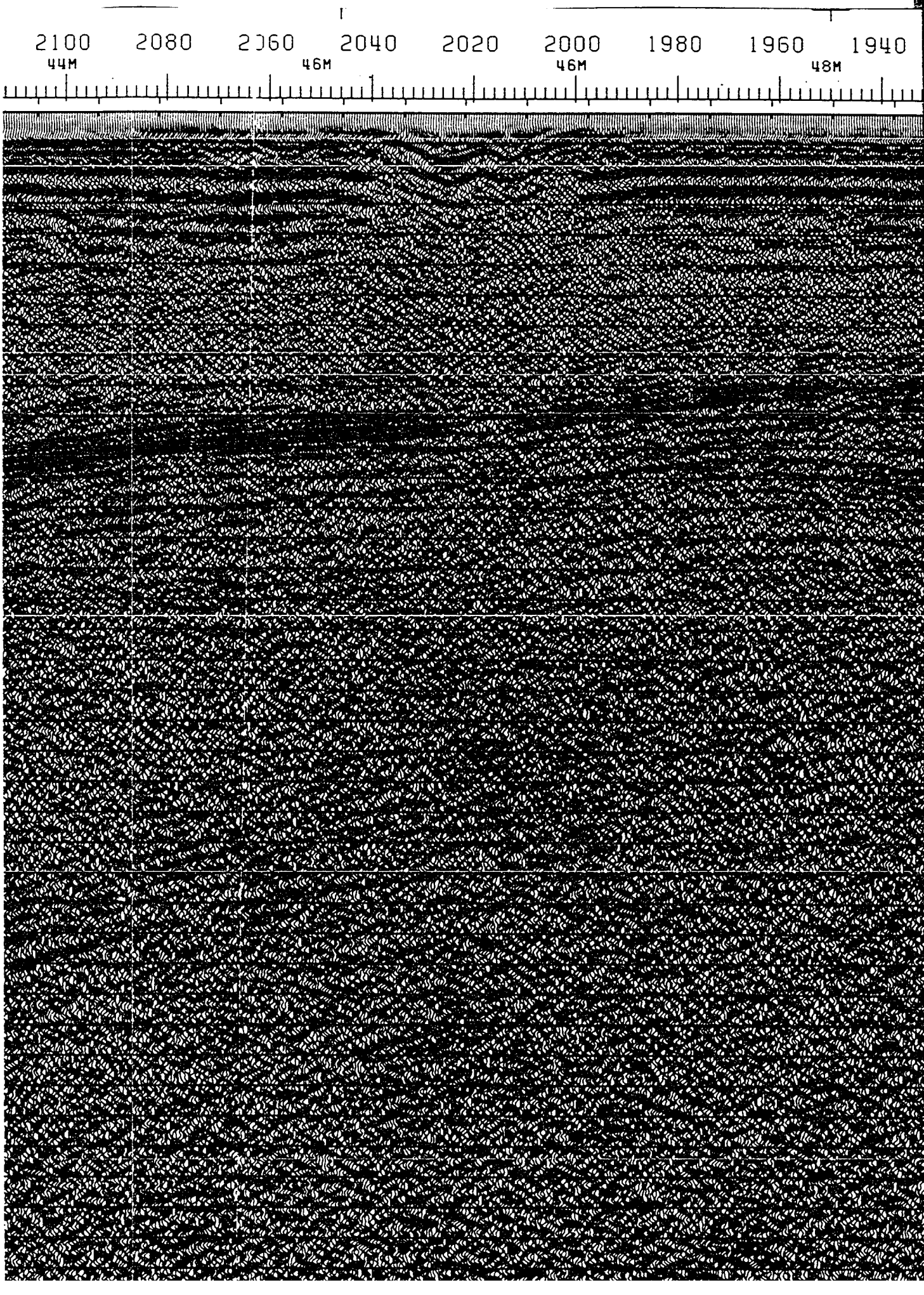
2100
2080
2060
2040
2020
2000
1980
1960
1940
44M
46M
46M
48M

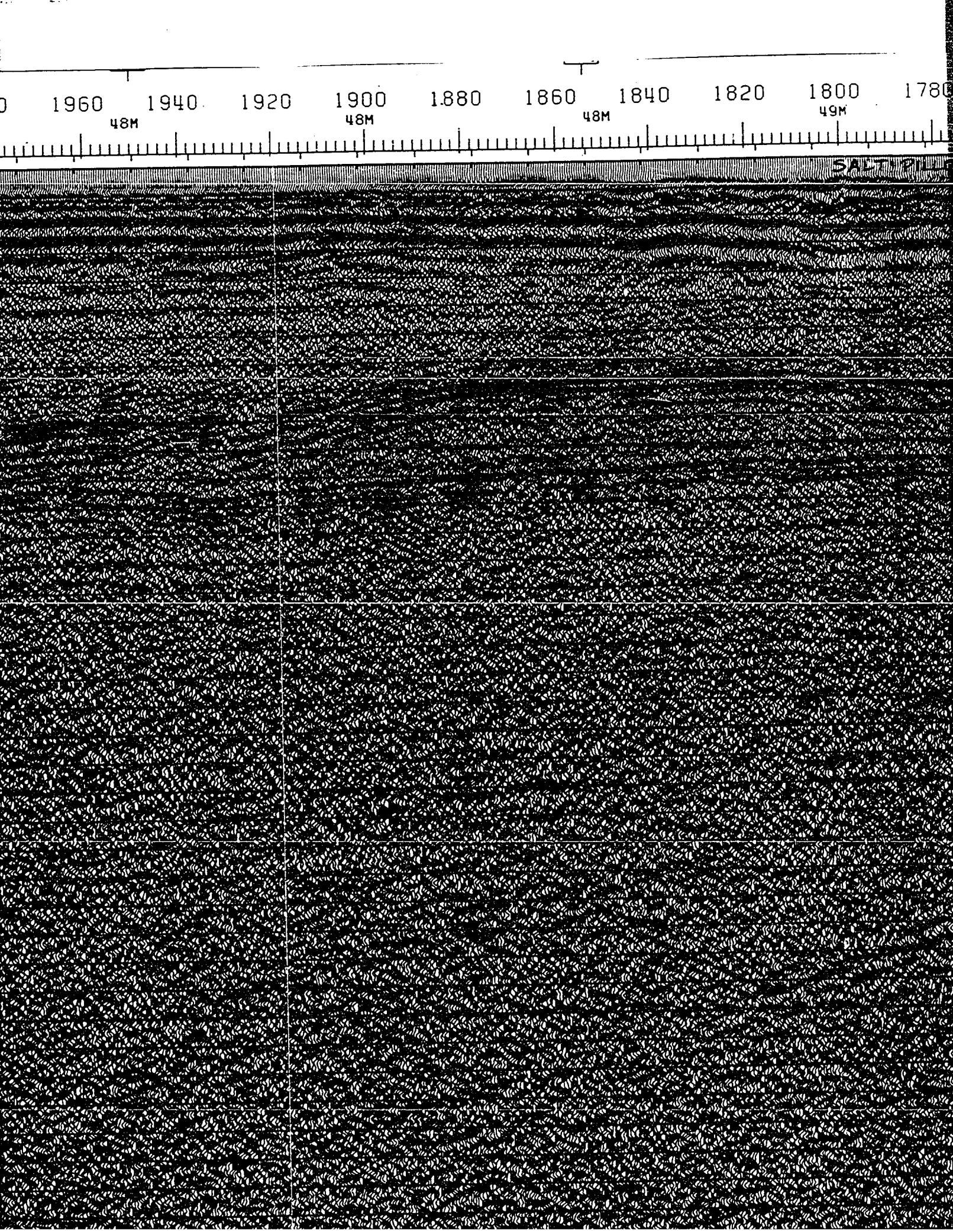
1960
1940
1920
1900
1880
1860
1840
1820
1800
48M
48M
48M
49M
SALT PILE

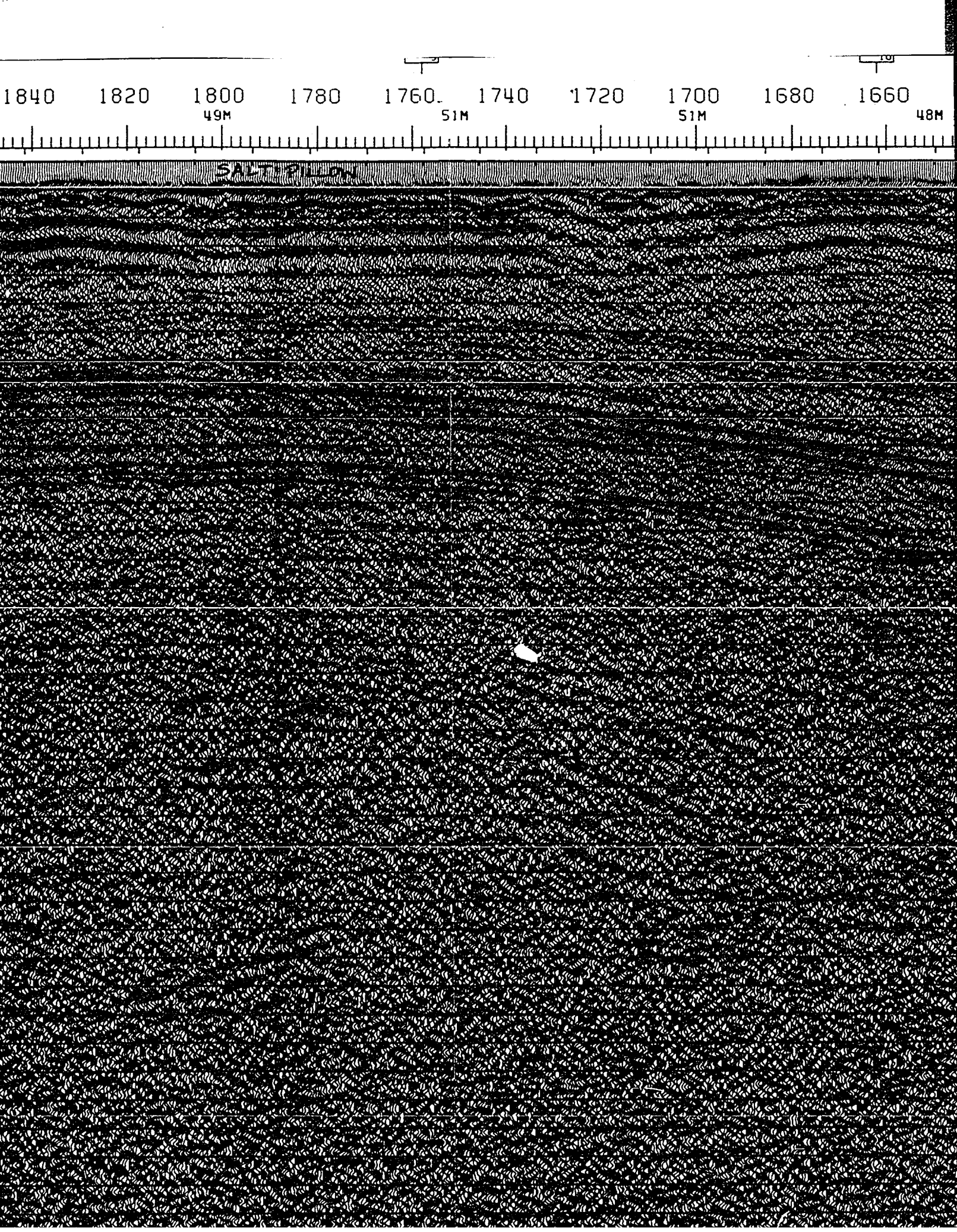
1840
1820
1800
49M
1780
1760
51M
1740
1720
1700
51M
1680
1660
48M
SALT PILLOW

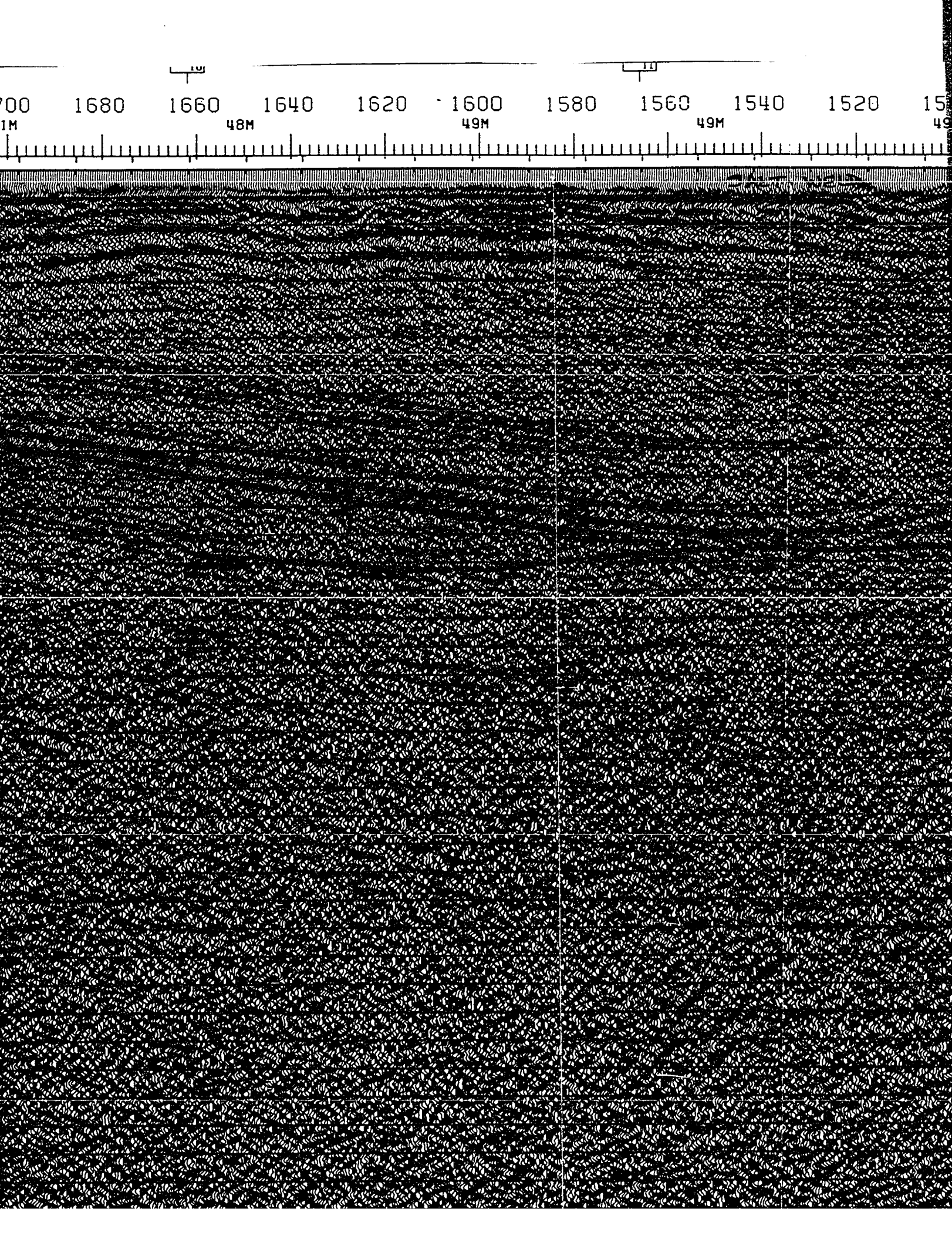
700
1680
1660
1640
1620
1600
1580
1560
1540
1520
48M
49M
49M

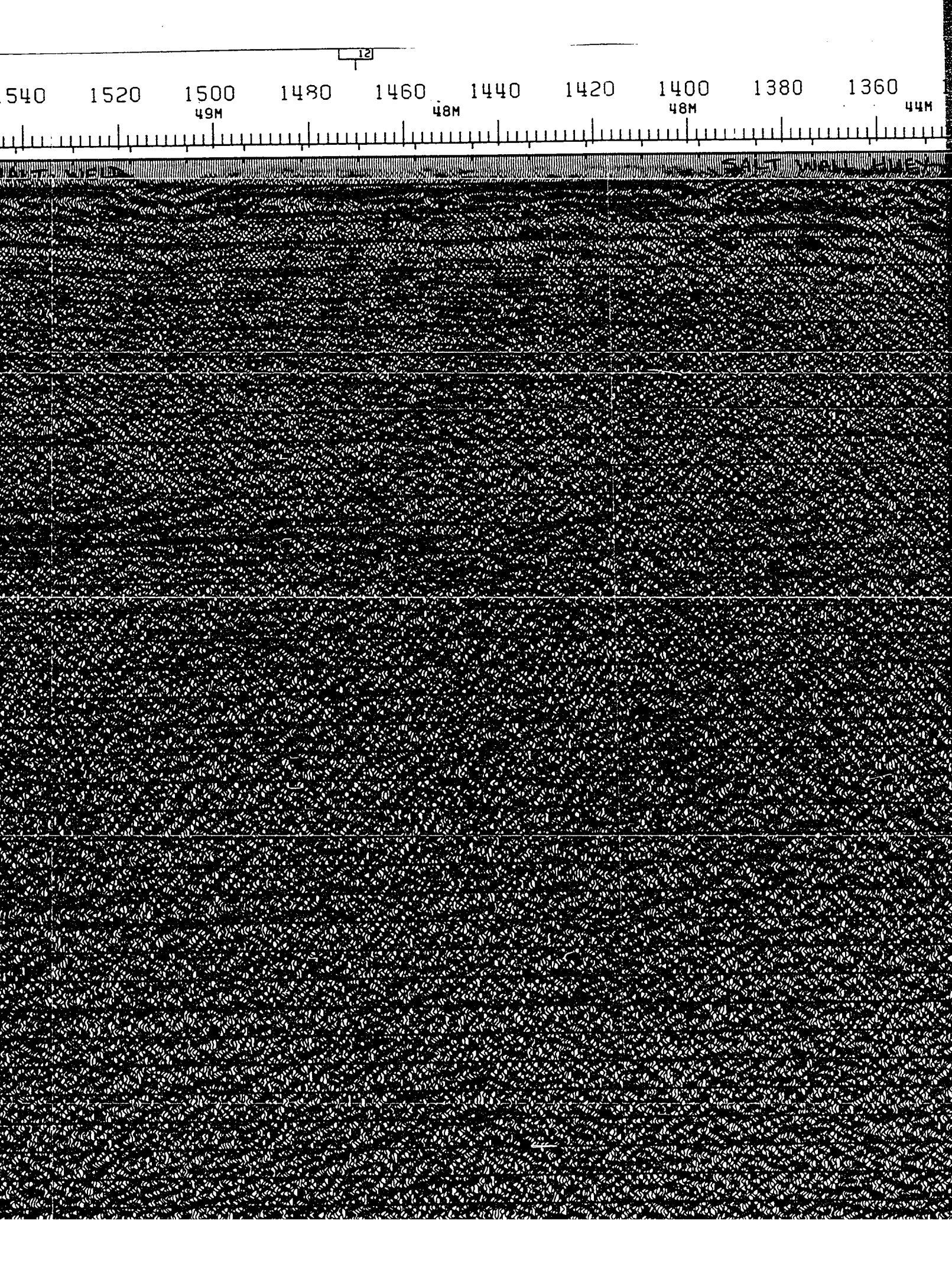
12
1540
1520
1500
1480
1460
1440
1420
1400
1380
1360
49M
48M
48M
44M

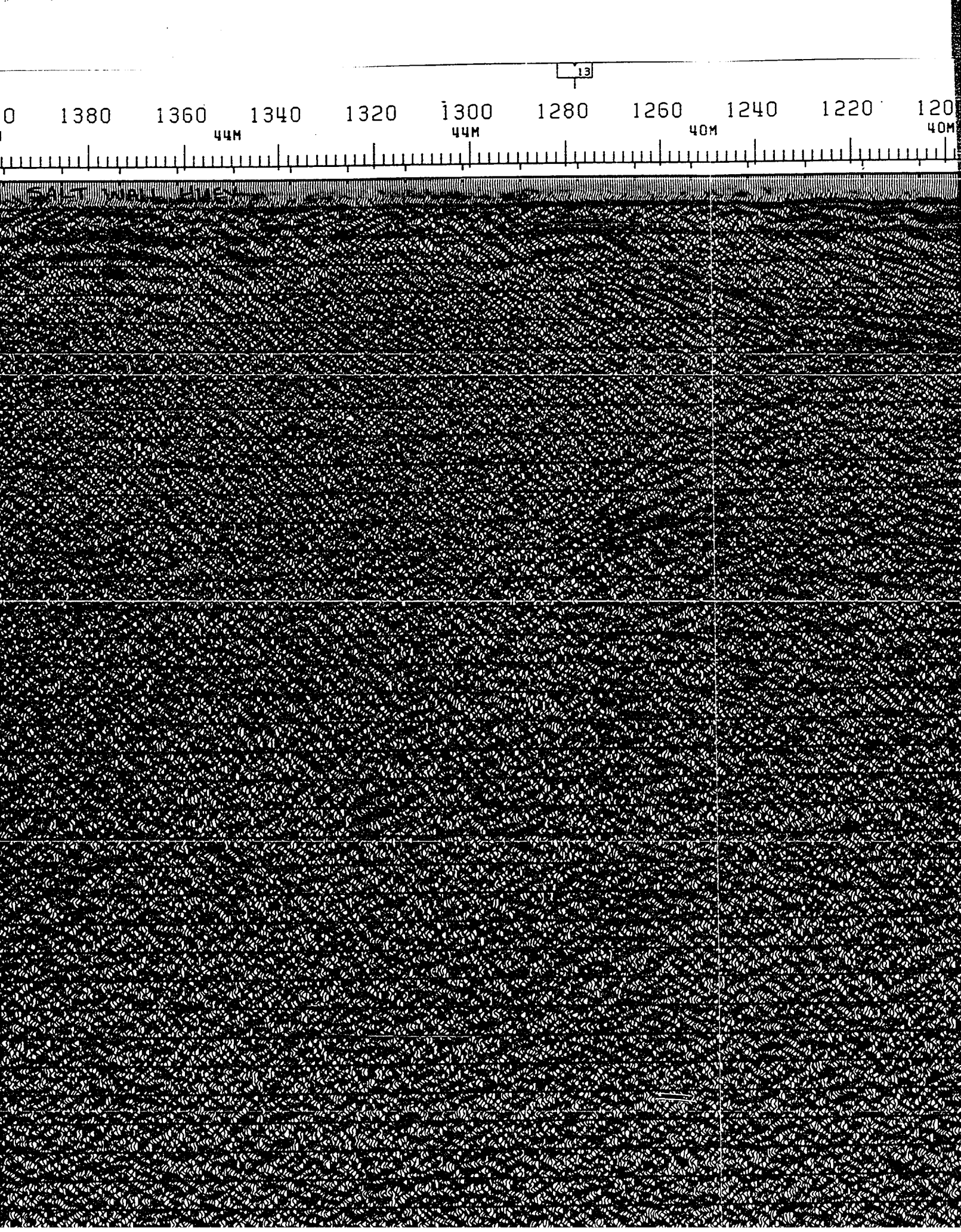
13
0
1380
1360
1340
1320
1300
1280
1260
1240
1220
120
44M
44M
40M
40M
SALT WALL CME

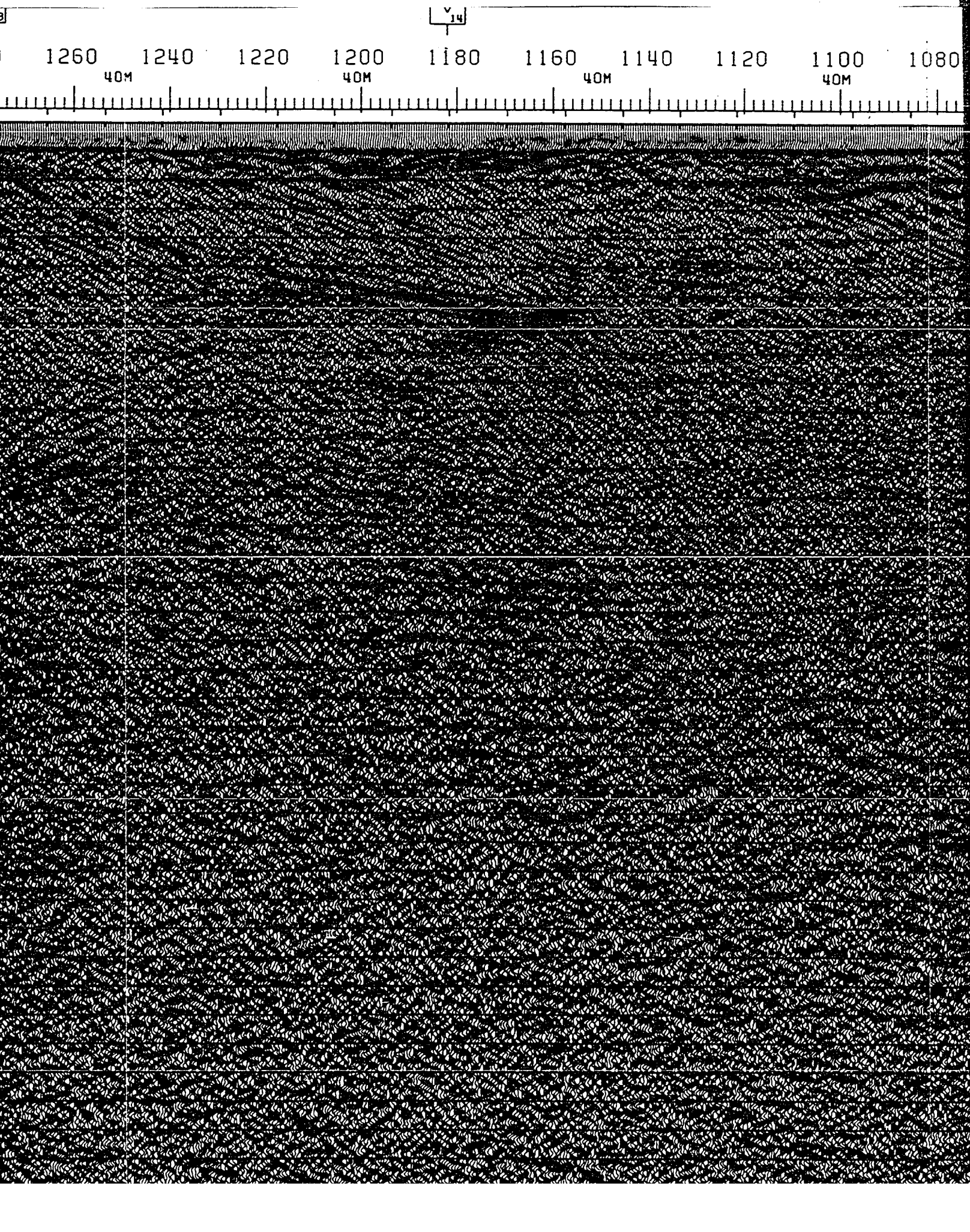
1260
1240
1220
1200
1180
1160
1140
1120
1100
1080
40M
40M
40M
40M

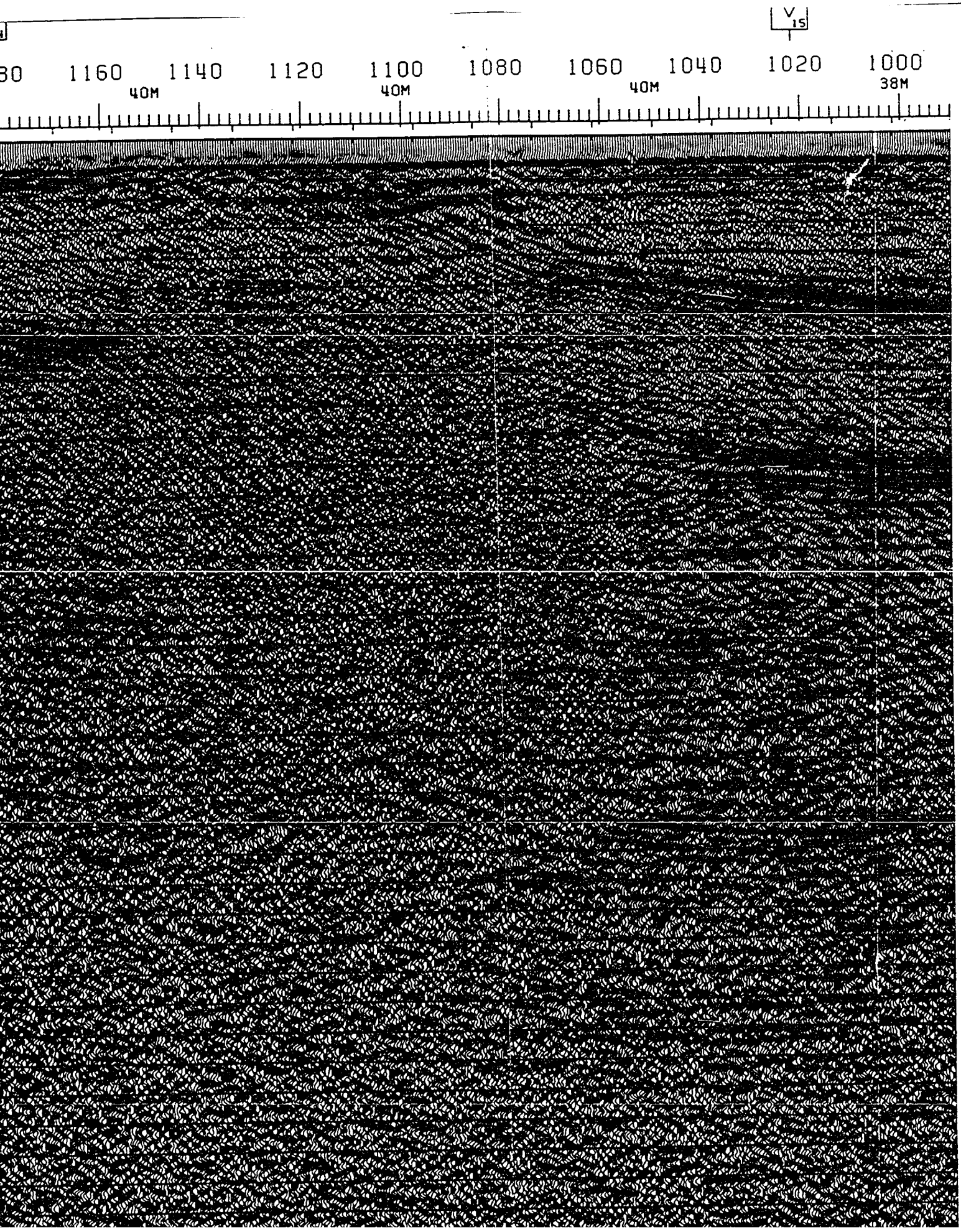
V
15
1160
1140
1120
1100
1080
1060
1040
1020
1000
40M
40M
40M
38M

79

INVERNESS FM.

PORT HOOD FM.

OJ NO: 8624 C4 9E LINE NO:

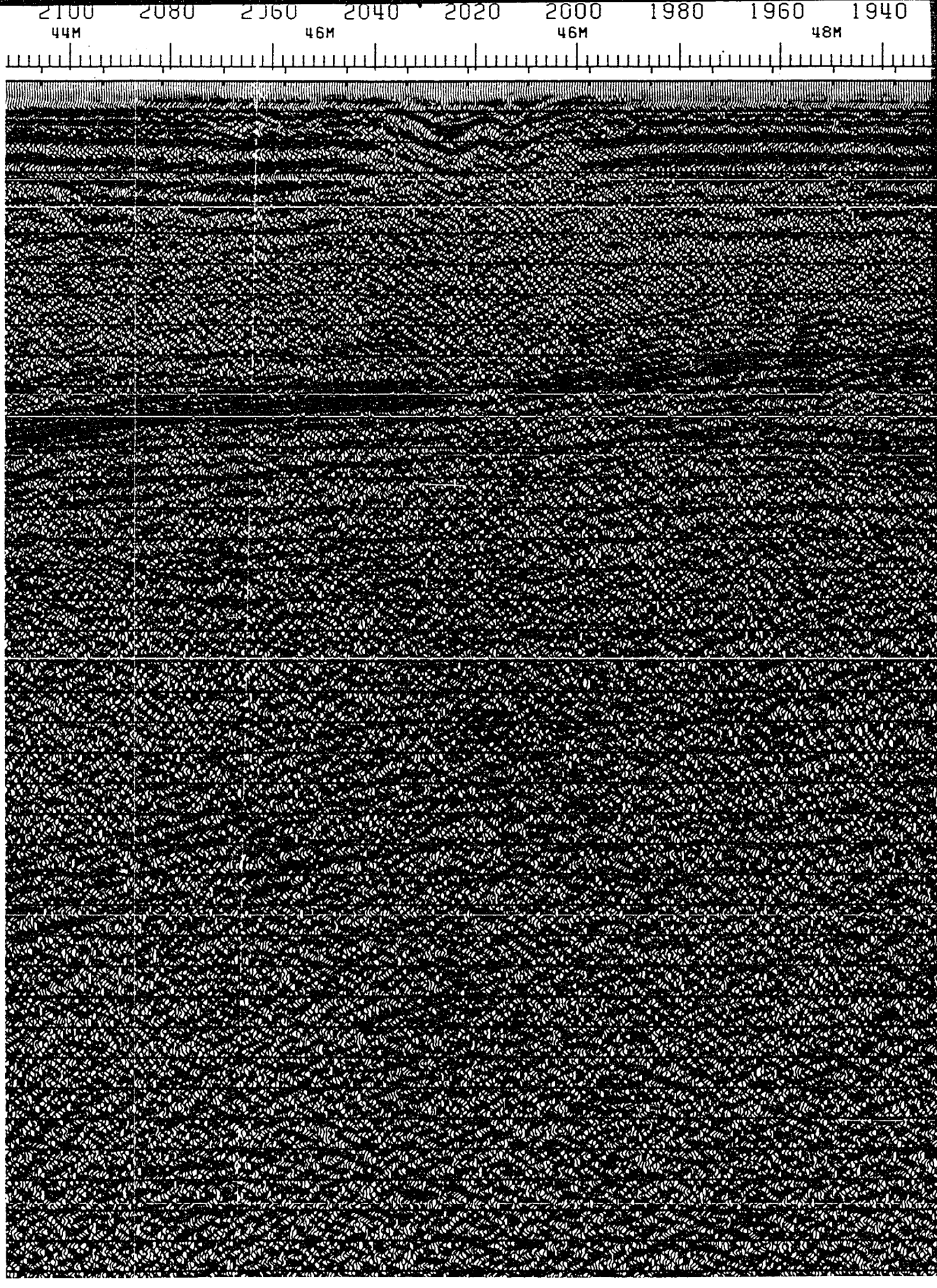
2100
2080
2060
2040
2020
2000
1980
1960
1940
44M
46M
46M
48M

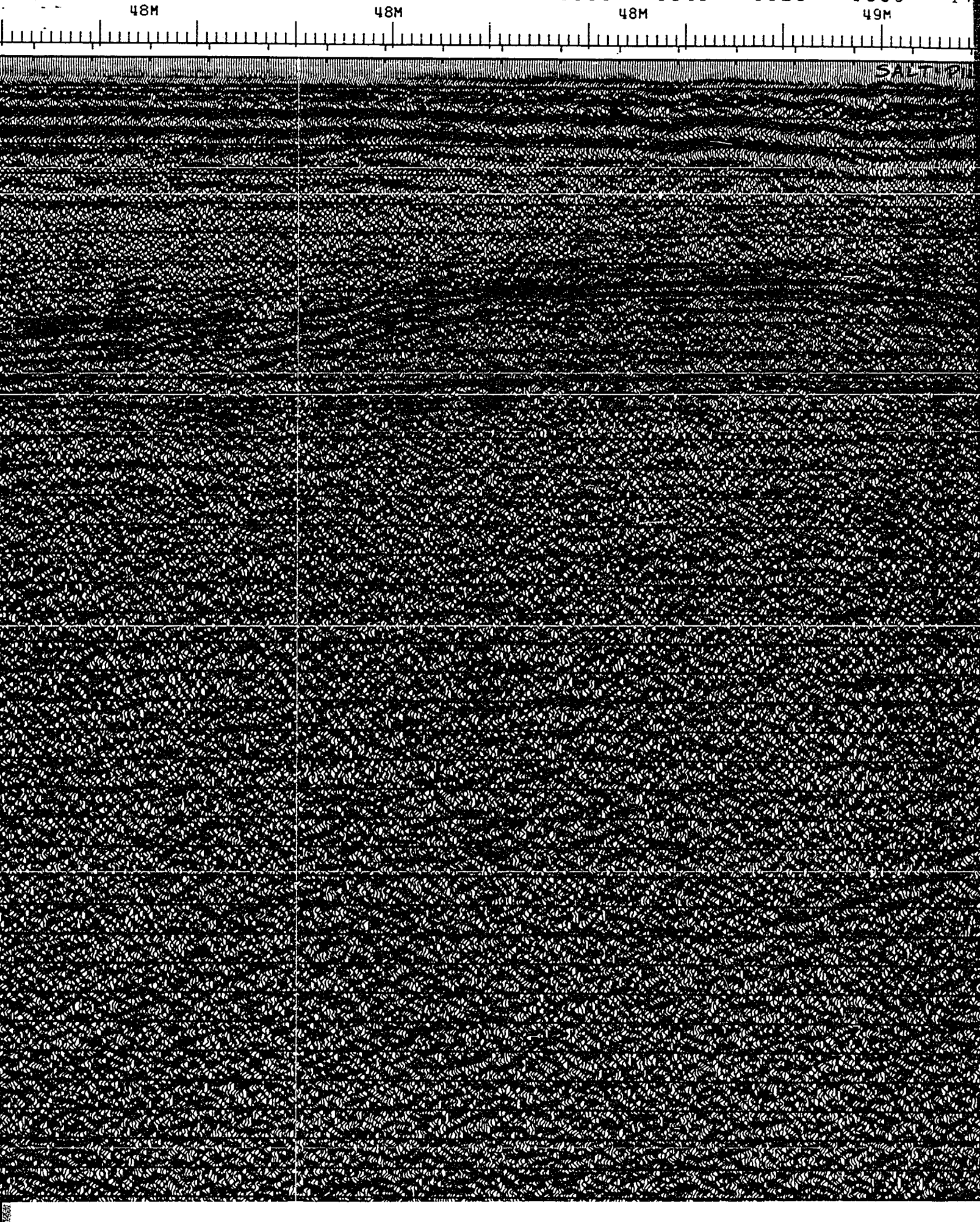
48M
48M
48M
49M
SALT

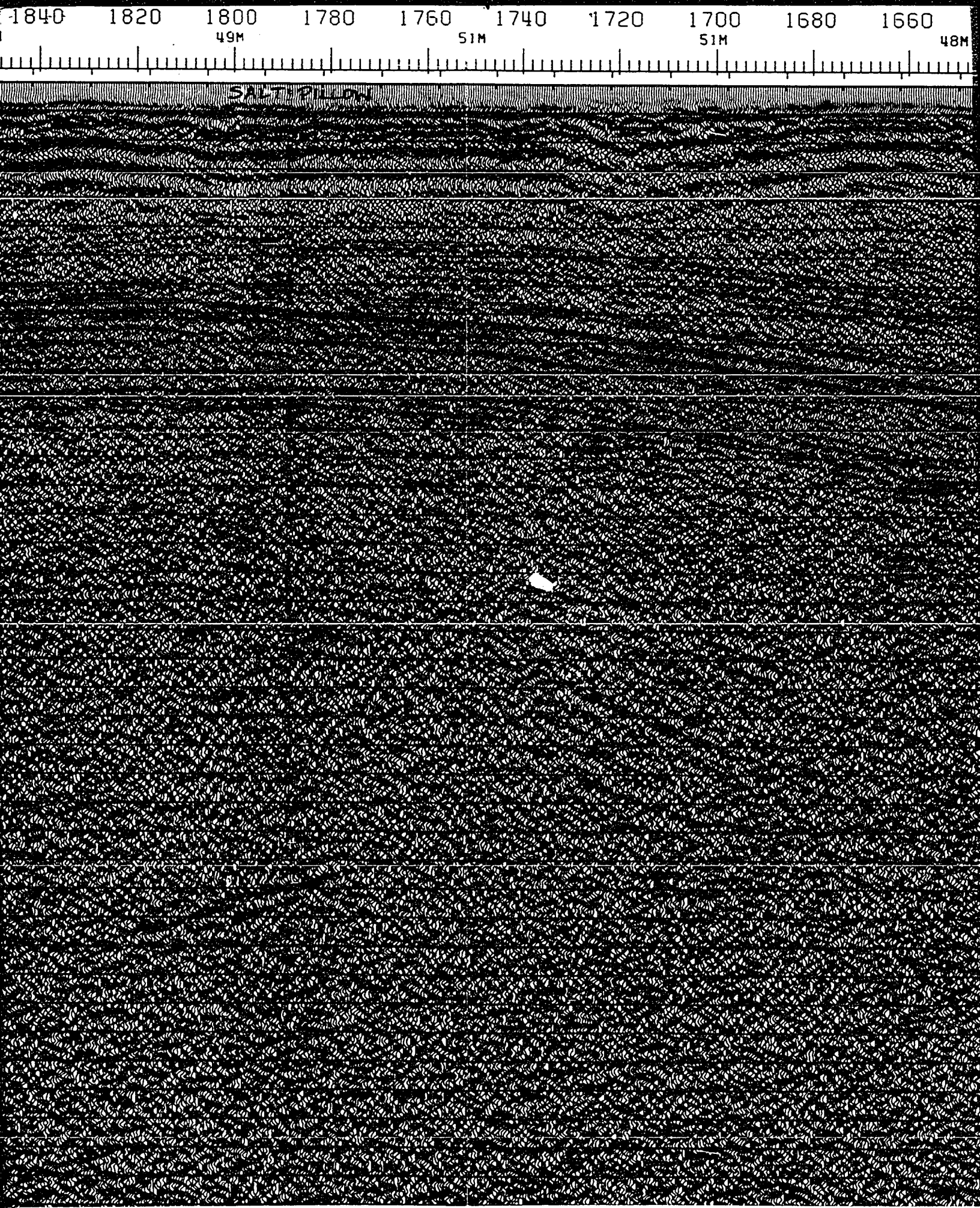
1840
1820
1800
1780
1760
1740
1720
1700
1680
1660
49M
51M
51M
48M
SALTPILLOW

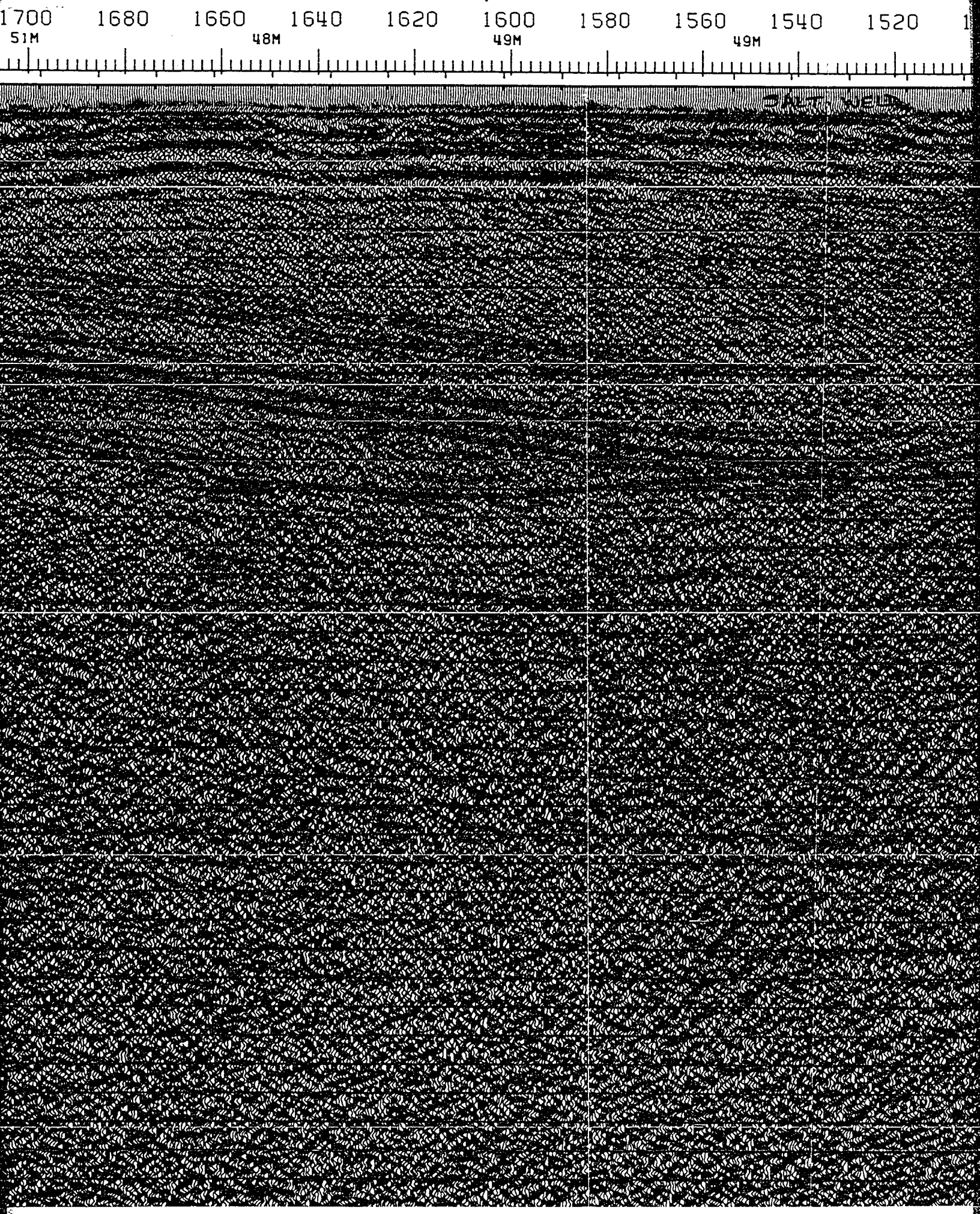
1700
1680
1660
1640
1620
1600
1580
1560
1540
1520
51M
48M
49M
49M
EAST WELL

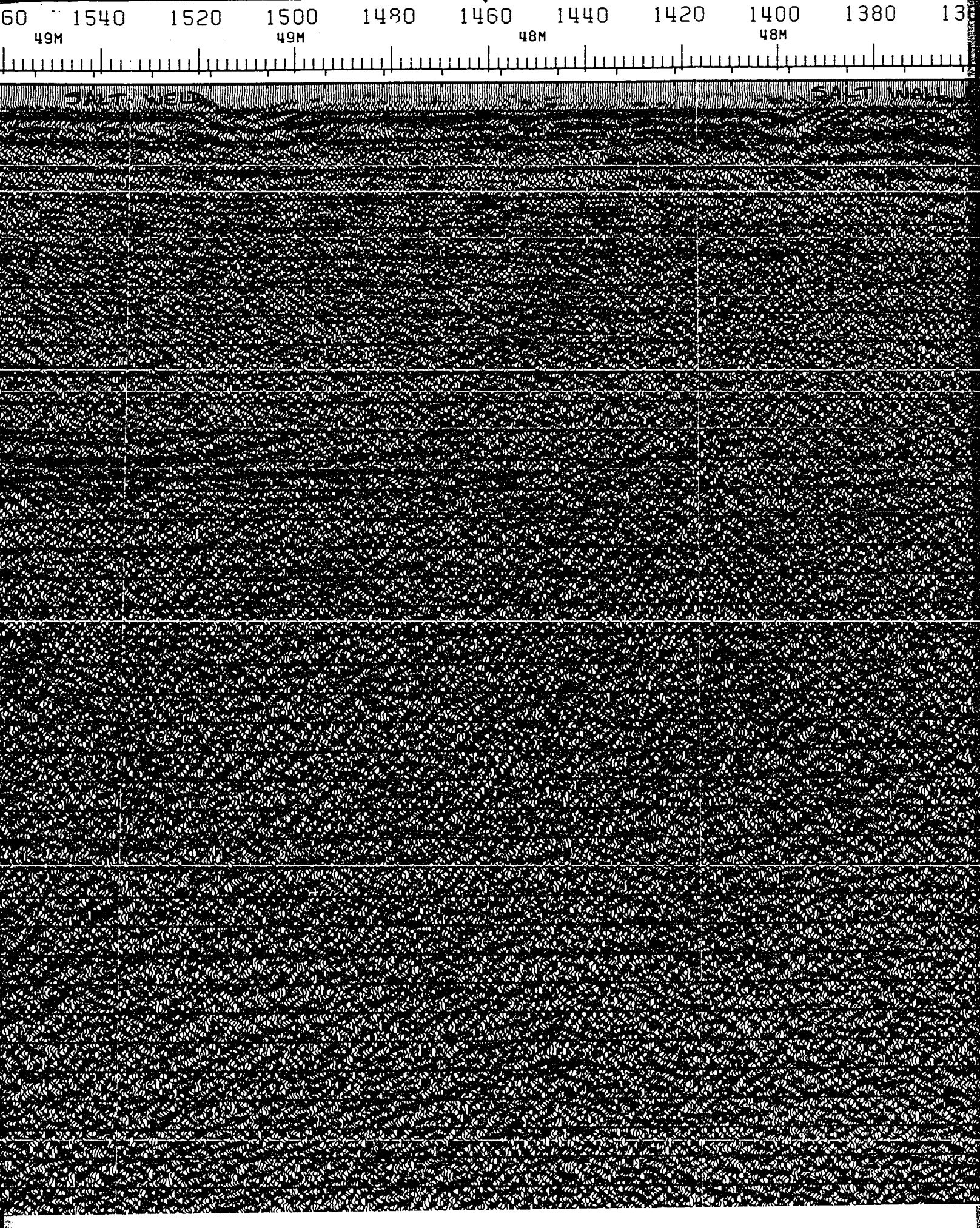
60 1540 1520 1500 1480 1460 1440 1420 1400 1380 13
49M
49M
48M
48M
SALT WELL
SALT WELL

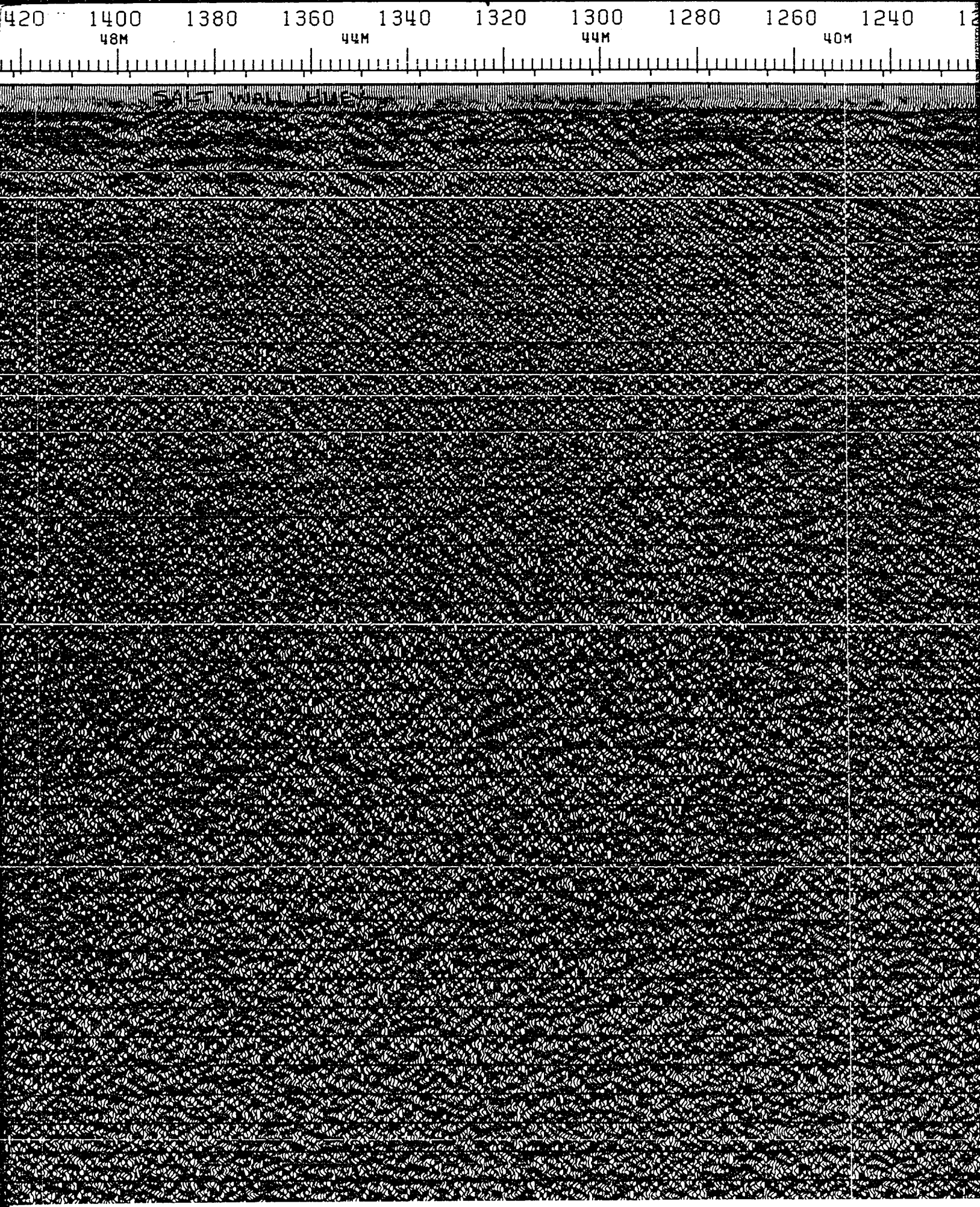
1420
1400
1380
1360
1340
1320
1300
1280
1260
1240
48M
44M
44M
40M
SALT WELL LIME


1260
1240
1220
1200
1180
1160
1140
1120
1100
1080
40M
40M
40M
40M

79

INVERNESS FM.

PORT HOOD FM.

PROJ. NO: 8624 C4 9E LINE NO:

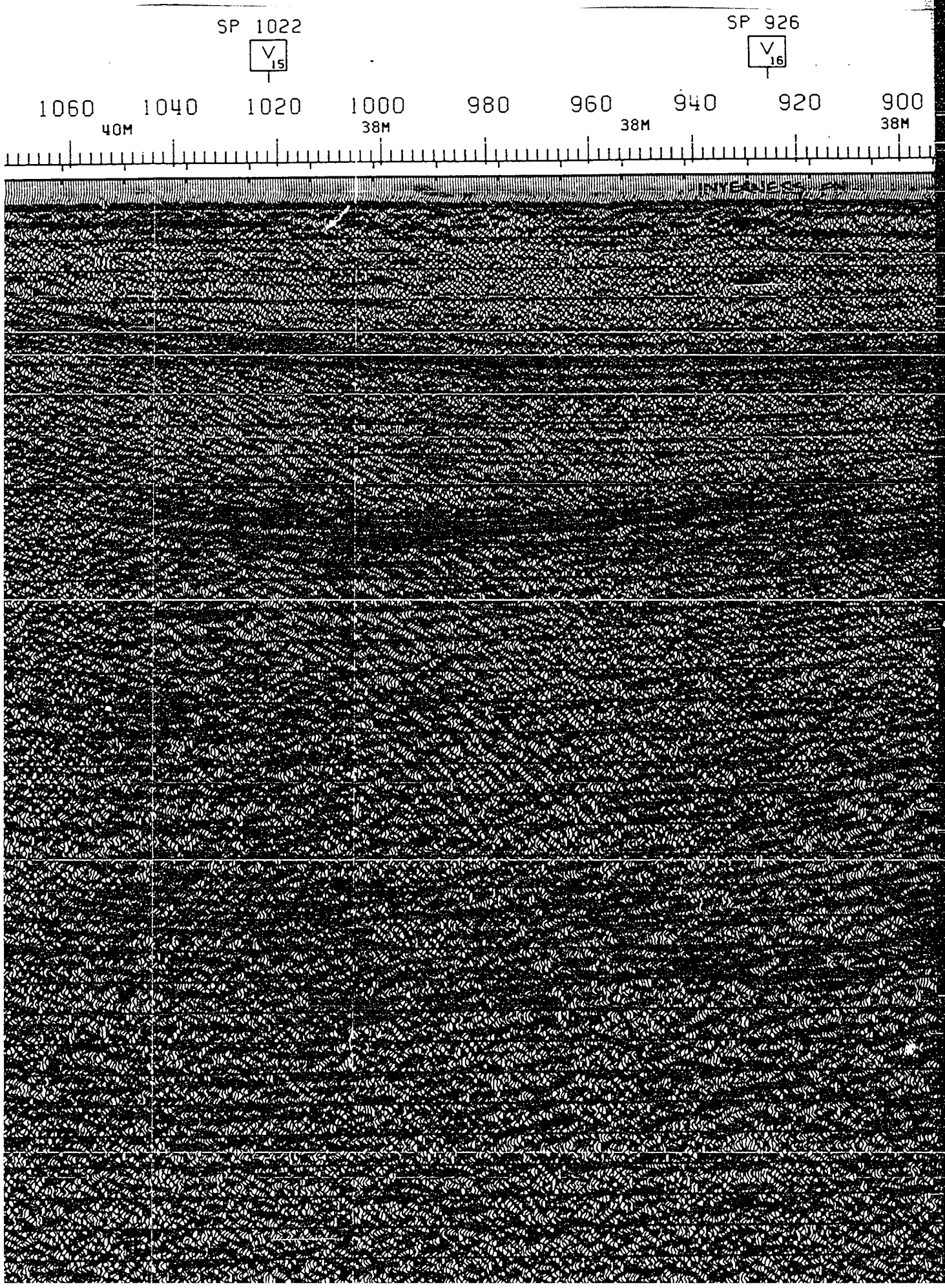
SP 1022
V15
SP 926
V16
1060
1040
1020
1000
980
960
940
920
900
40M
38M
38M
38M

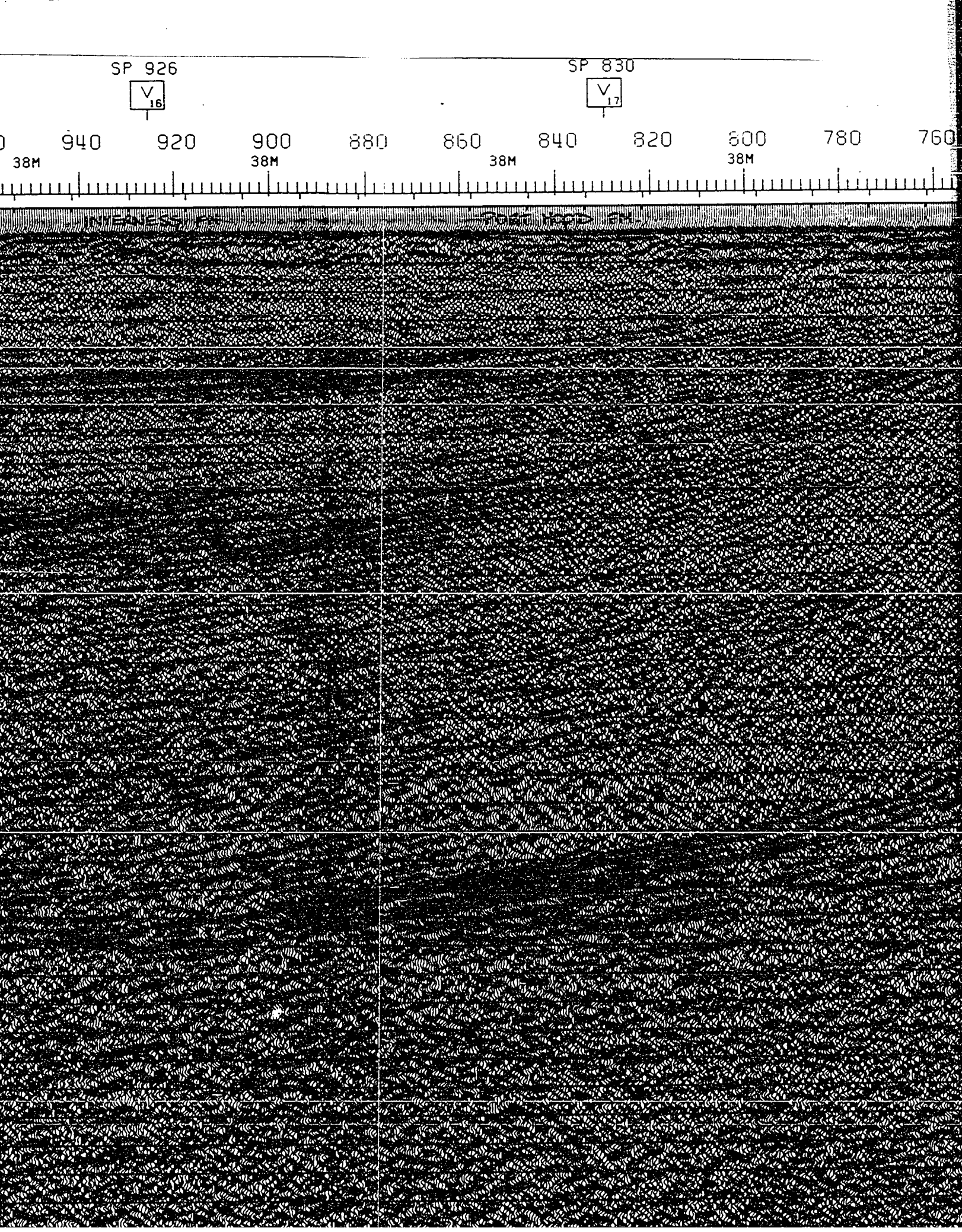
SP 926
V16
SP 830
V17
940
920
900
880
860
840
820
800
780
760
38M
38M
38M
38M

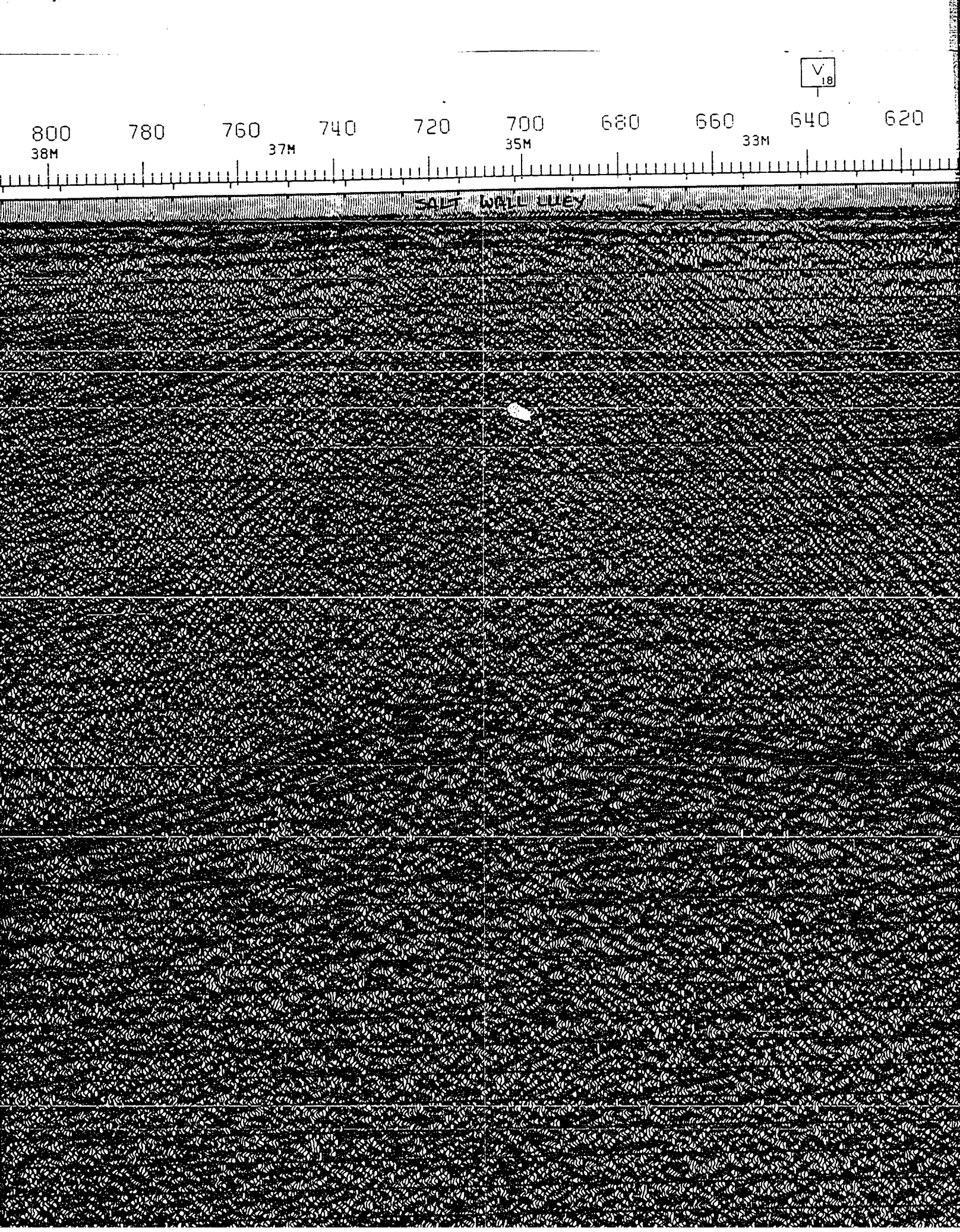
V 18
800
780
760
740
720
700
680
660
640
620
38M
37M
35M
33M
SALT WALL LUEY

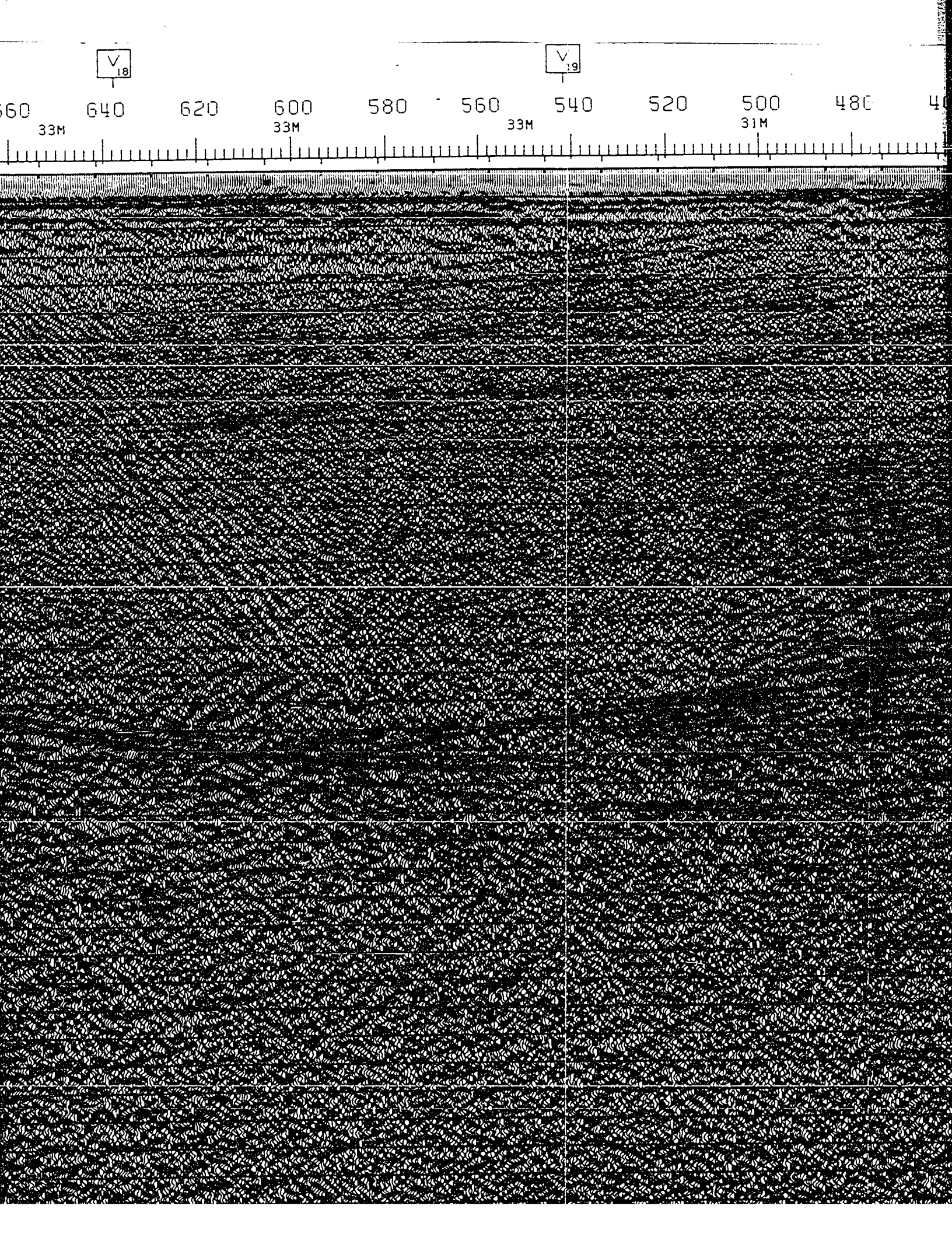
V18
V19
660
640
620
600
580
560
540
520
500
480
33M
33M
33M
31M

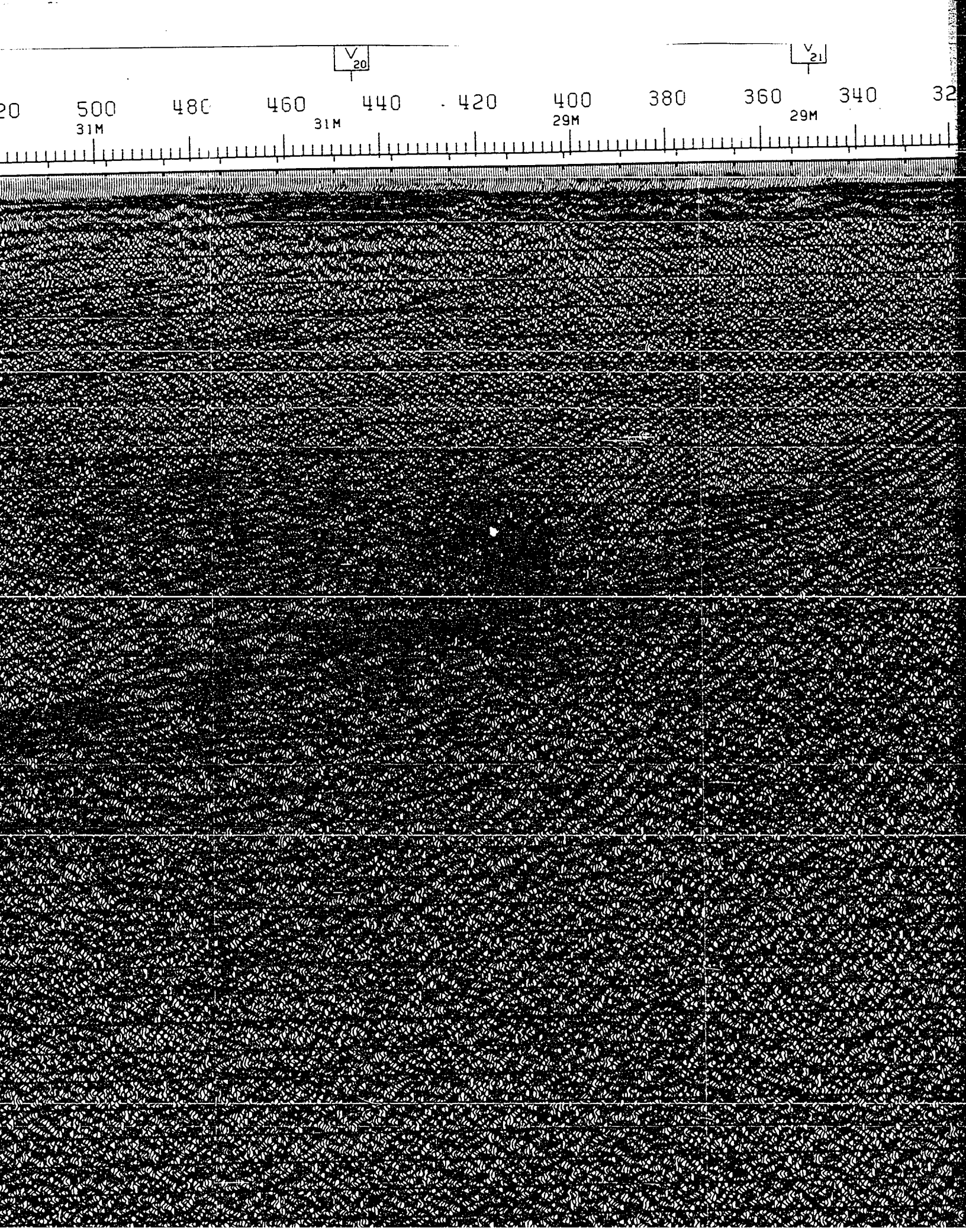
V20
V21
20
500
480
460
440
420
400
380
360
340
32
31M
31M
29M
29M

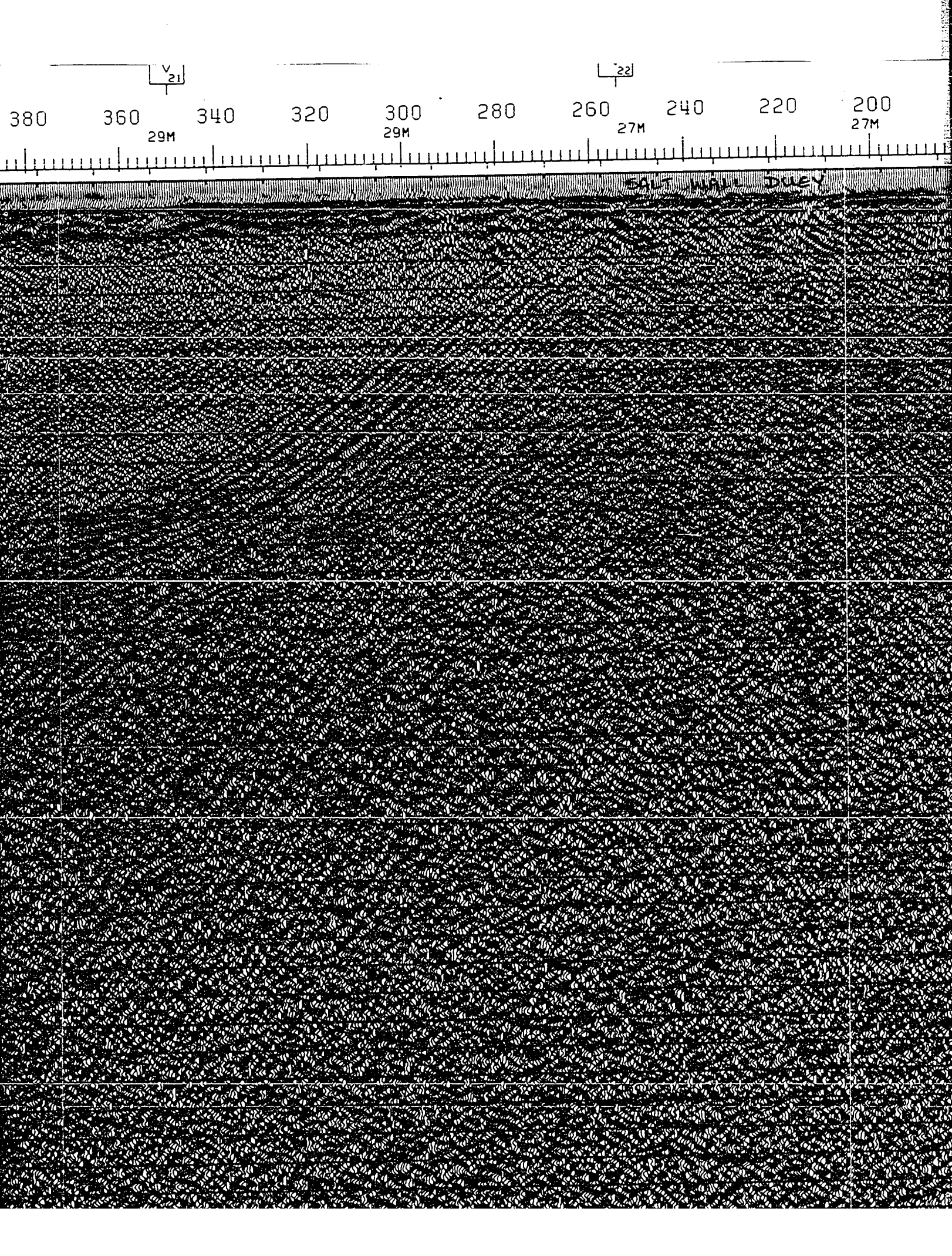
V21
22
380
360
340
320
300
280
260
240
220
200
29M
29M
27M
27M
SALT WALL DUEY

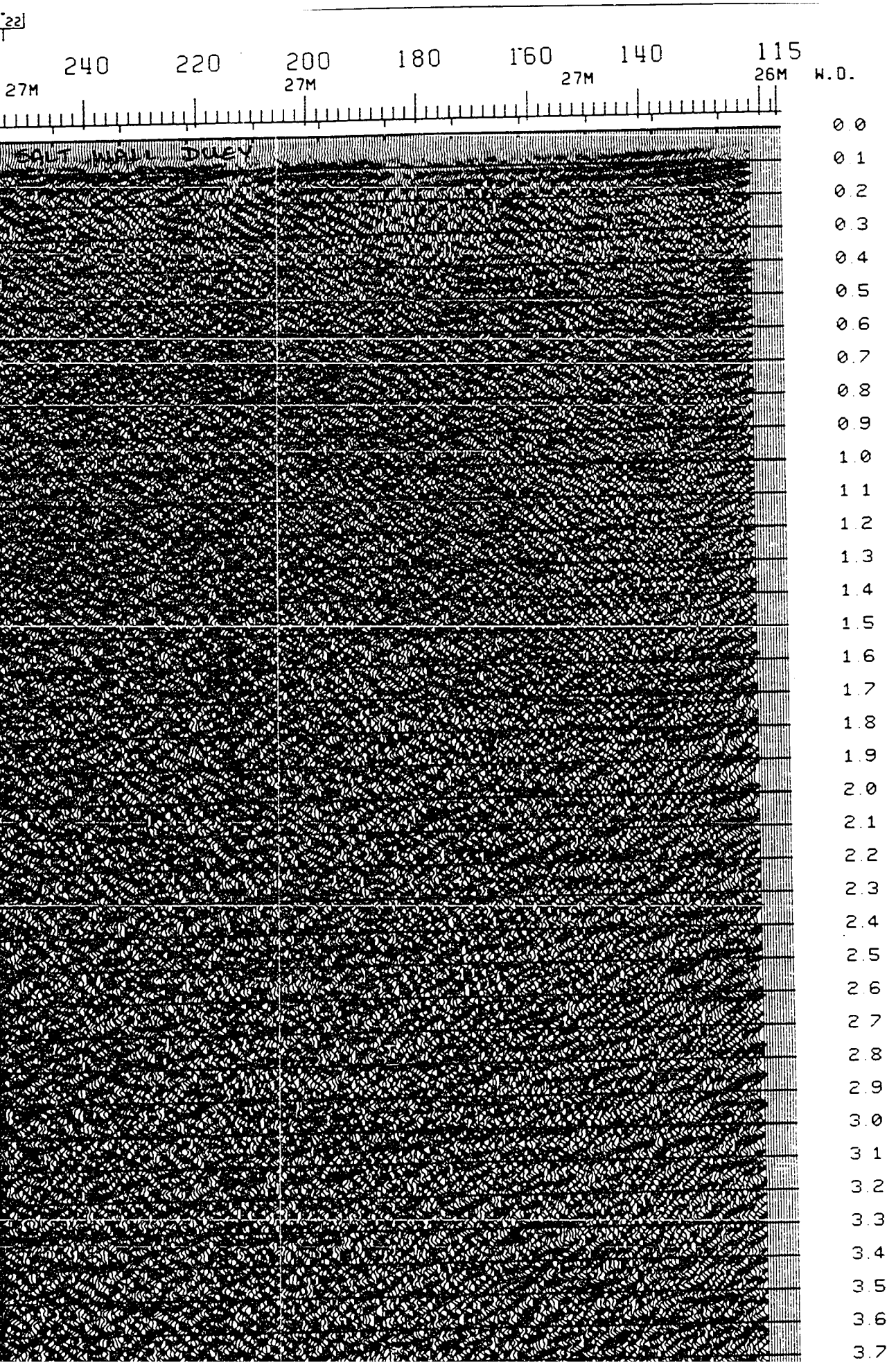

CHEVR

AR

SHOT BY WESTERN G
PROCESSED BY WEST

ENERGY SOURCE
CHARGE SIZE
NUMBER OF GUNS
GUN DEPTH
FIRING INTERVAL
SHOT POINT INTERV
DISTANCE OF SOURC

SYSTEM
AMPLIFIER
FILTER
SAMPLING INTERVAL
RECORD LENGTH
FORMAT

TYPE CABLE
CABLE LENGTH
CABLE DEPTH
LEAD IN
GROUP INTERVAL
NUMBER OF GROUPS
SPREAD

ROMS
CHANNELS PER ARR
WEIGHTS
NUMBER OF DATA C
CHANNEL INTERVAL

PROC

PRO
1. SIG
2. DEC
WI
LE
PR
3. NMO
4. REL
5. F-K
6. DEC
WI
LE
PR
7. FI
8. TI
9. GA

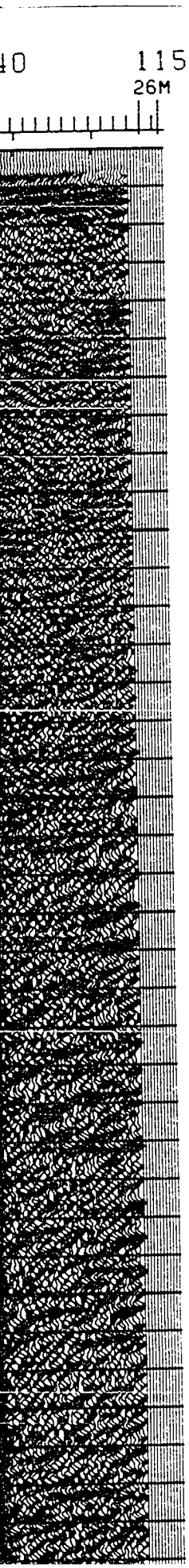

0.0
0.1
0.2
0.3
0.4
0.5
0.6
0.7
0.8
0.9
1.0
1.1
1.2
1.3
1.4
1.5
1.6
1.7
1.8
1.9
2.0
2.1
2.2
2.3
2.4
2.5
2.6
2.7
2.8
2.9
3.0
3.1
3.2
3.3
3.4
3.5
3.6
3.7

CHEVRON STANDARD LTD.

AREA: NORTHUMBERLAND STRAIT

SHOT BY WESTERN GEOPHYSICAL COMPANY PARTY 127 JULY 1981
PROCESSED BY WESTERN GEOPHYSICAL (CALGARY) GROUP 6 OCT 1981

RECORDING DATA

SOURCE

ENERGY SOURCE	AIR GUNS
CHARGE SIZE	1050 CU.IN
NUMBER OF GUNS	15
GUN DEPTH	6 M
FIRING INTERVAL	27 M
SHOT POINT INTERVAL	27 M
DISTANCE OF SOURCE TO ANTENNA	47 M

INSTRUMENTS

SYSTEM	KILOSEIS
AMPLIFIER	INST. FLOATING POINT
FILTER	L/9-H/450
SAMPLING INTERVAL	1 MS
RECORD LENGTH	5.0 SEC
FORMAT	SEG-D

CABLE

TYPE CABLE	STREAMER
CABLE LENGTH	2565 M
CABLE DEPTH	8 M
LEAD IN	187 M
GROUP INTERVAL	27 M
NUMBER OF GROUPS RECORDED	96
SPREAD	2752 M

ARRAY PARAMETERS

ROMS	7/21
CHANNELS PER ARRAY	8,50% OVERLAP
WEIGHTS	32,32,32,32,32,32,32,32
NUMBER OF DATA CHANNELS RECORDED	384
CHANNEL INTERVAL	6.67 M

PROCESSING SEQUENCE AND PARAMETERS

PROCESSING SAMPLING INTERVAL 4 MS

1. SIGNATURE DECONVOLUTION
2. DECONVOLVED BEFORE STACK
   - WINDOW LENGTH 2 ZONES OF 2500 MS
   - LENGTH OPERATOR 280 MS
   - PREDICTION DISTANCE 4 MS
3. NMO STACK 4800 %
4. RELATIVE AMP. COMPENSATION
5. F-K DOMAIN FILTER
6. DECONVOLVED AFTER STACK
   - WINDOW LENGTH 2 ZONES OF 2500 MS
   - LENGTH OPERATOR 300 MS
   - PREDICTION DISTANCE 20 MS
7. FINITE DIFFERENCE MIGRATION
8. TIME VARIANT FILTER

TIME		L.C. (HZ)	H.C.
1.00	SEC	12	60
3.00	SEC	8	45
5.00	SEC	8	30

9. GAIN (AMPLITUDE EQUALIZATION)

SOUTHEAST

EVRON STANDARD LTD.

AREA: NORTHUMBERLAND STRAIT

TERN GEOPHYSICAL COMPANY PARTY 127 JULY 1981
Y WESTERN GEOPHYSICAL (CALGARY) GROUP 6 OCT 1981

RECORDING DATA

SOURCE

CE	AIR GUNS
	1050 CU.IN
UNS	15
	6 M
RVAL	27 M
INTERVAL	27 M
SOURCE TO ANTENNA	47 M

INSTRUMENTS

	KILOSEIS
	INST. FLOATING POINT
	L/9-H/450
NTERVAL	1 MS
TH	5.0 SEC
	SEG-D

CABLE

	STREAMER
TH	2565 M
H	8 M
	187 M
RVAL	27 M
GROUPS RECORDED	96
	2752 M

ARRAY PARAMETERS

	7/21
ER ARRAY	8.50% OVERLAP
	32.32.32.32.32.32.32.32
DATA CHANNELS RECORDED	384
TERVAL	6.67 M

PROCESSING SEQUENCE AND PARAMETERS

PROCESSING SAMPLING INTERVAL 4 MS

1. SIGNATURE DECONVOLUTION
2. DECONVOLVED BEFORE STACK
   - WINDOW LENGTH 2 ZONES OF 2500 MS
   - LENGTH OPERATOR 280 MS
   - PREDICTION DISTANCE 4 MS
3. NMO STACK 4800 %
4. RELATIVE AMP. COMPENSATION
5. F-K DOMAIN FILTER
6. DECONVOLVED AFTER STACK
   - WINDOW LENGTH 2 ZONES OF 2500 MS
   - LENGTH OPERATOR 300 MS
   - PREDICTION DISTANCE 20 MS
7. FINITE DIFFERENCE MIGRATION
8. TIME VARIANT FILTER

TIME		L.C. (HZ)	H.C.
1.00	SEC	12	60
3.00	SEC	8	45
5.00	SEC	8	30

79

624 C4 9E LINE NO: 81-79-

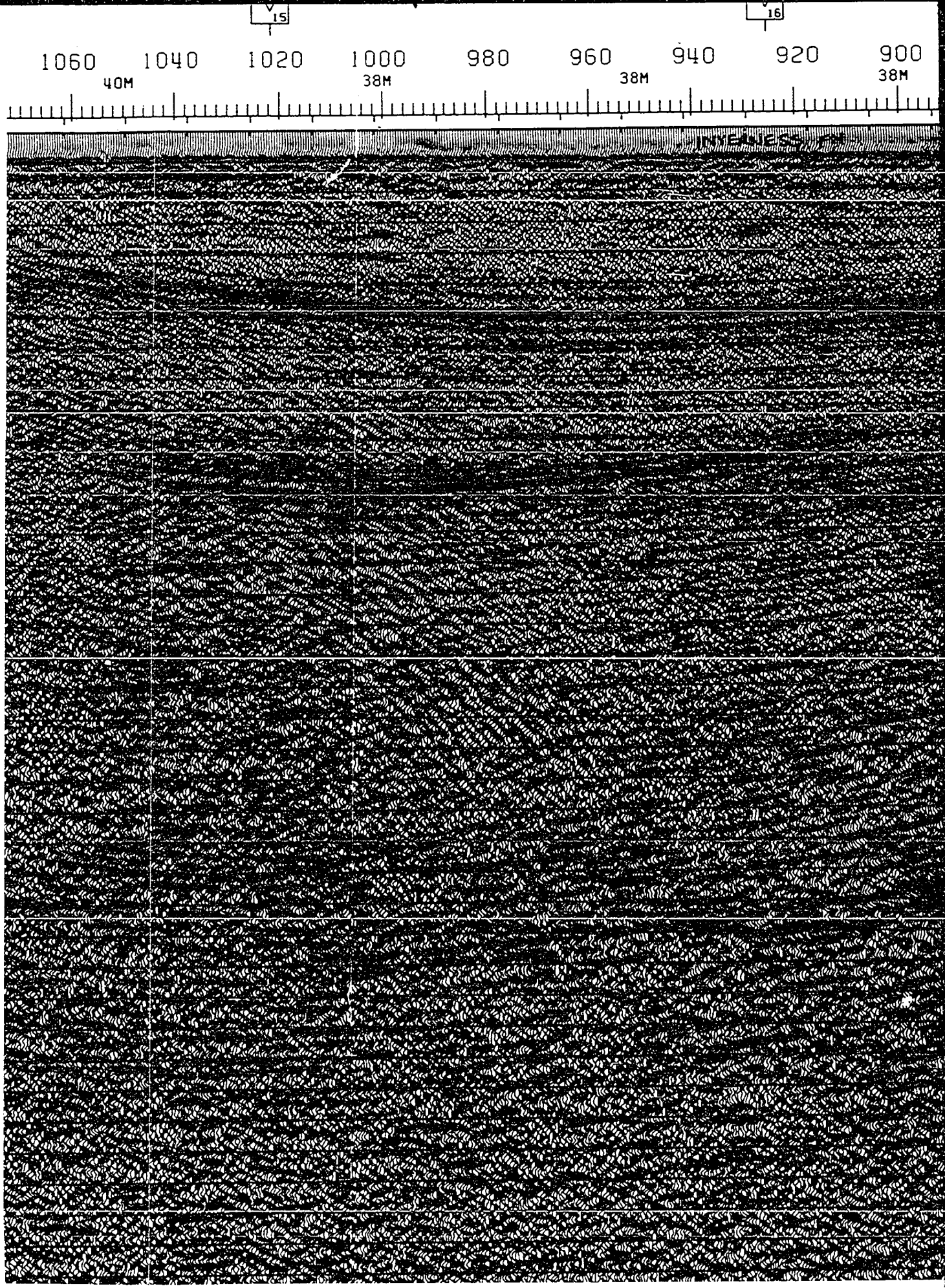
15
16
1060
1040
1020
1000
980
960
940
920
900
40M
38M
38M
38M

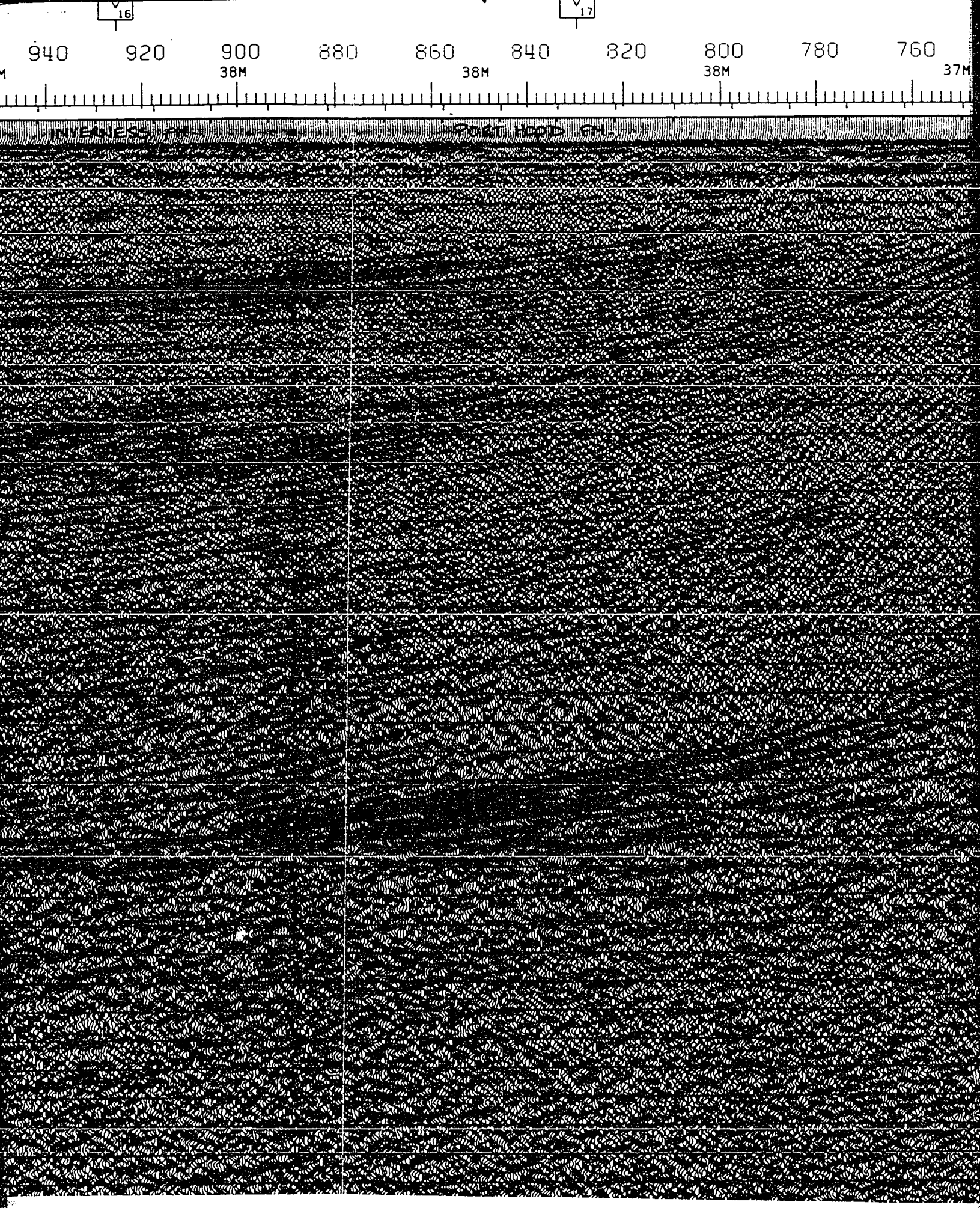
16
17
940
920
900
880
860
840
820
800
780
760
38M
38M
38M
37M
INVERNESS
PORT HOOD GM

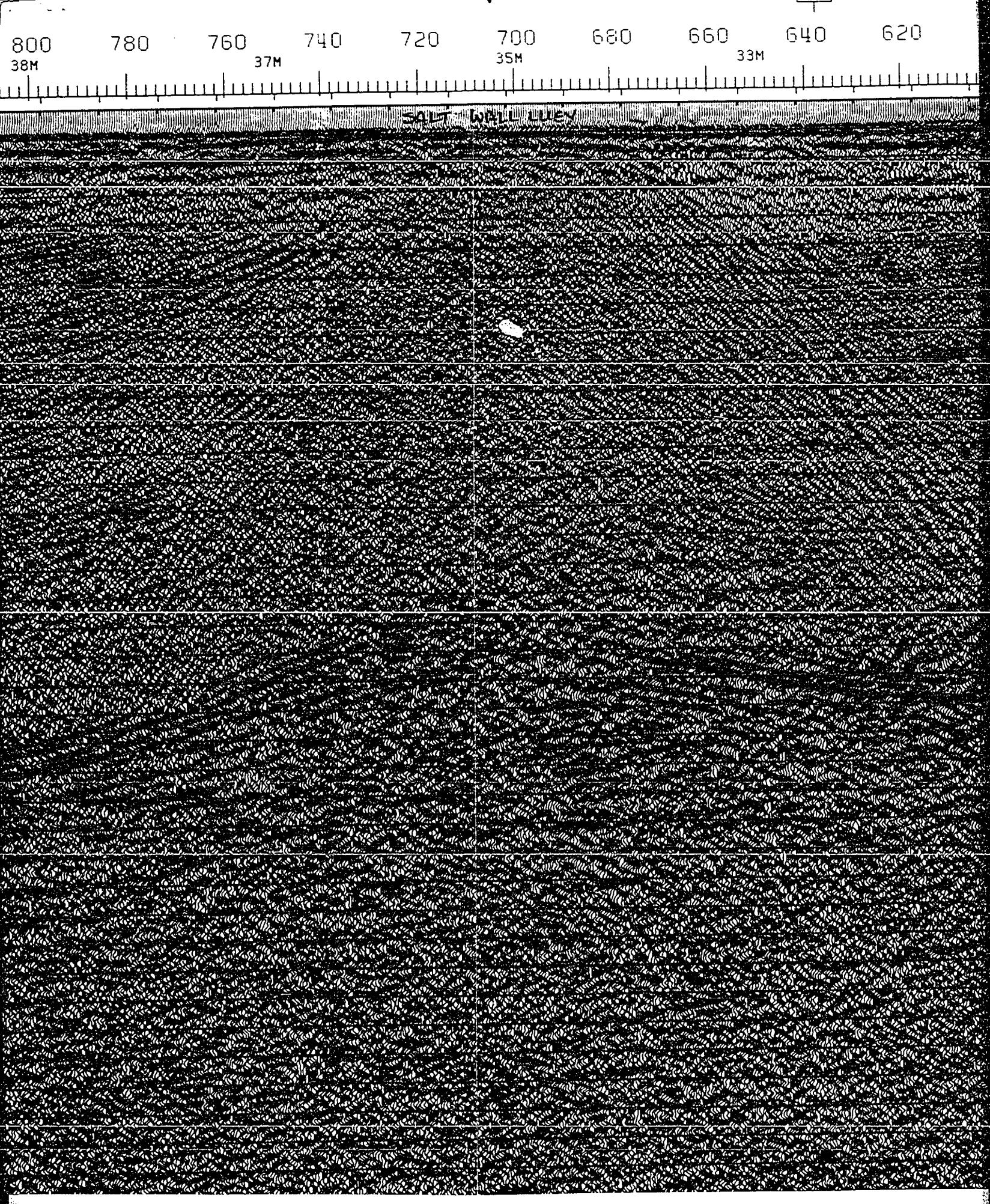
800
780
760
740
720
700
680
660
640
620
38M
37M
35M
33M
SALT WELL LUEY

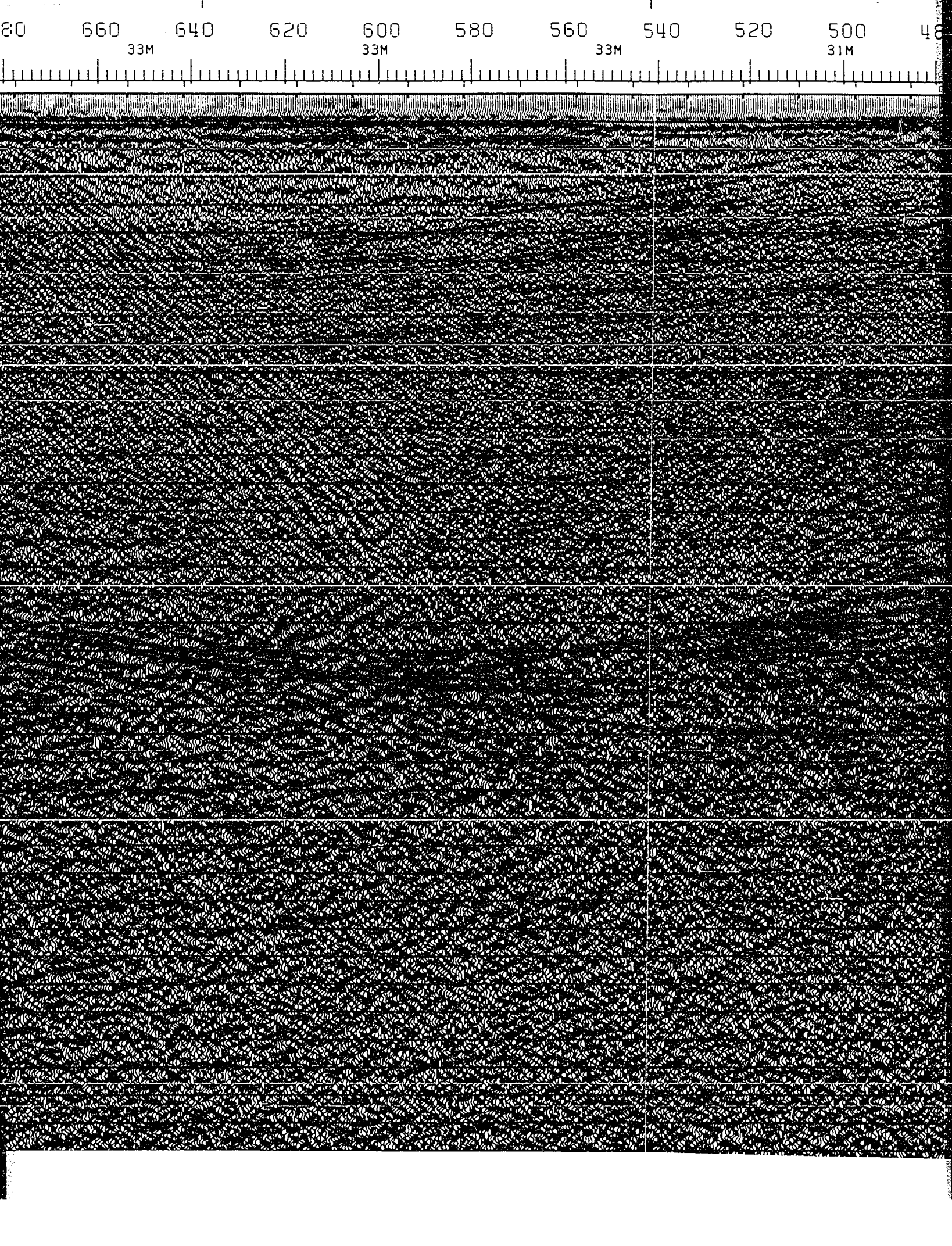
80
660
640
620
600
580
560
540
520
500
33M
33M
33M
31M

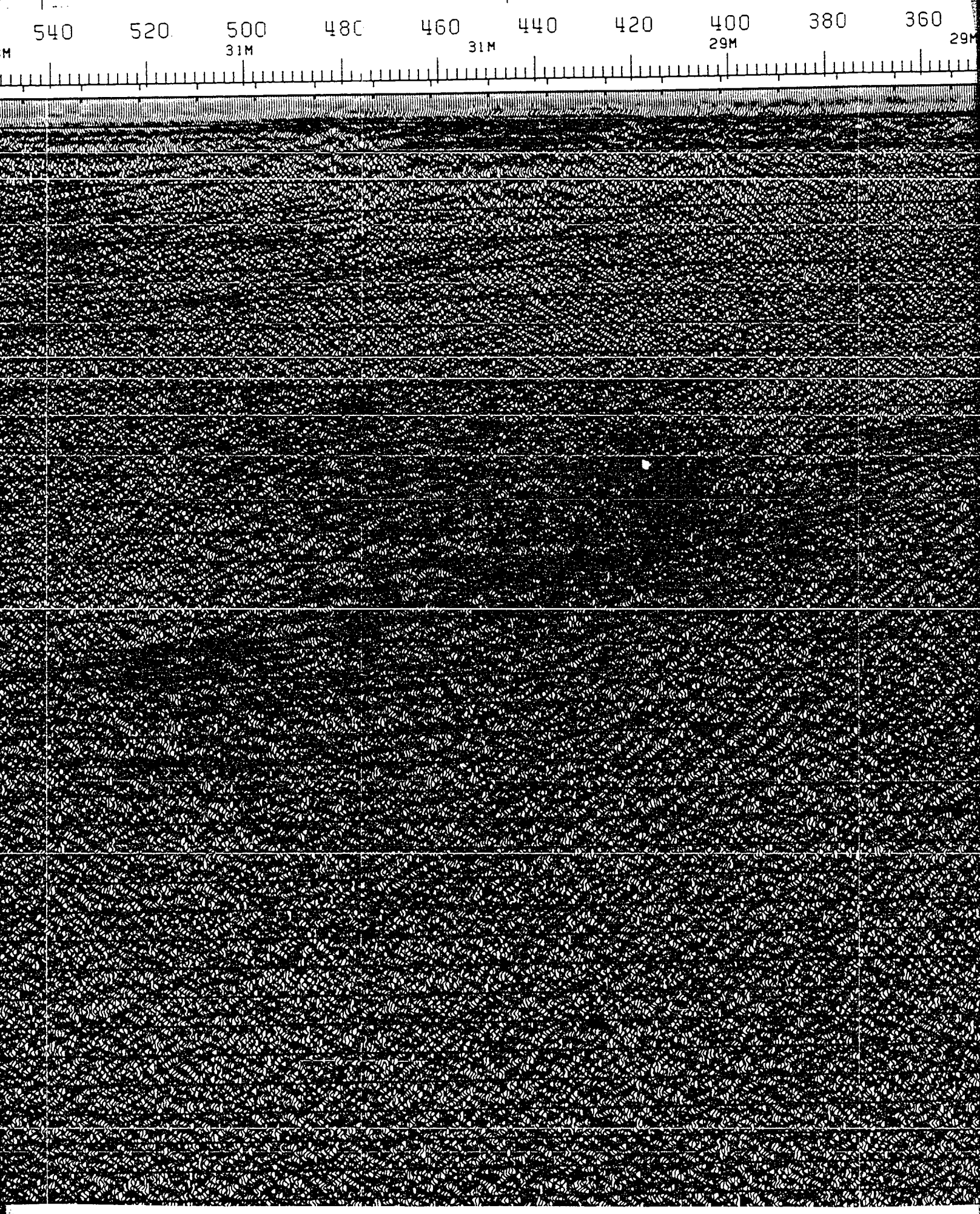
540
520
500
480
460
440
420
400
380
360
31M
31M
29M
29M

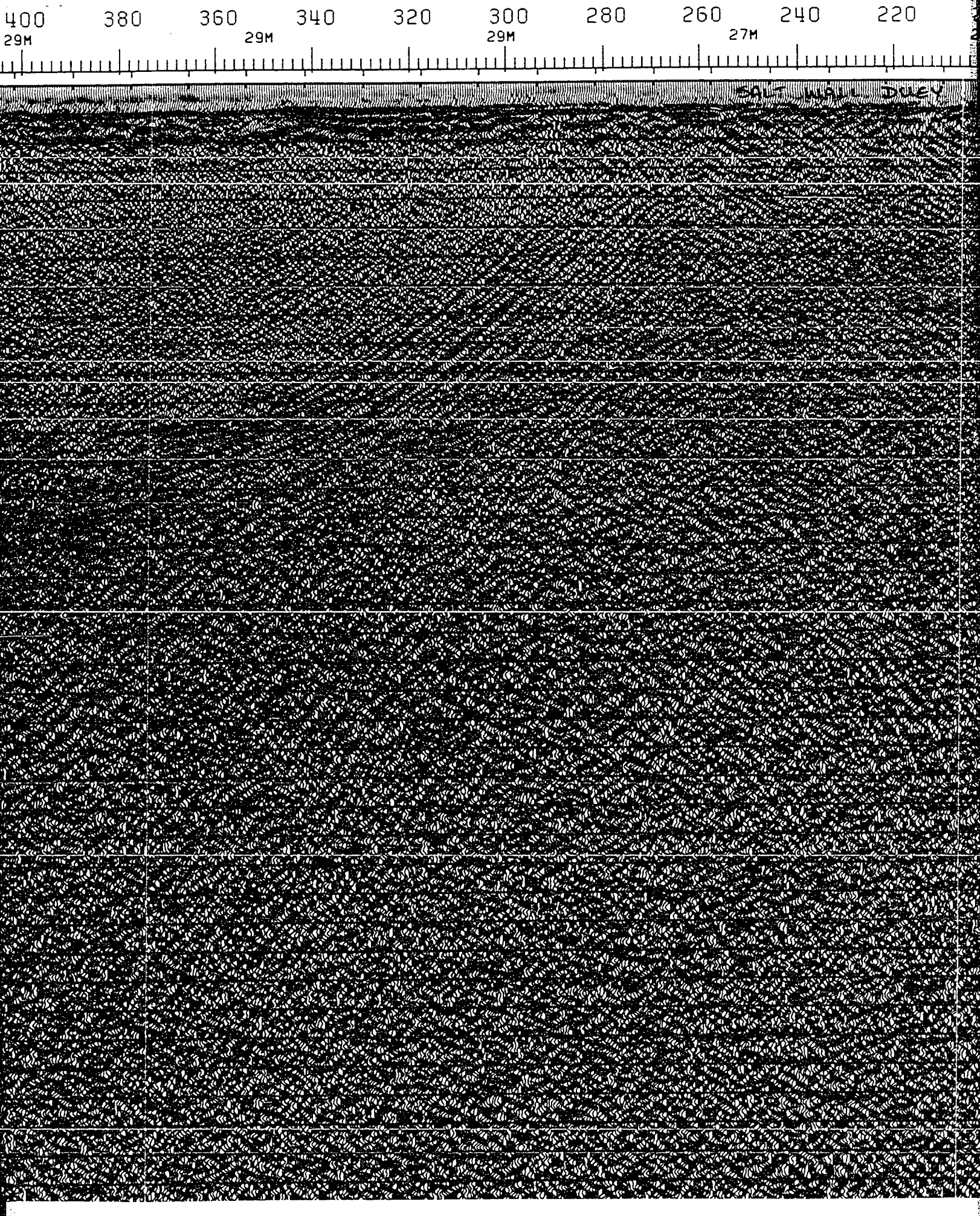
400
380
360
340
320
300
280
260
240
220
29M
29M
29M
27M

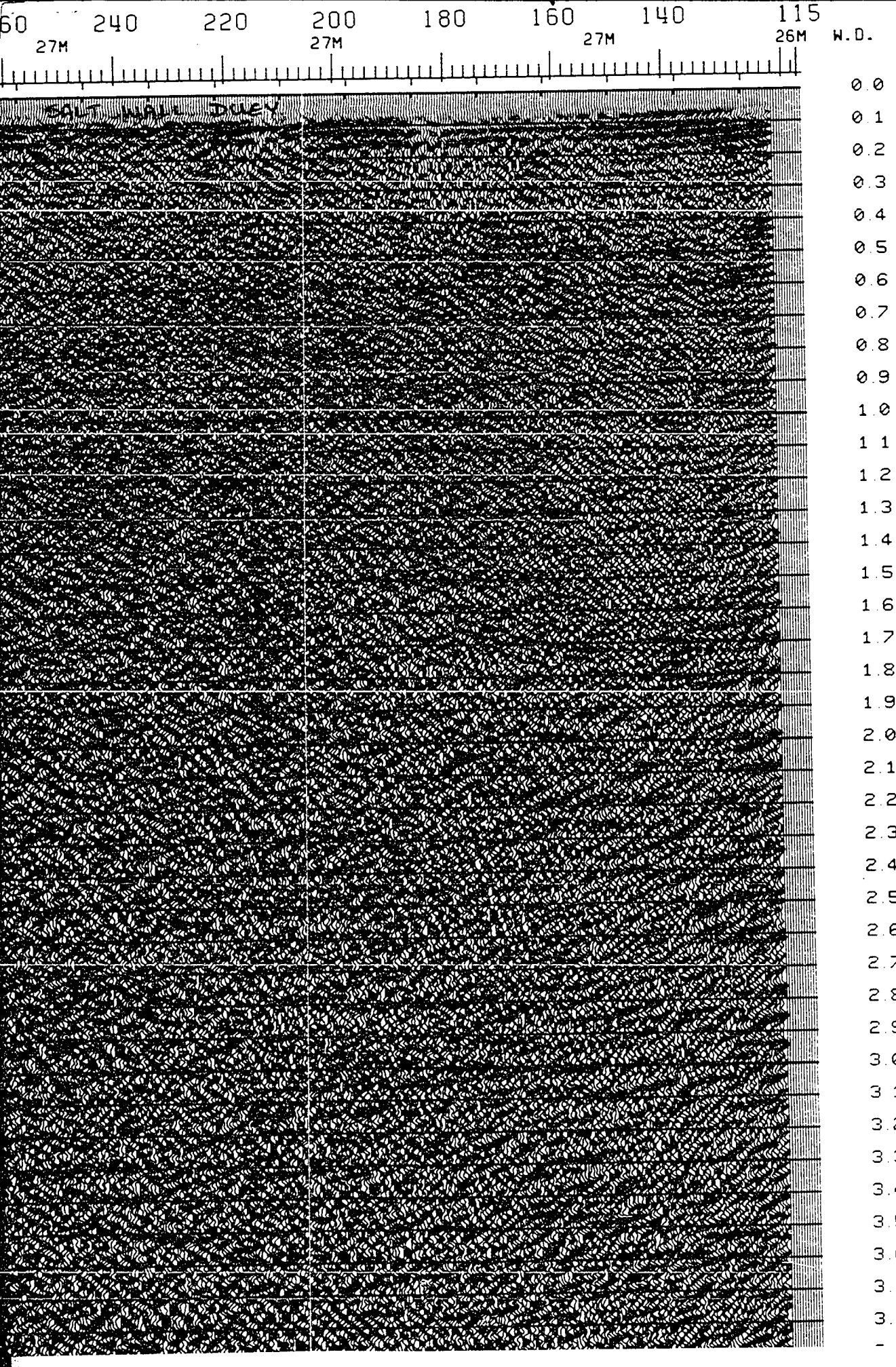

CHEV

SHOT BY WESTER
PROCESSED BY W

ENERGY SOURCE
CHARGE SIZE
NUMBER OF GUNS
GUN DEPTH
FIRING INTERVA
SHOT POINT INT
DISTANCE OF SO

SYSTEM
AMPLIFIER
FILTER
SAMPLING INTER
RECORD LENGTH
FORMAT

TYPE CABLE
CABLE LENGTH
CABLE DEPTH
LEAD IN
GROUP INTERVA
NUMBER OF GRO
SPREAD

ROMS
CHANNELS PER
WEIGHTS
NUMBER OF DAT
CHANNEL INTER

P

1.
2.
3.
4.
5.
6.
7.
8.
9.

47 M

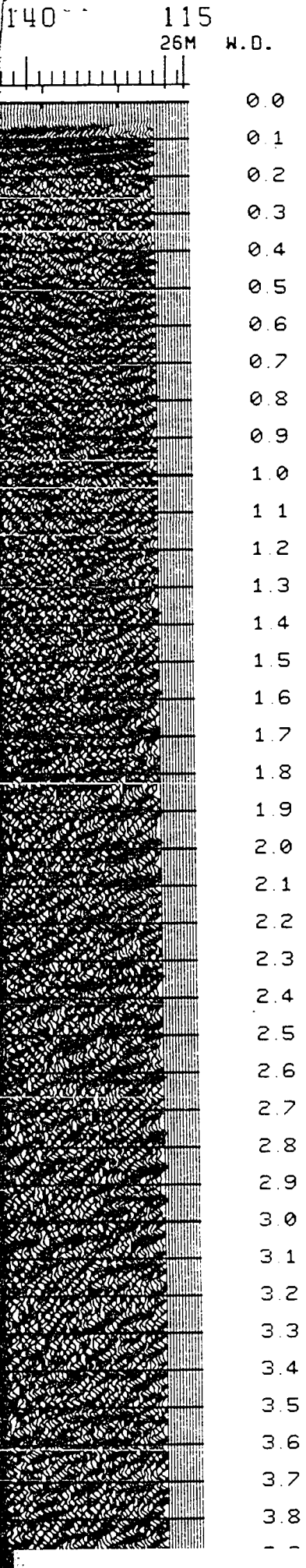

CHEVRON STANDARD LTD.

AREA: NORTHUMBERLAND STRAIT

SHOT BY WESTERN GEOPHYSICAL COMPANY PARTY 127 JULY 1981
PROCESSED BY WESTERN GEOPHYSICAL (CALGARY) GROUP 6 OCT 1981

RECORDING DATA

SOURCE

ENERGY SOURCE	AIR GUNS
CHARGE SIZE	1050 CU.IN
NUMBER OF GUNS	15
GUN DEPTH	6 M
FIRING INTERVAL	27 M
SHOT POINT INTERVAL	27 M
DISTANCE OF SOURCE TO ANTENNA	47 M

INSTRUMENTS

SYSTEM	KILOSEIS
AMPLIFIER	INST. FLOATING POINT
FILTER	L/9-H/450
SAMPLING INTERVAL	1 MS
RECORD LENGTH	5.0 SEC
FORMAT	SEG-D

CABLE

TYPE CABLE	STREAMER
CABLE LENGTH	2565 M
CABLE DEPTH	8 M
LEAD IN	187 M
GROUP INTERVAL	27 M
NUMBER OF GROUPS RECORDED	96
SPREAD	2752 M

ARRAY PARAMETERS

ROMS	7/21
CHANNELS PER ARRAY	8.50% OVERLAP
WEIGHTS	32.32.32.32.32.32.32.32
NUMBER OF DATA CHANNELS RECORDED	384
CHANNEL INTERVAL	6.67 M

PROCESSING SEQUENCE AND PARAMETERS

PROCESSING SAMPLING INTERVAL 4 MS

1. SIGNATURE DECONVOLUTION
2. DECONVOLVED BEFORE STACK
   - WINDOW LENGTH 2 ZONES OF 2500 MS
   - LENGTH OPERATOR 280 MS
   - PREDICTION DISTANCE 4 MS
3. NMO STACK 4800 %
4. RELATIVE AMP. COMPENSATION
5. F-K DOMAIN FILTER
6. DECONVOLVED AFTER STACK
   - WINDOW LENGTH 2 ZONES OF 2500 MS
   - LENGTH OPERATOR 300 MS
   - PREDICTION DISTANCE 20 MS
7. FINITE DIFFERENCE MIGRATION
8. TIME VARIANT FILTER

TIME		L.C. (HZ)	H.C.
1.00	SEC	12	60
3.00	SEC	8	45
5.00	SEC	8	30

9. GAIN (AMPLITUDE EQUALIZATION)

47 M

LEGEND

SOUTHEAST

VRON STANDARD LTD.

AREA: NORTHUMBERLAND STRAIT

ERN GEOPHYSICAL COMPANY — PARTY 127 — JULY 1981
WESTERN GEOPHYSICAL (CALGARY) — GROUP 6 — OCT 1981

79

RECORDING DATA

SOURCE

E	AIR GUNS
	1050 CU.IN
NS	15
	6 M
VAL	27 M
NTERVAL	27 M
SOURCE TO ANTENNA	47 M

INSTRUMENTS

	KILOSEIS
	INST. FLOATING POINT
	L/9-H/450
TERVAL	1 MS
TH	5.0 SEC
	SEG-D

CABLE

	STREAMER
H	2565 M
	8 M
	187 M
VAL	27 M
ROUPS RECORDED	96
	2752 M

ARRAY PARAMETERS

	7/21
R ARRAY	8.50% OVERLAP
	32,32,32,32,32,32,32,32
ATA CHANNELS RECORDED	384
ERVAL	6.67 M

PROCESSING SEQUENCE AND PARAMETERS

PROCESSING SAMPLING INTERVAL 4 MS

. SIGNATURE DECONVOLUTION

. DECONVOLVED BEFORE STACK

WINDOW LENGTH	2 ZONES OF 2500 MS
LENGTH OPERATOR	280 MS
PREDICTION DISTANCE	4 MS

. NMO STACK 4800 %

. RELATIVE AMP. COMPENSATION

. F-K DOMAIN FILTER

. DECONVOLVED AFTER STACK

WINDOW LENGTH	2 ZONES OF 2500 MS
LENGTH OPERATOR	300 MS
PREDICTION DISTANCE	20 MS

. FINITE DIFFERENCE MIGRATION

. TIME VARIANT FILTER

TIME		L.C. (HZ)	H.C.
1.00	SEC	12	60
3.00	SEC	8	45
5.00	SEC	8	30

. GAIN (AMPLITUDE EQUALIZATION)

LEGEND

VELOCITY FUNCTION

824 C4 9E LINE NO: 81-78-11

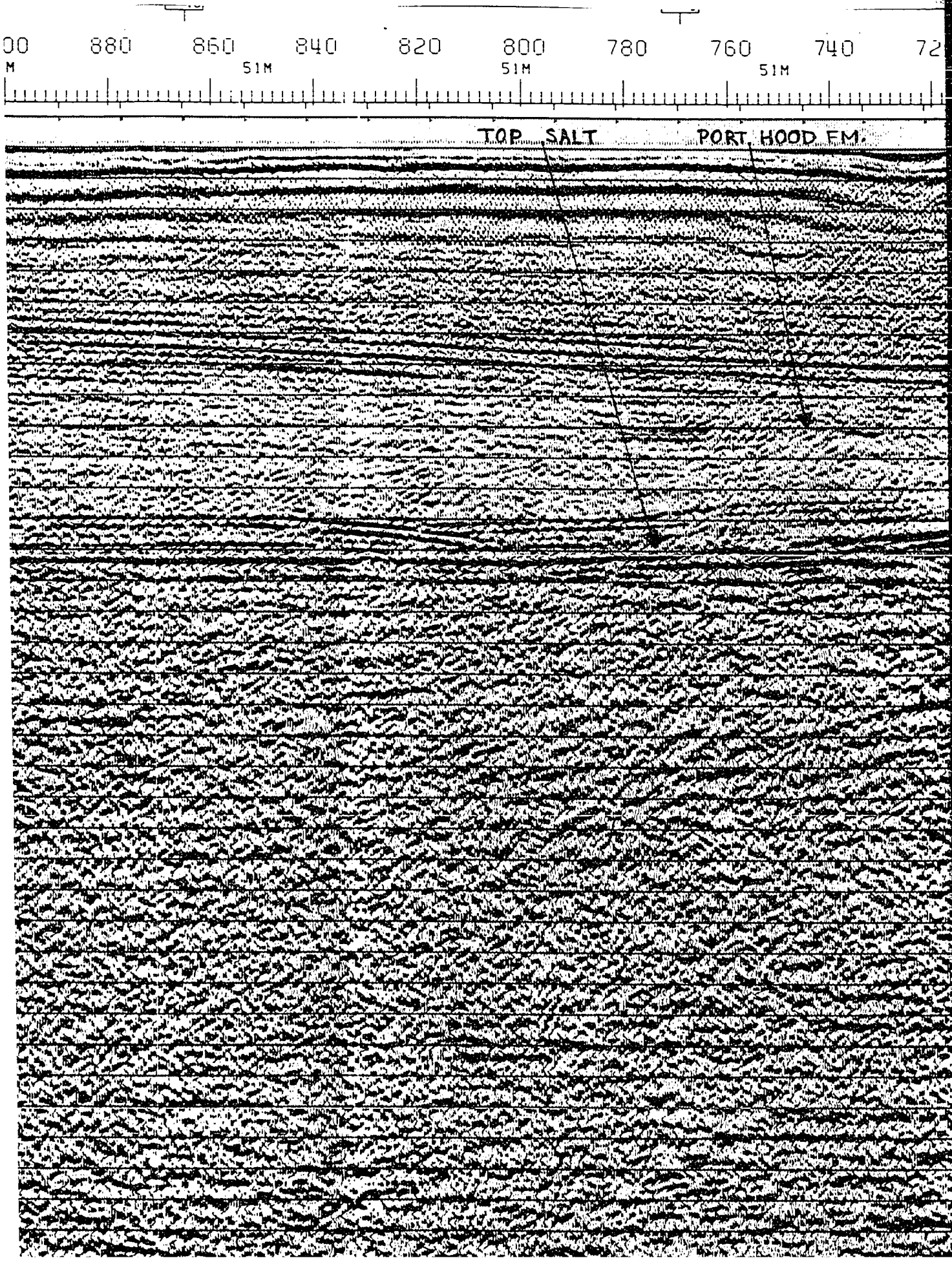
00 880 860 840 820 800 780 760 740 72
M
51M
51M
51M
TOP SALT
PORT HOOD FM.

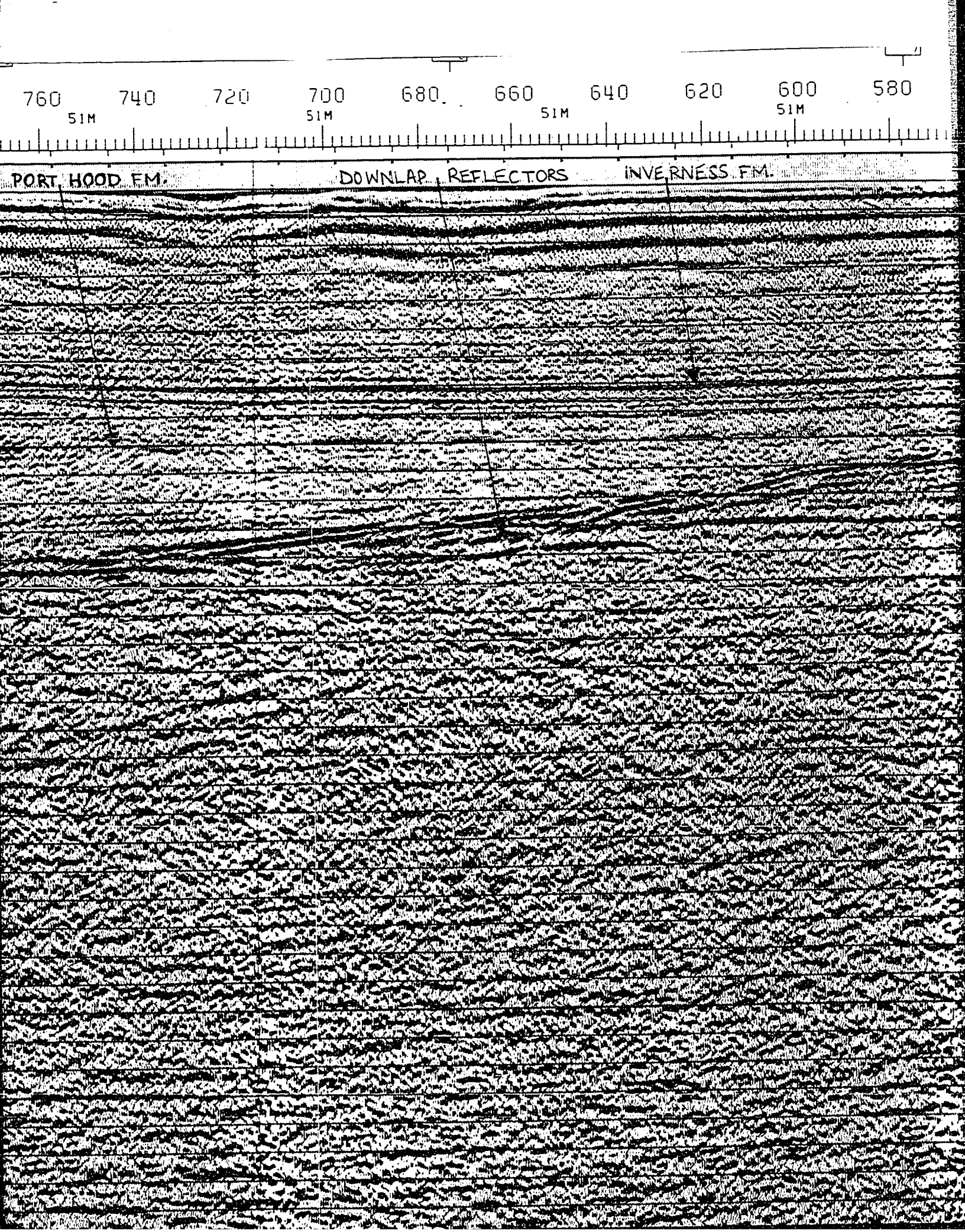
760
740
720
700
680
660
640
620
600
580
51M
51M
51M
51M
PORT HOOD FM.
DOWNLAP REFLECTORS
INVERNESS FM.

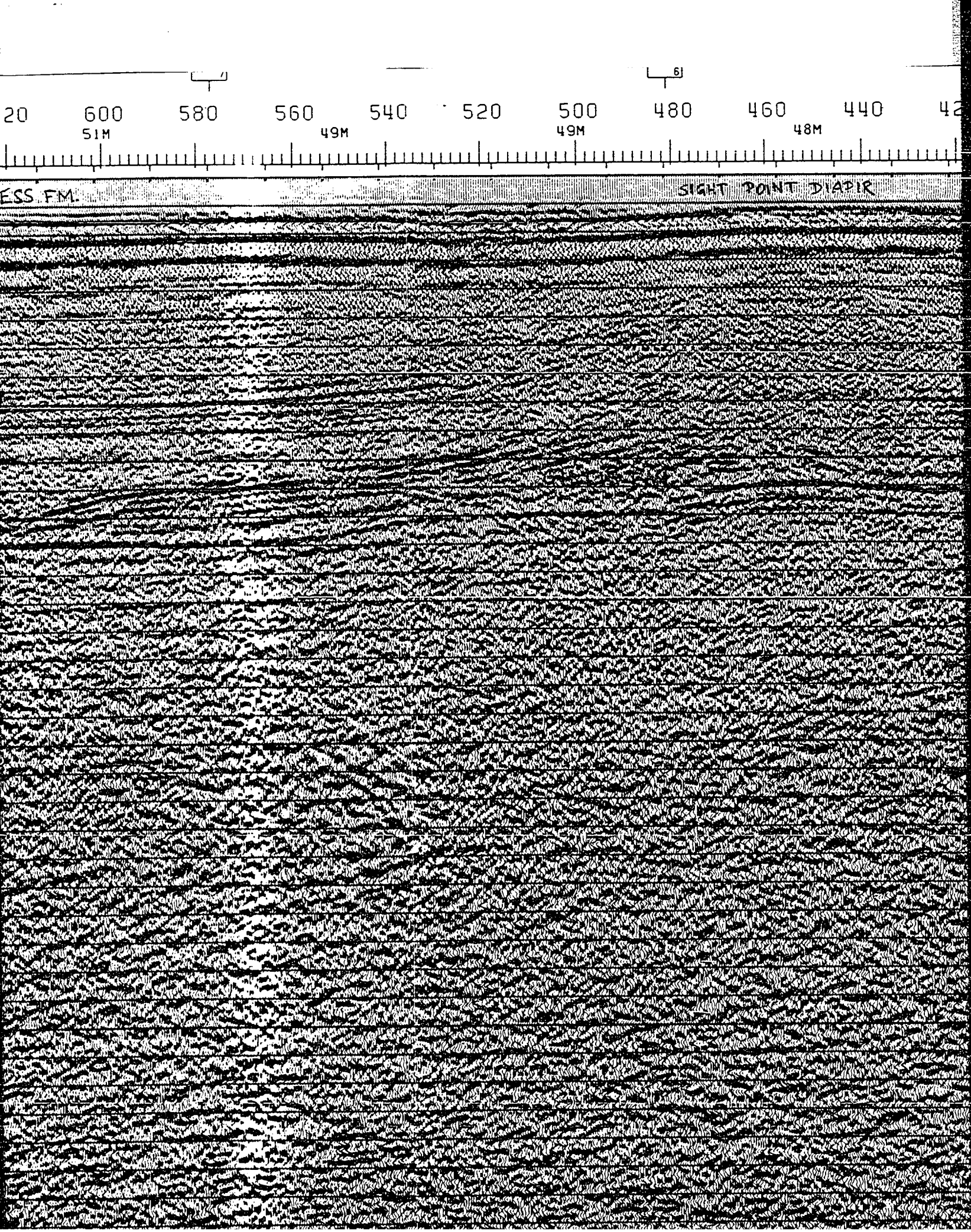
20
600
580
560
540
520
500
480
460
440
51M
49M
49M
48M
ESS FM.
SIGHT POINT DIAPIR

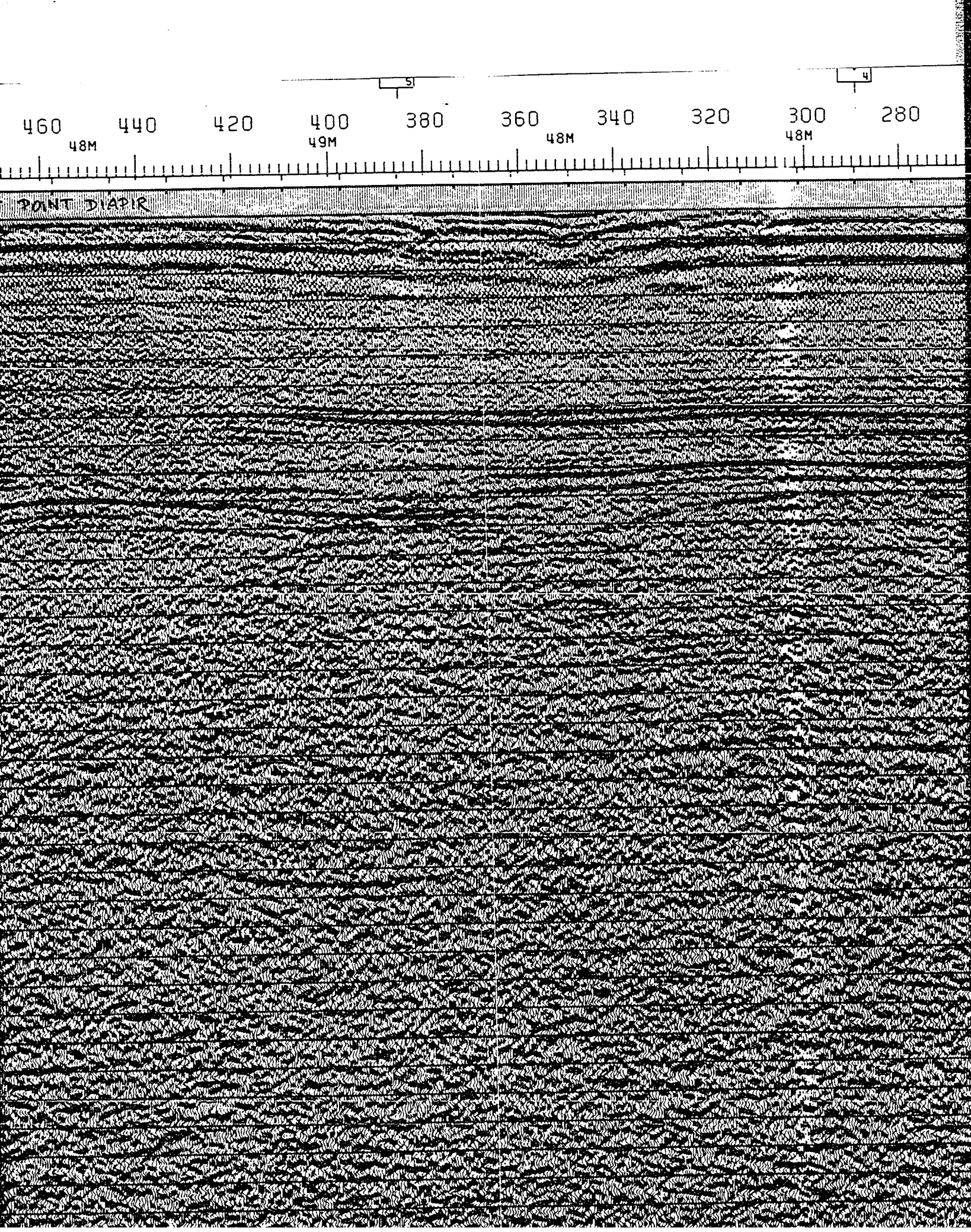
5
4
460
440
420
400
380
360
340
320
300
280
48M
49M
48M
48M
POINT DIAPIR

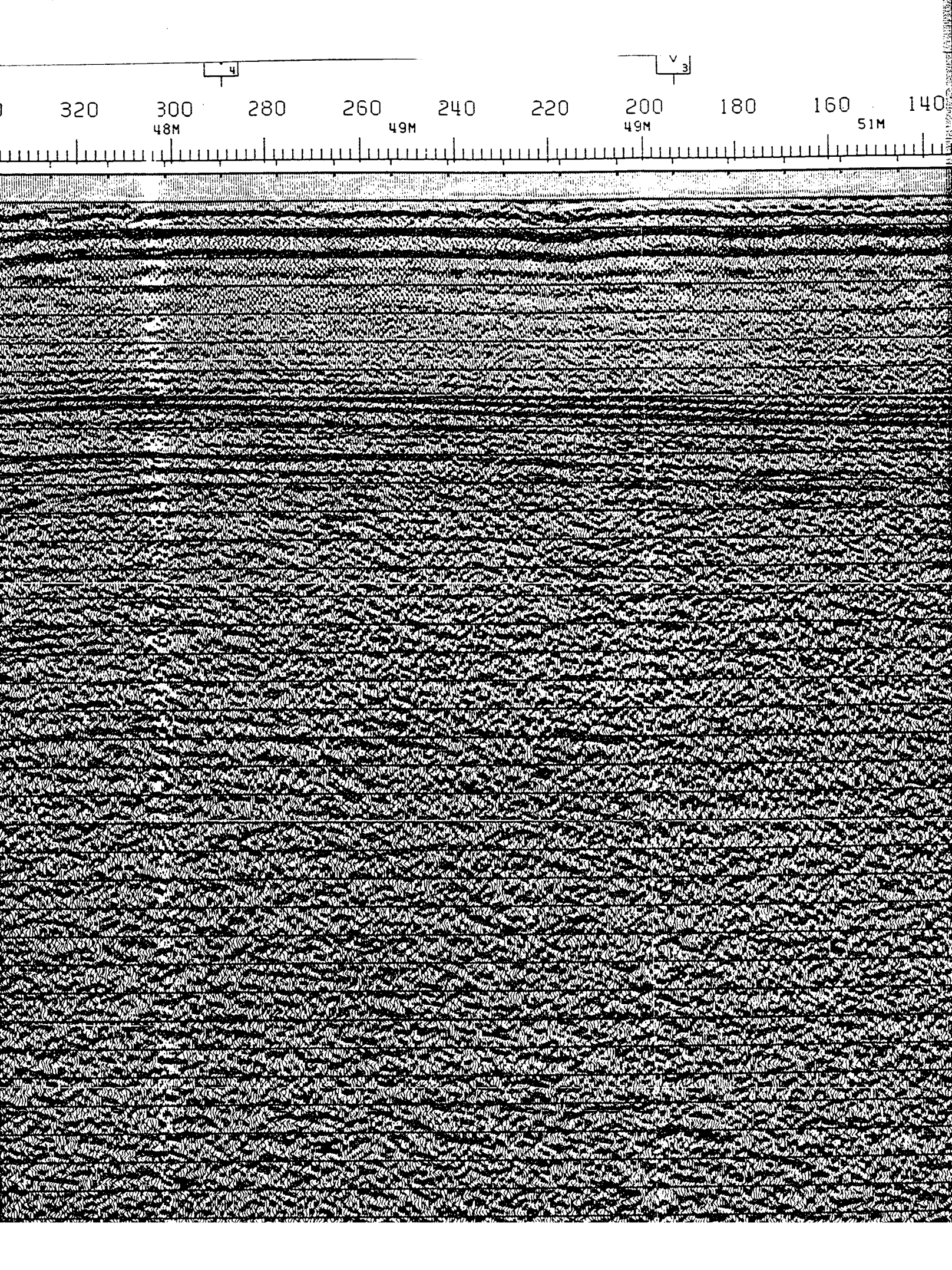
4
3
320
300
280
260
240
220
200
180
160
140
48M
49M
49M
51M

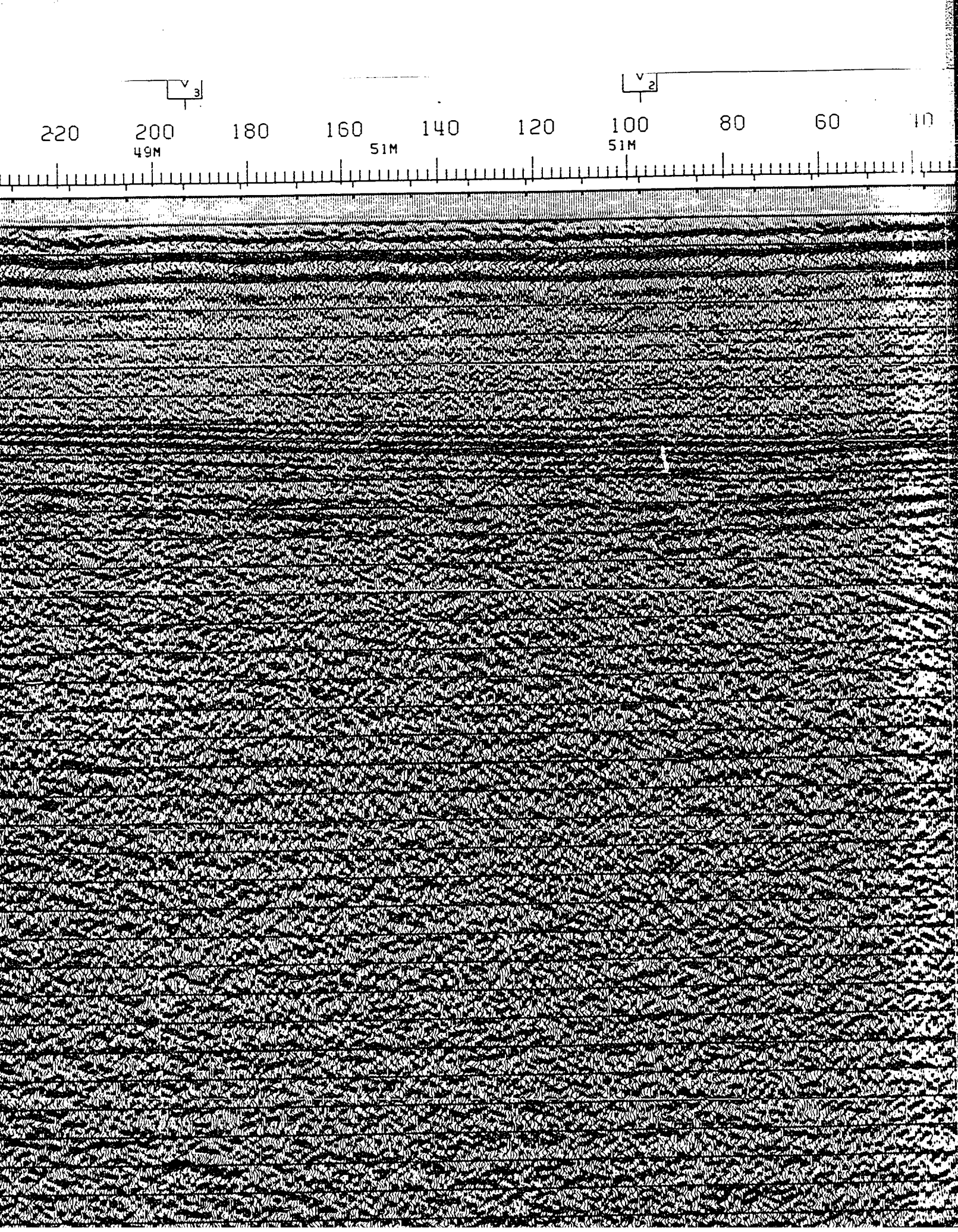
V3
V2
220
200
180
160
140
120
100
80
60
49M
51M
51M

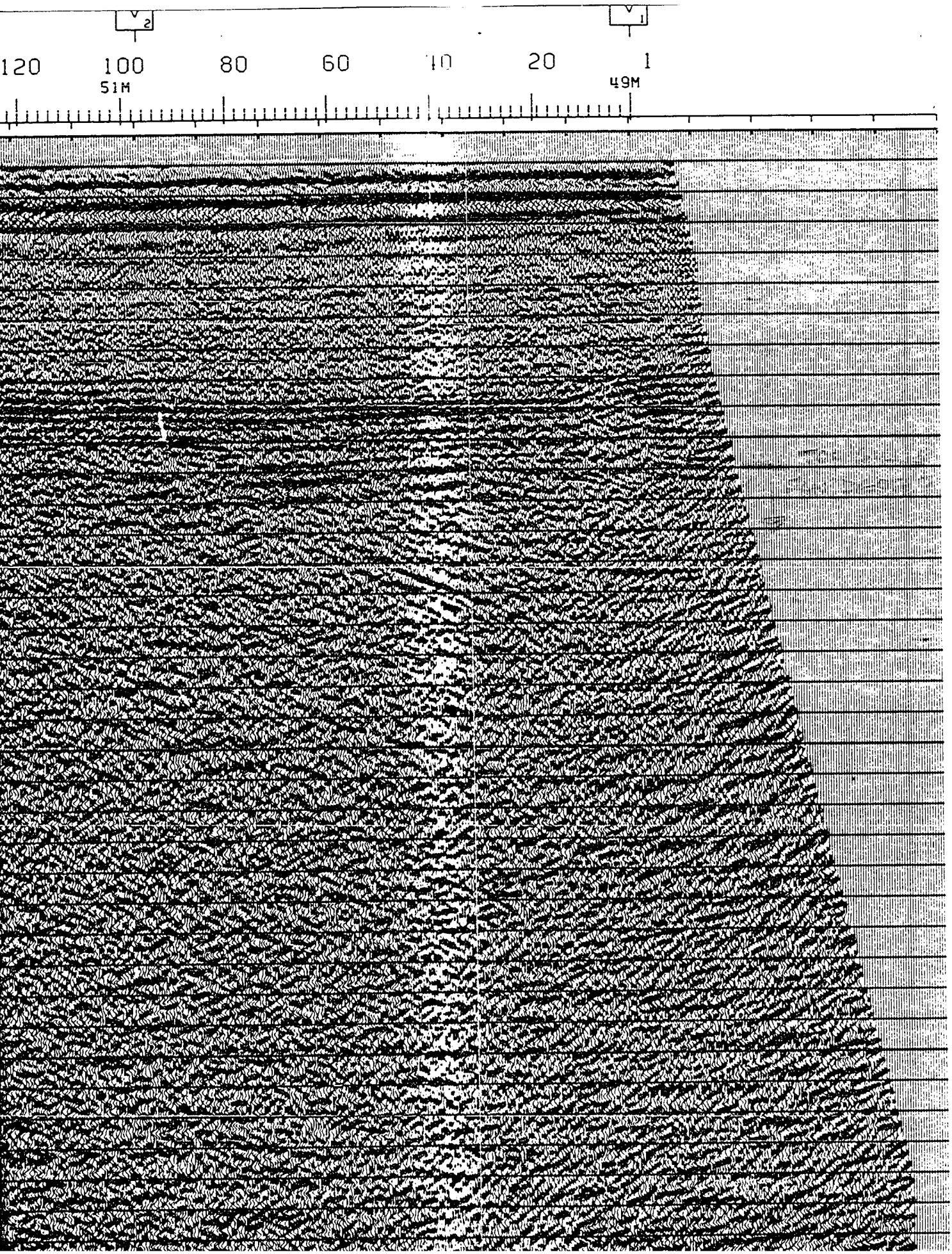
V2
V1
120
100
80
60
10
20
1
51M
49M
W.D.
0.0
0.1
0.2
0.3
0.4
0.5
0.6
0.7
0.8
0.9
1.0
1.1
1.2
1.3
1.4
1.5
1.6
1.7
1.8
1.9
2.0
2.1
2.2
2.3
2.4
2.5
2.6
2.7
2.8
2.9
3.0
3.1
3.2
3.3
3.4
3.5
3.6

1661 - 234 (1F-NW)

SOUTHWEST

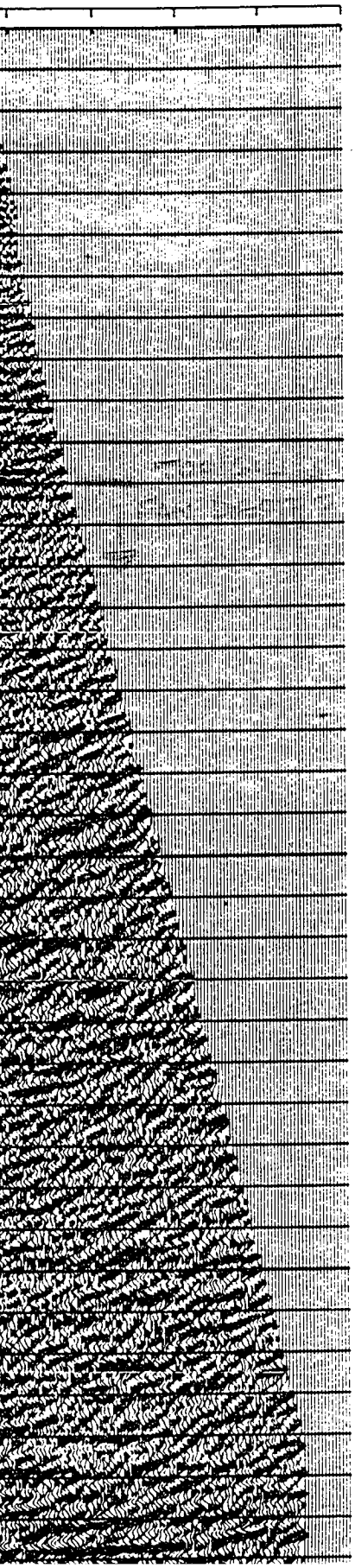

W.D.

0.0
0.1
0.2
0.3
0.4
0.5
0.6
0.7
0.8
0.9
1.0
1.1
1.2
1.3
1.4
1.5
1.6
1.7
1.8
1.9
2.0
2.1
2.2
2.3
2.4
2.5
2.6
2.7
2.8
2.9
3.0
3.1
3.2
3.3
3.4
3.5
3.6
3.7

CHEVRON STANDARD LTD.

AREA: NORTHUMBERLAND STRAIT

SHOT BY WESTERN GEOPHYSICAL COMPANY PARTY 127 JULY 1981
PROCESSED BY WESTERN GEOPHYSICAL (CALGARY) GROUP 6 OCT 1981

RECORDING DATA

SOURCE

ENERGY SOURCE	AIR GUNS
CHARGE SIZE	1050 CU.IN
NUMBER OF GUNS	15
GUN DEPTH	6 M
FIRING INTERVAL	27 M
SHOT POINT INTERVAL	27 M
DISTANCE OF SOURCE TO ANTENNA	47 M

INSTRUMENTS

SYSTEM	KILOSEIS
AMPLIFIER	INST. FLOATING POINT
FILTER	L/9-H/450
SAMPLING INTERVAL	1 MS
RECORD LENGTH	5.0 SEC
FORMAT	SEG-D

CABLE

TYPE CABLE	STREAMER
CABLE LENGTH	2565 M
CABLE DEPTH	8 M
LEAD IN	187 M
GROUP INTERVAL	27 M
NUMBER OF GROUPS RECORDED	96
SPREAD	2752 M

ARRAY PARAMETERS

ROMS	7/21
CHANNELS PER ARRAY	8.50% OVERLAP
WEIGHTS	32.32.32.32.32.32.32.32
NUMBER OF DATA CHANNELS RECORDED	384
CHANNEL INTERVAL	6.67 M

PROCESSING SEQUENCE AND PARAMETERS

PROCESSING SAMPLING INTERVAL 4 MS

1. SIGNATURE DECONVOLUTION
2. DECONVOLVED BEFORE STACK
   - WINDOW LENGTH 2 ZONES OF 2500 MS
   - LENGTH OPERATOR 280 MS
   - PREDICTION DISTANCE 4 MS
3. NMO STACK 4800 %
4. RELATIVE AMP. COMPENSATION
5. F-K DOMAIN FILTER
6. DECONVOLVED AFTER STACK
   - WINDOW LENGTH 2 ZONES OF 2500 MS
   - LENGTH OPERATOR 300 MS
   - PREDICTION DISTANCE 20 MS
7. FINITE DIFFERENCE MIGRATION
8. TIME VARIANT FILTER

TIME		L.C. (HZ)	H.C.
1.00	SEC	12	60
3.00	SEC	8	45
5.00	SEC	8	30

9. RMS GAIN (128-512 MS WINDOW)

1661 - 2334 (1F-NIN)

SOUTHWEST

16

RON STANDARD LTD.

AREA: NORTHUMBERLAND STRAIT

GEOPHYSICAL COMPANY	PARTY 127	JULY 1981
STERN GEOPHYSICAL (CALGARY)	GROUP 6	OCT 1981

RECORDING DATA

SOURCE	
	AIR GUNS
	1050 CU.IN
	15
	6 M
	27 M
RVAL	27 M
RCE TO ANTENNA	47 M
INSTRUMENTS	
	KILOSEIS
	INST. FLOATING POINT
	L/9-H/450
AL	1 MS
	5.0 SEC
	SEG-D
CABLE	
	STREAMER
	2565 M
	8 M
	187 M
	27 M
S RECORDED	96
	2752 M
ARRAY PARAMETERS	
	7/21
RAY	8.50% OVERLAP
	32.32.32.32.32.32.32.32
CHANNELS RECORDED	384
L	6.67 M

OCESSING SEQUENCE AND PARAMETERS

ROCESSING SAMPLING INTERVAL 4 MS
IGNATURE DECONVOLUTION
ECONVOLVED BEFORE STACK
INDOW LENGTH 2 ZONES OF 2500 MS
ENGTH OPERATOR 280 MS
REDICTION DISTANCE 4 MS
O STACK 4800 %
ELATIVE AMP. COMPENSATION
-K DOMAIN FILTER
ECONVOLVED AFTER STACK
INDOW LENGTH 2 ZONES OF 2500 MS
ENGTH OPERATOR 300 MS
REDICTION DISTANCE 20 MS
INITE DIFFERENCE MIGRATION
IME VARIANT FILTER

TIME		L.C. (HZ)	H.C.
1.00	SEC	12	60
3.00	SEC	8	45
5.00	SEC	8	30

NO: 8824 C4 9E LINE NO: 81

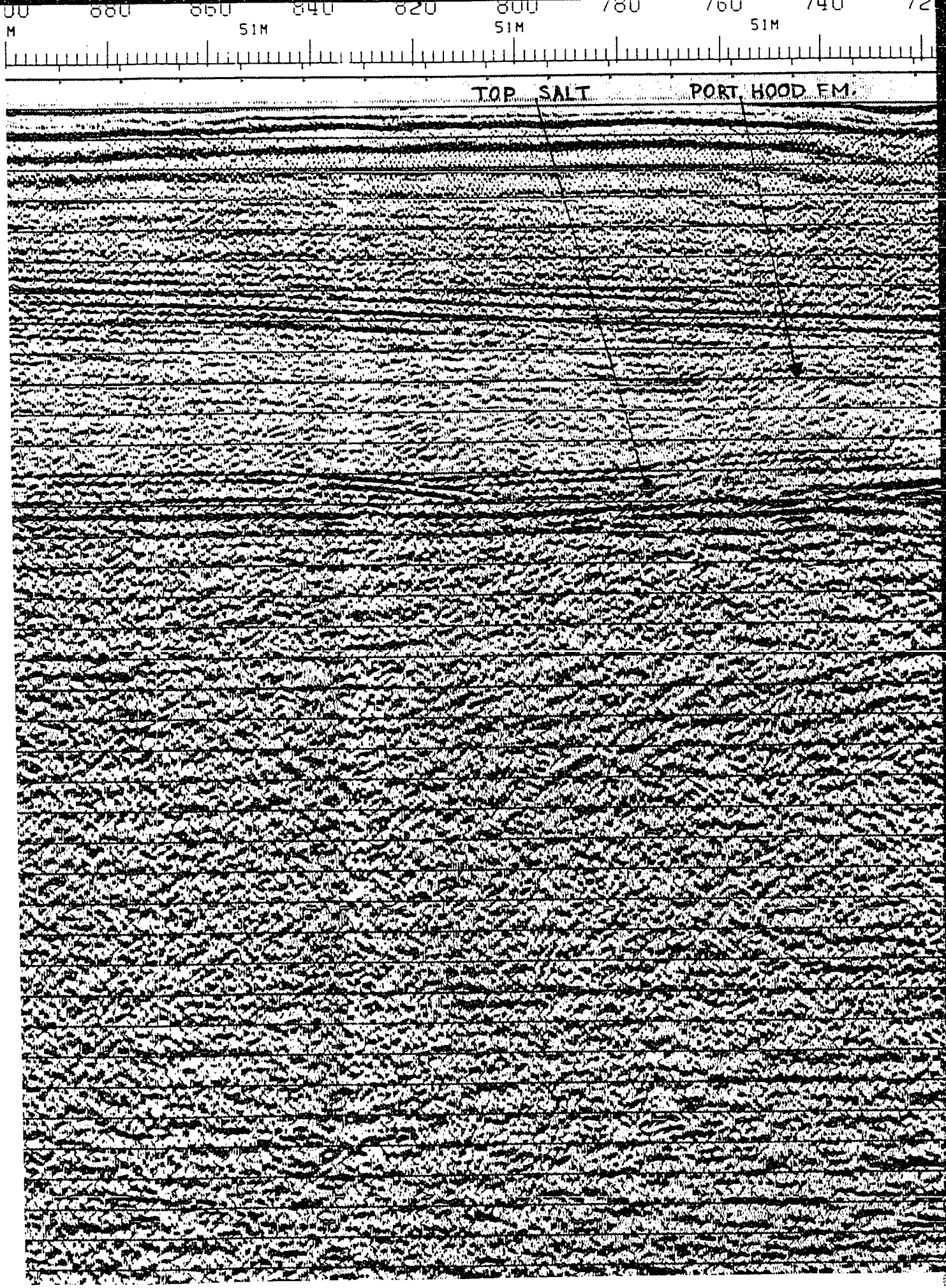
00 880 860 840 820 800 780 760 740 72
M
5IM
5IM
5IM
TOP SALT
PORT HOOD FM.


51M
51M
51M
51M
PORT HOOD FM.
DOWNLAP REFLECTORS
INVERNESS FM.

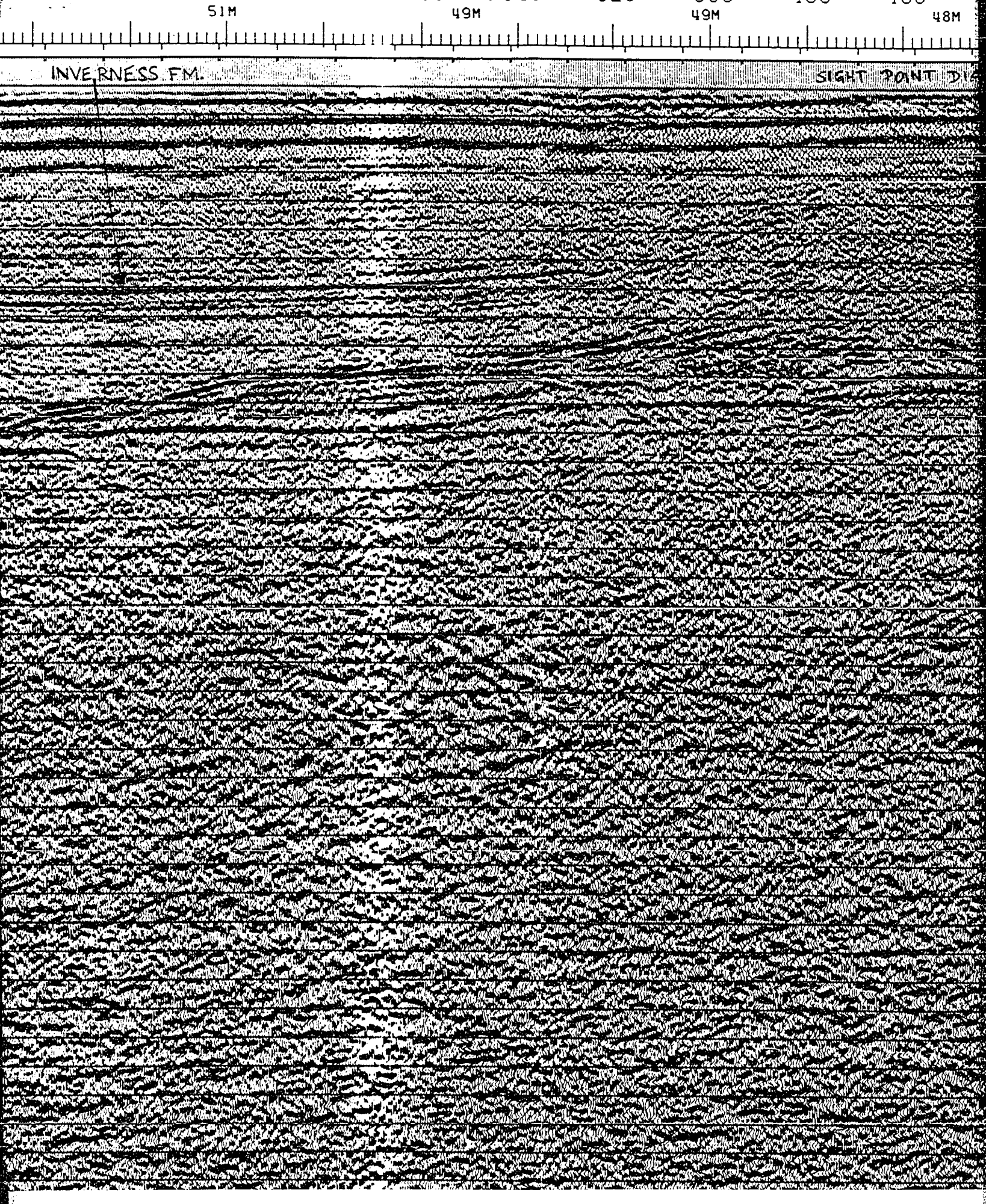
51M
49M
49M
48M
INVERNESS FM.
SIGHT POINT DI

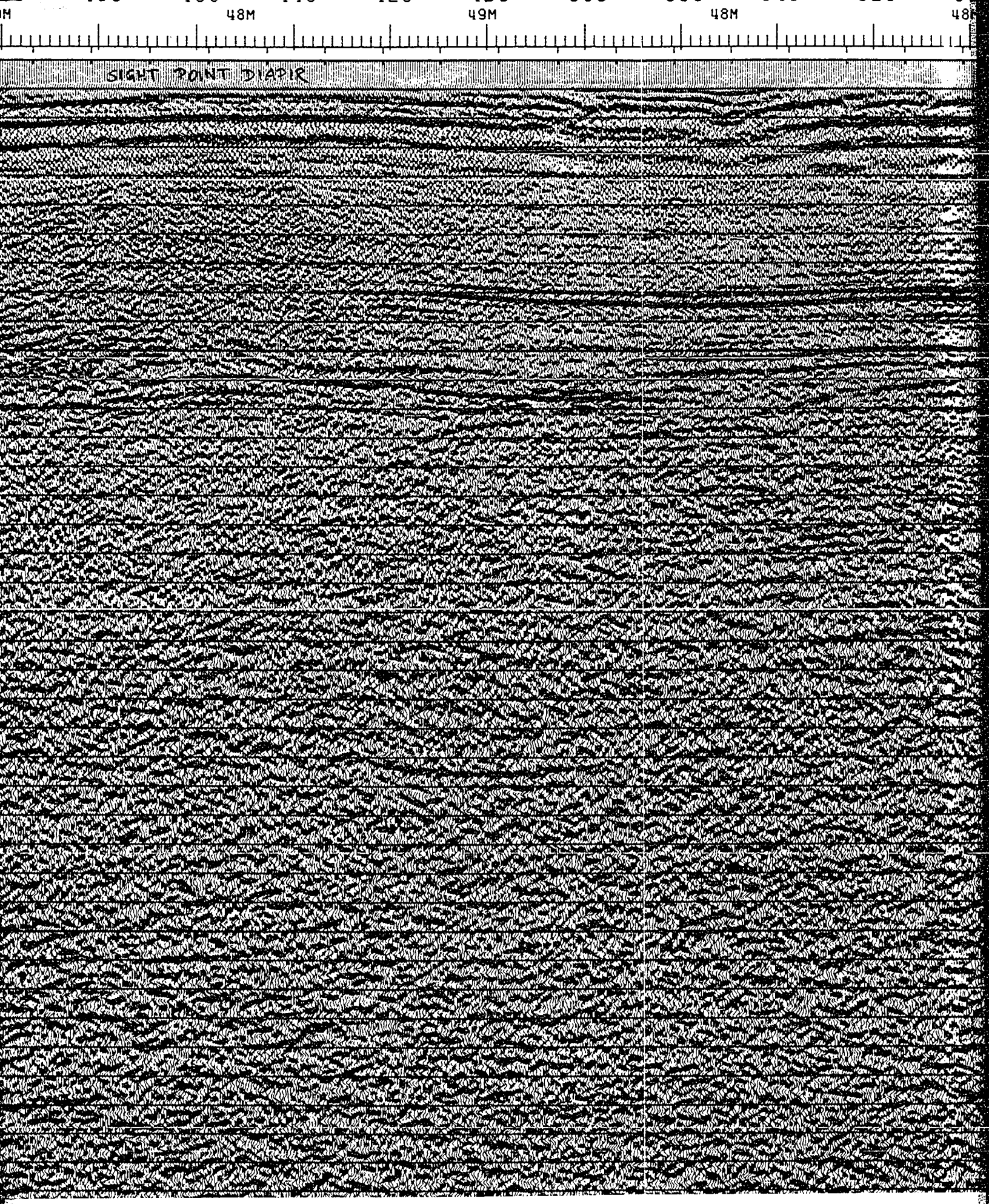
48M
49M
48M
SIGHT POINT DIAPIR

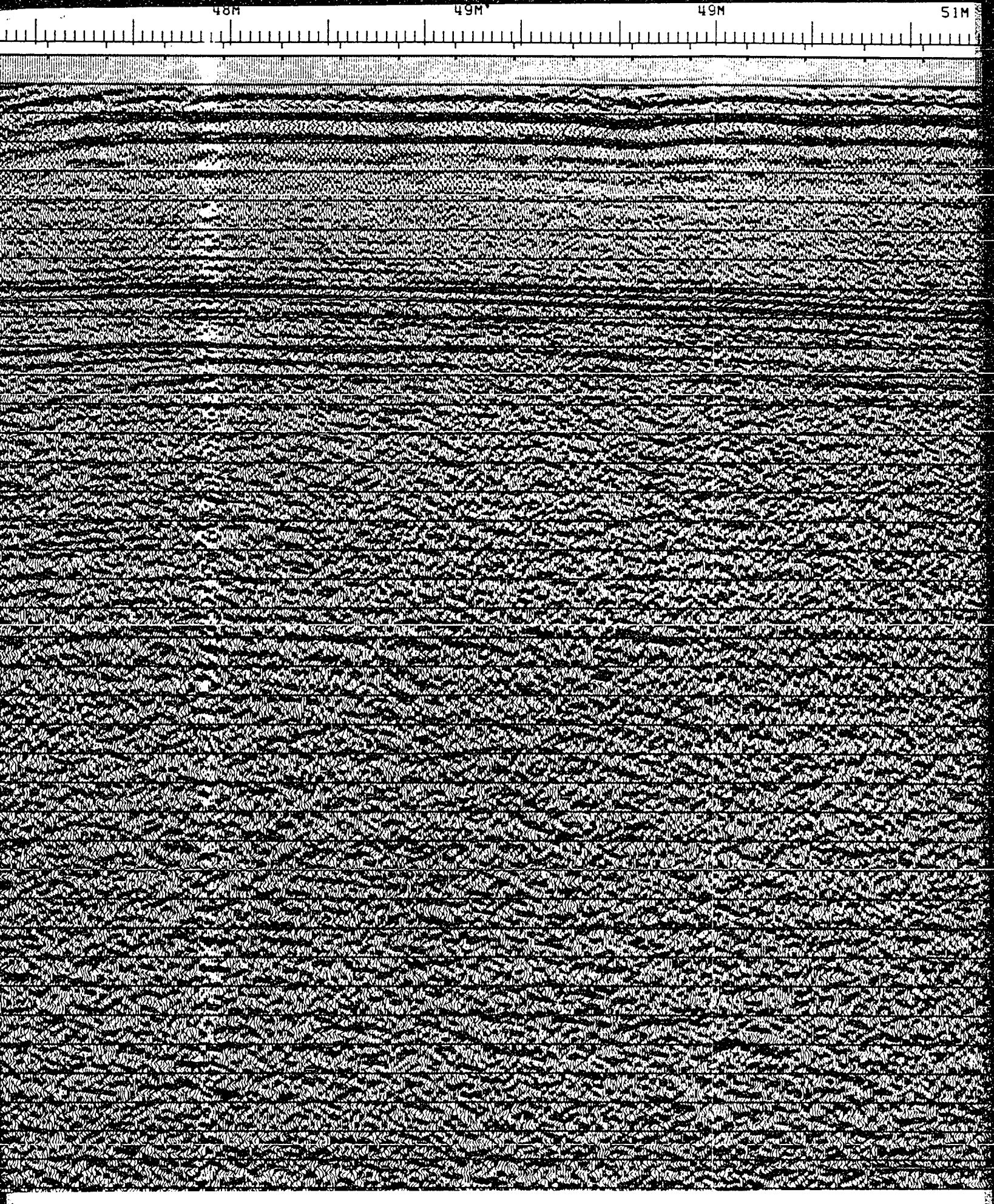
48M
49M
49M
51M

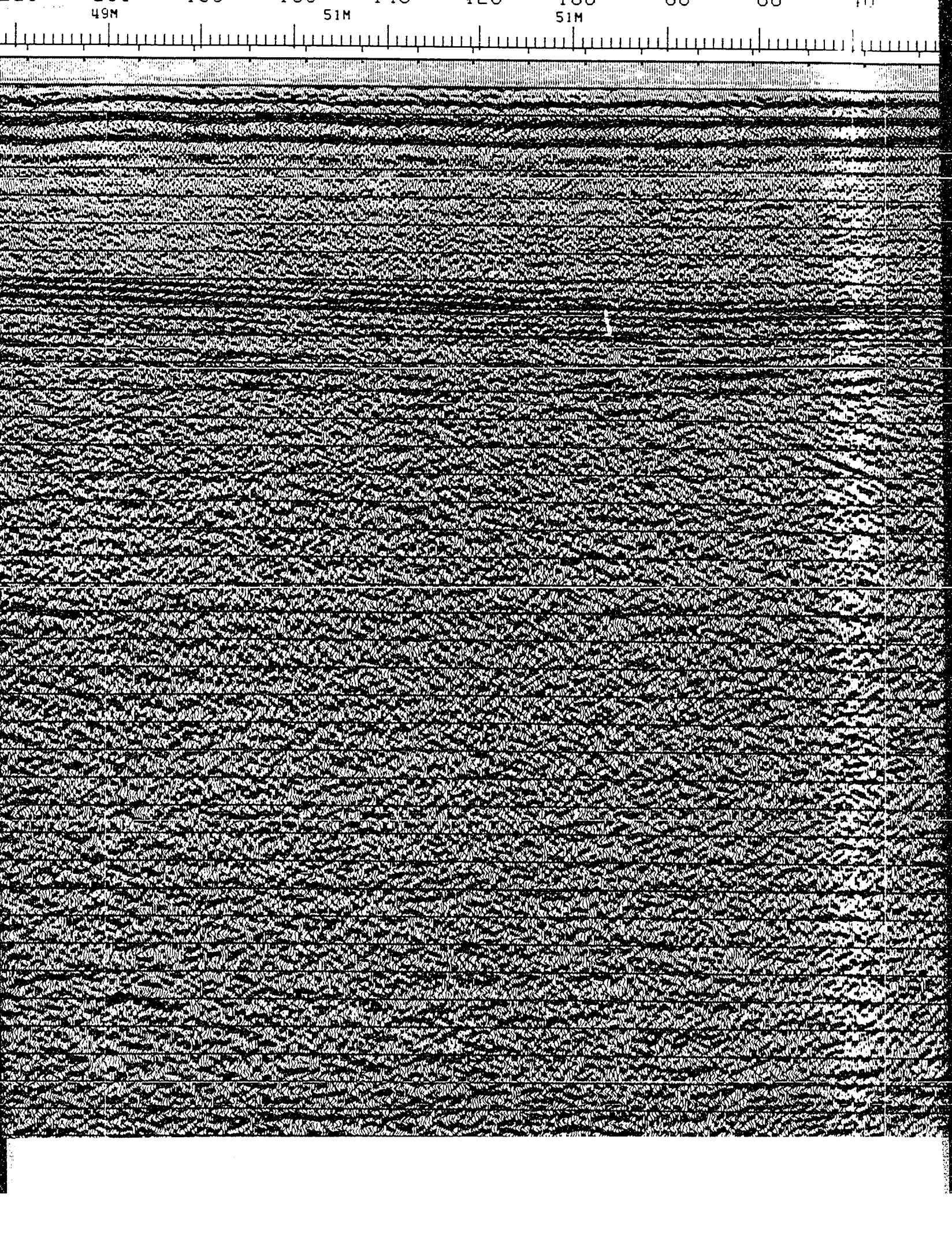
49M
51M
51M

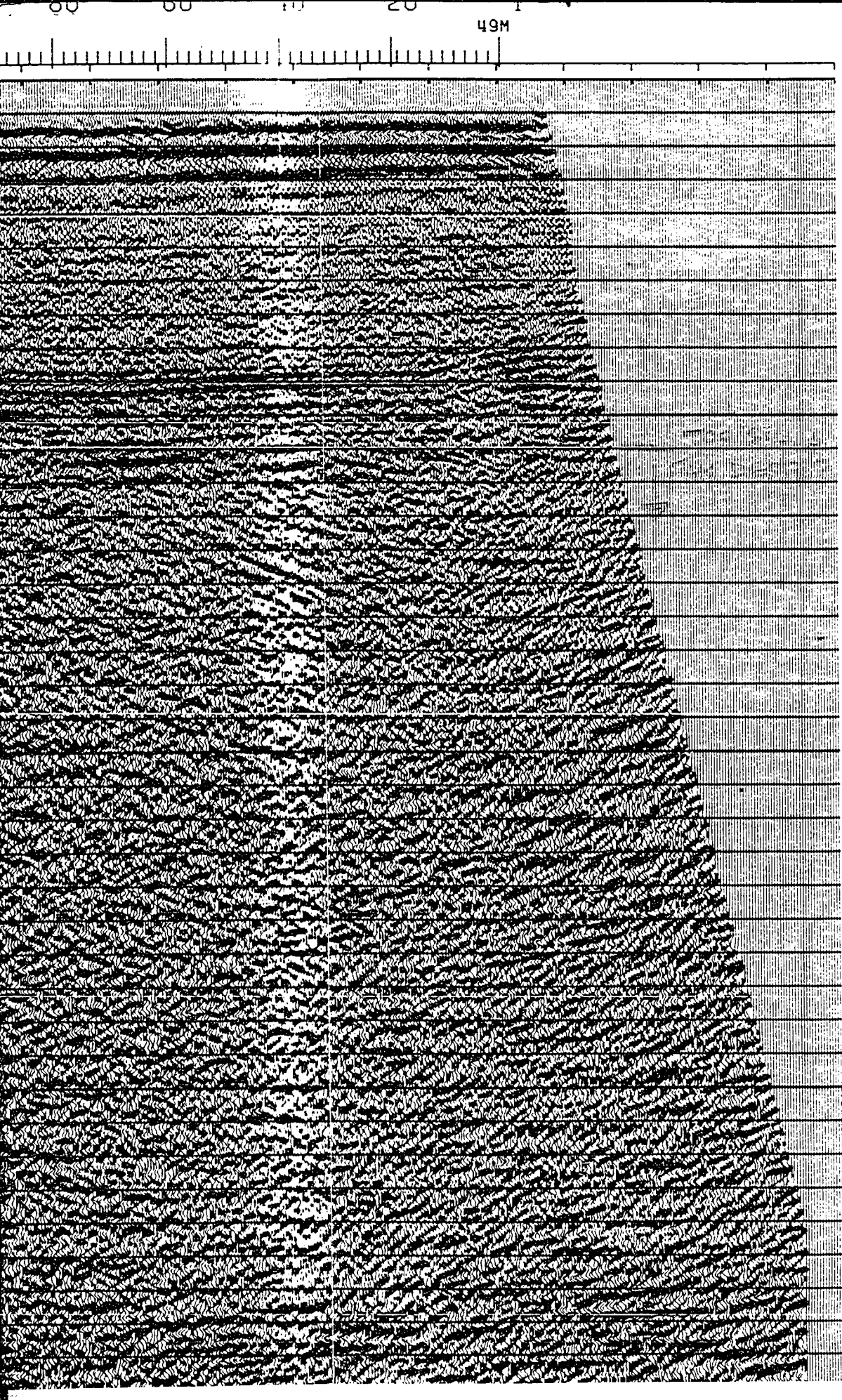

CHEV

SHOT BY WESTERN
PROCESSED BY WES

ENERGY SOURCE
CHARGE SIZE
NUMBER OF GUNS
GUN DEPTH
FIRING INTERVAL
SHOT POINT INTER
DISTANCE OF SOUR

SYSTEM
AMPLIFIER
FILTER
SAMPLING INTERVA
RECORD LENGTH
FORMAT

TYPE CABLE
CABLE LENGTH
CABLE DEPTH
LEAD IN
GROUP INTERVAL
NUMBER OF GROUPS
SPREAD

ROMS
CHANNELS PER ARR
WEIGHTS
NUMBER OF DATA C
CHANNEL INTERVAL

PROC

PRO
1. SIG
2. DEC
WI
LE
PR
3. NMO
4. REL
5. F-K
6. DEC
WI
LE
PR
7. FIN
8. TIM
9. RMS

47 M

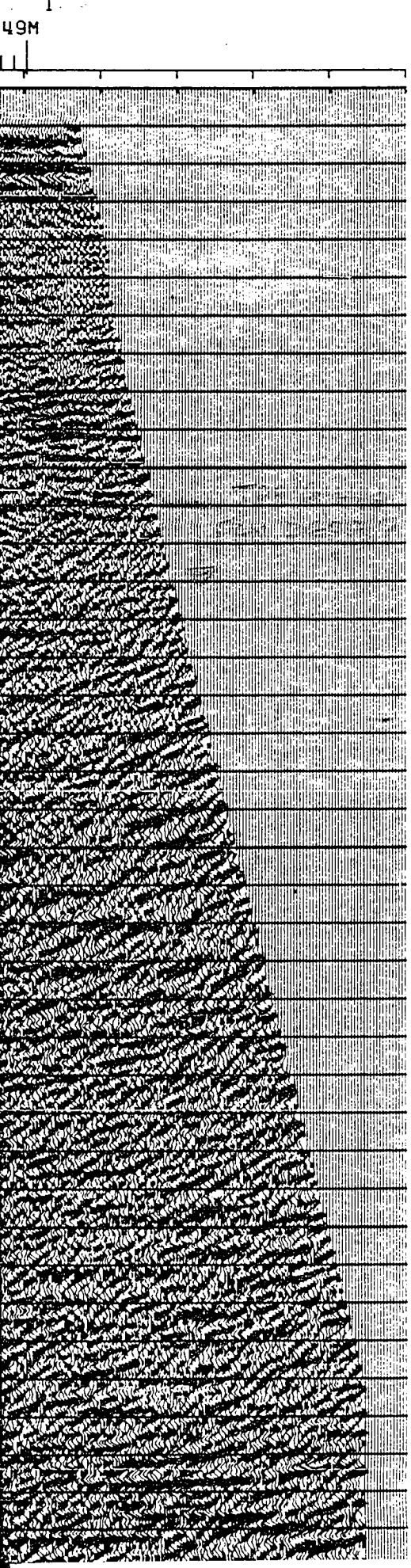

CHEVRON STANDARD LTD.

AREA: NORTHUMBERLAND STRAIT

SHOT BY WESTERN GEOPHYSICAL COMPANY PARTY 127 JULY 198
PROCESSED BY WESTERN GEOPHYSICAL (CALGARY) GROUP 6 OCT 1981

RECORDING DATA

SOURCE

ENERGY SOURCE	AIR GUNS
CHARGE SIZE	1050 CU.IN
NUMBER OF GUNS	15
GUN DEPTH	6 M
FIRING INTERVAL	27 M
SHOT POINT INTERVAL	27 M
DISTANCE OF SOURCE TO ANTENNA	47 M

INSTRUMENTS

SYSTEM	KILOSEIS
AMPLIFIER	INST. FLOATING POINT
FILTER	L/9-H/450
SAMPLING INTERVAL	1 MS
RECORD LENGTH	5.0 SEC
FORMAT	SEG-D

CABLE

TYPE CABLE	STREAMER
CABLE LENGTH	2565 M
CABLE DEPTH	8 M
LEAD IN	187 M
GROUP INTERVAL	27 M
NUMBER OF GROUPS RECORDED	96
SPREAD	2752 M

ARRAY PARAMETERS

ROMS	7/21
CHANNELS PER ARRAY	8.50% OVERLAP
WEIGHTS	32.32.32.32.32.32.32.32
NUMBER OF DATA CHANNELS RECORDED	384
CHANNEL INTERVAL	6.67 M

PROCESSING SEQUENCE AND PARAMETERS

PROCESSING SAMPLING INTERVAL 4 MS

1. SIGNATURE DECONVOLUTION
2. DECONVOLVED BEFORE STACK
   - WINDOW LENGTH 2 ZONES OF 2500 MS
   - LENGTH OPERATOR 280 MS
   - PREDICTION DISTANCE 4 MS
3. NMO STACK 4800 %
4. RELATIVE AMP. COMPENSATION
5. F-K DOMAIN FILTER
6. DECONVOLVED AFTER STACK
   - WINDOW LENGTH 2 ZONES OF 2500 MS
   - LENGTH OPERATOR 300 MS
   - PREDICTION DISTANCE 20 MS
7. FINITE DIFFERENCE MIGRATION
8. TIME VARIANT FILTER

TIME		L.C. (HZ)	H.C.
1.00	SEC	12	60
3.00	SEC	8	45
5.00	SEC	8	30

9. RMS GAIN (128-512 MS WINDOW)

47 M

LEGEND

W.D.

16

CHEVRON STANDARD LTD.

AREA: NORTHUMBERLAND STRAIT

SHOT BY WESTERN GEOPHYSICAL COMPANY PARTY 127 JULY 1981
PROCESSED BY WESTERN GEOPHYSICAL (CALGARY) GROUP 6 OCT 1981

RECORDING DATA

SOURCE

ENERGY SOURCE	AIR GUNS
CHARGE SIZE	1050 CU.IN
NUMBER OF GUNS	15
GUN DEPTH	6 M
FIRING INTERVAL	27 M
SHOT POINT INTERVAL	27 M
DISTANCE OF SOURCE TO ANTENNA	47 M

INSTRUMENTS

SYSTEM	KILOSEIS
AMPLIFIER	INST. FLOATING POINT
FILTER	L/9-H/450
SAMPLING INTERVAL	1 MS
RECORD LENGTH	5.0 SEC
FORMAT	SEG-D

CABLE

TYPE CABLE	STREAMER
CABLE LENGTH	2565 M
CABLE DEPTH	8 M
LEAD IN	187 M
GROUP INTERVAL	27 M
NUMBER OF GROUPS RECORDED	96
SPREAD	2752 M

ARRAY PARAMETERS

ROMS	7/21
CHANNELS PER ARRAY	8.50% OVERLAP
WEIGHTS	32.32.32.32.32.32.32.32
NUMBER OF DATA CHANNELS RECORDED	384
CHANNEL INTERVAL	6.67 M

PROCESSING SEQUENCE AND PARAMETERS

PROCESSING SAMPLING INTERVAL 4 MS

1. SIGNATURE DECONVOLUTION
2. DECONVOLVED BEFORE STACK
   - WINDOW LENGTH 2 ZONES OF 2500 MS
   - LENGTH OPERATOR 280 MS
   - PREDICTION DISTANCE 4 MS
3. NMO STACK 4800 %
4. RELATIVE AMP. COMPENSATION
5. F-K DOMAIN FILTER
6. DECONVOLVED AFTER STACK
   - WINDOW LENGTH 2 ZONES OF 2500 MS
   - LENGTH OPERATOR 300 MS
   - PREDICTION DISTANCE 20 MS
7. FINITE DIFFERENCE MIGRATION
8. TIME VARIANT FILTER

TIME		L.C. (HZ)	H.C.
1.00	SEC	12	60
3.00	SEC	8	45
5.00	SEC	8	30

9. RMS GAIN (128-512 MS WINDOW)

47 M

LEGEND

SOUTHWEST

16

ON STANDARD LTD.

SEA: NORTHUMBERLAND STRAIT

EOPHYSICAL COMPANY PARTY 127 JULY 1981
ERN GEOPHYSICAL (CALGARY) GROUP 6 OCT 1981

RECORDING DATA

SOURCE

	AIR GUNS
	1050 CU.IN
	15
	6 M
	27 M
AL	27 M
E TO ANTENNA	47 M

INSTRUMENTS

	KILOSEIS
	INST. FLOATING POINT
	L/9-H/450
	1 MS
	5.0 SEC
	SEG-D

CABLE

	STREAMER
	2565 M
	8 M
	187 M
	27 M
RECORDED	96
	2752 M

ARRAY PARAMETERS

	7/21
	8.50% OVERLAP
	32.32.32.32.32.32.32.32
ANNELS RECORDED	384
	6.67 M

SSING SEQUENCE AND PARAMETERS

ESSING SAMPLING INTERVAL 4 MS
ATURE DECONVOLUTION
NVOLVED BEFORE STACK
OW LENGTH 2 ZONES OF 2500 MS
TH OPERATOR 280 MS
ICTION DISTANCE 4 MS
STACK 4800 %
TIVE AMP. COMPENSATION
DOMAIN FILTER
NVOLVED AFTER STACK
OW LENGTH 2 ZONES OF 2500 MS
TH OPERATOR 300 MS
ICTION DISTANCE 20 MS
TE DIFFERENCE MIGRATION
VARIANT FILTER

TIME	L.C. (HZ)	H.C.
00 SEC	12	60
00 SEC	8	45
00 SEC	8	30

GAIN (128-512 MS WINDOW)

LEGEND

NO: 8824 C4 9E LINE NO: 81-1

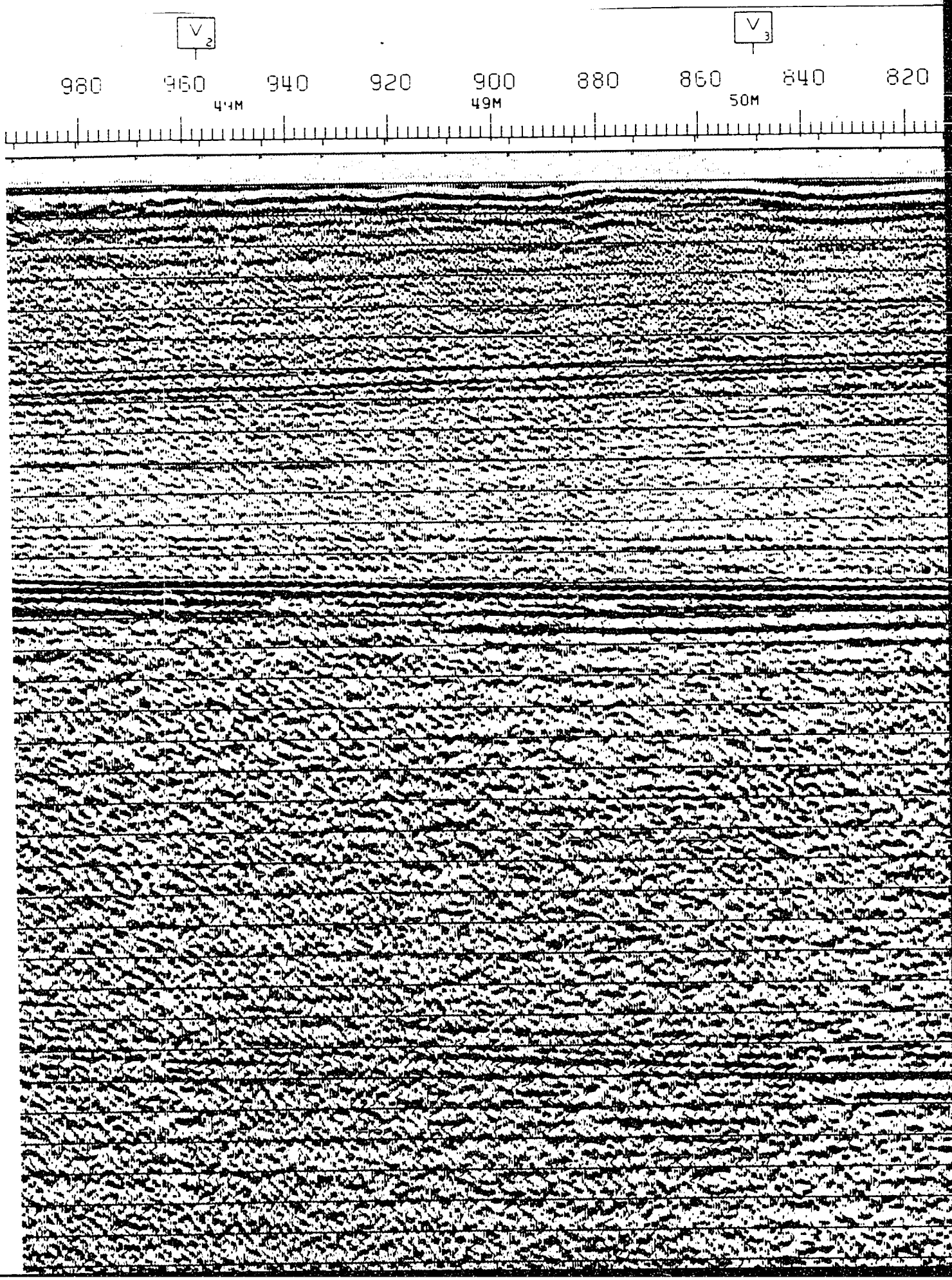
V2
V3
980
960
940
920
900
880
860
840
820
44M
49M
50M

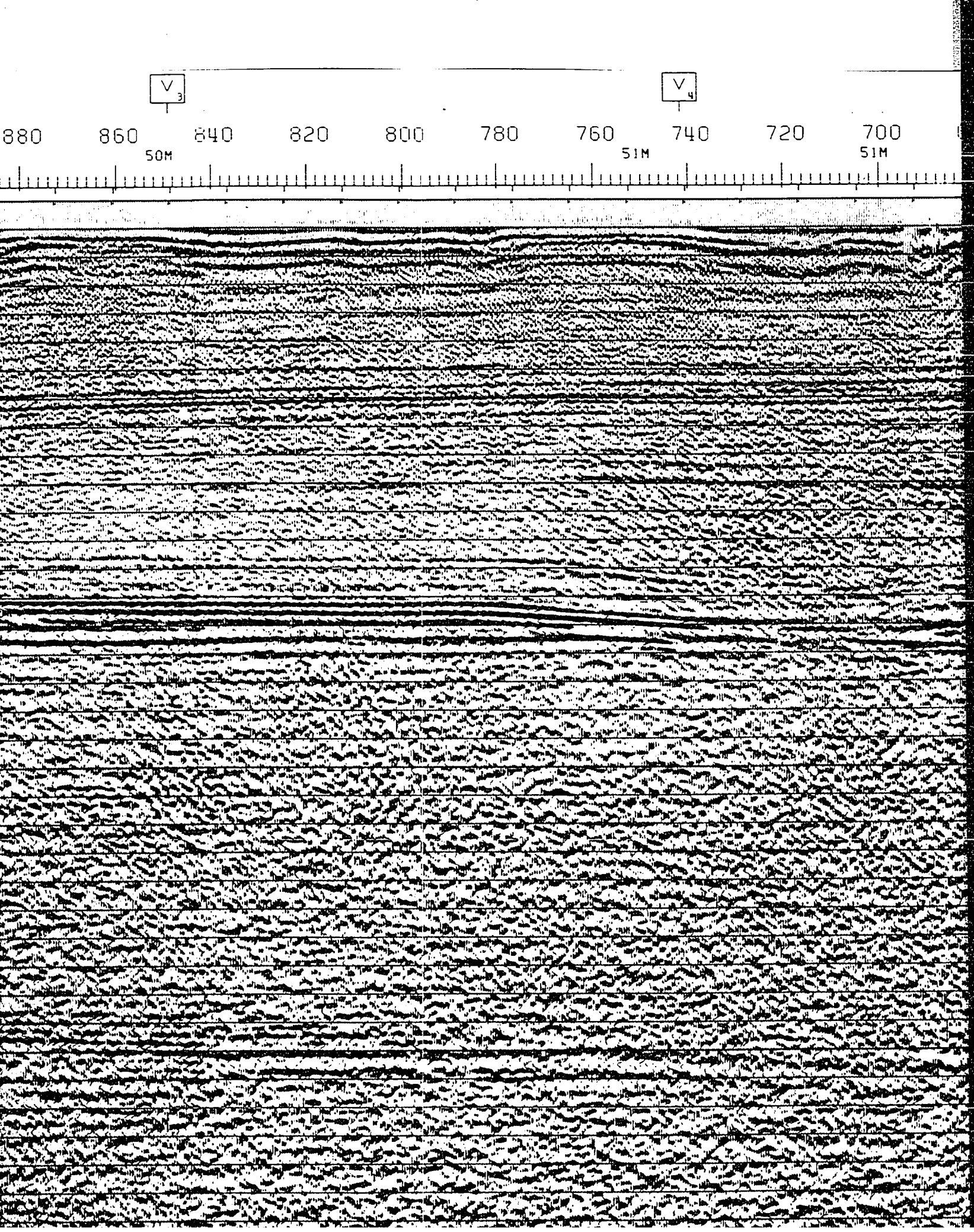
V3
V4
880
860
840
820
800
780
760
740
720
700
50M
51M
51M

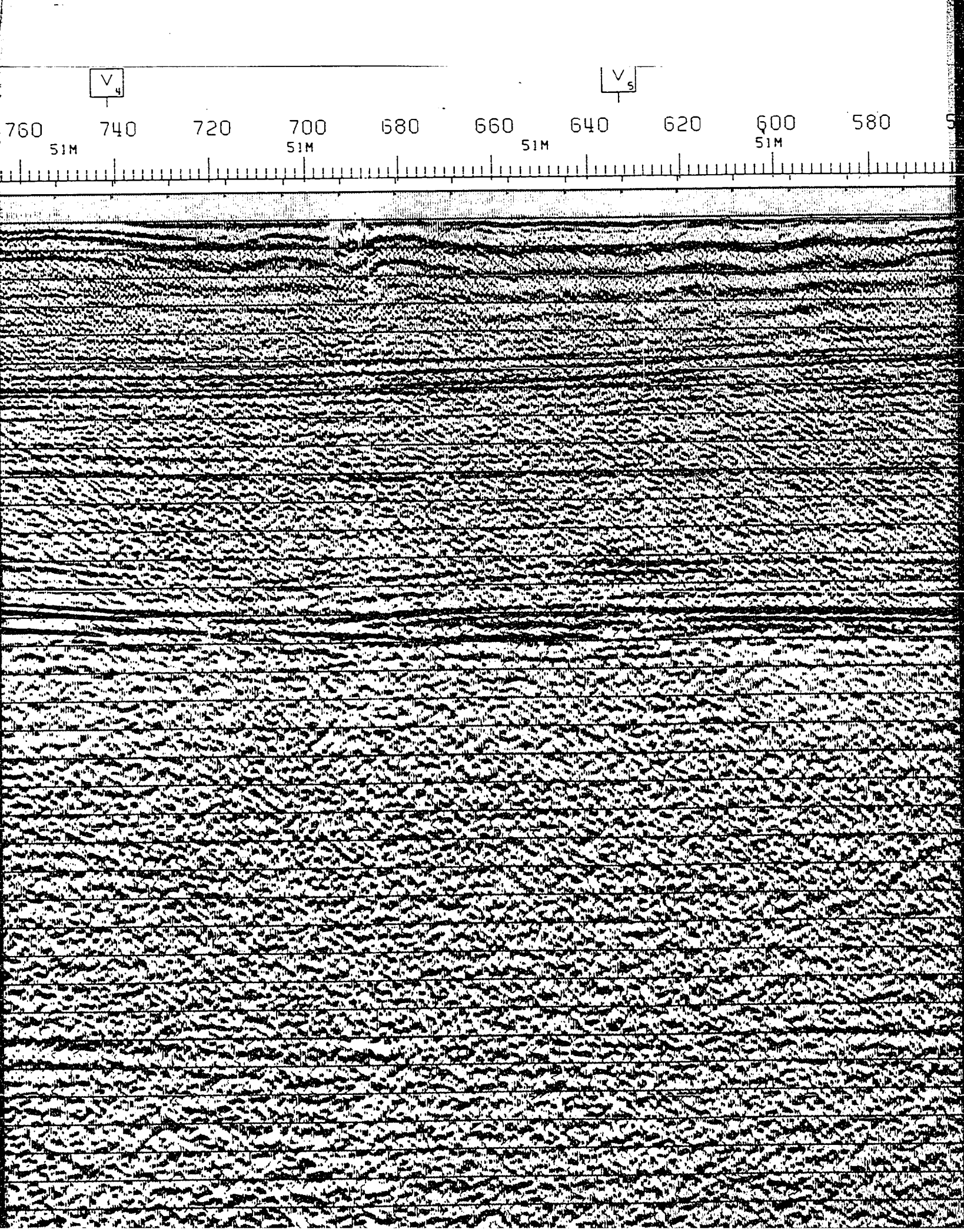
V4
V5
760
740
720
700
680
660
640
620
600
580
51M
51M
51M
51M

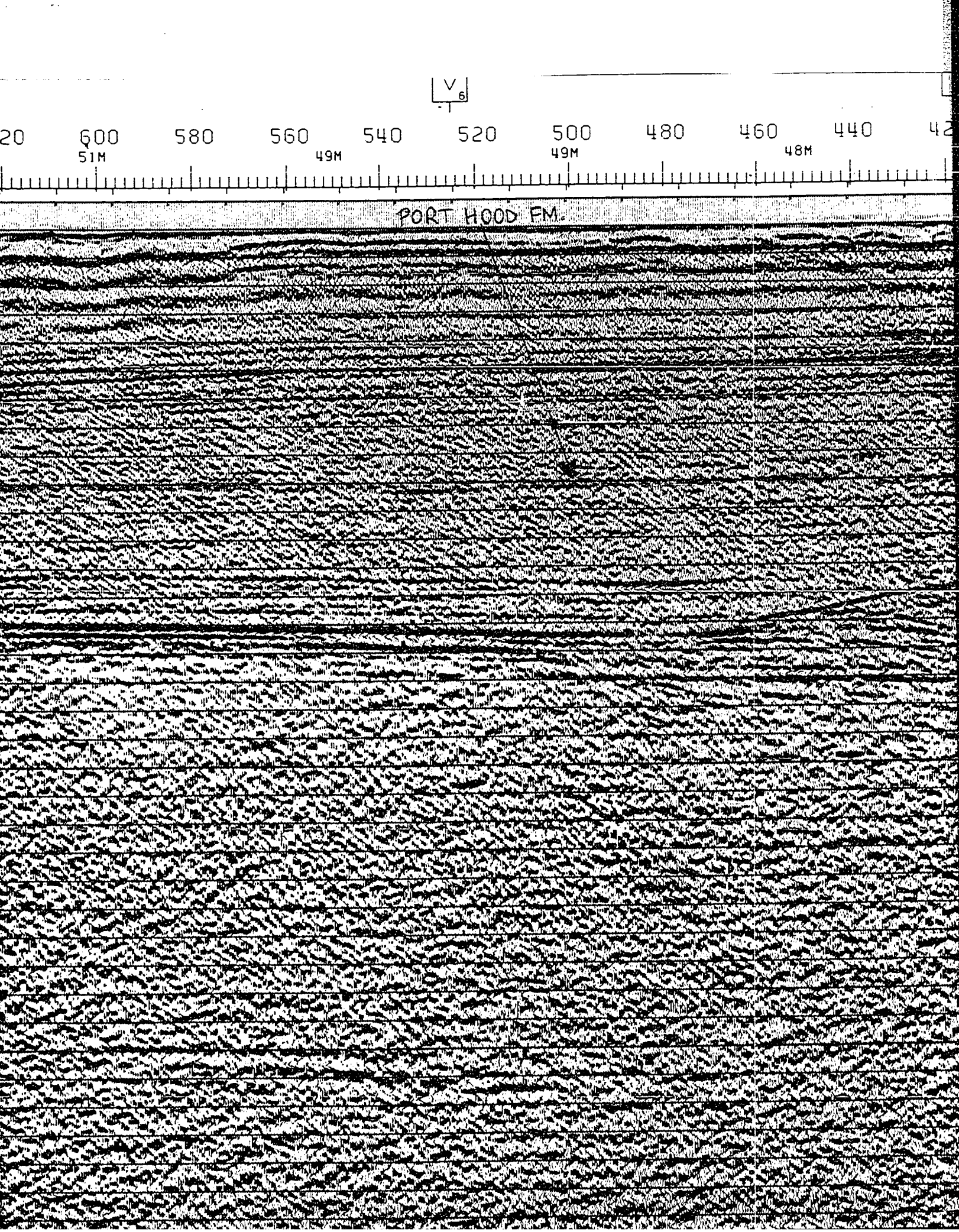
V6
620
600
580
560
540
520
500
480
460
440
51M
49M
49M
48M
PORT HOOD FM.

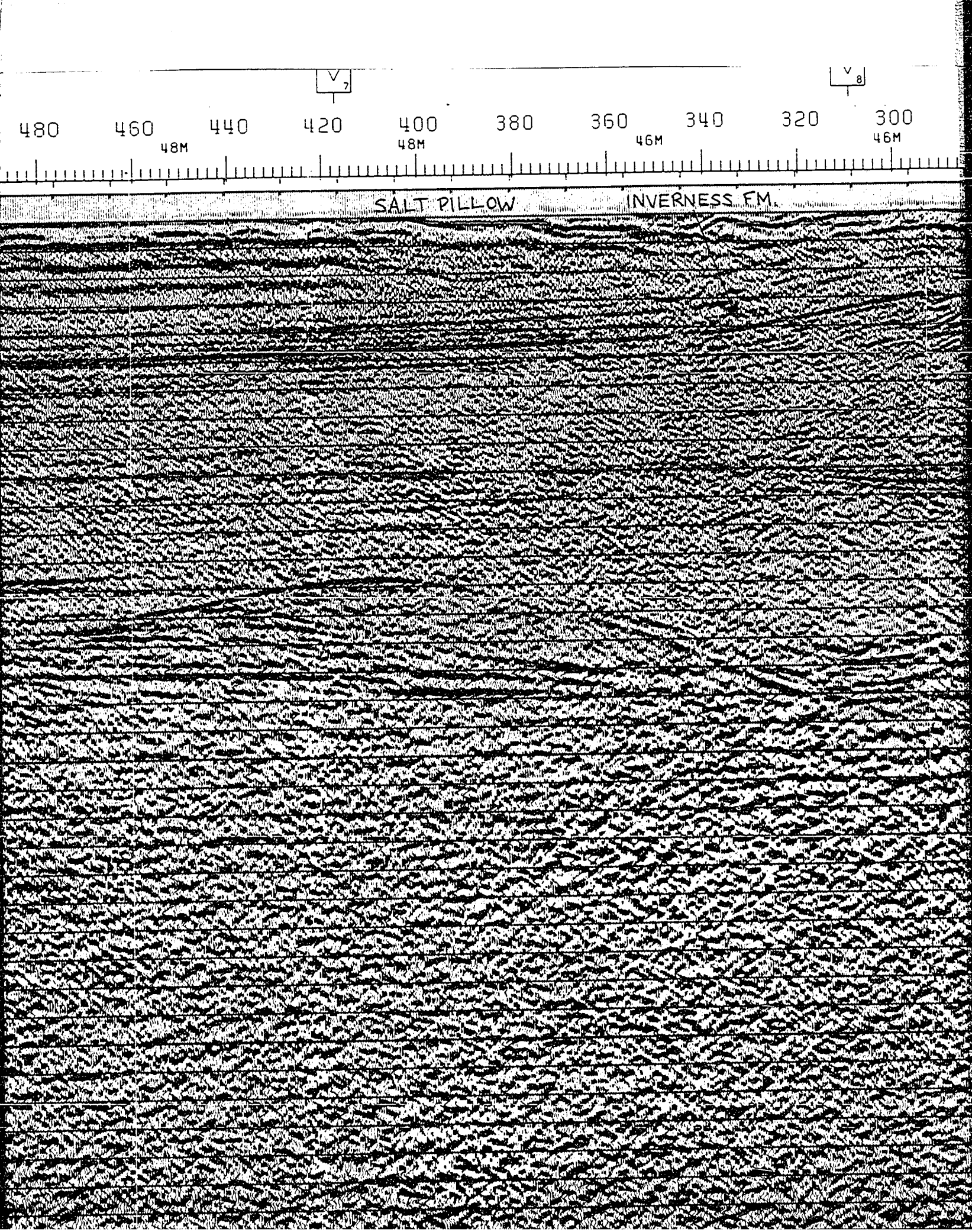
V7
V8
480
460
48M
440
420
400
48M
380
360
46M
340
320
300
46M
SALT PILLOW
INVERNESS FM.

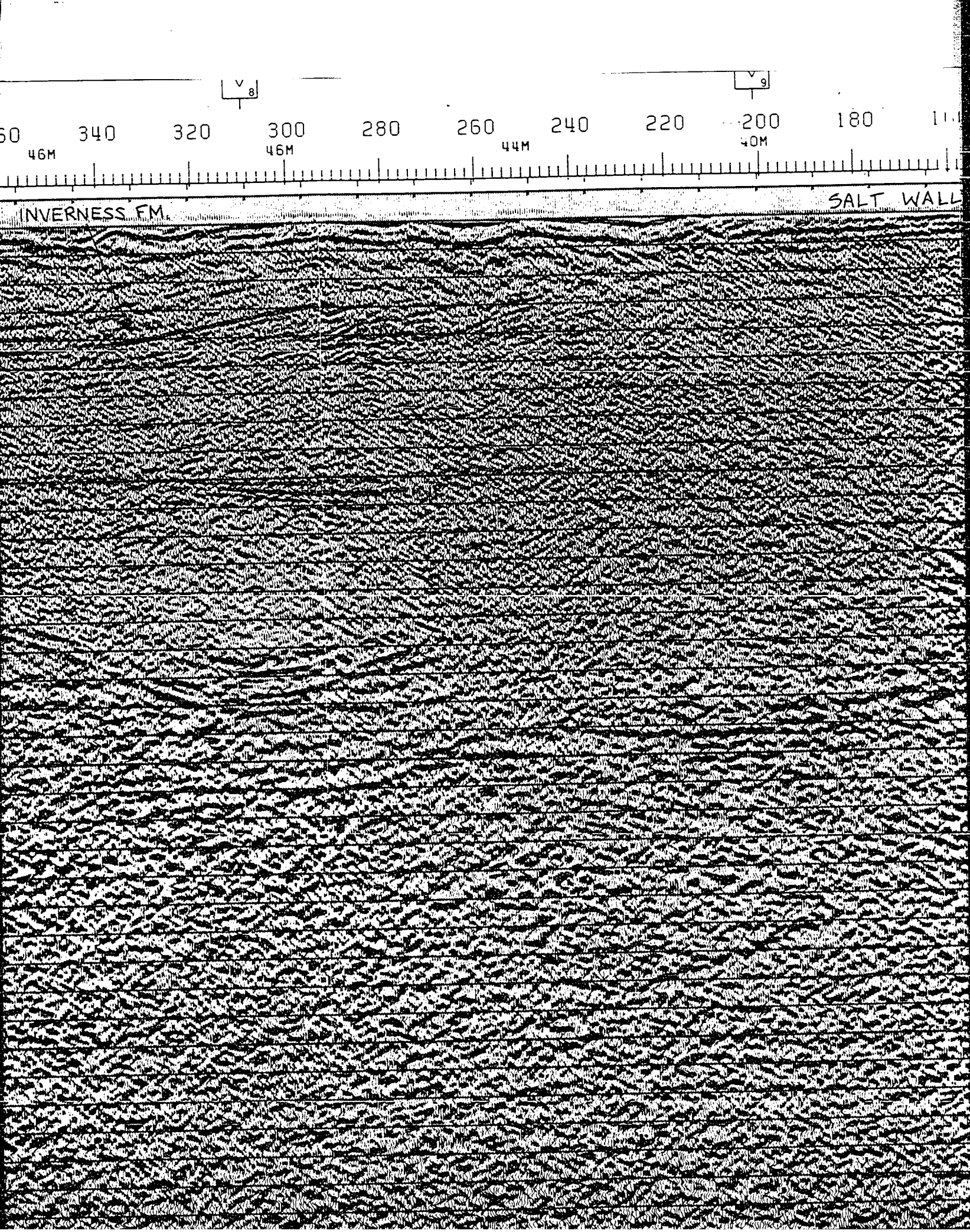
V8
V9
60
340
320
300
280
260
240
220
200
180
46M
46M
44M
40M
INVERNESS FM.
SALT WALL

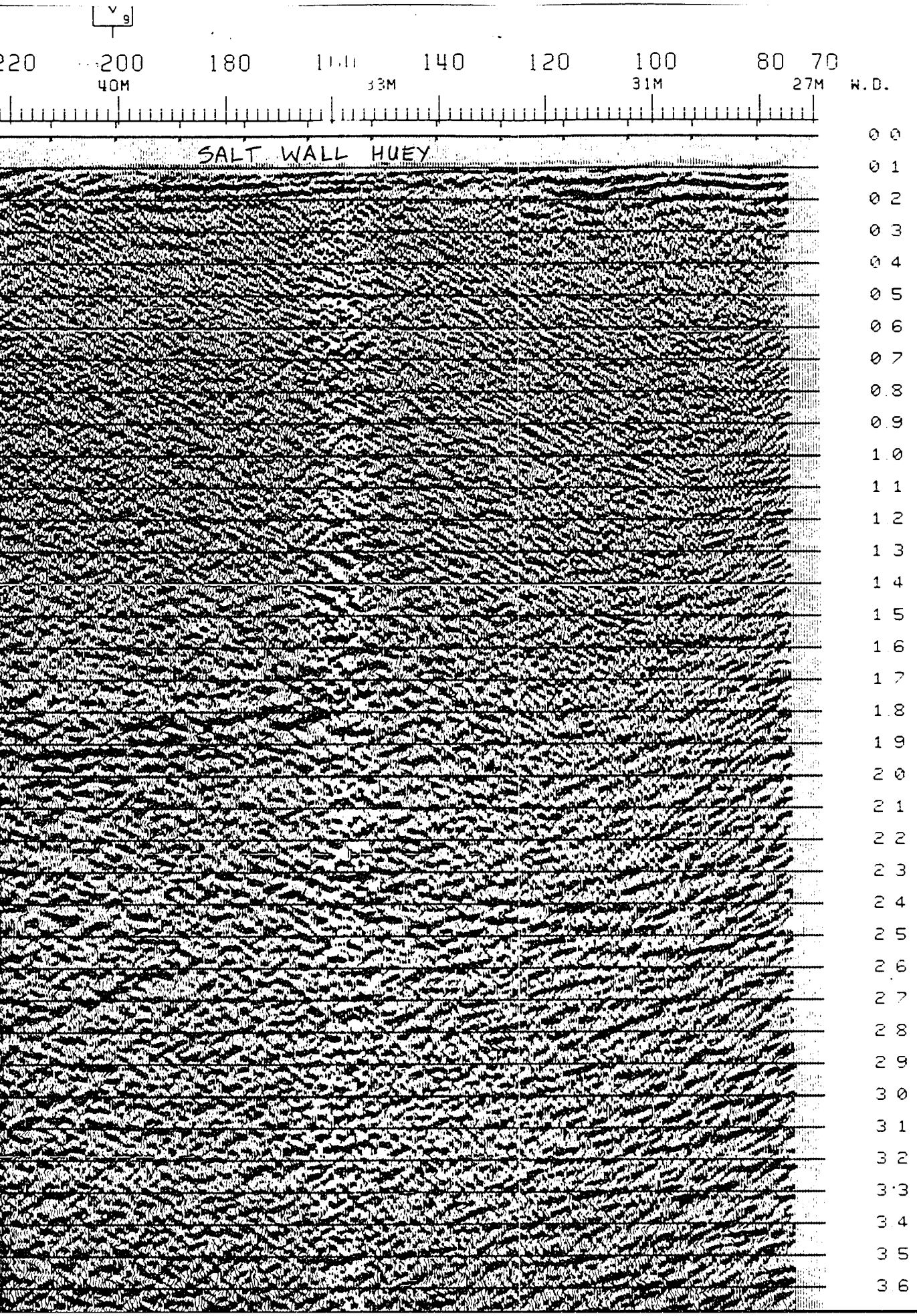

CH

SHOT BY WE
PROCESSED

ENERGY SOU
CHARGE SIZ
NUMBER OF
GUN DEPTH
FIRING INT
SHOT POINT
DISTANCE O

SYSTEM
AMPLIFIER
FILTER
SAMPLING I
RECORD LEN
FORMAT

TYPE CABLE
CABLE LENG
CABLE DEPT
LEAD IN
GROUP INTE
NUMBER OF
SPREAD

ROMS
CHANNELS P
WEIGHTS
NUMBER OF
CHANNEL IN

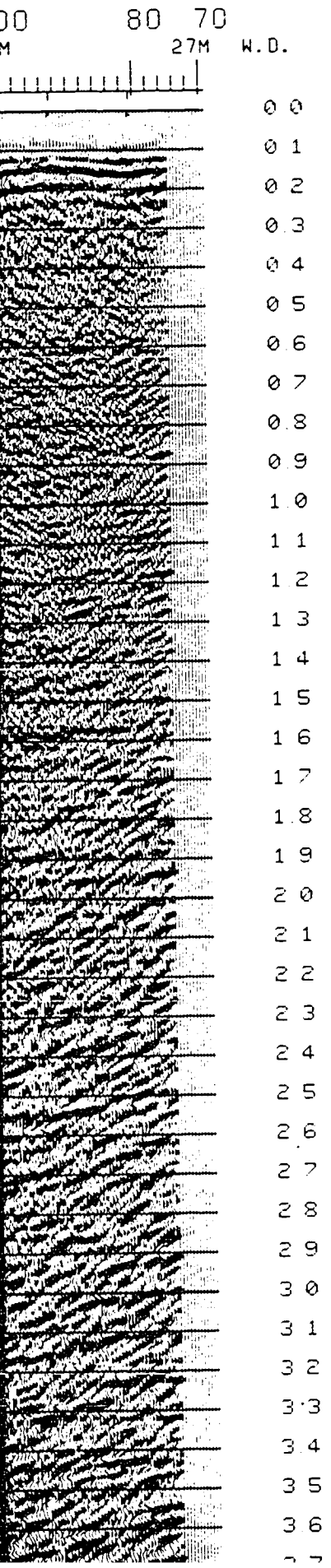

CHEVRON STANDARD LTD.

AREA: NORTHUMBERLAND STRAIT

SHOT BY WESTERN GEOPHYSICAL COMPANY PART 127 JULY 1981
PROCESSED BY WESTERN GEOPHYSICAL (CALGARY) GROUP 6 OCT-1981

RECORDING DATA

SOURCE

ENERGY SOURCE	AIR GUNS
CHARGE SIZE	1050 CU.IN
NUMBER OF GUNS	15
GUN DEPTH	6 M
FIRING INTERVAL	27 M
SHOT POINT INTERVAL	27 M
DISTANCE OF SOURCE TO ANTENNA	47 M

INSTRUMENTS

SYSTEM	KILOSEIS
AMPLIFIER	INST. FLOATING POINT
FILTER	L/9-H/450
SAMPLING INTERVAL	1 MS
RECORD LENGTH	5.0 SEC
FORMAT	SEG-D

CABLE

TYPE CABLE	STREAMER
CABLE LENGTH	2565 M
CABLE DEPTH	8 M
LEAD IN	187 M
GROUP INTERVAL	27 M
NUMBER OF GROUPS RECORDED	96
SPREAD	2752 M

ARRAY PARAMETERS

ROMS	7/21
CHANNELS PER ARRAY	8.50% OVERLAP
WEIGHTS	32.32.32.32.32.32.32.32
NUMBER OF DATA CHANNELS RECORDED	384
CHANNEL INTERVAL	6.67 M

PROCESSING SEQUENCE AND PARAMETERS

PROCESSING SAMPLING INTERVAL 4 MS

1. SIGNATURE DECONVOLUTION
2. DECONVOLVED BEFORE STACK
   - WINDOW LENGTH 2 ZONES OF 2500 MS
   - LENGTH OPERATOR 280 MS
   - PREDICTION DISTANCE 4 MS
3. NMO STACK 4800 %
4. RELATIVE AMP. COMPENSATION
5. F-K DOMAIN FILTER
6. DECONVOLVED AFTER STACK
   - WINDOW LENGTH 2 ZONES OF 2500 MS
   - LENGTH OPERATOR 300 MS
   - PREDICTION DISTANCE 20 MS
7. FINITE DIFFERENCE MIGRATION
8. TIME VARIANT FILTER

TIME		L.C. (HZ)	H.C.
1.00	SEC	12	60
3.00	SEC	8	45
5.00	SEC	8	30

9. RMS GAIN (128-512 MS WINDOW)

THEAST

71

OJ. NO: 8624 C4 9E LINE NO

NDARD LTD.

RLAND STRAIT

NY PARTY 127 JULY 1981
ICALGARY GROUP 6 OCT-1981

DATA

CE
AIR GUNS
1050 CU.IN
15
6 M
27 M
27 M
47 M

MENTS
KILOSEIS
INST. FLOATING POINT
L/9-H/450
1 MS
5.0 SEC
SEG-D

LE
STREAMER
2565 M
8 M
187 M
27 M
96
2752 M
AMETERS
7/21
8.50% OVERLAP
32.32.32.32.32.32.32.32
384
6.67 M

CE AND PARAMETERS

ING INTERVAL 4 MS
OLUTION
RE STACK
2 ZONES OF 2500 MS
280 MS
E 4 MS

MPENSATION
R
R STACK
2 ZONES OF 2500 MS
300 MS
E 20 MS
E MIGRATION
TER

L.C. (HZ)	H.C.
12	60
8	45
8	30

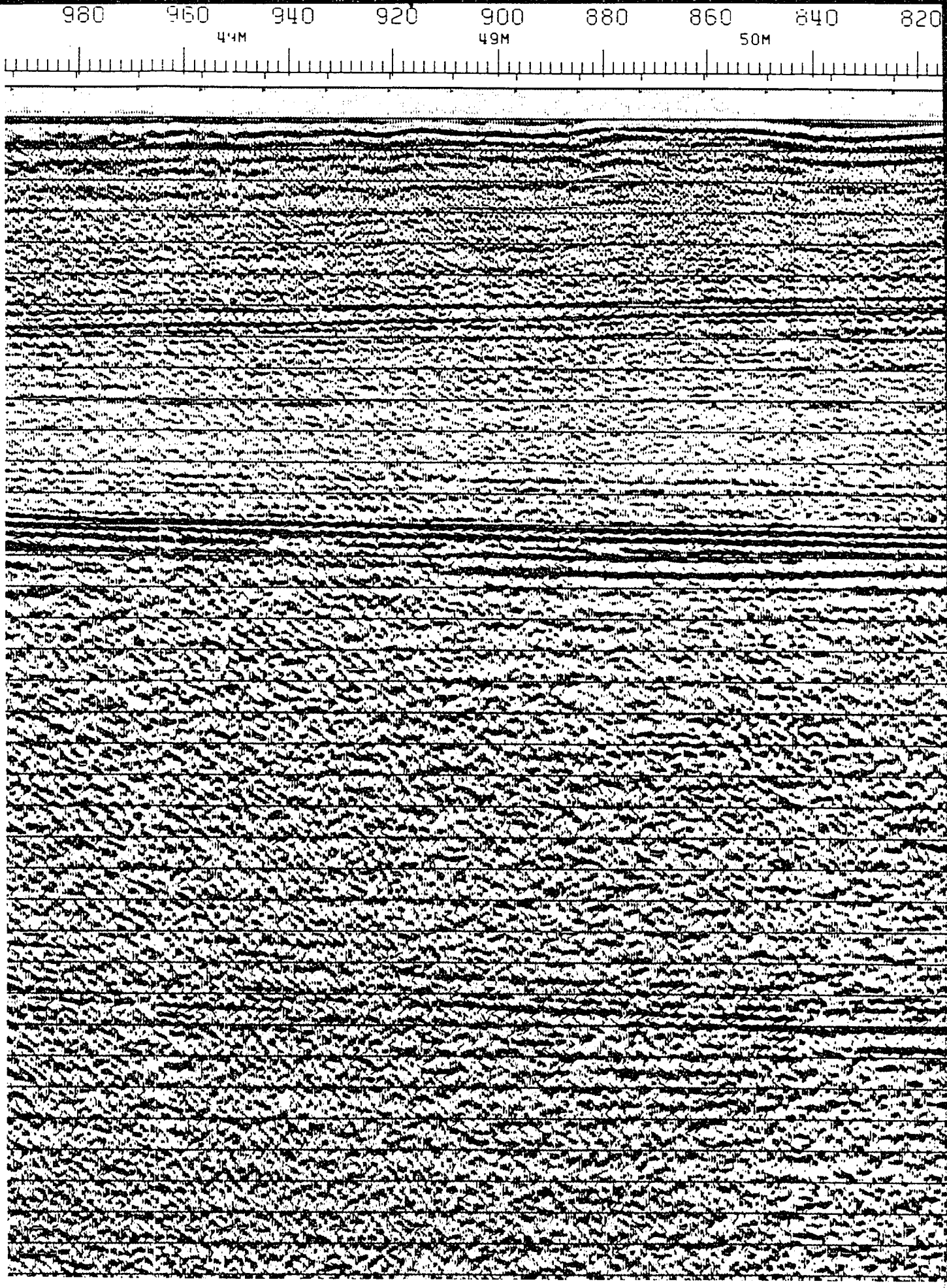
980
960
940
920
900
880
860
840
820
44M
49M
50M

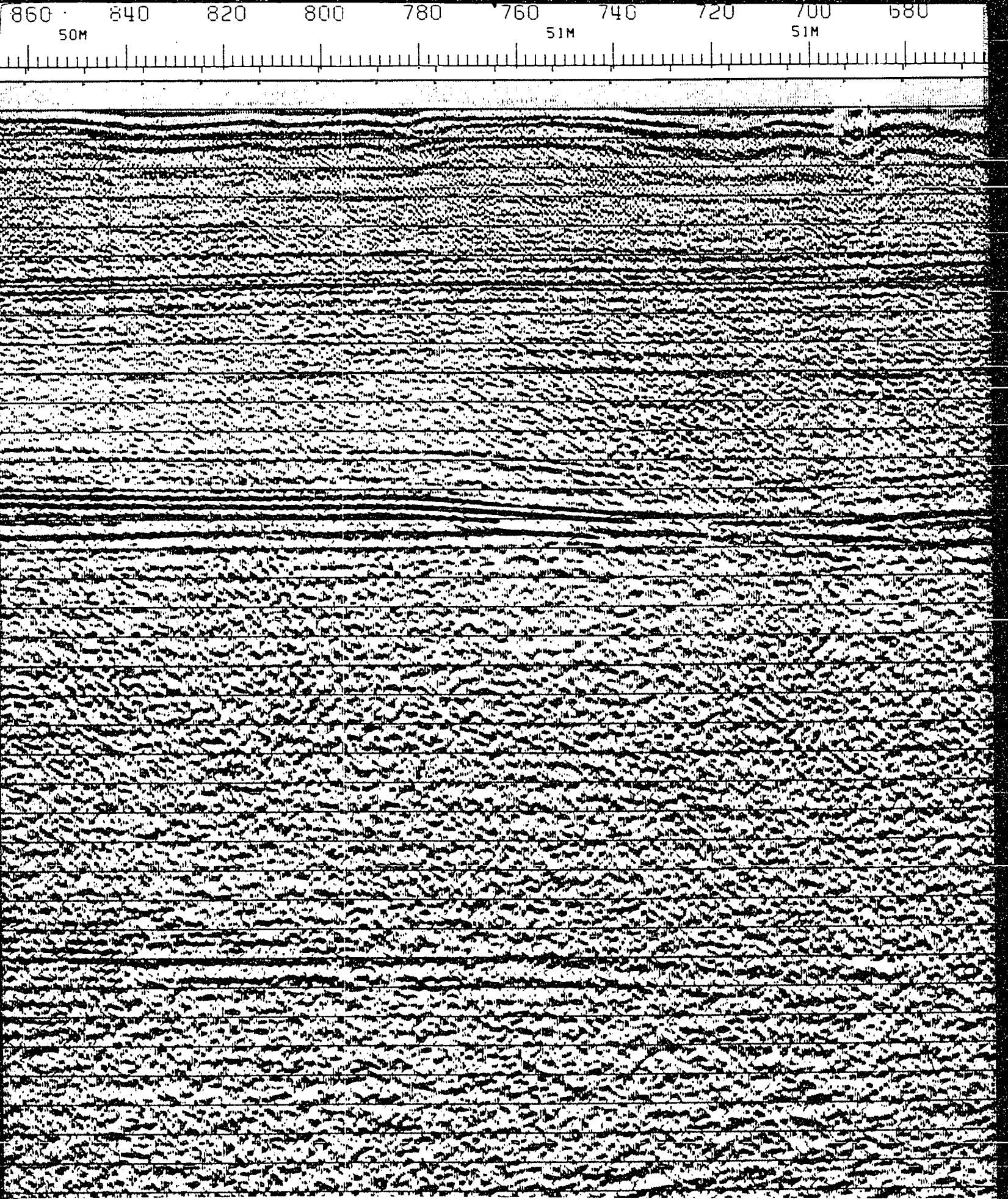
860
840
820
800
780
760
740
720
700
680
50M
51M
51M

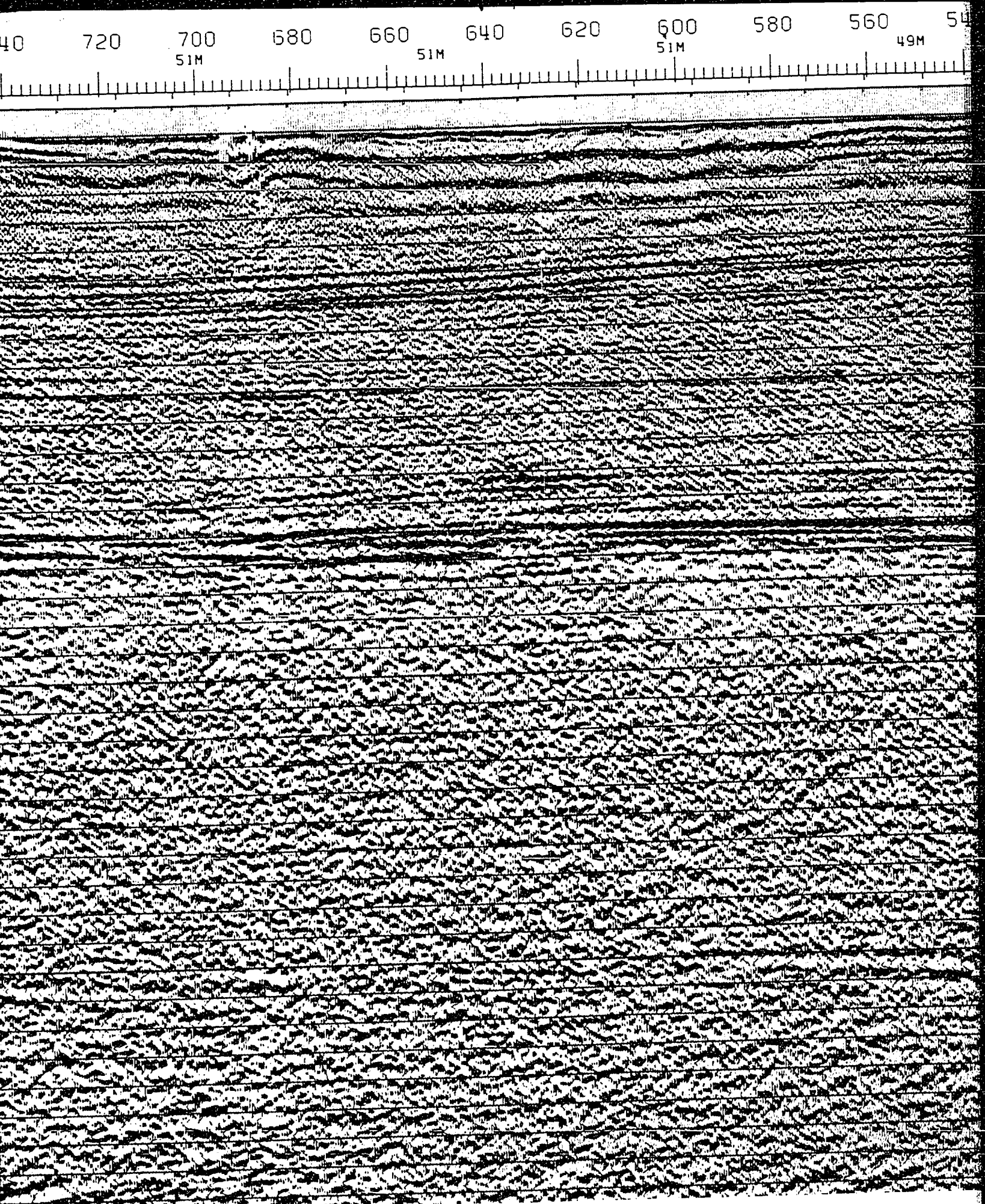
740
720
700
51M
680
660
51M
640
620
600
51M
580
560
49M

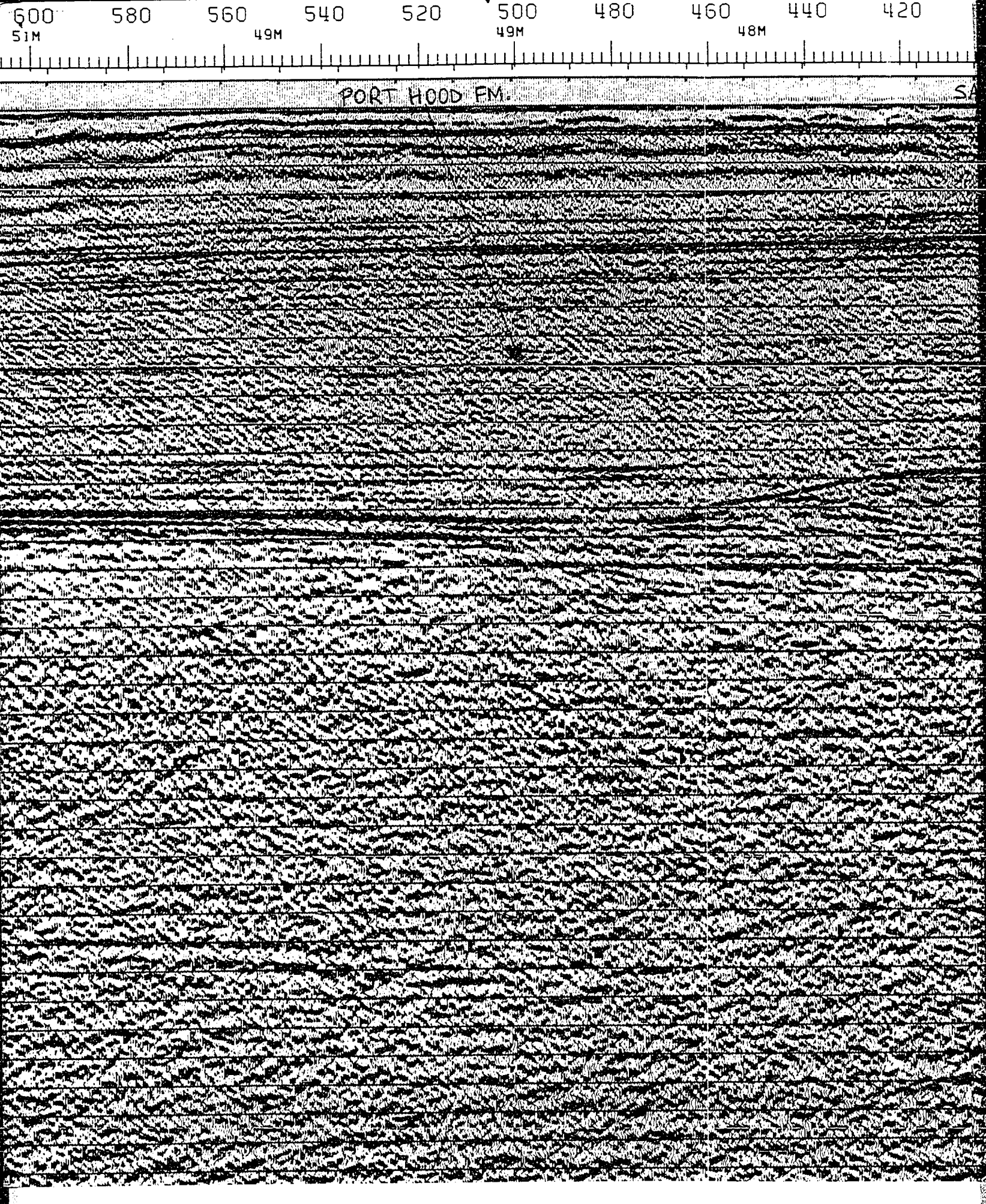
600
580
560
540
520
500
480
460
440
420
51M
49M
49M
48M
PORT HOOD FM.

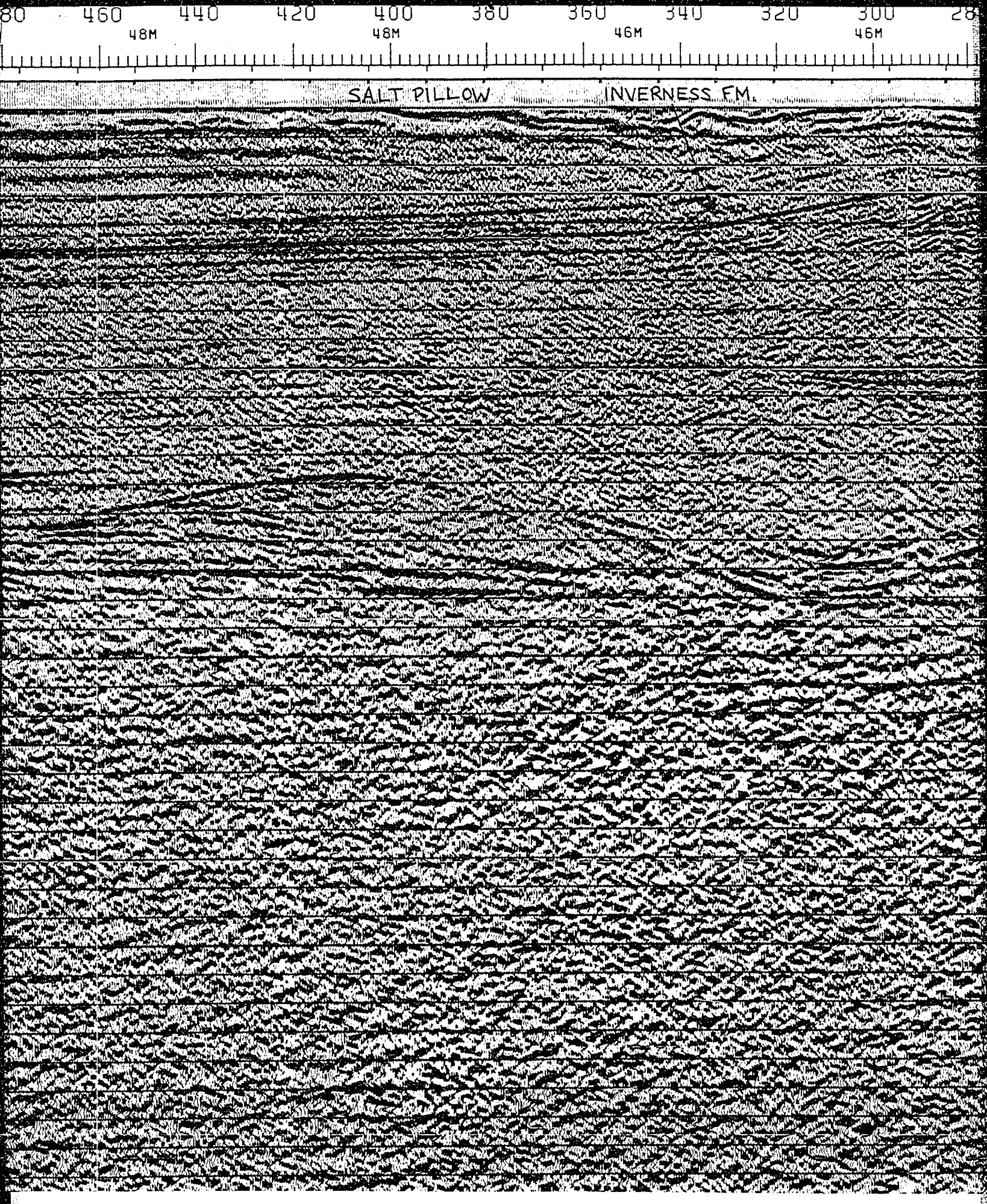
480
460
440
420
400
380
360
340
320
300
48M
48M
46M
46M
SALT PILLOW
INVERNESS FM.

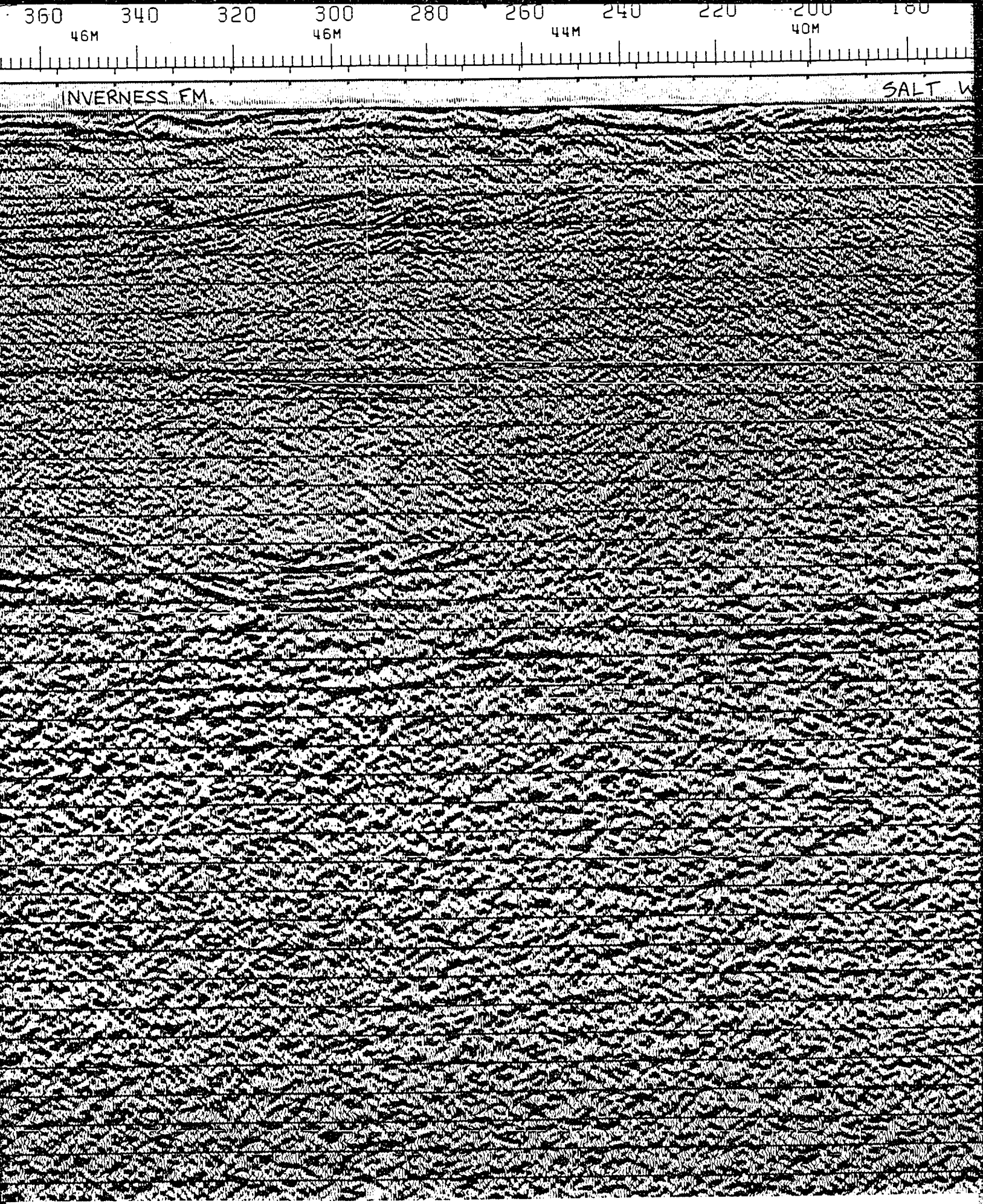
360
340
320
300
280
260
240
220
200
180
46M
46M
44M
40M
INVERNESS FM.
SALT W

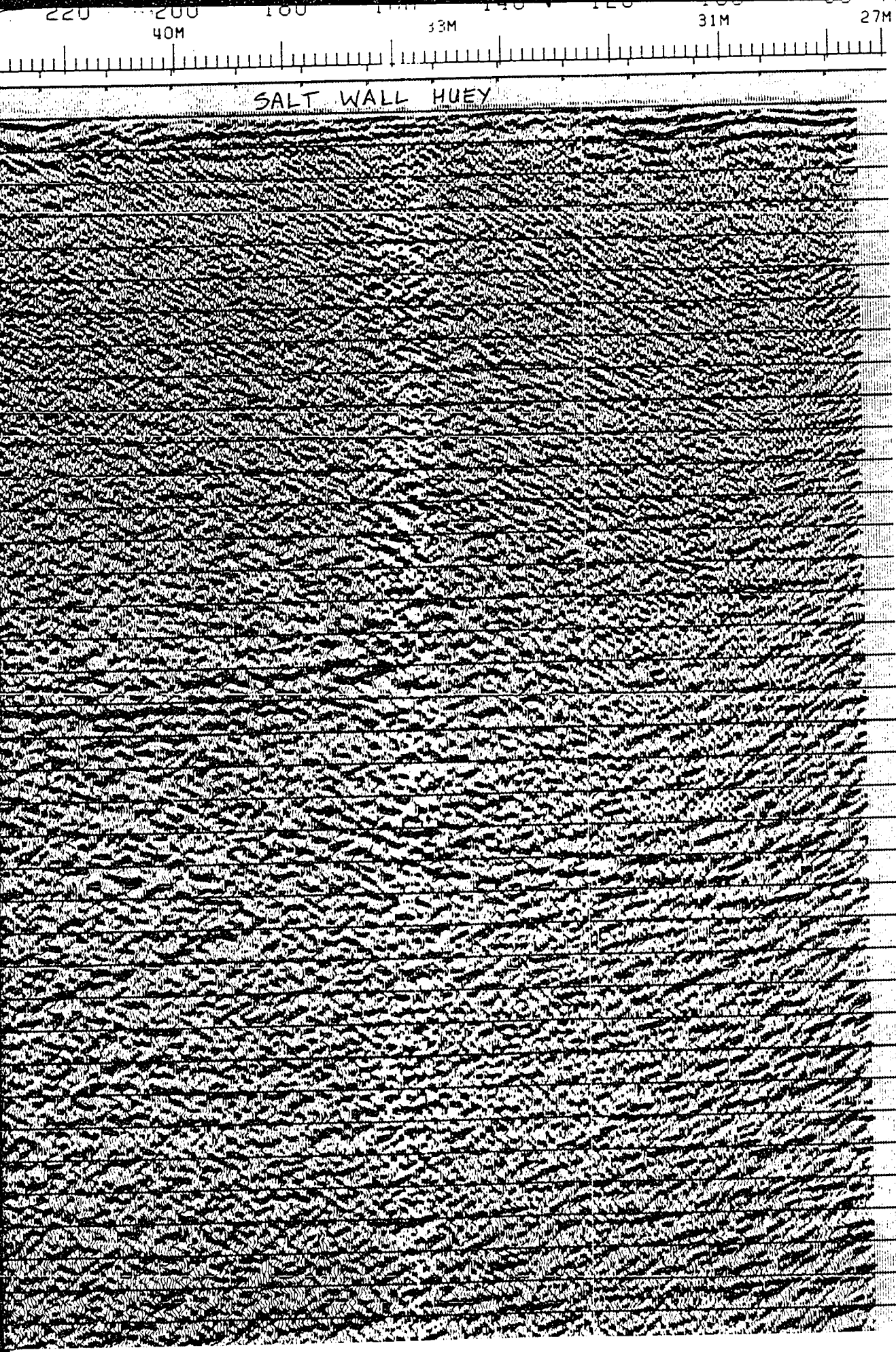
220
200
180
40M
33M
31M
27M
W.D.
SALT WALL HUEY
0 0
0 1
0 2
0 3
0 4
0 5
0 6
0 7
0 8
0 9
1 0
1 1
1 2
1 3
1 4
1 5
1 6
1 7
1 8
1 9
2 0
2 1
2 2
2 3
2 4
2 5
2 6
2 7
2 8
2 9
3 0
3 1
3 2
3 3
3 4
3 5
3 6
3 7
3 8

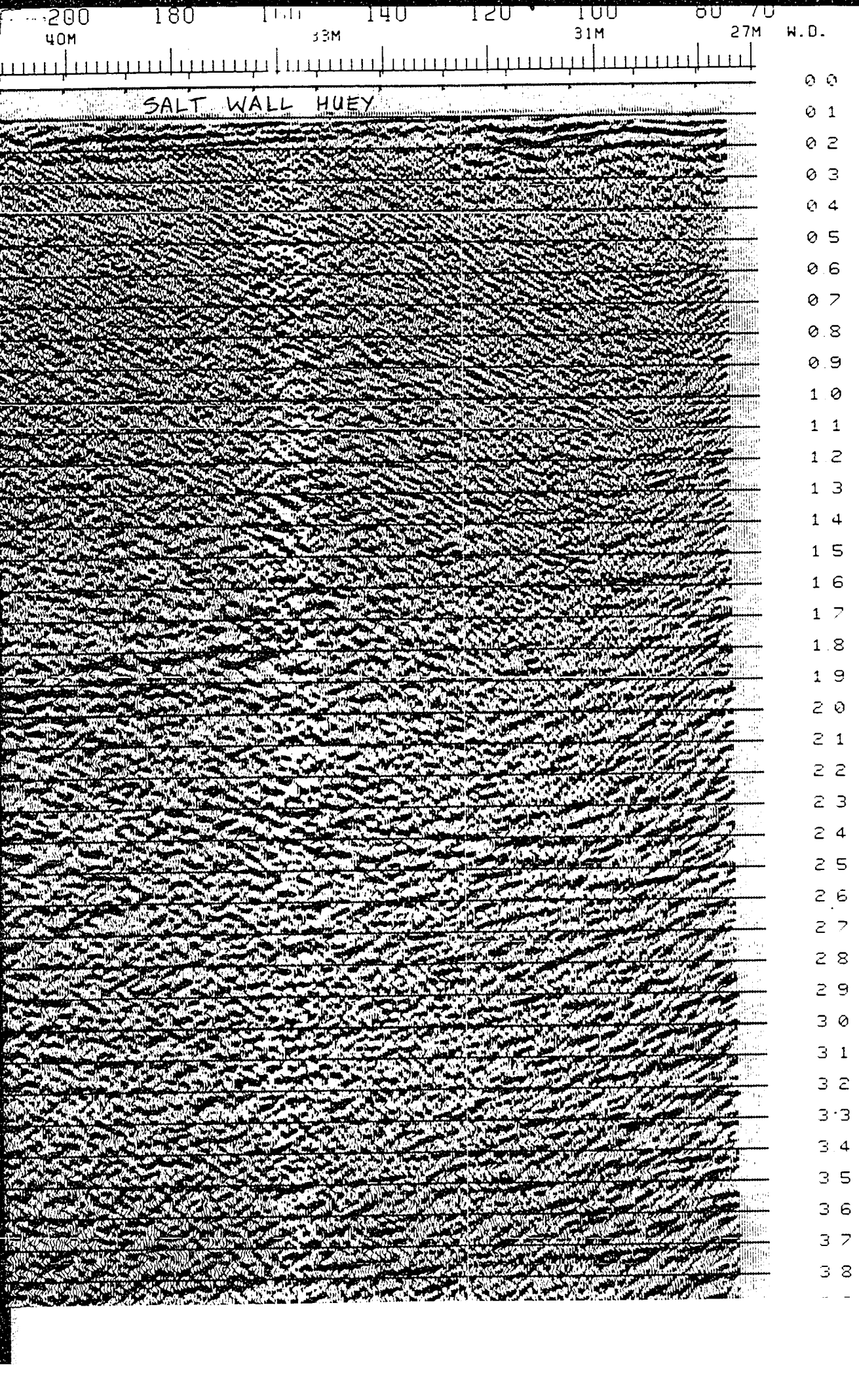

CHEV

SHOT BY WESTERN
PROCESSED BY WE

ENERGY SOURCE
CHARGE SIZE
NUMBER OF GUNS
GUN DEPTH
FIRING INTERVAL
SHOT POINT INTER
DISTANCE OF SOU

SYSTEM
AMPLIFIER
FILTER
SAMPLING INTERV
RECORD LENGTH
FORMAT

TYPE CABLE
CABLE LENGTH
CABLE DEPTH
LEAD IN
GROUP INTERVAL
NUMBER OF GROUP
SPREAD

ROMS
CHANNELS PER AR
WEIGHTS
NUMBER OF DATA
CHANNEL INTERVA

PRO

PR
1. SI
2. DE
W
LE
PR
3. NM
4. RE
5. F
6. DE
W
LE
PR
7. FI
8. TI
9. RM

47 M

70
27M W.D.

CHEVRON STANDARD LTD.

AREA: NORTHUMBERLAND STRAIT

SHOT BY WESTERN GEOPHYSICAL COMPANY PARTY 127 JULY 1981
PROCESSED BY WESTERN GEOPHYSICAL (CALGARY) GROUP 6 OCT. 1981

RECORDING DATA

SOURCE

ENERGY SOURCE	AIR GUNS
CHARGE SIZE	1050 CU.IN.
NUMBER OF GUNS	15
GUN DEPTH	6 M
FIRING INTERVAL	27 M
SHOT POINT INTERVAL	27 M
DISTANCE OF SOURCE TO ANTENNA	47 M

INSTRUMENTS

SYSTEM	KILOSEIS
AMPLIFIER	INST. FLOATING POINT
FILTER	L/9-H/450
SAMPLING INTERVAL	1 MS
RECORD LENGTH	5.0 SEC
FORMAT	SEG-D

CABLE

TYPE CABLE	STREAMER
CABLE LENGTH	2565 M
CABLE DEPTH	8 M
LEAD IN	187 M
GROUP INTERVAL	27 M
NUMBER OF GROUPS RECORDED	96
SPREAD	2752 M

ARRAY PARAMETERS

ROMS	7/21
CHANNELS PER ARRAY	8.50% OVERLAP
WEIGHTS	32.32.32.32.32.32.32.32
NUMBER OF DATA CHANNELS RECORDED	384
CHANNEL INTERVAL	6.67 M

PROCESSING SEQUENCE AND PARAMETERS

PROCESSING SAMPLING INTERVAL 4 MS

1. SIGNATURE DECONVOLUTION
2. DECONVOLVED BEFORE STACK
   - WINDOW LENGTH 2 ZONES OF 2500 MS
   - LENGTH OPERATOR 280 MS
   - PREDICTION DISTANCE 4 MS
3. NMO STACK 4800 %
4. RELATIVE AMP. COMPENSATION
5. F-K DOMAIN FILTER
6. DECONVOLVED AFTER STACK
   - WINDOW LENGTH 2 ZONES OF 2500 MS
   - LENGTH OPERATOR 300 MS
   - PREDICTION DISTANCE 20 MS
7. FINITE DIFFERENCE MIGRATION
8. TIME VARIANT FILTER

TIME		L.C. (HZ)	H.C.
1.00	SEC	12	60
3.00	SEC	8	45
5.00	SEC	8	30

9. RMS GAIN (128-512 MS WINDOW)

47 M

LEGEND

NDARD LTD.

BERLAND STRAIT

PANY PART1 127 JULY 1981
L (CALGARY) GROUP 6 OCT-1981

NG DATA

URCE
- AIR GUNS
- 1050 CU.IN.
- 15
- 6 M
- 27 M
- 27 M
- 47 M

AUMENTS
- KILOSEIS
- INST. FLOATING POINT
- L/9-H/450
- 1 MS
- 5.0 SEC
- SEG-D

ABLE
- STREAMER
- 2565 M
- 8 M
- 187 M
- 27 M
- 96
- 2752 M

ARAMETERS
- 7/21
- 8.50% OVERLAP
- 32.32.32.32.32.32.32.32

ED 384
- 6.67 M

NCE AND PARAMETERS

PLING INTERVAL 4 MS
NVOLUTION
ORE STACK
- 2 ZONES OF 2500 MS
- 280 MS

NCE 4 MS
%
OMPENSATION
TER
TER STACK
- 2 ZONES OF 2500 MS
- 300 MS

NCE 20 MS
NCE MIGRATION
ILTER

L.C. (HZ)	H.C.
12	60
8	45
8	30

512 MS WINDOW

LEGEND

71

OJ. NO: 8624 C4 9E LINE NO:

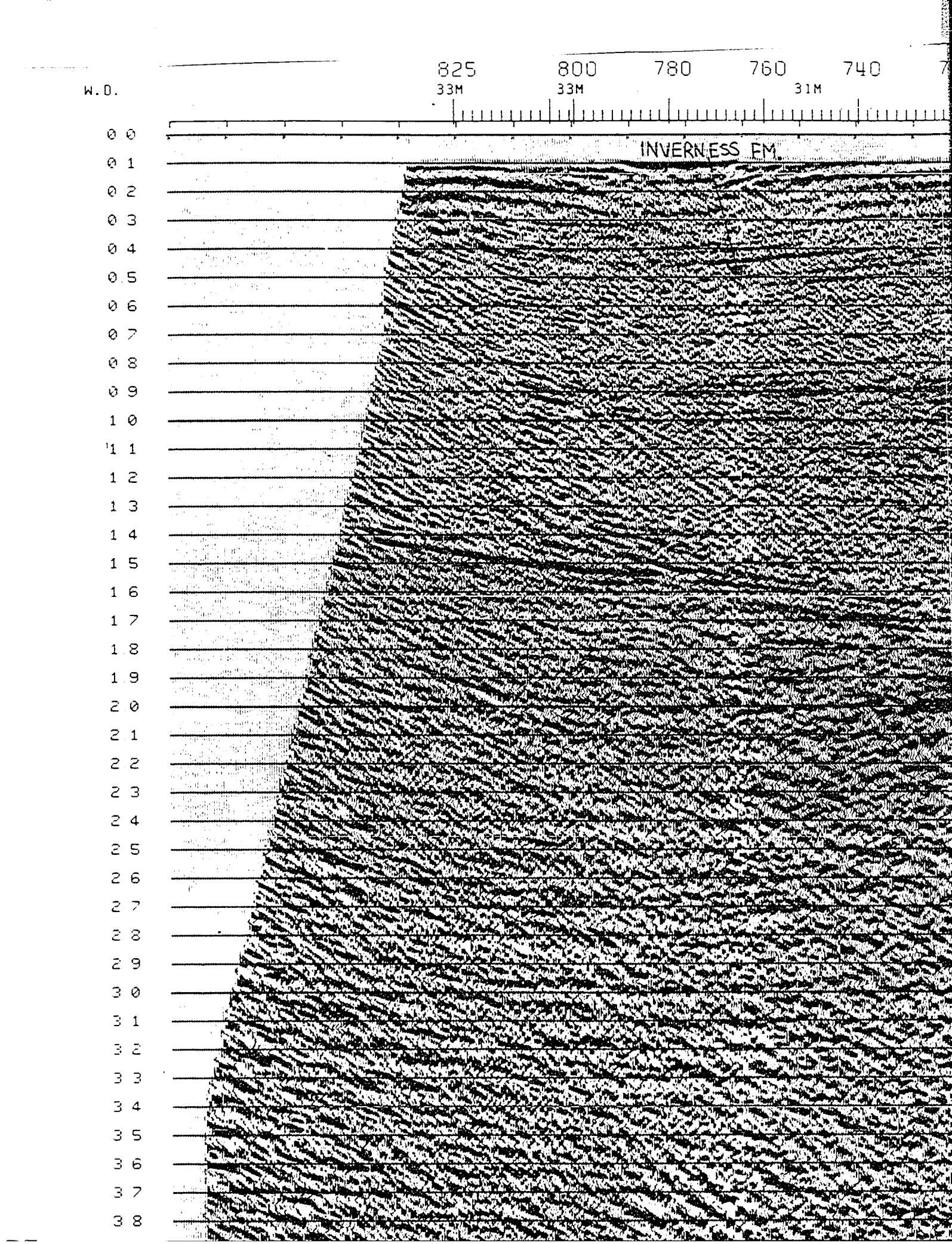
825
800
780
760
740
33M
33M
31M
W.D.
INVERNESS FM.
0 0
0 1
0 2
0 3
0 4
0 5
0 6
0 7
0 8
0 9
1 0
1 1
1 2
1 3
1 4
1 5
1 6
1 7
1 8
1 9
2 0
2 1
2 2
2 3
2 4
2 5
2 6
2 7
2 8
2 9
3 0
3 1
3 2
3 3
3 4
3 5
3 6
3 7
3 8

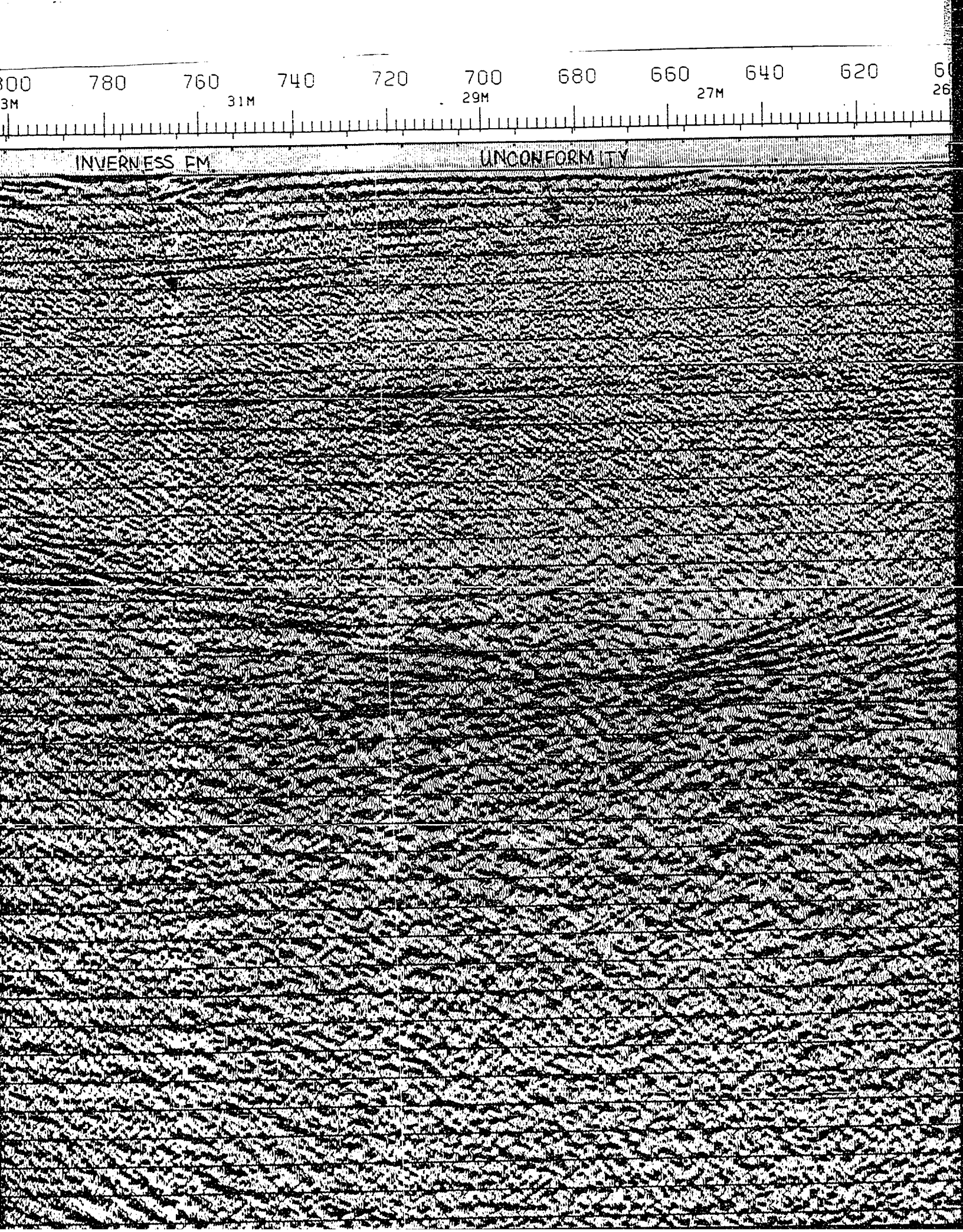
800
780
760
740
720
700
680
660
640
620
3M
31M
29M
27M
INVERNESS FM
UNCONFORMITY

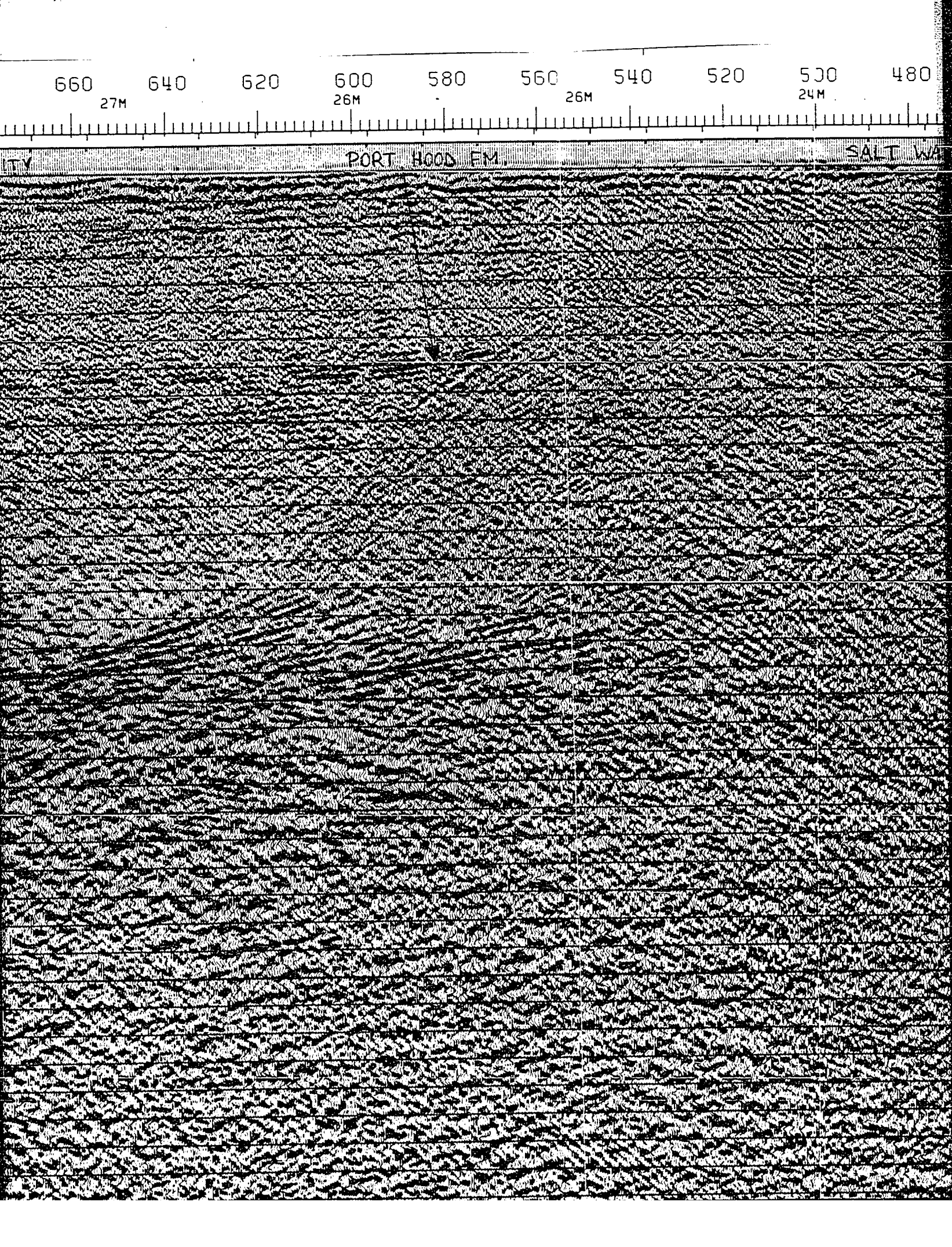
660
640
620
600
580
560
540
520
500
480
27M
26M
26M
24M
PORT HOOD FM.

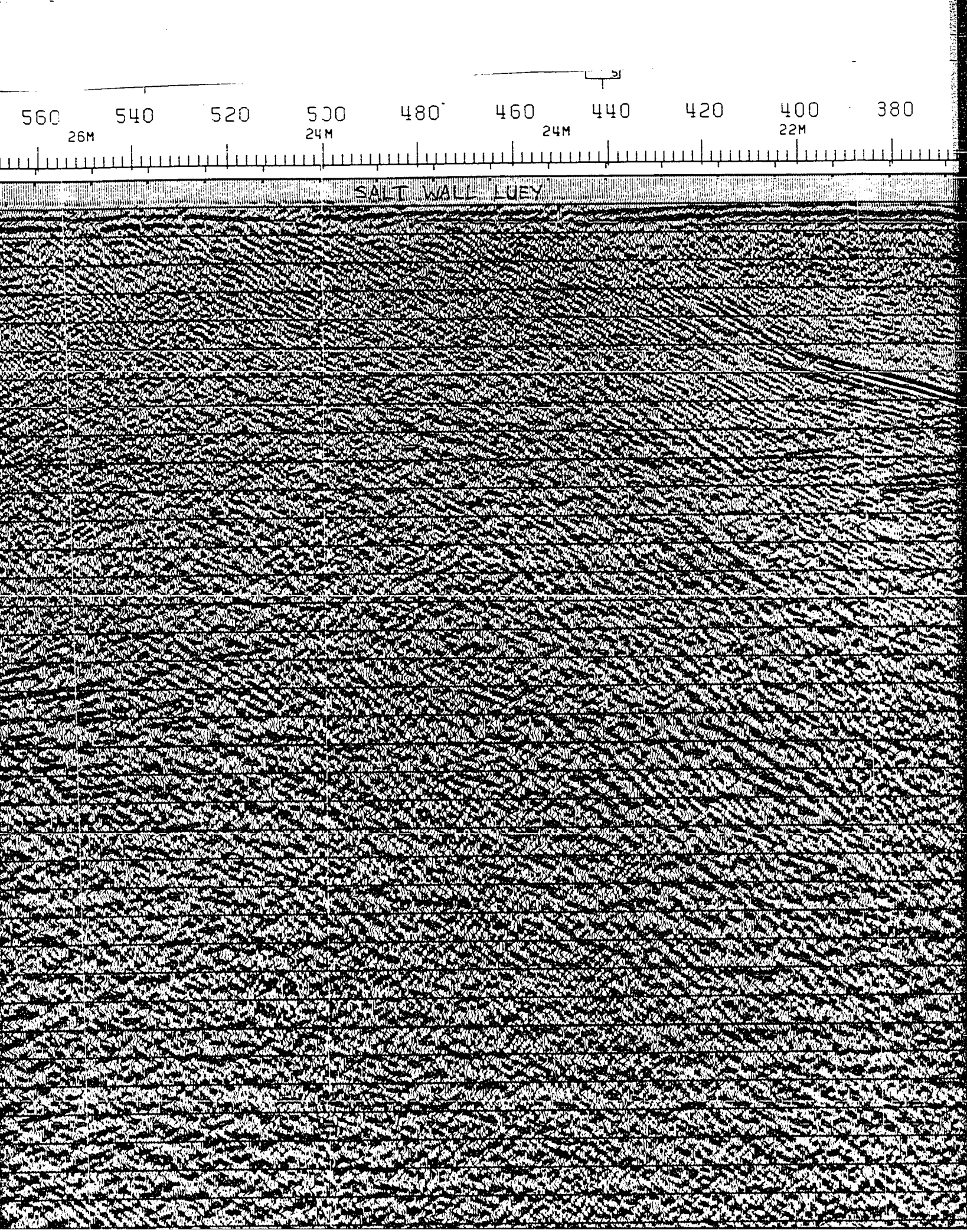
560
540
520
500
480
460
440
420
400
380
26M
24M
24M
22M
SALT WALL LUEY

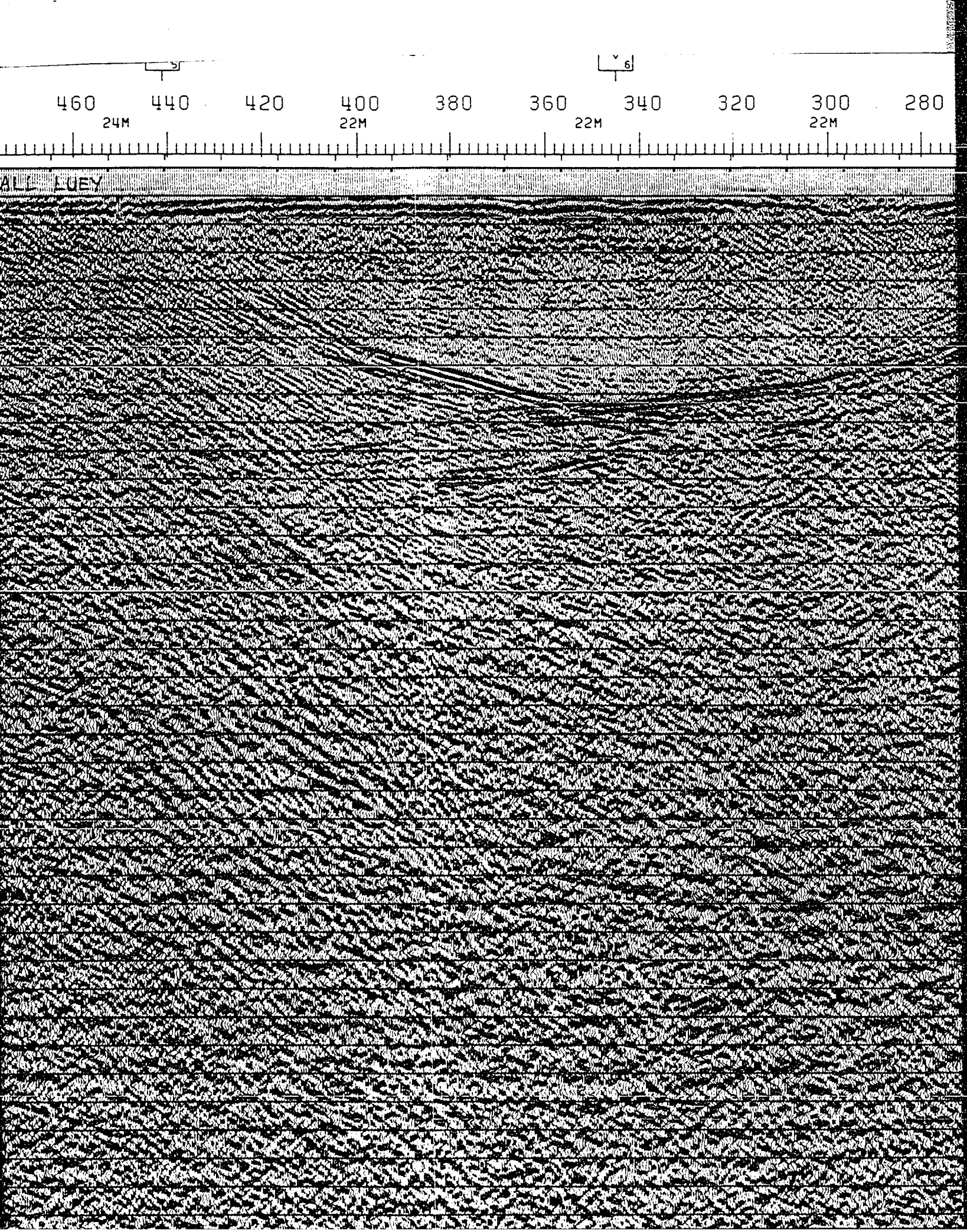
460
440
420
400
380
360
340
320
300
280
24M
22M
22M
22M
ALL LUEY

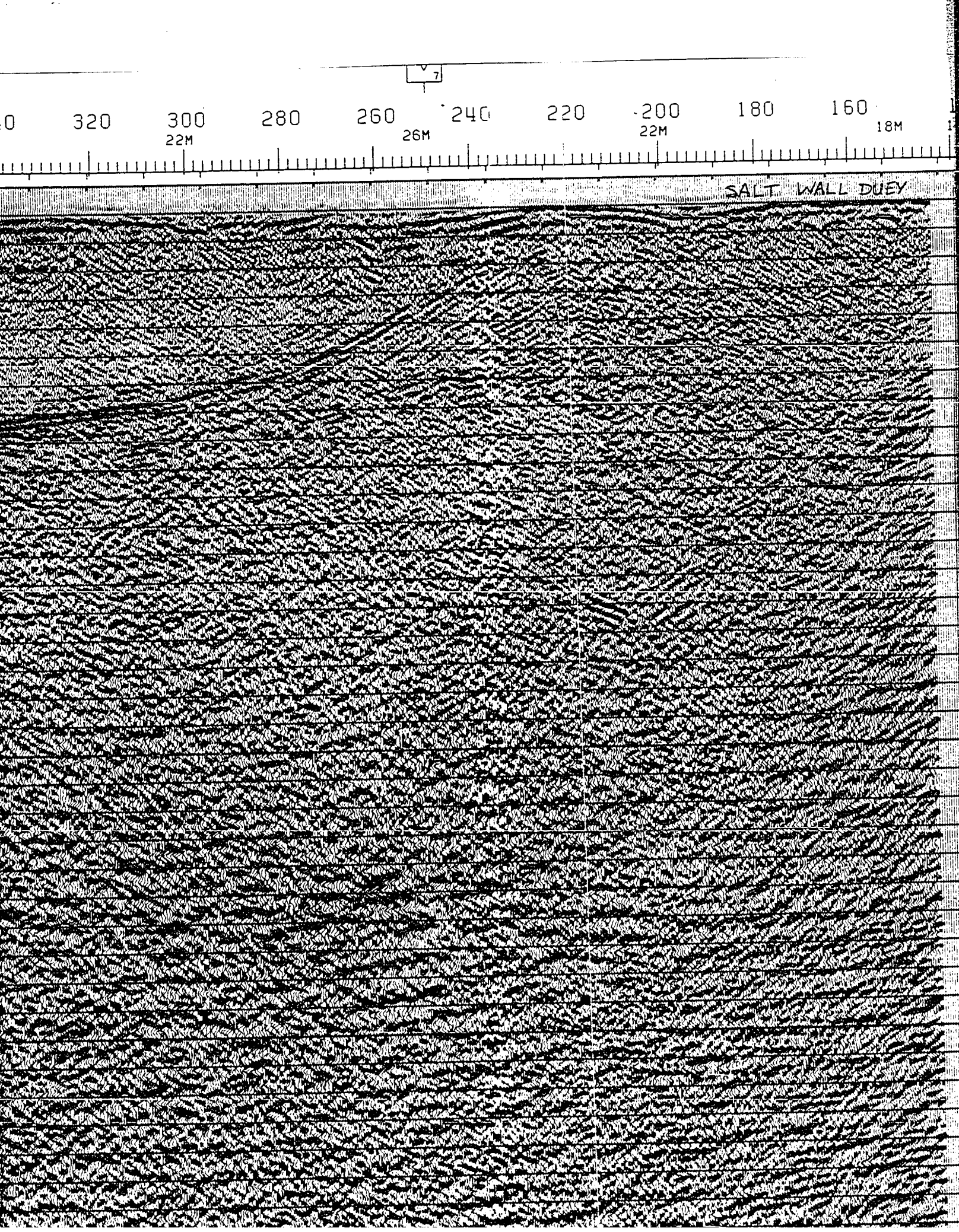
7
320
300
22M
280
260
26M
240
220
200
22M
180
160
18M
SALT WALL DUEY

SOUTH

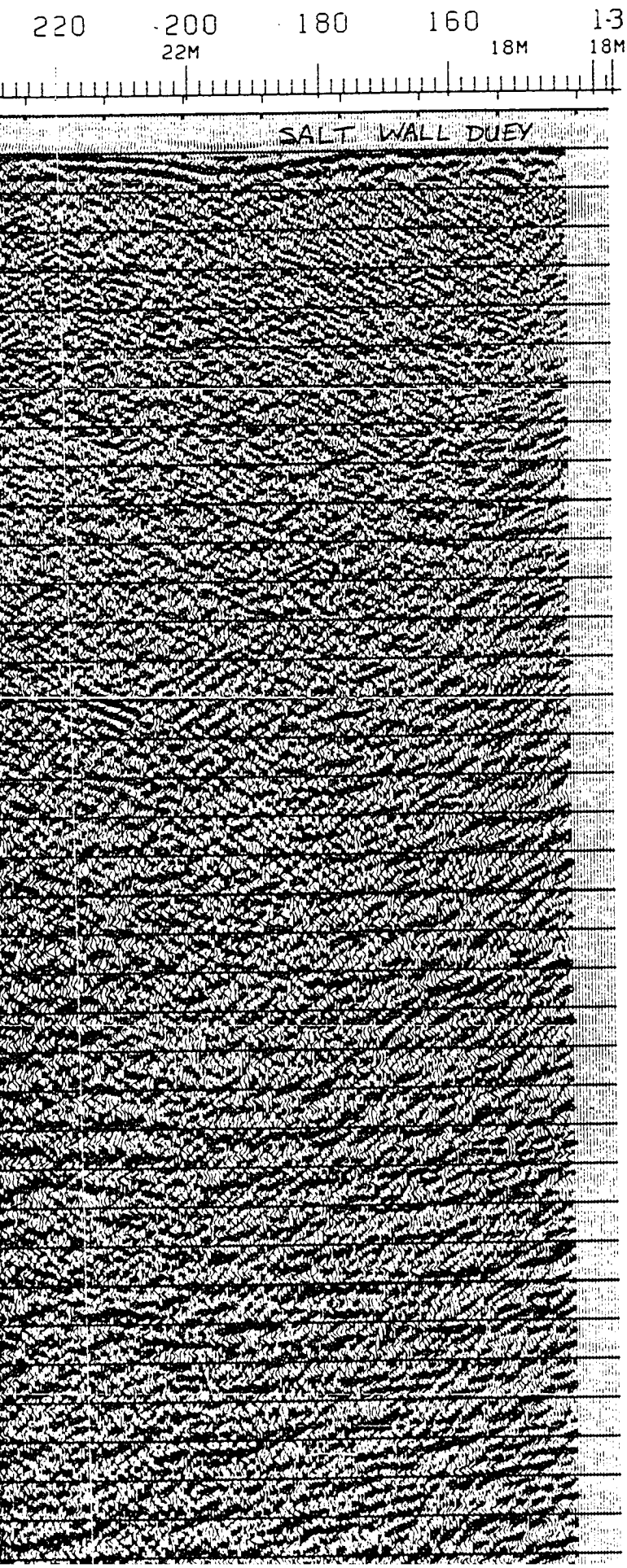

CHEVRON STANDARD

AREA: NORTHUMBERLAND ST

SHOT BY WESTERN GEOPHYSICAL COMPANY
PROCESSED BY WESTERN GEOPHYSICAL (CALGARY)

RECORDING DATA

SOURCE	
ENERGY SOURCE	AIR GUNS
CHARGE SIZE	1050 CU.
NUMBER OF GUNS	15
GUN DEPTH	6 M
FIRING INTERVAL	27 M
SHOT POINT INTERVAL	27 M
DISTANCE OF SOURCE TO ANTENNA	47 M
INSTRUMENTS	
SYSTEM	KILOSEIS
AMPLIFIER	INST. FL
FILTER	L/9-H/45
SAMPLING INTERVAL	1 MS
RECORD LENGTH	5.0 SEC
FORMAT	SEG-D
CABLE	
TYPE CABLE	STREAMER
CABLE LENGTH	2565 M
CABLE DEPTH	8 M
LEAD IN	187 M
GROUP INTERVAL	27 M
NUMBER OF GROUPS RECORDED	96
SPREAD	2752 M
ARRAY PARAMETERS	
ROMS	7/21
CHANNELS PER ARRAY	8.50% OV
WEIGHTS	32.32.32
NUMBER OF DATA CHANNELS RECORDED	384
CHANNEL INTERVAL	6.67 M

PROCESSING SEQUENCE AND PA

PROCESSING SAMPLING INTER

1. SIGNATURE DECONVOLUTION
2. DECONVOLVED BEFORE STACK
   - WINDOW LENGTH 2 ZONE
   - LENGTH OPERATOR
   - PREDICTION DISTANCE
3. NMO STACK 4800 %
4. RELATIVE AMP. COMPENSATIO
5. F-K DOMAIN FILTER
6. DECONVOLVED AFTER STACK
   - WINDOW LENGTH 2 ZONE
   - LENGTH OPERATOR
   - PREDICTION DISTANCE
7. FINITE DIFFERENCE MIGRATI
8. TIME VARIANT FILTER

TIME		L.C. (HZ)
1.00	SEC	12
3.00	SEC	8
5.00	SEC	8

9. RMS GAIN (128-512 MS WIND

SOUTHEAST

135
18M W.D.

0.0
0.1
0.2
0.3
0.4
0.5
0.6
0.7
0.8
0.9
1.0
1.1
1.2
1.3
1.4
1.5
1.6
1.7
1.8
1.9
2.0
2.1
2.2
2.3
2.4
2.5
2.6
2.7
2.8
2.9
3.0
3.1
3.2
3.3
3.4
3.5
3.6
3.7

CHEVRON STANDARD LTD.

AREA: NORTHUMBERLAND STRAIT

SHOT BY WESTERN GEOPHYSICAL COMPANY PARTY 127 JULY 1981
PROCESSED BY WESTERN GEOPHYSICAL (CALGARY) GROUP 6 OCT 1981

RECORDING DATA

SOURCE

ENERGY SOURCE	AIR GUNS
CHARGE SIZE	1050 CU.IN
NUMBER OF GUNS	15
GUN DEPTH	6 M
FIRING INTERVAL	27 M
SHOT POINT INTERVAL	27 M
DISTANCE OF SOURCE TO ANTENNA	47 M

INSTRUMENTS

SYSTEM	KILOSEIS
AMPLIFIER	INST. FLOATING POINT
FILTER	L/9-H/450
SAMPLING INTERVAL	1 MS
RECORD LENGTH	5.0 SEC
FORMAT	SEG-D

CABLE

TYPE CABLE	STREAMER
CABLE LENGTH	2565 M
CABLE DEPTH	8 M
LEAD IN	187 M
GROUP INTERVAL	27 M
NUMBER OF GROUPS RECORDED	96
SPREAD	2752 M

ARRAY PARAMETERS

ROMS	7/21
CHANNELS PER ARRAY	8.50% OVERLAP
WEIGHTS	32.32.32.32.32.32.32.32
NUMBER OF DATA CHANNELS RECORDED	384
CHANNEL INTERVAL	6.67 M

PROCESSING SEQUENCE AND PARAMETERS

PROCESSING SAMPLING INTERVAL 4 MS

1. SIGNATURE DECONVOLUTION
2. DECONVOLVED BEFORE STACK
   - WINDOW LENGTH 2 ZONES OF 2500 MS
   - LENGTH OPERATOR 280 MS
   - PREDICTION DISTANCE 4 MS
3. NMO STACK 4800 %
4. RELATIVE AMP. COMPENSATION
5. F-K DOMAIN FILTER
6. DECONVOLVED AFTER STACK
   - WINDOW LENGTH 2 ZONES OF 2500 MS
   - LENGTH OPERATOR 300 MS
   - PREDICTION DISTANCE 20 MS
7. FINITE DIFFERENCE MIGRATION
8. TIME VARIANT FILTER

TIME		L.C. (HZ)	H.C.
1.00	SEC	12	60
3.00	SEC	8	45
5.00	SEC	8	30

9. RMS GAIN (128-512 MS WINDOW)

SOUTHEAST

RON STANDARD LTD.

AREA: NORTHUMBERLAND STRAIT

GEOPHYSICAL COMPANY	PARTY 127	JULY 1981
STERN GEOPHYSICAL (CALGARY)	GROUP 6	OCT 1981

RECORDING DATA

SOURCE

	AIR GUNS
	1050 CU.IN
	15
	6 M
	27 M
RVAL	27 M
RCE TO ANTENNA	47 M

INSTRUMENTS

	KILOSEIS
	INST. FLOATING POINT
	L/9-H/450
L	1 MS
	5.0 SEC
	SEG-D

CABLE

	STREAMER
	2565 M
	8 M
	187 M
	27 M
S RECORDED	96
	2752 M

ARRAY PARAMETERS

	7/21
AY	8.50% OVERLAP
	32.32.32.32.32.32.32.32
CHANNELS RECORDED	384
	6.67 M

CESSING SEQUENCE AND PARAMETERS

OCESSING SAMPLING INTERVAL 4 MS
GNATURE DECONVOLUTION
CONVOLVED BEFORE STACK

NDOW LENGTH	2 ZONES OF 2500 MS
NGTH OPERATOR	280 MS
EDICTION DISTANCE	4 MS

D STACK 4800 %
LATIVE AMP. COMPENSATION
K DOMAIN FILTER
CONVOLVED AFTER STACK

NDOW LENGTH	2 ZONES OF 2500 MS
NGTH OPERATOR	300 MS
EDICTION DISTANCE	20 MS

ITE DIFFERENCE MIGRATION
E VARIANT FILTER

TIME		L.C. (HZ)	H.C.
1.00	SEC	12	60
3.00	SEC	8	45
5.00	SEC	8	30

83

J. NO: 8624 C4 9E LINE NO: _____

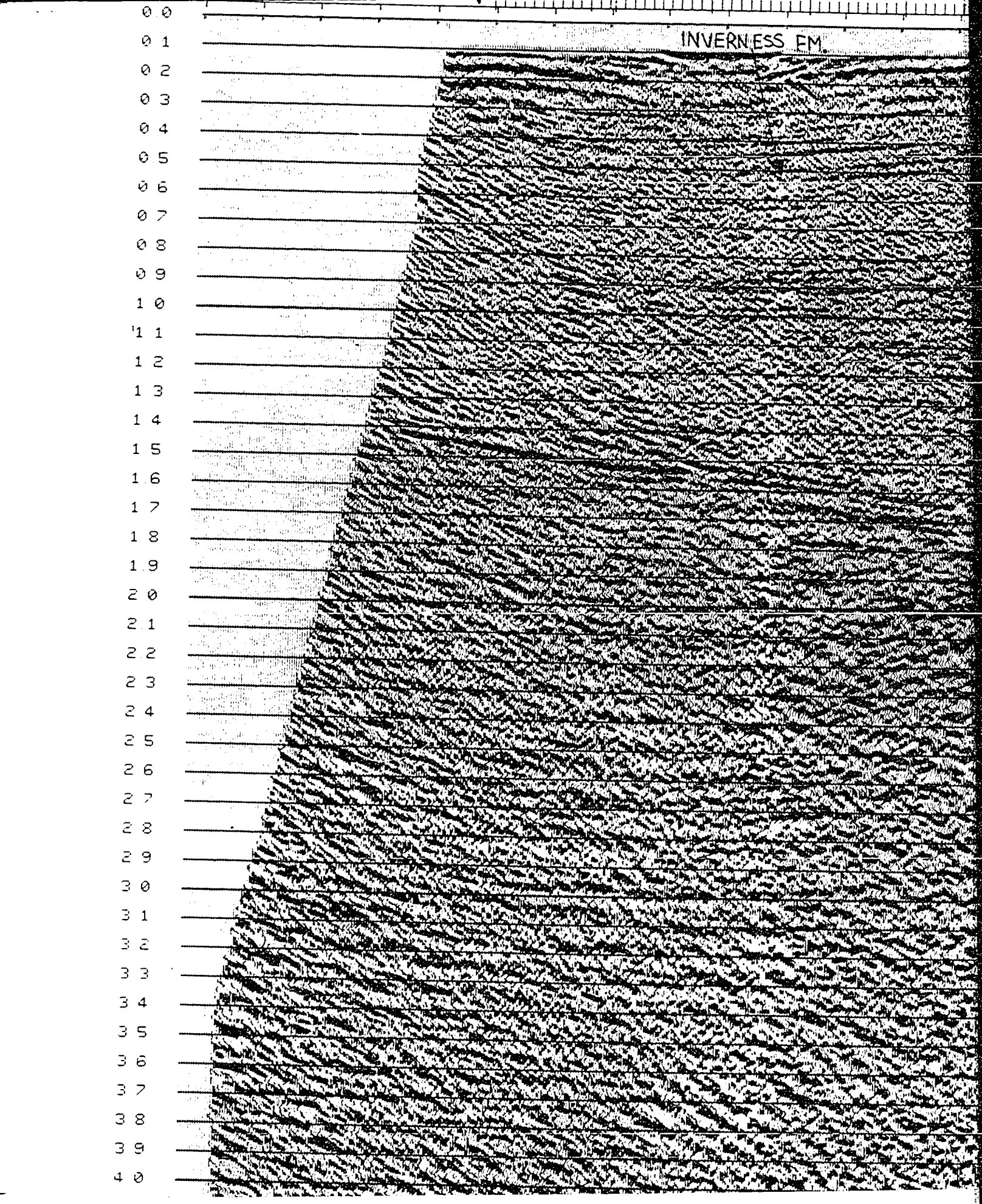
INVERNESS FM.
0 0
0 1
0 2
0 3
0 4
0 5
0 6
0 7
0 8
0 9
1 0
1 1
1 2
1 3
1 4
1 5
1 6
1 7
1 8
1 9
2 0
2 1
2 2
2 3
2 4
2 5
2 6
2 7
2 8
2 9
3 0
3 1
3 2
3 3
3 4
3 5
3 6
3 7
3 8
3 9
4 0

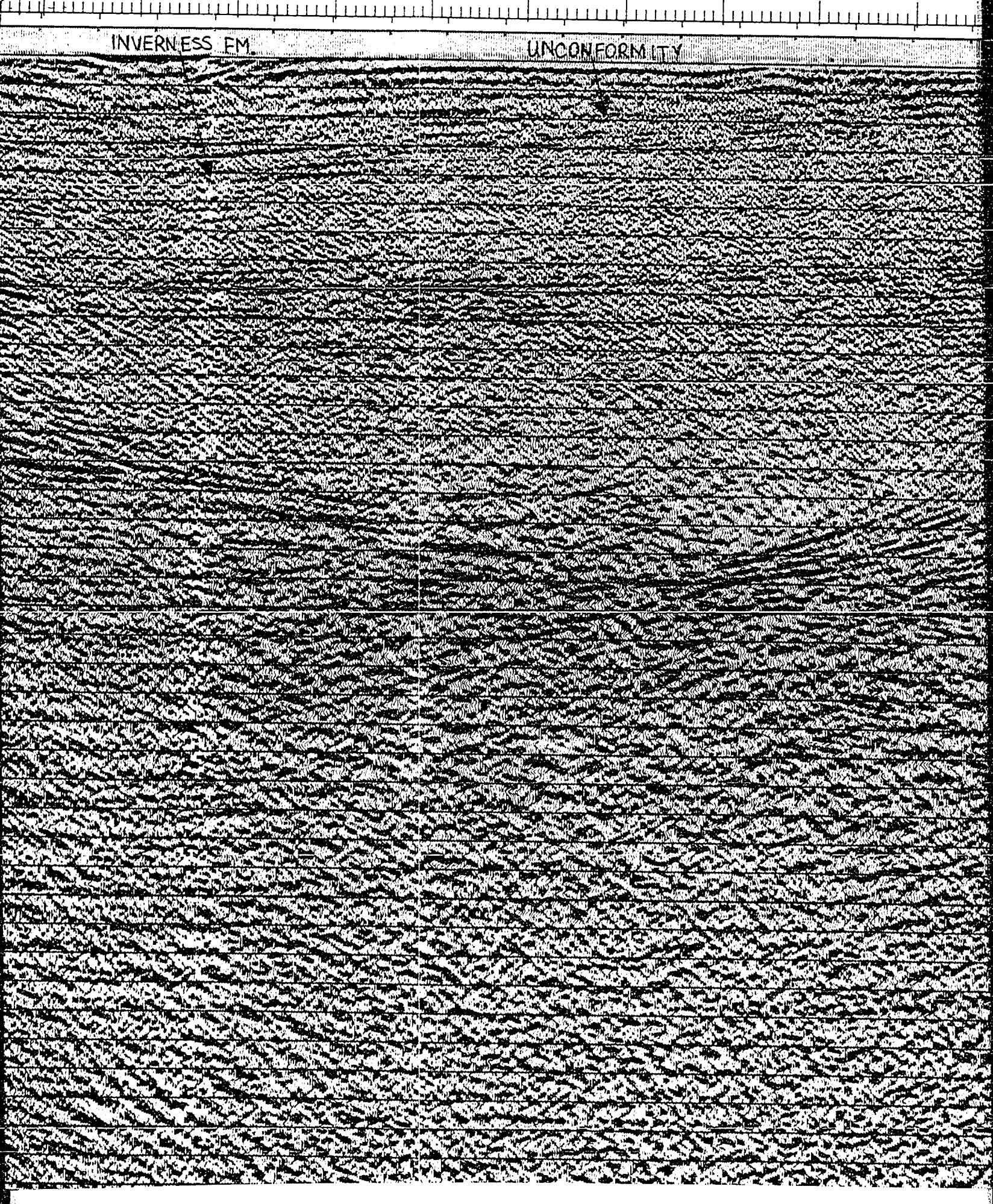
INVERNESS FM.
UNCONFORMITY

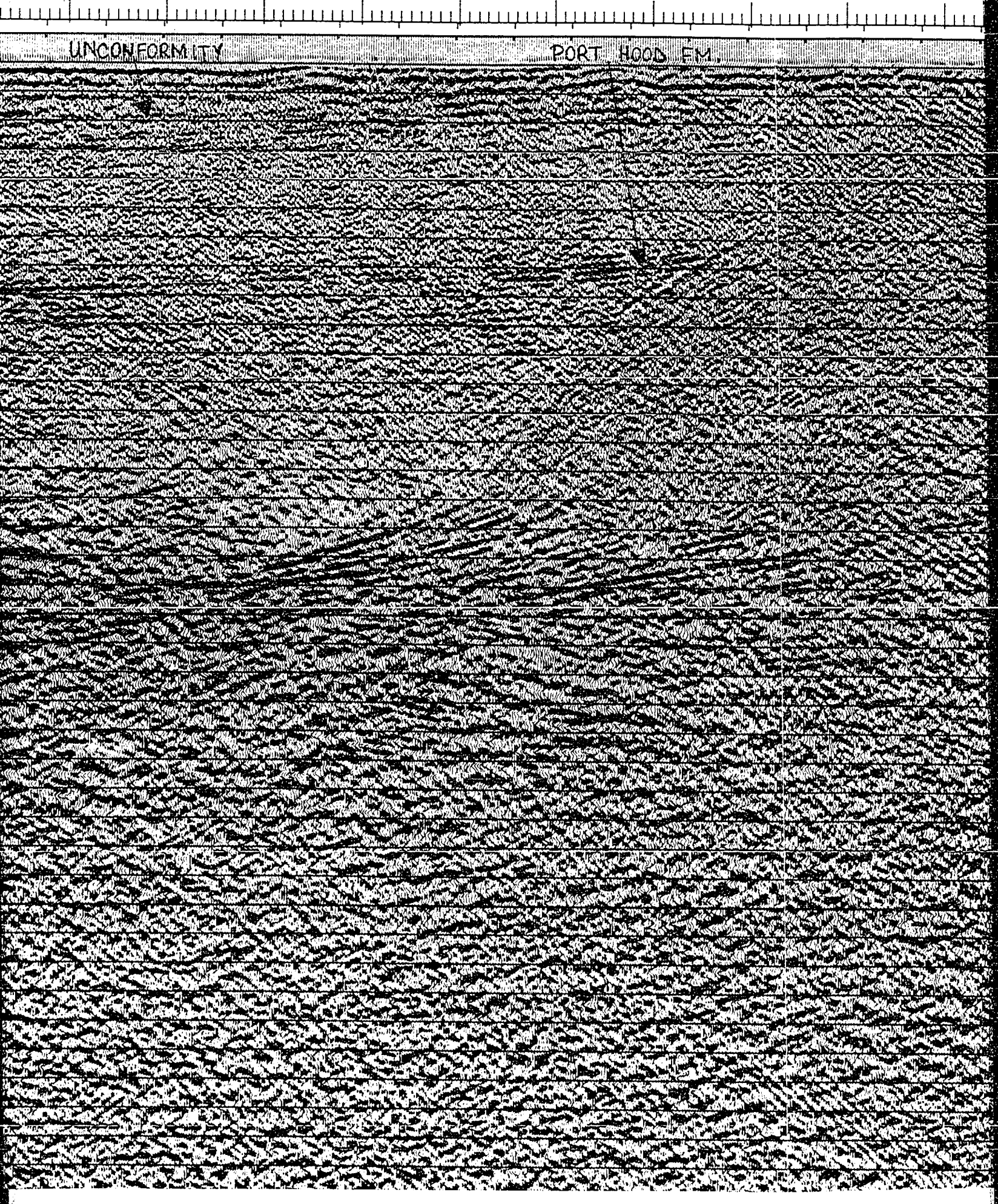
UNCONFORMITY
PORT HOOD FM.

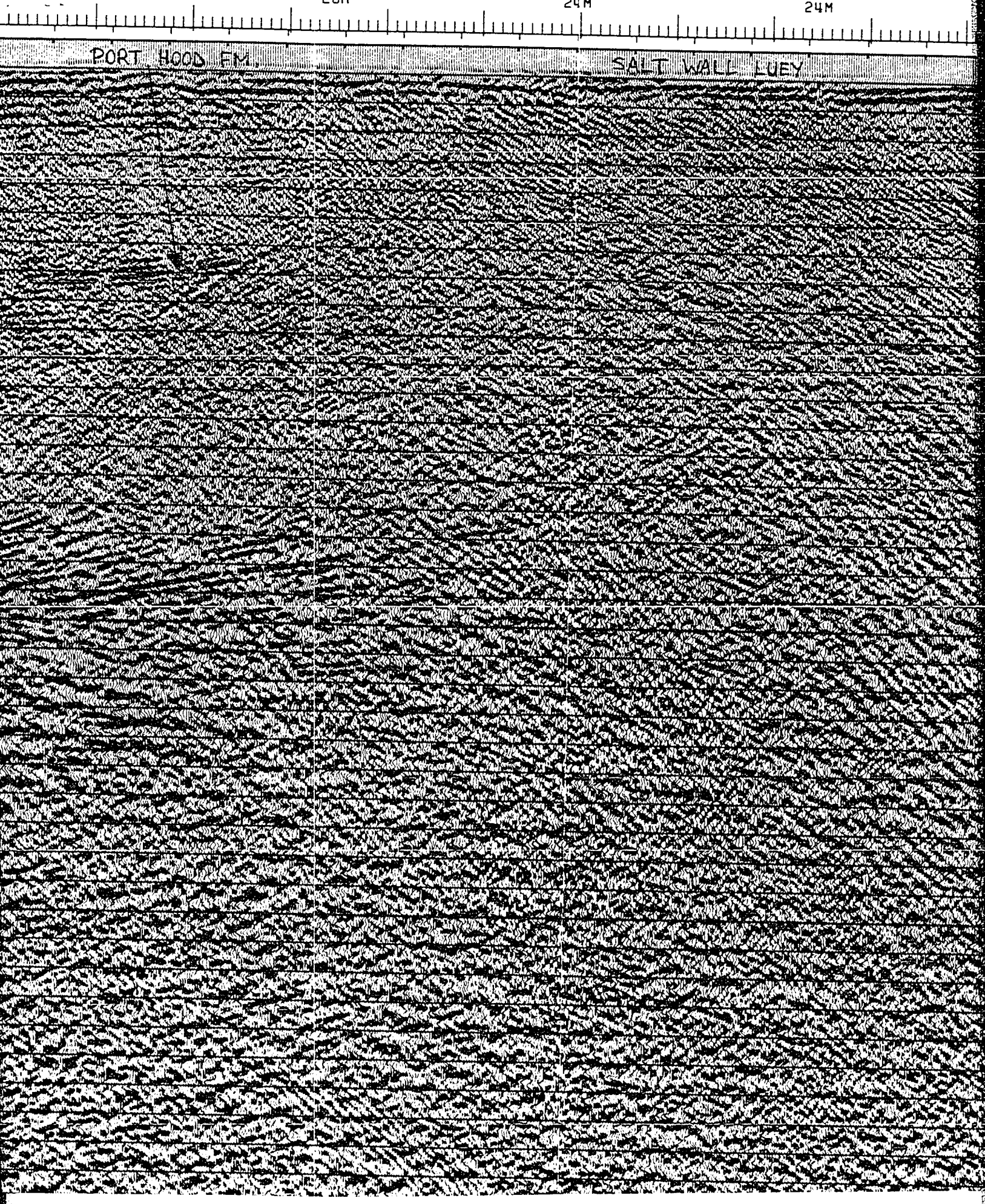
24M
24M
PORT HOOD FM.
SALT WALL LUEY

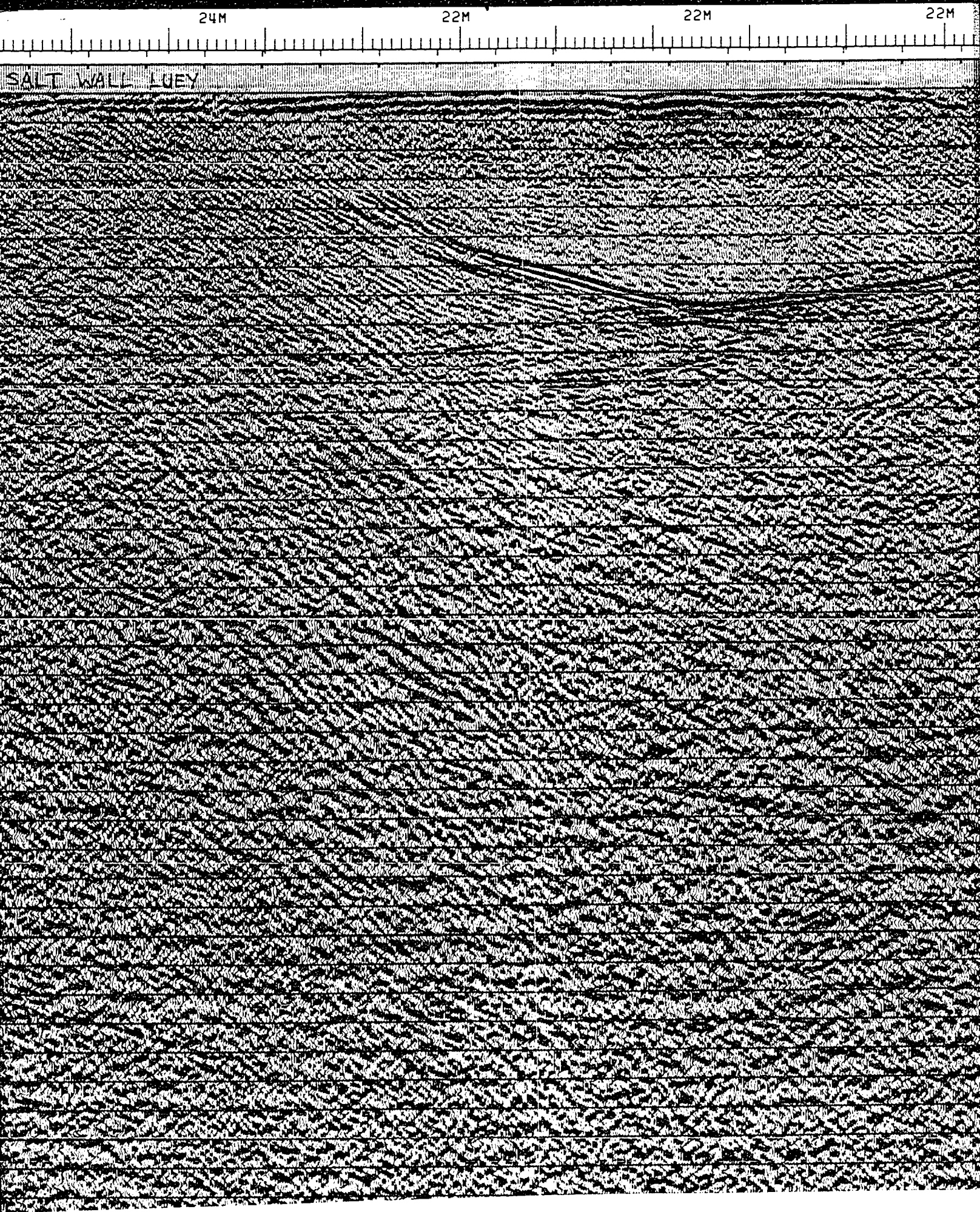
24M
22M
22M
22M
SALT WALL LUEY

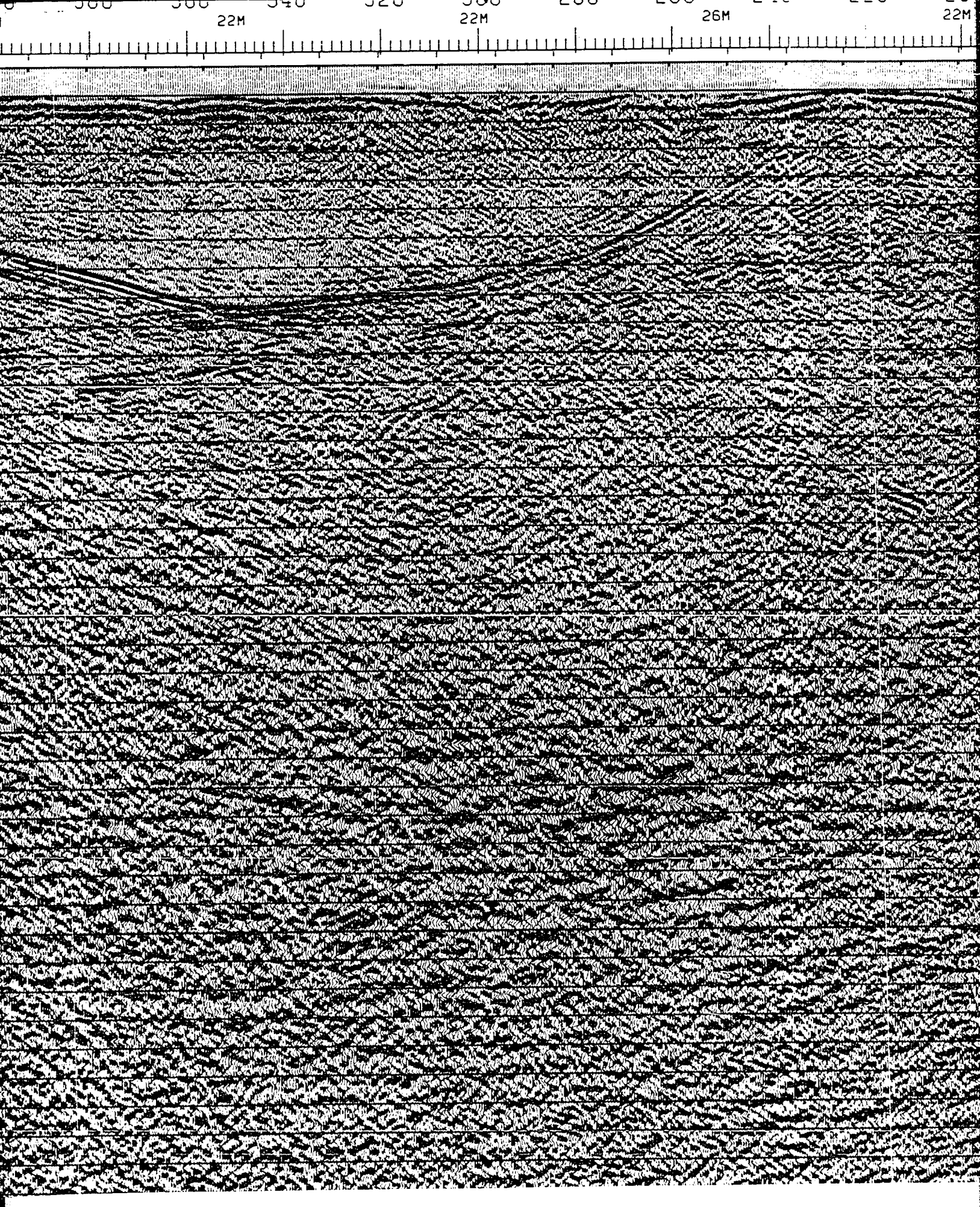
22M
22M
26M
22M

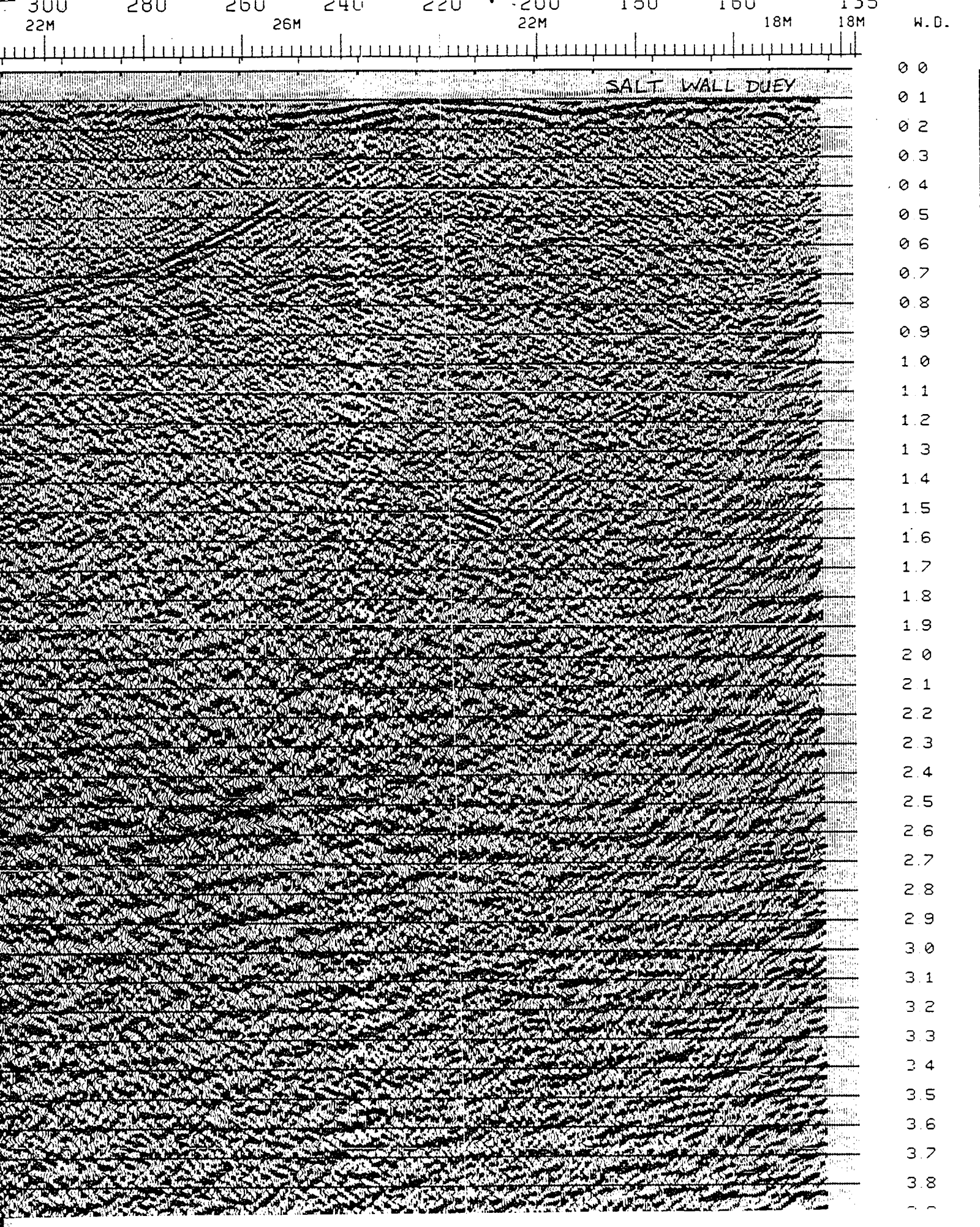
300
280
260
240
220
200
150
140
135
22M
26M
22M
18M
18M
W.D.
SALT WALL DUEY
0 0
0 1
0 2
0 3
0 4
0 5
0 6
0 7
0 8
0 9
1 0
1 1
1 2
1 3
1 4
1 5
1 6
1 7
1 8
1 9
2 0
2 1
2 2
2 3
2 4
2 5
2 6
2 7
2 8
2 9
3 0
3 1
3 2
3 3
3 4
3 5
3 6
3 7
3 8

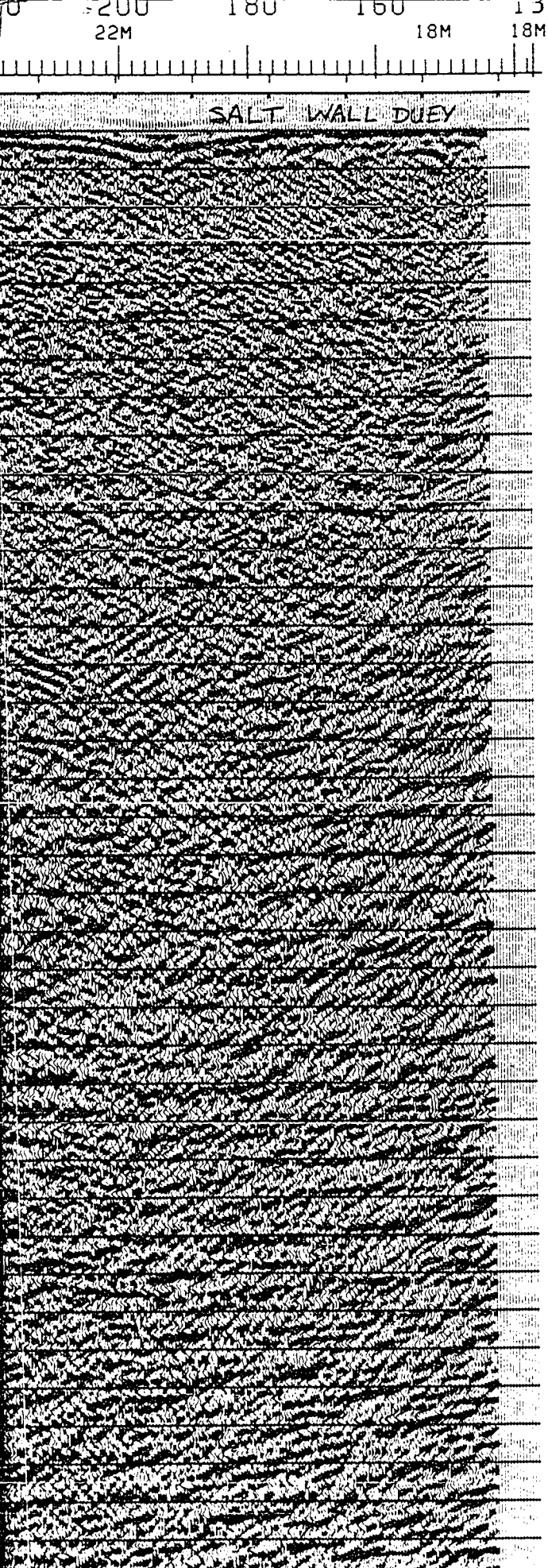

CHEVRON STANDARD L

AREA: NORTHUMBERLAND STRAIT

SHOT BY WESTERN GEOPHYSICAL COMPANY PARTY
PROCESSED BY WESTERN GEOPHYSICAL (CALGARY) GROUP

RECORDING DATA

SOURCE

ENERGY SOURCE	AIR GUNS
CHARGE SIZE	1050 CU.IN
NUMBER OF GUNS	15
GUN DEPTH	6 M
FIRING INTERVAL	27 M
SHOT POINT INTERVAL	27 M
DISTANCE OF SOURCE TO ANTENNA	47 M

INSTRUMENTS

SYSTEM	KILOSEIS
AMPLIFIER	INST. FLOATING
FILTER	L/9-H/450
SAMPLING INTERVAL	1 MS
RECORD LENGTH	5.0 SEC
FORMAT	SEG-D

CABLE

TYPE CABLE	STREAMER
CABLE LENGTH	2565 M
CABLE DEPTH	8 M
LEAD IN	187 M
GROUP INTERVAL	27 M
NUMBER OF GROUPS RECORDED	96
SPREAD	2752 M

ARRAY PARAMETERS

ROMS	7/21
CHANNELS PER ARRAY	8.50% OVERLAP
WEIGHTS	32.32.32.32.32
NUMBER OF DATA CHANNELS RECORDED	384
CHANNEL INTERVAL	6.67 M

PROCESSING SEQUENCE AND PARAMET

PROCESSING SAMPLING INTERVAL

1. SIGNATURE DECONVOLUTION
2. DECONVOLVED BEFORE STACK
   - WINDOW LENGTH 2 ZONES OF 2
   - LENGTH OPERATOR
   - PREDICTION DISTANCE
3. NMO STACK 4800 %
4. RELATIVE AMP. COMPENSATION
5. F-K DOMAIN FILTER
6. DECONVOLVED AFTER STACK
   - WINDOW LENGTH 2 ZONES OF 2
   - LENGTH OPERATOR
   - PREDICTION DISTANCE
7. FINITE DIFFERENCE MIGRATION
8. TIME VARIANT FILTER

TIME		L.C. (HZ)	H.C.
1.00	SEC	12	60
3.00	SEC	8	45
5.00	SEC	8	30

9. RMS GAIN (128-512 MS WINDOW)

47 M

LEGEND

CHEVRON STANDARD LTD.

AREA: NORTHUMBERLAND STRAIT

SHOT BY WESTERN GEOPHYSICAL COMPANY PARTY 127 JULY 1981
PROCESSED BY WESTERN GEOPHYSICAL (CALGARY) GROUP 6 OCT 1981

RECORDING DATA

SOURCE

ENERGY SOURCE	AIR GUNS
CHARGE SIZE	1050 CU.IN
NUMBER OF GUNS	15
GUN DEPTH	6 M
FIRING INTERVAL	27 M
SHOT POINT INTERVAL	27 M
DISTANCE OF SOURCE TO ANTENNA	47 M

INSTRUMENTS

SYSTEM	KILOSEIS
AMPLIFIER	INST. FLOATING POINT
FILTER	L/9-H/450
SAMPLING INTERVAL	1 MS
RECORD LENGTH	5.0 SEC
FORMAT	SEG-D

CABLE

TYPE CABLE	STREAMER
CABLE LENGTH	2565 M
CABLE DEPTH	8 M
LEAD IN	187 M
GROUP INTERVAL	27 M
NUMBER OF GROUPS RECORDED	96
SPREAD	2752 M

ARRAY PARAMETERS

ROMS	7/21
CHANNELS PER ARRAY	8.50% OVERLAP
WEIGHTS	32.32.32.32.32.32.32.32
NUMBER OF DATA CHANNELS RECORDED	384
CHANNEL INTERVAL	6.67 M

PROCESSING SEQUENCE AND PARAMETERS

PROCESSING SAMPLING INTERVAL 4 MS

1. SIGNATURE DECONVOLUTION
2. DECONVOLVED BEFORE STACK
   - WINDOW LENGTH 2 ZONES OF 2500 MS
   - LENGTH OPERATOR 280 MS
   - PREDICTION DISTANCE 4 MS
3. NMO STACK 4800 %
4. RELATIVE AMP. COMPENSATION
5. F-K DOMAIN FILTER
6. DECONVOLVED AFTER STACK
   - WINDOW LENGTH 2 ZONES OF 2500 MS
   - LENGTH OPERATOR 300 MS
   - PREDICTION DISTANCE 20 MS
7. FINITE DIFFERENCE MIGRATION
8. TIME VARIANT FILTER

TIME		L.C. (HZ)	H.C.
1.00	SEC	12	60
3.00	SEC	8	45
5.00	SEC	8	30

9. RMS GAIN (128-512 MS WINDOW)

47 M

LEGEND

SOUTHEAST

ON STANDARD LTD.

A: NORTHUMBERLAND STRAIT

PHYSICAL COMPANY PARTY 127 JULY 1981
N GEOPHYSICAL (CALGARY) GROUP 6 OCT 1981

RECORDING DATA

SOURCE
AIR GUNS
1050 CU.IN
15
6 M
27 M
27 M
TO ANTENNA 47 M

INSTRUMENTS
KILOSEIS
INST. FLOATING POINT
L/9-H/450
1 MS
5.0 SEC
SEG-D

CABLE
STREAMER
2565 M
8 M
187 M
27 M
CORDED 96
2752 M

ARRAY PARAMETERS
7/21
8.50% OVERLAP
32.32.32.32.32.32.32.32
NELS RECORDED 384
6.67 M

SING SEQUENCE AND PARAMETERS

SSING SAMPLING INTERVAL 4 MS
TURE DECONVOLUTION
VOLVED BEFORE STACK
W LENGTH 2 ZONES OF 2500 MS
H OPERATOR 280 MS
CTION DISTANCE 4 MS
TACK 4800 %
IVE AMP. COMPENSATION
OMAIN FILTER
VOLVED AFTER STACK
W LENGTH 2 ZONES OF 2500 MS
H OPERATOR 300 MS
CTION DISTANCE 20 MS
E DIFFERENCE MIGRATION
VARIANT FILTER

TIME	L.C. (HZ)	H.C.
0 SEC	12	60
0 SEC	8	45
0 SEC	8	30

AIN (128-512 MS WINDOW)

LEGEND

NO: 8624 C4 9E LINE NO: 81

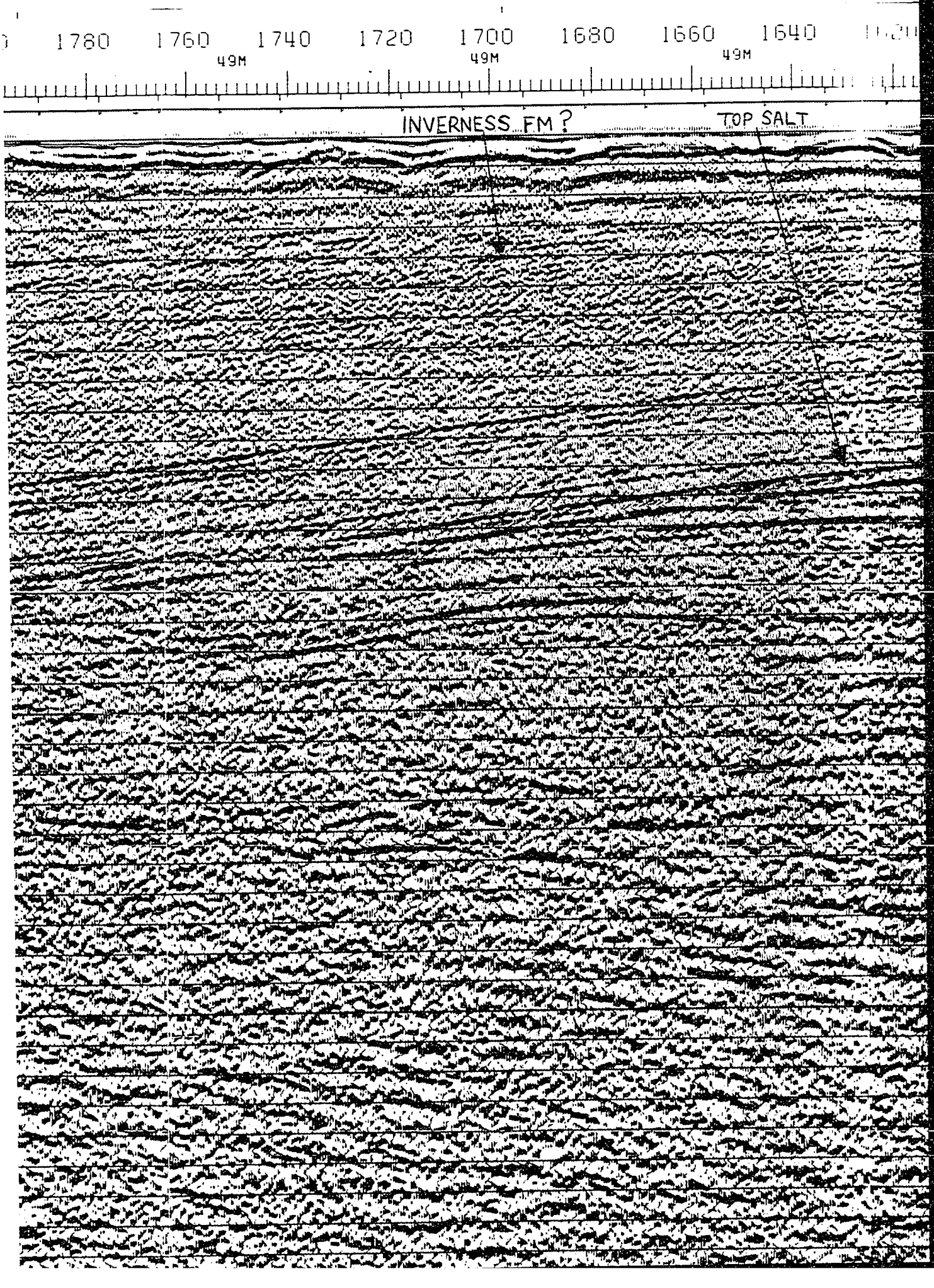
1780
1760
1740
1720
1700
1680
1660
1640
49M
49M
49M
INVERNESS FM ?
TOP SALT

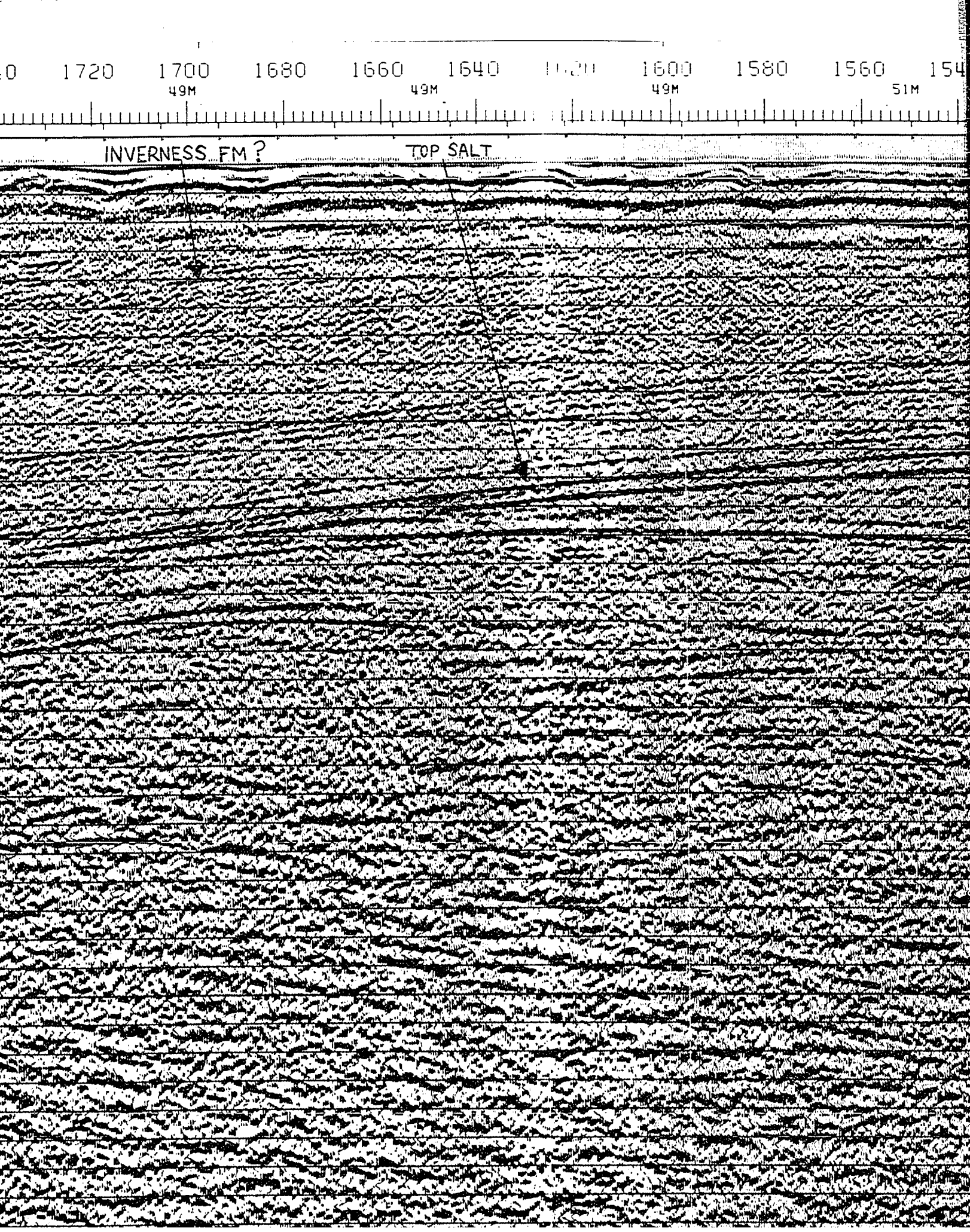
1720
1700
1680
1660
1640
1600
1580
1560
49M
49M
49M
51M
INVERNESS FM ?
TOP SALT

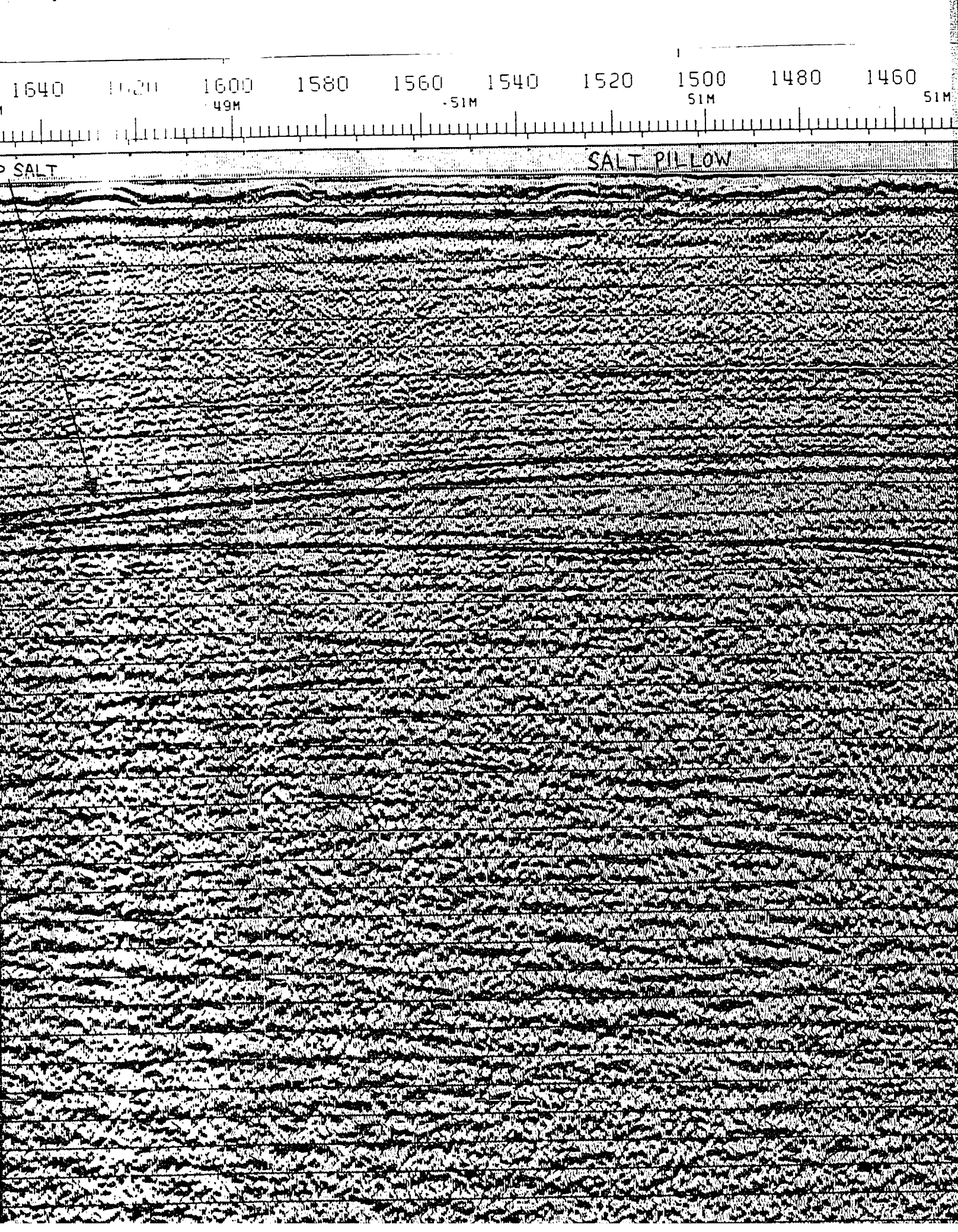
1640
1600
49M
1580
1560
-51M
1540
1520
1500
51M
1480
1460
51M
SALT
SALT PILLOW

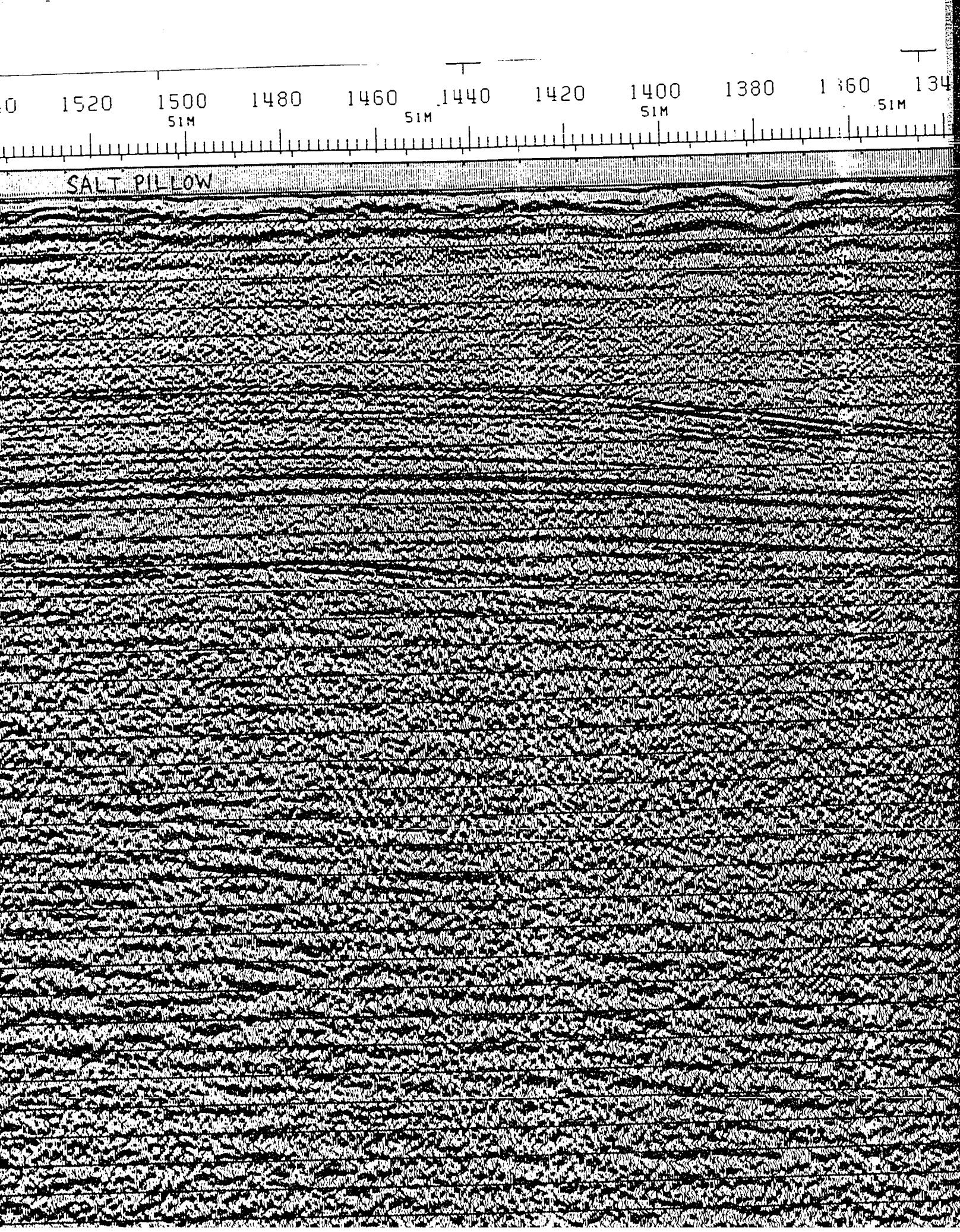
1520
1500
SIM
1480
1460
1440
SIM
1420
1400
SIM
1380
SIM
SALT PILLOW

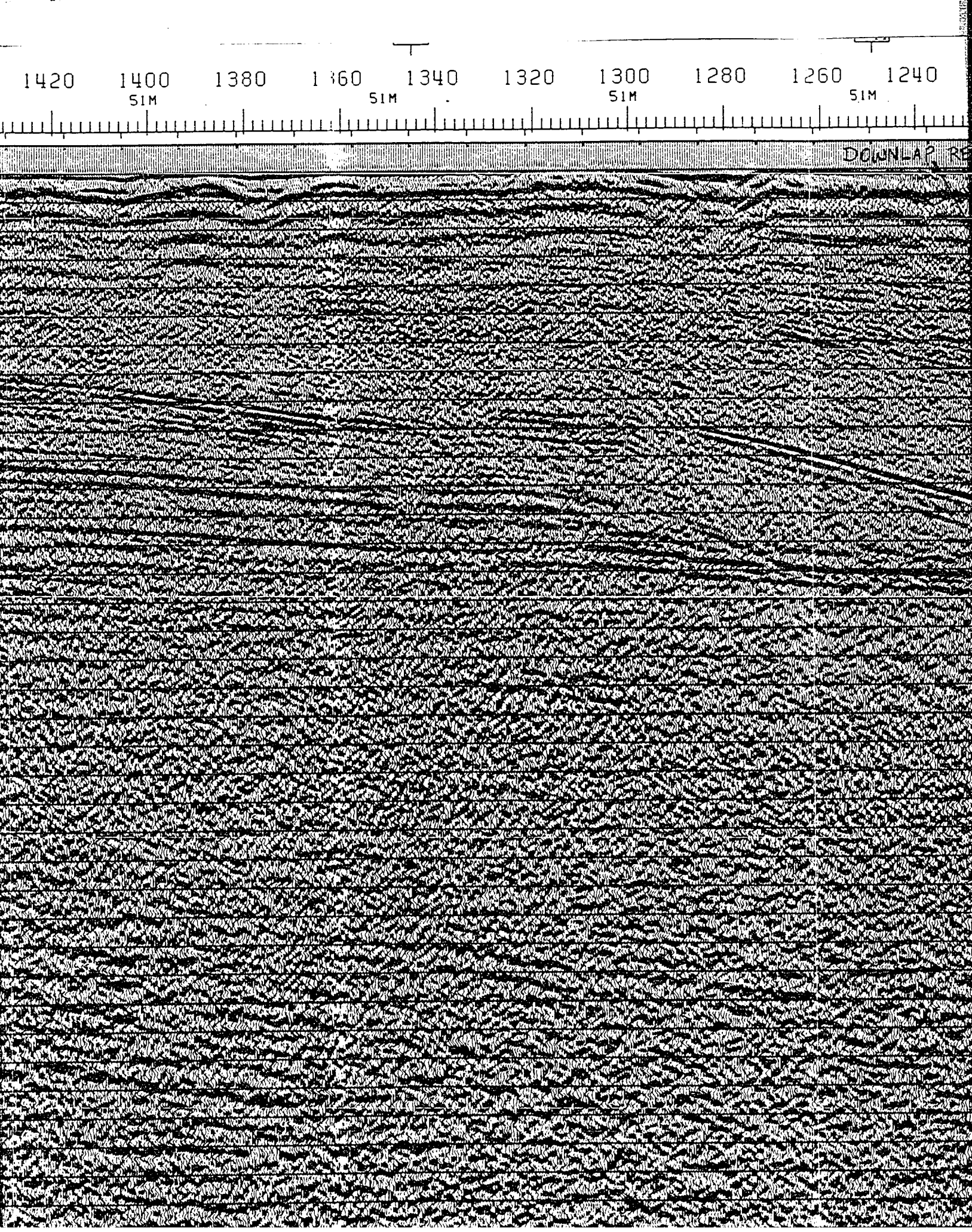
1420
1400
1380
1360
1340
1320
1300
1280
1260
1240
5IM
5IM
5IM
5IM
DOWNLAP RE

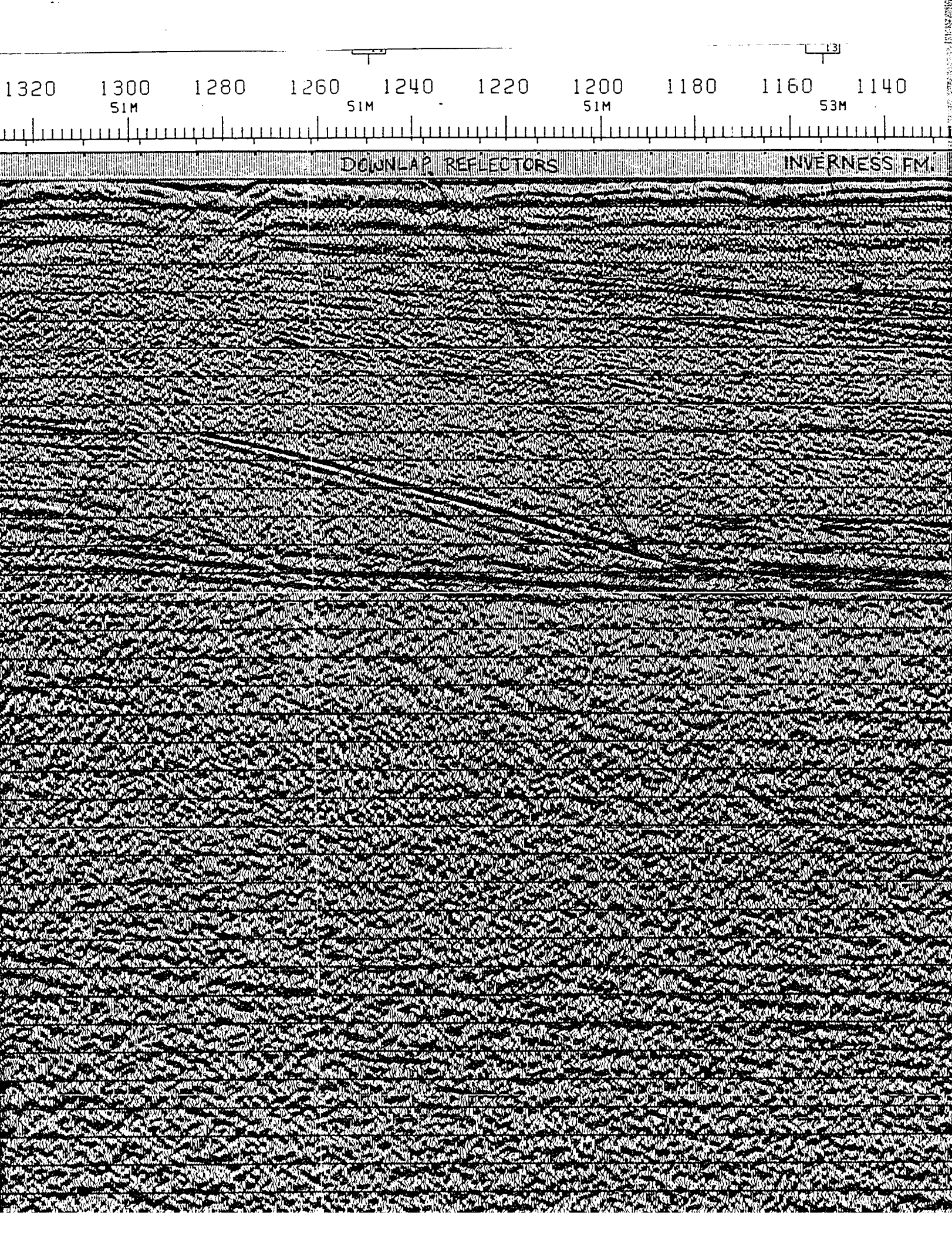
1320
1300
1280
1260
1240
1220
1200
1180
1160
1140
51M
51M
51M
53M
DOWNLAP REFLECTORS
INVERNESS FM.

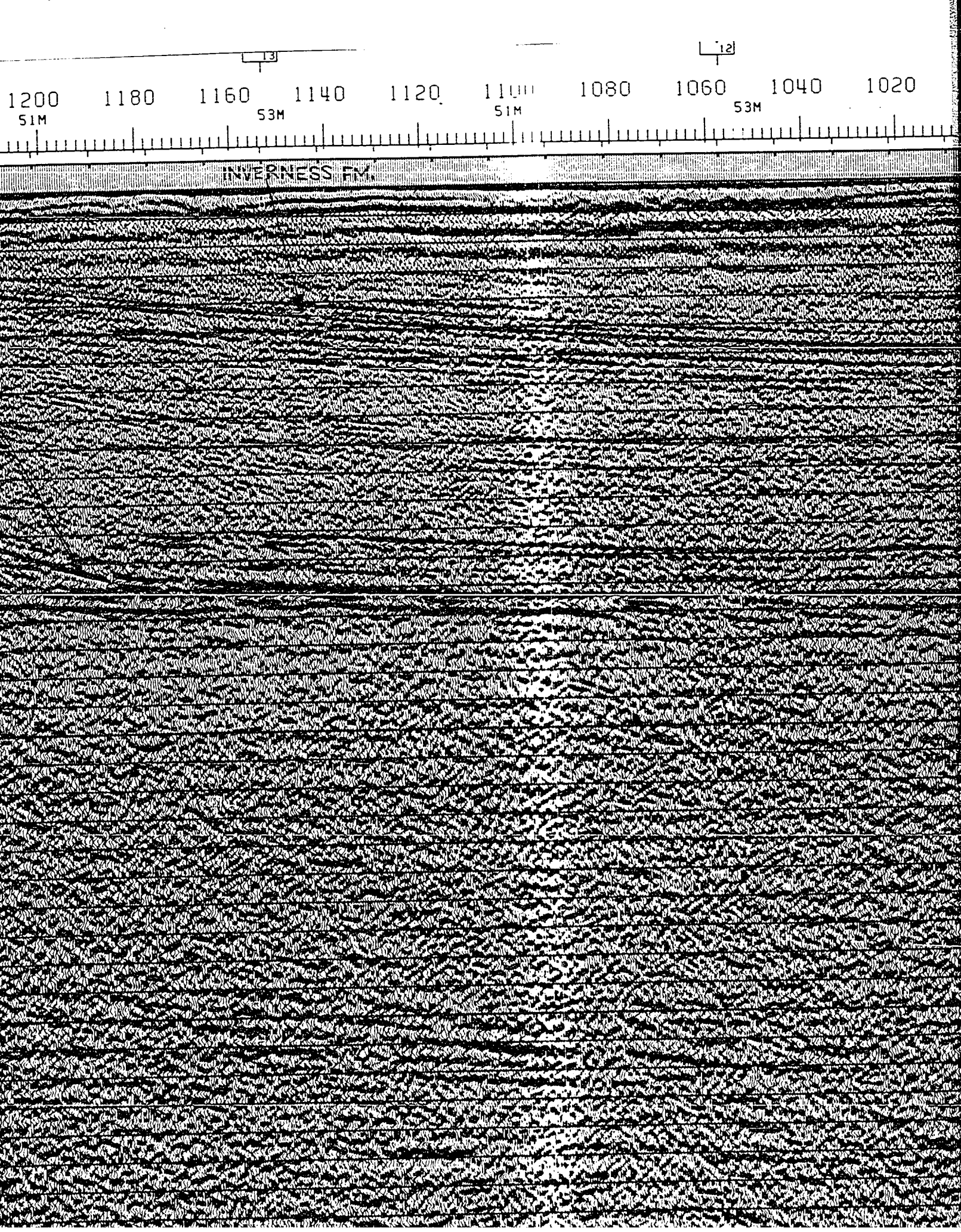
13
12
1200
1180
1160
1140
1120
1100
1080
1060
1040
1020
S1M
S3M
S1M
S3M
INVERNESS FM.

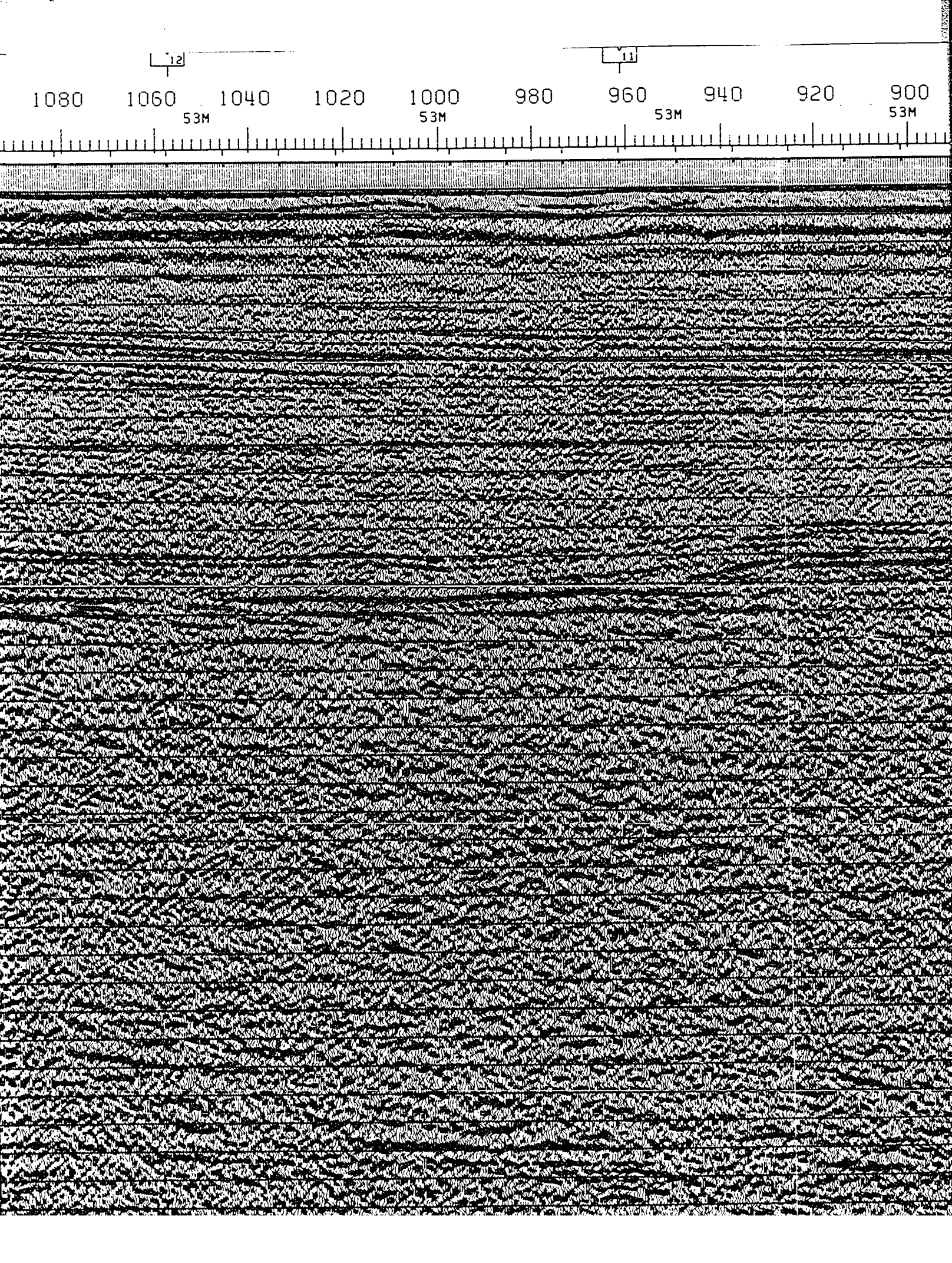
12
11
1080
1060
1040
1020
1000
980
960
940
920
900
53M
53M
53M
53M

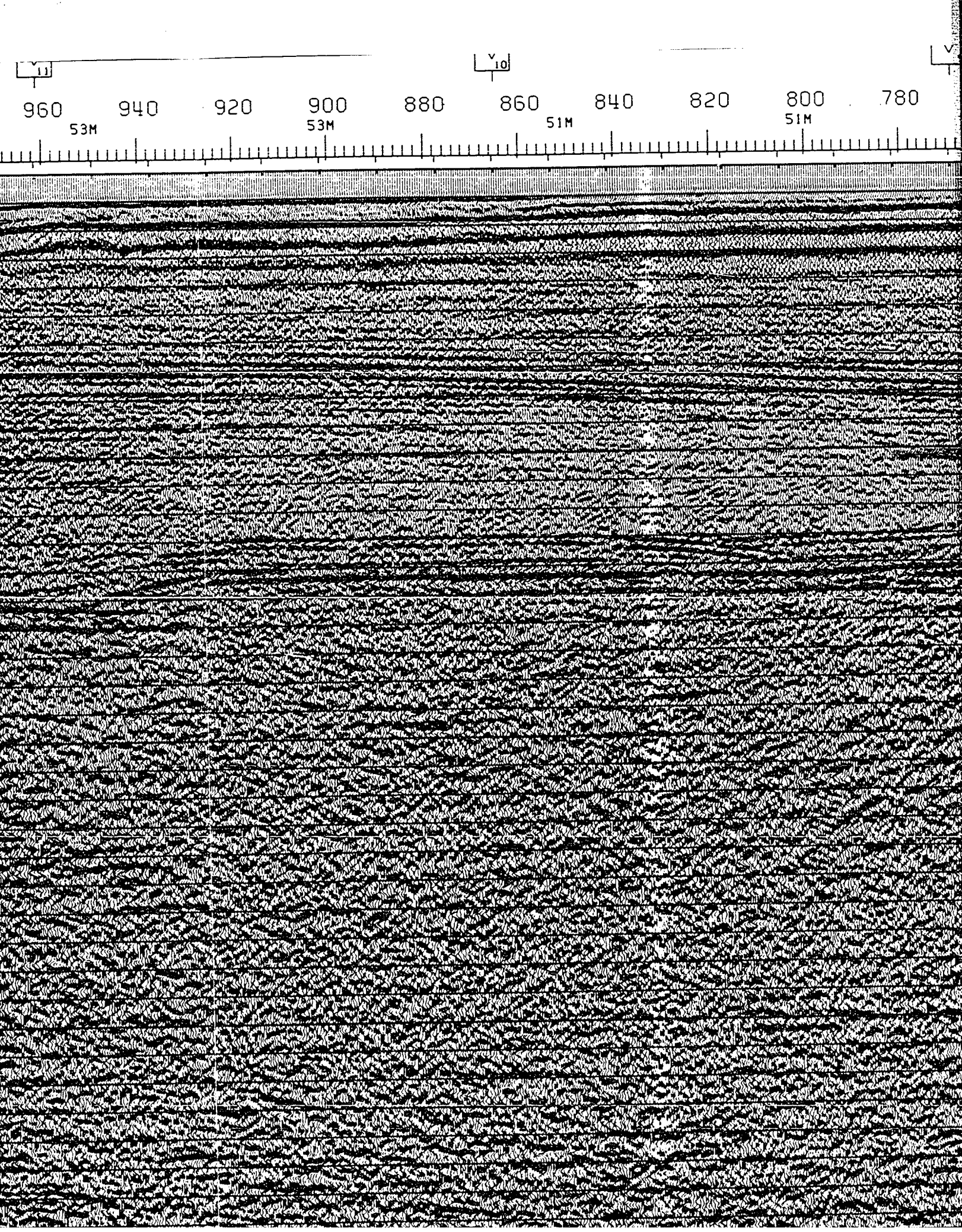
Y11
Y10
960
940
920
900
880
860
840
820
800
780
53M
53M
51M
51M

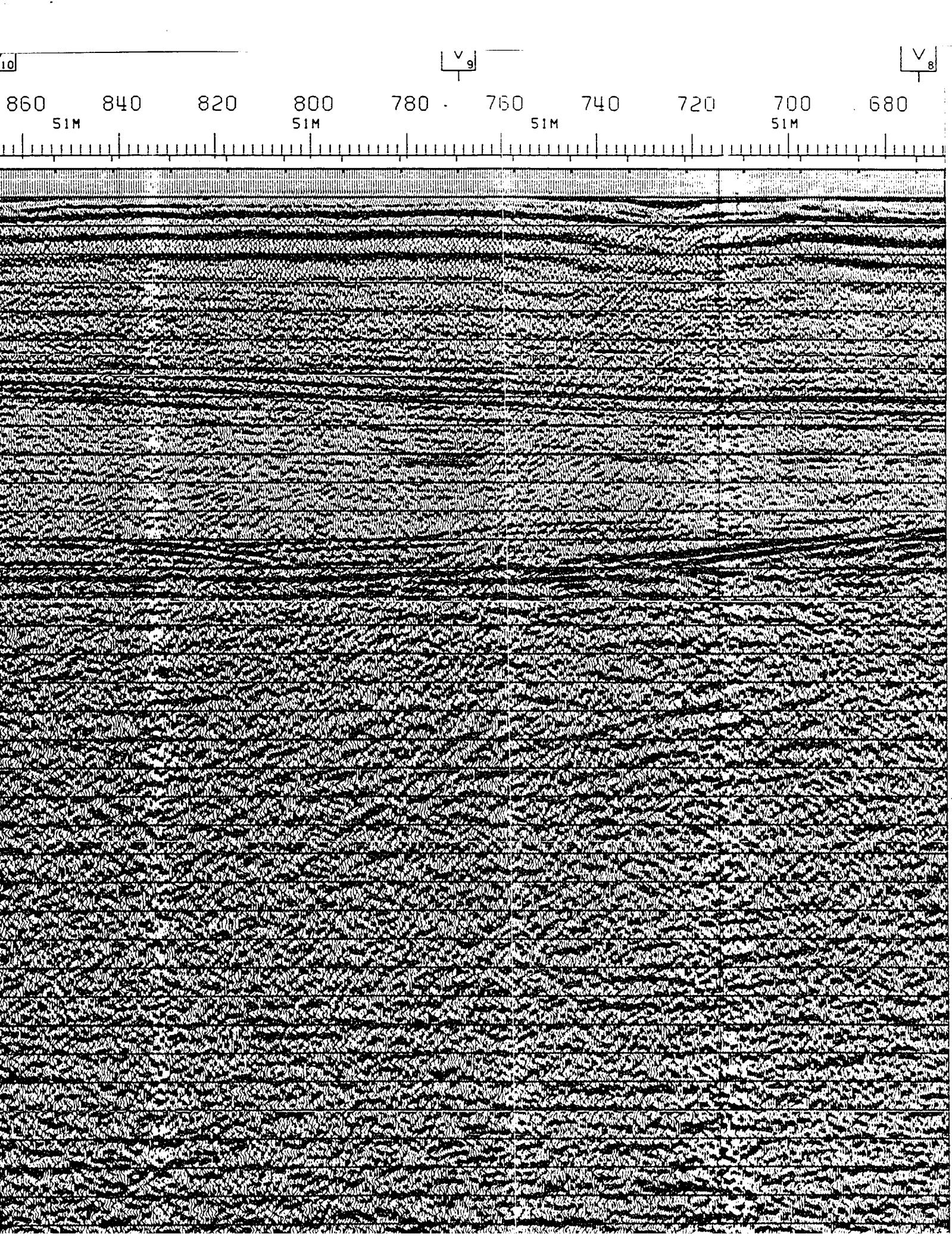
10
V 9
V 8
860
840
820
800
780
760
740
720
700
680
51M
51M
51M
51M

16

PROJ NO: 8824 C4 9E LINE

INVERNESS FM.

PORT HOOD FM.

END OF GILLIS FAN

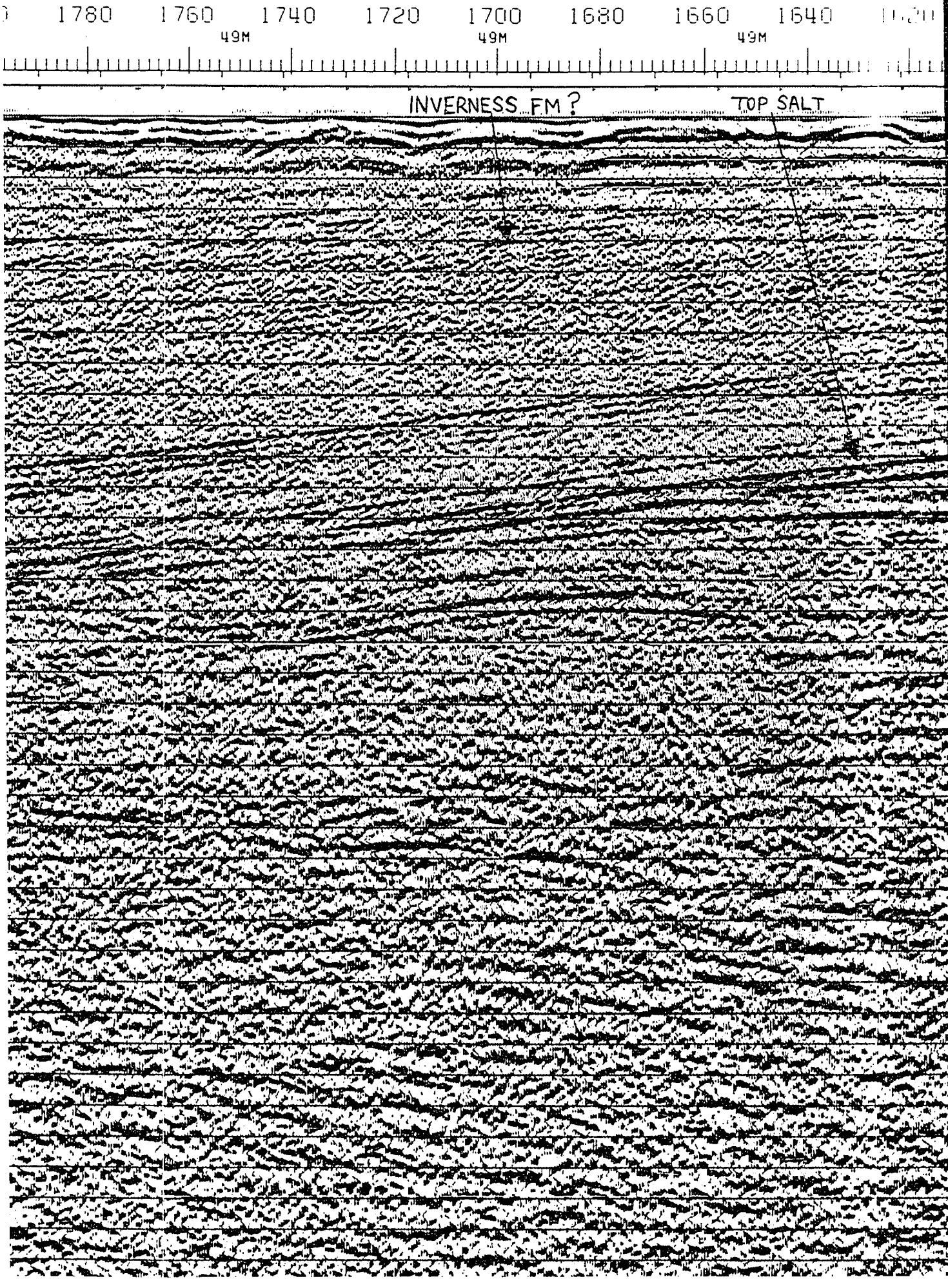
1780
1760
1740
1720
1700
1680
1660
1640
49M
49M
49M
INVERNESS FM ?
TOP SALT

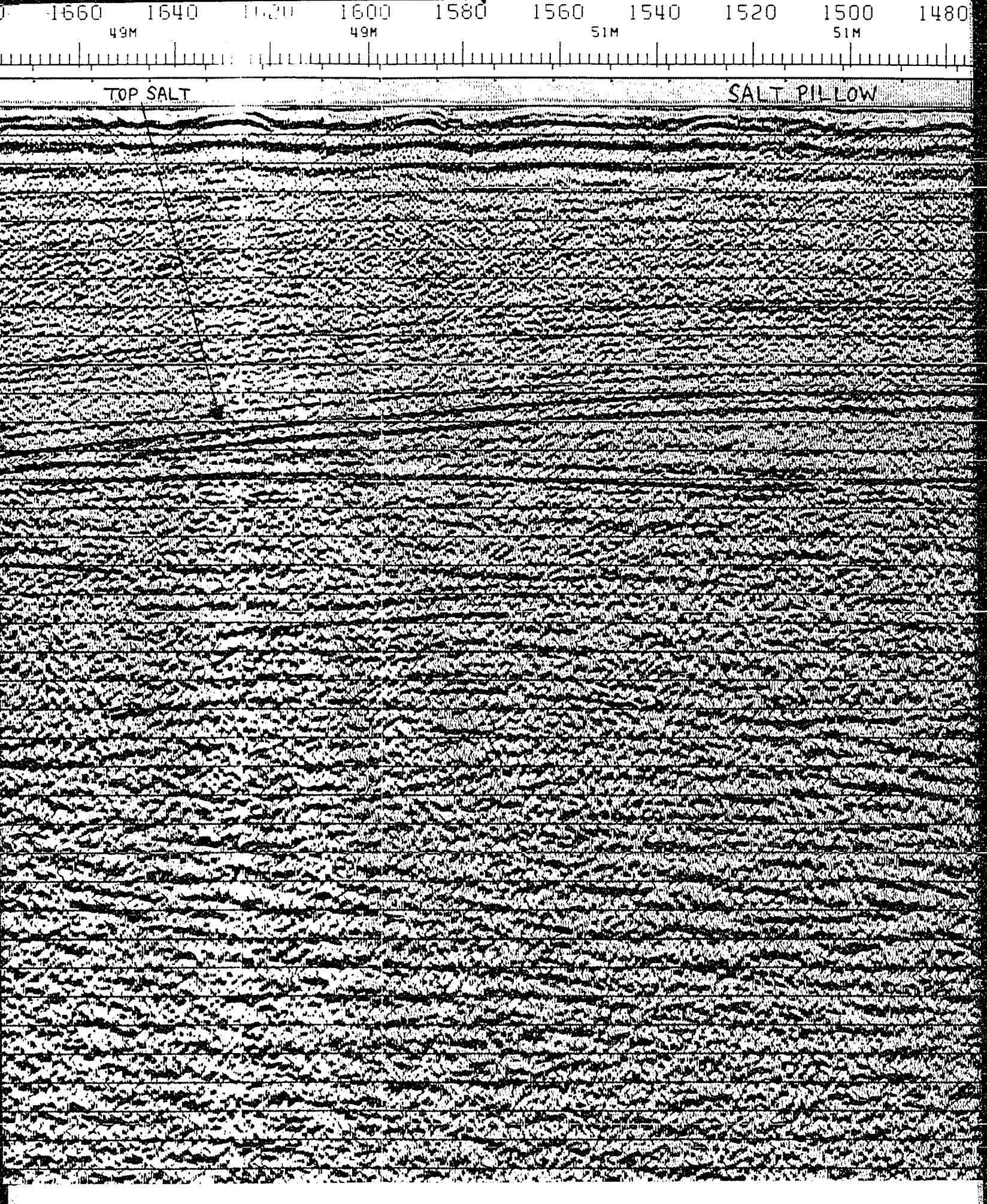
1660
1640
1600
1580
1560
1540
1520
1500
1480
49M
49M
51M
51M
TOP SALT
SALT PILLOW

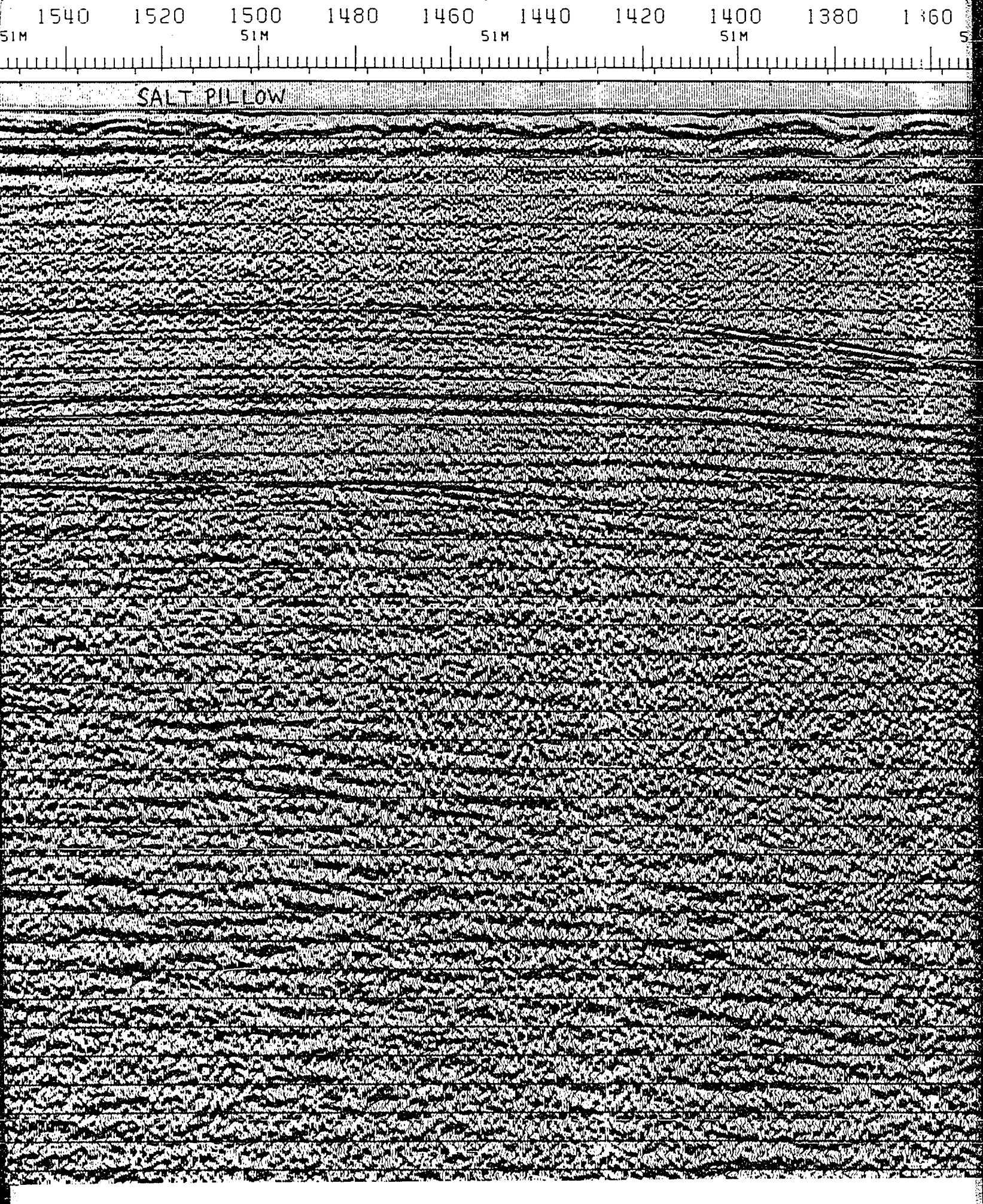
1540
1520
1500
1480
1460
1440
1420
1400
1380
SIM
SIM
SIM
SIM
SALT PILLOW

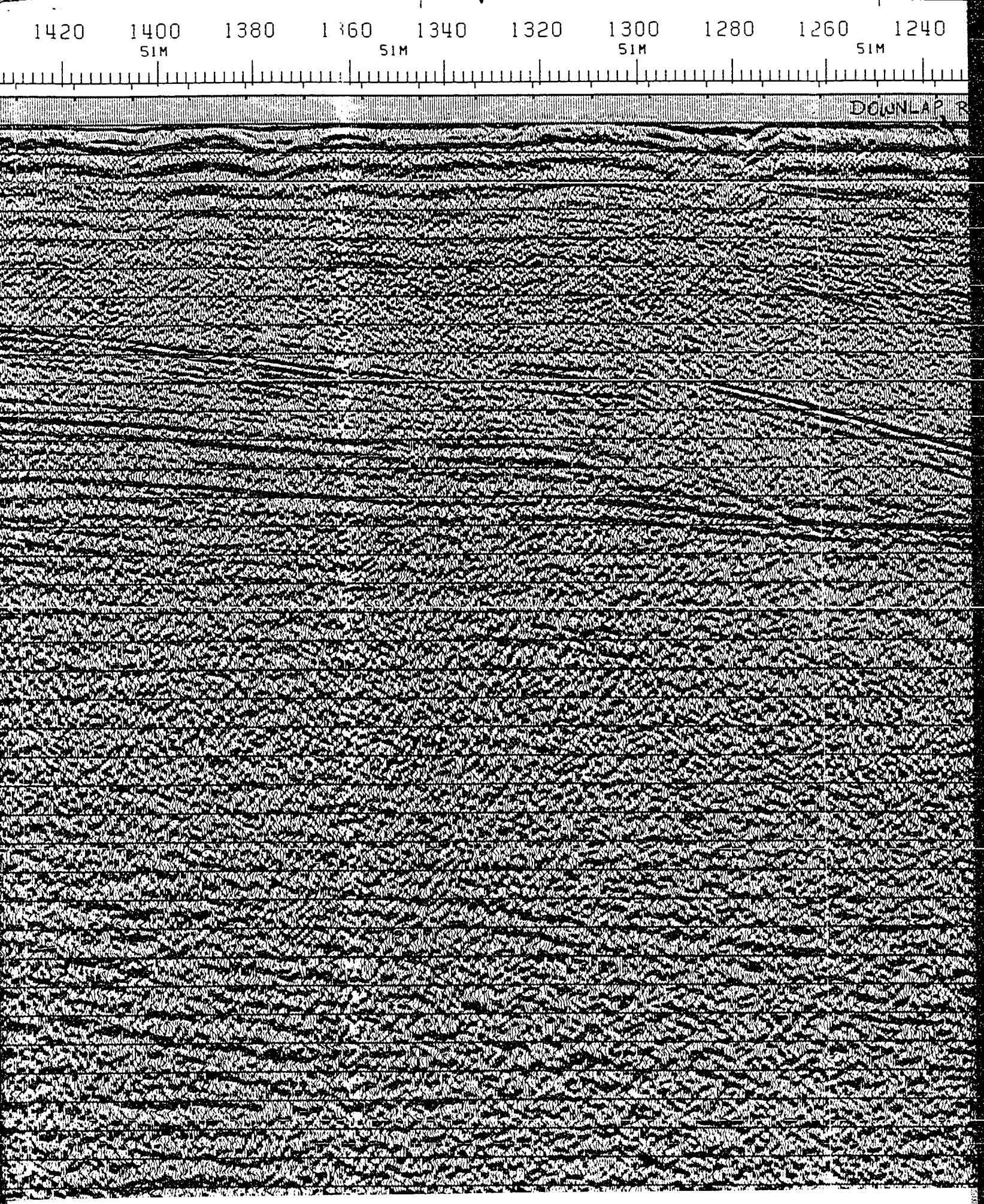
1420
1400
1380
1360
1340
1320
1300
1280
1260
1240
SIM
SIM
SIM
SIM
DOWNLAP R

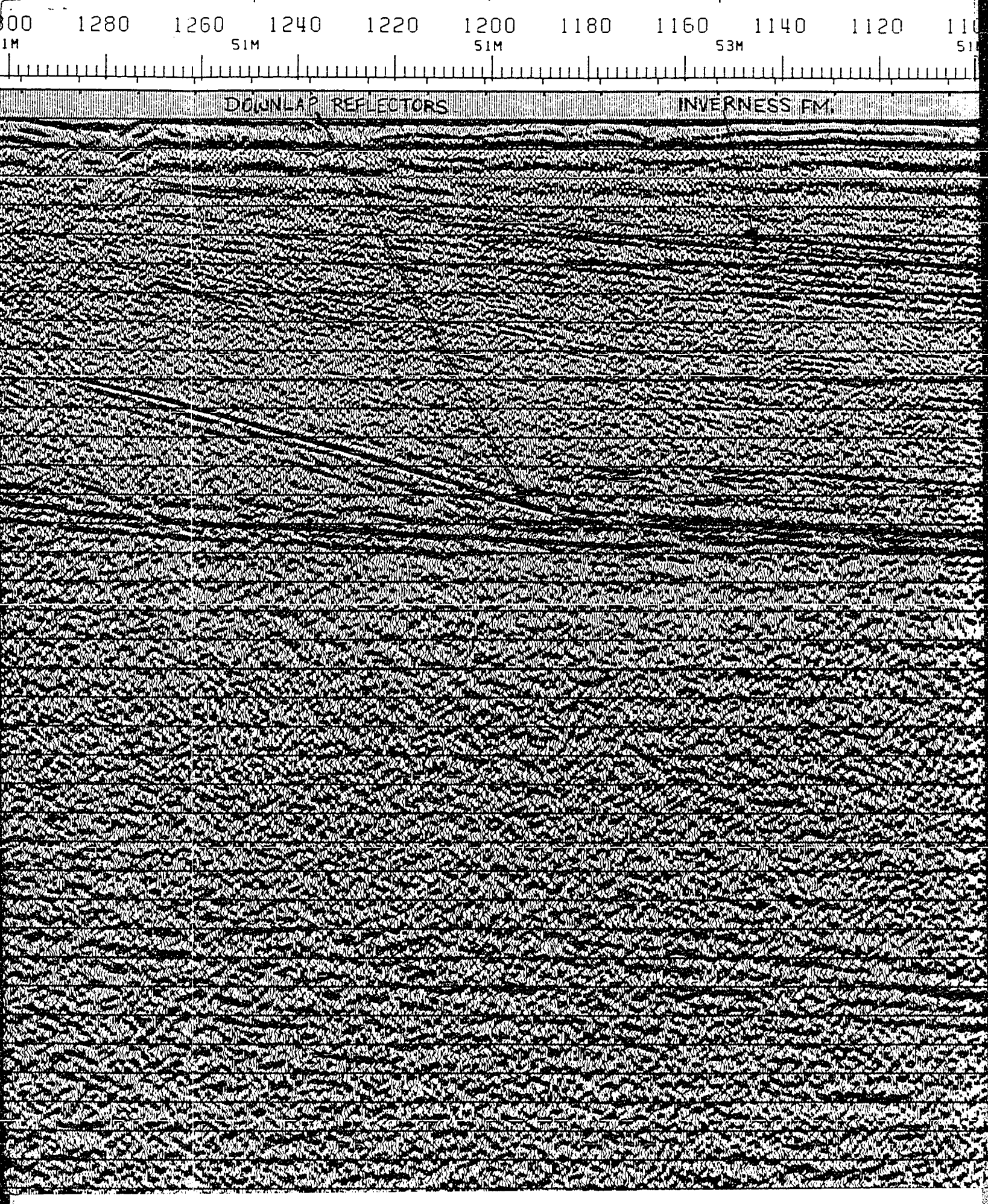
1300 1280 1260 1240 1220 1200 1180 1160 1140 1120 11
51M 51M 53M
DOWNLAP REFLECTORS
INVERNESS FM.

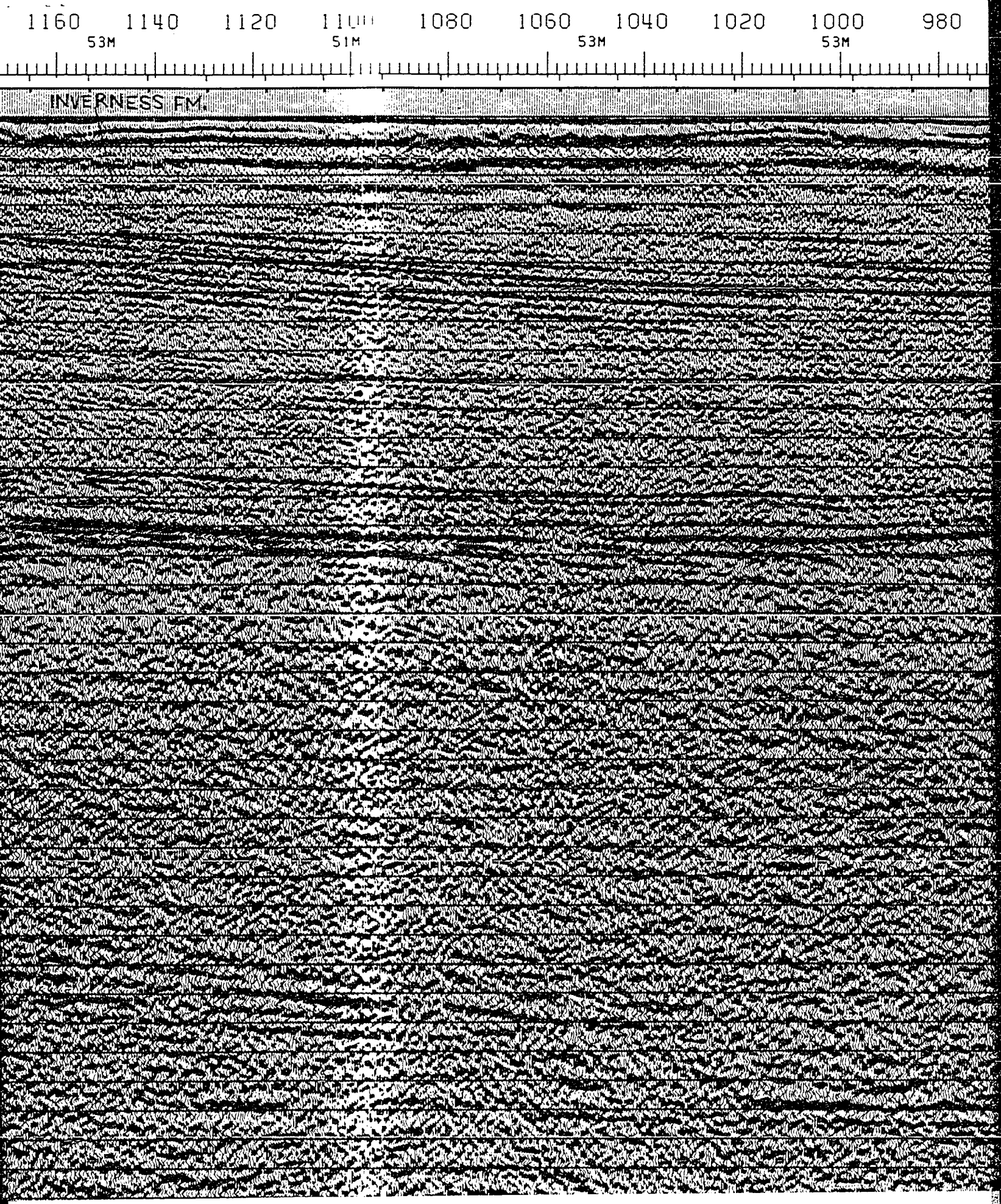
1160
1140
1120
1100
1080
1060
1040
1020
1000
980
53M
51M
53M
53M
INVERNESS FM.

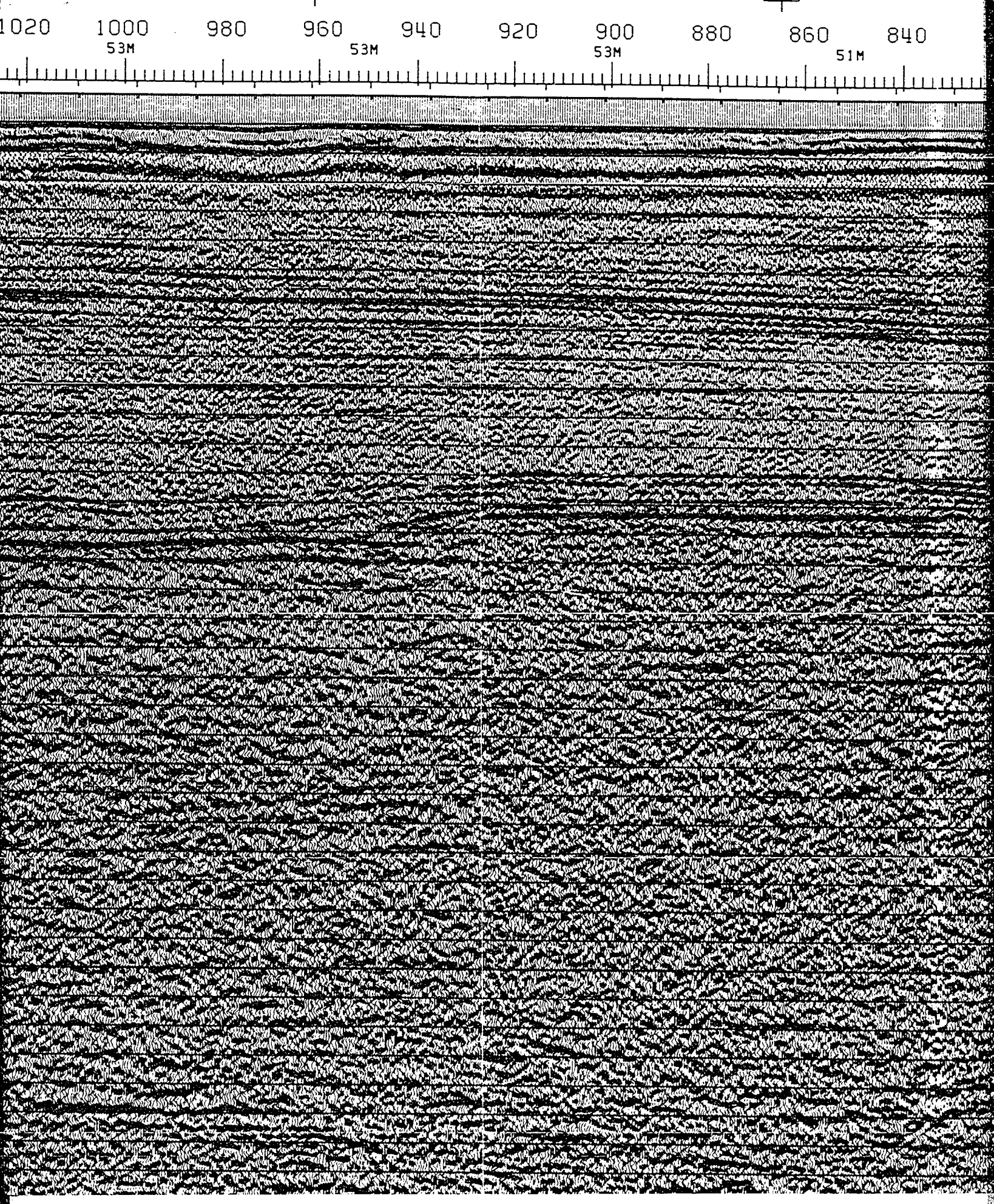
1020
1000
980
960
940
920
900
880
860
840
53M
53M
53M
51M

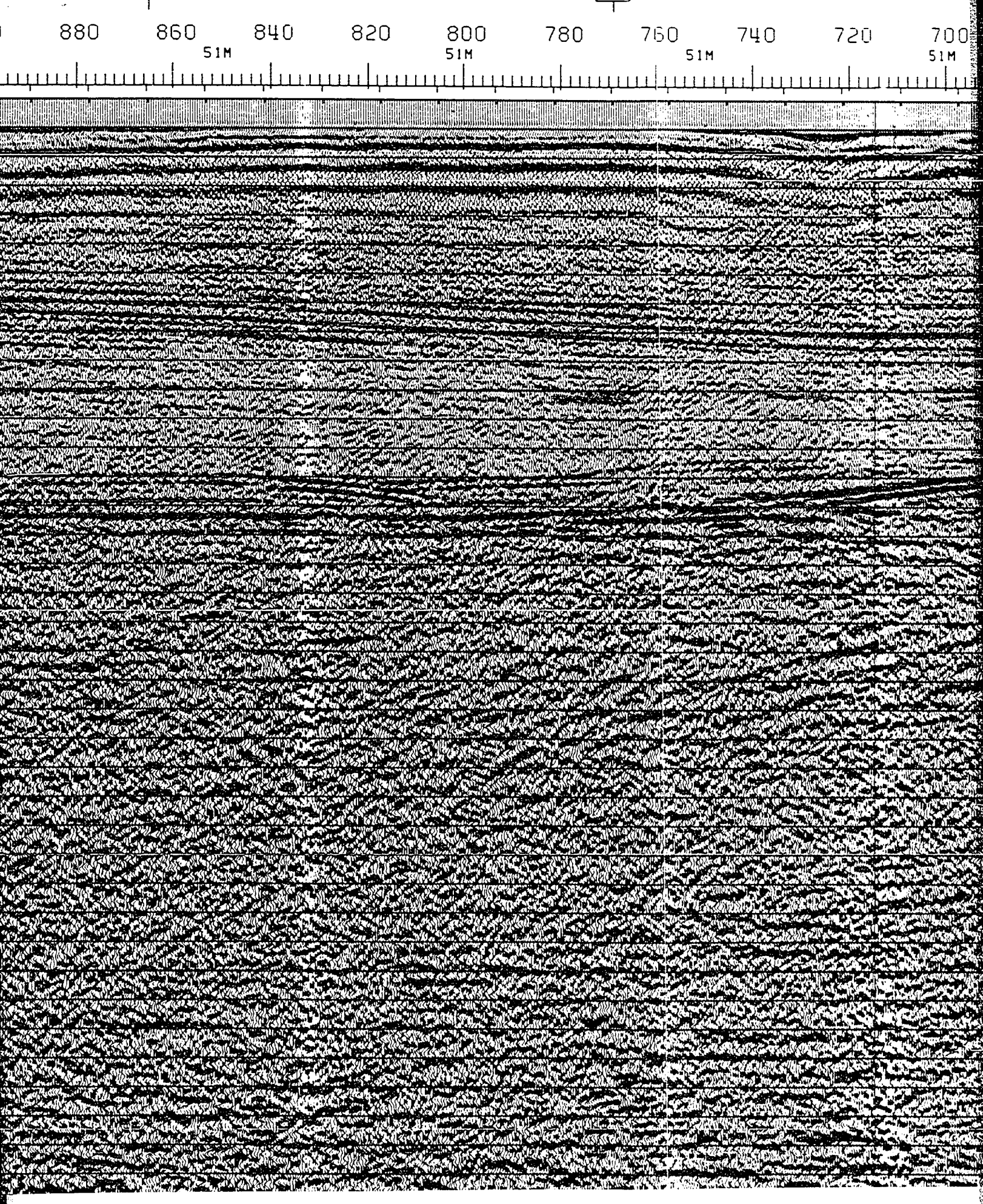
880
860
840
820
800
780
760
740
720
700
51M
51M
51M
51M

16

INVERNESS FM.

PORT HOOD FM.

END OF GILLIS FAN

PROJ. NO: 8824 C4 9E LINE

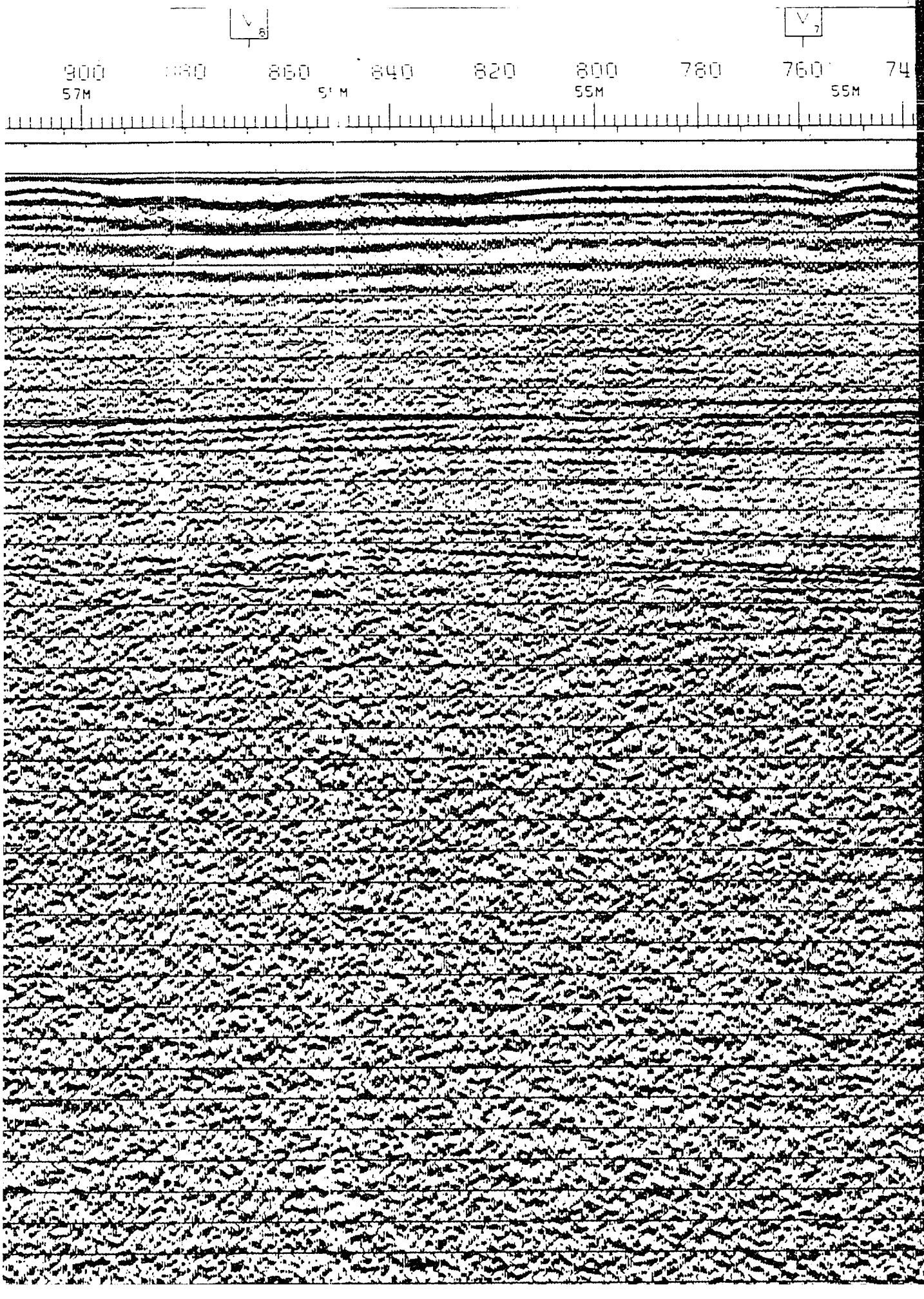
900
880
860
840
820
800
780
760
740
57M
55M
55M

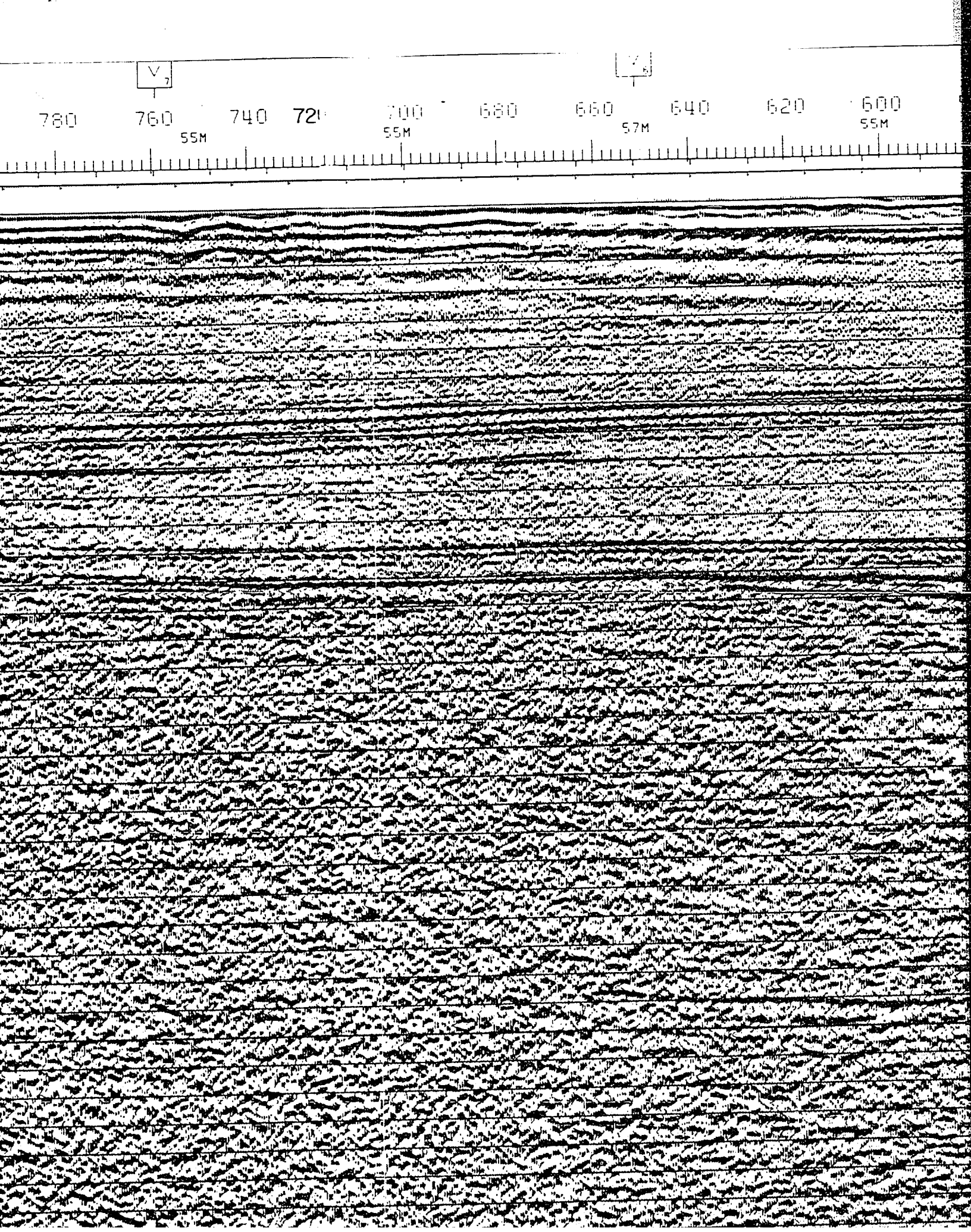
780
760
740
720
700
680
660
640
620
600
55M
55M
57M
55M

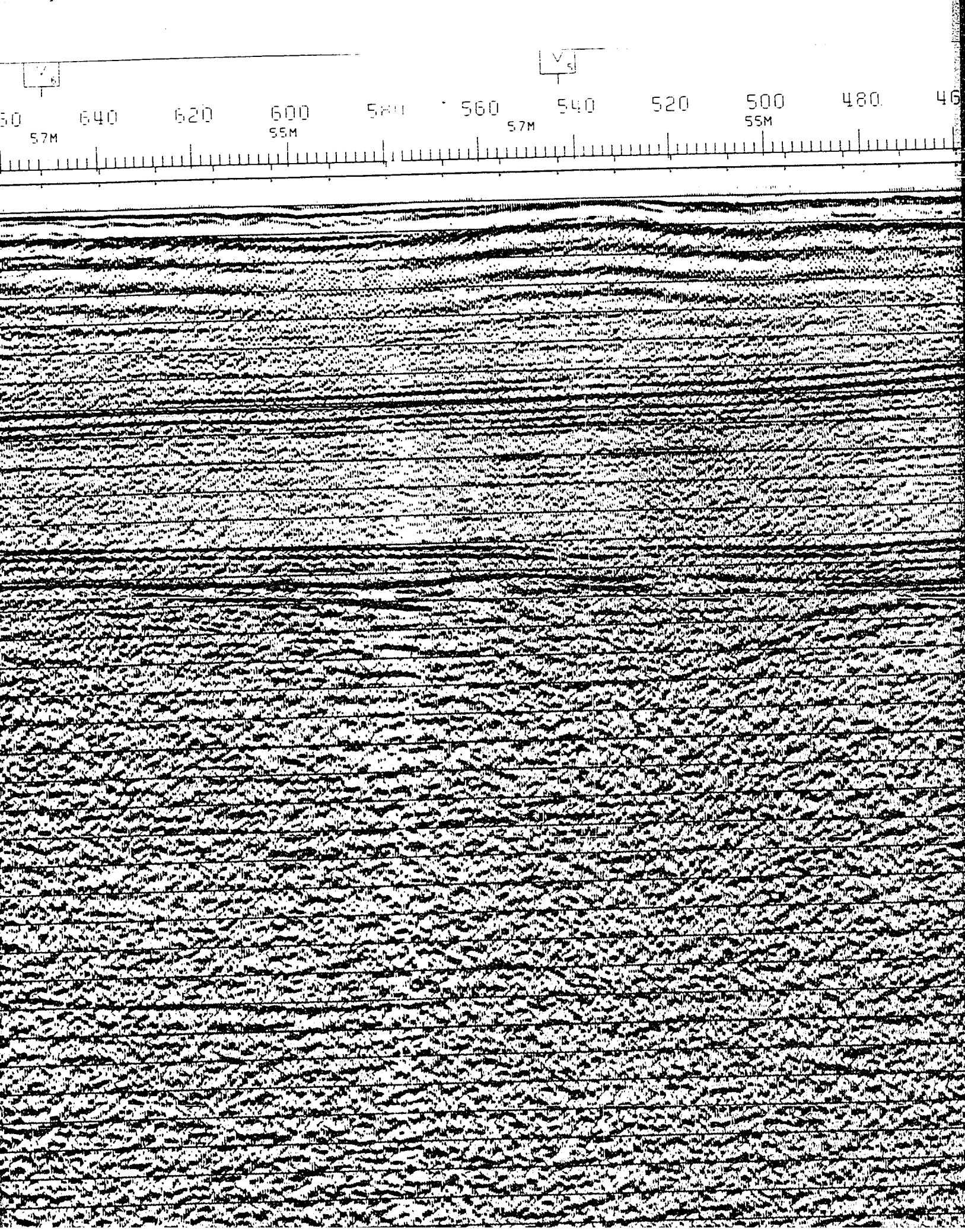
V6
V5
660
640
620
600
580
560
540
520
500
480
460
57M
55M
57M
55M

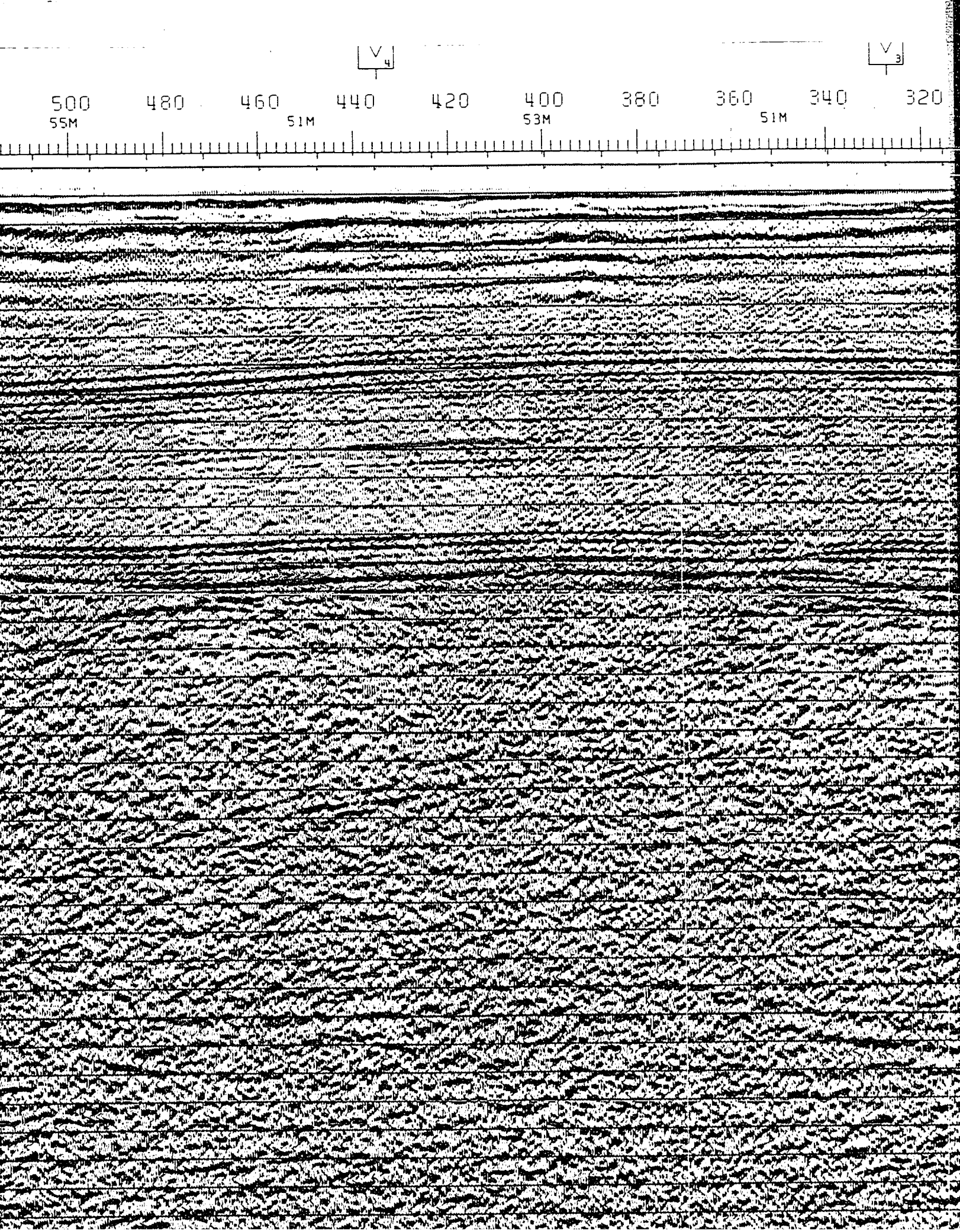
V4
V3
500
480
460
440
420
400
380
360
340
320
55M
51M
53M
51M

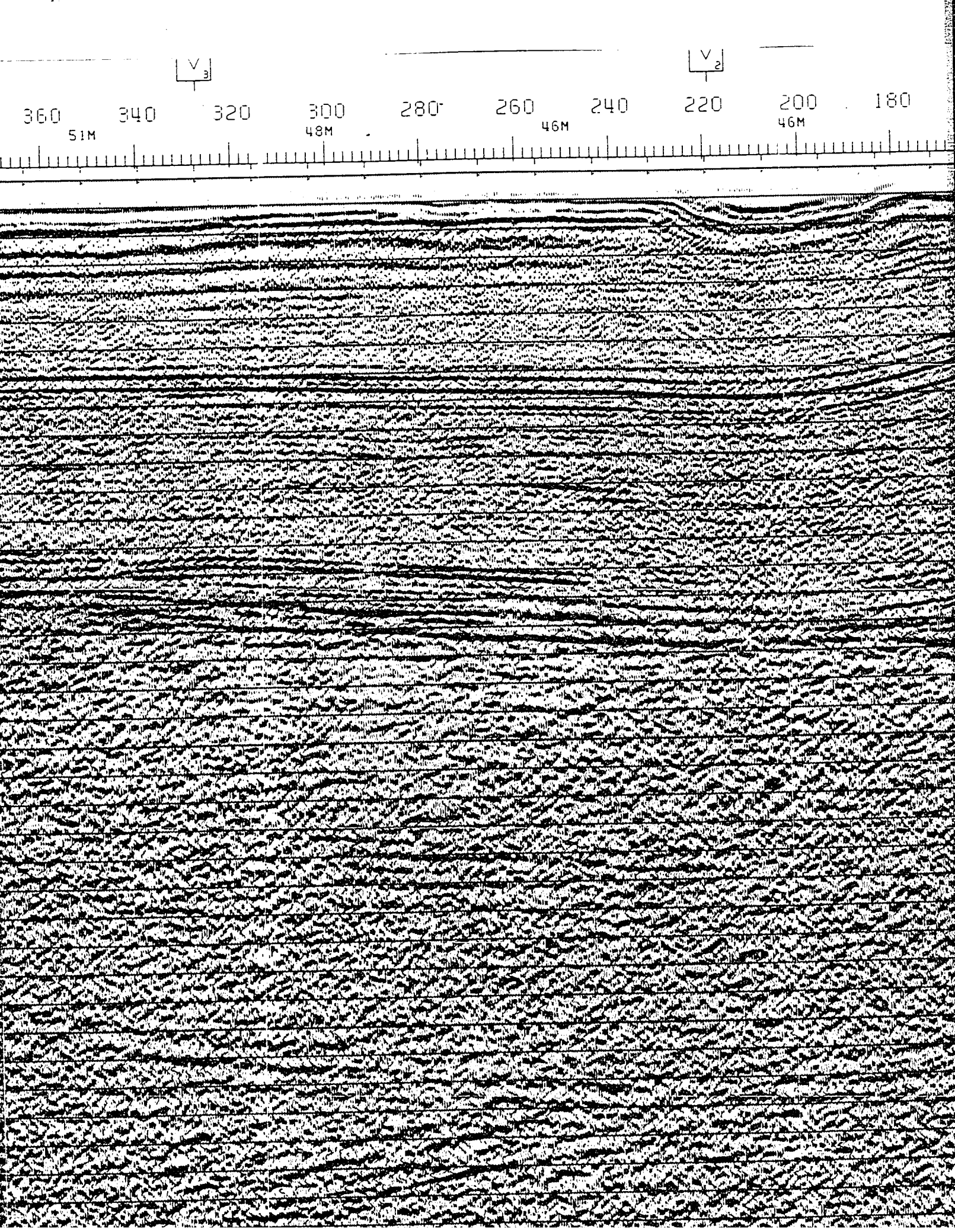
V3
V2
360
340
320
300
280
260
240
220
200
180
51M
48M
46M
46M

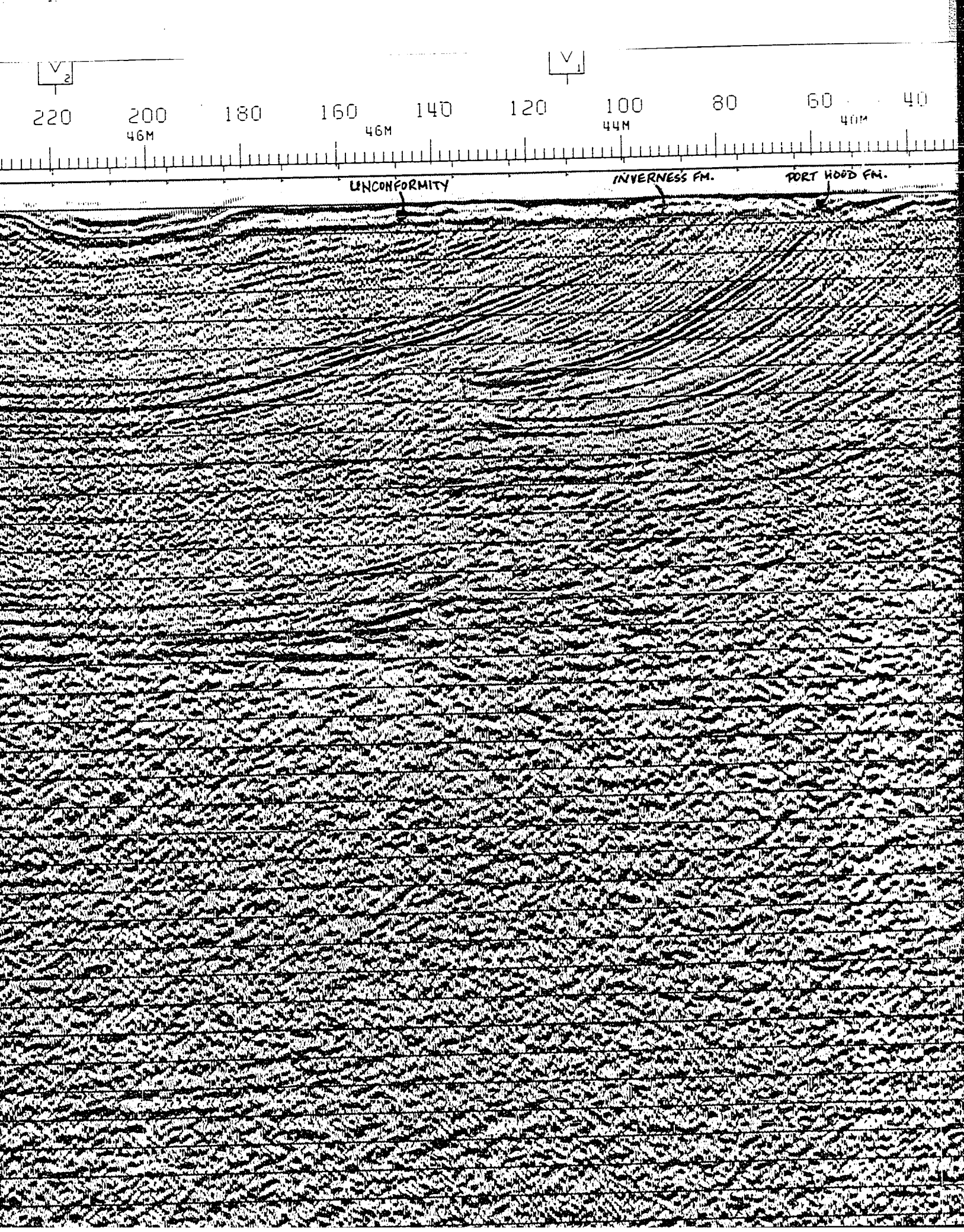
V2
V1
220
200
180
160
140
120
100
80
60
40
46M
46M
44M
40M
UNCONFORMITY
INVERNESS FM.
PORT HOOD FM.

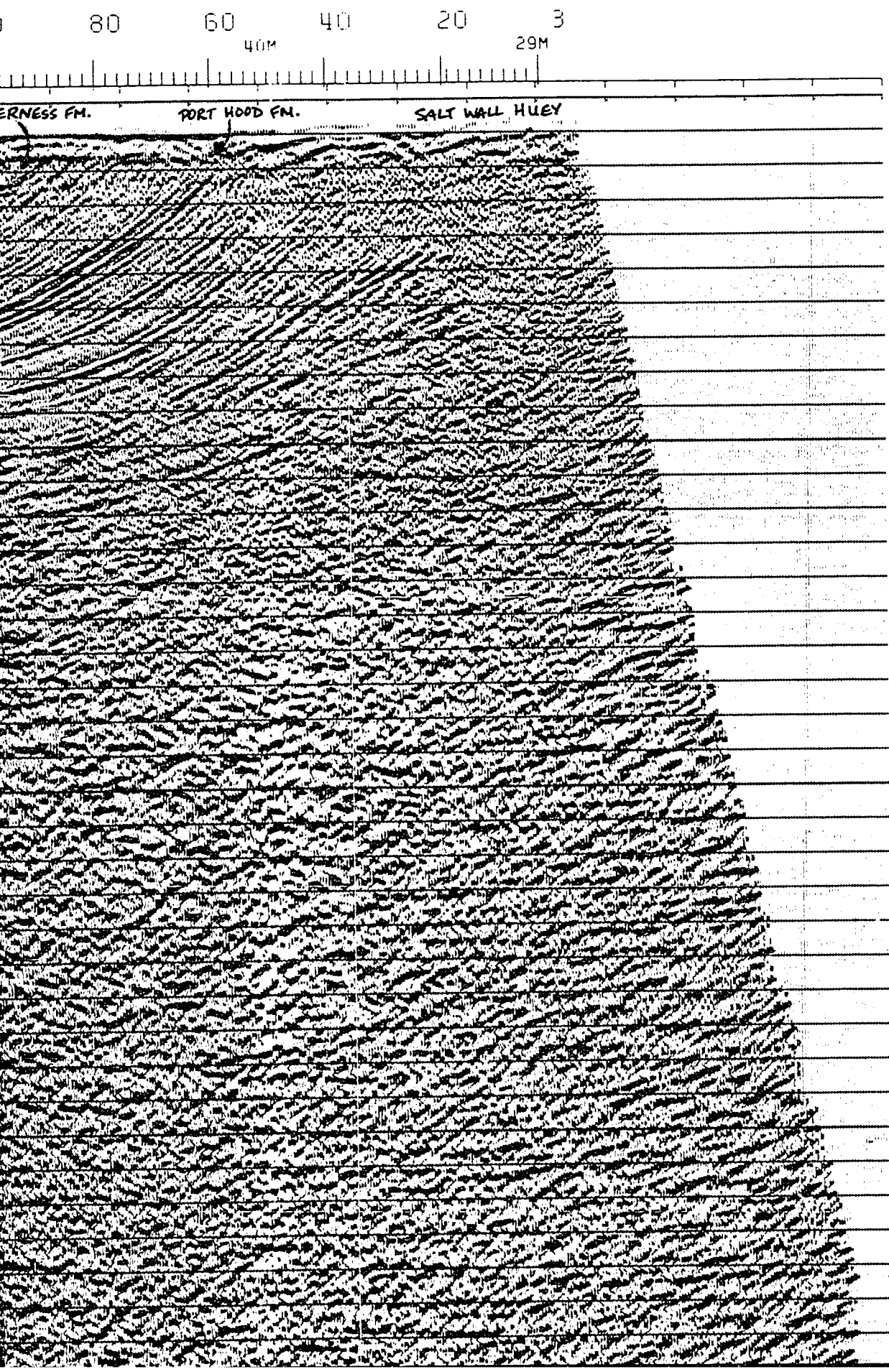

CHE

SHOT BY WESTE
PROCESSED BY

ENERGY SOURCE
CHARGE SIZE
NUMBER OF GUN
GUN DEPTH
FIRING INTERV
SHOT POINT IN
DISTANCE OF S

SYSTEM
AMPLIFIER
FILTER
SAMPLING INTE
RECORD LENGTH
FORMAT

TYPE CABLE
CABLE LENGTH
CABLE DEPTH
LEAD IN
GROUP INTERVA
NUMBER OF GRO
SPREAD

ROMS
CHANNELS PER
WEIGHTS
NUMBER OF DAT
CHANNEL INTER

P

1.
2.
3.
4.
5.
6.
7.
8.

NORTHWEST

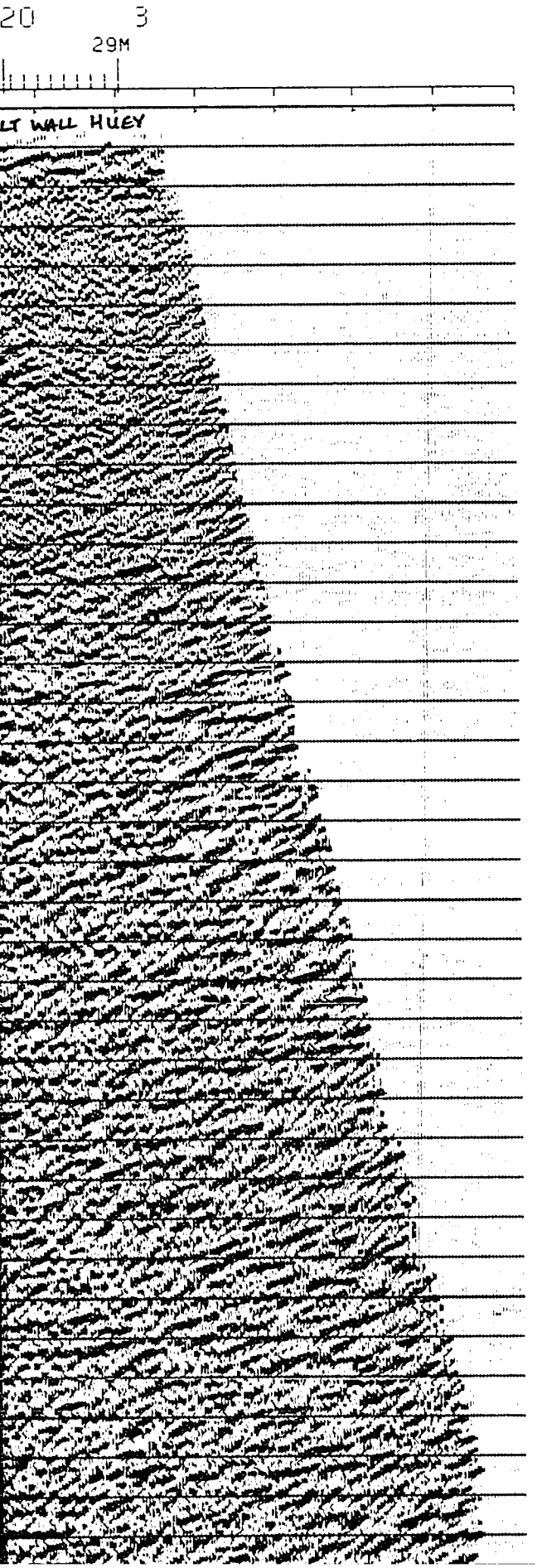

CHEVRON STANDARD LTD.

AREA: NORTHUMBERLAND STRAIT

SHOT BY WESTERN GEOPHYSICAL COMPANY PARTY 127
PROCESSED BY WESTERN GEOPHYSICAL (CALGARY) GROUP 6

RECORDING DATA

SOURCE

ENERGY SOURCE	AIR GUNS
CHARGE SIZE	1050 CU.IN
NUMBER OF GUNS	15
GUN DEPTH	6 M
FIRING INTERVAL	27 M
SHOT POINT INTERVAL	27 M
DISTANCE OF SOURCE TO ANTENNA	47 M

INSTRUMENTS

SYSTEM	MILOSEIS
AMPLIFIER	INST. FLOATING POINT
FILTER	L/9-H/450
SAMPLING INTERVAL	1 MS
RECORD LENGTH	5.0 SEC
FORMAT	SEG-D

CABLE

TYPE CABLE	STREAMER
CABLE LENGTH	2565 M
CABLE DEPTH	8 M
LEAD IN	187 M
GROUP INTERVAL	27 M
NUMBER OF GROUPS RECORDED	96
SPREAD	2752 M

ARRAY PARAMETERS

ROMS	7/21
CHANNELS PER ARRAY	8.50% OVERLAP
WEIGHTS	32.32.32.32.32.32.32.
NUMBER OF DATA CHANNELS RECORDED	384
CHANNEL INTERVAL	6.67 M

PROCESSING SEQUENCE AND PARAMETERS

PROCESSING SAMPLING INTERVAL 4 MS

1. SIGNATURE DECONVOLUTION
2. DECONVOLVED BEFORE STACK
   - WINDOW LENGTH 2 ZONES OF 2500 MS
   - LENGTH OPERATOR 280 MS
   - PREDICTION DISTANCE 4 MS
3. NMO STACK 4800 %
4. RELATIVE AMP COMPENSATION
5. F-K DOMAIN FILTER
6. DECONVOLVED AFTER STACK
   - WINDOW LENGTH 2 ZONES OF 2500 MS
   - LENGTH OPERATOR 300 MS
   - PREDICTION DISTANCE 20 MS
7. FINITE DIFFERENCE MIGRATION
8. TIME VARIANT FILTER

TIME		L.C. (HZ)	H.C.
1.00	SEC	12	60
3.00	SEC	8	45
5.00	SEC	8	30

W.D.

CHEVRON STANDARD LTD.

AREA: NORTHUMBERLAND STRAIT

SHOT BY WESTERN GEOPHYSICAL COMPANY PARTY 127 JULY 1981
PROCESSED BY WESTERN GEOPHYSICAL (CALGARY) GROUP 6 OCT 1981

RECORDING DATA

SOURCE

ENERGY SOURCE	AIR GUNS
CHARGE SIZE	1050 CU.IN
NUMBER OF GUNS	15
GUN DEPTH	6 M
FIRING INTERVAL	27 M
SHOT POINT INTERVAL	27 M
DISTANCE OF SOURCE TO ANTENNA	47 M

INSTRUMENTS

SYSTEM	KILOSEIS
AMPLIFIER	INST. FLOATING POINT
FILTER	L/9-H/450
SAMPLING INTERVAL	1 MS
RECORD LENGTH	5.0 SEC
FORMAT	SEG-D

CABLE

TYPE CABLE	STREAMER
CABLE LENGTH	2565 M
CABLE DEPTH	8 M
LEAD IN	187 M
GROUP INTERVAL	27 M
NUMBER OF GROUPS RECORDED	96
SPREAD	2752 M

ARRAY PARAMETERS

ROMS	7/21
CHANNELS PER ARRAY	8.50% OVERLAP
WEIGHTS	32.32.32.32.32.32.32.32
NUMBER OF DATA CHANNELS RECORDED	384
CHANNEL INTERVAL	6.67 M

PROCESSING SEQUENCE AND PARAMETERS

PROCESSING SAMPLING INTERVAL 4 MS

1. SIGNATURE DECONVOLUTION
2. DECONVOLVED BEFORE STACK
   - WINDOW LENGTH 2 ZONES OF 2500 MS
   - LENGTH OPERATOR 280 MS
   - PREDICTION DISTANCE 4 MS
3. NMO STACK 4800 %
4. RELATIVE AMP COMPENSATION
5. F-K DOMAIN FILTER
6. DECONVOLVED AFTER STACK
   - WINDOW LENGTH 2 ZONES OF 2500 MS
   - LENGTH OPERATOR 300 MS
   - PREDICTION DISTANCE 20 MS
7. FINITE DIFFERENCE MIGRATION
8. TIME VARIANT FILTER

TIME	L.C. (HZ)	H.C.
1.00 SEC	12	60
3.00 SEC	8	45
5.00 SEC	8	30

9. RMS GAIN (128-512 MS WINDOW)

NORTHWEST

67

NO: 8624 C4 9E LINE NO: 8

VRON STANDARD LTD.

AREA: NORTHUMBERLAND STRAIT

ERN GEOPHYSICAL COMPANY PARTY 127 JULY 1981
WESTERN GEOPHYSICAL (CALGARY) GROUP 6 OCT 1981

RECORDING DATA

SOURCE	
E	AIR GUNS
	1050 CU.IN
NS	15
	6 M
VAL	27 M
NTERVAL	27 M
SOURCE TO ANTENNA	47 M
INSTRUMENTS	
	KILOSEIS
	INST. FLOATING POINT
	L/9-H/450
ERVAL	1 MS
H	5.0 SEC
	SEG-D
CABLE	
	STREAMER
H	2565 M
	8 M
	187 M
VAL	27 M
ROUPS RECORDED	96
	2752 M
ARRAY PARAMETERS	
	7/21
R ARRAY	8.50% OVERLAP
	32.32.32.32.32.32.32.32
ATA CHANNELS RECORDED	384
ERVAL	6.67 M

PROCESSING SEQUENCE AND PARAMETERS

- PROCESSING SAMPLING INTERVAL 4 MS
- SIGNATURE DECONVOLUTION
- DECONVOLVED BEFORE STACK
  - WINDOW LENGTH 2 ZONES OF 2500 MS
  - LENGTH OPERATOR 280 MS
  - PREDICTION DISTANCE 4 MS
- NMO STACK 4800 %
- RELATIVE AMP COMPENSATION
- F-K DOMAIN FILTER
- DECONVOLVED AFTER STACK
  - WINDOW LENGTH 2 ZONES OF 2500 MS
  - LENGTH OPERATOR 300 MS
  - PREDICTION DISTANCE 20 MS
- FINITE DIFFERENCE MIGRATION
- TIME VARIANT FILTER

TIME		L.C. (HZ)	H.C.
1.00	SEC	12	60
3.00	SEC	8	45

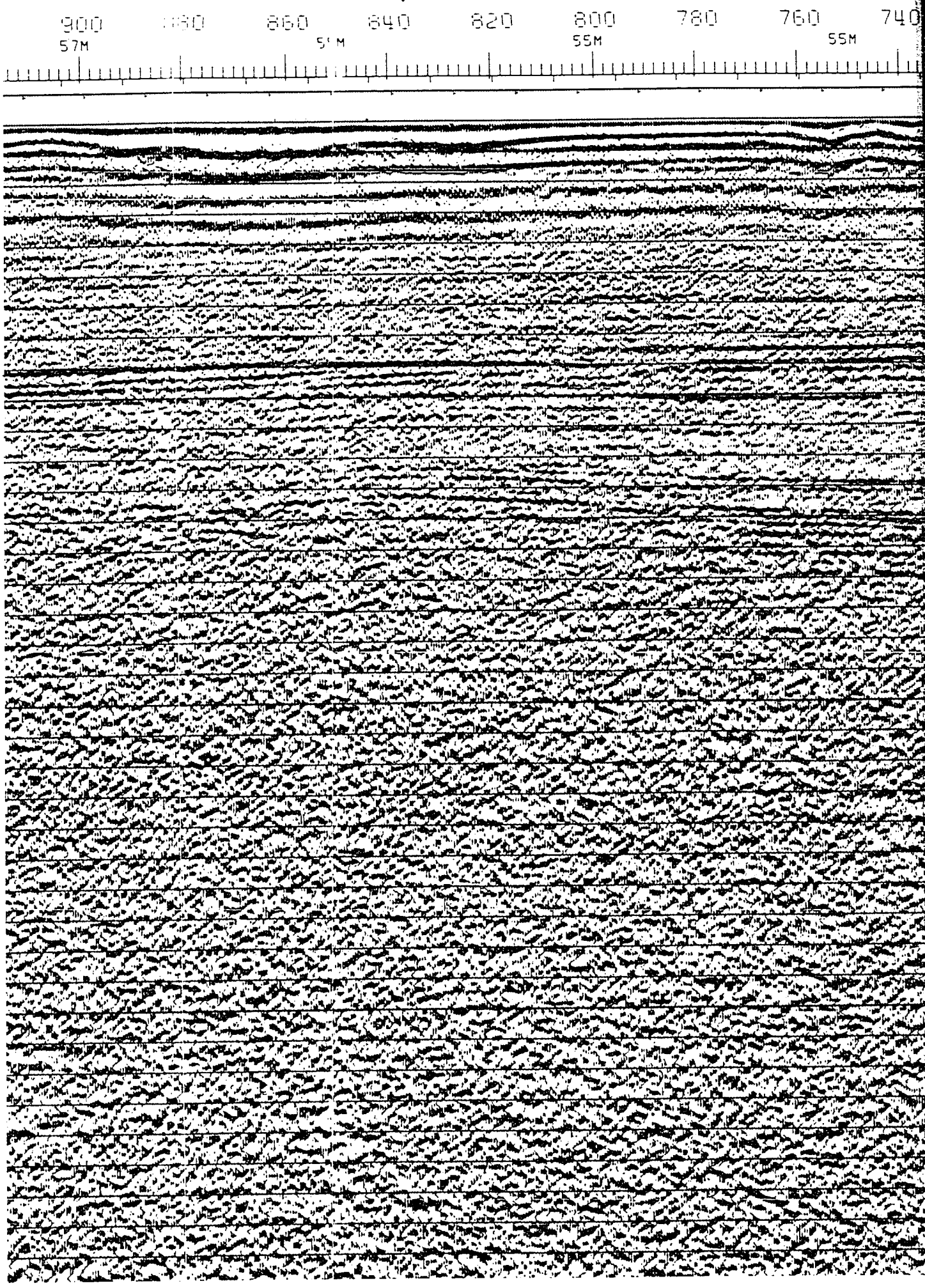
900
880
860
840
820
800
780
760
740
57M
55M
55M

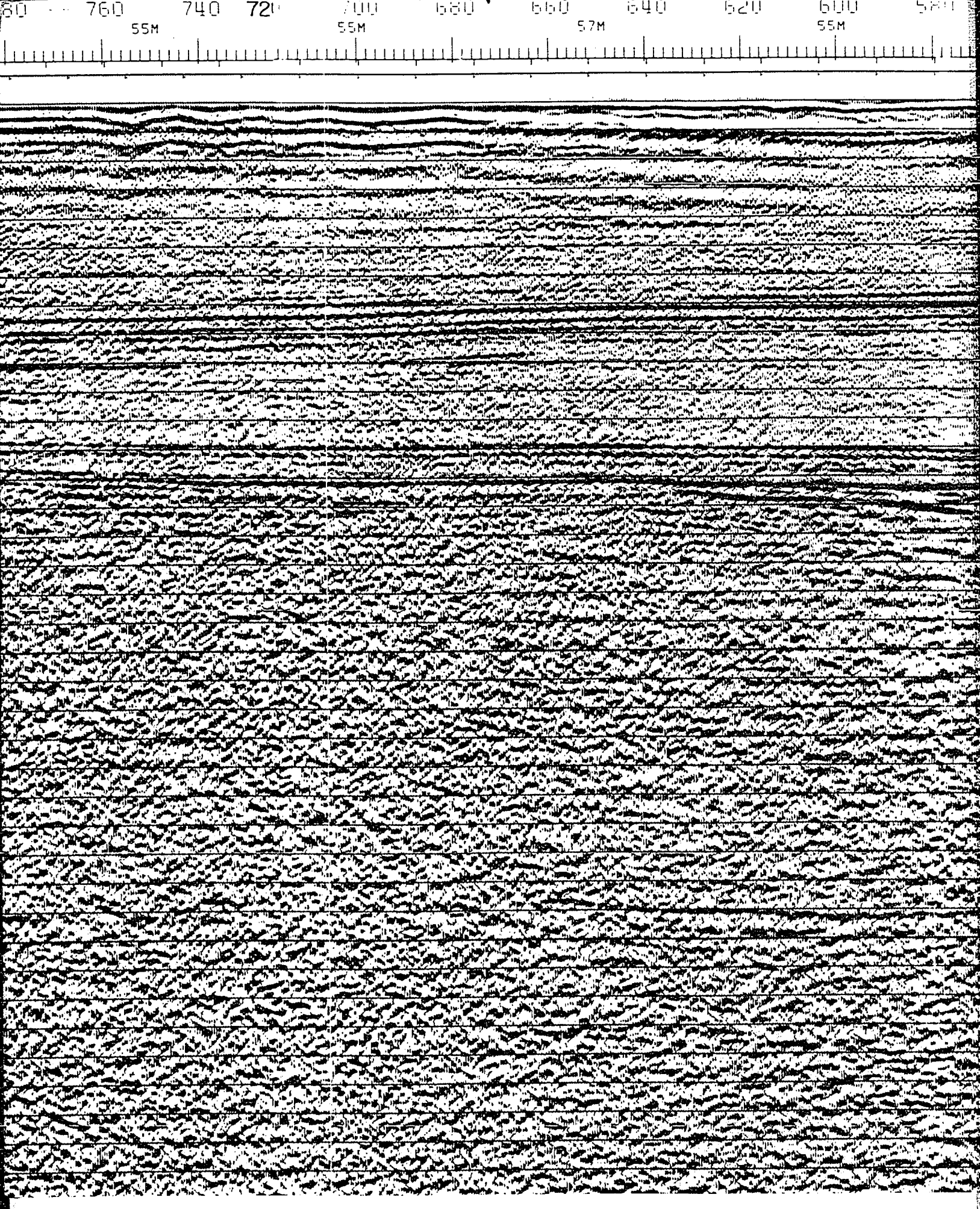
780
760
740
720
700
680
660
640
620
600
55M
55M
57M
55M

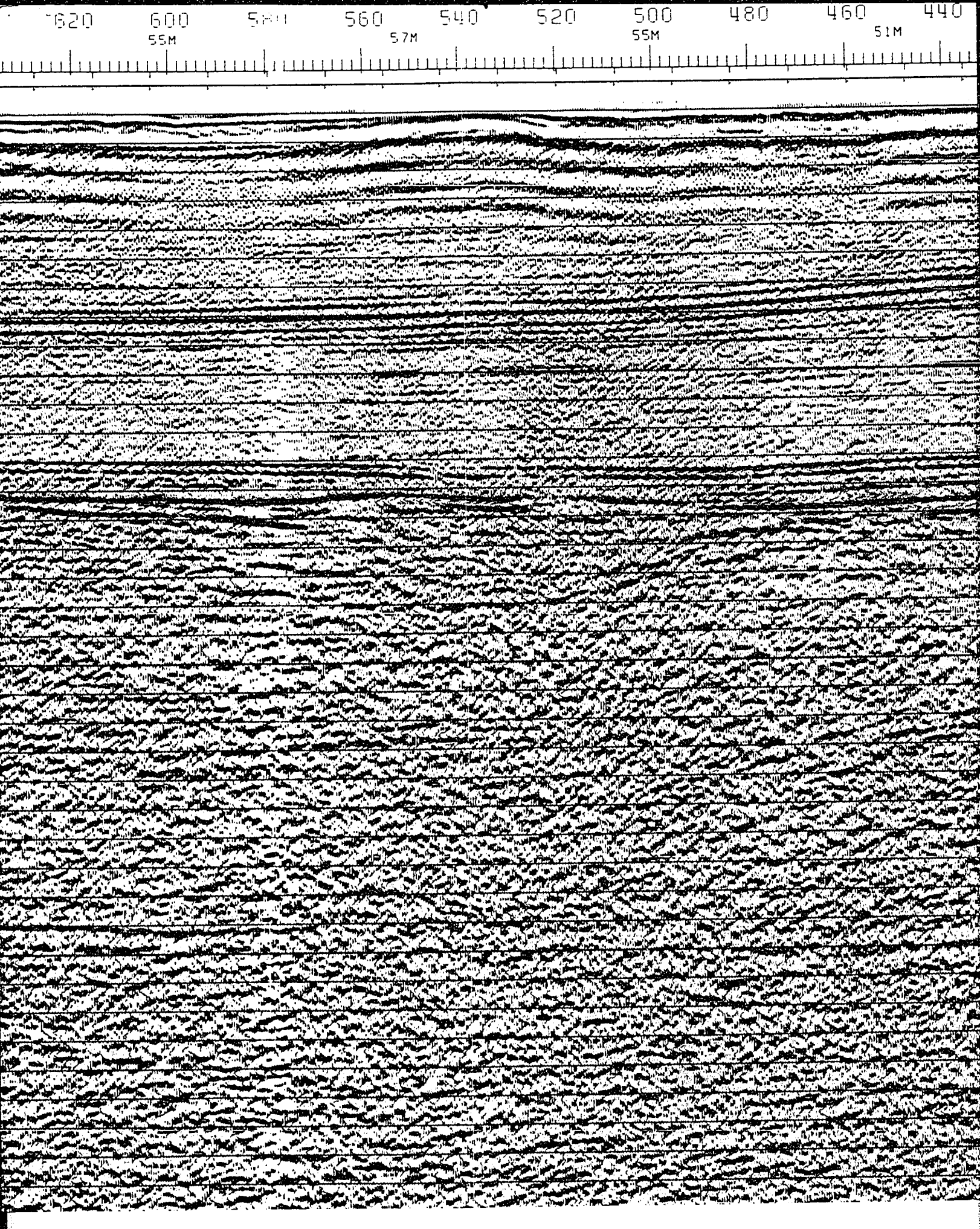
620
600
560
540
520
500
480
460
440
55M
57M
55M
51M

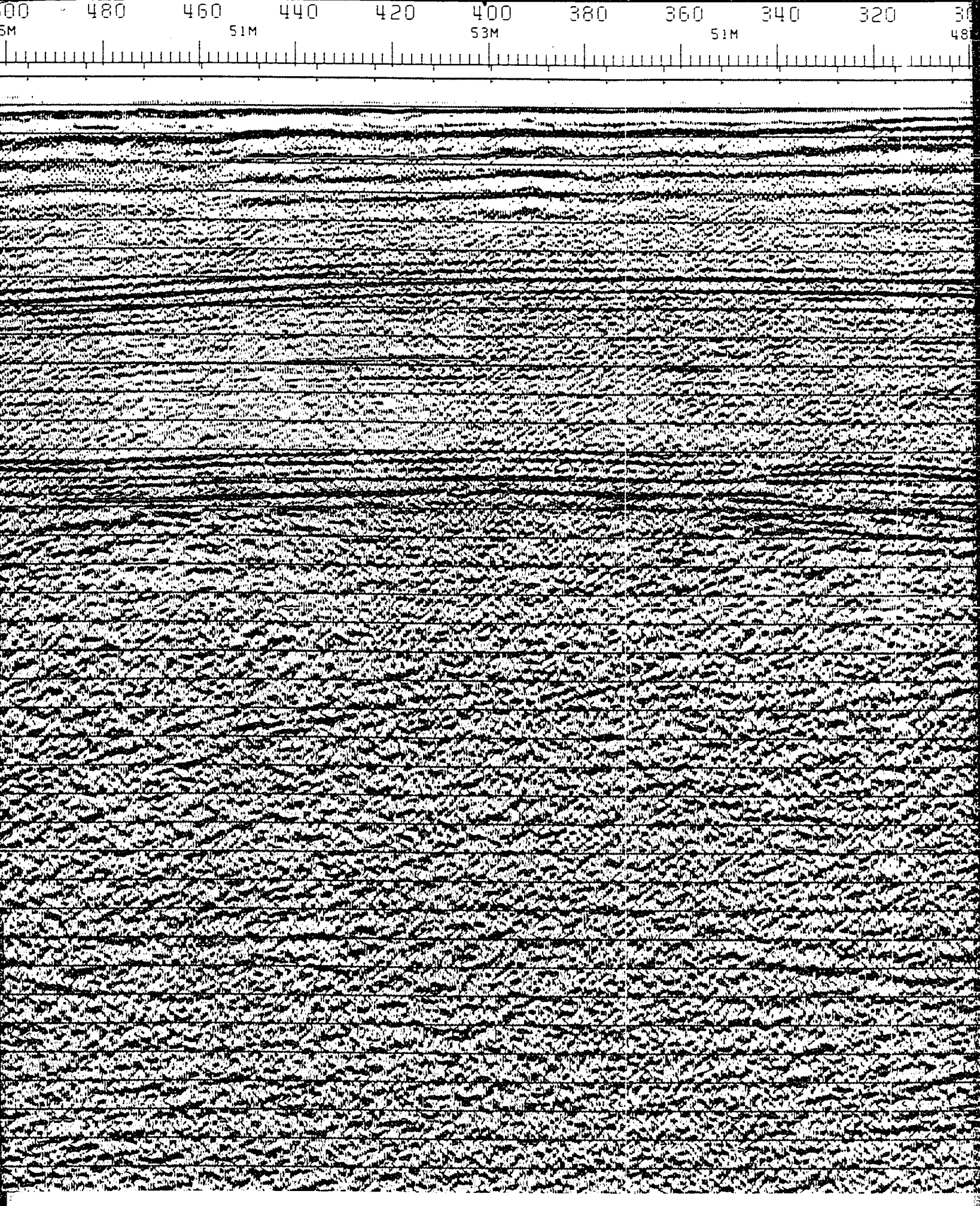
00
480
460
440
420
400
380
360
340
320
5M
51M
53M
51M
48

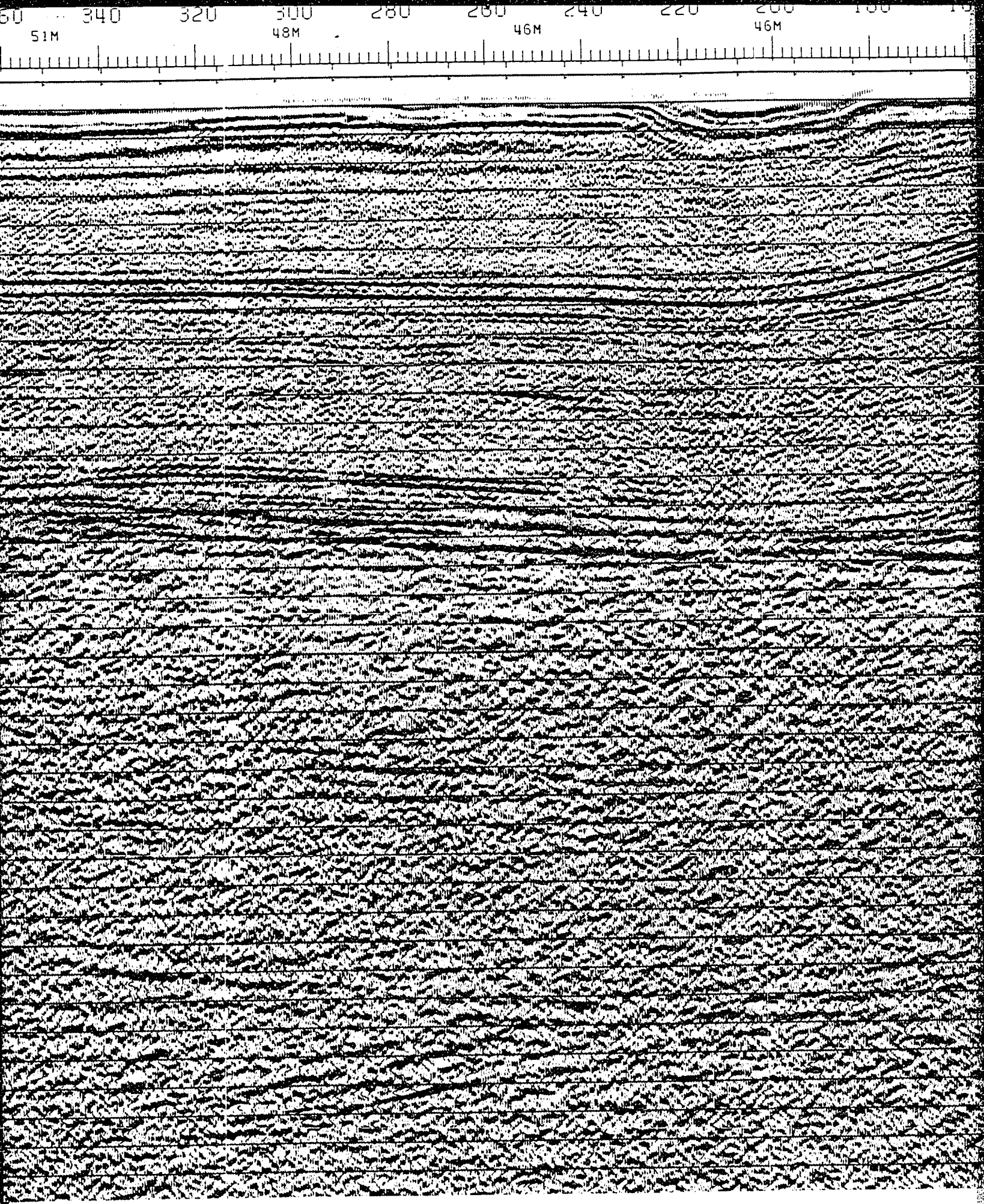
340
320
300
280
260
240
220
200
51M
48M
46M
46M

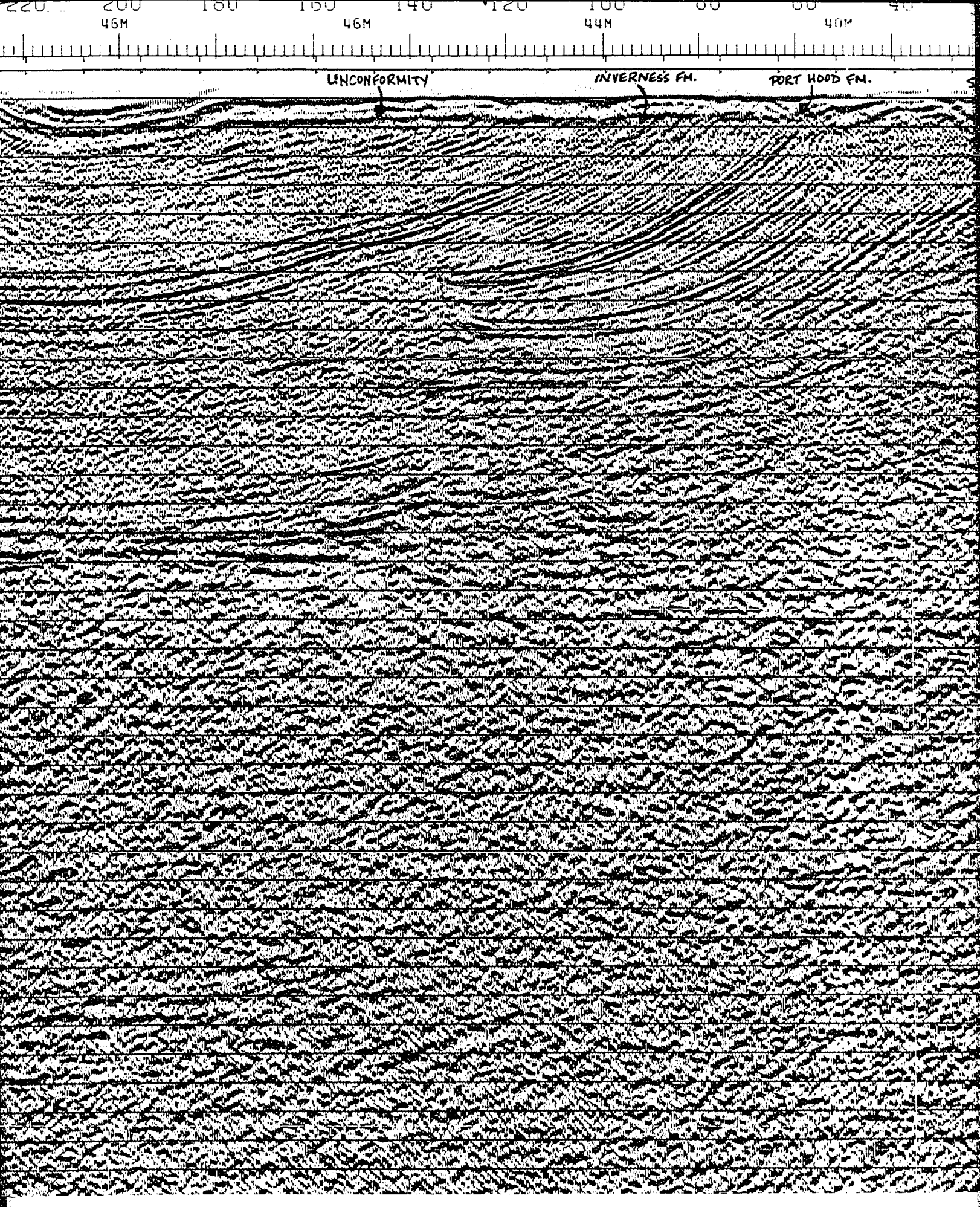
220
200
180
160
140
120
100
80
60
40
46M
46M
44M
40M
UNCONFORMITY
INVERNESS FM.
PORT HOOD FM.

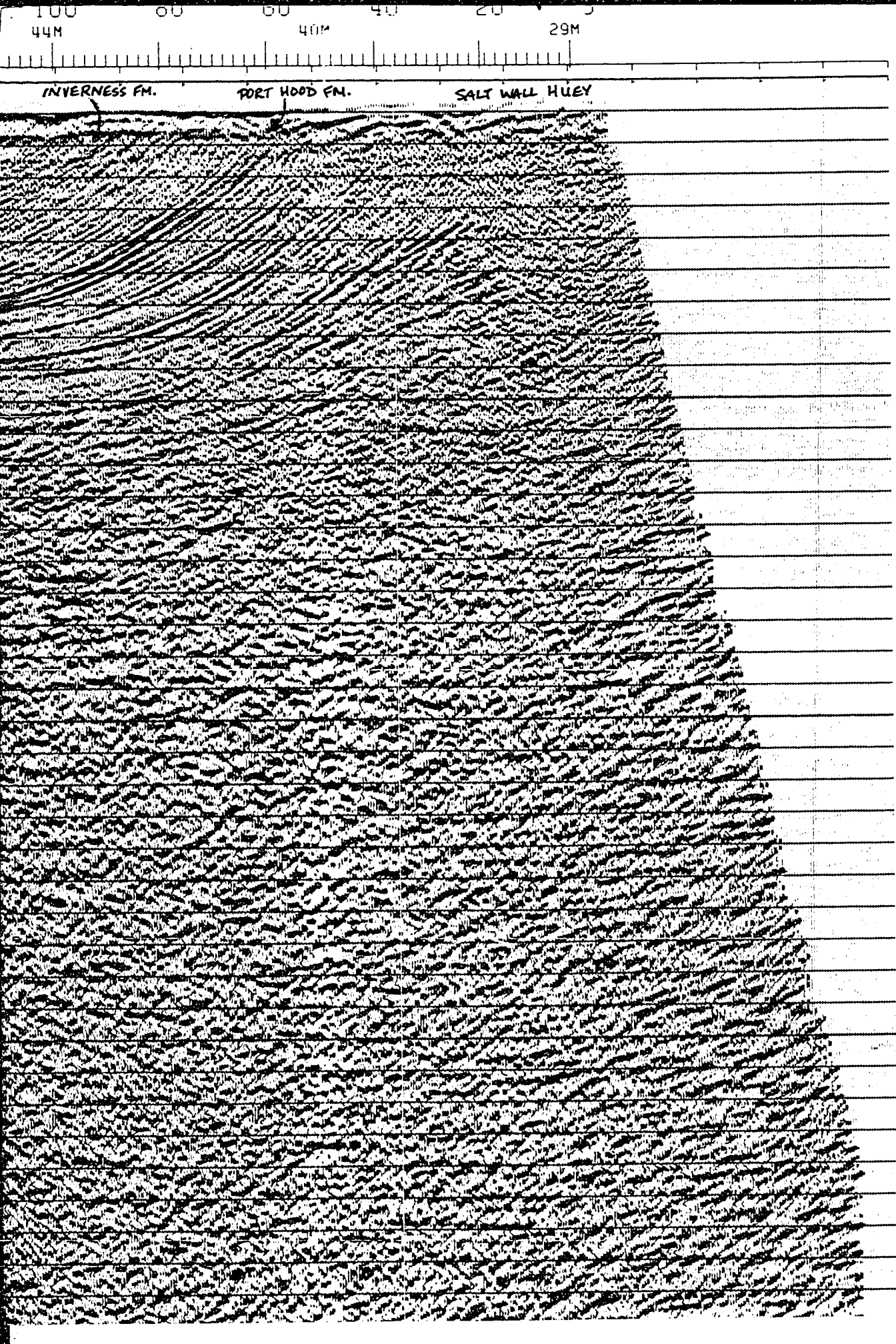

SHOT B
PROCES

ENERGY
CHARGE
NUMBER
GUN DE
FIRING
SHOT P
DISTAN

SYSTEM
AMPLIF
FILTER
SAMPLI
RECORD
FORMAT

TYPE C
CABLE
CABLE
LEAD I
GROUP
NUMBER
SPREAD

ROMS
CHANNE
WEIGHT
NUMBER
CHANNE

W.D.

CHEVRON STANDARD LTD.

AREA: NORTHUMBERLAND STRAIT

SHOT BY WESTERN GEOPHYSICAL COMPANY PARTY 127 JULY 1981
PROCESSED BY WESTERN GEOPHYSICAL (CALGARY) GROUP 6 OCT 1981

RECORDING DATA

SOURCE

ENERGY SOURCE	AIR GUNS
CHARGE SIZE	1050 CU.IN
NUMBER OF GUNS	15
GUN DEPTH	6 M
FIRING INTERVAL	27 M
SHOT POINT INTERVAL	27 M
DISTANCE OF SOURCE TO ANTENNA	47 M

INSTRUMENTS

SYSTEM	KILOSEIS
AMPLIFIER	INST. FLOATING POINT
FILTER	L/9-H/450
SAMPLING INTERVAL	1 MS
RECORD LENGTH	5.0 SEC
FORMAT	SEG-D

CABLE

TYPE CABLE	STREAMER
CABLE LENGTH	2565 M
CABLE DEPTH	8 M
LEAD IN	187 M
GROUP INTERVAL	27 M
NUMBER OF GROUPS RECORDED	96
SPREAD	2752 M

ARRAY PARAMETERS

ROMS	7/21
CHANNELS PER ARRAY	8.50% OVERLAP
WEIGHTS	32.32.32.32.32.32.32.32
NUMBER OF DATA CHANNELS RECORDED	384
CHANNEL INTERVAL	6.67 M

PROCESSING SEQUENCE AND PARAMETERS

PROCESSING SAMPLING INTERVAL 4 MS

1. SIGNATURE DECONVOLUTION
2. DECONVOLVED BEFORE STACK
   - WINDOW LENGTH 2 ZONES OF 2500 MS
   - LENGTH OPERATOR 280 MS
   - PREDICTION DISTANCE 4 MS
3. NMO STACK 4800 %
4. RELATIVE AMP COMPENSATION
5. F-K DOMAIN FILTER
6. DECONVOLVED AFTER STACK
   - WINDOW LENGTH 2 ZONES OF 2500 MS
   - LENGTH OPERATOR 300 MS
   - PREDICTION DISTANCE 20 MS
7. FINITE DIFFERENCE MIGRATION
8. TIME VARIANT FILTER

TIME		L.C. (HZ)	H.C.
1.00	SEC	12	60
3.00	SEC	8	45
5.00	SEC	8	30

9. RMS GAIN (128-512 MS WINDOW)

47 M

LEGEND

NORTHWEST

67

ØN STANDARD LTD.

REA: NORTHUMBERLAND STRAIT

EOPHYSICAL COMPANY PARTY 127 JULY 1981
ERN GEOPHYSICAL (CALGARY) GROUP 6 OCT 1981

RECORDING DATA

SOURCE
AIR GUNS
1050 CU.IN
15
6 M
27 M
AL 27 M
E TO ANTENNA 47 M

INSTRUMENTS
KILOSEIS
INST. FLOATING POINT
L/9-H/450
1 MS
5.0 SEC
SEG-D

CABLE
STREAMER
2565 M
8 M
187 M
27 M
RECORDED 96
2752 M

ARRAY PARAMETERS
7/21
Y 8.50% OVERLAP
32.32.32.32.32.32.32.32
ANNELS RECORDED 384
6.67 M

ESSING SEQUENCE AND PARAMETERS

CESSING SAMPLING INTERVAL 4 MS
NATURE DECONVOLUTION
ONVOLVED BEFORE STACK
DOW LENGTH 2 ZONES OF 2500 MS
GTH OPERATOR 280 MS
DICTION DISTANCE 4 MS
STACK 4800 %
ATIVE AMP COMPENSATION
DOMAIN FILTER
ONVOLVED AFTER STACK
DOW LENGTH 2 ZONES OF 2500 MS
GTH OPERATOR 300 MS
DICTION DISTANCE 20 MS
ITE DIFFERENCE MIGRATION
E VARIANT FILTER

TIME	L.C. (HZ)	H.C.
.00 SEC	12	60
.00 SEC	8	45
.00 SEC	8	30

GAIN (128-512 MS WINDOW)

LEGEND

NO: 8624 C4 9E LINE NO: 81-1

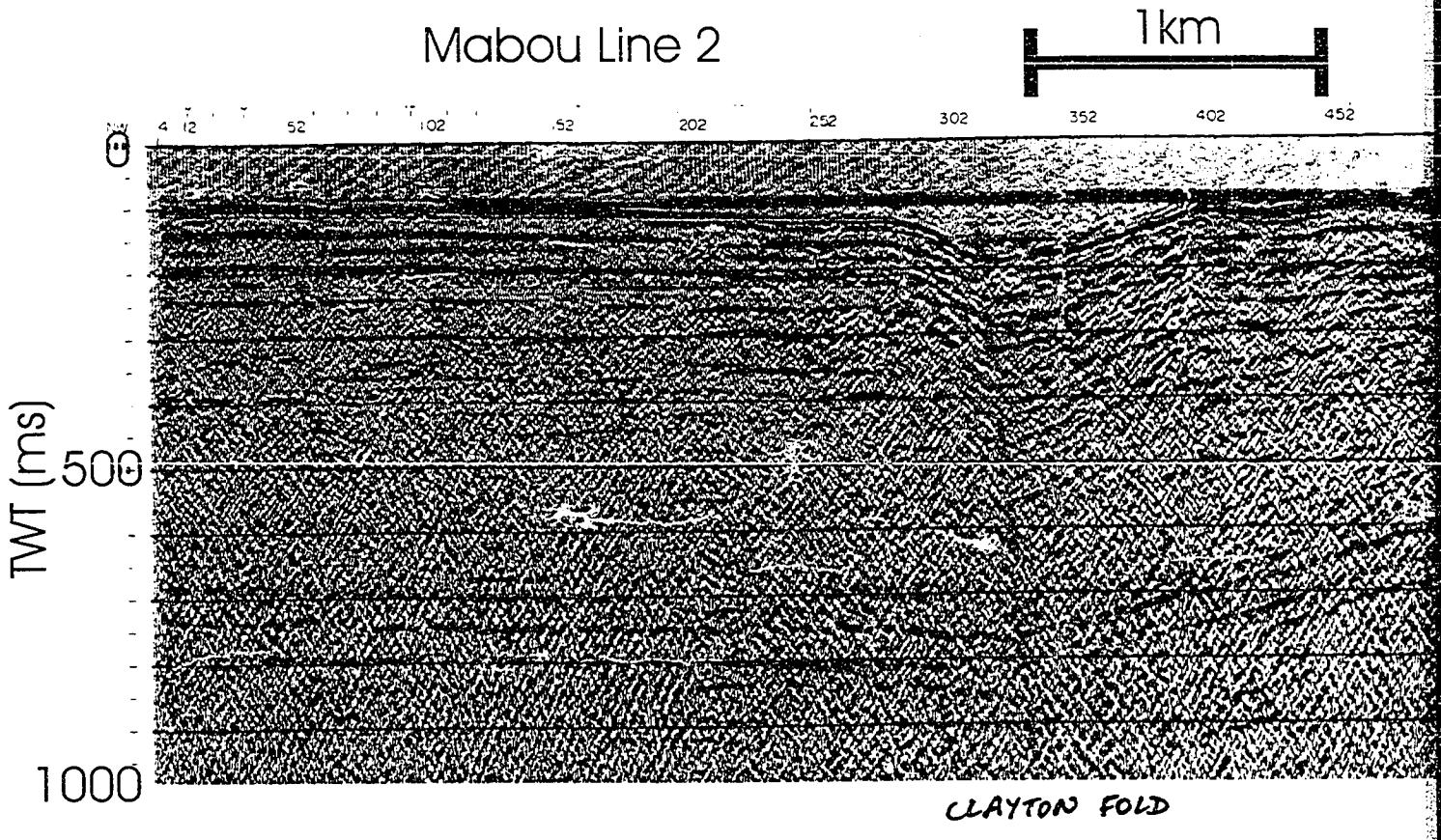
Mabou Line 2
1km
4
12
52
102
152
202
252
302
352
402
452
TWT (ms)
500
1000
CLAYTON FOLD

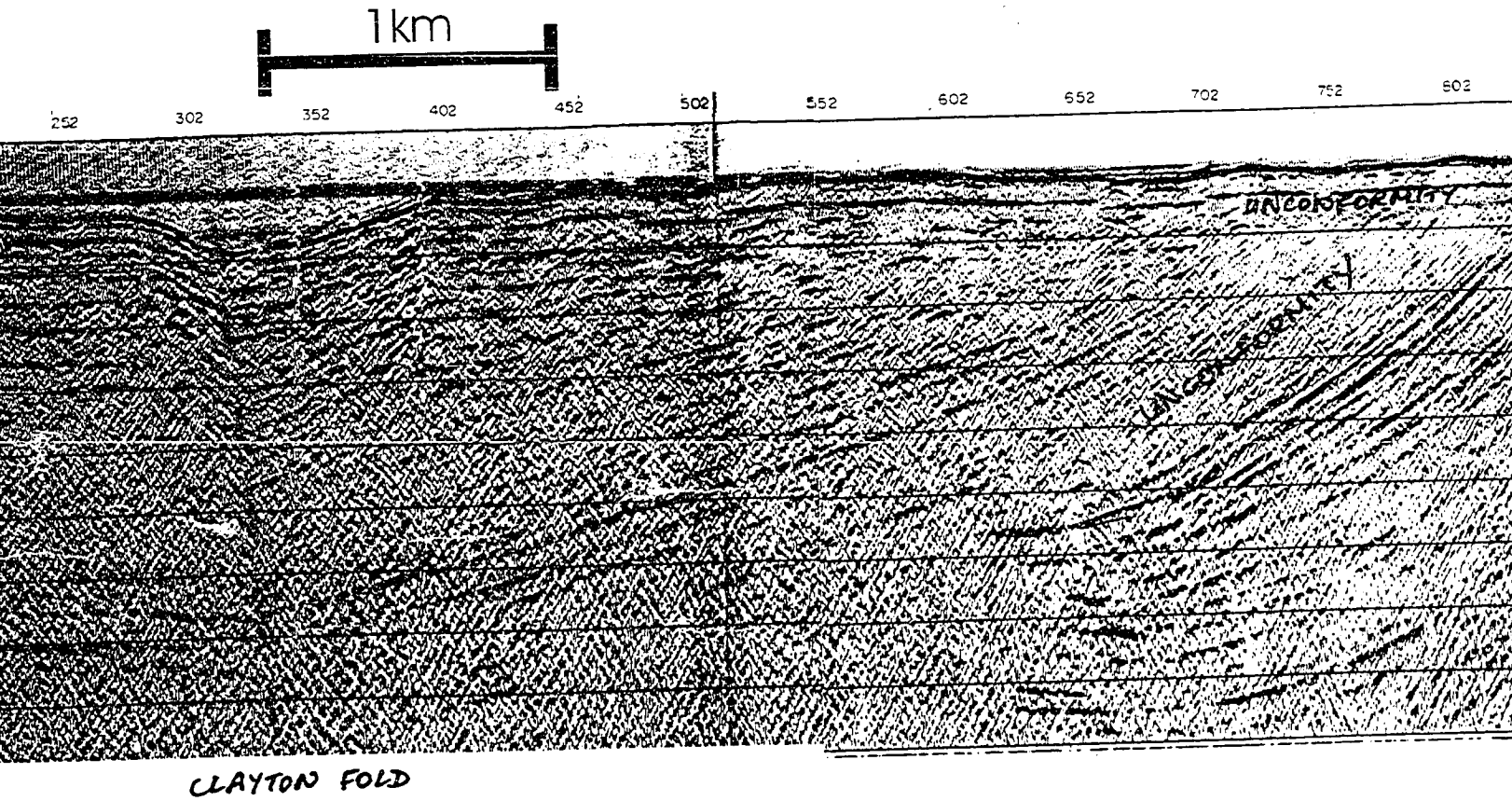

CLAYTON FOLD

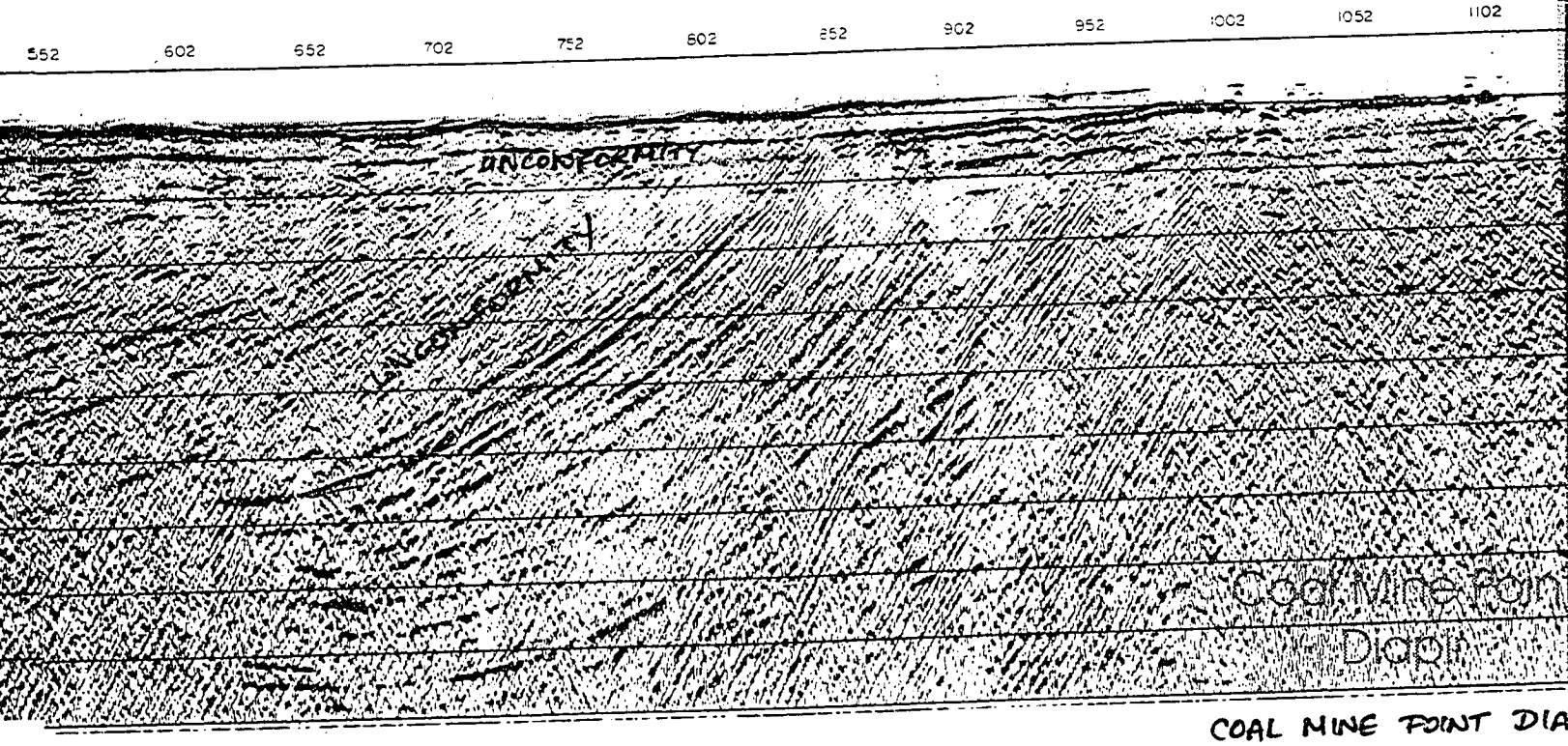

COAL MINE POINT DIA

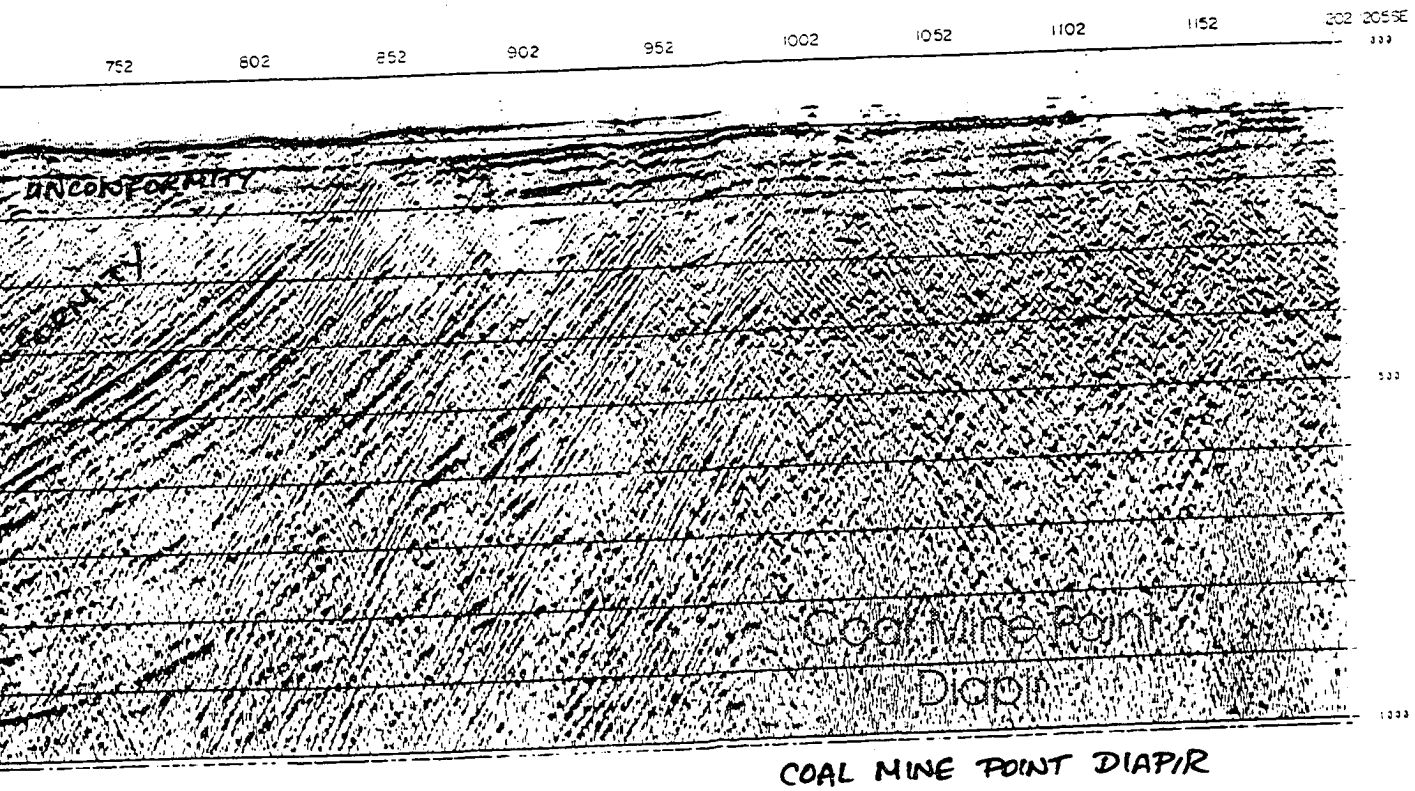

COAL MINE POINT DIAPIR

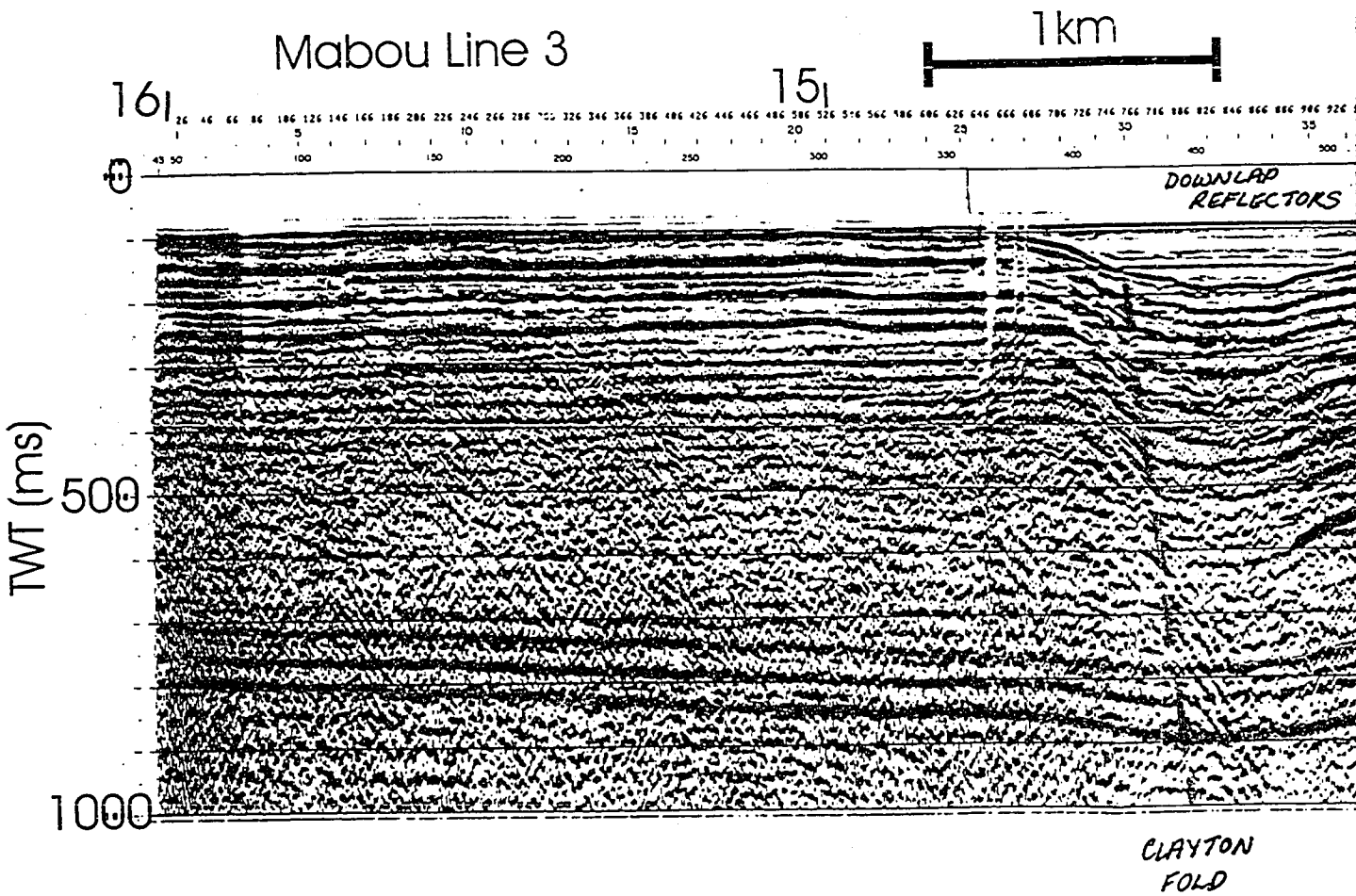
Mabou Line 3
1km
16
15
DOWNLAP REFLECTORS
TWT (ms)
500
1000
CLAYTON FOLD

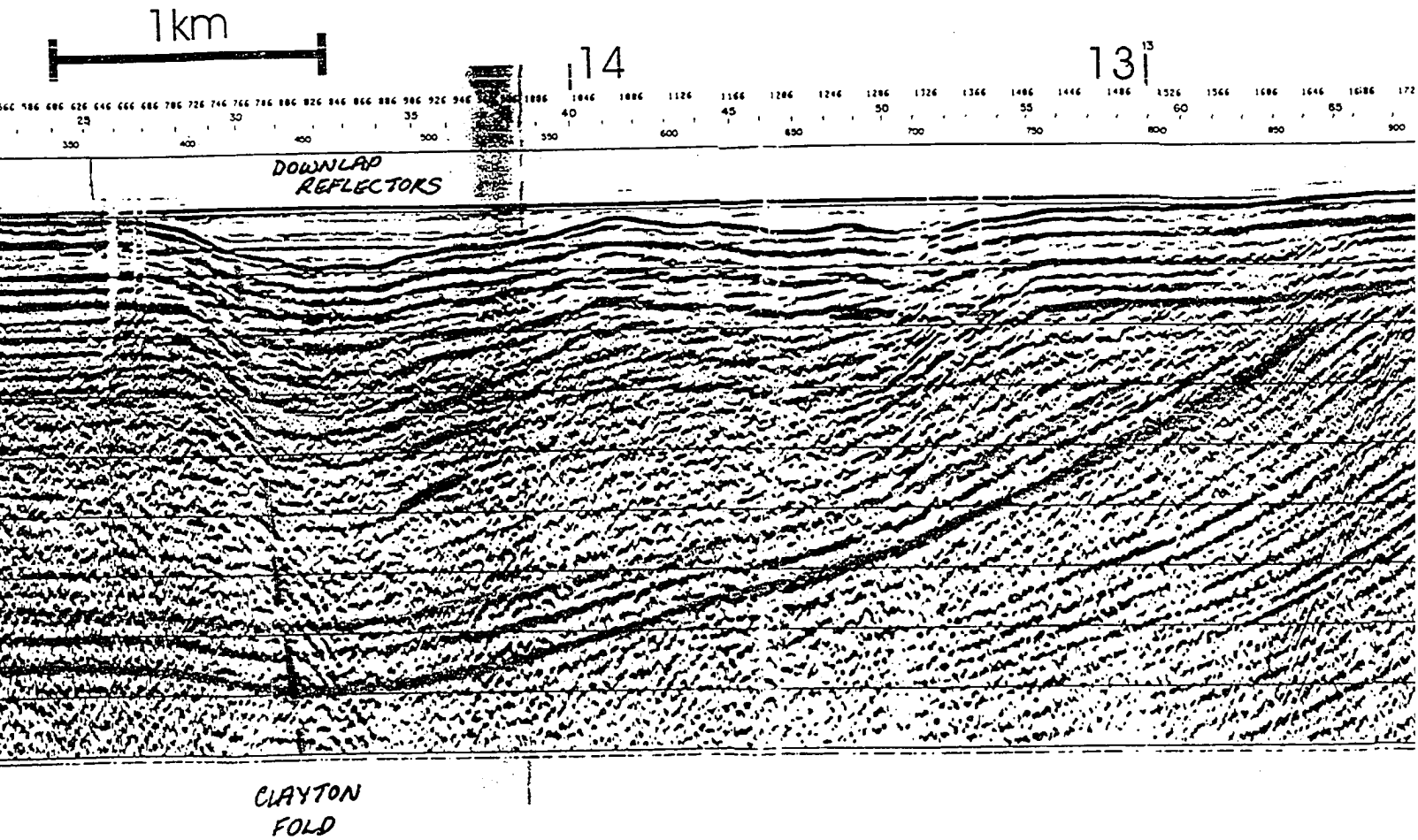
1km
14
13
DOWNLAP
REFLECTORS
CLAYTON
FOLD

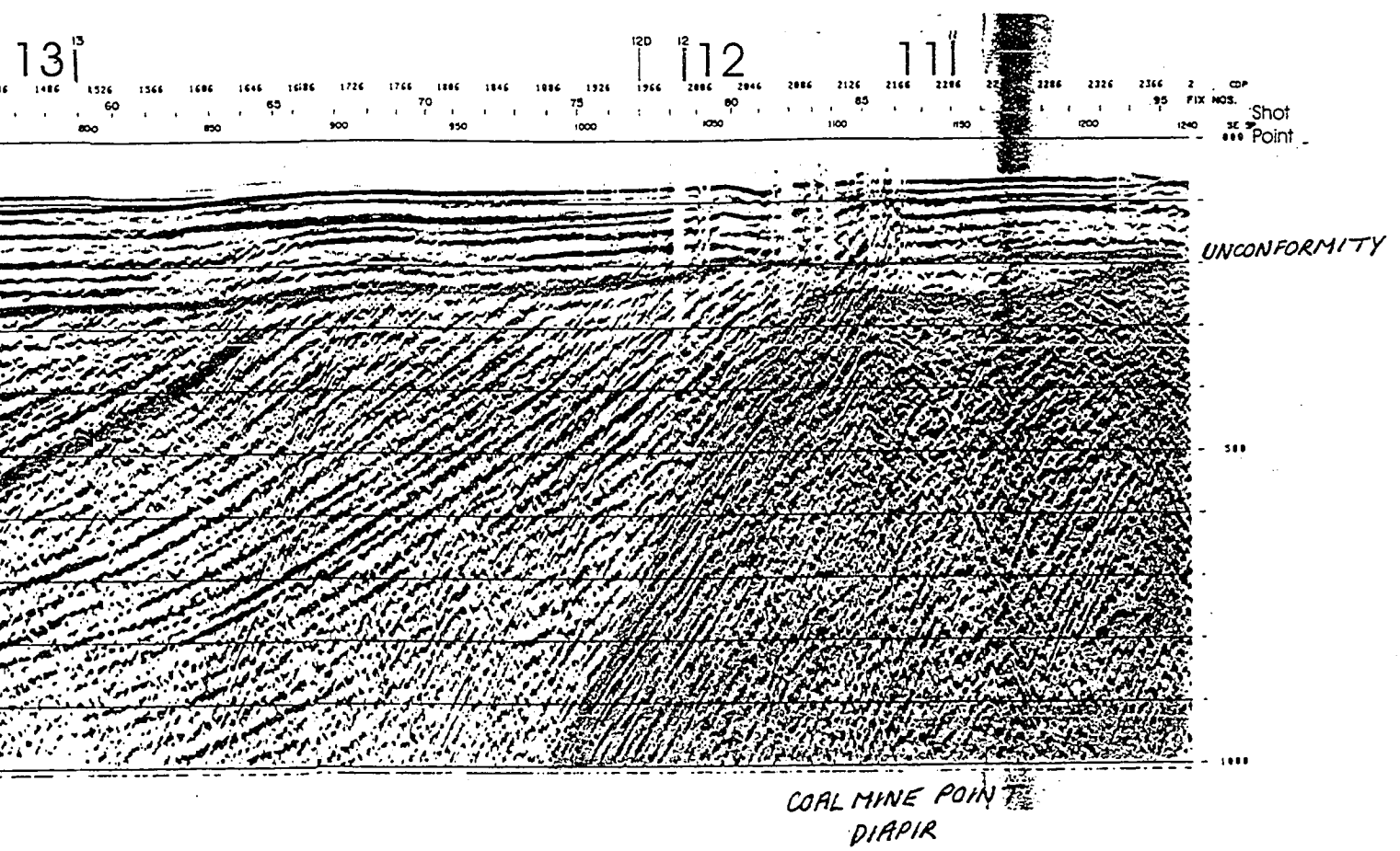
13
12
11
FIX NOS.
Shot Point
UNCONFORMITY
COAL MINE POINT
DIAPIR

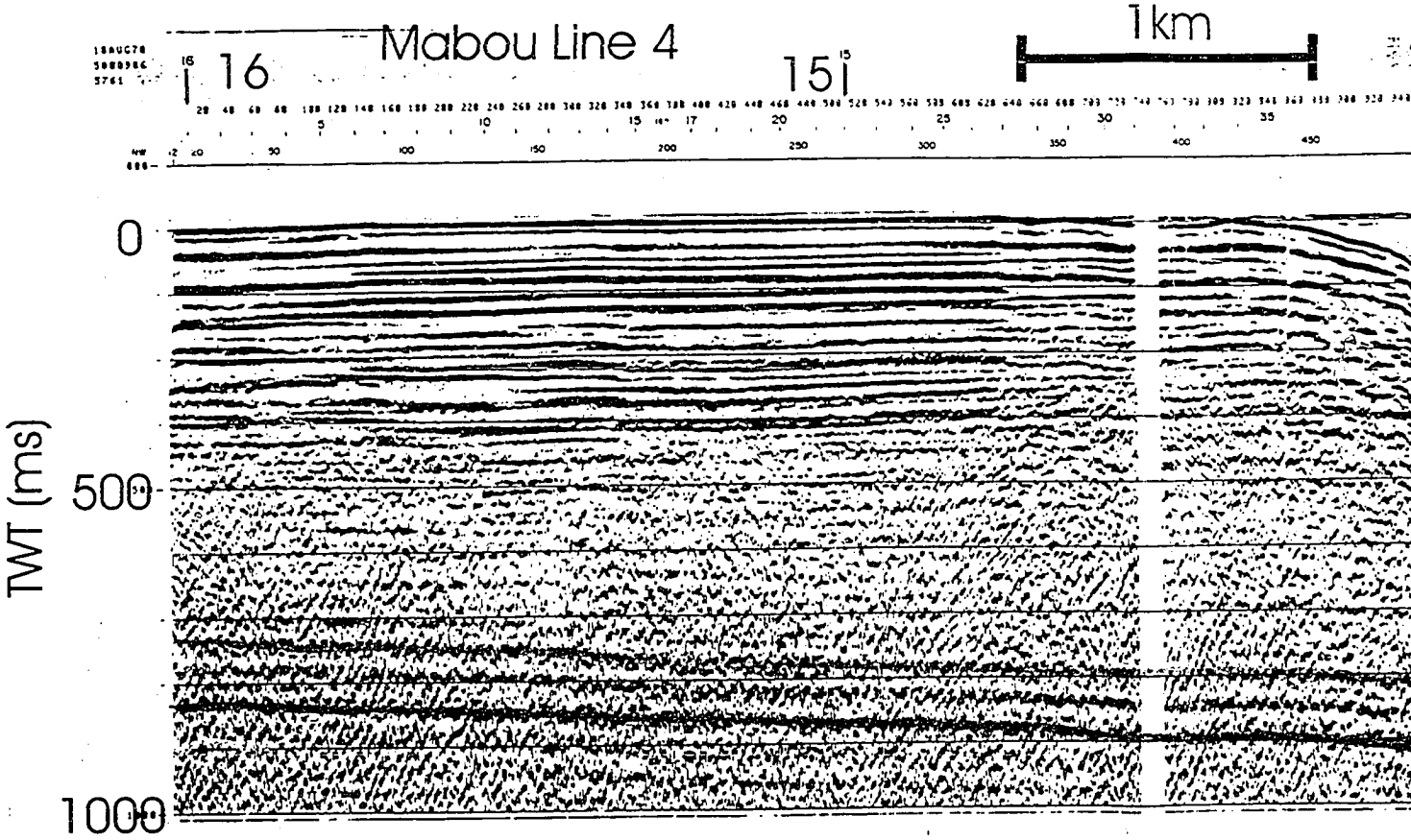
Mabou Line 4
16
15
1km
0
500
1000
TWT (ms)

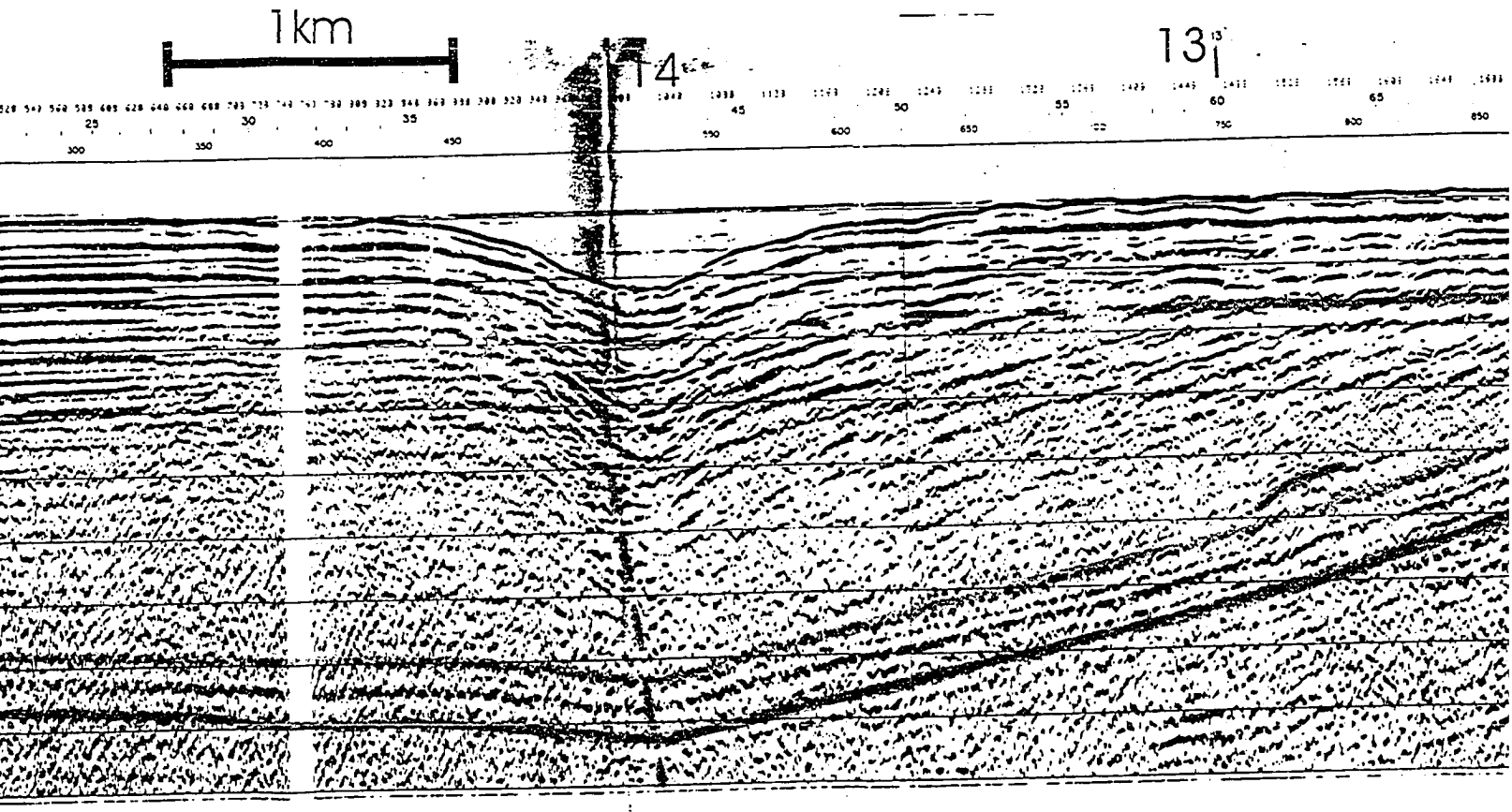
1km
14
13
CLAYTON
FOLD

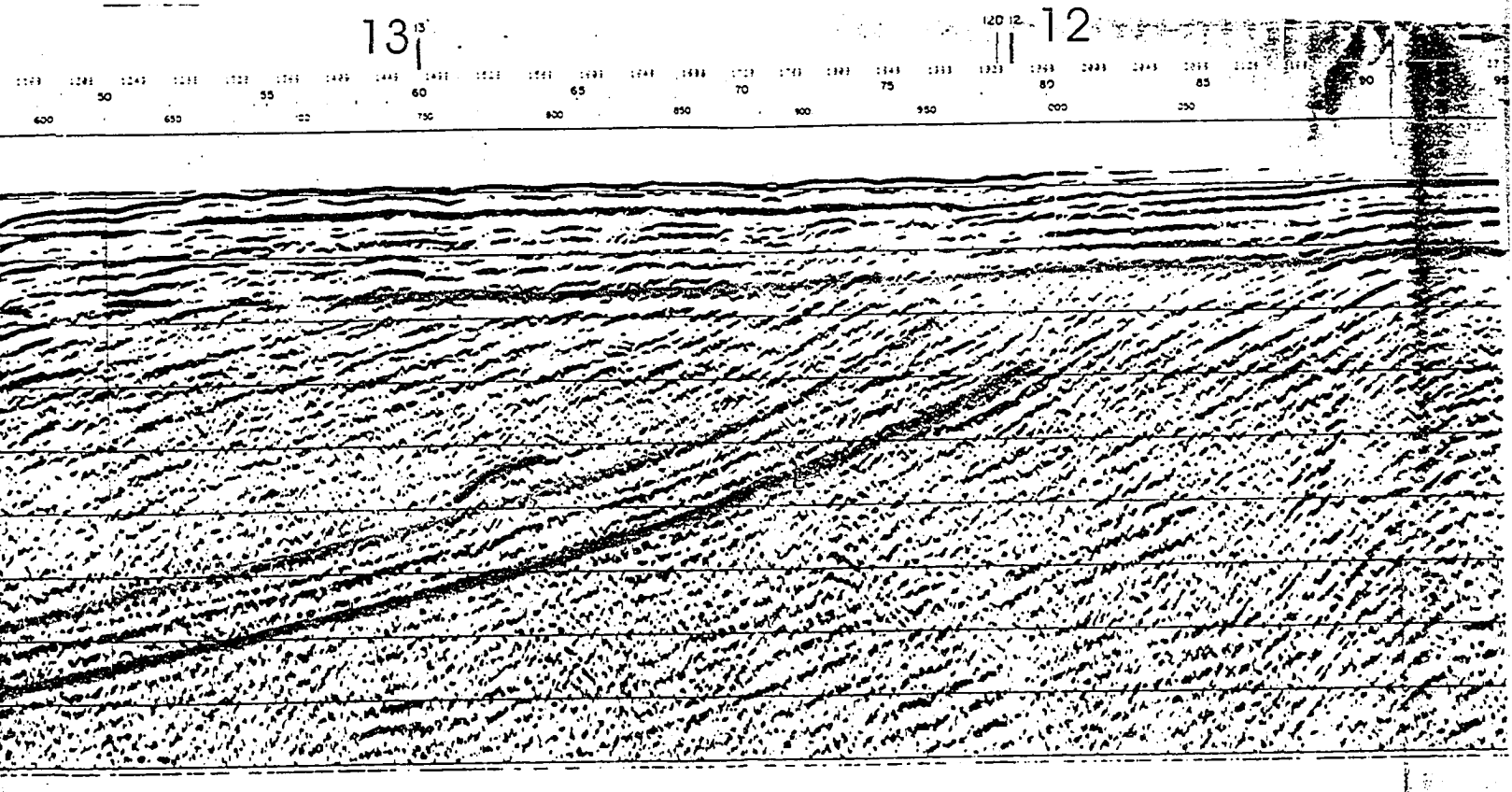
13
12
50
55
60
65
70
75
80
85
90
600
650
750
800
850
900
950

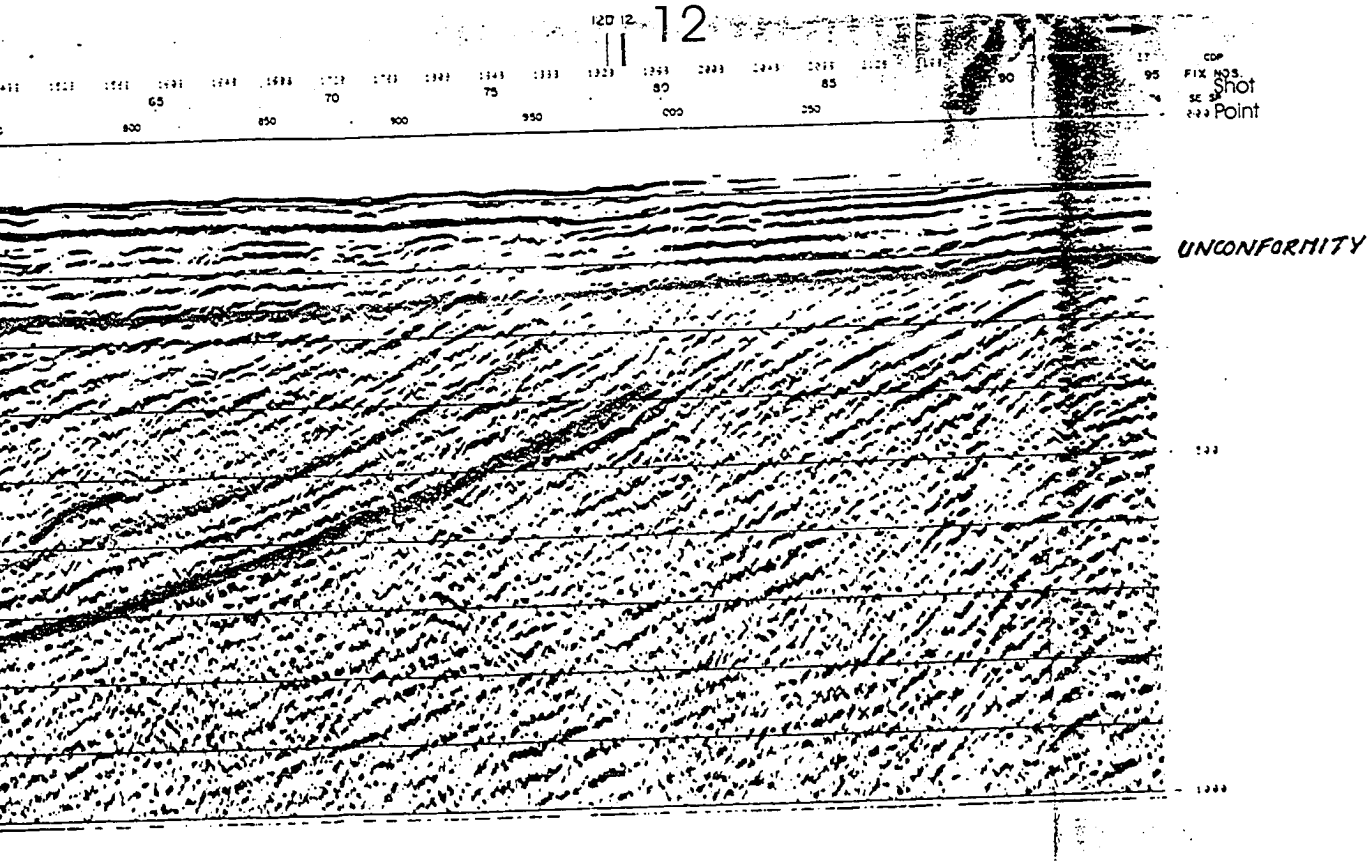
120 12
12
Shot
Point
UNCONFORMITY

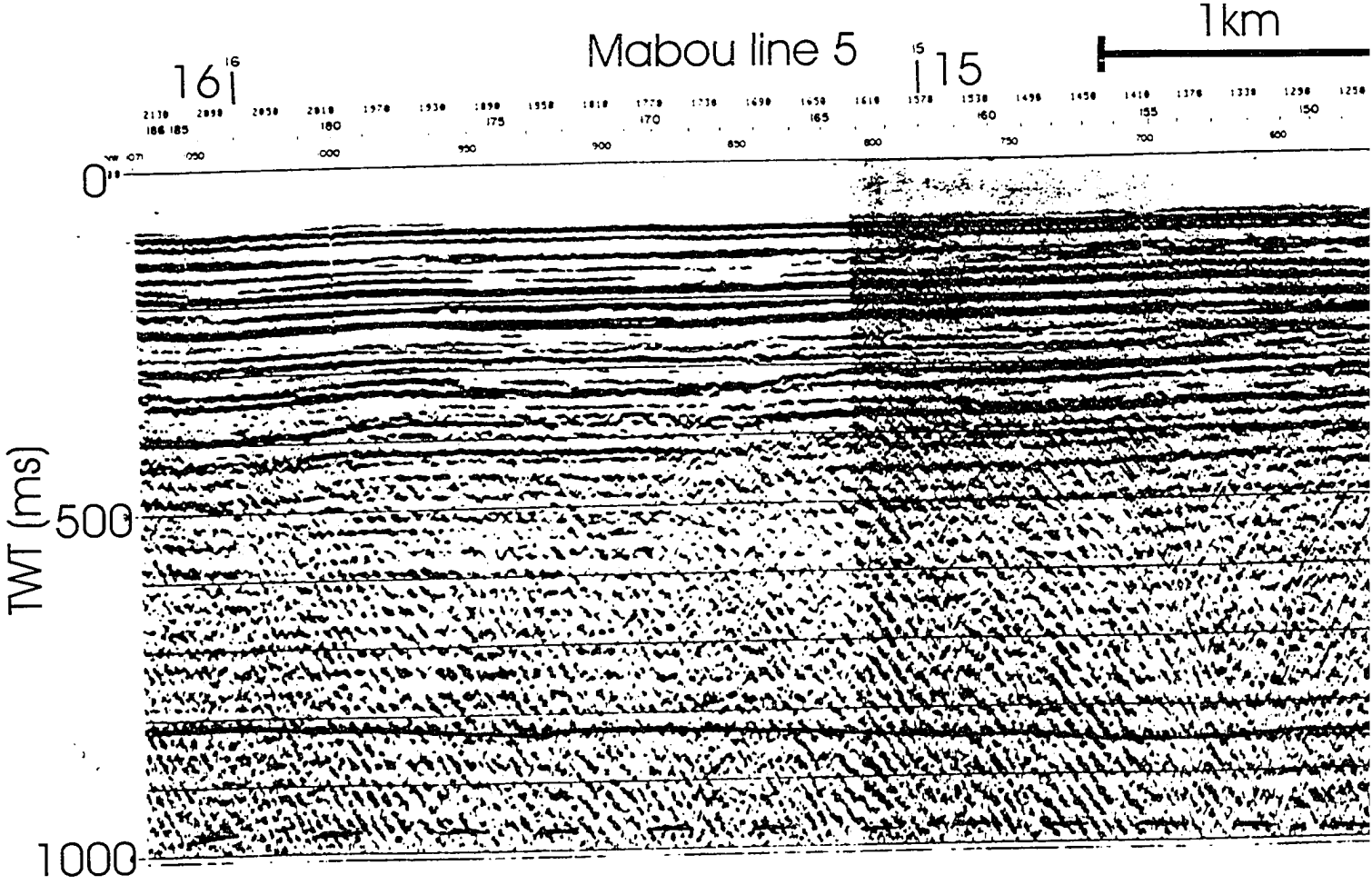
Mabou line 5
1km
16
15
TWT (ms)
0
500
1000

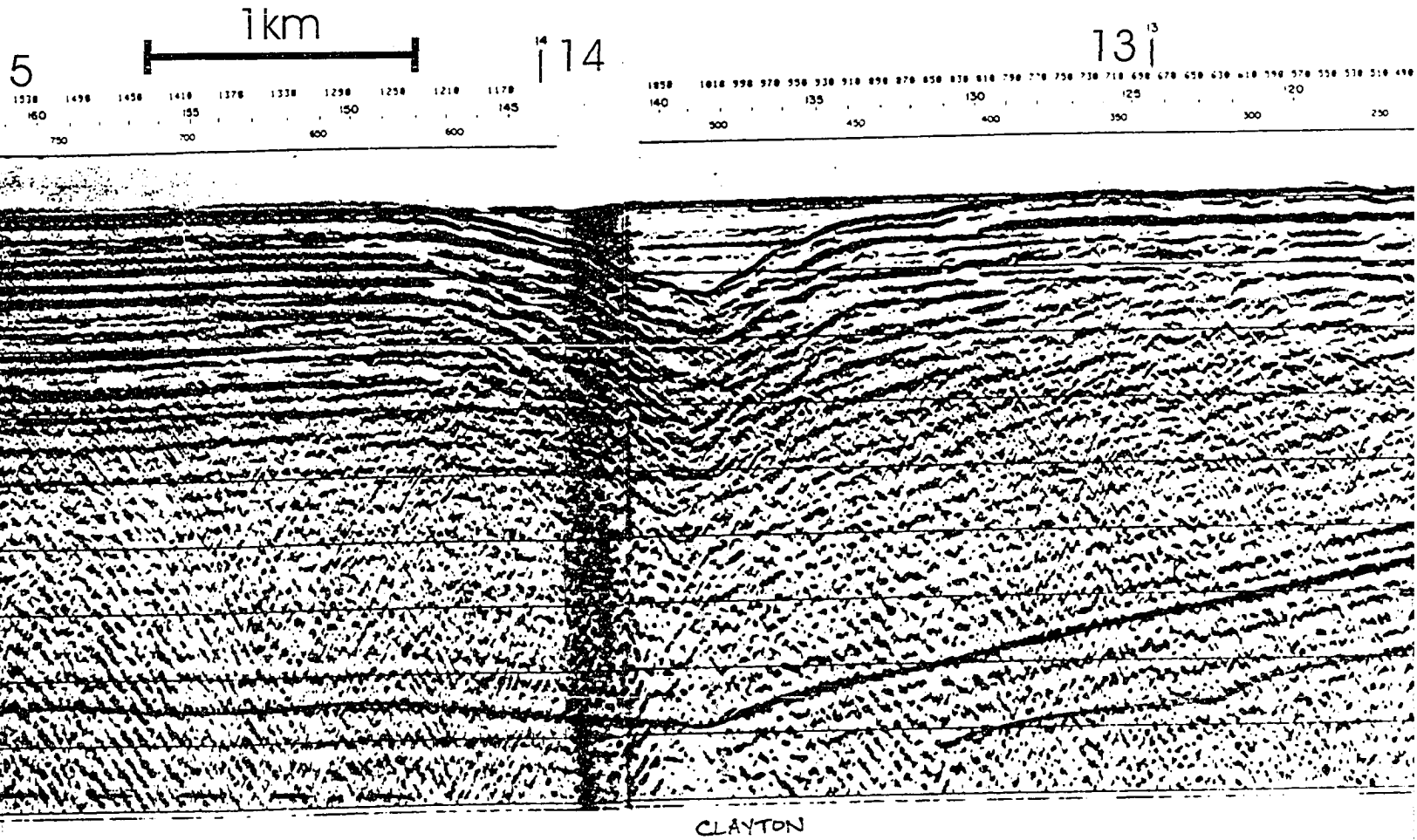
1km
5
14
14
13
13
CLAYTON
FOLD

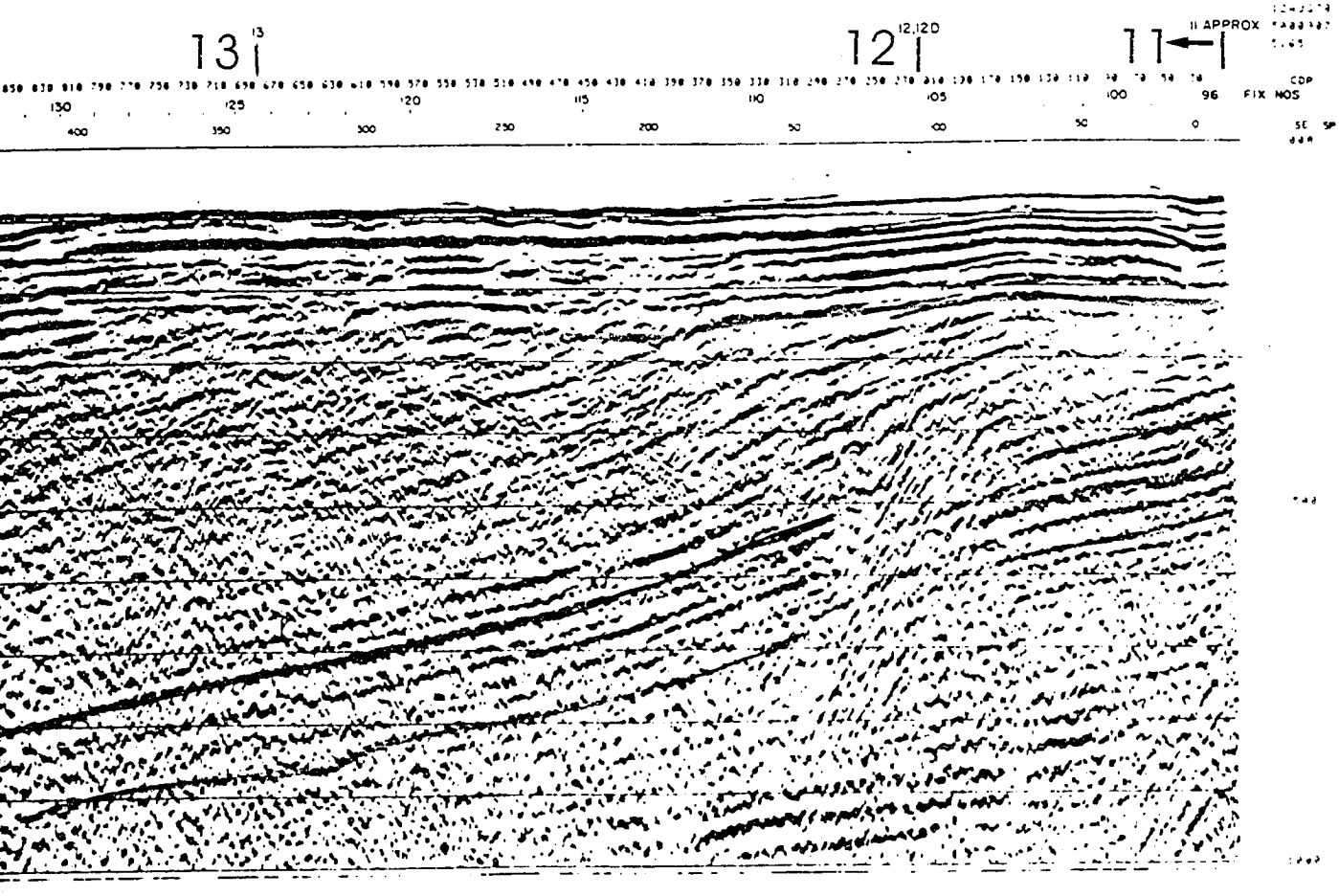
13
13
12,12D
12
11
APPROX
CDP
FIX NOS
130
125
120
115
110
105
100
96
400
350
300
250
200
50
0
SE
SP

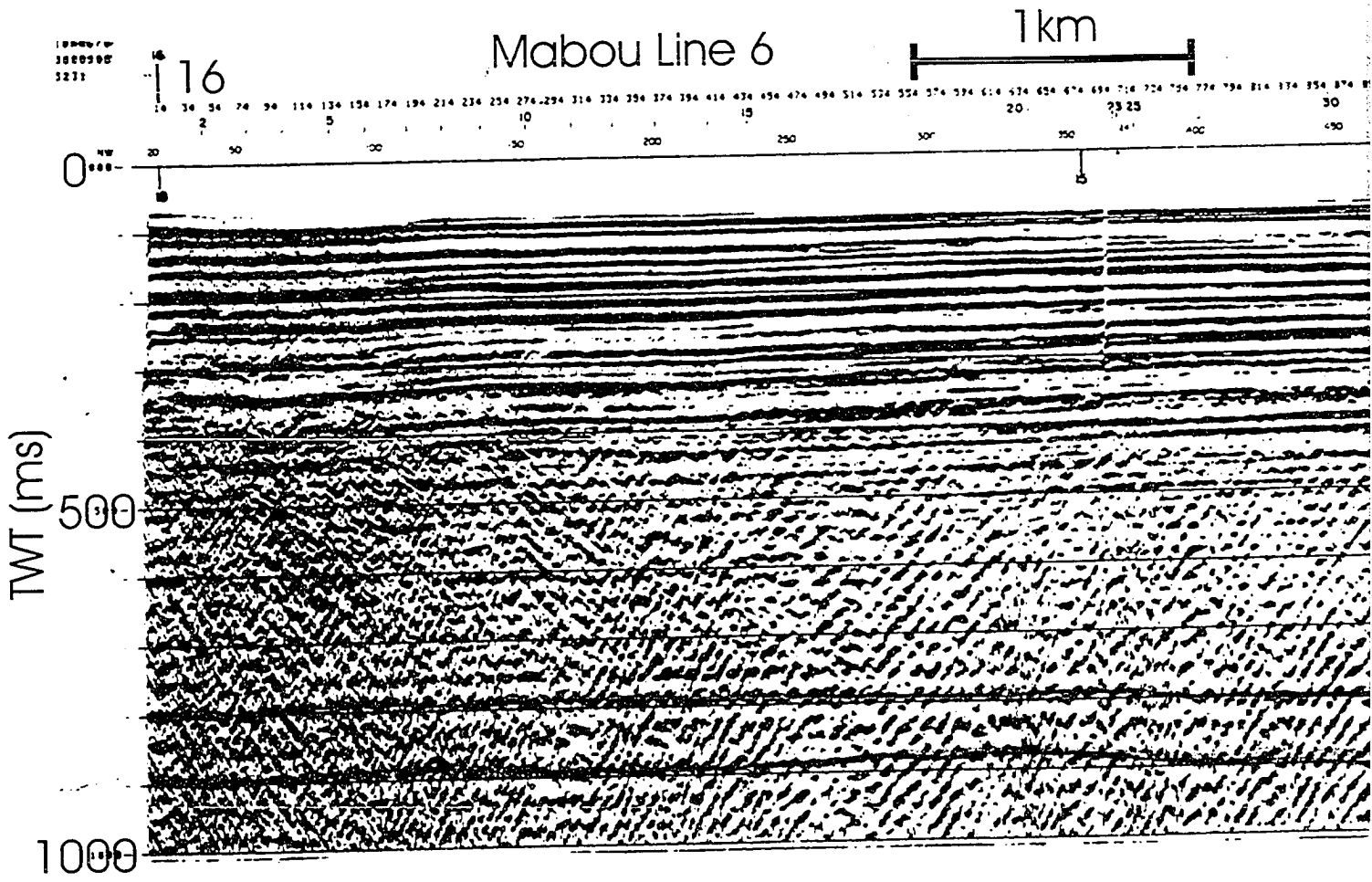
Mabou Line 6
1km
16
TWT (ms)
0
500
1000

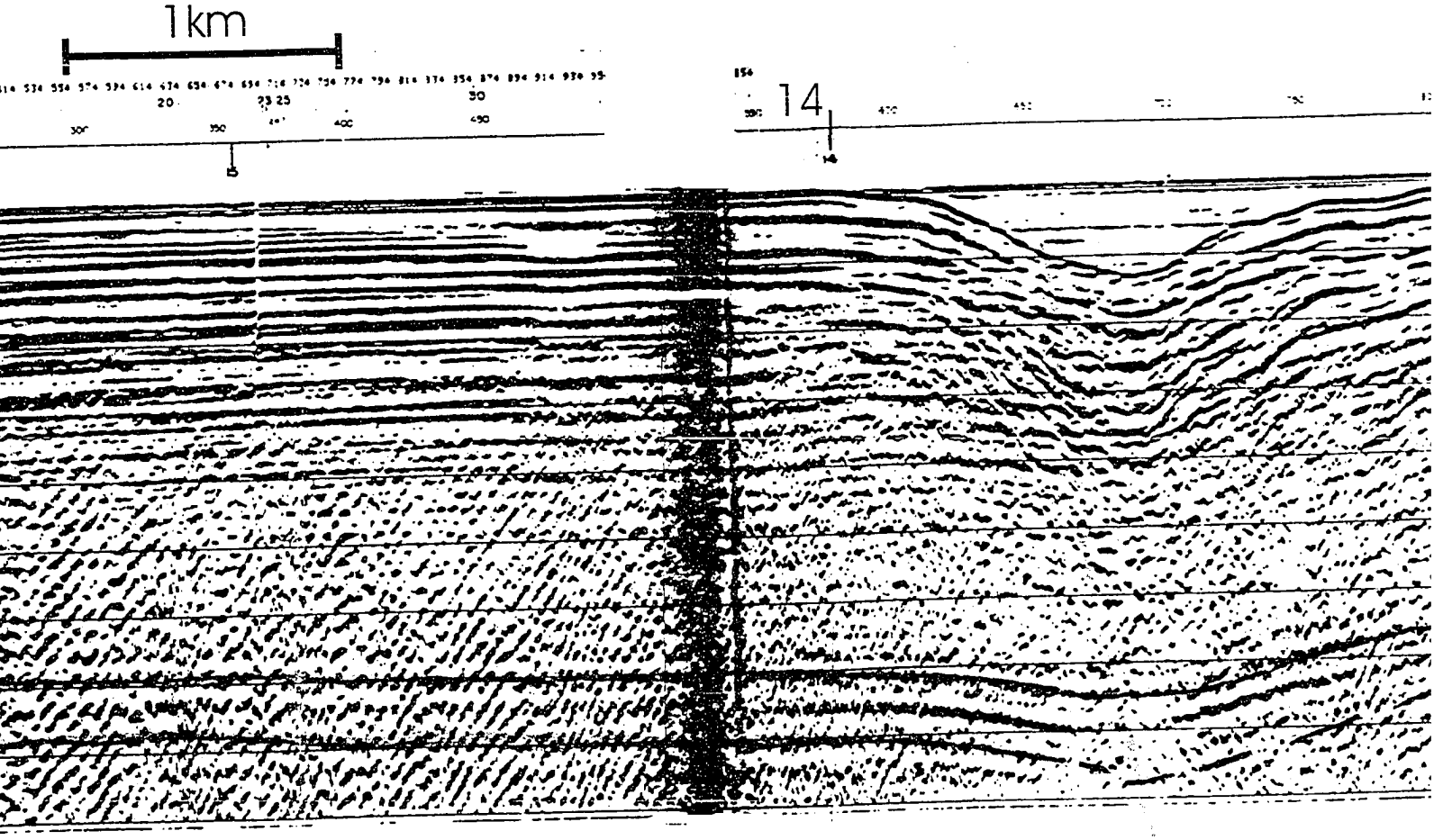

CLAYTON
FOLD

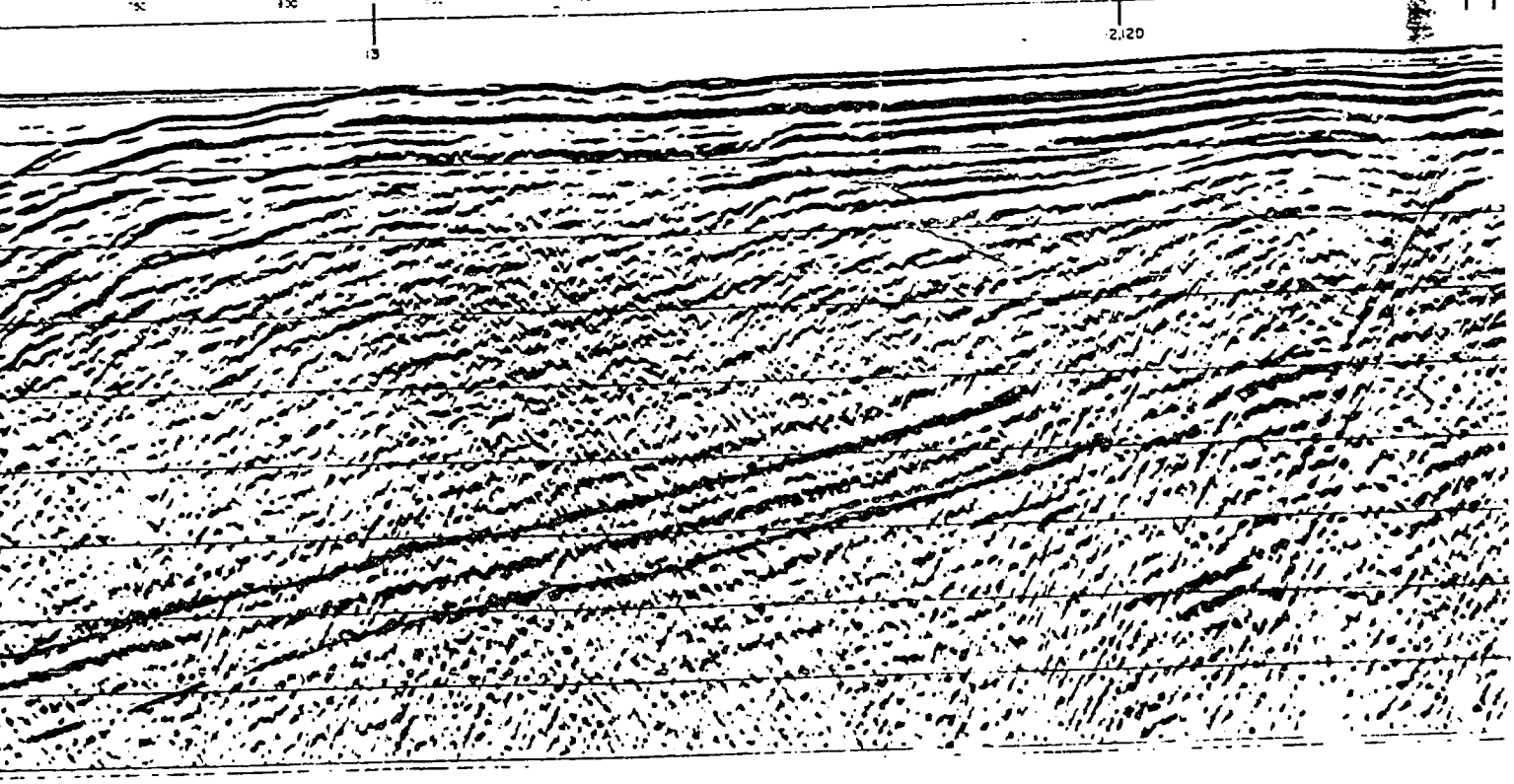

TON
D

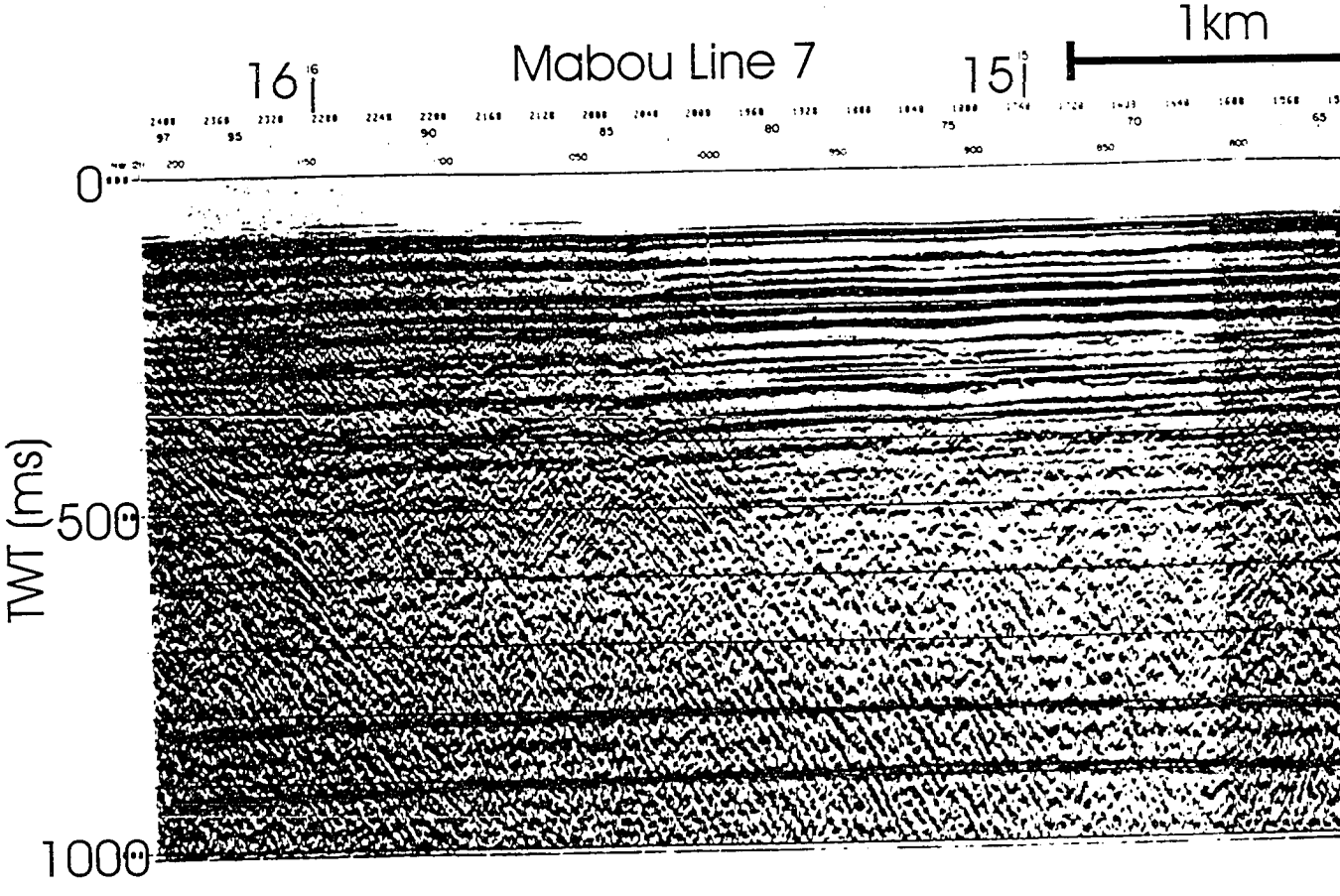
Mabou Line 7
1km
16
15
0
500
1000
TWT (ms)

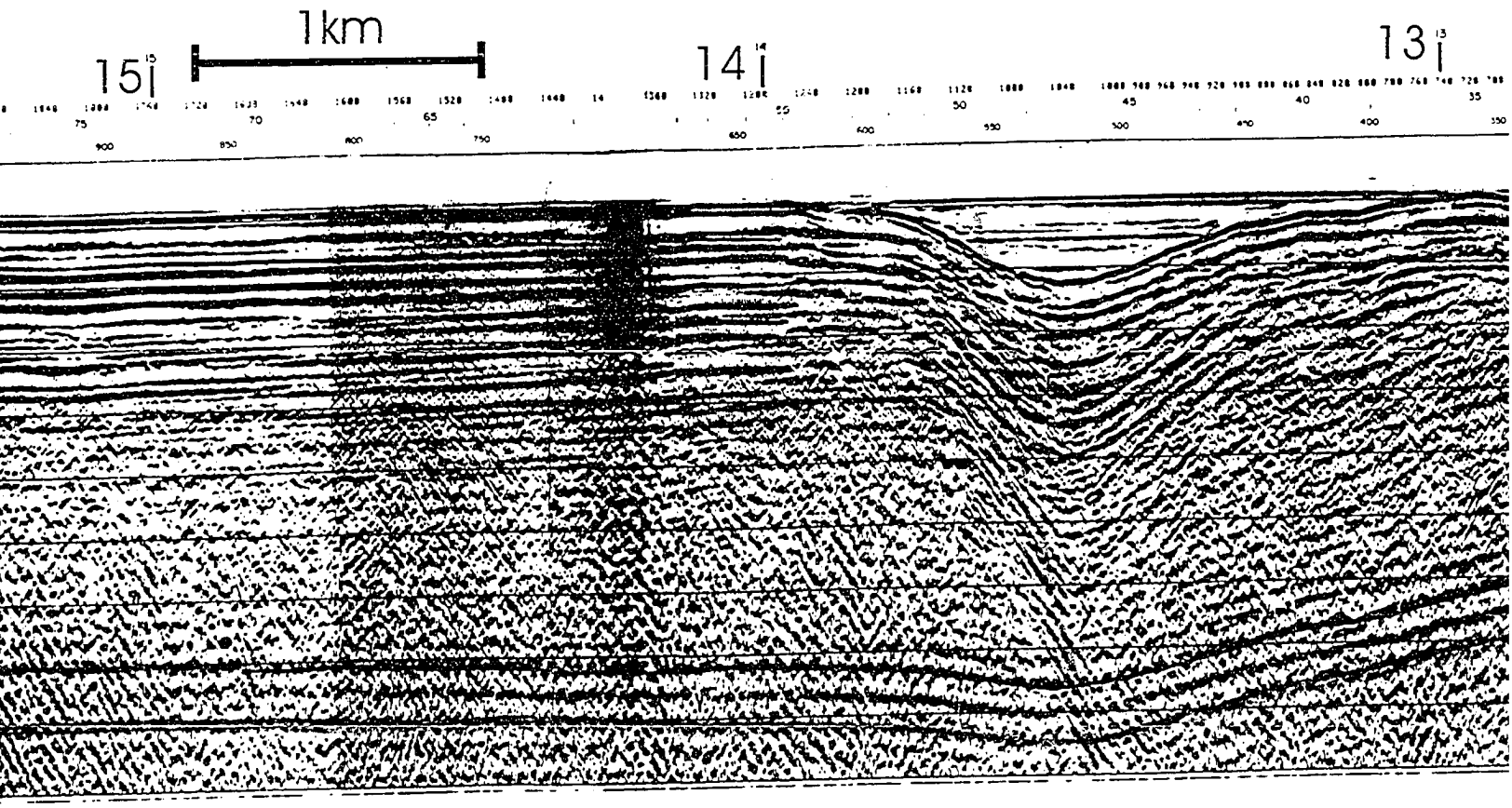

CLAYTON
FOLD

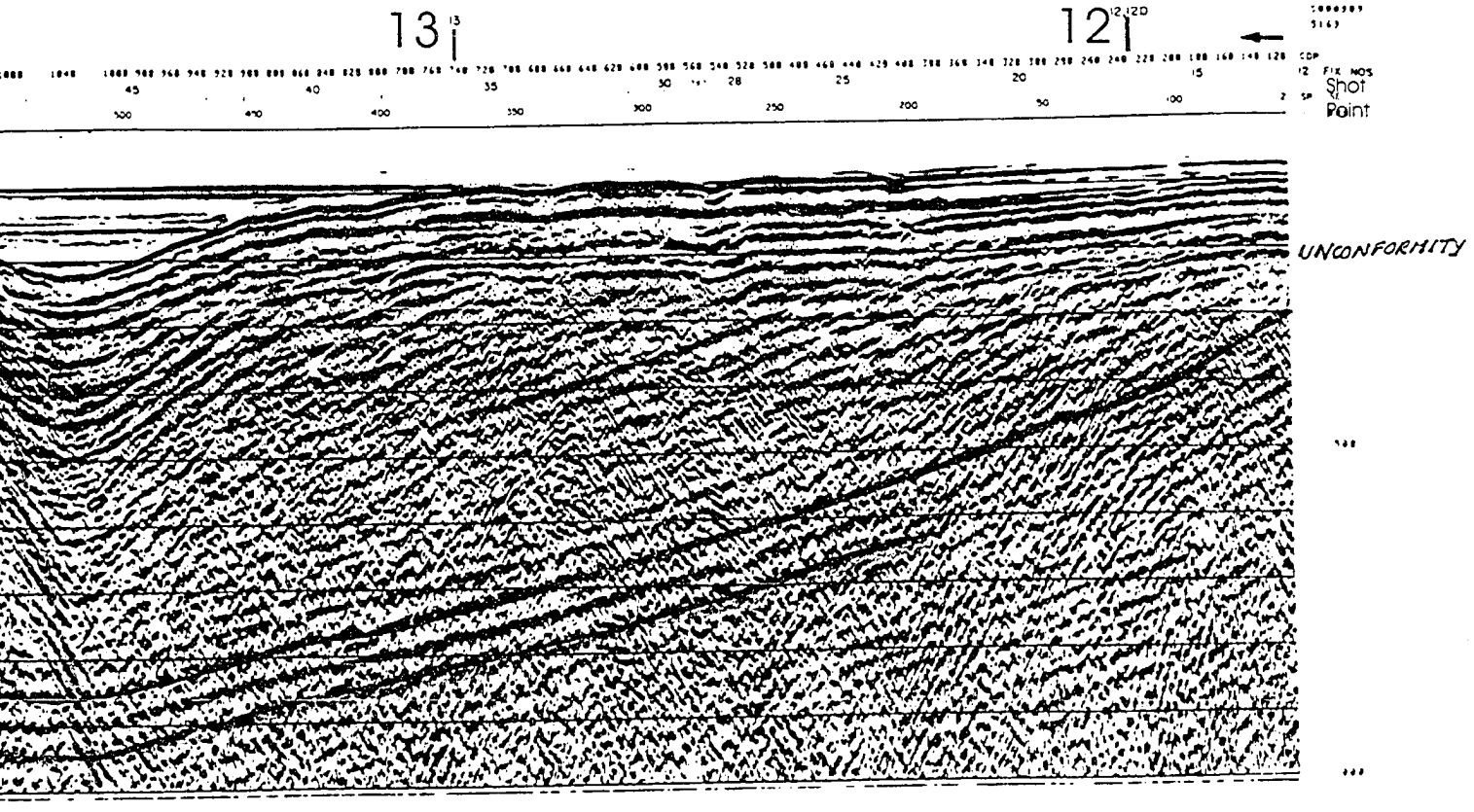

CLAYTON FOLD

Mabou line 8
DOWNLAP
REFLECTORS
1km
16
15
0
500
1000
TWT (ms)

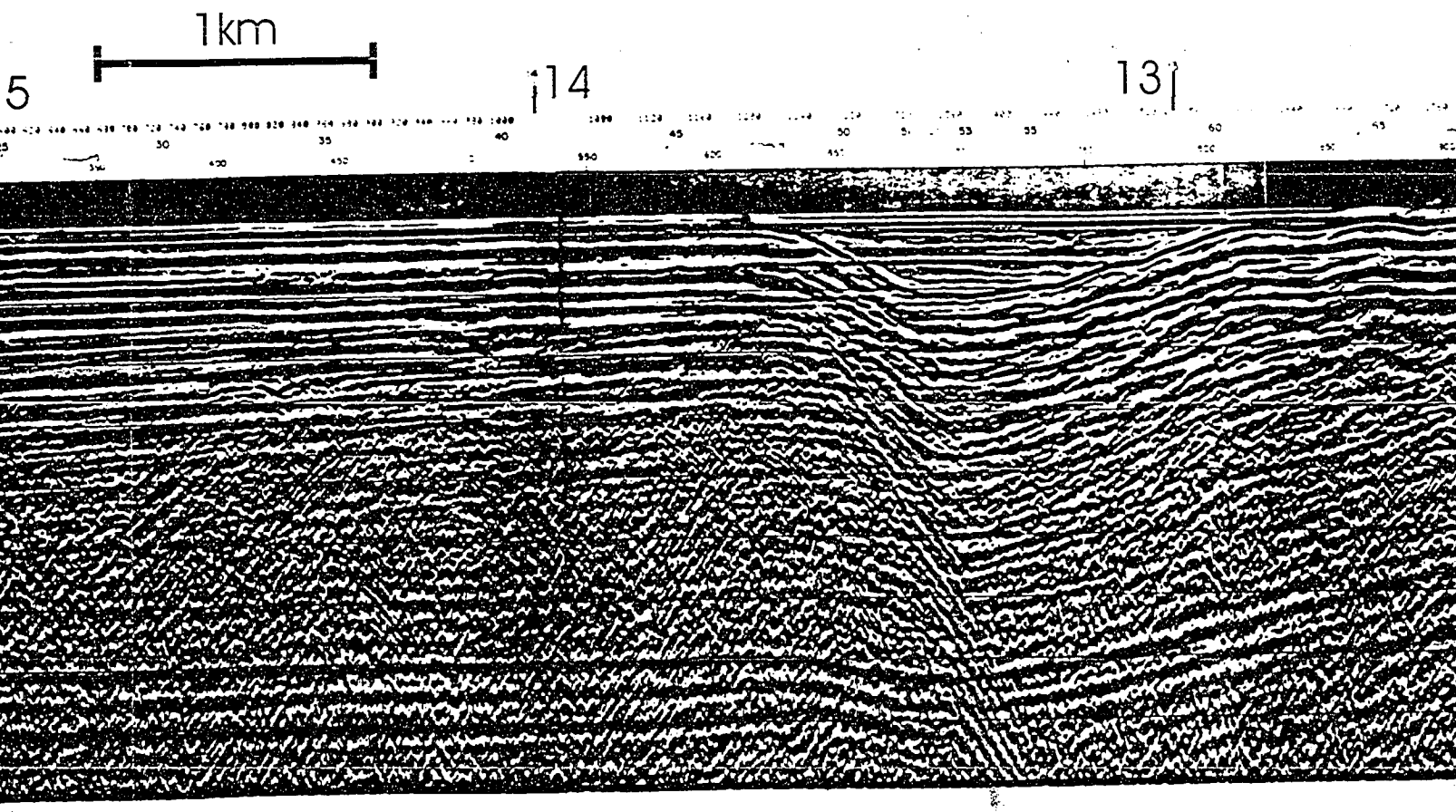

CLAYTON
FOLD

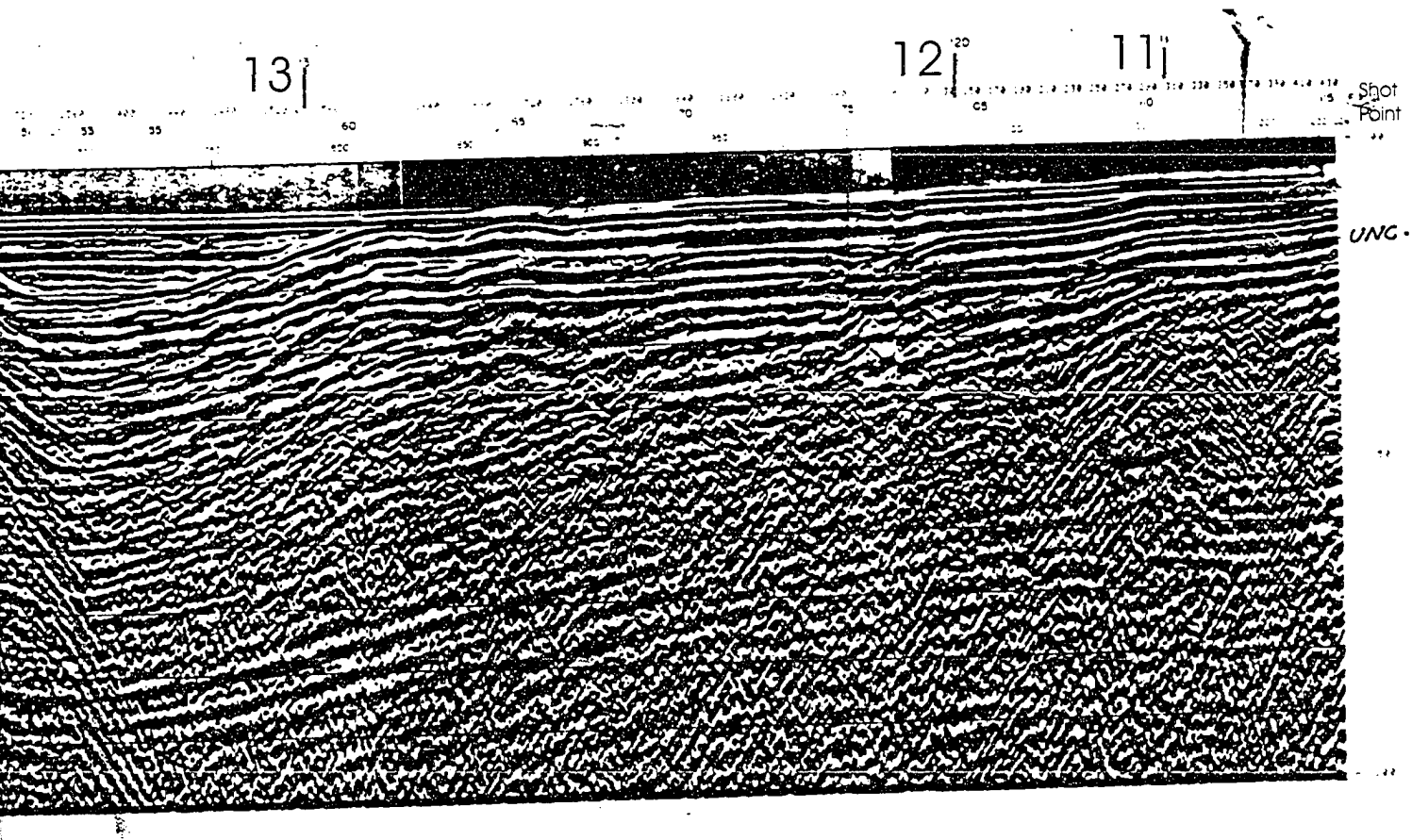

CLAYTON FOLD

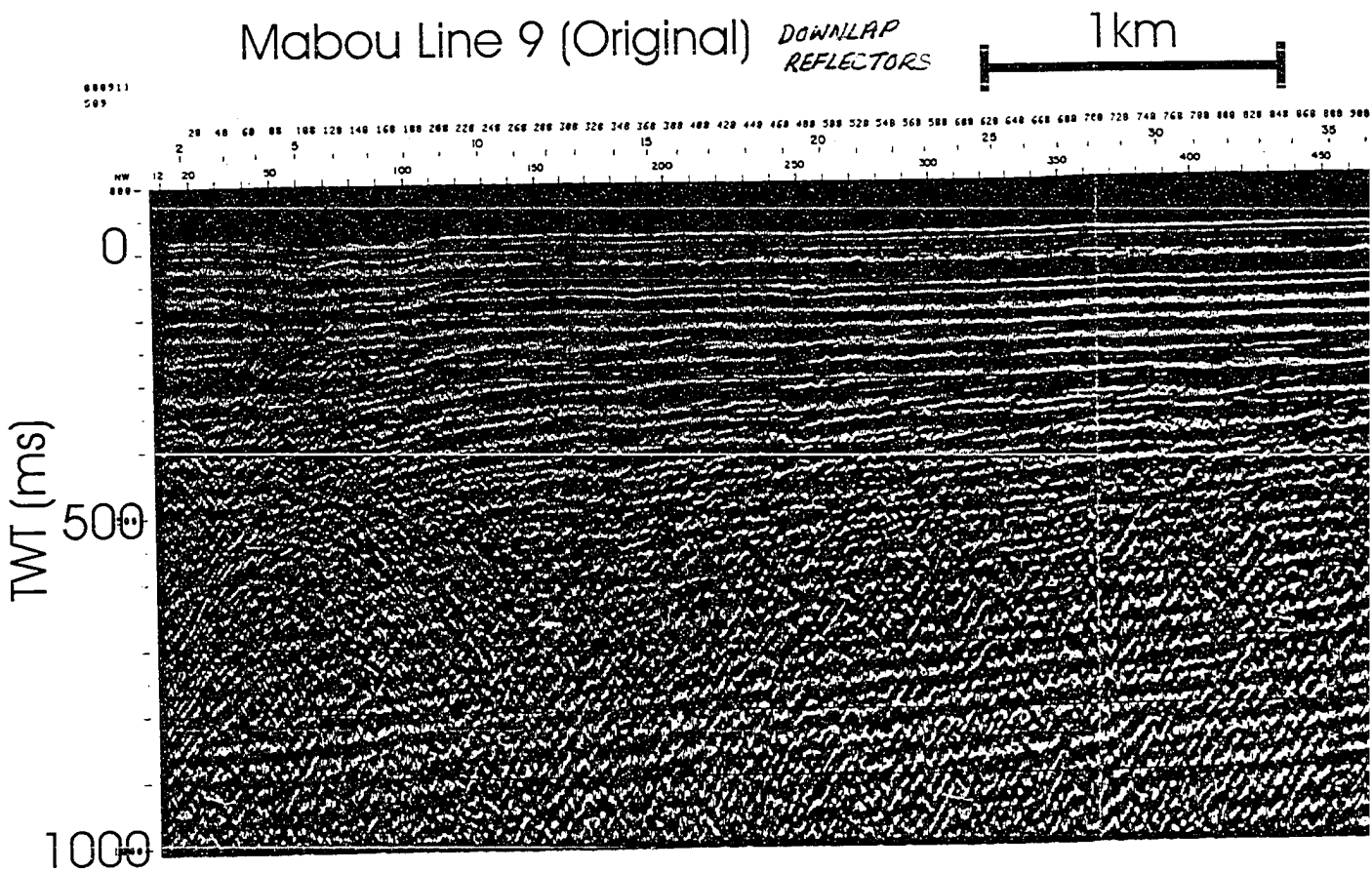
Mabou Line 9 (Original)
DOWNLAP REFLECTORS
1km
TWT (ms)
0
500
1000

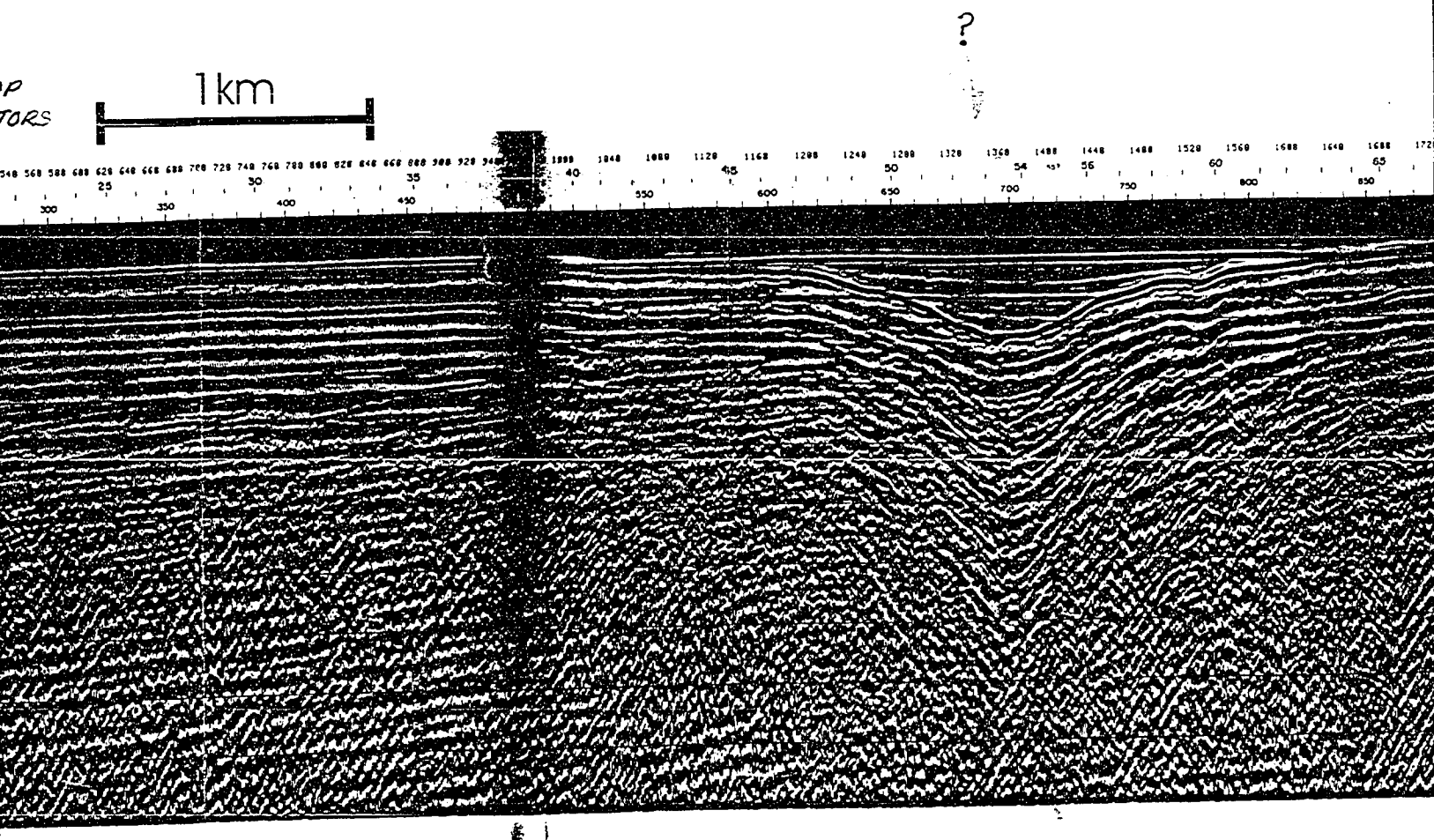
?
1km
CLAYTON
FOLD

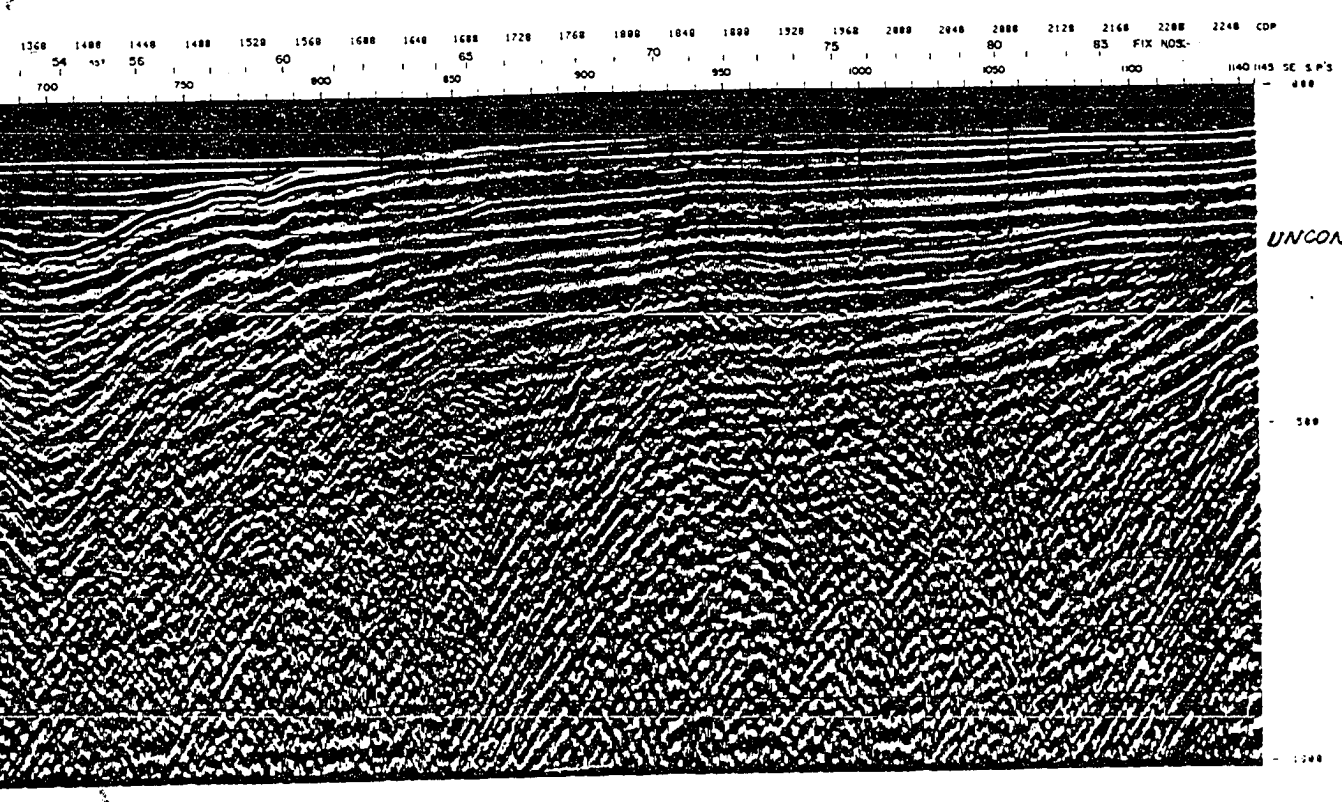

CLAYTON FOLD

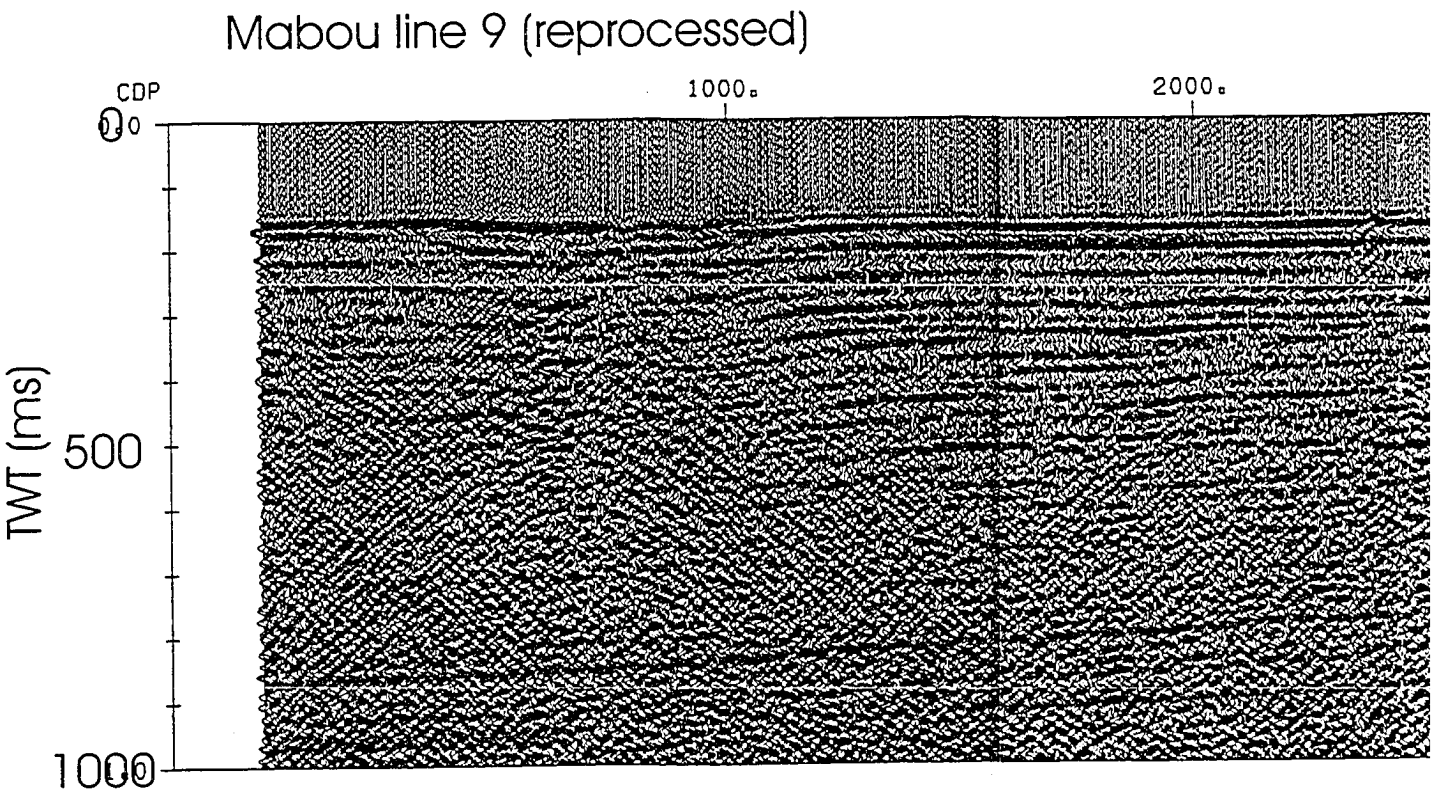
Mabou line 9 (reprocessed)
CDP
1000
2000
0.0
TWT (ms)
500
1000

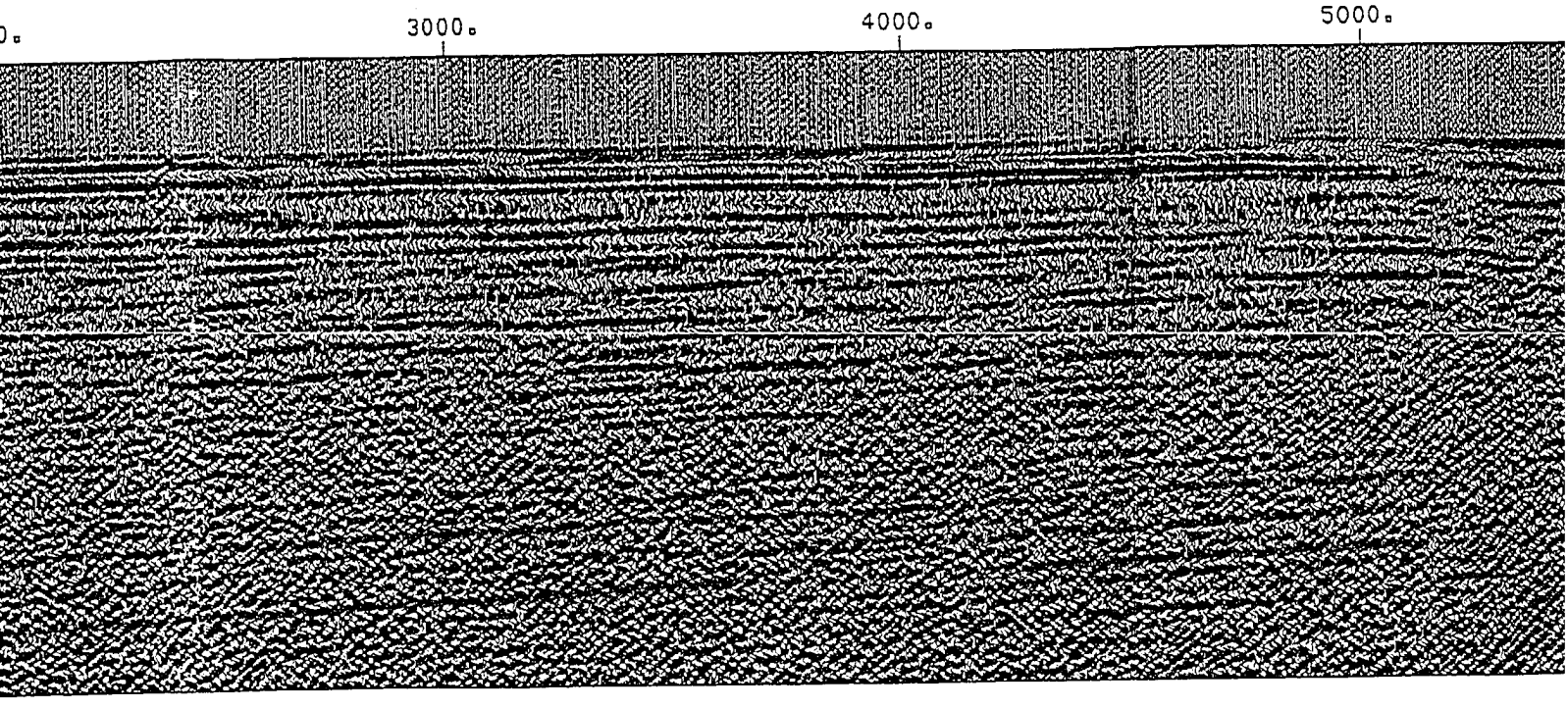
0.
3000.
4000.
5000.

?

5000.

6000.

7000.

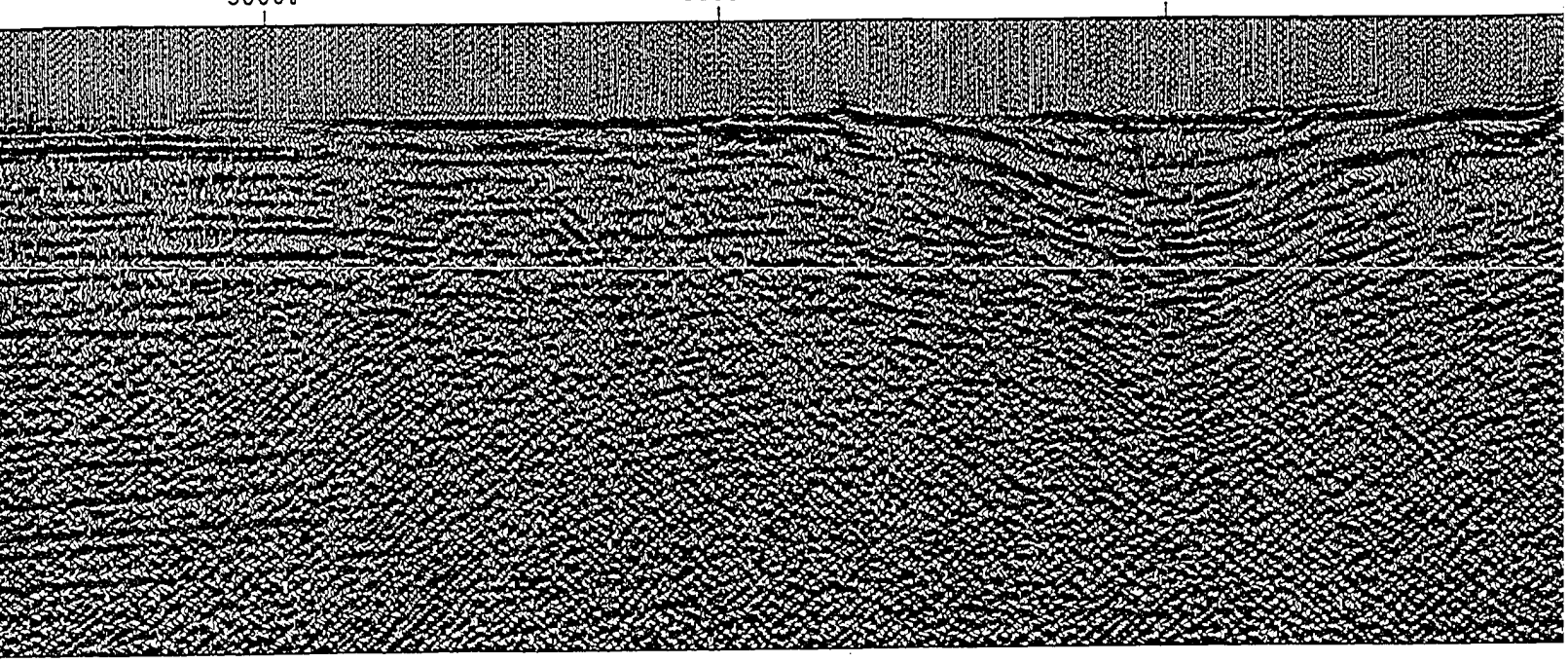

CLAYTON FOLD

?

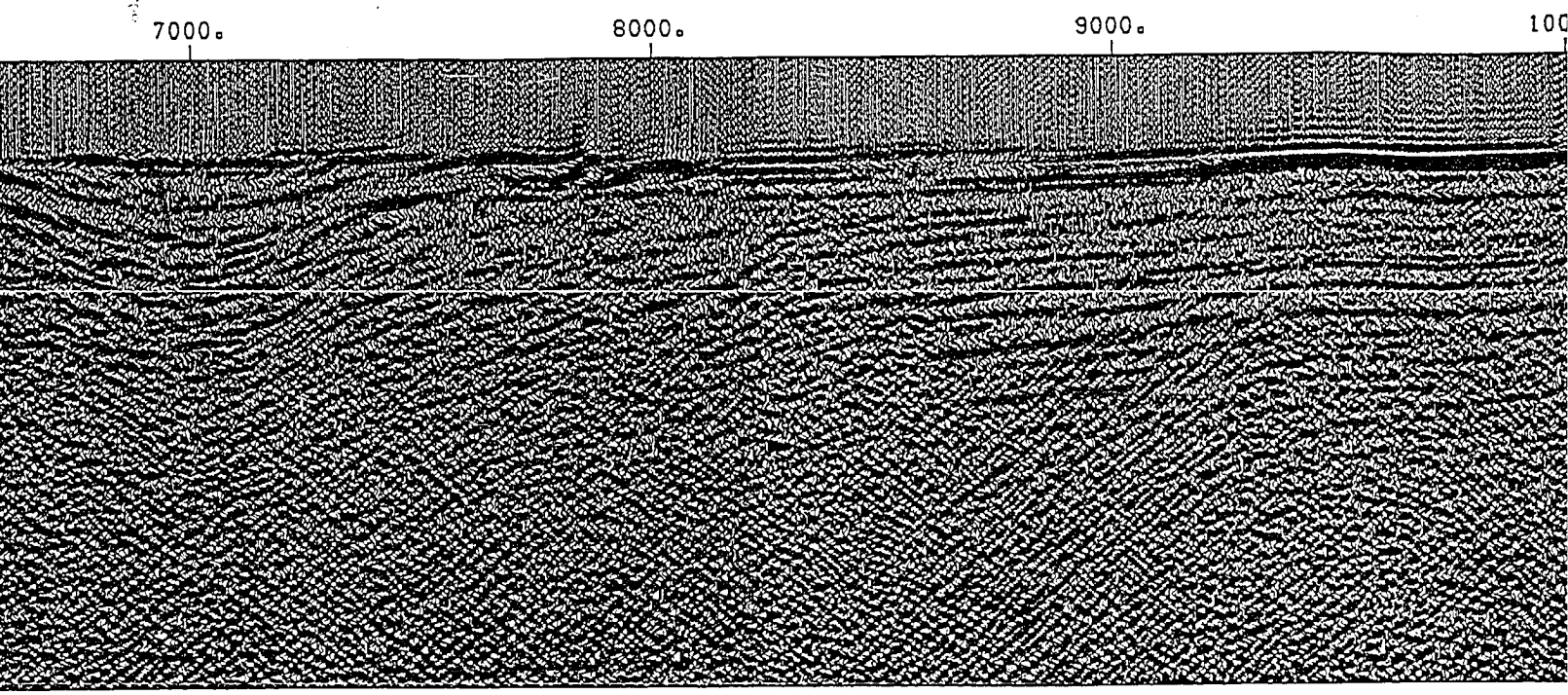

CLAYTON FOLD

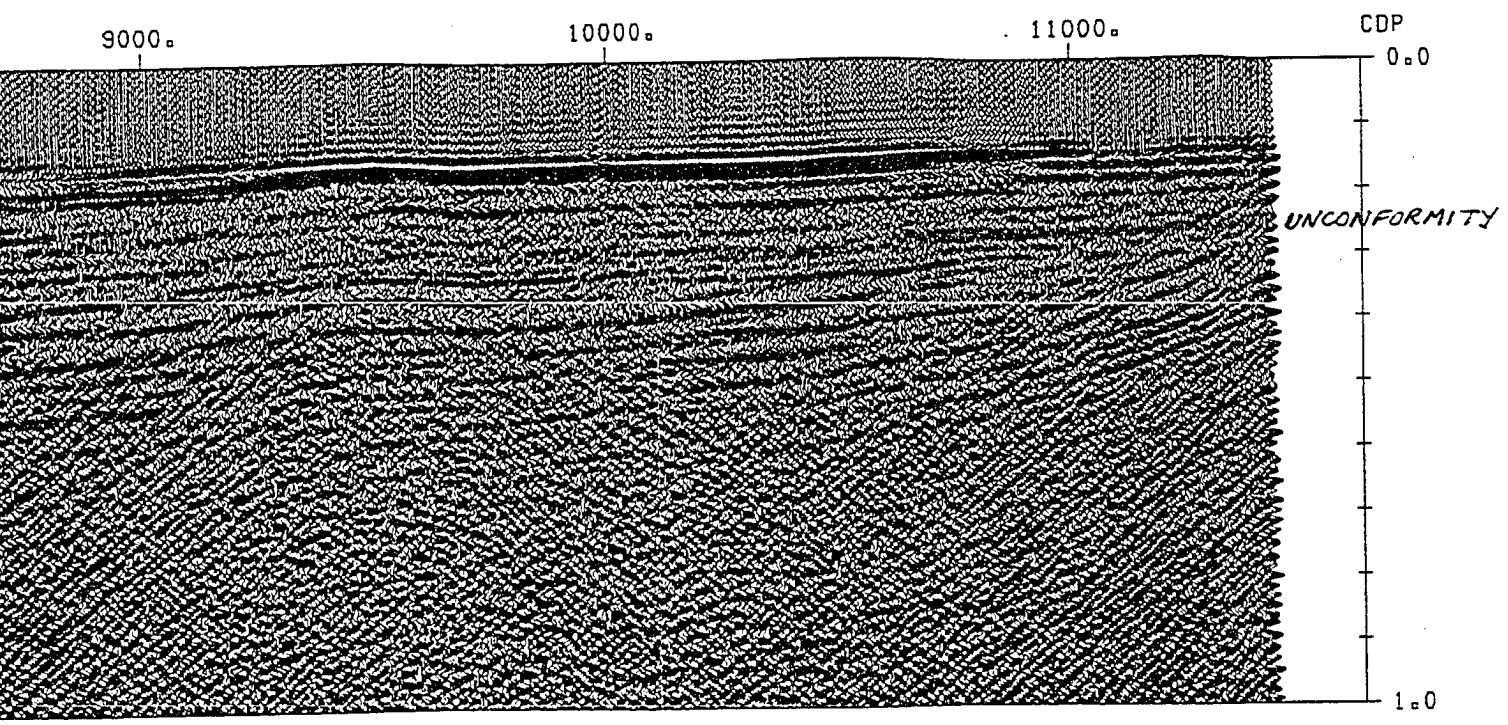
9000.
10000.
11000.
CDP
0.0
UNCONFORMITY
1.0

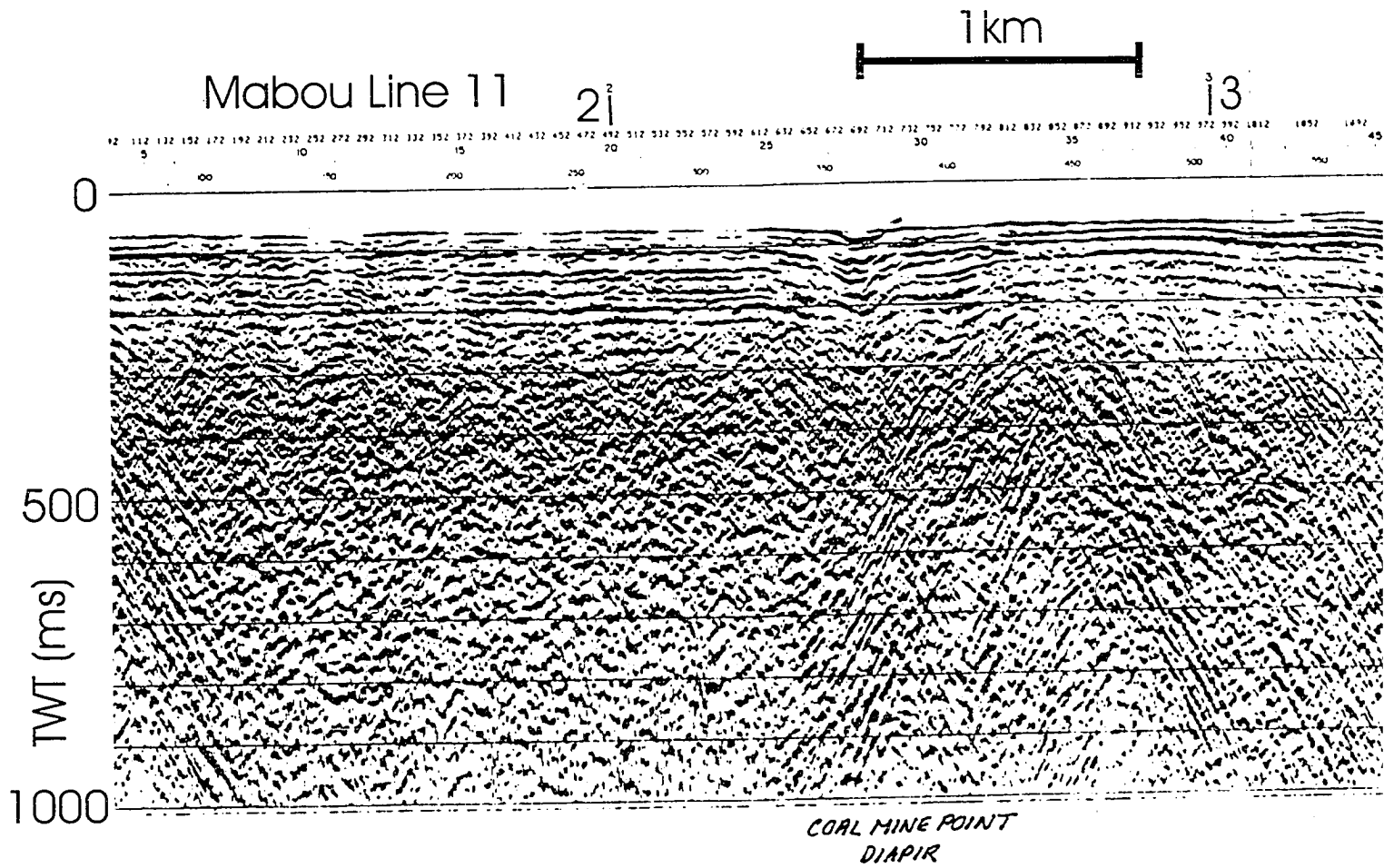
1km
Mabou Line 11
2
3
0
500
1000
TWT (ms)
COAL MINE POINT
DIAPIR

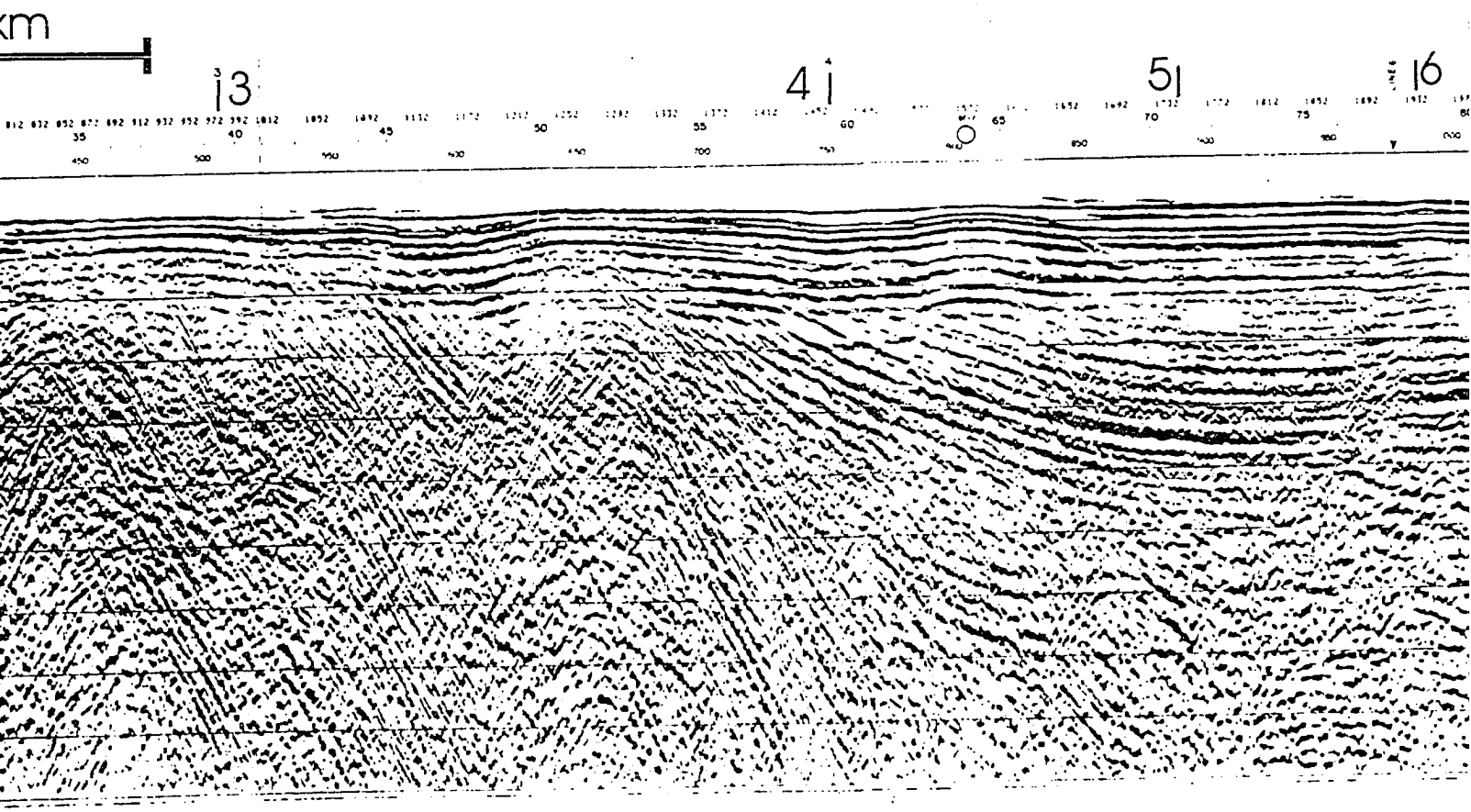
km
3
13
4
14
5
15
16
LINES

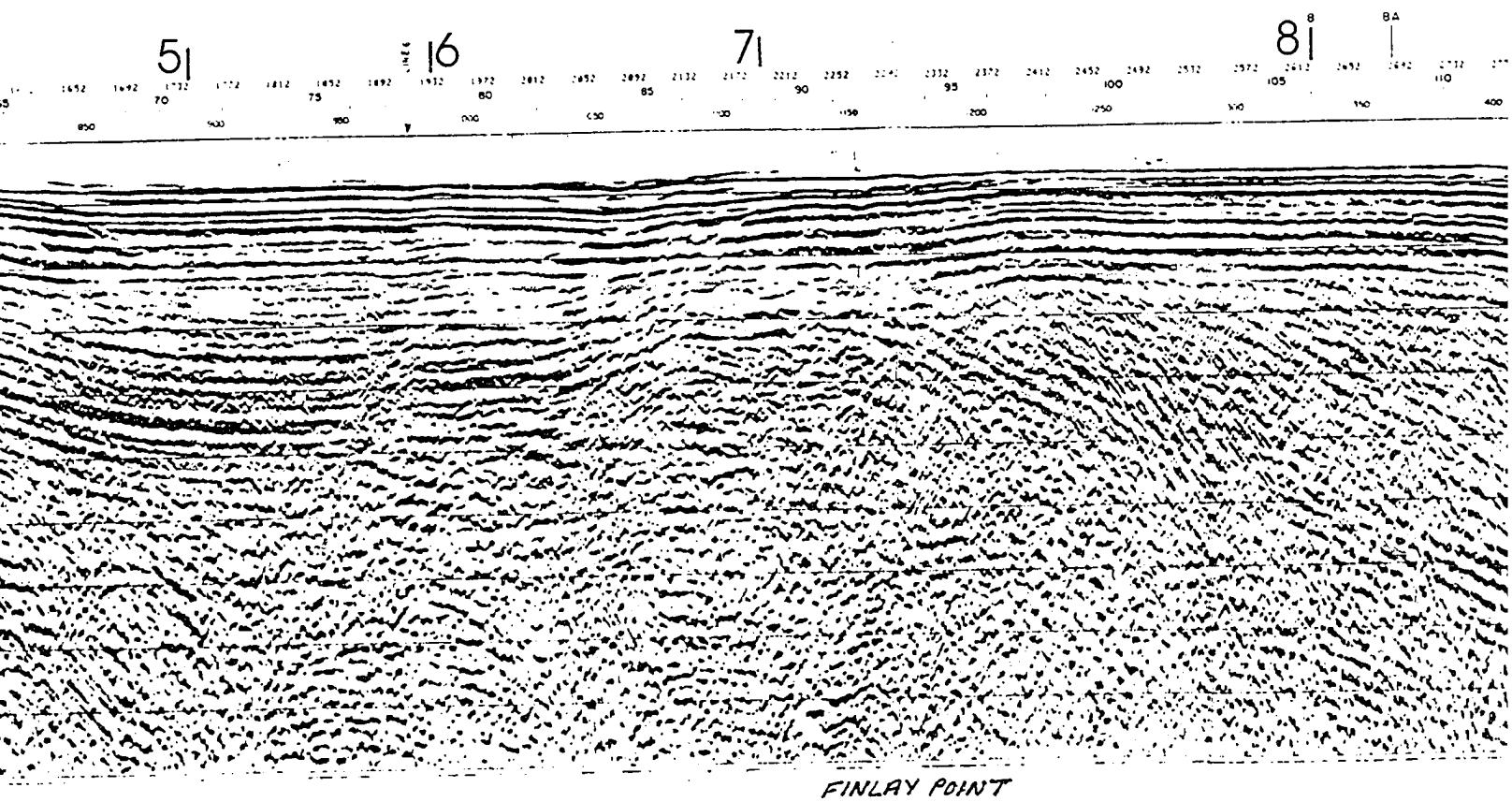

FINLAY POINT
DIAPIR

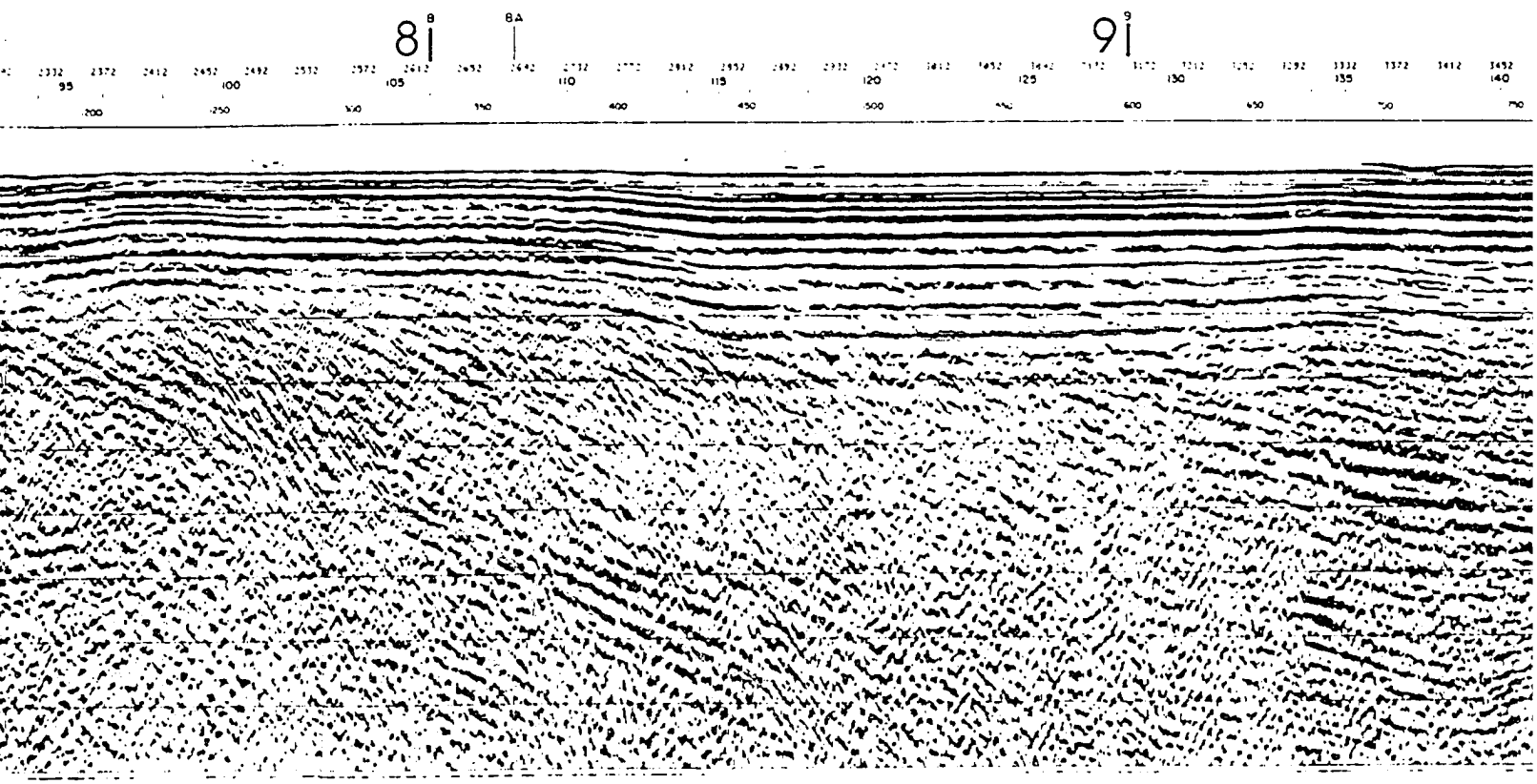

AY POINT
APIR

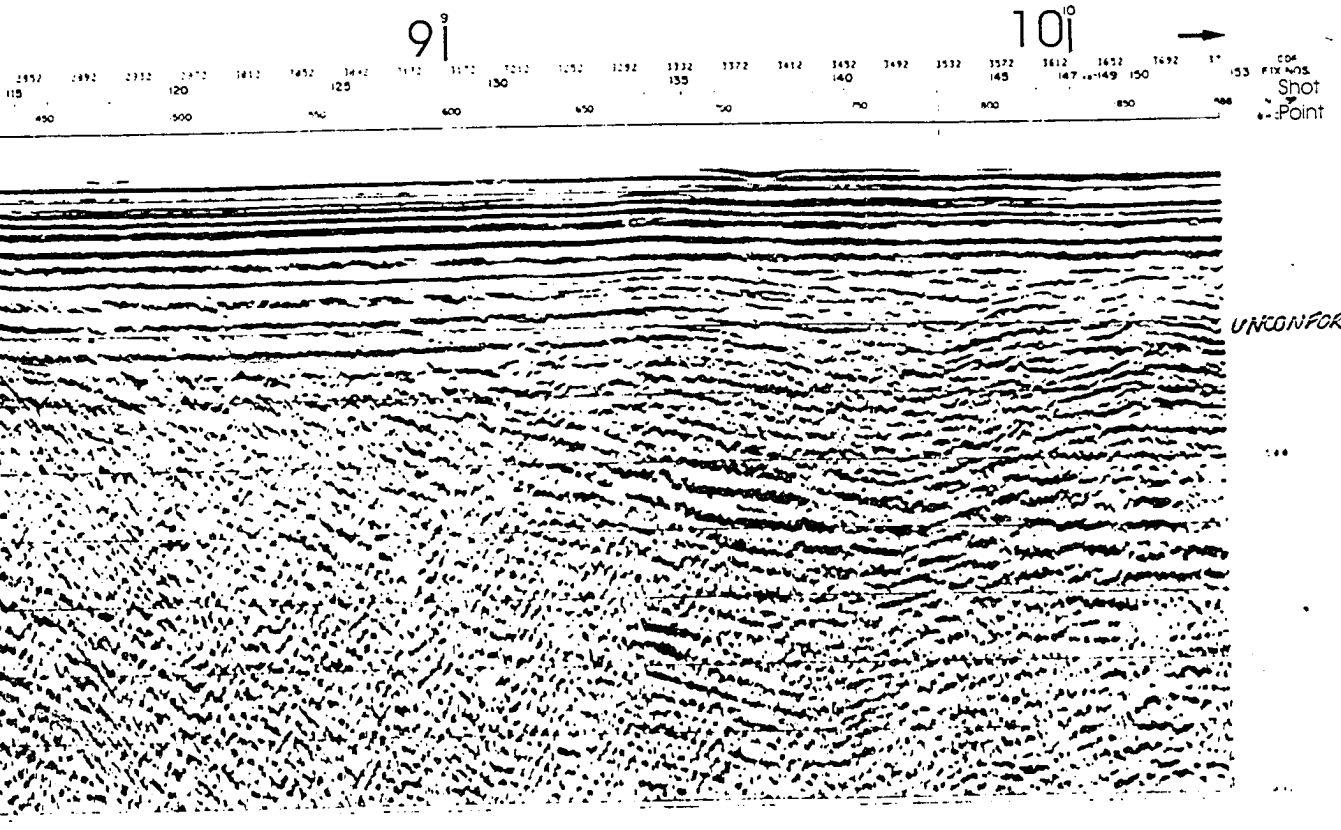
9
10
CDP FIX NOS.
Shot Point
UNCONFORMITY.

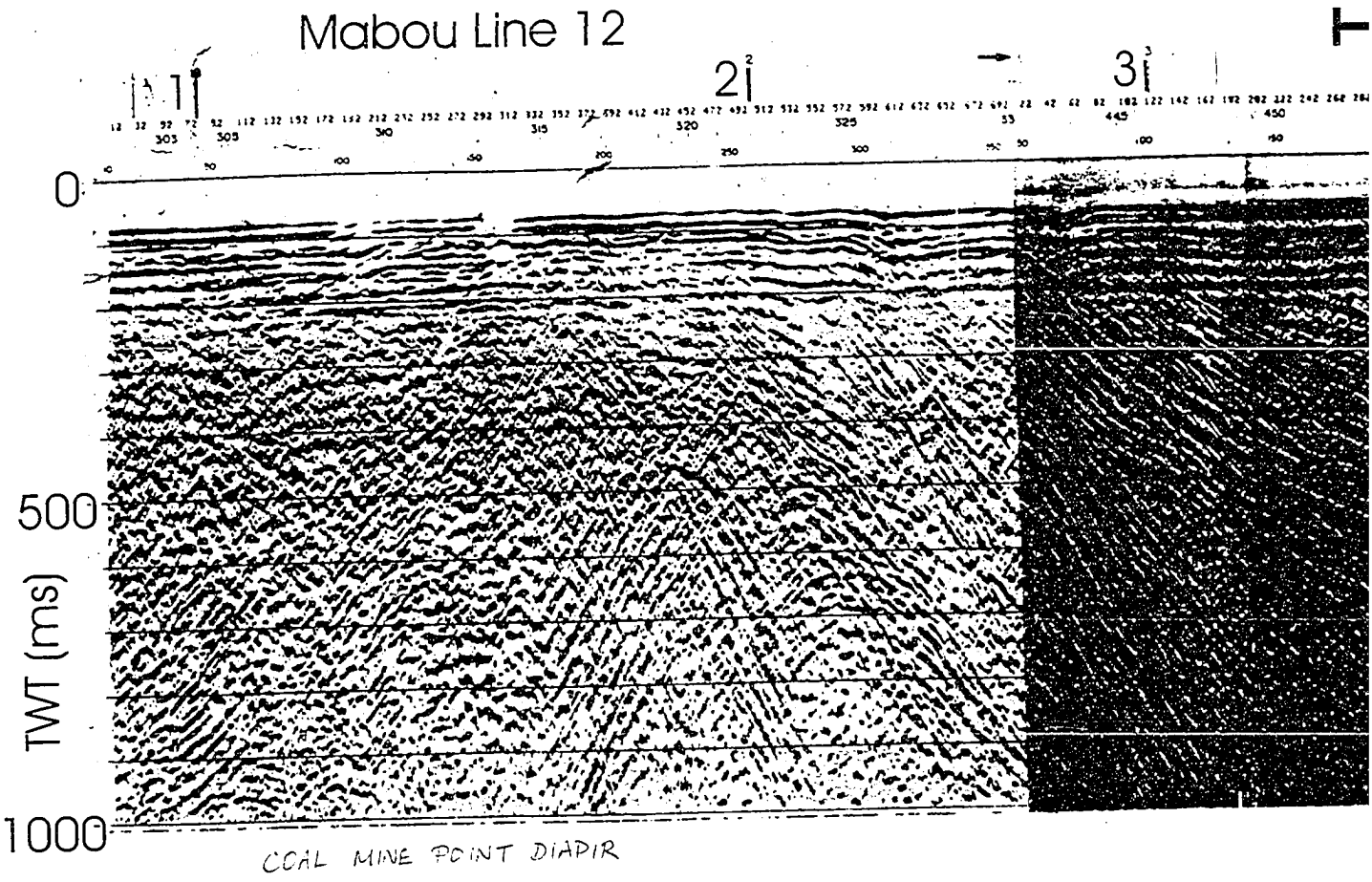
Mabou Line 12
1
2
3
0
500
1000
TWT (ms)
COAL MINE POINT DIAPIR

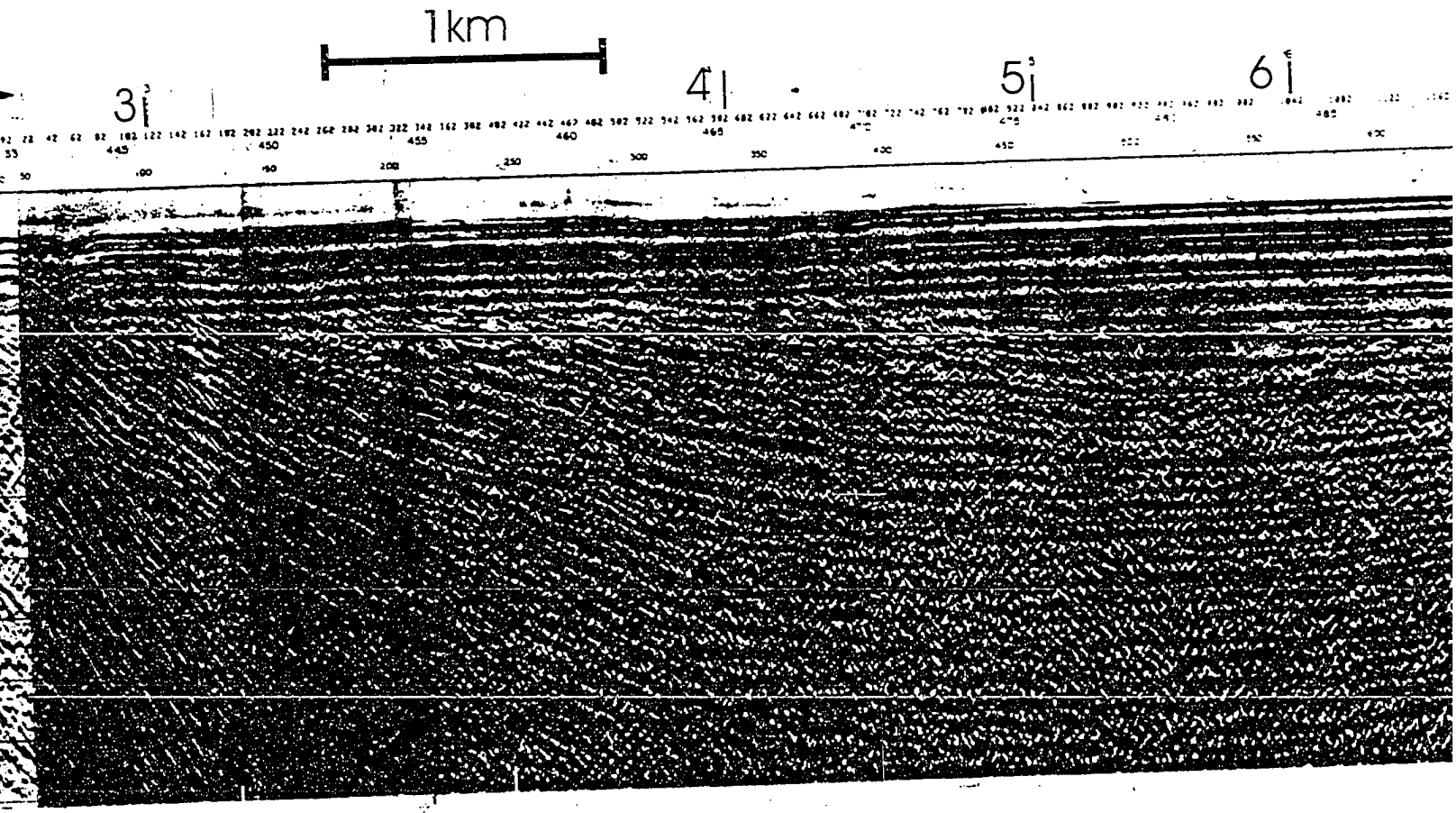
1km
3
4
5
6

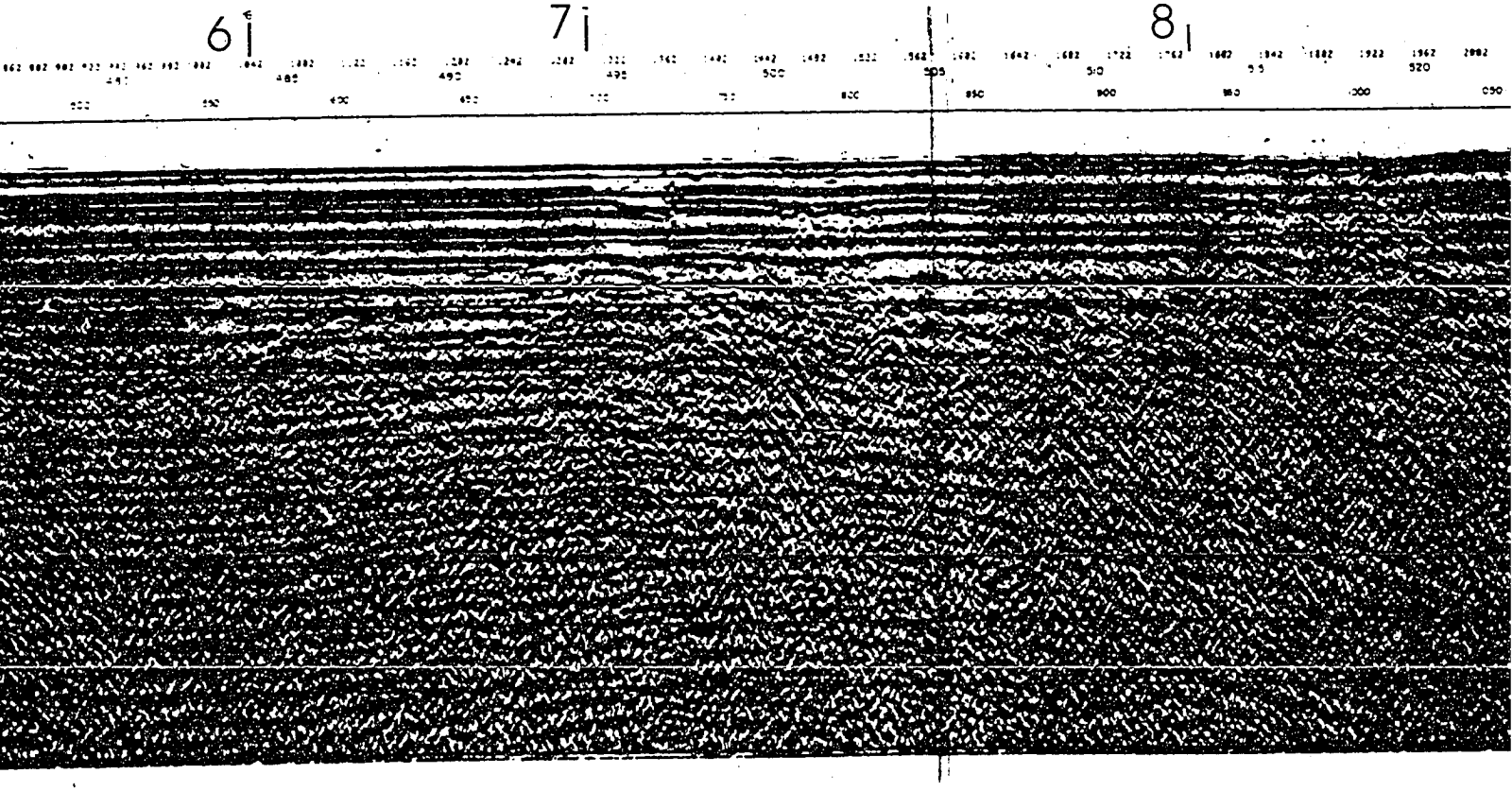
6
7
8

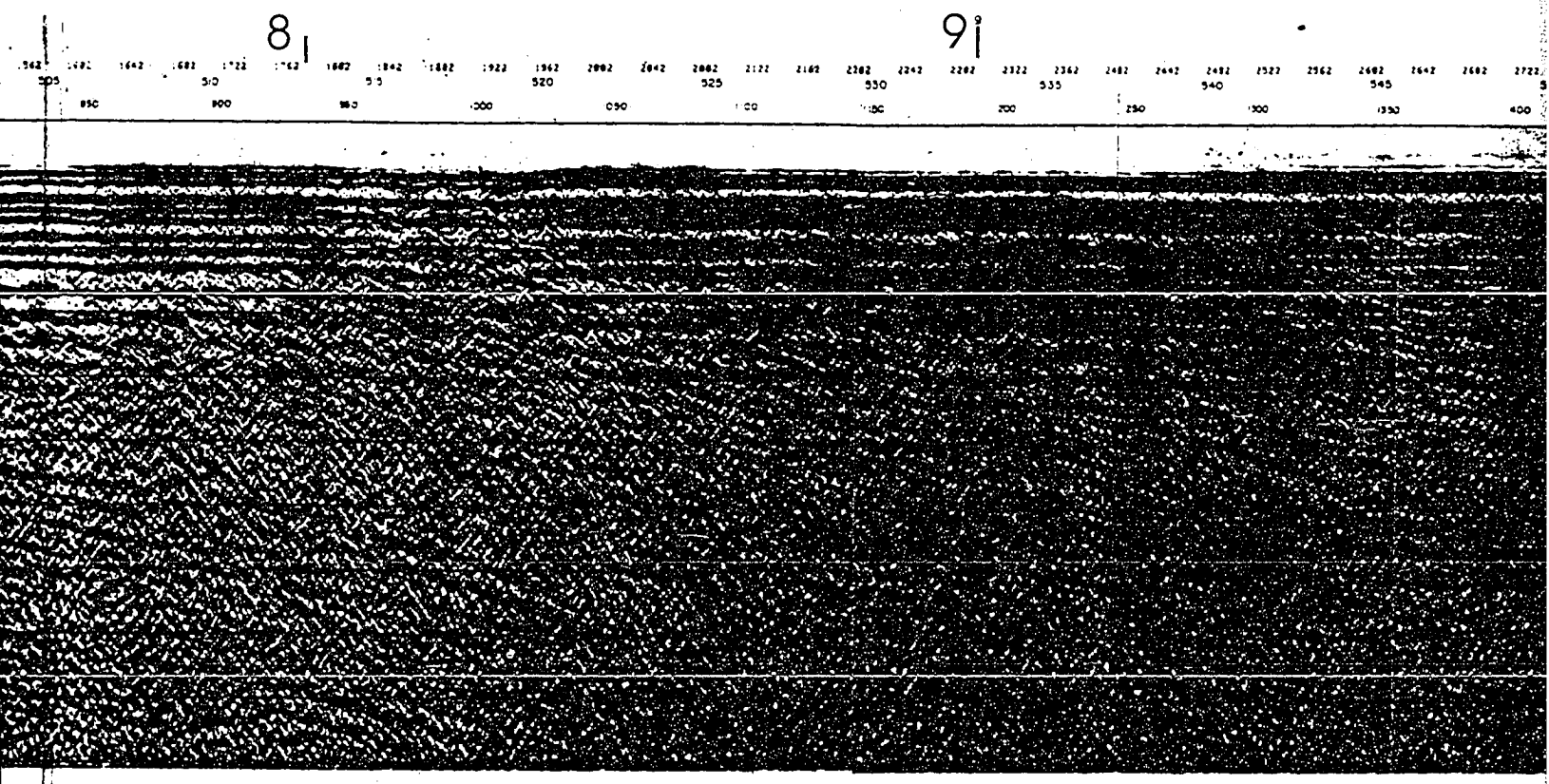
8
9

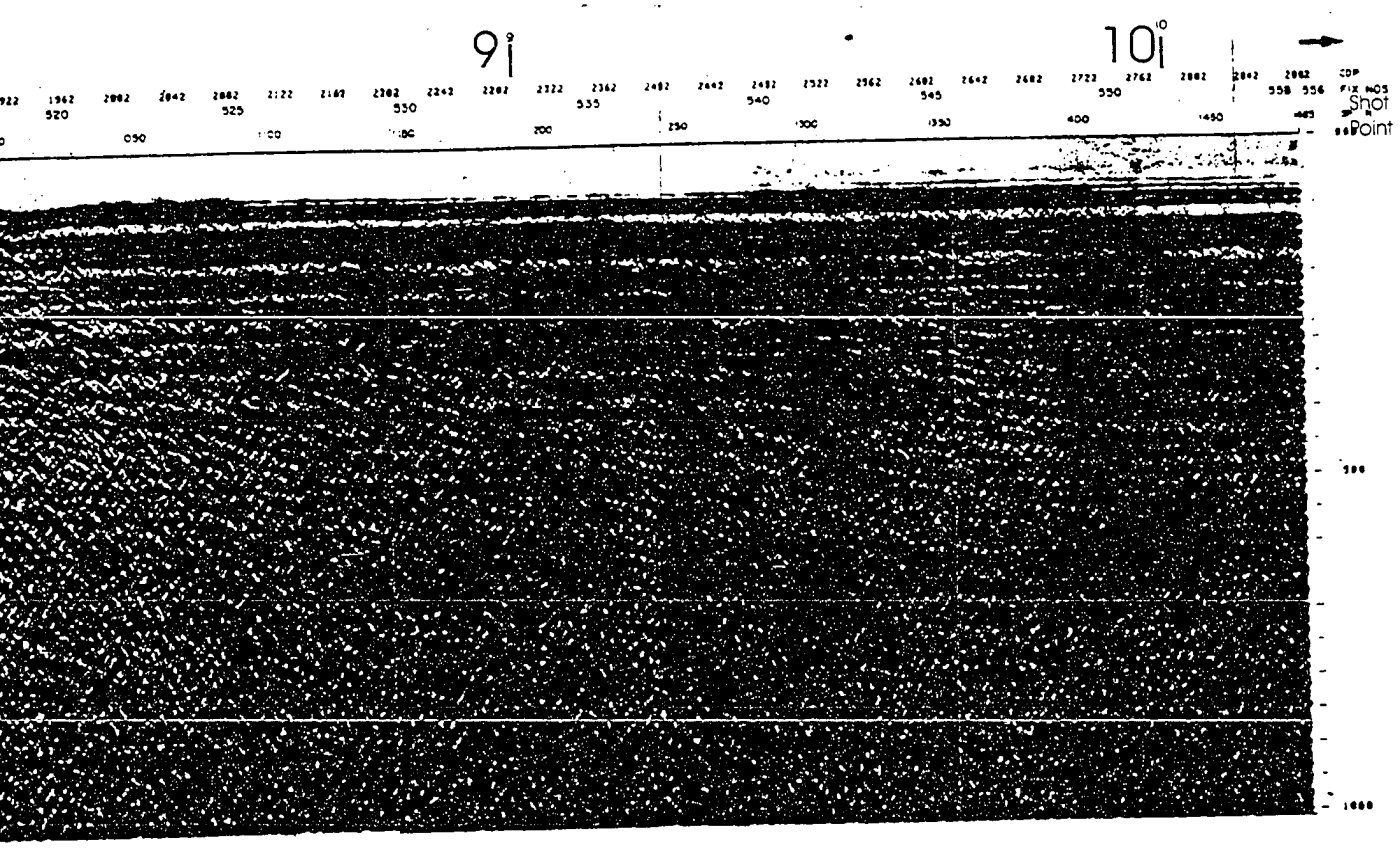
9
10
CDP
FIX NOS
Shot
Point

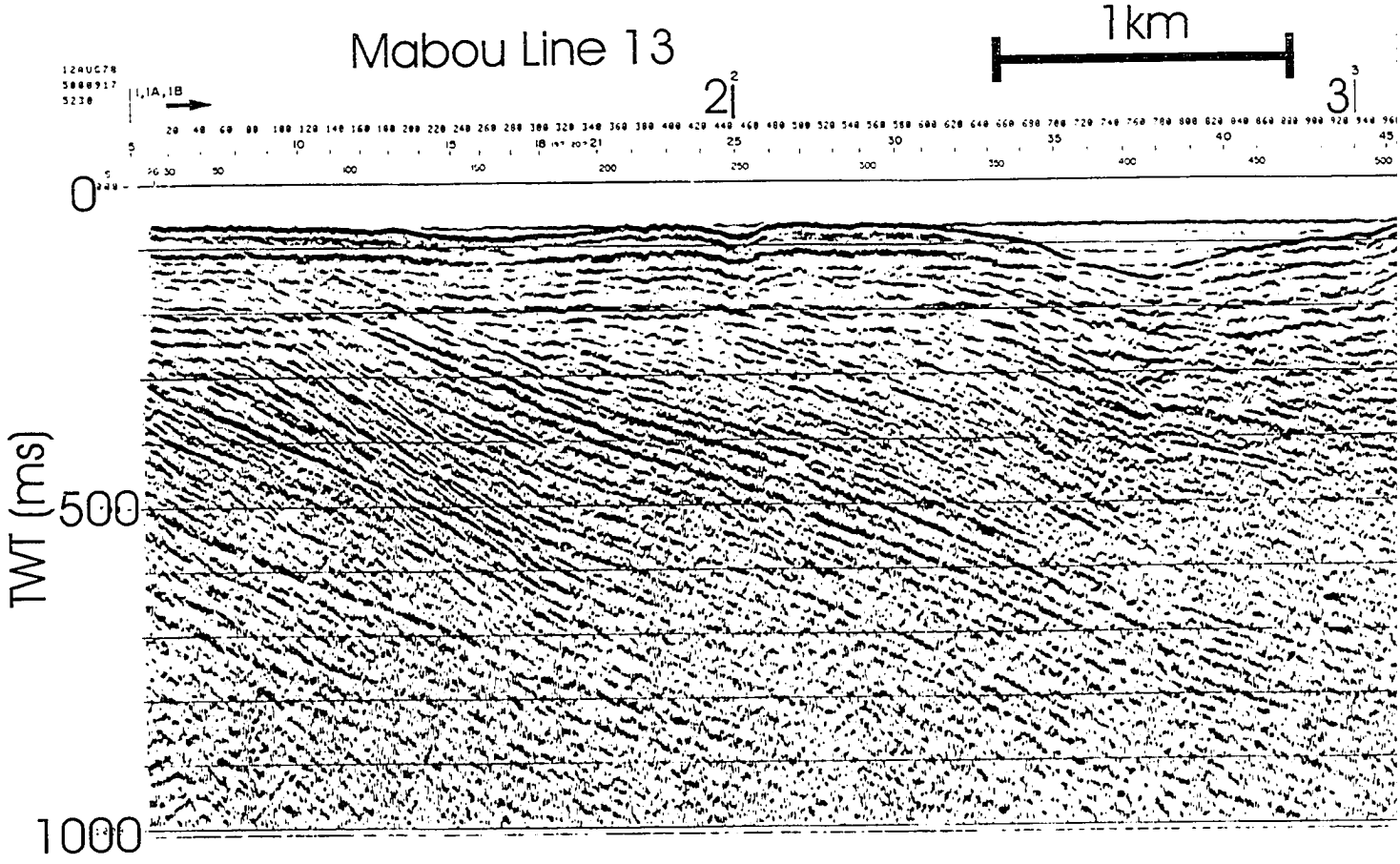
Mabou Line 13
1km
TWT (ms)
0
500
1000

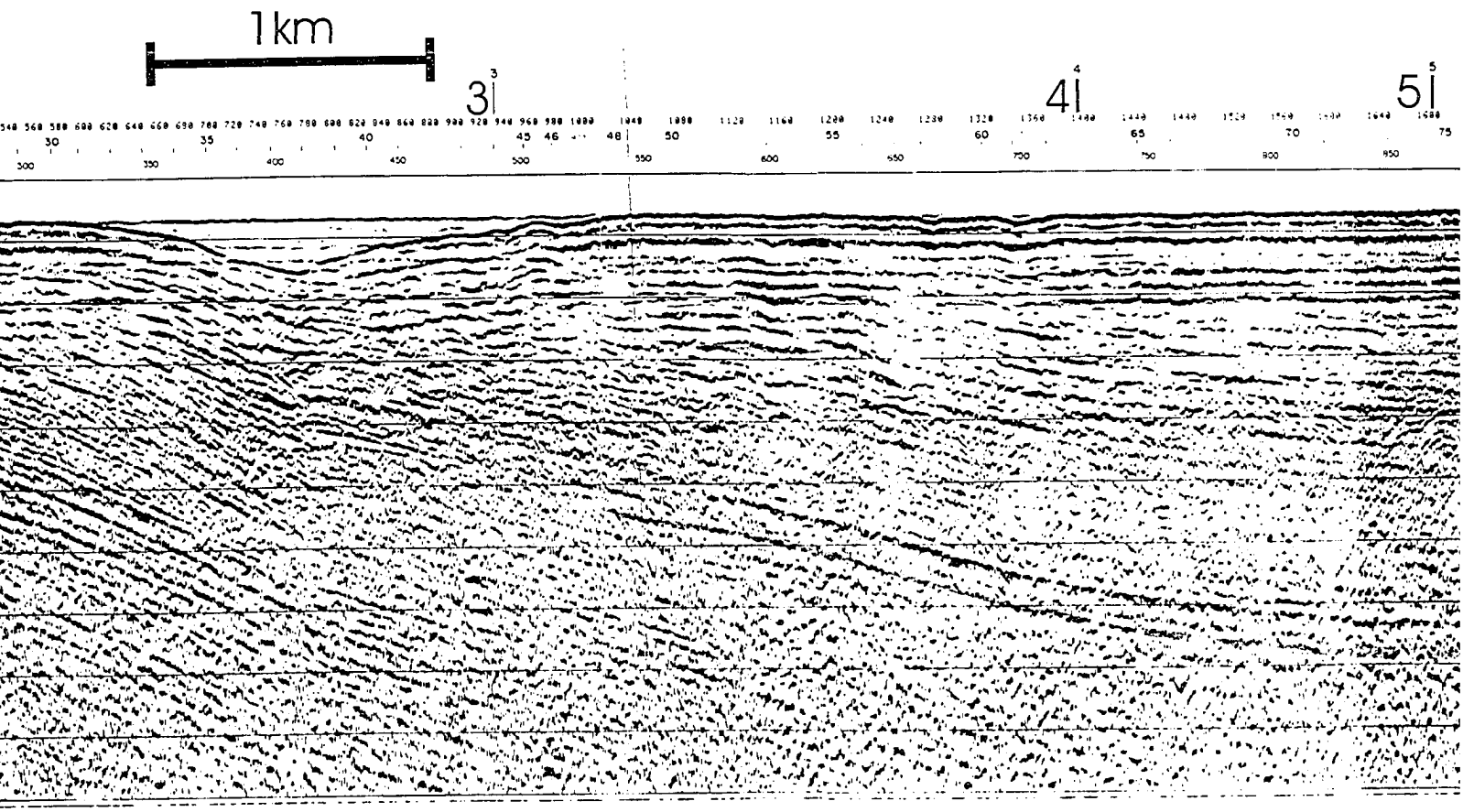
1km
3
4
5

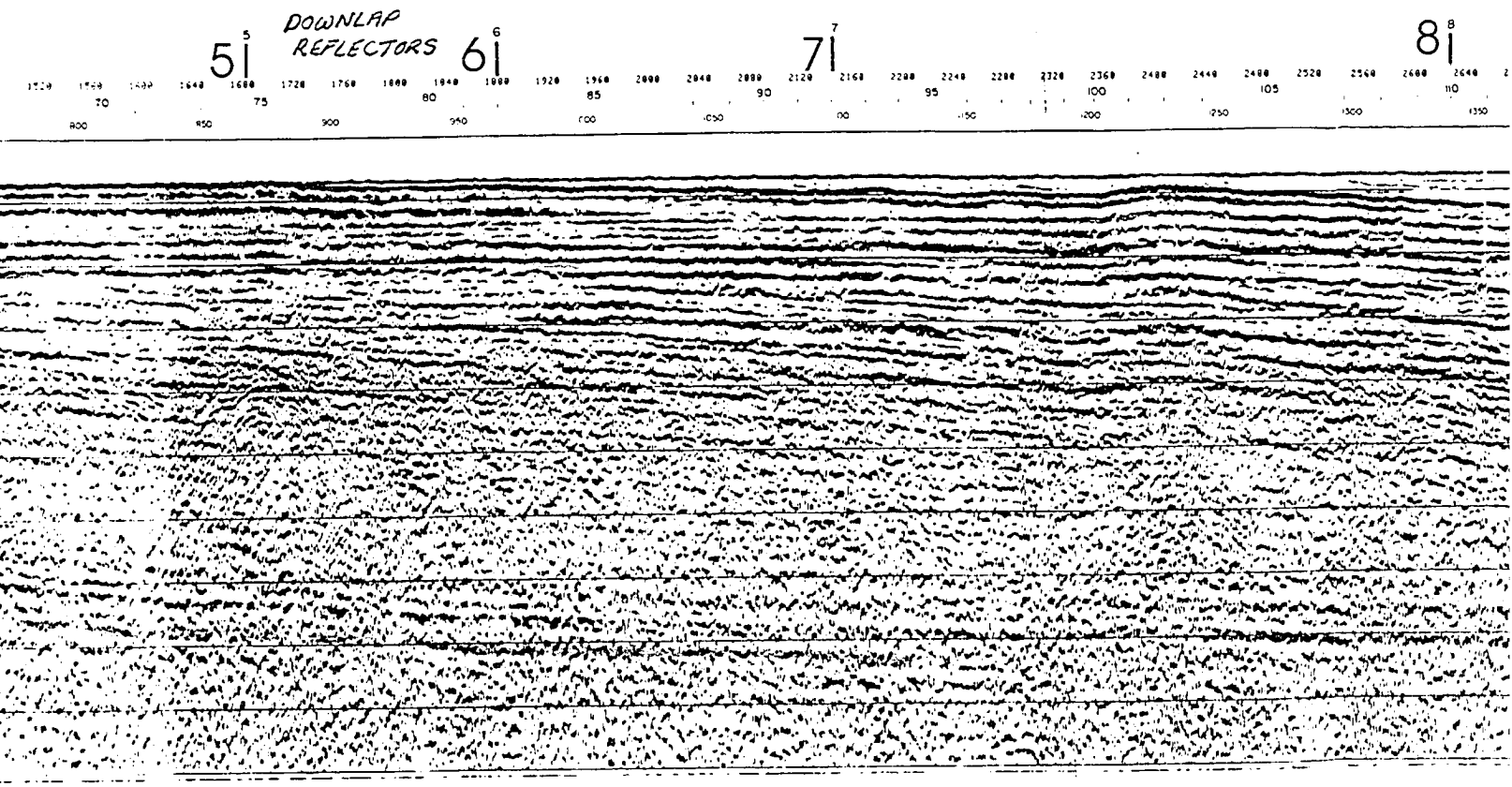
DOWNLAP
REFLECTORS
5
6
7
8

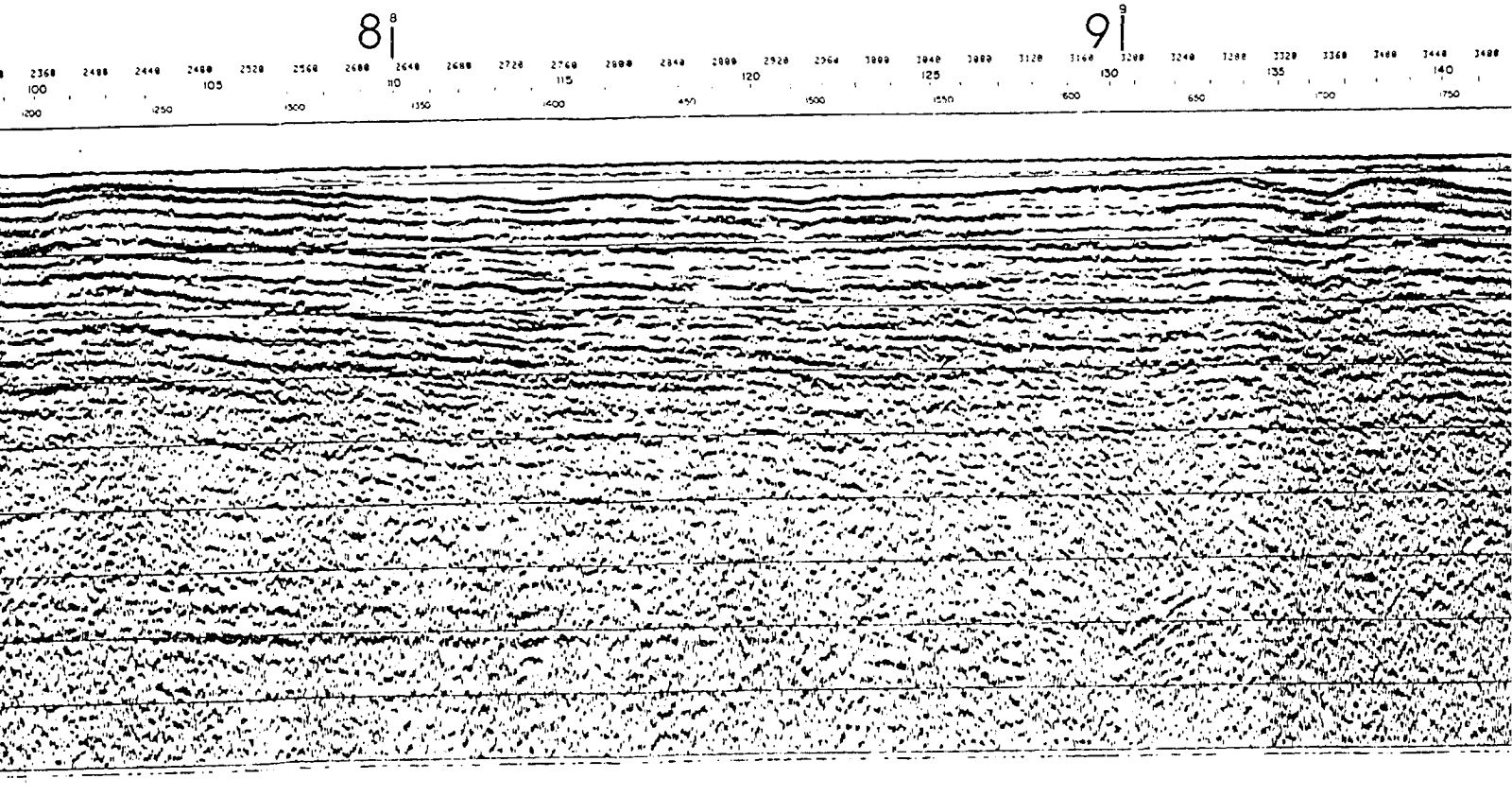
8
8
9
9
2360
2400
2440
2480
2520
2560
2600
2640
2680
2720
2760
2800
2840
2880
2920
2960
3000
3040
3080
3120
3160
3200
3240
3280
3320
3360
3400
3440
3480
100
105
110
115
120
125
130
135
140
1200
1250
1300
1350
1400
450
1500
1550
600
650
1700
1750

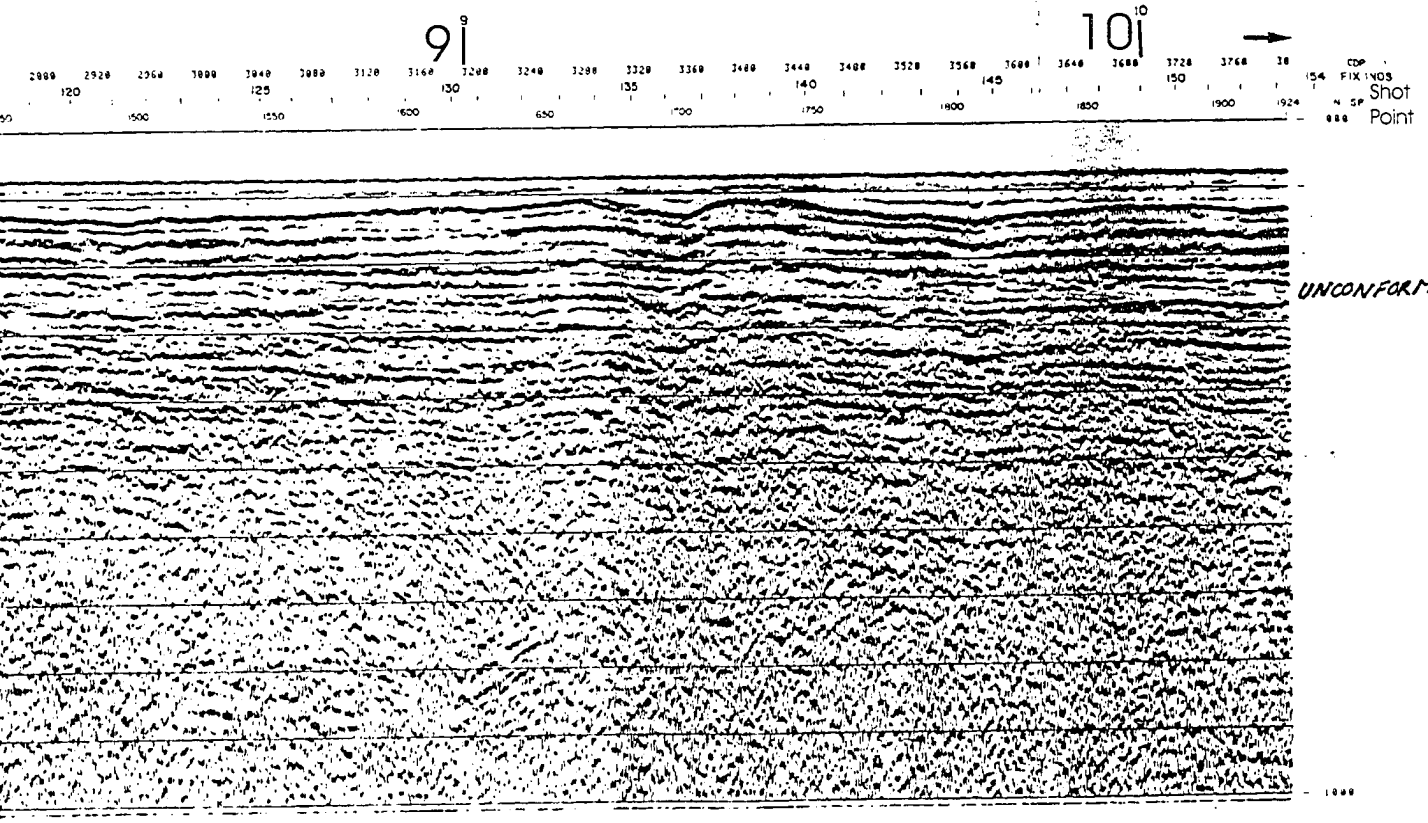
9
10
CDP
FIX NOS
Shot
Point
UNCONFORMITY

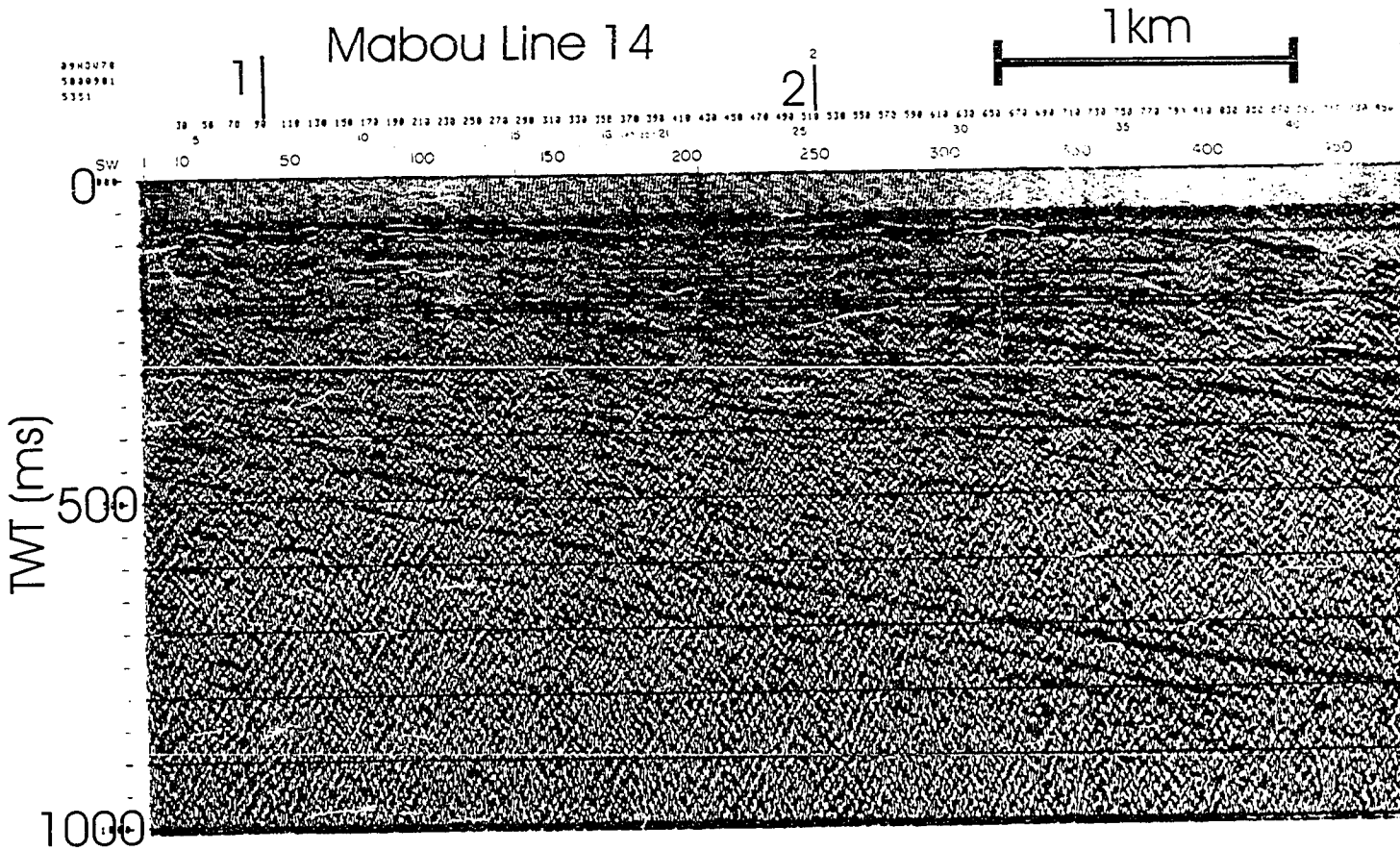
Mabou Line 14
1km
1
2
SW
TWT (ms)
0
500
1000

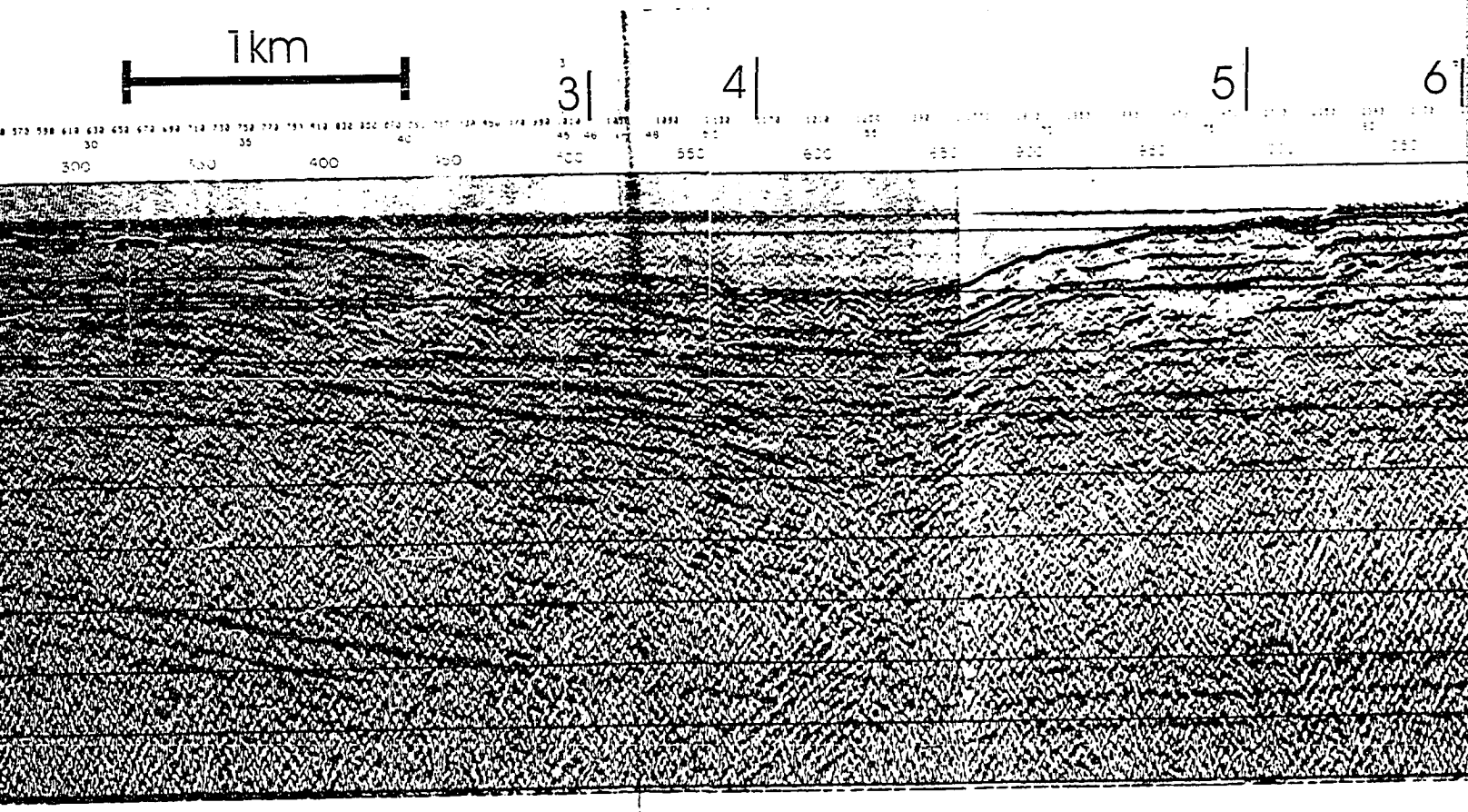

CLAYTON FOLD

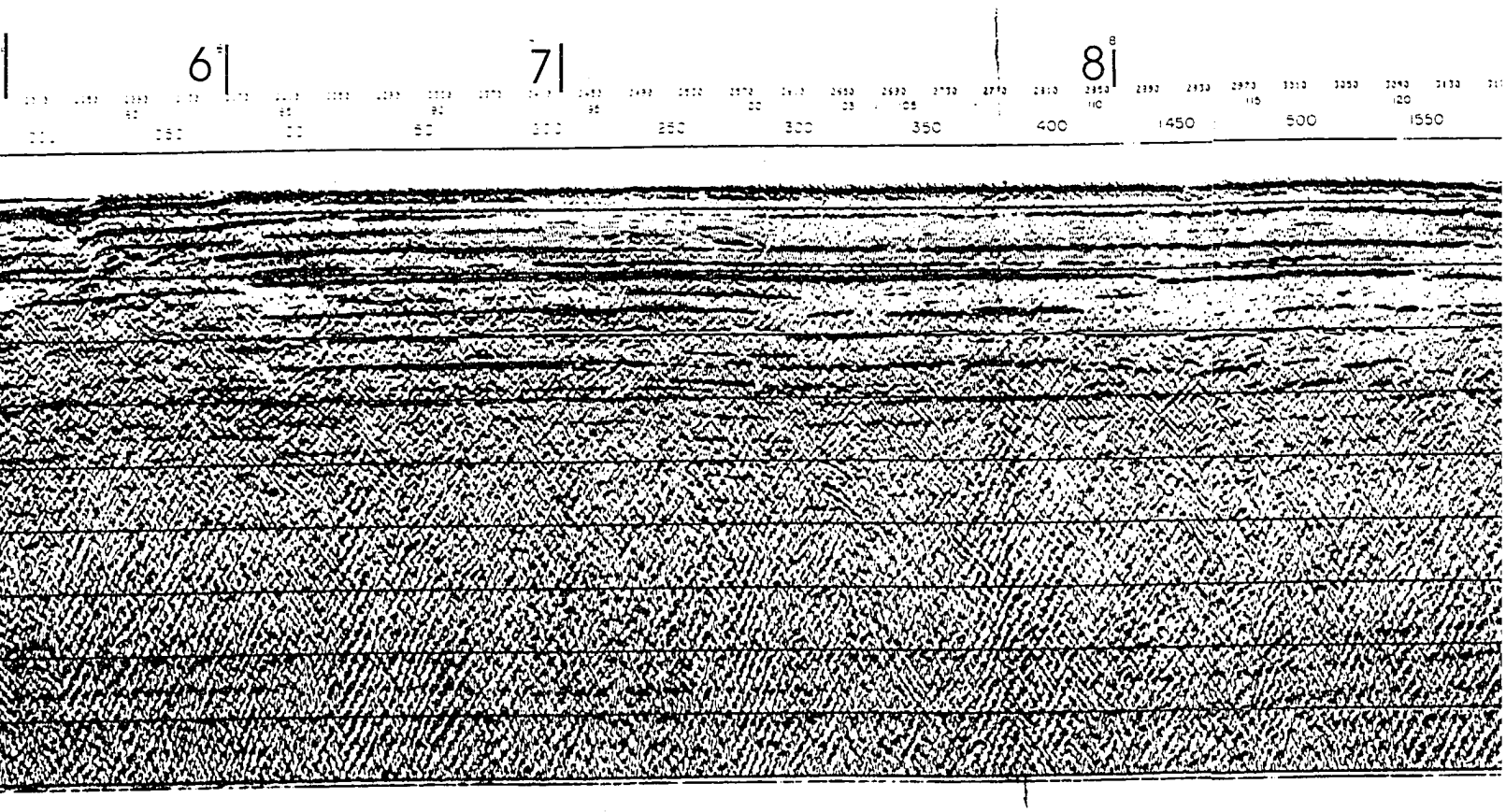
6
7
8
200
250
300
350
400
1450
500
1550

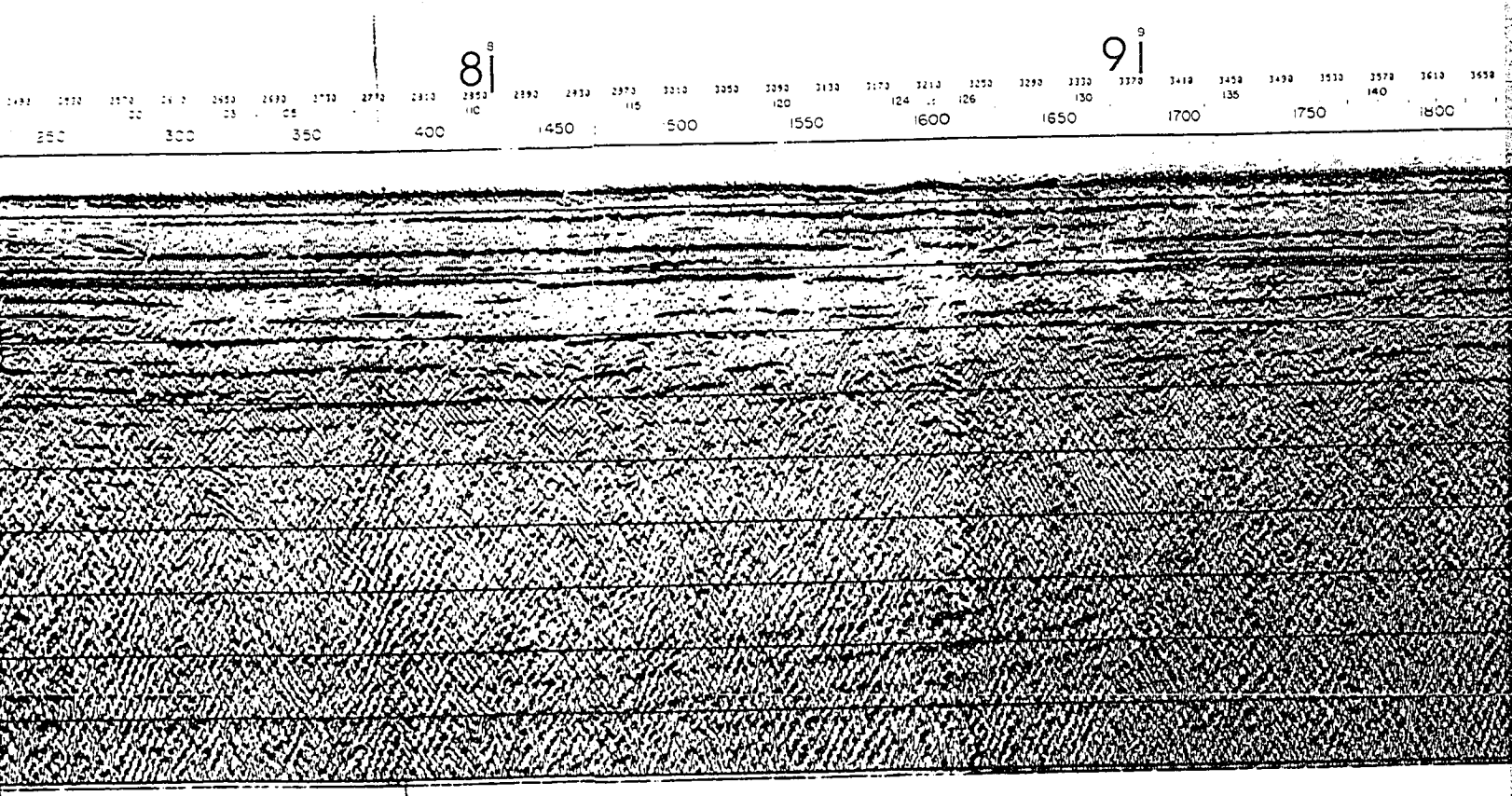
8
9
250
300
350
400
1450
500
1550
1600
1650
1700
1750
1800

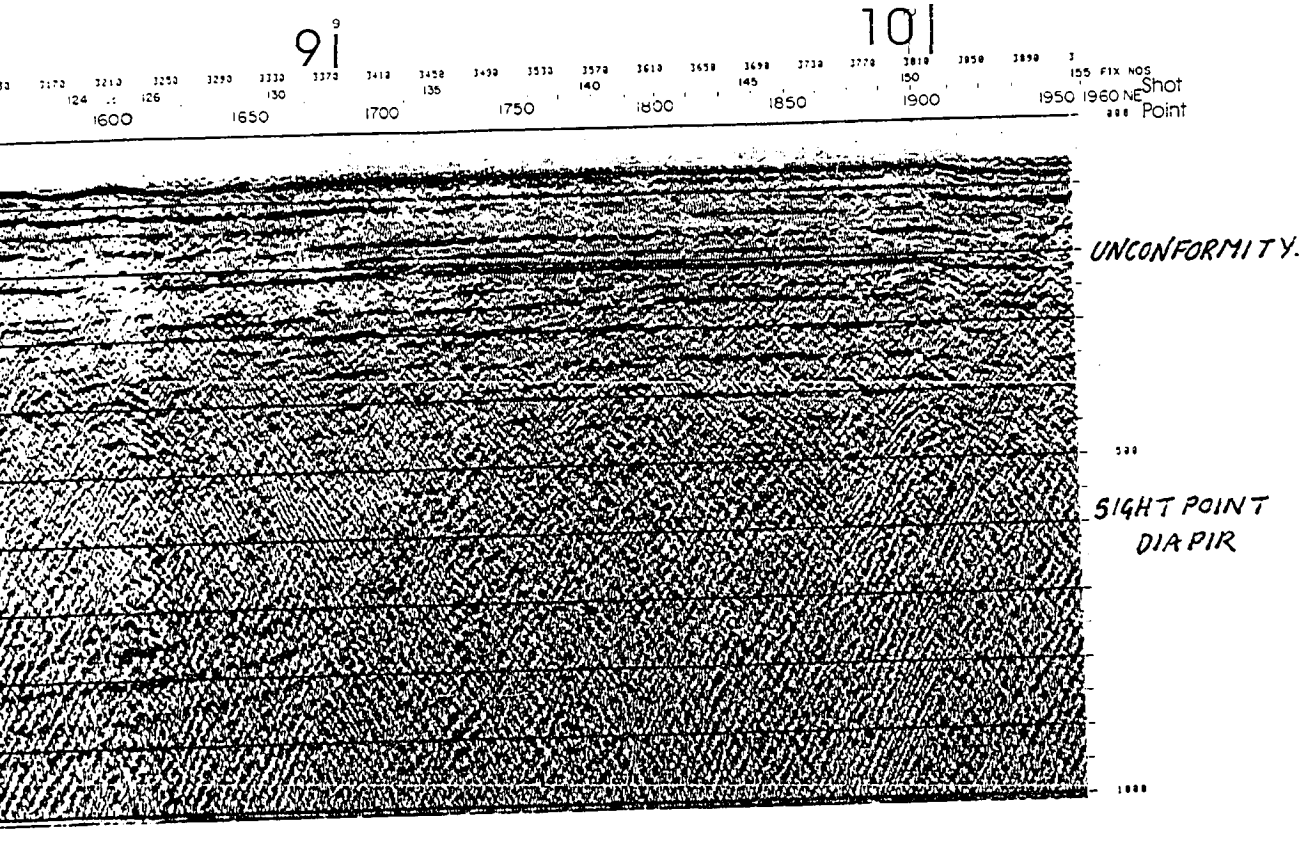
9
10
FIX NOS
Shot
Point
1600
1650
1700
1750
1800
1850
1900
1950
1960
UNCONFORMITY.
SIGHT POINT
DIAPIR

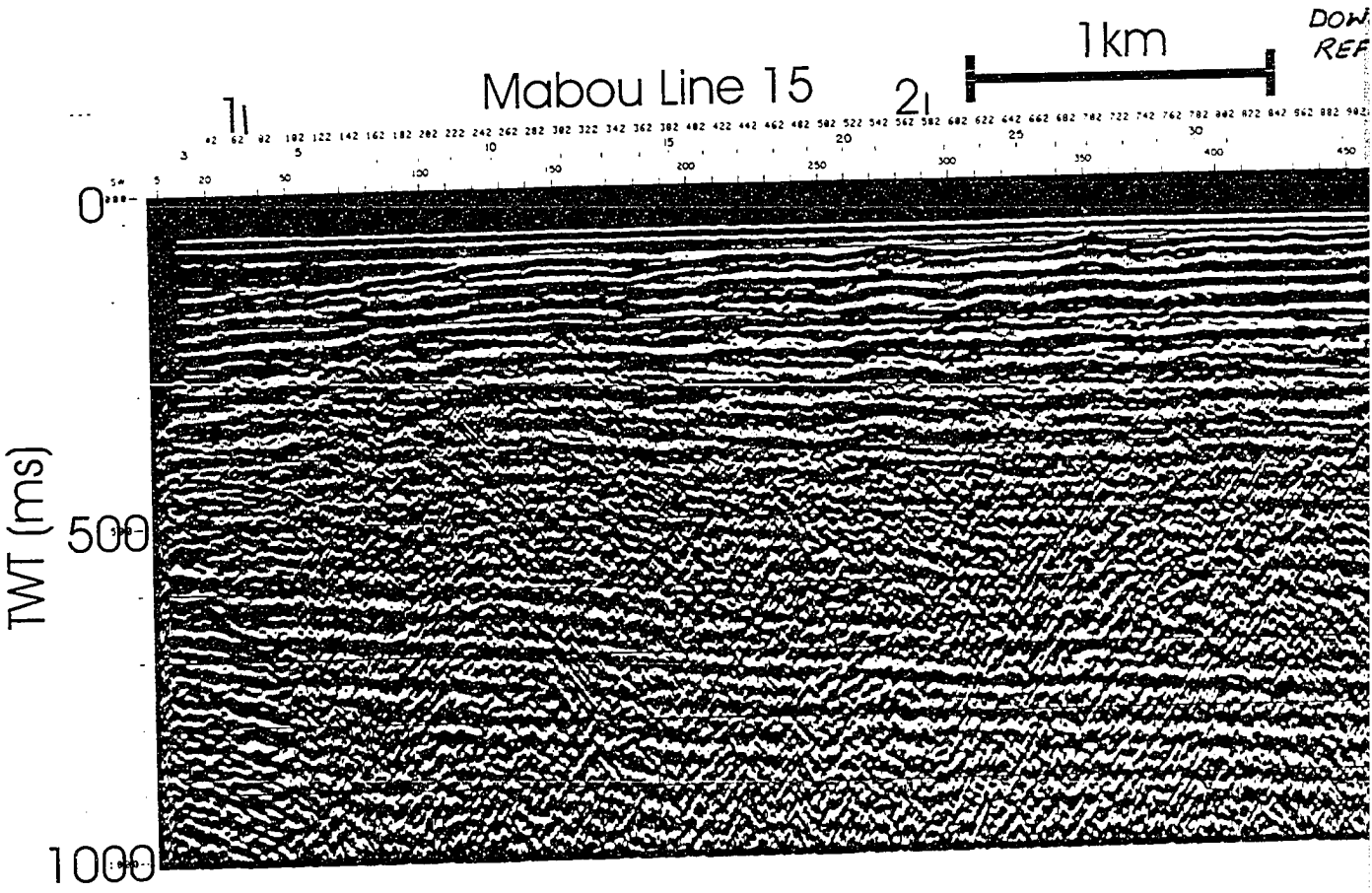
Mabou Line 15
1km
TWT (ms)
0
500
1000

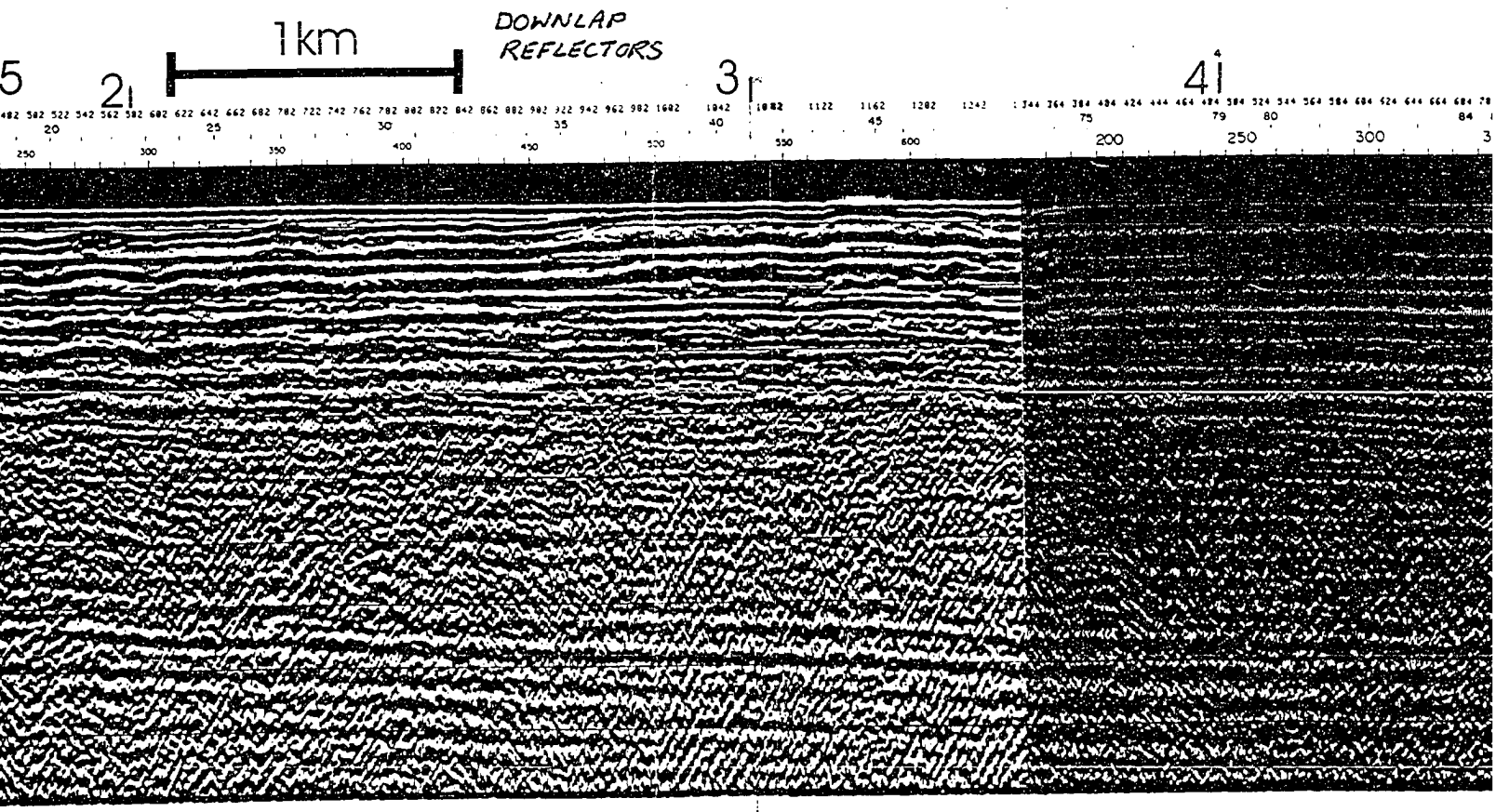
1km
DOWNLAP
REFLECTORS
5
2
3
4

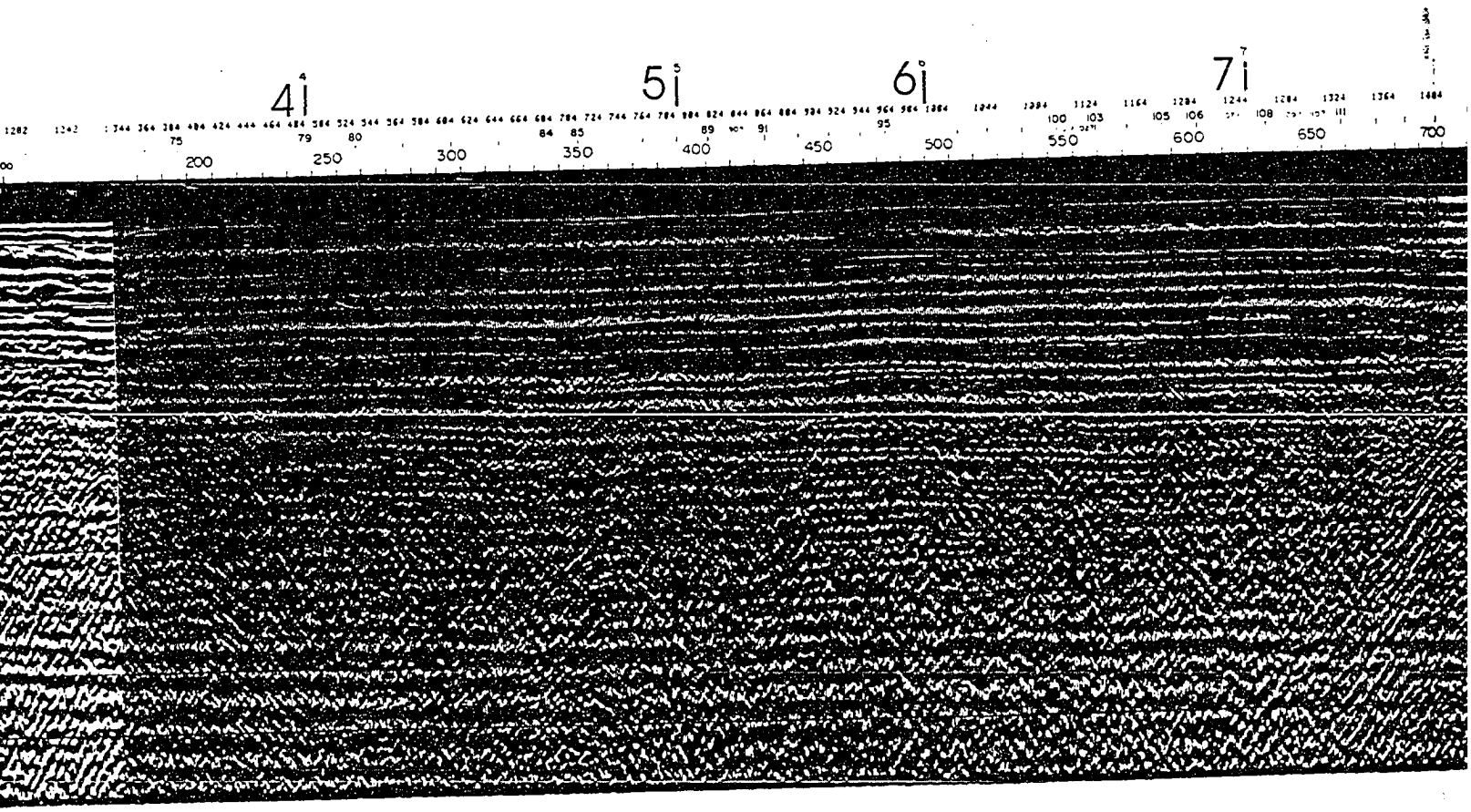
4i
5i
6i
7i
200
250
300
350
400
450
500
550
600
650
700

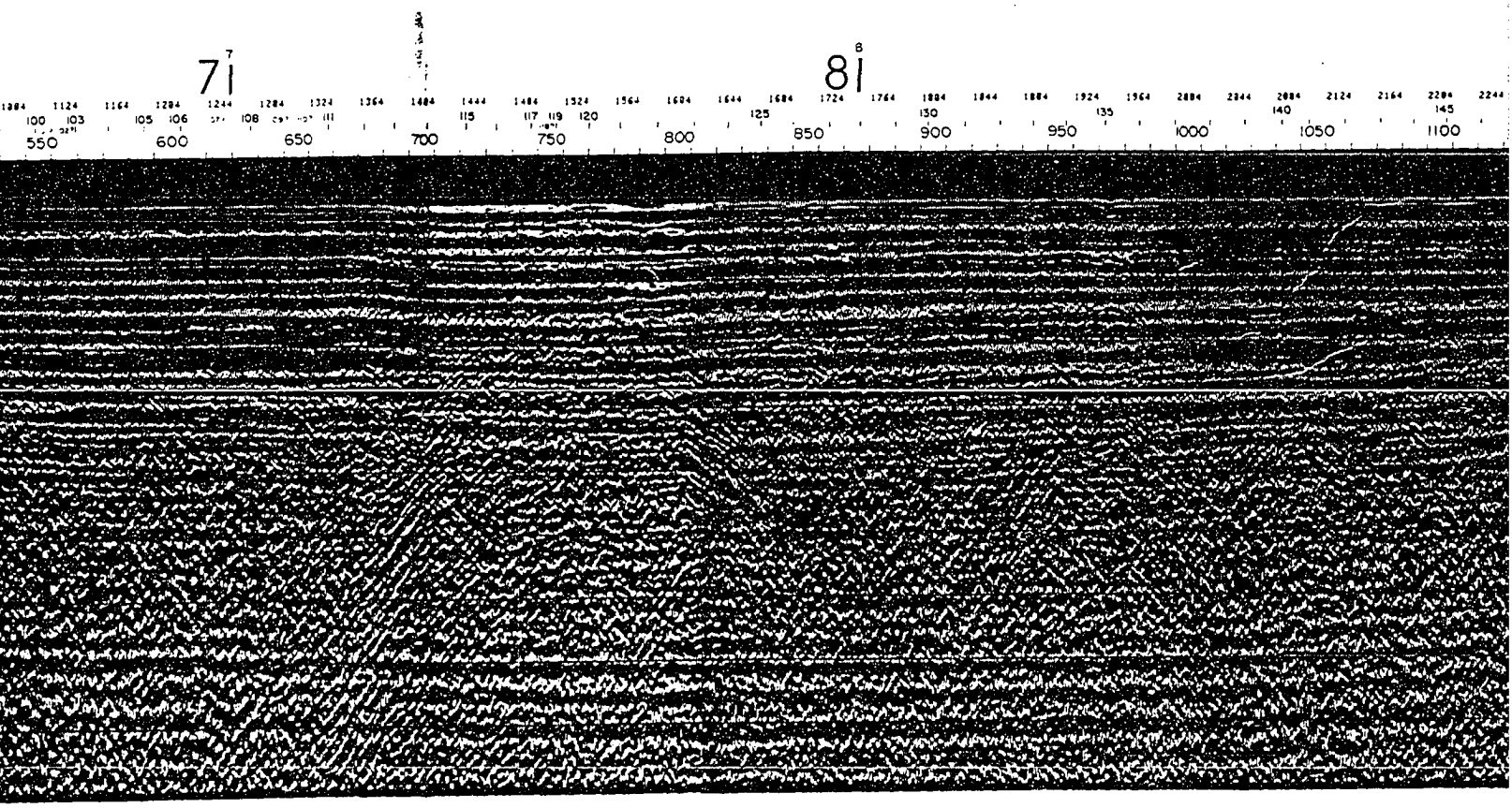
7
8
550
600
650
700
750
800
850
900
950
1000
1050
1100

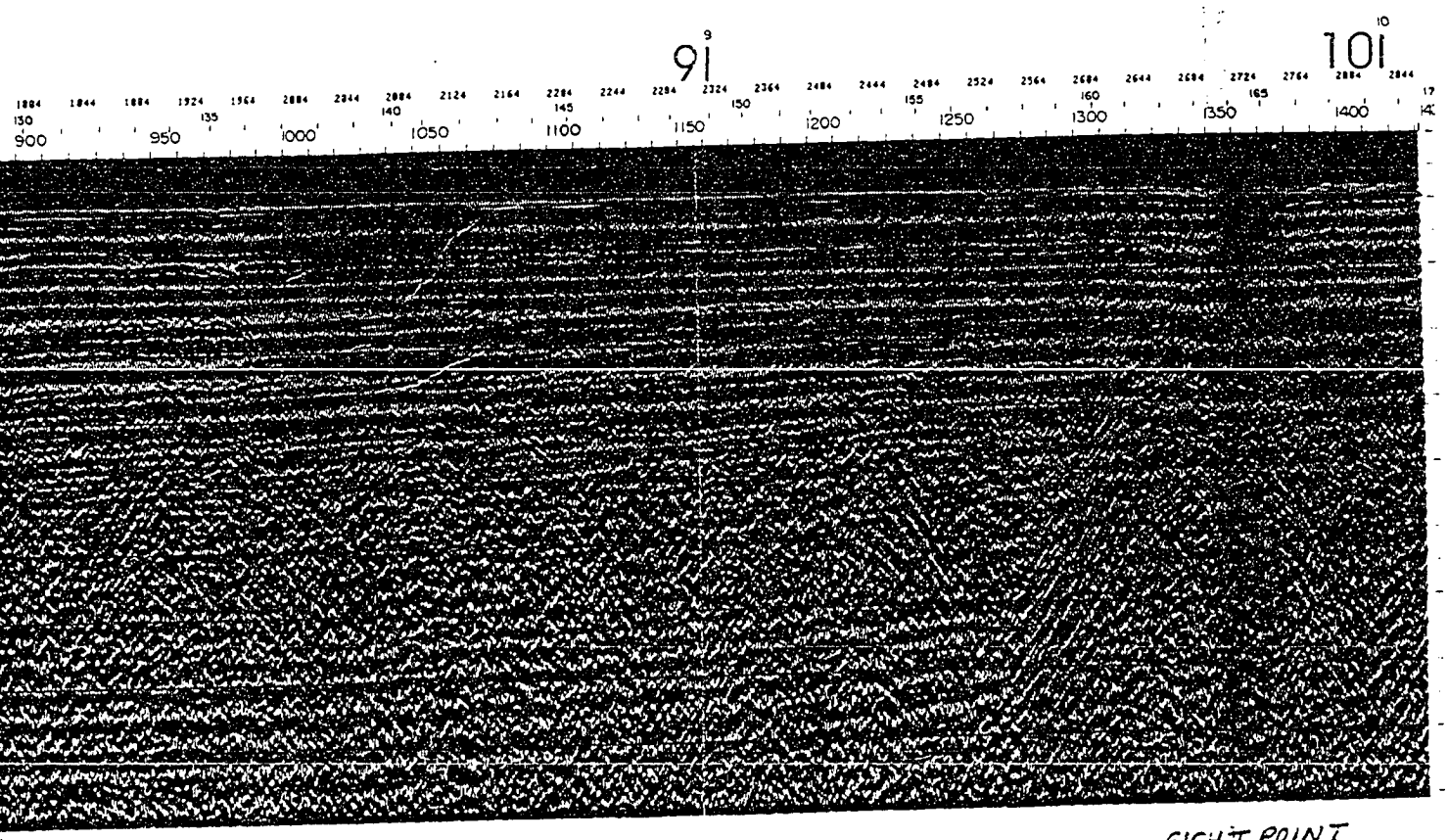

SIGHT POINT
DIAPIR

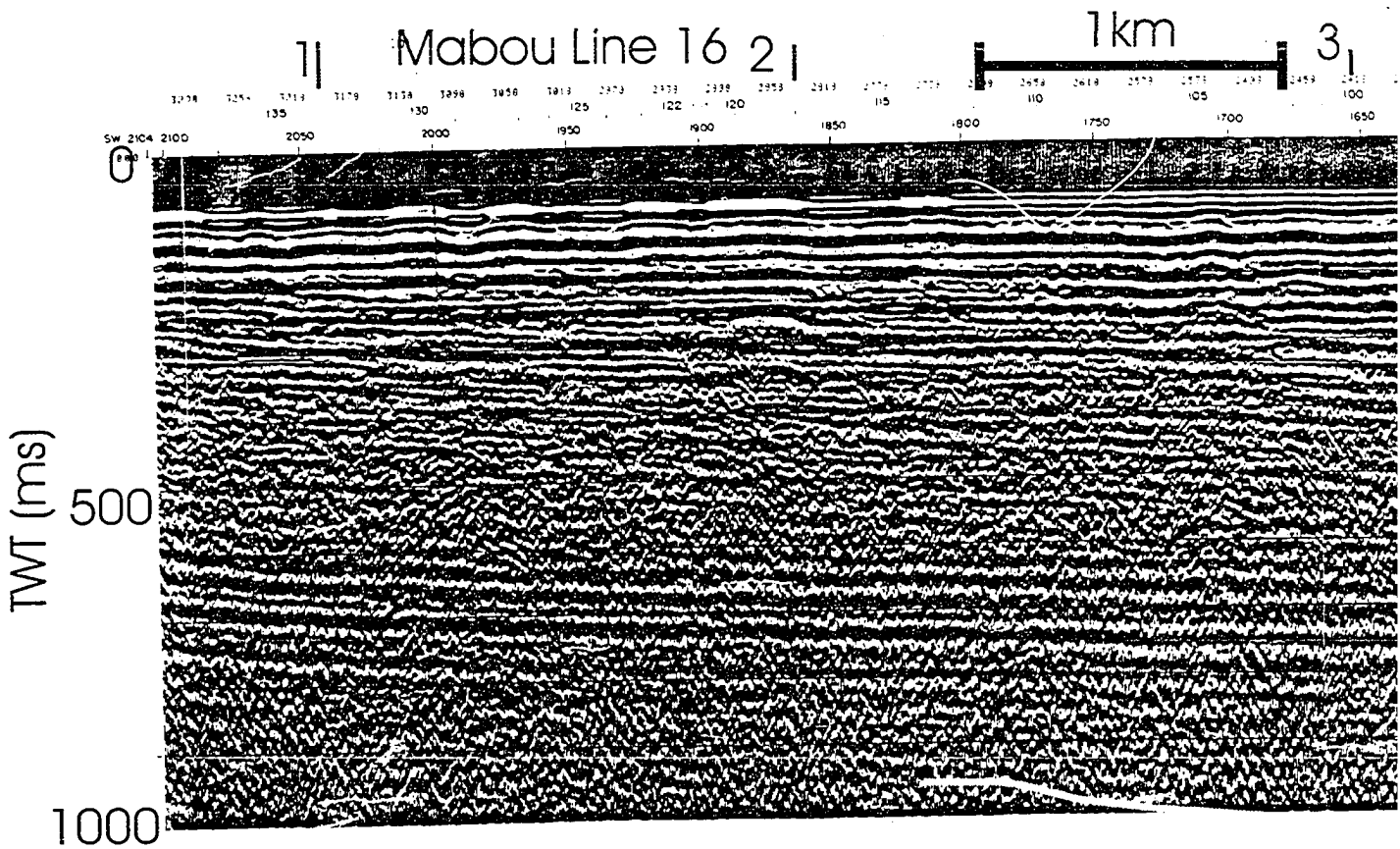
Mabou Line 16
1
2
3
1km
SW 2104 2100
2050
2000
1950
1900
1850
1800
1750
1700
1650
135
130
125
122
120
115
110
105
100
0
500
1000
TWT (ms)

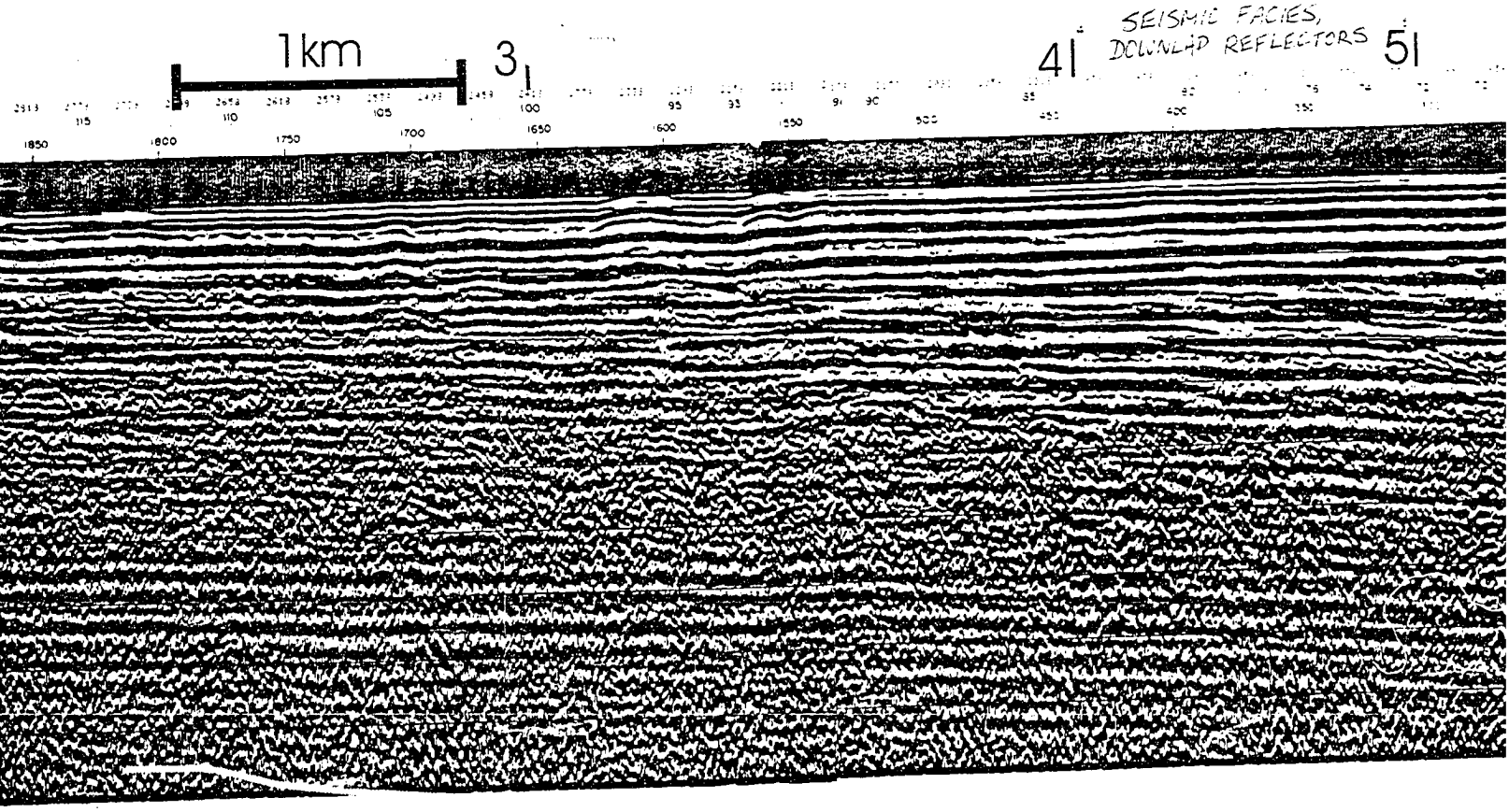
1km
3
4
5
SEISMIC FACIES,
DOWNLAP REFLECTORS

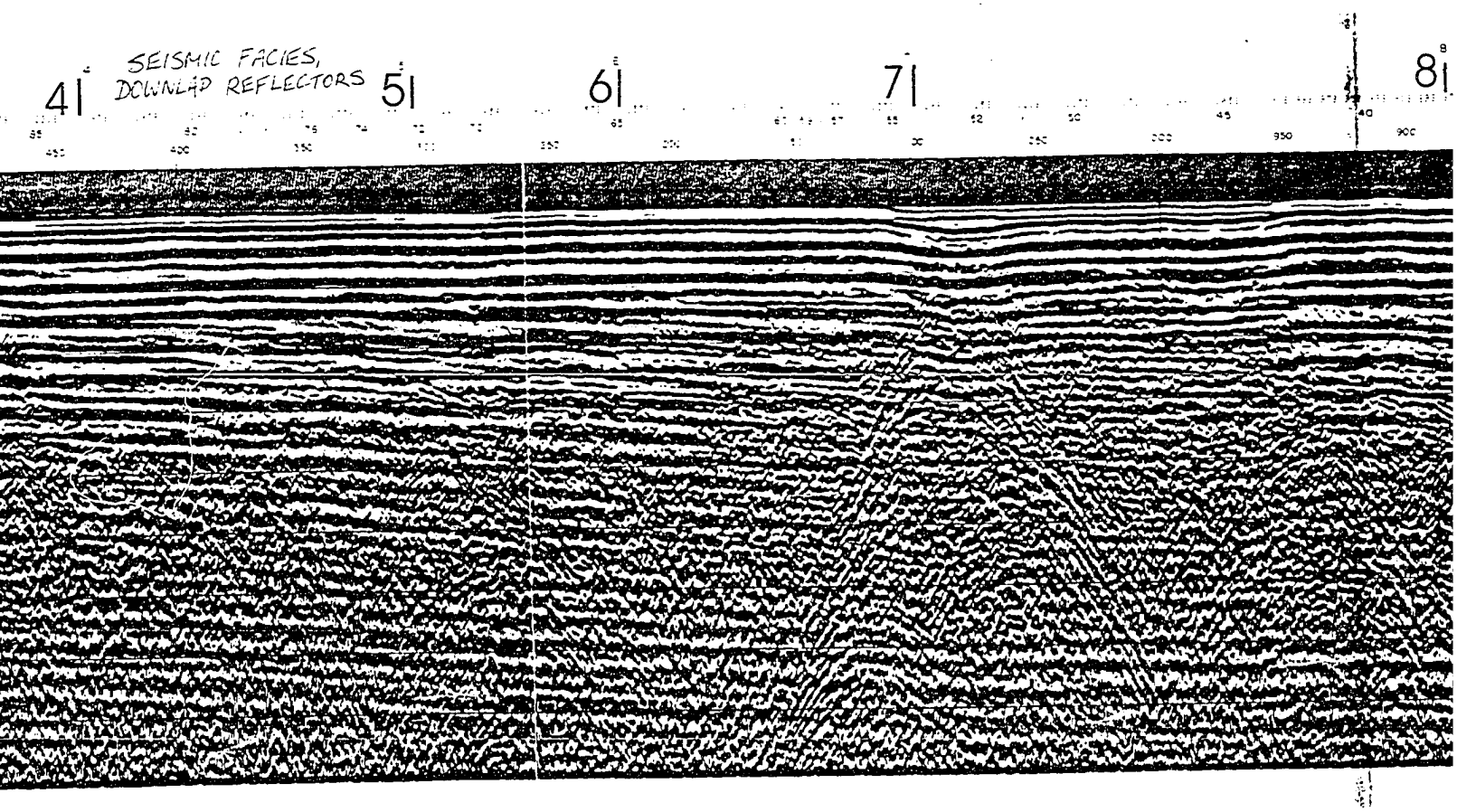
SEISMIC FACIES,
DOWNLAP REFLECTORS
4
5
6
7
8

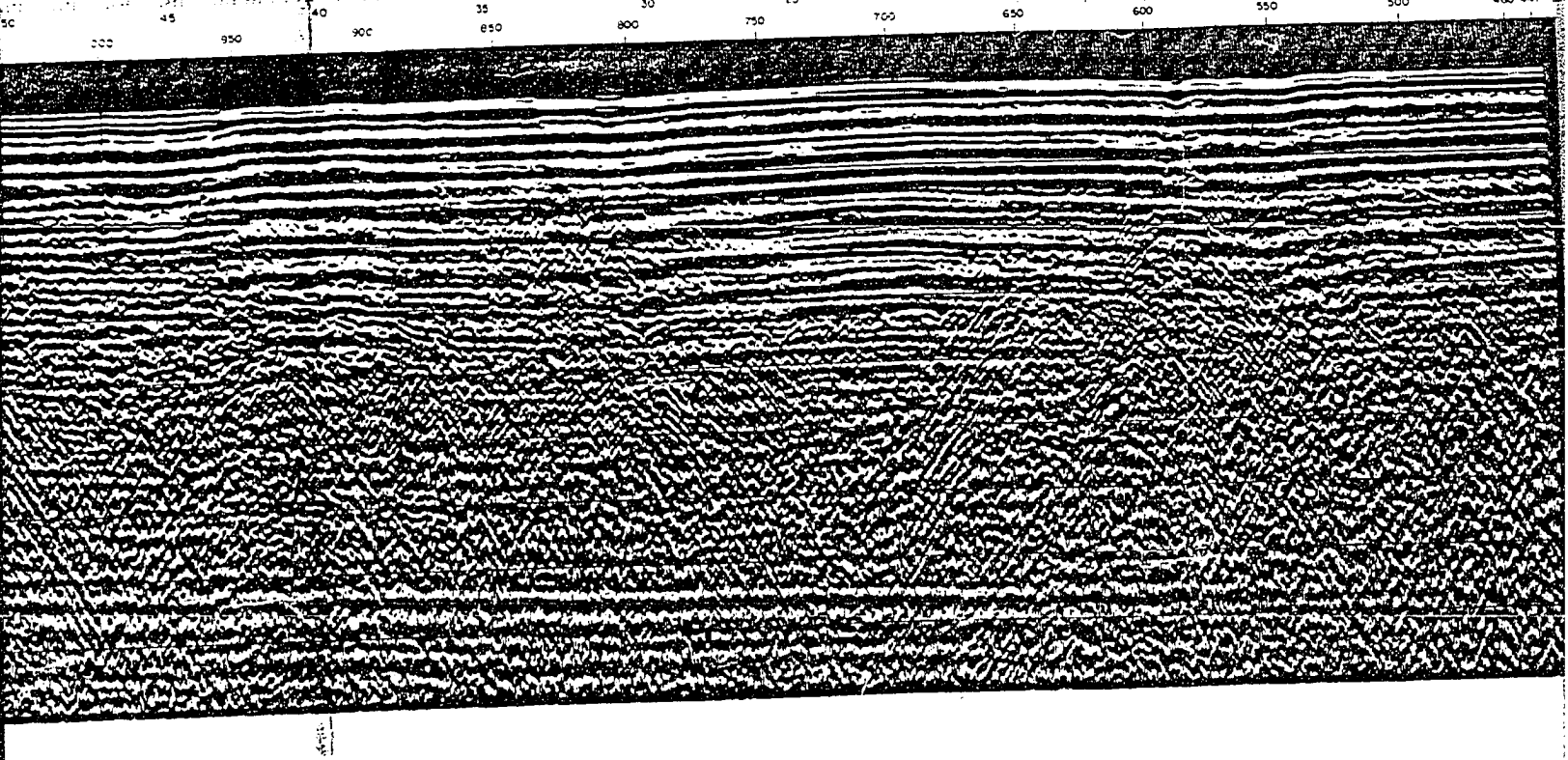
8
9
APPROX

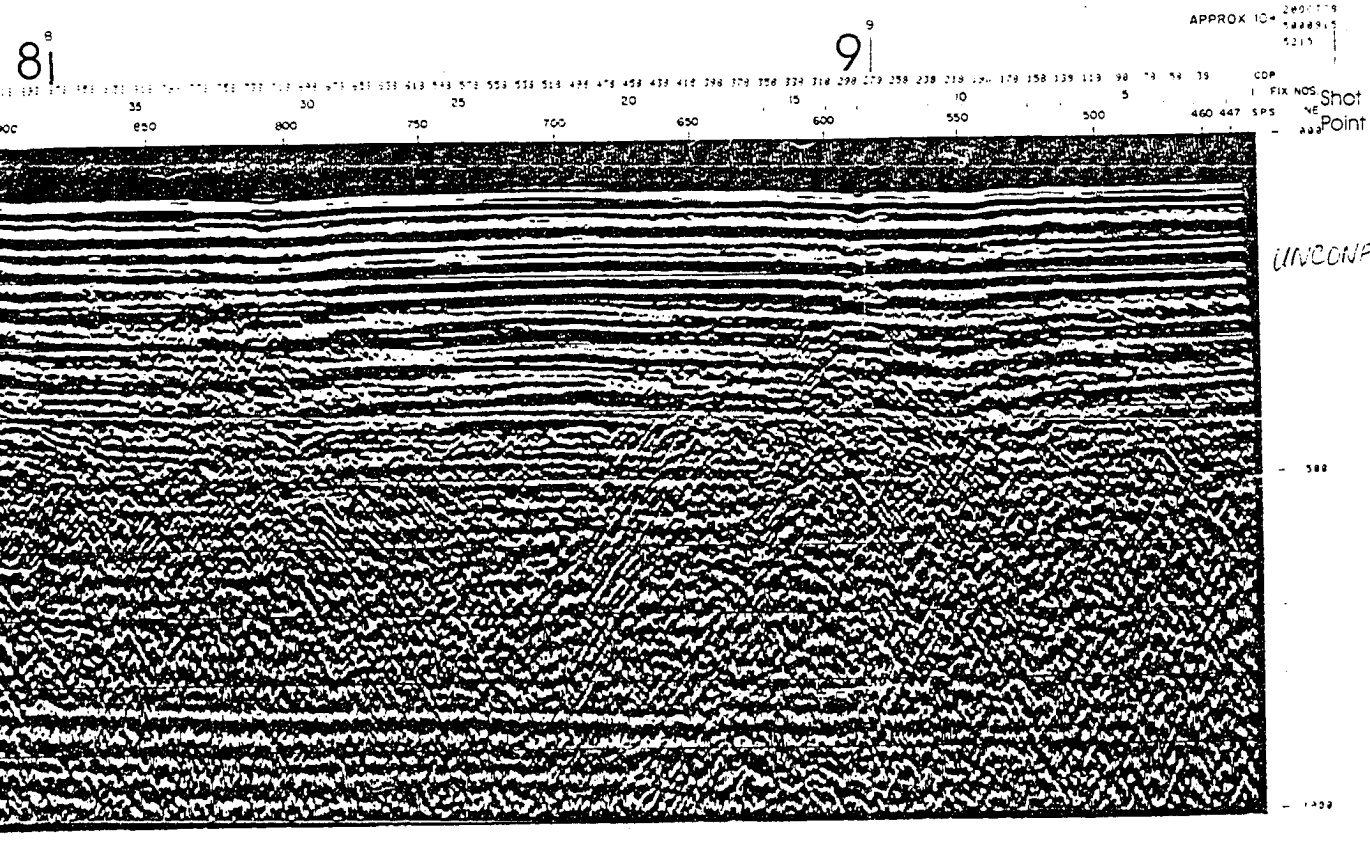
8
9
APPROX 10
CDP
FIX NOS
SPS
Shot Point
35
30
25
20
15
10
5
650
800
750
700
650
600
550
500
460 447
UNCONFORMITY

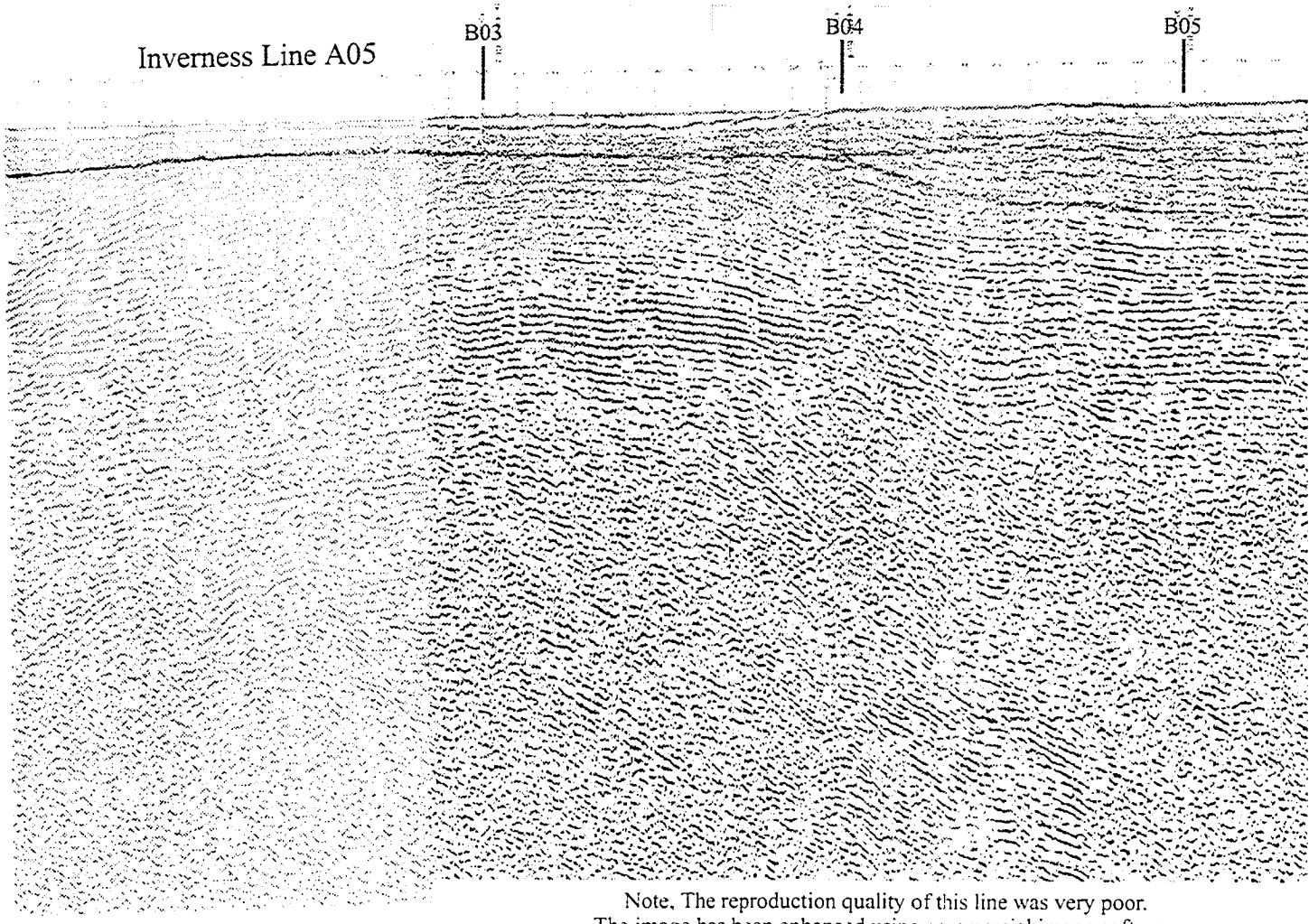

Note. The reproduction quality of this line was very poor.
The image has been enhanced using commercial image software

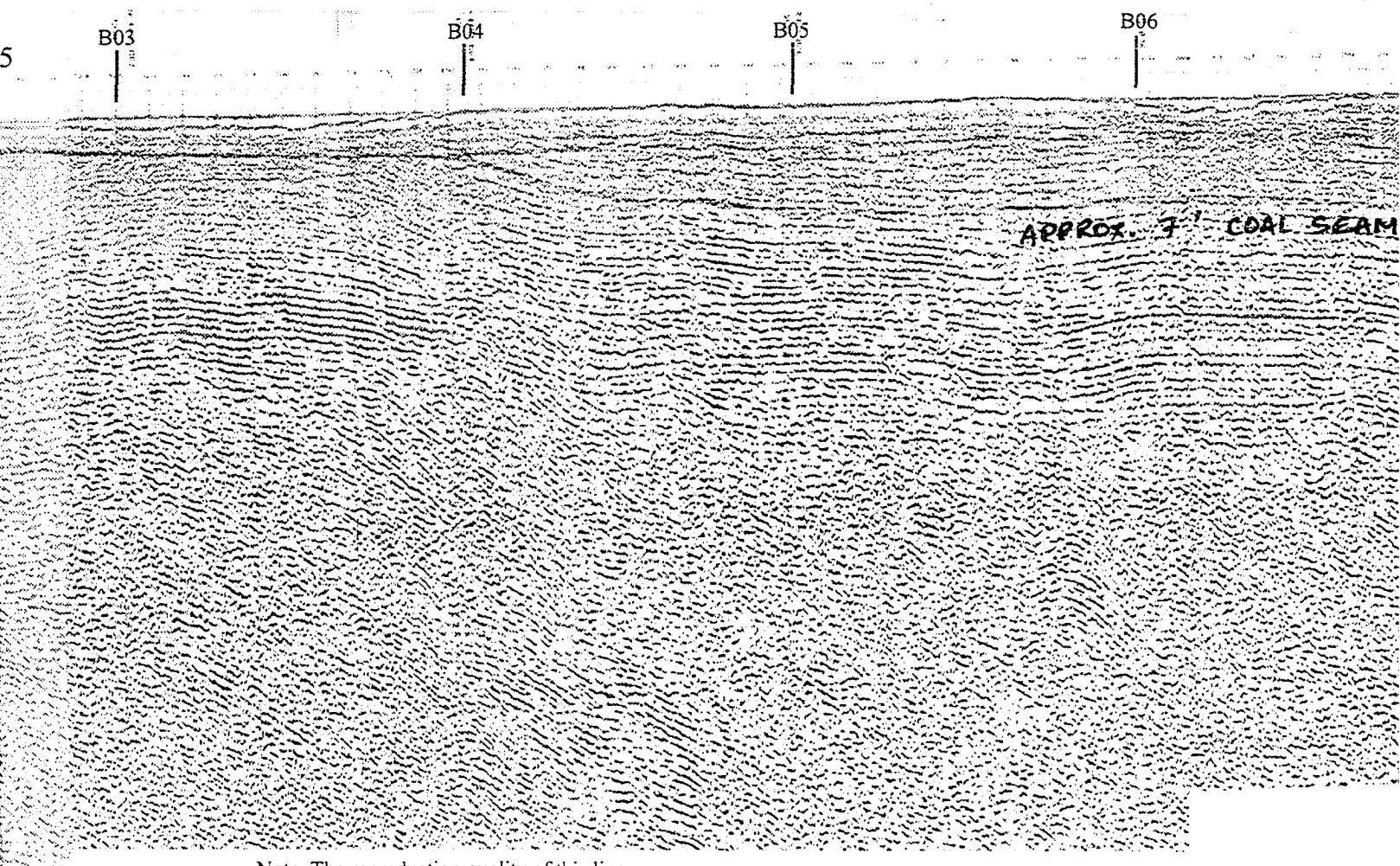

Note, The reproduction quality of this line was very poor.
The image has been enhanced using commercial image software

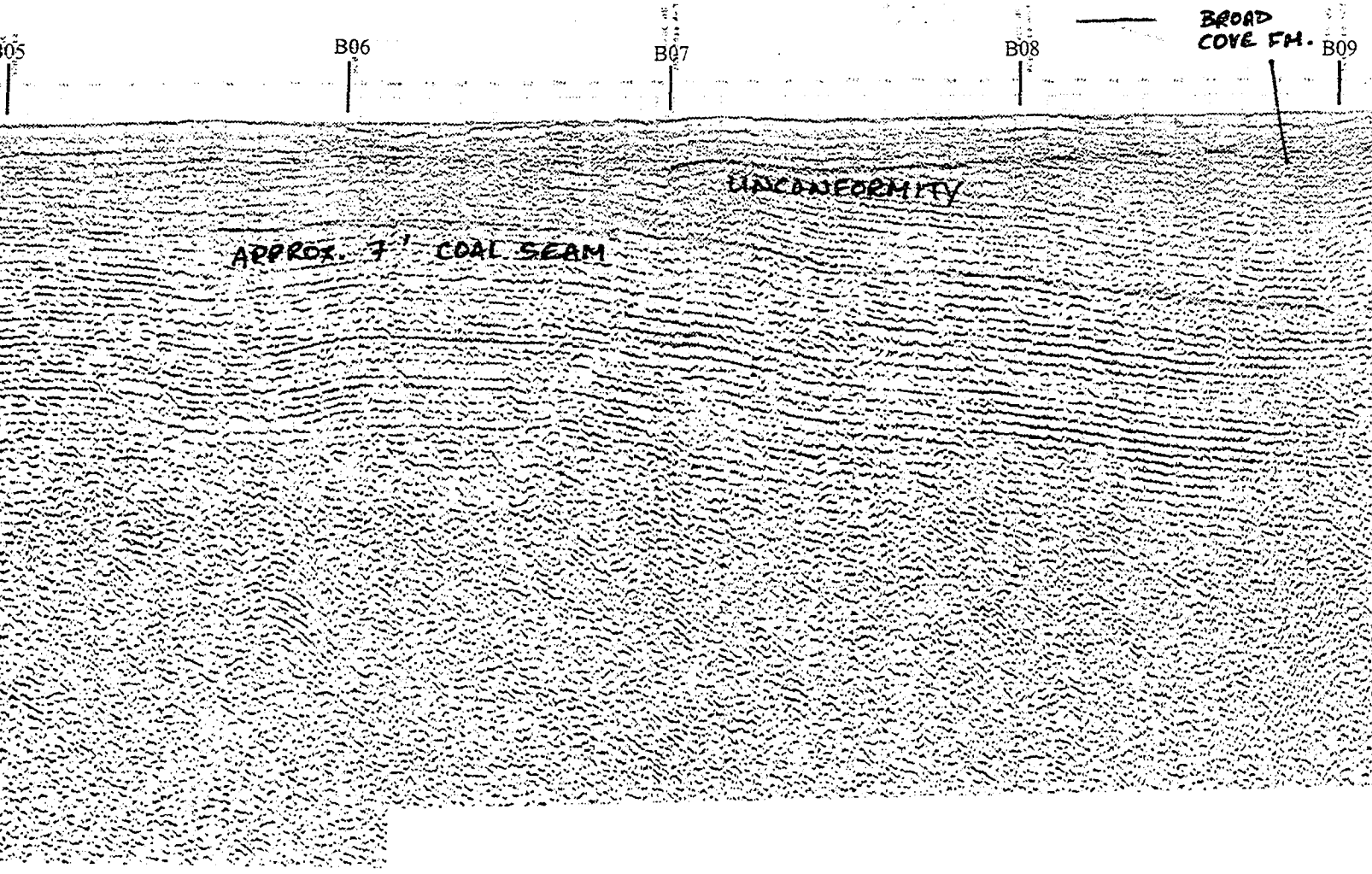
B05
B06
B07
B08
B09
BROAD COVE FM.
UNCONFORMITY
APPROX. 7' COAL SEAM

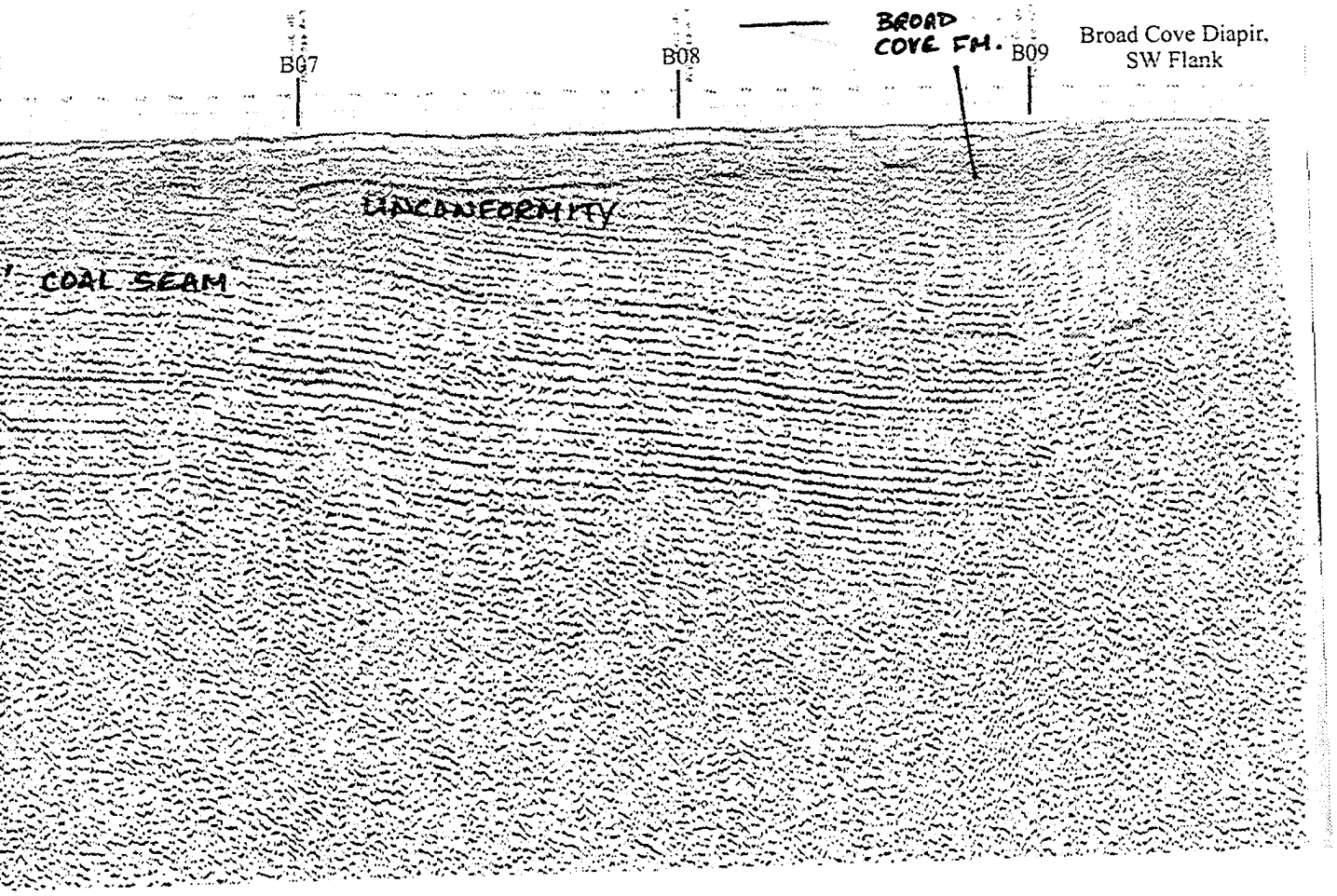
B07
B08
BROAD COVE FM.
B09
Broad Cove Diapir, SW Flank
UNCONFORMITY
COAL SEAM

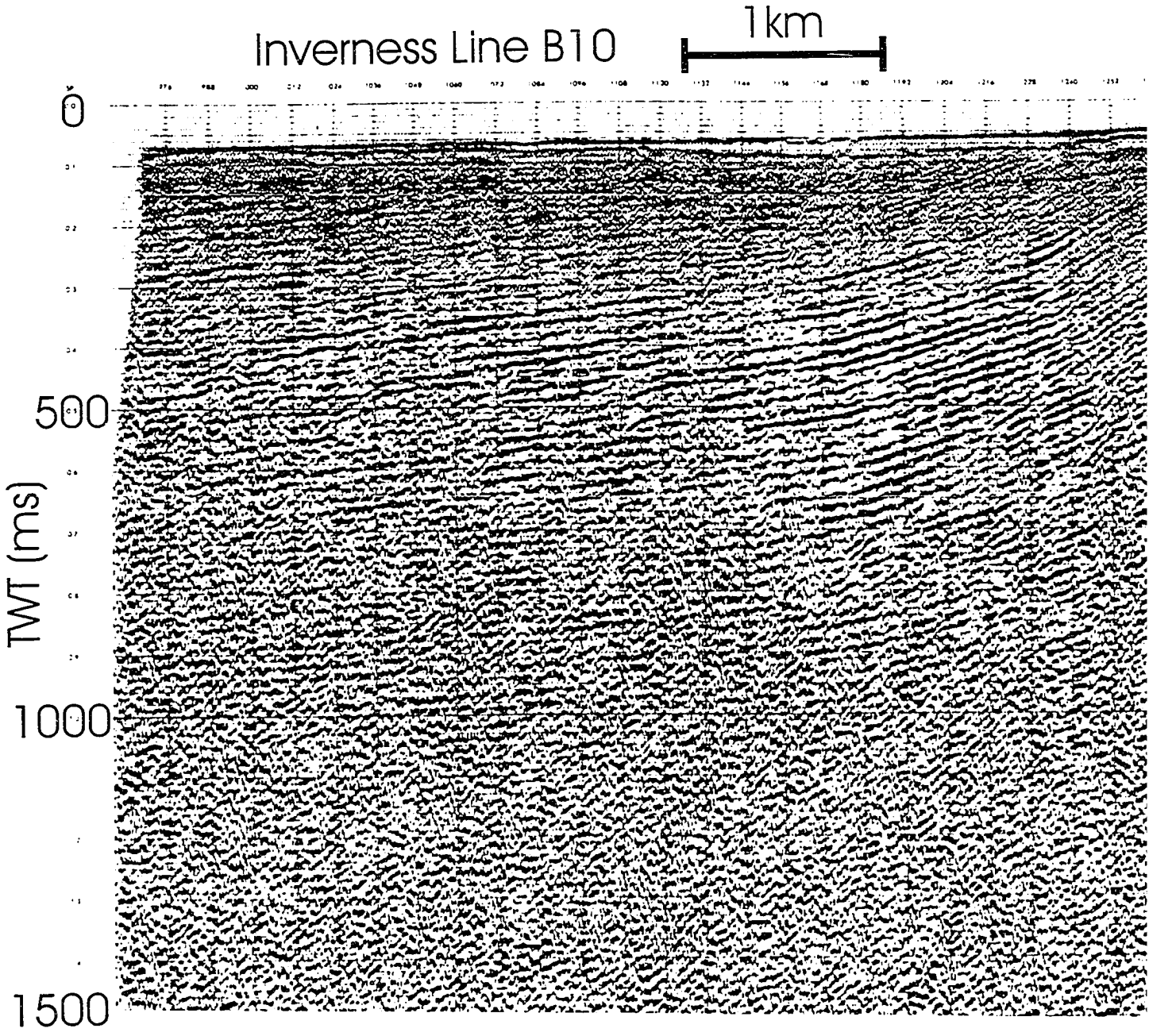
Inverness Line B10
1km
0
500
1000
1500
TWT (ms)

erness Line B10

1km

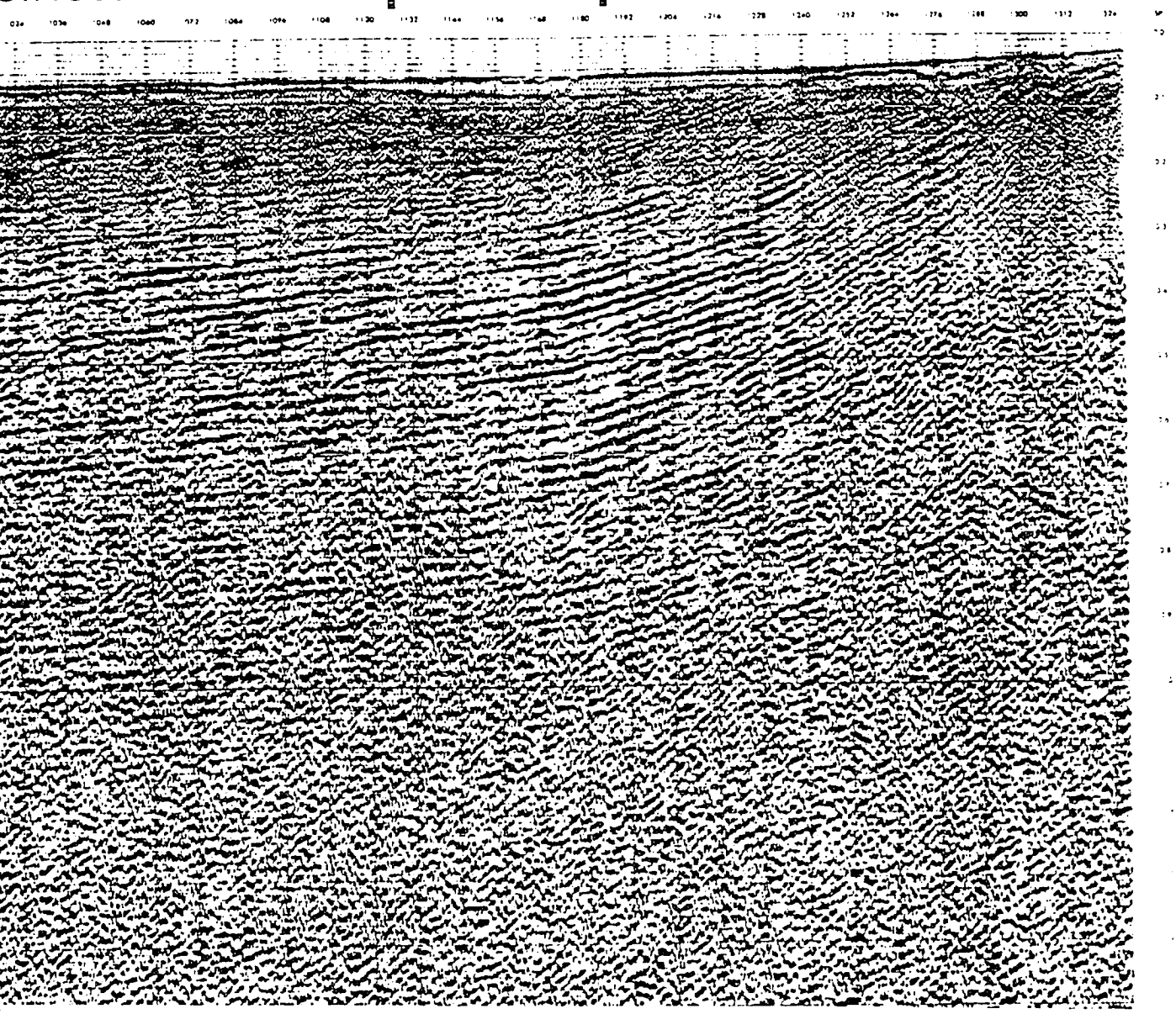

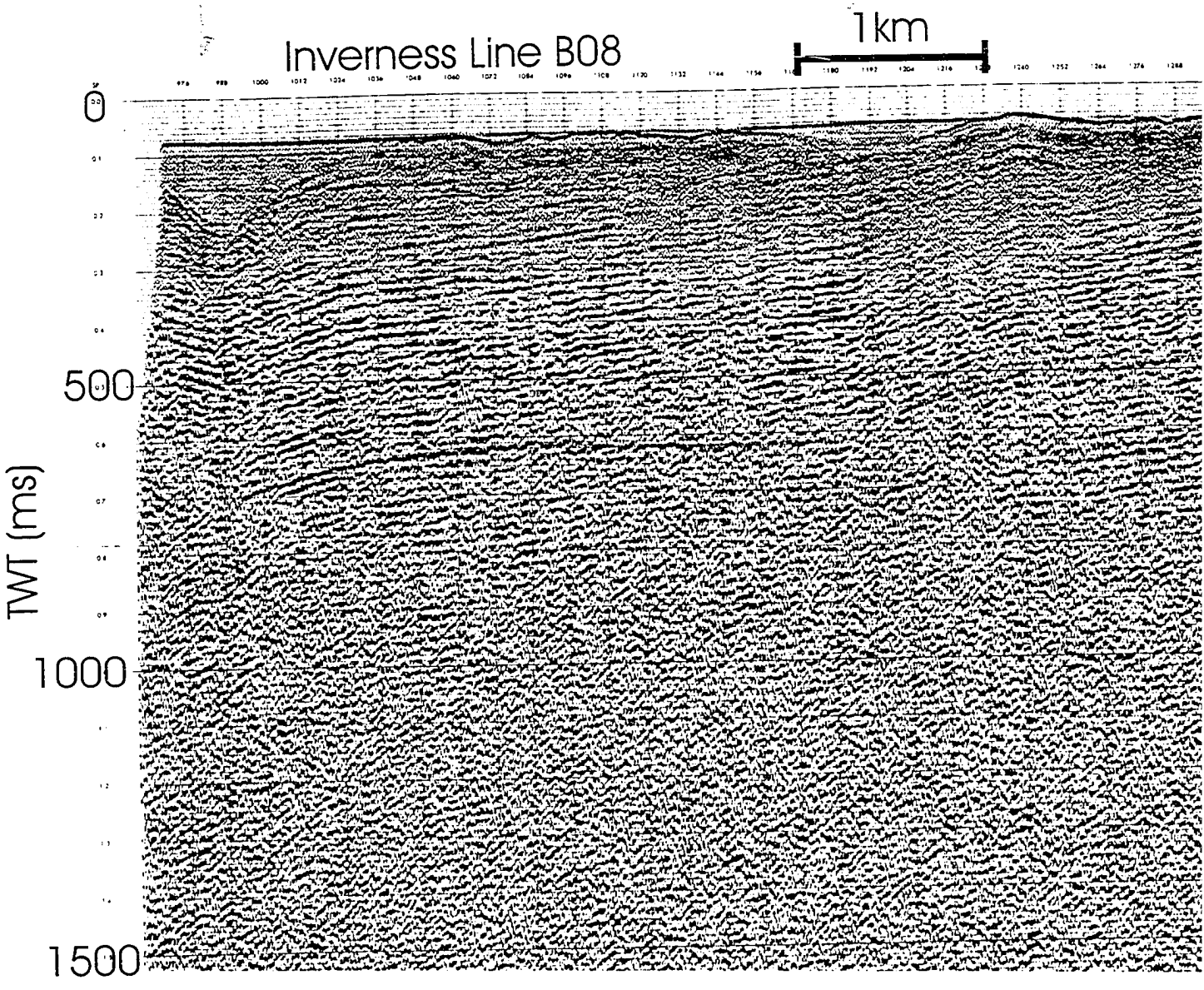
Inverness Line B08
1km
TWT (ms)
0
500
1000
1500

s Line B08

1km

A05

12-A05

Shot Point

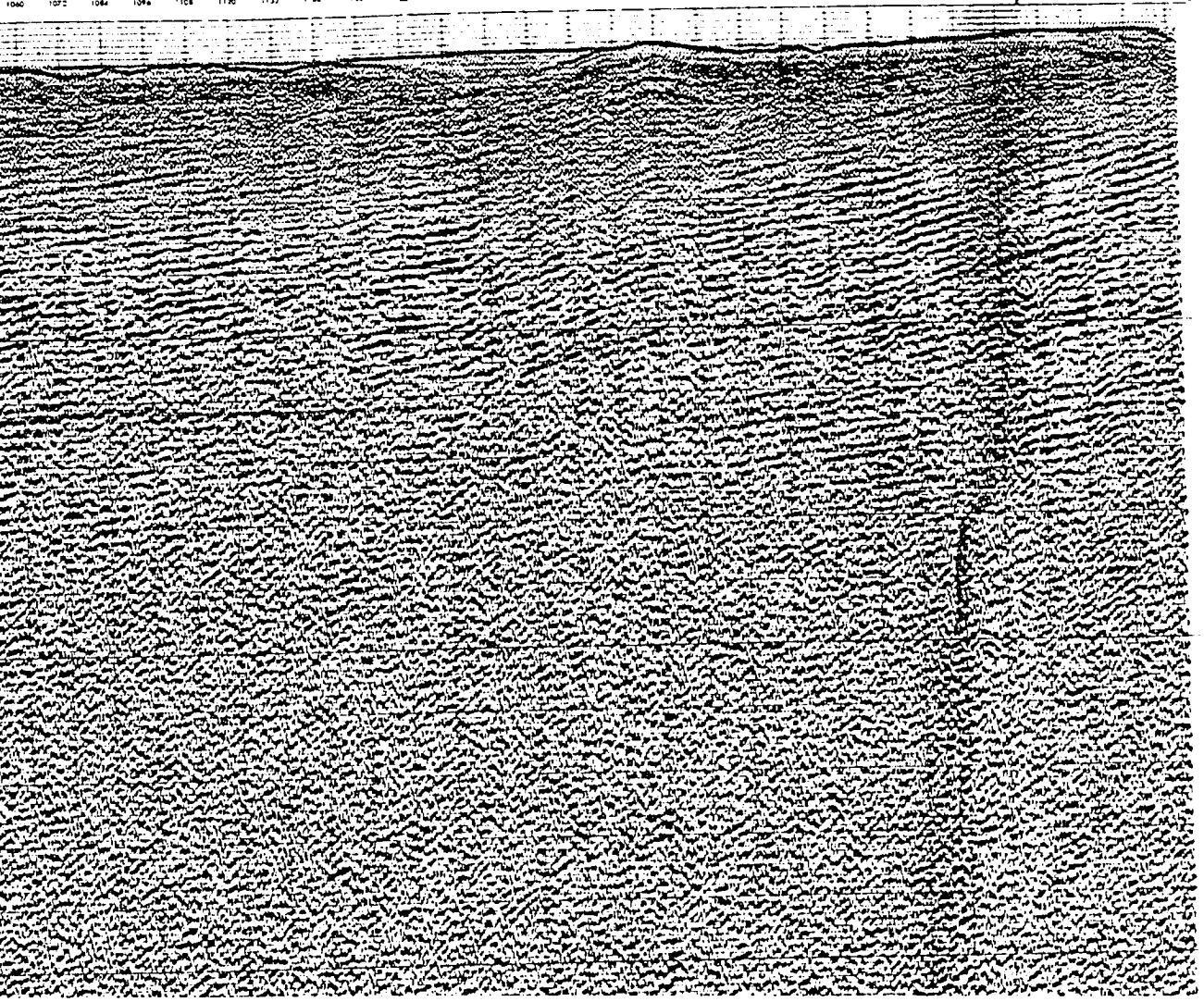

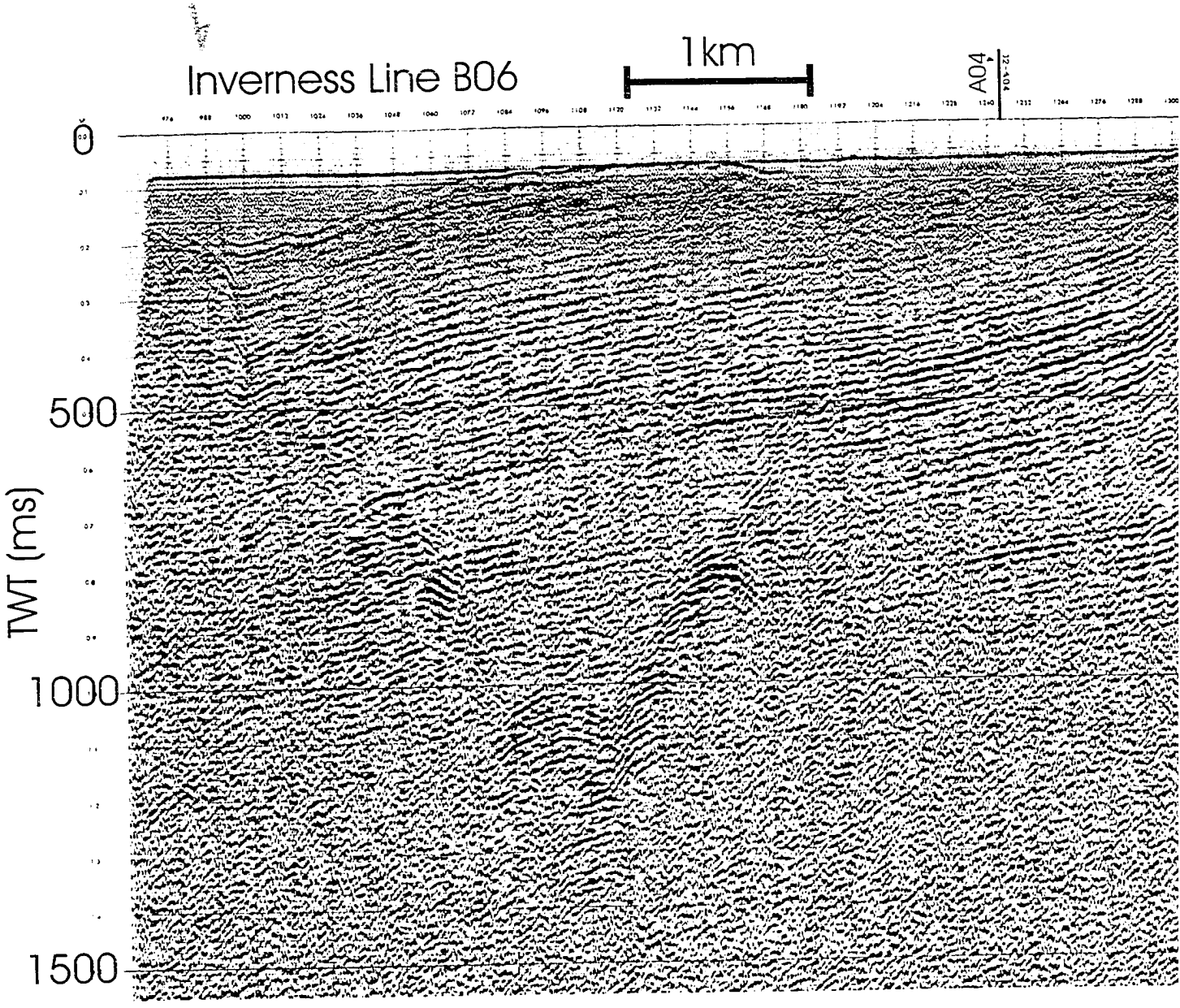
Inverness Line B06
1km
A04
0
500
1000
1500
TWT (ms)

Line B06

1km

A04

A05

Shot Point

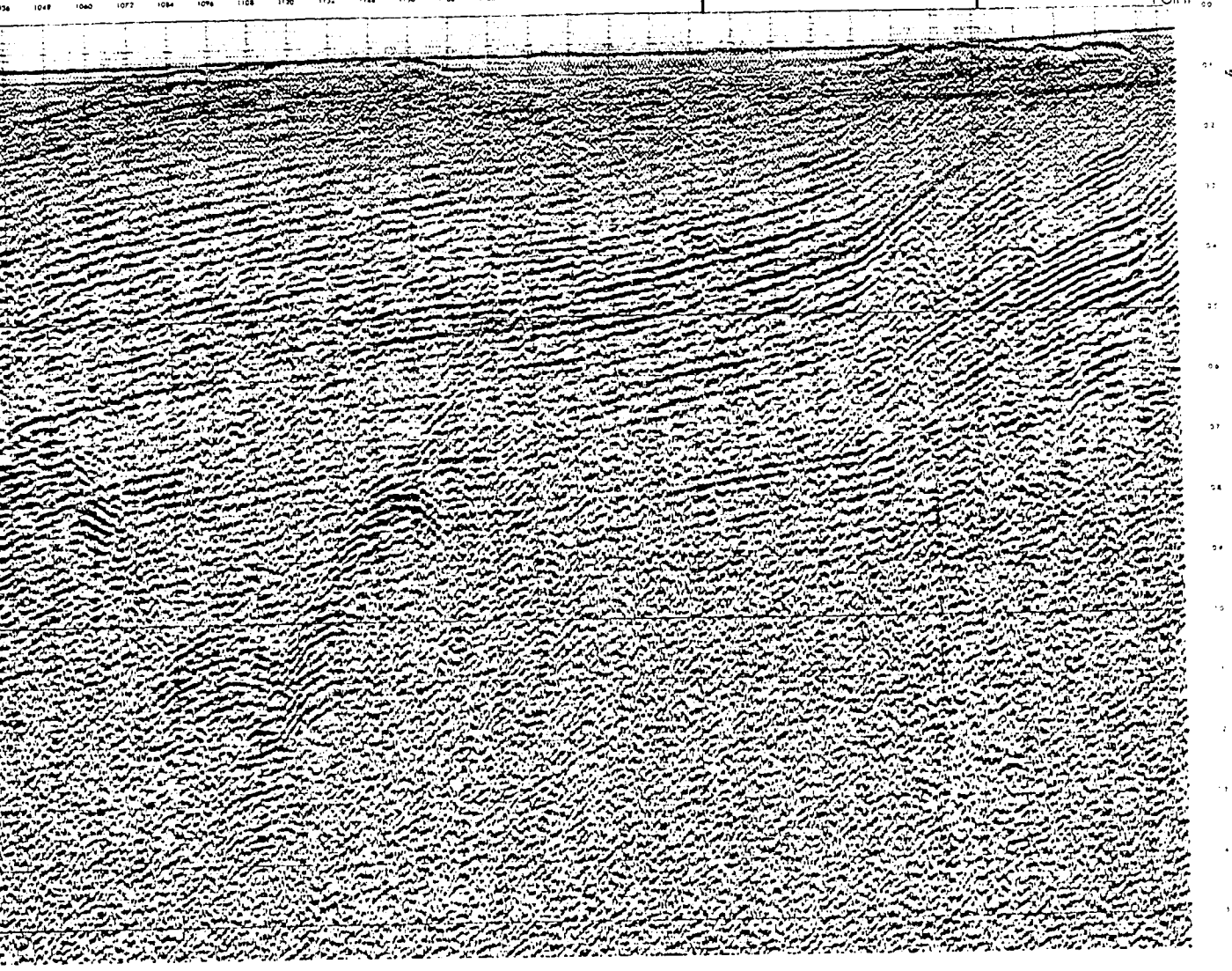

Inverness Line B03

1km

A04

TWT (ms)

0

500

1000

1500

ess Line B03

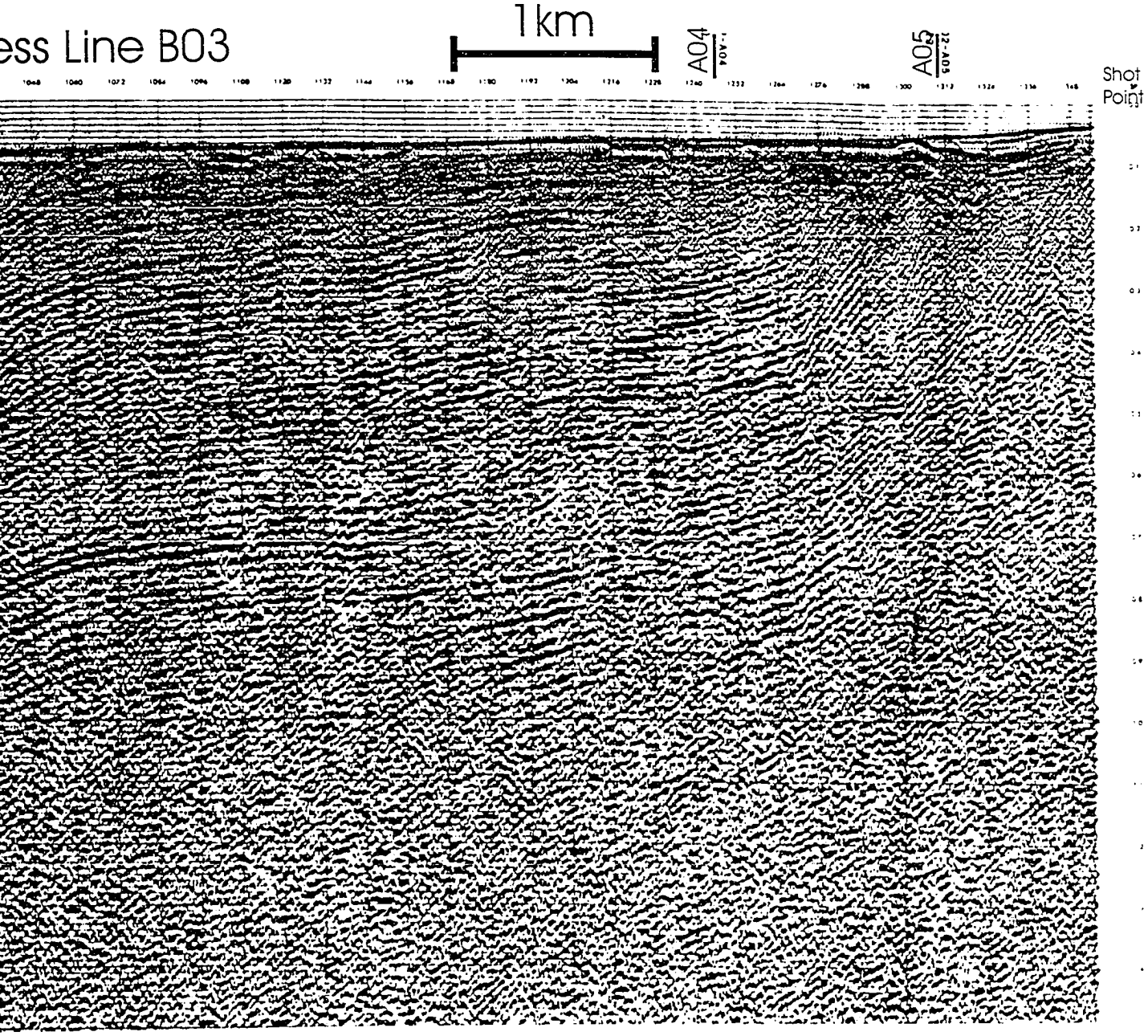

Inverness line B04
1km
A04
32-A04
976
988
1000
1012
1024
1036
1048
1060
1072
1084
1096
1108
1120
1132
1144
1156
1168
1180
1192
1204
1216
1228
1240
1252
1264
1276
0
0.1
0.2
0.3
0.4
500
0.6
0.7
0.8
0.9
1000
1.1
1.2
1.3
1.4
1500
TWT (ms)

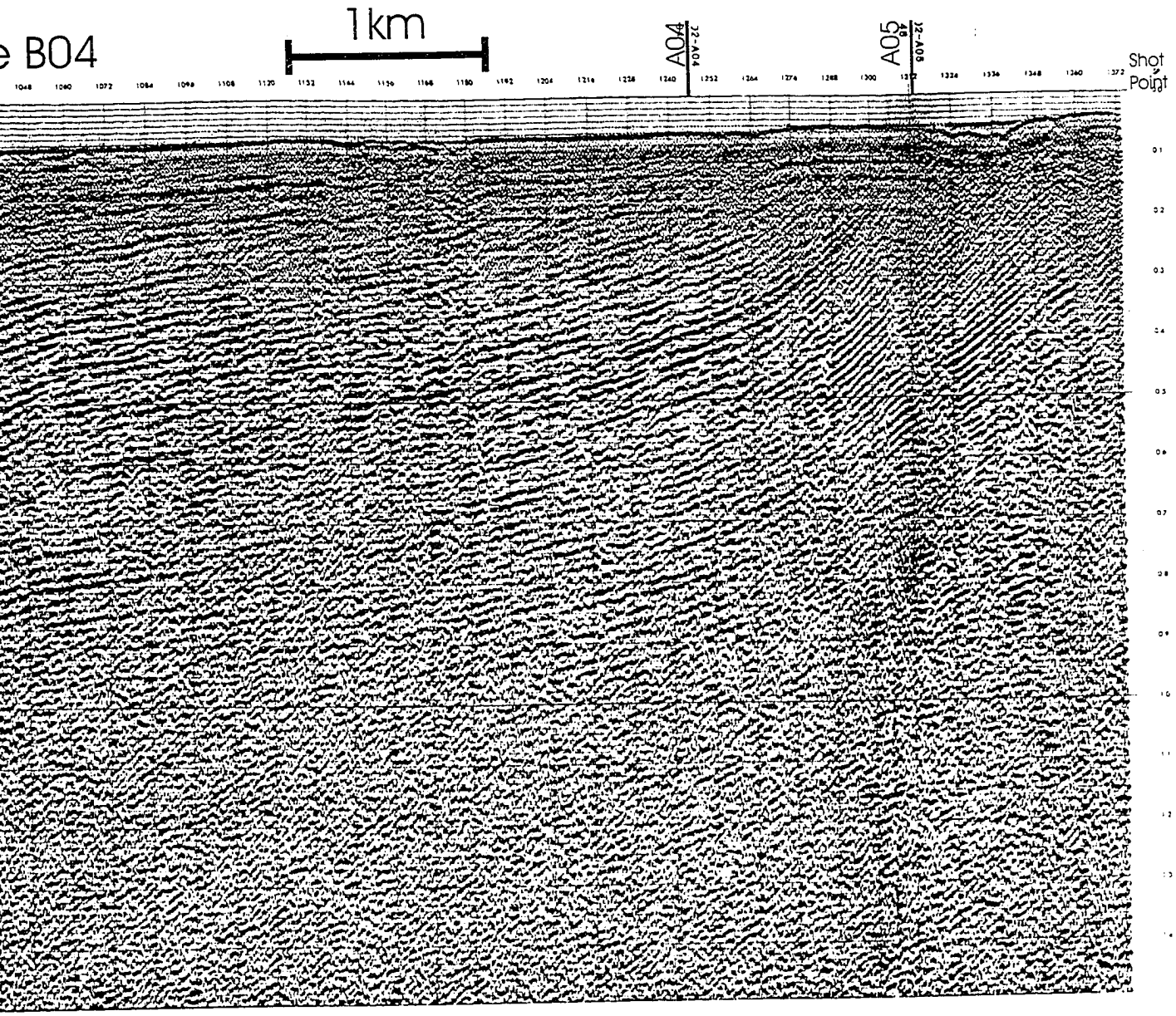
e B04
1km
A04
22-A04
A05
12-A05
Shot Point